

Table of Contents

1. Cover image
2. Title page
3. Table of Contents
4. Copyright
5. List of authors
6. About the authors
7. Preface
8. Acknowledgments

1. Dedication

9. Part One: The background to nuclear thermal-hydraulics

1. 1: Introduction

1. Abstract
2. Acknowledgments
3. Chapter foreword
4. Glossary

2. 2: A historical perspective of nuclear thermal-hydraulics

1. Abstract

2. Chapter foreword

3. 3: Parameters and concepts

1. Abstract

2. Chapter foreword

4. 4: Role of thermal-hydraulics in nuclear power plants: Design and safety

1. Abstract

2. Chapter foreword

10. Part Two: Thermal-hydraulics connections: The principles of thermodynamics and nuclear systems

1. 5: Balance equations

1. Abstract

2. Chapter foreword

3. 5.4 The time-averaged single-phase equations

4. 5.5 The space-time-averaged 1-D equations for single-phase flows

5. 5.6 The various approaches to two-phase flow modeling

6. 5.7 Time-averaged two-fluid equations

7. 5.8 The space averaged 1-D equations for two-phase flow

8. 5.9 The time-space averaged 1-D

equations for two-phase flow

9. 5.10 The 1-D two-fluid equations
as used in system codes
10. 5.11 Some simplified two-phase
models: HEM drift-flux model
11. 5.12 Characteristic velocities and
hyperbolicity
12. 5.13 Transport of interfacial area
and polydispersion models
13. 5.14 3-Field models in system
codes
14. 5.15 Summary remarks

2. 6: Target phenomena in nuclear thermal- hydraulics

1. Abstract
2. Acknowledgments
3. Chapter foreword
4. 6.5 Thermal-hydraulic phenomena
related to advanced water-cooled
reactors
5. 6.6 Thermal-hydraulic phenomena
for SCWRs
6. 6.7 Conclusions

11. Part Three: Nuclear thermal hydraulics modeling

1. 7: Heat transfer in nuclear thermal hydraulics

1. Abstract

2. Acknowledgments
3. Chapter foreword
4. Part 1: Principles and modeling
5. Part 2: Boiling Heat Transfer

2. 8: Pressure drops in nuclear thermal-hydraulics: Principles, experiments, and modeling

1. Abstract
2. List of symbols
3. Chapter foreword

3. 9: Constitutive equations

1. Abstract
2. Chapter foreword

4. 10: Special models for nuclear thermal hydraulics

1. Abstract
2. Chapter foreword

5. 11: The structure of system thermal-hydraulic (SYS-TH) code for nuclear energy applications

1. Abstract
2. Chapter foreword

6. 12: An overview of computational fluid dynamics and nuclear applications

1. Abstract
2. Chapter foreword
3. Part 1. Computational fluid dynamics for nuclear thermal hydraulics: The current overview
4. Part 2. Insights into computational fluid dynamics for nuclear power plant applications

12. Part Four: Applications of thermal-hydraulics in nuclear technology

1. 13: Verification and validation of system thermal-hydraulic computer codes, scaling and uncertainty evaluation of calculated code results

1. Abstract
2. Chapter foreword

2. 14: Best-Estimate Plus Uncertainty (BEPU) approach for accident analysis

1. Abstract
2. Acknowledgments
3. Chapter foreword

3. 15: Applications of SYS TH codes to nuclear

reactor design and accident analysis

1. Abstract
2. Acknowledgments
3. Chapter foreword

4. 16: Thermal-hydraulics aspects of key nuclear accidents

1. Abstract
2. Acknowledgments
3. Chapter foreword

13. Subject Index

14. Author Index

List of tables

1. Tables in 2

1. Table 2.1
2. Table 2.2

2. Table in 4

1. Table 4.1

3. Tables in 5

1. Table 5.1

2. Table 5.2
3. Table 5.3
4. Table 5.4
5. Table 5.5
6. Table 5.6

4. Tables in 6

1. Table 6.1
2. Table 6.2
3. Table 6.3
4. Table 6.4
5. Table 6.5
6. Table 6.6
7. Table 6.7
8. Table 6.8
9. Table 6.9
10. Table 6.10
11. Table 6.11
12. Table 6.12
13. Table 6.13

5. Tables in 7

1. Table 7.1
2. Table 7.2
3. Table 7.3
4. Table 7.4
5. Table 7.5
6. Table 7.6
7. Table 7.7

8. Table 7.8
9. Table 7.9
10. Table 7.10
11. Table 7.11
12. Table 7.12
13. Table 7.13
14. Table 7.14

6. Tables in 9

1. Table 9.1
2. Table 9.2
3. Table 9.3
4. Table 9.4
5. Table 9.5

7. Tables in 10

1. Table 10.1
2. Table 10.2
3. Table 10.3
4. Table 10.4

8. Tables in 12

1. Table 12.1
2. Table 12.2
3. Table 12.3
4. Table 12.4
5. Table 12.5
6. Table 12.6

9. Tables in 13

1. Table 13.1
2. Table 13.2
3. Table 13.3
4. Table 13.4
5. Table 13.5
6. Table 13.6
7. Table 13.7
8. Table 13.8

10. Tables in 14

1. Table 14.1
2. Table 14.2

11. Tables in 15

1. Table 15.1
2. Table 15.2
3. Table 15.3
4. Table 15.4
5. Table 15.5
6. Table 15.6
7. Table 15.7
8. Table 15.8
9. Table 15.9
10. Table 15.10
11. Table 15.11
12. Table 15.12
13. Table 15.13

14. Table 15.14
15. Table 15.15
16. Table 15.16
17. Table 15.17
18. Table 15.18
19. Table 15.19
20. Table 15.20
21. Table 15.21
22. Table 15.22
23. Table 15.23
24. Table 15.24
25. Table 15.25
26. Table 15.26
27. Table 15.27
28. Table 15.28
29. Table 15.29
30. Table 15.30
31. Table 15.31
32. Table 15.32
33. Table 15.33
34. Table 15.34
35. Table 15.35
36. Table 15.36
37. Table 15.37
38. Table 15.38

12. Tables in 16

1. Table 16.1
2. Table 16.2
3. Table 16.3
4. Table 16.4

5. Table 16.5
6. Table 16.6
7. Table 16.7
8. Table 16.8

List of figures

1. Figure in 1

1. Fig. 1.1

2. Figures in 2

1. Fig. 2.1
2. Fig. 2.2
3. Fig. 2.3
4. Fig. 2.4
5. Fig. 2.5
6. Fig. 2.6
7. Fig. 2.7
8. Fig. 2.8
9. Fig. 2.9
10. Fig. 2.10
11. Fig. 2.11

3. Figures in 3

1. Fig. 3.1
2. Fig. 3.2
3. Fig. 3.3

4. Fig. 3.4

4. Figures in 4

1. Fig. 4.1
2. Fig. 4.2
3. Fig. 4.3
4. Fig. 4.4
5. Fig. 4.5
6. Fig. 4.6
7. Fig. 4.7
8. Fig. 4.8
9. Fig. 4.9
10. Fig. 4.10

5. Figures in 5

1. Fig. 5.1
2. Fig. 5.2
3. Fig. 5.3
4. Fig. 5.4
5. Fig. 5.5
6. Fig. 5.6
7. Fig. 5.7
8. Fig. 5.8
9. Fig. 5.9

6. Figures in 6

1. Fig. 6.1
2. Fig. 6.2

7. Figures in 7

1. Fig. 7.1
2. Fig. 7.2
3. Fig. 7.3
4. Fig. 7.4
5. Fig. 7.5
6. Fig. 7.6
7. Fig. 7.7
8. Fig. 7.8
9. Fig. 7.9
10. Fig. 7.10
11. Fig. 7.11
12. Fig. 7.12
13. Fig. 7.13
14. Fig. 7.14
15. Fig. 7.15
16. Fig. 7.16
17. Fig. 7.17
18. Fig. 7.18
19. Fig. 7.19
20. Fig. 7.20
21. Fig. 7.21
22. Fig. 7.22
23. Fig. 7.23
24. Fig. 7.24
25. Fig. 7.25
26. Fig. 7.26
27. Fig. 7.27
28. Fig. 7.28
29. Fig. 7.29
30. Fig. 7.30

- 31. Fig. 7.31
- 32. Fig. 7.32
- 33. Fig. 7.33
- 34. Fig. 7.34
- 35. Fig. 7.35
- 36. Fig. 7.36
- 37. Fig. 7.37
- 38. Fig. 7.38
- 39. Fig. 7.39
- 40. Fig. 7.40
- 41. Fig. 7.41
- 42. Fig. 7.42
- 43. Fig. 7.43
- 44. Fig. 7.44
- 45. Fig. 7.45
- 46. Fig. 7.46
- 47. Fig. 7.47
- 48. Fig. 7.48
- 49. Fig. 7.49
- 50. Fig. 7.50
- 51. Fig. 7.51
- 52. Fig. 7.52
- 53. Fig. 7.53
- 54. Fig. 7.54
- 55. Fig. 7.55
- 56. Fig. 7.56
- 57. Fig. 7.57
- 58. Fig. 7.58
- 59. Fig. 7.59
- 60. Fig. 7.60
- 61. Fig. 7.61
- 62. Fig. 7.62

- 63. Fig. 7.63
- 64. Fig. 7.64
- 65. Fig. 7.65
- 66. Fig. 7.66
- 67. Fig. 7.67

8. Figures in 8

- 1. Fig. 8.1
- 2. Fig. 8.2
- 3. Fig. 8.3
- 4. Fig. 8.4
- 5. Fig. 8.5
- 6. Fig. 8.6
- 7. Fig. 8.7
- 8. Fig. 8.8
- 9. Fig. 8.9
- 10. Fig. 8.10
- 11. Fig. 8.11
- 12. Fig. 8.12
- 13. Fig. 8.13
- 14. Fig. 8.14
- 15. Fig. 8.15
- 16. Fig. 8.16
- 17. Fig. 8.17
- 18. Fig. 8.18
- 19. Fig. 8.19
- 20. Fig. 8.20
- 21. Fig. 8.21
- 22. Fig. 8.22

9. Figures in 9

1. Fig. 9.1
2. Fig. 9.2
3. Fig. 9.3
4. Fig. 9.4
5. Fig. 9.5
6. Fig. 9.6
7. Fig. 9.7
8. Fig. 9.8
9. Fig. 9.9
10. Fig. 9.10
11. Fig. 9.11

10. Figures in 10

1. Fig. 10.1
2. Fig. 10.2
3. Fig. 10.3
4. Fig. 10.4
5. Fig. 10.5
6. Fig. 10.6
7. Fig. 10.7
8. Fig. 10.8
9. Fig. 10.9
10. Fig. 10.10
11. Fig. 10.11
12. Fig. 10.12
13. Fig. 10.13
14. Fig. 10.14
15. Fig. 10.15
16. Fig. 10.16

17. Fig. 10.17
18. Fig. 10.18
19. Fig. 10.19
20. Fig. 10.20
21. Fig. 10.21

11. Figures in 11

1. Fig. 11.1
2. Fig. 11.2
3. Fig. 11.3
4. Fig. 11.4
5. Fig. 11.5
6. Fig. 11.6
7. Fig. 11.7
8. Fig. 11.8
9. Fig. 11.9
10. Fig. 11.10
11. Fig. 11.11
12. Fig. 11.12
13. Fig. 11.13
14. Fig. 11.14
15. Fig. 11.15
16. Fig. 11.16
17. Fig. 11.17
18. Fig. 11.18
19. Fig. 11.19
20. Fig. 11.20
21. Fig. 11.21
22. Fig. 11.22
23. Fig. 11.23
24. Fig. 11.24

- 25. Fig. 11.25
- 26. Fig. 11.26
- 27. Fig. 11.27
- 28. Fig. 11.28
- 29. Fig. 11.29
- 30. Fig. 11.30
- 31. Fig. 11.31

12. Figures in 12

- 1. Fig. 12.1
- 2. Fig. 12.2
- 3. Fig. 12.3
- 4. Fig. 12.4
- 5. Fig. 12.5
- 6. Fig. 12.6
- 7. Fig. 12.7
- 8. Fig. 12.8
- 9. Fig. 12.9
- 10. Fig. 12.10
- 11. Fig. 12.11
- 12. Fig. 12.12
- 13. Fig. 12.13
- 14. Fig. 12.14
- 15. Fig. 12.15
- 16. Fig. 12.16

13. Figures in 13

- 1. Fig. 13.1
- 2. Fig. 13.2

3. Fig. 13.3
4. Fig. 13.4
5. Fig. 13.5
6. Fig. 13.6
7. Fig. 13.7
8. Fig. 13.8
9. Fig. 13.9
10. Fig. 13.10
11. Fig. 13.11
12. Fig. 13.12
13. Fig. 13.13
14. Fig. 13.14
15. Fig. 13.15
16. Fig. 13.16
17. Fig. 13.17
18. Fig. 13.18
19. Fig. 13.19
20. Fig. 13.20

14. Figures in 14

1. Fig. 14.1
2. Fig. 14.2
3. Fig. 14.3

15. Figures in 15

1. Fig. 15.1
2. Fig. 15.2
3. Fig. 15.3
4. Fig. 15.4

5. Fig. 15.5
6. Fig. 15.6
7. Fig. 15.7
8. Fig. 15.8
9. Fig. 15.9
10. Fig. 15.10
11. Fig. 15.11
12. Fig. 15.12
13. Fig. 15.13
14. Fig. 15.14
15. Fig. 15.15
16. Fig. 15.16
17. Fig. 15.17
18. Fig. 15.18
19. Fig. 15.19
20. Fig. 15.20
21. Fig. 15.21
22. Fig. 15.22
23. Fig. 15.23
24. Fig. 15.24
25. Fig. 15.25
26. Fig. 15.26
27. Fig. 15.27
28. Fig. 15.28
29. Fig. 15.29
30. Fig. 15.30
31. Fig. 15.31
32. Fig. 15.32
33. Fig. 15.33
34. Fig. 15.34
35. Fig. 15.35
36. Fig. 15.36

37. Fig. 15.37
38. Fig. 15.38
39. Fig. 15.39
40. Fig. 15.40
41. Fig. 15.41
42. Fig. 15.42
43. Fig. 15.43
44. Fig. 15.44
45. Fig. 15.45
46. Fig. 15.46
47. Fig. 15.47
48. Fig. 15.48
49. Fig. 15.49
50. Fig. 15.50
51. Fig. 15.51
52. Fig. 15.52
53. Fig. 15.53
54. Fig. 15.54
55. Fig. 15.55
56. Fig. 15.56
57. Fig. 15.57
58. Fig. 15.58
59. Fig. 15.59
60. Fig. 15.60
61. Fig. 15.61
62. Fig. 15.62
63. Fig. 15.63
64. Fig. 15.64
65. Fig. 15.65
66. Fig. 15.66
67. Fig. 15.67
68. Fig. 15.68

69. Fig. 15.69

16. Figures in 16

1. Fig. 16.1

2. Fig. 16.2

3. Fig. 16.3

4. Fig. 16.4

Landmarks

1. Cover

2. Title page

3. Table of contents

1. iv

2. xi

3. xii

4. xii

5. xiv

6. xv

7. xvi

8. xvii

9. xviii

10. xix

11. xx

12. 1

13. 4

14. 5

15. 6

16. 7
17. 8
18. 9
19. 10
20. 11
21. 12
22. 13
23. 14
24. 15
25. 16
26. 17
27. 18
28. 19
29. 20
30. 21
31. 22
32. 23
33. 24
34. 25
35. 26
36. 27
37. 28
38. 29
39. 30
40. 31
41. 32
42. 33
43. 34
44. 35
45. 36
46. 37
47. 38

48. 39
49. 40
50. 41
51. 45
52. 46
53. 47
54. 48
55. 49
56. 50
57. 51
58. 52
59. 53
60. 54
61. 55
62. 56
63. 57
64. 58
65. 59
66. 60
67. 61
68. 62
69. 63
70. 64
71. 65
72. 66
73. 67
74. 68
75. 69
76. 70
77. 71
78. 72
79. 73

80. 74
81. 75
82. 76
83. 77
84. 78
85. 79
86. 80
87. 81
88. 82
89. 83
90. 84
91. 85
92. 86
93. 87
94. 89
95. 90
96. 91
97. 92
98. 93
99. 94
100. 95
101. 96
102. 97
103. 98
104. 99
105. 100
106. 101
107. 102
108. 103
109. 104
110. 105
111. 106

112. 107
113. 108
114. 109
115. 110
116. 111
117. 112
118. 113
119. 114
120. 115
121. 116
122. 117
123. 118
124. 119
125. 120
126. 121
127. 122
128. 123
129. 124
130. 125
131. 126
132. 127
133. 128
134. 129
135. 130
136. 131
137. 132
138. 133
139. 134
140. 135
141. 136
142. 137
143. 138

144. 139
145. 141
146. 143
147. 145
148. 146
149. 147
150. 148
151. 149
152. 150
153. 151
154. 152
155. 153
156. 154
157. 155
158. 156
159. 157
160. 158
161. 159
162. 160
163. 161
164. 162
165. 163
166. 164
167. 165
168. 166
169. 167
170. 168
171. 173
172. 174
173. 175
174. 176
175. 177

176. 178
177. 179
178. 180
179. 181
180. 182
181. 183
182. 184
183. 185
184. 186
185. 187
186. 188
187. 189
188. 190
189. 191
190. 192
191. 193
192. 194
193. 195
194. 196
195. 197
196. 198
197. 199
198. 200
199. 201
200. 202
201. 203
202. 204
203. 205
204. 206
205. 207
206. 208
207. 209

208. 210
209. 211
210. 212
211. 213
212. 214
213. 215
214. 216
215. 217
216. 218
217. 219
218. 220
219. 221
220. 222
221. 223
222. 224
223. 225
224. 226
225. 227
226. 228
227. 229
228. 230
229. 231
230. 232
231. 233
232. 234
233. 235
234. 236
235. 237
236. 238
237. 239
238. 240
239. 241

240. 242
241. 243
242. 244
243. 245
244. 248
245. 249
246. 250
247. 251
248. 252
249. 253
250. 254
251. 255
252. 256
253. 257
254. 258
255. 259
256. 260
257. 261
258. 262
259. 263
260. 264
261. 265
262. 266
263. 267
264. 268
265. 269
266. 270
267. 271
268. 272
269. 273
270. 274
271. 275

272. 276

273. 277

274. 278

275. 279

276. 280

277. 281

278. 282

279. 283

280. 284

281. 285

282. 286

283. 287

284. 288

285. 289

286. 290

287. 291

288. 292

289. 293

290. 294

291. 295

292. 296

293. 297

294. 298

295. 299

296. 300

297. 301

298. 302

299. 303

300. 304

301. 305

302. 306

303. 307

304. 308

305. 309

306. 310

307. 311

308. 312

309. 313

310. 314

311. 315

312. 316

313. 317

314. 318

315. 319

316. 320

317. 321

318. 322

319. 323

320. 324

321. 325

322. 326

323. 327

324. 328

325. 329

326. 330

327. 331

328. 332

329. 333

330. 334

331. 335

332. 336

333. 337

334. 338

335. 339

336. 340
337. 341
338. 342
339. 343
340. 344
341. 345
342. 346
343. 347
344. 348
345. 349
346. 350
347. 351
348. 352
349. 353
350. 354
351. 355
352. 356
353. 357
354. 360
355. 361
356. 362
357. 363
358. 364
359. 365
360. 366
361. 367
362. 368
363. 369
364. 370
365. 371
366. 372
367. 373

368. 374
369. 375
370. 376
371. 377
372. 378
373. 379
374. 380
375. 381
376. 382
377. 383
378. 384
379. 385
380. 386
381. 387
382. 388
383. 389
384. 390
385. 391
386. 392
387. 393
388. 394
389. 395
390. 396
391. 397
392. 398
393. 399
394. 400
395. 401
396. 402
397. 403
398. 404
399. 405

400. 406
401. 407
402. 408
403. 409
404. 410
405. 411
406. 412
407. 413
408. 414
409. 415
410. 416
411. 417
412. 418
413. 419
414. 420
415. 421
416. 422
417. 423
418. 424
419. 425
420. 426
421. 427
422. 428
423. 429
424. 430
425. 431
426. 432
427. 433
428. 434
429. 435
430. 436
431. 437

432. 438

433. 439

434. 440

435. 441

436. 442

437. 443

438. 444

439. 445

440. 446

441. 447

442. 448

443. 449

444. 450

445. 451

446. 452

447. 453

448. 454

449. 455

450. 456

451. 457

452. 458

453. 459

454. 460

455. 461

456. 462

457. 463

458. 464

459. 465

460. 466

461. 467

462. 468

463. 469

464. 470

465. 471

466. 472

467. 473

468. 474

469. 475

470. 476

471. 477

472. 478

473. 479

474. 480

475. 481

476. 482

477. 483

478. 484

479. 485

480. 486

481. 487

482. 488

483. 489

484. 490

485. 491

486. 492

487. 493

488. 495

489. 496

490. 497

491. 498

492. 499

493. 500

494. 501

495. 502

496. 503
497. 504
498. 505
499. 506
500. 507
501. 508
502. 509
503. 510
504. 511
505. 512
506. 513
507. 514
508. 515
509. 516
510. 517
511. 518
512. 519
513. 520
514. 521
515. 522
516. 523
517. 524
518. 525
519. 526
520. 527
521. 528
522. 529
523. 530
524. 531
525. 532
526. 533
527. 534

528. 535

529. 536

530. 537

531. 538

532. 539

533. 540

534. 541

535. 542

536. 543

537. 544

538. 545

539. 546

540. 547

541. 549

542. 550

543. 551

544. 552

545. 553

546. 554

547. 555

548. 556

549. 557

550. 558

551. 559

552. 560

553. 561

554. 562

555. 563

556. 564

557. 565

558. 566

559. 567

560. 568

561. 569

562. 570

563. 571

564. 572

565. 573

566. 574

567. 575

568. 576

569. 577

570. 578

571. 579

572. 580

573. 581

574. 582

575. 583

576. 584

577. 585

578. 586

579. 587

580. 588

581. 589

582. 590

583. 591

584. 592

585. 593

586. 594

587. 595

588. 596

589. 597

590. 598

591. 599

592. 600

593. 601

594. 602

595. 603

596. 604

597. 605

598. 606

599. 607

600. 608

601. 609

602. 610

603. 611

604. 612

605. 613

606. 614

607. 615

608. 616

609. 617

610. 618

611. 619

612. 620

613. 621

614. 622

615. 623

616. 624

617. 625

618. 626

619. 627

620. 628

621. 629

622. 630

623. 631

624. 632

625. 633

626. 634

627. 635

628. 636

629. 637

630. 638

631. 639

632. 641

633. 642

634. 643

635. 644

636. 645

637. 646

638. 647

639. 648

640. 649

641. 650

642. 651

643. 652

644. 653

645. 654

646. 655

647. 656

648. 657

649. 658

650. 659

651. 660

652. 661

653. 662

654. 663

655. 664

656. 665

657. 666

658. 667

659. 668

660. 669

661. 671

662. 672

663. 673

664. 674

665. 675

666. 676

667. 677

668. 678

669. 679

670. 680

671. 681

672. 682

673. 683

674. 684

675. 685

676. 686

677. 687

678. 688

679. 689

680. 690

681. 691

682. 692

683. 693

684. 694

685. 695

686. 696

687. 697

688. 698

689. 699

690. 700

691. 701

692. 702

693. 703

694. 704

695. 705

696. 706

697. 707

698. 708

699. 709

700. 710

701. 711

702. 712

703. 713

704. 714

705. 715

706. 716

707. 717

708. 718

709. 719

710. 720

711. 721

712. 722

713. 723

714. 724

715. 725

716. 727

717. 729

718. 733

719. 734

720. 735

721. 736

722. 737

723. 738

724. 739

725. 740

726. 741

727. 742

728. 743

729. 744

730. 745

731. 746

732. 747

733. 748

734. 749

735. 750

736. 751

737. 752

738. 753

739. 755

740. 756

741. 757

742. 758

743. 759

744. 760

745. 761

746. 762

747. 763

748. 764

749. 765

750. 766

751. 767

752. 768
753. 769
754. 770
755. 771
756. 772
757. 774
758. 775
759. 776
760. 777
761. 778
762. 779
763. 780
764. 781
765. 782
766. 784
767. 785
768. 786
769. 787
770. 788
771. 789
772. 790
773. 791
774. 792
775. 793
776. 794
777. 795
778. 796
779. 797
780. 798
781. 799
782. 800
783. 801

784. 802

785. 803

786. 804

787. 805

788. 806

789. 807

790. 808

791. 809

792. 810

793. 811

794. 812

795. 813

796. 814

797. 815

798. 817

799. 818

800. 819

801. 820

802. 821

803. 822

804. 823

805. 824

806. 825

807. 826

808. 827

809. 828

810. 829

811. 831

812. 833

813. 834

814. 835

815. 836

816. 837

817. 838

818. 839

819. 840

820. 841

821. 842

822. 843

823. 844

824. 845

825. 846

826. 847

827. 848

828. 849

829. 850

830. 851

831. 852

832. 853

833. 854

834. 855

835. 856

836. 857

837. 858

838. 859

839. 860

840. 861

841. 862

842. 863

843. 864

844. 865

845. 866

846. 867

847. 868

848. 869

849. 870

850. 871

851. 872

852. 873

853. 874

854. 875

855. 876

856. 877

857. 878

858. 879

859. 880

860. 881

861. 882

862. 883

863. 884

864. 885

865. 886

866. 887

867. 888

868. 889

869. 890

870. 891

871. 892

872. 893

873. 894

874. 895

875. 896

876. 897

877. 898

878. 899

879. 900

880. 901
881. 902
882. 903
883. 905
884. 908
885. 909
886. 910
887. 911
888. 912
889. 913
890. 914
891. 915
892. 916
893. 917
894. 918
895. 919
896. 920
897. 921
898. 922
899. 923
900. 924
901. 925
902. 926
903. 927
904. 928
905. 929
906. 930
907. 931
908. 932
909. 933
910. 934
911. 935

912. 936
913. 937
914. 938
915. 939
916. 940
917. 941
918. 942
919. 943
920. 944
921. 945
922. 946
923. 947
924. 948
925. 949
926. 950
927. 951
928. 956
929. 957
930. 958
931. 959
932. 960
933. 961
934. 962
935. 963
936. 964
937. 965
938. 966
939. 967
940. 968
941. 969
942. 970
943. 971

944. 972
945. 973
946. 974
947. 975
948. 976
949. 977
950. 978
951. 979
952. 980
953. 981
954. 982
955. 983
956. 984
957. 985
958. 986
959. 987
960. 988
961. 989
962. 990
963. 991
964. 992
965. 993
966. 994
967. 995
968. 996
969. 997
970. 998
971. 999
972. 1001
973. 1002
974. 1003
975. 1004

976. 1005
977. 1006
978. 1007
979. 1008
980. 1009
981. 1010
982. 1011
983. 1012
984. 1013
985. 1014
986. 1015
987. 1016
988. 1017
989. 1018
990. 1019
991. 1020
992. 1021
993. 1022
994. 1023
995. 1024
996. 1025
997. 1026
998. 1027
999. 1028
1000. 1029
1001. 1030
1002. 1031
1003. 1032
1004. 1033
1005. 1034
1006. 1035
1007. 1036

1008. 1037
1009. 1038
1010. 1039
1011. 1040
1012. 1041
1013. 1042
1014. 1043
1015. 1044
1016. 1045
1017. 1046
1018. 1047
1019. 1048
1020. 1049
1021. 1050
1022. 1051
1023. 1052
1024. 1053
1025. 1054
1026. 1055
1027. 1056
1028. 1057
1029. 1058
1030. 1059
1031. 1060
1032. 1061
1033. 1062
1034. 1063
1035. 1064
1036. 1065
1037. 1066
1038. 1067
1039. 1068

1040. 1069
1041. 1070
1042. 1071
1043. 1072
1044. 1073
1045. 1074
1046. 1075
1047. 1076
1048. 1077
1049. 1078
1050. 1079
1051. 1080
1052. 1081
1053. 1082
1054. 1083
1055. 1084
1056. 1085
1057. 1086
1058. 1087
1059. 1088
1060. 1089
1061. 1090
1062. 1091
1063. 1092
1064. 1093
1065. 1094
1066. 1095
1067. 1096
1068. 1097
1069. 1099
1070. 1102
1071. 1103

1072. 1104
1073. 1105
1074. 1106
1075. 1107
1076. 1108
1077. 1109
1078. 1110
1079. 1111
1080. 1112
1081. 1113
1082. 1114
1083. 1115
1084. 1116
1085. 1117
1086. 1118
1087. 1119
1088. 1120
1089. 1121
1090. 1122
1091. 1123
1092. 1124
1093. 1125
1094. 1126
1095. 1127
1096. 1128
1097. 1129
1098. 1130
1099. 1131
1100. 1132
1101. 1133
1102. 1134
1103. 1135

1104. 1136
1105. 1137
1106. 1138
1107. 1139
1108. 1140
1109. 1141
1110. 1142
1111. 1143
1112. 1144
1113. 1145
1114. 1146
1115. 1147
1116. 1148
1117. 1149
1118. 1150
1119. 1151
1120. 1153
1121. 1154
1122. 1155
1123. 1156
1124. 1157
1125. 1158
1126. 1159
1127. 1160
1128. 1161
1129. 1162
1130. 1163
1131. 1164
1132. 1165
1133. 1166
1134. 1167
1135. 1168

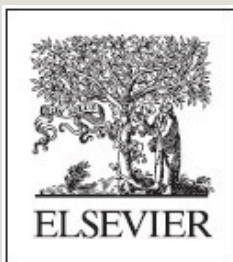
1136. 1169
1137. 1170
1138. 1171
1139. 1172
1140. 1173
1141. 1174
1142. 1175
1143. 1176
1144. 1177
1145. 1178
1146. pge1
1147. pge2
1148. pge3
1149. pge4
1150. pge5
1151. pge6
1152. pge7
1153. pge8
1154. pge9
1155. pge11
1156. pge12
1157. pge13
1158. pge14
1159. pge15
1160. pge16
1161. pge17
1162. pge18
1163. pge19
1164. pge20
1165. pge21

Thermal Hydraulics in Water-Cooled Nuclear Reactors

First Edition

Francesco D'Auria

University of Pisa, Italy



WP

WOODHEAD
PUBLISHING

An imprint of Elsevier



Table of Contents

Cover image

Title page

Copyright

List of authors

About the authors

Preface

Acknowledgments

Dedication

Part One: The background to nuclear thermal-hydraulics

1: Introduction

Abstract

Acknowledgments

Chapter foreword

Glossary

2: A historical perspective of nuclear thermal-hydraulics

Abstract

Chapter foreword

3: Parameters and concepts

Abstract

Chapter foreword

4: Role of thermal-hydraulics in nuclear power plants: Design and safety

Abstract

Chapter foreword

Part Two: Thermal-hydraulics connections: The principles of thermodynamics and nuclear systems

5: Balance equations

Abstract

Chapter foreword

5.4 The time-averaged single-phase equations

5.5 The space-time-averaged 1-D equations for single-phase flows

5.6 The various approaches to two-phase flow modeling

5.7 Time-averaged two-fluid equations

5.8 The space averaged 1-D equations for two-phase flow

5.9 The time-space averaged 1-D equations for two-phase flow

5.10 The 1-D two-fluid equations as used in system codes

5.11 Some simplified two-phase models: HEM drift-flux model

5.12 Characteristic velocities and hyperbolicity

5.13 Transport of interfacial area and polydispersion models

5.14 3-Field models in system codes

5.15 Summary remarks

6: Target phenomena in nuclear thermal-hydraulics

Abstract

Acknowledgments

Chapter foreword

6.5 Thermal-hydraulic phenomena related to advanced water-cooled reactors

6.6 Thermal-hydraulic phenomena for SCWRs

6.7 Conclusions

Part Three: Nuclear thermal hydraulics modeling

7: Heat transfer in nuclear thermal hydraulics

Abstract

Acknowledgments

Chapter foreword

Part 1: Principles and modeling

Part 2: Boiling Heat Transfer

8: Pressure drops in nuclear thermal-hydraulics: Principles, experiments, and modeling

Abstract

List of symbols

Chapter foreword

9: Constitutive equations

Abstract

Chapter foreword

10: Special models for nuclear thermal hydraulics

Abstract

Chapter foreword

11: The structure of system thermal-hydraulic (SYS-TH) code for nuclear energy applications

Abstract

Chapter foreword

12: An overview of computational fluid dynamics and nuclear applications

Abstract

Chapter foreword

Part 1. Computational fluid dynamics for nuclear thermal hydraulics: The current overview

Part 2. Insights into computational fluid dynamics for nuclear power plant applications

Part Four: Applications of thermal-hydraulics in nuclear technology

13: Verification and validation of system thermal-hydraulic computer codes, scaling and uncertainty evaluation of calculated code results

Abstract

Chapter foreword

14: Best-Estimate Plus Uncertainty (BEPU) approach for accident analysis

Abstract

Acknowledgments

Chapter foreword

15: Applications of SYS TH codes to nuclear reactor design and accident analysis

Abstract

Acknowledgments

Chapter foreword

16: Thermal-hydraulics aspects of key nuclear accidents

Abstract

Acknowledgments

Chapter foreword

Subject Index

Author Index



Copyright

Woodhead Publishing is an imprint of Elsevier

The Officers' Mess Business Centre, Royston Road, Duxford, CB22 4QH, United Kingdom

50 Hampshire Street, 5th Floor, Cambridge, MA 02139, United States

The Boulevard, Langford Lane, Kidlington, OX5 1GB, United Kingdom

© 2017 Elsevier Ltd. All rights reserved.

No part of this publication may be reproduced or transmitted in any form or by any means, electronic or mechanical, including photocopying, recording, or any information storage and retrieval system, without permission in writing from the publisher. Details on how to seek permission, further information about the Publisher's permissions policies and our arrangements with organizations such as the Copyright Clearance Center and the Copyright Licensing Agency, can be found at our website: www.elsevier.com/permissions.

This book and the individual contributions contained in it are protected under copyright by the Publisher (other than as may be noted herein).

Notices

Knowledge and best practice in this field are constantly changing. As new research and experience broaden our understanding, changes in research methods, professional practices, or medical treatment may become necessary.

Practitioners and researchers must always rely on their own

experience and knowledge in evaluating and using any information, methods, compounds, or experiments described herein. In using such information or methods they should be mindful of their own safety and the safety of others, including parties for whom they have a professional responsibility.

To the fullest extent of the law, neither the Publisher nor the authors, contributors, or editors, assume any liability for any injury and/or damage to persons or property as a matter of products liability, negligence or otherwise, or from any use or operation of any methods, products, instructions, or ideas contained in the material herein.

Library of Congress Cataloging-in-Publication Data

A catalog record for this book is available from the Library of Congress

British Library Cataloguing-in-Publication Data

A catalogue record for this book is available from the British Library

ISBN: 978-0-08-100662-7 (print)

ISBN: 978-0-08-100679-5 (online)

For information on all Woodhead publications visit our website at <https://www.elsevier.com/books-and-journals>



**Working together
to grow libraries in
developing countries**

www.elsevier.com • www.bookaid.org

Publisher: Joe Hayton

Acquisition Editor: Maria Convey

Editorial Project Manager: Ashlie Jackman

Production Project Manager: Mohana Natarajan

Cover Designer: Mark Rogers



List of authors

N. Aksan, *Paul Scherrer Institut, Villingen, Switzerland*

D. Bestion, *Atomic Energy Commission, Grenoble, France*

F. D'Auria, *University of Pisa, Pisa, Italy*

G.M. Galassi, *University of Pisa, Pisa, Italy*

H. Glaeser, *GRS, Garching, Germany*

Y. Hassan, *Texas A&M University, College Station, TX, United States*

J.J. Jeong, *Pusan National University, Pusan, South Korea*

P.L. Kirillov, *Institute of Thermal Physics and Nuclear Science in the State Scientific Centre of the Russian Federation, Obninsk, Russia*

C. Morel, *Atomic Energy Commission, Grenoble, France*

H. Ninokata, *Tokyo Institute of Technology, Tokyo, Japan*

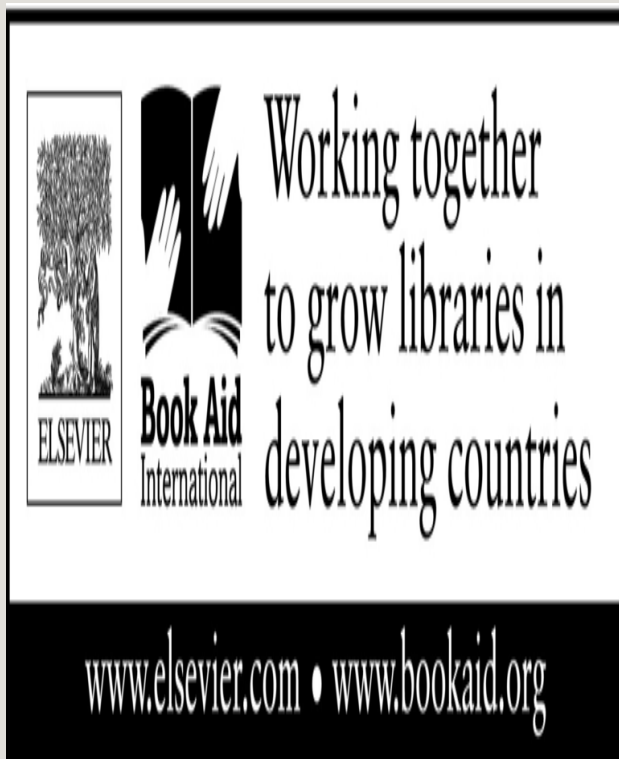
F. Reventos, *Polytechnic University of Catalonia, Barcelona, Spain*

U.S. Rohatgi, *Brookhaven National Laboratory, Upton, NY, United States*

R.R. Schultz, *Idaho National Engineering Laboratory, Idaho Falls, ID, United States*

K. Umminger, *AREVA, Erlangen, Germany*

About the authors



Nusret Aksan was born on Apr. 13, 1945 in Bursa, Turkey. He holds a BSc degree (1967) and an MSc degree (1969) in Mechanical Engineering from Middle East Technical University, Ankara, and an MSc degree (1971) in Nuclear Engineering from University of London. He has more than 45 years of experience in the nuclear engineering field. After working in the commissioning of Karachi Nuclear Power Plant (CANDU), he joined Paul Scherrer Institute, PSI (formerly Swiss Federal Institute for Reactor Research, EIR) and conducted two-phase flow and heat transfer research for Light Water Reactor (LWR) Safety (1973–2008). His

main area of interest is thermal-hydraulic safety analysis of nuclear reactor systems, LWRs, and Advanced LWRs. His five other areas of interest are: (1) Experimental data analysis, (2) modeling of phenomena, (3) computer code modeling and analysis, (4) licensing of nuclear power plants, and (5) active participation and leading roles in the work of various international organizations. Presently he is involved as an independent scientific and engineering consultant.



Dominique Bestion was born on Aug. 9, 1955. He graduated from an Engineering School in 1978 and got a PhD in Fluid Mechanics in 1982. He has been working at the Commissariat à l’Energie Atomique since 1983 in the Thermal-Hydraulic Department at CEA-Grenoble. He is currently a research director at CEA, “Professeur Chargé de Cours” at the Ecole Polytechnique and an editor at the Nuclear Engineering and Design Review. He has worked extensively in modeling two-phase flow and has been the project manager of the CATHARE code. He coordinated two-phase flow modeling activities in the NEPTUNE multiscale thermal-hydraulic project, in the NURESIM, NURISP, and NURESAFE European projects for a multidisciplinary and multiscale software platform. He coordinated a

Writing Group of OECD-CSNI on the application of CFD to nuclear reactor safety issues. His five areas of interest are: (1) Interfacial friction, (2) flashing and condensation, (3) two-phase modeling for SYS TH codes, (4) modeling for two-phase CFD, and (5) multiscale analysis of safety issues.



Francesco D'Auria was born on Aug. 28, 1954 in Benevento, Italy. He started his professional education at the University of Pisa where he got his Master's degree in Nuclear Engineering and his PhD in Nuclear Reactor Safety (1980). He became an assistant professor in 1981 in the same University and an associate professor in 1990 at University of Roma "La Sapienza." Since the year 2000 he is a chair professor at University of Pisa. He has been conducting research in nuclear thermal hydraulics since 1978. His five main areas of interest are: (1) TPCF and Blowdown, (2) scaling and design of ITF, (3) SYS TH code and nodalization qualification, (4) NC and BWR stability, and (5) development and application of uncertainty and BEPU methods. He has been an ANS member since 1981.



Giorgio (Maria) Galassi was born on Oct. 31, 1952 in Riccione, Italy. He got his Master's degree in Nuclear Engineering and the PhD in Nuclear Reactor Safety (1987) with a thesis dealing with the assessment of DBA and Post-DBA computer codes. From 1982 to 2015 he held the position of senior engineer at the Tuscany Region and from 1999 to 2016 has been a member of the "Consiglio del Programma di Dottorato di Ricerca in Ingegneria Nucleare e Sicurezza Industriale" of the University of Pisa. His five main topics of interest in nuclear thermal hydraulics are: (1) accuracy quantification and code validation, (2) counterpart tests and scaling, (3) BEPU, (4) ITF experiments, and (5) development and qualification of nodalization.



Horst Glaeser was born on Jan. 11, 1947 in Berlin, Germany. He got his PhD in Process Engineering in 1976 from Technical University Berlin, Germany. Later he worked in the design and construction of chemical plants and nuclear reprocessing plants at UHDE GmbH in Dortmund, Germany. He joined the Gesellschaft fuer Anlagen und Reaktorsicherheit (GRS) in Garching close to Munich, Germany in 1980. Since 2002 he has been the head of Cooling Systems Department at GRS until his retirement in Jul. 2014. Now he is a senior consultant in Nuclear Reactor Safety Analysis. His main interests are: (1) development of thermal-hydraulic computer codes and their verification and validation; (2) design, scaling, and evaluation of thermal-hydraulic experiments; (3) development and application of the GRS statistical uncertainty analysis method; (4) deterministic safety analyses and assessment for licensing of nuclear power plants; and (5) safety requirements and safety guides.



Yassin Hassan is a professor and head of the Department of Nuclear Engineering, Sallie and Don Davis'61 Professor of Engineering and Professor of the Department of Mechanical Engineering at Texas A&M University. Prior to joining Texas A&M in Sep. 1986, he worked for 7 years at Nuclear Power Division, Babcock & Wilcox Company, Lynchburg, Virginia. He received his MS and PhD in Nuclear Engineering from University of Illinois and MS in Mechanical Engineering from University of Virginia. His research interests are computational and experimental thermal hydraulics, reactor safety, laser-based flow visualization and diagnostic imaging techniques, system modeling, multiphase flow, transient and accident analyses, and advanced nuclear reactors. He is the editor-in-chief of the *Nuclear Engineering and Design Journal*.



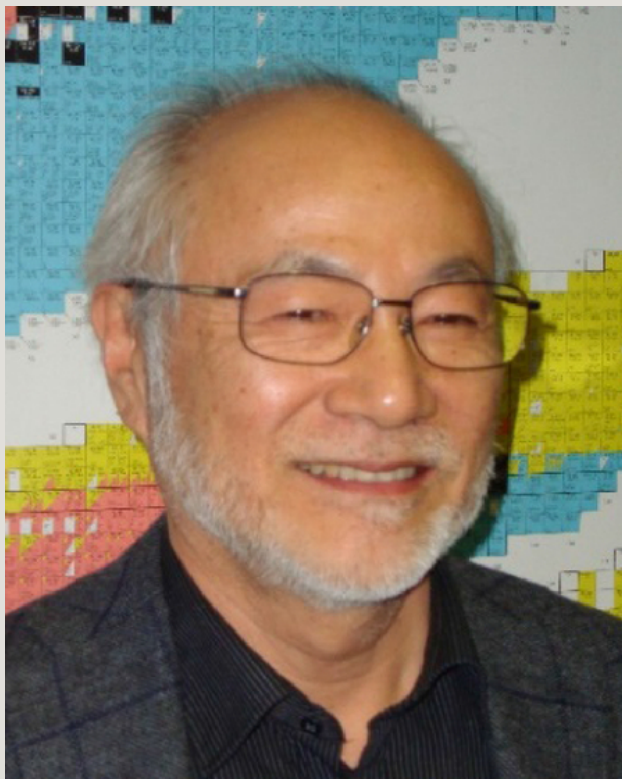
Jae Jun Jeong was born on Jan. 16, 1962 in Youngcheon, Korea. He joined Seoul National University (1980) and majored Nuclear Engineering there. He got his Masters and PhD degrees in Nuclear Engineering at Korea Advanced Institute of Science and Technology. Thereafter, he joined Korea Atomic Energy Research Institute (1990), where he had been responsible for the safety analysis of PWRs, the development and assessment of a TH system code, and a component-scale two-phase flow code. On Mar. 2011, he moved to the School of Mechanical Engineering, Pusan National University. His five main areas of interest are: (1) safety analysis, (2) TH system code, (3) component-scale code, (4) two-phase flow modeling, and (5) numerical methods for a two-phase flow.



Pavel Leonidovich Kirillov was born on Aug. 20, 1927, completed PhD in 1971 and became a professor (1971). He graduated from the Moscow Power Engineering Institute, specializing in Thermal Physics (1950). After graduation he worked at the Institute of Physics and Power Engineering (Obninsk) in various positions from research assistant to director (1950–95). Currently he is a director advisor at the Institute of Thermal Physics and Nuclear Science in the State Scientific Centre of the Russian Federation—Institute for Physics and Power Engineering named after A.I. Leypunsky. He taught at the Obninsk branch of Moscow Engineering Physics Institute (1956–96), was the head of departments “Thermal Physics” (1972–85), and “Nuclear Power Plants” (1985–92). He is a member of the International and Russian Engineering Academies, Honored Worker of Science and Technology (1988), Honorable Doctor of Obninsk State Technical University for Nuclear Energy, National Research Nuclear University, Moscow Engineering Physics Institute (2003), a member of the editorial board of “Atomic Energy.” He has more than 350 publications, including monographs, textbooks, handbooks, and 7 patents. He is an ASME member.



Christophe Morel was born on Mar. 31, 1969. He graduated from an Aerospace Engineer School in 1993 and got a PhD in Fluid Mechanics and Energetics in 1997. He has been working at the Commissariat à l'Energie Atomique for 20 years in the Thermal-Hydraulics Department at CEA-Grenoble. He currently works on numerical simulation for New Energies and Materials studies. He has been teaching Fluid Mechanics and Energetics in several Engineering Schools and Universities and has published a book on two-phase flow modeling for CFD application in 2015. His interests are numerical simulations in thermal, fluid mechanics (single phase or multiphase), solid mechanics applications, and thermoelectricity.



Hisashi Ninokata was born on Sept. 15, 1946 in Kagoshima Prefecture, Japan. He received his BA in Physics and MS and PhD in Nuclear Engineering from the University of Tokyo. He started working at Tokyo Electric Power Co., in 1977, was engaged in R&Ds of Japanese prototype LMFBR development from 1980, became a professor at Tokyo Institute of Technology in 1993, and later professor emeritus in 2012. Since 2012 he has been a professor at Dipartimento di Energia, Politecnico di Milano, Italy. His areas of interest include: (1) physical modeling of microscopic phenomena, (2) liquid metal boiling, (3) BWR subchannel analysis, (4) natural convection phenomena, and (5) uncertainty identification and quantification. He is a fellow of American Nuclear Society (ANS) and a recipient of the ANS Technical Achievement Award in Thermal Hydraulics.



Francesc Reventos was born on May 27, 1951 in Barcelona, Spain. He received his Doctor-Engineer (1982) at the “Institut National Polytechnique de Grenoble” (France). He became an attached professor in the Department of Physics at Technical University of Catalonia (UPC) collaborating also at the Institute of Energy Technologies of the same university. From 1985 to 2001, he was responsible for Plant Dynamic Analysis in the utility organization operating Ascó NPP and Vandellòs NPP, leading the preparation and qualification of the corresponding thermal-hydraulic models as well as its use in fields like operation support, probabilistic safety assessment, training, licensing, and fuel management. His teaching and research responsibilities encompass the areas of nuclear safety, reactor physics, plant dynamic analysis, thermal-hydraulic analysis, management of nuclear power plants and energy technology.



Upendra Singh Rohatgi was born in 1949 in Kanpur, India. He received his Bachelor of Technology degree in Mechanical Engineering from the Indian Institute of Technology, Kanpur. He then received his Masters and PhD degrees in Fluids and Thermal Sciences from Case Western Reserve University, Cleveland, OH in 1972 and 1975, respectively. He joined the scientific staff of Brookhaven National laboratory in 1975 in the Department of Applied Sciences. He is currently a senior scientist. He has contributed to US Nuclear Regulatory programs since 1975 in the areas of development and validation of reactor simulation codes, specifically TRAC, RELAP5, and RAMONA series of codes, and participated in the development of Code Scaling, Applicability, and Uncertainty (CSAU) methodology, the first method of estimating uncertainty in the code prediction. His expertise is in two-phase flows, nuclear simulation codes, LOCA and instabilities, scaling, and turbomachinery.



Richard R. Schultz received his PhD in Nuclear Science & Engineering (2010) from Idaho State University, Pocatello, ID; MSc in Mechanical Engineering (1971) from Rensselaer Polytechnic Institute, Troy, NY; and BSc in Mechanical Engineering (1967) from University of Florida, Gainesville, FL. He served in various positions including Professor of Practice—Texas A&M University; Distinguished Research Engineer (retired)—Idaho National Laboratory, Idaho Falls, Idaho; Research Professor—Idaho State University, Pocatello, ID. He has received several recognitions like Outstanding Engineer Award, 2013, School of Engineering, Idaho State University, Pocatello, ID; Fellow, ASME; Chair: ASME V&V 30 Standards Committee: V&V in Computational Simulation of Nuclear Systems Thermal Fluids Behavior. He has more than 40 years of professional experience in: (1) modeling and analyzing the steady-state and transient behavior of power plants and steam supply systems (PWRs, BWRs, gas-cooled reactors, and commercial steam supply systems); (2) V&V of advanced thermal-hydraulic (TH) engineering numerical models; (3) design, scaling, specification, and conduct of thermal-hydraulic experiments; and (4) evaluation of user-effect on application of advanced thermal-hydraulic software and BEPU techniques applied to advanced

thermal-hydraulic software.



Klaus Umminger was born on Jan. 13, 1956 in Oberlauda, Germany. After graduating from the Technical University of Munich (Diploma in Mechanical Engineering), he joined AREVA (formerly Siemens/KWU) in 1982, where he has been engaged in experimental projects in the field of reactor safety research and in the design of fluid instrumentation. Since 1995 he has been in charge of the large experimental program PKL. The PKL facility (operated at AREVA Germany) is used to investigate the T/H system behavior of PWRs during postulated accidents, since 2001 the PKL project has been continued as an international OECD project. His main areas of work include design, performance, interpretation of experiments for application in code validation, and experimental verification of AM measures for PWRs.



Preface

The technology created after the first self-sustainable nuclear chain reaction taking place in Chicago, USA, at the Chicago Pile-1, in 1942, under the leadership of Enrico Fermi (also called “architect of nuclear age”) constitutes the general framework for the nuclear reactor thermal-hydraulics and the present Book. This is the initiation of the Nuclear Power Plant (NPP) technology. Related cornerstone events or achievements can be summarized as follows:

- Production of electricity by the heat released through undergoing nuclear fission of uranium dioxide
- Use of water as coolant (and also as moderator in the majority of designs) for the region where the chain reaction is sustained, i.e., the core of the reactor
- Construction of large (high power) NPP units
- Safety and design needs for NPP as well as the advent of computational science

Thermal-hydraulics is one of the pillar disciplines to make possible the exploitation of the nuclear fission for the production of electrical power. The complexity and the relevance of the discipline can be depicted by three items:

(A) *Turbulence*: The existence of turbulence is known from several hundred years in single-phase flow conditions; at least, it was noticed by Leonardo da Vinci in the 16th century. Three questions can be formulated: (1) Does turbulence exist?, (2) What is turbulence?, and (3) Can we model turbulence? “Yes” can be the easy answer to the first question. The second question can be hardly answered, i.e., not covering all details of turbulence. “No” is the generic answer to the third question if all relevant appearances of turbulence in nature or man-made systems are considered. In nuclear thermal-hydraulics the intricacy is amplified by the presence

of two phases which interact by turbulence-controlled mass, momentum, and energy transfer processes.

(B) *Bubble motion*: I was visiting an Institute of National Academy of Science in Siberia at the time of Soviet Union. During my presentation about capabilities of thermal-hydraulic system codes a senior researcher who had a “personal” lab underground in the building asked: “How is it possible to predict transient evolutions of two-phase mixtures in complex systems when I cannot calculate the motion of a single bubble?” The problem is more challenging if production, growth coalescence, and collapse of a multitude of bubbles are concerned. Averaging is the answer to the question, but unpredictable errors are introduced.

(C) *Void fraction and neutron flux*: Massive boiling occurs in the core in design conditions of some reactors: two-phase mixture is responsible for generating thermal neutrons by the moderation process other than removing the fission energy. One key-affecting parameter is the amount of water mass in the region. In a high-velocity two-phase flow conditions, void fraction associated with flow regimes determines the fluid mass. Expertise in thermal-hydraulics is needed to determine void fraction with acceptable error including transient conditions: this is directly connected with a variety of flow configurations (flow regimes).

An attempt is made in the Book to provide a vision of nuclear thermal-hydraulics as it appears following more than half-a-century development. The idea is to cover from fundamentals to applications. This implies the consideration of a universe of topics, as discussed in Chapter 1, which may need an encyclopedia rather than a book. So, a window is opened to describe selected elements with emphasis to phenomena and basic principle equations on the side of fundamentals and nuclear reactors accident scenarios on the side of applications.

Currently system thermal-hydraulics codes are used to predict accident scenarios in nuclear reactors. Possibly in some future date computational fluid-dynamics codes (or sets of equations ready to be solved by computers) could be able to predict similar accident scenarios. In this respect, the computer codes constitute one of the central elements in the Book.

The processes of thermal-hydraulic phenomena identification and characterization, code development and validation, as well as scaling demonstration and prediction of errors of code calculations, i.e., uncertainty evaluation, may appear a matter for guru: rigorous procedures are not always applied or simply do not exist. This is also a consequence of some inadequate modeling of aspects in nature, behaviors like turbulence, and bubble motion and coalescence, already noted.

The vision provided in the Book is expected to be helpful in demonstrating the ability of thermal-hydraulics to address the needs in design and safety evaluation of existing nuclear reactors although this is achieved by those complex processes involving averaging techniques, validation, scaling, uncertainty, etc. Consequently, the Book may resemble as the description of a dynamic target rather than an archival product. However, inspiration for moving further the barriers of knowledge shall be attained from various discussed topics: the thermal-hydraulic phenomena and the accident scenarios are relevant in this connection.

The enormous research investment in the period 1970–1990 or 1970–2000, i.e., the golden period for research in nuclear thermal-hydraulics, provided the major source of knowledge to justify the Book. Sufficient understanding of phenomena for technological purposes and worldwide declining interest toward nuclear fission caused sharp decrease in financing and support of research in thermal-hydraulics in subsequent decades.

The grown expertise, sometimes of guru-type, is going to be lost because of retirement of top scientists acting during the golden period. The knowledge built may resemble a small town: the small town is now at risk to become a “Pompeii of the year 2020”; it can be buried by the dust of oblivion. Accidents like Chernobyl and, in a more powerful way, Fukushima mined the trustworthiness of nuclear technology: they are capable of producing the dust which is responsible for clouding the mind of decision makers. The Book contributes to the hope for knowledge preservation although coordinated efforts from all the stake-holders of nuclear technology are needed in this connection.

F. D'Auria, *September 2016, Pisa, Italy*



Acknowledgments

The adventure involved in producing a book like the present one may be undertaken by authors after decades of engagement where fundamental research and technology applications are intimately merged. The complexity of the topic “promotes” deep international cooperation.

The outcome of this is the unavoidable recognition that the work of several hundreds or even thousands of scientists and technologists contributed to the understandings depicted in this book. I feel profoundly indebted to each of them: everyone created or inspired a small stone of the mosaic which is described in the Book. An attempt to create a meaningful list of individuals to be acknowledged would imply an effort comparable to the effort set for producing the Book and still will not eliminate the risk of incompleteness.

Let me create below a pyramid of categories of persons to acknowledge.

The tip of the pyramid is constituted by:

- (a) The authors of chapters who have an expertise in the area far beyond my expertise and accepted the challenge to depict a new vision in the area.
- (b) The authors of documents listed in the references of each chapter: a few thousands names are now listed in alphabetic order at the end of the Book; they provide a sample picture of the expertise in nuclear thermal-hydraulics; I take the occasion here to apologize to the many leading scientists who are not considered in the list.

Further categories down to the base of the pyramid are:

- (c) Scientists and technologists who attended international working groups where I

participated, namely at the Organization for Economic Cooperation and Development (OECD) premises in Paris and at the International Atomic Energy Authority (IAEA) in Vienna: they provided unquantifiable amount of invaluable ideas, research results, and related information.

(d) Secretaries, managers, and directors of a variety of institutions I entered in contact: they ensure, sometimes by hidden efforts, the sustainability of research or the financing of knowledge.

(e) Members of international groups which have been functional for the activities I had the privilege to perform ranging in the areas of development, training, and application in nuclear thermal-hydraulics.

(f) Scientists part of established international contexts like American and European Nuclear Societies; Conferences frameworks like Nuclear Reactor Thermal-Hydraulics (NURETH), International Conference on Nuclear Engineering (ICONE), and International Congress on Advances on Nuclear Power Plants; and Journals like Nuclear Engineering and Design (NED), Science and Technology of Nuclear Installations (STNI), and Nuclear Engineering and Technology (NET).

(g) Colleagues (who tolerated my aversion to unnecessary red tape) and coworkers including Master and PhD students (a few hundreds) and technicians, in various universities of the world (mostly at University of Pisa).

(h) Teachers in Italy and at University of Pisa who opened the doors of knowledge and planned the bases for my professional career.

(i) My parents, relatives, and friends who created or accepted the conditions to perform the activities.

It is my pleasure here to remember my friends and leading scientists Nusret Aksan, Yassin Hassan, and Dominique Bestion who inspired or continuously drove or supervised many of the activities in nuclear thermal-hydraulics where I took part for including in the present Book.

I wish also to acknowledge the work done by Alessio Capperi at University of Pisa in deriving the list of authors of all references and in contributing to improve the editing of individual chapters.

The challenging (nuclear) technology supported by committed and dedicated people revealed the perfect environment for developing a research career. It is my

privilege to belong to this environment and, after decades of the working life, it is my pleasure to invite young generation scientists to enter this community and to tackle the many remaining issues in nuclear reactor thermal-hydraulics field.

However, for the sake of completeness of information, namely for young readers, I will not refrain to bring an unusual acknowledgement remark: this is for those who created hitches and tried to slow-down and stop research initiatives. This revealed an easier task for a technology which became unpopular and vulnerable during the last years (at least in some countries) because of and throughout misinterpreting, or putting within an obscure light, accidents which happened and are also discussed in the Book. Young researchers should expect artificial (man-created, external to the research environment) challenges and be ready to react.

Dedication

This book is dedicated to my teacher Bruno Guerrini and to my friend Emilio Vitale. Both were leaders who embraced the spirit of the Renaissance, paving the way for outstanding endeavors like the one resulting in this current effort. The passing away of Prof. Guerrini from natural causes was preceded by a tragic accident that, in the prime of his life, left Emilio in a twilight world. An easy path has been adopted by their successors that would appear to lead directly toward a new Middle Age. I can still tell Emilio this but he cannot react to the havoc that has been wreaked on great wisdom.

The Editor

Part One

The background to nuclear thermal- hydraulics

Introduction

F. D'Auria University of Pisa, Pisa, Italy

Abstract

The origins of nuclear thermal-hydraulics and its relevance within the technology for the production of electrical power are discussed together with the link with other disciplines. Nuclear power plant design and safety impose the needs for thermal-hydraulics and constitute the framework for the book. Computer codes and experiments are the outcome of five-six decades research to address those needs. The main scientists contributing to the development of the discipline are listed with some notes about their role. A universe of topics characterizes nuclear thermal-hydraulics. The vision provided for the universe reflects into the content of the book: topics range from phenomena in accident analysis, to balance and constitutive equations, development and validation of codes up to the best estimate plus uncertainty (BEPU) approach and the role of thermal-hydraulics for Three-Mile Island, Chernobyl, La Salle, Oskarshamn, and Fukushima events.

Keywords

Nuclear thermal-hydraulics; Accident analysis in NPP; Origin of thermal-hydraulics; Role of thermal-hydraulics in nuclear reactor safety; The computer codes in thermal-hydraulics; The BEPU (best estimate plus uncertainty) approach

Nomenclature

AA accident analysis

AM accident management

AMP accident management
procedures

AM-1 *Atom Mimy* (peaceful atom)—
First Nuclear Reactor in Soviet Union

ANS American Nuclear Society

AP-600 advanced PWR (e.g.,
including passive-safety systems)

AP-1000 advanced PWR (e.g.,
including passive-safety systems)

ASME American Society of
Mechanical Engineering

ATWS anticipated transient without

scram

BDBA beyond design basis accident

BEPU best estimate plus uncertainty

BoP balance of plant

BWR boiling water reactor

CCFL counter-current flow limitation

CFDs computational fluid-dynamics

CIWH condensation-induced water
hammer

CSNI Committee on the Safety of
Nuclear Installations

CVCS chemical and volume control
system

DBA design basis accident

DG diesel generator

DNS direct numerical simulation

DWI density wave instability

EBR-1 experimental breeder reactor
—First Nuclear Reactor in the United States

EC European Commission

ECC emergency core cooling

ECCS emergency core cooling system

EOP emergency operating
procedures

ESBWR economic simplified boiling water reactor

ESF engineered safety features

EVET equal velocities equal temperatures

FSI fluid-structure interaction

HEM homogeneous equilibrium model

HEU highly enriched uranium

HTC heat transfer coefficient

H&M heat and mass

IAEA International Atomic Energy Agency

IAT interfacial area transport

ITF integral test facility

I&C instrumentation and control

LBLOCA large break LOCA

LEU low enriched uranium

LOCA loss of coolant accident

LOFW loss of feed-water

LOOSP loss of on-site and off-site
power (or SBO plus DG failure)

MCP main coolant pump

MFB minimum film boiling

NEA Nuclear Energy Agency

NPP nuclear power plant

NPSH net positive suction head

OECD Organization for Economic
Cooperation and Development

ONB onset of nucleate boiling

PIE postulated initiating event

PSA probabilistic safety assessment

PTS pressurized thermal shock

PWR pressurized water reactor

RCS reactor coolant system

RHR residual heat removal

RIA reactivity-initiated accident

RPV reactor pressure vessel

RR research reactors

SBLOCA small break LOCA

SBO station blackout

SBWR simplified boiling water
reactor

SETF separate-effect test facility

SSC structures, system, and
components

SYS TH system thermal-hydraulics

SWINTH Specialists Workshop on
Advanced Instrumentation and
Measurement Techniques for Nuclear
Reactor Thermal Hydraulics

TMI Three-Mile Island

TPCF two-phase critical flow

UVUT unequal velocities unequal
temperatures

UVUTUP UVUT plus unequal
pressures

VVER (or WWER) water-cooled,
water-moderated energy reactors

WNA World Nuclear Association

Acknowledgments

I wish to acknowledge comments to the chapter received from D. Bestion, H.

Glaeser, and P. Kirillov. In particular, D. Bestion gave suggestion for the structure of the chapter, H. Glaeser performed a review of the original manuscript, and P. Kirillov provided a number of reference documents.

Chapter foreword

Top level researchers involved with applications and developments in thermal-hydraulics from all over the world cooperated to write the book.

Any scientist involved with nuclear thermal-hydraulics may take benefit from reading the book.

Reading this chapter is a prerequisite (not sufficient) for getting acquainted with the book.

Memorizing the authors of documents cited in **Chapter 1** and the topics, connected with thermal-hydraulics which are not discussed in the book (but are listed in **Chapter 1**) will be of great help for understanding the contents of the book.

1.1 Introduction

The composed word thermal-hydraulics, here preferred to thermo-hydraulics, thermal-hydraulics, and thermalhydraulics, derives from two Greek terms also used by Romans, which indicate heat and water, respectively. Thus, thermal-hydraulics is the discipline which studies the transient evolution of engineering systems where (hot-heated) water is the coolant fluid and, typically, heating and cooling or boiling and condensing processes occur.

Nuclear thermal-hydraulics addresses the performance of water-cooled reactors, typically water-moderated, i.e., the majority of research reactors (RR) and power plants. Selected features for the discipline can be listed as follows:

- design and safety of nuclear reactors highly depend upon thermal-hydraulics: this has been established since the beginning of the nuclear technology era;
- looking at the numerical simulation of phenomena,
- it shares with fluid-dynamics and gas-dynamics the difficulty associated with turbulence: in thermal-hydraulics the problem is even more complex because of the presence of two-phases;

○ time and space averaging is unavoidable: discontinuities including the interface between the phases are solved by continuum equations;

- approximation of results from numerical models and the need to bound the errors of calculations, i.e., the uncertainty, are a consequence of what written above;
- experiments are necessary and highly dependent upon geometric configurations: they are not conclusive for a suitable knowledge because performed at reduced scale in the case when power reactors are concerned;
- controversy in judging the quality, the applicability and the acceptability of experimental and numerical data to situations of technological interest is not surprising.

Thus, nuclear thermal-hydraulics can be considered as a sliding and lapsing technology. On the one hand, expertise based on decades of activity may reveal not sufficient to address targets put by design and safety of a variety of nuclear installations and, on the other hand a book built on weak foundations may not be justified. The former issue remains open. Otherwise, the present endeavor is an attempt to address the latter issue: technologists and scientists deeply involved with nuclear thermal-hydraulics after three dozen years activity (or more) are invited to be coauthors. The plan is to present as far as comprehensive vision of modern nuclear thermal-hydraulics assuming that rudimentary-established knowledge is available to readers.

The word nuclear associated with thermal-hydraulics testifies of the progress in knowledge achieved within the development of nuclear technology. Furthermore, the words system thermal-hydraulics (SYS TH) which should be seen as nuclear SYS TH, were proposed during the planning of the framework of the *Specialists Meeting on Transient Two-Phase Flow—System Thermal-hydraulics* organized by the Organization of Economic Cooperation and Development/Nuclear Energy Agency/Committee on the Safety of Nuclear Installations (OECD/NEA/CSNI), held in Aix-en-Provence (OECD/NEA/CSNI, 1992). The SYS TH acronym reflects the connection between the thermal-hydraulics and the nuclear system, namely the size of the concerned system and the interaction among phenomena which occur or are expected in complex geometrical configurations and in transient conditions during postulated accidents in nuclear reactors.

SYS TH, seen as an evolution of fundamental thermal-hydraulics and covering

nuclear thermal-hydraulics, constitutes the topic and the framework for the book.

The computational tools named SYS TH codes, which represent the baskets of expertise in the area, are the direct or the indirect target for individual chapters: emphasis is given to the development, the qualification, and the application of those codes for demonstrating the safety and the acceptability of nuclear installations. The bases, the applicability of the computational fluid-dynamics (CFDs), and its role in nuclear reactor safety and design are described to complement the vision provided for nuclear thermal-hydraulics.

1.1.1 Scope and framework

As far as possible comprehensive list of topics is introduced hereafter to define the framework of thermal-hydraulics. The necessarily reduced scope and framework for the textbook are discussed in the last paragraph of the section.

1.1.1.1 Origin of nuclear thermal-hydraulics

The word thermal-hydraulics has been associated with water and heat from its etymology. This already limited the scope of the book to water-cooled nuclear reactors. However, the word heat embeds concepts like material thermal properties, (thermal) energy balance, thermodynamic efficiency, and energy dissipation. Owing to this and based on the historical use of the word thermal-hydraulic, any process connected with heat generation and transfer has been considered as part of the discipline called thermal-hydraulics. Noticeably, thermal energy transport in sodium and gas-cooled reactors, natural circulation, and thermal mixing of lead-bismuth systems are important fragments in nuclear thermal-hydraulics.

Here in the book, the etymological origin of the word is kept, and at the same time the connection with the nuclear world is formally established. To the last aim, reference is made to the facility constructed by E. Fermi in Chicago to show the sustainability of the fission chain reaction. The nuclear thermal-hydraulics was born on Dec. 2, 1942 when Fermi triggered the fission reaction within the multiton graphite bricks pile. This ensured, other than neutron energy moderation capability and protection from radiations, suitable thermal capacity and heat sink to accommodate the fission power.

In Jul. 1951 the Congress of United States authorized the construction of the nuclear submarine which entered the sea on Jan. 17, 1955. In the mean time, according to World Nuclear Association (WNA, 2014) the first nuclear reactor to produce electricity, albeit in the amount of a few hundred watt, was the liquid metal-cooled EBR-1 reactor in Idaho: on Dec. 20, 1951 (Michal, 2001) “the liquid

metal flowed into water-jacketed pipes to form steam that turned a turbine.” The first substantial production of nuclear electricity, i.e., 5 MW, happened in Soviet Union by the water-cooled and graphite-moderated reactor called AM-1: the world first nuclear power electricity generator began the operation in Obninsk on Jun. 27, 1954.

So, nuclear thermal-hydraulics is unavoidable part of nuclear technology: the fission power heats up a material, i.e., typically the nuclear fuel, and processes are needed to transport the generated energy for application purposes, i.e., toward heat exchangers for the use of thermal power, toward the turbine for electricity for electric power or propulsion.

1.1.1.2 Single- and two-phase flows

Liquid-water or gas-water is commonly referred as liquid and steam or vapor, in the latter case leaving the word gas for superheated conditions. The thermodynamic evolutions of both individual liquid and steam fluids (1-phase or 1Φ) as well as of their mixtures, or two-phase flows (2-phases or 2Φ), constitute the topic of interest for nuclear thermal-hydraulics (e.g., Ishii, 1975; Yadigaroglu and Lahey, 1976). Furthermore, steam flows can be associated with noncondensable gas species of substances other than water, and liquid flows may transport solid particles like impurities including solid fission products or high-temperature boiling boric acid (typically measured in parts-per-million, ppm).

So, nuclear thermal-hydraulics deals with 1Φ and 2Φ water flows, plus noncondensable, plus solid impurities without treating the chemical interactions. However, as a noticeable exception, the metal-water chemical reaction which creates hydrogen at high temperature of a typically heating surface is within the boundary of interest.

1.1.1.3 Prominent scientists and textbooks

Technology needs associated with single- and two-phase flows occurred well before the nuclear era. The transition from horse power on the land or wind power on the sea to steam moved machinery imposed gathering expertise in thermal-hydraulics since the nineteen or even the late 18th century.

Following the creation of modern physics by G. Galilei (1564–1642), I. Newton (1642–1727), and L. Euler (1707–1783), selected prominent scientists who contributed to the development of thermodynamics at the basis of the modern thermal-hydraulics are J. Watt (1736–1819), J.B.J. Fourier (1768–1830), C.L. Navier (1785–1836), J.P. Joule (1818–1889), G. G. Stokes (1819–1903), J.A.

Froude (1818–1894), H. von Helmholtz (1821–1894), W.T. Kelvin (1824–1907), F. Grashof (1826–1893), O. Reynolds (1842–1912, e.g., see Reynolds, 1896), and M. Planck (1858–1947, see e.g., Planck, 1923). More recently, L. Prandtl (1875–1953, e.g., see Prandtl, 1956), T. von Kármán (1881–1963), K.E.W. Nusselt (1882–1957, e.g., see Nusselt, 1943), S. Nukiyama (1896–1983, e.g., see Nukiyama, 1966), A. Kolmogorov (1903–1987), L.D. Landau (1908–1968), A. V. Lykov (1910–1974, see, e.g., Lykov, 1958), and S. S. Kutateladze (1914–1986, see, e.g., Kutateladze, 1963) directly contributed to the bases of thermal-hydraulics even without taking a leadership in the application of the discipline to the nuclear technology.

Parallel to nuclear engineering and with limited interactions with it (i.e., at least in three cases before the start of the nuclear era, here fixed as 1942), thermal and fluid engineering/physics evolved during the first half of the 20th century. Fundamentals in those areas are also fixed by the textbooks by Gröber and Erk (1933), Reichardt (1941), Jakob (1949), Landau and Lifchitz (1954), Lykov and Mikhailov (1961), Bird et al. (1960), Spalding (1963), Sparrow and Cess (1966), and of Patankar and Spalding (1967) in addition to the references already listed in the previous section.

Rudimentary thermal-hydraulics, or elements and concepts in thermal-hydraulics, can be found in the pioneering nuclear engineering textbooks by Glasstone and Edlund (1952), Schultz (1955), Glasstone and Sesonske (1955), Stephenson (1958), and Etherington (1958), and later on by Lamarsh (1966), as well as by Margoulova (1969) in the former Soviet Union.

Nuclear thermal-hydraulics was inspired by the rudiments in the nuclear engineering textbooks rather than the textbooks in thermal and fluid engineering. Professor El-Wakil made the first effort to gather the concepts of nuclear thermal-hydraulics into a textbook (El-Wakil, 1962, 1971a,b).

The modern nuclear thermal-hydraulics can be associated with a couple dozen textbooks which are internationally spread and recognized. A representative and nonexhaustive list of those textbooks (reported in the order of publication date) includes names of key scientists in the area: Tong (1965), Wallis (1970), Tong and Weisman (1970), Collier (1975), Ishii (1975) (see also, Ishii and Hibiki (2006)), Incropera and Dewitt (1981), Delhay et al. (1981), Fenech (1981), Cumo (1982), Hsu and Graham (1986), Todreas and Kazimi (1990), Hewitt et al. (1992), Lahey and Moody (1993), Levy (1999), and Kirillov et al. (2010, 2013, 2014).

In order to complete, as far as possible, the current picture for reference books and scientists in nuclear thermal-hydraulics, the following needs to be considered:

- the reports issued by OECD/NEA and International Atomic Energy Agency (IAEA) dealing with application and needs in nuclear thermal-hydraulics (e.g., Aksan et al. (1987) and Lewis et al. (1989), from the side of OECD/NEA/CSNI and Allison et al. (2002) from the side of IAEA)
- the reports (code manuals) and the support papers describing SYS TH computer codes (e.g., starting from RELAP2, Moore and Rettig, 1968, to Berry et al., 2015) dealing with the RELAP7 under development now, and Bestion, 1990, dealing with the closure laws of the CATHARE code
- the CFD technology and the related CFD (and direct numerical simulation, DNS) codes (e.g., Hassan, 2005)
- the textbooks dealing with topics other than SYS TH in nuclear reactors where thermal-hydraulics has a key role, like Nuclear Plants (e.g., Knief, 2008; Cacuci, 2010; Oka, 2014; Murray and Holbert, 2014; Sjoden, 2015); nuclear fuel subchannel analysis (e.g., Ninokata and Aritomi, 1992); industrial plant safety (e.g., Banerjee, 2003); investigations into selected phenomena (e.g., Yadigaroglu, 1975); fluid-structure interactions (FSIs) (e.g., Païdoussis et al., 2014); thermal-hydraulic instrumentation (e.g., Mayinger, 1994); design of key components for nuclear and thermal plants (e.g., Cumo and Naviglio, 1990); even focused on centrifugal pumps (e.g., Gülich, 2010); steam generators (e.g., Annaratone, 2008); and turbines (e.g., Bloch and Singh, 2009)
- edited open access textbooks have been issued (e.g., Guillen, 2013), but focusing on CFD applications
- there are scientists who published outstanding papers during a time-span longer than half-a-century like Novak Zuber (see e.g., Zuber, 1958; Zuber, 2010) or scientists who published one paper which remained important for half-a-century, like Yamanouchi in relation to the reflood modeling idea (see, e.g., Yamanouchi, 1968) or scientists who devoted their half-a-century working life to a single thermal-hydraulic phenomenon like D.C. Groeneveld in relation to critical heat flux (see, e.g., Groeneveld, 1996)
- the integrated vision proposed by N. Kolev, with a series of five volumes dealing with multiphase flow dynamics (Kolev, 2015). This is the outcome of a lifetime effort for the author. Basilar physical phenomena are considered in the attempt to reconstruct complex system performance from the knowledge and the modeling of local interactions among substances: not only water but also molten materials interactions are concerned to deal with the severe accident conditions in NPP

The textbooks referenced in this section provide a snapshot idea, still narrow and incomplete, of the complexity of the nuclear thermal-hydraulics and, all together, constitute a challenge for the present book. Otherwise, links and interconnections between nuclear thermal-hydraulics and various topics including other disciplines relevant in nuclear technology and safety are considered below.

1.1.1.4 Journals, conferences, and the web

Nuclear thermal-hydraulics, like a variety of disciplines, has its space and interest in devoted journals, national and international conferences, and the web. Namely the web is not only a mirror for journal and conference papers but may include much more, like master theses, PhD dissertations, documents issued by institutions and companies, and lectures by professors and experts.

Providing lists of journals or conferences dealing with nuclear thermal-hydraulics is not the purpose here. Rather, the purpose here is to give an idea of the overall number of papers in the area and their rate of growth.

Starting from the 1950s and considering the exponential growth of the number of publications after the advent of computers and the internet, roughly 10,000–20,000 papers have been published within the nuclear thermal-hydraulics area. The current growth rate is around 1000 (papers)/year considering journals and conferences. This may also give an idea of the effort needed to follow or interpret developments in the area.

1.1.1.5 Education and training

Nuclear thermal-hydraulics is also the topic of education at universities, undergraduate, graduate, and PhD courses. Several tens of universities all over the world offer nuclear thermal-hydraulics courses: one may estimate in a few thousands of students per year, however largely changing in each country each year.

Specialized training courses exist, covering fundamentals and application topics in thermal-hydraulics (see the course organized in Zurich by Prof. G. Yadigaroglu) and the technology of using SYS TH codes (e.g., see Petruzzi et al., 2008).

The material in the book can be used for training and education in nuclear thermal-hydraulics.

1.1.1.6 The target NPP and the RR types, the structures, system, and components for concerned nuclear installations

The construction and the operation of Nuclear Power Plants shall be seen as the result of one among the most complex endeavors of the human minds: discoveries and technological applications from a variety of technological sectors are needed to design, construct, operate, and evaluate the safety of NPP.

The exploitation of fission reactions to produce thermal energy and, after proper transformation, mechanical or electrical power, is not exclusively connected with water. A variety of options are available, including gas or liquid metal as coolant, graphite as moderator, or even dissolving the nuclear fuel into the coolant, i.e., homogeneous reactors. However, strategic, financial, marketing, and technological reasons brought to the current (2016) situation where 99% of the operated NPP are cooled by water and more than 95% are cooled and moderated by water, whatever light or heavy. The use of water as coolant brought to the high pressure for the cooling loop encasing the nuclear core, e.g., in the range of 7–15 MPa, to ensure suitable thermal efficiency. The high pressure, the high operational power (up to 4500 MWt), and the power density (up to 100 kW/dm³ in core region, or 50 kW/m linear power for fuel pin) impose: (a) large geometry (up to around 300 m³) for the overall cooling system and (b) equivalent diameter of flow channels in the range around 0.01 m in the core region. All of this, combined with:

- possible neutron flux (reactivity) excursions translating into thermal power pulses
- unavoidable production of decay power (which cannot be stopped)
- unavoidable production of radioactive products (dangerous for humans and environment) which are kept into the fuel material part of the core

is at the basis of the needs or requirements for nuclear thermal-hydraulics at the levels of the design and the safety demonstration of nuclear installations.

The operational conditions and the system configuration of water-cooled RR, compared with NPP are characterized by: (a) much lower power (usually in the range of a few kW and anyway less than about 30 MW); (b) low-pressure values (in the large majority of cases, close to atmospheric values); and (c) much smaller geometric dimensions. However, challenges for nuclear thermal-hydraulics are not smaller than in the case of NPP, e.g., the predictions of margins to subcooled nucleate boiling and the natural circulation flowrate under flow reversal conditions.

The terms systems, structures, and components (SSC) include any hardware piece part of NPP or RR which is functional for the operation or to guarantee the safety. The SSC may have features either geometric or in terms of ranges of key variables

which require specific thermal-hydraulic modeling capabilities, like centrifugal pumps, steam separators, and containment. In the last case a specific paragraph below can be found.

1.1.1.7 Experiments and instrumentation

Any progress in 2 Φ nuclear thermal-hydraulics has been made possible by experiments. Experiments can be basic, like pressure drops in a cylindrical pipe and heat transfer between a wire and surrounding fluid, or make reference to NPP and RR, including SSC. Nonbasic experiments are generated from either separate-effect test facilities (SETF) or integral test facility (ITF) (e.g., Umminger and Del Nevo, 2012). Key issues for the experiments are the measurement errors, the time or space averaging, the perturbation introduced by the sensors, the difficulty to deal with heat losses, the role of radiation heat transfer when solid-surface temperatures overpass the threshold of about 500°C, the reproducibility mainly of transient experiments, the variance of measured data, and the suitability of needed scaling processes to demonstrate the similarity or the correspondence between gathered data and data expected in prototype systems.

Adopted instrumentation can be very simple and not expensive, like a thermocouple of the cost of 1 USD, or complex and expensive like gamma-densitometers and laser-doppler anemometry having costs up to 10⁶ USD per single instrument.

A few textbooks are aimed or restricted to experiments and instrumentation in nuclear thermal-hydraulics (e.g., Cumo, 1982); however, the majority of textbooks from previous paragraphs makes reference and gives proper consideration to experimental data.

Recently, following the OECD/CSNI Specialists Meeting on Advanced Instrumentation and Measurement Techniques held in Santa-Barbara, CA, USA, OECD/NEA/CSNI (1997), the Specialists Workshop on Advanced Instrumentation and Measurement Techniques for Nuclear Reactor Thermal Hydraulics (SWINTH) was organized in Livorno, Italy, Jun. 2016. This is going to be reflected in a special issue of the *Journal of Nuclear Engineering and Design* to be published in 2017–18, and constitutes the first of a kind of future workshops supported by NEA/CSNI also including the subject of instrumentation for the characterization of severe accidents (see e.g., Moretti, 2016). Issues related to experiments are marginally and occasionally considered in the book (e.g., Chapter 15).

1.1.1.8 Numerical methods and computer science

Nuclear thermal-hydraulics models and equations are typically nonlinear and need numerical methods to achieve solutions (e.g., Patankar, 1980). Programming of equations and achieving solutions need proper competence in computer science (e.g., Ferziger and Perić, 1999): numerical solution methods may affect substantially simulated performance of thermal-hydraulic systems (e.g., Ferreri and Ambrosini, 2002).

The design and the use of SYS TH codes are discussed in Chapter 11 and related verification and validation (V&V) and application are presented in subsequent chapters: all of this needs consideration and competence in the areas of numerical methods and computer science. However, numerical methods and computer science are outside the domain of interest for the book.

1.1.1.9 Nuclear safety, the licensing process, and the DBA (moving) boundaries

Nuclear reactor safety constitutes the essential technology for the exploitation of nuclear energy (e.g., Lewis, 1978). Furthermore, licensing shall be seen as the legal part of nuclear reactor safety: already in 1981, Prof. Okrent published a related book (Okrent, 1981). The key objective is to protect the humans and the environment from the radiations or from the contact with the radioactive nuclei mostly generated by fissions. Principles are established to this aim and are supported by regulatory requirements which become mandatory within the licensing process. Safety barriers and safety functions connect those requirements with the hardware of nuclear installations within a virtual environment known as Defense in Depth. Thermal-hydraulic parameters like pressure, fluid temperatures, and velocities must be under control to protect the barriers and safety functions.

As noticeable examples, the fuel clads and containments constitute barriers which can be broken due to high temperature and/or high pressure. High temperature in the core materials may be a consequence of inadequate cooling for the concerned fission power level. High pressure inside the clad and containment may derive by gas release from nuclear fuel or from loss of pressurized coolant from primary circuit, respectively. Ensuring protection of the barriers implies the design of the so-called engineered safety features (ESF), including the emergency core cooling systems (ECCSs) and the demonstration of related capabilities.

Key issue in this context is the determination of safety margins, or of the space which separates the safe operation from potentially dangerous conditions during the course of an accident. This is done by introducing the postulated accidents and,

shortly, the related design basis accident (DBA).

The ensemble of all hypothetical situations, and/or accidents and/or transients, against which a nuclear installation (typically a NPP) must be protected is called DBA envelope. The probability of the occurrence of any event plays a role in determining the envelope (see also below). The importance of the DBA envelope is associated with the regulatory requirements: whatever is inside the envelope must be known with the highest quality available at the time. This sets the boundary for thermal-hydraulics and for the present book. Thus, the book covers situations pertaining to the design and the nominal operating conditions of NPP and RR as well as accident situations until the loss of geometric integrity for the core. This also implies a space of knowledge outside the DBA envelope which is covered by accident management (AM) (see below).

Modern thermal-hydraulics received a decisive impulse from requirements set by regulatory authorities in each country (e.g., Reocreux, 1994, see also Chapter 2 of the book). Namely, requirements impose the demonstration of acceptability of ECCS in transient conditions; then, system and geometry complexities prevent the possibility of human mind solutions without the support of experiments and computational science; this opened the way to complex SYS TH codes; then, the issues came in relation to scaling, scaled experiments, V&V for computational tools and the uncertainty which characterizes the predictions by computational tools.

SYS TH may be seen as a key sector for nuclear safety and the mentioned topics are discussed in the book.

1.1.1.10 Severe accidents

Severe accidents did occur and may occur in NPP as well as in RR. Those events may imply damage to the core, the primary circuit, and eventually the containment. Severe accidents may cause serious damage to humans and the environment (see the fundamental book by Prof. Sehgal (2012)).

Other than proper competences and efforts, specific regulatory requirements exist and are needed to prevent severe accident evolutions and mitigate the consequences. Furthermore nuclear designers must be capable of demonstrating licensing acceptability of NPP and RR in relation to severe accident, and operators must be in the conditions to take decisions in case severe accidents occur.

Thermal-hydraulics has a key role in relation to the overall severe accident topic:

namely a “pure” thermal-hydraulics analysis is needed to analyze any transient since its beginning till the moment when core degradation occurs. However, severe accidents conditions and evolutions are beyond the domain of interest for the book.

1.1.1.11 Containment and RCS

The reactor coolant system (RCS) of any NPP is embedded into a protective structure called containment which also constitutes a safety barrier as already discussed. Unavoidably RCS and containment interact should an accident occur: in case of break occurrence in the RCS, the counter-pressure which develops in the containment caused by the release of steam water mixtures from RCS affects the flow-rate at the break; the fluid temperature and the liquid level in the sump affect the injection of ECCS in the long-term cooling period; in the case of boiling water reactors (BWRs) the role of the sump is taken by the pool of the wet-well region. Furthermore, hydrogen diffusion and transport may occur inside the containment also affected by temperature stratification and steam condensation at the walls. The last two phenomena are relevant for pressure build-up, containment cooling, and possible controlled releases to the environment.

The role of containment is essential should an accident occur. In the case of some advanced reactor designs like the advanced pressurized water reactor (PWR), or the AP-1000 (still prototypical design), the core cooling is ensured by the gravity and affected by the condensation phenomena (see also passive systems, below) occurring in the containment.

Thermal-hydraulic capabilities are needed to predict the containment performance.

1.1.1.12 Passive systems, reliability, and stability issues

Following the events of Three-Mile Island (TMI) in 1979 and more noticeably of Chernobyl in 1986, the so-called passive systems gained importance in the design and, recently, in the construction and operation of NPP. Components like accumulators and containments are already passive systems part of NPP design since the beginning of the nuclear era. Then, passive systems here are meant those systems introduced in the aftermath of the Chernobyl accident.

Noticeably, the original idea was that natural forces, gravity in particular, improve the reliability of core cooling (other than reducing the construction and the maintenance cost). Researches performed since the year 2000 showed that this is not correct (e.g., D'Auria and Galassi, 2000; Jafari et al., 2003; Marques et al., 2005). Reasons for this are:

- Passive systems, namely based on natural circulation involving a heat sink and a heat source at different elevations, never operate under (perfect) steady-state conditions: temperature, and/or pressure, and/or level, and/or exchanged/removed power change with time. Difficulties arise in demonstrating the reliability of passive systems because of the wide ranges of variations for governing parameters shall be investigated, and the combination of selected parameter values, even though in narrow ranges, may cause malfunctions.
- Boiling and condensation processes cannot be avoided in the majority of passive systems: the density changes associated with both processes makes those systems prone to instability.
- Minor changes in boundary conditions which are uninfluent upon system performance when pumps are installed, like $\pm 1^\circ$ inclination of horizontal pipes (specifically carrying two-phase mixtures), small leakages (unavoidable if large valves are present to isolate a large pressurized pipe), and heat losses (e.g., in the region where steam or two-phase flows are present) challenge the system performance and may largely reduce the reliability of the system.
- A stable natural circulation system characterized by a fixed power heat source may become unstable when the heat source power is generated by another natural circulation system, i.e., when the heat sink of a natural circulation system also constitutes the heat source for a downstream natural circulation system. This is the case when a passive cooling system is associated to the steam generator of a PWR. In this situation, oscillations in the passive system, i.e., downstream the steam generator may reflect in oscillations in the core flowrate, thus endangering core cooling.

Nuclear thermal-hydraulics is essential for the design of passive systems and for assessing the operational range of parameters.

1.1.1.13 Accident phenomenology

The knowledge in thermal-hydraulics evolved according to the given notes, see also Chapter 2, and complex phenomena occurring in case of accidents in NPP (i.e., the way they are understood today) had not a major role at the beginning of the nuclear era (year up to around 1970). However, the logical path for nuclear thermal-hydraulics became (starting from around 1970): [NPP-geometry-and-operating-conditions-&-design-requirements]+[DBA envelope]→[phenomena]→[range-of-variation-of-parameters-of-interest]→[requirements-&-development-for-thermal-hydraulics]. This (virtual)

view is pursued in the book, where phenomena discussed in Chapter 6 have the central role.

Scaling is the key issue here: the derivation of phenomena, their evolutions and the related variation ranges of important parameters, are based upon data measured in small size facilities compared with NPP, apart from a few exceptions. Ensuring a reasonable understanding, including predictive capabilities, of phenomena part of the DBA envelope in NPP, constitute the challenge for the specialists in thermal-hydraulics. This is a starting point for the definition of the objective of the book in Section 1.1.2.

1.1.1.14 Role of start-up and shutdown phenomena

Toward the end of 1980s it was realized that the risk of NPP during start-up and shutdown periods was not negligible compared with the risk during power operation. This triggered research and developments in various areas including thermal-hydraulics.

A distinction is made hereafter between nuclear thermal-hydraulics issues after power operation postulated initiating event (PIE) and after shutdown or start-up PIE: both situation types may have a relation with the DBA envelope.

- In the former case the problem to be addressed is the demonstration of adequacy of ECCS in satisfying licensing criteria for core cooling: components like centrifugal pumps injecting ECCS water are assumed to function properly even though failures are possible according to specifications from reliability analyses. Thermal-hydraulic competences are essential to provide a solution in terms of safety and licensing.
- In the latter case the problem is to determine what happens following the failure of residual heat removal (RHR) pumps typically starting from zero fission power operation. In this case thermal-hydraulic calculations also focus on determining the time available to operators before irreversible damage of the core. The solution is an improved design for pumps or of related operating conditions, rather than the outcome of a thermal-hydraulic calculation.

Thermal-hydraulic conditions challenging the RHR operation in the long term of accidents and the shutdown in NPP are in some cases similar in terms of range of variations for pressure, temperatures, and mass flows. This is also true in relation to RR operating conditions.

1.1.1.15 The accident management and the AM procedures (AMP)

The terms AM and AMP have been introduced in the 1990s. They indicate not only the possibility but also the need and the capability for the NPP operators to manage or drive any accident evolution. This is true for situations outside the DBA envelope, i.e., beyond design basis accident (BDBA) conditions, while for DBA conditions emergency operating procedures (EOP) are planned to support the operator actions.

Two categories can be distinguished for AMP in the concerned (BDBA) domain, respectively, aiming at preventing massive core degradation and mitigating the consequences of core melt including recovery of the plant. The phenomena expected to be relevant for the first category are considered in Chapter 6 and discussed in Chapter 15.

1.1.1.16 Connection with neutron physics, probabilistic safety assessment (PSA), radioprotection, chemistry, mechanics, nuclear fuel, electronics including instrumentation and control (I&C)

The application of thermal-hydraulics within NPP technology and nuclear reactor safety is not possible without an interaction with different disciplines: exceptions (i.e., thermal-hydraulics applications alone) also exist but are not universal and do not allow an overall safety assessment. In addition to textbooks dealing with other disciplines already cited in this chapter, in the following examples are given of connections between thermal-hydraulics and selected disciplines. The description below is not exhaustive or systematic; rather, it provides an idea of complexity in application of thermal-hydraulics to needs in NPP and RR technologies.

Neutron Physics. Thermal power is generated by neutrons and induced fissions. The neutron flux depends, among the other parameters upon temperature of moderator and fuel and, noticeably, upon density of moderator-coolant. Thus, fuel temperature and moderator density and temperature are calculated by thermal-hydraulics and affect instantaneous fission power. So any NPP or RR core-related analysis implies coupled neutron physics thermal-hydraulics calculations. A zero-dimensional neutron kinetics model was embedded into the primitive SYS TH codes since the end of 1960s (e.g., Lamarsh and Baratta, 2011). Toward the end of 1990s, three-dimensional core physics models were coupled with thermal-hydraulics codes (e.g., Ivanov and Baratta, 1999; see also D'Auria et al., 2004). This opened the way to the analysis of core transients involving local reactivity changes like those associated with boron mixing (e.g., Pla et al., 2010) and control rod ejection (e.g., Avvakumov et al., 2007).

PSA. Probabilistic safety assessment constitutes by itself a developed technology

(e.g., see Apostolakis and Moieni, 1987; Fulwood, 2000; Arkadov et al., 2012). Identification of all interactions between thermal-hydraulics and PSA is, again, beyond the scope here. In order to give an idea of the tight connection between PSA and thermal-hydraulics it is sufficient to recall that: (a) the transients part of the DBA envelope, i.e., those analyzed by thermal-hydraulics as given in **Chapter 15** of the book, need specifications for probability of occurrence; this also determines the acceptability criteria (e.g., IAEA, 2010a); (b) a transient thermal-hydraulic analysis is needed to determine the consequences of any accident relevant to PSA (e.g., IAEA, 2010b).

Radioprotection. Radioactivity and doses (e.g., Knoll, 2010) are concerned with the application of thermal-hydraulics. The amount of radioactivity releases from the core (or the source term calculation, e.g., Herviou, 2005), should an accident occur, and the possible paths to doses to humans or to radioactivity impact for environment need thermal-hydraulic calculations. One may also state that the atmospheric dispersion calculation for radioactive products (e.g., Thielen et al., 2007) is part of a nuclear reactor safety analysis based on thermal-hydraulics.

Chemistry. Chemistry of the coolant and, noticeably, the control and the transport of boron are needed for the long-term reactivity control or the fuel burn-up compensation of any NPP (e.g., Benedict et al., 1981): a devoted system called chemical and volume control system (CVCS) is designed, installed, and operated in each NPP. Time delays for boron arriving in the core since the injection time and mixing in regions like the down-comer or the lower plenum of the vessel need a thermal-hydraulic calculation (e.g., Theophanous and Shabana, 1991; Cheng et al., 2014). This is particularly true in case of anticipated transient without scram (ATWS). The calculation of the amount of hydrogen produced by the metal-water reaction (e.g., Baker and Just, 1962) and the transport of the H_2 gas into the containment (e.g., Camp et al., 1983; Royl et al., 2009; Xiao and Travis, 2013) need specific thermal-hydraulic analyses even in relation to accidents within the DBA envelope.

Mechanics. Eight examples are given hereafter of the interaction between mechanics and thermal-hydraulics (without having the target to provide a comprehensive view): (1) main coolant pump (MCP) transient operation, including the consideration of two-phase flows, cavitation and vibrations, and net positive suction head (NPSH) (e.g., Tuzson, 2000): various coupled set of mechanics and thermal-hydraulics equations are needed to address the MCP simulation; (2) Flap valve operation with changing pressure differences at the boundaries (e.g., Abu-Zeid, 2013): the inertia of the flap body (mechanics) is correlated with the pressure

difference calculated by thermal-hydraulics; (3) pressurized thermal shock (PTS) stresses are caused by imperfect mixing of cold liquid from ECCS injected in cold leg and challenge the reactor pressure vessel (RPV) integrity. PTS constitutes an example of multidisciplinary topic also involving, other than local thermal stresses, long-term damage to the vessel by neutron radiations (also affected by water density), material aging and embrittlement, welding technologies, crack growth and propagation, or fracture mechanics (e.g., IAEA, 2010c, see also Araneo and D'Auria, 2012); (4) condensation-induced water hammer (CIWH): the fast condensation causes the movement of liquid slug which may determine a dynamic load on piping and restraints (e.g., Schultz et al., 2001; Barna et al., 2010); (5) Thermal fatigue: this constitutes a long-term degradation mechanism important in NPP aging caused by fluid temperature stratification and turbulent mixing effects. Those effects induce continuous (e.g., during the life of the system) local mass flows of fluid having different temperatures which is at the origin of thermal stresses in the structures (see, e.g., Courtin, 2013); (6) Loads on RPV internals originated by pressure wave propagation from postulated break (e.g., Sokolowski and Koszela, 2012); (7) fluid-structure interaction: FSI constitutes a scientific and technological area dealing with loads on RPV internals caused by pressure wave (previous topic) as well as vibrations (e.g., Bungartz and Schäfer, 2006; see also the textbook by Païdoussis et al., 2014) already mentioned; (8) Jet impingement (and jet thrust) and pipe whip: the break of a pipe causes the release of the elastic energy stored in the pressurized structures (e.g., piping) which adds to the fluid-dynamic loads generated by the flow motion exiting the break. This generates (see, e.g., Vigni and D'Auria, 1979; D'Auria and Vigni, 1981): (a) loads on restraints; (b) mechanical and thermal loads by the jet impinging on close surfaces; (c) potential missiles including parts of components like rotor of a pump, blade of turbine, and pieces of broken material; and (d) pipe whip involving the displacement of piping.

Nuclear fuel. Any analytical simulation of NPP or of RR requires the modeling of nuclear fuel. Issues and challenges are connected with fuel, geometric, mechanical and physical or material properties which continuously change during the fuel life in the core. This is due to burn-up. Furthermore, the values of those properties depend upon thermal-hydraulic parameters, noticeably pressure and temperatures of the coolant and moderator (e.g., OECD/NEA/CSNI, 2010; see also Lisovsky et al., 2015).

Electronics including I&C. A wide number of parameters are continuously monitored during the operation of NPP. Connected systems, also identified as part of the I&C, have a role in determining the evolution of accidents, i.e., impacting

the thermal-hydraulic performance of the system and the thermal-hydraulic modeling (see, e.g., D'Auria et al., 2012b).

1.1.1.17 Scope and framework for the textbook

The huge space of interest, or scope and framework for nuclear thermal-hydraulics and SYS TH derives from the nonsystematic summary in the previous section. A textbook covering with sufficient detail each of the mentioned topics is well beyond the planning of the present effort. Nevertheless any of those topics may have a connection with what is discussed in the book. An attempt is made hereafter to summarize what of the considered topics is or is not part of the book.

- **Origin of nuclear thermal-hydraulics:** Chapter 2 deals with a vision of the history of SYS TH.
- **Single- and two-phase flows:** these are of main concern in Chapters 3–11; however, key concepts in fluid-dynamics and gas-dynamics are not discussed.
- **Prominent scientists and textbooks:** the idea is to not replicate the structure of any of the existing textbooks; the reader could derive from cited references the contributions to the knowledge in thermal-hydraulics by prominent scientists. However, partial duplication of fundamental concept cannot be avoided for subjects like definitions, balance equations, pressure drops, and heat transfer, e.g., Chapters 3, 5, 7, and 8. International reports issued by OECD/NEA and IAEA as well as reports documenting the features of SYS TH and of CFD codes constitute key references for the present book with related details in Chapters 9 and 11–15.
- **Journals, conferences, and the web:** a systematic review of publications (journals, conferences, and web) is beyond the scope for this textbook. However, latest developments in selected areas are considered.
- **Education and training:** the consideration of existing education and training courses is beyond the scope for the book. However, the book itself may become a reference for education and training courses.
- **The target NPP and the RR types, the SSC for concerned nuclear installations:** the reader of the book is expected to be familiar with the features of concerned NPP, RR, and SSC including containment. No devoted descriptions are part of the book.
- **Experiments and instrumentation:** experiments are unavoidable for the progress of nuclear thermal-hydraulics as already mentioned. Phenomena concerned in

Chapter 6 are derived from SETF and ITF experiments. However, description of experiments is not of direct interest. Instrumentation is also outside the scope for the book.

- Numerical methods and computer science: notwithstanding the need for numerical methods and competence in computer science for the development and the application of SYS TH codes, those topics are outside the scope for the book.
- Nuclear Safety, the licensing process, and the DBA (moving) boundaries: the reader of the book is expected to have fundamental knowledge of the nuclear reactor safety technology; otherwise, an idea of the licensing process can be derived from cited references. In Chapter 4 the needs from nuclear safety are considered, and results of application of thermal-hydraulics to nuclear safety are discussed in Chapters 14–16. The scope for the book in the concerned context is clarified by the statements at the following item.
- Severe accidents: the book does not cover severe accidents, i.e., the boundary of interest is set to the time of any accident or the reactor configuration when the core starts to be degraded. Two key reasons for this:
 - to keep as small as possible the size of the book (i.e., to avoid an encyclopedia),
 - the licensing requirements, the capabilities, the rigor and the quality of computational tools, and the amount of experimental investigations are different between the areas of thermal-hydraulics and severe accident.
- Containment and RCS: Containment is part of NPP and containment response is part of accident analysis (AA). Thus thermal-hydraulics of containment is part of the book, e.g., Chapter 4 in relation to needs for thermal-hydraulics, Chapter 6 in relation to occurring phenomena, Chapter 7 in relation to condensation heat transfer, and Chapter 15 in relation to containment performance in case of accidents.
- Passive systems, reliability, and stability issues: thermal-hydraulic phenomena expected due to the operation of passive systems are presented in Chapter 6. Furthermore, the SYS TH codes, Chapter 11, are capable to predict the transient performance of passive systems. Because of the mentioned complexities passive system deserves specific attention from the thermal-hydraulic community: this is out of the scope for the present book although passive system operation is considered in Chapter 15.

- The accident phenomenology: for the current vision, phenomena expected in NPP following off-normal conditions are at the bottom of the pyramid of knowledge for nuclear thermal-hydraulics. Phenomena are presented in Chapter 6.
- Role of start-up and shutdown phenomena: phenomena during RHR operation including start-up and shutdown in NPP are considered in Chapters 6 and 15. Reliability of RHR-related pumps and the best design of cooling loops are outside the scope for the book.
- The AM and the AM procedures (AMP): AM phenomena occurring to prevent severe core degradation are part of the scope of the book and discussed in Chapter 15.
- Connection with neutron physics, PSA, radioprotection, chemistry, mechanics, nuclear fuel, electronics including I&C: the application of nuclear thermal-hydraulics to safety and design of NPP and RR is not possible without the support of other disciplines, as it also derives from the cited references. However, technological and scientific aspects dealing with the connection between thermal-hydraulics and other disciplines as well as details related to any of those disciplines are beyond the scope of the book. An exception is constituted by Chapters 14 and 15. Namely Chapter 14 deals with best estimate plus uncertainty (BEPU) approach to the AA: details are provided in this chapter in relation to the connection between thermal-hydraulics and other disciplines. In a few cases, results of accident analyses discussed in Chapter 15 deal with “other disciplines.”

Computer codes in SYS TH (e.g., Miro et al., 1990) and CFD areas are within the scope and the framework of the book even though not explicitly part of the given list of topics. The computational tools, mainly the SYS TH codes, constitute the end product of the knowledge and the expertise in nuclear thermal-hydraulics: the related technology includes code development (e.g., Bestion, 1990; Jeong et al., 2010); code V&V (e.g., D'Auria et al., 2012a); code scaling (e.g., Glaeser and Karwat, 1993; D'Auria and Galassi, 2010; Rohatgi, 2015); and code application (e.g., Reventós et al., 2010); in this case, the evaluation of uncertainty in code predictions (e.g., D'Auria et al., 2008) is a requisite for the proper consideration of applications in nuclear reactor safety. Therefore, any concept or information reported in the book should be considered as relevant to the SYS TH code development or application processes (see also Section 1.1.3).

1.1.2 Objectives and target readers

Nuclear thermal-hydraulics appears like a universe of matters and themes: galaxies

and planetary systems of topics and skills can be distinguished and are needed for the proper comprehension of the discipline. In such a universe vision of thermal-hydraulics, Dr. Zuber already introduced the concept of quanta to deal with scaling (Zuber, 2010). Here we may add that black-holes in the knowledge of thermal-hydraulics still exist and may be associated with the modeling of turbulence at either the microscale or the macroscale levels including the occurrence of boiling and condensation in multifluid systems.

Then, a systematic and comprehensive treatment of all the matters and themes is not realistic or possible, and an encyclopedia, or a series of books, is needed to ensure reasonable covering of each matter. Rather one may note that a variety of textbooks (some of those included in the list of references) exist which address one or more individual topics in nuclear thermal-hydraulics: in this case, it is difficult to exceed their quality and novelty.

Here what are not the objectives of the present book can be stated: not to have a comprehensive covering or even mentioning of each important matter or theme in nuclear thermal-hydraulics; not moving the boundary of knowledge by considering quanta and black-holes mentioned above; not to replicate any existing textbook, rather referencing those books.

A number of requirements are identified hereafter. The objective for the book can be fixed as fulfilling those requirements.

- A novel approach, or a new vision, for nuclear thermalhydraulics is envisaged or attempted.
- Topics are discussed covering from fundamentals in thermal-hydraulics, i.e., mostly by referencing appropriate literature (e.g., textbooks), to applications in NPP design and safety technologies, including RR to the extent it is possible.
- The impulse given to the knowledge by needs of nuclear reactor safety, unavoidably connected with licensing rules, shall be recognized. The simplified chain is considered: regulatory goals→accident analysis→phenomena→transient thermal-hydraulic needs.
- From a logical view point and not necessarily connected with the order of chapters, a topdown approach is pursued: then, needs come first (basically Chapter 4) and applications are expected at the end (e.g., Chapters 15 and 16): noticeably, phenomena of interest come after the needs (e.g., Chapters 4 and 6, respectively).

- The technology impact is considered in each chapter (e.g., at least in introductory or closing remarks).
- The SYS TH code is seen throughout the book as the main/key repository of expertise in the area. This implies consideration of code development (namely thermal-hydraulic bases for development, e.g., **Chapters 9–11**), code V&V including the role of scaling and the evaluation of uncertainty (e.g., **Chapter 13**), the code application to NPP design and safety (e.g., **Chapter 14** dealing with the BEPU approach), and the results from AA (e.g., **Chapters 15 and 16**).

The innovation introduced with the book, other than transpiring from the requirements, is: (a) to shed light on the connection between fundamentals of thermal-hydraulics and application in nuclear technology; (b) to give emphasis to the V&V, scaling, and uncertainty evaluation including related motivations and procedures; (c) an as far as possible consistent formulation for the BEPU approach where the pivot role of nuclear thermal-hydraulics is established: this includes an integrated and nonconflicting role for DSA and PSA. Furthermore, the book has been written having in mind the targets to promote the application of SYS TH codes within the licensing process of existing and new nuclear reactors and to disseminate various steps of the BEPU approach to software technologies different from SYS TH.

An alternative and consistent formulation of the requirements/objectives and innovation introduced or expected for the book can be derived from the following statements.

1.1.2.1 Reformulation of the objective for the textbook

It is well clear that no numerical tool has the capability to predict the movement, growth, and collapse of a single bubble moving inside a liquid when condensation and evaporation processes take place. Similarly, there is no capability to simulate all the effects of turbulence even in single-phase flows, e.g., in predicting pressure drop at geometric discontinuity with an error which is acceptable for the design of thermal-hydraulic systems. Prediction capabilities are even poorer or nonexistent when a few bubbles move together and interact or when two-phase turbulence is considered, respectively. Decades of development since now, e.g., in the area of two-phase CFD, have not been sufficient to achieve a solution for the concerned computational challenges. So, the obvious question arises: how is it possible to predict transient two-phase mixture evolutions in complex geometrical systems like NPP or RR? Then the objective of the book is to address such a question.

The instant-simplified answer is as follows and may be seen as the reformulated objective for the book.

Time and space averaging is adopted in SYS TH codes, or approximate equations are solved by approximate numerical methods: the impacts of approximations upon the results, or the errors, are unknown. However, V&V procedures supported by experimental data and suitable scaling analyses allow the quantification of those errors. Qualified (as far as possible) uncertainty methods are established to this aim. In different terms, one may state that expertise including the knowledge of data measured in transient experiments is necessary to achieve qualified calculation results from application of thermal-hydraulics.

Definitely, side objectives for the book are on the one hand to recognize the irreplaceable role for SYS TH codes when establishing the safety of nuclear installations (i.e., determined on transients which involve two-phase fluid mixtures time evolutions) and on the other hand to clarify that rigorous V&V is needed and that any valuable set of SYS TH calculation results must be supported by an uncertainty evaluation.

1.1.2.2 To whom the book is addressed

Any scientist involved with nuclear thermal-hydraulics may take benefit from the book (as already mentioned in “Chapter foreword”). This is specifically true for code developers, nuclear thermal-hydraulic analysts, AA specialists including their supervisors and, more in general, nuclear safety technologists.

Students in the last years of engineering courses and masters or PhD student/researchers are expected to get acquainted with the vision of nuclear thermal-hydraulics from the reading of the book.

In all cases the knowledge of thermodynamics and nuclear thermal-hydraulics fundamentals is desirable, although not essential, for the comprehension of the concepts in the book.

1.1.3 Content

Nuclear SYS TH constitutes the content and the subject for the book (according to the title). Having recognized that it is not possible even to mention all important topics, a selection of themes and matters has been assembled to form the content. This shall be seen as a break-through of the universe of matters and themes mentioned in Section 1.1.1. Then, an attempt is made to link bases and applications of nuclear thermal-hydraulics; however, connections with other disciplines are

recognized as essential within the framework of applications and are not discussed in the book.

The sketch in Fig. 1.1, with short title for each chapter, provides an overall view for the content including the roadmap and the strategy for the book. The top row of the sketch synthesizes the framework for the book, i.e., the water-cooled NPP and RR configurations, plus the academic disciplines thermodynamics and thermal-hydraulics, plus the needs from (NPP and RR) design and safety technologies. Then the book is subdivided into three main parts, consistently with the objective in Section 1.1.2: Part One introduces the background and aims at clarifying the current vision for nuclear thermal-hydraulics, Part Two deals with features of the current SYS TH codes, and procedures for the consistent application of SYS TH codes and results are discussed in Part Three. Part Two has been further subdivided into two parts in the Contents to distinguish between connections of thermal-hydraulics and modeling.

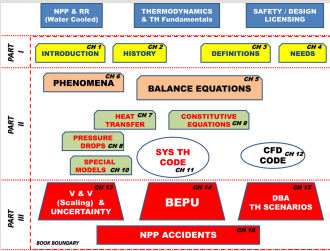


Fig. 1.1 Structure and content for the book.

Motivations and rationale for each chapter are given below (a short title for each chapter is also given, according to the boxes in Fig. 1.1). This also includes the discussion of critical aspects where applicable and (unfortunately) unavoidable repetitions of concepts.

1.1.3.1 Chapter 1: Introduction

The framework of nuclear thermal-hydraulics used for the planning and the issuing of the book is discussed in the present chapter.

1.1.3.2 Chapter 2: Historical remarks

The nuclear thermal-hydraulics discipline was developed following the need to demonstrate the NPP safety and, to a more limited extent, the NPP and the RR

design. As in all other fields where analytical methods are involved, nuclear thermal-hydraulics took benefit of the development of computers. Thermodynamics, rather than fluid-dynamics, is at the basis of the development of nuclear thermal-hydraulics together with experiments in complex two-phase situations, namely geometry, high power density, and pressure.

Mandatory licensing requirements originated by safety needs pushed huge investments in research which drove the developments in the area. All of this created a unique technology where highly geometry-dependent transient phenomena, sophisticated two-phase flow modeling, continuously advancing numerics science, and unavoidable empiricism derived from experiments are merged. This forms the iceberg knowledge which needs to be mastered and managed also for the use of new generation of scientists.

The objective and the motivation for this chapter are to trace the history of the discipline which is deemed necessary for its understanding and creating the perspectives for development.

1.1.3.3 Chapter 3: Definitions

Definitions may appear not necessary for an established discipline like nuclear thermal-hydraulics: all terms should have a consolidated meaning within the myriad and the variety of publications mentioned in Section 1.1.1. Unfortunately this is not the case, one reason being the complexity of the discipline which reflects in the difficulty of conjugating basic concepts like the principles of thermodynamics and complex displays like subcooled void appearance during depressurization which impact heat transfer and fission-generated power.

Then, objective and motivation for the chapter is to show the complexity of the nuclear thermal-hydraulics discipline from the point of view of what are called “definitions” (see below): then the chapter is complementary to the discussion in Section 1.1.1.

“Definitions” here imply in most cases providing a message which shows the difficulty associated with the concerned term. For instance, in the case of convection heat transfer coefficient (HTC), the huge number of variables which affect HTC are balanced by the simplicity of its correlation with heat flux and temperatures; in the case of turbulence, the lack of any direct predictive capability or the current status of the DNS is stressed; in the case of pressure drops at geometric discontinuity difficulties in measuring a free-from-(large or not-acceptable)-error value for the local coefficient arise because of need to distinguish

between reversible and irreversible contributions to the total pressure change: the problem becomes more complex when proper consideration must be given to the condition of fully developed flow.

Three categories of definitions are envisaged:

(A) Variables

(B) Phenomena

(C) Concepts

The variables include the fundamental quantities which are also part of balance equations, like temperature, pressure, velocity, material properties. Errors characterizing or expected from the measurement and the prediction by analytical tools of those quantities are outlined. The void fraction is introduced to characterize thermal-hydraulics. Furthermore non-dimensional quantities like Re , Pr , Nu , Fr are also part of this class. The derivation of key non-dimensional quantities in thermal-hydraulics and their physical meaning are discussed. Difficulties to apply those quantities in scaling analysis are mentioned: e.g., during a transient, at a given time, different Re values apply to different locations of the loop and a comprehensive mapping of Re values in the entire loop may not be possible with a scaling method alone not supported by a system code calculation.

Examples of discussed phenomena or concepts in thermal-hydraulics include natural circulation, two-phase critical flow (TPCF), Critical Heat Flux, blow-down, reflood and rewet, friction pressure drop (empirical) with main reference to two-phase flow multiplier, conduction heat transfer (theoretical, but utilizing the empirical/approximate Fourier law), convection heat transfer (empirical), and radiation heat transfer (supported by theory, but needing empirical parameters). Aspects connected with NPP and RR technology are emphasized.

The considered concepts encompass a variety of subjects and themes of the nuclear thermal-hydraulics universe, ranging from phenomena-modeling terms like drift flux formulation, to the characterization of equations like balance or conservation equations, constitutive or closure equations, state equations, to approaches to perform a calculation like conservative or best estimate, to modeling approaches like lumped parameter model or UVUT (unequal velocities unequal temperatures) model dealing with balance equations. Widely adopted terms like PIE, DBA, BDBA, and AM are clarified.

Within the class of concepts, a connection is created between nuclear thermal-hydraulics and fluid-dynamics and gas-dynamics, i.e., by including suitable definitions. Then, the concept of turbulence can be used to connect thermal-hydraulics with fluid-dynamics and gas-dynamics emphasizing the added complexity, as far as turbulence is concerned associated with void fraction: flow-regimes (bubbly, slug, churn, annular, etc.) can be seen as the connection between turbulence and two-phase flows.

1.1.3.4 Chapter 4: Needs

The development of nuclear thermal-hydraulics has several origins and motivations including thermodynamics and fluid-dynamics sciences: nuclear technology had an important role. In this chapter a reverse approach is pursued: starting points are the existing configurations, operating conditions, and safety aspects of NPP and RR; then an attempt is made to establish what capabilities are requested for nuclear thermal-hydraulics.

In order to accomplish this goal the following sectors, not independent among each other, are considered and reported hereafter together with examples of the origins of needs:

- Reactor coolant system for NPP: all water-cooled power reactor designs are included. Needs are identified which are associated with the design of core and other RPV internals, steam generators, separators, dryers (in the last two cases with main reference to BWRs), main coolant pumps, pressurizer, recirculation legs.
- Nonnuclear part of the NPP also known as balance of plant (BoP). The BoP has similar features for NPP and oil or coal fueled plants for electricity generation. However in the case of NPP the size of components, like turbines and condenser, may be larger than in conventional plants and the attention originally devoted (e.g., in the 1950s and 1960s) to maximize the thermal efficiency might have been lower (because of the smaller impact of the fuel upon the cost of the produced electricity). So, needs may derive from the modernization or revamping projects for existing NPP like decreasing pressure drops in the steam lines
- Containment: the designs of tight (or zero leakage target after DBA) containment for almost all NPP and of vented containments in “not-the-latest-generation” of Russian reactors need thermal-hydraulic capabilities. Interesting to note that controlled venting became a desirable feature after the Fukushima event in 2011. Containments equipped with pressure suppression pool of liquid need deep thermal-hydraulics competence (e.g., estimation of vibrations and loads on

compartment walls).

- **RR designs:** a variety of designs characterize the few hundreds RR now in operation. RR are equipped with highly enriched uranium (HEU) core or, the larger number, by low enriched uranium (LEU) core. Pool type or forced circulation RR are distinguished. Challenging topics for nuclear thermal-hydraulics are the evaluation of margins available to the onset of nucleate boiling (ONB) even during possible flow reversal consequence of main coolant pump trip, i.e., the pathway from downward forced circulation to upward natural circulation. The narrow passage for fluid across flat plate fuel elements also puts challenges to nuclear thermal-hydraulics.
- **Safety analysis of water-cooled reactors:** the needs for thermal-hydraulics primarily come from the licensing requirements, e.g., the ECCS design criteria. Updating of requirements and creating the link with computational capabilities constitute challenges for nuclear thermal-hydraulics applications. Needs and challenges for nuclear thermal-hydraulics are unavoidably defined outside the subject boundaries for the book: namely, the connection between nuclear thermal-hydraulics and neutron physics, nuclear fuel (modeling), chemistry (e.g., H_2 production), mechanics (e.g., FSIs, modeling of flap or inertia valves, modeling of the inertia of pump rotor, etc.), radioprotection (e.g., transport of radioactivity from core to containment) are at the origin of needs.

Addressing the listed topics constitutes motivation and objective for the chapter.

1.1.3.5 Chapter 5: Balance equations

Balance equations constitute the seed around which the predictive capabilities of nuclear thermal-hydraulics have been built with main reference to transient two-phase flow evolutions. This is the motivation for the chapter: predictive capabilities in thermal-hydraulics do not exist without these equations. Balance equations, synonymous of conservation equations, are established from the principles of science and technology: mass and energy balance are derived from mass conservation and the first principle of thermodynamics, and the momentum balance is derived from the first principle of mechanics. Nuclear reactor thermalhydraulics may be studied using a large variety of models which simplify more or less the physical reality.

The first problem of an engineer when investigating a reactor issue is to select the right degree of simplification depending on the situation and the required accuracy and reliability of the solution. Simplifications may result from the space and time

resolution and simulation tools include several scales from lumped parameter models to CFD and CMFD. 0-D, 1-D, 2-D, and 3-D models are available for single- and two-phase flow that use either time averaging or combined space-time averaging. Each approach uses a set of balance equations for mass, momentum, and energy, and the derivation of these equations may need complex mathematical developments which will not be presented in detail for all modeling scales, since reference books exist which may be referred to for readers who want to know more. Attention will be drawn on the physical assumptions and simplifications used at some steps of the derivation of equations and on the resulting limitations of the predictive capabilities.

The objective of this chapter is then to give a picture of all the available models with an evaluation of the predictive capabilities and limitations, on the degree of accuracy and reliability, and on the maturity of each model. More information will be given on 1-D models since they are the most currently used in design and safety studies using system codes. However 3-D models are also increasingly used, and the balance equations are also presented to introduce CFD and CMFD.

1.1.3.6 Chapter 6: Phenomena

The transient performance of NPP following plausible initiating events or accidents and also changes in operating conditions (e.g., start-up and shutdown) brings to the identification of phenomena. Phenomena are characterized by ranges of variations of significant parameters and may involve steady-state or transient conditions.

Thermal-hydraulic phenomena are important owing (at least) to the following reasons:

- (1) Experiments in thermal-hydraulics either “integral” or “separate-effect” type must be designed and executed in order to characterize the phenomena.
- (2) A variety of empirical or non-first-principle-derived formulations needs to be developed making reference to phenomena, e.g., including special models discussed in Chapter 10.
- (3) A comprehensive list of phenomena properly characterized by significant parameters is needed to ensure suitable validation for SYS TH codes as discussed in Chapter 13.

International activities performed at OECD/NEA/CSNI and by IAEA brought to the identification of phenomena in the following conditions (sample list):

- LBLOCA in PWR and VVER
- SBLOCA in PWR and VVER
- LOCA in BWR
- Separate-effect phenomena in BWR and PWR
- Shutdown conditions in PWR
- AM in PWR
- Containment response in PWR and BWR
- Performance of passive systems characterizing the coming reactor design
- Phenomena associated with RR

The motivation for the chapter derives from the needs (Chapter 4), and the objective is to create a comprehensive list of phenomena which are described in a (as far as possible) homogeneous way.

1.1.3.7 Chapter 7: Heat transfer

Heat transfer and pressure drops are the main targets within the design of thermal-hydraulics systems and a wide variety of approaches and precision needs have been established and are available.

Chapters 7 and 8 are planned to constitute a bridge between the past and the future for nuclear thermal-hydraulics: the evaluation of convection HTC has been among the most important research targets since the beginning of the nuclear era and is among the most important targets for the future with needs for increased calculation precision.

Selected important issues in the area which also constitute the motivation for the chapter are outlined hereafter. Those issues may imply the need for further development, for achieving common understanding and/or fixing precision goals for calculations.

- The convection HTC is defined on the basis of an empirical equation also known as Newton law. This makes possible the quantitative evaluation from experiments but implies the existence of a multidimensional surface where HTC is a function of dozens variables.

- Reflood heat transfer implies the definition of a HTC which assumes (very) high values for a few millimeter around the quench front; the reflood occurrence is associated with the quench front propagation and may be associated with a surface temperature also called minimum film boiling (MFB); in some situations, e.g., when a short (a few decimeters length) piece of fuel rods remains to be quenched, a sort of homogeneous-instantaneous reflood takes place.
- Heat transfer from fuel clad surface at high temperature in the conditions of interest for nuclear thermal-hydraulics on the one hand includes radiation and on the other hand may occur toward different fields of the same phase, i.e., liquid film and droplets. Modeling of both radiation heat transfer and liquid fields heat transfer poses challenges: the presence of spacer grids causes additional complexity to the modeling.
- Wall condensation occurs in containment during postulated accident conditions. Condensation is affected by the presence of noncondensable gases including H_2 and determines global convection motion of the fluid which at its time governs H_2 concentration, again putting a challenge to nuclear thermal-hydraulics.
- Conjugate heat transfer, in rough words connecting convection and conduction heat transfer, has already been known since decades; however related analytical formulations have not achieved maturity applicable to problems of technological interest.

The objective for the chapter is to present the current status and the vision for the future in this (selected) area of the thermal-hydraulic science.

1.1.3.8 Chapter 8: Pressure drops

Pressure drops and heat transfer are the main targets within the design of thermal-hydraulics systems and a wide variety of approaches and precision needs have been established and are available.

Chapters 7 and 8 are planned in the book also to constitute a bridge between the past and the future for nuclear thermal-hydraulics: the evaluation of pressure drops, at geometric discontinuities and in two-phase conditions, has been among the first targets since the beginning of the nuclear era and is among the most important targets for the future with needs for increased calculation precision.

Selected important issues in the area which also constitute the motivation for the chapter are outlined below. Those issues may imply the need for further development, for achieving common understanding and/or fixing precision goals

for calculations.

- Modeling of friction pressure drop in single-phase flows is based upon an empirical approach widely validated by experimental and theoretical data. This is not the case for two-phase flows where the ancient approach characterized by two-phase flow multiplier is adopted: this approach may have validity when fully developed flow conditions are established, i.e., a situation never verified when accident conditions in NPP are calculated.
- Pressure drops at geometric discontinuities in either in single- or two-phase conditions are currently modeled by the application of empirically based coefficients. Assumptions are needed to determine those coefficients from experiments and, usually, no dependence is available from Reynolds number and void fractions: the impact of assumptions and of the lack of specification of dependencies upon results of prediction is unknown. This may largely contribute to the uncertainty of SYS TH code predictions.
- Evaluation of pressure drop in case of sonic and supersonic velocity conditions implying formation of shock waves.
- Evaluation of acceleration pressure drops in a (not necessarily) closed boiling and condensing system where irreversibility of the thermodynamic process may add up in terms of complexity.

The objective for the chapter is to present the current status and the vision for the future in this (selected) area of the thermal-hydraulic science.

1.1.3.9 Chapter 9: Constitutive equations

Principles of thermodynamics and mechanics imply conservation of mass energy and momentum which give origin to the balance equations (Chapter 5). However, the same principles do not allow the characterization of the interactions between the phases also including the appearance of geometry-dependent flow patterns.

Thus, constitutive equations are needed to model the interactions between the phases and between each phase or field and the environment. As a target, the constitutive equations must account of all possible conditions and phenomena expected in NPP (and RR) within the DBA boundaries.

Selected important issues in the area which also constitute the motivation for the chapter are outlined below. Those issues may imply the need for further development, for achieving common understanding and/or fixing precision goals

for calculations.

- The words “closure equations” are also used and may embed the constitutive equations or may identify a class of equations having a mere numerical formulation which is focused at achieving hyperbolic solutions from balance equations.
- Water physical properties including derivatives are not usually classified as constitutive equations: nevertheless tight interactions are established between water properties and constitutive equations.
- Constitutive and/or closure equations may have an empirical nature where measurement errors and scatter of data are unavoidable: characterizing the impact of those errors and scatters upon the results obtained from solving balance equations coupled with constitutive equations may not have a commonly agreed answer.
- Assumptions are needed to create solvable sets of closure equations. As an example, reference can be made to the subdivision of wall heat flux, i.e., a unique value derived from experiments, into contribution terms to liquid, steam, and, in some cases, steam-liquid interface. Arbitrariness in the repartition is mitigated by consistency checks and partially validated “a-posteriori” making use of experimental data independent from those used to generate the original repartition.
- An additional level of arbitrariness and complexity, following-up to the item above (assumptions to create solvable sets of constitutive equations) occurs when either three fields or three dimensions are part of the concerned thermal-hydraulic model.

Objective for the chapter is to provide the current status in the areas of development and applications of constitutive equations and to provide evaluations or discussion upon the topics listed above.

1.1.3.10 Chapter 10: Special models

Reference is made here to the prediction of transient scenarios occurring in the concerned water-cooled reactors, i.e., NPP and RR. The physical systems, or the physical processes, or the phenomena which are not (or cannot be) modeled by what are called constitutive equations embedded into balance equations are considered in the category of special models. Namely, two broad categories of special models are distinguished, related to:

(A) components and

(B) physical processes or phenomena

Examples in the former category are: centrifugal pump, jet pump, steam separator, steam dryer, valves (various configurations), turbine.

Examples in the latter category are: pressure drop coefficients at geometric discontinuities (also discussed in **Chapter 8**), flooding and counter-current flow limitation (CCFL), TPCF when not derived from the set of balance and constitutive equations which are standard for a given SYS TH code, direct contact condensation typically at ECC port.

The motivation of the chapter is the importance of concerned components and physical processes or phenomena in the frame of the prediction of transient scenarios.

The objective of the chapter is the description of models which constitute essential parts of the SYS TH codes.

1.1.3.11 Chapter 11: SYS TH codes

The envisaged role of the SYS TH codes within the nuclear thermal-hydraulics and the pivot role for the same codes in the present book are discussed in this chapter.

As it may be derived from the notes in **Section 1.1.1**, the development of a SYS TH code needs a variety of expertise, or matter and themes of the thermal-hydraulic universe, including numerics, neutron physics, computer science, etc. Only thermal-hydraulics topics are discussed in **Chapter 11**.

Important aspects for best estimate SYS TH codes are (the last item below shall be considered a consequence of the previous ones):

- Demonstration of the qualification level
- User effect upon the results of the calculation
- Justification of the reason why approximate modeling may produce acceptable results
- Need and way to evaluate the uncertainty
- Acceptability by regulatory authorities

The motivation for Chapter 11 is the importance of the SYS TH code. The objectives are a contribution to establish the capabilities of the codes based on the thermal-hydraulics modeling and, as a consequence, in making robust the applications to NPP and RR technology.

1.1.3.12 Chapter 12: CFD codes

The computational fluid-dynamics (CFD) matter is apparently outside the main path across the nuclear thermal-hydraulics universe selected for the book. However, at least two reasons suggested the consideration of CFD codes in Chapter 12:

- (1) CFD technology has potential for further development in the future also connected with more powerful computing machines.
- (2) Currently the application of CFD codes provides an irreplaceable role to support SYS TH codes calculations in a large number of situations; examples of those situations are: PTS, boron mixing and transport, temperature stratification, H₂ transport in the containment.

CFD technology was born well before the advent of computers at the end of the 19th century; however only the availability of powerful computers after the 1970s, during the 20th century, allowed the application of CFD codes to problems of industrial interest. Key differences between SYS TH codes and CFD codes are connected with the turbulence modeling which is direct in the case of CFD and the averaging process (e.g., at cross section or volume levels) which in principle is not needed in the case of CFD codes. Namely convergence of results is expected with reduction in mesh sizes in CFD codes, while the same goal cannot be demonstrated in a general situation in the case of SYS TH codes. Moreover, in the case of CFD codes, attempts are made to reduce the dependence upon the empiricism which characterizes the modeling of SYS TH codes.

Currently debated aspects within the CFD technology are:

- Results are still mesh dependent: i.e., not only the convergence of results cannot be established in each application, but also changes in the mesh topology causes differences in results.
- Wall functions are needed, e.g., to take into account of friction or HTC: this implies reintroduction of empiricism, contrary to the no-empiricism target which

characterizes the development of CFD codes.

- Maturity and/or robustness of solutions for single-phase applications in nuclear reactor safety are claimed by code developers. However, this is not the case for two-phase applications.
- V&V methods including qualitative and quantitative acceptability targets are under discussion within the scientific community.
- Precision targets, as in the case of the SYS TH codes technology area, e.g., for punctual velocity vectors, pressure drop scalar between two positions, punctual mixing scalar, etc., are not established.

All of the above shall be seen as a framework for the motivation of the chapter. The objective of Chapter 12 is to present the current status of the development of CFD codes focusing on modeling, capabilities, and perspectives.

1.1.3.13 Chapter 13: Verification, validation, scaling, and uncertainty

This chapter can be characterized by the words “putting the right perspectives for exploiting the current capabilities of SYS TH codes.” This means addressing the areas of V&V, Scaling, and Uncertainty. Making use of some oversimplification, one may state that scaling (and scaling needs, see also “Glossary” below) is an outcome of V&V needs, as well as Uncertainty evaluation becomes a need following the evaluation of V&V results.

If one uses the human body to create a parallel with nuclear thermal-hydraulics where the body movement constitutes the application of the discipline, then the SYS TH code is the hearth of the body and V&V including scaling and Uncertainty constitutes the blood.

V&V, scaling, and uncertainty are the bridge between SYS TH codes development and the application in nuclear technology. As a result of decades of R&D (as already discussed) qualified numerical tools are available including capability to evaluate the uncertainty; however, applications in the licensing process do not exploit those capabilities and simplified (so-called conservative) methods are used. This situation may appear controversial.

Then, objectives and motivations for the chapter are to show the robustness of the

processes and the methodologies adopted for V&V, scaling, and uncertainty.

1.1.3.14 Chapter 14: BEPU approach

Several ways can be adopted to define BEPU, one of this being “*BEPU=connection between SYS TH code development and V&V, Scaling, Uncertainty on the one side and licensing process on the other side.*” Then, “*BEPU is the application of SYS TH codes.*”

The BEPU process shall be associated with the licensing process. The licensing process noticeably includes the PSA together with a number of methods not discussed in the present book; those methods including PSA need a cross-link with BEPU. AA is part of the licensing process.

Among the general attributes of AA, the first one shall be the compliance with the established regulatory requirements.

The second attribute deals with the adequacy and the completeness of the selected spectrum of events. The achievement of the spectrum of events (or envelope) shall be the result of the combined applications of deterministic and probabilistic methods.

The third attribute is connected with the knowledge base including that captured by the qualified computational tools and analytical procedures suitable for the analysis of transient conditions envisaged for individual (concerned) NPP.

The complexity of a NPP and/or the accident scenarios may prove challenging for a conservative analysis, thus justifying the choice for a BEPU approach. This implies two main needs for nuclear thermal-hydraulics: (a) to adopt the current computational tools, proving (to the regulatory authority) an adequate quality via suitable V&V and (b) to adopt a qualified uncertainty method.

The motivation for Chapter 14 is to establish a role for BEPU within science and technology, breaking the isolation which restricts now BEPU knowledge to a narrow group of specialists. The idea is to consider BEPU as an essential piece of nuclear thermal-hydraulics thus facilitating and spreading the application of SYS TH codes.

The objective of the chapter is to provide a suitable overview of the techniques and the procedures part of BEPU, giving proper emphasis to the benefits expected from its application.

1.1.3.15 Chapter 15: DBA calculations

AA constitutes one key branch of nuclear reactor safety and of NPP (and RR) safety demonstration as already mentioned. PIEs are at the origin of AA. The internal PIE need transient calculations: the most powerful tool to perform transient calculation is the SYS TH code. This constitutes the motivation for Chapter 15.

Answering the question “what calculations must be performed?” constitutes the preliminary question to be addressed before the application of SYS TH codes to the transient analysis. Addressing the questions brings to the DBA envelope for categories of NPP. Grouping of the events part of the DBA envelope by principal cause of the initiating events brings to the following list (categories of events):

- Reactivity anomalies due to control rod malfunctions
- Reactivity anomalies due to boron dilution or cold water injection
- Coast-down of the main circulation pumps
- Loss of primary system integrity (LOCA)
- Interfacing systems LOCA
- Loss of integrity of secondary system
- Loss of power supply
- Malfunctions in the primary systems
- Malfunctions in the secondary systems
- ATWS
- Accidents in fuel handling
- Accidents in auxiliary systems
- Accidents due to external events

The objective of Chapter 15 is to discuss results of sample NPP transient analyses performed by SYS TH codes. Results of calculations are synthesized by time trends, and a connection is established with phenomena presented in Chapter 6.

1.1.3.16 Chapter 16: Occurred NPP accidents: the thermal-hydraulics

Accidents have occurred in NPP (and RR) and are part of the history of nuclear technology. Those accidents had a noticeable impact upon the development of the technology and, unfortunately, a negative impact upon the exploitation of the technology for electricity production. This constitutes the motivation for Chapter 16 although this is an unexpected chapter for those who planned the development of nuclear thermal-hydraulics till the late 1970s of the previous century.

The considered nuclear events are listed below together with implications in nuclear thermal-hydraulics although recognizing in advance the low role that thermal-hydraulics competences and expertise had in the occurrence of the event or mitigating their consequences (where applicable).

Implications signify changes in the importance of sectors of thermal-hydraulics and investments to better address new challenges for nuclear technology derived from those accidents, i.e., lessons learned.

- TMI, Unit 2 (TMI-2), LOFW-SBLOCA combined event, March 1979. As a consequence of the event, focus of investigation in nuclear thermal-hydraulics was shifted from LBLOCA to SBLOCA: this means the shift from homogeneous conditions in the vessel to stratified conditions. This can also be translated as shift from HEM or EVET modeling to UVUT modeling. The TMI-2 event also triggered huge investments for experiments in large-scale ITFs.
- La Salle, Unit 2, and Oskarshamn, Unit 2, BWR stability events, respectively, Mar. 1988 and Feb. 1999. As a consequence of the first event, a systematic reevaluation of the capabilities to predict density wave instability (DWI) phenomena took place. This basically brought to understanding that DWI depend upon a large number of factors including their combined effect, and upon minor changes of each factor that are difficult to predict. However, DWI events appear to have an incubation period which is detectable making mild or negligible the safety impact of possible modeling inadequacies.
- Chernobyl, Unit 4, neutron flux and thermal power excursion event, April 1986. As a consequence of the event operator independent systems became a fashion in the new design. Thus the event triggered the appearance of passive systems and both new-generation PWR and BWR were equipped by passive systems, noticeably AP-600 (later on AP-1000) and SBWR (later on ESBWR).
- Fukushima, Units 1-3, LOOSP event, Mar. 2011. As a consequence of the event,

controlled containment venting, already introduced in Germany (a concept already part of the design of the early Soviet Union reactors to avoid the construction of containment walls resistant to the full pressure caused, e.g., by a LOCA) became of interest. The event also solicited more attention to low-probability situations (e.g., high-intensity earthquake in the deep water of ocean) which once occurred may reveal precursor with high probability of dangerous scenarios for the plant (e.g., the tsunami).

The objective for the chapter is to describe the transient thermal-hydraulic scenarios occurred during the concerned events. Some emphasis is given to consequences in the development of thermal-hydraulics.

1.1.3.17 Chapters interconnections

Chapters 1–4 are directly or indirectly connected among each other (namely Chapter 1 is connected to Chapters 2–4 and connections exists between Chapters 3 and 4) and to all remaining chapters.

Chapters 5–10 are directly connected to Chapter 11 (SYS TH code).

Chapter 11 (SYS TH code) is at the origin of Chapters 13–16. Thus, Chapter 11 plays a pivot role in the present book as already emphasized.

Additional key connections among chapters are:

- Chapters 4 and 6: the knowledge of thermal-hydraulic phenomena (Chapter 6) constitutes a need which is clarified in Chapter 4.
- Chapter 5 (balance equations) constitutes the framework and the basis for Chapters 9 and 10: namely, in case of Chapter 10 (special models), the situations which cannot be calculated by balance equations shall be dealt by special models; furthermore constitutive equations (Chapter 9) must be integrated into balance equations (Chapter 5). All together, Chapters 5, 9, and 10 constitute the input for Chapter 11 (SYS TH code). Chapter 5 shall also be seen as providing (partial) input to Chapter 12 (CFD code).
- Chapter 6 (phenomena) has direct connection and interrelation with Chapters 11, 13, and 15: the development of SYS TH codes (Chapter 11) needs the knowledge of phenomena; the validation of SYS TH codes (Chapter 13) must be based upon the phenomena; finally, phenomena must be derived from the envelope of DBA

(Chapter 15).

- The knowledge of subjects from Chapter 7 (heat transfer) and Chapter 8 (pressure drop) is embedded into the SYS TH code, thus creating a direct connection between those Chapters and Chapter 11.

- Chapter 9 (constitutive equations) shall be seen as a necessary support for (the solution of) balance equations discussed in Chapter 5. Both Chapters 5 and 9 provide input to the development of SYS TH code discussed in Chapter 11. Duplication of concepts appears unavoidable between Chapters 5 and 9 from the one side and Chapter 11 from the other side. However the authors made an effort to present complementary information and different viewpoints.

- The knowledge and the subjects from Chapter 10 (special models) are embedded into the SYS TH code thus creating a direct connection between this Chapter and Chapter 11. Furthermore pressure drop at geometric discontinuities are also discussed in Chapter 8.

- Chapter 11 (SYS TH code) is the end product of scientific competence and knowledge from Part Two of the book and, in a weaker sense, from Part One: the role of this chapter has already been discussed.

- Chapter 12 (CFD codes) has key connection in the book with Chapter 5 (balance equations) and Chapter 11 (SYS TH codes). In this last case, the connection is not only to provide support to the SYS TH code calculations but also to establish strategic difference in the two modeling approaches.

- Chapter 13 (V&V, scaling, and uncertainty) constitutes the articulated joint between Chapter 11 (SYS TH codes) and Chapter 15 (codes application to NPP), see also role of BEPU approach (Chapter 14).

- Chapter 14 (BEPU approach) shall be seen as having the upstream interface with Chapter 13 (V&V, scaling, and uncertainty) and the downstream interface with Chapter 15 (DBA calculations) when the licensing process is concerned.

- Chapter 15 (DBA calculations) is possible because of SYS TH (Chapter 11) codes application. In addition a link is established with phenomena in Chapter 6.

- Chapter 16, i.e., occurred NPP accidents, has weak connections with nuclear thermal-hydraulics. Rather, the nuclear thermal-hydraulics discipline and, noticeably, the SYS TH codes allowed or facilitated the understanding of the

progression of the events. An attempt is made in Chapter 16 to establish the connection between nuclear thermal-hydraulics and those NPP accidents.

Glossary

The book is devoted to researchers and scientists and professionals involved in safety analysis on both the industry side and the regulatory side as well as to students working for master or PhD theses, all of them having already expertise or suitable knowledge in nuclear technology. So in the Glossary only terms which may generate misunderstandings or not having wide diffusion and use are included.

Nuclear installation The ensemble of NPP and RR is characterized by the words nuclear installations in the present book.

Postulated accidents Thermal-hydraulic transient scenarios expected in nuclear installations following a PIE. Postulated accidents are used to evaluate the safety of individual NPP and RR. SYS TH codes supported by uncertainty evaluation are needed to calculate nuclear thermal-hydraulic scenarios during postulated accidents.

Scaling (or scale) Other than the words “validation or qualification” and “uncertainty or error in prediction” understandable in different

computational technologies, the word scaling is of key importance in nuclear thermal-hydraulics. Scaling indicates (need for) lacking information that is expected to characterize the transient performance of NPP. This implied and implies use of equations, development of methodologies, designing and execution of experiments, and gathering of data aimed at demonstrating the capability to understand the evolutions of two-phase mixtures in NPP conditions.

References

Abu-Zeid M.A. Finite element analysis for prediction hydraulic performance of a rectangular flap valve. *Int. J. Eng. Technol. Res.* 2013;2:1.

Aksan, N., Bessette, D., Brittain, I., D'Auria, F., Gruber, P., Holmström, H.L., Landry, R., Naff, S., Pochard, R., Preusche, G., Reocreux, M., Sandervag, O., Stadtke, H., Wolfert, K., Zuber, N., 1987. CSNI code validation matrix of thermo-hydraulic codes for LWR LOCA and transients. OECD/NEA/CSNI Report No. 132, Paris, France.

Allison, C., Balabanov, E., D'Auria, F., Jankowski, M., Misak, J., Salvatores, S., Snell, V., 2002. Accident analysis for nuclear power plants. IAEA Safety Reports Series No. 23, Vienna, Austria.

Annaratone D. *Steam Generators*. Berlin: Springer; 2008.

Apostolakis G., Moieni P. The foundations of models of dependence in probabilistic safety assessment. *Reliab. Eng.* 1987;18:3.

Araneo D., D'Auria F. Methodology for pressurized thermal shock analysis in nuclear power plant. In: Belov A., ed. *Applied Fracture Mechanics*. InTech; 2012.

Arkadov G., Getman A., Rodionov A. *Probabilistic Safety Assessment of Optimum Nuclear Power Plant Life Management*. Woodhead Publishing; 2012.

Avvakumov A., Malofeev V., Sidorov V., Scott H.H. *Spatial Effects and Uncertainty Analysis for Rod Ejection Accidents in a PWR*. NUREG/IA-0215 Washington, DC, USA: USNRC; 2007.

Baker Jr. L., Just, L.C., 1962. Studies of meta-water reactions at high temperatures – III – experimental and theoretical study of zirconium-water reactions. ANL 6548, Argonne, IL, USA.

Banerjee S. *Industrial Hazard and Plant Safety*. New York, NY, USA: Taylor & Francis; 2003.

Barna I.F., Imre A.R., Baranyai G., Ézsöl G. Experimental and theoretical study of steam condensation induced water hammer phenomena. *Nucl. Eng. Des.* 2010;240:146–150.

Benedict M., Pigford T.H., Levy H.W. *Nuclear Chemical Engineering*. New York, NY, USA: McGraw-Hill; 1981.

Berry, R.A., Peterson, J.W., Zhang, H., Martineau, R.C., Zhao, H., Zou, L., Andrs, D., 2015. RELAP-7 theory manual. INL/EXT-14-31366 (rev. 1), Idaho Falls, ID, USA.

Bestion D. The physical closure laws in the CATHARE code. *Nucl. Eng. Des.* 1990;124:3.

Bird R.B., Stewart W.E., Lightfoot E.N. *Transport Phenomena*. first ed. New York, NY, USA: John Wiley & Sons Inc.; 1960.

Bloch H.P., Singh M.P. *Steam Turbines, Design Applications and Re-Rating*. New York: McGraw-Hill; 2009.

Bungartz H.-J., Schäfer M. *Fluid Structure Interaction*. Berlin, Germany: Springer; 2006.

Cacuci D.G., ed. *Handbook of Nuclear Engineering*. Berlin, Germany: Springer; 2010.

Camp, A.L., Cummings, J.C., Sherman, M.P., Kupiec, C.F., Healy, R.J., Caplan, J.S., Sandhop, J.R., Saunders, J.H., 1983. Light water reactor hydrogen manual. Sandia Report NUREG/CR-2726, SAND82-1137, New Mexico, USA.

Cheng L.-Y., Baek J.-S., Cuadra A., Aronson A., Diamond D. *TRACE simulation of a BWR anticipated transient without scram leading to emergency depressurization*. In: ANS Annual Meeting, Reno, NV, USA; 2014.

Collier J.G. *Two Phase Flow and Heat Transfer in Water Cooled Nuclear Reactors, Lecture Series*. New Hampshire, USA: Dartmouth College; 1975.

Courtin S. High cycle thermal fatigue damage prediction in mixing zones of nuclear power plants: engineering issues illustrated on the FATHER case. *Procedia Eng.* 2013;66:240–249.

Cumo M. *Experimental Thermo-Technics*. (in Italian). Roma, Italy: ENEA Publisher; 1982.

Cumo M., Naviglio A. *Thermal Hydraulic Design of Components for Steam Generation Plants*. Boca Raton, FL: CRC Press; 1990.

D'Auria, F. (Project Coordinator), Bousbia Salah, A., Galassi, G.M., Vedovi, J., Reventos, F., Cuadra, A., Gago, J.L., Sjöberg, A., Yitbarek, M., Sandervag, O., Garis, N., Anher, C., Aragones, J.M., Verdù, G., Mirò, R., Hadek, J., Macek, J., Ivanov, K., Rizwan-Uddin, Sartori, E., Rindelhardt, U., Rohde, U., Frid, V., Panayotov, D., 2004. Neutronics/Thermal-Hydraulics Coupling in LWR Technology – CRISSUE-S (three volumes), Vol. I. OECD/NEA Report No. 4452, Paris, France.

D'Auria F., Bestion D., Jeong J.J., Kim M. *V & V in system thermal-hydraulics*. In: ASME Verification and Validation Symposium (V & V 2012) Meeting, Las Vegas, NE, USA, May 2–4; 2012a.

D'Auria, F., Galassi, G.M., 2000. Methodology for the evaluation of the reliability of passive systems. University of Pisa Report, DIMNP-NT 420(00)-rev. 1, Pisa, Italy, October.

D'Auria F., Galassi G.M. Scaling in nuclear reactor system thermal-hydraulics. *Nucl. Eng. Des.* 2010;240(10):3267–3293.

D'Auria F., Vigni P. *Fluid-dynamic analysis of steam-water flows from a pressure vessel*. In: Workshop on Jet Impingement and Pipe Whip, Genova, Italy, June 29–July 1; 1981.

D'Auria, F., Glaeser, H., Lee, S., Mišák, J., Modro, M., Schultz, R.R., 2008. Best estimate safety analysis for nuclear power plants: uncertainty evaluation. IAEA Safety Report Series No. 52, Vienna, Austria.

D'Auria F., Camargo C., Muellner N., Lanfredini M., Mazzantini O. The simulation of I & C in accident analyses of nuclear power plants. *Nucl. Eng. Des.* 2012b;250:656–663.

Delhaye J.M., Giot M., Rithmuller M.L., eds. *Thermohydraulics of the Two-Phase Systems for Industrial Design and Nuclear Engineering*. New York, NY, USA: Hemisphere Publishing Co. \McGraw-Hill Book Company; 1981.

El-Wakil M.M. *Nuclear Power Engineering*. New York, NY, USA: McGraw-Hill Book Company, Inc.; 1962.

El-Wakil M.M. *Nuclear Energy Conversion*. Scranton, PA, USA: Intext Educational Publisher; 1971a.

El-Wakil M.M. *Nuclear Heat Transport*. Scranton, PA, USA: Intext Educational Publisher; 1971b.

Etherington H., ed. *Nuclear Engineering Handbook*. New York, NY, USA: McGraw-Hill Book Company, Inc.; 1958.

Fenech H., ed. *Heat Transfer and Fluid Flow in Nuclear Systems*. Elmford, NY, USA: Pergamon Press Inc.; 1981.

Ferreri J.C., Ambrosini W. On the analysis of thermal-fluid-dynamic instabilities via numerical discretization of

conservation equations. *Nucl. Eng. Des.* 2002;215:153–170.

Ferziger E.H., Perić M. *Computational Methods for Fluid Dynamics*. Berlin, Germany: Springer; 1999.

Fulwood R.R. *Probabilistic Risk Assessment in Chemical and Nuclear Industries*. Oxford, UK: Butterworth-Heinemann Publisher; 2000.

Glaeser H., Karwat H. The contribution of UPTF experiments to resolve some scale-up uncertainties in countercurrent two phase flow. *Nucl. Eng. Des.* 1993;145:1–2.

Glasstone S., Edlund M.C. *The Elements of Nuclear Reactor Theory*. Princeton, NJ, USA: Van Nostrand Company, Inc.; 1952.

Glasstone S., Sesonske A. *Principles of Nuclear Reactor Engineering*. Princeton, NJ, USA: Van Nostrand Company, Inc.; 1955.

Gröber H., Erk S. *Die Grundgesetze Wärmeübertragung*. Berlin, Germany: Springer; 1933.

Groeneveld D.C. On the definition of critical heat flux margin. *Nucl. Eng. Des.* 1996;163:245–257.

Guillen D.P., ed. *Nuclear Reactor Thermal Hydraulics and Other Applications*. InTech Open Access; 2013.

Gülich J.F. *Centrifugal Pumps*. second ed. Berlin, Heidelberg: Springer; 2010.

Hassan Y.A. In: Buchlin J.M., ed. *Two-Phase Flow CFD in Nuclear Reactors (I)*. Berlin: Institute for Fluid Dynamics; 2005 published in the Industrial Two-Phase Flow CFD, Lecture Series 2005-04.

Herviou, K., 2005. Development of a methodology and of a computer tool for source term estimation in case of nuclear emergency in a Light Water Reactor (ASTRID). EC Report ASTRID/04.39.

Hewitt G.F., Delhay J.M., Zuber N., eds. *Post-Dryout Heat Transfer*. Boca Raton, FL, USA: CRC Press Inc.; 1992.

Hsu Y.Y., Graham R.W. *Transport Processes in Boiling and Two-Phase Systems*. Hinsdale, IL, USA: ANS Monograph; 1986.

IAEA. *Development and Application of Level 1 Probabilistic Safety Assessment for Nuclear Power Plants*. Vienna, Austria: IAEA; 2010a Safety Standard Series, SSG-3.

IAEA. *Development and Application of Level 2 Probabilistic Safety Assessment for Nuclear Power Plants*. Safety Standard Series, SSG-4 Vienna, Austria: IAEA; 2010b.

IAEA. *Pressurized Thermal Shock in Nuclear Power Plants: Good Practices for Assessment*. TECDOC 1627 Vienna, Austria: IAEA; 2010c.

Incropera F.P., Dewitt D.P. *Fundamentals of Heat Transfer*. New York, NY, USA: John Wiley & Sons; 1981.

Ishii M. *Thermo-Fluid Dynamic Theory of Two-phase Flow*. Paris, France: Eyrolles; 1975.

Ishii M., Hibiki T. *Thermo-Fluid Dynamics of Two-Phase Flow*. Berlin, Germany: Springer; 2006.

Ivanov K., Baratta A. *Coupling methodologies for best estimate safety analysis*. In: Int. Conf. on Mathematics, Computation, Reactor Physics and Environmental Analysis (M & C), Madrid, Spain; 1999.

Jafari J., D'Auria F., Kazeminejad H., Davilu H. Reliability evaluation of a natural circulation system. *Nucl. Eng. Des.* 2003;224:79–104.

Jakob M. *Heat Transfer*. New York, NY, USA: John Wiley & Sons Inc.; 1949.

Jeong J.J., Yoon H.Y., Park I.K., Cho H.K. The CUPID code development and assessment strategy. *Nucl. Eng. Technol.* 2010;42(6):636–655.

Kirillov P.L., Bobkov V.P., Zhukov A.V., Yur'ev Yu.S., eds. *Handbook on Thermohydraulic Calculations in Nuclear Power Engineering*. Moscow, Russia: IzdAt Publishing House; . *Hydrodynamic Calculations and Heat Transfer*. 2010;vol. 1 (In Russian).

Kirillov P.L., Zhukov A.V., Loginov N.I., Makhin V.M., Pioro I.L., Yur'ev Yu.S., eds. *Handbook on Thermohydraulic Calculations in Nuclear Power Engineering*. Moscow, Russia: IzdAt Publishing House; . *Nuclear Reactors, Structures and Core (Calculations), Heat Exchangers, Steam Generators, Heat Pipes*. 2013;vol. 2 (In Russian).

Kirillov P.L., Yur'ev Yu.S., D'Auria F., Migrov Yu.A., Soloviev S., eds. *Handbook on Thermohydraulic Calculations in Nuclear Power Engineering*. Moscow, Russia: IzdAt Publishing House; . *Thermohydraulic Processes under Transient and Irregular Regimes*. 2014;vol. 3 (In Russian).

Knief R.A. *Nuclear Engineering Theory and Technology of Commercial Nuclear Power (reprint of 1992, 2nd edition)*. Hinsdale, IL, USA: ANS; 2008.

Knoll G.F. *Radiation Detection and Measurement*. USA: John Wiley & Sons Inc.; 2010.

Kolev N. *Multiphase Flow Dynamics, Vols. I to V*. (various Editions) Berlin, Heidelberg: Springer; 2011–2015.

Kutateladze S.S. *Fundamentals of Heat Transfer*. London, UK: Edward Arnold Publishers Ltd.; 1963.

Lahey Jr. R.T., Moody F.J. *The Thermal-hydraulics of a Boiling Water Reactor*. Hinsdale, IL, USA: ANS Monograph; 1993.

Lamarsh J.R. *Introduction to Nuclear Reactor Theory*. Reading, MA, USA: Addison-Wesley; 1966.

Lamarsh J.R., Baratta A.J. *Introduction to Nuclear Engineering*. International Edition Upper Saddle River, NJ, USA: Prentice Hall; 2011.

Landau L., Lifchitz E. *Mécanique des Fluides (translated in French in 1971)*. (first Russian edition). Moscow, USSR: MIR; 1954.

Levy S. *Two-Phase Flow in Complex Systems*. New York, NY, USA: John Wiley & Sons Inc; 1999.

Lewis E.E. *Nuclear Power Reactor Safety*. New York, NY, USA: John Wiley & Sons, Inc.; 1978.

Lewis, M.J. (Ed.), Pochard, R., D'Auria, F., Karwat, H., Wolfert, K., Yadigaroglu, G., Holmstrom, H.L.O. (Lead Authors), 1989. Thermohydraulics of emergency core cooling in light water reactors – a state-of-the-art report. OECD/NEA/CSNI Report No. 161, Paris, France.

Lisovsky O., Cherubini M., Lazzerini D., D'Auria F. Base irradiation simulation and its effect on fuel behavior prediction by TRANSURANUS code: application to reactivity initiated accident condition. *Nucl. Eng. Des.* 2015;283:162–167.

Lykov A.V. *Transporterscheinungen in Kapillarporösen Körpern*. Germany: Springer Verlag; 1958.

Lykov A.V., Mikhailov Yu.A. *Theory of Energy and Mass Transfer*. New York, NY, USA: Prentice Hall; 1961.

Margoulova Th. *Le Centrales Nucléaires (translated in French in 1977)*. (first Russian edition) Moscow, USSR: MIR; 1969.

Marques M., Pignatelli J.F., Saignes P., D'Auria F., Burgazzi L., Muller C., Bolado-Lavin L., Kirchsteiger C., La Lumia V., Ivanov I. Methodology for the reliability evaluation of a passive system and its integration into a Probabilistic Safety Assessment. *Nucl. Eng. Des.* 2005;235:2612–2632.

Mayinger F., ed. *Optical Measurements*. Berlin, Heidelberg, Germany: Springer-Verlag GmbH; 1994.

Michal R. Nuclear news. *ANS*. (November):2001.

Miro J., Sonnenburg H.G., Steinhoff F., Teschendorff V., Forge A., Pochard R., Porracchia A. *Comparison of Thermal-Hydraulic*

Safety Codes for PWR Systems. London, UK: Graham & Trotman; 1990.

Moore, K.V., Rettig, W.H., 1968. RELAP2: a digital program for reactor blow-down and power excursion analysis. US DOE, IDO 17263, USA.

Moretti, F., 2016. Information about SWINTH and proposal for cooperation and support from WGAMA. 19th WGAMA Meeting, OED Conf. Centre, Sept. 23–26, 2016, Paris, France.

Murray R., Holbert K.E. An introduction to the concepts, systems and applications of nuclear processes. In: *Nuclear Energy*. seventh ed. Amsterdam: Elsevier; 2014.

Ninokata H., Aritomi M. *Sub-Channel Analysis in Nuclear Reactors*. Japan: Inst. of Applied Energy, Nihon Genshiryoku Gakkai; 1992.

Nukiyama S. The maximum and minimum values of heat transmitted from metal surface to boiling water under atmosphere pressure. *Int. J. Heat Mass Trans.* 1966;9:1419–1433 (also Journal of the Japan Society of Mechanical Engineers, 37, 206).

Nusselt W. *Teschnische Thermodynamik*. Berlin, Germany: Walter de Gruyter & Co; 1943.

OECD/NEA/CSNI. In: CSNI Spec. Meet. On Transient Two-Phase Flow - System Thermal-hydraulics, Aix-en-Provence Conference Proceedings, April 6–8, Paris, France; 1992.

OECD/NEA/CSNI, 1997. Proceedings of OECD/CSNI Specialists Meeting on Advanced Instrumentation and Measurement Techniques, Santa Barbara, CA, USA, March 17–20, 1997. NEA/CSNI/R(97)33, Paris, France.

OECD/NEA/CSNI, 2010. Nuclear Fuel Behavior under Reactivity Initiated Accident (RIA) conditions, NEA/CSNI/R(2010)1.

Oka Y., ed. *Nuclear Reactor Design*. Tokyo, Japan: Springer;

2014.

Okrent D. *Nuclear Reactor Safety: On the History of the Regulatory Process*. USA: University of Wisconsin Press; 1981.

Païdoussis M.P., Price S.J., de Langre E. *Fluid Structure Interactions*. Cambridge: Cambridge University Press; 2014.

Patankar S.V. *Numerical Heat Transfer and Fluid Flow*. Washington, NY, London: Hemisphere Publishing; 1980.

Patankar S.V., Spalding D.B. *Heat and Mass Transfer in Boundary Layers*. London, UK: Morgan-Grampian; 1967.

Petruzzi A., D'Auria F., Bajs T., Reventos F., Hassan Y. International course to support nuclear licensing by user training in the areas of scaling, uncertainty and 3D thermal-hydraulics/neutron-kinetics coupled codes: 3D S.UN.COP seminars. *Sci. Technol. Nucl. Install.* 2008;2008:1–16 Article ID: 874023.

Pla P., Parisi C., D'Auria F. *Boron Dilution and Boron Transport After SBLOCA in PWR and VVER-1000 Nuclear Reactors*. Germany: Lambert Academic Publishing; 2010.

Planck M. *Vorlesungen über die Theorie der Wärmestrahlung*. 4 Aufl. Germany: Leipzig; 1923.

Prandtl L. *Führer durch die Strömungslehre*. 4 Aufl. Braunschweig: Vieweg; 1956.

Reichardt H. Über eine Theorie der freien Turbulenz. *Angew. Math. Mech.* 1941;21(5):257–264 (Journal of Applied Mathematics and Mechanics).

Reocreux M. *Current and future trends in nuclear reactor thermal-hydraulics*. In: Int. Conf. New Trends in Nuclear System Thermal-Hydraulics, Pisa, Italy; 1994.

Reventós F., Llopis C., Batet L., Pretel C., Sol I. Analysis of an actual reactor trip operating event due to a high variation of neutron flux occurring in the Vandellòs-II nuclear power plant.

Nucl. Eng. Des. 2010;240:2999–3008.

Reynolds O. On the dynamical theory of incompressible viscous fluid and the determination of the criterion. *Philos. Trans. Royal Soc. London.* 1896;186:123–164.

Rohatgi U.S. In: Role of Scaling in Validation, Keynote at ASME Verification and Validation Symposium, Las Vegas, NV, USA; 2015.

Royle P., Travis J.R., Breitung W., Kim J., Kim S.B. GASFLOW validation with PANDA tests from the OECD SETH benchmark covering steam/air and steam/helium/air mixtures. *Sci. Technol. Nucl. Install.* 2009;2009:1–13 Article ID 759878.

Schultz M.A. *Control of Nuclear Reactors and Power Plants.* New York, NY, USA: McGraw-Hill Book Company, Inc.; 1955.

Schultz R.R., Kondo M., Anoda Y. In: Baseline Study to Model a Typical Condensation-Induced Water Hammer Event Measured at the Two-Phase Flow Test Facility (TPTF) in Japan, Pressure Vessel & Piping Conference, Atlanta, GA, USA, July 22–26; 2001.

Sehgal B.R. *Nuclear Safety in Light Water Reactors – Severe Accident Phenomenology.* Oxford, UK: Elsevier Academic Press; 2012.

Sjoden G.E. *Foundations in Applied Nuclear Engineering Analysis.* London, UK: Imperial College Press; 2015.

Sokolowski L., Koszela Z. RELAP5 capability to predict pressure wave propagation phenomena in single- and two-phase flow conditions. *J. Power Technol.* 2012;92:3.

Spalding D.B. *Convective Mass Transfer: An Introduction.* London, UK: Edward Arnold Publishers, Ltd.; 1963.

Sparrow E.M., Cess R.D. *Radiation Heat Transfer.* Belmont, CA, USA: Brooks/Cole Publishing Corp.; 1966.

Stephenson R. *Introduction to Nuclear Engineering.* New York,

NY, USA: McGraw-Hill Book Company, Inc.; 1958.

Theophanous T.G., Shabana E.A. Boron mixing in the lower plenum of a BWR. *Nucl. Eng. Des.* 1991;126:2.

Thielen H., Brücher W., Martens R., Sogalla M. *Advanced Atmospheric Dispersion Modelling and Probabilistic Consequence Analysis for Radiation Protection Purposes in Germany*. Germany: Springer; 2007.

Todreas N.E., Kazimi M. *Nuclear Systems (Vols. I and II)*. Washington, DC: Hemisphere Pub. Corp.; 1990.

Tong L.S. *Boiling Heat Transfer and Two-Phase Flow*. New York, NY, USA: John Wiley & Sons; 1965.

Tong L.S., Weisman J. *Thermal Analysis of Pressurized Water Reactors*. Hinsdale, IL, USA: ANS Monograph; 1970.

Tuzson J. *Centrifugal Pump Design*. New York: John Wiley & Sons Inc.; 2000.

Umminger K., Del Nevo A. Integral test facilities and thermal-hydraulic system codes in nuclear safety analysis. (Preface to Special Issue) *Sci. Technol. Nucl. Install.* 2012;2012:1–3 Article ID 826732.

Vigni P., D'Auria F. Unsteady two-phase jet forces (in Italian). *J. Nucl. Eng.* 1979;10:23–32.

Wallis G.B. *One Dimensional Two-Phase Flow*. New York, NY, USA: McGraw-Hill Book Company; 1970.

WNA. *Outline of History of Nuclear Energy*. www.world-nuclear.org/info/Current-and-Future-Generation/. 2014.

Xiao J., Travis J.R. How critical is turbulence modeling in gas distribution simulations of large-scale complex nuclear reactor containment? *Ann. Nucl. Energy*. 2013;56:227–242.

Yadigaroglu G. *Heat and Mass Transfer Between Droplets and the Atmosphere – State of the Art*. Berkeley, CA, USA: Department of

Nuclear Engineering, University of California; 1975.

Yadigaroglu G., Lahey Jr. R.T. On the various forms of the conservation equations in two phase flows. *Int. J. Multiphase Flow*. 1976;2:477–494.

Yamanouchi A. Effect of core spray cooling in transient state after loss of coolant accident. *Nucl. Sci. Technol*. 1968;11:541–558.

Zuber N. Stability of boiling heat transfer. *ASME Trans*. 1958;80:711–720.

Zuber N. Scaling: from quanta to nuclear reactors. *Nucl. Eng. Des*. 2010;240(8):1986–1996.

A historical perspective of nuclear thermal-hydraulics

F. D'Auria University of Pisa, Pisa, Italy

Abstract

Three main topics are concerned: (a) the definition of system thermal-hydraulics, (b) a historical outline, (c) elements for reflection when planning researches or improvement activities. The proposal of Interim Acceptance Criteria for Emergency Core Cooling Systems in 1971 by US AEC (United States Atomic Energy Commission) is recognized as the triggering event for modern system thermal-hydraulics. The complex codes and the foremost experimental programs (key ongoing projects are mentioned) shall be seen as the pillars for the discipline. The attempt to forecast developments in the area has been pursued without constraints connected with the availability of funds and considering potential industrial benefits or interests. Demonstrating the acceptability of current system thermal-hydraulics limitations and training in the application of those codes are mentioned as the main challenges for forthcoming research activities.

Keywords

System thermal-hydraulics; Licensing; A historical outline; The acceptance criteria for the ECCS design; Current challenges; Future developments in thermal-hydraulics

ADS Automatic Depressurization System

AEC Atomic Energy Commission (see USNRC)

AERB Atomic Energy Research Body in India

ALARA as low as reasonably achievable

AM Accident Management

AMG Accident Management Guidelines

ANE Annals of Nuclear Energy (Journal)

ANS American Nuclear Society

AOO anticipated operational occurrence

APEX name of ITF in the United States

APROS SYS TH code developed in Finland

APS American Physical Society

AP600, AP1000 reactor designed by Westinghouse

ASME American Society of Mechanical Engineers

ATHLET SYS TH code developed in Germany

ATLAS name of ITF in Korea

ATWS anticipated transient without
scram

BDBA beyond DBA

BE best estimate—also acronym for
a series of conferences

BEAU best estimate Analysis and
Uncertainty

BEM boundary element method

BEMUSE project in area of
uncertainty launched and completed
by CSNI

BEPU best estimate plus uncertainty

BETHSY name of ITF in France

BPG Best Practice Guidelines

BWR boiling water reactor

CANDU reactor designed by AECL in Canada

CASL DOE project

CATHARE SYS TH code developed in France

CCFL countercurrent flow limitation

CCTF name of large-scale SETF in Japan

CCVM Computer (or CSNI) Code Validation Matrix

CFD computational fluid dynamics

CFR Code of Federal Regulation

CHF critical heat flux

CIAU code with capability of
Internal Assessment of Uncertainty

CMT core makeup tank

CO containment

CRP Coordinated Research Project
(inside IAEA)

CRUD Chalk river unidentified
deposit

CSAU code scaling applicability and
uncertainty

CSNI Committee on the Safety of
Nuclear Installations of NEA

DBA design basis accident

DiD defense in depth

DNB departure from nucleate boiling

DOE see US DOE

DSA deterministic safety assessment
(or analysis)

EC European Commission

ECCS Emergency Core Cooling
Systems

EDB Experimental Data Base

EdF nuclear utility in France

EOP emergency operating procedure

EPRI Electrical Power Research
Institute

ERDA Energy Research and
Development Administration, see
USDOE

ESBWR reactor designed by General
Electric

ESF engineered safety features

ETFS Experimental Thermal and
Fluid Science (Journal)

ETN nuclear utility in Brazil

EUROFASTNET EC network for
planning TH project

FIST name of ITF in the United
States

FIX-II name of ITF in Sweden

FONESYS network of SYS TH code developers (see the web)

FSAR Final Safety Analysis Report

GIRAFFE name of ITF in Japan

GRNSPG Nuclear Research Group in San Piero a Grado

HDR name of large-scale SETF in Germany

H-F Henry-Fauske (TPCF model)

HT heat transfer

HTC heat transfer coefficient

IA interfacial area

IAC Interim Acceptance Criteria

IAEA International Atomic Energy
Agency

IJMF International Journal on
Multiphase Flow

IRSN Institute for Radiological
Protection and Nuclear Safety

IRWST in-reactor water storage tank

ISB name of ITF in Russia

ITF integral test facility

I&C instrumentation and control
(systems)

JHT Journal of Heat Transfer (of ASME)

KAERI Korea Atomic Energy Research Institute

KORSAR SYS TH code developed by Russia

LBLOCA large-break LOCA

LOCA loss-of-coolant accident

LOBI name of ITF of EC installed in Italy

LOFT name of ITF in United States

LSTF name of ITF in Japan

LUT look-up tables (for CHF)

MARS SYS TH code developed in Korea

MARVIKEN name of large-scale SETF in Sweden

MIST name of ITF in the United States

NASA nuclear utility in Argentina

NC natural circulation

NEA Nuclear Energy Agency of OECD

NED Nuclear Engineering and Design (Journal)

NET Nuclear Energy and Technology (Journal)

NK neutron kinetics

NPP nuclear power plant

NRC see USNRC

NRS Nuclear Reactor Safety
(technology)

NSC Nuclear Science Committee of
NEA

NT Nuclear Technology (Journal of
ANS)

NURESAFE EC project follow-up of
NURISP

NURESIM EC planning project based
on EUROFASTNET

NURETH Nuclear Reactor Thermal-

hydraulics (series of ANS conferences)

NURISP EC project follow-up of NURESIM

OECD Organization for Economic Cooperation and Development

PACTEL name of ITF in Finland

PANDA name of large-scale SETF in Switzerland

PIE postulated initiating event

PIPER-ONE name of ITF in Italy

PIRT phenomena identification and ranking table

PKL name of ITF in Germany

PMK name of ITF in Hungary

PNE Progress in Nuclear Energy
(Journal)

PORV pilot-operated relief valve

PREMIUM project in area of
uncertainty launched by CSNI

PRHR pressurized residual heat
removal (system)

PS primary system

PSA probabilistic safety assessment
(or analysis)

PSB name of ITF in Russia

PTS pressurized thermal shock

PUMA name of large-scale SETF in the United States

PWR pressurized water reactor

RCS reactor coolant system

RD-14M name of ITF in Canada

RELAP SYS TH code developed in the United States

RG Regulatory Guide (of USNRC)

ROSA-III name of ITF in Japan

R&D research and development

SAMG Severe Accident Management Guidelines

SBLOCA small-break LOCA

SBO Station Blackout

SBWR see ESBWR

SCTF name of large-scale SETF in Japan

SEMISCALE name of ITF in the United States

SETF separate effect test facility

SG steam generator

SILENCE Network of SYSTEM experimentalists (see the web)

SMR small and modular (or medium) reactor

SOAR State of the Art Report

SPACE SYS TH code developed in Korea

SPES name of ITF in Italy

SRS Safety Report Series (of IAEA)

SSG Specific Safety Guide (of IAEA)

STNI Science and Technology of Nuclear Installations (Journal)

SYS TH system thermal-hydraulics

TECC thermal-hydraulics of ECCS

THTF name of large-scale ITF in the United States

TF test facility

TM Technical Meeting (of IAEA)

TPCF two-phase critical flow

TPPD two-phase pressure drop

TRACE SYS TH code developed in the United States

UM name of ITF in the United States

UMAE uncertainty methodology based on accuracy extrapolation

UMS project in area of uncertainty launched and completed by CSNI

UPTF name of large scale-SETF in Germany

US DOE US Department of Energy

USNRC US Nuclear Regulatory
Commission

VVER-1000 reactor designed by
Gidropress in Russia

V&V verification and validation

XS cross section

W-Gama working group inside CSNI

3D three-dimensional

Chapter foreword

The nuclear thermal-hydraulics discipline was developed following the needs for nuclear power plants (NPPs) and, to a more limited extent, research reactors (RR) design and safety. As in all other fields where analytical methods are involved, nuclear thermal -hydraulics took benefit of the development of computers. Thermodynamics, rather than fluid dynamics, is at the bases of the development of

nuclear thermal-hydraulics together with experiments in complex two-phase situations, namely, geometry, high thermal power density, and pressure.

Mandatory licensing requirements originated by safety needs pushed huge investments since the end of 1960s during the past century which drove the developments in the area. All of this created a unique technology where highly geometry-dependent transient phenomena, sophisticated two-phase flow modeling, continuously advancing numerics science, unavoidable empiricism derived from experiments, are merged. This forms the knowledge which needs to be mastered and managed also for the use of new generations of scientists.

The objective and the motivations for this chapter are to trace the history of the discipline. This appears necessary for its understanding and creating perspectives for development.

Those perspectives also constitute the content for the chapter. However, caution or warning statement is introduced in advance when discussing perspectives for development in such a complex matter: a single scientist or even a group of scientists (or researchers) have little or no possibility, neither the capability, to streamline the forthcoming investments or to propose a roadmap for future activities.

A paper recently published by the author, D'Auria (2012), has been the inspiration basis for this chapter of the book.

2.1 Introduction

Thermal-hydraulics and system thermal-hydraulics (SYS TH) shall be seen as one of the five key disciplines essential for the progress in nuclear science, making reference to NPP design and Nuclear Reactor Safety (NRS) technologies. This is discussed in **Chapter 1** of the book. The other disciplines may be identified as neutron physics, structural mechanics, radioprotection, and reliability including statistics.

SYS TH deserves and achieves proper attention by national and international institutions engaged in NPP design and NRS. This is also true from the sides of research and development (R&D) and innovation.

Therefore, motivations are proposed hereafter to plan this chapter of the book. Reference is made to developments in a complex technology, i.e., SYS TH in the present case, which may require multimillion dollar investment to achieve concrete

improvements. A few, even contradictory concepts are discussed in the next paragraphs.

The epoch already started since two or three decades is characterized by fast increase in the easiness-to-travel and the communication power: in these conditions, political and market-driven decisions and large Institutions or Industry agreements may have contributed to average but also to overshadow the ideas of individuals. In the areas of science and technology, including the planning for the future, joint decisions constitute a democratic process. This also brings to minimize the resources for the development and, in generic terms, is functional in getting the peace of the humankind. However, the ideas of individuals in the research and innovations remain the engine for commercial success and advancements specifically when noncomplex technologies or fragments of complex technologies are involved. All of this depicts may be used to explain the current situation for nuclear thermal-hydraulics in the new millennium: many involved technologists and researchers, many ideas for innovations, and (very) slow perceptible progress. The developments in the area may be seen like the expansion of a marsh rather than the flow of a river in one direction.

The political and strategic importance of NPP design, construction, and operation and NRS with main reference to the acceptance criteria set by regulators, e.g., 10 CFR 50.46, USNRC (2015), bring to the following needs: (a) to construct and operate scaled facilities having “suitable-achievable” power, pressure, and geometric dimensions as part of the design and (b) to develop and qualify sophisticate computer codes (or computational tools). Endeavors associated with both SYS TH facilities and computational tools involve research groups formed by tens or several tens researchers and corresponding financial investments.

However, one may settle for nuclear thermal-hydraulics (and not only for this discipline) that:

- Averaging from several decision makers is a democratic process, and the “fashion-of-the-period” activities are privileged for funding.
- Targets set by individuals may become part of a dictatorial process if approved for development and may experience difficulties for fund raising; therefore, target set by individuals may remain hidden.
- (Brilliant) ideas of individuals may be overshadowed when important projects are concerned in complex technologies.

2.1.1 Key actors and stakeholders in nuclear thermal-hydraulics

It seems worthwhile to establish in advance a framework for key actors and stakeholders in nuclear reactor thermal-hydraulics (NURETH). The list below which is derived from the wider background discussed in Chapter 1 of the book (where more references can be found) may give an idea:

(1) Authors of textbook spread all over the world: El-Wakil, Tong-Weisman, Hsu, Collier, Lahey-Moody, Ishii, Todreas-Kazimi, and Levy are famous scientists who contributed to establish the NURETH technology.

(2) USNRC (US Nuclear Regulatory Commission): the role was to establish targets for the acceptability of NPP, consequently requesting a suitable level of knowledge and understanding in SYS TH.

(3) International Institutions, namely, OECD/NEA (Organization for Economic Cooperation and Development/Nuclear Energy Agency) and IAEA (International Atomic Energy Agency, Organism of the United Nations) which have the role to fix the status of knowledge, to spread the same knowledge as well as to identify perspectives for development.

(4) National Institutions, namely, EC (European Commission) and US DOE (US Department of Energy: the key role was to finance researches consistent with R&D investment strategies).

(5) Nuclear Industry, including vendors-designers (primarily, but not only Westinghouse, General Electric, Areva-Siemens-Framatome and Babcock & Wilcox) and utilities or associations of utilities (primarily, but not only EPRI and EdF) financed R&D in different sectors of thermal-hydraulics with the objectives of addressing regulatory needs and creating profits by better design.

(6) The NURETH series of conference within the framework of ANS (American Nuclear Society), started in 1980 (NURETH-01) with the 17th event (NURETH-17) to be held in 2017, can be used to synthesize the state of the art and the progress in the area: around 5000 papers coauthored by more than 6000 scientists are part of the proceedings of 16 conference events held so far.

(7) A dozen journals currently publish NURETH papers. A few journals in the previous century were leading nuclear SYS TH information: NED, NT, ANE, and PNE. More recently other journals have been founded and publish papers in the area like STNI and NET. Fundamentals of thermal-hydraulics can also be found in

ETFS, IJMF, and JHT.

2.1.2 Objective

The objective for the chapter is to provide a historical perspective for SYS TH, here distinguishing between basic and SYS TH. This is connected with characterizing perspectives in the development without constraints as budget, time schedules, fashion and roadmaps of established and ongoing projects, and strategies of the major stakeholders in the sector.

The given list of actors and stakeholders shall be considered to estimate the complexity of the endeavor of shaping the future for the NURETH.

Side or added objective for the chapter is to provide more insights for the understanding of nuclear thermal-hydraulics.

The current and the envisaged role of nuclear thermal-hydraulics inside NRS technology receive attention inside the chapter. This implies establishing a link with Chapter 14 of the book which deals with the best estimate plus uncertainty (BEPU) approach to exploit the capabilities of existing and qualified SYS TH codes (Chapter 11 of the book).

2.2 History for SYS TH and trends

This chapter aims at providing an outline of the history of development for nuclear thermal-hydraulics, i.e., the first objective for this chapter of the book. This is achieved by introducing at beginning the role of nuclear thermal-hydraulics within NRS. An attempt is made to minimize the duplication of concepts from Chapters 1 and 3 of the book. Moreover, based on the discussed history and interpretation is provided for current trends in SYS TH.

2.2.1 The role of nuclear thermal-hydraulics

The wide role of thermal-hydraulics in nuclear technology is outlined in Chapter 1 of the book. So, why NRS is of special concern here (i.e., in relation to nuclear thermal-hydraulics)? The answer is as follows. One key feature of nuclear thermal-hydraulics, which partly distinguishes it from other key disciplines relevant to nuclear technology (also mentioned earlier), is the importance and the complexity to deal with time changing or transient situations: this feature constitutes a need coming from NRS.

The NRS, as any technology, may be perceived as entailing two main parts, the

fundamentals and the application, plus the assessment. This is illustrated by the sketch in Fig. 2.1 (e.g., see D'Auria et al., 2015). An idea of the complexity of NRS, at least the part of it dealing with accident analysis, can also be derived from IAEA (2000), IAEA (2006), and IAEA (2009a).

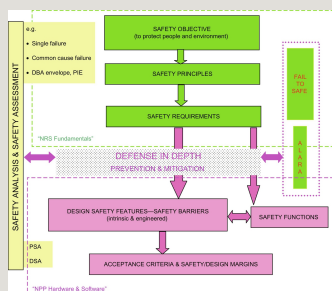


Fig. 2.1 Simplified sketch for Nuclear Reactor Safety technology and establishing the role of nuclear thermal-hydraulics.

The fundamentals (e.g., IAEA, 2000) include the key safety objective, i.e., to protect people and environment from ionizing radiations, the related safety principles and the safety requirements according to established IAEA nomenclature. The application (e.g., IAEA, 2006) makes reference to whatever is done for the design, the licensing, the construction, the displacement, the operation, and the decommissioning of any nuclear installation involving the presence of radioactive material (NPP equipped with water-cooled reactors are of concern, here). The assessment (e.g., IAEA, 2009a) implies establishing how to demonstrate that safety features introduced in the design are consistent with the safety objective.

The bases and the procedures which constitute the established defense in depth (DiD) framework shall be seen as the link between NRS fundamentals and application. Prevention and mitigation shall be distinguished in this connection, and DiD concepts apply in relation to both.

The NRS technology implies the existence of a road map originated at the established safety objective and becoming concrete with the design, construction, and operation (including the plant dismantling and the fuel cycle) of NPP or RR. Acceptable safety and/or design margins shall be demonstrated for each step of the process in compliance with the safety fundamentals. The safety and/or design margins imply the reference to acceptance criteria which are established by

devoted institutions, typically Regulatory Authority in the case of safety margins. Furthermore, concepts like fail-to-safe and as low as reasonably achievable (ALARA) are part of the overall picture.

The accomplishment of safety fundamentals in the NPP design is achievable by suitable safety analysis and assessment. A comprehensive Safety Analysis Report (also known as Final Safety Analysis Report, FSAR) for individual NPP provides the demonstration that the safety objective is met and, noticeably, that acceptable safety margins exist.

Here it appears worthwhile distinguishing between analysis and assessment: the former term relates to whatever is done by designers, vendors, or utilities to implement the fundamentals into the NPP (Hardware and Software), and the latter relates to confirmation activities typically performed under the responsibility of Regulatory Authority. Tools and procedures can be similar or even the same for analysis and assessment; however, specialist groups performing the activity shall be independent upon each other.

Probabilistic safety assessment (or analysis) (PSA), and deterministic safety assessment (or analysis) (DSA), constitute established categories within NRS technology. Assumptions, concepts, or procedures like single failure, design basis accident (DBA), and DBA envelope, event-tree, fault-tree, or uncertainty-evaluation are part of either PSA or DSA or both.

A path is established in Fig. 2.1 between the safety objective (top of the sketch) and the safety margins (bottom of the sketch). The safety functions are ensuring the integrity of the design-safety features and the safety barriers. Parameters characterizing the pink blocks part of the NPP hardware and software are object of calculations performed within the context of DSA and PSA. The concepts of prevention and mitigation are relevant to the overall road map and shall be considered as key elements of the DiD.

A comprehensive description of individual elements of the diagram is well beyond the purpose of the present paper. However, some insights are given below, in relation to the roles of PSA and DSA and the diagram-cross-cutting-issue constituted by licensing.

2.2.1.1 Role of PSA and DSA

The term DSA (IAEA, 2010a) are associated with the availability of qualified best estimate (BE) computational tools or codes, and it is in use since the 1990s.

However, conservative DSA constitutes key practice for the design and the safety confirmation of existing reactors, i.e., activities performed since 1950s. On the other hand, uncertainty is the key word for the application of BE codes.

The term PSA (IAEA, 2010b) are in use within the NRST since the issue of the WASH-700 (subsequently WASH-1400) by N. Rasmussen in the early 1970s. Three PSA levels are distinguished to estimate the risk; those levels cover the probability and the consequences (i.e., the radiological impact) of faulting events at any time of the NPP life. Noticeably, the calculation of consequences can only be done by DSA tools (see later).

Both DSA and PSA are needed for the issue of a consistent Safety Analysis Report (i.e., primarily Chapters 15 and 19 of the generally accepted FSAR structure). Furthermore, a variety of interactions are envisaged and do exists between the two NRS technology categories.

2.2.1.2 Role of nuclear thermal-hydraulics

The role of nuclear thermal-hydraulics within NRS as resulting from the (simplified) sketch of Fig. 2.1 shall be seen in the left part of the diagram: other than allowing the design of safety features and the safety barriers (pink region of the diagram), nuclear thermal-hydraulics is essential to link the fundamentals (green region in the diagram) and the application (pink region of the diagram). This brings to the demonstration of safety (and design) margins for any nuclear installations. Thus, nuclear thermal-hydraulics shall be embedded into procedures and processes which are part of PSA and DSA (dark-white column in the diagram).

2.2.2 Definitions

The distinction between basic thermal-hydraulics (simply, thermal-hydraulics), SYS TH, and computational fluid dynamics (CFD) in single- and two-phase flow is concerned hereafter, consequent to what discussed in Chapter 1 of the book. This is done with the understanding that commonly accepted (i.e., by the international scientific community) boundaries among those three sectors of knowledge do not exist and without the willingness to impose unnecessary new definitions.

- Thermal-hydraulics makes reference to single- and two-phase mixture performance whenever individual fluid or multifluids in steady and transient conditions are concerned. Different fields can be involved in each phase. The numerical domain for the solution of equations is assumed to be bounded by a solid surface and can be at “one-point” (giving rise to zero-dimensional (0D) or lumped-parameter models) and in an one-dimensional (1D), two-dimensional (2D)

or three-dimensional (3D), domain. The solid-surface-bounding hypothesis is straightforward for 0- and 1D situations, and a virtual solid surface may be considered in the 2- and 3D situations. Pursuing the numerical solution inside solid-bounded regions is known (sometimes and not necessarily) as porous media approach, or finite space averaged.

- SYS TH makes reference to geometry, materials, and boundary conditions which characterize a NPP. Experimental (or test) facilities (TF) and computational tools constitute pillars in SYS TH. In the case of TF, integral test facilities (ITF) and separate effects test facilities (SETF) shall be distinguished. ITF aim at “reproducing” (typically scaling-down) the overall reactor coolant system (RCS) performance and the SETF aim at “reproducing” limited space regions or components of the NPP during limited time periods following an accident. In the case of computational tools, the code and the input deck (or nodalization) shall be distinguished. Furthermore, the SYS TH code includes neutron kinetics and instrumentation and control (systems) (I&C) modeling capability. Qualification activities involving the so-called scaling issue shall be addressed in relation to the design of ITF and SETF and the related experiments as well as in relation to the computational tools (e.g., IAEA, 2002; D'Auria and Galassi, 2010). The following key branches in SYS TH can be distinguished, where the word “code” implies modeling and numerics developments and the word “experiment” implies suitable data base:

- Code1: SYS TH (codes)
- Code2: Subchannel (codes)
- Code3: Containment (codes)
- Code4: Specific phenomena, components, steady-state core, and CHF (codes)
- Experiment1: data from NPP measurements
- Experiment2: data from properly scaled ITF
- Experiment3: data from properly scaled SETF and selected “basic” experiments

- CFD makes reference, primarily to single-phase fluid dynamics and heat transfer. The two-phase capability for CFD is available, but far from being suitable for industrial needs for a broad range of applications, as discussed in Chapter 12 of the book. The numerical domain for the solution of equations is unbounded; 3D

geometry is adopted for the integration of the equations; the turbulence phenomenon has a direct connection with the solved equations and the computed unknowns; the linear dimension of the integration domain can be as small as 1/10 mm; variation profiles for quantities like velocity can be calculated inside a pipe for a cross section orthogonal to the flow axis. Pursuing the numerical solution in the unbounded fluid regions is known as open media approach.

The key difference between basic thermal-hydraulics and CFD may be identified as the modeling approach for two-phase mixtures and the related capability. When addressing the single-phase flow, geometry averaging assumptions adopted in thermal-hydraulics are not needed for CFD. The turbulence is calculated directly only in the case of CFD. Furthermore, the mesh (or calculation region) dimension reducing is expected to bring to convergence only in case of CFD.

The difference between SYS TH and basic thermal-hydraulics mostly applies when experiments and computational tools validation processes are planned. SYS TH implies the process of identification and characterization of phenomena which are relevant to the conditions of NPP (e.g., OECD/NEA/CSNI, 1987, 1993, 1996).

2.2.3 The history

The history of nuclear thermal-hydraulics can be covered in a number of ways which include: (a) the chronology of related events; (b) the list of topics of interest in different time periods; (c) the history of nuclear technology and/or NRS also connected with the occurred accidents and major (nuclear) catastrophes; and (d) the consideration of recognized achievements, like milestone reports issued by international institutions, publication of widely spread textbooks, findings from certain experiments, and availability of certain (also widely spread) computational tools.

Having in mind the motivation for introducing the history of thermal-hydraulics, i.e., to clarify the role of the discipline in NPP design and NRS technologies and to streamline possible future developments, an attempt is made hereafter to consider all together the ways (a) to (d).

The history shall start with the E. Fermi pile in 1942 (Dec. 2nd), as depicted in Fig. 2.2: several tons of graphite were assembled in the pile having a cross section $>20 \text{ m}^2$ in order to ensure suitable thermal capacity for dissipating the thermal power possibly produced by the chain fission reaction.

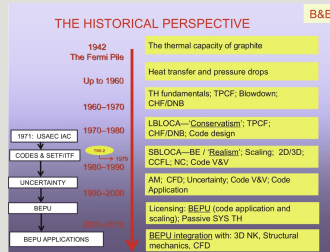


Fig. 2.2 A simplified sketch for the history of nuclear thermal-hydraulics.

Afterward, the design, the construction, and the operation of energy systems in the range from a few kW to thousands MW were possible with a parallel and consistent development of the thermal-hydraulics discipline.

2.2.3.1 The regulator history in the United States

A snapshot on the history of the Regulatory Authority in the United States, USNRC, appears worthwhile at this point (Bajorek, 2015).

In 1946 the Atomic Energy Commission (AEC) was established in order to foster and control the peacetime development of atomic science. The congressional act that created the AEC transferred from military to civilian control of many nuclear laboratories that were instrumental in the initial understanding of nuclear science and safety. It also put the AEC in the dual position of promoting the nuclear power industry and ensuring safety to the public.

In 1974 the AEC was replaced by the Energy Research and Development Administration (ERDA that later on originated the present Department of Energy, DOE) and the Nuclear Regulatory Commission, USNRC. In this moment the independent role (e.g., independent from industry and from promoters of nuclear technology) of USNRC became clear.

Following a long-lasting process (see also in the succeeding text) 10 CFR 50.46 and related Appendix K were formally published in Jan. 1974. Because technology was limited and there were few experimental studies available the rule and Appendix K restrictions were conservative. From the regulator's perspective the state-of-the-art, namely, in relation to nuclear thermal-hydraulics was poor and the restrictions associated to conservatism on the application of analysis methods were a reflection of that perception.

The demonstration of acceptable conservatism suddenly became an issue (Lewis et

al., 1975; Bajorek, 2015):

... If the degree of conservatism of the ECCS codes is to be established (assuming they are indeed conservative) then codes which predict the LOCA phenomena realistically must also be available for comparison.

The recommendations of the APS study group helped establish advanced code development programs and the experimental programs provided data for model development and assessment. USNRC initiated a broad series of research including large-scale system tests and support for the development and the validation of codes.

All of this enabled a rule change in 1988 which allowed “best estimate” loss-of-coolant accident (LOCA) calculations as an alternative to the models stipulated by Appendix K.

The depression in nuclear industry in the aftermath of the Chernobyl accident did not prevent the application of the 1988 rule to the licensing of core reload and changes in plant operating conditions such as power uprate (e.g., see Young et al., 1998; Martin and O'Dell, 2005).

In the mid-1990s Westinghouse submitted its application for design certification for the AP600, and General Electric submitted its application for the SBWR thus beginning a roughly 15-year period in which an emphasis was placed on advanced plants generally with passive cooling systems. The USNRC planned and executed related experimental programs which also covered the AP1000 design.

The current era started in 2011 with the events at Fukushima: since there has been diminished interest in the construction of new NPP in the United States and throughout the world with noticeable exceptions. Much of the interest in thermal-hydraulics from the USNRC transitioned from advanced plants to containment phenomena and severe accident analysis. This included focus on spent fuel pool thermal-hydraulics under LOCA conditions and filtered containment venting. Work on in-vessel thermal-hydraulics has been limited primarily to small modular reactors (SMRs). Furthermore, high burnup fuel received attention: research results have shown that hydrogen uptake into the cladding can affect integrity at high burnup (Billone et al., 2008) and it may be necessary to revise existing LOCA ECCS rule. The proposed new limits would restrict the maximum equivalent cladding reacted to lower than current values for high burnup fuel (USNRC, 2014).

In the area of nuclear fuel more consideration should be given to the modeling of oxide and crud.

2.2.3.2 Before 1960

The fission reaction offered (it still offers) innumerable possibilities to exploit the nuclear power: a wide variety of reactor designs have been conceived: breeding and a number of fuel cycles were and are possible. Water was selected as thermal power vector and nuclear system complexity became unavoidable: high pressure associated with suitable thermal efficiency opened the way to the possibility of LOCA. The large-break LOCA (LBLOCA) became of concern.

Accidents initiators and subsequent scenarios in NPPs were identified and characterized in order to demonstrate the safety of NPP since the 1950s, i.e., when computers did not exist. Experiments, pioneering thermal-hydraulics models, and engineering evaluations were at the bases of the reactor safety analyses at the time.

Nuclear thermal-hydraulics and reactor physics (or neutron kinetics) as well as nuclear fuel materials were subjects of integrated studies.

2.2.3.3 1960–70

Systematic thermal-hydraulic studies and experiments were conducted in the 1960s, noticeably concerning individual “physical” phenomena like two-phase critical flow (TPCF), critical heat flux, depressurization, and blowdown. Thermal-hydraulics became a “self-standing” discipline. The works by Zuber and Findlay (1965), Forslund and Rohsenow (1968), and Wallis (1969) give an idea of the interests at the time.

Several small-scale fundamental programs were launched and completed. New findings from those researches were considered in reactor safety and licensing documents. In the meantime, already in 1968, the seed of what would have become the reference computational tool in NRS adopted by several generations of researchers and analysts, the RELAP code, became available (Moore and Rettig, 1968).

2.2.3.4 1970–80

Massive use of computers for NRS started in the 1970s. The accident analysis could also benefit from primitive (SYS TH) numerical codes and from measurements taken in integral-system experiments. The nuclear regulatory point-of-view was established with the publication of the “Interim Acceptance Criteria

for ECCS” (1971) (USAEC, 1971). This triggered a wide variety of research aimed at the evaluation of safety margins and focusing on the estimation of the maximum temperature on the surface of fuel rods following LBLOCA. The Appendix K to the paragraph 10 CFR 50.46 of the Code of Federal Regulation followed in 1974. The issue of the “Interim Acceptance Criteria for ECCS” shall be taken as the starting date for “modern” SYS TH: competences were requested to comply with those criteria.

The technological community and the industry reacted to the request by regulators: comprehensive research projects were started in the experimental area as well as in the area of code development. Large experimental facilities were designed and operated, and the SYS TH codes were made available for transient analyses in NRS. Large-scale experimental ITF implied international cooperation projects, and “relevant” measured data were gathered to understand transient system thermal-hydraulic performance.

TPCF (see, e.g., D'Auria and Vigni, 1980) and CHF/DNB (critical heat flux/departure from nucleate boiling) (see e.g., Groeneveld, 1973) can be identified as the key thermal-hydraulic phenomena of interest during the decade associated with the LBLOCA scenario.

“Conservatism” (as already mentioned) is the key word which characterizes the application of Appendix K (to 10 CFR 50.46) in licensing analyses. During this decade the WASH-1400 or the “Rasmussen Report” was issued, putting the bases for the application of PSA in NRS; significant results from the execution of probabilistic analyses were produced (USNRC, 1975).

At the end of the decade, in 1979, the Three Mile Unit 2 accident happened (e.g., Henry, 2011). In the area of SYS TH, this shifted the attention from LBLOCA to small-break LOCA (SBLOCA) phenomena.

2.2.3.5 1980–90

Within the framework of SYS TH code use, the V&V (verification and validation) was soon recognized (e.g., D'Auria and Galassi, 1998) as a mandatory process to be completed before application of those computational tools to safety and licensing. In this context, the bases were set for addressing the scaling issue (e.g., D'Auria and Galassi, 2010) (see also Section 2.3 later). The reference SYS TH codes are APROS**, ATHLET*, CATHARE*, KORSAR*, MARS**, RELAP*, SPACE**, TRAC*, TRACE** (where: *=precursor code; **=lately developed code).

International activities were conducted at CSNI (Committee on the Safety of Nuclear Installations of OECD/NEA, Organization for Economic Cooperation and Development/Nuclear Energy Agency) proposing viable ways for V&V (OECD/NEA/CSNI, 1987, 1993, 1996). The importance of user effect upon the predictions was recognized (Aksan et al., 1993; Ashley et al., 1998; D'Auria, 1998) as well as the role of the input deck (or nodalization) and the related qualification (see, e.g., Bonuccelli et al., 1993).

The contribution to the understanding of NRS important phenomena from ITF experimental programs, conducted or initiated during this decade, shall be realized. Key acronyms for the ITF or large-scale SETF, within BWR (boiling water reactor), PWR (pressurized water reactor), and CANDU technologies are (related research programs may have developed in decades different from the current one in the cases identified by an asterisk: however, for the sake of synthesis all major research programs in SYS TH are listed hereafter in alphabetic order): APEX*, ATLAS*, BETHSY, CCTF, FIST, FIX-II, GIRAFFE, HDR, ISB, LOBI, LOFT, LSTF, MARVIKEN, MIST, PACTEL, PANDA, PIPER-ONE, PKL, PMK, PSB*, PUMA, RD-14M, ROSA, SCTF, SEMISCALE, SPES, UM, THTF, UPTF. In this framework, the 2D/3D international cooperation program (Damerell and Simons, 1992) (involving UPTF, SCTF, and CCTF) provided key information to address the scaling issue, i.e., connecting the measured data with expected NPP conditions, from the experimental viewpoint. Enormous benefits were gained in the area of demonstrating the SYS TH code capabilities.

CCFL (countercurrent flow limitation) (e.g., Glaeser, 1989) and NC (natural circulation) (e.g., D'Auria and Vigni, 1985; D'Auria et al., 1991) can be identified as the key thermal-hydraulic phenomena of interest during the decade associated with the SBLOCA event, together with reflood. The State of the Art Report on thermal-hydraulics of ECCS (OECD/NEA/CSNI, 1989) shall be mentioned in this context.

The words SYS TH were proposed (later on, those words had a spread use) inside the scientific community in the occasion of a specialists conference held in Aix-en-Provence (OECD/NEA/CSNI, 1992).

The need for uncertainty methods (UM) suitable for predicting unavoidable errors to be added to the results of calculations performed by system thermal-hydraulic codes became clear at the beginning of 1990s (or even at the end of 1980s). Working approaches were proposed; noticeably, the pioneering effort by USNRC shall be mentioned (USNRC, 1989a) which brought to the formulation of CSAU (code scaling and applicability and uncertainty). The phenomena identification and

ranking table (PIRT) process was proposed (see also later).

At the middle of the decade, in 1986, the Chernobyl Unit 4 accident happened (e.g., Khan, 1990). In the area of SYS TH, this moved increased attention toward passive systems and the processes for the design of AP-600 and SBWR had a strong impulse.

2.2.3.6 1990–2000

Addressing the uncertainty in SYS TH as a follow-up of V&V was at the center of the attention in the period. Following and considering the CSAU, the Wilks formulation and the UMAE (uncertainty methodology based on accuracy extrapolation) were proposed (Hofer, 1990; D'Auria et al., 1995). The UMS (Uncertainty Method Study) project was launched by the CSNI in 1993 and completed in 1998 (OECD/NEA/CSNI, 1998); the fundamental features of the UM were described into detail and suitable demonstration was achieved in relation to their robustness and qualification level.

The USNRC issued the Regulatory Guide (RG) 1.157 (USNRC, 1989b): the application of system thermal-hydraulic codes was envisaged, even though recommending the use of selected conservative models. Those models are concerned with phenomenological areas where the knowledge was not considered satisfactory. Requirements in the RG 1.157 did allow a few attempts of practical applications. However, Appendix K to 10 CFR 50.46 continued to be used during the decade for licensing purposes. The acronym BEPU started to circulate.

A break-through workshop for planning the future in SYS TH area was held in Annapolis (1996) under the combined effort by OECD/NEA and USNRC. The development of a new SYS TH code was launched (current name is TRACE), following identification of inadequacies of existing codes at the time. Noticeably, the key words “Internal Assessment of Uncertainty” were proposed during the workshop. At the end of the decade, CIAU (code with capability of Internal Assessment of Uncertainty) method was developed (D'Auria and Giannotti, 2000) and ready for practical applications. CIAU used UMAE (mentioned before) as the “engine” and the qualification tool for the process of code application.

The development of CFD technology, mostly connected with single-phase flows, had a strong impulse possible with the increase in computational power (Yadigaroglu et al., 2003).

The SYS TH coupling with 3D neutron physics was also made possible by the

availability of more powerful computers and numerical techniques (OECD/NEA, 2004).

2.2.3.7 2000–10

Applications of BEPU approaches in licensing processes, implying the exploitation of the capabilities of SYS TH codes and of UM, definitely started in the 2000s. The following key events, not an exhaustive list, not in the order of importance, not in the order of time, see also Petruzzi et al. (2005), give an idea of the technology development in the area:

(a) The KWU (NPP designer later on incorporated by Siemens, and lately became AREVA) on the behalf of the ETN (Brazilian utility owner for the nuclear plant) proposed a BEPU methodology to analyze the LBLOCA for the licensing of Angra-2 NPP in Brazil (KWU-Siemens, 1997). The submission was analyzed by the regulatory authority of the Country which also requested the application of different UM by assessor independent from AREVA.

(b) USNRC issued the RG 1.203, USNRC (2005), which provided clarification of the regulatory expectation for transient and accident analysis including the application of BEPU approaches.

(c) CSNI launched and completed the 6-year project BEMUSE. The aim was to demonstrate the maturity of UM and approaches with main concern to LBLOCA applications. The objective was achieved. However, differences among the results by participants (mainly in predicting reflood time) caused the need for a careful interpretation of related findings. The difficulty in harmonizing, from the side of applicants of UM, the choice of input uncertainty parameters and the related ranges of variations was an outcome from the project.

(d) Three important BEPU-concerned documents were issued by IAEA, two Safety Report Series, SRS 23 and SRS 52 (IAEA, 2002, 2008a), and one Specific Safety Guide, SSG-2 (IAEA, 2010a). The SRS 52 deals with the description of workable uncertainty approaches and methods. The SSG-2, dealing with DSA in general, proposes the BEPU approach in licensing as consistent with the technological state of the art in the area of accident analysis.

(e) BE conferences, BE-2000 and BE-2004, ANS (2000), and ANS (2004), respectively, were held under the auspices of the ANS. This series of conferences was actually continued by V&V Workshops in the United States held in Idaho Falls (Idaho), Myrtle Beach (North Carolina), and Las Vegas (Nevada), in 2008,

2010, and, up to now, till 2016, respectively, with the cooperation of the nuclear division of the ASME.

(f) The BEAU (application of the best estimate analysis and uncertainty) method was proposed by Canadian experts (Abdul-Razzak, 2009).

(g) A variety of BEPU (it shall be clear that the BEPU acronym is not always adopted) applications all over the world during the concerned decade, mostly within the license renewal framework, are summarized in the paper by Glaeser (2008).

The first decade of the current millennium is characterized by the application in NRS technology of the expertise in thermal-hydraulics: the BEPU approach constitutes the key word in this connection. The 2010s decade started with the submission of Chapter 15 of the FSAR of the Atucha-II NPP to the regulatory authority in Argentina, by the NASA utility. In this case, the entire Chapter 15 of the FSAR is based on the BEPU, and the approach itself was endorsed by the regulatory body (UNIPI-GRNSPG, 2008, see also D'Auria et al., 2012a,b).

2.2.3.8 2010–20

See the interpretation of current trends in Section 2.2.4.

2.2.3.9 History through the list of topics

List of topics can be identified from each nuclear thermal-hydraulic conference held in the last four of five decades. A recent summary provided by Yadigaroglu and Lakehal (2015), and related to NURETH series of conferences brought to the following list applicable to years 2013 and 2015:

- Multifield two-phase flow modeling (several sessions)
- Two-phase flow and heat transfer fundamentals (several sessions)
- Boiling and condensation fundamentals (several sessions)
- CHF and post-CHF heat transfer, flooding, and CCFL
- Advances in enhancement, understanding, and prediction of CHF and quenching (several sessions)
- Investigation of reflood phenomena (now in partially blocked core with fuel relocation)

- Operation and safety of existing reactors (several sessions)
- Safety systems and related phenomena
- NPP transient and accident analysis (several sessions)
- Plant system code development and validation (several sessions)
- Realistic BWR LOCA evaluation: methodology development and application
- Containment analysis (with V&V)
- Natural convection and mixing phenomena, modeling, and experiments
- Critical heat flux in a fuel bundle: modeling, prediction, and experimental measurements (several sessions)
- Core thermal hydraulics and subchannel analysis, fluid dynamics, and heat transfer
- Interfacial area (IA) transport
- Severe accident phenomenology (several sessions)
- Modeling and experiments of severe accidents (several sessions)
- Debris bed cooling

One may note the presence of “historical” words like CHF, CCFL, reflood, mixed with established concepts like V&V, modeling and experiments, and containment analysis, and “new comer” topics like IA transport and debris bed cooling. Furthermore, topics like severe accident phenomenology, modeling, and experiments of severe accidents and debris bed cooling although part of conference in nuclear thermal-hydraulics is not within the domain of interest for the present book, as already discussed in Chapter 1 of the book.

2.2.3.10 Summary of history in nuclear thermal-hydraulics

A summary of the history in nuclear thermal-hydraulics can be depicted as in Fig. 2.3 or can be based on the key words of Table 2.1.

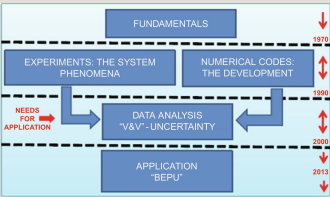


Fig. 2.3 Key elements in the history of nuclear thermal-hydraulics.

Table 2.1

Key words for a spot historic outline of system thermal-hydraulics

- ^a See Section 2.1 in this chapter of the book.
- ^b Acronym for an International Project.
- ^c See Section 2.3 in this chapter of the book.

One may see from Fig. 2.3 how fundamentals evolved into system experiments and numerical codes development. This gave origin to the data analysis and to V&V procedures and activities. Maturity of the nuclear thermal-hydraulics discipline is testified by the applications to NPP and NRS technologies; in the case of NRS, BEPU has a key role (as mentioned in Section 2.2.4 below and with more details in Chapter 14 of the book).

Key words for the TH spot historic outline can be found in Table 2.1. In the first row, the key “actors” and the “stakeholders” for the nuclear thermal-hydraulics discipline are listed as derived by the items (1)–(7) in Section 2.1 to this chapter of the book. The cross correlation between phenomena and key words representative of topics which form the nuclear thermal-hydraulics discipline (second column of the table) and selected reference documents or activities (third column of the table) provides a sample vision for the development of the discipline. Namely, starting from the second row of the table a few examples of cross correlations are provided:

(a) Convection heat transfer and friction pressure drops phenomena are addressed by numerical equations like the Dittus-Boelter one and by approaches like the two-phase multiplier—2nd concerned historical period.

(b) The evaluation of TPCF and blowdown phenomena is possible by models like the one proposed by Moody—3rd concerned historical period.

(c) The LBLOCA analysis (key topic in nuclear thermal-hydraulics) shall be performed in accordance with the Appendix K rule associated to the Interim Acceptance Criteria—4th concerned historical period.

(d) Validation and scaling activities shall be performed based on the knowledge synthesized in the USNRC Compendium—5th concerned historical period.

(e) Accident Management (AM) and UM are addressed in documents like those describing the CSNI Code Validation Matrices (CCVM and the UMS)—6th concerned historical period.

(f) Reference documents for the application of BEPU are constituted by the USNRC RG 1.203 and by the IAEA SRS 52—7th concerned historical period.

Table 2.1 provides a synthesis vision of nuclear thermal-hydraulics connecting with historical periods.

2.2.4 An interpretation of current trends

There are important research projects and initiatives in progress (reference year is 2015) in the area of SYS TH which also imply future plans and perspectives. A nonsystematic and (maybe) incomplete list of relevant programs, projects, or activity-frameworks includes (each of the given acronym corresponds to a web site where the reader can found detailed information; in the case of a few noticeable exceptions references are provided):

- Recent or ongoing projects on the side of EC: EUROFASTNET, NURESIM, NURISP, and NURESAFE
- Ongoing project on the side of US DOE: CASL
- OECD/NEA (CSNI & NSC) activities or projects: UAM, PREMIUM, W-Gama initiatives including ISP, “VVER-1000 Kalinin addressing NPP 3D

measurements,” and “Oskarshamn-II addressing the BWR stability issue”

- IAEA planning and carrying out CRP and TM, namely, in the areas of BEPU, connection DSA-PSA, CFD for NRS and thermal-hydraulics of innovative systems including SMR
- USNRC supporting the development of SYS TH codes (e.g., TRACE) and running the related CAMP program, other than continuously evaluating new reactors and updating the licensing process (in this last case with a number of connections with TH)
- ATLAS, MARS, and SPACE projects in Korea, all together constituting an integrated approach to SYS TH, involving experiments, modeling, and numerical development, namely, see the recent comprehensive paper by Song (2015)
- China and India designing and building or even operating large-scale thermal-hydraulic facilities and, China primarily, developing new system codes (e.g., AERB, 2010; Chang et al., 2011), respectively.
- FONESYS and SILENCE networks, established and recently launched, in the areas of code development and experimental programs, respectively.

Typical subjects for activities in progress or envisaged include (the list below shall be integrated with subjects mentioned in Section 2.2.3.9):

- Improvement in CHF database and understanding
- Improvement in reflood understanding
- Improving in understanding the role of spacer grids
- Finalizing, as far as possible, the development of IA transport models
- Coupling of SYS TH with other branches of nuclear technology: 3D NK, structural mechanics, nuclear fuel, etc.
- Improvement in CFD modeling including two phase
- Addressing the V&V of CFD
- Modeling of CRUD (Chalk river unidentified deposit) deposition

– Connection DSA-PSA

– Use of BE techniques in PSA

– Operation of experimental ITF or large-scale facilities, e.g., in Finland (PACTEL), Germany (PKL-III), Japan (LSTF), Korea (ATLAS), Switzerland (PANDA), Russia (PSB)

BEPU constitutes a further element to interpret current trends. This is mentioned in Section 2.3.16 hereafter and discussed with more details in Chapter 14 of the book.

2.3 The perspectives for SYS TH

This chapter aims at providing an outline of the current perspectives for the development of nuclear thermal-hydraulics, i.e., the second objective for this chapter of the book.

The historic outline in the previous section as well as the expectable incomplete list of key actors and stakeholders provides another picture of the “thermal-hydraulics universe” and of its complexity (Section 2.2.2 and Table 2.1). A broad set of activities is already ongoing (Section 2.2.3) in the same framework. Thus, the destiny of any individual or personal position for development may reveal impractical and unusable, as also discussed in the “Chapter foreword” of this chapter.

However, a list of envisaged ideas for the future is prepared looking from an optimistic viewpoint and in the attempt to invite the reader to a (further) reflection. The concerned domains for investigation include modeling features of computational tools, validation and application of those tools, and planning of experiments. The list unavoidably reflects the personal experience and shall not be seen as in competition with any ongoing international projects or with any similar list supported by proper contexts.

The envisaged needs in SYS TH, or better, elements for reflection may need elaborations and details beyond what is possible in one chapter of an edited book. Furthermore, what are called here envisaged needs or, better, elements for reflection shall be seen as complementary (or in addition) to the needs discussed in Chapter 4 of the book.

No attempt has been made to provide an order-of-importance for the issues concerned below and priority classification is left to the reader if deemed necessary.¹

Sixteen elements for reflection (or categories/targets for improvement) are considered. Interactions in virtual activities related to the elements are unavoidable although an attempt is made to select independent research topics. A description of each “element” is provided and rough proposals are formulated dealing with ideas to address the concerned open issues.

2.3.1 The “local form loss” coefficients (also reported as “K-factors” hereafter)

The K -factor is the multiplicative term to the product ρw^2 (where “ ρ ” is the “reference” density and “ w ” is the “reference” velocity of the concerned fluid) to calculate pressure drops at geometric discontinuities.

The origin of the issue lays in the derivation of the balance equations at the hearth of SYS TH codes: the balance equations are derived making reference to a geometric space without discontinuities (some advancement is proposed for the integration domain by TRACE code, but this is insufficient for practical applications). Therefore, the missing information about form loss coefficients at geometric discontinuities, either in the forward fluid motion direction, typically nominal conditions for the steady-state operation of NPP and ITF, or in the reverse direction (expected during a transient), must be fixed by the analyst or code-user. In a few situations tabulated (precalculated) or experimental data exist. In the largest majority of conditions the user must consider analogies with those data and/or “invent” a value based on his expertise.

The user has almost no possibility to estimate the effect of the not-fully developed flow upon the value of the “ K -factor.” Additional origins of misunderstandings and consequently of errors in the values of “ K -factors,” derives from inherent difficulties in gathering qualified experimental data: (a) irreversible pressure drops shall be distinguished from reversible pressure drops; (b) practical difficulties arise when measuring the pressure in narrow spaces and in complex geometries; (c) the influence of local velocities and of void fraction, other than the non-fully developed flow condition and the transient situation upon the adopted values of the coefficients, can be large and may require a broad range of experimental conditions. All of this is confirmed in a recent activity, Benhamadouce (2015), where making reference to spacer grids and high Re numbers, errors in the comparison between experimental and CFD calculated data in the range of 15%–

30% have been found.

The impact of the issue in NRS can be derived from the following: (1) many of the discrepancies among results of application of SYS TH codes to target cases (either of the same code or of different codes) is originated from the process of “fixing” the “ K -factors”; (2) in some cases, based on the comparison between experimental data and calculated results involving unacceptable discrepancies, code models other than the formulas for pressure drops are modified to minimize those discrepancies without accounting for the effect of the arbitrarily fixed “ K -factors”: this brings to never ending efforts for SYS TH code improvement.

The proposals to address the issue are:

- an effort shall be made to develop traceable procedures for calculating local form loss coefficients in cases of interest to the nuclear technology and/or supporting those procedures with a comprehensive data bank. Experiments and experimental conditions all over the world should be collected and archived. Examples for this could be the libraries for look-up tables for CHF and the microscopic XS (cross section) for neutrons.
- CFD computational tools, primarily in single-phase conditions, should be systematically used to generate proper values of K -factors in the situations of interest for NPP. Related results shall constitute a traceable support to the application of SYS TH codes. Specific attention shall be devoted to rounded or sharp edges.

2.3.2 The multi-D heat transfer coefficient surface

The convection heat transfer, i.e., one of the mechanisms for the transfer of thermal power between fluid and wall, is modeled by the well-established empirical relationships between the heat transfer coefficient (HTC) and the heat flux. This gives rise to the current need to use around two dozen correlations to cover the range of interest in NPP design and NRS, noticeably including the consideration of phenomena like CHF, reflood (also characterized by the acronym RNB and the MFB temperature), and condensation (also in the presence of noncondensable gases).

At least three fundamental issues of concern shall be identified in relation to the current status in predicting HTC:

- (a) The continuity among HTC values calculated from the various correlations, namely at the boundaries of the respective validity ranges.

(b) The repartition of heat flux from the wall to the fluid, distinguishing contributions to the gas and to the liquid phases and even directly (from wall) to the interface liquid-steam.

(c) Heat flux by radiation heat transfer adds to total heat flux and in some experimental situations (noticeably film boiling in the presence of fluid droplets) separation between convection and radiation becomes difficult to be quantified.

The proposal here, related to the issue (a), is to construct an as far as possible continuous multidimensional (multi-D) surface covering all the heat transfer regimes (examples of HT (heat transfer) regimes are nucleate boiling, saturated boiling, film boiling) and all the flow regimes (example of flow regimes are bubbly, slug, and annular flow). Reflood and condensation should be included in this picture. No proposal is formulated in relation to the issues (b) and (c) which also deserve proper consideration.

It should also be noted that the problem (i.e., of constructing a multi-D HTC surface) is quite well known in nuclear thermal-hydraulics and also applicable to other (nonnuclear) technologies (e.g., Divo et al., 2000, see also Tanaka and Dulikravich, 2000).

2.3.3 Energy and entropy balance following RCS blowdown and containment pressurization

The system of interest is a pressure vessel surrounded by full-pressure containment. The vessel is filled by high-pressure high temperature (two-phase fluid), and the containment is ideally isolated from the environment and filled by air at atmospheric conditions. The opening of a break in the pressure vessel triggers the “irreversible phenomenon” called blowdown or pressurized two-phase mixture discharge into the containment. The containment pressure increases, and energy exchanges with environment are (ideally) prevented. In this situation the entropy of the isolated system constituted by the vessel and the containment is expected to increase following the start of blowdown, i.e., an irreversible thermodynamic process for an isolated system. Results of code calculations are not consistent with what expected. This constitutes the issue.

In the case of SYS TH codes the difficulty may come in estimation the energy flowing out of the break (TPCF model results can be qualified against experimental data, and the same is more complex in relation to the energy flow out of the break).

Additional issues (or subissues) connected with the above include:

(a) Supersonic conditions. Supersonic conditions may occur in discharge pipes (e.g., the line connecting the PORV with the sump or the ADS 1–3 to the IRWST in the case of AP1000 design). Pressure drops in the discharge lines and mechanical loads upon constraints are affected by the occurrence of supersonic conditions.

(b) TPCF on-off. This is the situation which occurs when pressure difference between upstream (reactor pressure vessel side) and downstream (containment side) is not enough to provoke critical flow at the assigned throat and cycles of TPCF and “Bernoulli-flow” occur.

(c) TPCF location jumps. It is known since different decades that TPCF conditions in a nozzle may migrate (or jump) from one section to another. The same situation can be more complex inside a valve. TPCF location jumps may be originated by sharp edge cavitation: steam generated at any geometric discontinuity upstream an assigned critical section may cause the shift of the critical section at the upstream geometric discontinuity.

The capability to predict the discussed phenomena is not demonstrated. Recommendation here is to perform specific experiments and eventually to modify SYS TH codes. Again, as in the previous case, the problem is well known in nuclear thermal-hydraulics (e.g., D'Auria et al., 2003; IAEA, 2014; Qiu et al., 2015): the importance given to the problem constitutes the issue.

2.3.4 Precision targets

The word precision is not commonly used in SYS TH area. Common words, other than “error,” are “accuracy” and “uncertainty,” the former being the known error resulting from the comparison between measured and calculated data, and the latter being the unknown error in NPP predictions. The word precision may be used to encompass both the words and the concepts of accuracy and uncertainty. No values for precision or precision targets are fixed by any institution (or by stakeholders identified in Table 2.1). So the common practice is to produce new codes or improved code versions without knowing the target for acceptability.

The recommendation is to solicit the issuance of precision targets in SYS TH which also should be moving targets associated with the advancements in the technology and the understanding. In this case, the reluctance from all actors in nuclear thermal-hydraulics to fix the precision target constitutes the issue. An attempt to fix precision target for a narrow range of conditions can be found in D'Auria et al. (2004).

2.3.5 The application of CFD-like approaches to NPP design and NRS technologies

CFD has already been mentioned in Chapter 1 of the book (under the heading and in Section 1.1.1) and, more important, constitutes the topic for Chapter 12 of the book. CFD applications in NRS are the subject of many publications (e.g., see Bestion, 2014; Smith et al., 2008). Some notes consistent with those key documents are discussed hereafter to make self-standing this chapter of the book.

CFD technology impacted the area of NPP technology and NRS since the 1990, as already mentioned. The CFD code design targeting steady-state conditions, the lack of traceability of embedded equations (due to commercial reasons), the common assumption to neglect the pressure influence upon density changes, and the difficulty to model an entire NPP loop in two-phase conditions may represent obstacles for the application of CFD in accident analysis or may delay its full exploitation. Otherwise, the quality assurance and the needs from the DiD (see Fig. 2.1) impose the use of the best techniques (i.e., the least restrictive assumptions) and the possibility of “independent” checks.

CFD codes for single-phase flows may be seen as part of a mature technology ready for applications even for NPP design and NRS situations. The issue for full application to NPP design and mainly to NRS is the qualification:

- (a) Best Practice Guidelines (BPG) are available and may need enforcement and improvement
- (b) the convergence of results when the mesh sizes are decreased shall be demonstrated in any application
- (c) the demonstration of independence of results from mesh generation might be required

A further issue is related to the coupling between CFD and SYS TH codes. The coupled computational tool may generate inconsistent results (e.g., in a closed NC loop partly modeled by SYS TH and CFD codes): in fact CFD code results are (strongly) affected by boundary and initial condition values at the boundaries of the CFD domain of integration which are necessarily approximate (otherwise, CFD modeling of the entire loop is needed).

A recommendation is to use CFD for the evaluation of local pressure drops including derivation of direct and reverse K -factors (Section 2.3.1 above): properly qualified CFD codes and approaches may be exploited to generate a databank for

K-factors suitable for qualified SYS TH code applications.

Finally, CFD codes for two-phase flows are going to be developed. The full exploitation (the useful application) of the capabilities for those codes in NPP design and NRS may need decades or even never happen. Thus, two-phase CFD codes may not be strictly considered (within the present context) as part of the needs in SYS TH.

2.3.6 The thermal-hydraulics of passive systems

Passive systems and related thermal-hydraulics are part of the history for NPP design and NRS (e.g., IAEA, 2005, 2009b): the configuration of the RCS for both BWR and PWR (for instance) is determined considering the possibility to cool the core via NC, at least removing decay heat (e.g., D'Auria et al., 1991, 1997). Passive ECC systems and components like accumulators are installed in most of the NPP. The Chernobyl event in 1986 triggered new attention toward passive systems: new (i.e., other than accumulators) passive ECCS are part of NPP design, e.g., AP1000 and passive phenomena are at the basis of the RCS operation, e.g., ESBWR. Passive systems are also used in the category of “small” NPP, the so-called SMR (small and medium reactors or small modular reactors).

A not-comprehensive list of issues connected with the design and the operation of passive systems (again not in the order of importance) is given below:

(a) Stability of flow of two-phase mixture in a dozen meter high, large diameter riser of ESBWR.

(b) Triggering of NC flow-rate, in some cases consequence of opening of a valve: high values of flow-rate may cause too fast cooling and large dynamic loads on the structures.

(c) Stability issue: all NC systems are characterized by “small” driving forces (i.e., small related to a possible similar system equipped by a centrifugal pump).

“Small” perturbations may challenge the stability. The stability issue is even more complicated for the category of NC systems where boiling and condensation occur.

(d) The stability issue for “composite” systems: Either different NC systems are connected among each other by a heat exchanger (series connection, e.g., passive cooling of SG when PS is working in NC) or they are hydraulically connected (parallel connection, e.g., PRHR (pressurized residual heat removal), CMT (core makeup tank), and IRWST loops in AP1000). The issue here is that instability of one loop may propagate to connected loops: the stability issue must be addressed

for the entire system.

(e) The local pressure drop coefficients. The issue here, see also item (1) in the present list, is the precision needed for the “ K -factor” values: owing to the impact on stability (e.g., a “cliff-edge” type of thermal-hydraulic phenomenon) and to the “small” driving forces available, a higher precision is needed for the “ K -factor” values than needed for system equipped with energized pumps. Then, qualification results of calculations, without having access to suitable values for “ K -factors,” may reveal questionable.

(f) The reliability of passive systems constitutes a thermal-hydraulic issue not well established among designers of passive systems (e.g., Jafari et al., 2003).

2.3.7 The scaling issue and the experiments

Notwithstanding the large number of papers and reports related to scaling, the “scaling” still constitutes a controversy in SYS TH and applications, e.g., see the paper by D'Auria and Galassi (2010). The scaling issue in licensing is considered by D'Auria and Galassi (2010), who introduced the scaling pyramid to explain the current situation (Fig. 2.4) and proposed a roadmap for addressing the issue (Fig. 2.5). Even though there is no common acceptance for the proposed roadmap, the reader can refer to the last mentioned paper for details. The scaling issue for designing experiments is considered hereafter.

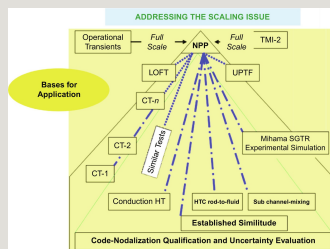


Fig. 2.4 The scaling pyramid proposed by D'Auria and Galassi (2010).

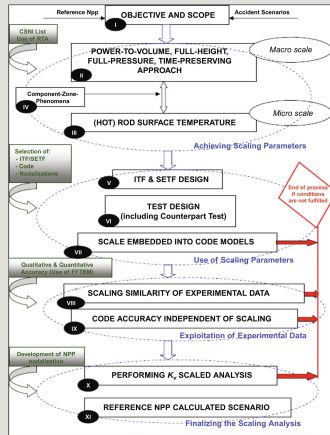


Fig. 2.5 The scaling road-map proposed by D'Auria and Galassi (2010).

SETF and ITF shall be distinguished when addressing the scaling issue for experiments.

The SETF design as well as the design of SETF experiments may or may not be connected with scaling: rather, the need to characterize a TH phenomenon, coming from the process of code validation, shall be at the basis of the SETF design. So, the connection between scaling and SETF may be weak and not further discussed here.

In the case of ITF a suitable design process shall include, namely, when the planned experiments are relevant for NRS, the consideration of principles like ALARA or the framework like DiD. ALARA imposes that the design effort shall be consistent with the safety relevance: in other terms inadequacy of budget may not justify the construction of a “very” (too) small facility or of a “short” (reduced height) facility. The framework of DiD imposes providing proper consideration to (in this case “the simulation of”) parameters affecting the safety functions and the integrity of safety barriers. Then, “the simulation of” PCT shall be considered a key target when designing ITF. This requirement may become more stringent when NC phenomena (or passive systems, see the item above) are involved in the simulation. The scaling-freedom in relation to the (design of a possible reduced) height for ITF offered by the so-called Ishii-scaling may reveal inconsistent with the DiD framework and the ALARA principle. Thus, basic limitations of the Ishii-scaling (actually reduced height is an interpretation of the Ishii papers) are:

- There is no criteria to determine an acceptable “shorter” length: i.e., to simulate

4 m of active length for the reference core (prototype) height one can choice 3.9 m or even 0.5 m in the model

- The rod surface temperature cannot be simulated to the best when shorter length is adopted because of the unknown relationship (this typically constitutes the objective of any experimental campaign) between linear power, HTC, and fluid dynamic conditions like local velocities and void fraction

Scaling is closely connected with experiments. The issue here is the preservation of Experimental Data Base (EDB). Preservation of EDB implies the characterization of what must be preserved and the gathering of the data: indications for the process can be found in the paper by Petruzzi et al. (2012).

Related to scaling issue and namely to the scaling in NRS, a comprehensive report is in preparation at the time of the writing of this chapter, within the framework of OECD/NEA/CSNI, called Scaling State of Art Report (S-SOAR) (see OECD/NEA/CSNI, 2016).

2.3.8 The V&V for SYS TH codes

As in the case of CFD (Section 2.3.5 above) the V&V subject has already been mentioned in Chapter 1 of the book (under the headings and in Section 1.1.1) and, more important, is the topic of Chapter 13 of the book. Furthermore, a recent IAEA report deals with a comprehensive vision for V&V (IAEA, 2015). A synthesis picture on the V&V for a SYS TH code derived from that report can be found in Fig. 2.6. Hereafter some notes supporting those key documents are discussed to make self-standing this chapter of the book.

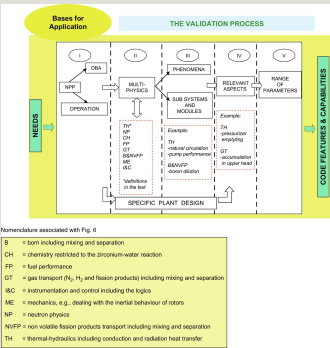


Fig. 2.6 A snapshot of the V&V for SYS TH codes (IAEA, 2015).

The V&V applies to SYS TH codes and, as such, shall be considered a technological branch established since the beginning of 1980. The precision targets, item (4) above, should be considered as a prerequisite for V&V and part of the present V&V issue. Additional aspects deal with the procedures for V&V and with the comparison between calculated and experimental data.

An attempt to synthesize current V&V understanding might be too long for the present chapter. So, the issues, or the element for reflections, are:

(a) Matrices for V&V should be available as a complement to code development (i.e., developmental assessment matrices) and should be endorsed by the scientific community based on fulfillment of acceptability conditions (e.g., see OECD/NEA/CSNI, 1993, 1996).

(b) Independent assessment matrices (i.e., matrices at the basis of code application), mostly dealing with Validation and not with verification, should also be available based on requirements: the exploitation of those matrices should be the basis and the prerequisite for any code application to NRS problems.

The recommendation here is to pursue the development and the application of those matrices and introduce acceptability requirements in connection with either the coverage-range of phenomena (see also Section 2.3.12 in this chapter), and the evaluation of comparison results coming from the use of the experiments part of the matrices (see also Section 2.3.4 in this chapter).

2.3.9 Uncertainty analysis

The uncertainty needs come from the V&V process. Evaluation of uncertainty must be connected with the application of BE SYS TH codes and must be supported by suitable UM. In other terms, one may state that the application of SYS TH code to the analysis of experimental data (e.g., obtained in ITF or SETF within the framework of [code-developers independent] validation activities) shows unavoidable errors, typically referred as accuracy; thus, errors shall be expected in the prediction of NPP transient scenario and are referred as uncertainty of code calculations. A recent IAEA report deals with current status of UM (IAEA (2008a). Uncertainty is the topic of Chapter 13 and also considered in Chapter 14 of the book. A synthesis picture providing an idea of UM can be found in Fig. 2.7. Hereafter some notes supporting those key documents are discussed to make self-standing this chapter of the book.

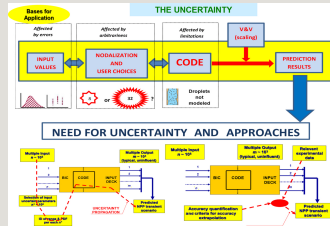


Fig. 2.7 A snapshot on the motivation and the processes to estimate the uncertainty of SYS TH code predictions.

International projects like UMS, BEMUSE, and PREMIUM are worthwhile to spread the expertise and shall be pursued. However looking from the exterior, e.g., from the side of scientists not part of the working teams, it definitely may appear that those initiatives bring more questions than answers, or more doubts than solutions.

Bifurcation analysis, or identification of cliff edges, is possible with current UM (e.g., see D'Auria et al., 2000).

The elements for reflection, or the issues for possible development, are:

- (a) The correct interpretation of results from international projects
- (b) The set-up and the acceptability procedure and criteria for V&V of UM
- (c) The integration of CIAU and GRS UM is desirable

The elements (a) and (b) are applicable to different areas of nuclear thermal-hydraulics and to other disciplines.

International projects like those mentioned above are important to achieve common understanding and even to open the way for further development in the concerned areas. However, in the general case because of (lack of) proper resources, (presence of) proprietary information and (need of) consensus among several participants from different Countries, written conclusions from the activities are smooth and may not reflect the current status. Therefore, item (a), expert-participant evaluation may be needed to supplement the information from the final report of the activities.

Any method or set of equations in nuclear thermal-hydraulics should be supported by a validation framework, item (b). In other words, because of lack of knowledge,

e.g., associated with turbulence modeling or to the evaluation of convection heat transfer, suitable proofs of validation and related documentation are strictly necessary for any method including UM.

An idea was launched to combine GRS and CIAU methods (Kovtonyuk et al., 2008) item (c). The completion of the activity, actually never started, may provide an additional proof of validation for both the methods.

2.3.10 Coupling with SYS TH

Starting from the 1960 the fundamental disciplines for NPP design and NRS followed separate paths for developments and related expertise was built in “separate compartments” as already discussed in Chapter 1 of the book. To some extent this was also true in relation to SYS TH if one consider computational tools in the analysis sectors of transient RCS performance, core design (primarily aimed at nominal conditions), subchannel analysis, and CO.

During the decade 1990–2000 the increase in computer power allowed the numerical coupling among codes in different areas like structural mechanics, neutron physics, CFD, and nuclear fuel, other than different branches in SYS TH. The SYS TH codes played a pivot role in this connection.

The coupling among codes implies addressing “numerical and informatics” interfaces between the codes and the computer-compilers. Those interfaces are not necessarily homogeneous at the design level for different codes and generate issues connected with the transfer of information among codes and with the selection of time step in transient calculations.

The elements for reflection and the recommendations are:

(a) To merge in one SYS TH code the capabilities of modeling RCS, core, subchannel, and CO: this brings the advantage of avoiding troublesome code coupling in some situations.

(b) To propose systematic V&V procedures for coupling, also involving acceptance criteria for the coupled results (e.g., see D'Auria et al., 2004, in relation to the coupling between SYS TH and 3D NK codes).

An example of cross correlation between codes, technological areas in NRS, and modeling of physical barriers, materials, and NPP components/systems can be seen in Fig. 2.8 (D'Auria et al., 2012a) (see also CFD coupling in Section 2.3.5 in this chapter).

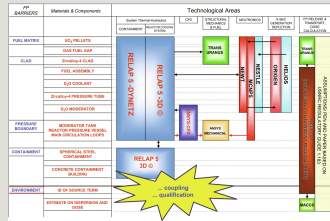


Fig. 2.8 Coupling between codes: cross correlation with technological areas in NRS and modeling of physical barriers, materials, and NPP components/systems (D'Auria et al., 2012a).

2.3.11 Modeling and structure for computational tools

The structure and the modeling of existing TH SYS codes (or computational tools) are based on the application of the “six-partial-derivative-balance-equations” to simulate the transient performance of the two-phase mixtures. Those equations shall be seen as the result of the application of the principles of thermodynamics and mechanics. However, approximations or even inadequacies (so far unavoidable) are part of the structure and the modeling, like (more details can be found in the paper by D'Auria et al., 1998):

- Two-phase flow regimes are not directly accounted.
- Averaging is needed at the levels of cross-sectional flow area, integration volume, and time; all of this is associated with the concept of control volume.
- Consideration of two (or three) fluid fields as solution domain (this may be seen as a consequence of the two items above).
- Need for a variety of constitutive and/(or) closure equations which are unavoidably used outside their range of applicability; this also implies the need of “virtual correlations” (or numerical terms) to get solutions within the real domain.

The concept of control volume implies the need to reconstruct the continuous reality (i.e., the NPP configuration) by more or less large pieces, thus introducing undue discontinuities at the connection faces. The well-known issue of “water-packing” is a consequence.

The V&V with main reference to the validation shall be seen as the only way to qualify and, eventually, to make acceptable those inadequacies.

Accident analysis constitutes an important part of the licensing. DBA, anticipated operational occurrence (AOO), beyond DBA (BDBA) as well as emergency operating procedure (EOP), and Accident Management Guidelines (AMG) constitute established concepts in accident analysis. Moreover, following the start of any accident (e.g., a PIE (postulated initiating event) part of the DBA envelope) I&C have the potential to bring the NPP far from the initial condition (e.g., D'Auria et al., 2012a).

The first element for reflection for accident analysis deals with the use of conservatism. The conservatism in input data, also known as “Option 2” in IAEA documents (e.g., see IAEA, 2008a, 2010a) does not ensure conservatism in the output (or code calculation results). Conservatism in the output can only be demonstrated when BEPU analyses are performed; otherwise adequacy of conservatism on the output can only be inferred by deep expertise. Thus, the IAEA “Option 2” should be considered as an “interim” option in the history of application of SYS YH codes to licensing.

The key issue in the case of accident analysis and licensing is the application of the BEPU approach also identified as “Option 3” in the IAEA documents (e.g., see IAEA, 2008a, 2010a). Pioneering efforts have been completed in this direction as discussed under the historic outline above. However, developments are needed to make traceable and robust the regulatory process, by addressing subissues like (not a comprehensive not a systematic list):

- use of 3D NK to determine the maximum linear power of individual fuel rods
- use of 3D NK to perform the transient analysis of events where nonhomogeneous core behavior is expected
- consideration of single failure
- consideration of the availability of systems and components part of the NPP (noticeably including engineered safety features, ESF)
- BEPU analysis of transients or situations identified as ATWS, SBO, and PTS (pressurized thermal shock)
- establish procedures for determining the worst break position and, at a higher level of detail, the break opening time which affect the calculation of mechanical load on internal and external components and structures

- establish procedures to account for the impact of burn-up upon the transient analysis

- establish procedure to calculate the quantities affecting the acceptance criteria other than the PCT and the H₂ production, i.e., the demonstration of core remaining intact (mostly mechanical loads at the transient start in case of LBLOCA) and the long-term core cooling involving the specific subissues of sump-recirculation, debris-effect, and, where applicable, containment leakages and long-term condensation.

Further elements for reflections are:

- (a) A procedure shall be established connecting the accident analysis with the design and the applicability domain of system codes: DBA envelope→TH phenomena→significant physical quantities (e.g., pressure, heat flux, flow-rate)→range of variations for those quantities and related combinations→design domain and V&V domain for SYS TH codes (e.g., see Fig. 2.6).

- (b) I&C simulation shall be part of the analysis of accidents (e.g., see D'Auria et al., 2012b).

The first recommendation also applies in relation to V&V for SYS TH codes (Section 2.3.8 in this chapter). The second recommendation also applies in relation to PSA and SYS TH (Section 2.3.13 in this chapter).

2.3.13 PSA and SYS TH

PSA process at any of the Levels 1, 2, or 3 requires deterministic calculations to establish the success of any sequence, decide about the failure modes of systems structures and components, and estimate the “source term.” Historically, approaches and computational tools have been adopted for deterministic calculations which are simplified in relation to the methods and the numerical codes available within the SYS TH domain (the reason for this being the huge number of requested calculations). Current controversial issue is constituted by the quality or the qualification level of the deterministic calculations which are used for PSA (e.g., see IRSN, 2013).

The role of I&C in PSA constitutes an additional concern. I&C systems and components are designed with the target of being uninfluential or providing benefits after any PIE. However, the complexity of the entire NPP system and the

interaction among various logics and components following any PIE has the potential to bring the NPP conditions far from the configuration associated with the originating PIE.

The issues or the elements for reflection are:

(a) The design of complex EOP and SAMG on the one hand and the availability of UM on the other hand, together with the advent of more powerful computers, impose reconsidering the use of simplified approaches when estimating the success of any sequence or when calculating radiological releases. This may imply the need for huge computational resources.

(b) The role of “deterministic” uncertainty shall be included in probabilistic results.

(c) I&C simulation shall be considered for PSA and DSA.

2.3.14 Severe accident and SYS TH

Making reference to the predicted evolution of any accident the intact (or nearly intact) core geometry is normally taken as the boundary between SYS TH and SA analyses. Furthermore, Severe Accidents are outside the domain of interest for this book as stated in Chapter 1.

The quality of DBA analyses (or of analyses performed within the DBA envelope) shall be distinguished from the quality of SA analyses or analyses involving core degradation. Enormous progresses have been made during the last two decades in the understanding of SA phenomena; however, the qualification level of results from SA analyses shall be considered far lower than the qualification level expected or achieved in the area of SYS TH analyses. A picture of the SA area can be obtained from documents (USNRC, 1995; OECD/NEA/CSNI, 2007, 2009; IAEA, 2008b).

The design impact from SA analyses shall be avoided or minimized, rather SA analyses shall be used to ensure thorough bases for nuclear technology understanding and supporting the decision of NPP staff in the unluckily SA situation. New systems to mitigate SA conditions may reveal improper and not in the direction of facilitating the operator actions and, even worse, can be the origin of new accident sequences (e.g., the undue flooding of reactor cavity during nominal operation).

Recommendations or elements for reflection are:

(a) The analysis until the prediction of important core degradation shall be performed by the BE SYS TH code. This is specifically true in relation to the calculation of the time of occurrence of degraded core conditions: in other terms, the use of simplified approaches might produce misleading results far from what can be reliably obtained by BEPU approach.

(b) SA codes results properly supported by SYS TH code results can be relevant for planning operator actions: optimized SAMG and connected procedures can be designed.

(c) Impact on the NPP hardware design from SA code results, even supported by SYS TH codes, should be avoided owing to the low qualification level, as already mentioned. Furthermore design changes caused by SA analyses should imply changes in the licensing approach which currently distinguishes between DBA and BDBA: DBA envelope shall be changed according to the design, and proper quality level should be ensured for SA computational tools.

2.3.15 User effect and training

The current user effect in the application of SYS TH codes and coupled codes undermines the applicability of those codes, the confidence toward the derived calculation results, and the possible benefits from code applications (e.g., see Aksan et al., 1993; Ashley et al., 1998; D'Auria, 1998; Petruzzi et al., 2005).

The effect of code-users upon “poor” code calculation results shall be seen similar to the effect of unexperienced drivers bringing top-quality bus or truck against a wall or out-of-the-road. In these cases (truck or bus off-road), little or no blame is put to the truck makers or designers, and discipline and training is invoked for drivers. In the case of SYS TH code, poor code calculation results are preferably attributed to poor code capabilities: codes appear unreliable and code development processes become repetitive and never-ending.

Elements for reflections are discussed later.

More focus should be on the qualification of researchers in SYS TH area, and additional emphasis should be given to the requested (mainly from the side of regulators) qualification level of code users. International programs are ongoing in this direction (e.g., Petruzzi et al., 2005), but they appear still weak and not properly supported by regulatory authorities. Targets and accomplishments for code users shall be connected with the number of year of experience and the modalities of performing the analysis (e.g., see IAEA, 2015). The role of input

deck, or the interface between the NPP reality and the code, should receive proper attention. Specific recommendations are:

- The input deck or the nodalization developed by group 1 of code-users should be “independently checked” by group 2 of code users.
- Proper acceptance criteria shall be used to endorse the quality of any input deck.
- The results of any safety or design relevant calculation should be “independently checked” and approved by a “supervisor” having at least 10 years documented expertise in SYS TH analyses.
- In addition to uncertainty analysis needed in conjunction with any BE code calculation, properly planned sensitivity analyses are necessary to minimize the risk of neglecting possible bifurcation or cliff-edge effects.

2.3.16 The BEPU approach

Only the definition of BEPU (approach), and key elements part of the approach are given here in order to complete the list of perspectives for the future in nuclear thermal-hydraulics. BEPU is discussed in the papers by D'Auria et al. (2012a) and D'Auria et al. (2012b). Details related to BEPU can be found in Chapter 14 of the book.

The following statements may help in providing an idea about BEPU:

- (a) BEPU is composed by the words best estimate (=the best one can do, within current technology—i.e., a moving target—in predicting/calculating an assigned, typically complex, transient scenario) and Uncertainty (=expected, or unavoidable, error associated to the calculation process).
- (b) The process of combined application of a SYS TH code and an UM, to the analysis of accident in NPP, is called BEPU.
- (c) BEPU can be seen as the connection between nuclear thermal-hydraulics and licensing (needs) (see also Fig. 2.11).

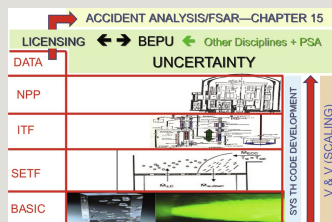


Fig. 2.11 The BEPU process focusing on accident analysis and Chapter 15 of FSAR (D'Auria, 2015).

(d) A metaphor has been used to describe BEPU (D'Auria, 2013). The knowledge acquired in nuclear thermal-hydraulics resembles a city suddenly abandoned by inhabitants: everything is there at rest, and no information is available to trigger the life in the city. A wild-experienced traveler arriving there feels lost and unable to use his competence and the existing and visible knowledge. In the allegory, the wild experienced traveler is the (expert) thermal-hydraulic specialist, the city and its components and systems is the nuclear thermal-hydraulic knowledge, and BEPU constitutes the civilization needed to make alive the city.

(e) BEPU constitutes a process which implies the widest exploitation of data and information in nuclear thermal-hydraulics: this can be derived from Fig. 2.11 (D'Auria, 2015).

The element for reflection is as follows: the application of BEPU is strongly recommended; benefits from the application can be listed and partly quantified (see also D'Auria et al. 2015); however, given those circumstances, neither Regulatory Authorities nor Nuclear Industry (more reasonable) is pushing for the application of BEPU.

2.3.17 Summary remarks

A synthesis of the items above is provided in Table 2.2. The following modalities or areas are proposed to plan possible improvements (third column in Table 2.2):

Table 2.2

Synthesis of (personal) views for perspectives in system

- The SYS TH code: this implies that improvements are expected for the codes and includes the (fundamental) modeling.
- Modeling: this implies that fundamental processes, or basic research, or experimental data are needed.
- Application: this deals with modalities and requirements for the processes and the procedures which foresee the application of computational tools and data to the NPP design, safety, or licensing. The word Application is adopted here to signify “exploitation of achieved knowledge and understanding in the technological practice.”
- Design: this implies that improvements are expected in the design of thermal-hydraulic systems.
- ITF design: this implies that improvements (or acceptable strategies) are expected in the design of new ITF.
- EDB: this should be taken as a synonymous of “EDB preservation” and implies that investments are expected in the area of preserving and storing experimental data.

It shall be noted how SYS TH code is both a target for improvement and a way to pursue envisaged improvements.

2.4 Conclusions

A noncomprehensive and nonsystematic review of perspectives and proposals for future activities in SYS TH has been performed and is applicable to NPP design and NRS frameworks. “Elements for reflection” are presented in the chapter.

Numerical codes and experimental facilities and the associated research programs and/or related data and applications constitute the hearth for SYS TH: the identification of numerical codes and experimental programs is provided in Section

2.2.2 and repeated in the “Nomenclature.”

A spot historic review brought to emphasize the publication of the Interim Acceptance Criteria for the design of ECCS, USNRC in 1971, as the triggering event for the development of modern nuclear thermal-hydraulics (or SYS TH). Other milestones are the achievement of qualification for SYS TH codes and their use inside the BEPU approach together with the development and the validation of UM.

Sixteen topics are discussed in the present chapter and shall be seen as the “elements for reflection.” These are reported in alphabetic order hereafter making reference to the key words in Table 2.2:

- Best-Estimate Plus Uncertainty (BEPU)
- CFD role for NPP design and NRS
- Coupling (with SYS TH codes)
- Licensing (implying application of SYS TH codes)
- Local form loss coefficients, “*K*-factors”
- Modeling and structure (of SYS TH codes)
- Multi-D heat transfer coefficient (HTC) surface
- Passive systems
- Precision targets
- PSA (connection with SYS TH code application)
- RCS depressurization and containment pressurization
- Severe accident (connection with SYS TH code application)
- Scaling and experiments
- Uncertainty methods
- User effect (and user training-qualification)

– Verification and validation (V&V)

Arbitrariness in the use of direct and reverse local pressure drop coefficients (K -factors) and inadequate qualification of code users undermined so far the confidence for the application of currently available SYS TH codes.

Procedures shall be established in a number of areas (identified as application in Table 2.2) which are consistent with the present level of knowledge, in order to make robust and reproducible the results from SYS TH code calculations. The BEPU approach noticeably falls in this category. “Closing the issue” in areas like Validation (rather than V&V), Scaling, and application of UM is also deemed possible based on the current understanding: spreading of available information within the scientific community may be worthwhile to reach consensus.

Improvements are considered necessary in areas like selected phenomena modeling, coupling among codes in different disciplines, the design of passive systems, the evaluation of related reliability, the interface between probabilistic and DSA, and the application of CFD codes. A peculiar area which deserves proper attention is the code-user training and qualification.

From a global perspective viewpoint, the results from envisaged activities should converge for a more efficient licensing process (and a better NPP design) minimizing the unavoidable lag between scientific and technological achievements and the practical applications.

Definitely, the implementation of the proposals, necessarily incomplete and not systematic, shaped in this chapter is expected difficult, and the practical relevance of those proposals may reveal questionable. Nevertheless, the provided discussion is expected to give a contribution for a deeper understanding of the nuclear thermal-hydraulics discipline.

References

Abdul-Razzak, A., 2009. Guidelines for application of the Best Estimate Analysis and Uncertainty (BEAU) methodology to licensing analysis in the Canadian CANDU Nuclear Power Industry, IAEA TM. Application of Deterministic Safety Analysis, Pisa, Italy, pp. 21–29.

AERB. In: The International Workshop on New Horizons in Nuclear Reactor Thermal Hydraulics and Safety, January 7–8, Niyamak Bhavan, Mumbai Region, India, Frequently Held Workshop; 2010.

Ahn S.H., Aksan N., Austregesilo H., Bestion D., Chung B.D., D'Auria F., Emonot P., Gandrille J.L., Hanninen M., Horvatić I., Kim K.D., Kovtonyuk A., Petruzzi A. FONESYS: the FORum & NETwork of SYStem thermal-hydraulic codes in nuclear reactor thermal-hydraulics. *Nucl. Eng. Des.* 2015;281:103–113.

Aksan S.N., D'Auria F., Staedtke H. User effects on the thermal-hydraulic transient system codes calculations. *Nucl. Eng. Des.* 1993;145(1):159–174.

ANS. In: Int. Meet. on Best-Estimate Methods in Nuclear Installation Safety Analysis (BE-2000), Washington, DC, USA, 10–13 November; 2000.

ANS. In: Int. Meet. on Best-Estimate Methods in Nuclear Installation Safety Analysis (BE-2004), Washington, DC, USA, 14–18 November; 2004.

Ashley, R., El-Shanawany, M., Eltawila, F., D'Auria, F., 1998. Good practices for user effect reduction. OECD/CSNI report NEA/CSNI/R(98)22, Paris, France.

Bajorek S.M. *A regulator's perspective on the state of the art in nuclear thermal-hydraulics*. In: NURETH-16 Conf., Chicago, IL, USA, August 30–September 4; 2015.

Benhamadouze S. *Pressure drop prediction using Code-Saturne in NESTOR CFD benchmark*. In: NURETH-16 Conf., Chicago, IL, USA, August 30–September 4; 2015.

Bestion D. *Validation data needs for CFD simulation of two-phase flow in a LWR core*. In: CFD4NRS-5 Conf., Zurich, September [Accepted for Publication in a Special Issue of Nuclear Engineering and Design]; 2014.

Billone, M., Yan, Y., Burtseva, T., Daum, R., 2008. Cladding

embrittlement during postulated loss-of-coolant accidents. USNRC NUREG/CR-6967, Washington, DC, USA.

Bonuccelli M., D'Auria F., Debrecin N., Galassi G.M. *A methodology for the qualification of thermal-hydraulic codes nodalizations*. In: International Top. Meet. on Nuclear Reactor Thermal-Hydraulics (NURETH-6), Grenoble, France; 1993.

Chang H., Li Y., Zhao R., Hu T., Wang H., Dai Q. Integral thermal-hydraulic test facilities to support the development of the large passive nuclear power plant in China. *Nucl. Safe. Simul.* 2011;2(4):317–325.

D'Auria F. *Proposal for training of thermal-hydraulic system codes users*. In: IAEA Spec. Meet. on User Qualification and User Effects on Accident Analysis for Nuclear Power Plants, Vienna, Austria; 1998.

D'Auria F. Perspectives in system thermal-hydraulics. *Nucl. Eng. Technol.* 2012;44(8):855–871.

D'Auria, F., 2013. Nuclear thermal-hydraulics: from fundamentals to applications. Conferencia pronunciada por el Dr. F. D'Auria el 18 de marzo (2013) en la Academia Nacional de Ciencias de Buenos Aires. Anticipo de Anales de la Academia Nacional de Ciencias de Buenos Aires – Buenos Aires, Argentina.

D'Auria F. *Presentation at panel 'data, data science and data-driven thermal-hydraulics'*. In: NURETH-16 Conf., Chicago, IL, USA, August 30–September 4; 2015.

D'Auria F., Galassi G.M. Code validation and uncertainties in system thermal-hydraulics. *Prog. Nucl. Energ.* 1998;33(1/2):175–216.

D'Auria F., Galassi G.M. Scaling in nuclear reactor system thermal-hydraulics. *Nucl. Eng. Des.* 2010;240(10):3267–3293.

D'Auria F., Giannotti W. Development of code with capability of internal assessment of uncertainty. *Nucl. Technol.*

2000;131(1):159–196.

D'Auria F., Galassi G.M., Vigni P., Calastri A. Scaling of natural circulation in PWR systems. *Nucl. Eng. Des.* 1991;2:187–206.

D'Auria F., Debrecin N., Galassi G.M. Outline of the uncertainty methodology based on accuracy extrapolation (UMAE). *Nucl. Technol.* 1995;109(1):21–38.

D'Auria, F., Galassi, G.M., Giannotti, W., 2003. Post-test analysis by Relap5/mod3.3 β of VVER-440 bubble condenser tests 01 to 05 performed in BC V-213 facility. University of Pisa Report, DIMNP-NT 509(03), Pisa Italy, July.

D'Auria, F. (Project Coordinator), Bousbia Salah, A., Galassi, G.M., Vedovi, J., Reventos, F., Cuadra, A., Gago, J.L., Sjoberg, A., Yitbarek, M., Sandervag, O., Garis, N., Anher, C., Aragones, J.M., Verdù, G., Mirò, R., Hadek, J., Macek, J., Ivanov, K., Rizwan-Uddin, Sartori, E., Rindelhardt, U., Rohde, U., Frid, V., Panayotov, D., 2004. Neutronics/thermal-hydraulics coupling in LWR technology – CRISSUE-S WP2: State-of-the-art report. OECD/NEA Report No. 5436, ISBN 92-64-02084-5, Paris, France.

D'Auria F., Camargo C., Mazzantini O. The Best Estimate Plus Uncertainty (BEPU) approach in licensing of current nuclear reactors. *Nucl. Eng. Des.* 2012a;248:317–328.

D'Auria F., Camargo C., Muellner N., Lanfredini M., Mazzantini O. The simulation of I & C in accident analyses of nuclear power plants. *Nucl. Eng. Des.* 2012b;250:656–663.

D'Auria F., Glaeser H., Kim M. *A vision for nuclear reactor safety*. In: 46th Jahrestagung Kerntechnik Annual Meeting on Nuclear Technology, Berlin, Germany, May 5–9; 2015.

Damerell, P.S., Simons, J.W., 1992. 2D/3D Program work summary report. GRS Report No. 100, ISBN 3-923875-50-9, Koln, Germany.

D'Auria, F., Vigni, P., 1980. Two-phase critical flow models.

OECD/NEA/CSNI Report No. 49, Paris, France.

D'Auria F., Vigni P. *Proposed set of criteria in designing nuclear power plants experimental simulators*. In: 3rd Int. Top. Meet. on Reactor Thermal-hydraulics (NURETH-3), Newport, RI, USA, October 15–18; 1985.

D'Auria F., Frogheri M., Monasterolo U. *Removable power by natural circulation in PWR systems*. In: ASME-JSME Conf. (ICONE-5), Nice, France, May 26–30; 1997.

D'Auria F., Chojnacki E., Glaeser H., Lage C., Wickett T. *Overview of uncertainty issues and methodologies*. In: Invited at OECD/CSNI Seminar on Best Estimate Methods in Thermal-Hydraulic Analyses, Ankara, Turkey, June 29–July 1; 1998.

D'Auria F., Giannotti W., Piagentini A. *Consideration of bifurcations within the internal assessment of uncertainty*. In: ASME-JSME Int. Conf. on Nuclear Engineering (ICONE), Baltimore, MD, USA, April 2–6; 2000.

Divo E., Kassab A.J., Kapat J.S., Tapley J. Determination of heat transfer coefficient maps using an inverse BEM algorithm. In: Tanaka M., Dulikravich G.S., eds. *Inverse Problems in Engineering Mechanics*. Oxford: Elsevier, Kidlington; 2000.

Forslund R.P., Rohsenow W.M. Dispersed flow film boiling. *J. Heat Transf.* 1968;90:399–407.

Glaeser H. *Analysis of down-comer and tie plate countercurrent flow in the Upper Plenum Test Facility (UPTF)*. In: NURETH-4 Conf., Karlsruhe, Germany; 1989.

Glaeser H. GRS method for uncertainty and sensitivity evaluation of code results and applications. *Sci. Technol. Nucl. Install.* 2008;2008:1–7.

Groeneveld, D.C., 1973. The thermal behavior of a heated surface at and beyond dry-out. PhD Thesis, University of Western Ontario, London, Canada.

Henry R.E. *TMI-2: An Event in Accident Management for Light-*

Water-Moderated Reactors. LaGrange Park, IL, USA: ANS; 2011.

Hofer E. *The GRS programme package for uncertainty and sensitivity analysis*. In: Seminar on Methods and Codes for Assessing the Off-Site Consequences of Nuclear Accidents, EUR 13013; Brussels, Belgium: CEC; 1990.

IAEA, 2000. Safety of nuclear power plants: design, requirements. NS-R-1, Vienna, Austria.

IAEA, 2002. Accident analysis for nuclear power plants. IAEA Safety Reports Series No. 23, ISSN 1020-6450; ISBN 92-0-115602-2, Vienna, Austria.

IAEA, 2005. Natural circulation in water-cooled nuclear power plants phenomena, models, and methodology for system reliability assessments. TECDOC 1474, Vienna, Austria.

IAEA, 2006. Fundamental safety principles, safety fundamentals. SF-1, Vienna, Austria.

IAEA, 2008a. Best estimate safety analysis for nuclear power plants: uncertainty evaluation. Safety Report Series, No. 52, Vienna, Austria.

IAEA, 2008b. Approaches and tools for Severe Accident Analysis for Nuclear Power Plants. Safety Report Series, No. 56, Vienna, Austria.

IAEA, 2009a. Safety assessment for facilities and activities, general safety requirements. GSR Part 4, Vienna, Austria.

IAEA, 2009b. Passive safety systems and natural circulation in water cooled nuclear power plants. TECDOC 1624, Vienna, Austria.

IAEA, 2010a. Deterministic safety analysis for nuclear power plants. IAEA SSG-2, Vienna, Austria.

IAEA, 2010b. Development and application of level 2 probabilistic safety assessment for nuclear power plants. Specific Safety Guide No. SSG-4, Vienna, Austria.

IAEA, 2014. Evaluation of advanced thermohydraulic system codes for design and safety analysis of integral type reactors. TECDOC 1733, Vienna, Austria.

IAEA, 2015. Verification and validation of system codes for nuclear safety analyses. Unpublished draft report, Vienna, Austria.

IRSN, 2013. ASAMPSA2 best practice guidelines for level 2 PSA development and applications. PSN-RES/SAG/2013-0177.

Jafari J., D'Auria F., Kazeminejad H., Davilu H. Reliability evaluation of a natural circulation system. *Nucl. Eng. Des.* 2003;224:79–104.

Khan S.A. The Chernobyl source term: a critical review. *Nucl. Saf.* 1990;31(3):353–374.

Kovtonyuk A., D'Auria F., Petruzzi A. *Proposal of integration between CIAU and GRS method for ATHLET code*. In: Presentation at a Meeting Held at GRS Headquarter, Garching, Germany, April 3; 2008.

KWU-Siemens, 1997. FSAR: Final Safety Analysis Report Central Nuclear Almirante Álvaro Alberto, Unit 2 – Rev. 0, September, Erlangen, Germany.

Lewis H.W., Budnitz R.J., Castleman A.W., Dorfan D.E., Finlayson F.C., Garwin R.L., Hebel L.C., Keeny Jr. S.M., Muller R.A., Taylor T.B., Smoot G.F., von Hippel F., Bethe H., Panofsky W.K.H., Weisskopf W.F. Report to the American Physical Society by the study group on light-water reactor safety. *Rev. Mod. Phys.* 1975;47:S1.

Martin R.P., O'Dell L.D. AREVA's realistic large break LOCA analysis methodology. *Nucl. Eng. Des.* 2005;235:1713–1725.

Moore, K.V., Rettig, W.H., 1968. RELAP2 – a digital program for reactor blowdown and power excursion analysis. IDO-17263, Idaho Falls, ID, USA.

OECD/NEA, 2004. Neutronics/thermal-hydraulics coupling in

lwr technology – three vols. OECD/NEA Report No. 4452, ISBN 92-64-02083-7 (Vol. I, 103 pages), Paris, France.

OECD/NEA/CSNI, 1987. CSNI code validation matrix of thermo-hydraulic codes for LWR LOCA and transients. CSNI, 132, Paris, France.

OECD/NEA/CSNI, 1989. Thermohydraulics of emergency core cooling in light water reactors—a state of the art report. OECD/CSNI 161, October, Paris, France.

OECD/NEA/CSNI. In: Proceedings of CSNI Spec. Meet. on Transient Two-Phase Flow – System Thermal-Hydraulics, Aix-En-Provence, France, April 6–8; 1992.

OECD/NEA/CSNI, 1993. Separate effects test matrix for thermal-hydraulic code validation: phenomena characterization and selection of facilities and tests. OCDE/GD(94)82, Paris, France.

OECD/NEA/CSNI, 1996. CSNI code validation matrix of thermo-hydraulic codes for LWR LOCA and transients. CSNI Report, 132-Rev. 1, Paris, France.

OECD/NEA/CSNI, 1998. [Authors: Wickett, T. (Ed.), D'Auria, F., Glaeser, H., Chojnacki, E., Lage, C. (Lead Authors), Sweet, D., Neil, A., Galassi, G.M., Belsito, S., Ingegneri, M., Gatta, P., Skorek, T., Hofer, E., Kloos, M., Ounsy, M., Sanchez, J.I]. Report of the Uncertainty Methods Study for advanced best estimate thermal-hydraulic code applications – volumes I and II. OECD/CSNI Report NEA/CSNI/R(97)35, Paris, France.

OECD/NEA/CSNI, 2007. State of art report on iodine chemistry. NEA/CSNI/R(2007)1, Paris, France.

OECD/NEA/CSNI, 2009. State of art report on nuclear aerosols. NEA/CSNI/R(2009)5, Paris, France.

OECD/NEA/CSNI, 2016. The scaling state of the art report – the S-SOAR. NEA/CSNI/R(2016)14, Paris, France.

Petruzzi A., D'Auria F., Bajs T., Reventos F. In: International

Training Program: 3D S.UN.COP-Scaling, Uncertainty and 3D Thermal-Hydraulics/Neutron-Kinetics Coupled Codes Seminar, ENC, Versailles, France; 2005.

Petruzzi A., Fiori F., Kovtonyuk A., D'Auria F. *Supporting qualified database for uncertainty evaluation*. In: Proceeding of ICAPP 2012, 12085, Chicago, IL, USA, June 24–28; 2012.

Qiu S.Z., Sun D.C., Tian W.X., Xiang Y., Su G.H., Zhang P. *Experimental and theoretical research on liquid entrainment in AP1000 ADS blow-down phase of SBLOCA*. In: NURETH-16 Conf., Chicago, IL, USA, August 30–September 4; 2015.

Smith, B.L., Bieder, U., Graffard, E., Heitsch, M., Henriksson, M., Höhne, T., Komen, E., Mahaffy, J., Moretti, F., Morii, T., Mühlbauer, T., Rohde, U., Scheuerer, M., Song, C.-H., Zigh, G., Andreani, M., Bestion, D., Ducros, F., Houkema, M., Lucas, D., Menter, F., Watanabe, T., 2008. Assessment of computational fluid dynamics (CFD) for nuclear reactor safety problems. NEA/CSNI/R(2007)13, Paris, France.

Song C.-H. *Issues and challenges on advanced thermal-hydraulic researches*. In: NURETH-16 Conf., Chicago, IL, USA, August 30–September 4; 2015.

Tanaka M., Dulikravich G.S., eds. *Inverse Problems in Engineering Mechanics*. Kidlington, Oxford: Elsevier; 2000.

UNIPI-GRNSPG, 2008. A proposal for performing the Atucha II accident analyses for licensing purposes. The BEPU Report – Rev. 3, Pisa, Italy [endorsed by Regulatory Authority in Argentina].

USAEC. *Interim Acceptance Criteria (IAC) for ECCS*. Washington, DC: USAEC; 1971.

USNRC, 1975. Reactor Safety Study – an assessment of accident risk in U.S. Commercial Nuclear Power Plants. WASH-1400, NUREG-75/014, Washington, DC, USA.

USNRC, 1989a. Quantifying reactor safety margins: application

of CSAU to a LBLOCA. NUREG/CR-5249, Washington, DC, USA.

USNRC, 1989b. Best-estimate calculations of emergency core cooling system performance. USNRC Regulatory Guide 1.157, Washington, DC, USA.

USNRC, 1995. Accident source terms for light water nuclear power plants. NUREG-1465, Washington, DC, USA.

USNRC, 2005. Transient and accident analysis methods. RG 1.203, USNRC, Washington, DC, USA.

USNRC, 2014. US Government, Federal Register Notice, 79 FR 16106, March 24.

USNRC, 2015. Code of Federal Regulation, Washington, USA [continuously updated – see the website of USNRC].

Wallis G.B. *One Dimensional Two-Phase Flow*. New York, NY: McGraw Hill; 1969.

Yadigaroglu G., Lakehal D. *Nuclear safety and thermal-hydraulics: personal thoughts and some recent progress*. In: NURETH-16 Conf., Chicago, IL, USA, August 30–September 4; 2015.

Yadigaroglu G., Andreani M., Dreier J., Coddington P. Trends and needs in experimentation and numerical simulation for LWR safety. *Nucl. Eng. Des.* 2003;221:205–223.

Young M.Y., Bajorek S.M., Nissley M.E., Hochreiter L.E. Application of code scaling applicability and uncertainty methodology to the large break loss of coolant. *Nucl. Eng. Des.* 1998;186:39–52.

Zuber N. Scaling: from quanta to nuclear reactors. *Nucl. Eng. Des.* 2010;240:1986–1996.

Zuber N., Findlay J.A. Average volumetric concentration in two-phase flow systems. *J. Heat Transf.* 1965;87:453–468.

¹ Commonly, this has been done in the past by adopting PIRT or related techniques. Then, the occasion is taken to state a view point in relation to PIRT. The present author expressed his doubts in relation to the use of the “ranking” process in SYS TH, since its presentation in 1989. Recently, the sentences by the key-proponent of the PIRT process, “... the PIRT process as presently implemented produces absolutely useless documents ... ranking is based purely on subjective opinions ...” (Zuber, 2010), put those doubts in the right perspective.

Parameters and concepts

F. Reventos Polytechnic University of Catalonia, Barcelona, Spain

Abstract

Parameters and concepts are introduced in order to provide a view of nuclear thermal hydraulics covering from the bases to the application of the discipline. Namely, selected cross-cutting issues from the thermal hydraulics universe are defined. This view is essential for understanding the content of the book and for self-confirming the level of understanding of thermal hydraulics by the reader. Two phase flows and heat transfer are concerned together with safety concepts. Examples moving from bases to applications are the fundamental relationship of thermal hydraulics involving quality, void fraction, slip ratio and pressure, the steam binding phenomenon, the design basis accident, the defense in depth, and the final safety analysis report.

Keywords

Fundamental thermal hydraulics relationship; Safety barriers; Passive systems; Emergency operating procedures; Accident management; Prevention and mitigation; Defense in depth (DiD); The nuclear reactor safety levels

Chapter foreword

In this chapter, a wide variety of parameters and concepts are introduced in order to provide a view of nuclear thermal hydraulics. The content covers from the bases

to the application of the discipline. This view is essential for understanding the content of the book: this is expected to be useful for the reader for self-confirming the level of understanding of thermal hydraulics.

3.1 General remarks on parameters and concepts

This chapter introduces parameters and concepts needed for subsequent developments along with the context in which the main developments of nuclear thermal hydraulics are built up.

Since the book includes from very fundamental topics in nuclear thermal hydraulics (or system thermal hydraulics) to advanced applications of thermal hydraulics in nuclear power plant (NPP) safety and design, the chapter intends to provide some discussion helpful to understand the boundaries of the whole text. It includes the concepts needed to depict the connection with fluid dynamics and gas dynamics emphasizing the added complexity. The concept of turbulence is commented with the aim of clarifying both the boundaries and the complexity.

The chapter is organized in several sections. Since two-phase flow and the heat transfer are the most relevant subjects that will appear in subsequent development, a full section is devoted to each of them.

Parameters and concepts needed for presenting two-phase flow are introduced connecting with the developments expected in the chapters of the book. The main parameters needed for two-phase flow theory, especially void fraction and quality, are introduced along with their relationship. Parameters involved in mass, energy, and momentum balance equations for two-phase flows are also introduced. Phenomena descriptions complete the notions needed for two-phase flow treatment (among them: flow regimes, natural circulation, critical flow, blowdown, etc.). Also a brief explanation on more simple approaches like homogeneous model, separate model, drift-flux model, or lumped parameter is included in order to illustrate the complexity of the involved physics. An outline of the so-called two-fluid model concludes the section.

In the second section, devoted to heat transfer, concepts and variables related to conduction, convection, and radiation are introduced. Such introduction is centered on characterization comments but it also includes the empirical and theoretical aspects needed for understanding the expected developments.

The following two sections are devoted to additional concepts to analytical and experimental thermal hydraulics. Parameters and concepts referred to system codes

and related subjects for the first and referred to test facilities and data management for the second.

A block of three other sections can be found in the continuation: concepts connected to design basis (DB), general safety concepts, and concepts related to deterministic safety analysis (DSA).

The last block includes two sections: concepts related to actual accidents and a miscellaneous section on concepts related to other uses thermal-hydraulic analysis.

Whenever it has been found interesting, the section includes also a kind of foreword with the aim of clarifying its context.

3.2 Concepts involved in two-phase flow developments

3.2.1 Context

3.2.1.1 Importance of two-phase flow

The analysis of water reactors thermal hydraulics needs to consider two-phase flow and related phenomena. Such phenomena that occur in normal operation in boiling water reactor (BWR) and also in specific components of pressurized water reactor (PWR) (mainly in steam generators, SGs) can also take place in accidental scenarios of both PWR and BWR. Most of the safety scenarios involve depressurization; among them loss of coolant accidents (LOCAs) and malfunction are related to pressure control or pressure relief valves. Once a depressurization occurs in a PWR, system saturation temperature could decrease and two-phase flow could appear. It also appears in advanced phases of most scenarios in which, due to decay heat and to the presence of water, vapor is produced in core and any mixture of water and vapor could flow driven by a break, by an injection, or by natural circulation. The importance of two-phase flow developments in the field of thermal hydraulics of nuclear systems has stressed in conferences (OECD/NEA/CSNI, 1992) as well as in internationally recognized textbooks (Tong, 1965; Wallis, 1969; Collier, 1975).

3.2.1.2 Multiscale and multiphysics

The scientific current approach to describe the involved scenarios includes multiscale calculations. Thermal-hydraulic analysis devoted to nuclear systems

must cover the whole range of modeling scales. By now, it is widely accepted that such scales are the following: system scale, subchannel scale, and CFD (computational fluid dynamics) scale.

The aim of the calculations at system scale is to predict the overall behavior of the plant, including the reactor and other components such as primary circuit, SGs, and pumps. System codes are the right tool to face the subject. Phenomena described at such scale are usually called system effects. System codes usually solve the problem using a 1D formulation for most of the modeled system and 3D options for the most relevant parts as the reactor vessel. System codes are widely used in thermal hydraulics of nuclear systems (Freixa et al., 2015a,b; IAEA, 2014).

The subchannel scale is also firmly established. It deals with the modeling of the reactor core or fuel bundles. To be stricter, at the definition level, this scale should be called component scale, given that, besides the core, different components have more detailed codes and models. Since the core is the component that more often is studied, it seems correct to nominate the scale as subchannel scale. At such scale, 3D aspects are taken into account and fuel bundles are modeled with enough detail in order to predict local cladding temperatures or DNB expected values. In an analogous way, SG or other heat exchanger tube bundles are modeled using specific codes at a similar level.

The third group is the so-called CFD scale. CFD produces simulations at an extremely finer scale. The studies at such scale are based on more advanced physical models, using nodalizations of a huge number of nodes and applying more updated numerical methods. Accordingly, the computing power needed is also huge and problem definition is rather complex (Smith et al., 2008). CFD codes are the tools and by now they are mainly used to clarify the behavior of local areas or critical components in specific scenarios.

Many initiatives have been carried out devoted to coupling thermal-hydraulic codes of different scale. In a similar way, there are also many initiatives connecting thermal-hydraulic codes with codes describing other physical aspects of the simulated scenario. Among them one can find either neutron physics, (Ivanov and Baratta, 1999; D'Auria et al., 2004; Pericas et al., 2013, 2016; Pericas, 2015) mechanical or severe accident codes (e.g., Pla, 2004; Espinosa-Paredes et al., 2012; IAEA, 2008b). Such activities are by now encouraged by the fact that computers are becoming faster every day. Multiscale and multiphysics platforms and projects are ongoing activities needed to be taken into account.

Neither the scale nor the fact of being coupled with other physical formulation

affects the thermal-hydraulic concepts introduced below. Comments will be added if needed.

3.2.1.3 Turbulence and two-phase flow

The essential characteristic of turbulent flow is its apparently chaotic property variation. In a turbulent flow pressure and velocity tend to change in space and time rapidly due to unsteady vortices that appear on many scales and interact among them. Reynolds number provides a first approach to limit the question: flows having a large Reynolds number (more than 5000) are typically turbulent. This is only a first approach and turbulence, despite the important analytical effort currently devoted to it, can be considered an unresolved problem.

The analysis of turbulent two-phase flow has some added difficulty. The above-mentioned chaotic property variations could change or even suppress any two-phase flow regime. At this point, it seems that to get an accurate picture of two-phase flow, turbulence has to be mastered previously.

Once again, experimentation is crucial to overcome the problem. Quite an important amount of tests related to two-phase flow have been performed and the observation of their results allows some confirmed outcome. Two-phase flow regimes have quite steady properties and transitions among them occur at definite values of key parameters. All this has some uncertainty, but it opens a possibility of going ahead with two-phase flow study. More detail on flow regimes and key parameters is given below.

3.2.1.4 Empirical database and instrumentation

An empirical database supports the use of equations, correlations, and codes. This is an important point since the validation of theories and practices depends on the right correspondence between what is defined and what is measured. The reliability of the database is supported by its systematic documentation and by the qualification process of facility instrumentation.

A huge database has been produced for many years and is now available for its use at the different level where it is needed (Addabbo et al., 2002; Pla et al., 2015, 2016b). It consists in separate effect and integral tests that were designed to support the developments devoted to predict the behavior of a reactor system in normal and abnormal or accident conditions. By now, after following an initiative of CSNI the results of such experiments are organized in two different matrices (separate effect and integral tests) that establish their suitability for each phase of the validation process of best estimate (BE) thermal-hydraulic computer codes

(Aksan et al., 1987; OECD/NEA/CSNI, 1992, 1993, 1996).

Instruments devoted to produce the measurement of the relevant parameters are needed for a complete qualification process devoted to certify its reliability. The design of such instruments has to assure the right correspondence between the signal produced and the physical parameter that the analyst is following. The complexity of thermal-hydraulic processes is an additional difficulty related to instrumentation design and setup. Another difficulty appears in the design and the qualification of most instruments that are required to be suitable for measuring parameters over wide ranges. For instance, the validity of thermocouples measuring temperatures in accidental scenarios is rather complex to certify.

3.2.2 Parameters and concepts

3.2.2.1 General aspects

The purpose of this section is to define the most relevant parameters that will be used in subsequent chapters related to two-phase flow. Again some recognized textbooks provide interesting details on such parameters and concepts, among them: El-Wakil (1962), El-Wakil (1971a), El-Wakil (1971b), Tong and Weisman (1970), Fenech (Ed.) (1981), and Todreas and Kazimi (1990). Parameters, usually known as water properties, are only mentioned when the added comments are significant enough for the specific development.

Two different comments are presented in this general section. They are related to intensive and extensive properties and also to time and volume averaging techniques.

By definition intensive properties are independent from the extent or the size of the system while extensive ones are dependent. Temperature is a good example of intensive property while mass and volume are examples of extensive properties.

Despite the extensive mass and volume, density and specific volume are intensive and can be easily written down in a table. Water property tables are very useful and most of the codes have their own versions of them.

Since thermal-hydraulic analysis deals with dynamic behavior of two-phase mixtures, discretization of time and space is an important issue. To do so, control volumes or space nodes on the one hand and time steps on the other hand are defined accordingly. Such definitions may change depending on the problem, and are significant to distinguish local from volume-average values and instantaneous

from time-averaged values.

Mass and energy conservation usually provide the criterion for averaging quantities. Such criterion is applied in a slightly different way in case of intensive or extensive properties. For extensive quantities like mass for example, the application is straightforward. For intensive properties like liquid water temperature, things are as follows: the volume-averaged temperature will be that of the liquid water at which mass and energy of the node are conserved.

Such considerations are usually taken into account when designing measurement techniques.

A similar rationale can be established in relation to instantaneous and time-averaged values.

3.2.2.2 Void fraction/quality

In a first and most intuitive approach, the void fraction (α) of a two-phase mixture is the volumetric fraction of a given control volume occupied by vapor.

Since different measurement techniques identify the cross section area (A) of a given channel and also the areas occupied by the gas (A_g) and the liquid (A_l), the void fraction is written:

$$\alpha = \frac{A_g}{A_g + A_l}$$

$$1 - \alpha = \frac{A_l}{A_g + A_l}$$

Void fraction is equal to 1 when all volume is vapor and 0 when it is liquid.

Similarly, quality (x) of a two-phase mixture is the mass fraction of vapor in a given control volume. If W_g is vapor mass flow and W_l is liquid mass flow then quality is written:

$$x = \frac{W_g}{W_g + W_l}$$

$$1 - x = \frac{W_l}{W_g + W_l}$$

Quality is equal to 1 when all volume is vapor and 0 when it is liquid.

3.2.2.3 Interfacial area/interfacial area concentration

Interfacial area, in a given control volume, is the area of contact between the two phases, liquid and vapor. It is usually described by means of the parameter defined as interfacial area concentration which is the area of contact between the two phases per unit of volume (Bestion and Serre, 2013). Such parameter is strongly connected with flow regimes that will be commented below. Characterizing such connection is an ongoing research activity that has had interesting results by now.

3.2.2.4 Mass velocity

The total mass flow (W) per unit of cross flow area is the so-called mass velocity (G):

$$W = W_g + W_l$$

$$G = \frac{W}{A}$$

Mass velocity is especially interesting in subchannel analysis since it is directly correlated with the remaining capability of extracting energy from a fuel bundle.

3.2.2.5 Equilibrium/subcooling/super-heating

As a general statement, two substances are in thermal equilibrium when there is no energy transfer between them; this is when they are at the same temperature. At a given pressure, there is a temperature, called saturation temperature, at which vapor and liquid coexist without exchanging any energy. At saturation temperature, vapor and liquid are in thermal equilibrium. It is useful, for further developments, to use saturation temperature as a kind of reference.

Thus, liquid with a temperature (T) below saturation is called subcooled and $\Delta T_{\text{SUB}} = T_{\text{sat}} - T$ is called subcooling.

And similarly, vapor at a temperature (T) higher than saturation is called super-heated and $\Delta T_{\text{SAT}} = T - T_{\text{sat}}$ is called super-heating.

3.2.2.6 Hydraulic diameter/Reynolds and Froude numbers

Hydraulic diameter (D_h) is defined as:

$$D_h = 4A/p$$

where A is the cross-sectional area and p is the wetted perimeter of the cross section.

It helps handling flow in noncylindrical tubes and channels. Using it, one can calculate different flow and heat transfer conditions in the same way as for a cylindrical tube.

The most used dimensionless numbers in two-phase flow are Reynolds number (Re) and Froude number (Fr).

Reynolds number (Re) is defined as:

$$Re = \rho \times v \times D_h / \mu$$

It is the ratio between inertia forces and viscous forces. When viscous forces are dominant Re has low values and flow becomes laminar, when inertia forces are dominant Re has higher values and flow becomes turbulent.

Froude number (Fr) is defined as:

$$Fr = v / \sqrt{(g \times L)}$$

It is the ratio between inertia forces and gravity forces. Froude number is crucial when determining the transition to stratified flows. When gravity forces are dominant flow becomes stratified.

3.2.2.7 Pressure drop

The difference in pressure between two points of a fluid system is known as pressure drop. Such difference can be due to static head, acceleration, friction, or local resistance.

Static head is originated between two points having different heights. The acceleration term, for a given fluid, is due to changes in cross area. Friction is caused by forces exerted between channel walls and the fluid as a consequence of wall roughness. Local resistance is due to changes in geometry like those produced by grids and elbows.

The proper evaluation of pressure drop is crucial in thermal-hydraulic analysis and becomes more complex when dealing with two-phase flow (Martinelli and Nelson, 1948; Lockhart and Martinelli, 1949). The start-up of natural circulation in any dynamic situation depends on the correct evaluation of pressure drops. Also, in

LOCA scenarios, the correct prediction of water mass distribution depends on the knowledge of pressure drops in the involved system. Once mass distribution is dynamically established versus time, core dry-out is also properly predicted.

3.2.2.8 Involved in balance equations

Balance equations usually considered in two-phase flow developments are conservation of mass, conservation of momentum, and conservation of energy.

Mass equation is usually postulated for a definite control volume. The most relevant parameters and concepts involved are commented.

Each phase has its own volume and velocities and densities are usually considered in their average value. If u_g and u_l are velocities of vapor and liquid phase, respectively, and ρ_g and ρ_l are densities of vapor and liquid phase, respectively, then

$$W_g = A_g \rho_g u_g = W \alpha$$

$$W_l = A_l \rho_l u_l = W (1 - \alpha)$$

The equation of conservation of mass is usually solved for each phase considering the existing mass of it in a given control volume and adding or subtracting any addition or removal of mass at the boundaries of the volume.

Vapor generation (due to boiling) and liquid generation (by condensation) are also terms of such balance. The accumulation of mass in a control volume equals the inlet/outlet of mass across its boundaries and the mass generated in it. Indeed, boiling and condensation correspond to this generation term, with the corresponding sign for each phase.

The equation of conservation of momentum is usually formulated for each phase considering the forces acting on it in a given control volume and equating it to the

change of momentum of the phase. Under these conditions, the most relevant parameters and concepts involved are commented.

The forces exerted by each phase against frictional resistance of channel wall in contact with it have the direction of the fluid and opposite sense.

The forces exerted by each phase against the other phase at the interfacial area have the direction of the fluid and opposite sense. Its magnitude is proportional to the relative velocity.

The forces due to static pressure against each phase could be calculated as $P \times A_g$ for vapor and $P \times A_l$ for liquid.

Since the weight of each phase is vertical, in a pipe having an angle θ with respect to horizontal direction, the force due to weight (per unit of volume) is computed as $\rho_g g A_g \sin \theta$ for vapor and $\rho_l g A_l \sin \theta$ for liquid.

A complete momentum equation for two-phase flow should also include a virtual mass term and the momentum production due to phase change.

Solving the resulting momentum equations has some additional complications since frictional resistance is difficult to handle. Pressure drop at geometric discontinuities is usually measured assuming that a fully developed flow is present and becomes an important source of uncertainty.

The energy balance equation is usually established in a definite control volume. The most relevant parameters and concepts involved are commented.

General parameters such as flow, velocity, or density are considered for each phase in a similar way as in the previous equations. Other relevant specific parameters are the change in enthalpy, the heat absorbed, and the work done. Variations in enthalpy are not commented since it is a state variable.

The heat absorbed by each phase could be provided by the other phase or by specific heat sources. Such source could be internal (chemical or nuclear reaction) or external (hot or cold wall).

The term “work done” (positive or negative) is only relevant in components producing or converting mechanical energy like turbines and compressors.

3.2.3 Phenomena

3.2.3.1 Flow-regime definition

Many experiments have been performed with heated and nonheated channels of different sizes and inclinations (mainly horizontal and vertical). From the observation of the results of such experiments important conclusions have been extracted.

This observation of results leads to the so-called flow-regime definition which is crucial in thermal hydraulics of nuclear systems. The development is highly motivated by the difficulties encountered in detailed calculations. As it has been said in a previous section, full 3D calculations with advanced physical models and detailed geometries are still difficult to carry out. Defining and improving the flow-regime definition methods, using the existing tests database, bring the analyst to something feasible and this is what induces the thermal-hydraulic community to follow this line. Some example will help understand the situations that are already tested.

In nonheated channels having at their inlet a two-phase flow, boiling will not be powered since no energy is added. Some energy exchange could take place depending on the subcooling of liquid and the super-heating of vapor.

In heated channels having at their inlet a two-phase flow (see e.g., Lahey and Moody, 1993) additional boiling could occur but this could be higher or lower depending again on the subcooling of liquid and the super-heating of vapor.

In horizontal channels having at their inlet a two-phase flow, gravity could produce phase separation depending on void fraction and velocity. Separated phases could easily get a different velocity for each phase. Friction between phases could appear so that they exchange momentum and alter again their relative velocities.

In vertical channels having at their inlet a two-phase flow, gravity could only produce phase separation if velocity is low and boiling is considerable.

The results of experiments fulfill two different purposes: characterizing flow regimes and establishing flow-regime maps.

A given group of experiments dealing with horizontal channels provides information useful to characterize the following flow regimes listed at increasing void fraction: bubbly, slug, annular mist, and dispersed (see Fig. 3.1). All these flow regimes are considered for this group at high values of mass velocity avoiding horizontal stratification in this first approach. Combinations of effects will come later along with comments on other relevant parameters. Characterization produced

by this first group of tests is the following:

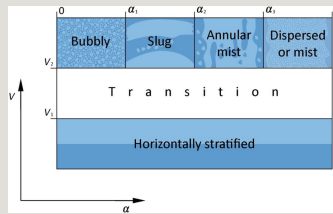


Fig. 3.1 Flow regimes in horizontal control volumes. Notes of lecture "Thermal-hydraulic Concepts" F. Reventos. UPC Master of Nuclear Engineering.

- Bubbly flow (very low void fraction): liquid appears as a continuous phase and vapor is formed by bubbles usually spherical and small.
- Slug flow (low void fraction): vapor bubbles are neither spherical nor small. Their diameter is close to that of the channel.
- Annular-mist flow (medium void fraction): liquid appears as a thick film in the vicinity of the wall and vapor is in the central part of the annulus.
- Dispersed flow (high void fraction): vapor appears as a continuous phase and liquid is formed by droplets or mist.

The considered group of experiments gives information helpful to derive the transitions from one regime to the other. Void fraction is the most relevant parameter to derive such transitions that are specific for horizontal channels. Despite being the most significant parameter, it is not the only one. This means that Fig. 3.1 is just quite a good approach that helps understand an approximate transition between different flow patterns. It is quite a good approach since some system codes are using similar flow-regime maps. Some authors suggest other more complex maps, and also research devoted to smooth flow pattern transitions is still an open item.

Other specific aspects of horizontal channels appear at lower values of mass velocity. The horizontally stratified flow occurs in situations where gravity becomes significant compared with inertia force, and thus produces phase separation. Once in a stratified pattern, if vapor velocity is increased, friction between phases will produce a wavy flow. Such flow does not appear in Fig. 3.1

map, since it appears after evaluating an additional parameter. Mass velocity and vapor-liquid relative velocity are the parameters driving specific transitions between flow regimes in horizontal channels.

Another group of experiments dealing with vertical channels provides the same information for vertical channels (see Fig. 3.2). At sufficient mean velocity to avoid vertical stratification and in pre-CHF (critical heat flux) situation, the basic flow regimes are the same than in horizontal channels.

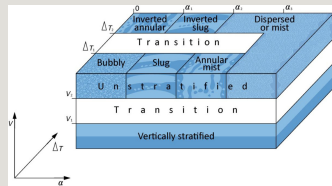


Fig. 3.2 Flow regimes in vertical control volumes. Notes of lecture "Thermal-hydraulic Concepts" F. Reventos. UPC Master of Nuclear Engineering.

Combining effects for vertical channels are more complex except for vertically stratified flow which is observed to appear for sufficiently low-mixture velocity. Transitions, in this case, depend mainly on one parameter.

The other specific aspect is connected with heat transfer (see Section 3.3) and has to do with a post-CHF situation. Since after CHF, an important amount of bubbles are formed and coalesced in the vicinity of the wall, each pattern will move to a new flow regime accordingly. Bubbly flow will move to inverted annular flow, slug flow to inverted slug flow, and annular-mist flow to dispersed flow. Transitions, in this case, depend not only on usual parameters like void fraction but also on the conditions of the heat transfer mode established at the wall.

At this point an important consistency check can be performed. Let us remind that ΔT is the difference between wall temperature and that of the bulk of the fluid. In the next section, it will be shown that once steam bubbles coalesce in the vicinity of the hot wall, heat transfer coefficient decreases and therefore ΔT increases. Inverted annular flow appears to be a thick vapor film in the vicinity of the wall and liquid is in the central part of the annulus, which is consistent with having a high ΔT and a rather low void fraction.

3.2.3.2 Natural circulation

Any closed circuit heated at its lower part and cooled at its upper part could start natural circulation. The driving force of such natural circulation is due to density difference between its cold and hot legs. Depending on the magnitude of density difference and the pressure drop along the circuit, equilibrium can be reached among involved parameters: power generated, natural circulation mass flow, and power extraction at the heat sink.

Such well-known phenomenon, which is widely used in heat transfer technology in conventional heat exchangers and evaporators, appears in NPPs in two different fields. The first one is related to some safety scenarios analyzed for current water reactors (D'Auria et al., 1991; IAEA, 2005) and the second one is related to third and fourth generation reactors (IAEA, 2009). The thermal-hydraulic analyst of nuclear plants needs to be able to face both. In a nuclear system such as the primary loop of a PWR, the reactor is supposed to act as thermal power generating device and SGs as heat sink.

3.2.3.3 Critical flow and choked flow

Increasing ΔP between upstream and downstream of a valve or junction results in the increase in the mass flow. Once ΔP becomes higher, a limiting value is observed after which mass flow rate does not increase anymore. Such value is called critical flow and the phenomenon occurs when fluid velocity reaches sound's speed. The phenomenon is due to a physical reason since mechanical perturbations propagate at sound's speed. Theoretical and empirical approaches are available to overcome the difficulty that appears when trying to solve momentum equation in such situation.

This phenomenon is extremely significant in nuclear safety since water reactors operate at a quite high pressure and so any break could produce a very high ΔP between the reactor coolant system (upstream of the break) and the reactor building space (downstream of the break). The accurate evaluation of mass flow through the break is crucial to match the right phenomenology of the scenario.

Mass flow rate when ΔP takes values within such critical interval is also called choked flow (due to the fact that it is limited or choked) and special models are needed in order to evaluate it (see Section 3.4.6).

3.2.3.4 Blowdown/reflood/rewet

Blowdown, reflood, and rewet are the three time phases expected to occur in a

large-break loss-of-coolant accident (LBLOCA) scenario (USNRC, 1987).

Blowdown is the first phase taking place just after the break. In this period a very high ΔP occurs between the reactor coolant system and the containment. For this entire time window, the break produces the driving force and an important amount of coolant mass is lost through the break at a time when pressure and saturation temperature rapidly decrease and vapor is formed. During the blowdown phase a quick dry-out is produced and heat transfer decreases a lot. Energy stored in the fuel results in a high peak of temperature.

Reflood is the second phase of an LOCA scenario. It starts when emergency core coolant injection brings water to the core. In this period, coolant in the core is vertically stratified, water level in reactor vessel increases progressively, and heat transfer comes to a rather complex situation. On the one hand heat transfer phenomena that appear are very different depending on their location, and on the other hand axial conduction in fuel becomes rather important due to temperature gradient. Water level in the core, in this situation is called quench front, increases at a rate that is a function of injected mass flow. Under the quench front, coolant is dominantly liquid (low void fraction) and bubbles are formed since cladding is still hot. In this situation flow regime is probably bubbly and convection mode nucleate boiling either subcooled or saturated. Above the quench front, coolant is dominantly vapor (high void fraction) and droplets are dragged by vapor produced under the front. In that other situation flow regime is probably dispersed or mist and convection mode is post-CHF.

Finally rewet is the last phase of an LOCA scenario. It starts when quench front reaches the upper part of the core. In this period, coolant is dominantly in liquid phase and heat transfer does not have any particular situation.

3.2.3.5 Reflux condenser mode

Reflux condenser mode is a cooling mechanism that could occur in a PWR usually in defined phases of small-break LOCA (SBLOCA) (Pretel, 1997). At a reduced inventory vapor is produced in the core and flows through the hot leg to SG U-tubes where it can condense, fall back to the vessel, and help cool the core. The secondary side of the SG has to be active (or at least full of water) to provide the condensing capability. Also, during such cooling mode counter current flow occurs in hot leg since vapor flows forward to the SG and liquid flows backward to the vessel.

3.2.3.6 Loop seal clearing

In the progression of an SBLOCA scenario, vapor is produced due to depressurization and heat addition from core decay power (Pretel, 1997). Such vapor could fill the upper parts of the primary side. More in detail, two different regions comprise such upper parts: on the one hand upper plenum, hot legs, pressurizer, and SG U-tubes and, on the other hand cold legs and downcomer upper ring. Liquid water is then cumulated in the lower parts of primary system especially reactor vessel and intermediate leg or loop seal. While vapor pressure in the upper head remains smaller than the compensating water column, loop seal water blocks its path and avoids the merging of water regions. During this interval, core uncover could occur. In the event of a pressure increase (due to additional vaporization) loop seal water could be cleared or displaced to cold leg and from there to the vessel. This phenomenon is known as “loop seal clearing.”

3.2.3.7 Steam binding

In the progression of an LOCA scenario, secondary pressure could become higher than primary pressure. This can happen after a loop seal clearing when vapor is the dominant phase of the fluid that fills the upper part of the primary side including SG U-tubes. In this situation such primary fluid could get heat from the secondary side and also from hot passive heat structures. As a consequence void fraction and primary pressure could increase and this could produce difficulties to the existing natural circulation or to the core level recover. This phenomenon is known as “steam binding.”

3.2.3.8 Boron dilution accidents

Boric acid is used as a soluble neutron absorber in the primary coolant of pressurized water reactors. In normal reactor operation the needed boron concentration is maintained by the volume control system. The event in which boron concentration in the core is accidentally reduced and produces the start of a reactivity excursion is called boron dilution accident (Freixa, 2007; Freixa et al., 2007, 2009a).

The most usual classification of boron dilution transients considers:

- External boron dilution. In such transients an injection of unborated water from outside the primary cooling system occurs
- Inherent boron dilution. In such transients a separation of primary coolant into highly borated water and almost boron-free water occurs. This process takes place

by evaporation and condensation.

Thermal-hydraulic analysis is highly involved in boron dilution transients. Both the build-up of a nonborated slug in the primary system and its transport to the core are connected with thermal-hydraulic phenomena. When the level in the reactor pressure vessel is low enough and core temperature is such that the coolant in that region boils, reflux-condensation conditions are established. Under such conditions, the steam produced condenses in SG tubes and almost boron free water is collected in a region of the primary system (usually in the loop seal) forming a nonborated slug. If a later natural circulation is established or a reactor coolant pump is restarted, the slug can be transported to the core and produce a reactivity excursion.

Experiments related to boron dilution scenarios were carried out in the last decade in the framework of two OECD projects, OCDE-SETH Project (2001–04) (OECD/NEA/CSNI, 2004) and OCDE-PKL Project (2004–07) (e.g., Mull et al., 2007; Umminger et al., 2012). Tests were performed at PKL facility and cover the most relevant involved scenarios. Analytical activities were also included in the projects (Freixa et al., 2009b; Reventós et al., 2008b).

3.2.3.9 Boron dilution/deboration

Boron dilution is the process where a local decrease in boron concentration in primary system occurs. Deboration is the process where a net loss of boron from primary system occurs, which implies a decrease in average boron concentration. In the same way, the following definitions are accepted as well: boration (the opposite of deboration), boron concentration recovery (the opposite of boron dilution), deboration rate (the rate of deboration), and dilution rate (the rate of boron dilution). These definitions were proposed by D'Auria et al. (2005), and are nowadays accepted within the international community.

3.2.4 Models and approximations

3.2.4.1 Homogeneous model

Solving two-phase flow equations is a complex task; different simplified approximations are available by now; among them are the homogeneous model, the separated flow model, and the drift-flux model.

The assumptions of the homogeneous model are the following:

- Liquid and vapor have equal velocities

- Liquid and vapor are in thermodynamic equilibrium
- A single friction factor suitable for the mixture is used

The model could produce suitable results not only when the differences between the properties of the liquid and vapor are not important (in the vicinity of the critical point) but also when the mass velocity of the two-phase flow is very high and flow regime is either bubbly or misty flow.

3.2.4.2 Separated flow model

The assumptions of the separated flow model are the following:

- Liquid and vapor velocities are not necessarily equal
- Liquid and vapor are in thermodynamic equilibrium
- An empirically correlated friction factor multiplier is used

The separated flow model has been successfully used for calculating the pressure drop in flow channels. As a general statement this model fits better at low mass velocity.

3.2.4.3 Drift-flux model

The drift-flux model is built on the concepts of drift velocity (which is the relative velocity between phases) and drift flux (which is the volumetric rate at which vapor passes forward or backward through the unit of area normal to the traveling flow).

The drift-flux model is currently used in different codes in thermal hydraulics of nuclear systems and other industries. It helps in analyzing systems behavior for quite different transient conditions. Simplicity and robustness are its most significant advantages.

3.2.4.4 Lumped parameter models

As a general statement lumped parameter models are built replacing in a more detailed model the behavior of a specific parameter by a tested correlation or logic. Its use is justified when the detailed code run is time consuming. The validity of the approach relies on that of the correlation or logic involved.

3.2.4.5 Two-fluid model

The state-of-the-art knowledge on thermal-hydraulic two-phase flow predictions is currently in between the approximations depicted above and the detailed simulations produced by CFD codes.

On the one hand, basic models (like homogeneous, separated flow, drift-flux model, or even some lumped parameter models) are good tools that help understand phenomena and calculate some specific scenarios, but they do not bring enough detail in many other situations. On the other hand, CFD studies, based on more advanced physical models, nodalizations, and numerical methods, are appropriate for certain aspects but they have two main drawbacks: a high computing effort is needed, and their validation process for usual nuclear safety scenarios is still not fully completed.

Nowadays, the most commonly used option is the so-called two-fluid model, which other authors may refer as the “flow pattern model” or even the *UVUT* model (where *U*=unequal; *V*=velocity; *U*=unequal; *T*=temperature). This approach allows the two phases to have unequal velocities and temperatures and it has the capability of building a more accurate picture of the thermal-hydraulic behavior of the scenario. This is the approach followed in most of the system codes used today.

Summarizing, since the so-called system codes are considered to be the main repository of expertise in the field of thermal hydraulics of nuclear systems, they are a reliable picture of the current option in the area. Such codes usually employ quite complex techniques that are nonhomogeneous and nonequilibrium two-phase flow models. Their two-fluid equations are formulated using volume and time-averaged parameters of the flow. Friction and heat transfer are formulated using bulk properties and empirical heat transfer coefficients. Flow regime information is supported by empirical results and accurately implemented.

3.3 Concepts involved in heat transfer developments

3.3.1 Context

3.3.1.1 Importance of heat transfer developments

The analysis of water reactors thermal hydraulics needs to consider heat transfer mainly in fuel elements in order to produce results needed by safety analysis (Kutateladze, 1963). Predictions of temperature distributions in fuel pins and reactor structures must be accurate since acceptance criteria of safety analysis are defined by means of limiting values of thermal parameters.

3.3.1.2 Scope

Most of the results needed by safety analysis and dealing with heat transfer are related to fuel. As a consequence, most of the efforts dedicated to improve predicting capabilities are also devoted to fuel. Heat transfer in fuel includes heat conduction, heat convection, and heat radiation.

Other areas and components of power plants are also needed for heat transfer calculations, among them: passive heat structures, electrical heaters, heat losses to environment, and heat exchangers.

Passive heat structures are usually metallic structures like the internals of reactor vessel or vessel walls or others in contact with the fluid of the analyzed system. Despite being passive, which means that they are not generating heat, the need of taking them into account is that they have an impact on certain scenarios storing thermal energy in certain periods of the transient and releasing it later.

Electrical heaters, like pressurizer heaters, are important for energy balances and for controlling pressure.

Heat losses to environment are sometimes negligible, for instance in a full size plant, but in experimental facilities this is not the case.

Finally, heat exchangers, mainly SGs, are crucial in many scenarios. Sometimes they are the essential components useful to perform an emergency function, and sometimes they are the components in which the initiator takes place, like in SG tube rupture.

3.3.1.3 1D/3D

The decision of using 1D or 3D option for a given calculation is rarely straightforward. 3D options could be better as a general statement since they are more detailed but sometimes it is not the case either because they do not add any specific interesting output to the established engineering goals or because their validation process is not complete and so their results are uncertain.

Heat transfer in nuclear fuel is a case in which 1D options work properly for many significant scenarios. Given the geometry and dimensions of a fuel rod, it is quite correct to consider that heat is transferred following the radial direction and almost no axial transfer takes place. This statement is valid for most of the involved

scenarios. Reflood situations are identified as different. During the reflood cold water fills only the lower part of the vessel while most of the core is noncooled and at high temperature. The axial temperature gradient is high and axial heat conduction is considerable, so a 3D option is needed.

Using 1D or 3D option is a decision to be made case by case.

3.3.2 Parameters and concepts

3.3.2.1 Related to power generation

Three different parameters are helpful for dealing with power generated or transferred: volumetric power, heat flux, and linear power.

Volumetric power (q''') is the thermal energy generation rate per unit of volume. Usually defined for the fuel pin, it is used in the general equation of heat conduction.

Heat flux (q'') is the rate of thermal energy transferred through a surface per unit of area. Usually defined for cladding surface, it is used to evaluate heat transfer by convection.

Linear power (q') is the thermal energy generation rate per unit of length of fuel rod. It is often used in safety statements.

3.3.2.2 Related to heat conduction

The general equation of heat conduction is obtained combining Fourier's law

$$\text{Heat flux} = -K(\text{temperature gradient})$$

$$q'' = -K \nabla T$$

with a balance equation

$$q'''(r,t) - \nabla q'' = \delta / \delta t (\rho c T)$$

$$q'''(r,t) - \nabla(-K \nabla(T(r,t))) = \delta / \delta t (\rho c T)$$

where K is the thermal conductivity and c is the specific heat of the solid where generation and conduction take place.

Usually the medium is isotropic and so, K is a scalar, in many cases only dependent on temperature. If the medium is not isotropic, K becomes a tensor and more complex options have to be considered.

If the equation is applied to fuel, $q''' \neq 0$ and the general equation will be integrated after calculating it as it follows:

- At power, it will be supplied by neutron physics formulation:

$$q'''(r,z) = K_f \Sigma_f \Phi(r,z)$$

where $\Sigma_f \Phi$ is fission rate at r, z location and K_f is the factor converting fissions/s in W.

- After a scram, either by a devoted table (like ANS79):

$$q''' / q_0''' = f(t_f, t_a)$$

where t_f =irradiation time and t_a =cooling time or by a specific code dealing with decay heat.

If the equation is applied to gap, $q'''=0$ and the general equation will be integrated considering it as a region with a given thermal resistance. The evaluation of such

resistance is rather complex and usually is not performed on line since it is based on the results of thermal-mechanical analysis of fuel rods as function of fuel burn-up.

If the equation is applied to cladding, $q'''=0$ and the general equation will be integrated accordingly.

3.3.2.3 Related to heat convection—general aspects

Heat convection is a mechanism of heat extraction from a hot wall by means of a fluid having a certain movement. The mechanism involves also molecular diffusion and the movement of the fluid could be forced (forced convection) or free (natural convection). Heat flux extracted by convection follows Newton's law:

$$q'' = h_s (T_{\text{wall}} - T_{\text{bulk}})$$

where h_s =convection heat transfer coefficient; T_{wall} =temperature of the hot wall (cladding) and T_{bulk} =average temperature of the fluid in the considered area.

Evaluating the convection heat transfer coefficient is rather complex and has been the object of important experimental activities. On the one hand, it depends on the convection mode (in some code manuals ambiguously called heat transfer mode), and on the other hand, its range of variation is very wide. Its units are W/(K m²) and some approximate values can be between 35,000 and 55,000 in a PWR nominal steady state and up to 5000 in one-phase natural circulation or 50 or less in a dry-out situation.

Convection mode depends on the mechanism of heat extraction. Besides the already mentioned conditions of movement and diffusion, there is another relevant aspect that becomes an additional difficulty in evaluating the coefficient; this is the vicinity of saturation. The convection modes resulting from this vicinity have a certain relation or proximity with flow regimes but they are essentially something different. The goal of the former is calculating heat transfer coefficient while that of the latter is allowing two-phase flow detailed studies.

Establishing a correlation for each and every heat transfer coefficient using data produced in specific experiments culminates the activities devoted to evaluate them.

3.3.2.4 Related to heat convection—pre-CHF convection modes

Convection to single phase liquid is the basic convection mode occurring when bulk temperature is far from saturation. It takes place in PWR at nominal steady state for most of the fuel rods mainly nearby core inlet and also for pins having a medium or low linear power (see Fig. 3.3).

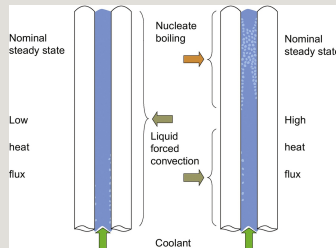


Fig. 3.3 Convection heat transfer modes at a PWR nominal steady state. Notes of lecture “First approach to reactor case” F. Reventos. UPC Master of Nuclear Engineering.

If bulk temperature is close to saturation (if ΔT_{SUB} is about a few °K) and that of the wall is about saturation, bubbles could be built up in contact with the hot wall extracting the needed latent heat from it. Since fluid is subcooled, the built up bubble could easily mix with liquid water and thus help general heat extraction. This mechanism occurs under certain conditions and is extremely positive since it helps heat transfer. As a consequence the temperature of the wall could stabilize at a lower value. This mechanism is called nucleate boiling (or subcooled nucleate boiling) and the heat transfer coefficient is greater than in previous situation. This convection mode takes place in PWR at nominal steady-state fuel rods having a higher linear power (see Fig. 3.4).

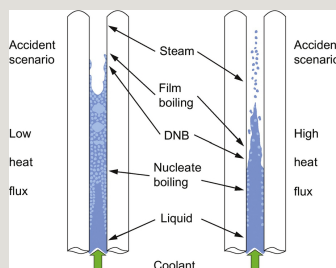


Fig. 3.4 Convection heat transfer modes in an accident scenario. Notes of

If bulk temperature is saturation (and so ΔT_{SUB} is 0) and that of the wall is slightly higher than saturation, bubbles in contact will be built up easily. Similarly bubbles could easily mix with liquid water and also help general heat extraction. The mechanism is then called saturated nucleate boiling. This convection mode takes place in most of the fuel rods of a BWR at nominal steady state as well as in accidental scenarios progression.

3.3.2.5 Related to heat convection—CHF/boiling crisis/post-CHF convection modes

The progress of the built up of bubbles at the hot wall and its subsequent coalesce produces a partial film covering its surface with the result of a strong reduction of heat transfer coefficient (Arias, 2009; Arias et al., 2009; Arias and Reventos, 2010). This phenomenon is known by many authors as boiling crisis and the value of heat flux at which it appears is called critical heat flux. The phenomenon could take place under three different circumstances. When previous heat transfer mode is nucleate boiling at a subcooled bulk temperature, it is called “departure from subcooled nucleate boiling” (DNB subcooled); when previous heat transfer mode is nucleate boiling at a saturated bulk temperature, it is called “departure from saturated nucleate boiling” (DNB saturated); and finally at liquid high enthalpy, it is called “dry-out.”

It is a phenomenon of high relevance for safety. When it takes place, the sudden reduction of heat transfer could produce the so-called burnout or physical destruction of the hot surface.

A huge amount of experiments have been performed to clarify the physics of the phenomenon itself and also to characterize the post-CHF heat transfer modes. Again the results of such experiments have been useful to establish correlations and look-up tables valid for the corresponding predictions.

3.3.2.6 Prandtl and Nusselt numbers

Besides Reynolds and Froude numbers already introduced in a previous section the most used dimensionless numbers in heat transfer developments are Prandtl number (Pr) and Nusselt number (Nu).

Prandtl number (Pr) is defined as:

$$Pr = \mu \times C_e / k$$

It is the ratio between momentum diffusion and heat diffusion.

Nüsselt number ($Nü$) is defined as:

$$Nü = h_s \times D_h / k$$

It is the ratio between convective and conduction heat transfer.

3.3.2.7 Related to heat radiation

The interest of thermal hydraulics of nuclear systems in radiation heat transfer is limited to the need of computing the rate of radiation exchanged between hot surfaces in an advanced phase of an accidental scenario assuming no participating media. Such interest is limited since disregarding the effect of heat radiation is usually slightly conservative and traditionally it has been ignored. The surfaces that might cool down by heat radiation need to have a line-of-sight or a reflection path through which they can communicate. The central problem is calculating view factors.

3.4 Additional concepts involved in analytical thermal hydraulics

3.4.1 Nuclear factors

Nuclear factors are ratios between parameters related to power generation. They are useful to understand radial and axial power distortion and helpful to produce a quick estimation of heat transfer on different areas of the reactor.

Radial nuclear hot channel factor (F_{RN}) is defined as the ratio between the average heat flux of the hot channel and the average heat flux of the whole core. A typical value of such factor at the beginning of cycle in a PWR can be about 1.5. At the

end of cycle such value is clearly reduced. In a similar way, radial nuclear channel (i) factor is the ratio between the average heat flux of the channel (i) and the average heat flux of the whole core.

Axial nuclear hot channel factor (F_{ZN}) is defined as the ratio between the maximum heat flux of the hot channel and the average heat flux of the hot channel. A typical value of such factor at the beginning of cycle in a PWR can be about 1.5. At the end of cycle such value is clearly reduced. In a similar way, axial nuclear channel (i) factor is the ratio between the maximum heat flux of the channel (i) and the average heat flux of the channel (i).

Total nuclear heat flux factor is defined as the ratio between the maximum heat flux of the hot channel and the average heat flux of the whole core. A typical value of such factor at the beginning of cycle in a PWR can be about 2.25 (obtained as 1.5×1.5). At the end of cycle such value is clearly reduced.

3.4.2 Engineering factors

Engineering factors are ratios between parameters related to two significant engineering concepts: tolerances and cross-flow paths. They are useful for a quick estimation on the impact of such phenomena. Engineering tolerances are one of the sources of uncertainty having an impact on heat transfer; the “engineering tolerances factor” (F_{QE}) is a simple figure that accounts for this. A typical value for F_{QE} is 1.03. Such factor helps computing the so-called total power peaking factor that has a typical value of 2.32.

$$F_Q^E = \text{Engineering tolerances factor}$$

$$F_Q = \text{Total power peaking factor}$$

$$F_Q = F_Q^N \times F_Q^E$$

The “enthalpy-rise hot channel factor” accounts for the effect of cross-flow paths in a PWR core. The mass interchange between parallel channels results usually in smoothing enthalpy rise. In an ideal situation assuming that coolant would be strictly associated to its fuel rod, $F_{\Delta H}$ and F_{RN} are identical. In practice cross flows produce a mixture among channels leading to moderate values of ΔH and then $F_{\Delta H}$ is slightly lower than F_{RN} . Typical values are 1.53 ($F_{\Delta H}$) and 1.56 (F_{RN}).

$$F_{\Delta H} = \Delta \text{Enthalpy}_{\text{Max}} / \Delta \text{Enthalpy}_{\text{Average}}$$

$$F_{\Delta H_i} = \Delta \text{Enthalpy}_i / \Delta \text{Enthalpy}_{\text{Average}}$$

3.4.3 System codes

System codes are devoted to solve six balance equations of mass, momentum, and energy (for liquid and steam). Such resolution is supplemented by a suitable set of closure laws. Equations are coupled with heat transfer models and sometimes with neutron kinetics coding. The two-phase flow field is organized in a number of control volumes connected by junctions. Thermal-hydraulic components such as separators, valves, accumulators, or pumps are also coded in order to complete the simulation of the described system.

Typically, system codes follow a finite difference method based on staggered grids to avoid the checkerboard problem (artificial pressure oscillations). Depending on the code, there are many options for temporal discretization. Options are chosen, with the goal of compromising a relatively large time step and a moderate computational cost. Spatial discretization is typically defined as a combination of the central difference and the upwind (donor-like) numerical schemes in order to guarantee maximum stability of the simulation.

The information describing the plant or the facility is read by the code in a file called “input deck.” Initial and boundary conditions of the scenario to be analyzed

are also included in the input deck. Nodalization is also in the input deck.

The results produced by code runs could be written down in an ASCII or binary file. The former can be directly accessed and the latter can be used to produce time trends of the key parameters or the results of the calculation.

Relap5 (developed by USNRC and USDOE), Cathare (developed by French CEA), Trace (developed by NRC), and Athlet (developed by German GRS) are the most used system codes.

3.4.4 Closure laws or constitutive equations

Closure laws or constitutive equations are the set of equations that handle mass, momentum, and energy exchanges between phases and also between each phase and the walls of the involved control volumes. Such laws, which are rigorously needed for solving the whole set of equations, are usually obtained empirically and based on separate effect experiments typically designed specifically for the purpose (Bestion, 1990).

Heat and mass transfer along with friction at the interface and from (or to) the wall are the most relevant closure laws.

3.4.5 Heat transfer correlations/look-up tables

Empirical information, usually about heat transfer, is provided to the code by means of correlations or look-up tables. Correlations exist for many important parameters of physical models. Technical literature supports and validates this information. This is the case of Dittus and Boelter (1930) correlation for heat transfer under forced convection and also for correlations like those of Kays, Churchill-Chu, Chen (Chen, 1966), Chen-Sundaram-Ozkaynak (Chen et al., 1977), Bromley (Bromley, 1950), Nusselt, Shah, or Colburn-Hougen. Look-up tables are used in system codes as another option to supply the values of some empirical information. They fit better some more complex functions of multiarguments. This is the case of Groeneveld look-up table for CHF evaluation (Groeneveld, 1973; Groeneveld et al., 1986, 1996).

3.4.6 Special models

System codes use to include special models. Such models are called by the main code when needed and interact with the equations to be solved in order to complete the description of the simulated scenario. Due to their relevance the following are briefly mentioned or depicted: choked flow, user-supplied hydrodynamic losses,

abrupt area change, and countercurrent flow limitation (CCFL).

As it has been anticipated in a previous section, most system codes include as special model a choked flow model. Such model is used to predict if the flow is choked at the considered junction (usually a break or a nozzle) and to calculate the expected mass flow under the special conditions established.

The issue of form hydrodynamic losses in junctions is related with what has been previously said in the section devoted to pressure drop and it is needed of some flexibility. In order to make available such flexibility, most system codes have a general user-specified form loss coefficient as an option. User-specified coefficients can be introduced and used by the code. This special model opens for the user the possibility of applying form coefficients directly taken from experiments, derived from its own calculations or from detailed codes.

Another special model, the so-called abrupt area change model, is related to the previous one. Quite often the code user can be connecting two nodes of different cross area in a junction having a sharp or abrupt edge. In such sudden enlargement or contraction of the equivalent pipe the known vena contracta effect will occur. This special model is often implemented with the purpose of avoiding repetitive calculations of the corresponding coefficients.

CCFL is a phenomenon that could occur in junctions with a partially closed structure in a situation having an ascending developed vapor flow and a countercurrent fall-back liquid. Such structures could include orifices, the upper core tie plate (Glaeser, 1989), SG tube support plates, or the entrance to the tube sheet in the SG at the inlet plenum. At low values of vapor mass flow rate, both countercurrent flows are perfectly compatible. In the event of increasing vapor mass flow, this could limit or even stop the gravity drainage of liquid.

The special models usually implemented in system codes are providing acceptable results if the user supplies the needed empirically determined coefficients that use to be specific for the involved detailed geometry.

3.4.7 Special components

System codes use to include special components. Such components are control volumes or junctions with some specific additional conditions interacting with the equations to be solved. Such specific conditions dependent on the component itself. Examples are shown below.

A SG separator works, providing centrifugal separation of liquid and vapor. Some

system codes include a nonmechanistic model that consists of a special volume with junction flows determined as a function of void fraction. At high void fractions the vapor junction ejects only vapor; at medium or low void fraction an empirical curve provides the results.

Valves are special junctions. They can be classified into different kinds, among them: those that open or close in a time step and those that open or close following the value of a given variable. Both cited kinds are driven by selected variables that connect hydrodynamics with protection and controls.

Accumulators are modeled in system codes as lumped-parameter component. Usually, a simple ideal gas equation of state is used to model the gas behavior during the discharge.

Pump components are also a special volume. The pump model is connected with the two-fluid hydrodynamic model and the head term appears in the momentum equation. Homologous curves provide pump information.

3.4.8 Nodalization/nodalization diagram

Spatial discretization of the two-phase flow field, in which equations are solved, is organized in control volumes connected by junctions and it is called nodalization. Sometimes the meaning of the word nodalization is extended to the whole set of parameters and information supplied by the user.

Nodalization diagram is a drawing or illustration showing control volumes with their connecting junctions. Such diagrams, when they have enough detail and are properly set, become very useful to understand, at first glance, the involved calculation.

3.4.9 User effect/good practices

An initial characterization of user effect was given in 1993 by Aksan et al. (1993).

Later on, in 1998, it had been defined by OECD/NEA as it follows: “User effects are any differences in calculations that use the same code version and the same specifications for a given plant or facility.” The document giving such definition (Ashley et al., 1998) analyzed also the main reasons explaining the appeared difference and established also a series of “good practices” devoted to avoid or minimize the user effect. Good practices are based on user training (D’Auria, 1998;

Petruzzi et al., 2008), user discipline, and quality assurance, and in a wider context with organization requirements and safety culture.

3.4.10 International standard problems

International standard problems (ISPs) are comparative exercises in which predictions or recalculations of a given physical problem with different best-estimate computer code are compared with each other and above all with the results of a carefully specified experimental study. Such exercises are organized within OECD/NEA framework since 1975 to increase confidence in the validity and the use of the different tools that are used in assessing the safety of nuclear installations. Extensive information is available. It includes reports on particular exercises (Kimber et al., 1998), compendium of groups of exercises (OECD/NEA/CSNI, 1997), or even articles on the results of revisiting any exercise with updated codes and models (Freixa et al., 2015a).

3.5 Additional concepts involved in experimental thermal hydraulics

3.5.1 Separate effect tests

Each separate effect test (SET) facility has been designed to investigate the local occurrence of a particular phenomenon. Usually, such facilities represent physically either some relevant zones of the NPP or some geometry in which the studied phenomenon can be identified and studied. The results of the experiments performed are used to validate the models created to describe the studied phenomenon. The final goal of the whole thing is to include the model in a system code.

The SET Validation Matrix is a document (OECD/NEA/CSNI, 1993), established under the auspices of OECD, devoted to identify the phenomena covered by the matrix and to give an outline of existing facilities and test types. The document manages to show a cross-reference matrix considering relationship between phenomena, test type, and facility.

3.5.2 Integral effects tests/integral test facilities

Each integral effects test (IET) performed in an integral test facility (ITF) has been designed to investigate the behavior of its reference plant under accidental conditions. All the significant components and systems of the involved NPP are reproduced usually at lower scale. For such reason scaling considerations have to

be considered in order to assure the suitability of the results. The expected results are the response of the plant to the simulated initiating events. The results are also used to improve models or to check code capabilities.

The IET Validation Matrix is a document, established under the auspices of OECD, devoted to identify the scenarios covered by the matrix and give an outline of existing facilities and test types.

PKL facility in Erlangen (Germany), LSTF in Tokaimura (Japan), and ATLAS in Daejeon (Korea) are three relevant ITFs currently in operation.

LOBI facility in Ispra (Italy), LOFT in Idaho Falls (Idaho, USA), and BETHSY in Grenoble (France) were ITFs operating in the past and currently dismantled.

3.5.3 Analytical support to experimental thermal hydraulics

The analytical support to experimental thermal hydraulics (Umminger et al., 2012) is based on calculations simulating the tests. Pretest calculations are usually performed before running the test and are devoted to complete test preparation or to clarify uncertain aspects of what is expected. Posttest calculations are performed after the test (e.g., Reventós et al., 2012). The results obtained are compared with experimental data and the comparison is useful in code and nodalization validation. Posttest can be open or blind. Both are helpful for validation and blind calculations have an additional outcome since they show the actual capabilities of predictive analysis.

3.5.4 Databases of experimental thermal hydraulics

The importance of experimental data production for code validation is clearly accepted. The databases of test results must be preserved and properly organized. Data need to be accessed and retrieved easily by analysts involved in their use (Addabbo et al., 2002).

The information stored in such databases includes basically files containing experimental data at different time frames (ASCII or binary formats) in order to facilitate the comparison between prediction and test results. Also typical documents related to experiments, among them the well-known Quick-Look Report (QLR) and Experimental Data Report (EDR), complete the information associated to each test.

The STRESA (Storage of Thermal Reactor Safety Analysis Data) web-based informatics platform is a good example of how such database can be implemented

(Pla et al. 2015, 2016b). In its current version STRESA is forming a network of nodes and storing data of an important amount of relevant thermal-hydraulic tests.

3.5.5 Scaling/scaling issue/addressing the scaling issue

Scaling in nuclear-thermal hydraulics constitutes the topic of an important document, completed in 2016 by a Specialist Scaling Group (SSG) formed in 2013 by the WGAMA (OECD/NEA/CSNI, 2016c). The document testifies not only the importance of scaling in nuclear technology, but also the controversial evaluations of scaling-related findings by the scientific community.

“Scaling,” “scaling issue,” and “addressing the scaling issue” indicate actions, methods, and techniques aimed at connecting the parameter values related to experiments with NPP conditions. Scaling is the process of demonstrating the applicability of any parameter value to the reactor conditions. Addressing the scaling issue refers to the process of demonstrating the applicability of data from models to prototype.

A general guideline for addressing the scaling issue can be found in USNRC code scaling, applicability, and uncertainty method (CSAU) (USNRC, 1989). It is an extensive work aimed at providing a suitable framework for uncertainty and accuracy analyses by the use of best-estimate codes. This methodology was presented as a response to the revision of the 10CFRpart 50 ECCS rule (USNRC, 2015), for which the evaluation of the acceptance criteria could be done using realistic codes under certain conditions, literally:

- Uncertainties in the analysis method and inputs must be identified and assessed so that uncertainty in the calculated results can be estimated
- There is a high level of probability that the criteria would not be exceeded

The document faces the scaling issue emphasizing the need of considering two main aspects:

- To evaluate the capability of BE codes to scale-up processes from reduced scale test facilities to full-scale NPPs
- To quantify the effects of scale distortion and/or a limited data base, on code uncertainty to calculate a safety parameter of interest, for example, peak clad temperature

Related to these concepts, several scaling criteria and scaling analysis methodologies can be found in the technical literature. Regarding scaling criteria and design of experimental facilities, one can find terms like linear scaling, power-to-volume scaling, and modified time preserving scaling. Regarding scaling analysis and experimental data extrapolation, hierarchical two-tiered scaling, Ishii three-level scaling, and fractional scaling analysis are the most common methodologies. Some of these techniques are depicted below.

3.5.6 Power-to-volume scaling

Power-to-volume scaling (or volume scaling) method conserves the time, length (or height), velocity, and heat flux equivalently to those of the prototype. A test facility designed following power-to-volume scaling has a full-height scale, while area and volume of the facility are reduced with the same scale. Experiments involved conserve also pressure, temperature, and time.

3.5.7 Hierarchical two-tiered scaling

Hierarchical two-tiered scaling (H2TS) is a comprehensive, systematic yet practical, auditable, and traceable methodology for evaluating the applicability of the experimental data from scaled-down facilities to NPP conditions, and hence, implicitly, the capability of the system codes and their special models (because they are qualified just at facility level) to scale-up TH data to full-scale plant conditions. It is based on the premise that each TH process that occurs in a system can be characterized by three parameters, volumetric concentrations, transfer areas, and time scales; and that all of them can be included just in the timescale parameter dependencies; hence, that is possible to determine TH process relevance with just one parameter. H2TS is divided into two levels of analysis: the “top-down system scaling analysis” and the “bottom-up process scaling analysis.”

3.5.8 Ishii three-level scaling

Ishii three-level scaling approach is a systematic methodology for designing IET facilities as well as analyzing their generated experimental data relative to prototype conditions. The bases of the methodology are the conservation principles and the constitutive laws. This approach is divided into three levels of analysis, integral system scaling, control volume scaling, and local phenomena scaling. The first two levels correspond to the top-down scaling and the third level represents the bottom-up scaling.

3.5.9 Fractional scaling analysis

Fractional scaling analysis (FSA) is a quantitative methodology based on the H2TS approach that has been developed to facilitate two aspects:

- scaling up of time-dependent evolution processes involving an aggregate of interacting modules and processes (such as a NPP)
- integration and organization of the information and data of interest to NPP design and safety analyses.

3.5.10 Scaling distortion

Scaling distortion refers to any discrepancy between the scaled and the referenced plant parameters. In a perfectly scaled experiment all the scaled parameters are equally reproduced at the intended scaled time. Only in very limited cases, like very specific SETs, perfect scaling is perfectly feasible. Usually, tests are rather complex and they involve phenomena that need diverse scaling criteria for the design of the scaled-down facility.

Following what is established in Buckingham π theorem, equations and laws can be written in nondimensional form. A long list of nondimensional groups can be generated to define similarity conditions. Nevertheless, all of them cannot be matched simultaneously in the design of scaled-down facilities, and distortions will appear once the analyst or the designer decides which are the most relevant to be preserved. Analysis and justification of such distortions is one of the most significant purposes of current scaling developments.

3.5.11 Counterpart tests/similar/special CP

Counterpart (CP) tests are tests performed in IET facilities of different scale with the same initial and boundary conditions. Their purpose is to study effect of scale in the behavior of the plant. If tests are properly designed and facilities have close configurations, similarities in the time trends of important parameters have to appear and the source of distortions have to be identified and explained. Such distortions have to be mainly due to differences in configuration (Martínez-Quiroga, 2014; Martinez-Quiroga et al., 2014; Martinez-Quiroga and Reventos, 2014).

Similar tests refer to some tests which, although they do not meet exactly the conditions of a CP test, have a great similarity in the initial and boundary conditions. Similar tests are at least useful to corroborate similarities expected in

time trends of main parameters.

A special CP test is a kind of scaled-down SET designed using full-scale test data as reference and having the goal of clarifying the same phenomena and processes. In special CP test, significant phenomena may be recorded at a higher level of detail.

3.5.12 Using system codes in scaling analysis

The use of system codes can help at every step of the analysis of complex transients. As said in OECD/NEA/CSNI (2016c): “System codes can reduce the cost of manpower by quickly doing evaluations that are done ‘by hand’ in H2TS and FSA. System codes are not an alternative to scaling analysis, but they are a tool for assisting scaling analysis and solving problems. For example, the identification of the phases of a transient may be easier after some preliminary simulations of the transient using system code, even before having simulated the transient with an appropriate IET.”

System codes also can identify (or help identify) the dominant processes and predict how the relative importance of each process may change all along the transient. They open the possibility of investigating phenomena that may be of second order importance, but might require some attention.

3.5.13 K_v -scaled calculations

A K_v -scaled calculation is a system code simulation in which defined IET conditions are scaled up to an NPP nodalization in order to reproduce the same scenario. It allows the behavior of the NPP and ITF nodalizations to be compared under the same conditions. Then it may be used to check the validity of the NPP nodalization and to improve it when needed.

In the framework of qualifying the NPP nodalization and meeting its quality assurance procedures, K_v -scaled calculations, introduced by D'Auria et al. (1995), are of great value because they allow testing their capabilities and the plant's response under accident conditions. One of the important points of this activity relies in calculating the NPP scaling factor (the K_v -factor) that was commonly computed as the ratio between the volume of the primary liquid of the NPP and the ITF. In addition, K_v -scaled calculations are also of great value for extrapolating code accuracy as described in the UMAE methodology. Many examples are available (e.g., D'Auria and Galassi, 2010).

Finally, the UPC scaling-up methodology (SCUP) (Martinez-Quiroga and

Reventos, 2014; Martinez-Quiroga et al., 2014; Martínez-Quiroga, 2014) established further the development of K_T -scaled calculations. Such method is a systematic approach for qualifying NPP nodalizations by extrapolating ITF posttest simulations. It includes defining and using concepts like “hybrid nodalization” and “scaled-up nodalization.”

Both concepts were shown to be necessary for justifying the qualitative discrepancies related to K_T -scaled calculations. “Scaled-up nodalizations” allow determining the scaling effects related with the criterion applied in the design of the ITF and “hybrid nodalizations” help the user to establish how differences in design modify the results of the experiment. To carry out these calculations specific software has been developed (Martínez-Quiroga, 2014).

3.6 Concepts connected with DB and licensing basis

3.6.1 Structures, systems, and components

The concepts of “structures,” “systems,” and “components” (SSCs) are well known and widely used in the current terminology of engineering and design. In this sense no definition is needed for each of them, but often, design or safety requirements are specified as applicable to all them. This is the case of Specific Safety Guide No. SSG-30, which establishes a set of requirements for all SSCs that are important for safety.

3.6.2 Acceptance criteria/design criteria

Both wordings are referred to the same essential functional and safety requirements of the design.

The words acceptance criterion and acceptance criteria are preferred when pointing out a statement that establishes the conditions that must be fulfilled by the designed SSC. It is used and defined in the DB.

The words design criterion and design criteria are more used in legislation, in standards, and in the licensing basis (see below). The NRC General Design Criteria established in Appendix A of 10CFR50 are a good example of general design criteria while velocities of fluids in a pipe established in an engineering handbook are a good example of detailed design criteria.

3.6.3 Design basis

The DB is defined as a set of conditions, needs, and requirements (including legal requirements) taken into account in designing a facility or product. The concept can be applied to a particular SSC or to the whole plant. The DB establishes the essentials of the engineering procedures needed to design the plant.

The DB of SSC is an engineering document (or part of a document) devoted to correlate the involved SSC with the scenario/s used for its design along with the criterion or criteria that will be considered in the corresponding acceptance.

Such scenarios and acceptance criteria are usually supported by standards, by regulations, or by engineering handbooks. For brand-new or very specific SSCs the supporting information could be also particular.

In the design development following what is established in the DB, a calculation and/or an engineering judgment must demonstrate that in each scenario, for a given dimensioning of the involved SSCs, the acceptance criteria are fulfilled. The DB is or has to be so, an adequate and self-standing guide for design activity. The DB has to be the central guideline for designing. For such reason it must be a concise document.

Additionally, the DB must classify SSCs and establish if they are safety related or not. It also facilitates performing design verification.

3.6.4 Licensing basis

A licensing basis is a complete and comprehensive set of regulations in force from which DB statements are retrieved. It is complemented by the set of terms and conditions imposed on the license and regulatory commitments adopted. It provides general criteria, scenarios, detailed criteria, standards, and codes.

Licensing basis is generic to an important extent and only plant specific in what results of commitments and complementary terms. In a different way DB is plant specific but it includes some more general statements defined in licensing basis. Both terms are quite often mixed in technical literature even though such error is not a strong inconvenience.

The licensing basis is toughly connected with safety regulations and the involved scenarios are design basis accidents (DBAs). If all considered safety-related SSCs and scenarios established fulfill their acceptance criteria, the involved SSC are properly designed and the plant can be licensed.

3.6.5 Quality attributes/availability/reliability

Modern system engineering usually includes rigorous treatment of quality requirements. A list of quality attributes can be long and rather different depending on the engineering field involved. In the context of nuclear safety, two of such attributes are especially significant: availability and reliability.

A system or a function is available when it is ready to operate. Availability tells information about the interval of time during which the system or function can actuate.

A system or a function is reliable when few failures are expected. Reliability tells information about the failure-free interval.

Both availability and reliability are highly appreciated in the design of safety systems. Probabilistic safety assessment (PSA) treats both in detail considering similarities and differences. Many provisions of system design are devoted to improve both at a time. Such provisions usually derive from general criteria.

3.6.6 Design basis accidents

DBAs are the scenarios considered in the licensing basis. They are the accident against which a NPP is designed according to established design criteria. They are also called “reference accidents,” and cited in this section due to their connection with licensing basis and DB. Their definition comes from a process called “grouping and bounding” that will be introduced in another section. DB classifies them, following their estimate frequency of occurrence:

- Standard Review Plan (USNRC, 2000) classifies them as anticipated operational occurrence (AOO) and postulated accidents
- Regulatory Guide 1.206 (USNRC, 1997) classifies them as Category 2 (moderate frequency), Category 3 (not frequent accidents), and Category 4

In an appropriate design, DBA are events for which the damage to the fuel and the release of radioactive material are kept within authorized limits.

3.6.7 DBA phenomenology

The most relevant DBAs are the following: LBLOCA, IBLOCA, SBLOCA, LOFW, SBO, LOOP, SGTR, and MSLB.

The initiating event of LOCA scenarios is usually a pipe break, but it can also be

the failure of any isolation valve connecting to the primary system. Depending on the size of the broken pipe, the scenario will be called large (LBLOCA), intermediate (IBLOCA), or small (SBLOCA) break. The expected phenomenology is specific for each kind of LOCA and, in fact, this is the most relevant aspect leading to classification. Despite this approximate break sizes are given as an approach of such classification.

In an LBLOCA scenario the main primary pipe is supposed to break in double guillotine; this means an equivalent break area of 200%. As a consequence, a quick depressurization occurs and different well-known two-phase flow phenomena take place. These are blowdown, refill, and reflood (see Section 3.2.3). Emergency core coolant system (ECCS) is designed to avoid an out-of-range increase of PCT.

In an SBLOCA the broken pipe has an area roughly in the range of 1% to 6%. Both limits can be discussed and are obviously questionable. The lower limit is related to high pressure injection system (HPIS) performance. Any “break” that can be compensated by HPIS is no more a break but a leakage. The other end of the interval is more ambiguous and related basically to phenomenology. The most relevant aspect of such phenomenology is that depressurization due to the break takes time and during all this time in which primary pressure remains at a considerable value, the only injection available is HPIS. Under these conditions and depending on circumstances, different events could occur. A dry-out and temperature excursion could take place. Vapor produced in the core could remain in the core or move to hot leg and SG U-tubes. A loop seal can be formed in the intermediate leg and it can be cleared depending on pressure evolution (see Section 3.2.3). Vapor produced can also condensate in SG U-tubes, fall back, and produce the so-called reflux-condenser cooling mode as explained before (see Section 3.2.3). DSA usually sweeps SBLOCA spectrum, but most of its concern is related to emergency operation since surveillance of critical parameters and manual actuations is crucial to face this group of scenarios. Among such manual actuations, cooling and depressurizing through the secondary side are the most significant ones. This is done manually by feeding the SGs with auxiliary feed water (AFW) and relieving vapor to the atmosphere or the condenser. Once primary pressure is reduced the break flow is consequently reduced too. Further reduction could bring the primary side to the set-point pressure needed for accumulator injection.

In an IBLOCA the broken pipe has intermediate area. Phenomenology is neither that of LBLOCA nor that of SBLOCA. Peak cladding temperature is expected to be solved by accumulators' injection.

The loss of FW (LOFW) is normally detected because the affected SG level decreases. An automatic turbine trip will occur and as a consequence, the scram. AFW will automatically start up and the recovery of the plant will be completed. Additional failures can be considered. If LOFW is in coincidence with loss of offsite power (LOOP), RCPs trip will take place and AFW will undergo additional difficulties either a delay due to diesel generator start-up or a flow reduction due to the fact that its flow will be limited to that of the turbo-pump (assuming that electrical pumps are not available). In this situation, one SG (at least 1 of 3) could assure a heat sink good enough for keeping core cooling by natural circulation in the primary side. Vapor produced will be sent to atmosphere through SG relieve valves.

In a LOOP scenario, all electrical equipment becomes unavailable. Later on Emergency Diesel Generator (EDG) starts up and in about 60 s safety systems are recovered following a definite sequence. Among unavailable components the most relevant are RCP, pressurizer heaters, and steam dump. LOOP produces RCP trip and directly or indirectly, the scram. From now on, the expected phenomena are the same as in an LOFW scenario (see previous paragraph).

In a station blackout (SBO) scenario, all electrical equipment become unavailable and EDG does not start up. In other words, SBO can be considered as a LOOP without any safety system is available. Besides all these, an additional failure must be taken into account. Since injection to RCP seals is also unavailable, a leakage through such seals must be assumed. Since seals could be further damaged during the progression of the accident, such leakage has to be estimated accordingly. AFW turbo-pump could remain available while vapor is still produced in the secondary side but such availability is also limited. For a certain time the plant, despite of being in an SBLOCA situation (due to seal leakage), can be cooled by natural circulation. This is done by feeding the secondary side using AFW turbo-pump. Since conditions that allow vapor production are also deteriorating, this situation is only guaranteed for a limited time, which is called SBO coping time. SBO coping time is specific for each plant and is in the range of some hours. To calculate it, information on times to recover availability of systems has to be taken into account and thermal-hydraulic calculations have to be performed. Recovering AFW, DC for instruments and valves and EDG are the crucial steps.

The SGTR is originated by the break of one or more tubes of an SG. In an SGTR the break brings water from the primary to the secondary side. The most important point of this scenario is that primary water, that could have some radioactivity, is flowing to secondary system that is not prepared to handle it. Studies of such

scenario are of two different kinds: DBA and emergency scenarios. For the DBA scenario some conservative assumptions are considered and a calculation is performed in order to estimate the maximum (or pessimistic) release of radioactivity to the atmosphere through broken SG relief valve. If such release is under the established limit, the DBA is positively evaluated. For the emergency scenario the general strategy is to minimize Δp from primary to secondary side in order to minimize leakage flow too. Once the rupture takes place scram will occur due to over temperature or low pressure and safety injection will automatically actuate. First steps of the corresponding procedure are devoted to identifying and isolating the broken SG. After doing so, radioactivity is confined to primary circuit and broken SG. Next actuations will be devoted to reduce primary pressure and to cool down the plant using intact SGs. Intact SGs are now fed with AFW and the vapor produced is relieved. Pressurizer spray is also used to reduce primary pressure and to limit break flow. Subcooling and core exit temperature are the parameters mainly surveyed.

A main steam line break (MSLB) accident in a PWR consists in a rupture of one steam line upstream of steam header. Immediately after the break, high differential pressure between steam lines causes the actuation of the HPIS, followed with no delay by reactor and turbine trips and steam isolation. As a result of the break, broken secondary loop mass flow will highly increase and produce an important heat extraction in the corresponding SG. The primary side of such SG will quickly cool to a temperature rather cold. When cold water reaches the core, it will be an asymmetric cooling in the core and a sudden positive reactivity feedback. One of the major concerns for the MSLB accident is the return to power and criticality. In conservative calculations, the MSLB scenario is usually based on assumptions that maximize the conditions for a return to power. One of such conditions could be assuming stuck-out control rod after the reactor trip.

3.6.8 Beyond design basis accidents/severe accidents

Beyond design basis accidents (BDBAs) are scenarios with boundary conditions more strict or rigorous than DBA.

Severe accidents are scenarios involving significant core degradation.

As it can be seen, Severe Accidents are part BDBA. Accidents belonging to the latter category and not to the former are mainly those in which damage is avoided by means of applying accident management (AM) strategies or actions.

3.6.9 Verification and validation

Verification and Validation are concepts used in many engineering fields. In a first approach, such concepts can be applied to any product, service, or system. In this context to verify is to check that the product, service, or system is built as intended and to validate is to check whether it works.

In the context of thermal hydraulics (D'Auria et al., 2012b; IAEA, 2015), verification of a model is the process of confirming that the model is correctly implemented with respect to its theoretical principles and equations. Similarly, validation of a model is the process of checking its accuracy in the representation of the real system.

Also in the context of thermal hydraulics, verification and validation could be applied to nodalizations (models or input decks) (Bonuccelli et al., 1993; Reventós et al., 2007a). The verification of a nodalization is the process of confirming that the nodalization is implemented using the documentation that properly describes the facility or the plant. Similarly, validation of a nodalization is the process of checking its accuracy in the representation of the dynamic behavior of the real plant. Methodologies exist to guide such processes.

3.7 General safety concepts

3.7.1 Safety objectives/safety culture

Fundamentals of safety of NPPs are explained in available documents of IAEA (International Atomic Energy Agency) (IAEA 2000, 2002, 2006).

The fundamental safety objective is to protect people and the environment from harmful effects of ionizing radiation. This means to guarantee that risk added by technology is affordable and avoiding fission products release is assured. To do so, it is necessary to establish and execute the engineering procedures devoted to accomplish the mentioned objective.

Safety culture is that type of organizational culture, where safety is a value of utmost priority, considered essential for the long-term success of the organization. The issue is to make that safety culture strong and sustainable so that safety becomes a primer responsibility of main focus for all types of activities. Nuclear safety has to be highly integrated in nuclear business.

3.7.2 Accident management/emergency operating procedures/severe accident management guidelines

AM is the systematic treatment or handling accident-related conditions with the purpose of preventing it, avoiding its escalation to more serious event and mitigating its consequences. In order to fulfill its goals AM establishes policies and plans that are identified as strategies, guidelines, and procedures. Procedures describe actions intending to be as concise as feasible. They establish a sequence of actions to be followed step by step. Guidelines are less strict since actions to be taken are needed of some evaluation. Strategies establish the general aspects of safety functions recovery.

Emergency operating procedures (EOPs) are designed with the goal of avoiding or delaying the accident progression to severe accident conditions. Bringing the plant to an optimal plant state is their general goal.

Severe accident management guidelines (SAMGs) are designed with the goal of mitigating severe accident consequences, by means of maintaining containment functions and minimizing radiation relief (inside and outside). Reaching a secure and stable plant condition at long term is their main goal.

3.7.3 Heat extraction safety relevance

The correct heat extraction from fuel keeps the integrity of the first safety barrier and avoids accidental radioactivity release. As a general statement when damage is avoided, accidental radioactivity release cannot progress.

3.7.4 Energy sources

Since damage can be produced by the failure of heat extraction, to predict the accident progression, complete studies of energy sources are needed. Some different energy sources have to be taken into account; among them are fission energy, stored energy, residual energy, and energy due to core degradation.

Fission energy is produced by fission reaction. Its calculation is usually performed by a neutron physics model. Such model can be rather simple as the so-called point kinetics (or zero-D) model or quite complete as those based on neutron diffusion, neutron transport, or Monte Carlo theories. The thermal-hydraulic analyst must decide on the need of coupling the involved code with any neutron-kinetics model and also on how detailed the related neutron physics model has to be.

Energy stored in fuel and structures is nonnegligible in some transient analyses. The amount of stored energy depends on materials' heat capacity and on temperature. As a general statement, stored energy is the most significant heat source at the early stages of most accidents. The blowdown dry-out in a LBLOCA

is an example of core heat-up produced by energy stored in the fuel. Another situation that has to do with stored energy is the injection of rather cold water in a way that it contacts hot structures of pipes and vessel. The energy stored in such structures will be partially absorbed by injected water that will increase its temperature, hence decreasing the cooling capability of the safety system.

Residual energy or decay heat is the energy produced by fission products within the fuel rods. When fission chain is stopped due to reactor scram, decay heat starts decreasing but it never becomes zero. Despite being a decreasing function, decay heat could produce damage by itself. The accurate evaluation of decay heat could be performed analyzing the built up and decay of fission products. Such calculation is connected with fuel burn-up, historical power, and also the time after scram. In practice some look-up tables are available and helpful to produce results that are good enough for safety and design purposes.

During core degradation many different chemical reactions could occur among fuel, structures, and degradation materials. Some of these reactions could be exoenergetic and become significant in powering core degradation. Among such reactions oxidation is the most relevant one. Oxidation could combine oxygen or water with zirconium, stainless steel, or other materials. Zirconium oxidation is exoenergetic at high temperature (more than 1000 K) and produces hydrogen that when combined with air could produce explosions. Safety limits are set to avoid such interactions.

3.7.5 Damage

Besides its essential goals of fulfilling acceptance criteria, thermal-hydraulic analysis of DBA is devoted to assure that damage is not involved in the progression of such scenarios. Although definitions are not fully established, authors use to distinguish between failure and damage when facing fuel behavior in an accident scenario. In most of technical literature, core damage occurs when strong degradation starts. Such degradation could include mechanical and chemical transformation (including strong cladding oxidation), components melting, and fission products release. All this would occur at high or very high temperatures. The value of 1200°C (or 2200°F) as cladding temperature, that is traditionally related with a well-known acceptance criterion in licensing basis, is indirectly used as the threshold of damage. In this sense, it is also accepted that other incipient degradation phenomena, for example, cladding oxidation at lower temperatures, are usually not pointed out core damage.

3.7.6 Safety functions

Safety functions are specific purposes that must be accomplished to assure the general safety objective. The accomplishment has to be performed in operational states, during and following DBAs and, to the extent practicable, during and following the considered plant conditions beyond DBA. The fulfillment of such functions is continuously checked in emergency operation. They constitute an important guideline for DBA and for emergency operation guide and procedures. General safety functions are the following: subcriticality, heat extraction, and radioactivity confinement.

Subcriticality is the safety function related to reactivity control. It is used and developed in the DB of systems dealing with reactivity control like control rods system, reactor protection system, and safety injection. In emergency operation, it generates the need of checking the ability to scram the reactor.

Heat extraction is the safety function related to removing heat from the core. It is used and developed in the DB of systems established to do so in any operational situation, like emergency core cooling. In emergency operation, it generates the need of checking the capability of doing so.

Radioactivity confinement is the safety function related to radioactivity control. It is used and developed in the DB of systems dealing with containment integrity and radioactivity extraction like containment building systems. In emergency operation, it generates the need of checking the availability of such systems.

3.7.7 Defense in depth

Following IAEA definition: defense in depth is a comprehensive approach to safety that has been developed by nuclear power experts to ensure with high confidence that the public and the environment are protected from any hazards posed by the use of nuclear power for the generation of electricity. The concepts of defense in depth and safety culture have served the nuclear power industry well as a basic philosophy for the safe design and operation of NPPs.

In such approach, it is established that the general objective of safety will be accomplished making provisions at different levels and considering different physical barriers to confine radioactivity.

3.7.8 Defense in depth levels

The five levels of actuation in defense in depth approach are the following:

Level 1 Prevention of abnormal operation and failures (provisions are made to avoid abnormal behavior).

Level 2 Control of abnormal operation and detection of failures (provisions are made to recover normal behavior).

Level 3 Control of accidents within the DB (provisions are made to avoid damage)

Level 4 Control of severe plant conditions, including prevention of accident progression and mitigation of the consequences of severe accidents (provisions are made to limit damage)

Level 5 Mitigation of radiological consequences of significant releases of radioactive materials (provisions are made to limit radioactivity release)

3.7.9 Safety barriers

Safety barriers are physical obstructions or walls established to confine the radioactive material at specified locations. Typically for water reactors, the considered barriers are the fuel cladding, the reactor coolant system pressure boundary, and the containment building. Some authors consider the fuel matrix as an additional safety barrier.

3.7.10 Safety systems/safety-related systems

Two kinds of systems are pointed out as important for safety: safety systems and safety-related systems.

Safety systems are systems directly necessary to assure the performance of safety functions. They are designed following specific codes and include protections and safeguards.

Protection systems use to monitor the operation of a component (usually the reactor) following the values of relevant parameters. Once any abnormal condition is detected through a critical value of the surveilled parameter, the system automatically initiates actions to prevent an unsafe situation. The most significant preventive action is usually to stop the equipment (to scram the reactor).

Engineered safeguards are SSCs designed to keep the safety functions. There are safeguards of different natures, among them: containment systems, emergency core cooling systems, secondary side safeguards, systems related to control room habitability and complementary systems.

In spite of control systems (or controls) contributing to levels 1 and 2 of defense in depth, they are not considered safety systems.

Safety-related systems are systems whose failure has a safety impact. They are classified in three categories: Safety Class 1, 2, and 3.

Safety Class 1 Systems are those whose failure could produce a LOCA (Category 3 or 4)

Safety Class 2 Systems are the rest of SSCs belonging to Reactor Coolant System pressure boundary.

Safety Class 3 Systems include those whose failure could produce a release to environment, those that support other safety systems and those controlling radioactivity.

3.7.11 Inherent safety/passive safety/active safety

Safety is highly integrated in design and performs properly because of many different implementations.

Among the different ways to perform safety in a plant, inherent safety is maybe the most effective. Inherent safety features are those that bring the plant to safe situation based on the initiator itself without the need of designing any additional safety system. Fail-safe designs are in this category. Current plants have only a few inherent safety features. Inherent safety is in the conceptual design of some future plants.

Passive safety is the one that brings the plant to safe situation-based passive systems actuation. A passive system performs its function without any manual action and without the need of electrical power. Second generation power plants have some passive safety system. Some of the third generation power plants are fully passive (Batet, 2004; IAEA, 2009).

So, safety in current plants, having a few inherent safety features and some passive safety system, is basically active. This means that to perform safety in current plants electrical power is needed in short term and manual actions are also needed at midterm. Some engineered features are needed to help availability of safety systems and thus avoid plant vulnerability. IAEA identifies and gives the definition (see below) of three of such features: redundancy, diversity, and independence. Design robustness is an additional feature connected with usual design practices.

Redundancy is the use of more than the minimum number of sets of equipment to fulfill a given safety function; it is an important design principle for achieving high reliability in systems important to safety and for meeting the single failure criterion for safety systems. Redundancy enables failure or unavailability of at least one set of equipment to be tolerated without loss of the function.

Diversity is applied to redundant systems or components that perform the same safety function by incorporating different attributes into the systems or components. Such attributes could be different principles of operation, different physical variables, different conditions of operation, or production by different manufacturers. Diversity helps minimize the risk of common cause failure.

Independence is accomplished in the design of systems by using functional isolation and physical separation:

- Functional isolation that should be used to reduce the likelihood of adverse interaction between equipment and components of redundant or connected systems resulting from normal or abnormal operation or failure of any component in the systems.
- Physical separation and layout of plant components that should use physical separation as far as practicable to increase assurance that independence will be achieved, particularly in relation to certain common cause failures.

Design practices consider robustness as an important additional feature that needs to be taken into account especially when reliability of systems involved is a first priority. The adequate size of safeguards is an example of design robustness.

3.7.12 International institutions

The Nuclear Energy Agency (NEA) is an OECD institution which strategic areas are the following:

- Serve as a forum for sharing and analyzing information and experience among member countries
- Foster international cooperation in the nuclear field
- Help member countries to pool and maintain their technical expertise and human infrastructure, and support their nuclear activities.
- Provide member countries with nuclear policy analyses

Activities and projects, conferences or specialist meetings (OECD/NEA/CSNI, 1992, 2000, 2011), and state-of-the-art reports (OECD/NEA/CSNI, 1989, 2016a) are the initiatives used for developing such strategic areas.

In EURATOM's tasks definition one can find statements related to research and safety such as promoting research and ensuring the dissemination of technical information; and establishing uniform safety standards to protect the health of workers and of the general public and ensure that they are applied.

And also, other statements related to: equitable supply of nuclear fuels (making certain, by appropriate supervision, that nuclear materials are not diverted to purposes other than those for which they are intended); exercise the right of ownership conferred upon it with respect to special fissile materials; exercise the right of ownership conferred upon it with respect to special fissile materials; establish with other countries and international organizations such relations as will foster progress in the peaceful uses of nuclear energy, and so on.

The former group results in the network of joint research centers all over Europe: Petten (Netherlands), Geel (Belgium), Karlsruhe (Germany), Ispra (Italy), and Sevilla (Spain). The latter results in all activities related with nuclear materials and peaceful uses of nuclear energy.

In the tasks definition of the IAEA one can find also statements related to research, science and technical information like: to encourage and assist research...; to make provision,..., for materials, services, equipment, and facilities to meet the needs; to foster the exchange of scientific and technical information on peaceful uses of atomic energy; to encourage the exchange and training of scientists and experts in the field of peaceful uses of atomic energy...

Tasks having a greater impact in development are maybe those related to: establish or adopt, in consultation and, where appropriate, in collaboration with the competent organs of the United Nations and with the specialized agencies concerned, standards of safety for protection.

3.8 Concepts related to DSA

3.8.1 Safety analyses

The IAEA Specific Safety Guide No. SSG-2 (IAEA, 2010a) defines safety analyses as: analytical evaluations of physical phenomena occurring at NPPs, made for the purpose of demonstrating that safety requirements, such as the

requirement for ensuring the integrity of barriers against the release of radioactive material and various other acceptance criteria, are met for all postulated initiating events that could occur over a broad range of operational states, including different levels of availability of the safety systems. There are two basic types of safety analysis: DSA and probabilistic safety analysis.

3.8.2 Deterministic safety analysis

Safety analysis devoted to study all initiators independently of the frequency is called deterministic safety analysis (IAEA, 2010a). This kind of analysis, in principle, has to face each and every mechanism leading to barrier failure, for each operation mode and for the whole operation range.

In practice, for each initiator, only a few limiting cases are analyzed. This is due to an important engineering activity called “grouping and bounding” that configures the practical scope and practice of DSA. Accidents are grouped. In each group a bounding representative is chosen or depicted in a way that the acceptance of the results of its analysis assures the acceptance of those of the other accidents of the group. To do so, the results of previous studies are taken into account, failure mechanisms are identified and compared, transient categorization is developed, and conservative assumptions are confirmed for all group members. The primary result of the “grouping and bounding” is a list of the bounding scenarios (also called DBA or reference accidents) and the ultimate result is the feasibility of DSA. Such DBA or reference accidents have already been cited in a previous section that stressed its connection with DB while in the present section they are mentioned emphasizing the way they are defined.

At this point, it can be established that DSA provides the verification of the design. For each finally considered scenario, it demonstrates the success of the involved SSC, as stated in the DB.

It is important to understand the scope and the objective of DSA.

It must be also pointed out that DSA does not provide any information on the overall risk of the plant or on the suitability of the DB. Another safety analysis will take care of this point.

3.8.3 Safety margin/safety limit

The acceptance criterion has been defined as a statement that establishes the

condition/s that must be fulfilled by the designed SSC. Most of the acceptance criteria defined in the licensing basis are set by selecting a key parameter and establishing a limiting value for it in a defined scenario. The limiting value is called safety limit and its difference with the calculated worse value is called safety margin.

3.8.4 DSA codes and methodologies

Four different options are currently available to face DSA:

- Conservative
- BE with conservative boundary conditions
- Best estimate plus uncertainty (BEPU) evaluation
- BE with systems availability supplied through probabilistic assessment

Each methodology uses its specific codes and procedures.

3.8.5 Conservative methodologies

A conservative approach is carried out replacing one or more parameters involved by values that will have an unfavorable effect in relation to the specific acceptance criteria. Plant conditions, physical models, as well as initial and boundary conditions used are set conservatively.

In conservative analyses, the single failure criterion is applied when determining the availability of systems and components. This establishes that the safety systems should be able to perform their specified functions when any single failure occurs. Besides such criterion, some others, related to plant status, are also considered: credit is not taken for operator action unless it limits conservatism and controls are not operated unless their actuation limits conservatism.

Finally some other conservatism is considered as related to calculating tools. Conservative codes are used. Such conservative codes are more simple than BE ones and their application has proved to be useful from the start of NPP technology.

The main drawback of conservative codes and methodologies is that they do not produce a realistic picture of accident phenomenology.

3.8.6 Methodologies using BE codes with conservative boundary conditions

Such kind of methodology tries to overcome the main drawback of the previous one. Using BE codes with conservative boundary conditions, a realistic picture of accident phenomenology is recovered and safety margins become clearer. Methodologies usually establish the main parameters that have to be considered and also the conservative value at which they have to be set.

3.8.7 BEPU methodologies

BEPUs evaluation methodologies analyze DBA in a realistic basis (IAEA, 2008a). Once a base case calculation is performed using a BE and a qualified nodalization, uncertainties have to be evaluated in order to establish error bands of the key parameters that allow checking the acceptance criterion. Such uncertainty evaluation can be performed following different procedures. Depending on the utilized procedures one can find statistical methodologies or methodologies based on accuracy extrapolation.

Statistical methodologies (Glaeser, 2008) are used to propagate input uncertainties and obtain output error bands on key parameters. Most of them are based on Wilks' theory (Wilks, 1941, 1942).

Methodologies based on accuracy extrapolation (D'Auria et al., 1995; D'Auria and Giannotti, 2000) use to derive error bands from an accuracy database obtained from posttest calculations performed with experiments of different facilities.

In the framework of OECD/NEA/CSNI activities, different comparative exercises have been carried out with the general objective of improving the capabilities of such techniques, among them: UMS (OECD/NEA/CSNI, 1998; Wickett et al., 1998) and BEMUSE (OECD/NEA/CSNI, 2006, 2007, 2008, 2009, 2011).

The debate on the lessons learned in BEMUSE activity produced an important amount of review articles (e.g., de Crécy et al., 2008; Pérez et al., 2010; Perez et al., 2011), conference papers (e.g., Glaeser et al., 2011; Reventós et al., 2011), and further developments (e.g., Perez et al., 2009; Pérez, 2011).

BEPU methods are now available and used by some organizations, see the following publications: D'Auria et al. (2012a) and Martin and O'Dell (2008).

3.8.8 Inverse methods

In modeling and simulation, the inverse method consists in a technique where model input parameters are estimated (with uncertainty) from comparison of model output magnitudes with experimental data. The solution of the inverse problem can include the processes of model calibration, model uncertainty quantification, or both. In the specific field of BEPU methodologies, such technique becomes helpful to derive uncertainties of selected input parameters from specific SET (or intermediate tests) measurements. OECD/PREMIUM is devoted to the quantification of model uncertainty. The objective of the PREMIUM (Post-BEMUSE Reflood Model Input Uncertainty Methods) benchmark is to progress on the issue of the quantification of the uncertainty of the physical models in system thermal-hydraulic codes by considering a concrete case: the physical models involved in the prediction of core reflooding. Two OECD/CSNI reports (OECD/NEA/CSNI, 2016a,b) describe the project. The former establishes the objectives along with the description of the methods used, while the latter gives the final results and identifies open items. Freixa et al. (2016) provide a comparison of two key methods used in PREMIUM.

3.8.9 Final safety analysis report

Final safety analysis report (FSAR) is a huge technical document that certifies the accomplishment of safety requirements of a plant. It is plant specific. It puts together the licensing basis (DB of all structures, systems, and components that are important for safety) as well as the results of calculations and engineering judgments that confirm its fulfillment. FSAR contains the verification of safety design.

3.9 Concepts connected with modern accident analysis

3.9.1 Context

An accident is defined as an undesired event that produces distortion in a preestablished process. Some authors add that such event results in damage and such damage could be human or material.

Advanced societies devote important efforts to minimize the number and the severity of accidents. Research, regulations, and accident investigation are some of the actions taken to fulfill such purpose. Accidents are investigated for legal

reasons or as part of a preventive strategy.

In the nuclear field, since the release of radioactivity to the environment is the event to avoid, all these investigations and preventive actions are more significant. Plant operator and safety authority conduct the investigations. Operators associations share experiences on actual accidents.

Since the behavior of the plants involved in actual accidents is often in discussions facing the preparation of new regulations or the launching of new research activities, it is important to bear in mind some specific background in actual accident concepts and phenomenology. To do so, the next section introduces some highlights on accident classification as well as some relevant notes on the three more significant accidents occurred: Three Mile Island, Chernobyl, and Fukushima.

3.9.2 Concepts

3.9.2.1 Classification and treatment

Accidents in NPPs are classified or treated using the following scales and groups: International Nuclear Event Scale (INES), estimated core damage frequency (CDF), and recurrent accidents.

The INES is the most used. It is properly a classification prepared by the IAEA. It classifies the events following their relevance from safety point of view in eight levels. Following INES classification criterion, the level of an event in INES scale is the highest of those corresponding to the three following factors: impact offsite, impact in-site, and degradation of defense in depth. Its highest level is level 7 defined as “events with large impact offsite having effects on health and environment.”

CDF is a PSA concept. In its use for event classification, it is calculated using the established PSA of the plant, quantifying the probability to bring the plant to a damage situation provided that the known failures have occurred. It is a good indicator of the severity of the event and it relies on the existing PSA of the plant.

This treatment is not properly a classification. Recurrent accidents are studied following the frequency of their initiators. The most relevant accidents in western water reactors are: loss of RHRS at mid-loop operation, error in valve operation, BWR instabilities, and SG tubes rupture.

3.9.2.2 Relevant notes on TMI-2 accident

The Three Mile Island accident occurred on March 28, 1979. It was rated as level five on the INES scale. The stuck-open of a pressurizer relief valve with the subsequent loss of primary coolant was a relevant accident cause, but the most significant failures were related to procedures and human factors. Operators failed to handle the situation after different misunderstandings of the state of the plant and the actions to be taken. The reactor core partially melted down. The main lesson learned from the accident was the need of a clear improvement in EOPs.

3.9.2.3 Relevant notes on Chernobyl accident

The Chernobyl accident occurred on April 26, 1986 (Martinez Val et al., 1990; Khan, 1990). It was rated as level seven on the INES scale. The reactor suffered a catastrophic power increase. Explosions took place. Radioactive materials were dispersed into the environment and graphite moderator was burned. The accident occurred during an experiment planned to test emergency core cooling additional capabilities. Some of the causes of the accident were identified as design deficiencies like the positive void reactivity coefficient or the fact that the reactor had not any hard containment vessel. Some others were related to operation procedures like disregarding the operating reactivity margin or switching-off reactor protections after having initiated the test. Most of the specialists agree that the lack of safety culture was the most relevant cause of the accident.

3.9.2.4 Relevant notes on Fukushima accident

Fukushima site underwent an earthquake and a tsunami on March 11, 2011 (OECD/NEA/CSNI, 2015). As a consequence, the plants lost their capability of cooling some of the reactors in operation and some of the spent fuel pools. Two units degraded severely and released substantial amounts of radioactivity to the environment. Several explosions of H_2 resulted in severe deterioration of the involved buildings. As said by L. E. Herranz “Fukushima: A multiple severe accident within a natural disaster.” The root cause of the accident was: Tsunami “sweep” away EDGs. Lessons learned bring technical community to seriously reconsider: maximum historical values of external causes, the so-called easy tasks, sites having more than one NPP, spent fuel storage and the availability of portable equipment to face SBO scenarios.

3.10 Concepts related to other uses of thermal-hydraulic analysis

3.10.1 Context

An important amount of analytical thermal hydraulics is performed in a framework slightly different from deterministic analysis. Three different areas are identified:

- Probabilistic safety assessment
- Emergency operation
- Support to plant operation

Many engineering organizations work on these three areas performing thermal-hydraulic calculations and some concepts need to be introduced.

3.10.2 Concepts

3.10.2.1 PSA sequences/success criteria

PSA (Apostolakis and Moieni, 1987) sequences are the scenarios involved in the construction of event trees. Thermal-hydraulic analysis of such sequences facilitates evaluating success criteria (IAEA, 2010b).

3.10.2.2 Emergency operating/strategies, guidelines, and procedures

The goal of emergency operation is to keep general and specific safety functions and to recover the plant back to normal procedures or to an optimal plant end state.

Optimal plant end state is a key concept in emergency operation in which radiation release is minimized, equipment release is minimized, and plant conditions are stable with equipment operating in long-term alignments.

Strategies, guidelines, and procedures are documents establishing the plans for emergency operation. They range from more generic to more detailed. Strategies are general processes and maneuvers such as secondary side cool down, primary feed and bleed, equalizing pressure, or facilitating natural circulation. Guidelines are recommendations and aims to be followed during emergency operation. Procedures are detailed practices that can be followed step by step.

3.10.2.3 Severe accident management guidelines

SAMGs (IAEA, 2008b) are plant-specific documents providing recommendations to meet safety requirement during a severe accident.

3.10.2.4 Support to plant operation: analytical tasks

The responsibilities of analysts involved in supporting plant operation are somewhat different from those of other analysts that currently produce usual thermal-hydraulic studies (Reventós et al., 2007a, 2008a). There could be some coincidences but usually their tasks are quite specific. Support tasks for commercial plants are something alive, and their guidelines strongly depend on organizational requirements, status of the plant, and availability of external help. Some of them are the following: supporting dialog with regulatory body and fuel designer, analyzing actual transients occurred in the plant (operating events) (Reventós et al., 2010), NPP start-up test analysis (Llopis et al., 2007), analysis of hypothetical transients (Reventós et al., 2007b; Freixa et al., 2015c; Pla et al., 2016a), transient analysis for training support, transient analysis for design modifications, supporting the design of control systems (Llopis, 2006) or improvement of plant availability.

References

- Addabbo, C., Annunziato, A., Aksan, N., D'Auria, F., Galassi, G.M., Dumont, D., Gaul, H.P., Umminger, K., Nilsson, L., Hofmann, D., Riikonen, V., Rigamonti, M., Steinhoff, F., Guba, A., Toth, I., 2002. Development and establishment of the CERTA network database. European Commission Report, CERTA/SC/D8 EUR 20421 EN, Brussels, Belgium, September.
- Aksan, S.N., Bessette, D., Brittain, I., D'Auria, F., Gruber, P., Holmström, H.L.O., Landry, R., Naff, S., Pochard, R., Preusche, G., Reocreux, M., Sandervag, O., Stadtke, H., Wolfert, K., Zuber, N., 1987. CSNI code validation matrix of thermo-hydraulic codes for LWR LOCA and transients. OECD/NEA/CSNI Report No. 132, Paris, France.
- Aksan S.N., D'Auria F., Staedtke H. User effects on the thermal-hydraulic transient system codes calculations. *Nucl. Eng. Des.* 1993;145(1 and 2):159–174.
- Apostolakis G., Moieni P. The foundations of models of dependence in probabilistic safety assessment. *Reliab. Eng.* 1987;18(3):177–195.
- Arias, F.J., 2009. Disquisition and hydrodynamics-

hydromagnetics aspects of film boiling heat transfer. PhD Thesis, UPC, Barcelona, Spain.

Arias F.J., Reventos F. Heat transfer enhancement in film boiling due to lift forces on the Taylor-Helmholtz instability in low forced convection from a horizontal surface. *J. Enhanc. Heat Transf.* 2010;17(2):1–97.

Arias F.J., Pla P., Reventos F. Thermocapillary on film boiling heat transfer from a non isothermal horizontal surface: a theoretical study from CANDU reactors. *Prog. Nucl. Energy.* 2009;51(6–7):672–675.

Ashley, R., El-Shanawany, M., Eltawila, F., D'Auria, F., 1998. Good practices for user effect reduction. OECD/CSNI Report NEA/CSNI/R(98)22, Paris, France.

Batet, L., 2004. Contribution to the development of passive safety systems for advanced light water reactors. PhD Thesis, UPC, Barcelona.

Bestion D. The physical closure laws in the CATHARE code. *Nucl. Eng. Des.* 1990;124(3):229–245.

Bestion D., Serre G. *Transport of interfacial area in system codes: status and perspectives*. In: NURETH-15, Pisa, Italy, May 12–15; 2013.

Bonuccelli M., D'Auria F., Debrechin N., Galassi G.M. A methodology for the qualification of thermal-hydraulic codes nodalizations. In: International Top. Meet. on Nuclear Reactor Thermal-Hydraulics (NURETH-6), Grenoble, France; 1993.

Bromley L.A. Heat transfer in stable film boiling. *Chem. Eng. Prog.* 1950;46:221–227.

Chen J.C. A correlation for boiling heat transfer to saturated fluids in convective flow. *Ind. Eng. Chem. Process Des. Dev.* 1966;5(3):322–327.

Chen, J.C., Sundaram, R.K., Ozkaynak, F.T., 1977. A phenomenological correlation for post-CHF heat transfer.

NUREG-0237, Washington, DC.

Collier J.G. *Two Phase Flow and Heat Transfer in Water Cooled Nuclear Reactors*. Hanover, NH: Dartmouth College; 1975 Lecture Series.

D'Auria F. *Proposal for training of thermal-hydraulic system codes users*. In: IAEA Spec. Meet. on User Qualification and User Effects on Accident Analysis for Nuclear Power Plants, Vienna, Austria; 1998.

D'Auria F., Galassi G.M. Scaling in nuclear reactor system thermal-hydraulics. *Nucl. Eng. Des.* 2010;240(10):3267–3293.

D'Auria F., Giannotti W. Development of code with capability of internal assessment of uncertainty. *Nucl. Technol.* 2000;131(1):159–196.

D'Auria F., Galassi G.M., Vigni P., Calastri A. Scaling of natural circulation in PWR systems. *Nucl. Eng. Des.* 1991;2:187–206.

D'Auria F., Debrecin N., Galassi G.M. Outline of the uncertainty methodology based on accuracy extrapolation (UMAE). *Nucl. Technol.* 1995;109(1):21–38.

D'Auria, F. (Project Coordinator), Bousbia, S.A., Galassi, G.M., Vedovi, J., Reventos, F., Cuadra, A., Gago, J.L., Sjoberg, A., Yitbarek, M., Sandervag, O., Garis, N., Anhert, C., Aragones, J.M., Verdù, G., Mirò, R., Hadek, J., Macek, J., Ivanov, K., Rizwan-Uddin, Sartori, E., Rindelhardt, U., Rohde, U., Frid, V., Panayotov, D., 2004. Neutronics/thermal-hydraulics coupling in LWR technology – CRISSUE-S (three volumes), Vol. I. OECD/NEA Report No. 4452, Paris, France.

D'Auria F., Galassi G.M., Giannotti W., Araneo D., Cherubini M., Del Nevo A. *The boron issue in PWR and VVER-1000, OECD/NEA/CSNI PKL project*. In: PKL Analytical Workshop; Pisa, Italy: University of Pisa; 2005.

D'Auria F., Camargo C., Mazzantini O. The Best Estimate Plus Uncertainty (BEPU) approach in licensing of current nuclear

reactors. *Nucl. Eng. Des.* 2012a;248:317–328.

D'Auria F., Bestion D., Jeong J.J., Kim M. V & V in system thermal-hydraulics. In: ASME Verification and Validation Symposium (V & V 2012) Meeting, Las Vegas, NV, USA, May 2–4; 2012b.

de Crécy A., Bazin P., Glaeser H., Skorek T., Joucla J., Probst P., Fujioka K., Chung B.D., Oh D.Y., Kyncl M., Pernica R., Macek J., Meca R., Macian R., D'Auria F., Petruzzi A., Batet L., Perez M., Reventos F. Uncertainty and sensitivity analysis of the LOFT L2-5 test: results of the BEMUSE programme. *Nucl. Eng. Des.* 2008;238(12):3561–3578.

Dittus F.W., Boelter L.M.K. Heat transfer in automobile radiators of the tubular type. Berkeley, CA: University of California; 443–461. *University of California Publications in Engineering.* 1930;Vol. 2.

El-Wakil M.M. *Nuclear Power Engineering.* New York, NY: McGraw-Hill Book Company; 1962.

El-Wakil M.M. *Nuclear Energy Conversion.* Scranton, PA: Intext Educational Publisher; 1971a.

El-Wakil M.M. *Nuclear Heat Transport.* Scranton, PA: Intext Educational Publisher; 1971b.

Espinosa-Paredes G., Batet L., Nuñez-Carrera A., Sugimoto J. Severe accident analysis in nuclear power plants. *Sci. Technol. Nucl. Install.* 2012;2012:2 Article ID 430471.

Fenech H., ed. *Heat Transfer and Fluid Flow in Nuclear Systems.* Elmford, NY: Pergamon Press Inc.; 1981.

Freixa, J., 2007. SBLOCA with boron dilution in pressurized water reactors. Impact on operation and safety. PhD Thesis, UPC, Barcelona, Spain.

Freixa J., Batet L., Pretel C., Reventós F. Boron transport model with physical diffusion for RELAP5. *Nucl. Technol.* 2007;160:205–215.

Freixa J., Reventos F., Pretel C., Batet L., Sol I. SBLOCA with boron dilution in pressurized water reactors. Impact on operation and safety. *Nucl. Eng. Des.* 2009a;239(4):749–760.

Freixa J., Reventós F., Manera A. *TRACE and RELAP5 thermal-hydraulic analysis on boron dilution tests at the PKL facility*. In: NURETH-13, Kanazawa, Japan, September 27–October 1; 2009b.

Freixa J., Perez-Ferragut M., Reventos F., Allison C.M., Hohorst J.K. *Revisiting ISP-13 with RELAP/SCDAPSIM/MOD3.5 using core SCDAP components*. In: NURETH-16, Chicago, IL, USA, September; 2015a.

Freixa J., Martínez-Quiroga V., Zerkak O., Reventos F. Modelling guidelines for core exit temperature simulations with system codes. *Nucl. Eng. Des.* 2015b;286:116–129.

Freixa J., Martínez-Quiroga V., Reventós F. *Core exit temperature response during an SBLOCA event in the Ascó NPP*. In: The 16th International Topical Meeting on Nuclear Reactor Thermal-Hydraulics, NURETH-16, Chicago, IL, USA, September; 2015c.

Freixa J., de Alfonso E., Reventos F. Testing methodologies for quantifying physical models uncertainties. A comparative exercise using CIRCE and IPREM (FFTBM). *Nucl. Eng. Des.* 2016;305:116–129.

Glaeser H. *Analysis of down-comer and tie plate counter-current flow in the Upper Plenum Test Facility (UPTF)*. In: NURETH-4 Conf., Karlsruhe, Germany; 1989.

Glaeser H. GRS method for uncertainty and sensitivity evaluation of code results and applications. *Sci. Technol. Nucl. Install.* 2008;7. doi:10.1155/2008/798901 2008, Article ID 798901.

Glaeser H., D'Auria F., De Crécy A., Reventós F. *Main results of the OECD best estimate methods*. In: Uncertainty and Sensitivity Evaluation (BEMUSE) Programme, NURETH-14, Toronto, CA,

September 25–30; 2011.

Groeneveld, D.C., 1973. The thermal behavior of a heated surface at and beyond dry-out. PhD Thesis, University of Western Ontario, London, CA.

Groeneveld D.C., Cheng S.C., Doan T. 1986 AECL-UO critical heat flux lookup table. *Heat Transf. Eng.* 1986;7(1–2):46–62.

Groeneveld D.C., Leung L.K.H., Kirillov P.L., Bobkov V.P., Smogalev I.P., Vinogradov V.N., Huang X.C., Royer E. The 1995 look-up table for critical heat flux in tubes. *Nucl. Eng. Des.* 1996;163:1–23.

IAEA. *Safety of Nuclear Power Plants: Design, Requirements*. Vienna, Austria: IAEA; 2000 NS-R-1.

IAEA. In: *Accident Analysis for Nuclear Power Plants*. Vienna, Austria: IAEA; . *IAEA Safety Reports Series*. 2002;No. 23 ISSN 1020-6450; ISBN 92-0-115602-2.

IAEA. *Natural Circulation in Water-Cooled Nuclear Power Plants Phenomena, Models, and Methodology for System Reliability Assessments*. Vienna, Austria: IAEA; 2005 TECDOC 1474.

IAEA. *Fundamental Safety Principles, Safety Fundamentals*. Vienna, Austria: IAEA; 2006 SF-1.

IAEA. In: *Best Estimate Safety Analysis for Nuclear Power Plants: Uncertainty Evaluation*. Vienna, Austria: IAEA; . *Safety Report Series*. 2008a;No. 52.

IAEA. In: *Approaches and Tools for Accident Analysis for Nuclear Power Plants*. Vienna, Austria: IAEA; . *Safety Report Series*. 2008b;No. 56.

IAEA. *Passive Safety Systems and Natural Circulation in Water Cooled Nuclear Power Plants*. Vienna, Austria: IAEA; 2009 TECDOC 1624.

IAEA. *Deterministic Safety Analysis for Nuclear Power Plants*. Vienna, Austria: IAEA; 2010a IAEA SSG-2.

IAEA. *Development and Application of Level 1 Probabilistic Safety Assessment for Nuclear Power Plants*. Vienna, Austria: IAEA; 2010b Safety Standard Series, SSG-3.

IAEA. *Evaluation of Advanced Thermohydraulic System Codes for Design and Safety Analysis of Integral Type Reactors*. Vienna, Austria: IAEA; 2014 TECDOC 1733.

IAEA. *Verification and Validation of System Codes for Nuclear Safety Analyses*. Vienna, Austria: IAEA; 2015 Draft to be issued.

Ivanov K., Baratta A. *Coupling methodologies for best estimate safety analysis*. In: Int. Conf. on Mathematics, Computation, Reactor Physics and Environmental Analysis (M & C), Madrid, Spain; 1999.

Khan S.A. The Chernobyl source term: a critical review. *Nucl. Saf.* 1990;31(3):353–374.

Kimber, G., Leveque, C., Lavialle, G., 1998. ISP-38 on BETHSY test 6.9C final report. NEA/CSNI/R(97)38, Vol. 1 and 2; Paris.

Kutateladze S.S. *Fundamentals of Heat Transfer*. London: Edward Arnold Publishers Ltd.; 1963.

Lahey Jr. R.T., Moody F.J. *The Thermal-Hydraulics of a Boiling Water Reactor*. Hinsdale, IL: American Nuclear Society Monograph; 1993.

Llopis, C., 2006. Modelos avanzados de sistemas de control y protección para reactores de agua a presión. Contribución a la seguridad y la disponibilidad (in Spanish). PhD Thesis, UPC, Barcelona, Spain.

Llopis C., Reventós F., Batet L., Pretel C., Sol I. Analysis of low load transients for the Vandellòs-II NPP: application to operation and control support. *Nucl. Eng. Des.* 2007;237(18):2014–2023.

Lockhart R.W., Martinelli R.C. Proposed correlation of data for isothermal two-phase, two-component flow in pipes. *Chem. Eng. Prog.* 1949;45:39–48.

Martin R.P., O'Dell L.D. Development considerations of AREVA NP Inc.'s realistic LBLOCA analysis methodology. *SSci. Technol. Nucl. Install.* 2008;2008(2008):13. doi:10.1155/2008/239718 Article ID 239718.

Martinelli R.C., Nelson D.B. Prediction of pressure drop during forced-circulation boiling of water. *Trans. ASME.* 1948;70:695–702.

Martinez Val J.M., Aragonés J.M., Mingues E., Perlado J.M., Velarde G. An analysis of the physical causes of the Chernobyl accident. *Nucl. Technol.* 1990;90(3):371–388.

Martínez-Quiroga, V., 2014. Scaling-up methodology, a systematic procedure for qualifying NPP nodalizations. Application to the OECD/NEA ROSA-2 and PKL-2 Counterpart test. PhD Thesis, UPC, Barcelona, Spain.

Martinez-Quiroga V., Reventos F. The use of system codes in scaling studies: relevant techniques for qualifying NPP nodalizations for particular scenarios. *Sci. Technol. Nucl. Install.* 2014;2014(2014):13 Article ID 138745.

Martinez-Quiroga V., Reventos F., Freixa J. Applying UPC scaling-up methodology to the LSTF-PKL counterpart test. *Sci. Technol. Nucl. Install.* 2014;2014(2014):18 Article ID 292916.

Mull, T., Umminger, K., Bucalossi, A., D'Auria, F., Monnier, P., Toth, I., Schwarz, W., 2007. Final report of the OECD-PKL project. NTCTP-G/2007/en/0009, Areva, Erlangen.

OECD/NEA/CSNI, 1989. Thermal-hydraulics of emergency core cooling in light water reactors—a state of the art report. OECD/CSNI 161, Paris, October.

OECD/NEA/CSNI. *System Thermal-hydraulics*. In: Proceedings of CSNI Spec. Meet. on Transient Two-Phase Flow, Aix-En-Provence, France, April 6–8; 1992.

OECD/NEA/CSNI, 1993. Separate effects test matrix for thermal-hydraulic code validation: phenomena characterization

and selection of facilities and tests. OCDE/GD(94)82, Paris, France.

OECD/NEA/CSNI, 1996. CSNI code validation matrix of thermo-hydraulic codes for LWR LOCA and transients. CSNI Report 132-Rev. 1, Paris, France.

OECD/NEA/CSNI, 1997. ISP-Brief descriptions 1975–1997. Report NEA/CSNI/R(97)3, Paris, France.

OECD/NEA/CSNI, 1998 [Authors: Wickett, T., D'Auria, F., Glaeser, H., Chojnacki, E., Lage, C., Sweet, D., Neil, A., Galassi, G.M., Belsito, S., Ingegneri, M., Gatta, P., Skorek, T., Hofer, E., Kloos, M., Ounsy, M., Sanchez, J.I.]. Report of the uncertainty methods study for advanced best estimate thermal-hydraulic code applications – volumes I & II. OECD/CSNI Report NEA/CSNI/R(97)35, Paris, France.

OECD/NEA/CSNI. In: OECD/CSNI Workshop on Advanced Thermal-hydraulics and Neutronics Codes: Current and Future Applications, Barcelona, Spain, April 10–13; 2000.

OECD/NEA/CSNI, 2004. OECD SETH project – final report of the PKL experimental programme part (2000–2004). NEA/CSNI/R(2004)24.

OECD/NEA/CSNI, 2006. BEMUSE phase II report, re-analysis of the ISP-13 exercise, post-test analysis of the LOFT L2-5 test calculation. NEA/CSNI/R (2006)2. Paris.

OECD/NEA/CSNI, 2007. BEMUSE phase III report, uncertainty and sensitivity analysis of the LOFT L2-5 test. NEA/CSNI/R(2007)4, Paris.

OECD/NEA/CSNI, 2008. BEMUSE phase IV report, simulation of a LB-LOCA in Zion nuclear power plant. NEA/CSNI/R(2008)6, Paris, France.

OECD/NEA/CSNI, 2009. BEMUSE phase V report, uncertainty and sensitivity analysis of a LB-LOCA in zion nuclear power plant. NEA/CSNI/R(2009)13, Paris, France.

OECD/NEA/CSNI, 2011. BEMUSE phase VI report, status report on the area, classification of the methods, conclusions and recommendations. NEA/CSNI/R(2011)4, Paris, France.

OECD/NEA/CSNI, 2015. Benchmark study of the accident at the Fukushima Daiichi nuclear power plant (BSAF Project). NEA/CSNI/R(2015)18, Paris, France.

OECD/NEA/CSNI, 2016a. PREMIUM a benchmark on the quantification of the uncertainty of the physical models in the system thermal-hydraulic codes: methodologies and data review. NEA/CSNI/R(2016)9, Paris, France.

OECD/NEA/CSNI, 2016b. Post-BEMUSE Reflood Model Input Uncertainty Methods (PREMIUM) Benchmark. Final report, approved in June 2016, to be issued, Paris, France.

OECD/NEA/CSNI, 2016c. The OECD/NEA/CSNI SOAR on scaling (S-SOAR) final report approved in June 2016, to be issued, Paris, France.

Pérez, M., 2011. Integration of a quantitative-based selection procedure in an uncertainty analysis methodology for NPP safety analysis. PhD Thesis, UPC, Barcelona, Spain.

Perez M., Reventós F., Wagner R., Allison C. In: Integrated Uncertainty Analysis Using RELAP/SCDAPSI M/MOD4.0, NURETH-13 Conf., Kanazawa, Japan, September 27–October 2; 2009.

Pérez M., Reventós F., Batet L., Pericas R., Toth I., Bazin P., de Crécy A., Germain P., Borisov S., Glaeser H., Skorek T., Joucla J., Probst P., Ui A., Chung B.D., Oh D.Y., Kyncl M., Pernica R., Manera A., D'Auria F., Petruzzi A., Del Nevo A. Main results of phase IV BEMUSE project: simulation of LBLOCA in an NPP. *Sci. Technol. Nucl. Install.* 2010;9 Article ID 219294.

Perez M., Reventos F., Batet L., Guba A., Tóth I., Miesusset T., Bazin P., de Crécy A., Borisov S., Skorek T., Glaeser H., Joucla J., Probst P., Ui A., Chung B.D., Oh D.Y., Pernica R., Kyncl M., Macek J., Manera A., Freixa J., Petruzzi A., D'Auria F., Del

Nevo A. Uncertainty and sensitivity analysis of a LBLOCA in a PWR nuclear power plant: results of the phase V of the BEMUSE programme. *Nucl. Eng. Des.* 2011;241:4206–4222.

Pericas, R., 2015. Contribution to the validation of best estimate plus uncertainties coupled codes for the analysis of NK-TH nuclear transients. PhD Thesis, UPC, Barcelona, Spain.

Pericas R., Ivanov K., Reventós F. *Comparison of best estimate plus uncertainties and conservative methodologies for a PWR MSLB analysis using coupled 3D neutron kinetics/thermal-hydraulic code.* In: NURETH-15 Pisa, Italy, May 12–15; 2013.

Pericas R., Ivanov K., Reventos F., Batet L. Code improvement and model validation for Ascó-II Nuclear Power Plant model using a coupled 3D neutron kinetics/thermal-hydraulic code. *Ann. Nucl. Energy.* 2016;87(Part 2):653–665.

Petruzzi A., D'Auria F., Bajcs T., Reventos F., Hassan Y. International course to support nuclear licensing by user training in the areas of scaling, uncertainty and 3D thermal-hydraulics/neutron-kinetics coupled codes: 3D S.UN.COP seminars. *Sci. Technol. Nucl. Install.* 2008;2008(1–16):16. doi:10.1155/2008/874023 Article ID 874023.

Pla, P., 2004. Assessment of size aspects in modelling molten fuel coolant interaction. PhD Thesis, UPC, Barcelona, Spain.

Pla P., Pascal G., Tanarro J., Annunziato A. The new STRESA tool for preservation of thermal-hydraulic experimental data produced in the European Commission. *Ann. Nucl. Energy.* 2015;85:893–902.

Pla P., Reventos F., Martin R.M., Strucic M., Sol I. Simulation of steam generator plugging tubes in a PWR to analyse the operating impact. *Nucl. Eng. Des.* 2016a;305:132–145.

Pla P., Tanarro J., Ammirabile L., Strucic M., Wastin F. *Long term preservation of knowledge in the area of nuclear thermal-hydraulics – the new STRESA database.* In: 11th Int. Conf. of Croatian Nuclear Society, Zadar, Croatia, June 5–8; 2016b.

Pretel, C., 1997. Análisis de transitorios con pérdida de refrigerante primario en reactores de agua a presión y optimización de la gestión de accidentes (in Spanish). PhD Thesis, UPC, Barcelona, Spain.

Reventós F., Batet L., Llopis C., Pretel C., Salvat M., Sol I. Advanced qualification process of ANAV NPP integral dynamic models for supporting plant operation and control. *Nucl. Eng. Des.* 2007a;237(1):54–63.

Reventós F., Batet L., Pretel C., Ríos M., Sol I. Analysis of the feed and bleed procedure for the Ascó NPP: first approach study for operation support. *Nucl. Eng. Des.* 2007b;237(18):2006–2013.

Reventós F., Batet L., Llopis C., Pretel C., Sol I. Thermal-hydraulic analysis tasks for ANAV NPPs in support of plant operation and control. *Sci. Technol. Nucl. Install.* 2008a;2008:13 Article ID 153858.

Reventós F., Freixa J., Batet L., Pretel C., Luebbesmeyer D., Spaziani D., Macek J., Kasahara F., Umminger K. An analytical comparative exercise on the OECD-SETH PKL E2.2 experiment. *Nucl. Eng. Des.* 2008b;238(4):1146–1154.

Reventós F., Llopis C., Batet L., Pretel C., Sol I. Analysis of an actual reactor trip operating event due to a high variation of neutron flux occurring in the Vandellòs-II nuclear power plant. *J Nucl. Eng. Des.* 2010;240(10):2999–3008.

Reventós F., Glaeser H., D'Auria F., De Crécy A. *Uncertainty and Sensitivity Analysis for a Nuclear Power Plant Large Break Loss of Coolant Accident (LB-LOCA) in the Context of OECD BEMUSE Programme.* In: NURETH-14 Conf., Toronto (Ca), September 25-30; 2011.

Reventós F., Pla P., Matteoli C., Nacci G., Cherubini M., Del Nevo A., D'Auria F. Consistent post-test calculations for LOCA scenarios in LOBI integral facility. *J. Sci. Technol. Nucl. Instal.* 2012;16 Article ID 474162.

Smith, B.L., Bieder, U., Graffard, E., Heitsch, M., Henriksson, M., Höhne, T., Komen, E., Mahaffy, J., Moretti, F., Morii, T., Mühlbauer, T., Rohde, U., Scheuerer, M., Song, C.-H., Zigh, G., Andreani, M., Bestion, D., Ducros, F., Houkema, M., Lucas, D., Menter, F., Watanabe, T., 2008. Assessment of Computational Fluid Dynamics (CFD) for nuclear reactor safety problems. NEA/CSNI/R(2007)13, Paris France.

Todreas N.E., Kazimi M. *Nuclear Systems (Vols I and II)*. New York, NY: Hemisphere Pub. Corp; 1990.

Tong L.S. *Boiling Heat Transfer and Two-Phase Flow*. New York, NY: John Wiley & Sons; 1965.

Tong L.S., Weisman J. *Thermal Analysis of Pressurized Water Reactors*. Hinsdale, IL: ANS Monograph; 1970.

Umminger K., Dennhardt L., Schollenberger S., Schoen B. Integral test facility PKL: experimental PWR accident investigation. *Sci. Technol. Nucl. Inst.* 2012;16 Article ID 891056.

USNRC, 1987. Compendium of ECCS research for realistic LOCA analysis. NUREG-1230, Washington, DC.

USNRC, 1989. Quantifying reactor safety margins: application of CSAU to a LBLOCA. NUREG/CR-5249, Washington, DC.

USNRC, 1997. Regulatory Guide 1.206 – Combined License Applications for Nuclear Power Plants.

USNRC, 2000. Draft Section 15.0.2, Review of Analytical Computer Codes. NUREG-0800 [Standard Review Plan for the Review of Safety Analysis Reports for Nuclear Power Plants], Washington, DC.

USNRC, 2015. Code of Federal Regulation, Washington, USA [continuously updated – see the website of US NRC].

Wallis G.B. *One Dimensional Two-Phase Flow*. New York, NY: McGraw Hill; 1969.

Wickett, T., Sweet, D., Neill, A., D'Auria, F., Galassi, G., Belsito, S., Ingegneri, M., Gatta, P., Glaeser, H., Skorek, T., Hofer, E., Kloos, M., Chojnacki, E., Ounsy, M., Lage Perez, C., Sánchez Sanchis, J.I., 1998. Report of the uncertainty methods study for advanced best estimate thermal hydraulic code applications, volume 1 (comparison) and volume 2 (report by the participating institutions). NEA/CSNI/R(97)35, Paris, France.

Wilks S.S. Determination of sample sizes for setting tolerance limits. *Ann. Math. Stat.* 1941;12:91–96.

Wilks S.S. Statistical prediction with special reference to the problem of tolerance limits. *Ann. Math. Stat.* 1942;13:400–409.

Role of thermal-hydraulics in nuclear power plants

Design and safety

R.R. Schultz Idaho National Engineering Laboratory, Idaho Falls, ID, United States

Abstract

Key questions addressed in the chapter are: Why nuclear thermal-hydraulics is needed? What are the roots for the development of analytical capabilities? Who (or which institution) is expected to drive the progress? Needs in thermal-hydraulics arise from design and safety. In the area of design focus is given to creating nuclear systems and components which are robust and reliable, have a long and trouble-free lifetime, are efficient and economical to operate, do not tend to stray into unwanted transient scenarios and are easy to inspect and maintain. In the area of safety focus goes on ensuring the nuclear systems and components always operate with operational margins consistent with the “defense-in-depth” approach required by the regulatory agencies. Licensing is the key word for deriving needs challenging design and safety thermal-hydraulic analyses. The needs at the basis of the design of computational tools are discussed.

Keywords

Elements for thermal-hydraulic assessment; Phenomena identification and ranking table (PIRT); The evaluation model concept; The validation pyramid; Safety margin; The acceptable error

Nomenclature

ASME American Society of
Mechanical Engineering

CFD computational fluid dynamics

CFR Code of Federal Regulation (in
USA)

ECCS emergency core cooling
systems

EM evaluation model

EMDAP evaluation model
development and application process

GT-MHR gas-turbine modular high
temperature reactor

GUM guide to the expression of uncertainty

IET integral effect test (facility)

ISO International Organization for Standardization

LBLOCA large break LOCA

LOCA loss-of-coolant accident

MMS method of manufactured solution

NPP nuclear power plant

NQA nuclear (grade) quality assurance

NRC Nuclear Regulatory Commission

PIRT phenomena identification and ranking table

PWR pressurized water reactor

R & D research and development

SAR safety analysis report

SET separate effect test (facility)

VHTR very high temperature reactor

V&V verification and validation

Chapter foreword

Following the definitions in nuclear thermal-hydraulics (Chapter 3 of the book), an attempt is made in the present chapter to establish the needs for the (nuclear thermal-hydraulics) discipline. The needs come from the design/operation of the nuclear power plants (NPPs), namely the water cooled nuclear reactors and from the safety evaluations. Focus is given in the chapter to the needs coming from safety, namely from the licensing process.

The needs shall translate into features of the computational tools as well as for the

procedures needed to prove their validity including the scaling capabilities. So, ideally the reader may jump from **Chapter 1** of the book (general overview of nuclear thermal-hydraulics) to **Chapter 4** (present chapter), to **Chapter 11** (the features of computational tools are discussed), to **Chapter 13** (the validation procedures and methods are described), and finally to **Chapter 15** (selected application results from computational tools are discussed).

Some information in the chapter is specifically related to gas-cooled reactors: that information is also applicable to the technology of water cooled reactors.

4.1 Introduction

Thermal-hydraulics is the physics of fluid flow, energy (e.g., heat) transfer, as well as the interactions between fluid flow, energy, and the surrounding structures. In nuclear systems, material interactions with nuclear radiation are also sometimes an important consideration. Therefore thermal-hydraulics in nuclear reactors is a very wide-ranging subject and includes such diverse topics as gravity-dominated stratified flow in pipes with a free surface—including hydraulic jumps, momentum-driven critical flow through passages and restrictions, fluid-structure interactions such as fluid jet impingement on structures, flow boiling and condensation, flow and heat transfer regimes for flow in various geometries at various orientations, energy generation and transfer to fluids and structures from nuclear sources, and a multitude of other phenomena. The study of these topics may range from one-dimensional to three-dimensional flow fields that interact with structures that may be represented as point to three-dimensional bodies with heat sources and/or sinks. For many of the scenarios which must be considered in nuclear reactors important variables and phenomena change as a function of time.

Thermal-hydraulic analyses are governed not only by their boundary and initial conditions, but also by limiting values of important figures-of-merit which define maximum or minimum acceptable limits stemming from design/operational or safety requirements. Therefore the thermal-hydraulic analysis objectives may often be separated into two broad categories:

- **Design:** limits defined to ensure the plant design is robust and thus can operate economically with minimal shutdowns and operational costs and
- **Safety:** limits defined by law or regulatory rules which are specified to protect public health or living standards.

4.1.1 Design

Thermal-hydraulic design analyses focus on creating nuclear systems and components which are robust and reliable, have a long and trouble-free lifetime, are efficient and economical to operate, do not tend to stray into unwanted transient scenarios leading to shutdowns that challenge equipment design limits, and are easy to inspect and maintain. A well-designed and operated nuclear system should be able to consistently achieve capacity factors in excess of 90% and have an operational lifetime which easily exceeds 30 years.

Because design analyses generally deal with normal operational conditions and the transition from one normal operational condition to another including power-up and shutdown, such analyses are generally centered on nonsafety grade equipment performance and phenomena that are known to affect plant efficiency, reliability, and long-term operations. Examples are:

1. *Efficiency*: steam separator and dryer performance for Rankine cycle plants; core power distributions (axial and radial) that match specifications; and uniform core inlet conditions. Optimization of such parameters enhances power output by enabling the plant to function at or near technical specification limits.

2. *Reliability and long-term operations*: unwanted fluid-structure interactions throughout the system, but particularly in the core at spacers and the steam generator (case of PWR) U-tubes—such as fretting; and factors which are known to cause crud formation in the core. By minimizing phenomena known to be adverse in the long-term plant reliability is enhanced and long-term operations assured.

Thermal-hydraulic analyses centered on the system design include numerical analysis tools which include those usually used for safety analyses such as (a) system analysis codes, fuel behavior codes, and containment performance evaluation tools, but also some not generally used for safety analyses such as (b) operational core power distribution analysis tools, computational fluid dynamics (CFD) and heat transfer numerical models, and many specialized thermal-hydraulic tools tuned for analysis of specialized operational conditions.

4.1.2 Safety

Thermal-hydraulic safety analyses focus on ensuring the nuclear systems and components always operate with operational margins consistent with the “defense-in-depth” approach required by the regulatory agencies. In essence, the principle of defense-in-depth requires four levels of protection of public health and safety to be present, as follows (Sorensen et al., 1999):

1. NPPs are designed to not fail for the range of normal and abnormal conditions they might reasonably experience during their operating life, including extreme natural phenomena and man-made hazards;
2. Redundant and diverse support systems are provided to detect initiating events or incipient failures and shut the reactor down before fuel damage can occur following events within the design basis;
3. Redundant and diverse emergency systems, including emergency core cooling and containment systems, are provided to limit the release of radioactivity to the environment and thereby mitigate accident consequences if the first two levels of defense fail; and
4. Reactors are sited remotely and emergency plans are prepared and practiced in advance with local and regional authorities to limit the public consequences of a catastrophic accident involving a large release of radioactivity.

Thermal-hydraulic analyses are important ingredients in all four of the defense-in-depth protection levels. Adherence to the defense-in-depth principle has resulted in less than 0.1 safety significant event annually per plant with no discernible radiological health effects from operations and incidents.

Because thermal-hydraulic safety analysis tools generally are used to assess the margin between calculated key figures-of-merit and limits for those figures-of-merit imposed on plant operations by national law, the analysis tools are assessed using a very rigorous protocol which has been closely examined and is monitored by the licensing authorities. Thermal-hydraulic tools used for safety analyses are usually system analysis tools, containment analysis tools, core performance tools, and fuel performance tools all created to study the behavior of the nuclear system under very adverse transient conditions which may lead to fission product release.

4.1.3 The role of thermal-hydraulics

Whether for the purposes of designing a nuclear system or demonstrating the safety of a nuclear system by meeting the necessary licensing requirements, these objectives are achieved by:

1. Identifying the nuclear reactor operational and accident envelopes,
2. Isolating the key phenomena in each of the plant scenarios that comprise the operational and accident envelopes,

3. Developing numerical models that accurately calculate the behavior of the key phenomena for the scenarios of interest,
4. Assessing the numeric models *to demonstrate their adequacy* for calculating the scenarios and thus calculate the nuclear reactor behavior for these scenarios in a manner which can be trusted by the plant designers and regulatory authorities, and
5. Performing the necessary calculations showing the subject nuclear reactor meets the necessary design and licensing requirements.

Thus the role of thermal-hydraulic analyses is to provide the necessary evidence to show the subject nuclear reactor meets the necessary design and licensing requirements by achieving the goals outlined in steps 1–5 mentioned previously.

4.1.4 Organization of Chapter 4

The role of thermal-hydraulics, as a key ingredient in the analysis of nuclear reactor design and licensing, is correlated directly with the types of analyses that must be performed, that is, the thermal-hydraulic analysis envelope. This topic is discussed in Section 4.2. Finally, Section 4.3 outlines how the analysis tools, that is, the numeric models, are demonstrated to be adequate for performing analyses of the key scenarios which must be analyzed.

4.2 The thermal-hydraulic analysis envelope

The design and safety requirements which underlie both the design and operation of a nuclear plant combine to form the operational and accident domain of the nuclear plant includes conditions (structural loads, temperatures, pressures, life expectancy, radiation levels, etc.) representative of:

- Normal operations (e.g., power production, shutdown, refueling),
- Anticipated operational occurrences (e.g., reactor trip, water hammer),
- Infrequent events or transients (e.g., loss of offsite power, loss of feedwater),
- Design basis events (e.g., floods, earthquakes, external man-made hazards), and
- Design basis accidents (e.g., loss of coolant, large reactivity changes).

The primary safety requirements that govern the design of NPPs in the United States are codified in Appendix A to 10 CFR 50, “General Design Criteria for Nuclear Power Plants.” From an international perspective, other nations have similar requirements which must be followed by both the designer and operator of the nuclear plant in that country.

The design basis for each NPP is described in its safety analysis report (SAR)—which must be produced in preliminary form by the plant designer for review by the regulatory authorities as well as the plant owner and other stakeholders prior to obtaining a license. The technical information contained in such reports includes the seismic, meteorological, hydrologic, and geologic characteristics of the plant site, “with appropriate consideration of the most severe of the natural phenomena that have been historically reported for the site and surrounding area and with sufficient margin for the limited accuracy, quantity, and time in which the historical data have been accumulated.” The SAR also contains safety assessments of the performance of the plant under a specified set of conditions that define a design envelope. All of those safety assessments are required to show that the reactor core is maintained in a coolable geometry and that there would be limited releases of fission products to the reactor coolant system or the reactor containment. In addition, the combination of site characteristics, demography, and plant design must be shown to meet certain radiation exposure criteria for offsite individuals in the event of an arbitrarily-large release of radioactive material from the reactor coolant system into the reactor containment.

The complete operational and accident domain of a nuclear plant, which makes up the plant's design basis, may be represented by the yellow region in the Venn diagram shown in Fig. 4.2. The owner of a nuclear plant will only qualify for an operating license if all of the operational conditions, infrequent events/transients, and design basis events/accidents are shown to result in conditions which do not violate national standards, laws, and operating requirements—such as, for example, 10 CFR 50 for the United States.

The design basis includes accident prevention and accident mitigation requirements for each NPP, for a defined scope of events. The requirements for all events within the design basis are that the fission process can be shut down, the reactor remains subcritical, the core can be cooled and its geometry maintained, coolant makeup can be supplied as needed, and, in the event of an accident involving core damage, any fission products released from the core can be controlled within a containment structure that assures limited radioactivity leakage to the environment. Information contained within the design basis for a particular

piece of equipment or building includes, for example, the specific functions to be performed and the specific values or ranges of values for conditions that serve as the bounds for its design. These conditions are derived from engineering analysis or experiments to predict the consequences of events postulated for design, including those in the preceding list. An important lesson learned from decades of operating NPPs is that rigorous configuration control must be applied, throughout a plant's operating life, to assure that the design basis is maintained.

A plant designer and a plant operator demonstrate that their nuclear reactor system does not violate national laws and national nuclear plant operational requirements and standards by using thermal-hydraulic analysis tools, that is, numeric models, which have been shown to be adequate for performing trustworthy predictions of the behavior of the nuclear plant for all the scenarios, conditions, and transients within the design envelope. The thermal-hydraulic tools themselves must be capable of calculating trustworthy analyses for a domain which either equals or exceeds the design envelope. The domain for which the thermal-hydraulic analyses may be used comprises the “calculational envelope” as shown in Fig. 4.1.

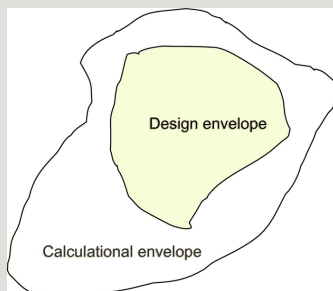


Fig. 4.1 Venn diagram showing relationship between the NPP system envelope and the thermal-hydraulic analysis calculational envelope (Venn, 1880, 1881).

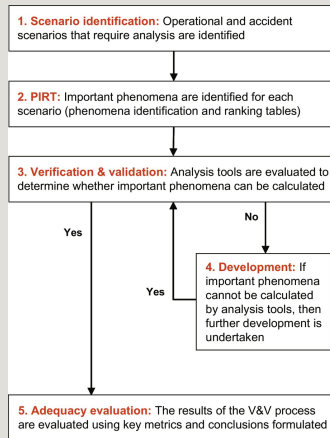


Fig. 4.2 PIRT informed R&D process.

4.3 Demonstration of thermal-hydraulic analysis tool adequacy

The process of qualifying software, for example, system analysis codes, such that the software is considered adequate for calculating the behavior of NPPs, is in concept relatively straightforward, even though there are many questions to be answered and the process itself is iterative. From a high-level perspective, the process consists of five stages (see Fig. 4.2) which must be exercised in their entirety for each NPP design. The five stages consist of the (1) identification of the scenarios of importance, (2) identification of the key phenomena for the scenarios of importance using a phenomena identification and ranking table (PIRT) process, (3) verification and validation (V&V) of the analysis tools/software, that is, determination of whether the tools to be used to analyze the scenario progressions are capable of calculating the important phenomena and figures-of-merit for the validation matrix, (4) correction or enhancement of existing software or possibly development of new software if necessary, and finally, (5) an adequacy evaluation. The function of the final stage, the adequacy evaluation, is to bring together all of the data—both experimental and calculational—obtained in the earlier steps—to enable a thorough review and conclusions to be formulated regarding whether the software is capable of making trustworthy predictions of the nuclear system behavior for the scenarios of interest. Therefore, software deemed adequate to calculate a particular plant scenario is capable of calculating the dominant phenomena and physics, with an acceptable calculational uncertainty that governs the behavior of the plant during the scenario in question.

Each of these stages consists of a number of important substages which will be discussed individually in the subsequent sections. It is important to note: following a positive outcome during the adequacy evaluation, the stage is set for obtaining uncertainty quantifications on the figures-of-merit required by the stakeholders—either for licensing or design purposes.

Online NPPs can only operate within limits defined by the capability of the licensee to demonstrate that the magnitude of all important figures-of-merit for plant safety parameters will not exceed acceptable limits. Thus a sufficient margin must be maintained so these figure-of-merits are not in danger of being violated. A figure-of-merit is a key parameter indicative of whether or not a safety limit or an equipment failure limit is in danger of being violated. For example, important figures-of-merit are fuel temperature, the quantity of water inventory in a light water reactor pressure vessel, and/or reactor vessel wall temperature. Although there are a number of figures-of-merit crucial to the operation of a power plant, for the sake of demonstrating the role of thermal-hydraulic tools/software, the fuel cladding temperature is perhaps the most common, particularly when considering safety limits during loss-of-coolant accidents (LOCAs) for online light water reactors.

Regardless of the figure-of-merit under consideration, each has the potential to affect the operational envelope of the plant in some way such that limits may be imposed resulting in special precautions, operational procedures, or equipment limitations to ensure the figure-of-merit is not challenged. In some cases, the limits translate to operating the plant at power levels below the designed power level. In other cases, the limits may translate to reducing the rate-of-change of an operational parameter in going from one condition to another, thus increasing the operational transit time. In any case, limits usually are accompanied with an economic penalty.

4.3.1 Software adequacy: A more detailed look at the process

To ensure that plant designer analyses adequately cover the operational and accident domain of concern, a number of methodologies have been developed. In the United States the NRC issued Regulatory Guide 1.203 which describes historically acceptable processes for the development and assessment of numeric models used to evaluate transient and accident behaviors that are within the design basis of a NPP. The process is known as the “Evaluation Model Development and Application Process” (EMDAP—see Fig. 4.3).

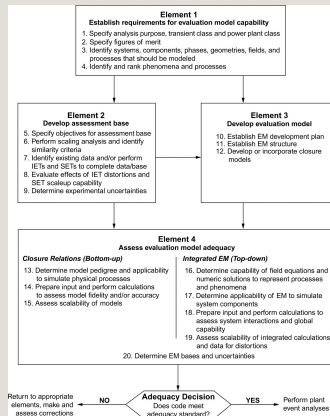


Fig. 4.3 Elements of evaluation model development and application process.

The term “evaluation model (EM)” is commonly used in the licensing arena to include all the numerical models used to calculate the nuclear system behavior, including system analysis and CFD software. The NRC EMDAP flow chart consists of four major elements followed by a final “Adequacy Decision” step.

4.3.1.1 Element 1

Element 1 establishes the plant scenario types and phenomena ranges that define the operational and accident envelopes for the plant of interest. It is common practice to combine these two envelopes to form a single operational/accident envelope for the system which may be represented by validation matrices specific to each scenario type. In the subsequent discussions this envelope will be called the design envelope as shown in Fig. 4.1. The envelope for the system is the domain within which the numeric models, which will be used to calculate the plant behavior, must be shown to be applicable and must be shown to be capable of calculating the key phenomena and figures-of-merit with an acceptable calculational uncertainty. Once the domain for adequacy evaluation is defined, then each scenario must then be dissected to isolate the regions where there are different controlling phenomena. Perhaps the most widely known example of a scenario being divided into regions where there are different controlling phenomena is the division of the light water reactor double-ended guillotine break, also known as the large break loss-of-coolant accident (LBLOCA) scenario, into the blowdown, refill, and reflood regions (USNRC, 1988). For each of these regions different phenomena dictate the scenario progression—and the dominant phenomena together with less important phenomena which must still be considered are

identified using a PIRT. The PIRT is an important ingredient to the adequacy evaluation because the identification of key phenomena points to the physics which must be adequately represented numerically in each region (Wilson and Boyak, 1998).

4.3.1.2 Element 2

Element 2 is focused on developing the “assessment base” which is equivalent to developing the validation matrices used as the validation calculation benchmarks. The validation matrices are comprised of the data from experiments that have a rigorous, scaled relationship to the prototype as well as known measurement uncertainties which are sufficiently low to enable high-fidelity validation calculations to be performed.

The set of experiments designed to generate validation data is based on nuclear reactor operational and accident envelopes. The envelopes, in turn, are composed of the various scenarios which may occur. For example, the operational envelope may be composed of a set of scenarios which include plant operation at various power levels—such as scenarios A–E shown in Fig. 4.4. The system of equations which describes the plant operational conditions for any region within a given scenario (e.g., the blue region within the scenario A domain) will change when a phenomenon or phenomena, which has negligible influence in the blue region, becomes influential, for example, the presence of subcooled boiling within the core denoted by the gold region within the scenario A domain. The boundary between the blue and gold regions denotes the change in the systems of equations which govern the thermal-hydraulic behavior in the two regions respectively.

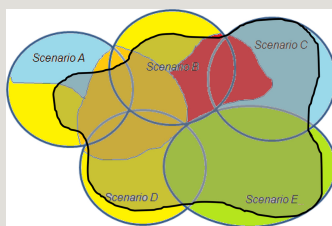


Fig. 4.4 Plant operating envelope (irregular curve) overlaid by plant operational scenarios. Regions within each scenario, denoted by different colors, denote domains a specific system of equations is applicable.

Such boundaries may signify changes to the systems of equations which, although significant enough to change the trajectory of the scenario progression, will not

lead to a reduction in the plant safety margin. Conversely, some boundaries represent the crossover to a region where a “cliff-edge” effect may occur, for example, critical heat flux in the core, which if encountered will lead to significant temperature increases in the core fuel rods.

This concept is important from several perspectives: (a) an important role of thermal-hydraulics analysis is to define the boundaries which separate the various regions within scenarios which reflect important changes in key characteristics of the governing equations² and (b) scaled experiments designed to generate validation data focus on characterizing the fluid/heat transfer behavior within each region as well as defining the boundaries between regions.

If the validation matrix used to qualify the numeric models is rigorously defined, the experiments properly scaled such that experimental distortions are both minimized and quantified, and the data have sufficiently low uncertainties, then the groundwork for completing the Element 4 numeric model validation and numeric models adequacy assessment is in place.

The design envelope for any nuclear plant is the domain of conditions and phenomena which the numeric models must be capable of calculating (see Figs. 4.1 and 4.5). The definition of the design envelope is addressed in Element 1 of the EMDAP. The region where the numeric models are valid, as confirmed by performing validation studies, is the calculational envelope and is the domain where the numeric models are shown to have the desired calculational fidelity. The numeric models calculational envelope must encompass the design envelope, as shown in Fig. 4.5, if the numeric models are to be used to calculate the projected behavior of the system for licensing studies.

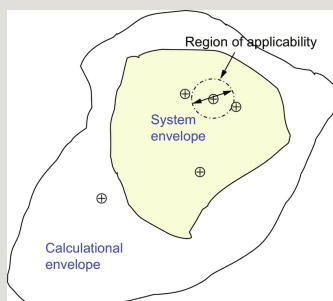


Fig. 4.5 Relationship of validation data to calculational and system envelopes.

The range of applicability for a given set of numeric models (the software) is in part determined by the physics and the numeric models contained within the software developed in Element 3. Therefore, the assessment or validation process, as implemented in Element 4, and the decision regarding the adequacy of the numerical models, must confirm that the software physics models properly calculate the key phenomena over the entire range of conditions encompassed by the calculation envelope. Success is only achieved when an adequate, high-fidelity data matrix and/or exact analytical solution set are available to benchmark the calculation results over the range of conditions that encompass the entire design envelope.

The data included in the validation matrix are indicated in Fig. 4.5 by \oplus where the + indicates the data coordinates and the circle around the + indicates the data uncertainty. An important point to be addressed is the applicability of the individual data points, and the validations that are performed on the basis of the selected data, to the region between the data points. The “region of applicability” for a particular data point within the validation matrix is indicated by the subdomain defined by the dotted line that surrounds an individual data point (see Fig. 4.5).

The validation matrix is constructed using specially designed experiments which are linked to the prototype by the scaling laws. Historically experiments such as LOFT, BETHSY, and ROSA were scaled using power-to-volume scaling with accommodations to achieve density-gradient scaling important for small break LOCA-related phenomena by using 1:1 height scaling (Ybarrondo et al., 1974; Levy, 1999). Over the last 20 years more advanced scaling techniques have been utilized including hierarchical two-tiered scaling as first proposed by Zuber (1991).

Using the scaling laws in an acceptable fashion, such as outlined in Zuber (1991), is crucial because when the numerical models are validated using data from correctly scaled facilities, as noted in Zuber et al. (1990): “Implicit to applications of computer codes to analyses of postulated accident events in nuclear plants is the premise that these codes have the capability to scale-up phenomena and processes from test facilities to full-scale plant conditions.”

These scaling methods typically include a combination of top-down and bottom-up scaling analyses. The top-down scaling approach is most applicable to the validation of system analysis codes and is usually performed for scaled integral experiments designed to simulate the integral behavior of the complete prototype plant. These scaled integral experimental facilities include simulation of most of the major components. On the other hand, the bottom-up scaling approach is useful

not only for system analysis software, but especially the validation of CFD software used to evaluate localized phenomena. The bottom-up scaling approach typically looks at phenomena occurring in individual components (local heat transfer, countercurrent flow, etc.) to confirm that scaling distortion do not occur at the local level or to quantify whatever distortion is present.

In the top-down scaling approach, the system to be addressed is defined, and the transient scenarios within the operational and accident domain are divided into several phases, and subphases if necessary. The system responses of interest in each phase are represented by the governing conservation equations that determine the behavior of the systems and/or components. These equations are then nondimensionalized and the nondimensional groups evaluated to determine the relative importance of each group. A set of nondimensionalized coefficients characterizing the system response, are then defined. The nondimensional groups from the calculated response of the prototype plant can then be compared with the measured data from the experimental facilities to quantitatively evaluate the scalability of the test facilities to the prototype plant for the parameters and scenarios of interest.

As indicated earlier, the bottom-up scaling approach is primarily concerned with localized phenomena, so it is primarily used to assess the applicability of individual models and correlations implemented into the system analysis and/or CFD software. This approach addresses the details lost in the averaging at the component level in the top-down scaling, thereby providing insights into qualitatively different responses between the test facility and plant. The bottom-up scaling approach is also useful in understanding apparent distortions between the test facility and plant that are observed but not easily explained by the nondimensional groups obtained from the top-down scaling approach. Identification and quantification of the distortions inherent to the experimental facility design and conditions are a key element of the process. This activity is identified as item 8 of the EMDAP Element 2 (see Fig. 4.1).

The data need for software validation depends on the particular software being considered. The system analyses software are used to analyze the overall behavior of the prototype reactor or experimental facility for selected scenarios in the operational or accident domain, while the CFD software are used to study more detailed flow behavior and the potential for hot spots and/or unacceptably large thermal gradients in localized areas of the reactor system. Depending on the particular application, the system analysis and CFD software may be used separately or coupled together to perform the analyses.

When new experimental facilities are required the design of these new facilities must be rigorous to ensure compliance with NRC requirements for licensing a new reactor plant, particularly an advanced reactor design with a limited history of regulatory review. Important features to be considered in the experiment design include: (1) assurance that the proposed experiment facility captures key phenomena being investigated; (2) the experiment is scaled to provide a direct link between the scaled facility and prototype plant; (3) the inherent distortions of the scaled experiments are identified and quantified; (4) adequate high-quality measurements are available to ensure that experimental data uncertainties are quantifiable and acceptable low; and (5) experiment results can be decomposed to the lowest level modeled by the software to ensure that system behavior at the component level is properly being calculated by the governing software physics.

All the data from the experimental facilities, taken together, form a data matrix. The data used in the validation of the numeric models form the validation matrix. Ideally the validation matrix data are defined in a sufficiently ordered manner—for example, as depicted in Fig. 4.6—such that the datasets are spaced at intervals sufficiently small that all of the system envelope domain is covered by either the data points or the combined subdomains of the individual data points as defined by the regions of applicability as shown in Fig. 4.5.

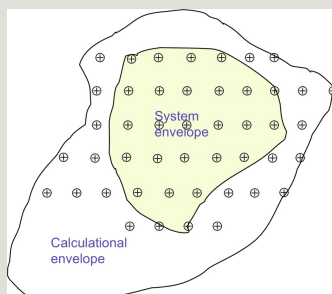


Fig. 4.6 Ideal coverage of the system envelope using an ordered validation matrix approach.

In general the data comprising the validation matrix may include NPP, integral facility, separate effects, and basic (sometimes called fundamental) experimental data. The relationship between these types of data is shown in a “validation pyramid” as illustrated in Fig. 4.7. The experiments performed to investigate and characterize the behavior of individual phenomenon are basic experiments and the data obtained from these experiments form the foundation of the validation

pyramid. Also forming the foundation of the pyramid are analytical solutions of the phenomena. Separate-effects experiments are designed to investigate and characterize the behavior of individual or a limited number of phenomena in a well-defined flow geometry, for example, turbulent flow in an inlet plenum. The separate-effects data obtained from such experiments form the next tier. The upper tiers of the validation pyramid are composed of the data obtained from integral-effects experiments and operational plants. The overall sum of the data forms the individual elements of the validation matrices.

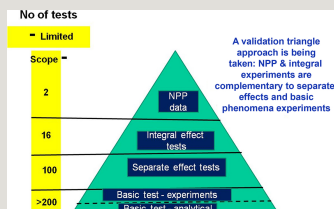


Fig. 4.7 The concept of a validation pyramid.

In principle, each of the experiments designs is related directly to the system envelope of the prototype for the key phenomena or figures-of-merit. Thus the ranges of the data measured in the experiments are quite important. The experimental data range of interest for the subject phenomena should be comparable to that of the prototype. An example comparison done for a very high temperature gas-cooled reactor separate-effects experiment is shown in Fig. 4.8 for Reynolds number (Re) and density ratio for density-gradient driven countercurrent stratified air-helium flow where the system envelope for a gas-turbine modular high temperature reactor (GT-MHR) is compared to the experimental envelope.

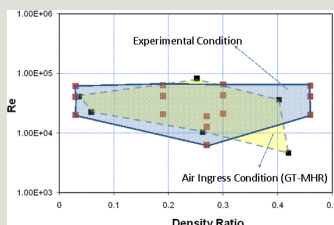


Fig. 4.8 Comparison of scaled experimental and prototype envelopes for key phenomena in a design basis scenario.

The experimental data quality must satisfy the requirements of Appendix B of Title 10 of the Code of Federal Regulations Part 50.46 and the ASME NQA-1 standard—in the United States—and comparable quality standards elsewhere internationally. To achieve this goal, the data should be generated in conformance with the practices and procedures described in the:

- i. International Organization for Standardization (ISO) guide to the expression of uncertainty in measurement (GUM)
- ii. ASME PTC 19.1-2005: Test Uncertainty standard.

4.3.1.3 Element 3

Element 3 activities are centered on the creation of the numeric models that make up the EM and thus are comprised of the physics and mathematical models, including the mathematical approximations, for example, finite difference models, finite element models, correlation approximations, etc. Many widely used numeric models describing thermal-hydraulics phenomena are already available. Examples of commonly used system analysis software include RELAP5, RETRAN, CATHARE, and TRACE. Examples of commonly used CFD software include Fluent, STAR-CCM+, and CFX. However, the existence of such software does not eliminate the need for both verification and validation of the software.

Stemming from the presence of readily available software, such as the important and commonly known examples given in the previous paragraph, verification of the numeric models and developmental validation of the existing software packages presently usually focuses on revisions and additions which are specific to advanced nuclear plant designs which have design features that are not present in online nuclear plants that were licensed and for which the above software have been found to be adequate and thus have been used to perform nuclear plant behavioral calculations for licensing submittals to the applicable regulatory agencies.

4.3.1.4 Element 4

Element 4 encompasses the creation of the input for the numeric models and the initial and boundary conditions for the numeric models. Subsequently the input models are verified and finally, the validation calculations are performed as a part of the Element 4 activities. The degree to which the numeric model validation calculations compare to the benchmark data is a primary ingredient in determining the adequacy of the numeric models for calculating the behavior of the system within the design envelope. At the conclusion of the Element 4 activities a decision

regarding the adequacy of the EM to calculate the scenarios, including consideration of the calculational uncertainty, within the system envelope may be made. To summarize the Element 4 activities, the verification and validation processes are discussed.

Verification

Practices and procedures are divided into several categories to indicate the goal and intent of each. These categories include code verification, code and calculation documentation, reduction of numerical error, quantification of numerical uncertainty, and calculation validation. Quantification of numerical uncertainty is discussed in some detail in Johnson et al. (2006). Validation, including calculation validation, is discussed in section “Validation.”

Code Verification: Code verification of system analysis codes is generally done via traditional techniques centered on first performing detailed reviews of the coding by parties which are independent of the code development group followed by a rigorous quality assurance protocol designed to track the code results obtained using verification benchmark problems with respect to known high-fidelity results.

Code verification of CFD codes involves the determination of coding correctness (Roache, 1998) a process separate from calculation verification (the quantification of numerical uncertainty). Users demand that the analysis software that will be applied to reactor safety analyses will already have been subjected to a variety of code verification tests. What will be required is documentation of these tests.

Only tests that exercise the options used in the particular computations need to be documented. The tests as a suite must be designed to exercise all the terms in the governing partial differential equations. For example, it is not adequate to only test the code on linearly varying solutions such as planar Couette flow, since this solution does not exercise vertical convection terms and others. The most complete and convincing type of code verification test uses the method of manufactured solutions or MMS (Roache, 1998) but this will not be required. If MMS is not used, it will probably be necessary to use a suite of test problems to demonstrate code correctness. For all of these problems, the observed rate of discretization error convergence should be documented and compared to a theoretical value for the discretization algorithms employed. If it is not, then more stringent requirements will be enforced during calculation certification (Johnson et al., 2006). The code verification must also include some data on the effect of iterative convergence criteria on numerical results (see Chapters 11–13 for details).

Code and Calculation Documentation: Software that is used for nuclear reactor safety analysis must be described in detail in code documentation. Such documentation should include describing equations used and their discretization as well as the basic methods used to obtain a solution. The truncation error and its formal order or accuracy should be given. The code documentation must include all details of implementation of the turbulence models used in calculations, for example, turbulence models for CFD software. The code documentation should be available for reference to reviewers who must review the associated calculational results.

For each calculation performed and submitted as a safety analysis, assumptions must be listed along with the details of the methods and models used. Other details, including but not limited to boundary and initial conditions, model constants (parameters), and other relevant information must also be provided. Options not used in the calculation need not be documented.

Reduction of Numerical Error: The reduction of numerical error is clearly a desirable objective for numerical calculations. Lessons have been learned about what not to do when using computational techniques for numerical analysis. These lessons-learned have been canonized in the requirements for manuscripts submitted to well-known journals such as the ASME Journal of Fluids Engineering. It therefore seems prudent to apply them to relevant software to reactor safety analysis. Examples of such requirements are those given in the ASME Journal of Fluids Engineering “Statement on Numerical Accuracy.” Details regarding the philosophy and meaning of the various key points are discussed in Johnson et al. (2006). Examples of the content include requirements that (a) methods must be at least second-order accurate in space, (b) grid independence or convergence must be established, and (c) in transient calculations phase error must be assessed and minimized.

Grid independence is the process of refining the grid from the starting point until numerical results stop changing or change by negligible amounts. Theoretically, the results will continue to change until the grid spacing approaches zero. The precision of the machine, however, will halt this process at a finite grid spacing. This is sometimes referred to as achieving machine zero (of the residuals). Not only is the process of obtaining grid independence important to reducing numerical errors, it is also a good way to obtain estimates of numerical uncertainty (see “Quantification of Numerical Uncertainty” in Johnson et al., 2006).

Iterative convergence relates to the number of iterations required to obtain residuals that are sufficiently close to zero, either for a steady-state problem or for

each time step in an unsteady problem. This error is in addition to the numerical error associated with the truncation error terms. Because of the well-known and unacceptable sensitivity of some commercial codes to the iteration tolerance and the too lax default tolerance, the final calculations must determine this effect. At least two levels of iteration tolerance must be shown and the sensitivity presented. For example, if results for a solution functional f are presented using a default iteration tolerance of (say) 10^{-3} reduction in residual from the initial condition, as required in Freitas et al. (2003), then another calculation with 10^{-4} will be required, and the sensitivity $f_{i0'}$ will be stated as the normalized % change in f per decade of change in iteration tolerance—as given in Eq. (4.1).

$$f_{i0'} = \frac{f(10^{-3}) - f(10^{-4})}{f(10^{-3})} \times 100 \quad (4.1)$$

The normalization can be based on $f_{\text{norm}} = f(10^{-3})$ when divides by near zero are not a problem, otherwise by another appropriate normalization. The final test of sufficient tightness of the iterative tolerance will be the acceptability of the final results based on estimation of numerical uncertainty and validation metrics.

For transient calculations, the same convergence criterion should apply as for spatial convergence (grid independence). The time step should be refined until negligible change is obtained. Also, though not required by the *Journal of Fluids Engineering*, it is recommended that the time-wise discretization scheme should be second-order accurate or better. While there are other practices to reduce numerical error, the above will constitute the required practices for reactor safety analysis at the present time. Other practices that reduce numerical error are certainly allowed and even encouraged.

Validation

Whether or not software is adequate for performing best-estimate VHTR analyses is determined using both “top-down” and “bottom-up” evaluations, as summarized in Fig. 4.9 and described in this section.

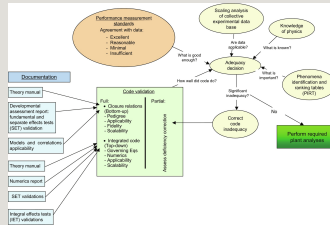


Fig. 4.9 VHTR system design software—elements of adequacy evaluation and acceptance testing practices.

“Bottom-Up” Code Adequacy: Bottom-up evaluation of code adequacy entails examination of four features: the pedigree, applicability, fidelity, and scalability of the code under consideration.

The pedigree of a systems code consists of its history, its development procedures, and the basis for each correlation that is used in the code. Any correlations, data sources, and approximations used in the code must be documented in textbooks, laboratory reports, papers, etc. The uncertainty data used to bound the correlation(s), data, and approximations such as instrumentation and data system uncertainties must be included in the documentation. The basis for the uncertainties should be traceable and reproducible. The assumptions and limitations of the models must be known and documented.

The applicability of a systems code depends on the range of use of each of its correlations, data, and approximations. Those ranges must be documented and referenced. Finally, the range of applicability claimed in the code manual should be consistent with the pedigree, or, if a greater range is claimed, the justification for the increase in range must be reported.

The fidelity of a systems code means the degree to which the code's predictions agree with physical reality. High fidelity requires that the mathematical models and correlations used in the code are not altered in an ad hoc manner from their documented formulation. A code is validated when it is shown that the code's predictions of key parameters agree within allowable tolerances with experimental data. The validation effort should be complete for all the key phenomena in the events of interest. Finally, benchmarking studies may either supplement the validation effort or make up the validation effort if appropriate standards are available, for example, comparisons of code calculation with a closed form solution.

“Bottom-up” scaling stems from the need to:

- Build experimental facilities that model the desired full-scale system.
- Closely match the expected behavior of the most important transient phenomena in the scenarios of interest.
- Demonstrate the applicability of data from a scaled facility to a full-scale system and to defend the use of data from a scaled facility in a code used to calculate the behavior of a full-scale system.
- Relate a calculation of a scaled facility to a calculation of a full-scale system.

Scalability studies are usually performed to scale key parameters for a portion of the system behavior, not to correlate global system behavior. Therefore, scalability analyses consist of four steps: (1) isolate the “first-order” phenomena, (2) characterize the “first-order” phenomena, (3) convert the defining equations into nondimensional form, and (4) adjust the experimental facility conditions to give equivalent behavior with the full-scale system within the limitation of the facility (or nearly equivalent, based on nondimensional numbers that follow from Step 3).

As implied in the earlier discussion, “bottom-up” code adequacy techniques focus principally on closure relationships. Thus, the field equations used in the code must be correctly formulated and programmed. In addition, the field equations must be reviewed by the scientific community, and its agreement on the correct formulation and insertion of the governing equations in the code must be obtained.

“Top-Down” Code Adequacy: The “top-down” approach for ensuring code adequacy focuses on the capabilities and performance of the integrated code. The top-down approach consists of four parts: numerics, fidelity, applicability, and scalability.

Numerics. Evaluation of the numerical solution considers convergence, stability, and property conservation.³ Again, agreement by the scientific community on acceptable convergence, stability, and property conservation must be obtained.

Fidelity. The fidelity of the code is demonstrated by performing thorough code assessments based on applicable integral-effects and separate-effects data. The data are part of an agreed-upon code assessment matrix constructed based on the transients of importance and the key phenomena for each phase of the transients.

Applicability. The code must be shown to be capable of modeling the key

phenomena in the system components and subsystems by conducting thorough validation studies. The key phenomena are identified in the PIRT. The method to determine whether the code is capable of modeling key phenomena is to compare the calculation produced by the code to data that have known uncertainties. For example, “excellent” agreement between the code calculation and data is achieved if the calculated value is at all times within the data uncertainty band.

The degree of agreement between the code calculation and the data is generally divided into four categories as given in Table 4.1. A more rigorous definition is given by Schultz (1993). A code is considered adequate in applicability when it shows either excellent or reasonable agreement with the highly ranked phenomena (sometimes identified as the dominant phenomena) for a transient of interest. If the code gives minimal or unacceptable agreement, additional work must be performed, which may range from additional code development to additional analyses if needed to better understand the phenomena.

Table 4.1

Code adequacy identifiers

--

Scalability. Experimental scaling distortions are identified and isolated, for example, inappropriate environmental heat losses that stem from the larger surface-to-volume ratios that are inherent to scaled facilities. Finally, an effort to isolate all code scaling distortions is performed through code assessment calculations. Scaling distortions may arise from an inappropriate use of a correlation developed in a small-scale system when applied to a full-scale system.

4.3.2 Software tool selection and software development

When confronted with the need to calculate key phenomena for an advanced nuclear plant, it is inevitable that analysts will be required to choose one software tool over another. This will be particularly true of system analysis software and CFD software. To assist the analyst in formally choosing software, a methodology

is given in Fig. 4.10 where a flow chart summarizes key factors and questions such as:

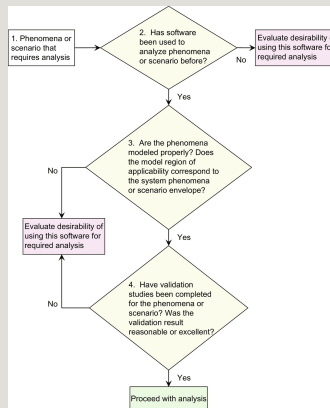


Fig. 4.10 Flow chart to evaluate applicability of analysis software.

- Has the software ever been used to analyze the phenomena or scenario? By answering this question the analyst may be introduced to references and other experts who have applied the software to similar phenomena or scenarios. Hence a body of useful information may be available.
- Are the phenomena modeled properly? And does the model region of applicability correspond to the system phenomena or scenario envelope? These questions may be most easily answered by using the required manuals and documentation identified in Fig. 4.8, for example, models and correlations, theory manual, scaling relationships and applications, developmental assessment reports, validations.
- Have validation studies been completed for the phenomena or scenario? Were the validation results reasonable or excellent (as defined in Table 4.1)—or were the results minimal or unacceptable? If a body of validation results are not available, or if the validation results were not “reasonable” as a minimum, then either the software should not be used or it should be validated to ensure that the calculated results are reliable rather than misleading.

Only when acceptable answers are obtained for the questions listed earlier, can the software under consideration be used for the required analysis with confidence.

References

Freitas C.J., Ghia U., Celik I., Roache P.J., Raad P. *ASME's quest to quantify numerical uncertainty*. In: 41st Aerospace, Sciences Meeting, Reno, NV, USA, 6–9 January; 2003.

Johnson R.W., Guillen D.P., Gallaway T. *Processes and procedures for application of cfd to nuclear reactor safety analysis*. In: INL/EXT-06-11789, Idaho Falls, ID, USA, September; 2006.

Levy S. *Two-Phase Flow in Complex Systems*. New York, NY, USA: John Wiley & Sons; 1999.

Roache P.J. *Verification and Validation in Computational Science and Engineering*. Albuquerque, NM, USA: Hermosa Publishers; 1998.

Schultz R.R. *Next generation nuclear plant – high-level functions and requirements: Addendum 1, requirements for system design models*. In: INEEL/EXT-03-01163, Addendum 1, Idaho Falls, ID, USA, December; 1993.

Sorensen J.N., Apostolakis G.E., Kress T.S., Powers D.A. In: On the Role of Defense in Depth in Risk-Informed Regulation, Probability and Safety Analysis Conference, Washington, DC, USA, August 22–25; 1999.

USNRC. *Compendium of ECCS Research for Realistic LOCA Analysis*. USNRC NUREG-1230 Washington, DC, USA: USNRC; 1988.

Venn J. On the diagrammatic and mechanical representation of propositions and reasonings. *London Edinburgh Dublin Philos. Mag. & J. Sci.* 1880;9:1–18.

Venn J. *Symbolic Logic*. London, UK: MacMillan; 1881.

Wilson G.E., Boyak B.E. The role of the PIRT process in experiments, code development and code applications

associated with reactor safety analysis. *J. Nucl. Eng. Des.* 1998;186:23–37.

Ybarrondo L.J., Fabic S., Griffith P., McPherson G.D. In: Examination of LOFT scaling, Winter Annual Meeting of the ASME, paper 74-WA/HT-53, New York, NY, USA; 1974.

Zuber, N., 1991. Appendix D: A Hierarchical Two-Tiered Scaling Analysis, An Integrated Structure and Scaling Methodology for Severe Accident Technical Issue Resolution, US NRC NUREG/CR-5809, November.

Zuber N., Wilson G.E., Boyack B.E., Catton I., Duffey R.B., Griffith P., Katsma K.R., Lellouche G.S., Levy S., Rohatgi U.S., Wulff W. Quantifying reactor safety margins, part 5: evaluation of scale-up capabilities of best estimate codes. *J. Nucl. Eng. Des.* 1990;119:97–107.

¹ The term “assessed” includes verification and validation of the numerical models using a top-down and bottom-up protocol which has been rigorously examined and is approved by the licensing authorities.

² Such changes may occur when the fluid behavior moves into the region of applicability of various correlations.

³ Property conservation issues arise when two calculations of the same property are performed by a systems code using two different algorithms or methods. This practice may follow in an effort to enhance the accuracy of the code result. Because the two methods are likely to calculate slightly different values of the same property such as pressure, property conservation must be considered.

Part Two

Thermal- hydraulics connections: The principles of thermodynamics and nuclear systems

Balance equations

D. Bestion; C. Morel Atomic Energy Commission, Grenoble, France

Abstract

Any investigation of a nuclear thermal-hydraulic issue either by hand calculations or using more or less sophisticated simulation tools requires first a difficult selection of the right degree of simplification of equations depending on the situation and on the expected accuracy and reliability of the solution. An effort is made to present the subject in steps of increasing difficulty and to show differences and similarities between balance equations in system thermal-hydraulics and in computational fluid-dynamics. This may help the reader to find his own path toward the understanding of the complex nuclear thermal-hydraulics. Attention is drawn on the physical assumptions and simplifications used in the derivation of equations and on the resulting limitations of the predictive capabilities. The chapter gives a picture of the available models with an evaluation of the predictive capabilities, the limitations, and the maturity of each model.

Keywords

Balance equations; Thermal-hydraulics fundamentals; Time averaging; Space averaging; Direct numerical simulation; Approaches to two-phase flow modeling; Drift-flux model

Nomenclature

Acronyms

BWR boiling water reactor

CFD computational fluid dynamics
(numerical solution of 3-D equations
of fluid dynamics)

CHF critical heat flux

CMFD computational multifluid
dynamics (numerical solution of 3-D
equations for multiphase or
multifluid flow)

DES detached eddy simulation

EVET equal velocity equal
temperature

HEM homogeneous equilibrium
model

IA interfacial area concentration

ITM interface tracking method

IRT interface reconstruction
technique

LBLOCA large break loss of coolant
accident

LES large eddy simulation

LEIS large-eddy and interface
simulation

PDE partial differential equation

PWR pressurized water reactor

RANS Reynolds average Navier-
Stokes

RHS right-hand side

TIA transport of interfacial area

UVUT unequal velocity unequal temperature

VLES very large eddy simulation

Symbols latin

A surface (m^2)

A cross-sectional area of a duct (m^2)

a_i interfacial area concentration (m^{-1})

C wall contour in a cross section of a duct

C_s pressure wave (sound) celerity
(m/s)

C_p heat capacity at constant pressure
(J/kg/K)

C_d drag coefficient

C_f friction coefficient

C_i interface contour in a cross
section of a duct

C_k wall contour in a cross section of
a duct in contact with phase k

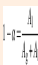
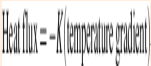
C_α void wave celerity (m/s)

C_μ turbulent viscosity coefficient


D diameter (m)

D mass diffusivity (m^2/s)


D_h hydraulic diameter (m)

 specific external forces (usually limited to gravity: ) (N/m^3)

F_{ik} interfacial momentum transfer to phase k per unit volume (N/m^3)

 gravity acceleration vector (m/s^2)

g_i gravity acceleration vector components (m/s^2)

g_z gravity acceleration projected along  axis (m/s^2)

G mass flux ($\text{kg}/\text{m}^2/\text{s}$)

G_k mass flux of phase k ($\text{kg}/\text{m}^2/\text{s}$)

h specific enthalpy (J/kg)

h_k specific enthalpy of phase k (J/kg)

h_{ksat} specific saturation enthalpy of phase k (J/kg)

h_{lv} latent heat (J/kg)

H_k time- and/or space-averaged specific enthalpy of phase k (J/kg)

j_k local superficial velocity of phase k (m/s)

J diffusive flux

J_{kt} turbulent flux of ψ_k

J_k area-averaged superficial velocity of phase k (m/s)

k turbulent kinetic energy (m^2/s^2)



mass flowrate (kg/s)



mass flux ($\text{kg}/\text{m}^2/\text{s}$)



mass flowrate of phase k (kg/s)

M_{ik} interfacial force per unit volume
(N/m^3)

M_{ikD} drag force per unit volume (N/m^3)

M_{ikL} lift force per unit volume (N/m^3)

M_{ikAM} added mass force per unit
volume (N/m^3)

M_{ikTD} turbulent dispersion force per
unit volume (N/m^3)



unit vector normal to interface-oriented outside phase k

Nu Nusselt number

p pressure (Pa)

P space-time averaged mixture pressure (Pa)

Pr Prandtl number



heat flux vector (W/m_2)

q_j conduction heat flux vector components (W/m_2)

q_{ext} volumetric external energy source, e.g., due to radiation (W/m_3)



heat flux vector in phase k (W/m_3)

q_{kj} conduction heat flux vector
components in phase k (W/m_2)

q_{ik} heat flux per unit volume from
interface to phase k (W/m_3)

q_{idl} heat flux per unit volume from
interface to droplet (W/m_3)

q_{ivdl} heat flux per unit volume from
vapor to interface of droplet (W/m_3)

q_{icl} heat flux per unit volume from
interface to continuous liquid (W/m_3)

q_{ivcl} heat flux per unit volume from
vapor to interface of continuous
liquid (W/m_3)

q_{kjt} turbulent heat diffusion vector
components in phase k (W/m_2)

q_w wall heat flux (W/m²)

q_{wk} wall heat flux to phase k (W/m²)

Q volume flowrate (m³/s)

Q_k volume flowrate of phase k (m³/s)

Q_{ik} interface-to-phase k interfacial energy transfer rate per unit volume (W/m³)

Re Reynolds number

R_k surface fraction of phase k (in 1-D equations)

R_{ij} Reynolds stress tensor

s specific entropy (J/K/kg)

t time (s)

T temperature (K)

T stress tensor (KPa)

u specific internal energy (J/kg)

$$\mathbf{u} = \frac{\mathbf{u}_2}{\mathbf{u}_1 + \mathbf{u}_2}$$

velocity vector (m/s)

\mathbf{v}_j velocity vector components (m/s)

$$\mathbf{v}_k = \mathbf{v}_k \cdot \mathbf{v}_k$$

velocity vector in phase k (m/s)

$\mathbf{v}_{k,j}$ velocity vector components for phase k (m/s)

$$\mathbf{F}_Q = \mathbf{F}_Q^k \times \mathbf{F}_Q^L$$

component of velocity of interface normal to the interface

V volume (m³)

\mathbf{V} time- and/or space-averaged velocity (m/s)

\mathbf{V}_k time- and/or space-averaged velocity of phase k (m/s)

\mathbf{V}_{idl} interfacial axial velocity at continuous liquid interface (m/s)

\mathbf{V}_{icl} interfacial axial velocity at continuous liquid interface (m/s)

Y_k mass concentration of species k

Symbols greek

α_k space-time fraction of phase k

β added mass coefficient

γ slip ratio

δ_{32} Sauter mean diameter

ε_k local time fraction of phase k

ε dissipation rate ($m_2/s_3 = W/kg$)

λ heat conductivity ($W/m_2/K$)

μ dynamic viscosity ($kg/s/m$)

ν kinematic viscosity (m_2/s)

Γ_{ik} interface-to-phase k interfacial mass transfer rate per unit volume ($kg/m_3/s$)

Γ_{vcl} interfacial mass transfer rate per unit volume from continuous liquid to vapor ($kg/m_3/s$)

Γ_{vdl} interfacial mass transfer rate per unit volume from dispersed liquid to

vapor ($\text{kg}/\text{m}^3/\text{s}$)

Γ_d mass transfer rate per unit volume
by droplet deposition ($\text{kg}/\text{m}^3/\text{s}$)

Γ_e mass transfer rate per unit volume
by droplet entrainment ($\text{kg}/\text{m}^3/\text{s}$)

σ surface tension (N/m)

ρ density (kg/m^3)

ρ_k density of phase k (kg/m^3)

ρ_m mixture density (kg/m^3)

σ surface tension (N/m)

τ_{ij} viscous stress tensor components
(Pa)

τ_{wk} wall friction force applied to

phase k (Pa)

ϕ porosity

ϕ volumetric source of ψ

χ_f fluid characteristic (or indicator)
function

ψ specific quantity

χ_k phase characteristic (or indicator)
function

Symbols other scripts

 viscous stress tensor components
(Pa)

Subscripts and superscripts

AM relative to the added mass force

c relative to continuous field

cl relative to continuous liquid field
(in a 3-field 2-phase flow of a fluid
with its vapor)

dl relative to dispersed liquid field
(in a 3-field 2-phase flow of a fluid
with its vapor)

d relative to dispersed field

cl relative to continuous liquid

dl relative to dispersed liquid

D relative to drag force

f relative to liquid phase in a gas-
liquid two-phase flow

g relative to gas phase in a gas-liquid

two-phase flow

k relative to phase k or field k

i relative to interface

i i th component

j j th component

ki relative to phase k or field k at interface

k relative to wall

l relative to liquid phase (in a two-phase flow of a fluid with its vapor)

L relative to lift force

m relative to a mixture

sat relative to a saturation

S relative to a surface

t relative to turbulence

TD relative to turbulent dispersion force

v relative to vapor phase (in a two-phase flow of a fluid with its vapor)

x,y,z coordinates

z curvilinear abscissa

Double averaged quantities in single-phase flow

$F_{\Delta H_i} = \Delta \text{Enthalpy}_i / \Delta \text{Enthalpy}_{\text{Average}}$ space-time averaged density

$$\mathbf{P} \triangleq \widehat{\bar{p}} = \langle \bar{p} \rangle^S$$

space-time averaged pressure

$$\mathbf{V} \triangleq \widetilde{\widetilde{v_z}} = \frac{\langle \overline{\rho v_z} \rangle^S}{\langle \bar{\rho} \rangle^S} = \frac{\langle \bar{\rho} \widetilde{v_z} \rangle^S}{\langle \bar{\rho} \rangle^S}$$

mass-weighted space-time velocity

$$\mathbf{H} \triangleq \widetilde{\widetilde{h}} = \frac{\langle \overline{\rho h} \rangle^S}{\langle \bar{\rho} \rangle^S} = \frac{\langle \bar{\rho} \widetilde{h} \rangle^S}{\langle \bar{\rho} \rangle^S}$$

mass-weighted space-time enthalpy

Double averaged quantities in two-phase flow

$$\mathbf{Q}_k \triangleq \widehat{\bar{\rho}}_k^k = \frac{\langle \overline{\chi_k \rho_k} \rangle^S}{\alpha_k}$$

space-time phase average density

$$\mathbf{Q}_m \triangleq \alpha_v \mathbf{Q}_v + \alpha_l \mathbf{Q}_l$$

space-time mixture average density

$$\mathbf{P}_k \triangleq \widehat{\bar{p}}_k^k \triangleq \frac{\langle \overline{\chi_k p_k} \rangle^S}{\alpha_k}$$

space-time phase

average pressure

$$P \triangleq \alpha_v P_v + \alpha_l P_l$$

space-time
mixture average pressure

$$V_k \triangleq \overline{v_{zk}} \triangleq \frac{\langle \overline{\chi_k \rho_k v_{zk}} \rangle^S}{\langle \overline{\chi_k \rho_k} \rangle^S} = \frac{\langle \overline{\chi_k \rho_k v_{zk}} \rangle^S}{\alpha_k \widehat{\rho_k}}$$

$$j_k \triangleq \overline{\chi_k v_{zk}} = \epsilon_k \overline{v_{zk}^k}$$

$$j \triangleq j_v + j_l$$

$$J_k \triangleq \langle j_k \rangle^S = \langle \epsilon_k \overline{v_{zk}^k} \rangle^S$$

$$J_k \triangleq J_v + J_l$$

$$v_k \triangleq \frac{J_k}{\alpha_k} = \frac{\langle \overline{\chi_k v_{zk}} \rangle^S}{\langle \overline{\chi_k} \rangle^S}$$

average velocity

$$G_k \triangleq \alpha_k Q_k V_k = \overline{\langle \chi_k \rho_k v_{zk} \rangle}^S \quad \text{phase mass flux}$$

$$G \triangleq G_v + G_l \quad \text{mixture mass flux}$$

$$H_k \triangleq \widetilde{h}_k^k = \frac{\overline{\langle \chi_k \rho_k h_k \rangle}^S}{\overline{\langle \chi_k \rho_k \rangle}^S} = \frac{\widehat{\rho_k h_k}^k}{\widehat{\rho_k}^k} \quad \text{mass-weighted space-time phase average enthalpy}$$

$$H_m \triangleq \frac{\alpha_v Q_v H_v + \alpha_l Q_l H_l}{Q_m} \quad \text{mass-weighted space-time mixture average enthalpy}$$

$$\widehat{H}_k \triangleq \frac{\overline{\langle \chi_k \rho_k v_{zk} h_k \rangle}^S}{\overline{\langle \chi_k \rho_k v_{zk} \rangle}^S} = \frac{\alpha_k \overline{\langle \rho_k v_{zk} h_k \rangle}^S}{G_k} \quad \text{mass flux-weighted space-time phase average enthalpy}$$

$$\widehat{H}_m \triangleq \frac{G_v \widehat{H}_v + G_l \widehat{H}_l}{G} \quad \text{mass flux-weighted space-time mixture average enthalpy}$$

$$x \triangleq \frac{\alpha_v Q_v}{Q_m} \quad \text{static quality}$$

$$X \triangleq \frac{G_v}{G} \quad \text{dynamic quality}$$

$$X_{th} = \frac{\widehat{H}_m - h_{lsat}}{h_{vl}} \quad \text{thermodynamic quality (or equilibrium quality)}$$

Non-dimensional quantities

Bo Bond number (Eötvös)

$$Bo = \frac{g \Delta \rho L^2}{\sigma}$$

Fr Froude number $Fr = \frac{v}{\sqrt{gD}}$

J_k^* non-dimensional superficial velocity of phase k (m/s²)

$$J_k^* = \frac{\sqrt{\rho_k} J_k}{\sqrt{g \Delta \rho D}}$$

K_k Kutateladze number for phase k

$$K_k = \frac{\sqrt{\rho_k} J_k}{(g \Delta \rho \sigma)^{1/4}}$$

Re Reynolds number $Re = \frac{vD}{\nu}$

We Weber number $We = \frac{\rho \Delta V^2 L}{\sigma}$

Operators

∇ gradient operator

$\nabla \cdot$ divergence operator

$\nabla^2 = \Delta$ Laplacian operator

$\vec{A} \vec{B}$ dyadic product of vectors
(= tensor)

$\vec{A} \cdot \vec{B}$ scalar product of vectors

(= scalar)

$A:B$ double-dot product of 2 tensors

(= scalar)

tT transpose tensor

Time averaging operators

$$\bar{f} \triangleq \frac{1}{T} \int_T f dt \quad \text{time averaging}$$

$$\tilde{f} \triangleq \overline{\rho f} / \bar{\rho} \quad \text{mass-weighted time averaging}$$

$$\bar{f}^k \triangleq \overline{\chi_k f_k} / \overline{\chi_k} \quad \text{phase time averaging}$$

$$\tilde{f}_k^k \triangleq \frac{\overline{\chi_k \rho_k f_k}}{\overline{\chi_k \rho_k}} = \frac{\overline{\epsilon_k \rho_k f_k}}{\overline{\epsilon_k \rho_k^k}} = \frac{\overline{\rho_k f_k^k}}{\overline{\rho_k^k}} \quad \text{phase mass-weighted time averaging}$$

Space averaging operators

$$\langle f \rangle^L \triangleq \frac{1}{L} \int_L f \, dl$$

space averaging
over one dimension

$$\langle f \rangle^S \triangleq \frac{1}{A} \int_A f \, ds$$

area averaging

$$\langle f \rangle^V \triangleq \frac{1}{V} \int_V f \, dv$$

volume averaging

$$\langle f(x, y, z, t) \rangle^{\theta} \triangleq \iiint_{R^3} g(x' - x, y' - y, z' - z, t) \cdot f(x', y', z', t) dx' dy' dz'$$

volume filtering

$$\check{f} \triangleq \frac{\langle \rho f \rangle^S}{\langle \rho \rangle^S}$$

mass-weighted area
averaging

$$\widehat{f}_k^k \triangleq \frac{\langle \chi_k f_k \rangle^S}{R_k}$$

phase area averaging

$$\check{f}_k^k \triangleq \frac{\langle \chi_k \rho_k f_k \rangle^S}{\langle \rho_k \rangle^S}$$

phase mass-
weighted area averaging

Space-time averaging operators

$$\hat{\bar{f}} \triangleq \langle \bar{f} \rangle^S \quad \text{space-time averaging (time-area averaging)}$$

$$\tilde{\bar{f}} \triangleq \frac{\langle \rho \bar{f} \rangle^S}{\langle \bar{\rho} \rangle^S} \quad \text{mass-weighted space-time averaging}$$

$$\hat{\bar{f}}_k^k \triangleq \frac{\langle \overline{\chi_k f_k} \rangle^S}{\alpha_k} \quad \text{phase space-time averaging}$$

$$\tilde{\bar{f}}_k^k \triangleq \frac{\langle \overline{\chi_k \rho_k f_k} \rangle^S}{\langle \overline{\chi_k \rho_k} \rangle^S} = \frac{\widehat{\rho_k f_k}^k}{\widehat{\rho_k}^k} \quad \text{mass-weighted phase space-time averaging}$$

Chapter foreword

It is mandatory for any scientist working with nuclear thermal-hydraulics, namely for those who use computer codes, to know the balance equations, their starting point, and the unavoidable approximations needed to achieve a solution.

The balance equations constitute the bases for the modern computational tools in thermal-hydraulic. An effort was made (by the author of the chapter) to track the subject in steps of increasing difficulty till the description of current trends and foreseeable developments. One key issue considered in the chapter is the distinctions and the similarities between balance equations which are at the bases of system thermal-hydraulics and computational fluid-dynamics.

The complexity of the topic should not discourage the reader from getting insights into the equations; rather, this should encourage him to find his own path toward the understanding of the nuclear thermal-hydraulics.

5.1 Introduction to balance equations

The objective of this chapter is to give minimum information to engineers on most current systems of equations used to describe and predict single- and two-phase flow in nuclear reactor thermal-hydraulic studies. Various modeling approaches are possible, and a few reference books exist on the mathematical derivation of the systems of equations (Delhay et al., 1981; Lahey and Moody, 1993; Ishii and Hibiki, 2011; Morel, 2015). Fundamental research in the area was also done by Boure (see, e.g., Boure, 1975). Details of all existing approaches will not be repeated here, and the following sections are focused on some important aspects of the most common set of equations used in system codes and some computational fluid dynamics (CFD) codes. Attention will be drawn on the physical assumptions and simplifications used to derive the equations and on the resulting limitations of the predictive capabilities.

After having recalled the basic principles of thermodynamics and fluid mechanics, the local instantaneous mass, momentum, and energy equations are given. Then, the various approaches to single- and two-phase flow modeling are presented and classified. The time-averaged, single-phase equations are derived to introduce the CFD approach and the turbulence modeling. The space averaged 1-D equations for single-phase flow are derived as they may be a very reasonable approximation in many situations. Then two-phase modeling is considered in the frame of the two-fluid approach. Time-averaged, two-fluid equations are given, and the derivation of space averaged 1-D equation is summarized in view of identifying the most important simplifications, before presenting the time-space averaged 1-D two-fluid system of equation as it is used in current system codes. Some simple two-phase models, such as the homogeneous equilibrium model (HEM), and the drift flux model are here presented as simplifications of the two-fluid model although they were previously developed, in order to better identify the degree of approximation

as function of the flow regime. Some recent advances on two-phase flow modeling include transport of interfacial area (TIA) and the three-field model. Equations used in these new approaches are also given.

5.2 The principles of thermodynamics and mechanics

All fluids considered in reactor thermal-hydraulics are here considered as Newton-Stokes fluids. They may be present as a single-component (species) fluid or multicomponent fluid. They may be present as a single-phase liquid, a single-phase gas, or even as a two-phase gas-liquid. It may happen that a dominant species (e.g., water) is present in both liquid and vapor phases with some other species present as noncondensable gas in a gas mixture or diluted in liquid (boron, nitrogen,...).

5.2.1 The local instantaneous equations

The three basic equations result from the basic principles:

- mass conservation
- Newton's second law of motion applied to fluid flow
- energy conservation (first principle of thermodynamics)

Let us consider a fluid volume $V(t)$ limited by a surface $A(t)$ as in Fig. 5.1. One may consider the variation of some specific quantity ψ using the general conservation equation:

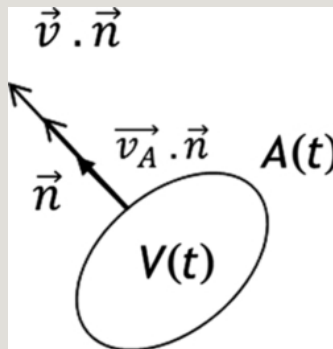


Fig. 5.1 Volume $V(t)$ limited by a surface $A(t)$.

$$\frac{d}{dt} \left(\int_{V(t)} \rho \psi dv = \int_{V(t)} \rho \phi dv - \int_{A(t)} \rho \psi \left(\vec{v} - \vec{v}_A \right) \cdot \vec{n} da - \int_{A(t)} (J \cdot \vec{n}) da \right) \quad (5.1)$$

$$-\int_{A(t)} \rho \psi \left(\vec{v} - \vec{v}_A \right) \cdot \vec{n} da$$

where $\int_{A(t)} \rho \psi \left(\vec{v} - \vec{v}_A \right) \cdot \vec{n} da$ is the flowrate of ψ entering through $A(t)$ and:

\vec{n} is the unit vector directed outside $V(t)$

ρ is the fluid density (kg/m³)

$\vec{v} = \frac{dx}{dt} \vec{e}_1 + \frac{dy}{dt} \vec{e}_2 + \frac{dz}{dt} \vec{e}_3$ is the velocity vector (m/s)

\vec{v}_A is the surface velocity vector (m/s)

ϕ is the volumetric source of ψ within $V(t)$

J is the diffusive flux of ψ through A

Mass momentum and total energy balance equations can be written considering the respective ψ , ϕ , and \vec{J} given in Table 5.1.

Table 5.1

Volumetric source and surface source in mass momentum and total energy equations

--	--

$\vec{f} = \frac{1}{\rho} \frac{d\vec{p}}{dt} \vec{e}_1 + \frac{1}{\rho} \frac{d\vec{q}}{dt} \vec{e}_2 + \frac{1}{\rho} \frac{d\vec{r}}{dt} \vec{e}_3$ is the specific external force (J/kg or m/s²) usually limited to gravity force (

$$\vec{F} = \vec{g}$$

T is the stress tensor (Pa or N/m²)

$$\vec{q}$$

is heat flux vector (W/m²)

q_{ext} is the external volumetric source of energy (usually radiation)

The Leibniz rule applied to a sufficiently regular function $f(x, y, z, t)$ writes:

$$\frac{d}{dt} \int_{V(t)} f \, dv = \int_{V(t)} \frac{\partial f}{\partial t} \, dv + \int_{A(t)} f \vec{v}_A \cdot \vec{n} \, da$$

Applied to $f=1$ it shows that:

$$\int_{A(t)} \vec{v}_A \cdot \vec{n} \, da = \frac{dV(t)}{dt}$$

$$\vec{a}$$

The Gauss theorem applied to a vector \vec{a} and a tensor B writes:

$$\int_{V(t)} \nabla \cdot \vec{a} \, dv = \int_{A(t)} \vec{a} \cdot \vec{n} \, da$$

$$\int_{V(t)} \nabla \cdot B \, dv = \int_{A(t)} B \cdot \vec{n} \, da$$

Using Leibniz rule and Gauss theorem, one can write all terms of the balance Eq. (5.1) using only volume-averaged terms. Applied to an elementary volume of fluid,

it results in local instantaneous mass, momentum, and energy equations (see Delhaye et al., 1981).

The mass balance equation or continuity equation is:

$$\frac{\partial \rho}{\partial t} + \nabla \cdot (\rho \vec{v}) = 0$$

The momentum balance equation is:


$$\frac{\partial \rho \vec{v}}{\partial t} + \nabla \cdot (\rho \vec{v} \vec{v}) - \rho \vec{F} - \nabla \cdot \vec{T} = 0$$

The total specific energy (internal energy+kinetic energy) balance equation is:

$$\frac{\partial}{\partial t} \left[\rho \left(u + \frac{v^2}{2} \right) \right] + \nabla \cdot \left[\rho \vec{v} \left(u + \frac{v^2}{2} \right) \right] - \rho \vec{F} \cdot \vec{v} - \nabla \cdot (\vec{T} \cdot \vec{v}) + \nabla \cdot \vec{q} = d_{tot}$$

u is the specific internal energy

$v^2 = \vec{v} \cdot \vec{v}$ is the specific kinetic energy (m²/s²)

T is split into a pressure tensor and deviator stress tensor 

$$\mathcal{T} \triangleq T + p I$$

τ_{ij} are the components of tensor 

p is the pressure (Pa)

I is the identity tensor

Separating the contributions of pressure and



$$\frac{\partial}{\partial t} \left(\rho \left(u + \frac{v^2}{2} \right) \right) + \nabla \cdot \left[\rho \vec{v} \left(u + \frac{v^2}{2} \right) \right] - \rho \vec{F} \cdot \vec{v} + \nabla \cdot (\rho \vec{v}) - \nabla \cdot (\tau \cdot \vec{v}) + \nabla \cdot \vec{q} = q_{in}$$

A total specific enthalpy equation can be written as:

$$\frac{\partial}{\partial t} \left(\rho \left(h + \frac{v^2}{2} \right) \right) + \nabla \cdot \left[\rho \vec{v} \left(h + \frac{v^2}{2} \right) \right] - \rho \vec{F} \cdot \vec{v} - \nabla \cdot (\tau \cdot \vec{v}) + \nabla \cdot \vec{q} = q_{in}$$

h is the specific enthalpy

$$h = u + \frac{p}{\rho}$$

The momentum equation can then be written as

$$\frac{\partial \rho \vec{v}}{\partial t} + \nabla \cdot (\rho \vec{v} \vec{v}) + \nabla p - \rho \vec{F} - \nabla \cdot \tau = 0$$

and can be projected along each coordinate in a Cartesian frame, using summation on repeated indices:

$$\frac{\partial \rho v_j}{\partial t} + \frac{\partial \rho v_i v_j}{\partial x_i} + \frac{\partial p}{\partial x_j} - \rho F_j - \frac{\partial \tau_{ij}}{\partial x_i} = 0$$

$$\frac{v^2}{2}$$

One can also write an equation for the specific kinetic energy by multiplying

the momentum energy by the velocity vector $\vec{u} = \frac{\vec{A}_2}{\vec{A}_1 + \vec{A}_2}$

$$\frac{\partial \rho^2}{\partial t} + \nabla \cdot \left(\rho \vec{v} \frac{v^2}{2} \right) - \rho \vec{F} \cdot \vec{v} + \vec{v} \cdot \nabla p - \vec{v} \cdot \nabla \cdot T = 0$$

which can be subtracted from total energy or total enthalpy equations to obtain internal energy and enthalpy equations:

$$\frac{\partial \rho u}{\partial t} + \nabla \cdot \left(\rho \vec{v} u \right) + p \nabla \cdot \vec{v} - T : \nabla \vec{v} + \nabla \cdot \vec{q} = q_{ext}$$

$$\frac{\partial \rho h}{\partial t} + \nabla \cdot \left(\rho \vec{v} h \right) - \frac{\partial p}{\partial t} \vec{v} \cdot \nabla p - T : \nabla \vec{v} + \nabla \cdot \vec{q} = q_{ext}$$

The flow can be solved by using a system of equations with the mass balance, the momentum balance, and one of the various forms of energy or entropy equations

complemented with equations of state and expressions of $\vec{u} = \frac{\vec{A}_2}{\vec{A}_1 + \vec{A}_2}$ and $\vec{q} = -\lambda \nabla T$.

The Fourier law is used for $\vec{q} = -\lambda \nabla T$:

$$\vec{q} = -\lambda \nabla T$$

λ is the heat conductivity (W/m/K)

In Newton-Stokes fluid, $\vec{\tau} = \eta \nabla \vec{v}$ writes:

$$T = -\frac{2}{3}\mu \nabla \cdot \vec{v} + \mu \left(\nabla \cdot \vec{v} + \nabla \cdot \vec{v} \right)$$

μ is the dynamic viscosity (kg/m/s)

The thermodynamic state of a single-phase single-component fluid is characterized by the knowledge of two independent state variables such as pressure and temperature (p, T) or (p, h) , (p, u) .

Let us consider that (p, h) are chosen as independent variables, the necessary equations of state are:

$$\rho(p, h); T(p, h); \mu(p, h); \lambda(p, h)$$

Combining above equations can then result in three equations with three

independent unknowns p , h , and $\theta = \frac{h}{T}$ such as:

$$\frac{\partial \rho}{\partial t} + \nabla \cdot (\rho \vec{v}) = 0$$

$$\frac{\partial \rho \vec{v}}{\partial t} + \nabla \cdot (\rho \vec{v} \vec{v}) + \nabla p - \rho \vec{F} - \nabla \cdot \left(\frac{2}{3} \mu \nabla \cdot \vec{v} + \mu \left(\nabla \cdot \vec{v} + \nabla \cdot \vec{v} \right) \right) = 0$$

μ is often considered as nearly homogeneous so that:

$$\frac{\partial \rho \vec{v}}{\partial t} + \nabla \cdot (\rho \vec{v} \vec{v}) + \nabla p - \rho \vec{F} - \mu \left(\frac{1}{3} \nabla \cdot \vec{v} + \nabla^2 \vec{v} \right) = 0$$

$$\frac{\partial}{\partial t} \left[\rho \left(h + \frac{v^2}{2} \right) - p \right] + \nabla \cdot \left[\rho \vec{v} \left(h + \frac{v^2}{2} \right) \right] - \rho \vec{F} \cdot \vec{v} - \nabla \cdot (T \cdot \vec{v}) - \nabla \cdot (\mu \nabla T) = q_{ext}$$

Momentum equation for each component is:

$$\frac{\partial \rho v_{ij}}{\partial t} + \frac{\partial \rho v_i v_{ij}}{\partial x_j} + \frac{\partial p}{\partial x_j} = -\rho g_j + \mu \left[\frac{\partial^2 v_{ij}}{\partial x_i^2} + \frac{1}{3} \frac{\partial^2 v_i}{\partial x_j \partial x_i} \right]$$

The entropy equation writes:

$$\rho \frac{ds}{dt} = \frac{q_{ext}}{T} - \nabla \cdot \left(\frac{\vec{q}}{T} \right) + \frac{T : T}{2\mu T} + \frac{\lambda (\nabla T)^2}{T^2}$$

The two last terms of the entropy equation are the irreversible entropy sources associated to viscous dissipation and heat conduction.

The second principle of thermodynamics just indicates that $\mu > 0$ and $\lambda > 0$.

The single-component single-phase flow equations of Newton-Stokes fluid can be summarized as in the following if we use the total enthalpy equation. Note that the principal variables are here p , h , and $\alpha = \frac{h_2}{h_1 + h_2}$.

Basic equations: 1-Component 1-phase flow equations for a Newton-Stokes fluid

Principal variables: p , $\alpha = \frac{h_2}{h_1 + h_2}$, h

$$\frac{\partial \rho}{\partial t} + \nabla \cdot (\rho \vec{v}) = 0$$

$$\frac{\partial \rho}{\partial t} + \nabla \cdot \left(\rho \vec{v} \right) + \nabla p - \rho \vec{F} - \mu \left(\frac{1}{3} \nabla \nabla \cdot \vec{v} + \nabla^2 \vec{v} \right) = 0$$

$$\frac{\partial}{\partial t}\left[\left(\frac{\rho}{\rho_0}\right)^{\frac{\gamma}{\gamma-1}}\right]-\rho\left[\vec{v}\cdot\left(\frac{\gamma}{\gamma-1}\vec{\hat{v}}\right)\right]-\rho\vec{F}\cdot\vec{v}-\nabla\cdot\left(\vec{v}\cdot\nabla\right)-\nabla\cdot\lambda\nabla\vec{v}=\omega$$

$$T=-\frac{2}{3}\mu \nabla \cdot \vec{v} \; I + \mu \left(\nabla \vec{v} + {}^t \nabla \vec{v} \right);$$

$$\rho=\rho(p,h);T=T(p,h);u=\mu(p,h);\lambda=\lambda(p,h)$$

In a multicomponent fluid flow with n species, $n-1$ equations are added to predict mass concentration of each species.

$$\frac{\partial \rho Y_k}{\partial t} + \nabla \cdot \left(\rho Y_k \vec{v} \right) = \nabla \cdot \left(\overrightarrow{\dot{m}_{Y_k}} \right) + S_{Y_k}$$

$$\overrightarrow{\dot{m}_{Y_k}} = D_{Y_k} \nabla Y_k$$

which can be written as:

$$\frac{\partial \rho Y_k}{\partial t} + \frac{\partial \rho v_j Y_k}{\partial x_j} = \frac{\partial}{\partial x_j} \left(D_{Y_k} \frac{\partial Y_k}{\partial x_j} \right) + S_{Y_k}$$

Y_k is the mass concentration of species k

ρ is the density of the mixture

$$\sum_{k=1,n} Y_k = 1$$

where $\overrightarrow{m_{Y_k}}$ is the diffusion mass flux vector of component k within the mixture (kg/m²/s)

One may choose $(p, h, Y_{k=2,n})$ as independent variables, and the necessary equations of state are then functions of $2+n-1$ state variables:

$$\rho(p, h, Y_{i=2,n}) ; T(p, h, Y_{i=2,n}) ; \mu(p, h, Y_{i=2,n}) ; \lambda(p, h, Y_{i=2,n})$$

5.2.2 Some properties of the local instantaneous equations

It is not yet proven that this set of equations is a well-posed problem as defined by Jacques Hadamard, which requires three conditions:

1. A solution exists
2. The solution is unique
3. The solution's behavior changes continuously with the initial conditions

The third condition is directly linked to the predictability of fluid flows since it is related to the sensitivity to initial conditions. An exponential sensitivity would result in an ill-posed problem and a high sensitivity may give at least an ill-

conditioned problem.

It is simply “believed” that fluid equations are exact and correspond to a well-posed problem—even if the demonstration is still open to mathematicians—but it is observed that turbulence may result in a rather high sensitivity to initial conditions. It is also observed that macroscopic quantities (time averaged, space averaged, or space-time averaged quantities) have a lower sensitivity to initial conditions. This opens the possibility to predict macroscopic fluid flow parameters using averaged balance equations.

Fluid flow equations are strongly nonlinear, which may explain the rather high sensitivity to initial conditions. The main source of nonlinearity is the advection term in momentum equations.

The turbulent nature of many flows induces a chaotic or stochastic character and a large spectrum of flow fluctuations including very small scales. This makes it practically impossible to solving the local instantaneous equations. Analytical exact solutions are not known in (almost) all cases of interest and numerical solutions are and will remain for a long time beyond the capabilities of current computers.

Since exact equations cannot be solved, simplified, and/or averaged equations must be used to predict fluid flows. The main difficulty of industrial thermal-hydraulic studies is to apply the right simplification to exact equations to give an approximate solution with a sufficient degree of confidence. The next sections will present some of the simplified set of equations used in nuclear thermalhydraulics.

5.3 The various approaches to single-phase modeling

One can classify single-phase modeling approaches (Bestion et al., 2011) first with regard to the space dimension of the model, considering 0-D, 1-D, 2-D, and 3-D models. Then, to be more specific one may consider the type of time and/or space averaging which is used. 3-D models are often called CFD models. They can be split first into 3-D for porous body and 3-D CFD in an open medium approach.

RANS-type models, LES-type models, and direct numerical solution (DNS) are the three main categories of single-phase CFD models in open medium, see Table 5.2. RANS models are the most commonly used in nuclear reactor applications, and they include a large variety of turbulence models. Some recommendations were made by the Writing Group of OECD-WGAMA for selection of the model

according to the application for reactor safety analysis (Mahaffy 2007).

Table 5.2

Characteristics and modeling needs of the various types of single-phase CFD



5.3.1 RANS-type models

Time or ensemble averaging of local instantaneous equations (mass momentum and energy) is a common way to derive equations for the so-called Reynolds average Navier-Stokes (RANS) approach. Although time averaging and ensemble averaging are different, they can reasonably be considered as equivalent (ergodicity) in steady or quasi-steady flows where the RANS approach is applied. Since closure laws (e.g., for Reynolds stress) are almost systematically validated against time averaged measured flow parameters, one may consider that practical validated RANS model are time-averaged models. Time-averaged equations are supposed to filter all turbulent eddies and to predict only a mean velocity field. The time averaging affects both time and space resolution in an Eulerian approach since eddies are transported by the mean flow. The most popular RANS model ($k-\epsilon$) uses a two-equation turbulence model with the Boussinesq approximation and a turbulent viscosity. Many variations of two-equation turbulence modeling exist such as $k-l$, $k-\omega$, SST, RNG- $k \epsilon$, $k-\epsilon-V_2$, nonlinear $k-\epsilon$. RANS was initially devoted to steady flow but may be also applied to some unsteady or transient flow (U-RANS or T-RANS) if the time scale of the mean flow is larger than the time scale of the largest eddies. It has been shown that a RANS approach could predict the large-scale Von Karman alleys in the wake of the cylinder provided that the numerical scheme does not induce artificial numerical viscosity.

RANS-type models require closure models for Reynolds stress tensor and turbulent diffusion of heat. Wall functions are required for both momentum and energy to avoid too fine meshes close to the walls. The modeling effort is rather heavy since models for Reynolds stress require additional equations with several closure laws.

5.3.2 Scale/eddy-resolving-type models

When the computational grid is not sufficient to resolve the entire spectrum of scale (from integral to Kolmogorov ones), a space filter is applied to the basic balance equations. This allows predicting large eddies (or sometimes called super-grid scale), whereas the effects of smaller eddy have to be modeled in a statistical way. This is the basis of the large eddy simulation (LES). The detached eddy simulation (DES) and very large eddy simulation (VLES) belong to the same class of scale/eddy-resolving models. Some hybrid methods between U-RANS and LES exist such as scale adaptive simulation (SAS). LES requires a transient calculation with rather fine 3-D space nodalization; high-order space discretization scheme and high-order time integration method are needed, which make the method much more CPU time demanding than RANS methods. Statistical models are required to mimic the diffusive effects of the unresolved subgrid scales (called simply “subscale” in the VLES context) on momentum and energy transfers. Very often turbulent viscosity and diffusivity models are used. Wall functions are also required for both momentum and energy to avoid fine meshes near the walls. However the modeling effort is much lighter than for RANS.

5.3.3 Direct numerical solution (DNS)

Direct numerical simulation just solves exact local instantaneous equations without any averaging or filtering. In turbulent flow this requires that the nodalization is extremely fine to be able to capture the smallest eddies at the Kolmogorov scale. This approach being extremely CPU costly is limited to some investigations of simple problems to create reference solutions or “numerical experiments” in view of assessing other approaches.

5.3.4 Locality and universality of the modeling

Both RANS- and LES-type methods require some closure laws for additional terms of equations coming from the averaging of filtering procedure. The modeling of these terms most often assumes a kind of “principle of locality” where the physics of the process to model depends only on local flow variables (i.e., velocity, density, internal energy) and their time and space local derivatives. This is the case for the treatment of Reynolds stresses and turbulent heat fluxes in both RANS- and LES-type methods. The only exceptions to this principle of locality are the so-called wall functions where some closure terms depend on the distance to a wall. This allows using rather coarse nodalization in high shear regions close to a wall.

It must be stressed that the principle of locality is much more relevant in a LES-type method than in a RANS approach. The subgrid local turbulent viscosity at a

given point $P(x, y, z, t)$ of a flow in a LES approach models only effects of small eddies which are close to point P . In a RANS approach the effects of the largest eddies on local physics have also to be modeled, and such large eddies depend on flow conditions far from the point P . This is a reason why different RANS model options are recommended for different flows like a boundary layer, wake, mixing layer, or jet, whereas LES best models tend to be more universal. In RANS approach, local models are much more geometry dependent than in LES. One may also consider that only DNS provides a full application of the principle of locality since the only transfers that are present are molecular transfers, which are expressed as functions of the first derivatives (Fourier law, Newtonian fluid law).

One may define a figure of merit to quantify the degree of locality and then the degree of universality of a model which would give five stars to the DNS *****, four stars **** to the LES, three stars *** to the RANS, two stars ** to the 2D, only one star* to porous-3D and to 1D, and no star to 0D.

5.4 The time-averaged single-phase equations

5.4.1 Reynolds averaging—time averaging

Time averaged single-phase equations are used in single-phase RANS CFD models. CFD is presented in more detail in Chapter 12. So these equations are just rapidly presented here in view of using them for double-space time-averaging of 0-D, 1-D, 2-D, and 3-D models for porous body.

When boundary conditions of a flow are steady—not considering turbulent fluctuations—time-averaged equations are used. The Reynolds averaging was applied to steady or quasi-steady flows where time scales of mean flow variations are significantly larger than time scales of turbulent fluctuations. Time averaging over a time period T is:

$$\bar{f} = \frac{1}{T} \int_T f dt$$

$$f \triangleq \overline{f} + f'$$

If variations of \overline{f} over a time scale T is negligible, then

$$\overline{f'} = 0$$

The properties of the Reynolds averaging are such that:

$$\overline{cf} = c\overline{f} \text{ if } c = cte$$

$$\overline{\overline{f}} = \overline{f}$$

$$\overline{f\overline{g}} = \overline{f}\overline{g}$$

$$\overline{\frac{\partial f}{\partial x}} = \frac{\partial \bar{f}}{\partial x}$$

$$\overline{\frac{\partial f}{\partial t}} = \frac{\partial \bar{f}}{\partial t}$$

One can consider three level of compressibility of the fluid:

1. Incompressible flow for low Mach flow without dilatation:

$$\rho = \rho_0 = cte$$

2. Dilatable flow for low Mach flow with dilatation:

$$\rho = \rho_0 [1 - \beta(T - T_0)]$$

3. Compressible flow:

$$\rho = \rho(P, T)$$

In the most general case one may average local instantaneous equations and obtain

the following mass, momentum, and total enthalpy equations:

$$\frac{\partial \overline{\rho}}{\partial x} + \frac{\partial \overline{\rho v_j}}{\partial x_j} = 0$$

$$\frac{\partial \overline{\rho v_j}}{\partial t} + \frac{\partial \overline{\rho v_j v_l}}{\partial x_l} + \frac{\partial \overline{p}}{\partial x_j} = -\overline{\rho} g_t + \mu \left[\frac{\partial^2 \overline{v_j}}{\partial x_t^2} + \frac{1}{3} \frac{\partial^2 \overline{v_l}}{\partial x_j \partial x_l} \right]$$

$$\frac{\partial}{\partial t} \left[\overline{\rho u} + \frac{\overline{\rho v^2}}{2} \right] + \nabla \cdot \left[\overline{\rho u \vec{v}} + \frac{\overline{\rho \vec{v} v^2}}{2} \right] - \overline{\vec{F}} \cdot \overline{\rho \vec{v}} - \nabla \cdot \left(\overline{T \cdot \vec{v}} \right) + \nabla \cdot \overline{\vec{q}} = \overline{q_w}$$

$$\frac{\partial}{\partial t} \left[\overline{\rho \overline{u}} + \frac{\overline{\rho \overline{u^2}}}{2} \right] + \nabla \cdot \left[\overline{\rho \overline{u \vec{v}}} + \frac{\overline{\rho \vec{v} \overline{u^2}}}{2} \right] - \overline{\vec{F}} \cdot \overline{\rho \vec{v}} - \nabla \cdot \left(\overline{T \cdot \vec{v}} \right) + \nabla \cdot \overline{\vec{q}} = \overline{q_w}$$

It is usual to define mass-weighted average quantities of velocity, internal energy, or enthalpy

$$\widetilde{v_j} = \overline{\rho v_j} / \overline{\rho}$$

$$\widetilde{u} = \overline{\rho u} / \overline{\rho}$$

$$\widetilde{h} = \overline{\rho h} / \overline{\rho}$$

Mass balance equation is thus simplified

$$\frac{\partial \overline{\rho}}{\partial t} + \frac{\partial \overline{\rho \widetilde{v}_j}}{\partial x_j} = 0$$

But the averaging of the nonlinear momentum balance advection term induces an additional tensor \overrightarrow{T}^t of components R_{ij}

$$\overrightarrow{T}^t \triangleq \overline{\rho \widetilde{\vec{v}} \widetilde{\vec{v}}} - \widetilde{\overline{\rho \vec{v}} \vec{v}}; \quad R_{ij} \triangleq \overline{\rho \widetilde{v}_i \widetilde{v}_j} - \widetilde{\overline{\rho v_i} v_j}$$

R_{ij} is called the Reynolds stress tensor

The averaging of the nonlinear enthalpy balance advection term induces also an additional vector term \overrightarrow{q}^t which is a turbulent heat transfer: or

$$\overrightarrow{q}^t \triangleq \overline{\rho h \widetilde{\vec{v}}} - \widetilde{\overline{\rho h} \vec{v}}; \quad q_j^t \triangleq \overline{\rho h \widetilde{v}_j} - \widetilde{\overline{\rho h} v_j}$$

5.4.2 Incompressible flow

In the case of an incompressible flow:

$$\frac{\partial \overline{v_j}}{\partial x_j}=0$$

$$\overline{\rho v_i v_j} \triangleq \rho \overline{v_i v_j} + \rho \overline{v_i' v_j'}; \quad R_{ij} = \overline{\rho v_i' v_j'}$$

$$\overline{\rho h v_j} \triangleq \rho \overline{h v_j} + \rho \overline{h' v_j'}; \quad q_j' = \overline{\rho h' v_j'}$$

$$\frac{\partial \overline{v_j}}{\partial t} + \frac{\partial \overline{v_i v_j}}{\partial x_i} + \frac{1}{\rho} \frac{\partial \overline{p}}{\partial x_j} = -g_j - \frac{\partial R_{ij}}{\partial x_i} + \nu \left[\frac{\partial^2 \overline{v_j}}{\partial x_i^2} \right]$$

$$\frac{\partial}{\partial t}\left[\rho\left(h+\frac{\overline{v}^2}{2}+k\right)-\overline{p}\right]+\nabla\cdot\left[\rho\left(\frac{\overline{\overline{h\overline{v}}+\overline{v}v^2}}{2}\right)\right] \\ -\rho\overline{\overline{F}}\cdot\overline{\overline{v}}-\nabla\cdot\left(\overline{T\cdot\overline{v}}\right)+\nabla\cdot\left(\overline{\overline{q}}+\overline{\overline{q'}}\right)=\overline{q_{ext}}$$

$$k=\frac{1}{2}\overline{v_i'v_i'} \qquad C_p=ct$$

is the turbulent kinetic energy when

$$\overline{\rho h v_j} \triangleq \rho \overline{h v_j} + \rho C_p \overline{T^{\prime} v_j'}; q_j' = \rho C_p \overline{T^{\prime} v_j'}$$

$$q_j^t$$

This shows that R_{ij} and q_j^t are representing, respectively, a transport of momentum and energy by velocity fluctuations. By analogy with transport by

molecular agitation, they were first modeled as diffusive terms.

A usual modeling consists in using a turbulent viscosity and turbulent conductivity:

$$T' \triangleq R_{ij} = -\rho \overline{v'_i v'_j} = \rho \left[-\frac{2}{3} k \delta_{ij} + \nu_t \left(\frac{\partial \bar{v}_i}{\partial x_j} + \frac{\partial \bar{v}_j}{\partial x_i} \right) \right]$$

$$q'_j = \rho C_p \overline{u'_j T'} = -\lambda_t \frac{\partial \bar{T}}{\partial x_j} \lambda_t = \frac{C_p \mu_t}{Pr_t}$$

$$\overline{u'_j Y'_k} = -D_{Y_{kt}} \frac{\partial \bar{Y}_k}{\partial x_j} D_{Y_{kt}} = \frac{\nu_t}{Sc_t}$$

Considering an isotropic turbulent viscosity one can model it as a product of a turbulent length scale l with a turbulent velocity scale v'

$$\nu_t \sim l v'$$

Following Kolmogorov, in high Reynolds number flows the dissipation ε is controlled by inertial processes and does not depend on viscosity. Then from dimensional analysis one can write:

$$\varepsilon \sim \frac{v'^3}{l}$$

Using the turbulent kinetic energy k as the square of the velocity scale:

$$\nu_t \sim \frac{v'^4}{\varepsilon} = C_\mu \frac{k^2}{\varepsilon}$$

This relation opens the way to the very popular k - ε turbulence model which requires transport equations for k and ε . It belongs to the first-order RANS models.

Many other turbulence model exist for R_{ij} and q'_j . More advanced second-order RANS models write separate equations for each component of the R_{ij} tensor and

\vec{q} vector which may be complemented by equations for ε , temperature variance $k_\theta = T'^2$, and its associated dissipation ε_θ .

5.4.3 Closure of the time-averaged equations

In order to close the system of time-averaged equations, some simplifications and models are necessary:

- A choice is first made of using only time averaging of all variables or using mass-weighted averaging of velocity and enthalpy
- Expression for R_{ij} : models developed first for incompressible flows were extrapolated to compressible flow with some adaptation
- Expression for q_j : models developed first for incompressible flows were extrapolated to compressible flow with some adaptation

$$\frac{\overline{\rho v^2}}{2}$$

- Expression for:

$$\overline{\rho \frac{v^2}{2}} \cong \bar{\rho} \frac{\bar{v}^2}{2} + \bar{\rho} k$$

- it may be approximated by

$$\frac{\bar{v}^2}{2} \gg k$$

neglected considering that:

$$\overline{\rho \frac{v^2}{2}} \cong \bar{\rho} \frac{\tilde{v}^2}{2} + \bar{\rho} k$$

- it may be also approximated by

$$\frac{\tilde{v}^2}{2} \gg k$$

neglected considering that:

$$\nabla \cdot (\overline{T \cdot \vec{v}})$$

- Expression for may require simplification of average of products:

$$\nabla \cdot (\overline{T \cdot \vec{v}}) \cong \nabla \cdot (\bar{T} \cdot \vec{v})$$

○

$$\nabla \cdot (\overline{T \cdot \vec{v}}) \cong \nabla \cdot (\tilde{T} \cdot \tilde{v})$$

○ or

A possible set of time-averaged equations for a single-component single-phase flow equations of Newton-Stokes fluid can be summarized as follows if we use the total enthalpy equation and if we use the mass-weighted velocity and enthalpy.

Note that the principal variables are here \bar{p} , \tilde{h} , and \tilde{v}_j :

Time-averaged equations: 1-Component 1-phase flow equations for a Newton-Stokes fluid

Principal variables: $\bar{p}, \vec{\tilde{v}}, \tilde{h}$

$$\frac{\partial \bar{p}}{\partial t} + \nabla \bar{p} \cdot \vec{\tilde{v}} = 0$$

$$\frac{\partial \vec{\tilde{p}}}{\partial t} + \nabla \vec{\tilde{p}} \cdot \vec{\tilde{v}} + \nabla \vec{p} = + \vec{\tilde{p}} \cdot \vec{g} + \nabla \cdot (\vec{T} + \vec{T}')$$

$$\frac{\partial}{\partial t} \left[\vec{p} \left(\vec{\tilde{h}} + \frac{\vec{v}^2}{2} \right) - \vec{p} \right] + \nabla \cdot \left[\vec{p} \cdot \vec{\tilde{v}} \left(\vec{\tilde{h}} + \frac{\vec{v}^2}{2} \right) \right] \\ = \vec{F} \cdot \vec{p} \cdot \vec{\tilde{v}} + \nabla \cdot \left[(\vec{T} + \vec{T}') \cdot \vec{\tilde{v}} \right] + \nabla \cdot \left(\vec{q} + \vec{q}' \right) + \vec{q} \cdot \vec{\omega}$$

$$T = -\frac{2}{3} \mu \nabla \cdot \vec{\tilde{v}} I + \mu \left(\nabla \vec{\tilde{v}} + {}^t \nabla \vec{\tilde{v}} \right) ; \vec{\tilde{q}} = -\lambda \nabla T$$

$$\vec{p} = p(\rho, \tilde{h}); \vec{T} = T(\rho, \tilde{h}); \mu = \mu(\rho, \tilde{h}); \lambda = \lambda(\rho, \tilde{h})$$

+ expressions or equations for \vec{T}' and \vec{q}'

One can notice that time averaging only adds \vec{T}' and \vec{q}' in momentum and energy equations.

5.5 The space-time-averaged 1-D equations for single-phase flows

1-D equations are commonly used to describe flows and heat transfers in circuits. It can result from space averaging over the cross section of the duct and produces a set of three partial derivative equations function of time and curvilinear abscissa. It is applicable to ducts with continuous cross-sectional area and is not adapted to abrupt area changes. Another approach is the use of successive “control volumes” where equations are integrated over a volume between two sections of the duct. This produces interconnected zero-D differential equations function of time only rather than real 1-D equations. This allows abrupt area changes and may be equivalent to 1-D equations when the distance between the sections tends to zero.

5.5.1 The 1-D equations for single-phase flow

The derivation of space-time-averaged equations in 1-D is a very common approach for flows in pipes and ducts. As shown by Delhaye et al. (1981) one can proceed in two ways: first space averaging then time averaging or time averaging then space averaging. In the case of single-phase flow, the second approach is summarized here.

One will use here the set of time-averaged equations given in Section 5.4 where \bar{p} , \tilde{h} , and \tilde{v}_j are the principal variables, which can also be written (with summation on repeated indices):

$$\frac{\partial \bar{p}}{\partial t} + \frac{\partial \bar{p} \tilde{v}_j}{\partial x_j} = 0$$

$$\frac{\partial \bar{p} \tilde{v}_j}{\partial t} + \frac{\partial \bar{p} \tilde{v}_i \tilde{v}_j}{\partial x_i} + \frac{\partial \bar{p}}{\partial x_j} = -\bar{p} g_j + \frac{\partial}{\partial x_j} (\bar{\tau}_{ij} - R_{ij})$$

$$\frac{\partial \left[\bar{p} \left(\bar{s} + \frac{v^2}{2} \right) - p \right]}{\partial t} + \frac{\partial \left[\bar{p} \tilde{v}_j \left(\bar{s} + \frac{v^2}{2} \right) \right]}{\partial x_j} - \bar{p} g_j \tilde{v}_j - \frac{\partial \left((\bar{\tau}_{ij} - R_{ij}) \tilde{v}_j \right)}{\partial x_j} + \frac{\partial \left(\bar{q} + \bar{q}_r \right)}{\partial x_j} = \bar{q}''$$

Now one must average these equations on the cross section of a duct using the following notation

$$\langle f \rangle^S = \frac{1}{A} \int_A f \, ds$$

Fig. 5.2 shows a portion of a duct with the following notations:

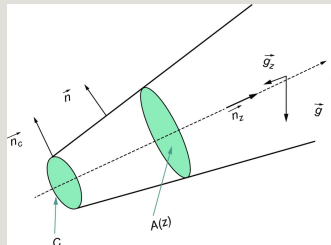


Fig. 5.2 Portion of a duct.

z is the curvilinear abscissa of the duct

$A(z)$ is the cross-sectional area

C is the contour of A



\vec{n} is the vector normal to the duct wall directed to the exterior of the duct



\vec{n}_c is the vector normal to the contour C directed to the exterior of the duct



\vec{g}_z is the gravity acceleration vector projected along z axis

One will use a particular form of the Leibniz rule

$$\frac{d}{dt} \int_A f(x, y, z, t) da = \int_A \frac{\partial f}{\partial t} da + \int_C f \vec{v} \cdot \vec{n} \frac{dC}{\vec{n} \cdot \vec{n}_C}$$

Since there is no flow through the wall $\vec{v} \cdot \vec{n} = 0$ and:

$$\left\langle \frac{\partial f}{\partial t} \right\rangle^S = \frac{\partial \langle f \rangle^S}{\partial t}$$

Notation: $\hat{f} = \langle \bar{f} \rangle^S$

One will use a particular form of the Gauss theorem applied to a vector \vec{B} or a tensor T

$$\int_A \nabla \cdot \vec{B} da = \frac{\partial}{\partial z} \int_A B_z da + \int_C \vec{n} \cdot \vec{B} \frac{dC}{\vec{n} \cdot \vec{n}_C}$$

$$\vec{B} = \vec{n}_z \Rightarrow \frac{\partial A}{\partial z} = - \int_C \vec{n} \cdot \vec{n}_z \frac{dC}{\vec{n} \cdot \vec{n}_C}$$

$$\int_A \nabla \cdot T da = \frac{\partial}{\partial z} \int_A \vec{n}_z \cdot T da + \int_C \vec{n} \cdot T \frac{dC}{\vec{n} \cdot \vec{n}_C}$$

5.5.1.1 Mass balance equation

$$\begin{aligned} \left\langle \frac{\partial \rho}{\partial t} + \nabla \cdot (\bar{\rho} \vec{v}) \right\rangle^S &= \frac{\partial \langle \bar{\rho} \rangle^S}{\partial t} + \left\langle \nabla \cdot (\bar{\rho} \vec{v}) \right\rangle^S = \frac{\partial \langle \bar{\rho} \rangle^S}{\partial t} + \frac{1}{A} \frac{\partial}{\partial z} \int_A \bar{\rho} \vec{v}_z da \\ &= \frac{\partial \langle \bar{\rho} \rangle^S}{\partial t} + \frac{1}{A} \frac{\partial A \langle \bar{\rho} \vec{v}_z \rangle^S}{\partial z} = 0 \end{aligned}$$

One may define a space-time-averaged velocity

$$V \triangleq \frac{\langle \bar{\rho} \tilde{v}_z \rangle^S}{\langle \bar{\rho} \rangle^S} = \frac{\langle \bar{\rho} \tilde{v}_z \rangle^S}{\hat{\rho}}$$

$$A \frac{\partial \hat{\rho}}{\partial t} + \frac{\partial A \hat{\rho} V}{\partial z} = 0$$

5.5.1.2 Energy equation

$$\frac{\partial \rho \left(\bar{h} + \frac{\tilde{v}^2}{2} \right) - \bar{\rho}}{\partial t} + \frac{\partial \bar{\rho} \tilde{v}_j \left(\bar{h} + \frac{\tilde{v}^2}{2} \right)}{\partial x_j} - \frac{\partial (\overline{\tau_{ij}} + R_{ij}) \tilde{v}_j}{\partial x_j} + \frac{\partial \bar{q}_i + \tilde{q}_i}{\partial x_i} = \bar{q}_{\omega}$$

$$\left\langle \frac{\partial \bar{\rho} \left(\bar{h} + \frac{\tilde{v}^2}{2} \right) - \bar{\rho}}{\partial t} \right\rangle^S = \frac{\partial \langle \bar{\rho} \tilde{h} \rangle^S}{\partial t} + \frac{\partial \langle \bar{\rho} \frac{\tilde{v}^2}{2} \rangle^S}{\partial t} - \frac{\partial \langle \bar{\rho} \rangle^S}{\partial t}$$

Let us define the mass-weighted space-time average enthalpy H and the space-time average pressure P

$$H \triangleq \frac{\langle \bar{\rho} \tilde{h} \rangle^S}{\langle \bar{\rho} \rangle^S};$$

$$P \triangleq \langle \bar{p} \rangle^S = \hat{p}$$

An approximation is necessary for the second term

$$\left\langle \bar{\rho} \frac{\widetilde{v}^2}{2} \right\rangle \cong \langle \bar{\rho} \rangle^s \frac{V^2}{2}$$

$$\left\langle \frac{\partial \bar{\rho} \left(\widetilde{h} + \frac{\widetilde{v}^2}{2} \right) - \bar{p}}{\partial t} \right\rangle = \frac{\partial \bar{\rho} H}{\partial t} + \frac{\partial \bar{\rho} \frac{V^2}{2}}{\partial t} - \frac{\partial P}{\partial t}$$

$$\left\langle \frac{\partial \bar{\rho} \widetilde{v}_z \left(\widetilde{h} + \frac{\widetilde{v}^2}{2} \right)}{\partial t} \right\rangle^s = \frac{1}{\Lambda} \frac{\partial \Lambda \left\langle \bar{\rho} \widetilde{v}_z \left(\widetilde{h} + \frac{\widetilde{v}^2}{2} \right) \right\rangle^s}{\partial t} = \frac{1}{\Lambda} \frac{\partial \Lambda \left(\bar{\rho} \widetilde{v}_z h \right)^s}{\partial t} + \frac{1}{\Lambda} \frac{\partial \Lambda \left(\bar{\rho} \widetilde{v}_z \frac{v^2}{2} \right)^s}{\partial t}$$

Again the averaging of the advection term induces an additional term q_{zd} :

$$q_z^d \triangleq \left\langle \bar{\rho} \widetilde{v}_z \widetilde{h} \right\rangle^s - \widehat{\rho} V H$$

q_{zd} is called a “dispersion” term and has an axial diffusive effect on H

An approximation is necessary for the second term

$$\left\langle \bar{\rho} \widetilde{v}_z \frac{\widetilde{v}^2}{2} \right\rangle^s \cong \langle \bar{\rho} \rangle^s V \frac{V^2}{2}$$

$$\left(\frac{\partial \bar{\rho} \, \tilde{v}_i \left(\tilde{h} + \frac{\tilde{v}^2}{2}\right)}{\partial x_j}\right)^S = \frac{1}{A} \frac{\partial}{\partial x_i} \left[\bar{\rho} \, \tilde{v}_z \left(\tilde{h} + \frac{\tilde{v}^2}{2}\right) da = \frac{1}{A} \frac{\partial A}{\partial z} \left\langle \bar{\rho} \, \tilde{v}_z \left(\tilde{h} + \frac{\tilde{v}^2}{2}\right) \right\rangle^S \right. \\ \left. = \frac{1}{A} \left[\frac{\partial A \bar{\rho} V H}{\partial z} - \frac{\partial A q_z^H}{\partial z} + \frac{\partial A \bar{\rho} W \frac{V^2}{2}}{\partial z} \right] \right.$$

$$\langle \bar{\rho} g_i \, \tilde{v}_i \rangle^S \cong \widehat{\rho} g_z V$$

$$\left\langle \frac{\partial (\mathbf{r}_J - \mathbf{R}_J)}{\partial x_j} \tilde{\mathbf{v}}_i \right\rangle^S = \frac{1}{A} \frac{\partial}{\partial z} \left[A < \left((\bar{T} + T^i) \cdot \vec{\tilde{v}} \right) \vec{n}_i >^S \right]$$

$$\left\langle \frac{\partial \left(\vec{q}_i^* + \vec{q}_i^*\right)}{\partial y_j} \right\rangle^S = \frac{1}{A} \frac{\partial}{\partial x_i} A (\bar{q}_i + q_i^*)^S + \frac{1}{A} \frac{\partial}{\partial x_i} \left[\pi \cdot \left(\vec{q} + \vec{q}_i^*\right) \frac{d\mathbf{C}}{d\left(\vec{q} + \vec{q}_i^*\right)} \cdot \frac{1}{A} \frac{\partial A (\bar{q}_i^* + q_i^*)^S}{\partial z} \right] + \frac{1}{A} C_{q_i}$$

Cq_w is the wall heat transfer term

$$A \frac{\partial}{\partial t} \left[\bar{\rho} \left(H + \frac{V^2}{2} \right) - P \right] + \frac{\partial}{\partial z} \left[A \bar{\rho} V \left(H + \frac{V^2}{2} \right) \right] - A \bar{\rho} g_z V = \\ \frac{\partial}{\partial z} A < \left((\bar{T} + T^i) \cdot \vec{\tilde{v}} \right) \vec{n}_i >^S - \frac{\partial A q_z^{eff}}{\partial z} + C q_w + A \bar{\rho} c_{ei}$$

$$q_z^{eff} \triangleq \widehat{\rho}_Z + \langle q_z^t \rangle^S + q_z^d = -(\lambda + \lambda_t + \lambda_d) \frac{\partial T}{\partial z}$$

q_{zeff} is the effective axial diffusion-dispersion term

The axial contribution of the stress tensor $\overline{\boldsymbol{T}} + \boldsymbol{T}^t$ is usually neglected so that the equation writes:

$$A \frac{\partial}{\partial r} \left[\bar{\rho} \left(H + \frac{V^2}{2} \right) - P \right] + \frac{\partial}{\partial z} \left[A \bar{\rho} V \left(H + \frac{V^2}{2} \right) - A \bar{p}_0 V = C q_w + A \bar{\rho}_{\text{ref}} - \frac{\partial M_z^d}{\partial z} \right]$$

The effective axial diffusion-dispersion term may be neglected when heat sources at the wall have a much higher impact than axial diffusion.

5.5.1.3 Momentum equation

One can apply the particular form of the Leibniz rule and Gauss theorem to the vectorial equation and then project along z axis or apply the particular form of the Leibniz rule and Gauss theorem to the equation projected along z axis.

$$\int_A \frac{\partial \bar{\rho} \tilde{v}_z}{\partial t} dS = A \left\langle \frac{\partial \bar{\rho} \tilde{v}_z}{\partial t} \right\rangle^S = A \frac{\partial \langle \bar{\rho} \tilde{v}_z \rangle^S}{\partial t} = A \frac{\partial \bar{\rho} V}{\partial t}$$

$$A \left\langle \nabla \cdot \left(\bar{\rho} \tilde{v}_z \vec{\tilde{v}} \right) \right\rangle^S = \frac{\partial A \langle \bar{\rho} \tilde{v}_z \tilde{v}_z \rangle^S}{\partial z}$$

One must define a momentum axial dispersion term T_{zd}^d

$$T_{zd}^d \triangleq \langle \bar{\rho} \tilde{v}_z \tilde{v}_z \rangle^S - \bar{\rho} V V$$

$$A \left\langle \nabla \cdot \left(\bar{\rho} \tilde{v}_z \vec{\tilde{v}} \right) \right\rangle^S = \frac{\partial A \langle \bar{\rho} \tilde{v}_z \tilde{v}_z \rangle^S}{\partial z} = \frac{\partial A \bar{\rho} V V}{\partial z} + \frac{\partial T_{zd}^d}{\partial z}$$

The contribution of pressure term is split into an axial gradient and a contribution Fp along the duct wall contour C :

$$A \left\langle \frac{\partial p}{\partial z} \right\rangle^S = A \left\langle \nabla \bar{p} \cdot \vec{n}_z \right\rangle^S = \frac{\partial A \langle \bar{p} \rangle^S}{\partial z} + A \int_C \bar{p} \cdot \vec{n}_z \cdot \vec{n}_z \frac{dC}{\vec{n}_c \cdot \vec{n}} = \frac{\partial A P}{\partial z} + Fp$$

with:

$$Fp = \int_C \bar{\rho} \vec{n} \cdot \vec{n}_z \frac{dC}{\vec{n}_c \cdot \vec{n}}$$

The local time-averaged pressure at wall is split into the space-time-averaged pressure P and a local-time-averaged pressure difference $\delta \bar{p}$

$$\bar{\rho} = \langle \bar{\rho} \rangle^S + \delta \bar{\rho} = P + \delta \bar{\rho}$$

$$Fp = -P \frac{dA}{dz} + \int_C \delta \bar{\rho} \vec{n} \cdot \vec{n}_z \frac{dC}{\vec{n}_c \cdot \vec{n}} = -P \frac{dA}{dz} + F'p$$

with

$$F'p = \int_C \delta \bar{\rho} \vec{n} \cdot \vec{n}_z \frac{dC}{\vec{n}_c \cdot \vec{n}}$$

then:

$$A \left\langle \frac{\partial \bar{\rho}}{\partial z} \right\rangle^S = A \frac{\partial P}{\partial z} + F'p$$

No difficulty with the external force (gravity) term:

$$\langle \bar{\rho} g_z \rangle^S = \widehat{\rho} g_z$$

Two contributions of the deviator stress tensor:

$$\lambda \left(\nabla \cdot (\vec{T} + \vec{T}^t) \cdot \vec{n}_i \right)_C = - \frac{\partial}{\partial t} A \cdot \vec{n}_i \cdot (\vec{T} + \vec{T}^t) \cdot \vec{n}_i > + \left(\vec{n}_i \cdot (\vec{T} + \vec{T}^t) \cdot \vec{n}_i \right) \frac{dC}{d\vec{n}_i \cdot \vec{n}_i}$$

The first right-hand side (RHS) term is usually small and neglected. The second RHS term is the wall friction term.

$$-C\tau_w \triangleq \int_C \vec{n} \cdot (\vec{T} + \vec{T}^t) \cdot \vec{n}_i \frac{dC}{n_i \cdot \vec{n}}$$

Finally:

[image]

F_p is nonzero when the duct shape or cross section is not constant ($\vec{n} \cdot \vec{n}_z \neq 0$)

It takes geometrical effects on pressure forces into account and is usually modeled as a singular pressure loss:

$$-F'p = A \left(\frac{\partial P}{\partial z} \right)_{sing} = -A \frac{K_{sing}}{\delta z} \rho \frac{V^2}{2}$$

It can play an important role in singular geometry such as convergent, divergent, bend, and any other complex geometry which can influence the flow. The form-loss coefficient K_{sing} depends on the geometry and may be a function of the

$$Re = \frac{\rho V D_h}{\mu}$$

Revnolds number, D_h being the hydraulic diameter

$$D_h = \frac{4A}{C}$$

$$-F'p = + (p_p - \langle p \rangle) \frac{dA}{dz}$$

As for the last dispersion term:

$$\frac{\partial AT_z^d}{\partial z} = \frac{\partial A \left(\langle \bar{\rho} \tilde{v}_z \tilde{v}_z \rangle^s - \hat{\rho} V V \right)}{\partial z}$$

it is zero in established flow (transverse profiles of \tilde{V}_z does not depend on z) in a constant cross-section duct ($A = Ct$). In nonestablished flow in a constant cross-section duct, it is most often neglected. In variable cross section or in the presence of complex geometry, its effect may be modeled together with $F'p$ as a geometrical effect.

These equations must be complemented by equations of state which are necessarily approximated due to averaging of nonlinear functions such as:

$$\hat{\rho} = \left\langle \overline{\rho(p,h)} \right\rangle^s \cong \rho(P,H) = \rho \left(\langle \bar{p} \rangle^s, \frac{\langle \bar{\rho} \bar{h} \rangle^s}{\langle \bar{\rho} \rangle^s} \right)$$

These equations must be complemented by closure laws for τ_w , K_{sing} , q_w , and q_{zeff}

Usual expressions for τ_w and K_{sing} are of the following form:

$$\tau_w = Cf(Re)\rho \frac{V^2}{2}; \quad Cf = aRe^{-b}; \quad K_{sing} = cRe^{-d}$$

Usual expressions for q_w and q_{zeff} are:

$$q_w=h(T_w-T)=\frac{\lambda Nu(Re,Pr)}{D_h}(T_w-T); \;\; Nu=C\,Re^a\,Pr^b$$

$$q_z^{eff} = -\lambda^{eff} \frac{\partial \bar{T}}{\partial z}$$

The resulting set of 1-D equation is then:

1-D 1-Phase equations: 1-Component 1-phase flow space-time-averaged equations

Principal variables: P, V, H

$$A\frac{\partial \widehat{\rho}}{\partial t}+\frac{\partial A\widehat{\rho}V}{\partial z}=0$$

$$A\frac{\partial \widehat{\rho}V}{\partial t}+\frac{\partial A\widehat{\rho}^2V}{\partial z}+A\frac{\partial P}{\partial z}=\widehat{p}\widehat{\rho}_z-C\tau_w-A\frac{K_{drag}}{Rz}\frac{V^2}{2}$$

$$A\frac{\partial}{\partial t}\left[\left(\theta+\frac{V^2}{2}\right)\cdot\theta\right]+\frac{\partial}{\partial z}\left[\theta V\left(\theta+\frac{V^2}{2}\right)\right]-\kappa_0\theta\cdot V-C\tau_w+\kappa_0\frac{\partial}{\partial z}\left(\frac{\partial\theta}{\partial z}\right)$$

$$\tau_w=Cf(Re)\rho\frac{V^2}{2}; \; K_{drag}=K_{drag}(Re); \; Re=\frac{\widehat{\rho}VD_h}{\mu}$$

$$h_w = h(T_w - T) + \frac{\Delta h_{ref}(P, T)}{\rho_w} (T_w - T); \quad q_w'' = -\rho_w \frac{\partial T}{\partial x}; \quad Pr = \frac{\rho_w c_p \mu}{k}$$

$$P = \bar{p}(\bar{r}); \quad H = \frac{(\rho \bar{h})^2}{\rho^2}; \quad \bar{p} = \bar{p}(P, H); \quad \bar{\mu} = \bar{\mu}(P, H); \quad \bar{k} = \bar{k}(P, H); \quad T = T(P, H)$$

+ expressions for C_f , K_{sing} , Nu and λ_{eff}

5.5.2 Predictive capabilities of the 1-D set of equations

One may note that usual expressions for wall friction and wall heat transfers use the “principle of locality” of the modeling where the physics of the process to model depends only on local flow variables (i.e., velocity, pressure, enthalpy) and their time and space local derivatives. It assumes that the knowledge of the local instantaneous principal variables (P , V , H) is sufficient to model the process. Moreover algebraic expressions are most often used without partial derivatives. This corresponds to the assumption of a quasi-steady quasi-established flow. The quasi-steady approximation is a reasonable approach when time scales of the process are small compared to time scale for variations of principal variables. The quasi-established flow is a reasonable approach in case of a regular geometry after some distance from entry (say $Z/D > 50$) when radial profiles of velocity and temperature are similar (not dependent on abscissa). It also requires that time scales of the process are small compared to transit time scales V/L .

The set of equation is able to give very good predictions of many 1-phase flows with heat transfers. Main limitations are:

- If the flow is not really one-dimensional, i.e., if the direction of the flow is not unique in a section of the duct, for example, when buoyancy forces induce natural circulation cells in the duct, pressure, and temperature field cannot be precisely described by 1-D equations;
- Closure laws for τ_w and q_w are available for a simple geometry like a circular pipe, a square or rectangular duct, an annulus, but predictive capabilities in more complex geometry (rod bundle) may require that specific closure laws are established based on prototypical experiments.

- In case of a local complex geometry, no universal model can predict singular pressure losses. Specific form loss coefficients have to be used depending on the geometry, but the 1-D model cannot predict it by itself. The geometrical effects on wall heat transfer may also be very important. Usually any perturbation of the flow which increases turbulence may increase heat transfer coefficient. 1-D model cannot predict this effect by itself.
- Rapid transient conditions may require more sophisticated wall momentum and heat transfers depending on partial derivatives of V , H , and T_w .
- Nonestablished flow exist in a significant part of any industrial systems and using classical closure laws for established flow may involve some inaccuracy of predictions.

5.6 The various approaches to two-phase flow modeling

One can classify two-phase modeling approaches (Bestion et al., 2011) in a similar way as was done for single phase in Section 5.3. Classification is made with regard to the space dimension of the model, considering 0-D, 1-D, 2-D, and 3-D models. Then, to be more specific one may consider the type of time and/or space averaging which is used. 3-D models of two- or multiphase flow are often called computational multifluid dynamics (CMFD). They are split first into 3-D for porous body and 3-D CFD in an open medium approach.

RANS-type time-averaged models, LES-type space-filtered models, and DNS type models are the three main categories of two-phase CFD models in open medium (see Table 5.3). Due to a much higher complexity of two-phase flow compared to single-phase flow, 1-D models are the most mature and commonly used in nuclear reactor applications. 3-D RANS models are also progressively used for some reactor issues, but there is no mature 3-D CMFD model in an open medium covering all flow regimes. A modeling covering all flow regimes is still a challenge (see Bestion, 2014).

Table 5.3

Classification of Eulerian fluid dynamic simulation approaches for two-phase CFD

5.6.1 Time space and phase averaging in two-phase flow

Phase averaging means that a multiplication of local instantaneous equations by a phase indicator function (or phase characteristic function) is made before a time or a space averaging.

Let χ_k be the phase indicator function (see Fig. 5.3) of phase k :

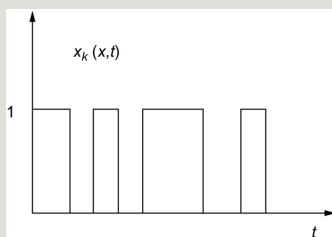


Fig. 5.3 Definition of time fractions for phase k .

$$\chi_k(x, y, z, t) = 1 \quad \text{if point } (x, y, z) \text{ is occupied by phase } k \text{ at time } t$$

$$\chi_k(x, y, z, t) = 0 \quad \text{if point } (x, y, z) \text{ is not occupied by phase } k \text{ at time } t$$

In a two-phase flow, with liquid and gas

$$\chi_g + \chi_l = 1$$

A two-phase flow can be split into several fields including, for example, a continuous liquid field, a continuous gas field, one or Nb bubble fields, and one or Nd droplet fields. In this case, a field averaging means that local instantaneous equations are multiplied by field indicator (or characteristic) functions before a time or a space averaging.

Let us define some useful quantities and operators.

with

$$\iiint_{R^3} g(x, y, z) dx dy dz = 1$$

The filter function g may be a uniform function over a distance δ_f

One can notice:

$$R_k \check{f}_k^k = \langle \chi_k f_k \rangle^S$$

5.6.2 CMFD models

Five types of Eulerian two-phase CFD approaches for open medium are distinguished in Table 5.3. They differ by the treatment applied to basic mass,

momentum and energy balance equations. The four successive choices can be made successively:

1. Multiplication or not of mass momentum and energy equations by the phase indicator functions (for each phase in the two-fluid approach) or multiplication by the field indicator functions (for each field for a multifield approach)
2. Time averaging or not
3. Space filtering or not
4. Addition of an interface tracking method (ITM) or interface reconstruction technique (IRT) for some or all interfaces or not

These choices allow to distinguishing various methods according to the following aspects:

- Phase averaging or field averaging:
 - Mixture model under Homogeneous and Algebraic Slip
 - Two-fluid model
 - Multifield models
- Filtering turbulent scales and two-phase intermittency scales:
 - All turbulent and two-phase scales are filtered (RANS type models)
 - Only some scales are filtered (LES type models)
 - All scales are predicted or simulated (DNS type models)
- Treatment of Interfaces
 - Use of ITM
 - Use of Interface Reconstruction method
 - Use of a pure statistical treatment of interfaces

As a result of the various choices three kinds of interface treatment are possible:

- *Deterministic interface*: or simulated interface: an interface is said “deterministically treated” when its space and time position is simulated or actually predicted without any simplification. This requires the use of an ITM.
- *Statistical Interface*: An interface is said “Statistically treated” when a space or time averaging or filtering procedure does not allow to predicting its space and time position. Only statistical or averaged information on several interfaces may be predicted through quantities such as a void fraction, or an interfacial area density. This is the case for small bubble and droplet interfaces of Figs. 5.3 and 5.4.

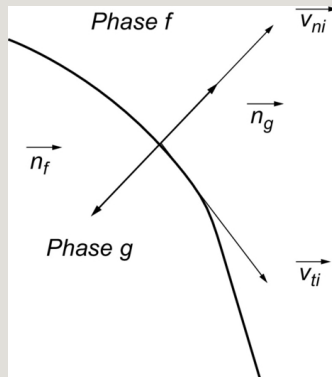


Fig. 5.4 Interface between phases f and g .

- *Filtered interface*: An interface is considered as “Filtered Interface” when its space and time position is predicted with some filtering of the smaller scale deformations. This filtering may result either from space filter or time averaging.

The modeling of wall transfers, interfacial transfers, interfield transfers, and turbulent transfers depends on the approach. Each approach is described in short here below.

5.6.2.1 The pseudo-DNS method

The pseudo-DNS does not apply any space or time averaging of the equations. However some ITM is required to tracking the interface. A one-fluid approach is used. Additional models are often required, for example, for implementing a film splitting criterion when two bubbles coalesce or for the contact angles at a triple line solid-liquid-gas. Such additional models are the reason why in two-phase flow the word DNS must be replaced by pseudo-DNS since some very small scale

physics is not solved but only modeled.

Since no averaging or filtering is used, pseudo-DNS should be able to simulate all interfaces including the smaller-scale interface deformations and to predict the smaller-scale eddies up to the Kolmogorov dissipative scale. Since even pseudo-DNS requires extremely expensive CPU cost, its use is restricted to the investigation of very small scale flow processes as a complement to experimental investigations and as a support for the modeling and validation of more macroscopic approaches.

The pseudo-DNS can in principle simulate all flow regimes but is in practice limited by the extremely expensive CPU time which is required.

5.6.2.2 The RANS method

The RANS method (or U-RANS) is the most simple, the cheapest (in terms of CPU), the most advanced, and the most used available two-phase CFD method. All turbulent scales and all two-phase intermittency scales are filtered. All interfaces are statistically treated. The method is applied to steady flows or quasi-steady (U-RANS) flows when the time scales of variation of mean variables are larger than the largest time scales of turbulence and two-phase intermittency (time between passage of two interfaces at a given point).

In case of stratified flow or annular flow, large interfaces (free surface or film interface) can be treated as “filtered interfaces.” RANS is in principle compatible with all two-phase flow regimes provided that they are steady or quasi-steady. For dispersed bubbly flow or dispersed droplet flow, the condition is easy to satisfy. For separate-phase flows (stratified flow, annular flow), the averaging filters interfacial waves in a way which is not fully clear: although the RANS modeling of turbulent diffusion prevents simulation of large eddies it does not prevent irrotational waves to be predicted resulting from Kelvin-Helmholtz instability. Therefore RANS and URANS are compatible with the statistical interfaces and to some filtered interfaces.

For slug and churn flow regimes with large bubbles (either Taylor bubbles in slug flow or distorted large bubbles in churn flow) the intermittency due to the passage of these bubbles corresponds to rather large time scales. Since the RANS filters even these large scales it is not able to predict this intermittency, but the average behavior can be predicted.

RANS is compatible with all the possible choices for the number of fields,

including single-fluid, two-fluid, and all kinds of multifield models.

5.6.2.3 The LES with deterministic interface

The LES with deterministic interface combines a filtering of turbulent fluctuations with an ITM used for all interfaces. This method was first proposed by Toutant et al. (2009a,b), Bois et al. (2010), Magdeleine et al. (2010), Lakehal (2008), and Lakehal et al. (2008), for free surface flow. The concept has been since then better reformulated by Lakehal and Labois (2011), who refer to it as LEIS, short for large-eddy and interface simulation (LEIS).

5.6.2.4 The LES with statistical interfaces

When the largest interfacial scale is rather small and significantly smaller than the largest turbulent eddies, a LES method is applicable with a filters scale smaller than the larger eddies but larger than the two-phase scale to allow a statistical treatment. The idea was first developed by Lakehal (2002), who put the filtered two-fluid equations on firmer grounds and proposed a bubble-induced diffusion model incorporated within the Dynamic Procedure of Lilly and Germano (see Lilly, 1991). It was since then applied with some success to some turbulent dispersed flow by Dhotre et al. (2007), Dhotre et al. (2008), Niceno et al. (2008), and Ničeno et al. (2009).

Such a method is clearly much less CPU consuming than the pseudo-DNS and the LES with deterministic interface, but it is restricted to some flow situations, typically the dispersed bubble or dispersed drops where the large eddies are much larger than the largest bubbles or eddies. In slug or churn flow where the largest bubbles and the largest eddies are of the size of the geometrical dimensions of the flow (such as a Hydraulic diameter) this method is clearly not applicable.

This method is compatible with the two-fluid model and multifield models where the dispersed bubbles or droplets may be treated by size groups.

5.6.2.5 The hybrid LES method with both filtered and statistical interfaces

This hybrid method filters the smaller eddies and treats statistically the small droplets or small bubbles, while the other interfaces are simply filtered and treated as large interfaces. The space filter eliminates the smaller bubbles which are treated statistically, and it thickens and filters the interface of the large bubble which may

be reconstructed with a simplification of the shape.

Lakehal (2010) discussed the difficulties of this method in comparison to the LES with simulated interfaces.

It may be a promising way of modeling the most complex two-phase flow (such as churn or slug flow) at a reasonable CPU cost without filtering the large two-phase structures like RANS does. However the closure issue is rather complex, and the present state of the art is not very well advanced.

This method is compatible with the two-fluid approach and with multifield models. A fourfield model with a continuous gas field, a continuous liquid field, a dispersed bubble field, and dispersed droplet field may help to reconstruct the large filtered interfaces and to model the mass transfers between continuous and dispersed fields.

This method includes much more closure terms to model than the LES with deterministic interfaces. In particular the effects due to subgrid waves of large interfaces have to be modeled.

It was observed that many applications which use an ITM pretend to be of the LES type with deterministic interfaces although they are actually hybrid methods. The interface tracking by the ITM is “underresolved” and simulated interfaces are “filtered interfaces” instead of “deterministic interfaces.” All effects due to subgrid waves of large interfaces should be added in the modeling.

5.6.2.6 Locality and universality of the modeling

The “principle of locality of the modeling” is used in two-phase CFD as it is used in single-phase CFD since closure laws are expressed only as functions of local flow variables (i.e., velocity, density, internal energy) and their time and space derivatives. Here the exceptions to this principle of locality are the so-called wall functions where some closure terms depend on the distance to a wall and the equivalent for large interfaces which may be called “interfacial functions.” This allows using rather coarse nodalization in high shear regions close to a wall or close to a large interface.

It was stressed that the principle of locality is more relevant when the processes to model at point $P(x,t)$ depend on flow conditions close to the point P . In single-phase CFD the principle of locality is better satisfied in LES type method than in a RANS approach since the subfilter local turbulent viscosity in a LES approach

models only effects of small eddies which are close to point P . In two-phase, there are small interfaces (small bubbles and droplets) and also large-scale interfaces such as the large distorted bubbles in churn flow, the free surface in stratified flow, and the film surface in annular flow. Therefore in the flow regimes with large interfaces like slug and churn flow, the principle of locality may only be reasonably applied in LES with deterministic or filtered interfaces

5.6.2.7 Applicability and degree of maturity of the various CMFD approaches

Table 5.4 summarizes the applicability and degree of maturity of the various two-phase CFD approaches to every flow regime. It may be seen that only two modeling approaches can be applied to simulate physical situations where all two-phase flow regimes may occur: the RANS (or URANS) and the LES with filtered and statistical interfaces. However the former is more mature than the latter. The pseudo-DNS and the LES with deterministic interfaces can address all flow regimes but are practically limited by the required CPU time which is prohibitive in the most complex flows. The LES with statistical interfaces cannot treat “large interfaces” and is intrinsically limited to dispersed flows.

Table 5.4

Applicability and degree of maturity of the various two-phase CFD approaches to every flow regime including CPU cost

Applied, is applicable and has been applied; not possible, cannot be applied due to intrinsic limitations; possible, can be applied but not very mature; expensive, requires a very high CPU time; too expensive, unaffordable with current computer power.

5.7 Time-averaged two-fluid equations

Phase time averaging or field time averaging is the most natural approach to extend CFD RANS models to two-phase flow, Fig. 5.4. It consists in multiplying basic equations by the phase indicator function χ_k of phase k .

The derivation of equations is presented in detail by Ishii and Hibiki (2011), and various methods are also presented for dispersed flow by Morel (2015).

Following Ishii and Hibiki (2011), a general form of transport equation for a specific quantity integrated over time period Δt is (see Fig. 5.3):

$$\frac{\partial \epsilon_k \bar{\rho}_k^k \bar{\psi}_k^k}{\partial t} + \nabla \cdot \left(\epsilon_k \bar{\rho}_k^k \bar{v}_k^k \bar{\psi}_k^k \right) + \nabla \cdot \left[\epsilon_k \left(J_k^k + J_k^s \right) \right] \\ = \epsilon_k \bar{\rho}_k^k \bar{\phi}_k^k + \frac{1}{\Delta t} \sum_{\text{vol}} \left\{ \frac{1}{V_{\text{vol}}} \left[\bar{n}_k \cdot \rho_k \left(\vec{v}_k - \vec{v}_i \right) \psi_k \right] + \bar{n}_k \cdot J_k \right\}$$

ϕ_k is the volumetric source of ψ_k in phase k

J_k is the diffusive flux of ψ_k in phase k

Mass momentum and total energy balance equations can be written considering the respective ψ_k , ϕ_k , and J_k , as given in Table 5.5.

Table 5.5

Volumetric source and surface source in mass momentum and total energy equations

--	--



is the specific external force on phase k (N/kg or m/s²) usually limited to

gravity force ($\vec{F} = \vec{g}$)

T_k is the stress tensor in phase k (Pa or N/m²)



is the heat flux vector in phase k (W/m²)

q_{ext} is the external volumetric source of energy (usually radiation)



\vec{n}_k is the unit vector normal to the interface oriented outside of phase k



\vec{v}_k^+ is the component of velocity of interface normal to the interface



\vec{v}_k^+ is the component of velocity of interface tangential to the interface

J_{kt} is the turbulent flux of ψ_k

$$J_k^t \triangleq \frac{\overline{\chi_k \rho_k \vec{v}_k \psi_k}}{\epsilon_k} - \overline{\rho_k} \vec{v}_k^k \widetilde{\psi_k^k}$$

This term results from averaging of a product for convection terms.

The second RHS term takes account of convective and diffusive fluxes through all interfaces which passed at point x during the period of time Δt .

One obtains the following set of phase mass, momentum, and energy equations:

$$\frac{\partial \epsilon_k \overline{\rho_k^k}}{\partial t} + \nabla \cdot \left(\epsilon_k \overline{\rho_k^k} \vec{v}_k^k \right) = \frac{1}{\Delta t} \sum_j \left\{ \frac{1}{V_{int}} \left[\vec{n}_k \cdot \rho_k \left(\vec{v}_k^k - \vec{v}_j^k \right) \right] \right\} \Delta \gamma_a$$

γ_{jk} is the time averaged interfacial mass transfer per unit volume (kg/m³/s)

$$\begin{aligned} & \frac{\partial \epsilon_k \overline{\rho_k^k} \vec{v}_k^k}{\partial t} + \nabla \cdot \left(\epsilon_k \overline{\rho_k^k} \vec{v}_k^k \vec{v}_k^k \right) + \epsilon_k \nabla \overline{p_k^k} \\ & = \epsilon_k \overline{\rho_k^k} \vec{g} + \nabla \cdot \left[\epsilon_k \left(\overline{T_k} + T_k^k \right) \right] + \vec{M}_{ik} \end{aligned}$$

$$\vec{M}_{ik} = \frac{1}{\Delta t} \sum_j \left\{ \frac{1}{V_{int}} \left[\vec{n}_k \cdot \rho_k \left(\vec{v}_k^k - \vec{v}_j^k \right) \vec{v}_k^k \right] - \vec{n}_k \cdot T_k \right\}$$

A very common approximation is to consider a unique pressure for both phases:

$$\overline{p_f}^f = \overline{p_g}^g = \overline{p}$$

M_{ik} is the time-averaged interfacial momentum transfer per unit volume (N/m³)

The first term is usually modeled as:

5.8.2.3 Energy balance of phase *k*

Time derivative term

Let us define the mass-weighted phase space average enthalpy:

$$\overline{H}_k^k = \frac{\langle \rho_k h_k \rangle_k^S}{\widehat{\rho}_k^k}$$

$$\int_{\Omega_k} \frac{\partial \rho \left(h + \frac{v^2}{2} \right)}{\partial t} dA = \frac{\partial \Omega_k \langle \rho_k \left(h_k + \frac{v_k^2}{2} \right) \rangle_k}{\partial t} = \frac{\partial A R_k \widehat{\rho}_k^k \left(\widehat{h}_k^k + \frac{V_k^k}{2} \right)}{\partial t}$$

An approximation was necessary for the kinetic energy term:

$$\langle \rho_k \frac{v_k^2}{2} \rangle_k \cong \widehat{\rho}_k^k \frac{\overline{V}_k^k}{2}$$

Advection term

$$\int_{\Omega_k} \nabla \cdot \rho \vec{v} \left(h + \frac{v^2}{2} \right) dA = \frac{\partial A R_k \langle \rho_k v_k h_k \rangle_k^S}{\partial t} + \frac{\partial A R_k \left(\rho_k v_k \frac{v_k^2}{2} \right)_k^S}{\partial t} + M H_k + E C_k \\ \cong \frac{\partial A R_k \widehat{\rho}_k^k \widehat{V}_k^k \left(\widehat{h}_k^k + \frac{\widehat{V}_k^k}{2} \right)}{\partial t} + \frac{\partial A R_k d_k^d}{\partial t} + M H_k + E C_k$$

MH_{ik} and EC_{ik} are the volumetric energy transfer through interface

$$MH_{ik} = - \int_{C_i} \rho_k \left(\vec{v}_k - \vec{v}_i \right) h_k \cdot \vec{n}_k \frac{dC_i}{\vec{n}_k \cdot \vec{n}_{kC}}$$

$$EC_{ik}=-\int_{\vec{C_i}}\rho_k\left(\overrightarrow{v_k}-\overrightarrow{v_i}\right)\frac{v_k^2}{2}\cdot\overrightarrow{n_k}\frac{dCi}{\overrightarrow{n_k}\cdot\overrightarrow{n_{kC}}}$$

MH_{ik} and EC_{ik} are usually modeled as:

$$MH_{ik}=A\Gamma_{ik}\overset{\smile}{H_k^k}$$

$$EC_{ik}=\Gamma_{ik}\frac{V_i^2}{2}$$

Again the averaging of the advection term induced an additional dispersion term q_{kzd}^d .

$$q_{kz}^d\triangleq\langle\rho_kv_{kz}h_k\rangle_k^S-\widehat{\rho_k^k}\overset{\smile}{V_k^k}\overset{\smile}{H_k^k}$$

q_{kzd}^d can be modeled as:

$$q_{kz}^d=\lambda_{kz}^d\frac{\partial \overset{\smile}{T_k^k}}{\partial z}$$

Pressure term:

$$\int_{A_k} \frac{\partial p}{\partial t} dA = A \frac{\partial R_k \langle p_k \rangle_k^S}{\partial z} = A \frac{\partial R_k \widehat{\rho_k^k}}{\partial t}$$

Contribution of the deviator stress tensor

$$\int_{A_k} \nabla \cdot T \cdot \vec{v} \, dA = \frac{\partial}{\partial z} A_k \vec{v_k} \cdot \left(T_k \cdot \vec{n_z} \right)_k^S + EF_k + EP_k$$

This first term is often neglected.

The second term EF_{ik} is a work of interfacial friction and can be modeled as:

$$EF_{ik} = \tau_{ik} V_i$$

The third term EP_{ik} is a work of interfacial pressure and can modeled as:

$$EP_{ik} = EP'_{ik} - P \frac{\partial R_k}{\partial t} \cong -P \frac{\partial R_k}{\partial t}$$

Gravity term

$$\int_{A_k} \rho \vec{g_z} \cdot \vec{v} \, dA = A_k \langle \rho_k g_z u_{kz} \rangle_k^S = A R_k \widehat{\rho_k^k} \vec{V_k^k} \cdot \vec{g_z}$$

Heat flux term:

$$\begin{aligned} - \int_{A_i} \nabla \cdot \vec{q} \, dA &= - \frac{\partial}{\partial z} A_i \left(\vec{q}_i \cdot \vec{n}_i \right)_i - \int_{C_i} \vec{n}_i q_i \frac{dC}{\vec{n}_{ic} \cdot \vec{n}_i} - \int_{C_i} \vec{n} \cdot \vec{q}_i \frac{dC}{\vec{n} \cdot \vec{n}_i} \\ &= - \frac{\partial A_i q_{oi}}{\partial z} + C_i q_{oi} + A_i q_{oi} \end{aligned}$$

with:

$$C_i q_{oi} \triangleq - \int_{C_i} \frac{\vec{n}_k \cdot \vec{q}_k}{\vec{n}_k \cdot \vec{n}_{ci}} \frac{dC}{\vec{n}_{ci} \cdot \vec{n}_k}; A q_{ik} \triangleq - \int_{C_i} \frac{\vec{n}_i q_i}{\vec{n}_{ic} \cdot \vec{n}_i} \frac{dC}{\vec{n}_{ic} \cdot \vec{n}_i}$$

$$\sum_k q_{ik} + \Gamma_{ik} \tilde{H}_k^k = 0$$

$$\begin{aligned} & \frac{\partial R_i \widehat{\rho}_k^k}{\partial t} \left(\vec{H}_k^k + \frac{\vec{V}_k^k}{2} \right) + \frac{\partial A R_i \widehat{\rho}_k^k \vec{V}_k^k}{\partial z} \left(\vec{H}_k^k + \frac{\vec{V}_k^k}{2} \right) \\ & - A R_i \frac{\partial P}{\partial t} + \frac{\partial A R_i (q_{iz} + q_{iz}^k)}{\partial z} = + A R_i \widehat{\rho}_k^k \vec{V}_k^k \cdot \vec{g}_z \\ & + C_i q_{oi} + A q_{oi} + A \Gamma_{ik} \left(\vec{H}_k^k + \frac{V_k^2}{2} \right) + A \tau_{ik} V_i + A q_{iu} \end{aligned}$$

Considering orders of magnitudes, it is found that the diffusion-dispersion term and the term $\tau_{ik} V_i$ are often small compared to others and are neglected.

5.8.3 The space-phase averaged equations for stratified flow

The case of a stratified flow in a horizontal or inclined duct is particular since the interface has a simple shape, and the pressure field in a cross section may be reasonably approximated. Therefore, the integration of pressure forces is easier than in more complex flow regimes.

Having in mind that the main difficulty in horizontal legs is to correctly predict the stratification occurrence and the characteristics of stratified flow, attention was paid in the CATHARE code development to derive the best possible system of

equations.

The CATHARE code two-fluid 6-equation model able to describe stratified flows was derived by de Crecy (1986), who also analyzed its properties, Fig. 5.8. Assuming:

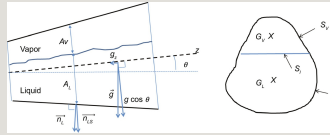


Fig. 5.8 Stratified flow.

- A hydrostatic transverse pressure gradient
- Vapor and liquid densities uniform over the cross section
- Continuity of pressure across the interface (no surface tension effect and no pressure jump induced by mass transfer)

In such conditions pressure terms can be calculated and momentum equations are written as:

$$\begin{aligned} A \frac{\partial R_i \rho_i V_i^2}{\partial t} + \frac{\partial A R_i \rho_i V_i^2}{\partial z} + A R_i \frac{\partial P}{\partial z} + A f_i \frac{\partial R_i}{\partial z} \Delta t + A \rho_i G_i - D_i \\ = A R_i \rho_i g_i - A \tau_{ik} - C_i \tau_{ik} + A \Gamma_{ik} V_i \end{aligned}$$

with:

$$g_z = -g \sin \theta$$

$$\Delta_k = -\rho_k g \sin \theta (X_k - X_i)$$



Δ_k is the pressure difference between the average pressure p_k in phase k and pressure at the interface p_i

$$f_i=R_g\Delta_l-(1-R_g)\Delta_v+R_g(1-R_g)\frac{\partial(\Delta_v-\Delta_l)}{\partial\alpha}$$

$$G_z=R_g(1-R_g)\frac{\partial(\Delta_v-\Delta_l)}{\partial z}$$

$$D_k=\int\limits_{S_k}\overrightarrow{n_z}\cdot\overrightarrow{n_k}[p_k(x,y,z)-p_i]\overrightarrow{n_k}\cdot\overrightarrow{n_{ks}}\frac{ds}{n_k\cdot n_{ks}}$$

$$\epsilon_v=1;\epsilon_l=-1$$

For each phase k , D_k takes into account the pressure difference due to gravity between the interface and the wall perimeter in contact with phase k .



D_k and Δ_k are terms dependent on the pipe shape. In the particular case of a square duct, the following expressions are found:

$$G_z=A^{3/2}\varepsilon_k\alpha(1-\alpha)\frac{\rho_m}{2}\frac{\partial g\cos\theta}{\partial z}$$

$$f_i=R_g\big(1-R_g\big)(\rho_L-\rho_V)g\cos\theta A^{1/2}$$

$$\Delta_k=\frac{1-\alpha_k}{4}f_i$$

$$\rho_m=R_g\rho_V+\big(1-R_g\big)\rho_L$$

The momentum equation is:

$$\begin{aligned} &A\frac{\partial R_g\bar{\rho}_L^2V_L^2}{\partial t}+\frac{\partial AR_g\bar{\rho}_L^2V_L^2}{\partial z}+AR_L\frac{\partial P}{\partial z}\\ &+\Delta_L\frac{\partial A}{\partial z}+At_dG_z-D_L=AR_L\bar{\rho}_L^2g_z-At_{da}-C_L\tau_{at}+AF_dV_L\\ &-Af_L\frac{\partial R_L}{\partial z}+\frac{1-R_L}{4}\frac{\partial A}{\partial z}+A^{1/2}r_LR_L(1-R_L)\frac{\rho_L}{2}\frac{\partial g\cos\theta}{\partial z} \end{aligned}$$

The expression for f_i in a circular pipe should include a shape function of void fraction which is often forgotten and replaced with 1.

In the CATHARE code 1-D module (de Crecy, 1986; Bestion and Serre, 2012), f_i is written:

$$f_i=R_g\big(1-R_g\big)(\rho_L-\rho_V)g\cos\theta D$$

$$f_i\frac{\partial R_k}{\partial z}$$

The $f_i\frac{\partial R_k}{\partial z}$ term controls the characteristic velocity corresponding to void fraction waves which are shallow water waves at the free surface of the stratified

flow (see Bestion and Serre, 2012).

The properties of the momentum equations in stratified flow are illustrated in Fig. 5.9 where water is injected very slowly at the entrance of a pipe with area restriction and enlargement followed by a bend. Gas velocity is zero at the entrance and pressure is imposed at the outlet. It is shown that the water level plotted from the predicted void fraction respect a horizontal free surface even in varying diameter zones and in the bend. This is the result of the last three terms of the momentum equations.

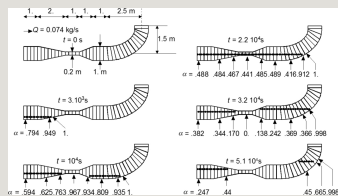


Fig. 5.9 Liquid level at rest in a pipe with varying diameter and inclination.

5.9 The time-space averaged 1-D equations for two-phase flow

Let us define some simple notations for space-time phase-averaged parameters:

$$\overline{q_{kz}} = \frac{1}{L} \int_0^L q_{kz} dz$$

In momentum equations a turbulent stress contribution q_{kz} resulting from time averaging of convection term is added to the dispersion term q_{kzd} .

In energy equations a turbulent heat flux contribution T_{kz} resulting from time averaging of convection term is added to the dispersion term T_{kzd} .

Some minor approximations are still necessary to derive time-space averaged 1-D equation.

Simplified notations and approximations:

$\overline{\Gamma_{ik}}$ is simply noted: Γ_{ik}

$\overline{V_i}$ is simply noted: V_i

with the following approximation: $\overline{\Gamma_{ik} V_i} \cong \Gamma_{ik} V_i$

$\overline{F_k^{AM}}$ is simply noted: F_{kAM}

$\overline{\tau_{ik}}$ is simply noted: τ_{ik}

$\overline{C_k}$ is simply noted: C_k

$\overbrace{\tau_{wk}}$ is defined as: $\overline{C_k \tau_{wk}} \triangleq \overline{C_k} \overbrace{\tau_{wk}}$ is simply noted: τ_{wk}

$\overline{f_i \frac{\partial R_k}{\partial z}}$ is modeled as a term of the form: $\widehat{f_i} \frac{\partial \alpha_k}{\partial z}$ and $\widehat{f_i}$ is simply noted: f_i

$\overbrace{q_{wk}}$ is defined as: $\overline{C_k q_{wk}} \triangleq \overline{C_k} \overbrace{q_{wk}}$ is simply noted: q_{wk}

$\overline{q_{ik}}$ is simply noted: q_{ik}

$\overline{q_{kext}}$ is simply noted: q_{kext}

This results in the following system of equations:

1-D two-fluid equations

Principal variables: $\alpha_g, P, V_g, V_f, H_g, H_l$

$$A\frac{\partial \alpha_k Q_k}{\partial t} + \frac{\partial A \alpha_k Q_k V_k}{\partial z} = A \Gamma_{ik}$$

$$\begin{aligned} &A\frac{\partial \alpha_k Q_k^{(1)}}{\partial t} + \frac{\partial A \alpha_k Q_k^{(1)} V_k}{\partial z} + A \alpha_k \frac{\partial V_k}{\partial t} + V_k \frac{\partial \alpha_k}{\partial t} + \alpha_k \frac{\partial V_k}{\partial z} \\ &= A \alpha_k Q_k \frac{\partial}{\partial z} = \frac{\partial A \alpha_k \left(V_k + V_k^2 \right)}{\partial z} - A \alpha_k V_k \frac{\partial}{\partial z} - A \alpha_k \frac{\partial V_k}{\partial z} + A V_k^2 \frac{\partial}{\partial z} + A V_k \frac{\partial}{\partial z} \\ &A\frac{\partial \alpha_k \left(V_k + \frac{V_k^2}{2} \right)}{\partial t} + \frac{\partial A \alpha_k V_k \left(V_k + \frac{V_k^2}{2} \right)}{\partial z} - A \alpha_k \frac{\partial V_k}{\partial z} = \frac{\partial A \alpha_k \left(V_k^2 + V_k^3 + V_k^4 \right)}{\partial z} \\ &= A \alpha_k Q_k V_k + C_k Q_k + A Q_k + A V_k \left(V_k + \frac{V_k^2}{2} \right) + A V_k V_k + A Q_k \end{aligned}$$

$$\sum_i x_i = 1, \sum_i x_i \cdot l_i = 0, \sum_i x_i = 0, \sum_i l_i^{(m)} = 0, \sum_i x_i \cdot l_i^{(m)} = 0, \sum_i x_i \cdot f_i \cdot H_i = 0$$

$$q_{kz} + q_{kz}^t + q_{kz}^d = -\lambda_k^{eff} \nabla T_k$$

$$Q_0 = p_1(P,H_1) \circ T_1 = T_1(P,H_1) \circ p_0 = p_0(P,H_1) \circ i_0 = i_0(P,H_1)$$

$$+ \hspace{1cm} expressions \hspace{1cm} or \hspace{1cm} equations \hspace{1cm} for \\ \tau_{ik}, T_{kz}^t, T_{kz}^d, q_{ik}, \overrightarrow{q}_k^t, C_k, \tau_{wk}, q_{wk}, \delta P_{ksing}, F_k^{AM}, \lambda_k^{eff}$$

5.10 The 1-D two-fluid equations as used in system codes

System codes such as CATHARE (Bestion, 1990), RELAP-5 (RELAP5/MOD3, 1998), and TRACE (TRACE V5.0, 2007) use the 1-D two-fluid equations as in Section 5.9 below with some differences. TRACE writes volume-averaged equations on a part of a duct between two sections. Equations are somewhat similar to the discretized form of 1-D equations when a staggered grid is used.

Axial diffusion and dispersion terms of momentum are never modeled and may be partly modeled through the singular pressure loss term.

Momentum equation may be written using the secondary form (CATHARE, RELAP-5) instead of the conservative form:

$$A\alpha_k Q_k \frac{\partial V_k}{\partial t} + A\alpha_k Q_k V_k \frac{\partial V_k}{\partial z} + A\alpha_k \frac{\partial P}{\partial z} + A f_k' \frac{\partial \alpha_k}{\partial z} + E_k \frac{\partial A}{\partial z} \\ = A\alpha_k Q_k E_k - A \tau_{sk} - C_k \tau_{sk} - A\alpha_k \frac{\partial P_{\text{source}}}{\partial z} + A F_k^{MW} + A f_{sk}(V_k - V_i)$$

$$g_k \frac{\partial A}{\partial z}$$

The term $g_k \frac{\partial A}{\partial z}$ is not present in all codes and may be present (in the Cathare code) only for stratified flow for which an expression was derived.

$$f_i \frac{\partial \alpha_k}{\partial z}$$

The term $f_i \frac{\partial \alpha_k}{\partial z}$ is present in all codes for stratified flow and may be present (in the Cathare code) for all flow regimes.

Axial diffusion and dispersion terms of energy are not included in standard models but some options may exist and may be actuated for some specific transients. Axial diffusion and dispersion terms of mass concentrations of transported species like boron or radio-active components, which are treated as passive scalars, may also be added on option.

Energy equation may be written as a total enthalpy equation (CATHARE) or as internal energy equation (RELAP-5) or as total energy equation (TRACE):

$$A \frac{\partial \alpha_k Q_k U_k}{\partial t} + \frac{\partial A \alpha_k Q_k V_k U_k}{\partial z} = -A P \frac{\partial \alpha_k}{\partial t} - P \frac{\partial A \alpha_k V_k}{\partial z} \\ + C_k q_{w,k} + A q_{sk} + A f_{sk} H_K + A q_{lec,k} + D_k$$

D_k is a viscous dissipation in phase k

$$\begin{aligned} A \frac{\partial \alpha_0 Q \left(U_i + \frac{V_i^2}{2} \right)}{\partial t} + \frac{\partial \alpha_0 Q V_i \left(U_i + \frac{V_i^2}{2} \right)}{\partial z} + \frac{\partial \alpha_0 V_i P}{\partial z} = A \alpha_0 R_i V_i \\ + C_1 q_{1,2} + A q_{12} + \Delta \Gamma_d H_{12} + A \tau_{12} V_i + A \tau_{13} V_i + A q_{12,2} \end{aligned}$$

5.11 Some simplified two-phase models: HEM drift-flux model

5.11.1 From one- to two-fluid models

Historically, two-phase steam-water flows were first described as a one-fluid forming a homogeneous mixture following approximately the single-phase set of equations with some minor modifications. A 1-D one-fluid 3-equation two-phase flow model was the first set of equations used to describe steam-water flow in a reactor. It can use both mechanical and thermodynamic equilibrium in the HEM or it may accept some velocity difference (slip between phases) expressed by an algebraic relation. Before going to the 1-D 6-equation two-fluid model, some 4-equation or 5-equation models were used in some codes for steam-water flow to describe thermodynamic nonequilibrium of one phase or both phases.

In two-phase steam-water flow, the interface between phases is at saturation temperature. A phase can be at thermodynamic equilibrium in a two-phase system

when it is at saturation temperature ($T_k = T_{sat}(P)$). A phase can be out of thermodynamic equilibrium in a two-phase system when it is either

subcooled ($T_k < T_{sat}(P)$) or superheated ($T_k > T_{sat}(P)$)

Phases may have different velocities when different forces are applied to them. For example the gravity force being proportional to the phase density creates some differences between phases. Also the same friction force along walls is not applied to both phases, which may affect the two velocities. Mechanical interactions between phases (drag force, added mass force) tend to couple phases and to reduce the slip between phases. As a result of all forces there may be an equilibrium slip between phases. Due to different inertia of phases—corresponding to different densities—there may be some acceleration of phases before reaching an equilibrium slip which may be expressed as an algebraic relation between gravity, drag, and wall friction forces. The simplest assumption considers an equilibrium slip with no velocity difference. This corresponds to an infinite drag coefficient. A more realistic assumption considers that phases are always at equilibrium slip: only

an algebraic relation between phase velocities is sufficient. The most realistic treatment is to consider the different inertia of phases, which requires separate momentum equations for each phase. Table 5.6 summarizes the existing models from one-fluid to two-fluid system of equations.

Table 5.6

The various steam water models from 1-fluid to 2-fluid system of equations

--

Let us define some quantities:

--

5.11.2 The homogeneous equilibrium model (HEM)

The HEM is the simplest model to describe a steam-water flow. It assumes that both phases are tightly mechanically and thermally coupled so that they have the

same mean velocity $(V_v = V_l)$ and the same temperature. Since the two-phase mixture is supposed to be at thermodynamic equilibrium, it results that both phases are at saturation temperature when they coexist.

The 1-D HEM model is here reestablished starting from the 1-D two-fluid formulation.

Adding the two phasic mass balance equations provides the mixture mass balance equation. Adding the two phasic momentum balance equations provides the mixture momentum balance equation. Adding the two phasic total enthalpy balance equations provides the mixture total enthalpy balance equation. The

variations of kinetic energy and the work of gravity are neglected. The axial diffusion and dispersion terms are also neglected.

5.11.2.1 A single set of equations from single-phase liquid to single-phase steam

The one-fluid HEM model is able to treat continuously a flow of subcooled water which receives heat, vaporizes progressively up to a full superheated vapor flow which can then be cooled and condensate to come back to a pure liquid flow.

Depending on the value of the mean mixture enthalpy one can consider three cases, giving the following set of equations with P , G , and H being the three principal variables:

1-D HEM equations

Main variables: P, G, \hat{H}_m

$$A \frac{\partial \rho_m}{\partial t} + \frac{\partial AG}{\partial z} = 0$$

$$A \frac{\partial G}{\partial t} + \frac{\partial A G^2}{\partial z} + A \frac{\partial P}{\partial z} = A p_m g_z - C \tau_w - A \frac{\partial p_{\text{stat}}}{\partial z}$$

$$A \rho_m \frac{\partial H_m}{\partial t} + A G \frac{\partial \hat{H}_m}{\partial z} - A \frac{\partial P}{\partial t} = C q_w$$

$$\widehat{H}_m < h_{\text{sat}} : X_{\text{th}} \equiv \frac{H_1 - h_{\text{sat}}}{h_{\text{fg}}} < 0; a_1 = x = X = 0$$

$$H_m=\widehat{H}_m=H_L;\rho_m=\rho_l(P,H_L);T=T_l(P,H_L)$$

$$\widehat{H}_m>h_{\text{isat}}:X_0\triangleq\frac{H_c-h_{\text{isat}}}{h_{\text{cr}}}>1;\alpha_x=x=X=1$$

$$H_m=\widehat{H}_m=H_L;\rho_m=\rho_l(P,H_L);T=T_l(P,H_L)$$

$$h_{\text{isat}}\leq \widehat{H}_m\leq h_{\text{isat}}+\Delta<X_0<1;\;X_0=X=x=-\frac{\widehat{H}_m-h_{\text{isat}}}{h_{\text{cr}}}$$

$$H_m=\widehat{H}_m=xh_{\text{isat}}+(1-x)h_{\text{isat}}$$

$$\alpha_x=-\frac{\left(\widehat{H}_m-h_{\text{isat}}\right)\rho_{\text{isat}}}{\left(h_{\text{isat}}-\widehat{H}_m\right)\rho_{\text{isat}}+\left(\widehat{H}_m-h_{\text{isat}}\right)\rho_{\text{isat}}}$$

$$\rho_m=\frac{\rho_{\text{isat}}\rho_{\text{isat}}h_{\text{cr}}}{\left(h_{\text{isat}}-\widehat{H}_m\right)\rho_{\text{isat}}+\left(\widehat{H}_m-h_{\text{isat}}\right)\rho_{\text{isat}}}$$

+ expressions for $\tau_w,\delta p_{sing},q_w$

5.11.2.2 Predictive capabilities of the 1-D HEM set of

equations

Although the 1-D HEM set of equations looks very close to the single-phase 1-D set of equation the predictive capabilities are much worse and can be very poor depending on the two-phase flow situation. Main limitations are:

- The no-slip assumption is almost always far from the reality and is the main source of error. It may be a reasonable approximation only in the case of a bubbly flow with very small bubbles. It is totally wrong in separate-flow, such as annular flow and stratified flow and is also a bad approximation for droplet flow.
- The thermodynamic equilibrium of both phases does not allow good prediction of condensing flow and in post-CHF conditions with inverse-annular, inverse-slug, and dispersed flow.
- Closure laws for τ_w and q_w are available but are much more complex and must take into account a large number of flow regimes and heat transfer regimes. There are generally much less accurate than closure laws of single phase flow.

5.11.3 The drift flux model

The drift flux model was the first approach which could better model the mechanical interactions between phases and describe the slip between phases.

It can easily be obtained from simplification of the two-fluid model only if phase density variations within the time-space averaging domain are neglected.

Let us define some quantities:

$$\mathcal{V}_v = \int_V \mathbf{v}_v \cdot \mathbf{e}_z dV$$

and dividing by a_v obtain the drift flux identity:

$$\mathcal{V}_v = CoJ + V_{gj}$$

where the difference between the average gas velocity \overline{V}_v and the mixture superficial velocity J is due to two effects:

- void and velocity profiles effects when $Co \neq 1$

- average local slip between phases through $V_{gj} \neq 0$

An approximation neglecting the density variations within the time-space averaging domain simplifies expressions of accumulation and advection terms of the equations.

One can then consider that:

$$V_k \triangleq \frac{\langle \overline{\chi_k \rho_k v_{zk}} \rangle^S}{\langle \overline{\chi_k \rho_k} \rangle^S} \cong \mathcal{V}_k = \frac{\langle \overline{\chi_k v_{zk}} \rangle^S}{\langle \overline{\chi_k} \rangle^S}$$

$$H_k \triangleq \overline{\overline{h}}_k \triangleq \frac{\langle \overline{\chi_k \rho_k h_k} \rangle^S}{\langle \overline{\chi_k \rho_k} \rangle^S} \cong \widehat{\overline{h}}_k = \frac{\langle \overline{\chi_k h_k} \rangle^S}{\langle \overline{\chi_k} \rangle^S}$$

Provided that good models are available to express Co and V_{gj} , the simple algebraic relation between the phase velocities and the void fraction can eliminate one partial differential equation (PDE) of the 1-D 6-equation 2-fluid model:

$$V_v(1 - Co\alpha_v) = Co(1 - \alpha_v)V_l + V_{gj}$$

It can also be used together with a 1-D 3-equation model (using thermodynamic equilibrium) to remove the main drawback of the HEM model.

5.11.3 Drift-flux model versus two-fluid model

Let us consider momentum equations of the two-fluid model and in the drift flux approach. In the two-fluid model one writes two-phase momentum equations:

$$\begin{aligned} &A\frac{\partial \alpha_k \varrho_k V_k}{\partial t} + \frac{\partial A \alpha_k \varrho_k V_k V_z}{\partial z} + A \alpha_k \frac{\partial P}{\partial z} + A f_i \frac{\partial \alpha_k}{\partial z} + g_k \frac{\partial A}{\partial z} \\ &= A \alpha_k \varrho_k g_z - A \tau_{ik} - C_k \tau_{wk} - A \alpha_k \frac{\delta P_{ksing}}{\delta z} + A F_k^{IM} + A \Gamma_{ik} V_i \end{aligned}$$

One can write the mixture momentum equation by adding them:

$$\begin{aligned} &A\frac{\partial \alpha_k \varrho_k V_k + \alpha_l \varrho_l V_l}{\partial t} + \frac{\partial A [\alpha_k \varrho_k V_k V_z + \alpha_l \varrho_l V_l V_l]}{\partial z} + A \frac{\partial P}{\partial z} + (g_l + g_k) \frac{\partial A}{\partial z} \\ &= A \varrho_m g_z - C_l \tau_{wl} - C_k \tau_{wk} - A \left(\frac{\alpha_l \delta P_{lsing} + \alpha_k \delta P_{ksing}}{\delta z} \right) \end{aligned}$$

and one can obtain a “cross-momentum equation” by elimination the pressure gradient term between the two-phase equations:

$$\begin{aligned} &A \left[\alpha_l \frac{\partial \alpha_k \varrho_k V_k}{\partial t} - \alpha_l \frac{\partial \alpha_l \varrho_l V_l}{\partial t} \right] + \alpha_l \frac{\partial A \alpha_k \varrho_k V_k V_z}{\partial z} - \alpha_l \frac{\partial A \alpha_l \varrho_l V_l V_l}{\partial z} \\ &= -A f_i \frac{\partial \alpha_k}{\partial z} - [g_l \alpha_l - \alpha_l g_l] \frac{\partial A}{\partial z} - A \alpha_l \alpha_k [q_l - q_k] g_z \\ &\quad - A \tau_{li} - C_l \alpha_l \tau_{wl} + C_k \alpha_l \tau_{kl} - A \alpha_l \alpha_k \left(\frac{\delta P_{ksing}}{\delta z} - \frac{\delta P_{lsing}}{\delta z} \right) + A F_k^{IM} + A \Gamma_{li} V_i \end{aligned}$$

$$\left(\frac{\partial}{\partial t} \cong 0\right)$$

Let us consider a quasi-steady flow and quasi-established flow

$$\frac{\partial \alpha_v}{\partial z} \cong 0; \frac{\partial V_k}{\partial z} \cong 0$$

$$g_v \cong 0; \delta P_{ksing} \cong 0)$$

without strong geometrical complexity (

and without big interfacial mass transfer ($\Gamma_{iv} V_i$ term is negligible) this cross momentum equation is simplified:

$$A \tau_{lv} \cong -A \alpha_v \alpha_l [q_l - q_v] g_z - C_v \alpha_l \tau_{vl} + C_l \alpha_v \tau_{lv}$$

In such conditions, the force balance between phases is reduced to equilibrium between drag force gravity, and wall friction forces. Considering a dispersed gas phase and a continuous liquid as encountered in bubbly, slug and churn flow, in a vertical channel at moderate velocity, wall friction terms may be significantly smaller than interfacial friction due to a much higher interfacial area than wall friction area. Then a rough approximation in vertical upward oriented flow leads to:

$$\tau_{iv} \cong \alpha_v \alpha_l [q_l - q_v] g$$

This simple balance between buoyancy and drag forces has a clear similarity with the drift flux models where the drift velocity models are of the following form:

$$V_{gj} = C \sqrt{\frac{g \Delta \rho \delta}{\rho_l}}$$

where δ is a length scale characteristic of the bubble size. This expression can be obtained from a balance between buoyancy B and drag force D applied to a bubble of size:

$$B \sim g \Delta \rho \delta^3; D \sim C_d \rho_l \delta^2 V_{gj}^2$$

If the drag coefficient is assumed constant and if δ is proportional to the Laplace scale, one obtains the form of Zuber and Findlay (1965), model for churn-turbulent bubbly flow:

$$V_{gj} \sim \left[\frac{g \Delta \rho \sigma}{\rho_l^2} \right]^{0.25}$$

If the drag coefficient is assumed constant and if δ is bounded by the duct diameter, one obtains the form of Zuber and Findlay model for slug flow:

$$V_{gj} \sim \sqrt{\frac{g \Delta \rho D}{\rho_l}}$$

From the drift flux equation, V_{gj} general expression, and simplified cross-momentum equation, one can obtain an expression of the interfacial friction which is consistent with a drift flux model:

$$\tau_n = \alpha_v \alpha_l \varrho_l \frac{V_{gj}^2}{C^2 \delta} = \alpha_v \alpha_l \varrho_l (1 - Co \alpha_v)^2 \frac{(V_v - C_d V_l)^2}{C^2 \delta}$$

$$C_\alpha = \frac{Co(1 - \alpha_v)}{(1 - Co \alpha_v)}$$

This simply shows that a drift flux approach can be equivalent to a full two-fluid 6-equation model when the approximations made in the simplified cross-momentum equation are valid. When some simplifications are not justified a full two-fluid 6-equation model may have better capabilities.

In situations where inertial forces are not negligible compared to buoyancy, drag, and friction forces, the drift flux may be significantly worse than the full 6-equation model. For example:

- Droplet flow: a water droplet created at a quench front during a core reflooding process is entrained by steam but it does not reach an equilibrium slip within the core.

- Stratified flow: in a stratified flow, due to a weak coupling between phases, many situations cannot be predicted precisely by an algebraic slip since the

$$Af_i \frac{\partial \alpha_v}{\partial z}$$

term is not negligible and also some acceleration terms may play a significant role in the phase slip.

$$\frac{\partial}{\partial t} \cong 0$$

- Transient flow: when $\frac{\partial}{\partial t} \cong 0$ is no more valid in cross-momentum equation, the algebraic slip relation is not valid.

$$\frac{\partial \alpha_v}{\partial z} \cong 0; \frac{\partial V_k}{\partial z} \cong 0$$

- Nonestablished flow: when $\frac{\partial \alpha_v}{\partial z} \cong 0; \frac{\partial V_k}{\partial z} \cong 0$ is no more valid in cross-momentum equation, the algebraic slip relation is not valid.

- High condensation and flashing flows: such flows are usually accelerating flows and the term $\Gamma_v V_i$ is no more negligible.

5.12 Characteristic velocities and hyperbolicity

The notion of well-posedness was introduced by Hadamard in his analysis of the nature of mathematical modeling. According to Hadamard's classification, well-posedness requires the existence and uniqueness of the solution of the model and that the solution depends in continuous fashion on the initial and boundary data. This requisite is induced by the fact that it is necessary to ensure that a small perturbation in the data should give rise to a small variation of the solution at any point of the domain at a finite distance from the boundaries.

A first-order conservative set of PDE is well posed if and only if it is hyperbolic. As shown in Sections 5.4 and 5.7 the 1-D systems of equations for single phase and for two-phase flow are not first order since there are diffusion terms. However, they are often neglected, and the system becomes a first-order conservative set of PDE.

A set of PDEs as a function of time and space is said hyperbolic when all the roots of the characteristic equation are real.

More precisely, let a 1-D system of equation be written in the following form:

$$A \frac{\partial X}{\partial t} + B \frac{\partial X}{\partial z} = C$$

X is the vector of state variables; A, B are matrices and C is the vector of sources/sinks.

The characteristic equation is

$$Det(B - \lambda A) = 0$$

In the 1-D 1-phase 3-equation model this is a third-order polynomial function with three roots:

$$\lambda_1 = V$$

is the transport velocity of enthalpy

$$\lambda_{2,3} = V \mp C_s$$

are the propagation velocities of pressure (sound) waves.

$$\frac{1}{C_s^2} = \left(\frac{\partial \rho}{\partial P} \right)_s$$

is the celerity is related to the compressibility of the fluid and is usually considered as an isentropic compressibility since time scales of pressure fluctuations are small compared to heat conduction time scales.

In the 1-D two-fluid 6-equation model this is a sixth order polynomial function with six roots.

When solving this equation for a 1-D two-fluid 6-equation model, one obtains:

$\lambda_1 = V_g$ is the transport velocity of gas enthalpy,

$\lambda_2 = V_l$ is the transport velocity of liquid enthalpy,

$\lambda_{3,4} = W_\alpha \mp C_\alpha$ are the propagation velocities of void waves,

$\lambda_{5,6} = W_s \mp C_s$ are the propagation velocities of pressure (sound) waves.

A problem was raised when the two-fluid single pressure set of equation was found not hyperbolic when no closure law uses partial derivatives. In particular the propagation velocities of void waves may be imaginary. This may induce an unstable void wave which increases in amplitude very rapidly. Such a system could not be used in any numerical tool.

$$f_i \frac{\partial \alpha_v}{\partial z}$$

Then it was observed that terms like the added mass force or the term can change the nature of the system and make it hyperbolic. It was also found that a nonhyperbolic system of equations could be solved in some codes without being unstable. From the initial problem two new problems arise:

1. Should a nonhyperbolic system of equations be prohibited in two-fluid modeling?
2. What way should be followed to make the two-fluid model hyperbolic?

Different answers were given to both questions.

The second-order diffusive terms that have been neglected in the establishment of the 6-equation model would have made the system parabolic and thus probably well posed. At least they can stabilize highest frequency waves. Also many transfer terms of the equations like wall friction and interfacial friction can induce dissipation which may stabilize the lower frequency waves but it is not demonstrated that this is sufficient. A complex stability analysis would be necessary which is not currently available. Two answers to question 1 were given:

- A very pragmatic point of view has been developed: the second-order diffusive

terms that have been neglected in 6-equation model are small compared to numerical diffusion, and the cell size used is such that there is no need to add this second-order terms. This point of view requires cells large enough to prevent instability through numerical diffusion. However, when decreasing the mesh size, numerical diffusion is decreased and the possible unstable nature of equation is revealed. In this approach, no convergence in cell size is possible.

- Although diffusion terms could stabilize high-frequency waves, it is more convenient to use a system of equation which is hyperbolic without diffusion.

For the second answer to question 1 there are also two answers to question 2:

$$f_i \frac{\partial \alpha_v}{\partial z}$$

- Using the added mass force and the $f_i \frac{\partial \alpha_v}{\partial z}$ to guaranty the hyperbolicity is artificial and one should use an unconditionally hyperbolic system of equation without such closure differential terms. For example a 7-equation model with two phasic pressures is unconditionally hyperbolic. A seventh equation is added (usually a void fraction equation) leading to a new and very difficult closure problem which can be understood as finding a model for a relaxation time to the single pressure model, this relaxation time being very difficult to understand and to measure.

$$f_i \frac{\partial \alpha_v}{\partial z}$$

- Using the added mass force and the $f_i \frac{\partial \alpha_v}{\partial z}$ term is justified by the physics of two-phase flow. However, the expression for f_i is not known for all flow regimes in two-phase flow and can only be approximated after some simplifying assumptions are made. Adding a condition that these terms make the system hyperbolic may be justified if the condition remains compatible with the limited understanding of the complex physics. This position is illustrated here below.

The characteristic equation of the CATHARE 1-D 6-equation model was calculated by making some simplifying assumptions.

$$f_i \frac{\partial \alpha_v}{\partial z}$$

Both the added mass force (with a coefficient β) and the $f_i \frac{\partial \alpha_v}{\partial z}$ terms are used in momentum equations. When calculating the two characteristic velocities relative to void fraction waves, it was assumed that the two densities are constant, (infinite

sound speed) and only mass and momentum equations are used. The following velocities were found:

$$\lambda_{3,4}=W\mp C_{\alpha}$$

$$W_{\alpha}=\frac{\alpha_l\rho_g^{am}V_G+\alpha_G\rho_l^{am}V_l}{\alpha_l\rho_g^{am}+\alpha_G\rho_l^{am}}$$

$$C_{\alpha}^2=\frac{f_i\rho_m^{am}-\alpha(1-\alpha)\rho_l^{am}\rho_g^{am}(V_G-V_l)^2}{\rho_m^{am2}}$$

With:

$$\rho_k^{am}=\rho_K+\beta\rho_m$$

$$\rho_m=\alpha_G\rho_G+\alpha_L\rho_L$$

$$\rho_m^{am}=\alpha_L\rho_g^{am}+\alpha_G\rho_l^{am}$$

One can see that the void waves velocities can only be real if $C_{\alpha}^2>0$

which gives the condition:

$$f_i > f_{ihyp} = \frac{\alpha(1-\alpha)\rho_l^{am}\rho_g^{am}(V_G - V_l)^2}{\rho_m^{am}}$$

Since this form is close to the formulation suggested by Stuhmiller (1977), it was accepted and it was chosen to satisfy this condition in Cathare. One can see that the added mass force does not play here any role in the hyperbolicity, and one may obtain an hyperbolic system of equation without added mass force provided that:

$$f_i > f_{ihyp} = \frac{\alpha(1-\alpha)\rho_g\rho_l(V_G - V_l)^2}{\rho_m}$$

The Athlet code (Lerchl and Austcberegesilo, 2013) uses a slightly different form of f_i as:

$$f_i = C\alpha\rho(V_G - V_l)^2$$

where the C value can also provide hyperbolicity and stability.

5.13 Transport of interfacial area and polydispersion models

Two-phase flow have a complex nature with a large diversity of length scales associated to bubbles size, droplet size, distance between bubbles or droplets, film thickness, turbulent eddy sizes, wavelength at a free surface or a film surface. Similarly a large variety of time scales can be identified. All basic processes such as mass momentum and energy transfers at walls and interfaces which have to be modeled depend on the length scales which also depend on the flow regime. Transport equations may be added to predict evolution of some scales such as turbulent scales. The first approach in two-phase flow modeling was to write an

equation for interfacial area concentration a_i which may be defined as the ratio of interface area (IA) to the volume of a two-phase mixture. Transport equation for interfacial (TIA) was developed in both system codes in a 1-D approach and 3-D CMFD. TIA focused on bubbly flow and on droplet flow. Three main reasons promoted the use of a transport equation for interfacial area (TIA) in system codes.

Nonestablished flows: it was observed that dispersed bubbly flow and droplet flows have a mean bubble and drop size which depends on several mechanisms such as break up, coalescence, nucleation, collapse, and interfacial mass transfer. Some of these phenomena have relatively long relaxation times which are larger than convective time scales so that the “average size” is not an “equilibrium size” which can be expressed based only on local principal variable of the two-fluid 6-equation model used in current system codes. TIA is capable to better model such nonestablished flows by taking relaxation times into account provided that source and sink terms are modeled and validated.

Flow regime transitions: it was observed that many flow regime transitions are corresponding to a change of IA: bubbly-to-slug flow or bubbly-to-churn flow result from a coalescence process which decreases IA, bubbly-to-stratified flow transition also results from bubble sedimentation and coalescence of bubbles. Therefore TIA should be used for a prediction of some flow regime transition and could also model intermediate states between two flow regimes. Other flow regime transitions such as the onset of droplet entrainment increases IA dramatically but the governing phenomenon is an interfacial instability. One may distinguish transitions which result from a change on IA from transitions which induce a change of IA.

Interfacial transfers: interfacial transfers of mass, momentum, and energy depend on IA (or on drop/bubble size, for example). Therefore a dynamic prediction of IA would also improve the prediction of interfacial friction and interfacial heat transfers which control void fraction and slip between phases and also phase temperatures and mass transfers by vaporization and condensation.

Usual expressions of interfacial friction and interfacial heat transfers in system codes are of the form:

$$\tau_i = -a_i C_i \frac{\rho}{2} |V_v - V_l| (V_v - V_l)$$

$$q_{ik} = a_i h_{ik} (T_{sat} - T_k)$$

Let us consider a dispersed flow with a continuous phase c and a dispersed phase d (bubbles or drops) with a particle number density n_d and a Sauter mean diameter δ_{32} .

5.13.1 Monodispersed approximation:

The simplest assumption is to consider a population of uniform size spherical particles. In this case simple relations exist between a_i , dispersed phase fraction α_d , δ_{32} , and n_d .

$$a_i = \frac{6\alpha_d}{\delta_{32}}; n_d = \frac{6\alpha_d}{\pi\delta_{32}^3}$$

Usual expressions for interfacial friction and heat transfer coefficients h_{id} in dispersed flow are:

$$\begin{aligned}\tau_{id} &= -C_d(Re_d) \frac{\pi\delta_{32}^2}{4} n_d \frac{\rho_c}{2} |V_d - V_c|(V_d - V_c) \\ &= -\frac{3\alpha_d}{4\delta_{32}} C_d \rho_c |V_d - V_c|(V_d - V_c)\end{aligned}$$

$$q_{id} = \frac{6\alpha_d}{\delta_{32}} h_{ik} (T_{sat} - T_d) = \frac{6\alpha_d \lambda_c Nu_d}{\delta_{32} \delta_{32}} (T_{sat} - T_d)$$

with:

$$Nu_d = a Re_d^p Pr_c^q; Re_d = \frac{\rho_c (V_d - V_c) \delta_{32}}{\mu_c}; Pr_c = \frac{\mu_c C p_c}{\lambda_c}$$

Both models need expressions for δ_{32} or a_i or n_d .

5.13.2 Monodispersed approximation with algebraic interfacial area:

In standard industrial fully validated versions of system codes only algebraic expressions of δ_{32} or a_i or n_d are available. It is often assumed that a droplet or bubble diameter is equal to the limiting value corresponding to a critical Weber number:

$$We_{crit} = \frac{\rho_c (V_d - V_c)^2 \delta_{32}}{\sigma}$$

This assumes that all droplets or bubbles have reached the maximum diameter above which they would be broken. It is clear that this is a very strong assumption which cannot be valid except in some particular situations.

5.13.3 Monodispersed approximation with dynamic interfacial area modeling

A more general approach within the monodispersed approximation consists in writing a transport equation for a_i or n_d . The derivation of such equations can be found in Ishii and Hibiki (2011), or in Morel (2015).

$$\frac{\partial n_d}{\partial t} + \nabla \cdot n_d \mathbf{v}_n = \Phi_n^{Nuc} + \Phi_n^{Col} + \Phi_n^{Coa} + \Phi_n^{BU}$$

$$\frac{\partial a_i}{\partial t} + \nabla \cdot a_i \mathbf{v}_i = \frac{2a_i}{3a_{d,i}} \left(\Gamma_d - a_i \frac{\partial \Gamma_d}{\partial t} - a_i N_d \nabla \Gamma_d \right) + \Phi_n^{Nuc} + \Phi_n^{Col} + \Phi_n^{Coa} + \Phi_n^{BU}$$

\mathbf{v}_n or \mathbf{v}_i have to be modeled and the dispersed phase velocity \mathbf{v}_d is most often used. The following source and sink terms have also to be modeled.

Φ_{nNuc} is the source term of n_d due to nucleation (creation of bubble by flashing or boiling or drop creation by condensation)

Φ_{nCol} is the sink term of n_d due to collapse (vaporization of a drop or condensation of a bubble)

Φ_{nCoa} is the sink term of n_d due to coalescence

Φ_{nBU} is the source terms of n_d due to break up

$\Phi_{a_i}^{Nuc}$ is the source term of a_i due to nucleation

$\Phi_{a_i}^{Col}$ is the sink term of a_i due to collapse

$\Phi_{a_i}^{Coa}$ is the sink term of a_i due to coalescence

$\Phi_{a_i}^{BU}$ is the source terms of n_d due to break up

with the relations:

$$\Phi_{a_i}^{Coa} = 12\pi \left(\frac{\alpha_d}{a_i}\right)^2 \Phi_n^{Coa}; \quad \Phi_{a_i}^{BU} = 12\pi \left(\frac{\alpha_d}{a_i}\right)^2 \Phi_n^{BU}$$

5.13.4 Polydispersed dynamic modeling with the method of statistical moments

A more complex modeling consists in predicting the bubble or drop size distribution along the flow.

The bubble diameter distribution function $f(\delta; x, t)$ is defined such that $f(\delta; x, t)d\delta dx$ represents the probable number of bubbles in a volume element dx at time t ,

having their diameters in the interval $[\delta, \delta + d\delta]$

The j th order moment of the bubble diameter distribution function is defined by:

$$S_j(x,t) \triangleq \int_0^\infty \delta^j f(\delta; x, t) d\delta$$

The four first-order moments give the bubble number density, the product of the bubble number density n_d by the mean bubble diameter δ_{10} , the IA a_i , and the fraction of dispersed phase α_d :

$$S_0 = n_d; S_1 \triangleq n_d \delta_{10}; S_2 = \frac{a_i}{\pi}; S_3 = \frac{6\alpha_d}{\pi}$$

The Sauter mean diameter is the ratio:

$$\delta_{32} = \frac{S_3}{S_2}$$

A transport equation for the moment S_j can be written as:

$$\frac{\partial S_j}{\partial t} + \nabla \cdot (S_j v_j) - j \dot{D}_{j-1} S_{j-1} = P_j$$

where closure relations are necessary for the transporting velocity v_j , the mean

bubble or drop growth rate \dot{D}_j , and the source term P_j .

Selecting a law of distribution function and writing transport equations for some moments, one can predict the evolution with x and t of the distribution. This was tested with log-normal and quadratic laws by Zaepffel et al. (2012), since these are simple laws which can be defined by the knowledge of only two statistical moments.

When a bubble size distribution function is known one can express the liquid-to-interface heat transfers as:

$$q_{il} = \left[n_d \pi \int_{\delta_{min}}^{\delta_{max}} \delta f(\delta) Nu(\delta) d\delta \right] \lambda_c (T_{sat} - T_c)$$

which is likely to be more precise than the monodispersed expression.

5.13.5 Polydispersed dynamic modeling with a multifield approach

Another approach for modeling polydispersion is the multisize group (MUSIG) method where mass balance equations are written for different size groups of bubbles or drops with all transfers between groups being modeled. This provides a discrete function f . The MUSIG model was developed and validated (Krepper et al., 2011) to describe the bubble size polydispersion, where the disperse phase is divided into a number of groups, each group being characterized by its volume fraction and velocity field by writing several mass and momentum equations. This approach has already proven good capabilities to capture the different behavior of small and large bubbles and the influence on the formation of a certain flow pattern.

5.13.6 Predictive capabilities of the monodispersed and polydispersed approaches

Using a simple algebraic model for the interfacial area provides an average bubble size—the Sauter mean diameter—which cannot take all effects into account. Coalescence and break-up may have rather long relaxation times so that equilibrium between them is not reached in the situation of interest. Moreover boiling and condensation may affect the size and depart from equilibrium.

Using a transport equation for either the bubble number density or the IA may improve the prediction of coalescence and break-up. However there are common limitations of both algebraic and dynamic “monodispersed” bubble size models since almost all dispersed flow of interest in reactor thermalhydraulics have a rather large bubble and drop size distribution.

In order to go beyond these limitations, polydispersed models offer much better inherent capabilities but require a huge effort for modeling coalescence and fragmentation

A state of the art in using monodispersed or polydispersed approaches can be found in Krepper et al. (2011), for CMFD and status and perspective for TIA in system codes was presented by Bestion and Serre (2013). Some conclusions are:

- TIA models available today cover only a very small fraction of the flow situations of interest.
- The analysis of some flow regimes with new measurement giving access to IA and bubble size distribution has confirmed that almost all flow are nonestablished flows. In such condition an algebraic IA modeling has many limitations, a TIA equation brings some added value.
- A polydispersion modeling would be necessary to get a very significant progress.

5.14 3-Field models in system codes

When a phase is present in both a dispersed field and a continuous field it may happen that both fields have very different behaviors. Using a simple mass, momentum, and energy equation for both fields may not be able to predict important phenomena. This was identified in nuclear reactor thermalhydraulics particularly for annular-mist flow where the liquid is present with droplets in the core steam flow and films along the walls. A similar situation may exist in horizontal pipes when there is a free surface and a steam flow carrying droplets above. This may be encountered in a boiling water reactor (BWR) core in normal and abnormal situation and in some accidental situations in a pressurized water reactor (PWR). 3-field models were then developed to better capture the physics of the flow. Film velocity is usually small (of the order of a few cm/s or mm/s), whereas droplets may be entrained at higher velocities (several m/s) in the gas phase. It may happen that both liquid fields are countercurrent with falling films and upward flowing droplets. The interest of a 3-field model for a large break loss of coolant accident (LBLOCA) simulation was presented by Valette et al. (2009).

1-D 3-field equations are derived following the same method as for the two-fluid by multiplying by field characteristic functions of vapor χ_v , continuous liquid χ_{cl} and dispersed liquid χ_{dl} before applying time and space averaging.

New transfers are defined:

$$\Gamma_{vcl} = -\Gamma_{clv}$$

is the interfacial mass transfer from continuous liquid to vapour (kg/m³/s)

$$\Gamma_{vdl} = -\Gamma_{dlv}$$

is the interfacial mass transfer from dispersed liquid to vapour (kg/m³/s)

Γ_d is the mass transfer from dispersed to continuous liquid by droplet deposition (kg/m³/s)

Γ_e is the mass transfer from continuous to dispersed liquid by droplet entrainment (kg/m³/s)

q_{idl} is the heat flux per unit volume from interface to droplet (W/m³)

q_{ivdl} is the heat flux per unit volume from vapour to interface of droplet (W/m³)

q_{icl} is the heat flux per unit volume from interface to continuous liquid (W/m³)

q_{ivcl} is the heat flux per unit volume from vapour to interface of continuous liquid (W/m³)

V_{idl} is the interfacial axial velocity at dispersed liquid interface (m/s)

V_{icl} is the interfacial axial velocity at continuous liquid interface (m/s)

$$Af_{ivcl} \frac{\partial \alpha_{cl}}{\partial z}$$

The term may be modeled as the equivalent term in two-fluid for stratified flow

$$Af_{ivdl} \frac{\partial \alpha_{dl}}{\partial z}$$

The term may be modeled as the equivalent term in two-fluid for dispersed flow

An added mass term AF_{vAM} is used for interactions between gas in bubbly flow and continuous liquid, but there is no need to use such a term for interactions between droplets and gas which would have a minor effect on droplet behavior.

It is assumed that there is no direct contact between dispersed liquid and walls since drops would deposit in pre-CHF conditions and would bounce in post-CHF

conditions. Then there is no wall friction for droplets, no wall direct heat transfer

$$g_{dl} \frac{\partial A}{\partial z}$$

for droplets, no

$$A \alpha_{dl} \frac{\delta P_{dlsing}}{\delta z}$$

term, and no

term.

The set of equation is given below for the case where axial diffusion-dispersion terms are neglected.

1-D 3-field equations for gas-continuous liquid-droplets

Principal variables: $\alpha_v, \alpha_{cl}, P, V_v, V_{cl}, V_{dl}, H_v, H_{cl}, H_{dl}$

$$A \frac{\partial \alpha_v Q_v}{\partial t} + \frac{\partial A \alpha_v Q_v}{\partial z} = A \Gamma_{vcl} + A \Gamma_{vdl}$$

$$A \frac{\partial \alpha_{cl} Q_{cl}}{\partial t} + \frac{\partial A \alpha_{cl} Q_{cl}}{\partial z} = A \Gamma_{clv} + A \Gamma_{clg} - A \Gamma_{cl}$$

$$A \frac{\partial \alpha_{dl} Q_{dl}}{\partial t} + \frac{\partial A \alpha_{dl} Q_{dl}}{\partial z} = A \Gamma_{dlv} - A \Gamma_{dl} + A \Gamma_{cl}$$

$$\begin{aligned} A \frac{\partial \alpha_v V_v}{\partial t} + \frac{\partial A \alpha_v V_v}{\partial z} &= A \alpha_v \frac{\partial V_v}{\partial t} + A \alpha_v \frac{\partial V_v}{\partial z} + A \alpha_v \frac{\partial V_v}{\partial t} + A \alpha_v \frac{\partial V_v}{\partial z} \\ &= A \alpha_v \frac{\partial V_v}{\partial t} + A \alpha_v \frac{\partial V_v}{\partial z} + A \alpha_v \frac{\partial V_v}{\partial t} + A \alpha_v \frac{\partial V_v}{\partial z} \end{aligned}$$

$$\begin{aligned} A \frac{\partial \alpha_{cl} V_{cl}}{\partial t} + \frac{\partial A \alpha_{cl} V_{cl}}{\partial z} &= A \alpha_{cl} \frac{\partial V_{cl}}{\partial t} + A \alpha_{cl} \frac{\partial V_{cl}}{\partial z} + A \alpha_{cl} \frac{\partial V_{cl}}{\partial t} + A \alpha_{cl} \frac{\partial V_{cl}}{\partial z} \\ &= A \alpha_{cl} \frac{\partial V_{cl}}{\partial t} + A \alpha_{cl} \frac{\partial V_{cl}}{\partial z} + A \alpha_{cl} \frac{\partial V_{cl}}{\partial t} + A \alpha_{cl} \frac{\partial V_{cl}}{\partial z} \end{aligned}$$

$$\begin{aligned} &A\frac{\partial \mathcal{M}_{\mathcal{G},\mathcal{G}}V_{\mathcal{G}}}{\partial t} - \frac{\partial \mathcal{M}_{\mathcal{G},\mathcal{G}}V_{\mathcal{G}}}{\partial t} + A\mathcal{M}_{\mathcal{G},\mathcal{G}}\frac{\partial P}{\partial t} + A\mathcal{M}_{\mathcal{G},\mathcal{G}}\frac{\partial \mathcal{M}_{\mathcal{G}}}{\partial t} \\ &= A\mathcal{M}_{\mathcal{G},\mathcal{G}}\mathcal{G}_{\mathcal{G}} - A\mathcal{G}_{\mathcal{G}} + A\mathcal{G}_{\mathcal{G}}V_{\mathcal{G}} - A\mathcal{G}_{\mathcal{G}}V_{\mathcal{G}} + A\mathcal{G}_{\mathcal{G}}V_{\mathcal{G}} + A\mathcal{G}_{\mathcal{G}}V_{\mathcal{G}} \end{aligned}$$

$$\begin{aligned} &A\frac{\partial \mathcal{M}_{\mathcal{G}}\left(\mathcal{M}_t+\frac{V_{\mathcal{G}}}{2}\right)}{\partial t} - \frac{\partial \mathcal{M}_{\mathcal{G}}\mathcal{V}\left(\mathcal{M}_t+\frac{V_{\mathcal{G}}}{2}\right)}{\partial t} - A\mathcal{M}_{\mathcal{G}}\frac{\partial P}{\partial t} \\ &= A\mathcal{M}_{\mathcal{G}}\mathcal{V}\mathcal{V} + \mathcal{C}_{\mathcal{G},\mathcal{G}} + A\mathcal{G}_{\mathcal{G}} + A\mathcal{G}_{\mathcal{G}} + A\mathcal{G}_{\mathcal{G}}\mathcal{V}\mathcal{V} - A\mathcal{G}_{\mathcal{G}}\left(\mathcal{M}_t+\frac{V_{\mathcal{G}}}{2}\right) - A\mathcal{G}_{\mathcal{G}}\left(\mathcal{M}_t+\frac{V_{\mathcal{G}}}{2}\right) + A\mathcal{G}_{\mathcal{G}} \end{aligned}$$

$$\begin{aligned} &A\frac{\partial \mathcal{M}_{\mathcal{G}}\left(\mathcal{M}_t+\frac{V_{\mathcal{G}}}{2}\right)}{\partial t} + \frac{\partial \mathcal{M}_{\mathcal{G},\mathcal{G}}V_{\mathcal{G}}\left(\mathcal{M}_t+\frac{V_{\mathcal{G}}}{2}\right)}{\partial t} - A\mathcal{M}_{\mathcal{G}}\frac{\partial P}{\partial t} \\ &= A\mathcal{M}_{\mathcal{G},\mathcal{G}}V_{\mathcal{G}} + \mathcal{C}_{\mathcal{G},\mathcal{G}} + A\mathcal{G}_{\mathcal{G}} + A\mathcal{G}_{\mathcal{G}}\left(\mathcal{M}_t+\frac{V_{\mathcal{G}}}{2}\right) \\ &\quad - \mathcal{G}_{\mathcal{G}}\left(\mathcal{M}_t+\frac{V_{\mathcal{G}}}{2}\right) + \mathcal{G}_{\mathcal{G}}\left(\mathcal{M}_t+\frac{V_{\mathcal{G}}}{2}\right) + A\mathcal{G}_{\mathcal{G},\mathcal{G}} \end{aligned}$$

$$\begin{aligned} &A\frac{\partial \mathcal{M}_{\mathcal{G}}\left(\mathcal{M}_t+\frac{V_{\mathcal{G}}}{2}\right)}{\partial t} + \frac{\partial \mathcal{M}_{\mathcal{G},\mathcal{G}}V_{\mathcal{G}}\left(\mathcal{M}_t+\frac{V_{\mathcal{G}}}{2}\right)}{\partial t} - A\mathcal{M}_{\mathcal{G}}\frac{\partial P}{\partial t} \\ &= A\mathcal{M}_{\mathcal{G},\mathcal{G}}V_{\mathcal{G}} + \mathcal{C}_{\mathcal{G},\mathcal{G}} + A\mathcal{G}_{\mathcal{G}} + A\mathcal{G}_{\mathcal{G}}\left(\mathcal{M}_t+\frac{V_{\mathcal{G}}}{2}\right) \\ &\quad + A\mathcal{G}_{\mathcal{G}}\left(\mathcal{M}_t+\frac{V_{\mathcal{G}}}{2}\right) + \mathcal{G}_{\mathcal{G}}\left(\mathcal{M}_t+\frac{V_{\mathcal{G}}}{2}\right) - \mathcal{G}_{\mathcal{G}}\left(\mathcal{M}_t+\frac{V_{\mathcal{G}}}{2}\right) + A\mathcal{G}_{\mathcal{G},\mathcal{G}} \end{aligned}$$

$$\begin{aligned} f_{\mathcal{G}} &:= -f_{\mathcal{G}} = \frac{\mathcal{G}_{\mathcal{G}} + \mathcal{G}_{\mathcal{G}}}{\mathcal{G}_{\mathcal{G}}} f_{\mathcal{G}} := -f_{\mathcal{G}} = \frac{\mathcal{G}_{\mathcal{G}} + \mathcal{G}_{\mathcal{G}}}{\mathcal{G}_{\mathcal{G}}} f_{\mathcal{G}} \\ &:= -f_{\mathcal{G}} f_{\mathcal{G}}^{\mathcal{G}} := -f_{\mathcal{G}}^{\mathcal{G}} \end{aligned}$$

$$\alpha_t + \alpha_{\mathcal{G}} + \alpha_{\mathcal{G}} = \mathbb{E}_{\mathcal{G}}[\mathcal{P}_{\mathcal{G}}H_t] - \mathbb{E}_t[\mathcal{P}_{\mathcal{G}}H_t] - \mathbb{E}_t[\mathcal{P}_{\mathcal{G}}H_t] - \mathbb{E}_t[\mathcal{P}_{\mathcal{G}}H_t] - \mathbb{E}_t[\mathcal{P}_{\mathcal{G}}H_t]$$

+ expressions for $\Gamma_e, \Gamma_d, f_{\text{ivdl}}, f_{\text{ivcl}}, g_v, g_{cl}, \tau_{\text{idb}}, \tau_{\text{ivcl}}, q_{\text{icl}}, q_{\text{ivcl}}, q_{\text{idl}}, q_{\text{ivdl}}, C_k, \tau_{\text{wk}}, q_{\text{wk}}, \delta P_{\text{ksing}}, F_{\text{vAM}}, V_{\text{icl}}, V_{\text{idl}}$

5.15 Summary remarks

The equations at the basis of computational tools adopted for transient analysis of water-cooled nuclear reactors have been presented. Those equations have a broad validity which derives from their origin, i.e., the principles of thermodynamics and mechanics. Continuum body assumption is invoked in order to translate the principles into workable equations for fluids either single- or multiple phase.

The process for development of the equations has been outlined in this chapter starting from the fundamentals and involving steps of increasing complexity. The set of six PDEs dealing with steam and water mixture is also known as unequal velocity unequal temperature (UVUT): qualified sets of UVUT-PDE, including the constitutive/closure equations (Chapter 9), which are implemented in current system thermal-hydraulic codes, shall be considered the key outcome of decades of research in nuclear thermal-hydraulics (Chapter 2); the same equations also constitute a synthesis of knowledge and the state of the art in the area.

Time and space averaging constitute at the same time unavoidable processes for achieving a solution and sources of approximations in the results of the numerical integration which are difficult to be quantified.

Nevertheless the translation of the equations into the algebraic form necessary for numerical computation and the solution of the algebraic equations have been marginally considered in this chapter (more information is given in Chapter 11).

The distinction between open and porous media modeling approaches is discussed: the former deals with the CFD-like codes and includes the DNS codes; the latter deals with system thermal-hydraulics and may be characterized by the amount and type of closure models (i.e., including constitutive equations) which are needed for achieving a solution. Actually, only in the case of single-phase DNS, closure models can be avoided for predicting fluid transient evolutions at the expenses of computational power that is impractical for NPP applications. More information about current CFD models can be found in Chapter 12.

Special topics related to the nature and the structure of the balance equations are also considered in the present chapter. These are listed below together with summary notes:

(a) *The HEM* also called equal velocity equal temperature (EVET): steam and liquid form a compressible fluid.

(b) *The drift flux model*: this can be considered an attempt to establish a relationship between liquid and steam velocities in a gravity environment; the drift

flux model, as conceived in the 1960s, can be derived by introducing approximations to the UVUT momentum equation.

(c) *The hyperbolicity of the solution*: the issue of hyperbolicity is connected with the numeric solution of the UVUT set of equations and has been thoroughly investigated for the case of 1-D models. Nonhyperbolicity or lack of hyperbolicity of a set of equations implies non-real roots for the characteristic equation and may cause abortion of a calculation process.

(d) *The CFD modeling*: this is considered by the paragraph above and included in this list for the sake of completeness.

(e) *The Transport of Interfacial Area*: efforts in the last two decades attempting to introduce an additional equation (and additional unknown) to the existing set of balance equations did not demonstrate yet to be able to catch the complex two-phase phenomena even in a limited range of conditions, noticeably droplet and bubbly flows, considered in modeling. The polydispersed modeling approach may reveal more promising in this area.

(f) *The 3-D modeling*: all major thermal-hydraulic system codes have a three-dimensional modeling capability; however, systematic and comprehensive validation demonstrations are not achieved. Differences in relation to 3-D open media and porous media approaches are important, as discussed in the chapter.

(g) *The multifield modeling*: the complex nature of two-phase flow imposes the consideration of multifields in modeling. The capability appears important for modeling of reflood, with main reference to the flow configuration from the quench front where droplets are entrained up to upper plenum, hot legs, and steam generators where they can deposit and vaporize. This complex behavior has an important impact on the overall reflooding process.

It may be noted that the last three topics constitute areas for current research in relation to which industrial applications are not fully mature at the time of this writing. Furthermore, a problem common to the TIA approach, the 3-D modeling (at least in porous media) and the multifield modeling, derives from the difficulty in utilizing the huge and expensive experimental data base available in nuclear thermal-hydraulics (see Chapter 6): the same level of information from experiments which is suited for 1-D modeling needs to be extended to more complex modeling approach. New experimental programs with advanced local measurement techniques are then necessary.

This chapter constitutes a hinge, or has the pivot role, for all the chapters. Namely, the development of equations is the technology response to needs established in **Chapter 4** within the framework in nuclear thermal-hydraulics set by **Chapters 1–3**. The equations in this chapter are supplemented by constitutive/closure equations in **Chapter 9** and constitute the basis for the code discussed in **Chapter 11**. The code must have the capability to predict phenomena in **Chapter 6** and shall undergo the process of validation discussed in **Chapter 13**. The envisaged framework for code applications and the results from calculation of transient scenarios are discussed in **Chapters 14 and 15**, respectively.

References

- Bestion D. The physical closure laws in the Cathare code. *Nucl. Eng. Des.* 1990;124:229–245.
- Bestion D. The difficult challenge of a two-phase CFD model for all flow regimes. *Nucl. Eng. Des.* 2014;279:iv–v.
- Bestion D., Serre G. On the modelling of two-phase Flow in horizontal legs of a PWR. *Nucl. Eng. Technol.* 2012;44:8.
- Bestion D., Serre G. *Transport of interfacial area in system codes: status and perspectives*. In: NURETH-15, Pisa, 12–15 May; 2013.
- Bestion D., Coste P., Niceno B., Mimouni S., Lakehal D., Bartosiewicz Y. Two-phase CFD: the various approaches and their applicability to each flow regime. *Multiph. Sci. Technol.* 2011;23(2–4):101–128.
- Bois G., Jamet D., Lebaigue O. *Towards large eddy simulation of two-phase flow with phase-change: direct numerical simulation of a pseudo-turbulent two-phase condensing flow*. In: 7th International Conference on Multiphase Flow, ICMF 2010, Tampa, FL, 30 May–4 June; 2010.
- Boure J.A. *On a unified presentation of the non-equilibrium two-phase flow model*. In: Lahey Jr., G.B.Wallis R.T., eds. ASME Annual Winter Meeting, Houston, TX; 1975.
- de Crecy F. Modeling of stratified two-phase flow in pipes, pumps and other devices. *Int. J. Multiphase Flow.* 1986;12:307–323.
- Delhaye J.M., Giot M., Riethmuller M.L. *Thermohydraulics of Two-Phase Systems for Industrial Design and Nuclear Engineering*. New York: McGraw-Hill; 1981.
- Dhotre M.T., Smith B., Niceno B. CFD simulation of bubbly

flows: random dispersion model. *Chem. Eng. Sci.* 2007;62:7140–7150.

Dhotre M.T., Niceno B., Smith B. Large eddy simulation of a bubble column using dynamic sub-grid scale model. *Chem. Eng. J.* 2008;136:337–348.

Ishii M., Hibiki T. *Thermo-Fluid Dynamics of Two-Phase Flow*. second ed. New york: Springer; 2011.

Koncar B., Morel C., Mimouni S., Vyskocil L., Galassi M.C. CFD modeling of boiling bubbly flow for DNB investigations. *Multiph. Sci. Technol.* 2011;23(2–4).

Krepper E., Morel C., Niceno B., Ruyer P. CFD modelling of adiabatic bubbly flow. *Multiph. Sci. Technol.* 2011;23:2–4.

Lahey Jr. R.T., Moody F.J. *The Thermal-hydraulics of a Boiling Water Reactor*. Hinsdale, IL: ANS Monograph; 1993.

Lakehal D. On the modelling of multiphase turbulent flows for environmental and hydrodynamic applications. *Int. J. Multiphase Flow*. 2002;28:823–863.

Lakehal D. *LEIS for the prediction of turbulent multifluid flows applied to thermal hydraulics applications*. In: Int. Meet XCFD4NRS, Grenoble, 10–12 September; 2008.

Lakehal D. LEIS for the prediction of turbulent multifluid flows applied to thermal-hydraulics applications. *Nucl. Eng. Des.* 2010;240:2096–2106.

Lakehal D., Labois M. A new modelling strategy for phase-change heat transfer in turbulent. *Int. J. Multiphase Flow*. 2011;37:627–639.

Lakehal D., Fulgosi M., Banerjee S., Yadigaroglu G. Turbulence and heat transfer in condensing vapor-liquid flow. *Phys. Fluids*. 2008;20.

Lerchl G., Austcberegesilo H. *ATHLET Mod 3.0 Cycle A.—models and methods*. In: GRS-P-1/Vol. 4, Garching, July; 2013.

Lilly D.K. A proposed modification of the Germano Subgrid-Scale Closure Method. *Phys. Fluids A*. 1991;4(3):633–635.

Lucas D., Coste P., Höhne T., Lakehal D., Bartosiewicz Y., Bestion D., Scheuerer M., Galassi M.C. CFD modeling of free surface flow with and without condensation. *Multiph. Sci. Technol.* 2011;23(2–4).

Magdeleine S., Mathieu B., Lebaigue O., Morel C. *DNS up-scaling applied to volumetric interfacial area transport equation*. In: 7th International Conference on Multiphase Flow (ICMF 2010), Tampa, FL, 30 May–4 June; 2010.

Mahaffy J., ed. *Best Practice Guidelines for the Use of CFD in Nuclear Reactor Safety Applications*. Paris: OECD, Nuclear Energy Agency; 2007 Technical Report, NEA/CSNI/R(2007)5.

Morel C. *Mathematical Modelling of Disperse Two-Phase Flow*. Cham, Switzerland: Springer-Verlag; 2015.

Niceno B., Dhotre M.T., Deen N.G. One equation sub-grid scale (SGS) modeling for Euler-Euler large eddy simulation (EELES) of dispersed bubbly flow. *Chem. Eng. Sci.* 2008;63:3923–3931.

Ničeno B., Boucker M., Smith B.L. Euler-Euler large eddy simulation of a square cross-sectional bubble column using the neptune CFD code. *Sci. Technol. Nucl. Ins.* 2009.

RELAP5/MOD3. *Code manual volume I: code structure, system models and solution procedure*. In: NUREG/CR-5535; Washington, DC: USNRC; 1998.

Stuhmiller J.H. The influence of interfacial pressure forces on the character of two-phase flow model equations. *Int. J. Multiphase Flow*. 1977;3:551–560.

Toutant A., Chandesris M., Jamet D., Lebaigue O. Jump conditions for filtered quantities at an under resolved interface. Part 1: theoretical development. *Int. J. Multiphase Flow*. 2009a;35(12):1100–1118.

Toutant A., Chandesris M., Jamet D., Lebaigue O. Jump

conditions for filtered quantities at an under resolved interface.
Part 2: a priori tests. *Int. J. Multiphase Flow*.
2009b;35(12):1119–1129.

TRACE V5.0, 2007. Theory Manual—Field Equations, Solution Methods and Physical Models, USNRC, Washington, DC.

Valette M., Pouvreau J., Bestion D., Emonot P. *Revisiting large break LOCA with the CATHARE 3 three field model*. In: NURETH 13, Kanazawa, 27 September–2 October; 2009.

Zaepffel D., Morel C., Lhuillier D. A multi-size model for boiling bubbly flows. *Multiph. Sci. Technol*. 2012;24(2):105–179.

Zuber N., Findlay J.L. Average volumetric concentration in two-phase systems. *J. Heat Transf*. 1965;453–468.

Target phenomena in nuclear thermal-hydraulics

N. Aksan *Paul Scherrer Institut, Villigen, Switzerland*

Abstract

Nuclear power plants, namely water-cooled nuclear reactors, constitute complex systems operated at conditions which put continuous challenges to materials, structures, and components. This is specifically true in the case of postulated accidents. The knowledge of the evolution of postulated accidents is mandatory to determine the challenges. The reactor design basis environment is considered ending-up in the so-called design basis accident. Postulated accidents or transient scenarios are decomposed by thermal-hydraulic phenomena. Following three decades work in the area, about more than 100 phenomena are found as reasonable to characterize expected transient scenarios in water-cooled reactors. Identification and (mostly qualitative) characterization of phenomena constitute the topic of the chapter. Phenomena are expected to be part of the modeling capabilities of computational tools.

Keywords

Accident scenarios; Thermal-hydraulic phenomena; Separate effect tests; Integral effect tests; Small-scale facilities; Design of experiments; Scaling

Nomenclature

ABWR advanced boiling water reactor (BWR)

ADS automatic depressurization system

ALWR advanced light water reactor

AM accident management

AP1000 or AP600 advanced pressure water reactor-1000

ARDs advanced reactor designs

ATWS anticipated transient without scram

BIC boundary and initial conditions

BMFT The Federal Ministry for Research and Technology of the

Federal Republic of Germany

BWR boiling water reactor

CCF countercurrent flow

CCFL countercurrent flow limitation

CCVM computer code validation
matrix

CHF critical heat flux

CMT core makeup tank

CRGT control rod guide tube

CSNI Committee on the Safety of
Nuclear Installations (of OECD/NEA)

DBA design basis accident

DNB departure from nucleate boiling

DP differential pressure

ECCI emergency core cooling
injection

ECCS emergency core cooling system

EPR European pressurized water
reactor

ESBWR economic simplified boiling
water reactor

FCO forced convection

GDCS gravity-driven cooling system

HPLWR high performance light
water reactor

HT heat transfer

HTD heat transfer deterioration

IC isolation condenser

ILOCA interfacing LOCA

IBLOCA intermediate-break LOCA,
see also MBLOCA

ISP International Standard Problem

KWU Kernkraftwerk Union

LBLOCA large-break loss of coolant
accident

LOCA loss of coolant accident

LOFW loss of feedwater

LOOSP loss of off-site power

LP lower plenum

LWR light water reactor

MBLOCA medium-break LOCA, see also IBLOCA

MSLB main steam line break

NC natural circulation

NCO natural convection

NEA Nuclear Energy Agency

NPP nuclear power plant

OECD Organization for Economic Cooperation and Development

OTSG once-through steam generator

P pressure

PCCS passive containment cooling system

PCEI parallel channel effects and instabilities

PD pressure drop

PH phenomenon

PHWR pressurized heavy water reactor designed by KWU (G)

PRZ pressurizer

PTS pressurized thermal shock

PWRs pressurized water reactors

PWR-O PWR equipped with OTSG

QF quench front

RCS reactor coolant system

RIA reactivity-initiated accident

RPV reactor pressure vessel

SBLOCA small-break loss of coolant accident

SBO station black out

SCWR super critical water reactor

SET, SETF separate effects test (SET) facility

SG steam generator

SGTR steam generator tube rupture

SHD shutdown (accident conditions)

SNB subcooled nucleate boiling

SOAR state-of-the-art report

T temperature

UP upper plenum

US NRC United States Nuclear
Regulatory Commission

UTP upper tie plate

VVER (WWER) water-cooled water-
moderated energy reactors designed

Acknowledgments

Dedicated to my parents Meliha and Hüseyin Aksan, my family Berrin Aksan, Elif Aksan Akkaya, Ercan Akkaya, Defne Akkaya, Celine Le Roch, Gökhan Aksan. Thank you for your patience, love, and support throughout the years.

Special thanks to Paul Scherrer Institut, Villigen and Würenlingen, Switzerland (especially, Dr. G. Markoczy, Prof. Dr. G. Yadigaroglu, G. Varadi, and Dr. J. Dreier) for providing me the means and support to carry out the work in this writing. Further appreciations are to International Organizations, OECD/NEA/CSNI, Paris, France (especially, David Bessette, Heikki Holmstrom, Javier Reig), IAEA, Vienna, Austria (especially, John Cleveland, Sama Bilbao y Leon, Katsumi Yamada), and US NRC, Rockville, Maryland, USA for providing the necessary international working environment and support. The author is grateful to F. D'Auria (University of Pisa, Italy), H. Glaeser (GRS Garching, Germany), K. Wolfert (GRS Garching, Germany), C. Richards (AEA Technology, Winfrith, UK), J. Lillington (AEA Technology, Winfrith, UK), R. Pochard (IPSN: DPEI-CEA/FAR, Fontenay-Aux-Roses, France), and A. Sjöberg (Studsvik Eco & Safety AB, Nyköping, Sweden), A. Annunziato (JRC, Ispra, Italy), P. Marsili (ENEA, Rome, Italy), C. Renault (CEA, Cadarache, France), who are also contributors to separate effects (SET) and integral test facilities (ITF) Matrices work.

Chapter foreword

Nuclear power produces 15% of the world's electricity. Many countries are planning to either introduce nuclear energy or expand their nuclear generating capacity. Design organizations are incorporating both proven means and new approaches for reducing the capital costs of their advanced designs. In the future newest nuclear plants will be of evolutionary design, often pursuing economies of scale. In the longer term, innovative designs could help to promote a new era of nuclear power.

Since the mid-1980s it has been recognized that the application of passive safety systems (i.e., those whose operation takes advantage of natural forces such as convection gravity), can contribute to simplification potentially improve economics of new nuclear power plant (NPP) designs. The IAEA Conference on

The Safety of Nuclear Power: Strategy for the Future, which was convened in 1991, noted that for new plants “the use of passive safety features is a desirable method of achieving simplification increasing the reliability of the performance of essential safety functions, should be used wherever appropriate.” Some new designs also utilize natural circulation (NC) as a means to remove core power during normal operation. The use of passive systems can eliminate the costs associated with the installation, maintenance, operation of active systems that require multiple pumps with independent redundant electric power supplies. However, considering the weak driving forces of passive systems based on NC, careful design analysis methods must be employed to ensure that the systems perform their intended functions.

To support the development of advanced water-cooled reactor designs with passive systems, investigations of NC are conducted in several IAEA Member States with advanced reactor development programs. To foster international collaboration on the enabling technology of passive systems that utilize NC, the IAEA initiated a Coordinated Research Project (CRP) on Natural Circulation Phenomena, Modelling and Reliability of Passive Systems that Utilize Natural Circulation in 2004. As one output of this CRP, this publication describes passive safety systems in a wide range of advanced water-cooled NPP designs with the goal of gaining insights into the system design, operation, and reliability.

The identification and the characterization of thermal-hydraulic phenomena expected during postulated accident scenarios in light water cooled reactors (LWRs) including Advanced Water Cooled Reactors (AWCRs), and Supercritical Water Cooled Reactors (SCWRs), constitute the topic of this chapter. The knowledge of thermal-hydraulic phenomena is the essential component of the development of nuclear thermal-hydraulics subject area.

6.1 Introduction

For the analyses of transients and loss of coolant accidents (LOCAs) in light water reactors (LWRs) thermal-hydraulic computer codes have been developed over the last 40 years. Starting with relatively simple computer codes in the early 1970s, a continuous development of the codes has been made with respect to a more realistic description of thermal-hydraulic phenomena and a more detailed system representation.

At the beginning of the 1970s, codes for the analysis of large-break loss of coolant accidents (LBLOCAs) had been requested. The codes were based on the homogeneous equilibrium model (HEM), assuming equal velocities and

temperatures of vapor and liquid phases. The next effort in code development was directed by the demand for the simulation of transients and small break accidents. The implementation of new models allowed for the separation of vapor and liquid by gravity. The representation of primary and secondary side with control systems and balance of plant models were extended.

In the middle of the 1970s, the development of a new generation of thermal-hydraulic codes was initiated to provide analytical tools for a more realistic simulation of LWR behavior under transient and accident conditions. Thermal and mechanical nonequilibrium phenomena have been taken into account. The effects of noncondensables and boron tracking have been considered. These codes allow the simulation of transients, the entire range of break sizes as well as beyond design basis accidents (DBAs) including accident management (AM) procedures with operator interventions.

Parallel to the development of the analytical tools a large variety of experimental programs have been executed to improve the understanding of thermal-hydraulic phenomena, to study system behavior, and to provide the required database for code development and code validation. A very high number of separate effects tests (SETs) have been performed for the development and validation of code models. SETs investigate individual phenomena under clear boundary conditions. While in the 1970s the experiments were conducted mainly on small-scale test facilities, in the 1980s more attention has been directed to integral effect tests simulating system behavior, and emphasizing scaling. For example, in 1986, the first tests at the test facility UPTF, a representation of a four-loop 1300 MWe PWR with upper plenum (UP), downcomer, and the main coolant pipes in full-scale reactor geometry, were performed (US NRC, 1987).

The overall results of the code calculations are validated mainly by data from integral test facilities representing the primary and secondary coolant systems. While in the early 1970s the experiments were focused on large-break issues, in the following, up to now, parallel to the advancement in code development, integral tests have been carried out to investigate LWR system behavior during transients, small breaks, transients under shutdown (SHD) conditions, and beyond DBAs. In addition to the results of integral tests, LWR plant data of transients or accidents are being used to validate the predictive capability of the codes.

Construction of code validation matrices is an attempt to collect together the best sets of test data for code validation and improvement from the wide range of experiments that have been carried out world-wide in the field of thermal-hydraulics. The first formulation of a validation matrix was proposed by Wolfert

and Frisch (GRS) (1983). This activity was taken by a CSNI subgroup to establish matrices for PWR and boiling water reactor (BWR). During this activity a number of related works were performed by experts in the field and reports were published. These activities also included the identification and characterization of thermal-hydraulic phenomena for the current generation of LWRs.

Already in the year 1987, the OECD/NEA Committee on the Safety of Nuclear Installations (CSNI) published a document that identified systematically a set of physical phenomena and tests, which were considered to provide the best basis for the assessment of the performance of thermal-hydraulic codes, "CSNI Code Validation Matrix of Thermohydraulic Codes for LWR LOCA and Transients" (OECD/NEA, 1987). The report included all typical phenomena expected to occur in plant transients and LOCA analyses. As follow up, state-of-the-art report (SOAR) on thermohydraulic of emergency core cooling in LWRs, Lewis et al. (1989) emphasized the importance of phenomena identification for transient analysis of LWRs. After publishing these two reports, it turned out that continued comparison of calculations with additional SET data is also necessary to consider particular applications of codes, especially where a quantitative evaluation of prediction accuracy is required for best estimate computer codes, as well as for code model improvement. Based on these needs, the OECD/NEA-CSNI issued an independent and separate two-volume report on SETs validation matrix (Aksan et al., 1994). An updated integral test validation matrix report was also worked on and issued (Annunziato et al., 1996). In addition, to set-up validation matrices for Russian pressurized water-cooled and water-moderated energy reactor (VVER (WWER)) analyses, an International Working Group was formed on the initiative of the Federal Ministry for Research and Technology (BMFT) of the Federal Republic of Germany. A further evaluation of the VVER matrices was performed by an OECD/NEA Support Group (2001). One of the few advanced water-cooled reactor studies within OECD/NEA-CSNI was directed to some characteristics of advanced reactor designs (ARDs), for example, AP600, SBWR, advanced boiling water reactor (ABWR), EPR, PIUS, etc. In this status report, specific needs for thermal-hydraulic codes together with the identified relevant and important thermal-hydraulic phenomena for ARDs are summarized with the purpose of providing some guidance in development of research plans for considering further code development and assessment needs and for the planning of experimental programs (Aksan and D'Auria, 1996). These identified phenomena for ARDs are in addition to the relevant thermal-hydraulic phenomena identified for the current generation LWRs.

As part of the IAEA's overall effort to foster international collaborations that strive

to improve the economics and safety of future water-cooled NPPs, an IAEA CRP was started in early 2004. This CRP, entitled Natural Circulation Phenomena, Modeling and Reliability of Passive Safety Systems that Utilize Natural Circulation, focused on the use of passive safety systems to help meet the safety and economic goals of a new generation of advanced NPPs. This CRP has been organized within the framework of the IAEA Department of Nuclear Energy's Technical Working Groups for Advanced Technologies for LWRs and heavy water reactors (the TWG-LWR and the TWG-HWR) and provided an international cooperation on research work underway at the national level in several IAEA Member States.

The use of passive safety systems such as accumulators, condensation and evaporative heat exchangers, and gravity-driven safety injection systems eliminate the costs associated with the installation, maintenance, and operation of active safety systems that require multiple pumps with independent and redundant electric power supplies. As a result, passive safety systems are being considered for numerous reactor concepts (including in Generation III and III+ concepts) and are expected to find applications in the Generation IV reactor concepts, as identified by the Generation IV International Forum (GIF). Another motivation for the use of passive safety systems is the potential for enhanced safety through increased safety system reliability.

The CRP on NC and passive safety systems benefits from earlier IAEA activities that include developing databases on physical processes of significant importance to water-cooled reactor operations and safety, for example, in the area of thermal-hydraulic phenomena in advanced water-cooled reactors, recent IAEA activities have assimilated data internationally on heat transfer (HT) coefficients and pressure drop (PD) (IAEA and Aksan, 2001); and have shared information on NC data and analytical methods (IAEA and Aksan, 2001), and on experimental tests and qualification of analytical methods (IAEA and Aksan, 2000). In order to establish the progress of work in this CRP, an Integrated Research Plan with description of the tasks addressing the objectives of the CRP was defined. These tasks are:

- establish the state-of-the-art on NC,
- identify and describe reference systems,
- identify and characterize phenomena that influence NC,
- examine application of data and codes to design and safety,

- examine the reliability of passive systems that utilize NC.

The activity under the first task is aimed at summarizing the current understanding of NC system phenomena and the methods used experimentally to investigate and model such phenomena. In November 2005, the IAEA issued a technical document (IAEA and Aksan, 2005), developed by the collaborative effort of the CRP participants and with major contributions from some selected experts in the CRP, aimed at documenting the present knowledge in six specific areas: advantages and challenges of NC systems in advanced designs, local transport phenomena and models, integral system phenomena and models, NC experiments, advanced computation methods, and reliability assessment methodology.

The activity for the third task is aimed at identifying and categorizing the NC phenomena of importance to advanced reactors and passive safety system operations and reliability. This task is the major link between the second and the fourth tasks. During the phase to perform the activities on the mentioned tasks, one of the unique features was to collect and include plant design descriptions with a strong emphasis on passive safety systems of the specific design. These descriptions of the passive safety systems were considered during the phenomena identification and characterization process by the group of experts. As basis for the phenomenon (PH) identification for AWCs, earlier works performed within the OECD/NEA framework during 1983 to 1997 were in detail considered (OECD/NEA, 1987; Lewis et al., 1989; Aksan et al., 1994; Annunziato et al., 1996; Aksan and D'Auria, 1996). The list of relevant phenomena established in Aksan and D'Auria (1996) has been taken as basis for the AWCs work and been modified according to the reactor types and passive safety systems considered. It is to be also noted that in identifying the relevant thermal-hydraulic phenomena in the list which is provided in Section 6.5, expert judgment is the main contributor.

IAEA-TECDOC-626 provides definitions for safety-related terms as applied to advanced reactors (IAEA, 1991). In that document, the concepts of passive and active safety systems are defined and discussed. The definition of a passive safety system is as follows: *Either a system which is composed entirely of passive components and structures or a system which uses active components in a very limited way to initiate subsequent passive operation.* Four categories were established to distinguish the different degrees of passivity.

This chapter will provide some details on the important and relevant thermal-hydraulic phenomena for current generation LWRs (e.g., PWRs, BWRs, and VVERs) including separate effect and integral effect phenomena, AWCs (AP1000, ESBWR, EPR, VVER-1200, etc.), and SCWRs (super critical water

reactors). These identified phenomena are the backbone of subject area of the nuclear reactor thermal-hydraulics and helps to define the research and development activities in the experimental and analytical field.

6.2 Classification of thermal-hydraulic phenomena for set

The basic conservation equations used in thermal-hydraulic two-phase flow models for analyzing LWR systems under normal and off-normal operating conditions describe the transport of mass, momentum, and energy of the steam and water. These local instantaneous partial differential equations are generally integrated over a control volume of the fluid to result in a set of finite difference equations (algebraic equations) which can be solved numerically by known algorithms. When making the integration some kind of averaging procedure is applied which implies that the resulting equations will loose the capability to resolve phenomena in a microscale sense. Thus phenomena such as turbulent fluctuations will either be ignored or integrated into correlations. Only the average three-dimensional, time-varying characteristics of the flow over a scale dictated by the size of the mesh cells can be retained. The most commonly used averaging procedure includes double averages, in time and space. The procedure generates distribution coefficients for different transport phenomena. These coefficients appear as the ratio of the averages of products divided by the products of the averages. Due to lack of information on these coefficients they are usually taken to be unity (Yadigaroglu et al., 1990).

In earlier two-phase models the fluid was treated as a homogeneous mixture of liquid and vapor and consequently only three conservation equations were needed to describe the two-phase flow. In the HEM the phases are assumed to move with the same velocity and also exist at the same temperature. An extension to the mixture model is the drift flux model in which the relation between the phasic velocities is described through an algebraic equation, thus allowing for slip between the phases (Sonnenburg, 1990). In further developed models, the conservation equations are set up for each phase separately, and six equations are used (two-fluid two-phase flow models). Additional equations can be incorporated in the models to account for liquid solutes and noncondensable gases. The significant property of the two-fluid model is that it allows the two phases to have different velocities and temperatures. Consequently, this type of model has the potential to calculate the effects of phase separation and thermal nonequilibrium.

The two-phase flow model is in most cases simplified to be a one-dimensional

model whether it is a mixture or two-fluid model. Then possible three-dimensional effects cannot be taken into account, but have to be included by means of special process models (e.g., special models for simulating the phenomena associated with subcooled ECC injection into a voided pipe) and by simulating the actual flow path by the appropriate connections of a number of one-dimensional flow paths.

There are two-phase models that retain some three-dimensional characteristics, although simplifications in the equations are usually introduced in order to make system calculations practical. Despite the simplifications, these models have the potential to simulate three-dimensional effects which can be most important, for example, in some time windows of a LBLOCA, where flow redistributions are supposed to occur in the reactor vessel.

In order to solve the set of finite difference equations, closure or constitutive equations are required, along with relations describing the steam-water properties under different conditions. In this context the steam-water properties are assumed to be well known for most of the application ranges and associated tables and functions are supposed to be adequately programmed in any of the used codes. The same is also assumed to be true for needed derivatives of the properties.

The constitutive equations describe the HT between wall structures and the two-phase fluid, the interphase mass, momentum, and HT, and the wall to fluid drag. The wall HT and the wall drag to each phase are dependent on the extent of the wall contact of the phase and the associated transfer process, whereas the interphase exchange of mass, momentum, and energy depends on the interfacial area along with associated interphase transport processes. In view of the averaged nature of the conservation equations as mentioned above, the wall contact of the phases and the interfacial area has to be expressed as volume based or averaged quantities. The adequate description of the interfacial area density, and thus the prevailing flow regimes, and the wall to fluid and interphase transport processes is one of the most important requirements for accurate modeling of the two-phase flow behavior.

Most of the constitutive equations are based on correlations with different levels of empiricism, from pure empirical models to models based on physical principles and with possibly only a few constants that have to be evaluated from experimental data. Pump degradation curves at two-phase conditions are examples of the former while models for frictional PDs can be examples of the latter. In some cases, the inherent capabilities of the two-fluid model are not fully exploited and a separate special process model or correlation is utilized. An example is the modeling of critical flow (Yadigaroglu et al., 1990). The integration of the two-fluid

conservation equations is able to predict a choked condition. Choking calculations in a component with a smooth area change could be done by using a sufficiently fine axial mesh and noting the occurrence of the critical conditions. However, this requires a very fine mesh to adequately predict the critical conditions.

The interactions of different correlations along with the conservation equations will constitute a code's capability to simulate important phenomena during the course of an LOCA or transient. It is essential to identify each relevant PH and to ascertain that the specific PH is adequately simulated by the code. This is usually done by comparing the code's results from simulations of well-defined tests carried out in properly designed test facilities with the test data. In this context a distinction is made between integral tests and SETs.

Integral tests are carried out in scaled test facilities and provide data on the overall behavior of a simulated reactor system during an LOCA or transient. These tests are being used for code assessment purposes relating to overall reactor behavior. A definition of sets of such tests (matrices) has been provided in OECD/NEA (1987). These facilities have a complicated configuration and are expensive to operate. Compromises, for instance with respect to scaling to real plants, are inevitable. Also the instrumentation for measurements of parameters governing different two-phase flow phenomena is limited. This makes the integral tests less suitable for detailed investigations of specific two-phase flow phenomena. As a consequence, this also requires in assessment analyses that the code user is very confident of which phenomena prevail during the course of a transient in order to avoid "good results but for the wrong reasons" (compensating errors).

SETs are employed not only to develop correlations of specific processes but also to investigate individual or localized two-phase phenomena which in most cases are dependent on several specific processes. These kinds of tests are also used to characterize the behavior of single components such as pumps or steam separators.

The interactions with other phenomena or components as in a full-scale LWR are either imposed by external boundary conditions on the test, or are purposely eliminated. In fact, an important consideration in the design of SETs is to have well-defined boundary conditions. In some cases, the test section in a SET is locally in full scale or very near to full scale. This minimizes the concern about scale effects. On the other hand, in all SETs it is important to evaluate the influence of the chosen boundary conditions on measured parameters.

In SETs the instrumentation for measurements of two-phase flow parameters can be quite extensive. Thus data for assessment of details of the models used in the

codes to simulate localized phenomena can be provided, and this can help in understanding the interactions of different processes that combine to produce the overall phenomena of interest. The data have also proved to be valuable when evaluating prediction uncertainties of specific phenomena at or near full scale.

As part of the definition of integral test matrices in OECD/NEA (1987), different phenomena were identified. In particular, phenomenological windows were distinguished in the case of:

- LBLOCAs in PWRs,
- small- and intermediate-break LOCAs and transients in PWRs,
- LOCAs in BWRs,
- transients in BWRs.

Typical scenarios simulated in the integral test facilities constituted the basis for this analysis. The consideration of presumed evolution paths of accidents in the reference plants (PWRs and BWRs) also played a role in this connection. The phenomena were identified essentially on the basis of the experience of the individual members of the Writing Group that was formed to investigate the simulated scenarios. Those identified phenomena formed a first basis for a more detailed list of relevant phenomena.

An expansion of that list covering different important LOCA phenomena was presented for both BWRs and PWRs in Lewis et al. (1989). A weighting and appraisal of each PH were also included. The main support for these phenomena was provided by a number of integral and SETs. That list of phenomena is the basis for the one given in Table 6.1. Only minor modifications were introduced in the list. Apart from some rearrangement a new group named “Basic Phenomena” has been added. Each PH in this group can be characterized as independent of other phenomena and is of a constitutive nature for the two-phase flow.

Table 6.1

List of thermal-hydraulic phenomena



In this section, the identification of the relevant two-phase flow phenomena is made and a short description of each PH is provided. A total of 67 phenomena is identified and the resulting phenomena list is given in Table 6.1. As stated above the identification is based on the phenomena list in OECD/NEA (1987). All representative phenomena occurring during an LOCA or transient is included, although several phenomena are combined under a general heading in some cases such as various instances of countercurrent flow limitation (CCFL), and of critical flow. It should also be realized that some phenomena are dependent on each other, for instance spray effects and condensation. It will be seen that there are several different types of phenomena, varying from those such as interphase friction which is a very basic attribute of a two-phase flow, to those such as loop seal clearing, which is essentially a system PH, localized in its occurrence but very dependent on events and conditions elsewhere in the loop. In such cases the influences from the loop have to be provided as boundary conditions.

Some groups of phenomena are linked. In this case an introductory description prefaces the group to avoid repetition of material. For instance, CCFL can occur at a variety of locations in an LWR. CCFL is very geometry dependent and encompasses a wide range of situations, requiring data from different types of SET facilities. Nevertheless, some aspects of CCFL are common to all these circumstances.

In some cases, there is an apparent overlap of the phenomena description, since the same PH occurs in combination with other phenomena. The intention has been, though, to provide the information without repetition, as far as possible.

6.3 Characterization of thermal-hydraulic phenomena for set

A brief description of each of the 67 phenomena listed in Table 6.1 is provided in this section.

This indicates the interpretation that has been put on the PH for the purposes of assessing suitable SET data. Thus, for example, it will be seen that the term horizontal stratified flow has been used to include the PH of thermal stratification as well as aspects of two-phase stratified flow associated with the presence of a surface. The description also indicates where in a reactor system, and under what

circumstances, the PH is likely to occur. The discussion of the PH should indicate features such as the degree of scale or geometry dependence, which affect the range of data likely to be necessary for code model validation.

Some groups of phenomena are linked. In this case an introductory description prefaces the group to avoid repetition of material. For instance, CCFL can occur at a variety of locations in an LWR. CCFL is very geometry dependent and encompasses a wide range of situations, requiring data from different types of SET facilities. Nevertheless, some aspects of CCFL are common to all these circumstances.

In some cases, there is an apparent overlap of the phenomena description, since the same PH occurs in combination with other phenomena. The details and specifics of overlaps and clarifications are provided in detail for each specific PH.

6.3.1 Basic phenomena

Basic phenomena are the transfer processes at the interface between different fluids (liquid and steam or a noncondensable gas) and solid surfaces facing the fluid. They comprise momentum, heat, and mass transfer which have been divided into evaporation due to depressurization (Section 6.3.1.1), evaporation due to heat input (Section 6.3.1.2), condensation due to pressurization (Section 6.3.1.3), condensation due to heat removal (Section 6.3.1.4), interfacial friction in vertical flow (Section 6.3.1.5), interfacial friction in horizontal flow (Section 6.3.1.6), and wall to fluid friction (Section 6.3.1.7), PDs at geometry discontinuities (Section 6.3.1.8), and pressure wave propagation (Section 6.3.1.9).

In the six equation models used in some thermal-hydraulic safety computer codes, the constitutive laws are intended to model these basic transfers between phases. The method of discretization for the fluid dynamics, and the numerical solution, significantly affect the calculation of pressure wave propagation.

Basic phenomena govern all the fluid behavior during an accident sequence, so they are inevitably important for nuclear safety.

In most cases of practical interest there is no direct measurement of basic phenomena for two-phase flow. They can be only evaluated on the basis of global measurements (e.g., DP , P , T).

Models are necessary to evaluate the basic transfers from the global measurements. From these models correlations are set up. But it is important to realize that the use of these correlations is not independent of the chosen model. Normally the

correlations should be used in a way which is consistent with their derivation. Usually the basic phenomena (Sections 6.3.1.1–6.3.1.7) are treated as independent of modeling.

With the present state of knowledge, models employed in codes give a large range of differences on evaluation of basic phenomena, Forge et al. (1988). But the global thermal-hydraulic behavior is nevertheless predicted quite similarly by different approaches, Ambrosini et al. (1988).

6.3.1.1 Evaporation due to depressurization

A good illustration of the PH is the case of water and saturated steam in an adiabatic cylinder with a piston. By increasing the volume with the piston, one can observe a sudden pressure decrease followed by a pressure increase due to vaporization of the liquid. The common understanding is that there is a delay before vaporization begins and then a gradual return to thermodynamic equilibrium. The delay depends on water purity which means that the presence and the number of microscopic nucleation sites play a role.

In a closed cylinder of fixed dimensions, the pressure variation can be obtained by extracting a certain amount of liquid at the bottom or steam at the top.

Another way to depressurize the two-phase fluid is to use a steady-state flow in a Venturi nozzle. In this case the fluid acceleration is the main source of depressurization and induces steam evaporation. A strong gradient of pressure can be obtained in a steady state with this process.

In the real experiments, the perfect adiabatic situation is not reached. There is always heat exchange with walls, and heat losses.

In blowdown experiments the flow can enhance transfer phenomena between phases.

This PH gives a major contribution to the general behavior during the course of an accident, for example, pressure evolution, upstream flow conditions at the breach, stagnation point for LBLOCAs.

This PH is easily predicted under the thermal and mechanical equilibrium conditions that occur in slow transients (in which mass and energy conservation are important but the kinematics are not). It is the prediction of departures from the equilibrium behavior that is of particular interest in the safety context.

6.3.1.2 Evaporation due to heat input

Evaporation of liquid due to heat input is one of the most essential phenomena occurring both in normal and off-normal operation of LWRs. The evaporation or boiling process on a heated surface is a very effective HT mode with more than one order of magnitude higher HT coefficient than for single-phase convection. On the other hand, at high heat flux on the heated surface, or when a high vapor content has accumulated under forced flow conditions, a sudden deterioration of the effective boiling HT mode can occur which can be hazardous to the heated surface.

Because of its contribution to determining boiling HT and dry-out phenomena, a relatively detailed description of the nucleation process is given below. HT from a heated surface is described in Section 6.3.12.

The evaporation process implies that vapor bubbles can be created and then are able to grow within the liquid. This requires that bubble nuclei are present and that the surrounding liquid is somewhat superheated. The nucleation process is described in terms of the difference of free energy between existing small vapor clusters in a liquid and the surrounding liquid (Hsu and Graham, 1986).

The free energy will reach a maximum as a function of increasing vapor cluster radius and then decrease. When the cluster radius is less than this critical radius, the natural tendency is for the vapor cluster to collapse since this will reduce free energy. On the other hand, if the cluster radius is greater than the critical value, an increase in the cluster size will also reduce free energy and thus a spontaneous growth of the cluster will occur. The vapor clusters with sizes greater than the critical value will serve as nuclei for vapor bubbles.

In the case when a solid heated surface is immersed into a liquid, the free energy difference required for nucleation is usually smaller than for the case of a homogeneous liquid. The reason is that on the solid surface small cavities exist which will act as nucleation sites. The liquid temperature gradient across the thermal boundary layer adjacent to the heated surface will determine the bubble growth.

When a bubble leaves the heated surface (or collapses) relatively cold liquid will replace the space earlier occupied by the bubble. This liquid is gradually heated by transient conduction until the temperature is high enough to allow for a new bubble to grow. The period until the appearance of the second bubble is called the waiting period. Following the appearance of the bubble, the growth period starts. During this period the bubble will grow because of evaporation taking place at the vapor-liquid interface and also to some extent from the microlayer of liquid at the bubble

base. The adjacent liquid is subjected to enhanced convection because of bubble agitation. The growth period terminates with bubble departure or collapse. Then the process repeats itself and a new bubble is created.

When the thermal boundary layer temperature is increased, more nucleation sites are activated. The bubble frequency at each site is increased, while the waiting period is decreased. A multibubble region will be established in which the creation of one bubble is strongly influenced by existing adjacent bubbles. Also coalescence of bubbles in the thermal boundary layer will occur, and this will be increased with heat flux. As a result liquid access to the heated surface will be restricted and momentary dry patches will begin to form. When this situation is reached the heat flux is approaching the critical heat flux (CHF).

The evaporation process due to heat input is a basic PH that contributes substantially to determining the overall course of an accident or transient event. The evaporation and coalescence of bubbles occurring at small scales give rise to different macroscopic two-phase flow regimes. The associated HT in the different regimes determines the maximum fuel temperature encountered during subsequent phases of a transient and, for example, the quenching velocity of the fuel during the reflood phase of an LOCA. The evaporation is also a basic process when a three-dimensional distribution of vapor and liquid is developed in pressure vessel plena after an accident and in a steam generator (SG) secondary side.

6.3.1.3 Condensation due to pressurization

In the case of the experiment described in Section 6.3.1.1, by reducing the volume with the piston, one can observe a sudden increase of pressure followed by a small decrease due to condensation of steam. In a closed cylinder of fixed geometry, the pressure increase can be obtained by injection of saturated water at the bottom or saturated steam at the top. This effect is also very sensitive to the film condensation process which occurs as walls become subcooled when pressure increases. It is possible that this condensation process is more important than the condensation at the interface.

In real experiments the same remarks as in Section 6.3.1.1 apply. The pressurization is, generally, due to injected subcooled water (e.g., safety injection).

The PH contributes to the general behavior of the pressurizer (PRZ) which governs the pressure evolution of transients such as anticipated transients without scram (ATWS), and feed and bleed procedures for transients such as a loss of feedwater (LOFW). Pressure recovery in the upper head at the end of some transients and SG

secondary side behavior in the case of tube rupture are related to this PH, and void collapse in the upper head during refill and reflood of the core at high pressure may delay core recovery.

6.3.1.4 Condensation due to heat removal

Condensation of vapor due to heat removal is an essential PH occurring in certain phases of normal and off-normal operation of LWRs and in various types of condenser equipment. The mode of condensation can be classified as dropwise or film-wise condensation on a solid surface, or as direct contact condensation on the surface of a subcooled liquid.

Dropwise and film-wise condensations are obtained on surfaces with temperatures below the saturation temperature in a superheated or saturated vapor environment. The exact mechanism of initiation of condensation is not yet fully understood. However, the consensus view is that the initiation of condensation starts in small surface cavities which contain liquid with enough subcooling. The magnitude of the subcooling depends on the curvature of the liquid surface that faces the vapor.

If the condensed liquid does not wet the surface the condensate will form droplets that run off the surface depending on the surrounding flow velocity, surface conditions, and surface inclination. This is known as dropwise condensation.

If the liquid wets the surface, or the dropwise condensation is intense enough, a continuous liquid film will be created and will cover the surface. This mode of condensation has a much lower HT coefficient than the dropwise mode. However, film-wise condensation is the predominant mode and is usually assumed when specifying correlations for condensation HT coefficients on a surface. These correlations are almost entirely based on Nusselt's theory.

Direct contact condensation is obtained when existing subcooled liquid droplets are passing through a saturated or superheated vapor environment. An example of this kind of condensation will be the spraying in a PWR PRZ. Relatively cold liquid will be provided as spray by means of spray nozzles in the PRZ top. The condensation will take place at the surface of the droplets and the temperature of the droplets will gradually increase as the droplets pass through the vapor phase. The spray flow rate is normally rather high compared with the amount of vapor being condensed and hence the droplet radius will increase only by a small amount.

The amount of condensed vapor will depend on the temperature difference between

the vapor and liquid droplets, the droplet size, the droplet transit time in the vapor phase, and on vapor and liquid properties.

The condensation processes due to heat removal are important during some parts of the course of evolution of an accident in LWRs and generally in condensers.

In condensers the condensation of vapor takes place on the shell side while the cooling liquid passes on the tube side in the usually horizontal tubes. The tubes are often arranged in a triangular pattern in such a way that the condensate can drain as freely as possible due to gravity and at the same time allow for high vapor velocities at low PDs within the condenser.

During the course of a small-break loss of coolant accident (SBLOCA) in a PWR, a situation can occur where vapor from the more or less uncovered core flows through the hot leg and condenses on the hot-leg side of the SG tubes. The condensed liquid flows back due to gravity along the tube wall and back through the hot leg to the core. This mode of cooling the core is quite effective and is characterized as the reflux condensation mode. The condensation in the SG tubes will basically be of the film-wise type.

The spray process is important in PRZ control and for the effectiveness of emergency core cooling in BWRs.

6.3.1.5 Interfacial friction in vertical flow

The momentum transfer between phases is principally a function of relative velocity between steam and water, of fluid densities and of a so-called interfacial friction coefficient which is highly dependent on flow regime. For vertical flow the basic flow regimes are bubbly flow, slug flow, chum flow, annular flow, and inverted annular flow (Govier and Aziz, 1976). The interfacial friction in general is highest in those flow regimes which result in high interfacial areas. In relating the interphase friction to the difference in average phase velocities, the effect of nonuniform velocity (velocity profile) needs to be considered, as does the effect of averaging flow structures (e.g., use of a single droplet diameter). Although interfacial friction is a basic PH, it is still a highly complex one, in which much simplification must be done to reduce it to a one-dimensional two-fluid description.

The interfacial friction has a direct influence on carryover and carryunder: entrainment and de-entrainment of water by steam. During core uncover, the swell level is related to interfacial drag. If the friction is high, the swell level is higher. This PH, coupled with wall friction, also influences CCFL.

To study the fundamentals of this PH air-water flow is useful (no heat and mass transfer).

Interphase friction is a key PH affecting the overall fluid behavior in a system under two-phase conditions, and its correct modeling is crucial for the adequate prediction of a number of other phenomena. This PH, together with wall-to-fluid friction (see Section 6.3.1.7), contributes to determining PD for two-phase flow in vertical situations. It governs phase separation and swell level particularly in the core, and so it is of high relevance for reactor safety.

6.3.1.6 Interfacial friction in horizontal flow

On the same physical basis as described in Section 6.3.1.5, the interfacial friction in horizontal flow is highly influenced by flow regime. Possible flow regimes are bubbly flow, plug flow, stratified flow, wavy flow, slug flow, and annular flow (Delhaye et al., 1981). It also influences countercurrent flow (CCF) in stratified conditions, and CCFL (Hewitt, 1989). At high flow rates horizontal and vertical flows behave similarly. There are major differences, resulting from the effects of phase separation, at low flows.

This PH, together with wall-to-fluid friction (see Section 6.3.1.7), contributes to PD for two-phase flow in horizontal conditions. It plays a role in the reflux condenser heat removal mode and also in the rate at which water can drain from the upper parts of the circuit to the core.

6.3.1.7 Wall-to-fluid friction

Wall-to-fluid friction causes, as is well known, a force opposite to the direction of the motion of the fluid. In single-phase fluid dynamics, the force is known to be dependent upon the cross-section average squared velocity and fluid density and upon external parameters. These parameters are the roughness of the walls and the equivalent diameter of the flow duct. The fluid viscosity also plays a role in the determination of the friction coefficient.

In two-phase flows, the wall-to-fluid interaction may depend greatly upon flow regime and local void fraction.

The PH gives a significant contribution to the overall PDs in a plant during normal and off-normal conditions. Essentially, three kinds of geometric situations can be distinguished in a nuclear reactor system concerning the wall-to-fluid friction:

(a) large plena,

(b) piping,

(c) core and SGs.

The last item (c) is characterized by small values of equivalent diameter.

6.3.1.8 PDs at geometric discontinuities

Important pressure variations occur due to abrupt changes of geometry in any thermal-hydraulic system including variations of curvature. Void fractions, cross-section profile of the fluid velocities and geometric peculiarities of the system (e.g., shape of the edges that constitute the discontinuity) are among the main parameters that affect the PH.

Strong three-dimensional flow paths may occur in the proximity of abrupt geometry variations making difficult analytical modeling and a complete experimental characterization of the PH.

The prediction of this PH is essential to evaluate scenarios in the plant. The following main zones are relevant as far as local PDs are concerned:

(a) inlet and outlet of the core;

(b) inlet and outlet of the vessel;

(c) inlet and outlet of the U-tube bundle in primary and secondary sides of PWR SGs;

(d) bypass flow paths, mostly inside the vessel;

(e) special components like pumps, steam separators, and valves.

6.3.1.9 Pressure wave propagation

Because the primary system's coolant is subcooled everywhere except in the PRZ, extremely rapid decompression occurs following an almost instantaneous rupture of the primary system piping. The pressure can fall well below the hot-leg saturation pressure (12 MPa), to around 5 MPa. The subsequent motion of decompression waves through the piping and vessels induces severe dynamic loads on their internal structures. The larger the breach, the larger are the instantaneous differences of pressure applied to structures. The decompression waves have a smaller effect for smaller breaches. On the secondary side in the case of a steam line break, pressure waves can propagate and induce dynamic loads on elbows.

Later in the transient in the case of a large amount of steam in the primary or secondary side, the injection of the cold water can cause a condensation shock and a related water hammer, for example, on dead ends or bends.

The BWR vessel has the same features as the secondary side of SGs in PWRs as far as the propagation of pressure waves is concerned. Sudden condensation and evaporation are a consequence of the transit of pressure waves attenuation of the amplitude is strongly affected by the geometry and by the average value of void fraction (including the degree of subcooling) in a given volume.

Core internals have to be designed to withstand these dynamic loads without severe deformation in order to ensure that a coolable geometry is retained during a large breach LOCA. Severe deformation could also prevent the control rods from entering the core. For most plants the control rods are not essential during a LBLOCA in a PWR, because coolant voids and the boron injected with the ECC water will make the reactor subcritical anyway. It is nevertheless good engineering practice and essential for small breaches to ensure that the reactor is scrammed.

Condensation shock and related water hammer can damage pipes and some problems have been experienced on the secondary side for some plants.

Positive pressure propagation causes void collapse in the BWR core and may be the origin of a significant neutron flux excursion. The interaction between neutronics and thermal-hydraulics in the case of instability may also be affected by the propagation of small pressure waves (e.g., initial perturbation).

Furthermore, especially in the case of LBLOCA (steam line or recirculation line break), pressure wave propagation from the break toward the vessel may cause significant loads on internal structures and damage to the systems relevant to safety.

6.3.2 Critical flow

When a flow discharges from a reservoir at higher pressure to a reservoir at lower pressure through a joining pipe, providing the pressure difference is not too large, the rate of flow will be determined by the size of the pressure difference and (inter alia) the wall frictional losses at the pipe walls, entrance, and exit. If the ratio of the upstream to downstream pressure is large enough, however, the flow is found to be independent of the downstream reservoir conditions, and the flow is said to be critical, or choked. In single-phase flow this condition is simply interpreted: the speed of the flow at some point along the flow path, the choke plane, is then equal

to the maximum speed at which pressure disturbances can propagate within the flow. Such a situation is conceptually simpler in the case of flow through a pipe, where the flow is essentially one-dimensional, than for flow through a short constriction such as a break in the side of a pipe, or a valve, where multidimensional effects can be more important (Brittain et al., 1982).

The three cases of breaks, valves, and pipes are treated separately below. For the purposes of discussion the term “pipe” is taken to apply to a constant cross-section duct with a length to diameter ratio (L/D) greater than 5. In practice there will be a gradual change in behavior as the length of a duct with critical flow at exit is increased from $L/D < 1$ to $L/D \gg 1$, and the choice of 5 is rather arbitrary. Length of the flow path affects velocity profile development, the degree of thermal disequilibrium between phases, and the importance of wall friction. Two possible sites for choking in a LBLOCA, in addition to the break itself, are the PRZ surge line and the pump. No specific SETs relating to either of these two cases have been found. The PRZ surge line should in principle be covered by the database for critical flow in pipes. The pump rotor and diffuser have a more complex geometry, and present problems akin to those encountered in valves. In addition the rotor may be spinning or locked.

The CSNI published a State of the Art Report on critical flow modeling in OECD/NEA/CSNI (1982) which covered both critical flow models and experimental data. An extended review of the models is reported in the technical addendum to this report (D'Auria and Vigni, 1980).

6.3.2.1 Critical flow in breaks

When a break occurs in a separating wall structure between a high and low pressure system the flow through the break will be dependent on conditions upstream the break and on the break area and shape. Critical flow through a break is similar to critical flow through a nozzle, but because the geometry of the break can encompass any shape, location, and size from a small crack to a complete 200% guillotine break in a flow pipe, multidimensional effects and losses are important but also difficult to account for accurately.

For a guillotine break in a large pipe the flow will pass across the entire break area cross-section in a rather homogeneous way but for a small break the geometry of the break and the upstream flow pattern close to the break is of great importance. At low flow rates stratification effects upstream of the break are crucial to the flow rate. Under such conditions, the orientation of the break relative to the liquid-vapor interface governs the actual flow rate and this is also likely to change during the

course of drainage through the break. Two-phase flow processes influencing the flow rate through a break in a horizontal pipe include upstream flow regime transitions, liquid entrainment in the break flow, and vapor pull-through.

The critical flow through breaks is a very important element in analyzing plant behavior during the course of the complete spectrum of LOCAs. The break flow determines the depressurization rate of the system and the time to core uncover which in turn are of major concern for when and how different mitigation auxiliary systems will be initiated and function. Because of the empirical nature of critical flow models as well as the arbitrariness in location, orientation, shape, and size of a break, the licensing requirements of a plant include that a spectrum of postulated breaks is analyzed. It is important that in such analyses that the envelope of the influences from the break conditions can be found.

6.3.2.2 Critical flow in valves

Critical flow through a valve is essentially no different from critical flow through a nozzle, but because the geometry of the flow path through a valve is variable, and usually more complicated than a nozzle, multidimensional effects and losses are likely to be more important and more difficult to account for. Several studies have shown that the choking position and the effective minimum area in a valve are not always easy to determine. They may even vary with downstream conditions. There are many different types of valves, and because of the uncertainties inherent in using 1-D models, data from at least a scaled version of the relevant geometry is highly desirable if reasonably accurate critical flow predictions are required.

Critical flow through valves is an important element in many analyses of plant behavior. In safety assessments it is central to the stuck open PRZ valve LOCA, ATWS, LOFW, and accident recovery procedures based on dumping primary side coolant.

6.3.2.3 Critical flow in pipe

In a constant cross-section pipe choking is expected to occur at the pipe exit. In this case the flow rate is still influenced by the entrance losses and wall friction in the pipe since these produce a fall in pressure before the choke point is reached. Thus L/D is an important parameter in determining critical flow from pipes. Pipe length is also important in determining the degree of thermal and mechanical disequilibrium in the critical flow. The experimental evidence suggests that unless the pipe is very short, even in the absence of significant wall friction the phases will approach thermal equilibrium at the choke plane. The relative importance of length, and length to diameter ratio are discussed in Holmes and Allen (1990). It is

also assumed that for critical flow in pipes slip ratios are close to unity.

The subject of critical flow through cracks is closely related to that occurring in pipes, being dominated by friction and the attainment of thermal equilibrium.

A pipe break is a prime mechanism for initiating an LOCA. The pipe involved could be a main coolant pipe, in which case complete severance leads to a LBLOCA, or a pipe connected to the main coolant loop (e.g., an emergency core cooling system (ECCS) line) which could lead to an intermediate or SBLOCA. The flow rate from the pipe is an important factor in determining the course of the resulting transient. The way in which the flow evolves as a function of time can be different for the case of a small broken pipe from that corresponding to a small hole in a large pipe even when the initial break flow is the same in both cases. In many licensing applications the actual flow rate through a break of a given size is not required because what is of interest is the behavior of a plant for a range of break sizes. Exceptions are the determination of the maximum flow from particular types of break (for instance from an instrument penetration in the pressure vessel), and the likely flow from a broken SG tube.

6.3.3 Phase separation/vertical flow with and without mixture level

Flow regimes in two-phase conditions are included under the title “phase separation/vertical flow with and without mixture level”; this comprises the limit case of stagnant or nearly stagnant two-phase mixture when all the liquid is collapsed in the bottom of the vertical component. The consideration of the so-called mixture level is also part of this section.

Three subsections have been distinguished owing to their relevance in nuclear reactor thermal-hydraulics and to the differences in the flow regimes that are a consequence of the geometry and of the boundary conditions (essentially, heat input in the case of the core)

- pipes and plena,
- core,
- downcomer of the vessel.

The first item essentially includes the SG tubes, both primary and secondary sides, and the vertical parts of the PRZ surge line and of the hot and cold legs of PWR main loops. The subitem plena include all the zones of the primary and secondary

sides where the fluid velocities are substantially lower than the neighboring zones. Examples of this are the lower and UP of the vessel (in both BWR and PWR), the steam dome of the SGs, the inlet and outlet chamber of the SG primary side, and the PRZ. Stratified conditions are typical of plena, particularly the lower plenum (LP) of both PWR and BWR, while several slow regimes may occur and are important in vertical pipes and in other types of plena (e.g., SG chambers, see also Section 6.3.7.5).

All flow and HT regimes occur in the core region of BWR under nominal conditions and are expected for PWR during off-normal conditions (second item). The difference between the two kinds of reactor is the possibility of cross flow in PWR that is inhibited in BWR owing to the presence of the fuel boxes.

The third item has been introduced mainly to take account of the complex three-dimensional situations occurring in a PWR vessel downcomer during several kinds of accidents: the ECC bypass/downcomer penetration, specifically considered as item 21 in Table 6.1, is an example of this.

6.3.3.1 Phase separation/vertical flow with and without mixture level—pipes and plena

Steam and liquid phases remaining at rest or flowing cocurrently in vertical channels tend to separate owing to either the gravity force or the inertia forces, both essentially driven by the different density of the two phases. With the phases at rest or moving at very low velocity, gravity dominates and the PH is very simple with the lighter phase stratifying in the upper part of the available volume. Essentially, the only physical aspect to be considered in modeling this situation is the time required to reach a stable condition starting from mechanical nonequilibrium (e.g., liquid in the upper part of a voided system).

The situation is much more complex in a flowing system: various flow configurations may occur as a function of system parameters (e.g., equivalent diameter, flow area, geometric flow path, wall HT, etc.), of the fluid thermodynamic parameters (e.g., pressure, liquid and steam velocities, void fraction, etc.) and of the fluid properties. The well-known flow regime zones are the result of the interaction of the parameters mentioned. The formation of a mixture level is also a consequence of the interaction between the phases in flowing and/or wall-heated two-phase fluid systems. Finally, special flow regimes may occur in the case of strong mechanical and/or thermodynamic nonequilibrium such as in the case of abrupt area change or reflood.

The PH is relevant to nuclear reactor safety because of the significant dependence

of the values of PDs and HT upon the flow regimes. The prediction of flow regime may be important in the case of BWR (nominal conditions) or BWR and PWR (conditions of accidents without scram) in the evaluation of local void fraction, and as a consequence, in predicting neutron flux.

6.3.3.2 Phase separation vertical flow with and without mixture level—core

Phase separation in the core will develop during some phases of an LOCA in PWRs and under normal and off-normal conditions in BWRs. The separation effect is caused by gravity, inertia, or drag dominated forces acting on the phases along with the density difference between the phases.

At low flow velocities and accelerations, gravity will cause the phases to stratify. If the transient is slow enough there may also be time for thermal nonequilibrium to develop. Vapor and droplets can be driven out of the mixture creating a mixture level. This type of separation can be found, for example, toward the end of the blowdown phase of an LOCA. The rate of phase separation will depend on parameters controlling the velocity of rising bubbles in the liquid and the stability of the separated flow interface, such as bubble size, geometry, and different types of drag (form, interfacial, and wall) and pressure gradient. The HT from the fuel cladding to the fluid is highly dependent on the location of the mixture level. Below the level, the HT coefficient can be quite high, resulting in moderate fuel temperatures, whereas the conditions above the level can be the opposite.

At higher flow velocities the vapor-liquid interface will be distributed in the flow creating complex two-phase flow patterns which are dependent on different parameters. Governing system parameters are, for example, core flow area and geometry, possibly spacer vanes characteristics, etc., while fluid thermodynamic parameters are pressure, phase velocities, void fraction, etc. This flow behavior is typical in BWRs at normal and off-normal conditions and in PWRs at LOCA conditions.

Another form of phase separation that can occur in the core is droplet entrainment and de-entrainment. In this case liquid droplets can be entrained from for instance a mixture surface by means of the vapor flow. The liquid droplets carried along in the vapor flow will enhance the downstream cooling of the core.

The phase separation in the core is crucial for the fuel-coolant HT during some phases in LOCAs in both PWRs and BWRs and during normal operation in a BWR. This process determines for instance the quenching of the core during an LOCA and consequently has great impact on the fuel maximum temperature.

6.3.3.3 Phase separation vertical flow with and without mixture level—downcomer

Phase separation with and without mixture level in vertical flow is mainly determined by gravity or inertia forces, both essentially influenced by density of the gas and liquid phases. If the phases are at rest or moving at very low velocity the gravity force dominates and the lighter phase separates in the upper part of the downcomer. One aspect is the time required to obtain a stable condition starting from well-mixed two-phase distribution situations.

In a flowing system the flow regimes are dependent on void fraction and mass fluxes of steam and water and dimensions of the downcomer flow path. The formation of the mixture level is also dependent on the evaporation of water at the hot downcomer walls, if the walls are still at higher temperatures compared with the water during or after blowdown. If the flow is directed from the downcomer to the cold leg(s) the flow conditions in the cold leg are affected (e.g., cold-leg break flow rate, pressure decrease in the system, etc.).

The downcomer collapsed water level is the driving force for core reflood and consequently core cooling conditions. The phase separation in the downcomer influences the water inventory loss during blowdown via a cold-leg break due to its influence on the pressure loss mainly in the broken loop and on the critical flow rate at the break.

6.3.4 Stratified flow in horizontal pipes

At high velocities the flow of a two-phase mixture in a horizontal pipe can be fairly homogeneous. As the velocity falls the gravitational forces tending to cause phase separation across the direction of flow become more important compared with the inertial forces. The ratio of these forces is expressed by the Froude number, a key number in describing stratified flows. The occurrence of stratified flow has a significant effect on a number of two-phase flow processes. Interfacial friction and the interfacial area for HT are much reduced compared to other flow regimes, and in branching flows the occurrence of stratified flow can significantly alter the flow quality within a branch. Stratified flow conditions are a prerequisite for CCF in a horizontal pipe.

Adjacent flow regimes range from bubbly (at low gas flow velocity and low void fraction) through plug flow and slug flow to wavy-annular flow (at high gas velocity and high void fraction). The transition between stratified and nonstratified

flow is often not a sharp one. For instance the boundary between stratified and slug flow can be difficult to define. When the slug frequency is low the flow retains many of the characteristics of purely stratified flow.

The prediction of behavior within the stratified regime requires knowledge of appropriate wall friction, interphase friction, and HT relationships. These are less difficult to determine than for other more complex flow regimes, although these relationships depend on whether the stratified surface is smooth or wavy. However, inhomogeneous effects within the liquid phase, such as thermal stratification, are more noticeable in this low flow regime. The extent to which inlet effects influence the flow regime (when the flow is not fully developed) is still not fully understood.

It should be noted that stratified flow is not confined to horizontal pipes, but can occur in quite steeply inclined pipes.

The main sites for stratified pipe flow are the hot legs, the cold legs, and the loop seals of a PWR. Stratified flow can also occur in auxiliary piping such as feedwater lines. The development of stratified conditions in the hot legs is closely bound up with the transition from NC to refluxing, and the draining of the SG tubes in an LOCA. Its occurrence in the cold legs affects the condensation rates of steam on the ECCS liquid in SBLOCA. Where a break in the primary circuit occurs in a horizontal pipe, the break flow is much more strongly dependent on the orientation of the break once the flow in that pipe has become stratified, when the break flow quality becomes very level dependent. Similar considerations apply to a stuck open PRZ valve during LOCA. Flow stratification was found to occur in LOFT at reduced primary inventory even while the primary pumps were still running.

Thermal stratification within the liquid phase is an important consideration in the determination of thermal stresses associated with ECC injection.

6.3.5 Phase separation at branches

At low velocities, where the flow tends to stratify, phase separation at branches is dominated by gravity effects. In this case the flow through the branch will be liquid rich, if the branch is at the bottom of the pipe and, gas rich, if it is at the top. In general the branch flow quality will be greatly dependent on the liquid level in the main pipe. Liquid entrainment and vapor pull through, which are primarily inertial effects, both exert a powerful influence on this relationship.

At high velocities the effect of inertial forces on branching flow becomes dominant: the heavier phase (liquid) tends to flow in the straight direction, while

the lighter one (steam) is more easily diverted by the low pressure in the side junction of the branch. This causes in most cases a larger void fraction in the side pipe with respect to the value at the branch inlet. The mechanism is multidimensional and is significantly affected by all the geometric peculiarities of the system.

The flow regime also plays an important role in this connection; as an example, in bubbly or slug flow the steam phase can prefer to flow in the side branch as mentioned above, but in annular flow, the liquid on the walls may be diverted more easily to the side branch.

Branching situations can occur in LOCA scenarios at break locations. The prediction of the phase separation at branches is important for evaluating the energy and mass lost from the system. Vapor pull-through and liquid entrainment are examples of phenomena expected.

Other typical branching configurations include the connections of the main piping with the vessel and of the surge line with the hot leg in the PWR.

6.3.6 Entrainment/de-entrainment

Droplet entrainment and de-entrainment are also forms of phase separation and are related to interface friction dependent on the flow regime. Water can, for example, be entrained by sufficiently high steam velocities from the bottom of the reactor vessel and be carried out of the vessel. This water can be lost from the liquid inventory in the pressure vessel.

Compared to phase separation in vertical flow with and without mixture level (Section 6.3.3), entrainment and de-entrainment processes are more related to high void fraction flows including void fraction discontinuities.

The main source of entrainment, in the case of core uncover, is the core, where steam is produced. Another place closely connected to the core is the UP where both entrainment and de-entrainment can occur. These phenomena also take place in the downcomer, mainly in the case of reverse steam flow for LBLOCAs. SG mixing chambers, SG tubes, and the hot legs, in the case of ECCS injection, are also affected by these phenomena.

For a given mass inventory, entrainment and de-entrainment influence the mass distribution in the primary circuit and as a consequence the available mass inventory in the core. So they have consequences on core cooling and are relevant for nuclear safety.

The important parameters related to entrainment and de-entrainment to be measured are the droplet sizes and distribution, the interfacial area, the field of velocities. Only limited global measurements are available based mainly on DP measurements. Catch tanks are also used, and carryover tanks are available.

The present state of knowledge is limited to allow a detailed description of these phenomena. Only global correlations are available. The geometry of internals and geometric discontinuities also play an important role in relation to this PH. This limits the degree of extrapolation of particular models.

6.3.6.1 Entrainment/de-entrainment in the core

Droplet entrainment and de-entrainment are forms of phase separation. Water can, for example, be entrained by sufficiently high steam velocities from the bottom of the reactor vessel and be carried out of the vessel. Thus water can be lost from the liquid inventory in the vessel. Droplets carried out of the reactor core by rising steam during reflooding can be de-entrained by impinging on the various structures situated in the UP and, consequently, may fall back into the core.

Entrainment of liquid droplets by the flow of steam has considerable influence on the effectiveness of emergency core cooling. The importance of the entrainment has been especially recognized associated with heat and mass transfer processes during LOCAs, in particular, during the recovery phase of these accidents through reflooding of a core. In this case entrainment improves HT, since droplets act as a heat sink through droplet evaporation. This will lead to lower vapor superheat and improved cooling of fuel rods. Indeed, the hot portion of the fuel rods in the core is cooled by the mixture of steam and entrained droplets. Liquid entrainment affects the liquid core inventory and is also important in the determination of the CHF location. Another indirect effect of the entrainment is that the vaporization of the droplets carried to SGs pressurizes the UP and prevents the core water level from rising (i.e., steam binding effect). Liquid de-entrainment occurs when water entrained in the steam generated in the core is removed from the steam flow at other places in the core, UP, or beyond. De-entrainment occurs from gravitational and inertial forces. It is enhanced when flow slows down because of a flow area increase or when it changes direction to pass around flow obstructions or structures or to turn out through a nozzle. De-entrainment removes entrained water from the two-phase flow mixture. De-entrained water that accumulates in the core and UP provides a source of water for core cooling supplementing the cooling by bottom reflood. This enhances core cooling near fuel assembly grid spacers and is also important for the upper regions of the core. Clearly, such entrainment and de-entrainment phenomena are controlled by interfacial shear. Correct modeling of the

interfacial shear force is crucial for the adequate prediction of a number of phenomena and interfacial shear models also vary according to the flow regimes.

The importance of the entrainment and de-entrainment in a core has been recognized associated with heat and mass transfer processes during LOCAs, in particular, during the recovery phase of these accidents through reflooding of a core and also under boil-off situations. Since these phenomena will lead to improved cooling of the fuel rods, the knowledge of the extent of entrainment and de-entrainment is necessary to predict the hydrodynamic and thermal response in the core.

6.3.6.2 Entrainment/de-entrainment in the UP

These phenomena are very much related to the entrainment and de-entrainment in the core (Section 6.3.6.1). Some of the carryover out of the core will be captured in the water pool, which may form on the upper core support plate, and by UP structures. Pool formation refers to the collection of water in the UP during reflood. The source of this water is entrained water carried up from the core which is then de-entrained in the UP. The UP contains a great deal of internal structures that act as a steam separator to de-entrain liquid in the two-phase flow. In addition, the drop in flow velocities from the core to the UP allows gravitational separation of liquid from steam. The flow behavior of a collected pool may be highly three-dimensional because of the tendency of the water pool to collect in low flow areas and in regions near walls and structures. UP pool formation is important to ECCS performance during an LOCA. The reasons can be summarized as: the pool, particularly due to its multidimensional nature, provides a source of additional cooling water for the core; de-entrainment and pool formation reduce carryover to the SG; the pool can reduce the flooding rate by creating a static head PD in the UP.

The extent of liquid carryover to the UP is expressed by the liquid carryover rate fraction, that is, the ratio of total liquid mass flow rate out of the core to the liquid mass entering the core. Liquid carryover reduces the rate of accumulation of water within the core and provides a source of water for de-entrainment in the UP or beyond. Carryover has a major effect, because the rate of advance of the quench front (QF) is tied directly to the increase in core mass inventory, and is therefore highly relevant to reactor safety.

6.3.6.3 Entrainment/de-entrainment in the downcomer

In a large cold-leg break LOCA, the beginning of the “reflood” phase occurs when the reactor vessel water level reaches the bottom of the core. This creates a seal

between the core and the downcomer, and further ECC water injection tends to fill the downcomer to near the cold-leg elevation. The difference in water level between the downcomer and the core provides the driving head for core flooding. This driving head also creates a pressure difference from the top of the core to the top of the downcomer which tends to cause core steam generation to flow out of the core and through the loops to the downcomer. In combined injection PWRs, essentially all of the steam flow is condensed by hot-leg and/or cold-leg ECC water and there is no steam flow into the downcomer. In cold-leg injection or downcomer injection PWRs, steam flows to the downcomer via intact loops or vent valves. Some of the steam is condensed by ECC injected in the cold legs or in the downcomer. Any steam not condensed, along with steam generated in the downcomer due to superheated walls, flows circumferentially around the downcomer and out of the broken cold leg, potentially entraining and carrying away a portion of the ECC water (Damerell and Simons, 1993b). Some de-entrainment may occur due to higher inertia of the water droplets compared with the steam phase where the flow changes its direction from the downcomer to the broken leg.

The PH is mainly important if a large cold-leg break occurs and the ECC water is injected only at the cold side of the reactor (into the cold legs or into the downcomer). The circumferential flow of steam around the downcomer and the generation of steam on superheated downcomer walls tend to entrain ECC in the downcomer region. The interaction of steam flow, wall boiling, and ECC entrainment is important since it affects the water level in the downcomer. Reduction of the downcomer liquid level below the level (which is at the bottom of the cold-leg nozzles) reduces the available driving head and tends to reduce the core flooding rate. This prolongs quench times and potentially allows higher clad temperatures in the core.

The PH is not important if subcooled ECC water is injected at the hot side of the reactor vessel and condenses a considerable steam flow from the core to the hot legs. The PH is not important for intermediate and small breaks (rupture area less than 25% of maximum pipe area connected with the pressure vessel) since the circumferential steam flow in the downcomer is not high enough to cause a significant entrainment.

6.3.6.4 Entrainment/de-entrainment in SG tubes

In the case of high steam flow rate droplets can be entrained into the SG tubes, from the mixing chambers. In the case where the SG is a heat source (such as a large break accident) the droplets may vaporize creating additional steam binding.

This entrainment process is strongly connected with the behavior of fluid in the mixing chambers.

This PH contributes to the so-called steam binding for LBLOCAs.

For a smaller break size, entrainment contributes to reducing the two-phase NC, to producing reverse flow in some SG tubes and to reducing mass inventory in the core.

6.3.6.5 Entrainment/de-entrainment in SG mixing chambers

Mixing chambers, by reducing the steam velocity, have a large impact on the phase separation process and can reduce droplet entrainment in SG tubes. But when a mixture level appears within a mixing chamber a sufficiently high steam flow can also generate droplets with consequences for fluid behavior in the SG tubes (see Section 6.3.6.4).

As in Section 6.3.6.4, this PH contributes to steam binding for large break and to flow distribution in U-tubes (3-D effects) for smaller sizes of break and NC conditions. It also influences the mass distribution in the primary circuit.

6.3.6.6 Entrainment/de-entrainment in the hot leg with ECC injection (PWR)

A pressure difference exists from the UP to the downcomer through the loops, if a large break occurs at the cold-leg side of one of the primary coolant loops, or if condensation occurs in the SG primary side in a small-break scenario. The pressure difference causes a steam flow from the UP to the SGs. ECC water injected into the hot legs via a special nozzle (Hütze in KWU PWR) at the bottom of the hot legs, for instance, may be entrained toward the SG by sufficiently high steam velocities. The entrained water may reach the SG tubes where it may evaporate in the large break case. The evaporated water is no longer available for core cooling. On the other hand, the pressure in the SG primary side increases due to the evaporation, reducing the steam velocity toward the SG, or even causing a steam flow from the SG to the UP. Consequently, the total ECC water injected into the hot legs will be delivered into the UP for a certain time span, causing an oscillatory flow in the hot legs.

In the case of condensation in the SG the condensed water flows back toward the UP. Due to the decreasing steam flow in the SG the entrained water also flows back to the hot leg toward the UP.

Since the hot-leg ECC injection water is subcooled (injection temperature 30–35°C) the condensation may cause a water plug to form in the hot legs where ECC water is injected. The plug formation is dependent on the steam flow rate in the hot leg and condensation potential of the ECC water. The hot-leg ECC injection entrainment behavior is mainly determined by condensation (see Section 6.3.7.6). An oscillatory plug flow establishes itself or a stable stratified flow occurs depending on these parameters. The whole process is closely connected with CCFL including condensation and momentum effects of the ECC water injection.

The amount of ECC water injected into the hot legs (i.e., via the special nozzles at the bottom of the hot legs in some reactors) reaching the core is important for emergency core cooling effectiveness. The water entrained in the steam flow is lost for core cooling at first. The pressure increase due to evaporation of entrained water in the SG may support the ECC water delivery subsequently, resulting in an oscillating ECC water delivery to the UP. SCTF test results show that core quench in a LBLOCA is delayed by approximately 15 s, if ECC water is injected into the UP intermittently instead of continuously.

6.3.7 Liquid-vapor mixing with condensation

Direct contact condensation of steam on cold water is a very efficient heat removal mechanism which often takes place at very rapid heat and mass transfer rates. Violent pressure oscillations due to the rapid condensation of steam and the resulting volume reductions have been observed in several situations when a subcooled liquid is brought into intimate contact with steam. For example, such oscillations can take place at the ECC injection points. The mixing of liquid and vapor has an effect on the magnitude of the interfacial area and consequently, in conjunction with temperature differences between steam and water, it determines the condensation efficiency. The mixing is mainly influenced by the void fraction and the mass fluxes of steam and water as well as steam and water temperatures and other properties.

Condensation processes are relevant to reactor safety in that they

- reduce the reactor primary side pressure below the set points for low pressure ECCSs by SG secondary side heat removal and high pressure ECCS injection,
- reduce steam flows which otherwise reduce water delivery to the core due to CCFL, as shown by experiments in UPTF (Damerell and Simons, 1993a,b; Riegel, 1990a,b); however, a higher steam upflow to the condensation location preventing water delivery has occurred in small-scale facilities like LOBI,

- reduce pressure in the UP region (by means of hot-leg ECC injection) to support a faster reflood of the core.

Condensation may be reduced if noncondensable gases, for example, nitrogen from the accumulators, are present, see **Section 6.3.25**.

The measurement of condensed steam is mainly performed by measurements of mass flow, water inventories, temperatures, pressures, void fractions (gamma-densitometer, pressure difference). The interfacial area has not yet been measured successfully.

Computer code models describe mixing and condensation in the way that interphase heat and mass transfer rates are empirically correlated to the flow regimes which are assumed to occur (Forge et al., 1988). An interfacial area then needs to be specified, which is difficult for all flows except for well defined, gravity-separated flow conditions (see **Section 6.3.8**). The flow map is not used explicitly in every computer code, but implicitly in the transfer laws. It is not clear, if these flow regime maps are scale independent (Lewis et al., 1989; Yadigaroglu et al., 1990).

Interfacial heat and mass transfer laws and the resulting condensation models are mainly determined by the interfacial area models that the computer codes use (Fletcher and Schultz, 1992). In the three-dimensional, highly unsteady two-phase flow situation, interfacial area and surface temperature can change rapidly. Two fluid codes employ an average interfacial area over a chosen numerical cell size which, in practice, is orders of magnitude larger than the characteristic turbulent mixing dimensions or the molecular transfer dimensions of the flow in or perpendicular to the main flow directions (e.g., turbulent mixing length or thermal boundary layer thickness). Thus predictions of mixing and condensation are often dependent on the discretization chosen for a problem (Yadigaroglu et al., 1990; Forge et al., 1988; OECD/NEA, 1989). The stability of the calculations is particularly sensitive to pressure spikes from artificial water packing.

Liquid-vapor mixing with condensation is of special interest in the core, downcomer, UP, LP, SG mixture chamber (PWR) and in the ECC water injection regions in the hot and cold legs (PWR) (Hafner and Fischer, 1990). The differences in geometry and boundary conditions cause differences in the flow regimes of the different locations. Spray cooling effects for BWRs are covered by **Section 6.3.9.1**.

6.3.7.1 Liquid-vapor mixing with condensation—core

Liquid-vapor mixing in the core occurs during ECC water injection in order to prevent overheating of the core. Subcooled ECC water may enter the core from the cold injection location via the downcomer and LP or from the hot-leg injection location via the UP down to the core.

Condensation on subcooled water entering the core removes a part of the heat in the core. Local reduction of steam flow and consequently higher water delivery under CCF conditions may occur due to condensation in the core. Fast water delivery to the core is essential for emergency core cooling. The PH is relevant for plant with combined injection, UP or upper head injection.

6.3.7.2 Liquid-vapor mixing with condensation—downcomer

Subcooled ECC water is injected into the cold legs or into the downcomer directly depending on reactor design. The injected water flows down the downcomer, and, on its way down, the water is warmed up mainly due to steam condensing on the water interface.

Direct contact condensation on the ECC water which is injected into the cold legs or directly into the downcomer has an influence on the CCF in the downcomer region. The upward flowing steam is reduced by the condensation rate. Consequently, the water downflow rate toward the core can increase. The condensation rate again is dependent on the downward water mass flow rate. The main water downflow was observed in UPTF tests below the cold legs which are farthest from the broken cold leg. In small-scale facilities like LOBI, however, an opposite effect was observed. Condensation at the accumulator ECC water injection location caused a high steam upflow in the downcomer which prevented water downflow for some time.

Condensation in the cold legs and in the downcomer is ranked as very important for LBLOCA refill in a four-loop PWR (Wilson et al., 1990).

Steam condensation causes a warm-up of the subcooled ECC water which may reduce pressurized thermal shock (PTS) in the reactor vessel wall, in the case of high pressure ECC water injection.

6.3.7.3 Liquid-vapor mixing with condensation—UP

Liquid-vapor mixing with condensation is important in the case of UP and hot-leg ECC injection in PWRs and in BWRs. It is highly dependent on the injection device, for example, whether injection is via spray systems or nozzles in the UP or hot leg.

Condensation in the UP may decrease the steam binding effect substantially and consequently may allow faster reflood of the core.

Direct contact condensation on the ECC water in the UP has an influence on the CCF in the UP and especially in the upper tie plate (UTP) region at the top of the core. The upward flowing steam is reduced by the condensation rate. Consequently, the water downflow rate into the core can increase. The condensation rate is dependent on downward water mass flow rate.

6.3.7.4 Liquid-vapor mixing with condensation—LP

At the end of the blowdown period of a LBLOCA, the depressurization of the reactor coolant system (RCS) allows the ECCS to inject subcooled water into the system. When this cold water comes into intimate contact with the superheated steam or saturated two-phase mixture intense condensation occurs with associated pressure oscillations. The ECCS water will penetrate the downcomer as described in Section 6.3.7.2 and reach the LP of the vessel. At this instant the refill period starts. Refill will be terminated when the LP water level reaches the bottom end of the core. Some water could remain in the LP after the blowdown and the amount of water has a high impact on the fuel cladding temperature. Evaporation and the entrainment of liquid droplets, which to some extent pass through the core, limit the fuel cladding temperature. Also some subcooled water could enter the LP from leakage in the control rod drives (BWR) and contribute to the water contents of the plenum.

When the ECCS water reaches the LP, the water will partly be evaporated on the superheated mechanical structures but will also contribute to the condensation of the existing saturated or superheated vapor in a complicated manner. The ECCS water has a strongly three-dimensional random distribution when it enters the LP because of the CCF in the downcomer. This will become even more pronounced in the LP because of the complex evaporation on irregular shaped and distributed structures and the simultaneous condensation of existing vapor.

Direct-contact condensation often takes place at very rapid heat and mass transfer rates. Thus the condensation of vapor can lead to the occurrence of violent pressure fluctuations.

Liquid-vapor mixing in the LP is an important PH, as it influences the fuel temperature through related entrainment and vaporization processes. The entrained liquid and vapor will partly pass through the core and enhance the core HT, and the final cooling of the core.

6.3.7.5 Liquid-vapor mixing with condensation—SG mixing chambers (inlet/outlet plenum)

The SG mixing chambers connect the RCS piping with the SG tube bundle. Because of the geometrical shape of these chambers high turbulence and effective mixing can be expected even at rather low flow conditions. Thus the inlet conditions to the tube bundle can in most cases be assumed fairly uniform across the tube bundle flow area.

However, during the course of SBLOCAs, situations occur when the NC in the loops can no longer be sustained because of the liquid inventory being insufficient to allow flow over the top of the U tubes. Complete phase separation occurs and at further loss of liquid inventory CCF develops in the hot legs. Thus saturated or slightly superheated vapor flows from the core through the hot leg into the SG mixing chamber and up into the tube bundle. If the secondary side of the SG has a temperature lower than the saturation temperature of the primary side, condensation of vapor in the tubes will be initiated. The condensate will fall back down the tubes due to gravity and CCF will be prevailing in those parts of the U tubes. The liquid will enter the mixing chamber in which stratification occurs. Some condensation of the vapor in the chamber can be expected. The liquid flows “over the edge” of the SG nozzle into the hot leg and back to the core where it evaporates. The process is known as reflux condensation and can contribute significantly to the cooling of the core.

The condensation in the SG tubes is not likely to be uniform and is also oscillatory in nature because of the behavior of the condensation process. As a result the condensate flow into the mixing chamber will be quite nonuniform and this along with the stratification will create multidimensional effects that will have some influence on, for instance, the reflux condensation process. Also it is quite possible that the conditions in each SG can be different, which may contribute to asymmetric behavior of the loops.

At low flow or almost stagnant conditions the liquid-vapor mixing in the SG mixing chambers will have some influence on the SG efficiency as a heat sink. In the reflux condensation mode, the detailed processes in the SG tubes will be governed by for instance the multidimensional conditions in the mixing chamber. However, the exact details of the conditions in the mixing chamber seem to be of second order importance in most situations because the large HT area of the SGs (sized to remove full power) is more than adequate for decay heat removal. Exceptions can occur when HT efficiency in the SGs is greatly reduced by the presence of noncondensables or by dryout of the secondary side.

6.3.7.6 ECC injection in hot and cold leg

Depending on the ratio of steam flow rate in the cold or hot leg to the condensation potential of the ECC water, a stratified flow pattern or a water plug will be established in these legs. Conditions favoring plugging are most likely to be found in a LBLOCA scenario. While the mechanisms of plug onset are the same during condensation and adiabatic flows, an additional mechanism takes place during condensation due to the local decrease in pressure in the pipe as a result of volume reduction of the steam. Plug formation causes an intermittent water delivery to the downcomer or the UP, respectively. Plug formation delays the water delivery to the core region.

Those water plugs which are formed in the hot legs (in spite of the nozzle momentum toward the UP) enter the SG tubes and steam is generated. The increased pressure in the SG pushes the plug toward the UP. A new plug is formed after the old plug is delivered to the UP such that an intermittent water delivery to the UP, and subsequently into the core, occurs.

The temperature of the plug end faces in the cold legs increases up to saturation temperature due to steam condensation. Consequently, the condensation decreases and the plug is delivered to the downcomer. A new plug is formed after delivery of the old one. This process causes an intermittent water delivery to the downcomer.

ECC water delivery from the hot- and cold-leg injection locations toward the core is essential for effective performance of the ECCS. Small delays in ECC water delivery are produced due to plug formation in the legs.

6.3.8 Condensation in stratified conditions

When the flow is stratified with subcooled liquid, experiments have shown that due to liquid temperature stratification, the condensation rate is relatively low because the liquid *interface* is close to the saturation temperature of steam.

Condensation in stratified conditions plays an important role in the behavior of the PRZ (Section 6.3.8.1), the SG primary side (Section 6.3.8.2), and the SG secondary side (Section 6.3.8.3). In these components a so-called piston effect can occur, that is, an increase of pressure, sometimes limited by safety valves, following cold water injection. In horizontal pipes condensation in stratified conditions can occur during emergency cooling water injection and can cause water hammer (Section 6.3.1.9).

Condensation in stratified conditions governs the pressure behavior during

recovery procedures and the mass distribution in the circuits, and so is relevant to nuclear safety.

The important parameters are the vertical temperature profile, local heat and mass transfer, local liquid and steam velocities, and void fraction. Often only P and DP measurements, and limited temperature measurements, are available—densitometer measurements are sometimes available in pipes. The database is generally poor.

This PH is not well predicted by codes mainly due to 1-D assumptions (1 liquid temperature). Codes generally predict too large a condensation rate.

Generally, a fine mesh nodding can improve code calculation results for vertical components because that gives a better simulation of the water temperature profile. Justified user guidelines are strongly recommended.

6.3.8.1 Condensation in stratified conditions—PRZ (PWR)

During recovery procedures the safety injection system refills the primary side. When the water enters the surge line, and then the PRZ, condensation occurs. But with stratified conditions in the PRZ heat and mass transfer are limited. The so-called piston effect can occur and the pressure increases, which induces some condensation.

Condensation in stratified conditions governs the pressure behavior at the end of recovery procedures, and can make it difficult to reach the set point for the normal residual heat removal system.

6.3.8.2 Condensation in stratified conditions—SG primary side

During the course of an accident, in the case of refilling of the primary side with stopped pumps the water level there rises into the SG primary side. Steam is compressed by subcooled water and condensation occurs. But the PH is complicated by axial heat conduction in the large number of tubes and depends on the secondary side conditions. This can be complicated by the presence of noncondensable gas (Section 6.3.25). In these conditions NC is difficult to reestablish.

This PH is related to the pressure behavior of the primary side during recovery procedures after an accident. The pressure influences the injected water flow rate, so there is a feedback in influence on the condensation. Finally the total amount of injected water is dependent on condensation.

6.3.8.3 Condensation in stratified conditions—SG secondary side

In the case of stratification in the SG secondary side, different behavior can be expected depending on the water level, the recirculation flow, and the geometry. This problem is encountered in the particular case of a steam generator tube rupture (SGTR) where the intact SGs are used to cool down the primary side. After a certain time the riser becomes cooler than the downcomer and the recirculation can reverse.

If the upper recirculation flow path is close to the water level, significant condensation occurs. If this flow path is below the water level the condensation is strongly reduced and the so-called piston effect becomes important.

This PH governs the pressure behavior in the SG in the case of SGTR so it has significant effects on the amount of primary fluid flowing to the secondary side and also to fission product release by the SG safety relief valves. (Fission product transport and distribution themselves are not considered in this writing.)

6.3.8.4 Condensation in stratified conditions—horizontal pipe

The typical case is associated with HPIS flow in the cold leg during a SBLOCA. For example, in the ISP18 test in LOBI a large temperature difference (100 K) was observed in a 50 mm cold-leg pipe over a period of at least 1000 s.

This behavior (stable build-up of a large steam/liquid temperature difference) is due to liquid temperature stratification. The liquid interface reaches saturation temperature and the condensation rate becomes lower.

The mass distribution in the primary circuit depends on the condensation PH in connection with bypass flows. The pressure behavior is also governed by condensation.

6.3.9 Spray effects

The phenomena that occur when a more or less subcooled liquid is sprayed into a zone containing superheated steam or two-phase mixture (usually at high void fraction), are considered in this section.

Three subitems have been distinguished essentially to emphasize the influence that the geometry of the system may have upon the evolution of the phenomena:

- core in the case of a BWR,
- PRZ in the case of a PWR,
- secondary side in the case of once-through steam generators (OTSGs).

Spraying of liquid in the UP zone of BWR is essential to quench core rods from the top in the case of inadequate effectiveness of the low pressure injection system. Flooding situations typically occur at the top of the fuel elements and obstruct the downward liquid flow. The distance of the sprayers from the core upper plate, the subcooling of the sprayed liquid and the distribution of droplet diameters, are parameters affecting the PH.

Spray in the upper part of PRZ (steam zone) is used to control the pressure during nominal conditions and minor transients in PWR plants. The liquid is directed from the cold leg downstream of the main circulation pumps and arrives at the PRZ top with a subcooling of about 60 K. The sprayed droplets may interact with the PRZ walls and decrease the stored heat of the structures. Spraying of liquid in the PRZ may prevent the so-called piston effect.

Injection of a liquid spray into the secondary side of a voided OTSG occurs as a consequence of auxiliary feedwater intervention. The effects of this are essentially two: firstly, there is direct HT to the superheated steam (decrease of stored heat and condensation), or to the saturated steam (condensation). Secondly there is direct HT with primary side. In this last case the HT depends upon the geometric configuration of the SG tubes and the thermal-hydraulic conditions of primary side fluid.

6.3.9.1 Spray effects—core

The ECCS of a BWR is designed to spray liquid into the steam filled UP region of a BWR, downstream of the core. The low pressure core spray (LPCS) starts to inject water when the pressure reaches values below about 2 MPa. In BWR-6-type reactors a high pressure system (high pressure core spray, HPCS) working in a similar way to the LPCS is also installed. The injection set point pressure is higher than the nominal pressure of the reactor.

The spray of the liquid into the UP creates condensation of steam and, owing to flooding, a liquid level may form on the top of the upper core plate. Three-dimensional phenomena occur and make possible the breakdown of CCFL in some bundles, leading to liquid falling down to the LP. This can facilitate the bottom up quench of the fuel bundles.

In the case of liquid formation in the UP, the liquid level may reach the elevation of the spray nozzles that are located a few tens of centimeters above the top of the core. At this time the liquid mass may soon become subcooled making more effective the condensation of the steam coming from the core. The final result is the CCFL-break down and the penetration of the liquid into the core.

At a basic level, the heating of the sprayed droplets and the consequent condensation of steam, constitute the main PH occurring in the case of spray. The size of the droplets (distribution of diameter), the spray angle, and the degree of subcooling are the main parameters affecting the PH apart from the total sprayed flow rate. The distance between the spray nozzles and the upper core plate and the interaction among the various jets, can also play a role in the evolution of the PH.

The actuation of spray systems (especially of the LPCS) is required in the case of major accidents for the plant such as LBLOCA or SBLOCA. The ability to maintain the system within safety limits closely depend upon the capability of the LPCS or HPCS to quench the core.

6.3.9.2 Spray effects in the PRZ

Liquid spray into the top of the PRZ is used to control the PRZ pressure by reducing it. (Pressure increase can be obtained by heaters.) Spray water is taken from the cold leg downstream of the main circulation pump, so the subcooling in normal operating condition is about 50 K. In most of the reactors, a small flow (of the order of 1 kg/s) flows continuously through the line connecting the cold leg with the PRZ, in order to prevent thermal shock problems in the case of sudden operation.

In the case of undesired PRZ pressure increase, the spray valve is open to control the pressure. Two main phenomena occur:

- (a) direct condensation between spray droplets and steam,
- (b) heating of the sprayed droplets due to direct HT from the PRZ wall.

Both the above effects contribute to lowering the pressure. The size of the droplets and the spray angle are the main parameters affecting the PH (droplet temperature is fixed and droplet velocity and PRZ pressure can also play a role). The amount of space occupied by steam, including the distance between the spray nozzle and the actual PRZ level are also important.

Finally, in some cases a shield is installed inside the PRZ to protect the PRZ wall

from thermal shock.

Actuation of the PRZ spray system will occur during the normal operation of the plant. In the case of off-normal transients like steam line closure, turbine trip, LOFW, etc., opening of the valve may occur but, usually, the delivered flow rate is not sufficient to stop the pressure increase (opening of the PRZ relief valve is necessary).

Considering the above the spray effect in the PRZ cannot be considered highly relevant from a safety point of view. This consideration obviously does not exclude the possibility that spurious actuation of the spray valve may be the origin of a more complex transient for the plant.

6.3.9.3 Spray effects in OTSG secondary sides (PWR)

Auxiliary feedwater is injected into the SG secondary side via a spray system. The water is heated up and evaporated by the hot water on the primary side flowing through the SG tubes.

The feedwater inlet into the OTSG secondary side downcomer of US OTSG PWRs is performed via a ring-pipe with holes. No spray system is designed for feedwater inlet into the German OTSG plant. A simple pipe connection to the OTSG secondary side downcomer is installed. The German OTSG auxiliary feedwater inlet is constructed as a ring with holes to inject radially directly into the secondary side. The US OTSG auxiliary feedwater is injected radially by a nozzle directly into the secondary side. The US OTSG nozzle is located close to the top of the secondary side whereas the German OTSG plant, auxiliary feedwater ring is located close to the bottom. The primary side water flow in normal operation is downward within the SG tubes. A design goal of the auxiliary feedwater spray system is to prevent thermal stress as much as possible. The spray effect is not considered highly relevant from a safety point of view but it may determine the number of SG tubes wetted by the auxiliary feedwater.

6.3.10 Countercurrent flow/countercurrent flow limitation

At high flow rates the gas and liquid phases in a two-phase flow move down the pressure gradient in the same direction. At lower flow rates, however, the existence of a gravitational field can result in the significantly different velocities for the two phases, and it is possible for liquid to flow downward while the lighter gas phase flows upward. This is CCF, and it can occur in vertical pipes and inclined pipes, and in horizontal pipes in stratified flow (Bankoff and Lee, 1985, 1986).

There is a limit on the rate at which liquid can flow down for a given gas upflow, which is known as the CCF limit. The term “flooding” is sometimes used to mean the CCF limit, but it can also be used for the special case of zero liquid phase penetration down the duct. In this document the former interpretation is used.

If the liquid flow rate is held constant, while the gas upflow is slowly increased, the onset of flooding often occurs abruptly, accompanied by a change of the flow regime from a relatively separated flow, to a chum flow pattern.

Flooding is a local PH, and often takes place at the entrance or exit of a piping section. The flooding characteristics are thus fairly sensitive to the local geometry. Flooding in some geometries, such as the hot leg/SG inlet plenum, has been found to display significant hysteresis with respect to gas flow rate.

CCFL is also of importance in calculating flow behavior at a perforated plate (such as the UTP). Here the question is how fast can water, which may have formed a pool on top of the plate, drain through (some of) the perforations against a given steam flow from below the plate. This is more like flow through a set of parallel tubes than CCFL in a single tube, and is likely to be quite asymmetric in character.

If the liquid phase is subcooled then condensation will reduce the volumetric flow of steam as the steam proceeds along the duct. This can modify the flooding behavior appreciably.

In the following discussion CCFL associated with specific regions within an LWR are described. These are

- upper tie plate (UTP),
- channel inlet orifices (BWR),
- hot and cold leg,
- SG tube (PWR),
- downcomer,
- surge line (PWR).

6.3.10.1 CCF/CCFL at the UTP

CCF of steam and water through the UTP is a multidimensional PH. It can occur

due to water being de-entrained in the UP flowing back to the core region, or because ECC water is injected into the UP or into the hot legs.

CCFs of steam (or steam/water mixtures) and water play an important role regarding the distribution of coolant in the primary system both in PWRs and BWRs. In CCF a limiting condition appears first when the downward flow of liquid is influenced by the upward flow of vapor. Any increase of vapor flux then leads to a reduction in the liquid counterflow until, eventually, this becomes zero and the incoming liquid may be carried upward with the gas flow. CCFL tends to occur at flow cross-section restrictions, like the tie plate, where the gas velocity is a maximum (Siebe and Stumpf, 1990).

Many CCFL data have been obtained with air and water. For steam/water the CCFL situation may be different due to steam condensation on subcooled ECC water resulting in a reduced steam upflow rate. Steam condensation reduces the vapor flux, allowing a greater liquid flux which in turn increases condensation. This process may lead to a complete water “break-through.”

If the up flow consists of a two-phase gas/droplet flow at the CCFL location the momentum of the entrained droplets opposes the liquid downflow leading to more limitation of the liquid downflow rate.

In some PWR designs the ECC injection location is not only on the cold side of the primary system but also on the hot side. The injection locations are, for example:

- into the hot legs via a special “Hütze” nozzle at the bottom of the hot legs directed toward the UP, and into the cold legs,
- into the UP via two injection nozzles (low pressure coolant injection system), and into the cold legs (high pressure coolant injection system and accumulators).

Either de-entrained water from the UP, or ECC water injected into the hot legs and into the UP, has to flow down through the UTP countercurrently to steam generated within the reactor core or to steam generated by evaporation due to depressurization or to steam expansion due to depressurization. The steam flows toward the broken loop hot leg. The injected water is needed in the core region to prevent overheating. The limited water delivery into the core can delay the core reflood. UTP CCFL has a high ranking of importance for UP or hot-leg ECC injection during LBLOCA refill and reflood phases.

6.3.10.2 CCF/CCFL at channel inlet orifices (BWR)

Fuel rod bundles of BWRs are equipped with side-inlet orifices at the bottom. These side orifices have different flow cross-sections in order to control the radial power profile of the core during normal reactor operation. CCFL can occur in the side-inlet orifices under accident conditions. Water evaporation in the LP causes a steam upflow (see Section 6.3.14) which can limit the draining of the fuel rod bundles (Sun, 1979).

BWR core bundles form parallel channels with different heating powers, and in accident situations there would be nonuniform liquid hold up and steam flow distribution among the bundles.

The first limiting condition appears in a CCF situation when the downward flow of liquid in the channels is influenced by the upward flow of vapor. Any increase of vapor flux then leads to a reduction in the liquid counterflow until, eventually, this becomes zero. CCFL tends to occur at flow cross-section restrictions like the channel side-inlet orifices, where the gas velocity is a maximum. Marked differences in the behavior of individual channels can be expected.

Limiting draining of the fuel rod channels due to CCFL in the side-inlet orifices at the bottom of the fuel channels is important for cooling of the fuel rods during blowdown, refill, reflood, and spray periods.

6.3.10.3 CCF/CCFL in the hot and cold legs

Under certain circumstances the high and low density phases of a two-phase mixture can flow in opposite directions within a pipe. The driving force for such flows is gravity. For CCF to occur in a horizontal pipe the flow must be stratified, and the driving force corresponds to changes of liquid level along the pipe. For a given liquid depth at the pipe inlet, increasing the countercurrent gas velocity will tend to reduce the liquid flow rate. Complete CCFL, often known as “flooding,” when the liquid phase can no longer flow against the gas, will occur when the stratified flow regime breaks down. A typical mechanism for this to occur is for waves on the liquid surface to develop to the extent of bridging the pipe and producing slug flow, but other mechanisms are possible. CCFL behavior can be substantially modified when significant subcooling is present in the liquid phase, since condensation of the steam phase changes the steam flow along the pipe (Macken, 1990).

In inclined pipes the driving force for CCF is larger than in horizontal pipes when the liquid is in downflow. An inclined pipe of significant length is, however, unable to sustain liquid upflow, and at a transition from the horizontal to an

upwardly inclined direction churn flow can develop.

CCFL in the hot legs is associated with behavior in the inclined pipe sections leading to the SGs. CCFL in this part of the circuit could affect the rate of liquid drain back from the SG tubes to the core in a small LOCA. This in turn would affect the depth to which the core became uncovered. Furthermore, in order for reflux condensing to occur, it is necessary that the steam flow produced by core decay heat and flashing in the vessel is less than that required to cause flooding in the hot legs. CCFL is also of interest in the case of injection of ECCS into the hot legs, where in order for the injected water to flow directly to the vessel it must flow against steam exiting the vessel.

CCFL may also occur in the horizontal part of the cold legs and is effectively involved in the PH of loop seal clearing, in the intermediate leg.

6.3.10.4 CCF/CCFL in SG tubes

CCFL can occur within the vertical tubes of the SG at the tube plate. As the hot legs and SG inlet plena empty during a SBLOCA, liquid can be held up within the SG tubes by steam produced within the reactor vessel which is flowing into the SGs. If the direction of heat flow is from primary to secondary some of this steam is condensed within the tubes. CCFL in SG U tubes is characterized by nonuniform parallel channel behavior, that is, nonuniform liquid hold up and steam flow rate. Some of the tubes may be flooded, while others are cleared (D'Auria and Galassi, 1990).

CCFL at the inlet to the SG tubes will affect the rate of liquid drain back from the SG tubes to the core in a small LOCA. This in turn affects the depth to which the core uncovers. Significant drain back occurs when NC is terminated by the build-up of steam in the down side of the SG tubes. Furthermore, it is necessary that the steam flow produced by core decay heat and flashing in the vessel is less than that required to cause flooding at the tube plate to prevent a build-up of liquid in the SG tube upsides later on in an LOCA, if reflux cooling is to be sustained. The build-up of liquid would again have the effect of depressing the core mixture level.

CCFL is less likely to occur in the downward side of the SG tubes.

6.3.10.5 CCF/CCFL in the downcomer

CCFs of steam (or steam/water mixtures) and water play an important role regarding the distribution of coolant in the primary system both in PWRs and BWRs. In CCF a limiting condition appears first when the downward flow of

liquid is influenced by the upward flow of vapor. Any increase of vapor flux then leads to a reduction in the liquid counterflow until, eventually, this becomes zero. The liquid which cannot flow down may be carried upward with the gas flow. CCFL tends to occur at flow cross-section restrictions like the downcomer, where the gas velocity is a maximum.

ECC water is injected into the cold legs or directly into the downcomer. The injected water is needed to refill the LP and reflood the core in an LOCA situation. This water has to flow countercurrent to steam flowing upward toward the broken loop cold leg. Downcomer CCF may limit the water delivery into the LP. Additional steam production in the downcomer may occur, if some of the injected water evaporates due to the hot downcomer walls. This hot wall effect is more pronounced in small-scale test facilities than in large-scale facilities due to the different ratio of structure surface to downcomer volume.

CCF in the downcomer is a multidimensional PH, and the flows of steam and liquid are far from evenly distributed around the downcomer annulus (Mullen et al., 1992).

Many CCFL data have been obtained with air and water. For steam/water the CCFL situation may be different due to steam condensation on subcooled ECC water resulting in a reduced steam upflow rate. Steam condensation reduces the vapor flux, allowing a greater liquid flux which in turn increases condensation. This process may lead to a complete water “break-through.” In small-scale facilities like LOBI, however, an opposite effect was observed. Condensation at the accumulator ECC water injection location caused a high steam upflow in the downcomer which prevented water downflow for some time.

If the upflow consists of a two-phase gas/droplet flow at the CCFL location the momentum of the entrained droplets is opposing the liquid downflow leading to more limitation of the liquid downflow rate.

ECC water injected into the downcomer or into the cold legs has to flow downward through the downcomer in order to refill the LP and subsequently the total core to prevent overheating. This water flow can be limited by steam flowing upward through the downcomer. Consequently, the core reflood can be delayed. Downcomer CCFL is one of the most important phenomena during the refill phase of a LBLOCA in PWRs (OECD/NEA, 1989; Wilson et al., 1990).

6.3.10.6 CCF/CCFL in the PRZ surge line

The PRZ surge line contains both horizontal and vertical sections of large diameter (around 0.3 m ID) piping. If fluid is discharged from the top of the PRZ, by opening the PRZ valve, for instance, there is the possibility that under two-phase primary circuit conditions steam flowing to the PRZ will delay or prevent liquid draining back from the PRZ to the primary circuit. CCFL could occur in the horizontal sections or at the upward elbows in the system.

CCFL in the surge line has a direct bearing on faults such as the stuck open PORV (power operated relief valve). It results in the liquid level within the PRZ being decoupled from that within the rest of the primary circuit, as in the TMI-2 accident. It also has implications for use of the PRZ PORV in AM procedures; for instance, if the PORV is discharging to depressurize the primary side, liquid held within the PRZ may not be available to supplement the inventory of the primary loop.

6.3.11 Global multidimensional fluid temperature, void, and flow distribution

Phenomena in this section address mainly the three-dimensional flow behavior in selected components compared with phenomena described in Section 6.3.3. Global distribution means large-scale behavior of the fluid temperature, void, and flow distribution within special components such as the UP, core, downcomer, or SG secondary side. Nearly all two-phase flow phenomena are inherently three-dimensional and unsteady on a fluid-element scale, for example, in a droplet and in the gas field around a droplet. Also turbulent fluctuations are ignored in all practical problems, and space-time averaging of the conservation equations filters them out. Only the average three-dimensional, time-varying characteristics of the flow over the size of the numerical mesh cells can be retained. Within this average framework, the terms for the production and convection of fluxes of mass, momentum, and energy are all specified in a mathematically rigorous form (Yadigaroglu et al., 1990; OECD/NEA, 1989). However, the averaging process generates unknown distribution coefficients for the convective terms and several unknown coefficients for the wall and interface transport terms. Distribution coefficients are usually taken to be unity. Transport or constitutive relationships are often assumed to be algebraic relationships involving parameters such as friction factors, drag coefficients, and HT coefficients, derived from the fully developed situation and related to one-dimensional variables such as the cross-sectional average velocity—all these have to be established empirically.

On the other hand, three-dimensional phenomena are sometimes very evident, even

dominating the local thermal-hydraulics, in large size flow passages of the primary system, such as the UP in the reactor vessel, the core and the downcomer in a PWR. Mixing, condensation, and CCF of liquid and vapor during ECC injection are typical examples which give rise to three-dimensional velocity, temperature, and void distributions in these regions. One-dimensional mixture and one-dimensional two-fluid models can only average these three-dimensional effects into their one-dimensional framework, which may penalize the scaling and generality of their prediction capabilities. Thus, uncertainties introduced by the one-dimensional approximation have to be assessed from near full-scale experiments.

UPTF results indicate that the larger the size of a flow passage (such as the reactor vessel downcomer, or the UP and core), combined with nonuniform geometric distribution of water inlet and flow outlet, the more multidimensional the flow distribution becomes (Glaeser, 1992). Fluids of different density and different direction of flow find it much easier to establish their own preferred flow paths in which the flow is predominantly cocurrent rather than countercurrent.

The two-fluid code TRAC allows a three-dimensional representation of the pressure vessel. However, interface transfer like shear stress, heat and mass transfer between the fluid in neighboring fluid is included only where there is bulk flow exchange between the cells (Glaeser, 1990a,b). The averaging process within the cells is described above.

One of the major sources of uncertainty in current thermal-hydraulic computer code simulation is the fact that it is not adequately known for all flow situations, how to describe the local interfacial area density and the momentum, mass, and energy transfer rates at those interfaces, irrespective of the computational cell size.

All the above considerations specifically address the geometric configuration of the primary circuit of PWRs. Nevertheless, these are essentially valid for BWRs, for which case the following aspects can be added:

- The multidimensional behavior in the lower plenum occurs as in the case of PWRs with the additional complexity arising from the presence of the control rod guide tubes (CRGTs) with related CCFL and delayed flashing phenomena.
- The multidimensional behavior in the core originates from the interaction of single channels, where the flow can be locally two-dimensional, from channel to channel and involve multidimensional interchange with the upper and lower plena. Additional detail can be found in Section 6.3.11.2.

– The multidimensional behavior in the UP is less complex than in the PWR case because of the geometrical configuration that allows only vertical flows from core to separators; in fact no horizontal connections corresponding to PWR hot legs are present. The injection of spray systems inside this zone creates thermodynamic situations that are similar to those created in the case of hot-leg injection in a PWR (see also Section 6.3.9.1). Multidimensional phenomena may take place in the steam dome in the case of a main steam line break (MSLB) or during the period of actuation of the fast depressurization system (ADS, automatic depressurization system), also causing eccentric loading of the internal structures. These are not further considered here because of their low relevance in terms of safety and to the global behavior of the system.

– The geometric dimensions of the vessel downcomer (thickness and flow area) are much greater in a BWR compared with a PWR. This makes the 3-D behavior of the BWR vessel downcomer less important compared to the PWR. The relatively small ratio between the feedwater flow area and the downcomer cross-section area (in comparison with the ratio of cold leg area to downcomer cross-section area in a PWR) also reduces three-dimensionality. Three-dimensional effects can occur in the case of the break of one recirculation line (for additional details, see Section 6.3.11.3) while limited or no (in the majority of BWRs) 3-D effects are expected following the injection of emergency cooling system water.

Phenomena in this section also incorporate the PH of temperature stratification. Temperature stratification in the water in the LP and in the U tubes of the SGs are not specifically addressed in this section, but may have an influence on the system behavior, if this water is pushed to other locations (e.g., into the core). Its relevance to nuclear safety is considered to be low.

6.3.11.1 Global multidimensional fluid temperature, void, and flow distribution—UP

The flow in the UP is three-dimensional. During the blowdown period of a LBLOCA, for example, water is delivered from the PRZ and the SG primary side into the UP via the hot legs.

In the case of hot-leg ECC water injection, water is injected toward the UP via a special nozzle at the bottom of each hot leg. The water jet is directed out of the hot legs horizontally into the UP. The ECC water impinges on the columns (guide tubes) in the UP and is directed downward.

The water downflow location in the UP determines the downflow location through the upper end box, including the UTP, into the core region. This observation has

been made in UPTF and other large-scale test facilities like SCTF and CCTF (Damerell et al., 1993a,b; MPR Associates, 1990). The magnitude of the cross-section of the ECC water downflow in the UP and in the core is important for partially cooling the core during the end of blowdown and refill period of a postulated LOCA. Multidimensional effects are also of prime importance in estimating fuel rod damage during the heat-up period. The UP multidimensional flow is one of the most important phenomena during refill and reflood with hot leg or UP ECC injection.

The liquid inventory in the UP is relevant for steam binding, if no subcooled ECC is injected into the UP (only cold leg or downcomer injection). The UP liquid inventory for all injection designs may be important for washout of fission products released from defect fuel rods. (Fission product transport and distribution themselves are not considered in this chapter.)

6.3.11.2 Global multidimensional fluid temperature, void, and flow distribution—core

During normal operation of a PWR the core is completely covered with water whereas in a BWR the steam is produced in the core. Even when the core is liquid covered, flow patterns, which are essentially three-dimensional rather than 1-D, can be set up. In the case of an accident the water level may drop and the cooling of the core has to be reestablished by means of the ECC system.

Cold-leg injection leads to a core refill from the bottom upwards. The combined cold- and hot-leg ECC injection or the hot leg only injection leads to a local top-down cooling of the core in addition to refilling from the bottom. The hot-leg ECC injection water flows down within preferred flow paths. The precursory cooling in these water downflow locations is higher than in the steam dominated core regions. The precursory cooling may reduce the possible fuel rod damage during the heat-up period.

A three-dimensional distribution of water downflow and steam upflow establishes itself above the swell level in the core. After the start of bottom reflood the void fraction and flow distribution determines the further core cooling.

There is also some local top down water flow in the core from the PRZ and the SGs during blowdown.

In the case of BWRs the different parallel channels bounded by the fuel boxes may cause different flow regimes (Dix, 1983): three of these may occur at the same time during a typical LOCA transient. In the peripheral region of the core, where the

coolant is sprayed, and in the bypass region, where there is almost no power production, the subcooled liquid may flow downward from UP to LP (CCFL breakdown condition), thus condensing almost all the steam eventually produced. In other zones of the core, a few fuel channels vent the flashing vapor from the LP which results in cocurrent upflow condition of steam and entrained droplets in those channels. At the same time the remaining parts of the fuel channels may experience typical CCFL conditions at the bottom, with level formation inside the fuel bundles (see Section 6.3.10.2).

Looking at the overall scenario, a typical horizontal “sandwich” situation is expected with level formation in the LP (the steam is produced due to boil-off caused by the depressurization), core (the steam is produced by the evaporation of the coolant and by depressurization), and UP (the liquid is produced by the de-entrainment of droplets from core and by the injection of the spray systems).

The cooling of the core by means of available remaining water or by injected subcooled ECC water is the most essential safety aspect. The increase of water inventory by means of ECC injection determines the HT from the fuel rods.

Three-dimensional flow is important for combined injection (into hot and cold legs during refill), and is ranked important for cold-leg injection only during reflood in LBLOCA (OECD/NEA, 1989; Wilson et al., 1990).

The 3-D flow behavior is important in the case of BWRs considering that the flow patterns discussed above constitute a typical configuration for the core.

6.3.11.3 Global multidimensional fluid temperature, void, and flow distribution—downcomer

During the blowdown and LP refill of an LOCA, the ECC water injected into the cold legs flows down the downcomer below the injection cold legs, if the steam upflow is sufficiently low. With increasing steam upflow the water downflow may be limited (see Section 6.3.10.5).

If the collapsed water level is higher than the bottom of the downcomer (above the lower edge of the downcomer skirt) the steam upflow from the core is stopped.

During core reflood, the water level in the downcomer approaches the bottom of the cold-leg height. An azimuthal steam flow is directed from the intact cold legs to the broken cold leg within the downcomer, which may entrain water from the downcomer through the broken cold leg. Consequently, the downcomer liquid head, which is the driving force for core reflood, is reduced.

The distribution of the down flowing ECC water in the downcomer has an influence on the water delivery to the LP which may be limited by steam upflow. Multidimensional effects are ranked as being important during LBLOCA refill (OECD/NEA, 1989; Wilson et al., 1990).

A reduction of the downcomer liquid head may reduce the driving force for core reflood.

During subcooled ECC water injection into hot water the temperature distribution in the downcomer may be of interest for evaluating the PTS stress on the reactor vessel wall.

6.3.11.4 Global multidimensional fluid temperature, void, and flow distribution—SG secondary side

In the SG secondary side there are several areas where multidimensional effects are of high importance and will influence the overall behavior of the primary to secondary side HT. The flow rate on the secondary side is determined by NC, and small changes to void and temperature distributions can have a substantial impact on the flow conditions and hence on the local HT. This has been demonstrated, for example, at feed and bleed operation of the auxiliary feedwater flow in the case of loss of main feedwater, where subcooled auxiliary feedwater is mixed with the vapor in the SG downcomer (D'Auria et al., 1993).

At the top of the downcomer subcooled feedwater is mixed with saturated liquid which is returning from the separators and dryers. Some vapor will be present in this separated liquid flow (carryunder) which will be condensed on contact with the feedwater. The feedwater is provided fairly uniformly around the top of the downcomer resulting in rather uniform downcomer flow conditions.

At the bottom of the downcomer the flow enters the riser where the liquid is heated to saturation and boiling starts. Baffle plates will force the flow to pass the tube bundle in a transverse direction along with its main axial direction. This increases the HT coefficient on the tubes outer surface.

The two-phase flow enters the steam separators located at the top of the riser. The number of separators can vary from only a few to a vast number in parallel. They all rely on separation due to centrifugal forces. The two-phase mixture is set into rotation by means of swirl vanes at the separator inlets. The liquid will then be “spilled” over the separator top edge and will fall back to downcomer.

The vapor with some liquid droplets (carryover) then enters the dryers in the

steam-generator dome. In the dryers the remaining liquid is separated from the vapor and is feedback to the downcomer. The vapor passes through the SG outlet nozzle and enters the steam line.

Multidimensional effects prevail at almost every location in the flow path due to the system geometry, and the mixing of liquid and vapor. However, the most important parts are the riser and the steam separators.

In the riser the baffle plates force the two-phase flow into a zigzag flow path. Behind the plates and tubes eddies will be created, which will strongly influence the two-phase flow pattern and the interfacial area distribution. It is likely that a dispersed regime will be promoted even under conditions where other flow regimes normally would prevail. As mentioned above also the HT on the outer surface of the tubes will be augmented compared to ordinary pipe flow because of the crossflow nature of the flow.

In the separators, three-dimensional effects will be introduced through the circulation of the flow. These effects will govern the actual separation of the two-phase mixture and will determine the carryunder and carryover fractions in the separated flow. The interfacial area and the slip are of essential importance for the separation behavior. The presence of a preheater in some SG designs produces additional multidimensional effects.

During the course of intermediate and SBLOCAs it is essential to keep the heat sinks as intact as possible to mitigate the consequences of the transients. However, the detailed conditions of the SG secondary side are not of crucial importance in this respect, and neither are the two-phase multidimensional characteristics of the secondary flow in many cases. It has been found, though, that the conditions in the downcomer in some cases have influenced the overall SG behavior.

6.3.12 Heat transfer

The HT between wall structures and fluid is an essential heat transport mechanism in LWRs for transporting the heat generated in the core to the turbines. In the first step, the heat is transferred in the core from fuel to fluid. The SG tubes transmit the heat between the high pressure primary side and low pressure secondary side. The safety aspects of the HT are mostly related to the core region.

The fuel cladding temperature is usually near the saturation temperature of water. During an accidental increase in power, or decrease of flow and pressure, a

deterioration in the HT process is possible. The surface temperature increases to such a high level that the heated surface can no longer support continuous liquid contact. This PH is called boiling crisis or dryout depending on the mechanism leading to the event. The key question is how efficiently the deteriorated HT mechanism can remove heat generated in the core after the reactor shutdown. The HT problems are both global in the case of core uncover and local for high power rods.

Due to the inadequate understanding of HT mechanisms, an empirical approach is often necessary. This approach requires the derivation of empirical HT correlations for each HT configuration, resulting in numerous correlations for each HT mode. Some correlations are based on the phenomenological basic formulations for explaining the parametric tendencies, but typically some key parameters are required for fitting against the experimental data.

At the present time, quite a large selection of HT correlations exists in the world literature and many correlations are derived from a large database. Most of the HT correlations are based on tube data, since the simplest test geometry is a heated tube. Extrapolation of the tube correlations to other geometries (bundles, annuli) is common practice in reactor safety analysis. In principle no new SETs are needed for the more accurate calculations of HT in expected incidents. The problem for model development is inadequate measurements of local parameters needed for developing models of HT mechanisms for two-fluid codes.

6.3.12.1 Natural or forced convection (FCO) in the core, in the SG, and at structures

Either FCO or natural convection (NCO) can occur when single-phase liquid, vapor, or two-phase flow is present. During normal operation of a PWR the FCO to single-phase water is the main HT regime in the primary coolant system. In the core, subcooled boiling may also occur. During normal operation of a BWR FCO to single-phase liquid in the core occurs only in the lower entrance region, while two-phase forced convective HT is the HT regime in the upper part of the core.

NC of the single-phase water may occur, if the reactor is scrammed and the main coolant pumps are switched off due to different water densities in the hot part (core, UP, and hot part of SGs) and the cooler part of the primary system (cold side of SG U tubes and downcomer). In this situation forced or NCO HT (depending on the Reynolds number of the flow) can occur at any of the components involved.

Two-phase natural convective HT is important for the HT from the core to the SG secondary side in the case of small leak scenarios.

Two-phase convective HT is described in Sections 6.3.11.2–6.3.11.4.

Cooling of the core and the primary side fluid inventory via the SG has the highest priority in nuclear reactor safety. Apart from core and SG HT an additional heat input may be relevant from hot structure material to the primary side water or steam during blowdown, for example, and the heat loss from the primary side to the environment through the vessel and piping structure material may affect the system behavior during long transients.

6.3.12.2 Subcooled and nucleate boiling HT

The transition from single-phase liquid HT to nucleate boiling takes place, once the wall temperature exceeds the temperature for onset of nucleate boiling. According to one hypothesis, the condition for nucleation and thus the onset of subcooled boiling is the point where the convective heat flux and boiling heat flux are equal. More refined treatment of nucleation can be derived by considering the temperature profile in the region adjacent to the wall.

Fully developed subcooled boiling does not exist immediately the surface exceeds the saturation temperature. A region of partial boiling exists between the subsaturation zone and fully developed subcooled boiling.

The heat flux/surface temperature relationship in the fully developed region is independent of velocity and subcooling and may be correlated by the equations of the type obtained from pool boiling experiments, where the constant coefficients are mainly functions of the pressure, and the heat flux is a function of the wall superheating with an exponent $n=2, \dots, 4$.

Saturated nucleate boiling starts when the bulk liquid temperature equals saturation temperature. In saturated boiling the HT consists of two contributions, a nucleate pool boiling term and a convective term. The Chen correlation (Hsu and Graham, 1986) is an example of this kind of formulation. The FCO contribution is multiplied by a two-phase factor F and the nucleate boiling term by the suppression factor S when the local quality increases.

The nucleation term represents the normal nucleation caused by the nucleation sites on the wall. The convective term is an effect of the forced vaporization through the annular liquid layer on the wall.

The nucleate boiling region is an essential part of the HT curve. The onset of nucleate boiling has an effect on the void profile and thus on the nuclear power profile in the BWR core. In the PWR core no bulk boiling is expected, but

subcooled nucleate boiling (SNB) can occur in the top third of the core. The possible local voiding thus generated has the unwanted side effect of disturbing the neutron power profile.

Nucleate boiling is particularly relevant in special cases such as ATWS in BWRs.

6.3.12.3 Departure from nucleate boiling/dryout

A large number of terms have been used in the literature to denote the occurrence of CHF: burnout, dryout, boiling crisis, CHF, and DNB. The term DNB is usually reserved for the occurrence of CHF in the subcooled region caused by microlayer evaporation under a bubble. Typical mechanisms creating this kind of situation are the depressurization of the flow channel increasing the wall superheating, decreasing the liquid subcooling, and perhaps creating a bulk boiling in the liquid together with a strong nucleate boiling.

Dryout refers to the CHF occurrence caused by evaporation of the wall liquid film in the annular flow regime. When three fluid fields are considered in an annular flow pattern, vapor, liquid film, and droplets entrained from the liquid core, the hypothesis is that the boiling crisis in annular film occurs when the liquid film is depleted by evaporation and entrainment. A typical situation creating this kind of CHF pattern is a stationary boiling channel in stationary forced flow conditions, where an annular flow pattern exists.

The following observed asymptotic trends are valid for the CHF:

- local subcooling increases CHF,
- CHF approaches pool boiling CHF at low flows,
- CHF approaches zero for quality (void fraction) approaching unity,
- CHF reaches a maximum in the pressure (P) range of 3–4 MPa,
- CHF approaches zero when P approaches critical pressure,
- the existence of spacers in the bundle increases CHF rate.

For steady-state operation of the reactor the avoidance of CHF is one of the main criteria in acceptance of the plant power level. Taking into account the peaking

factors for the maximum power fuel bundle and for the maximum power fuel rod, no CHF is allowed during steady-state conditions. Rods experiencing CHF may be damaged.

The criterion is also used in anticipated transients, when the plant protection systems are operating normally.

In accidents including LOCA or in transients with an additional failure of plant protection systems, CHF at least in the hottest rods may be expected, and as a consequence the rods may be damaged causing a release of radioactivity to the coolant. During LOCA the occurrence of CHF initiates the core heat up period.

6.3.12.4 Post-CHF HT

The post-CHF regime means in general the regime where the hot wall temperature or lack of coolant does not allow liquid to contact the surface. The HT models considered under this title are the transition boiling, film boiling, HT to the droplet dispersed mixture, and convection to single-phase steam. Above the dryout type of CHF the coolant in the flow channel consists of a mixture of droplets and steam when the annular liquid film has evaporated. After the DNB type of CHF the hot surface temperature prevents the turbulent mixture of coolant and steam wetting the wall. During quasi-stationary conditions in the core after core uncover only steam exists above the swell level. All these modes are considered as post-CHF HT.

Transition boiling is a special HT mode because the heat flux generally declines with an increase in surface temperature. The HT area is bounded by the CHF and minimum heat flux. Transition boiling can be understood as a combination of unstable film boiling with low HT capability and nucleate boiling with high HT capability alternating on the heated surface. In high quality region most of the transition boiling is due to convection to the droplets impinging on the superheated steam layer in the vicinity of the wall. The increase of mass flux increases the transition boiling rate and liquid subcooling has a similar effect.

During film boiling, the heated surface is cooled by radiation, by FCO to vapor, and by interaction of the liquid and the heated surface. The vapor may become highly superheated and its temperature is controlled by HT from the wall and to the liquid phase in the chain wall-vapor-liquid. Liquid in the form of a dispersed spray of droplets is encountered at void fractions in excess of 80% (liquid deficient flow regime) and in the form of a continuous liquid core (inverted annular film boiling) usually encountered at void fractions below 30% (inverted annular flow regime).

The transition regime between these two flow regimes takes place usually in the form of a churn turbulent liquid dispersed flow.

Of the film boiling regimes the liquid dispersed regime with droplets (after dryout, above liquid swell level) is most commonly encountered and has been well studied. In a phenomenological model it is assumed that HT takes place in two steps: from the heated surface to vapor and from the vapor to the droplets. The axial gradients of the droplet size are evaluated from the heat balance data and the droplet size is used for the interfacial drag and HT correlations. The wall temperature is found from the vapor temperature using a superheated steam HT correlation. In the model a direct droplet-wall interaction can be modeled, as well. The droplet dispersed HT regime exists during the emergency core cooling above the swell level as a consequence of droplet entrainment. In BWR HT, the cooling effect of spray droplets is essential.

Phenomenological models have also been developed for the inverted annular flow regime. In the basic formulation, the balance equations are written for the vapor film between the surface and liquid core. The wall-steam friction is calculated for the laminar or turbulent steam layer and for an average HT coefficient the length is integrated from the beginning of the film to the start of unstable wave formation in the liquid-steam interface.

Phenomenological correlations are also developed to predict the degree of thermal nonequilibrium. The degree of the nonequilibrium is expressed by actual and equivalent equilibrium qualities.

For steady-state operation, the prediction of the post-CHF HT is not essential, because the existence of CHF is itself interpreted as a cause of the fuel damage. For BWR some attempts have been made to allow for local CHF and to demonstrate safety by using post-CHF HT models. After some fuel rod damage, as a consequence of CHF in the BWR bundle, the avoidance of CHF has been retained as an acceptance criterion. In transient analysis the evaluation of the post-CHF HT is needed but also in this case the existence of CHF in the hot channel/hot rod is interpreted as a cause of the rod damage.

In accidents with loss of reactor coolant inventory the HT in the post-CHF mode controls the maximum temperature of the fuel. If the temperature exceeds 800°C, the heat production by cladding oxidation becomes a significant contributor to the further core heat up rate. During a quasi-stationary core uncovering the HT capability of steam depends on the boiling rate below the swell level and in this case the maximum core temperatures depends on simple energy balance rules.

During the emergency core cooling after a LBLOCA the cooling by the droplet-steam mixture is essential both for bottom reflooding and UP spray injection. Quite soon after the reflooding water enters the core, the temperature increase in the upper part may be stopped due to the steam cooling caused by the droplets. Also, as soon as spray droplets impinge on the hottest parts of the core, the cladding temperature starts decreasing. Thus the post-CHF HT is the main contributor to limiting maximum cladding temperatures in the core and preventing damage by oxidation.

6.3.12.5 Radiation HT

Thermal radiation will transfer energy both from surface to surface and from surface to the two-phase flow. Exchange of thermal radiation with the two-phase flow will mainly consist of absorption in the two-phase flow, mainly in the droplets. Due to the relatively low temperature the emission of the two-phase mixture is negligible. The radiation HT becomes important in addition to other HT modes when the structure temperature locally exceeds the saturation temperature by 200 K. These kind of high temperatures are possible only in the core with pure steam, with droplet-steam mixture or with inverted annular flow regime. Typically the net radiative heat flux streams from the highest temperature regions into colder parts, being partially absorbed in the fluid.

The radiation flux from the solid surface consists of two contributions: a radiated flux which is a function of the surface temperature to the fourth power, and a partial reflection of the incoming radiation.

Steam and liquid emit radiation in principle, but the emission is small compared to that of surfaces. Both liquid and steam absorb radiation. In practice the absorption by steam is negligible. The density of liquid water is large enough to absorb all radiation in the space between fuel rods, for instance if an inverted annular flow regime with a continuous liquid core fills the flow channel. For droplet dispersed mixture only a part of the radiation is absorbed and the rest streams to the next surface.

Before emergency cooling water enters the core during an LOCA during which the core has become uncovered, the radiation HT between structures is the most significant HT balancing the local temperature differences. The net heat flux is directed from the hottest rods to the cooler ones. In the BWR bundle the channel wall finally absorbs the heat streaming from the central parts of the fuel element. This heat flux chain between different rod and channel wall creates inside a fuel bundle a temperature profile, where the central rods are in a higher temperature

than the peripheral ones. Due to its strong dependence on the fuel temperature the radiation may effectively prevent the temperature rise and prevent cladding oxidation.

6.3.12.6 Condensation in SG tubes and on structures

The condensation of steam on structures whose surfaces are below saturation temperature can be an efficient means of removing heat from a coolant system. On vertical and inclined surfaces the condensation of steam produces a thin film of liquid which is continuously removed by gravity. The rate of HT is dependent on the subcooling of the surface, and the thickness that the liquid film attains—HT is limited by conduction through the film. The HT coefficient is also affected by the steam flow rate to some degree, through its influence on the film thickness and state. The presence of small amounts of noncondensable gas in the vapor can result in a drastic reduction in condensation rates under stagnant conditions. This is because the flow of steam toward the condensing surface produces an increase in the concentration of the noncondensable gas at the interface, and the presence of the noncondensable lowers the saturation temperature of the steam.

In parallel channels, condensation can give rise to instabilities with different tubes going through a refilling and siphoning cycle at different times (D'Auria et al., 1990).

Condensation within SG tubes is an important mechanism for the removal of decay heat. Provided that the secondary side of the SG is cooled the primary pressure will closely follow the saturation pressure of the secondary side when the SG tubes contain steam. This enables reflux cooling to remove decay heat satisfactorily following an LOCA, and permits primary depressurization via secondary side cooldown when the primary circuit is voided above the core. Because of the large area available within the SG tubes, however, the exact magnitude of the condensation HT coefficient is not critical at decay heat levels. Only when the secondary side coolant level was very low or substantial quantities of noncondensable gas were blocking the SG tubes would the condensation rate be expected to limit the overall HT.

Condensation on external structures such as pipe walls or within the PRZ steam space can occur in transients where the pressure rises, with the effect of reducing the rate of pressure rise.

6.3.13 QF propagation/rewet

The reflooding and quenching phenomena are important for LWRs. Indeed, it is

usually postulated that the core is uncovered and overheats due to decay heat from the fission products and the energy stored prior to LOCA during the so-called blowdown phase of the LOCA. In PWRs, the core is recovered, that is, the overheated rods are quenched and adequate HT is reestablished, by reflooding from below. ECC injection at the top of the core, or combined top and bottom injection are, however, also practiced in certain types of PWRs. In BWRs, the hot fuel rods may be quenched by a spray that forms a liquid film flowing down and cooling the rods as well as the walls of the “channels” containing the rod bundles and also the water rods in the rod bundles.

Water is forced into the core by the ECCS via bottom flooding (PWRs) or top spray (BWRs) in order to stop overheating of the fuel rods and reestablish cooling. Otherwise, cladding oxidation, zircaloy-water chemical reaction or clad melting and the consequent release of radioactive products can occur.

Reflooding refers to a particular mode of postburnout cooling of a hot channel by refilling it with coolant. Quenching or rewetting of the hot surface occurs during reflooding. Quenching refers to the transition from a mode of HT characterized by total or almost total absence of liquid contacts with the wall to one where the wall is essentially wetted by the liquid. The HT coefficient increases dramatically following quenching.

As a result of the high temperatures attained by the clad before the emergency coolant arrives, water does not initially wet the hot clad surface. Rewetting or quenching of hot surfaces occurs when the coolant reestablishes contact with the dry surface. The surface temperature corresponding to the achievement of liquid-solid contact is the rewetting or quenching temperature. The temperature of the fuel pellets and fuel clad is reduced by heat conduction and convection to the coolant. As the coolant rises in a hot channel or in the overheated nuclear fuel rod bundle, complex HT and two-phase flow phenomena take place and also the succession of regimes moves gradually up the rod bundle channels. The hot surfaces along the channels experiences in turn free- or forced-convection cooling by steam, dispersed-flow film boiling, inverted-annular film boiling, transition boiling, nucleate boiling, and finally single-phase convection to the liquid. Almost, all the HT modes listed under HT (Section 6.3.12) are encountered during reflooding and quenching phase.

During reflow multidimensional flow patterns occur in the core and UP due to: Flow rates and flow regimes are such that gravitational forces are of the same order as inertial forces; nonuniformities in core power distribution and differences in resistance to flow through the intact and broken hot legs tend to promote

multidimensional effects; as the flow passes through the UP it must flow around several structural elements and additionally the flow behavior of a collected pool in the UP may be highly three-dimensional.

Another important PH, observed in the PWR integral system LBLOCA experiments, was core wide cooling of the fuel cladding and quench during the blowdown phase. This PH is important regarding heat up of the core, because it removes a large part of the stored energy from the fuel during the early phases of the transient. The blowdown-phase quench was caused by the hydraulic response of the primary system during the transition from subcooled to saturated choked flow at the break and by the operational characteristics of the primary system coolant pumps. The rapid cooling of the cladding is primarily a result of low-quality, high upward core flow at 7 MPa pressure range. The correlations currently used in the advanced codes cannot handle adequately such blowdown quench phenomena and also no directly applicable separate effects type experimental database exists.

QF propagation/rewet on fuel rods and, also channel walls and water rods (BWR) will be presented below, in some detail.

6.3.13.1 QF propagation/rewet on fuel rods

QF progression has been an interesting physical PH studied intensively over the last four decades. After a LBLOCA has occurred the core is empty and adiabatic heat up is possible. Emergency coolant injection by bottom reflooding creates a rising quenching front, and upper head injection or core spray injection a falling film, sputtering front. Many experiments in 1970s and 1980s were done for understanding and visualization of the reflooding front movement. Visual demonstrations with an overheated, red-colored rod enclosed in a glass tube demonstrated clearly that quenching to the saturated temperature takes place in a distance of a few millimeters.

In the boiling curve, QF propagation means a movement from the film boiling HT mode through transition boiling to the nucleate boiling regime. In a quenching front the axial temperature gradient of the cladding may be so large that a significant part of the heat in the unwetted part is removed by the axial conduction in the cladding. For a fast front movement this gradient may be quite different between the inner and outer cladding surfaces. But other mechanisms may also support conduction-controlled quenching or be a main contributor to the cooldown close to the saturation temperature. These are transition boiling caused by the collapse of the liquid-vapor interface in the inverted annular film boiling regime

and droplet impingement through the steam layer in the transverse direction toward the wall.

During the LBLOCA the first cladding heat up is caused by the stagnation of flow going through the core. Soon after this large mass flow rates may exist in the core first in the negative flow direction and later in the positive direction. This high mass flux rate may be enough for cooling the cladding along the whole core length without a specific quenching front (Aksan et al., 1989).

The conduction controlled quenching mechanisms for a rising reflooding front and a falling film front are quite similar. In the wetted region the heat is transferred, in both cases, by nucleate boiling and later by convection. In the unwetted part, the heat is removed by convection to vapor or to droplet-vapor mixture or by inverted annular flow film boiling during bottom reflooding. Precursory cooling effects support the QF movement.

The rewetting characteristics of the overheated core after the large LOCA was one of the most interesting research topics in 1970s and 1980s, and still has a significant influence on acceptance criteria in licensing and probabilistic safety assessment safety analyses. The main interest is related to the maximum temperature in the core, but this turn-over temperature is determined by the liquid dispersed flow well before quenching. Depending on the amount of water available the cooldown takes place earlier or later.

The large temperature gradient in the cladding gives rise to a mechanical stress on the cladding, and it may affect fuel damage and radioactivity leakages. The rapid temperature drop is also associated with strong steam generation and this may have an effect on system characteristics including:

- liquid entrainment rate,
- CCFL in the UTP,
- steam binding in the SG,
- multidimensional flow distribution in the core.

6.3.13.2 QF propagation/rewet on channel walls and water rods (BWR)

Following hypothetical complete emptying of the core in BWR-type reactors (e.g., as a consequence of a LBLOCA in one circulation line), both rod cladding and fuel

box surfaces attain temperatures well above the saturation temperature of the fluid. (Usually the system pressure is around a few tenths of an MPa in these conditions.)

At a given time, the reflood process starts, caused usually both by the injection of cold liquid through the LPCI (low pressure coolant injection) and the LPCS. The former system injects water into the downcomer or inside the core bypass region; in both cases the liquid reaches the LP and enters the core from the bottom. In the latter system, the liquid is sprayed at the top of the core and creates a QF traveling from top to bottom.

Phenomena like CCFL, entrainment, PDs, etc., are very important for predicting the transient evolution in these conditions.

The reflood PH inside each fuel bundle follows the same mechanisms described in Section 6.3.13.1. The fuel box walls play a special role that can be outlined as follows:

(a) Due to the fact that there is essentially no power production and initial temperatures before reflood are slightly lower than cladding temperatures, reflood occurs earlier along the fuel box walls than adjacent to the fuel rods (the thickness of fuel boxes, which is far greater than the rod cladding thickness, does not appear to have a significant role in relation to the different rewet times between the rods and the fuel box walls).

(b) Because they cool earlier, the walls constitute a heat sink for the rods and make easier the reflood in the rods themselves; radiation HT plays a role in this regard.

(c) As an additional consequence of the first item, the liquid injected by the LPCI or sprayed by the LPCS can penetrate to the LP preferentially along the fuel box walls and contribute to reflooding of the core rods.

The local mechanism of reflood, including the two-dimensional nature of the PH, is the same as described in Section 6.3.13.1.

The rewetting of fuel box walls gives an important contribution to core reflood. In this sense the present PH is as relevant as the reflood in the core rods. The same considerations as in the previous paragraph apply in this case.

6.3.14 LP flashing

When a pool containing saturated or subcooled liquid is subjected to depressurization, the system pressure acting on the liquid itself may reach the

saturation pressure corresponding to the initial liquid temperature. In this case a more or less violent vaporization (flashing) may occur depending upon the depressurization rate. (High purity water bounded by a surface with negligible nucleation sites—a very flat surface—may behave in a different way; in particular, several tens of degrees of liquid superheating can be expected. This is not of interest in practical reactor situations.)

During flashing (nearly) homogeneous nucleation occurs in the bulk of the liquid, and the gas bubbles produced may entrain a large mass of liquid toward the upper parts of the pool (LP in this specific case).

The PH is significantly affected by the geometry of the system, shallow pools giving rise to more violent flashing than tall ones containing the same volume of liquid.

The liquid entrained in the steam flowing toward the upper part of the vessel both in BWR and PWR systems, in most of the situations of practical interest, may give a significant contribution to core cooling. In the case of LBLOCA, the PH may contribute to early core quench observed in the experiments performed in integral test facilities. The LP vaporization occurring late in the transient in the case of a large break may lead to the occurrence of flooding, thus preventing or limiting the flow of injected liquid into the downcomer. The last PH is more relevant for PWR systems. In the case of BWR, rapid boiling in the LP may prevent the fall back of liquid from the core making rod cooling more efficient.

6.3.15 Guide tube flashing (BWR)

As indicated in the heading, the PH is typical of a BWR. From a phenomenological point of view, the substance of Section 6.3.14 is also applicable here. The particular geometry and the presence of relatively small holes (orifices) at the top of the guide tubes govern the development of the PH and make it distinct from LP flashing.

The liquid initially contained in the CRGTs is slightly more subcooled than the remaining LP liquid. For this reason, flashing during a given transient is delayed with respect to LP flashing. Level swell is also limited by the abovementioned orifices.

In view of the above this PH could be considered less important than the previous one as far as nuclear reactor safety is concerned. Nevertheless, it may affect the core thermal-hydraulic behavior later in a transient (with respect to LP flooding).

6.3.16 One- and two-phase impeller-pump behavior

In single-phase conditions the dimensionless pump characteristics are almost independent of the fluid (liquid, gas, steam). The small variations are mainly due to viscous properties connected to recirculation losses, shock losses on the impeller, and fluid friction (Comolet, 1976).

In two-phase flow the torque and head characteristics are affected by so-called degradation which is a function of void fraction, pressure, and flow rate. The main causes of the degradation seem related to phase separation in the impeller due to centrifugal forces, with liquid phase acceleration and relative deceleration of the gas or steam. The pre- and postrotations of fluid in the inlet and outlet pipes play a part in this issue. All these phenomena depend on the type (centrifugal, axial, mixed flow) and geometry of the pump.

For all LOCAs with running pumps, the pump performance is important. For large LOCAs the behavior of the intact loop pumps plays a role in determining the position of the stagnation points in the primary circuit.

For SBLOCAs the pump behavior plays a role in steam-water mixing and core cooling.

6.3.17 One- and two-phase jet-pump behavior

In normal operating conditions the jet pump operates as a single-phase ejector and is installed in the lower part of the downcomer (BWR-3, 4, 5, and 6). The driving flow provided by the external recirculation pumps is injected in the upper part of the ejector (converging section) and creates depressurization in the throat. The downcomer fluid is accelerated by the pressure difference created and mixes with the driving flow in the diverging part of the jet pump.

When recirculation pumps stop, as in most transients, the jet pumps behave exactly as ventures connecting the LP with the downcomer. In the case of main coolant pump cavitation, steam may flow out of the top nozzles completely preventing the correct operation of the device.

The component has a critical relevance in terms of nuclear reactor safety in the case of LOCA involving the break of a recirculation line. Owing to its axial elevation, the jet pump prevents mass depletion from the core region; so its mechanical integrity is of vital importance.

In the case of off-normal conditions, the jet pump simply introduces an extra PD in

the flow path from LP to downcomer and vice versa. Consequently, no new phenomena are expected in this case.

An exception may be the jet pump behavior during pump coast down. Possible unstable behavior may cause neutron flux instabilities or interact with the neutron flux. This last aspect may have some safety relevance.

6.3.18 Separator behavior

Separators are installed in the vessel of a BWR and in the secondary side of SGs equipped with U-tubes (PWR). The basic function is to separate the steam from the two-phase mixture coming either from the core (BWR) or from U-tubes riser (PWR), allowing (near) pure steam to flow to the turbine.

In all cases, the separation process is based on the larger inertia of the liquid phase with respect to the steam phase: the upward flowing two-phase mixture is constrained to rotate. In this way, the steam can continue to flow upward while the liquid droplets impinge on the walls and are drained downward to the downcomer (of the main vessel or of the SG in BWR and PWR cases).

The separation efficiency largely depends upon the average velocity of the incoming mixture. At very low velocity the separator essentially behaves as a simple flow obstruction.

The component behavior has no direct relevance in terms of nuclear reactor safety for PWRs and in most cases for BWRs. An exception, in the case of BWR, is that the PDs introduced in the riser zone can facilitate the occurrence of core thermohydraulic-neutronic instabilities.

6.3.19 Steam dryer behavior

The steam dryer allows the achievement of a vessel exit quality of near to one (0.999). The working principle is similar to the one adopted for the separator and exploits the different inertia of the light (steam) and heavy (liquid) phases. The two-phase mixture exiting from the separator (quality range between 0.98 and 0.99) flows horizontally in parallel flow paths created between adjacent undulated plates. The steam phase flows across, while the liquid droplets unavoidably impinge against the wall and are drained to the bottom of the dryer and toward the downcomer.

Considerations already detailed in Section 6.3.18 are also valid in this case. As in the case of the separator, the component behavior has no direct relevance in terms

of nuclear reactor safety in PWR. The dryer does, however, contribute to the PD introduced in the riser zone of a BWR and therefore can facilitate the occurrence of core thermohydraulic-neutronic instabilities.

6.3.20 Accumulator behavior

When, in an LOCA, the primary pressure in a PWR falls below the set point for accumulator injection, the driving gas within the accumulator can expand, delivering borated water (boratec) coolant to the primary circuit. The rate of delivery of the flow depends on the resistance of the accumulator line (important in LBLOCA) and on the expansion characteristic of the driver gas (dominant effect for SBLOCA). The latter depends on the HT processes occurring between the gas and the accumulator structure and the liquid interface. The rate of accumulator delivery may also be influenced by feedback between the accumulator flow and the system pressure. Condensation on the injected liquid can lower the circuit pressure, increasing the flow and lowering the pressure further. On the other hand, accumulator injection can cause an increase in primary pressure (e.g., by reflooding the core and increasing heat input to the fluid), reducing the flow rate. The combination of local and system effects can possibly give rise to instabilities in the accumulator flow rate.

When the liquid within the accumulator is exhausted the cover gas can flow into the primary circuit. The presence of a noncondensable gas in the primary can then modify the coolant distribution and the HT processes, particularly condensation. The emptying of the accumulator could be modified by the formation of a vortex at the outlet pipe.

Under the near adiabatic conditions occurring in the LBLOCA the cover gas temperature can fall to subzero (°C) temperatures, leading to the possibility of frost forming in the accumulator lines.

The accumulators form a key element of the safety injection systems for dealing with LOCA. In a LBLOCA, they provide the principal means of limiting the peak clad temperature by refilling the vessel after blowdown and initiating reflood. In SBLOCA (particularly in beyond DBA scenarios where the HPIS is assumed to fail) the accumulators also play an important role in preventing or limiting core uncover. The role of the accumulators in a range of accident scenarios is discussed in OECD/NEA (1989).

6.3.21 Loop seal filling and clearance

In most current PWR designs, the primary piping from the outlet of the SGs

descends to a level roughly corresponding to half way down the core before rising to enter the pump inlet from below. During an LOCA when the primary circuit is partially voided, liquid present in the U bend of this intermediate leg can form a barrier to the flow of steam around a loop. This liquid plug is said to form a loop seal. A pressure difference across the loop seal which is greater than the hydrostatic pressure arising from the height of the pump inlet side of the intermediate leg is necessary before steam can displace the loop seal.

The manner and extent of the displacement of the liquid from the loop seals depends on the steam supply characteristics. At reduced steam velocities and low liquid subcoolings the expulsion of fluid will be incomplete. This aspect of loop seal behavior is closely connected with the PH of countercurrent flooding limitation (CCFL). However, the pipe sizes of interest are very much larger than those studied in most SETs.

When the loop seals clear, their liquid contents are displaced into the reactor vessel, producing a rapid refill. The number of loop seals clearing, which depends for instance on the size of the break, affects the total amount of water added. How many loops need to clear is determined by the balance between the frictional PD around the cleared loops and the hydrostatic pressure difference corresponding to the depth of the loop seal.

It is possible for loop seals to reform, after they have cleared. Back flow of ECCS from the cold legs through the pump is limited by the height of the impeller and the diffuser geometry, but can occur if there is a general flow reversal, or if the level in the cold leg is high enough. Condensate from the down side of the SG tubes also can provide a contribution to the reforming of the loop seals.

The loop seals have a particularly significant effect on the behavior of a plant in a small cold-leg break LOCA. Until at least one of the loop seals has cleared steam produced in the core cannot reach the break, and the pressure in the primary system remains high, at a level determined by the secondary side pressure. Furthermore, as the liquid content of the primary side falls, the hydrostatic head of the liquid trapped in the pump inlet causes the liquid level in the core region to be depressed by an amount equal to the depth of the loop seal. This can lead to uncovering of the core. Loop seal reformation could impair long-term cooling after a LBLOCA by causing periodic depression of the mixture level in the core.

6.3.22 ECC bypass/downcomer penetration

The ECC bypass and downcomer penetration PH is a combination of three

phenomena already described (Rohatgi et al., 1990):

- CCF or CCFL in the downcomer (see Section 6.3.10.5),
- liquid-vapor mixing with condensation in the downcomer (see Section 6.3.7.2),
- entrainment/de-entrainment in the downcomer (see Section 6.3.6.3).

These three phenomena contribute to ECC bypass/downcomer penetration. This PH is listed separately because of its importance to ECC water injection performance. Complete ECC bypass occurs, if the steam upflow rate is so high that it does not permit any liquid downflow through the downcomer. All the injected ECC water is carried out through the broken cold leg by the steam flow. This may be caused by high steam upflow in the downcomer (as CCFL), increased steam upflow due to pressure decrease at the condensation location in the cold leg and upper part of the downcomer, as well as high azimuthal steam velocities from the intact cold legs to the broken cold leg during LBLOCA blowdown (as entrainment). Downcomer penetration is partial or complete water downflow of the injected ECC water through the downcomer at lower steam upflow or lower azimuthal steam flow.

ECC water injected into the cold legs or directly into the downcomer has to flow downward through the downcomer in order to refill the LP and subsequently reflood the total core to prevent overheating. This water flow can be limited by upward and/or azimuthal steam flow. ECC bypass and penetration is ranked to be very important during LBLOCA refill (OECD/NEA, 1989; Wilson et al., 1990).

6.3.23 Parallel channel instabilities

The term “parallel channel instabilities” includes a broad range of instabilities that may occur in a system owing to the presence of a boiling boundary. Any boiling channel, even if operated in an open loop mode, may give rise to instabilities that can be detected as pressure, flow rate, temperature, void fraction, etc., oscillations (OECD/NEA/CSNI, 1990).

There are several reasons for instabilities including static (e.g., Ledinegg) or dynamic (e.g., density wave) ones. The most studied instability mode is just called a density-wave instability: a perturbation in a boiling channel inlet flow rate may result in a perturbation of the PDs across the channel; this may reflect back to the channel inlet, strengthening the initial flow rate variation (unstable system) or smoothing it (stable channel). A special case of “stable oscillations” may also occur.

The cases of interest essentially include a closed loop where the boiling channel is one of the parts of the system, and a single channel that constitutes the entire system, bounded by upper and LP with imposed conditions is the other; multiple parallel boiling channels are of considerable interest in the BWR technology. The core of a BWR can be considered as a unique channel: in this case parallel channels are constituted by the bypass and the downcomer. A single core channel can also be considered for instability purposes: in this case the other channels are the parallel channels that may interact to some extent with the other external channels (bypass and core).

This very short survey gives an idea of the number of thermal-hydraulic unstable situations that may occur in a BWR. The complexity increases, if one considers the neutron flux which may oscillate and interact with thermal-hydraulic instabilities (neutronic-thermal-hydraulic feedback).

So far, two general kinds of instabilities measured in BWR plants have attracted the attention of technologists:

- (a) core wide oscillations: the neutron flux oscillates with same frequency and amplitude in all parts of the core;
- (b) regional oscillations: at least two parts of the core oscillate with different frequencies.

It seems easy to imagine that a very limited number of channels or even a single channel can oscillate at its own characteristic frequency and amplitude in a core that may remain stable.

The PH is relevant in nuclear reactor safety. With reference to the BWR flow map (power versus core flow rate) a zone has been found, from operational experience, where the occurrence of instabilities is very probable. This is characterized by power and core flow rate around 40% and 30% of the nominal value, respectively. Operation in this zone may be necessary following a pump trip or during plant start-up transients.

6.3.24 Boron mixing and transport

Boron is a highly neutron absorbing material and will consequently strongly affect the core power when inserted or removed from the core. Thus boron mixing and transport will not directly influence the thermal-hydraulics (if one neglects possibly minor chemical effects) but will do so indirectly through the core power which is a thermal-hydraulic boundary condition. In PWRs, boron is added to the coolant-

moderator and its concentration will control the long-term variation of core reactivity. Because of the high liquid velocity in the RCS, the added boron will be mixed quite homogeneously with the coolant without steep gradients, and its transport through the RCS will closely follow the liquid transport.

However, there are low flow conditions, for example, at idle reactor coolant pumps, when the pump power has temporarily been lost, when inhomogeneous boron concentration can be attained in the loops with rather steep concentration gradients. In this case, the diffusion of boron within the liquid can be quite substantial and thus the boron transport will be different from the liquid flow.

The boron concentration will influence the PWR core power through reactivity feedback effects. The boron content impacts the moderator temperature reactivity coefficient and the boron concentration reactivity coefficient. For a fresh normal PWR core in equilibrium conditions (beginning of life) high boron concentration (1600–2000 ppm) will cause the former to be slightly positive at low moderator temperatures (300–400 K) and less positive at higher temperatures. At lower concentrations it is always negative and more negative at higher temperatures. The boron concentration coefficient is always negative being more negative at low concentrations and temperatures.

Boron mixing and transport within the RCS is of crucial importance for core power control in LWRs. The mixing and transport of boron influences through reactivity feedback the local core power during normal and off-normal operation of PWRs and during off-normal operation of BWRs.

During normal operation of a PWR the initial excess reactivity of a fresh core is compensated by adding boron to the coolant. This added boron is gradually decreased as the fuel burnup increases in order to keep the core reactivity essentially constant throughout the core lifetime.

It is also a well-known fact that a PWR cannot be kept in a subcritical cold SHD condition immediately after refueling without the boron concentration in the coolant being above some value despite all the control rods being inserted. Thus the boron concentration and its mixing and transportation with the coolant is also of major concern at SHD conditions.

During a LBLOCA, the core fission power will almost immediately be terminated because of global core voiding and associated loss of moderation. However, during the reflood period it is essential that the injected relatively cold ECCS water has some level of boration in order to avoid possible local recriticalities of the core.

During a SBLOCA in a PWR with U-tube SGs it has been found that in the reflux condensation phase there exists a mechanism which can accumulate boron-free condensate in the loop seal (Hyvarinen, 1992). Analyses of externally caused boron dilution transients suggest that the SBLOCA in this case could become a reactivity-initiated accident (RIA) initiator.

It has also been found that in some specific cases during SHD conditions in a PWR, there could be situations where pronounced heterogeneities in the boron concentration can develop and thus can potentially cause a RIA (Jacobson, 1992).

6.3.25 Noncondensable gas effect (PWR)

The presence of a noncondensable gas in the primary circuit plays a role in mechanical and thermal fluid behavior. Noncondensables are mainly nitrogen from the accumulator injection or hydrogen from clad oxidation.

In the case of nitrogen injection, the mechanical effects are related to gas expansion in the cold leg and the upper part of the downcomer. The momentum-transfer between the gas, steam, and liquid increases the liquid velocity. This has an impact on the downcomer water penetration and on water bypass to the break.

The thermal effect is related to the change in HT laws, particularly for the condensation process produced by noncondensables.

Both effects are associated with the end of accumulator injection. When nitrogen enters the cold leg, the mixing of gas with liquid stops oscillation due to plug formation. This is due to the compressibility of gas liquid mixture and to the reduction in condensation rate.

Within the primary circuit the gas migrates from its injection or generation point. There are several mechanisms for migration: the entrainment of gas by flowing steam, the gravity forces arising from density differences and diffusion driven by the concentration gradient. In the SG, due to condensation in the tube inlet region and the flow of steam toward the SG, noncondensable gas stays at the top of the U-tubes and can limit NC.

This PH could have some influence on the general thermal-hydraulics behavior for LBLOCA but is of most relevance to accidents with NC phases.

6.3.26 LP entrainment

In the case of a LBLOCA, the reverse flow in the core goes to the LP where saturated liquid is still present. Depending on steam flow and water level, liquid can be entrained to the downcomer, then to the break. Oscillatory behavior can occur. This PH depends on the geometry and on LP internal structures.

This PH has a direct impact on the nature of reverse flow in the downcomer during LBLOCAs as well as on break flow and ECCS bypass.

6.4 Thermal-hydraulic phenomena for integral facilities (PWRs, BWRs, VVERs)

Thermal-hydraulic phenomena identification and characterization has been done for PWRs, BWRs, and VVERs within the OECD/NEA-CSNI framework. The results of this work have been described and introduced in different tables in Sections 6.4.1–6.4.3.

6.4.1 Thermal-hydraulic phenomena for integral facilities of PWRs

The analysis and the classification of off-normal events which may happen in a real system are slightly different for PWRs and BWRs, although in both cases a simple classification based on rupture area has been preferred. For PWRs the following classes of accidents were selected:

- (1) Large breaks (rupture area greater than 25% of the maximum pipe area connected with the pressure vessel A_{\max});
- (2) Small and intermediate breaks with UTSG (rupture area less than or equal to 25% A_{\max});
- (3) Small and intermediate breaks in PWRs with OTSG;
- (4) Transients, where upset conditions are created by single or multiple failures of one or more systems in the plant;
- (5) Transients at shutdown conditions;
- (6) Accident management for a nondegraded core.

Large break LOCAs (item 1), are dominated by inertia effects and characterized by strong rather homogeneous steam/water flow distribution inside the primary loop, in particular during the depressurization period.

For small break LOCAs (item 2), gravity and stratification effects are important phenomena to be simulated. Intermediate break LOCAs (item 2) as well may contain features related to both LB and SB LOCAs. The actual subdivision between items (1), (2), and (3) depends in general upon the size of the plant, the position of the break and the status of the pumps (on or off); the boundary selected (25% A_{\max}) must be seen as approximate and somewhat arbitrary.

Transient with single or multiple failures (item 4) is mainly determined by the sequence of operation of valves, pumps, and engineered safety features.

Transients at shutdown conditions (item 5) is mainly related to the so-called mid-loop plant operations, which are characterized by the atmospheric pressure in the primary system (with openings or not) and the water level at the height of the loop connections to the reactor vessel.

Accident management for a nondegraded core (item 6) contains accident management measures for a nondegraded core to prevent core degradation and damage.

In the term “phenomena” all the important thermal-hydraulic aspects expected to occur during the accident are included; “type of test” relates to the definition of the experiment simulating a characteristic accident scenario. Phenomena, test types, and test facilities are identified and selected essentially on the basis of the personal experience of the experts assigned to perform the work.

The correlation between phenomena and test type in the tables is given three levels:

- Occurring, which means that the particular phenomenon is occurring in that kind of test type (plus (+) sign in the matrix);
- Partially occurring: only some aspects of the phenomenon are occurring (open circle (o) in the matrix);
- Not occurring (dash (–) in the matrix).

Widely used nomenclature has been adopted in the identification of phenomena and test types. The test types are identified and described in some detail in the Appendix A of Annunziato et al. (1996), and the phenomena are defined also in some detail in the Appendix B of the same report. For a better understanding of the tables, it is useful to describe one or two lines of each one of those tables.

“The Large Break Matrix” is given in Table 6.2. As an example, consider the ECC bypass and penetration phenomenon. It is considered to be of high importance for refill tests but of limited interest in blowdown and reflood tests. Another example is quench front propagation. This phenomenon has been considered suitable for indirectly heated rods, not suitable for directly heated rods. Indirectly heated rods simulate better the heat capacity effect of the nuclear fuel rod, but they cannot take into account the effect of the gas gap of the nuclear fuel rod.

Table 6.2

Cross reference matrix for large breaks in PWRs

--

“The Small and Intermediate Breaks Matrices in PWRs with UTSG and OTSG” are given respectively in Tables 6.3 and 6.4. It should be noted that, among the phenomena, the “structural heat and heat losses” phenomenon has been considered in order to emphasize the noticeable distortions introduced by the heat release from structures in the scaled-down facilities with respect to the plant behavior; this is due to the larger values of structural masses and structure-to-fluid heat exchange areas relative to the volume-scaled values.

Table 6.3

Cross reference matrix for small and intermediate breaks in PWRs with UTSG

--

(1) This phenomenon is related to the scaled test facilities. (2) For intermediate breaks, phenomena included in large break reference matrix could also be important.

Table 6.4

Cross reference matrix for small and intermediate breaks in PWRs with OTSG (in addition to the matrix for PWRs with UTSG)

(1) This phenomenon is related to the scaled test facilities. (2) For intermediate breaks, phenomena included in large break reference matrix could also be important.

A relatively large number of test types, total of seven, have been considered to emphasize that a number of different transients are possible under the general category of Small Break LOCA.

Quench front propagation has been considered suitable for indirectly heated rods, not suitable for directly heated rods. As already mentioned above, indirectly heated rods simulate better the heat capacity effect of the nuclear fuel rod, but they cannot take into account the effect of the gas gap of the nuclear fuel rod.

“The matrix for small and intermediate breaks in PWRs with once through steam generators (OTSG)” is given in **Table 6.4**. Twenty-seven phenomena, and seven test types are included. The “structural heat and heat losses” phenomenon is included by the same arguments as given above.

“The transient matrix” is given in **Table 6.5**. The following observations can be added to those in the preceding three sections:

Table 6.5

Cross reference matrix for transients in PWRs

(1) Valve flow behavior will be strongly design- and type-dependent, specific experimental data should be used, if available. (2) This phenomenon is related to the scaled test facilities. (3) Isolation of one or more steam generators.

- some of the phenomena discussed in the SB and IB matrix are relevant in the present case and they are not repeated in this table;
- thermal-hydraulic nuclear feedback is a phenomenon which characterizes some of the transients: for this reason, LOFT test facility (which was equipped with a nuclear core) was judged to be more suitable than the other experimental loops in operation;
- the experience gained from incidents occurring in power plants is potentially of great importance, as is that from the analysis of data from start up, shut down, and other maneuvers.

Table 6.6 is a cross-reference matrix dedicated to “transients at shutdown,” that is, corresponding to accident scenarios with the plant in shutdown conditions (control rods inserted). A separate matrix has been prepared in order to emphasize the importance of these transients with respect to safety issues and to the challenge for codes at low pressure conditions.

Table 6.6

Cross reference matrix for transients at shutdown conditions in PWRs

--

(1) Dependent on opening location; + pressurizer manway open; – pressurizer manway shut.

Four test types have been considered for shutdown conditions (three of them relating to loss of RHR at mid-loop operation, and one to boron dilution at shutdown). The cold overpressure transients have not been included in the matrix because the thermal-hydraulics is quite simple (mostly single phase liquid flow) and the phenomena associated are not expected to challenge significantly thermal-

hydraulic codes.

Among the 24 phenomena mentioned in these tables for PWRs, 20 have been taken from the small break LOCAs and transients matrices and are not specific to transients at shutdown conditions. However, it has been considered that shutdown conditions required a particular attention because of specific thermal-hydraulic conditions (atmospheric pressure) for which the validity of computer codes has to be demonstrated.

Table 6.7 is the cross-reference matrix for “Accident Management for a nondegraded core in PWRs.” With respect to the initial version of the report, this is a new matrix. However, the phenomena are basically those identified for small break LOCAs and transients in PWRs. This is because AM scenarios are initiated by the same events as small break LOCAs and transients, but are terminated by appropriate operator actions according to AM procedures.

Table 6.7

Cross reference matrix for accident management for a nondegraded core in PWRs



(1) This phenomenon is related to the scaled test facilities.

The five test types selected in this matrix refer to the intrinsic nature of the AM procedure considered except one, which refers to failure in plant operation (SGTR with multiple failure).

6.4.2 Thermal-hydraulic phenomena for integral facilities of BWRs

For BWRs, almost all the plants now in operation are equipped with an Automatic Depressurization System (ADS), and therefore, even a small break LOCA is characterized by a fast depressurization following the actuation of this device. Thus, as a difference from the PWR case, only two tables have been considered: a LOCA table and a transient table. In the Transient table, start-up tests, frequent

operational transients and ATWS have been included. For both plant types, tables are composed of two elements, related to the following items: “Phenomena versus Test Types.”

The LOCA matrix is given in Table 6.8. The analysis of off-normal events in actual nuclear plants is potentially valuable, especially with reference to scaling and simulation problems. The “structural heat and heat losses” phenomenon is included by the same arguments as given in Section 6.4.1.

--	--

Table 6.8

Cross reference matrix for LOCA in BWRs

(1) This phenomenon is related to the scaled test facilities.

A relatively large number of test types, six, has been considered to emphasize that a number of different transients are possible under the general category of blowdown.

The transient matrix is given in Table 6.9. The following observations can be done in addition to those in the preceding section on PWRs:

--	--

Table 6.9

Cross reference matrix for transients in BWRs

(1) Two-phase pump behavior is of interest for certain special ATWS and inadvertent increase of steam flow transients. (2) This phenomenon is related to the scaled test facilities.

- Almost all of the phenomena discussed in the LOCA matrix are also important for transients, but for brevity they are not repeated in this table;
- Thermal-hydraulic nuclear feedback is the phenomenon which characterizes some of the transients. Due to this reason, actual BWR plants have been judged much more suitable than the other experimental loops already in operation;
- The experience gained from off-normal events occurring in real plants is potentially of great importance, as is that from the analysis of data from start up, shut down, and other test or operational maneuvers.

6.4.3 Thermal-hydraulic phenomena for integral facilities of VVERs

In addition, to set-up validation matrices for Russian Pressurized Water-cooled and Water-moderated Energy Reactor (WWER or VVER) analyses, an international Working Group was formed on the initiative of the Federal Ministry for Research and Technology (BMFT) of the Federal Republic of Germany. A further evaluation of the WWER matrices was performed by a CSNI Support Group. Based on these CSNI matrices the lists of phenomena have been reviewed and adopted to the characteristics of WWER-440 and WWER-1000 systems, respectively.

Germany, Hungary, Russia, Slovak Republic, Poland, and Ukraine has been formed on the initiative of the BMFT of the Federal Republic of Germany, giving the task to GRS in close co-operation with the Nuclear Protection and Safety Institute (IPSN) of France in May 1993 to elaborate the topic “Verification Matrix for Thermal-hydraulic System Codes Applied for WWER Analysis.”

The topic was combined with the objective of a co-operation to formulate an internationally agreed WWER-specific validation matrix as a supplement to the existing OECD/NEA-CSNI code validation matrix for PWRs with U-tube steam generators as presented in Annunziato et al. (1996).

Based on the CSNI cross reference matrices the lists of phenomena have been reviewed and adopted to the characteristics of WWER-440 and WWER-1000 systems respectively, and the lists of test facilities suitable for code assessment have been formed.

The above tasks have been performed successfully by the Working Group under the leadership of GRS in close co-operation with IPSN during 1993–95, and the results were published by Liesch and Réocreux (1995).

The selection of tests from the large number of experiments proposed has to be continued, in order to get the ones which are the most suitable for code assessment with respect to a given phenomenon or test type.

As a consequence, these activities will continue under the auspices of the OECD/NEA. Therefore, in June 1995 a new Support Group has been installed to continue

with the further evaluation of the matrices, concentrating on three tasks:

- description of WWER-specific phenomena and safety relevance,
- optimization of the WWER-specific code validation matrices,
- development of criteria for the data bank storage of experimental data valid for the matrices.

As a result of this work, WWER validation matrix has been completed and published in 2001 (OECD/NEA, 2001). In the following three tables, as in the case of PWRs and BWRs, phenomenon versus test type specific for VVER-440 and VVER-1000 will be presented for Large Break LOCA which includes 16 phenomena and 3 test types (Table 6.10), Small and Intermediate Leaks which includes 27 phenomenon and 8 test types (Table 6.11), and Transients which includes 11 phenomenon and 9 test types (Table 6.12). It is to be noted that the majority of these phenomena for PWRs are also relevant to WWERs.

Table 6.10

Cross reference matrix for large breaks in VVERs

--

(1) These phenomena are not covered in the OECD/NEA-CSNI Matrix for PWRs.

Table 6.11

Cross reference matrix for small and intermediate leaks in VVERs

--

(1) These phenomena are not covered in the OECD/NEA-CSNI Matrix for PWRs. (2) This phenomenon is related to the scaled test facilities.

Table 6.12

Cross reference matrix for transients in VVERs

--

(1) These phenomena are not covered in the OECD/NEA-CSNI Matrix for PWRs. (2) For phenomena requiring separate effects test, e.g., pressurizer behavior. (3) This phenomenon is related to the scaled test facilities.

6.5 Thermal-hydraulic phenomena related to advanced water-cooled reactors

This section will provide the relevant thermal-hydraulic phenomena for advanced light water reactor (ALWR) designs including the reactor designs employing passive safety systems, in addition to the relevant thermal-hydraulic phenomena identified for the current generation of LWRs in Sections 6.3 and 6.4.

IAEA-TECDOC-626 provides definitions for safety-related terms as applied to advanced reactors (IAEA, 1991). In that document, the concepts of passive and active safety systems are defined and discussed. The definition of a passive safety system is as follows: *Either a system which is composed entirely of passive components and structures or a system which uses active components in a very limited way to initiate subsequent passive operation.* Four categories were established to distinguish the different degrees of passivity. Thermal-hydraulic phenomena and related parameter ranges that characterize the performance of passive systems do not differ, in general, from phenomena that characterize the performance of systems equipped with active components. This is specifically true for transient conditions occurring during safety relevant scenarios. In other words, one can say that friction PDs or HT coefficients are affected by local velocity and void fraction and not by the driving force that establishes those conditions, for

example, gravity head or centrifugal pump. The same can be repeated for more complex phenomena like two-phase critical flow or countercurrent flow limiting.

Thus, a large number of thermal-hydraulic phenomena that are expected to occur in passive systems during transients and accidents are classified in the OECD/NEA/CSNI documents “separate effect” (SE) and “integral effect” (IE) reported in Aksan et al. (1994) and Annunziato et al. (1996), hereafter. However, specific layout of passive systems and combination of parameter ranges brought the need of expanding the original list of phenomena in the mentioned references. This was done in Aksan and D'Auria (1996), where mainly the passive systems proposed at the time of issuing of the report were considered.

As part of the IAEA's overall effort to foster international collaborations that strive to improve the economics and safety of future water-cooled NPPs, an IAEA CRP was started in early 2004. This CRP, entitled Natural Circulation Phenomena, Modeling and Reliability of Passive Safety Systems that Utilize Natural Circulation, focused on the use of passive safety systems to help meet the safety and economic goals of a new generation of advanced NPPs. This CRP has been organized within the framework of the IAEA Department of Nuclear Energy's Technical Working Groups for Advanced Technologies for LWRs and HWRs (the TWG-LWR and the TWG-HWR) and provided an international cooperation on research work underway at the national level in several IAEA Member States.

The use of passive safety systems such as accumulators, condensation, and evaporative heat exchangers, and gravity-driven safety injection systems eliminate the costs associated with the installation, maintenance, and operation of active safety systems that require multiple pumps with independent and redundant electric power supplies. As a result, passive safety systems are being considered for numerous reactor concepts (including in Generation III and III+ concepts) and are expected to find applications in the Generation IV reactor concepts, as identified by the Generation IV International Forum (GIF). Another motivation for the use of passive safety systems is the potential for enhanced safety through increased safety system reliability.

The CRP on NC and passive safety systems benefits from earlier IAEA activities that include developing databases on physical processes of significant importance to water-cooled reactor operations and safety, for example, in the area of thermal-hydraulic phenomena in advanced water-cooled reactors, recent IAEA activities have assimilated data internationally on HT coefficients and PD (IAEA and Aksan, 2001); and have shared information on NC data and analytical methods (IAEA and Aksan, 2001), and on experimental tests and qualification of analytical methods

(IAEA and Aksan, 2000). In order to establish the progress of work in this CRP, an Integrated Research Plan with description of the tasks addressing the objectives of the CRP was defined. These tasks are:

- establish the state-of-the-art on NC,
- identify and describe reference systems,
- identify and characterize phenomena that influence NC,
- examine application of data and codes to design and safety,
- examine the reliability of passive systems that utilize NC.

The activity under the first task is aimed at summarizing the current understanding of NC system phenomena and the methods used experimentally to investigate and model such phenomena. In November 2005, the IAEA issued a technical document (IAEA and Aksan, 2005), developed by the collaborative effort of the CRP participants and with major contributions from some selected experts in the CRP, aimed at documenting the present knowledge in six specific areas; advantages and challenges of NC systems in advanced designs, local transport phenomena and models, integral system phenomena and models, NC experiments, advanced computation methods, and reliability assessment methodology.

The activity for the third task is aimed at identifying and categorizing the NC phenomena of importance to advanced reactors and passive safety system operations and reliability. This task is the major link between the second and the fourth tasks. During the phase to perform the activities on the mentioned tasks, one of the unique features was to collect and include plant design descriptions with a strong emphasis on passive safety systems of the specific design. These descriptions of the passive safety systems were considered during the phenomena identification and characterization process by the group of experts. As basis for the PH identification for AWCs, earlier works performed within the OECD/NEA framework during 1983 to 1997 were in detail considered. These are:

- code validation matrix of thermal-hydraulic codes for LWR LOCA and transients (OECD/NEA, 1987),
- SOAR on thermohydraulic of emergency core cooling in LWRs (Lewis et al., 1989),
- SET validation matrix for LWRs (Aksan et al., 1994),

- integral facility tests validation matrix for LWRs (Annunziato et al., 1996),
- status report on relevant thermal-hydraulic aspects of ARDs (Aksan and D'Auria, 1996).

Since the Generation III and III+ reactor designs contain technological features that are common to the current generation reactors, the phenomena identified during the work performed for first item to fourth item can be used as base knowledge. The fifth item provides the important and relevant thermal-hydraulic phenomena for ARDs in addition to the relevant thermal-hydraulic phenomena identified for the current generation of LWR. The list of relevant phenomena established in Aksan and D'Auria (1996) has been taken as basis for the AWCRs work and been modified according to the reactor types and passive safety systems considered. It is to be also noted that in identifying the relevant thermal-hydraulic phenomena in the list which is provided in Table 6.13, expert judgment is the main contributor.

Table 6.13

Identification and characterization of phenomena for advanced water-cooled reactor designs including natural circulation and passive safety systems

--

The “expanded” OECD/NEA list of phenomena for passive systems was upgraded in IAEA CRP on Natural Circulation Phenomena, Modeling and Reliability of Passive Safety Systems that Utilize Natural Circulation, considering the recently proposed passive systems by the industry. The identification and characterization of additional (i.e., with reference to the original SE and IE lists) phenomena for passive systems are presented in Table 6.13, which includes two main columns, other than the first column with numbering, which is consistent with the phenomena numbering in Aksan and D'Auria (1996):

- Column 1: phenomena number,

- Column 2: phenomena identification,
- Column 3: phenomena characterization based upon the individual phenomena description.

The content of Table 6.13 is self-standing and directly understandable. In addition, the supportive description of the individual phenomena is also provided in order to be clearly explanatory about each PH. However, the following additional items should be noted:

- Specific geometry configurations or range of variations of affecting thermal-hydraulic parameters justify the presence of phenomena at rows 2, 5, 6, 7, and 14 in both the present list and the list in Aksan et al. (1994). This is specifically true in the case of PH 6 (NC) that is expected to occur whenever a gravity environment exists.
- NC is also at the origin of the core makeup tank (CMT) performance, PH at row 15 in Table 6.13. However, the simultaneous presence of stratification in the tank, the possible condensation with level formation inside the tank, the specific loop connection and the values of boundary and initial conditions, suggest the consideration of a separate PH.

This section will provide some details on the important and relevant thermal-hydraulic phenomena for current generation AWCRs (AP1000, ESBWR, EPR, VVER-1200, MASLWR, CAREM, SMART, etc.) in Table 6.13. Detailed descriptions of the 15 phenomena related to AWCRs as listed are also given.

6.5.1 Behavior in large pools of liquid

Large pools of water (e.g., up to several thousand cubic meters) at near atmospheric pressure are incorporated into several advanced designs. These large pools provide a heat sink for heat removal from the reactor or the containment by NC, as well as a source of water for core cooling. Examples include the pressure suppression pool (wet-well) of the ESBWR, the in-containment refueling water storage tank of the AP-1000, the pool of the emergency condenser of the SWR-1000 and the gravity-driven water pool of the AHWR.

Large pools may have a very wide spectrum of geometric configurations. HT in a limited zone in terms of volume (e.g., by condensing injected steam or by HT from an isolation condenser, IC) does not imply homogeneous or nearly homogeneous temperature in the pool. Three-dimensional convection flows develop affecting the

HT process, which results in a temperature stratification.

Steam generated by HT or following injection may be released from the pool into the containment and influences the increase of the containment pressure. Compared to a homogeneous temperature distribution, the fluid at the top of the pool may reach the saturation temperature while the bulk fluid is subcooled. The evaporation from the top of the pool results in a pressure increase in the containment. Therefore, the temperature stratification influences plant design. The three-dimensional nature of the temperature stratification requires appropriate modeling.

6.5.2 Effects of noncondensable gases on condensation HT

Condensation occurs when the temperature of vapor is reduced below its saturation temperature. Presence of even a small amount of noncondensable gas (e.g., air, N₂, H₂, He, etc.) in the condensing vapor leads to a significant reduction in HT during condensation. The buildup of noncondensable gases near the condensate film inhibits the diffusion of vapor from the bulk mixture to the liquid film. The net effect is to reduce the effective driving force for heat and mass transfer. This PH is the concern of industrial applications and nuclear reactor systems.

In nuclear plants, the condensation of steam in the presence of noncondensable gas becomes an important PH during LOCA when steam released from the coolant system mixes with the containment air. Besides this, nitrogen gas in accumulators is a source of noncondensable gas, which can affect the condensation HT inside the SG tubes of NPPs, and may affect the CMT performance. The effect of noncondensable gases on condensation HT is also relevant to certain decay heat removal systems in ARDs, such as passive containment cooling systems (PCCSs).

The effect of noncondensable gases on the condensation of steam has been extensively studied for both natural and FCO flows. In each of them, geometries of interest (e.g., tubes, plates, annulus, etc.) and the flow orientation (horizontal, vertical) can be different for various applications. The condensation HT is affected by parameters such as mass fraction of noncondensable gas, system pressure, gas/vapor mixture Reynolds number, orientations of surface, interfacial shear, Prandtl number of condensate, etc. Multicomponent noncondensable gases can be present.

6.5.3 Condensation on containment structures

This PH involves heat and mass transfer from the containment atmosphere toward

the surrounding structures. This PH would occur in existing reactors in the case of a coolant release into the containment. It also occurs in advanced designs where containment surfaces are cooled externally, usually by natural mechanisms. Good examples are the designs of the AP series by Westinghouse, where the steel containment is cooled externally by water flowing on its exterior surface from a reservoir above the containment, and by ascending air driven by buoyancy.

Steam condensation is largely affected by conditions which can be split into two groups depending on the relevance of the physical dimensions of the system. The “scale-independent factors” are variables like the fraction of noncondensables, the pressure, the gas composition and so on, the effect of which could be well investigated through separate effect tests. The “scale-dependent factors” are those phenomena that require to be investigated in actual or scaled geometries (i.e., integral effect tests) since physical dimensions largely influence their quantitative effect. Examples of this kind are the NCO process at both sides of the metallic structures and the potential gas stratification.

6.5.4 Behavior of containment emergency systems

Nuclear power reactor containments are equipped with safety systems which protect the containment integrity under various accident conditions. The focus of this PH is the NC cooling and HT in various containment passive cooling systems under accident conditions to remove the energy out of the containment by NC and condensation HT. Typical systems are the tube condensers such as the PCCS and external air cooling system or external liquid film cooling and internal condensation of steam in the containment by NC. The major purpose of these containment systems is to protect the containment under both DBAs and severe accidents involving serious core damages and to prevent the significant release of radioactive materials to the atmosphere. These systems are required to remove the load on the containment from the LOCAs and other accidents by removing the heat but containing the mass within the structure. Most of load comes from the released steam from the primary coolant system due to the LOCA or venting of the pressure relief valves. The major part of the noncondensable gases consists of the original containment atmosphere such as air or nitrogen, however, with the core damage, hydrogen or fission gases can be also released into the containment atmosphere. The thermal-hydraulic phenomena of importance are tube surface condensation with noncondensable gases, NC of steam and noncondensable gases, degradation of condensation by the accumulation of noncondensable gases and purging of noncondensable gases from condenser systems. The PCCS can be vertical or horizontal tube condensers in external water pool, exposed condenser tube system

in the containment cooled by NC water through the tubes from the external pool or by external air circulation and others.

6.5.5 Thermo-fluid dynamics and PDs in various geometrical configurations

PD is the difference in pressure between two points of interest in a fluid system. In general, PD can be caused by resistance to flow, changes in elevation, density, flow area, and flow direction. PDs in NC systems play a vital role in their steady state, transient, and stability performance.

It is customary to express the total PD in a flowing system as the sum of its individual components such as distributed pressure loss due to friction, local pressure losses due to sudden variations of shape, flow area, direction, etc., and pressure losses (the reversible ones) due to acceleration (induced by flow area variation or by density change in the fluid) and elevation (gravity effect). An important factor affecting the pressure loss is the geometry. In a nuclear reactor, we have to deal with several basic geometrical shapes (circular pipes, annuli, etc.) and a number of special devices like rod bundles, heat exchangers, valves, headers, plenums, pumps, large pools, etc. Other factors are concerned with the fluid status (single or two phase/one-component, two-component, or multicomponent), the flow nature (laminar or turbulent), the flow pattern (bubbly, slug, annular, etc.), the flow direction (vertical upflow, downflow, inclined flow, horizontal flow, CCF, etc.), flow type (separated and mixed), flow paths (one-dimensional or multidimensional, open or closed paths, distributor or collector), and the operating conditions (steady state or transient).

An important focus of this PH is the geometric conditions that hinder the establishment of fully developed flow especially when the fluid in question is a mixture of steam, air, and water. This complex thermo-fluid dynamic PH warrants special attention. However, it is worth mentioning here that though in many systems like the primary system of a NPP, flow is mostly not fully developed, PD relationships used in these systems are invariably those obtained for developed flow. This practice is also experimentally proved to be more than adequate in most of the cases. However, in some specific cases like containment internal geometry, it is necessary to consider thermos-fluid dynamics in the developing region.

A final, very important, issue is concerned with the driving force depending on whether the flow is sustained by a density difference in the fluid (NC) or by a pump (FCO), or whether there will be feedback between the pressure loss and the extracted power or not. Normally the pressure loss inside a device depends on the

nature of flow through the device and not on the nature of driving head causing the flow. However, under some circumstances, because of local effects, the pressure loss may get influenced by the nature of driving force.

6.5.6 Natural circulation

The complex set of thermal-hydraulic phenomena that occur in a gravity environment when geometrically or materially distinct heat sinks and heat sources are connected by a fluid can be identified as natural circulation. No external sources of mechanical energy for the fluid motion are involved when NC is established.

The above definition includes the situations of a heater immersed into a fluid, of an open flame in the air, of a chimney-driven fire, of in-surge of hot fluid into a pool of cold liquid, and of a heat source and sink (e.g., heater and cooler) consisting of separated mechanical components connected by piping and situated at different gravity elevations. NC also drives the occurrence of stratification in horizontal pipes.

Within the scope of this document, this PH involves the following system configurations:

- (a) Heat source and sink of primary loop constituted, respectively, by core and SG, or boiler, or primary side of heat exchanger, with core located at a lower elevation.
- (b) Heat source and sink inside the pressure vessel, constituted, respectively, by core and (typically annular-like region of) vessel downcomer. “Steady-state” NC between core and downcomer occurs owing to continuous cooling of the downcomer fluid by a heat exchanger (boiler or SG) or by continuous inlet of feedwater liquid at a temperature lower than core outlet temperature.
- (c) Cooling of the containment atmosphere by a closed loop.

In the current generation of nuclear plants, the NC core power removal capability is exploited for accident situations to demonstrate the inherent safety features of the plant (with the noticeable exception of the Dodewaard commercial BWR unit, shutdown in 1997). The NC is also occurring during various phases of the refueling.

In future generation of nuclear plants, NC is planned to be used for ensuring the nominal operating conditions and for achieving safe cooling following accidents in a wider spectrum than foreseen for current generation reactors.

6.5.7 Steam-liquid interactions

Large pools may have a very wide spectrum of geometric configurations. HT in one very limited zone in terms of volume (e.g., by condensing injected steam or by HT from a passive containment cooler) does not imply homogeneous or nearly homogeneous temperature in the pool. Many containment phenomena require steam-liquid interface. Steam discharge into a suppression pool of BWR is a good example of this case. After break-up of the originally created bubbles in the suppression pool, the subsequent formation of bubble plumes takes place. Consequently, complete condensation occurs and this induces mixing in the pool, the process is being determined by single- and two-phase NC. It is important to understand the break-up and plume-stirring process and mechanisms, because the system pressure ultimately controlled by the pressure in the vapor space above the water surface in the suppression chamber. This pressure is the sum of the partial pressures of steam and gas, the former controlled by the temperature at the pool surface. In turn, the pool surface temperature depends on the efficiency of steam condensation in the pool, and the degree of mixing in the pool.

The following is a listing of the steam-liquid interactions related phenomena:

- Direct contact condensation of steam in pool water.
- Bubble formation and break-up and the subsequent formation of bubble plums.
- Break-up and plume-stirring process and mechanisms inducing mixing in the pool.

As example for steam-liquid interactions can be given passive containment cooling (PCC) venting into the suppression pool of ESBWR and also injection of steam-gas mixture through a downcomer vent line into the suppression pool.

6.5.8 Gravity-driven cooling and accumulator behavior

Gravity-driven cooling provides emergency core cooling water by gravity draining, in events with loss of coolant. This system requires a large volume of water above the core, plus additional depressurization capacity, so that the primary coolant

system can be depressurized to allow for gravity flow from the elevated suppression pool. Since there are no large reactor vessel pipes at or below the core elevation, this design ensures that the core will remain covered by water during all DBAs. In general, gravity-driven cooling concept is mainly based on the depressurization of the reactor pressure vessel (RPV) to sufficiently low pressures to enable reflood of the core by gravity feed from an elevated pool. When the gravity-driven cooling operates, the gravity drain flow rate to the RPV depends on the piping geometry, the state of the fluid, and the pressure conditions in both the water pool and the RPV. Flow entering the RPV during the later stages of blowdown during a postulated LOCA must be sufficient to keep the nuclear core flooded. The system which provides gravity-driven cooling is a simple and economical safety system.

The following is a listing of the gravity-driven cooling-related phenomena:

- Depressurization of the RPV by discharging through depressurization valves into the drywell and increase of pressure in the upper part of containment.
- Evaporation in the RPV due to depressurization.
- Friction in the gravity-driven cooling system (GDCCS) and injection lines including the valves in these lines.
- Large amounts of cold water immediately floods the lower parts of the RPV, causing:
 - collapse of voids,
 - condensation of steam,
 - suppression of boiling,
 - increase of water level inside the RPV.
- Condensing of steam out of the RPV and drywell gas space until air accumulates on the primary sides of the PCCS, resulting in termination of steam condensation.

As examples for GDCCS can be given GDCCS of ESBWR and passive core flooding system (HA-2 hydraulic accumulators of the second stage) of WWER-1000/392 and passive core flooding systems (ECCS tank) of WWER-640/407.

6.5.9 Liquid temperature stratification

Nuclear reactors that implement NC passive safety systems may produce large temperature gradients in their working fluid as a result of local cooling caused by emergency core coolant (ECC) injection or local heating caused by steam condensation or heat exchanger HT. Thermal stratification arises because the low flow condition typically encountered in a NC system greatly reduces the amount of fluid mixing that can occur. Examples of thermal stratification during ECC injection include the formation of cold plumes in the downcomer, and liquid thermal stratification in the LP, cold legs, and loop seals.

ECC injection into horizontal piping partially filled with steam also results in liquid temperature stratification. The cooler liquid condenses the steam forming a saturated layer of liquid water on top of the subcooled liquid layer. This saturated layer is at a higher temperature than the subcooled layer, resulting in a stratified temperature condition. The formation of the saturated layer may mitigate occurrences of condensation-induced water hammer events.

Liquid temperature stratification can also arise in passive safety systems such as the NC-driven CMTs and the large liquid-filled tanks that serve as the heat sink for reactor core or containment passive cooling systems. Steam vented into the large safety tanks condenses in the cold liquid producing hot rising plumes that form thermal layers at the free surface of the tank. Thermal layers having different temperatures grow with time to create a large temperature gradient in the liquid.

6.5.10 Behavior of density locks

The stability of interface of the density locks, especially when two density locks are present, appears a critical aspect. Possible long-term variations of static head in the pool (e.g., due to stratification or heating) may change the interface position in each density lock and consequently stability characteristics.

6.5.11 Behavior of check valves

Check valves connect the primary circuit with very large volumes through large pipes. Conditions in the piping with check valves may arise that cause rapid condensation on one side resulting in slam closure of the valve. The small diving forces may not be sufficient to reopen the valves again. The failure to open may prevent the coolant to flow into the primary circuit; the failure to close may cause draining of the primary circuit; and in addition opening and closure cycles critical oscillations in the flow rates.

6.5.12 Critical and supercritical flow in discharge pipes and valves

Under this item, shock waves, supercritical flow in long pipes, and behavior of multiple critical sections are included, see also Govier and Aziz (1976).

6.5.13 Behavior of emergency heat exchangers and ICs

The removal of decay heat from a nuclear core can be accomplished by passive means using either an emergency heat exchanger or an IC, depending on the system design. In some advanced pressurized water reactors (PWRs), the emergency heat exchanger decay heat removal system consists of a closed loop that includes a shell and tube heat exchanger immersed in a large liquid pool that is elevated above the core. The relative elevation between the heat source and heat sink creates a buoyancy-driven NC flow that eliminates the need for a pump. Decay heat is removed from the core by convective HT from the fuel to the single-phase liquid in the reactor vessel. The heat stored in the liquid is carried by NC to the emergency heat exchanger. Heat is transferred from the fluid through the emergency heat exchanger tubes into the pool by three mechanisms: single-phase convective HT at the tube inside surface, heat conduction through the tube walls, and nucleate boiling at the tube outside surface. Some advanced PWRs use the SG as an intermediate emergency heat exchanger with a passively cooled, NC feedwater loop.

Some ABWRs use ICs as the means of removing core decay heat. The IC consists of a shell and tube heat exchanger immersed in a large liquid pool elevated above the core. In a BWR, core decay heat is removed by nucleate boiling. The steam generated by this process is condensed inside the IC tubes creating a low pressure region inside the tubes which draws in additional steam. Thus the driving mechanism for the flow is steam condensation. Heat is transferred through the IC tubes into the pool by three mechanisms: single-phase steam condensation (phase change) at the tube inside surface, heat conduction through the tube walls, and convective HT at the tube outside surface. The condensate is returned as a single-phase liquid to the reactor vessel by gravity draining. Performance of the IC can be affected by the presence of noncondensable gases.

The following is a listing of the emergency heat exchanger-related local phenomena:

- emergency heat exchanger loop flow resistance,

- buoyancy force,
- single-phase convective HT,
- shell-side nucleate boiling HT.

The following is a listing of the IC-related local phenomena:

- IC loop flow resistance,
- low pressure steam condensation,
- condensation HT in the presence of noncondensable gases,
- shell-side convection HT,
- condensate/steam CCFLs.

6.5.14 Stratification and mixing of boron

Boric acid is introduced into the reactor coolant to control long-term reactivity. Forced coolant circulation during normal operation ensures that the boric acid is homogeneously distributed in the RCS so that the boron concentration is practically uniform. Decrease of the boron concentration results in an increase of the reactivity. Causes for decreasing of boron concentration are injection of coolant with less boron content from interfacing systems (external dilution) or separation of the borated reactor coolant into highly concentrated and diluted fractions (inherent dilution). Examples of external dilution are the injection of coolant of reduced boron concentration by the makeup system, and injection of low-boron pump sealing water into the primary system. Inherent dilution can occur after reflux condenser HT or back flow from the secondary system in the case of primary-to-secondary leakage accidents.

Operation in the reflux condenser mode over a lengthy period of time could occur in the event of SBLOCA concurrent with limited operability of the emergency core cooling (ECC) systems. In such an event the condensate descending down the cold-leg SG tubing into the SG outlet plenum and from there into the pump seal could form slugs of low-boron water. On restoration of NC after refilling of the RCS such slugs would be transported toward the reactor core. However, on their way to the core, they would be mixed in the cold-leg piping, the RPV downcomer and the LP and thus increase in boron concentration. Restarting of a reactor coolant pump (RCP) after a SBLOCA or a SGTR is very unlikely to occur as such events

can be clearly identified on the basis of measured data and starting of an RCP is an action which would provide several individual actions and therefore some time. Assuming that an inadvertent demineralized water injection into one loop was to occur before starting of the RCP in this loop in spite of the monitoring and measurement of the boron concentration of the water injected into the RCS, a slug of demineralized water moves toward the core inlet after pump start. Mixing of the diluted slug with the ambient coolant of higher boron content provides the only mitigation mechanism before the slug enters the core.

The main mixing mechanism in the case of the low-boron water slug accelerated by the RCP start is turbulent mixing between the fluid flows having different velocities whereas in the case of reestablishing the NC after a reflux condensation phase the main mixing mechanism is buoyancy-driven turbulent mixing. The density differences between the fluids are due to the temperature and the boron concentration differences.

6.5.15 CMT behavior

Several ARDs implement CMTs to provide NC cooling to the core. CMTs are elevated tanks connected to the reactor vessel and primary loop at the top and bottom of the tank. Special lines connect the bottom of the tank with the vessel, and are termed direct vessel injection. In connection to this, an important interaction occurs between the CMT, the accumulator and the IRWST also considering the actuation signal for automatic depressurization. The tanks are filled with cold borated water and can provide coolant injection at system pressure. The tanks are normally isolated from the reactor vessel by an isolation valve located at the bottom of the vessel. The fluid is always sensing full system pressure through the top connection line. In the event of an emergency, the bottom isolation valve is opened to complete the NC loop and permitting cold borated water to flow to the core. The relative elevation between the core and the CMT and the density difference between the hot primary system water and the cold CMT water creates a buoyancy-driven NC flow that eliminates the need for a pump. Decay heat is removed from the core by convective HT from the fuel to the single-phase liquid in the reactor vessel. CMT behavior includes NC, liquid thermal stratification in the tank, and liquid flashing during plant depressurization.

6.6 Thermal-hydraulic phenomena for

SCWRs

SCWR has been currently chosen by Generation IV International Forum as one of the reactor designs to be investigated. It is the only water-cooled NPP studied under the Generation IV framework. In Europe, investigations on the SCWR concept have been integrated into a joint research project, called high performance light water reactor (HPLWR), which is a LWR operating at supercritical pressure (25 MPa). HPLWR is cofunded by the European Commission and has been worked out by a consortium of 10 partners from 8 European countries as their contribution to the Generation IV International Forum. The concept is based on a RPV similar to a PWR, but designed for a higher pressure of around 25 MPa. Other plant characteristics of the HPLWR include also a coolant heat up from 280°C to more than 500°C (Squarer et al., 2003). At these conditions, water changes its phase continuously from liquid to steam without boiling, so that a boiling crisis in the core can be physically excluded. As in a BWR, the high temperature steam is fed directly to the high pressure turbine, so that a closed primary cycle like in a PWR can be omitted. Steam separators or primary pumps, which are needed in BWRs, are not required either.

The high steam enthalpy increases the power density of the steam cycle by more than 40%. The envisaged net efficiency of 44% exceeds by far those of conventional LWR (Bittermann et al., 2004). It is expected that the HPLWR will be more economical than conventional LWRs (Bittermann et al., 2003), it will have a higher efficiency and thus a better fuel utilization, which also produces less waste per kWh, but it still fulfills the high safety standards of third generation nuclear plants, for example, EPR, SWR1000 (Aksan et al., 2003). Key advantages of this concept shall be a significant reduction of equipment, resulting in a smaller building volume and consequently of plant erection costs, compared with conventional PWR design, and lower fuel costs thanks to the higher thermal efficiency, keeping the safety features at least as advanced as with third generation LWRs.

During the safety analysis studies for the HPLWR, one of the initial phase activities was to identify the new additional thermal-hydraulic phenomena which needs to be considered for the thermal-hydraulic safety analysis. As a result of these investigations, a list of thermal-hydraulic phenomena for HPLWR conditions has been identified and selected in addition to the phenomena included in earlier studies mentioned in Sections 6.3 and 6.4. These are:

- thermal-physical properties near and at supercritical conditions,

- critical flow during depressurization from supercritical conditions,
- pressure loss characteristics of supercritical water (SCW),
- HT characteristics of SCW,
- reflooding for tight lattice geometry at low pressure,
- boil-off for tight lattice geometry at low pressure,
- instability and NC in supercritical pressure systems.

Above six identified thermal-hydraulic phenomena for HPLWR have also been confirmed for other SCWR designs (eight different concepts including SCWR using heavy water) during investigations and studies carried out (2007–12) by a group of scientists in the Cooperated Research Program (CRP) of IAEA on “HT Behaviour and Thermohydraulics Code Testing for Super Critical Water Cooled Reactors (SCWRs)” (IAEA and Aksan, 2014)

6.6.1 Thermal-physical properties near and at supercritical conditions

HT at supercritical pressure is mainly characterized by the thermal physical properties which vary strongly, especially near the pseudocritical line. Fig. 6.1 shows the specific heat as a function of pressure and temperature.

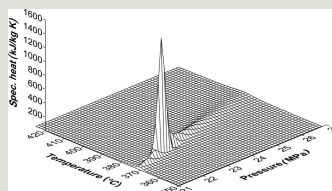


Fig. 6.1 Specific heat of water (Wagner and Kruse, 1997).

It is seen that at each pressure there is a local maximum of the specific heat capacity. In the subcritical pressure range the maximum specific heat locates on the saturation line. At the critical point ($P=22.1$ MPa, $T=374^{\circ}\text{C}$) specific heat has its maximum value. In supercritical pressure range, the line connecting the maximum values of the specific heat is called pseudocritical line (PCL), as shown in Fig. 6.2.

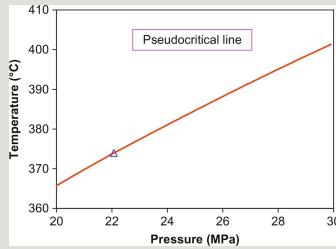


Fig. 6.2 Pseudocritical line PCL in a P - T diagram.

It is seen that the pseudocritical temperature increases with increasing pressure. At a pressure of 25 MPa the pseudocritical temperature is 384°C. The specific heat at the critical point is as high as 5600 kJ/kg K, which is more than 1000 times higher than that at room temperature. Near the pseudocritical line the density decreases dramatically. There exists a large peak of the thermal expansion coefficient, which behaves very similar to the specific heat. Thermal conductivity decreases with increasing temperature. It shows, however, a local maximum near the pseudocritical point. Beyond the pseudocritical temperature thermal conductivity decreases sharply. Similar behavior shows also the dynamic viscosity. Due to the sharp increase in specific heat capacity, there exists a large peak of the Prandtl number at the pseudocritical point.

It has been found that near the critical point, thermal-physical properties obtained from different sources might deviate strongly from each other, especially as related to specific heat and thermal conductivity. This is due to the steep variation of the fluid properties, leading to a less accurate interpolation and a lower measurement accuracy. A comparison between two water-steam tables in use at EDF has shown a deviation of up to 35% for thermal conductivity and up to 10% for heat capacity at a condition close to the critical point. If the physical properties are showing these types of deviations, the physical parameters, which describe certain PH, for example, HT coefficient will also show some calculated differences. Consequently, it is important to use the same or at least similar steam tables for the application and use of different computer codes within a design or safety-related project, when analysis work is performed.

Based on the experience gained and the critical review performed during the HPLWR project, it was recommended that the steam tables of IAPWS-97 and IAPWS-95, whichever relevant was well accepted by international institutions and, therefore, should be taken as reference. Due to the large expenditure needed for the

implementation of such a steam table into the existing codes, it is not required to use unique steam table for each of the code, but the deviation (compared to IAPWS-97, respectively to IAPWS-95) of the steam tables used should be clearly indicated. The International Association for the Properties of Water and Steam (IAPWS) is an international, nonprofit association of national organizations concerned with the thermo-physical properties of water and steam, particularly those properties of high temperature steam, water, and aqueous systems that are relevant to thermal power cycles and other industrial applications. The IAPWS released its formulation for general and scientific use in 1995. IAPWS-95 is a state-of-the-art accurate representation and covers the entire range of light water properties (Wagner and Kruse, 1997). At the limit boundaries, ideal gas behavior is satisfied and at the other “residual” behavior.

6.6.2 Critical flow during depressurization from supercritical conditions

Critical flow is defined as the maximum flow that can pass through an opening for a given thermodynamic condition. Under this definition, numerous different configurations are possible: orifices or long tubes, single-phase flow or two-phase flow, rough or smooth tubes, sharp or round entrances, etc. All of these configurations affect the flow in their own manner and thus have to be characterized upon the specific application, in this case, an LOCA of a SCWR.

When a fluid discharges from a high pressure and high temperature system, a “choking” or critical condition occurs, and the flow rate no longer increases as the downstream pressure is further decreased. During a postulated LOCA of a PWR the break flow will be subject to this condition (see Section 6.3.2 for details). An accurate amount of the critical flow rate is important for the evaluation of the reactor safety, because this flow rate controls the loss of coolant inventory and energy from the system, and thus has a significant effect on the accident consequence. A depressurization event or LOCA is particularly of a concern for the SCW reactor safety due to the lower coolant inventory compared to a typical PWR for the same power output. This lower coolant inventory would result in a faster transient response of the reactor dominated by the discharge flow rate. Critical flow is coupled with drastic depressurization and vaporization, and the flow rate is heavily dominated by the vapor content or quality of the vapor, which is closely related with the onset of vaporization and the interfacial interaction between phases. This presents a major challenge for the estimation of the flow rate due to the lack of the knowledge on those processes, especially under the conditions of interest for the SCWR. High pressure depressurization leading to

critical flow has been investigated extensively, in both experimental and theoretical ways. These studies have mostly been conducted with subcritical pressure or ideal gases well above the vapor dome, as presented in number of comprehensive reviews. Selected examples of these reviews can be given as in Levy et al. (1982) and Lee and Swinnerton (1983), and Saha (1978), but little work has been done near or above the thermodynamic critical point. To the author's knowledge, the available experimental data for SCW are those obtained by Lee and Swinnerton (1983) at a maximum temperature of 402°C and by Chen with a maximum temperature of 474°C (Chen et al., 2009). Based on the limited data of supercritical fluids, the critical flows at conditions above the pseudocritical point seem to be fairly stable and consistent with the subcritical HEM predictions. Further, in this regime the flows tend to be lower than those in the two-phase region. Thus the major difficulty in the prediction of the depressurization flow rate remains in the region where two phases coexist, that is, within the two-phase portion of the vapor dome. In this region, the flow rate is strongly affected by the nozzle geometry and tends to be unstable. Various models for this region have been developed with different assumptions, for example, the HEM and Moody model (Moody, 1965), and the Henry-Fauske nonequilibrium model (Henry and Fauske, 1971) are currently used in subcritical pressure reactor safety design (Ardron and Furness, 1976). It appears that some of these models could be reasonably extended to above the thermodynamic pseudocritical point. The more stable and smaller flow observed in conditions above the pseudocritical point suggests that even though SCWR designs have a smaller coolant inventory, the safety implications of an LOCA and the subsequent depressurization from supercritical conditions may not be as severe as expected and the limiting accident scenario may be driven by the critical flow within the subcritical pressure region.

6.6.3 Pressure loss characteristics of SCW

Pressure losses in the heat transport system have a direct impact on the pump capacity and the power output, affecting the capital and operating costs. In addition, these losses affect the local flow conditions along the fuel assembly impacting the HT characteristics. Depending on the design, the pressure loss components consist of frictional loss, form losses (such as valves and elbows), head loss due to gravity, and loss due to acceleration. A significant portion of the overall pressure loss occurs in the core region (particularly over the bundle assembly). Therefore, it is important to evaluate the core pressure loss accurately (see also Sections 6.3.1.7 and 6.3.1.8).

6.6.4 HT characteristics of SCW

In supercritical fluids, the properties change rapidly with the temperature, especially in the pseudocritical region. Here, the local HT coefficient varies significantly, depending on flow conditions and the value of the heat flux. Effect of heat flux, together with the thermo-physical properties variations needs to be understood, based on experimental, numerical, and theoretical data available in order to be able to predict the onset of heat transfer deterioration (HTD).

As already indicated in Section 6.6.1, a large variation of thermal physical properties occurs near the pseudocritical line. This would lead to a strong variation in HT coefficient. Just considering simply for single-phase steam flow near and at supercritical conditions, the Dittus-Boelter equation gives at the pseudocritical point ($T=384^{\circ}\text{C}$) a HT coefficient of about $40 \text{ kW/m}^2\text{K}$, more than twice of that at low temperature (e.g., 300°C) and five times of that at high temperature (e.g., 500°C). This shows clearly that due to the variation in thermal physical properties, HT coefficient varies strongly near the pseudocritical line. The closer the pressure to the critical point is, the higher is the peak of the HT coefficient.

As indicated and agreed in the open literature, the actual HT coefficient deviates from the Dittus-Boelter equation, especially near the pseudocritical line. At low heat fluxes, HT coefficient is higher than the values predicted by Dittus-Boelter. This PH is called HT enhancement. At high heat fluxes the HT coefficient is lower than that computed by the Dittus-Boelter equation. At a low heat flux the wall temperature behaves smoothly and increases with increasing bulk temperature. The difference between the wall and the bulk temperature remains small. At a high heat flux a similar behavior of the wall temperature is expected, except for the bulk temperature approaching the pseudocritical value. In this case a sharp increase in the wall temperature can occur. The wall temperature decreases again, when the bulk temperature exceeds the pseudocritical value. This large increase in the wall temperature is referred to *heat transfer deterioration*. In the literature there is still no unique definition for the onset of HTD, because the reduction in HT coefficient, or the increase in the wall temperature behaves rather smoothly, compared to the behavior of the boiling crisis at which a much sharper increase in the wall temperature takes place.

6.6.5 Reflooding for tight lattice geometry at low pressure

The concept and also the geometric arrangement of HPLWR core, as example of SCWRs, differs drastically from conventional LWR concepts by the use of SCW to achieve higher core outlet temperatures. The fuel assembly design examples are based on tight lattice geometry and also have different configurations (Hofmeister et al., 2005). Considering these types of fuel assembly arrangements, tight lattice geometry and special arrangements of fuel rods is considered to be a solution. In general, quenching and rewetting phenomena process defined and described in Sections 6.3.13.1 and 6.3.13.2 for SET is valid also for tight lattice geometries. But it has to be considered that specific reflooding modeling and experiments are needed for selected geometrical consideration.

6.6.6 Boil-off for tight lattice geometry at low pressure

As already mentioned and considered in Section 6.6.6, CHF and post-CHF HT phenomena defined for SET in Sections 6.3.12.3–6.3.12.5 are valid also for tight-lattice geometries. But it has to be considered that specific CHF and post-CHF HT models and experiments are needed for selected geometrical consideration.

6.6.7 Instability and NC in supercritical pressure systems

The design of SCW-cooled reactors poses new challenges in relation to the prediction of some basic phenomena, whose characteristics are relatively well known at subcritical pressure. In particular, stability and NC phenomena observed in single-phase conditions at subcritical pressures become more complex at supercritical pressures because of the strong variability of thermodynamic and thermophysical properties. Moreover, categories adopted for dealing with two-phase flow phenomena must be updated to deal with supercritical pressure flow regimes, having in principle a simpler structure than the corresponding two-phase flow ones, though they anyway involve uneven distributions of lighter and heavier fluids within the channel cross-section. Flow instabilities and NC, being dealt with in this section, have been the subject of major experimental and modeling efforts at subcritical pressures. Some of these studies belong to both aspects, since a quite populated intersection of the two categories is represented by the interesting domain of NC instabilities. In single-phase flow, in particular, apart from turbulence and acoustic effects, which are beyond the scope of this section, instabilities mainly occur in NC systems, being driven by a mechanism explained with effective elementary arguments by Welander in 1967 (Welander, 1967). In that work, it was suggested that pockets of fluid with perturbed temperature may

emerge from the heat source and/or the sink, affecting the fluid residence time along the loop and being damped or amplified as a consequence of the subsequent passages through the heater and the cooler. This mechanism was proposed on the basis of numerical computations and was confirmed later on by further experimental and computational studies, focusing on different interesting aspects affecting the PH (see, e.g., Creveling et al., 1975). A remarkable feature of the observed behavior is its chaotic character, mainly caused by the fact that the growth of flow perturbations frequently leads to flow reversal; as a consequence, the system is seen to continuously switch from clockwise to counterclockwise flow directions and vice versa, showing a high sensitivity to initial conditions. Two-phase flow instabilities are mainly connected with the behavior of boiling channels that are recognized to be susceptible to different instability mechanisms, having a “static” or a “dynamic” nature (see, e.g., Lahey and Moody, 1993). The discrimination among the two categories of instabilities is introduced considering whether their occurrence can be explained on the basis of the static internal PD versus flow characteristic of the system. The Ledinegg “excursive” instability mechanism (Ledinegg, 1938) is representative of the category of static instabilities, while density wave, PD oscillations and thermal oscillations are mechanisms which belong to the second category. Of these instabilities, density waves represent the most relevant instability mechanism for nuclear reactor applications since, in combination with neutronic feedback, it is responsible for observed space and time oscillations of BWR core power. These instabilities have been the subject of extensive studies, summarized in review papers and SOARs (March-Leuba and Rey, 1993). Basic experimental investigations (see, e.g., D’Auria et al., 1997) allowed grasping the main features of involved phenomena, gaining the basic understanding necessary for analytical developments. An interesting body of information about reactor plant events is also available (see D’Auria et al., 1997). Models for predicting the unstable behavior of boiling systems have been set up and qualified by applications ranging from the scale of experimental facilities to the full reactor scale (see, e.g., D’Auria et al., 1997). Both time-domain (i.e., transient) and frequency-domain (i.e., linearized) models are available to estimate the stability thresholds of even very complex systems. NC phenomena have also been thoroughly studied at subcritical pressures, both in single- and two-phase flow conditions. The relevance of this PH for nuclear reactors is well known, since NC involves several regimes of reactor operation. As previously mentioned, NC and stability phenomena have an extensive intersection in single- and two-phase flows. A limited list of relevant aspects relating NC at subcritical pressures is reported hereafter:

- Different single- and two-phase NC modes appear during start-up, under normal

operating conditions and postulated LWR accidents, as observed in experiments and code predictions (see, e.g., D'Auria and Frogheri, 2002).

- NC is relied upon for decay heat removal from the nuclear reactor core and/or the containment system; in particular, passive decay heat removal by NC represents one of the most important features in advanced (Gen III) and innovative (Gen IV) reactors.
- Different modes of flow instabilities are recognized in NC boiling systems, adding additional phenomena to be addressed to those already observed in boiling channels (see, e.g., D'Auria and Frogheri, 2002).
- The vast body of information from experimental and theoretical researches on stability and NC performed at subcritical pressures constitutes a useful background also for SCW reactor applications, at least in view of two main aspects.
- The knowledge acquired on fundamental phenomena can be helpful in supporting the new developments required for supercritical pressure conditions, provided that analogies and differences between the two operating regions (subcritical and supercritical) are properly identified.
- Part of the operational and perturbed evolution of SCW reactors will occur at subcritical pressures, directly involving operating conditions for which previous knowledge is immediately applicable.

In particular, stability has been addressed as an issue of great importance for SCWR design, owing to the fact that heated channels with supercritical pressure fluids are assumed to be susceptible to similar instability phenomena as observed in boiling channels. In fact, the transition across the pseudocritical temperature can be considered as a sort of “pseudoboiling” PH, leading to denser fluid at channel inlet and lighter one at the outlet. This is one of the reasons why the basic understanding and the numerical tools developed for two-phase flow instabilities are found immediately available for being converted for supercritical pressure instabilities. The scarcity of relevant experimental data on instabilities in supercritical pressure systems is presently a problem to be coped with in order to ascertain that this process of knowledge transfer from one research field to another is made without forgetting any important difference. On the other hand, NC at supercritical conditions has been the subject of a number of experiments performed in past and recent times. Experimental facilities working at supercritical pressures, in particular, sometimes made use of NC even when the primary focus was on different aspects (e.g., HT). However, in these cases their data on NC may be

insufficiently detailed to allow for meaningful analytical conclusions. Though relevant experiments and modeling tools are already available in this field, there is still the need for further understanding and specific assessment.

6.7 Conclusions

The knowledge of thermal-hydraulic phenomena is the backbone and essential element for the development of nuclear thermal-hydraulics subject area. Consequently, thermal-hydraulic phenomena have been collected from OECD/NEA-CSNI and IAEA activities which were covering design basis accidents or courses of events “before loss of core integrity” for LWRs, AWCs, and SCWRs. The same phenomena may be important in different evolutions for single- and two-phase flows. This collection of phenomena can be used to prove the applicability and quality of best-estimate thermal-hydraulic system computer codes.

In this chapter, about 12 water cooled reactor designs were considered. These are being PWR-U-tube steam generator, PWR-once-through steam generator, PWR-horizontal steam generator (VVER-440 and VVER-1000), BWR, AP1000, APR1400, EPR, ESBWR, ABWR, small modular reactors (e.g., SMART, MASLWR CAREM), and SCWR.

The phenomena are identified from experiments and through the expertise of the international experts who were involved in the various related activities. The results of the work performed covers at least about 40 years of activity performed at different times within OECD/NEA-CSNI and IAEA. List of tables including thermal-hydraulic phenomena is applicable to the entire class of light water cooled reactors (LWRs). All identified phenomena should be modeled according to the state of the art knowledge. System thermal-hydraulics codes constitute the source of expertise associated with considered phenomena and the best and unique tool to calculate accident scenarios, including the course of events. In addition, these best estimate computer codes are the depository of the collected knowledge with all available elements, models of the phenomena, experiments for validation, etc.

Comprehensive experimental and code development research activities have been conducted, also very intensely at an international level, in the past three to four decades in relation to the understanding of thermal-hydraulic phenomena and for establishing related code predictive capabilities for existing nuclear power reactors. In the same context, research activities also addressed some of the phenomena for passive systems and also for SCWRs. However, a systematic effort for evaluating the level of understanding of thermal-hydraulic phenomena for passive systems

and also for supercritical water conditions with connected code capabilities appears to be limited and in general lacking.

The knowledge and the understanding of phenomena is a prerequisite for performing meaningful accident analysis. The presented information can be used as part of the qualification process for system code calculations.

References

- Aksan, N., D'Auria, F., 1996. Relevant thermal hydraulic aspects of advanced reactor design – status report. OECD/NEA Report, NEA/CSNI/R (96)22, Paris.
- Aksan, S.N., Modro, S.M., Berta, V.T., Wahba, V.T., 1989. Review of LOFT large break experiments. US NRC Report, NUREG/IA-0028.
- Aksan, N., D'Auria, F., Glaeser, H., Pochard, R., Richards, C., Sjöberg, A., 1994. Separate effects test matrix for thermal-hydraulic code validation. (a) Volume I: phenomena characterisation and selection of facilities and tests, (b) Volume II: facility and experiment characteristics. OECD/NEA Report, NEA/CSNI/R (93)14/Part 1 and Part 2, Paris.
- Aksan N., Schulenberg T., Squarer D., Cheng X., Struwe D., Sanchez V., Dumaz P., Kyrki-Rajamaki R., Bittermann D., Souyri A., Oka Y., Koshizuka S. *Potential safety features and safety analysis aspects for high performance light water reactor (HPLWR)*. In: Int. Conf. on Global Environment and Advanced Nuclear Power Plants (GENES4/ANP2003), Kyoto, Japan; 2003.
- Aksan S.N., Ambrosini W., Ammirabile L., Anderson M., Bae Y.Y., Chen Y., Churkin A., Hanninen M.J., Jackson J.D., Kirillov P.L., Leung L., Novog D., Pioro I., Razumovskiy V., Vijayan P., Xiaojing L., Yamada K. *Heat Transfer Behavior and Thermo-Hydraulics Code Testing for Supercritical Water Cooled Reactors (SCWRs)*. Vienna, Austria: IAEA; 2014 IAEA-TECDOC-1746.
- Ambrosini W., D'Auria F., Grassi W., Vigni P. *Accuracy in the prediction of two-phase flow regimes*. In: Eurotherm Sem. No. 3: Modeling of Nuclear and Advanced Heat Transfer Components,

Bologna, Italy, June 14–15; 1988.

Annunziato, A., Glaeser, H., Lillington, J., Marsili, P., Renault, C., Sjöberg, A., 1996. CSNI integral test facility validation matrix for the assessment of thermal-hydraulic codes for LWR LOCA and transients. OECD/NEA Report, NEA/CSNI/R (96)17, Paris.

Ardron K.H., Furness R.H. A study of the critical flow models used in reactor analysis. *Nucl. Eng. Des.* 1976;39:257–266.

Bankoff S.G., Lee S.C. A brief review of countercurrent flooding models applicable to PWR geometries. *Nucl. Saf.* 1985;26(2):139–152.

Bankoff S.G., Lee S.C. A critical review of the flooding literature. In: Hewitt G.F., Delhay J.M., Zuber N., eds. *Chapter 2 Multiphase Science and Technology*. New York, NY: Hemisphere Publishing Corporation; 1986.

Bittermann D., Squarer D., Schulenberg T., Oka Y. *Economic prospects of the HPLWR*. In: Int. Conf. GENES4/ANP2003, Paper 1003, Kyoto, Japan; 2003.

Bittermann D., Starflinger J., Schulenberg T. *Turbine technologies for high performance light water reactors*. In: Proceedings of ICAPP Conf., Paper 4195, Pittsburgh, PA, USA; 2004.

Brittain, I., Karwat, H., D'Auria, F., Vigni, P., Hall, D.G., Reocreux, M., 1982. CSNI critical flow modelling in nuclear safety. NEA/OECD Report (CSNI Report No. 4), ISBN 92-64-12366-0, Paris, France, November.

Chen Y., Yang C., Zhang C., Zhao M., Du K. *An experimental study of critical flow of water under near-critical and supercritical pressures*. In: Presented at the 13th International Topical Meeting on Nuclear Reactor Thermal Hydraulics (NURETH-13), N13P1048, Japan; 2009.

Comolet R. *Mécanique Expérimentale des Fluides, Bd. 2:*

Dynamique des Fluides Réels. Paris, France: Masson; 1976.

Creveling H.F., De Paz J.F., Baladi J.Y., Schoenals R.J. Stability characteristics of a single-phase free convection loop. *J. Fluid Mech.* 1975;67(1):65–84.

Damerell, P.S., Simons, J.W. (Eds.), 1993a. 2D/3D Program work summary report. International Agreement Report, USNRC NUREG/IA 0126, Washington, DC, USA.

Damerell, P.S., Simons, J.W. (Eds.), 1993b. Reactor safety issues resolved by the 2D/3D program. International Agreement Report, USNRC NUREG/IA 0127, Washington, DC, USA.

D'Auria, F. (Ed.), et al., 1997. State-of-the-Art Report on Boiling Water Reactor Stability. NEA/CSNI/R(96)21, OCDE/GD(97)13, OECD/NEA Paris, 1997.

D'Auria F., Frogheri M. Use of a natural circulation map for assessing PWR performance. *Nucl. Eng. Des.* 2002;215:111–126.

D'Auria F., Galassi G.M. Characterization of instabilities during two-phase natural circulation in PWR typical conditions. *Exp. Therm. Fluid Sci.* 1990;3:90.

D'Auria, F., Vigni, P., 1980. Two-phase critical flow models. CSNI Report No. 49, Paris, France, May.

D'Auria F., Debrecin N., Galassi G.M., Galeazzi S. Application of RELAP5/MOD3 to the evaluation of loss of feedwater in test facilities and in nuclear plant. *Nucl. Eng. Des.* 1993;141(3).

Delhaye J.M., Giot M., Riethmuller M.L., eds. *Thermal-Hydraulics of Two Phase Systems for Industrial Design and Nuclear Engineering*. Washington, DC: McGraw Hill; 1981.

Dix G.E. *BWR loss of coolant technology review*. In: 2nd Int. Top. Meeting on Nuclear Reactor Thermalhydraulics, Santa Barbara, CA, USA, January 11–14; 1983.

Fletcher, C.D., Schultz, R.R., 1992. RELAP5/MOD3 Code

Manual: User's Guidelines. EGG-2596, USNRC NUREG/
CR-5535, Vol. 5, Washington, DC, pp. 5-7-5-8.

Forge, A., Pochard, R., Porraccia, A., Miro, J., Sonnenburg, H.G., Steinhoff, F., Teschendorff, V., 1988. Comparison of thermal-hydraulic safety codes for pwr systems. Gesellschaft für Reaktorsicherheit GmbH (GRS), Federal Republic of Germany, CEC Report EUR 11522, Graham & Trotman.

Glaeser, H., 1990a. Post test calculations of UPTF test 12 with the advanced computer code TRAC-PF1/MOD1. GRS-A-1 727, Garching, Germany.

Glaeser, H., 1990b. Post test calculation of UPTF test 13 with the advanced computer code TRAC-PF1/MOD1. GRS-A-1 728, Garching, Germany.

Glaeser H. Downcomer and tie plate countercurrent flow in the upper plenum test facility (UPTF). *Nucl. Eng. Des.* 1992;113:259-283.

Govier G.W., Aziz K. *The Flow of Complex Mixtures in Pipes*. New York: Van Nostrand Reinhold Company; 1976.

Hafner W., Fischer K. Contact condensation effects in the main coolant pipe. In: Krischer W., ed. *Reactor Safety Research – The CEC Contribution*. London: Elsevier Applied Science; 1990:197-206.

Henry R.E., Fauske H.K. The two-phase critical flow of one-component mixtures in nozzles, orifices, and short tubes. *ASME Trans. C, J. Heat Transf.* 1971;93(2):179-187.

Hewitt G.F. *Countercurrent two-phase flow*. In: Hewitt G.F., ed. Proc. 4th Int. Topical Meeting on Nuclear Reactor Thermal-Hydraulics (NURETH-4), Vol. 2, Karlsruhe, Germany; 1989.

Hofmeister J., Schulenberg T., Starflinger J. *Optimization of a fuel assembly for a HPLWR*. In: Proc. of ICAPP'05, Paper No. 5077, Seoul, Korea; 2005.

Holmes, B.J., Allen, E.J., 1990. A review of critical flow data

for pressurized water reactor safety studies. AEEW-R 2592, Winfrith, UK.

Hsu Y.Y., Graham R.W. *Transport Processes in Boiling and Two-Phase Systems*. Chicago, IL: ANS Publisher; 1986.

Hyvarinen J. *An inherent boron dilution mechanism in pressurized water reactors*. In: CSNI Specialist Meeting on Transient Two-Phase Flow, OECD/NEA/CSNI, Aix-en-Provence, France; 1992.

IAEA. *Safety Related Terms for Advanced Nuclear Plants*. Vienna, Austria: IAEA; 1991 IAEA-TECDOC-626.

IAEA, Aksan (Chairman of CRP) N. *Thermo-Hydraulic Relationships for Advanced Water Cooled Reactors*. Vienna, Austria: IAEA; 2001 IAEA-TECDOC-1203.

IAEA, Aksan (Chairman of the Technical Meeting) N. *Experimental Tests and Qualification of Analytical Methods to Address Thermo-hydraulic Phenomena in Advanced Water Cooled Reactors*. 2000 IAEA-TECDOC-1149, Vienna, Austria.

IAEA, Aksan (Chairman of CRP) N. *Natural Circulation in Water Cooled Nuclear Power Plants: Phenomena, Models, and Methodology for System Reliability Assessments*. 2005 IAEA-TECDOC-1474, Vienna.

IAEA, Aksan (Chairman of CRP) S.N. *Heat Transfer Behaviour and Thermohydraulics Code Testing for Supercritical Water Cooled Reactors (SCWRs)*. 2014 Vienna, Austria, IAEA-TECDOC-1746. See also Aksan et al., 2014, above.

Jacobson, S., 1992. Risk evaluation of local dilution transients in a pressurized water reactor. Division of Energy Systems, Dept. of Mechanical Engineering, Dissertation No. 275, Linköping, Sweden.

Lahey R.T., Moody F.J. *The Thermal-Hydraulics of a Boiling Water Reactor*. American Nuclear Society; 1993.

Ledinegg M. Instability during Natural and Forced Circulation. *Die Wärme*. 1938;vol. 16.

- Lee, D.H., Swinnerton, D., 1983. Evaluation of critical flow for supercritical steam-water. NP-3086.
- Levy, S., Abdollahian, D., Healzer, J., et al., 1982. Critical-flow data review and analysis. EPRI-NP-2192.
- Lewis, M.J.† (Ed.), Pochard, R., D'Auria, F., Karwat, H., Wolfert, K., Yadigaroglu, G., Holmstrom, H.L.O. (Lead Authors), 1989. Thermohydraulics of emergency core cooling in light water reactors – a state-of-the-art report. OECD-NEA-CSNI Report No. 161, Paris, France.
- Liesch, K., Réocreux M., 1995. Concerted Actions on Safety Research for WWER Reactors: Verification Matrix for Thermal-hydraulic System Codes Applied for WWER Analysis. Common Report IPSN/GRS No. 25, Paris-Garching (France and Germany).
- Macken, N.A., 1990. Momentum effects on countercurrent flow in a horizontal pipe with saturated conditions. Siemens Work Report 4200 90/09, Erlangen, Germany.
- March-Leuba J., Rey J.M. Coupled thermo-hydraulic-neutronic instabilities in boiling water nuclear reactors: a review of the state of the art. *Nucl. Eng. Des.* 1993;145:97–111.
- Moody F.J. Maximum flow rate of a single component, two-phase mixture. *ASME Trans. C, J. Heat Transf.* 1965;87(1):134–142.
- MPR Associates, 1990. Summary of results from the UPTF downcomer separate effects tests, comparison to previous scaled tests and application to U.S. pressurized water reactors. MPR-1163, USA, July.
- Mullen, E., Stumpf, H.J., Siebe, D.A., 1992. Summary of downcomer injection phenomena for UPTF and TRAC posttest analyses. Los Alamos National Laboratory document LA-CP-92-188, Los Alamos, NM, USA.
- OECD/NEA, 1987. CSNI code validation matrix of thermal-

hydraulic codes for LWR LOCA and transients. OECD-NEA-CSNI Report No. 132, Paris.

OECD/NEA, 1989. State of the art report (SOAR) on thermal-hydraulics of emergency core cooling in light water reactors. OECD-NEA-CSNI Report No. 161, Paris.

OECD/NEA and A Report by OECD Support Group, 2001. Validation matrix for the assessment of thermal-hydraulic codes for VVER LOCA and transients. NEA/CSNI/R (2001) 4, Paris, France.

OECD/NEA/CSNI, 1982. CSNI State of the Art Report on Critical Flow Modelling in Nuclear Safety. CSNI SOAR No. 4.

OECD/NEA/CSNI. In: USNRC and CSNI International Workshop on Boiling Water Reactor Stability, Brookhaven, October 17–19; 1990 CSNI Report 178, Paris, France.

Riegel, B., 1990a. Post test calculation of UPTF test 8 with the advanced computer code TRAC-PF1/MOD 1. GRS-A-1666, Garching, Germany.

Riegel, B., 1990b. Post test calculation of UPTF test 9 with the advanced computer code TRAC-PFI/Mod 1. GRS-A-1738, Garching, Germany.

Rohatgi, U.S., Neymotin, I.Y., Jo, J., Wulff, W., 1990. Bias in peak clad temperature predictions due to uncertainties in modelling of ECC bypass and dissolved non-condensable gas phenomena. Brookhaven National Laboratory, USNRC NUREG/CR-5254, Washington, DC, USA.

Saha, P., 1978. A review of two-phase steam-water critical flow models with emphasis on thermal non-equilibrium. BNL-NUREG-50907.

Siebe, D.A., Stumpf, H.J., 1990. Posttest analysis of the upper plenum test facility downcomer separate effects tests with TRAC-PF1/MOD2. Los Alamos National Laboratory, LA-CP-90-299, Los Alamos, NM, USA.

Sonnenburg, H.G., 1990. Analysis of UPTF-test 26 run 230 by ATHLET-code with full-range drift flux model. GRS-A-1 723, Garching, Germany.

Squarer D., Schulenberg T., Struwe D., Oka Y., Bittermann D., Aksan S.N., Maraczy C., Kyrki-Rajamäki R., Souyri A., Dumaz P. High performance light water reactor. *Nucl. Eng. Des.* 2003;222:167–180.

Sun H. *Flooding correlations for BWR bundle upper tie plate and side-entry orifices*. In: Second Multi-Phase Flow and Heat Transfer Symposium Workshop, Miami Beach, FL, USA; 1979.

US NRC, 1987. Compendium of ECCS research for realistic LOCA analysis. US NRC Report NUREG-1230, Washington, USA.

Wagner W., Kruse A. *The Industrial Standard IAPWS-IF97 for the Thermodynamic Properties and Supplementary Equations for Other Properties – Properties of Water and Steam*. Heidelberg, Germany: Springer-Verlag; 1997.

Welander P. On the oscillatory instability of a differentially heated fluid loop. *J. Fluid Mech.* 1967;29(1):17–30.

Wilson G.E., Boyack B.E., Catton I., Duffey R.B., Griffith P., Katsma K.R., Lellouche G.S., Levy S., Rohatgi U.S., Wulff W., Zuber N. Quantifying reactor safety margins part 2: characterization of important contributors to uncertainty. *Nucl. Eng. Des.* 1990;119(1):17–31.

Wolfert, K., Frisch, W., 1983. Proposal for the formulation of a validation matrix. OECD/NEA-CSNI-SINDOC (83) 117, Paris, France.

Yadigaroglu, G., Andreani, M., Aksan, S.N., Analytis, G.Th., Lubbesmeyer, D., Olek, S. 1990. Modelling of thermohydraulic emergency core cooling phenomena. Labor für Thermohydraulik, Paul Scherrer Institut, PSI Report No. 27, Wurenlingen.

Part Three

Nuclear thermal hydraulics modeling

Heat transfer in nuclear thermal hydraulics

*P.L. Kirillov**; *H. Ninokata†* · *Institute of Thermal Physics and Nuclear Science in the State Scientific Centre of the Russian Federation, Obninsk, Russia*
† Tokyo Institute of Technology, Tokyo, Japan

Abstract

Power removal capability from structures housing the nuclear fuel is determined by heat transfer. Convection heat transfer in two-phase conditions sets the limits for the production of fission power. The amount of thermal power per unit area exchangeable from a solid to the two-phase mixture may suddenly change for two or three orders of magnitude (even more in certain conditions) when parameters like void fraction of fluid velocities reach some threshold values. Failures of safety barriers in transient condition can also be associated with step variations of heat transfer. The importance of heat transfer in nuclear thermal hydraulics is depicted by previous statements: this is the motivation for the chapter. The complexity of heat transfer mechanisms, involving the description of related features, is the key message expected for the reader from the present chapter.

Keywords

Heat transfer; Convection; Conduction; Radiation; Reflood; Critical heat flux; Condensation; Droplet cooling; Film boiling; Nucleate boiling

Nomenclature

a thermal diffusivity, m^2/s ; the
sound velocity, m/s ; eccentricity, m ;
gas absorption coefficient

A cross-section area of the channel,
 m^2 ; absorbance

c speed of light, m/s

c_p specific heat, $\text{J}/(\text{kg K})$

D diameter (shell), m ; fuel rod
diameter, m ; transmittance

d diameter (pipe), m

f frequency, s^{-1}

g gravitational acceleration, m^2/s

G mass flux ($=\rho w$, kg/m²/s) or mass flow ($=\rho wA$, kg/s)

h height (ribs, channel, etc.), m;
enthalpy, kJ/(kg)

j volumetric flux, m/s

L, l length, m

m volume porosity; added mass, kg

M mass, kg

n number of tubes, ribs, pumps, ..., etc.

q' linear heat rate, W/m

q* or *q'' heat flux, W/m²

q_v or q''' volumetric power density,
W/m₃

Q volumetric flow, m₃/s; total
energy, kJ

p pressure, Pa

P wetted perimeter, m; fuel rod
pitch, m

r, R radius, m

R thermal resistance, (m²K)/W;
reflectance; gas constant

s spacing, m (of rod or pipe
arrangement); slip ratio; cross
sectional area, m²

T temperature, K

ν specific volume, m^3/kg

V volumetric flow, m^3/s

w velocity, m/s

x vapor quality (static; flowing); also relative enthalpy

Z axial coordinate

Greek symbols

α Heat transfer coefficient, $\text{W}/(\text{m}^2\text{K})$; kinetic energy coefficient

β thermal expansion coefficient ($1/\text{K}$); angle; condensation coefficient

δ thickness; height roughness, m

Δ equivalent roughness, m

Δh_{fg} latent heat (heat of evaporation), J/kg

ζ local resistance coefficient

ε emissivity

η efficiency, coefficient of performance

Θ ratio (R_1/R_2 ; d_1/d_2 ; T_w/T_0)

λ thermal conductivity, W/(m K);
wave length, m

μ viscosity, Pa s

ν kinematic viscosity, m^2/s ;
frequency of light, 1/s

ρ density, kg/m^3

σ surface tension, N/m^2

σ_0 Stefan-Boltzmann constant, $\text{W}/(\text{m}^2\text{K}^4)$

τ shear stress, N/m^2 ; time, s

φ vapor volumetric fraction (void fraction); angle

ψ coefficient of two-phase flow inhomogeneity

ξ accommodation constant (defined by Eq. (7.114))

ω cross-sectional area, m^2 ; angular frequency ($2\pi f$), $1/\text{s}$

Subscripts/Superscripts/

Indices

0 black body

c convection

g gas (vapor-phase)

ib, ob onset boiling, boiling
beginning

max maximum

min minimum

r, R radiation

S, sat saturation or saturated

sub subcooled

v vapor

λ conduction

+ nondimensional quantity

av average

f fluid (liquid-phase)

hn homogeneous nucleation

in entrance

MFB minimum film boiling

out exit

red reduced

s surface

T turbulent

W wall; condensate film surface

— averaging sign (over-bar)

Acknowledgments

The current chapter is based on Chapters 5, 6, 7, 11, 12, and 13 of the book “Handbook On Thermohydraulics Calculations In Nuclear Power Engineering, Vol. I,” by PL Kirillov, VP Bobkov, AV Zhukov and Yuriev Y, IzdAT, Moscow (2010) under the general editorship of one of the two authors.

The authors acknowledge the help of Dr. G. Bogoslovskaya in translating Russian text into English and that, without her help, this chapter was not possible. Also noting the original book was contributed by many colleagues in the thermal hydraulics community in Russia, the authors express sincere gratitude to the staff of thermal and other departments IPPE, Obninsk Institute of Atomic Energy—National Nuclear University (MEPhI) whose research results are reflected.

Chapter foreword

In recent years, there is a tendency to use the numerical experiment in connection to the rapid development of computer technology. Admit that it is a right direction to pursue, it does not relieve engineers totally from a deep understanding of the physical processes, for “a correct statement of the problem—half the solution.” Many try to solve the problems of computational methods, no experimental work. Quality of Direct Numerical Simulation (DNS) is almost equivalent to experiment. However DNS requires by far more computing resources and speed than available even in the near future. Other computational approaches than DNS require physical models that must be constructed based on experimental information. Here, caution is needed. Once Einstein said that *Mathematics are well and good but nature keeps dragging us around by the nose*. One can fairly accurately carry out all the calculations and their results will be different from what happens in the

experiments, not by 5% or 10%, but 100%. But the theoretician can be led by the nose for only himself alone, and in engineering world, we are talking to hundreds and thousands people to construct nuclear power plants! The expression by Pyotr L. Kapitsa “Experiment is forever!” fits in our thermal hydraulics perfectly.

Another trend of the modern approach to the design of advanced nuclear power—the transition from the calculation of average values for local, which is particularly important when designing intense nodes of the reactor core, steam generators, heat exchangers (Schlünder et al., 1983). This requires detailed knowledge of distributed parameters, detailed coolant flow and temperature distributions, the surface temperature distribution, and uncertainties to consider the account for possible deviations from the calculated actual values. Such an idea is constantly being implemented and put into practice guide authors.

In the preparation of the manuscript, data are based on not only known and proven works, reference books, but information available from the scientific and technological IAEA reports, international conferences, scientific information databases leading domestic and foreign organizations. While at the end of this chapter is a list of reference sources, useful reference books, and reports in connection to Part I are listed here.

General:

Birds, R.B., Stewart, W.E., Lightfoot, E.N., 2007. Transport Phenomena, second ed. John Wiley & Sons, Inc., New York.

Todreas, N.E., Kazimi, M.S., 2012. Nuclear Systems—I. CRC Press, Taylor & Francis.

Heat conduction:

Berman, B.R., 1976. Thermal Conduction in Solids. Oxford University Press, New York.

Grimvall, G., 1999. Thermophysical Properties of Materials. Enlarged and revised ed. Elsevier.

Chaikin, P.M., Lubensky, T.C., 1995. Principles of Condensed Matter Physics. Cambridge University Press.

Carslaw, H.S., Jaeger, J.C., 1959. Conduction of Heat in Solids, second ed.

Clarendon Press, Oxford, UK.

Schneider, P.J., 1973. Conduction. In: Rohsenow, W.H., Hartnett, J.P. (Eds.), Handbook of Heat Transfer. McGraw-Hill Book Co.

Convective heat transfer:

Kaviany, M., 2001. Principles of Convective Heat Transfer, second ed. Springer.

Kays, W.M., Crawford, M.E., 1993. Convective Heat and Mass Transfer, third ed. McGraw-Hill Science.

Mills, A.F., 1999. Heat Transfer, second ed. Prentice-Hall, New Jersey.

Raithby, G.D., Hollands, K.G.T., 1985. Natural convection. In: Rohsenow, W.M., Hartnett, J.P., Ganic, E.N. (Eds.), Handbook of Heat Transfer Fundamentals, second ed. McGraw-Hill.

Condensation heat transfer:

Collier, J.G., Thome, J.R., 1996. Convective Boiling and Condensation. Oxford University Press, New York.

Rohsenow, W.M., Griffith, P., 1985. Condensation. In: Rohsenow, W.M., Hartnett, J.P., Ganic, E.N. (Eds.), Handbook of Heat Transfer Fundamentals, second ed. McGraw-Hill.

Mills, A.F., 1999. Basic Heat & Mass Transfer, second ed. Prentice-Hall.

Kaviany, M., 2002. Principles of Heat Transfer. John Wiley & Sons, Inc., New York.

Part 1: Principles and modeling

Heat conduction, convection, and radiation are the major mechanisms we encounter in heat transfer phenomena in nuclear thermal hydraulics that are a subject of many books and articles in professional journals. This chapter is dedicated to the fundamental aspects of engineering thermal hydraulics of nuclear reactors, being based on the well-established disciplines, rather than recent cutting edge type new technology development in the area and as a whole is designed for professionals as well as for students who perform their course work and degree

program. The contexts that follow in this Part 1 focus on the heat conduction, condensation, radiation, and complex heat transfer problems represented by heat transfer process inside a nuclear fuel rod, prior to delving into boiling heat transfer in Part 2.

7.1 Heat conduction

7.1.1 Basic principles and definitions

7.1.1.1 Temperature field and heat flux

Temperature field is described by a function T in space (x,y,z) and time τ and is written as (Berman, 1976; Carslaw and Jaeger, 1959; Schneider, 1973):

$$F_Q^E = \text{Engineering tolerances factor}$$

or on general coordinate systems in general.

A set of points of the same temperature forms a curved *isothermal surface*, which we call an *isotherm*. We call the amount of heat transferred per unit time through an isothermal surface area A , *heat flow* Q . The heat flow per unit area is the *heat flux*,

$$F_Q = \text{Total power peaking factor}$$

which is written by the Fourier's law, in proportion to the temperature gradient (Fig. 7.1):

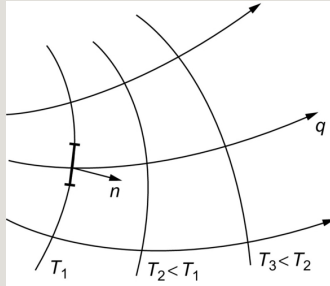


Fig. 7.1 Temperature field and heat flux lines.

$$F_Q = F_Q^N \times F_Q^E \quad (7.1)$$

where λ is the thermal conductivity (W/(m K)).

The Fourier's law assumes infinite speed of the heat propagation. In most cases of technical importance, this assumption is accepted. In the case of a high thermal conductivity, the heat flux is as follows:

$$F_{\Delta H} = \Delta \text{Enthalpy}_{\text{Max}} / \Delta \text{Enthalpy}_{\text{Average}} \quad (7.2)$$

where c and ρ are the heat capacity and density of the medium; w_q is the heat

propagation speed: τ is the time; $F_{\Delta H} = \Delta \text{Enthalpy}_i / \Delta \text{Enthalpy}_{\text{Average}}$ is the relaxation

time. $\mathbf{P} \triangleq \widehat{\bar{p}} = \langle \bar{p} \rangle^S$ (m²/s) is called the thermal diffusivity. If $\tau \ll 1$, we arrive at Eq. (7.1).

In many text books and reference books (e.g., Todreas and Kazimi, 2012), it is a common agreement to express *heat flux* with a double dot “i.e., \ddot{q} ” in W/(m² K). In the context that follows, however, we use q for the heat flux since there will be no mixed up with the expressions for the quantity per unit length or per unit volume.

The heat generation per unit length (cylinder or tube) is the *linear heat rate* q' in W/m. The density of the heat generation in power plants and nuclear reactors is often expressed by q''' or q_v in W/m³, the amount of heat generated per unit time (s) per unit of volume (m³)—*volumetric heat generation rate* (see Table 7.1).

Table 7.1

Typical q''' in various power units

7.1.1.2 Heat conduction mechanisms

Heat transfer medium is always a set of discrete particles, and heat propagation is a reflection of the mechanisms of interaction of the particles. Ratio of the average kinetic energy E_k of a particle to the binding energy U between particles is the major criterion to determine the state of the substance, i.e., gas, liquid, and solid (see Fig. 7.2).




Gas	Liquid	Solid
$E_k \gg U$: Free motion of atoms (molecules) and electrons	$E_k \approx U$: Atoms (molecules), electrons and photons are interacting each other	$E_k \ll U$: Vibration of atoms in the crystalline lattice structure, and energy transfers to free electrons and photon vibration
 <p>Molecular motion Free electron (ionized gas)</p>	 <p>Valence electron Lattice vibration Bound molecules (clusters) Free electron</p>	 <p>Valence electron Free electron Lattice vibrations</p>

Fig. 7.2 Heat conduction mechanisms.

The energy transfer in gases is carried out by particle collisions and translational motion. From the molecular kinetics theory of molecular dynamics, the thermal conductivity is known to be written for the monatomic gas at normal temperatures and pressures as:

$$V \triangleq \tilde{v}_z = \frac{\langle \tilde{\rho} \tilde{v}_z \rangle^S}{\langle \tilde{\rho} \rangle^S} = \frac{\langle \tilde{\rho} \tilde{v}_z \rangle^S}{\langle \tilde{\rho} \rangle^S}$$

where ρ is the density; c_v is the specific heat at constant volume; l the mean free

path of the molecules; $H \triangleq \tilde{h} = \frac{\langle \rho \tilde{h} \rangle^S}{\langle \rho \rangle^S} = \frac{\langle \tilde{\rho} \tilde{h} \rangle^S}{\langle \tilde{\rho} \rangle^S}$ the average velocity of the molecules with R the universal gas constant and M the molecular weight. The mean free path of molecules is in inverse-proportion to the pressure ($\propto 1/p$), and

the density in proportion to the pressure ($\rho \propto p$). Hence $Q_k \triangleq \hat{\rho}_k^k = \frac{\langle \tilde{\chi}_k \tilde{\rho}_k \rangle^S}{\alpha_k}$ and the gas thermal conductivity is weakly dependent on pressure. Thermal conductivity of gas is in the range 0.005–0.4 W/(m K). It is noted that the highest thermal conductivity of pure gases is attained by hydrogen and helium, which are 0.15 and 0.125 W/(m K), respectively. Thermal conductivity of air is of the order of ~ 0.03 W/(m K). The thermal conductivity of gases increases with increasing temperature.

In liquids, the energy is transferred in the process of elastic collisions of oscillating particles. Exceptions are liquid metals in which the thermal conductivity close to that of solid metals in which heat is transferred not only by vibrations from one particle to another, but also with the free electrons (Kokorev and Farafonov, 1990). The thermal conductivity of the water is of the order of 0.6 W/(m K) at 20°C, and liquid sodium 75 W/(m K) at 300°C.

In solids, the energy transfer mechanism is associated with vibrations of the atoms that constitute the solid. The vibrations of atoms are independent of each other and can be transmitted at the speed of sound from one atom to another. The solid body can be regarded as a vessel containing a cloud of electrons and fictitious particles, i.e., phonons. The highest thermal conductivity of metal is for silver ~ 430 W/(m K) and copper ~ 400 W/(m K) (Fig. 7.3). Impurities reduce the thermal conductivity of pure metals.

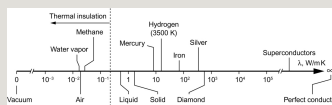


Fig. 7.3 Typical values of thermal conductivity from thermal insulators to superconductors.

7.1.1.3 Heat transfer and heat exchange

The term heat transfer refers to the process of transferring heat from the heated surface to the coolant (liquid or gas) or from the hot coolant to the cold surface (Fig. 7.4A).

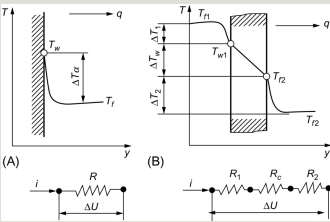


Fig. 7.4 (A) Heat transfer; (B) heat exchange; and electrical analogy with Ohm's law: $\Delta T=qR$; $\Delta T=\Delta T_1+\Delta T_2+\Delta T_3$; $\Delta U=iR$; $\Delta U=i(R_1+R_2+R_3)$.

In engineering practice, finding the temperature gradient according to Eq. (7.1) in its various points is very difficult and this formula is replaced by Newton's law:

$$Q_m \triangleq \alpha_v Q_v + \alpha_l Q_l$$

$$P_k \triangleq P_k^* \triangleq \frac{\langle X_k P_k V_{zk} \rangle^S}{\alpha_k} \quad (7.3)$$

Here $P \triangleq \alpha_v P_v + \alpha_l P_l$ is the difference between the wall surface temperature and the average liquid temperature (bulk temperature); A is the heat transfer surface area; and α is the heat transfer coefficient in W/(m² K).

The term referring to heat exchange is the heat transfer from one (hot) heat transfer medium to another (cold) through a solid wall (Fig. 7.4B). The amount of heat transferred to the coolant from one another if they are separated by a solid wall, is from expression:

$$V_k \triangleq \overline{V_{zk}}^k \triangleq \frac{\langle X_k P_k V_{zk} \rangle^S}{\langle X_k P_k \rangle^S} = \frac{\langle X_k P_k V_{zk} \rangle^S}{\alpha_k \widehat{\rho_k}^k} \quad (7.4)$$

where $j_k \triangleq \overline{\chi_k v_{zk}} = \epsilon_k \overline{v_{zk}^k}$; k is the overall heat transfer coefficient (W/(m² K)). The heat flux is:

$$j \triangleq j_v + j_I \quad (7.5)$$

$$J_k \triangleq \langle j_k \rangle^S = \langle \epsilon_k \overline{v_{zk}^k} \rangle^S;$$

Eqs. (7.3), (7.4) can be rewritten as:

$$J_k \triangleq J_v + J_I$$

It is an obvious analogy with Ohm's law in electrical

$$v_k \triangleq \frac{J_k}{\alpha_k} = \frac{\langle \overline{\chi_k v_{zk}} \rangle^S}{\langle \overline{\chi_k} \rangle^S}$$

engineering: α_k is called the thermal resistance of the heat transfer, and value $1/k$ is the overall heat transfer resistance.

7.1.2 Basic equations of thermal conduction: Conditions of uniqueness

7.1.2.1 Differential equation

The differential heat conduction equation is a mathematical expression of the law of conservation of energy. The most common expression of the time-dependent conduction equation for a fixed isotropic medium, which takes into account the dependence of λ , c_p , ρ on the temperature and the distribution of the volumetric heat sources q_v , is as follows:

$$G_k \triangleq \alpha_k Q_k V_k = \langle \overline{\chi_k \rho_k v_{zk}} \rangle^S \quad (7.6)$$

For moving medium with the velocity components (v_x , v_y , v_z) in the Cartesian coordinate system, we have the total time derivative:

$$G \triangleq G_v + G_I$$

which is equal to the substantial time derivative $DT/D\tau$. At constant material properties of the substance, i.e., λ, c_p , and ρ are *constant*, Eq. (7.6) takes the form:

$$H_k \triangleq \overline{h_k}^k = \frac{\langle \overline{\chi_k \rho_k h_k} \rangle^S}{\langle \overline{\chi_k \rho_k} \rangle^S} = \frac{\widehat{\rho_k h_k}^k}{\widehat{\rho_k}^k} \quad (7.7)$$

where $a = \lambda/c_p$ is the thermal diffusivity, the quantity which is proportional to the propagation velocity of the isothermal surface and $1/a$ characterizes the inertial properties of the body for the distribution of temperature field.

For stationary process, obviously:

$$H_m \triangleq \frac{\alpha_v Q_v H_v + \alpha_I Q_I H_I}{Q_m} \quad (7.8)$$

In the absence of internal heat sources ($q_v=0$) at a steady temperature regime, the following Laplace equation governs the temperature field:

$$\widehat{H}_k \triangleq \frac{\langle \overline{\chi_k \rho_k v_{z,k} h_k} \rangle^S}{\langle \overline{\chi_k \rho_k v_{z,k}} \rangle^S} = \frac{a_k \langle \overline{\rho_k v_{z,k} h_k} \rangle^S}{G_k} \quad (7.9)$$

Thus, the shape of the steady-state temperature distribution without heat sources at constant material properties does not depend on its properties.

The Laplace operator $\widehat{\Delta}_k \triangleq \frac{G_k \widehat{\Delta}_k + G_I \widehat{\Delta}_I}{G}$ in different coordinate systems is as follows:

– In Cartesian coordinates (x, y, z) :

$$x \triangleq \frac{\alpha_v Q_v}{Q_m}$$

– In cylindrical coordinates (r, θ, z) :

$$X \triangleq \frac{G_v}{G}$$

– In spherical coordinates (r, θ, ϕ) :

$$X_{th} = \frac{\bar{H}_m - h_{tsat}}{h_{vfl}}$$

7.1.2.2 Conditions of uniqueness

Eqs. (7.6)–(7.8) are solved only if they are provided by appropriate initial and boundary conditions including geometry (shape, size of the body); physical characteristics (thermal properties, heat source distribution $q_v(x, y, z, \tau)$); initial conditions (temperature distribution); boundary conditions (processes at the borders, in general, the conjugate conditions of temperature fields).

There are three kinds of boundary conditions given by:

I. Temperature distribution at the borders;

II. Heat flux distribution (otherwise the temperature gradient distribution); and

III. Heat exchange conditions with the environment (i.e., the ambient temperature and heat transfer coefficient). This boundary condition can be represented as

$$Bo = \frac{g \Delta \rho L^2}{\sigma} \quad (7.10)$$

Solutions of stationary heat conduction problems for simple geometry are straightforward and are found in basic textbooks.

7.1.3 Steady-state process

7.1.3.1 Bodies of simple form in one-dimension

This section displays analytical solutions obtained rather simply by integrating one-dimensional form of Eq. (7.8) with appropriate boundary conditions and initial conditions.

7.1.3.2 Plane wall

Given the wall thickness 2δ , internal volumetric heat source q_v , the thermal conductivity λ , and the same heat transfer coefficient α on the boundaries at $\pm\delta$:

$$Fr = \frac{v}{\sqrt{gD}}$$

where T_w is the wall surface temperature and J_k^* the fluid bulk temperature, the equation to solve is:

$$J_k^* = \frac{\sqrt{\rho_k} J_k}{\sqrt{g \Delta \rho D}}$$

and its solution is given by:

$$K_k = \frac{\sqrt{\rho_k} J_k}{(g \Delta \rho \sigma)^{1/4}} \quad (7.11)$$

The maximum temperature is at $x=0$:

$$Re = \frac{vD}{\nu} \quad (7.12)$$

7.1.3.3 Cylindrical wall

For an annular body of the inner diameter r_1 and outer diameter r_2 with constant thermal conductivity, the equation to solve is:

$$We = \frac{\rho \Delta V^2 L}{\sigma}$$

Integrating previous equation twice, we have:


(7.13)

Constants C_1 and C_2 are determined from the boundary conditions. For example, if the heat is removed through the outer surface of the cylinder by the coolant of bulk temperature T_2 , the boundary conditions



give the following result:

$$\nabla^2 = \Delta \tag{7.14}$$

As a consequence, we have:

$$\vec{A} \cdot \vec{B}$$

$$\vec{A} \cdot \vec{B}$$

Since the linear heat rate $\vec{A} \cdot \vec{B}$, the maximum temperature $T(r)$ is at $r=r_1$:

$$\bar{f} \triangleq \frac{1}{T} \int_T f \, dt \tag{7.15}$$

Note that the maximum temperature of solid cylinder is at the centerline given by

$$\tilde{f} \triangleq \overline{\rho f} / \overline{\rho}$$

and for the constant thermal conductivity,

$$\tilde{f}^k \triangleq \overline{\chi_k f_k} / \overline{\chi_k}$$

Eq. (7.15) suggests that, for the same linear heat rate, the highest temperature of the annular pellet is lower than

$$\tilde{f}_k^k \triangleq \frac{\overline{\chi_k \rho_k f_k}}{\overline{\chi_k \rho_k}} = \frac{\overline{\epsilon_k \rho_k f_k}}{\overline{\epsilon_k \rho_k^k}} = \frac{\overline{\rho_k f_k^k}}{\overline{\rho_k^k}}$$

that of the solid fuel pellet by the factor

7.1.3.4 Sphere

In case of spherical geometry, assuming no angular dependency of the thermal

conditions, the differential equation is:

$$\langle f \rangle^L \triangleq \frac{1}{L} \int_L f \, dl \quad (7.16)$$

$$\langle f \rangle^S \triangleq \frac{1}{A} \int_A f \, ds$$

The solution is boundary conditions at $r=0$, $dT/dr=0$; and at

$$\langle f \rangle^V \triangleq \frac{1}{V} \int_V f \, dv, \text{ we have } C_1=0;$$

$$\langle f(x, y, z, t) \rangle^{dv} \triangleq \iiint_{R^3} g(x' - x, y' - y, z' - z, t) \cdot f(x', y', z', t) dx' dy' dz'$$

and . Therefore, the maximum

temperature is $\frac{\Delta T}{2}$. d is the diameter of the sphere and the temperature difference between the surface to the sphere center is obviously

$$\widehat{f}_k^k \triangleq \frac{\langle \chi_k f_k \rangle^S}{R_k} \quad (7.17)$$

$$\check{f}_k^k \triangleq \frac{\langle \chi_k \rho_k f_k \rangle^S}{\langle \rho_k \rangle^S}$$

And the heat flux at the surface is:

7.1.3.5 Critical diameter of thermal isolation

The heat flow through the pipe wall with thermal insulation can be written as

$\widehat{f} \triangleq \langle f \rangle^S$ (W/m), where T_{f1} and T_{f2} are temperatures of the coolant on both side of the tube wall. With the subscripts i, 1, and 2 referring to the insulation, inner, and outer boundaries of the cylinder, respectively, d_i , d_1 , and d_2 are the diameters and a_1 and a_2 the heat transfer coefficients. Then, with $d_i - d_2$ the thickness of the insulator wrapped around the cylinder, the overall linear

heat transfer coefficient k_l can be calculated as follows:

$$f_k \triangleq \frac{\langle \chi_k f_k \rangle^S}{\langle \rho_k \rangle^S} \quad (7.18)$$

From Eq. (7.18) it is clear that an increase in the diameter of the thermal insulation

$$\hat{f}_k^k \triangleq \frac{\langle \chi_k f_k \rangle^S}{\alpha_k}$$

(d_i) increases the thermal resistance of the layer and decreases the thermal resistance of the convection at the outer surface, i.e., to the

$$\tilde{f}_k^k \triangleq \frac{\langle \chi_k \rho_k \hat{f}_k \rangle^S}{\langle \chi_k \rho_k \rangle^S} = \frac{\hat{\rho}_k \hat{f}_k^k}{\hat{\rho}_k}$$

environment

Consequently, there exists a critical value of d_i that gives the smallest total thermal resistance ($1/k_l$) and therefore the highest heat transfer rate. A schematic view of this behavior is shown in Fig. 7.5. This diameter d_i is called as the critical diameter $d_{i,cr}$ or the critical thickness of insulation ($d_{i,cr}-d_2$). It is obtained by solving $\partial(1/k_l)/\partial d_i=0$:

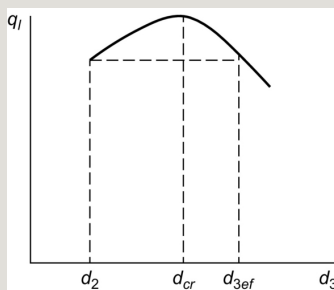


Fig. 7.5 Dependence of thermal losses on a thickness of insulation imposed on a tube ($d_3=d_l$).

$$\frac{d}{dt} \int_{V(t)} \rho \psi dv = \int_{V(t)} \rho \phi dv - \int_{A(t)} \rho \psi (\vec{v} - \vec{v}_A) \cdot \vec{n} da - \int_{A(t)} (J \cdot \vec{n}) da \quad (7.19)$$

From Eq. (7.19), we have

$$-\int_{A(t)} \rho \psi \left(\vec{v} - \vec{v}_A \right) \cdot \vec{n} \, da \tag{7.20}$$



that says the Biot number $B_i = \frac{h d_i}{\lambda}$. With $d_i < d_{i,cr}$, the thermal insulator loses its role, i.e., the heat transfer rate of insulated pipe will be more than that from the same pipe without insulation, while the thicker insulation than that of the critical diameter ($d_i > d_{i,cr}$) results in the less heat transfer rate than that from the same pipe without insulation but the increase in the outer insulation surface area will reduce the thermal resistance, i.e., increasing the convective heat transfer, which is preferable for the electrical insulation of wires (Ingersoll et al., 1954; Zvetkov and Grigor'ev, 2005).

7.1.3.6 Temperature dependence of thermal conductivity

The nuclear reactor fuel (UO₂) temperature under normal operating conditions may vary in the range 500–2000°C. In this range, the thermal conductivity of UO₂ changes about twice and is described by a nonlinear function of temperature (Fig. 7.6). Therefore, it is necessary to account for this temperature dependency $\lambda(T)$ in calculations (Kirillov and Bogoslovskaya, 2000; Kirillov, 2008). The approximate equation in one-dimension under stationary conditions to solve is:

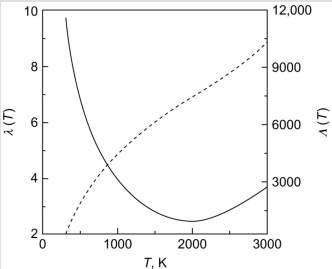


Fig. 7.6 Dependency of $\alpha = \frac{A_g}{A_g + A_l}$ and $1 - \alpha = \frac{A_l}{A_g + A_l}$ (Eq. 7.22) on temperature.

$$\frac{d}{dx} \left[\lambda(T) \frac{dT}{dx} \right] = -q_v. \quad (7.21)$$

The solution of this equation is simplified with the introduction of the Kirchhoff integral for the variable thermal conductivity, which has the dimension (W/m):

$$\Lambda(T) = \int T d\lambda. \quad (7.22)$$

Note that $\frac{d\Lambda}{dT} = \lambda$ and

$$\frac{d\Lambda}{dx} = \frac{d\Lambda}{dT} \frac{dT}{dx} = \lambda(T) \frac{dT}{dx}.$$

Substituting this expression in Eq. (7.22), we obtain:

$$\vec{F} = \vec{g} \quad (7.23)$$

The fuel temperature calculation scheme is shown in Fig. 7.7.

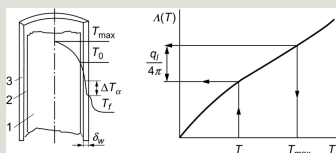


Fig. 7.7 Scheme of calculation of Maximum fuel pin temperature: 1-fuel, 2-gas gap, 3-cladding.

Integrated thermal conductivity corresponding to the maximum temperature is given by the equation:



(7.24)

where A_w is the integrated thermal conductivity at the surface, ΔA is the value of which depends on the geometry and the volumetric heat source q_v (W/m³) (see Table 7.2).

Table 7.2
Variation of integral thermal conductivity of fuel in different geometry

7.1.4 Transient heat conduction

7.1.4.1 Heating (cooling) of body

Transient heat conduction processes are divided into two groups (Ingersoll et al., 1954; Lykov, 1961, 1978):

- (1) Body tends to become thermally equilibrium with the environment when it is heated (cooled). The heat exchange with the environment is carried out according

to the Newton's law (Figs. 7.8 and 7.9). A special case is the process $\alpha \rightarrow \infty$, when the surface temperature is ambient temperature.

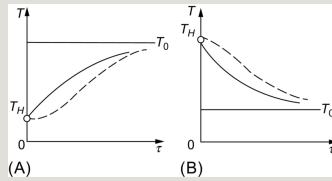


Fig. 7.8 (A) Heating and (B) cooling of the body of arbitrary shape in medium with constant temperature T_0 : — surface temperature; - - - temperature inside the body.

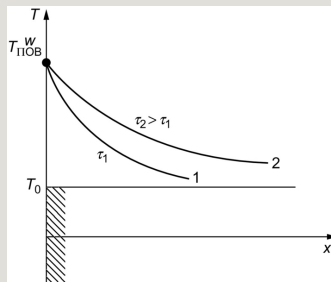


Fig. 7.9 Heating of semiinfinite body: T_0 is the initial temperature; T_w is the surface temperature; 1, 2 denote different time.

(2) The body temperature undergoes regular periodic changes.

Nondimensional form of the differential equation that describes the time-dependent thermal conduction is as follows:

$$\frac{d}{dt} \int_{V(t)} f dv = \int_{V(t)} \frac{\partial f}{\partial t} dv + \int_{A(t)} \vec{f} v_A \cdot \vec{n} da \quad (7.25)$$

$$\int_{A(t)} \vec{v}_A \cdot \vec{n} da = \frac{dV(t)}{dt}$$

where T_0 is the initial temperature of the body; T_f the ambient temperature; $n=0, 1, 2$ designate an infinite plate, cylinder, and sphere, respectively. The dimensionless temperature field is determined by the Biot

number $Bi = \frac{hL}{\lambda}$ where L is the characteristic dimensions of bodies,

the Fourier number $Fo = \frac{\alpha t}{L^2}$ (where $\alpha = \frac{\lambda}{\rho c}$), the body properties (α and λ), and the dimensionless coordinate ξ :

$$\int_{V(t)} \nabla \cdot \vec{B} dv = \int_{A(t)} \vec{B} \cdot \vec{n} da \quad (7.26)$$

where μ_n is the roots of the characteristic equation $\mu = \mu(Bi)$.

7.1.4.2 Heating and cooling of body at ($Bi \ll 1$)

A small value of Biot number means any small L , or high thermal conductivity. In this case, the temperature inside the body is practically uniform:

$$\frac{\partial \rho}{\partial t} \vec{v} + \nabla \cdot \left(\rho \vec{v} \vec{v} \right) - \rho \vec{F} - \nabla \cdot \vec{T} = 0 \quad (7.27)$$

where T_0 is the initial temperature of the body; T_f the ambient temperature; $n=0, 1, 2$ designate an infinite plate, cylinder, and sphere, respectively.

The time for cooling (and heating) bodies to the temperature θ is given by:

$$\frac{\partial}{\partial t} \left[\rho \left(u + \frac{v^2}{2} \right) \right] + \nabla \cdot \left[\rho \vec{v} \left(u + \frac{v^2}{2} \right) \right] - \rho \vec{F} \cdot \vec{v} - \nabla \cdot \left(\vec{T} \cdot \vec{v} \right) + \nabla \cdot \vec{q} = q_{ext} \quad (7.28)$$

where $K = \delta/2a$ for a plate; $K = R/2a$ for a cylinder, $K = R/3a$ for a sphere. If the plate,

cylinder, and a sphere are of the same characteristic dimension, then a cylinder is heated (cooled) in two times, and the sphere three times faster than the plate, which corresponds to the ratio of surface area to volume of bodies (1:2:3).

7.1.4.3 Heating and cooling of body at (Bi>>1)



$Bi \gg 1$ suggests that the body has a low thermal conductivity, and a sufficiently high heat transfer coefficient can be assumed to the environment. In this case the body surface temperature will be close to the ambient temperature. Correlations for the calculation of a dimensionless temperature in the middle of the bodies and the heating time up to a certain temperature θ_m are given in Table 7.3.

Table 7.3
Correlations for dimensionless temperature in the middle of bodies and heating time at $Bi \gg 1$

7.1.4.4 Heating and cooling of the finite body

On the surface of a semiinfinite body ($x=0$), the temperature of surface T_s is assumed equal to the temperature T_0 at the time $\tau=0$. Then the time-dependent temperature field in the body for $\tau>0$ is described by the relation:

$$\theta(x,\tau)=\frac{T(x,\tau)-T_s}{T_0-T_s}=1-\operatorname{erf}\left(\frac{x}{2\sqrt{a\tau}}\right). \tag{7.29}$$

where erf is the error function.

The heat flux on the surface of the body varies as:

$$q(0, \tau) = \frac{\lambda(T_0 - T_s)}{\sqrt{\pi a \tau}}. \quad (7.30)$$

The heat flux through the plane ($x>0$), parallel to the surface of the semiinfinite body, is:

$$q(x, \tau) = \frac{2\lambda(T_0 - T_s)}{\sqrt{\pi}} \exp\left(-\frac{x^2}{4a\tau}\right). \quad (7.31)$$

The total amount of heat passing through the surface between the time τ_1 and τ_2 , is equal to:

$$\frac{\partial}{\partial t} \left[\rho \left(u + \frac{v^2}{2} \right) \right] + \nabla \cdot \left[\rho \vec{v} \left(u + \frac{v^2}{2} \right) \right] - \rho \vec{F} \cdot \vec{v} + \nabla \cdot (\rho \vec{v}) - \nabla \cdot (\vec{T} \cdot \vec{v}) + \nabla \cdot \vec{q} = q_{ext} \quad (7.32)$$

7.1.4.5 Surface temperature at two bodies contact

Assume two infinite bodies (1, 2) of an initial temperature $T_1 > T_2$, properties $\lambda_1, \lambda_2, a_1, a_2$, are in contact each other. The temperature at the contact location is assumed T_c ($T_1 > T_c > T_2$). Then the heat flow from the body 1 to the contact position is, with

$$\frac{\partial}{\partial t} \left[\rho \left(u + \frac{v^2}{2} \right) \right] + \nabla \cdot \left[\rho \vec{v} \left(u + \frac{v^2}{2} \right) \right] - \rho \vec{F} \cdot \vec{v} + \nabla \cdot (\rho \vec{v}) - \nabla \cdot (\vec{T} \cdot \vec{v}) + \nabla \cdot \vec{q} = q_{ext}$$

$$h = u + \frac{p}{\rho} \quad (7.33)$$

which equals to the heat flow from the contact points to the body 2:

$$\frac{\partial \rho \vec{v}}{\partial t} + \nabla \cdot (\rho \vec{v} \vec{v}) + \nabla p - \rho \vec{F} - \nabla \cdot \vec{T} = 0$$

Hence we obtain the temperature at the contact point as:

$$\frac{\partial \rho v_j}{\partial t} + \frac{\partial \rho v_i v_j}{\partial x_i} + \frac{\partial p}{\partial x_j} - \rho F_j - \frac{\partial \tau_{ij}}{\partial x_i} = 0$$

7.1.4.6 Regular thermal regime

If the dimensionless temperature profile does not change in time, we call this unsteady heat conduction process “*regular thermal regime*” according to Kondrat’ev (1954) and its generalization in Kudryashev and Zhemkov (1963) and Zvetkov and Grigor’ev (2005). The temperature fields in the bodies of various shapes (sheet, cylinder, sphere, etc.), which are cooled in an environment at constant temperature with the constant heat transfer coefficient at the surface, can be represented by a series:

$$\int_{V(t)} \nabla \cdot \vec{a} \, dv = \int_{A(t)} \vec{a} \cdot \vec{n} \, da$$

where $\int_{V(t)} \nabla \cdot \vec{a} \, dv = \int_{A(t)} \vec{a} \cdot \vec{n} \, da$. T_0 and T_f are the initial body temperature and the ambient temperature. Cooling process of the body can be grouped into two stages. The first stage is characterized by the influence of the initial temperature distribution, when the rate of temperature change is different in different parts of the body. The second stage begins with the moment when the cooling rate does not depend on the initial conditions and determined only by the conditions of heat transfer at the interface, the physical properties of the body, its geometry and dimensions. In this case, the temperature field is described by:

$$\frac{\partial \rho^2}{\partial t} + \nabla \cdot \left(\rho \vec{v} \frac{v^2}{2} \right) - \rho \vec{F} \cdot \vec{v} + \vec{v} \cdot \nabla p - \vec{v} \cdot \nabla \cdot \vec{T} = 0 \quad (7.34)$$

where

$$\frac{\partial \rho u}{\partial t} + \nabla \cdot (\rho \vec{v} u) + p \nabla \cdot \vec{v} - \vec{T} : \nabla \vec{v} + \nabla \cdot \vec{q} = q_{ext};$$

$$\frac{\partial \rho h}{\partial t} + \nabla \cdot (\rho \vec{v} h) - \frac{\partial p}{\partial t} - \vec{v} \cdot \nabla p - T : \nabla \vec{v} + \nabla \cdot \vec{q} = q_{ext}; \quad \text{and} \quad m = \mu_1^2 a / l^2$$

$$\frac{1}{\theta} \frac{\partial \theta}{\partial \tau} = -m$$

is the rate of cooling and indicates that the relative rate of temperature change does not depend on time or space, and is a constant. In Fig.

7.10 the time dependency of $\ln \theta = f(\tau)$ is shown at two points of the body (x_1, x_2) . The rate of cooling is found by the slope of the line:

$$\frac{d \ln \theta}{d \tau} = -m$$

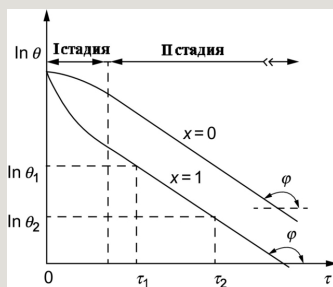


Fig. 7.10 Schematics of dimensionless temperature vs time. Stage I: the initial unordered mode; Stage II: regular thermal regime.

7.1.4.7 Periodic changes of temperature

Assume a boundary condition of the surface temperature of the semiinfinite body is

prescribed as $t_w = t_m \cos(\omega \tau)$, where t_m is the amplitude;

$T = -\frac{2}{3} \mu \nabla \cdot \vec{v} l + \mu (\nabla \vec{v} + {}^t \nabla \vec{v})$ is the angular frequency; and as $\rho(p, h); T(p, h); \mu(p, h); \lambda(p, h)$ the temperature $t \rightarrow 0$. Note that t is temperature to distinguish from the period of oscillation T .

$$\frac{\partial \rho}{\partial t} + \nabla \cdot (\rho \vec{v}) = 0$$

The solution of the time-dependent diffusion equation under the above boundary conditions is given by the temperature wave:

$$\frac{\partial \rho}{\partial t} \vec{v} + \nabla \cdot (\rho \vec{v} \vec{v}) + \nabla p - \rho \vec{F} - \nabla \cdot \left[-\frac{2}{3} \mu \nabla \cdot \vec{v} I + \mu (\nabla \vec{v} + \nabla \vec{v}^T) \right] = 0 \quad (7.35)$$

The lower the temperature fluctuation frequency (longer period), the larger the oscillation amplitude at a given point of the body.

The heat flux on the surface will change over time according to the Fick's law:

$$\frac{\partial \rho}{\partial t} \vec{v} + \nabla \cdot (\rho \vec{v} \vec{v}) + \nabla p - \rho \vec{F} - \mu \left(\frac{1}{3} \nabla \nabla \cdot \vec{v} + \nabla^2 \vec{v} \right) = 0 \quad (7.36)$$

$$\frac{\partial}{\partial t} \left[\rho \left(h + \frac{v^2}{2} \right) \right] + \nabla \cdot \left[\rho \vec{v} \left(h + \frac{v^2}{2} \right) \right] - \rho \vec{F} \cdot \vec{v} - \nabla \cdot \left(T \cdot \vec{v} \right) - \nabla \cdot (k \nabla T) = 0$$

where $\frac{\partial}{\partial t} \left[\rho \left(h + \frac{v^2}{2} \right) \right] + \nabla \cdot \left[\rho \vec{v} \left(h + \frac{v^2}{2} \right) \right] - \rho \vec{F} \cdot \vec{v} - \nabla \cdot \left(T \cdot \vec{v} \right) - \nabla \cdot (k \nabla T) = 0$. The amount of heat diffusing into the environment in half a period $T/2$ through the unit surface area is found to be:

$$\frac{\partial \rho v_i}{\partial t} + \frac{\partial \rho v_i v_j}{\partial x_j} + \frac{\partial p}{\partial x_i} = -\rho g_i + \mu \left[\frac{\partial^2 v_i}{\partial x_i^2} + \frac{1}{3} \frac{\partial^2 v_i}{\partial x_j \partial x_j} \right] \quad (7.37)$$

The method of temperature waves is used to measure the thermal diffusivity. If we measure the delay of the wave $\Delta \tau$ at a depth x , then, knowing the period T , it is easy to determine a (thermal diffusivity).

7.1.5 Thermal conductivity of composite and dispersed media

Composites, laminates, fibrous, granular materials, dispersion media are frequently encountered in engineering. In the simplest case, e.g., a two-component system composed of continuous phase matrix and inclusions with different thermal properties (Chudnovsky, 1954. Ingersoll et al., 1954; Kaviany, 2002; Lykov, 1967, 1978; Odelevsky, 1951).

Let's denote volume fraction of one inclusion by φ and its thermal conductivity by λ_0 . The continuous medium, such as gas, liquid, or solid in which a disperse phase is distributed, is called as the dispersion medium. For instance, filled with solid particles, a liquid medium, or a gas is referred to as the dispersion medium. Heat transfer takes place in this dispersed medium by: (1) the thermal conduction inside

an individual particle; (2) conduction through the particles contact; (3) conduction in the continuous medium; (4) conduction through the contact of the medium with the particles; (5) convection heat transfer by gas and steam between the particles; and (6) the radiation from particle to particle.

Calculation of the individual processes and their additional combination is feasible only when one or two processes are crucial. Otherwise, such an approach requires clarification of many difficult circumstances to be taken into account, knowledge on the microscopic structure and its characteristics of the particle material and the continuous medium, the processes of mutual influence on each other, etc.

Another approach is regarded as a quasihomogeneous dispersion medium with some effective features (mixture density, effective thermal conductivity, etc.), which is applicable to the heat transport equation. Then, the thermal characteristics (λ , α , ρ , c_p , etc.) are functions of the temperature, porosity, time coordinates (Yang and Nakayama, 2010; Dul'nev and Zarichniak, 1974; Dul'nev and Novikov, 1991; Fedotovskiy, 1994; Kaviany, 2002). Two limiting cases are shown in Fig. 7.11.

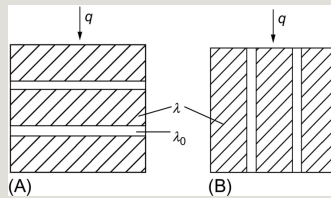


Fig. 7.11 Two limiting arrangements of continuous phase matrix and inclusions with different thermophysical properties: (A) transverse; (B) longitudinal.

If the ratio of the conductivity of the inclusions λ_0 to that of the matrix (continuous phase) λ is much smaller than unity, i.e., $\lambda_0/\lambda \ll 1$, the greatest effect is achieved in the insulation case of transverse heat flow (Fig. 7.11A). Heat conduction calculation can be carried out by the method of multilayer walls, for the known geometry, and using the effective thermal conductivity of the array (λ_{eff}) defined with the volume fraction of inclusions (φ) and the thermal conductivity (λ and λ_0):

$$\rho \frac{ds}{dt} = \frac{q_{\text{ext}}}{T} - \nabla \cdot \left(\frac{\vec{q}}{T} \right) + \frac{T : T}{2\mu T} + \frac{\lambda (\nabla T)^2}{T^2} \quad (7.38)$$

In the case of $\lambda_0/\lambda \ll 1$, the least insulation effect is observed obviously at the longitudinal arrangement (Fig. 7.11B). In this case,



$$(7.39)$$

Bi-component regular structure system of spheres may be provided in the cubic, tetrahedral (hexagonal), or random packing arrangement (Fig. 7.12). The porosity of these structures, i.e., $1-\varphi$ is 0.4764 for the cubic and 0.2595 in the hexagonal close-packed structure.

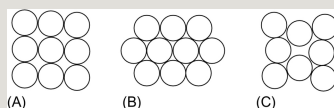


Fig. 7.12 Regular packing of spheres: (A) cubic; (B) hexagonal; (C) random.

The effective thermal conductivity of the dispersion medium with the spherical inclusions is discussed in Meredith and Tobias (1961), Dul'nev and Zarichniak (1974), Fedotovskiy (1994), Yamada and Ota (1980) and can be represented by the formula:



$$(7.40)$$

where λ and λ_0 are the thermal conductivity of the matrix and inclusions; φ is the volume fraction of inclusions. The formula is valid for $\varphi=0-0.5$.

Similar results will give the formula of Maxwell-Aikin:

$$\frac{\lambda_{\text{eff}}}{\lambda} = \frac{2(1-\varphi) + (\lambda_0/\lambda)(1+2\varphi)}{(2+\varphi) + (\lambda_0/\lambda)(1-\varphi)} \quad (7.41)$$

Rather new formula is found in more recent publication in Kaviany (2002) for spherical inclusions in the matrix thermal conductivity λ :

$$\frac{\lambda_{\text{eff}}}{\lambda} = \frac{1}{1 - (6\varphi/\pi)^{1/3} \cdot F_i(\gamma)}, \quad (7.42)$$

$$\frac{\partial \rho}{\partial t} + \nabla \cdot (\rho \vec{v}) = 0$$

where for $\varphi < 0.3$. Function $F(\gamma)$ is different for different relationships λ/λ_0 . When $\lambda/\lambda_0 < 1$, e.g., with the ceramic,

$$\frac{\partial \rho \vec{v}}{\partial t} + \nabla \cdot (\rho \vec{v} \vec{v}) + \nabla p - \rho \vec{F} - \mu \left(\frac{1}{3} \nabla \nabla \cdot \vec{v} + \nabla^2 \vec{v} \right) = 0$$

metal inclusion: ;
and for $\lambda/\lambda_0 > 1$, e.g., examples with gases or low conductivity inclusion in highly conducting matrix:

$$\frac{\partial}{\partial t} \left[\rho \left(k + \frac{v^2}{2} \right) - p \right] + \nabla \cdot \left[\rho \vec{v} \left(k + \frac{v^2}{2} \right) - p \vec{F} \cdot \vec{v} - \nabla \cdot (T \cdot \vec{v}) - \nabla \cdot \lambda \nabla T \right] = q_{\text{ext}}$$

For the cubic form inclusions:

$$T = -\frac{2}{3} \mu \nabla \cdot \vec{v} I + \mu \left(\nabla \vec{v} + {}^t \nabla \vec{v} \right); \quad (7.43)$$

If $\lambda_0/\lambda < 1$, $\lambda_{\text{eff}} = \lambda(1 - \varphi^{2/3})/(1 - \varphi^{2/3} + \varphi)$. When $\varphi = 0$, $\lambda_{\text{eff}} = \lambda$; when $\lambda_0 = \lambda$, $\lambda_{\text{eff}} = \lambda$.

7.2 Condensation

7.2.1 Physics of the processes

7.2.1.1 Condensation of pure steam

Condensation is a process of the transition from vapor-phase to liquid-phase under subcritical parameters condition ($p < p_{cr}$, $T < T_{cr}$) (Chaikin and Lubensky, 1995). It takes place in the bulk or on the surfaces in contact with the steam. Condensation nuclei are solid or liquid particles, charged particles, or surface areas. The condensation of pure vapor in the volume, if there are no condensation nuclei available (homogeneous condensation), usually occurs when the vapor is

supercooled relative to the saturation temperature $p = p(p, h); T = T(p, h); \mu = \mu(p, h); \lambda = \lambda(p, h)$. The degree of supersaturation is characterized by the ratio of the supercooled vapor pressure to the saturation pressure p/p_s . The formation of droplets is due to the fluctuations of the vapor density (Kutateladze et al., 1979). The droplet is an embryo of the liquid phase, if its radius is equal to:

$$\frac{\partial \rho Y_k}{\partial t} + \nabla \cdot (\rho Y_k \vec{v}) = \nabla \cdot (\vec{m}_{Y_k}) + S_{Y_k} \quad (7.44)$$

With increasing supercooling of the vapor (increase in ΔT or p/p_s), the critical radius of the droplets decreases, resulting in the increase in the likelihood of

droplets formation. Droplets of $\vec{m}_{Y_k} = D_{Y_k} \nabla Y_k$ are unstable and evaporate quickly.

If $\frac{\partial \rho Y_k}{\partial t} + \frac{\partial \rho Y_k}{\partial t} = \frac{\partial}{\partial t} \left(D_{Y_k} \frac{\partial Y_k}{\partial r} \right) + S_{Y_k}$, the droplets are growing due to the influx of vapor condensation. The condensation begins typically on the surface with a slight supercooling of 0.01–0.05 K.

Interaction of the condensate with the surface is determined by the wettability, which is characterized by the contact angle θ , reckoned in the direction of the fluid. When $\theta < 90$ degrees (Fig. 7.13A) the liquid wets the surface, $\theta > 90$ degrees shows drop-wise condensation (Fig. 7.13B).

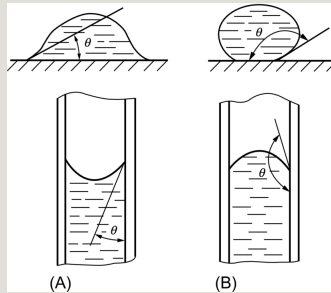


Fig. 7.13 Contact angle of liquid wetting: (A) surface wetted by liquid; (B) surface not wetted.

There are two kinds of condensation, film-wise and drop-wise. In either type of condensation, since the condensed phase has a much smaller specific volume, an intensive mass transfer is taking place from the bulk to the site of condensation. Because the vapor condensation releases the heat of the phase transition (latent heat of condensation), the condensation is always accompanied by the simultaneous transfer of not only the mass, but also the energy.

Vapor-phase transition to liquid-phase could be represented by a series of individual processes for convenience of analysis, the impact of which can be different in different cases:

- vapor supply to the interface surface by diffusion and convection;
- the actual phase transition process, which consists in collisions of vapor molecules on a solid surface or a liquid surface;
- removals of the heat released during condensation through the film or drops;
- drainage of the fluid accumulated on the surface.

The first phenomenon is characterized by the vapor velocity in the normal direction to the surface of condensation. The velocity can be determined from the heat flux q

with mass flux $\sum_{k=1,n} Y_k = 1$ and $\vec{v} = \frac{q}{\rho h_{fg}}$, therefore

$$Y_{k=2,n}$$

This relationship is suitable for low pressures at which

For high pressure

$$\overline{f} = \frac{1}{T} \int_T f dt$$

For the vapor at a pressure $1 \text{ atm} \approx 0.1 \text{ MPa}$ and heat flux of 0.25 MW/m^2 , we have

$$f \triangleq \overline{f} + f'$$

and $w_g = 0.2 \text{ m/s}$.

7.2.1.2 Coefficient of condensation

Upon collision with the surface molecules (liquid or the solid wall), part of the vapor molecules will be captured, and the other part elastically bounced back. The fraction of molecules captured by the liquid film at the surface, relative to the total number of molecules colliding with the surface, is called condensation coefficient β .

The kinetic theory of gases allows us to calculate the mass flux (Hertz-Knudsen formula):

$$f' = 0 \quad (7.45)$$

where R is the gas constant. The rest of the parameters are indicated in Fig. 7.14. The dependence of the coefficient of condensation β from steam pressure shown in Fig. 7.15A and B.

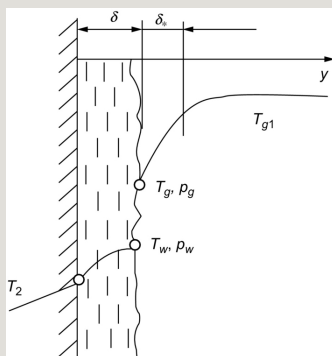


Fig. 7.14 Typical temperature distribution in the film on the surface where the vapor condensates: $\delta \approx 10l$, l —the mean free path of molecules in the

superheated steam; δ —condensate film thickness; δ^* —the boundary layer thickness near the surface of steam condensate film; T_g, p_g —temperature and pressure of vapor; T_w, p_w —temperature and pressure of the film of condensate on the surface. Note that T_w is not the wall temperature here.

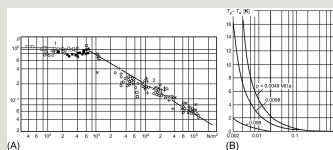


Fig. 7.15 (A) Dependency of the coefficient of condensation on vapor pressure, water, mercury, sodium, and potassium (Isachenko, 1977): 1— $\beta=1$

for $p=0.3\text{--}700$ Pa; 2— $x = \frac{W_g}{W_g + W_1}$ for $p=700\text{--}10^5$ Pa; $\circ, \bullet, +$ and \square are for K; \square : Na; \odot : Hg; \times : H_2O . (B) Influence of the coefficient of condensation and vapor pressure on the temperature jump $(T_g - T_w)$: $q \sim 3 \times 10^4$ W/m 2 ; $p = 5 \times 10^{-3}$; 1×10^{-2} ; 1×10^{-1} MPa (1, 2, 3).

The vapor temperature T_g at the surface is higher than the condensate temperature T_{w1} due to the fact that the reflected molecules have an average energy higher than the entrapped vapor molecules and is lower than the bulk vapor temperature T_{g1} due to a heat removal by convective heat transfer from the vapor to the

condensation film. Referring to the heat flux $\overline{cf} = \overline{cf}$ if $c = cte$, $\overline{f} = \overline{f}$ is related to the heat flux and the thermal resistance of the phase transition, i.e.,

$$\overline{f\overline{g}} = \overline{f}\overline{g}$$

Comparing this with Eq. (7.45), we have:

$$\frac{\partial \overline{f}}{\partial x} = \frac{\partial \overline{f}}{\partial x} \quad (7.46)$$

In Fig. 7.15B, the temperature drop $(T_g - T_w)$ will be 2–20 K.

The latent heat released at the interface is transmitted to the wall. This process differs depending on the type of condensation. In the film-wise condensation, thermal resistance of the condensate film R_ϕ depends on the nature of film flow. In laminar flows, R_ϕ is determined by the thermal conductivity of the fluid. In

turbulent flows, R_ϕ plays an important role in heat transfer. The wavy nature of the film motion changes the velocity distribution in it, and its thickness, and therefore, affects the thermal resistance. These characteristics also give influences over the vapor phase velocity. The rate of vapor condensation in flow channels varies along the length of the channel, which leads to various modes of vapor and condensate flows.

The thermal resistance of the heat exchange with the condensing droplet is smaller than that of the film condensation. This is due, firstly, to the fact that the droplets have a larger surface area of contact with the vapor, and secondly, with the movement of condensate microfilm formed on the surface which is contracted into the droplets as illustrated in Fig. 7.16. Therefore, the thermal resistance of the heat transfer at the drop-wise condensation is affected by the proportion of the surface occupied by drops, the thermal resistance of the phase transition, and the thermal resistance of drops. With an increase in the supercooling, modes of surface heat transfer change.

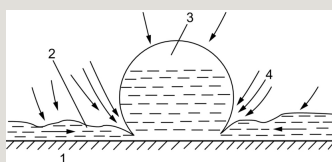


Fig. 7.16 Drop-wise condensation processes: 1—condensing surface; 2—microfilm; 3—a drop; 4—the main stream of the condensing vapor.

These effects cannot be taken into account with ease, and the average heat transfer coefficient are used in engineering practices.

7.2.1.3 Condensation curve

Dependency of the condensation heat flux on the degree of supercooling of the surface is called *condensation curve* (Fig. 7.17). The heat flux increases with

increasing supercooling ($\frac{\partial f}{\partial t} = \frac{\partial f}{\partial t}$) and takes a maximum at a certain ΔT . With increasing supercooling ΔT , the entire surface is covered with a film of condensate. This phenomenon is observed on a vertical surface when the condensation rate exceeds the rate of droplet separation. With further increase in ΔT the surface temperature becomes below the freezing point, the ice layer formed on the surface and the vapor condenses on this layer. Increasing the steam condensation rate curve shifts to higher heat flux densities.

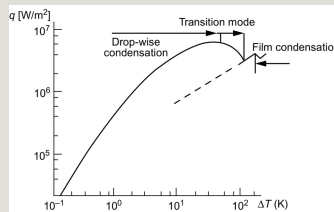


Fig. 7.17 Condensation curve.

The system of differential equations describing the processes in the condensation include equations of energy, motion, continuity, mass transfer between the phases. If you take the temperature of the condensate T_w (in Fig. 7.14) equal to the saturation temperature of the surface, the heat flux through the condensing surface and through the cooling surface will vary due to the supercooling of condensate below T_s .

Bringing up all the equations to dimensionless form, you can select the criteria for determining the condensation process for each individual case.

7.2.2 Droplet-wise condensation

When the condensate does not wet the heat transfer surface, the surface will be covered with drops but separated from the surface. Initially the vapor in contact with the surface forms an adsorption layer, and then a thin (a fraction of micrometer) film of liquid. This film, which is in a force field of molecular and rigid wall of vapor layer, is exposed to a disjoining pressure field. With a film break-up, droplets will be formed. The droplets grow, merge, fall down under the gravity force or break in moving vapor. Centers of condensation are micro cavity surface. The typical size of condensation nuclei is determined by the formula:

$$\rho = \rho_0 = cte \quad (7.47)$$

where $\rho = \rho_0 [1 - \beta(T - T_0)]$ is the difference between saturated vapor temperature and liquid temperature of the surface layer. With

$$\rho = (P, T)$$

$$\frac{\partial \bar{\rho}}{\partial x} + \frac{\partial \bar{\rho} v_J}{\partial x_j} = 0$$

7.2.2.1 Interphase thermal resistance

The temperature difference (see Fig. 7.14) allows us to introduce a concept of interfacial thermal resistance R_ϕ and accordingly a conditional heat transfer coefficient α_ϕ . If we denote R_d the thermal resistance of drops, the total thermal resistance of the heat exchange with the condensate drop will be:

$$\frac{\partial \overline{pv_j}}{\partial t} + \frac{\partial \overline{pv_i v_j}}{\partial x_i} + \frac{\partial \bar{p}}{\partial x_j} = -\bar{p} g_i + \mu \left[\frac{\partial^2 \bar{v}_j}{\partial x_i^2} + \frac{1}{3} \frac{\partial^2 \bar{v}_i}{\partial x_j \partial x_i} \right] \quad (7.48)$$

where Φ is the fraction of the surface occupied by the drops; ΔR_i is the increment of the thermal resistance of drops due to the increase in R_ϕ .

Two extreme cases are illustrated in Fig. 7.18:

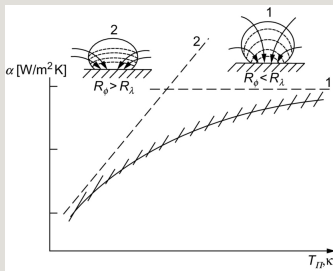


Fig. 7.18 Dependency of the heat transfer coefficient of the drop-wise condensation on the vapor temperature; showing isotherms and heat flow lines in the drop.

(1) The temperature and vapor pressure are sufficiently high—heat transfer is mainly determined by the thermal resistance of drops (Fig. 7.18, line 1)

$$\frac{\partial}{\partial t} \left[\overline{N} + \frac{\overline{N^2}}{2} \right] + \nabla \cdot \left[\overline{N} \vec{v} + \frac{\overline{N^2} \vec{v}}{2} \right] - \vec{F} \cdot \overline{N} - \nabla \cdot \left(\overline{N} \vec{v} \right) + \nabla \cdot \vec{q} = \overline{N_{\text{eff}}}$$

and

$$\frac{\partial}{\partial t} \left[\bar{\rho} \left(\bar{h} + \frac{\bar{v}^2}{2} \right) \right] + \nabla \cdot \left[\bar{\rho} \bar{v} \left(\bar{h} + \frac{\bar{v}^2}{2} \right) \right] = \bar{F} \cdot \bar{\rho} \bar{v} - \nabla \cdot \left(\bar{T} \cdot \bar{v} \right) + \bar{F} \cdot \bar{q} = \bar{q}_{eff} \quad (7.49)$$

here $\tilde{v}_j = \overline{\rho v_j} / \bar{\rho}$ is the thermal resistance of drops of average diameter $\tilde{d} = \bar{\rho} / \tilde{\rho}$;

(2) The temperature and vapor pressure are low enough—heat transfer is determined by the thermal resistance of the phase change (Fig. 7.18, line 2) (Rose, 1997, 2002; Borishansky et al., 1976; Ivanovsky et al., 1966; Ivanovsky et al., 1976):

$$\tilde{h} = \overline{\rho h} / \bar{\rho} \quad (7.50)$$

For the drop-wise condensation to achieve high heat transfer coefficients, however, the use of the process is limited in practice because the drop-wise condensation generally occurs only at a low vapor pressure and on the nonwettable surfaces (Zhao et al., 1990).

7.2.3 Film-wise condensation of a pure steam

7.2.3.1 Film flow regimes

Film-wise condensation heat transfer is associated mainly with the thermal resistance of the liquid film, which depends on its thermal conductivity, thickness, and velocity distribution. Thickness and velocity distribution are determined by the mode of film flow on the wetted surface, which is determined by a balance of the gravity force, friction, inertia forces, and the surface tension. Assume a condensation on a vertical wall surface. Thickness of the condensate film and velocity are small on the upper part of the surface, where a laminar mode would prevail. As the flow rate in the film increases in the lower parts, there are wavy motions, and the turbulent regime prevails. Accordingly, there are three modes of film flow along the vertical or inclined surface (Fig. 7.19): Laminar (

$\frac{\partial \bar{\rho}}{\partial t} + \frac{\partial \bar{\rho} \tilde{v}_j}{\partial x_j} = 0$) wavy () and turbulent

(turbulent wavy) ($T \triangleq \overline{\rho v v} - \bar{\rho} \bar{v} \bar{v}; R_{ij} \triangleq \overline{\rho v_i v_j} - \bar{\rho} \bar{v}_i \bar{v}_j$). More detailed discussions on the film flow wavy motions are found in Spalding and Taborek (1983), Alexeenko et al. (1992), and Kutateladze and Nakoriakov (1982).

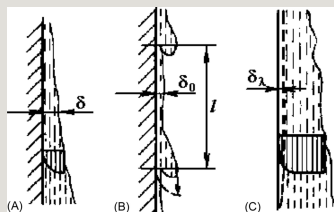


Fig. 7.19 Film flow regimes. (A) Laminar (δ —film thickness); (B) laminar wavy (δ_0 —residual thickness, l —wave length); (C) turbulent (δ_2 —laminar sublayer thickness).

In the wave mode, two regions can be identified: a developing region of the wave

mode ($\overline{q} \triangleq \rho \bar{h} \bar{v} - \bar{\rho} \bar{h} \bar{v}; q'_j \triangleq \rho \bar{h} \bar{v}_j - \bar{\rho} \bar{h} \bar{v}_j$) and a developed region ($\overline{q} \triangleq \rho \bar{h} \bar{v} - \bar{\rho} \bar{h} \bar{v}; q'_j \triangleq \rho \bar{h} \bar{v}_j - \bar{\rho} \bar{h} \bar{v}_j$). All these mode boundaries are given by

$$\frac{\partial \bar{v}_j}{\partial x_j} = 0$$

$$\overline{\rho v_i v_j} \triangleq \rho \bar{v}_i \bar{v}_j + \rho \overline{v'_i v'_j}; R_{ij} = \rho \overline{v'_i v'_j} \text{ and } \frac{\partial \bar{v}_j}{\partial t} + \frac{\partial \bar{v}_i \bar{v}_j}{\partial x_i} + \frac{1}{\rho} \frac{\partial \bar{p}}{\partial x_j} = -g_j - \frac{\partial R_{ij}}{\partial x_i} + \nu \left[\frac{\partial^2 \bar{v}_j}{\partial x_i^2} \right]$$

$$\rho \bar{h} \bar{v}_j \triangleq \rho \bar{h} \bar{v}_j + \rho \overline{h' v'_j}; q'_j = \rho \overline{h' v'_j} \text{ where } \frac{\partial}{\partial t} \left[\rho \left(\bar{h} + \frac{\bar{v}^2}{2} + k \right) - \bar{p} \right] + \nabla \cdot \left[\rho \left(\frac{\bar{h} \bar{v} + \bar{v} \bar{v}^2}{2} \right) \right]$$

$-\rho \bar{F} \cdot \bar{v} - \nabla \cdot (\bar{T} \cdot \bar{v}) + \nabla \cdot (\bar{q} + \bar{q}') = \bar{q}_{ext}$, L is the length or diameter of the section [m]; V is the volumetric flow per unit length [m³/s]; q is the heat flux [W/

$$m^2]; \text{ and } k = \frac{1}{2} \overline{v'_i v'_i}.$$

Heat transfer mechanism in a laminar mode depends on the conductivity and film thickness of the condensate. In the wave development region, the heat transfer is enhanced due to the convective mixing and increase in the interfacial surface area. Within a zone where there is a periodic wavy motion, the heat transfer is determined by the thermal resistance of the residual liquid film layer, in which the

waves move.

7.2.3.2 Vertical surfaces: Laminar flow

Consider condensation of dry saturated steam fixed on a vertical surface, whose temperature is T_w . Theory of the heat transfer process is established by Nusselt.

The following assumptions are made:

- inertia forces are small compared to the forces of gravity and viscosity;
- heat through the film is transferred only by conduction, convective transfer, and thermal conductivity along the film are not considered;
- temperature of the outer surface of the film is equal to T_s ;
- physical parameters of the film are independent of temperature;
- friction at the interface of the liquid-vapor absent, assuming the smooth film surface and small surface tension forces.

Heat transfer is carried out only by thermal conduction. Then, with the equations

$$C_p = ct \quad \text{and} \quad \overline{\rho h v_j} \triangleq \overline{\rho h v_j} + \rho C_p \overline{T v_j'}; q_j^l = \rho C_p \overline{T v_j'}, \text{ we have:}$$

$$\overline{\rho h v_j} \triangleq \overline{\rho h v_j} + \rho C_p \overline{T v_j'}; q_j^l = \rho C_p \overline{T v_j'} \quad (7.51)$$

Thus, the problem of determining the heat transfer coefficient is reduced to finding the film thickness $\delta(x)$, which is obtained from the equations of motion and heat balance equation; x is the coordinate.

The film thickness is given by:

$$T^t \triangleq R_{ij} = -\rho \overline{v_i' v_j'} = \rho \left[-\frac{2}{3} k \delta_{ij} + \nu_t \left(\frac{\partial \bar{v}_i}{\partial x_j} + \frac{\partial \bar{v}_j}{\partial x_i} \right) \right] \tag{7.52}$$

Hence, the local heat transfer coefficient is:

$$q_j^t = \rho C_p \overline{u_j' T'} = -\lambda_t \frac{\partial \bar{T}}{\partial x_j} \quad \lambda_t = \frac{C_p \mu_t}{Pr_t} \tag{7.53}$$

The average heat transfer coefficient

$$\overline{u_j' Y_{k'}} = -D_{Y_{kt}} \frac{\partial \bar{Y}_k}{\partial x_j} \quad D_{Y_{kt}} = \frac{\nu_t}{Sc_t} \tag{7.54}$$

$$\nu_t \sim l \nu'$$

where h is the height of plate, $\nu_t \sim l \nu'$. From this equation, it is well understood that the average heat transfer coefficient decreases with an increase in the height h and the temperature difference ΔT .

Eq. (7.54) is expressed in terms of Nusselt number:

$$\epsilon \sim \frac{\nu'^3}{l} \tag{7.55}$$

with

$$\nu_t \sim \frac{\nu'^4}{\epsilon} = C_\mu \frac{k^2}{\epsilon}$$

$Pr = c_p \mu / \lambda$, $k_\theta = T'^2$ and $\frac{\rho \nu^2}{2}$. Eq. (7.55) is valid when $\rho \nu \omega_j \delta l \mu_f < 200$,

7.2.3.3 Laminar-wavy flow

In the laminar-wavy film flow, a large quantity of liquid mass is transported in the waves, and major thermal resistance is at the thin film of condensate with “residual” thickness δ_0 (see Fig. 7.19B). The residual thickness δ_0 virtually does not change with the condensate flow, i.e., a flow rate increase does not increase δ_0 , but reduces the wavelength l . This wavy regime does not develop within the short period time of existence of this thin layer, which is of the order of wave oscillation period. In this case, as for the laminar flow of the film $\alpha = \lambda / \delta_0$. The average heat transfer coefficient of the film flow of the laminar wave character is given by:

$$\frac{\overline{\rho} \overline{v^2}}{2} \cong \overline{\rho} \frac{\overline{v^2}}{2} + \overline{\rho} k \quad (7.56)$$

where

$$\frac{\partial \bar{v}_j}{\partial t} + \frac{\partial \bar{v}_i \bar{v}_j}{\partial x_i} + \frac{1}{\rho} \frac{\partial \bar{p}}{\partial x_j} = -g_j - \frac{\partial R_{ij}}{\partial x_i} + \nu \left[\frac{\partial^2 \bar{v}_j}{\partial x_i^2} \right]$$

The relation holds for

$$\frac{\overline{\rho} \overline{v^2}}{2} \cong \overline{\rho} \frac{\overline{v^2}}{2} + \overline{\rho} k$$

In the wave development within the condensate film, the heat transfer coefficient is independent of the geometrical dimensions and is a function of the physical properties of the liquid film. The model will cover a range of $Re=200-10^3$.

The influence of the wavy film motion and a variation of the physical parameters in temperature on the heat transfer coefficient is accounted for by two correction factors to α_0 :

$$\frac{\overline{v^2}}{2} \gg k \quad (7.57)$$

Here α_0 is the heat transfer coefficient calculated by Eqs. (7.51)–(7.53), with physical parameters evaluated at T_s ; $\epsilon_v = Re^{0.053}$ is the correction due to the wave motion for $Re < 10^2$ and may be given by another expression

$$\nabla \cdot (\overline{\mathbf{T} \cdot \vec{v}}) \cong \nabla \cdot (\overline{\tilde{\mathbf{T}} \cdot \vec{v}})$$

is the amendment due to a variation of the fluid properties in the film section. These correlations are valid for

$$\nabla \cdot (\overline{\mathbf{T} \cdot \vec{v}}) \cong \nabla \cdot (\overline{\tilde{\mathbf{T}} \cdot \vec{v}})$$

and

$$\frac{\partial}{\partial x} \left(\overline{\mathbf{T} \cdot \vec{v}} \right) \cong \frac{\partial}{\partial x} \left(\overline{\tilde{\mathbf{T}} \cdot \vec{v}} \right)$$

Here assumed is the wall suitable for transferring the heat released on the surface of the film due to condensation. The conclusion remains valid if, instead of the heat of condensation, we use a substitute of an effective heat of condensation, which takes into account the liquid film supercooling and change the temperature profile:



Another prerequisite consideration for the solution has been the neglect of the inertia forces in the film and in the vapor. The influence of these forces may not be neglected, at least for two reasons: (1) steady-state vapor flow should show acceleration to the speed of the film interface boundaries; (2) the condensate flow would accelerate when it flows downward. When

$$K = \frac{1}{2} \frac{v_i v'_i}{v_i v'_i}$$

$K > 5$ and $Pr = 1-100$, the inertial forces can be ignored, since their effect on the heat transfer coefficient would be of only a few percent. Consideration of inertial forces is important when $K < 5$ for fluids of $Pr > 1$ and liquid metals of $Pr \ll 1$, i.e., in the critical region with large temperature differences, and in the case of condensation of metal vapor (Fig. 7.20).

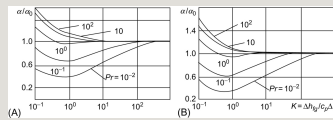


Fig. 7.20 Influences of inertia forces of condensate film laminar flows on the convective heat transfer: (A) Flat vertical surface; (B) horizontal circular tube; α is the heat transfer coefficient, from the Nusselt number calculated by Eqs. (7.51), (7.53).

7.2.3.4 Turbulent-wave flow

If greater than the critical Reynolds number ($Re_{cr} \approx 1600$), the film flow becomes turbulent. Increase in the hydraulic flow resistance of the film and increase in its thickness should cause a reduction of α . However, turbulence increases the effective thermal conductivity of the film flow (Isachenko, 1977; Labuntzov, 1960). When $Pr \geq 1$ the turbulence factor is more important and leads to higher heat transfer coefficient. For $Pr \ll 1$ (liquid metals), turbulence of the film does not play a big role in increasing the *effective thermal conductivity* () and the main factor is the increase in the film thickness that causes a reduction in heat transfer, even when compared with laminar flow (in Borishansky et al., 1976).

In the case of condensation on inclined surfaces, the gravitational acceleration g is modified to be its projection onto the axis x , i.e., $g \cos \varphi$. Here φ is the angle between the vertical axis (gravity force direction) and x :



$$(7.58)$$

7.2.3.5 Horizontal tubes and rod bundles

Condensation on the horizontal circular pipes (φ -variable). Noting $\delta \ll d$ (=pipe diameter) and under the conditions of the laminar condensate film flow and with $T_w = \text{const}$, we have an approximation of the average heat transfer coefficient:

$$\frac{\partial \bar{\rho}}{\partial t} + \nabla \bar{\rho} \vec{v} = 0 \quad (7.59)$$

or in the form of the Nu -number correlation when $\frac{\rho v^2}{2}$:

$$\frac{d}{dx} \left[\rho \left(\delta + \frac{1}{2} \delta^2 \right) - \rho \right] + \rho \cdot \left[\rho \cdot \vec{v} \left(\delta + \frac{1}{2} \delta^2 \right) \right] = \rho \cdot \left[\rho \cdot \vec{v} + \rho \cdot \left[\left(\vec{v} + \vec{v}^2 \right) \cdot \vec{v} \right] + \rho \cdot \left(\vec{v} + \vec{v}^2 \right) + \rho \cdot \vec{v} \right] \quad (7.60)$$

Eqs. (7.59), (7.60) are approximate. The more exact calculation can be made incorporating the laminar and turbulent wave modes as suggested in Sukhatme (1990), Labuntzov (1960), and Tanasawa (1994). The wave mode to horizontal

$$\vec{T} = -\frac{2}{3}\mu \nabla \cdot \vec{v} I + \mu \left(\nabla \vec{v} + {}^t \nabla \vec{v} \right); \vec{q} = -\lambda \nabla \vec{T}$$

and

pipes develops when

$$\bar{p} = p(\bar{p}, \bar{h}); \bar{T} = T(\bar{p}, \bar{h}); \bar{\mu} = \mu(\bar{p}, \bar{h}); \bar{\lambda} = \lambda(\bar{p}, \bar{h})$$

if . When $q = \text{const}$, 0.728 in Eqs. (7.58), (7.59) is set equal to 0.693.

Average heat transfer coefficient of the stationary vapor flow in a bundle of horizontal pipes depends weakly on the relative distance between the tubes, dripping characteristics from the pipes and other parameters, and generalized dependencies mentioned previously (see Fig. 7.21).

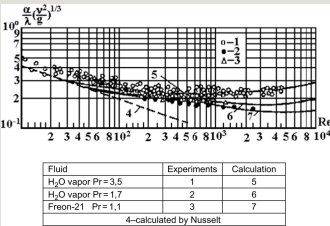


Fig. 7.21 Intensity of heat transfer by condensation.

The heat transfer rate on a horizontal tube surface is higher than on a vertical surface, since the film thickness is less than the average. Condensation of the vapor occurs on the horizontal tube banks, condensate flows from the upper to the lower pipe, and the liquid layer is increased on the lower pipes and tends to decrease the heat exchange, but the liquid film is turbulent induced by falling jets on the surfaces of lower rows of the tube bank. Therefore, the nature of heat transfer depends on the steam supply, its speed and the layout of the beam.

7.2.3.6 Condensation of superheated and wet vapor

When the superheated (δT) vapor condensates, the condensation latent heat Δh_{fs} are transferred with the heat of superheating $c_{pf}\delta T$, then Δh_{fs} is replaced by

$(\Delta h_{fg} + c_{pg} \delta T)$, so the heat transfer coefficient of the superheated vapor will be:

$$\alpha = \alpha_s \sqrt[4]{\frac{\Delta h_{fg} + c_{pg} \delta T}{\Delta h_{fg}}} \quad (7.61)$$

Here α_s is the heat transfer coefficient of dry saturated vapor.

Condensation of the wet steam having a quality $x < 1$ releases an amount of the heat equal to $\Delta h_{fg}x$ per kg. Therefore, for an approximation the following can be accepted

$$\alpha \approx \alpha_s \sqrt[4]{x}. \quad (7.62)$$

In many cases of practical importance, with small overheating or at low humidity, where $(1-x) < 0.1$, the heat transfer coefficient is $\alpha \approx \alpha_s$.

7.2.3.7 Condensation of metal vapor

Intensity of the heat transfer with metal vapor condensation depends little on the nature of the flow of the condensate film due to the high thermal conductivity of the metals. The decisive role in this case is played by the following two effects:

- (1) the dominant thermal resistance is the phase transition (at relatively low temperatures and pressures, the vapor condensation rate $\beta < 1$);
- (2) the presence of noncondensable gases in the vapor, whose effect is very difficult to estimate.

When $p < 10^3$ Pa, $\beta = 1$. With increasing pressure condensation coefficient decreases

according to $\beta = 20 / \sqrt{p}$.

7.2.4 Film condensation of flowing steam

7.2.4.1 Vertical surface

Vapor flow has a dynamic effect on the phase interface, speeding up or slowing down the condensate film flow. If the steam flows downward (direction coincides with the direction of gravity), the film speed increases, the thickness decreases, and the heat transfer rate increases. When the steam flows upward, hampering the condensate film, and increasing its thickness, there is a wave mode, and the heat transfer coefficient can be reduced. With further increase in the vapor-phase velocity, the interphase friction force increases and drags the film upward, its thickness is reduced and the heat transfer coefficient (Fig. 7.22) increases again. At this high speeds of the vapor, a break-up of the film is likely and the liquid droplets are entrained to the vapor flow, which leads to a reduction in the film thickness and to a sharp increase in the heat transfer coefficient (Gogonin, 2006; Labuntzov, 1960).

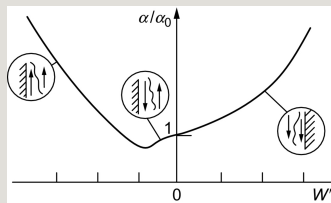


Fig. 7.22 The change of heat transfer coefficient with vapor velocity w_g .

Steam-vapor flow acts on the condensate film flow so that it not only changes the film thickness, but also leads to a perturbation of the film flow, accelerates a transition from laminar to turbulent flow. Therefore, a molecular heat transfer is supplemented by turbulent transfer even at low Re .

7.2.4.2 Horizontal tubes and rod bundles (Breber et al., 1980; Labuntzov, 1957; Sukhatme, 1990)

Calculation of heat transfer in a horizontal tube bundle is complicated due to: (1) a decrease in steam velocity due to partial condensation as the steam moves in the tube bundle; (2) an increase in the condensate film thickness on the lower tube bank by a drainage from the upper to the lower tubes, which largely depends on the geometry of the tube array configuration. Usually tube bundle layouts of

condensers are complex, making it difficult to put theoretical and even experimental results into practice. Therefore, it is often the case that condensation calculations in tube bundles are made based on the correlations and models developed in industry.

7.2.4.3 Condensation inside tube

Vapor condensation inside a tube is more complex phenomena than the stationary or moving steam condensation on the surface (Spalding and Taborek, 1983; Miropol'sky, 1962). The film of condensate is exposed to the steam flow in a pipe. The rate of vapor condensation decreases in length of the tube and the condensate flow rate increases. Assume steam quality $x > 1$ (saturated or superheated steam) in the inlet portion of the pipe, the whole pipe cross section is occupied by the steam. Downstream two-phase flow structure depends on the balance among the gravity and friction, vapor flow acting on the condensate film, and volumetric relationship of fluid and steam. Single-phase vapor flow at the tube inlet is usually in the turbulent flow regime. It can be replaced on the laminar flow. Although laminar, the condensate films may show turbulent motions near the inlet due to increased condensate flow rate and enters again into the laminar flow regime, where the steam flow velocity will drop and become low. Sketch of a horizontal pipe flow regimes of vapor and liquid is shown in Fig. 7.23.

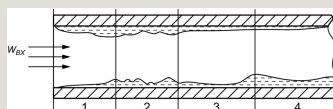


Fig. 7.23 Scheme condensation and flow conditions inside the horizontal pipe (by Breber et al., 1980): 1—initial portion; 2—section of the turbulent film movement; 3—section with laminar film movement; 4—stream.

In horizontal tubes a strong nonuniformity will be found in the condensate distribution over the cross section, leading to a considerable temperature difference of top and bottom of the tube.

Theoretical solutions would be obtained, typically applicable for a narrow range of parameters. Therefore, heat transfer calculations are carried out, knowing the steam

velocity w_0 at the inlet or total mass flow rate, where ρ and w are the mixture density and velocity. The latter, although it is convenient for calculations, but is rather notional.



Condensing vapor behaviors in a vertical tube differ depending on the direction of flow of the vapor. In the case of countercurrent flow at low speeds (10–5 m/s), flooding may occur. At high speeds (15–30 m/s), the liquid portion breaks down from the film surface (Gogonin, 2006).

Under superheated vapor complete condensation in a pipe, where the vapor enters and exits as a supercooled liquid, it is possible to distinguish four characteristic sections along the tube as shown in Fig. 7.24:

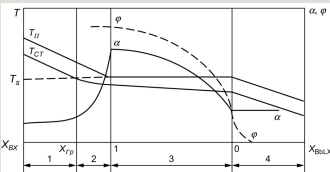


Fig. 7.24 Modes and heat transfer characteristics of complete condensation of the superheated steam inside the tube (φ is the vapor void fraction).

(1) cooling of the superheated steam by condensation heat transfer $T_g > T_s$,

$$\frac{\partial \bar{p}}{\partial t} + \frac{\partial \bar{p} \bar{v}_j}{\partial x_j} = 0, \quad \frac{\partial \bar{p} \bar{v}_j}{\partial t} + \frac{\partial \bar{p} \bar{v}_j}{\partial x_j} + \frac{\partial \bar{p}}{\partial x_j} = -\bar{p} g_j + \frac{\partial}{\partial x_j} (\bar{c}_{ij} - R_{ij})$$
. In this section, $\frac{\partial}{\partial t} \left(\frac{1}{2} \bar{v}^2 \right) + \frac{\partial}{\partial x_j} \left(\bar{v} \bar{v}_j \right) = \frac{\partial}{\partial t} \left(\frac{1}{2} \bar{v}^2 \right) + \frac{\partial}{\partial x_j} \left(\bar{v} \bar{v}_j \right) = \frac{\partial}{\partial t} \left(\frac{1}{2} \bar{v}^2 \right) + \frac{\partial}{\partial x_j} \left(\bar{v} \bar{v}_j \right)$,

$$\langle f \rangle^s = \frac{1}{A} \int_A f \, ds$$
.

(2) condensation of superheated vapor $T_g \geq T_s$,

(3) Condensation of saturated vapor $\frac{d}{dt} \int_{V_k} f(x_j, t) \, dV = \int_{V_k} \frac{\partial f}{\partial t} \, dV + \int_{V_k} \frac{\partial f}{\partial x_j} \bar{v}_j \, dV = \frac{dC}{dt}$, $\vec{v} \cdot \vec{n} = 0, 1 \geq x \geq 0$.

(4) condensate cooling $\langle \frac{\partial f}{\partial t} \rangle^s = \frac{\partial \langle f \rangle^s}{\partial t}$, $\vec{v} \cdot \vec{n} = 0, x < 0$.

Here, is the relative enthalpy with i_{CM} the mixture enthalpy, and x_{Tp} is the relative enthalpy at which vapor condensation begins.

7.2.5 Condensation of vapor-gas mixture

7.2.5.1 Mechanisms of heat transfer: three thermal resistances

A presence of noncondensable gases in the vapor-steam changes the heat transfer mechanism significantly. Pressure of the gas-vapor mixture is approximately uniform in the cross section of the volume, but since the vapor partial pressure in a condensation surface is less than in the core flow, the gas concentration at the surface is higher than in the bulk (Fig. 7.25; Isachenko, 1977). As a result, there are two opposite diffusion processes: one diffusion of the gas mixture toward the film and the other diffusion of the gas away from the wall. The resulting mixture flow is zero but the vapor flow is not zero. The films of noncondensable gas are a barrier to incoming vapor to the film. The heat transfer coefficient in the presence of noncondensable gases decreases sharply and depends on the three thermal resistances—condensate film resistance R_{film} , interfacial thermal resistance R_{ϕ} , and the diffusion thermal resistance (resistance to steam supply to the condensation surface) R_{dif} .

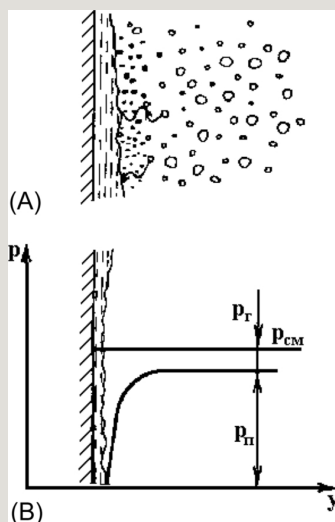


Fig. 7.25 Condensation surface conditions: (A) scheme of distribution of molecules at the condensation surface: •—gas molecules; ○—vapor molecules. (B) Distribution of partial pressures of steam and gas at the surface.

$$\int_A \nabla \cdot \vec{B} \, da = \frac{\partial}{\partial z} \int_A B_z \, da + \int_C \frac{\vec{n} \cdot \vec{B}}{\vec{n} \cdot \vec{n}_C} \, dC \quad (7.63)$$

This thermal resistance is a sum of the temperature differences ΔT_{film} , ΔT_ϕ , and

$$\vec{B} = \vec{n}_z \Rightarrow \frac{\partial A}{\partial z} = - \int_C \vec{n} \cdot \vec{n}_z \frac{dC}{\vec{n} \cdot \vec{n}_C} \Delta T_{diff} \text{ i.e.,}$$

At moderate (not too low) pressure we can neglect the thermal resistance of the phase transition:

$$\int_A \nabla \cdot T da = \frac{\partial}{\partial z} \int_A \vec{n}_z \cdot T da + \int_C \vec{n} \cdot T \frac{dC}{\vec{n} \cdot \vec{n}_C} \quad (7.64)$$

When calculating the thermal resistance of the diffusion account for the intensity of

the supply of heat by convection $\left\langle \frac{\partial \rho}{\partial t} + \nabla \cdot (\rho \vec{v}) \right\rangle^s = \frac{\partial \rho^s}{\partial t} + \left\langle \nabla \cdot (\rho \vec{v}) \right\rangle^s = \frac{\partial \rho^s}{\partial t} + \frac{1}{A} \frac{d}{dt} \int_A \rho \vec{v} \cdot d\vec{v}$ and that by condensing

vapor, where $V \triangleq \frac{\langle \rho \vec{v}_z \rangle^s}{\langle \rho \rangle^s} = \frac{\langle \rho \vec{v}_z \rangle^s}{\rho}$ is the vapor mass flux to the condensation surface; β is the mass transfer coefficient (m/s); c_s and c_w are the vapor concentration in kg/m³. Hence, we come up with:

$$A \frac{\partial \hat{\rho}}{\partial t} + \frac{\partial A \hat{\rho} V}{\partial z} = 0 \quad (7.65)$$

Here a is the conditional that takes into account the processes of heat and mass transfer in the gas-vapor mixture and the convective heat transfer through the film. Fig. 7.26 shows how the temperature field is distributed near the condensation surface with increasing number of noncondensable gases in the steam.

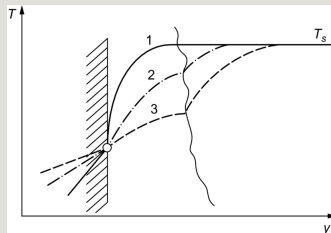


Fig. 7.26 Changes in temperature field near the condensation surface with increasing amount of noncondensable gases ($1 < 2 < 3$).

The intensity of condensation increases with increase in pressure. In Fig. 7.27 shown are the effects of the volume of gas content and pressure on the heat transfer coefficient.

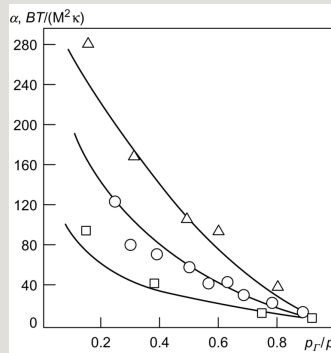


Fig. 7.27 The effect of pressure and partial pressure of the gas in the condensation heat transfer coefficient of the steam from the steam-air mixture, \square $p=0.1-0.3$ MPa; \circ $p=0.4-0.8$ MPa; \triangle $p=2.2-3.0$ MPa.

7.2.6 Condensation at direct contact of the phases

Relevant to severe accidents evaluation of nuclear power reactors, it is important to consider the processes of condensation in direct contact of two phases, which play an important role in nuclear reactor safety analysis. These include:

- (1) Condensation of large vapor bubbles in the fluid (vapor and water mixing under the ECCS operation modes);
- (2) Condensation of vapor in the liquid (water and vapor mixing in the reactor vessel);
- (3) Condensation of steam on the subcooled droplets (ECCS spray);
- (4) Condensation on free surfaces.

A major difficulty in these problems is associated with defining the interface area per unit volume.

7.2.6.1 Condensation in subcooled liquid

Vapor condensation in the subcooled liquid flow is popular and observed, e.g., in

the channels and pipings of boiling water reactors, steam generators, mixers of vapor and liquid.

There are two stages in the collapse of vapor bubbles: at a large radius, the rate of change in the radius of a bubble is determined by the intensity of the interface heat transfer, while at a small radius, the main role is played by the inertia force. The first stage accounts for most of the lifetime of the vapor bubble, so it is more important. A detailed discussion on the bubble radius change in the subcooled liquid is found in Florschuetz and Chao (1965).

The condensation of vapor bubbles flowing out of the nozzle into the subcooled turbulent flow, can be estimated as in the following. The rate of collapse of the

vapor bubble is described by
$$\frac{\partial \bar{p} \left(\tilde{h} + \frac{\tilde{v}^2}{2} \right) - \bar{p}}{\partial t} + \frac{\partial \bar{p} \tilde{v}_j \left(\tilde{h} + \frac{\tilde{v}^2}{2} \right)}{\partial x_j} - \bar{\rho} g_i \tilde{v}_i - \frac{\partial (\bar{\tau}_{ij} + R_{ij}) \tilde{v}_i}{\partial x_j} + \frac{\partial \bar{q}_j + \bar{q}_j}{\partial x_j} = \bar{q}_{ext}$$
, where the heat transfer coefficient can be found from the approximate relations for heat transfer solid sphere:

$$\left\langle \frac{\partial \bar{p} \left(\tilde{h} + \frac{\tilde{v}^2}{2} \right) - \bar{p}}{\partial t} \right\rangle = \frac{\partial \langle \bar{p} \tilde{h} \rangle^s}{\partial t} + \frac{\partial \left\langle \frac{\tilde{v}^2}{2} \right\rangle^s}{\partial t} - \frac{\partial \langle \bar{p} \rangle^s}{\partial t} \quad (7.66)$$

where $H \triangleq \frac{\langle \bar{p} \tilde{h} \rangle^s}{\langle \bar{p} \rangle^s}$; is the surface velocity. This relationship gives satisfactory results for $P \triangleq \langle \bar{p} \rangle^s = \hat{P}$, $p=1-6$ MPa, $Re=2000-3000$.

When the vapor jet injection is made into a large amount of subcooled liquid, condensation is characterized by an unstable boundary and changes in transient velocity profile. Evaluation of heat exchange between the vapor flow and liquid volume can be made by empirical relations $Nu=F(Re, Pr)$.

7.2.6.2 Condensation on liquid subcooled jet

Suppose a large volume is filled with vapor at a saturation temperature. A liquid jet at a temperature T_0 is lower than the saturation temperature ($T_0 < T_s$) and is fed through a hole of diameter d into this volume with a mass flow W_f [kg/s]. If the jet of a length $x=l$ condenses the amount of vapor G_k [kg/s], the heat balance equation

can be written as:

$\left\langle \bar{\rho} \frac{\tilde{v}^2}{2} \right\rangle \cong \langle \bar{\rho} \rangle^s \frac{V^2}{2}$; here T_0 and T_l are the average temperature of liquid-phase on the cross section at $x=0$ and $x=l$.

Condensation of the vapor will stop when the temperature of the liquid at the end of the jet reaches T_s . The quantity of heat transmitted by the vapor condensation to

the jet, can be computed as $\left\langle \frac{\partial \bar{\rho} \left(\tilde{h} + \frac{\tilde{v}^2}{2} \right) - \bar{p}}{\partial t} \right\rangle = \frac{\partial \bar{\rho} H}{\partial t} + \frac{\partial \bar{\rho} \frac{V^2}{2}}{\partial t} - \frac{\partial \bar{p}}{\partial t}$ where $\frac{\partial \bar{\rho}}{\partial t} \frac{V^2}{2}$ is the average heat transfer coefficient along the length; A is the area of the surface

of the jet; $q_z^d \triangleq \left\langle \bar{\rho} \tilde{v}_z \tilde{h} \right\rangle^s - \hat{\rho} V H$ is the

mean log temperature difference. Because $\left\langle \bar{\rho} \tilde{v}_z \frac{\tilde{v}^2}{2} \right\rangle^s \cong \langle \bar{\rho} \rangle^s V \frac{V^2}{2}$, the relationship between the coefficient of heat transfer and heating jets is of the form:

$$\left\langle \frac{\partial \rho \left(\tilde{h} + \frac{\tilde{v}^2}{2} \right)}{\partial t} \right\rangle = \frac{1}{A} \frac{\partial}{\partial t} \int \rho \left(\tilde{h} + \frac{\tilde{v}^2}{2} \right) dV = \frac{1}{A} \frac{\partial}{\partial t} \left(\rho \frac{V^2}{2} \right) = \frac{1}{A} \left[\frac{\partial \rho}{\partial t} \frac{V^2}{2} + \rho \frac{\partial V^2}{\partial t} \right] \quad (7.67)$$

The heat transfer theory for the case of condensation of steam on the liquid jet (laminar and turbulent) has been developed only with considerable simplifications.

7.2.6.3 Condensation on dispersed liquid spray jet

Vapor condensation on the spray jet is considerably more intense than that in the continuous stream case due to a sharp increase in the surface area of the liquid-vapor contact. This process of droplet condensation can be represented with two stages.

In the first stage, the droplet surface is heated from its initial temperature T_0 to T_s . The rate of process is determined by the thermal resistance at the interface, which

depends on the pressure. $\langle \bar{\rho} g_i \tilde{v}_i \rangle^s \cong \hat{\rho} g_z V$ and the condensation coefficient β .
 For water $\left\langle \frac{\partial (\tilde{t}_d - R_d) \tilde{v}_i}{\partial t} \right\rangle = \frac{1}{A} \frac{\partial}{\partial t} \left[A \left\langle \left(\tilde{T} + T \right) \cdot \tilde{v} \right\rangle_n^s \right]$ [(m² K)/W].

The rate of condensation in the second stage is determined by the heat removal process from the surface to inside the droplet, i.e., thermal resistance of drops. Influence of the convection on heat transfer inside the drop is low and, therefore,

the resistance of the drop depends on the thermal conductivity of the liquid and the radius of the droplet. Hence, to obtain the heat transfer of drops, a classical solution approach is applied to the heat conduction problem for a solid sphere:

$$\left(\frac{\partial \bar{q}}{\partial \bar{r}} + \frac{\bar{q}}{\bar{r}} \right)^S = -\frac{1}{A} \frac{\partial}{\partial \bar{r}} \left(\bar{r}^2 + \bar{r}_c^2 \right)^S + \frac{1}{A_c} \left(\bar{r} + \bar{r}_c \right) \frac{dC}{d\bar{r}} = -\frac{1}{A} \frac{\partial}{\partial \bar{r}} \left(\bar{r}^2 + \bar{r}_c^2 \right)^S + \frac{1}{A} C_{D0} \quad (7.68)$$

Solving the heat transfer problem on the dispersed jet is regarded not yet completed due to a lack of a number of factors to be considered (spectrum of droplets, deformation, different types of coagulation or decay of the drops, etc.). For more information, see Berman et al. (1983) and Isachenko (1977).

7.2.7 Enhancement of heat transfer at condensation

When the thermal resistance of the condensate film (R_{film}) is large compared to other thermal resistances, for the enhancement of heat transfer it is necessary to reduce this resistance. One method of reducing this resistance is to make a transition to the drop-wise condensation. Other methods are based on an artificial reduction of the condensate film thickness by the employment of vertical pipes with ribbed or corrugated surfaces instead of smooth pipes. The ribs may be of very different forms—two-dimensional or three-dimensional (Fig. 7.28). The issue has been extensively discussed in open literatures. In the review by Sukhatme (1990), for example, you can find the information to optimize the geometry and dimensions of the finned tubes. The presence of corrugations leads to the fact that the condensate film curved surface.

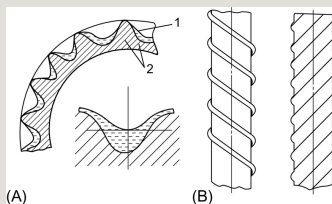


Fig. 7.28 Ribbed and corrugated pipes for heat transfer enhancement: (A) finned tube cross section: 1—condensate film; 2—tube wall; (B) types of protrusions on the tube surface.

Under the influence of the surface tension forces, the condensate moves from a crest to a trough and the film thickness decreases for a greater portion of the condensate film surface, and therefore, the thermal resistance of heat transfer (Fig. 7.28A). Twisted ribs on the vertical tubes contribute to further enhancement of heat transfer coefficient due to the fact that the liquid film is formed on a short stretch, before drainage through the spiral protrusions (Fig. 7.28B).

For the vertical tubes, the heat transfer will increase until the area occupied by the ribs is around 10% of the total surface area. A further increase in the number of ribs has little effect. Enhancement of heat transfer with the ribs on vertical tube surfaces is effective as long as the ribs are not flooded with the condensate.

For the horizontal tubes, the presence of transverse or cross-ribs facilitates withdrawal of the condensate film and improves the heat transfer coefficient. This effect is associated with a decrease in film thickness on the edge, while the main mass of the condensate quickly drains down along the troughs (Fig. 7.29). The effectiveness of cross-ribs sharply decreases with decreasing distance between the ribs.

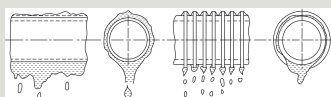


Fig. 7.29 Dripping films with a horizontal smooth pipe and ribbed pipe.

One of the attractive methods that have been reported recently is coating tube surfaces. It provides a constant drop-wise condensation on the surface of copper tubes (Zhao et al., 1990). This is achieved by coating the surface with the Cu-Cr-N 0.9 mm thick alloy layer. The coating is carried out by the ion implantation of Cr and N so that the crystal structure of the surface layer of copper is transformed into amorphous. The thermal resistance of the coating has become negligible and the heat transfer coefficient is 20–40 times higher than that for the film condensation.

7.3 Radiative heat transfer

7.3.1 Basic principles

Thermal radiation is a portion of the process of energy propagation by means of electromagnetic waves. When it is in thermodynamic equilibrium with a substance, we call it an equilibrium radiation. The radiation results from changes in electronic, vibrational, and rotational states of the atoms-molecules and the *emission* of the radiant energy takes place as a result of irregular deceleration of charged particles (electrons, ions) in the media. The reverse process is then what occurs when radiant energy impinges on a solid surface and causes its temperature rise (*absorption*).

From a corpuscular point of view, the radiant energy is emitted and absorbed in discrete forms of the electromagnetic waves, which could be described as if particles with mass zero and charge zero, i.e., photons are carrying energy with the speed of light c . The photon energy is $h\nu$, where

$$\frac{\partial}{\partial t} \left[\bar{\rho} \left(H + \frac{V^2}{2} \right) - P \right] + \frac{\partial}{\partial z} \left[A \bar{\rho} V \left(H + \frac{V^2}{2} \right) \right] - A \bar{\rho} g_z V =$$

$$\frac{\partial}{\partial z} A < (\bar{T} + T') \cdot \bar{v} \rangle \hbar \nu > s = - \frac{\partial A q_{eff}}{\partial z} + C q_w + A \bar{\rho} c_{ext}$$
 is the Planck constant, ν is the frequency of an electromagnetic wave. Note that the photon has momentum $h\nu/c$.

The wavelength λ , characterizing an electromagnetic wave, is related to its frequency ν by the equation $\frac{d}{dt} \left[\left(\frac{d}{dt} \right)^2 + \left(\frac{d}{dt} \right)^2 \right] = - \left(\frac{d}{dt} + \frac{d}{dt} \right) \frac{d}{dt}$. The speed of light $\bar{T} + T'$ ($=299,792,458$ m/s exactly) in vacuum.

$$\frac{\partial}{\partial t} \left[\frac{\partial}{\partial t} \left(\frac{\partial}{\partial t} \right) \right] = \frac{\partial}{\partial t} \left[\frac{\partial}{\partial t} \left(\frac{\partial}{\partial t} \right) \right] = \frac{\partial}{\partial t} \left[\frac{\partial}{\partial t} \left(\frac{\partial}{\partial t} \right) \right]$$
 in gases, and in other media
$$\frac{\partial}{\partial t} \left[\frac{\partial}{\partial t} \left(\frac{\partial}{\partial t} \right) \right] = \frac{\partial}{\partial t} \left[\frac{\partial}{\partial t} \left(\frac{\partial}{\partial t} \right) \right] = \frac{\partial}{\partial t} \left[\frac{\partial}{\partial t} \left(\frac{\partial}{\partial t} \right) \right]$$
. The ratio $\frac{\partial}{\partial t} \left[\frac{\partial}{\partial t} \left(\frac{\partial}{\partial t} \right) \right] = \frac{\partial}{\partial t} \left[\frac{\partial}{\partial t} \left(\frac{\partial}{\partial t} \right) \right] = \frac{\partial}{\partial t} \left[\frac{\partial}{\partial t} \left(\frac{\partial}{\partial t} \right) \right]$ is refractive index. The frequency does not change when the electromagnetic wave passes through from one medium to another, but the wavelength because the light speed changes. Distribution of radiation energy per frequency (or wavelength) is radiation spectrum.

The spectrum of equilibrium radiation is independent of the nature of the substance and determined by Planck's law of radiation. Thermal radiation field in the electromagnetic spectrum covers a range of wavelengths $\sim 10^{-7}$ – 10^{-4} m (see Fig. 7.30), i.e., in the visible and infrared regions (Hackford, 1960). The visible part of the spectrum covers a wavelength of 0.40 – 0.76 μm . The infrared region of the spectrum consists of a near-infrared region (0.76 – 25 μm) and the far infrared region (25 – 1000 μm). A main portion of the thermal radiation energy falls on the wavelengths region of 0.76 – 15 μm , i.e., lies in the near infrared. Radiation in the visible region of the spectrum is significant only at very high temperatures.

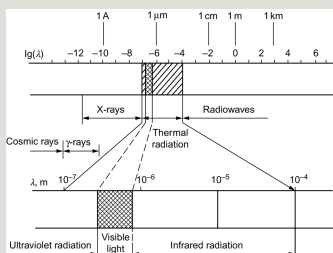


Fig. 7.30 Portion of the thermal radiation in the electromagnetic spectrum.

Thermal radiation can be viewed as a surface phenomenon because thin surface layers (–0.001 to 1 mm) on the body are involved in the radiative heat transfer.

Bodies can radiate energy of all wavelengths $A\left(\frac{\partial \vec{p}}{\partial t}\right) = A\left(\nabla \vec{p} \cdot \vec{n}\right) = \frac{\partial A \langle \vec{p} \rangle^S}{\partial t} + A\left(\vec{p} \cdot \vec{n} \cdot \frac{\partial \vec{C}}{\partial t} - \frac{\partial \vec{C}}{\partial t} \cdot \vec{n}\right) + Fp$ (a continuous spectrum) or selectively to a specific wavelength range (selective spectrum). With a change in temperature, not only the intensity but also structure of the radiation (spectrum) varies. There are monochromatic and full (integral) radiation modes. *Monochromatic radiation* corresponds to that of a narrow wavelength range

$$Fp = \int_C \vec{p} \cdot \vec{n} \cdot \vec{n}_z \frac{dC}{n_c \cdot n}$$

Integral radiation (full spectrum) is associated with the total radiant energy emitted from a body Q (W); in the entire wavelength range $0 < \lambda < \infty$, the integral flux density of the (hemispherical) radiation, i.e., the radiation flux emitted from the unit area per unit time we call *emittance* (or *emissive power*)

$$\vec{p} = \langle \vec{p} \rangle^S + \delta \vec{p} = P + \delta \vec{p} \quad (\text{W/m}^2). \text{ Thus}$$

Emittance in an infinitesimal range of wavelengths divided by this interval is called the *spectral density* of radiation flux (spectral or monochromatic emittance):

$$Fp = -P \frac{dA}{dz} + \int_C \vec{p} \cdot \vec{n} \cdot \vec{n}_z \frac{dC}{n_c \cdot n} = -P \frac{dA}{dz} + Fp \quad (\text{W/m}^3).$$

The amount of energy, emitted per unit time in the angular direction ψ the elementary area dA , per unit solid angle ω and per unit area of the projection onto a plane perpendicular to the direction of radiation, is called the *brightness* (intensity) of radiation:

$$F'P = \int_C \delta \vec{p} \cdot \vec{n} \cdot \frac{dC}{\vec{n}_c \cdot \vec{n}} \quad (7.69)$$

$$A \left\langle \frac{\partial \vec{p}}{\partial z} \right\rangle^s = A \frac{\partial P}{\partial z} + F'p$$

is called the spectral brightness.

Thermal radiation energy impinging on the body can be absorbed, reflected, or can pass through the body:

$$\langle \vec{p} g_z \rangle^s = \hat{p} g_z \quad (7.70)$$

where A , R , and D correspond to the absorbance, reflectance, and transmittance (transparency) of the material body. Here note that A is a fraction of absorption and should be distinguished from the area A in m^2 . Particular cases of this equation leads us to concepts of ideal bodies, i.e.,

$A=1$; $R=D=0$ —absolutely blackbody;

$D=1$; $A=R=0$ —completely transparent;

$R=1$; $A=D=0$ —absolutely mirror.

Dry air, mono- and di-atomic gases at temperatures below 3000 K can be regarded as transparent (diathermic).

Most of the solids are opaque, so that $D=0$ and $A+R=1$. In this case, the reflectivity and absorptivity of the body are interconnected. A blackbody does not exist, and usually $A < 1$ (gray body). In general, the absorbance depends on the wavelength. Such substances show selective absorption (see Fig. 7.31). Classification of different types of radiation is shown in Fig. 7.32. There, E is the *own* radiation; E_{inc} is the *incident* of radiation on the body; $E_{abs}=AE_{inc}$ is the *absorption* of radiation; $E_{ref} = (1-A)E_{inc}$ is the *reflected* radiation. A sum of the own and reflected radiations is called the *effective* radiation $E_{eff} = E + E_{ref} = E + (1-A)E_{inc}$. It is noted that E_{abs} , E_{ref} , and E_{eff} are linear functions of E_{inc} . Properties (spectral content) of their own and the reflected radiations may be different.

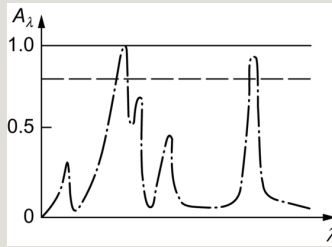


Fig. 7.31 Absorption of different material bodies: — ideal blackbody; - - - gray body; - · - · - selective absorption body.

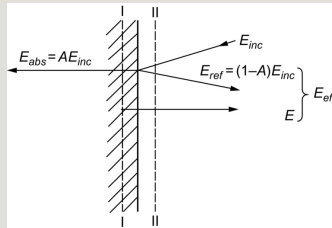


Fig. 7.32 Classification of different types of radiation; I and II are the layers infinitesimally close to the surface.

Thermal radiation flux can be given from the heat balance. For the plane I-I (Fig. 7.32), we have:

$$\lambda \left(\nabla \cdot (\vec{T} + \vec{T}') \cdot \vec{n}_c \right) = \frac{\partial}{\partial t} \left(A \langle \vec{n}_c \cdot (\vec{T} + \vec{T}') \cdot \vec{n}_c \rangle + \int_C \vec{n} \cdot (\vec{T} + \vec{T}') \cdot \vec{n}_c \right) \frac{dC}{d\vec{n}_c \cdot \vec{n}} \quad (7.71)$$

For the plane II-II in Fig. 7.32:

$$-C \tau_w \triangleq \int_C \vec{n} \cdot (\vec{T} + \vec{T}') \cdot \vec{n}_c \frac{dC}{n_c \cdot \vec{n}} \quad (7.72)$$

By eliminating E_{inc} from these equations yields:

[image]

or

$$\vec{n} \cdot \vec{n}_z \neq 0 \quad (7.73)$$

More discussions on radiation heat transfer are provided in many monographs and text books, e.g., by Adrianov (1972), Blokh (1962), Cess (1964), Klimenko and Zorin (2001), Spalding and Taborek (1983), and Sparrow and Cess (1978).

7.3.2 Laws of thermal radiation

Thermal radiation laws apply to the equilibrium radiation of blackbody.² When all the bodies that are involved in the system take the same temperature,

$-F_p = A \left(\frac{\partial p}{\partial z} \right)_{\text{avg}} = -A \left(\frac{K_{\text{avg}}}{\delta z} \right) \frac{V^2}{2}$ and the radiation is called as equilibrium (black). A heated blackbody emits photons, the spectrum of which depends only on the temperature. In the case of a gray body, radiation spectrum depends, besides the wavelength, on physical properties and surface conditions of the body, and can only be determined experimentally.

7.3.2.1 Planck's law (Fig. 7.33)

Spectral distribution of the radiation flux of a blackbody is expressed by a function of the wavelength and temperature.

$$Re = \frac{\rho V D_h}{\mu} \quad (7.74)$$

where C_1 —first radiation constant; C_2 —second radiation constant, λ —wave length (m); T —absolute temperature (K). All the fundamental constants are shown in Table 7.4.

Table 7.4

Fundamental constants in the law of radiation

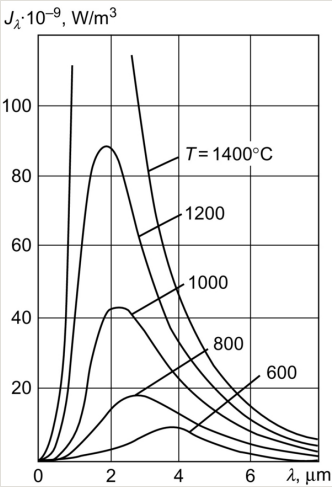


Fig. 7.33 Graphical representation of the Planck's law.

Another expression for this law is using $\lambda = n c_0 / \nu$:

$$D_h = \frac{4A}{C} \tag{7.75}$$

where h is the Planck's constant; k is the Boltzmann constant; c_0 is the speed of

light in vacuum and $A \left(\nabla \cdot \left(\vec{p}_0, \vec{r} \right) \right)^s = \frac{\partial A \left(\vec{p}_0, \vec{r} \right)^s}{\partial \epsilon} = \frac{\partial A \left(\vec{p}_0, \vec{r} \right)^s}{\partial \epsilon} + \frac{\partial A \left(\vec{p}_0, \vec{r} \right)^s}{\partial \epsilon}$ is the refractive index of the medium.

With the Stefan-Boltzmann constant σ , the law in the form of:

$$\frac{\partial AT_z^d}{\partial z} = \frac{\partial A \left(\langle \tilde{\rho} \tilde{v}_z \tilde{v}_z \rangle^S - \tilde{\rho} V V \right)}{\partial z} \quad (7.76)$$

leads to a conclusion that $J_{0z}/(\sigma m_3 T_3)$ is a function of only one variable $n\lambda T$.

Two limiting cases of the Planck's law are in the following:

(1) with $\tilde{\rho} = \left(\rho(p, H) \right)^+ \cong \rho(P, H) = \rho \left(\frac{\partial h}{\partial p} \right)^+$, i.e., at high temperatures or long wavelengths $\tau_w = Cf(Re)\rho \frac{V^2}{2}$; $Cf = aRe^{-b}$; $K_{sing} = cRe^{-d}$ (m K)

$$q_w = h(T_w - T) = \frac{\lambda Nu(Re, Pr)}{D_h} (T_w - T); \quad Nu = C Re^p Pr^q$$

where $C_3 = 2.60110 \cdot 10^{-8}$ W m/K. This expression is known as the *Rayleigh-Jeans law*.

(2) with $q_z^{eff} = -\lambda^{eff} \frac{\partial T}{\partial z}$ (or $h\nu \gg kT$), i.e., at low temperatures or short wavelengths $A \frac{\partial \tilde{\rho} V}{\partial t} + \frac{\partial A \tilde{\rho} V V}{\partial z} + A \frac{\partial P}{\partial z} = \hat{\rho} g_z - C \tau_w - A \frac{K_{sing}}{\delta z} \rho \frac{V^2}{2}$ (m K), the Planck's law becomes the *Wien's law*:

$$\lambda \frac{\partial}{\partial \lambda} \left[\hat{\rho} \left(H + \frac{V^2}{2} \right) - P \right] + \frac{\partial}{\partial z} \left[\hat{\rho} V \left(H + \frac{V^2}{2} \right) \right] - \hat{\rho} g_z = C_0 + \hat{\lambda}_{eff} \frac{\partial h \nu}{\partial z} \quad (7.77)$$

The position of maximum of the radiation intensity is obtained from Eq. (7.74), equating $dJ_\lambda/d\lambda$ zero. As a result,

$$\tau_w = C_f(Re)\rho \frac{V_\infty^2}{2}; \quad K_{\text{sing}} = K_{\text{sing}}(Re); \quad Re = \frac{\rho V D_0}{\mu} \quad (7.78)$$

These expressions are called the *Wien's displacement law*. For example, maximum solar emission is observed at $q_w = h(T_w - T) = \frac{\lambda Nu(Re, Pr)}{D_h}(T_w - T); \quad q_z^{\text{eff}} = -\lambda^{\text{eff}} \frac{\partial T}{\partial z}; \quad Pr = \frac{\mu C_p}{\lambda}$, which suggests that the sun's surface temperature is about 6100 K.

Maximum radiation intensity corresponding to the wavelength is determined from the relation:

$$P = \langle \bar{p} \rangle^S; \quad H = \frac{\langle \bar{p} \bar{h} \rangle^S}{\langle \bar{p} \rangle^S}; \quad \hat{p} = p(P, H); \quad \mu = \mu(P, H); \quad \lambda = \lambda(P, H); \quad T = T(P, H) \quad (7.79)$$

with $C_4=1.33 \times 10^{-5} \text{ W}/(\text{m}^3 \text{ K}^5)$.

Stefan-Boltzmann law: A total amount of energy radiated by a blackbody per unit time per unit area in the entire range of wavelengths (frequencies), i.e., the total blackbody radiation flux is obtained by an integral of spectral distribution of Planck's law, Eq. (7.74):

$$\chi_k(x, y, z, t) = 1 \quad (7.80)$$

$$\chi_k(x, y, z, t) = 0$$

where $\sigma = 5.67 \times 10^{-8} \text{ W}/(\text{m}^2 \text{ K}^4)$ is the Stefan-Boltzmann constant (radiation constant of absolute blackbody).

For gray bodies, own radiation is proportional to the fourth power of the temperature. Then the Stefan-Boltzmann law takes the following form:

$$\chi_g + \chi_I = 1 \quad (7.81)$$

where $\langle f \rangle^L \triangleq \frac{1}{L} \int_L f dl$ is the thermal emissivity (integral emissivity or emissivity).

Kirchhoff's law establishes a relationship between emittance and absorbance of any material (gray and black) bodies in thermodynamic equilibrium. The ratio of emittance (E) of the gray body to its dimensionless coefficient of absorption A given by Eq. (7.70) is constant for a given temperature and equal to the emittance of the blackbody:

$$\langle f \rangle^S \triangleq \frac{1}{A} \int_A f ds \quad (7.82)$$

Because $\langle f \rangle^V \triangleq \frac{1}{V} \int_V f dv$, the essence of Kirchhoff's law reduces to the statement that, in thermodynamic equilibrium, absorbance and the thermal emissivity of the surface are numerically equal: i.e.,

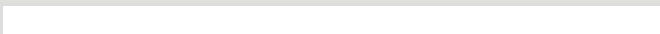
$$\left\| \left(x, y, z \right) \right\| \triangleq \left\| \left(\frac{x^2}{a^2} + \frac{y^2}{b^2} + \frac{z^2}{c^2} - 2\frac{xy}{ab} - 2\frac{xz}{ac} - 2\frac{yz}{bc} \right) \right\| \quad (7.83)$$

For majority of the surfaces encountered in engineering processes, the temperature dependence of $\epsilon(T)$ is weak in general. Detailed characterization of the radiating surface is a spectral thermal emissivity:

$$\iiint_{R^3} g(x, y, z) dx dy dz = 1 \quad (7.84)$$

which is a ratio of the spectral radiation flux of the material to that of the blackbody.

The emissivity of some materials of nuclear engineering is shown in the following:



Corium (core melt) $\varepsilon=0.85$ for $T_{m,p}=2850$ K, where ε is the integrated emissivity (Harding et al., 1989).

Lambert's cosine law determines the distribution of radiant intensity of a blackbody in directions. The radiation flux per unit area in a certain direction (E_ψ) is proportional to the radiation flux in a direction normal to the surface (E_n) and the cosine of the angle (ψ) between two directions:

$$\bar{f} \triangleq \frac{1}{T} \int_T f dt \quad (7.85)$$

When the radiation obeys Lambert's law, the brightness does not depend on the direction. Fig. 7.34 shows a qualitative distribution of the relative emittance of different bodies in all directions.

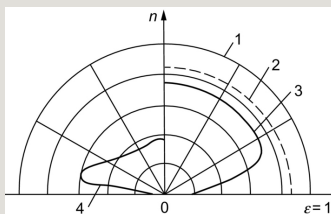


Fig. 7.34 The distribution of the relative emittance of different bodies depending on the direction: 1—blackbody; 2—gray body; 3—oxidized metals, dielectrics, wood, paper; 4—polished metals.

A body, that obeys Lambert's law, is called the diffuse emitter, while the radiation of actual solid materials obeys Lambert's law only partially. Metals exhibit a maximum emission intensity at $\psi=40\text{--}80$ degrees, i.e., observed from the surface at a considerable angle. Dielectrics give the greatest intensity of radiation in the normal direction $\psi=0\text{--}60$ degrees and low value in the range of high angles ψ .

In radiation characteristics of actual bodies, a conventional temperature is

introduced along with the degree of blackness (thermal emissivity) as shown in the following.

Radiation temperature (T_{rad}) is a conventional temperature of a blackbody for the same radiation flux as that from the body under consideration:

$$\epsilon_k \triangleq \overline{\chi_k} = \frac{1}{T} \int_T \chi_k dt = \frac{T_k}{T}. \quad \text{From the Stefan-Boltzmann law}$$

$$\tilde{f}_k^k \triangleq \frac{\int_A \chi_k f_k ds}{AR_k}. \quad \text{Therefore}$$

$$R_k \tilde{f}_k^k = \langle \chi_k f_k \rangle^S \quad (7.86)$$

Color temperature (T_c) is a conventional blackbody temperature at which the ratio of the spectral intensities at two wavelengths (colors) is the same as that of the

$$\tilde{f}^k \triangleq \frac{\int_T \chi_k f_k dt}{\int_T \chi_k dt}.$$

considered body Using the Wien's law, we obtain:

$$\frac{1}{T_c} = \frac{1}{T} - \frac{\ln(\epsilon_{\lambda_1}/\epsilon_{\lambda_2})}{C_2 \left(\frac{1}{\lambda_1} - \frac{1}{\lambda_2} \right)}. \quad (7.87)$$

Bright temperature (T_b) is determined by equating the brightness of blackbody and

$$\tilde{f} \triangleq \frac{\langle pf \rangle^S}{\langle p \rangle^S}, \quad \text{i.e.,}$$

the body under consideration

$$\hat{f}_k^k \triangleq \frac{\langle \chi_k f_k \rangle^S}{\alpha_k} \quad (7.88)$$

Relations linking T_{rad} , T_c , and T_b with T are the basis of the methods to measure high temperatures by optical methods (pyrometers—radiant color luminance).

7.3.3 Radiation characteristics

In describing the radiative properties of actual bodies, the use is made of relative dimensionless quantities and properties in linking real and ideal bodies.

Relative emissivity ε (thermal emissivity) is a ratio of the real radiation surface energy of to that of an ideal blackbody at a same temperature and other conditions being equal.

Absorptivity A is a ratio of the energy absorbed by the surface to the energy absorbed by the blackbody irradiated by a same incident radiation flux, and other conditions being equal.

Reflectivity R is a ratio of the energy reflected by the surface to the energy reflected by ideally reflecting (mirror) surface irradiated by the same incident radiation flux and other conditions being equal.

Transmissivity D (transparency) of the material is a ratio of the energy transmitted through the material to the incident radiation energy.

In practice, it is more convenient to work with the averaged radiation properties over all directions. Thus, considering the energy emitted by the element of the body surface into all directions over that element suggests a hemispherical emittance or the degree of blackness. Depending on whether it is over an entire range or a narrow range of wavelengths, we have the total (integral) or monochromatic (spectral) hemispherical emissivity. Similarly, corresponding radiation properties are defined for reflectivity and absorptivity of the surface.

Radiation characteristics of real bodies depend on the wavelength of the radiation, surface temperature, and the direction of the emitted or the incident radiation. The surface, which has the same emissivity and absorbance at all wavelengths refers to

gray bodies: $\overline{\overline{f_k}}^k \triangleq \frac{\langle \overline{\chi_k \rho_k f_k} \rangle^S}{\langle \overline{\chi_k \rho_k} \rangle^S} = \frac{\widehat{\rho_k f_k}}{\widehat{\rho_k}}$ and $\frac{\partial \langle \overline{\chi_k \rho_k} \rangle^S}{\partial T} + \nabla \cdot \left(\varepsilon_k \rho_k^{-1} \overline{\overline{q_k}}^k \right) + \nabla \cdot \left[\varepsilon_k (J_k^+ + J_k^-) \right] = \varepsilon_k \rho_k^{-1} \overline{\overline{q_k}}^k + \frac{1}{\Delta} \sum \left(\frac{1}{r_{ik}} \left[\overline{\overline{q_k}}^k \cdot \mathbf{r}_{ik} (\overline{\overline{q_k}}^k \cdot \mathbf{r}_{ik}) + \overline{\overline{q_k}}^k \cdot \mathbf{J}_k \right] \right)$. The gray body is an idealized concept just because at the real bodies, these radiation properties are dependent on the wavelength.

Integral emissivity of metals is

$$\varepsilon = 0.576 \sqrt{\rho_e T} - 0.124 \rho_e T. \quad (7.89)$$

Here ρ_e is the electrical resistivity (Ωcm); T in K.

Spectral emission of pure metals in a short wavelength region of the spectrum ($\lambda < 0.5 \mu\text{m}$) is more than half of the blackbody radiation at the same temperature. When $\lambda > 1 \mu\text{m}$, the spectral emissivity of most metals ≈ 0.05 – 0.1 . For example, to improve the thermal insulation properties, the walls of cylinders, flasks, and Dewar

vessels are coated by silver ($\varepsilon = 0.02 - 0.03$) or aluminum ($\varepsilon = 0.02 - 0.03$).

Water and ice have a higher emissivity for the longwave thermal radiation. Mono- and di-atomic gases (He, H₂, N₂, etc.) are practically transparent to the thermal radiation, i.e., neither absorb nor emit radiation. Tri-atomic gases (H₂O, CO₂, SO₂, NO₂, etc.) have high emissivity and absorptivity. They absorb and emit at specific intervals (bands) of wavelengths and transparent at the remaining of the spectrum.

Emission from gas deviates from the fourth power law. For example:

$$E_{\text{CO}_2} = 3.5 \times 10^{-7} (pl)^{0.33} T^{3.5}$$

where p is the partial pressure and l is the path length along the propagation. However, in engineering applications, we use the fourth power law, for the sake of convenience, and the deviation is taken care of by the relative emissivity of gas:

$$\varepsilon_g = \varepsilon_{g,0} \left(\frac{p}{p_0} \right)^n \left(\frac{l}{l_0} \right)^m \quad (7.90)$$

$\varepsilon(T, pl)$ are given in the form of graphs for each gas. Issues related to the radiation heat transfer in high temperature gases are discussed in detail in Golovnyov et al. (1984).

Reflectivity of the body $\rho_k \triangleq \frac{\vec{X}_k \rho_k \vec{V}_k \psi_k}{\varepsilon_k} - \frac{\vec{X}_k \rho_k \vec{V}_k \psi_k}{\rho_k \vec{V}_k \psi_k}$ depends on directions of the incident and reflected radiation (Kitzel', 1973). Extreme cases of reflections from surfaces are diffuse and specular reflection. A diffuse surface reflects the incident beam so that the intensity of reflected radiation is the same for all the reflection angles (Fig. 7.35). A specular surface reflects the beam at the same angle just in the same way

as a mirror does. The surface is a mirror when its roughness is much smaller than the wavelength of the incident beam. Thus, the same surface can become diffuse or mirror, depending on the incident radiation wavelength.

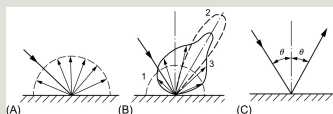


Fig. 7.35 Types of reflective surfaces: (A) diffuse; (B) actual; (C) specular. 1—Reflectance for short wavelength; 2—reflectance for long wavelength; 3—integrated reflectance (over all wavelength).

Fig. 7.36 shows the dependence of the reflection coefficient of the paint at different angles of incident and reflected radiation.

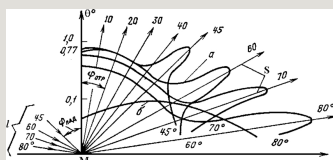


Fig. 7.36 Dependence of the brightness coefficient of the coatings on the angles between incident and reflection beams: a—white shiny surface; b—black matte finish.

White (color) materials can have a high reflection coefficient for short-wave radiation and are “black” for the longwave. Due to the selectivity of reflectance bodies, the latter depends essentially on the temperature of the incident radiation source.

Transparency (transmissivity) of the bodies for thermal radiation may be visible even for relatively thick layers. It is so-called greenhouse effect due to the high transparency glass for shortwave solar radiation and extremely low opacity to the longwave infrared radiation. Bodies that are completely opaque in the visible spectrum at normal temperatures can be transparent to the thermal radiation at high temperatures (e.g., porcelain, BeO, etc.).

7.3.4 Radiation heat transfer between bodies

First let's consider the heat exchanges between two parallel plates of infinite length (1) and (2), which are separated by infinite transparent medium. Calculation of radiation heat transfer is carried out according to the formula:

$$\frac{\partial \epsilon_k \bar{\rho}_k}{\partial t} + \nabla \cdot \left(\epsilon_k \bar{\rho}_k \vec{v}_k \right) = \frac{1}{\Delta t} \sum_j \left\{ \frac{1}{v_{ij}} \left[\bar{n}_i \rho_i (\vec{v}_i - \vec{v}_j) \right] \right\} \cdot \vec{v}_k \quad (7.91)$$

where
$$\frac{\partial \epsilon_k \bar{\rho}_k}{\partial t} + \nabla \cdot \left(\epsilon_k \bar{\rho}_k \vec{v}_k \right) + \epsilon_k \nabla \bar{p}_k = \epsilon_k \bar{\rho}_k \vec{g} + \nabla \cdot [\epsilon_k (\bar{T}_k + T_k^t)] + \vec{M}_{ik}$$
 is the reduced emissivity of the system; ϵ_1, ϵ_2 are the surface emissivity; T_1 and T_2 are the surface temperatures (K).

The total amount of heat transferred from surface 1 to surface 2 is:

$$\vec{M}_{ik} = \frac{1}{\Delta t} \sum_j \left\{ \frac{1}{v_{ij}} [\bar{n}_i \cdot \rho_i (\vec{v}_i - \vec{v}_j) \cdot \vec{v}_k] - \bar{n}_i \cdot T_k \right\} \quad (7.92)$$

Here, A is the surface area (m²).

7.3.4.1 Arbitrary arrangement of two surfaces

The geometry of the system is taken into account by means of integral angular radiation coefficients (irradiance coefficients). The angular coefficient determines the amount of diffusely distributed radiation energy, which is transferred from one surface to another. The physical meaning of the angular coefficient can be understood by the following example. The radiation flux leaving the surface 1, is evenly distributed over the surface of hemisphere. In this space over the surface 1, the other surface 2 is located with a certain area which makes a solid angle φ_{12} . Then, this angle determines the portion of the radiant energy that falls from the

surface 1 to surface 2:
$$\bar{p}_f^f = \bar{p}_g^g = \bar{p} \quad \text{and} \quad \varphi_{21} = \frac{Q_{2 \rightarrow 1}}{Q_2}$$
 The first subscript refers to the emitting surface and the second to the irradiated surface. The angular coefficients φ possess the reciprocity with the exposed area A :

$$\varphi_{12} \cdot A_1 = \varphi_{21} \cdot A_2. \quad (7.93)$$

The angular coefficient is dimensionless ($\varphi < 1$), reflecting the purely geometrical features of the placement of the two bodies in space. There are graphic-analytical and experimental methods for determining the angular coefficients.

When the surface area receiving the heat is small, corresponding angular coefficient is also small. In a closed system, all the radiation energy originating from any surfaces is distributed over the rest of the surfaces of the system so that

$$\sum_{j=1}^n \varphi_{ij} = 1$$

, where n is the number of surfaces, forming a closed system.

The heat flow between two gray bodies with temperatures T_1 and T_2 in accordance with the Stefan-Boltzmann law

$$Q_{12} = \sigma_0 [T_1^4 A_1 \varphi_{12} - T_2^4 A_2 \varphi_{21}]$$

or using the property of reciprocity,

$$Q_{12} = \sigma_0 (T_1^4 - T_2^4) A_1 \varphi_{12} = \sigma_0 (T_1^4 - T_2^4) A_2 \varphi_{21}. \quad (7.94)$$

Full radiant flux for a system consisting of a gray body is given by:

$$Q_{12} = \sigma_0 \varepsilon_{red} (T_1^4 - T_2^4) A_1 \varphi_{12}. \quad (7.95)$$

$$\varepsilon_{red} = \frac{1}{1 + \varphi_{12} \left(\frac{1}{\varepsilon_1} - 1 \right) + \varphi_{21} \left(\frac{1}{\varepsilon_2} - 1 \right)}$$

where is called as a reduced degree of blackness of a pair of bodies and is an optical and geometrical parameter. The value of $A_1 \times \varphi_{12} = H_{12}$ is called the mutual radiation surface of bodies. Q_{12} are in (W).

7.3.4.2 Heat transfer between body and shell

Assume one body is in a cavity of another body and their sizes are given. With the surface areas (A_1 , A_2) and temperature (T_1 , T_2) being given and noting the absorption coefficients can be set equal to the emissivity (ϵ_1 and ϵ_2), then the calculation of an amount of heat transmitted from one surface (1) to the other surface (2) will be:

$$Q_{12} = \frac{\sigma_0 (T_1^4 - T_2^4) A_1}{\frac{1}{\epsilon_1} + \left(\frac{1}{\epsilon_2} - 1 \right) \frac{A_1}{A_2}}. \quad (7.96)$$

If the surface area of the body in the cavity is much less than the surface of the shell ($A_1 \ll A_2$) or $\epsilon_2 = 1$, Eq. (7.96) takes the form:

$$Q_{12} = \sigma_0 \epsilon_1 (T_1^4 - T_2^4) A_1. \quad (7.97)$$

If $A_1 \cong A_2$ we will arrive at the parallel plate formula, Eq. (7.92).

Many other specific problems and solutions are found in Siegel and Howell (1981).

7.3.5 Heat transfer in absorbing and emitting environments

Electromagnetic wave, as it passes through a medium, interacts with the particles of the medium and undergoes scattering and absorption processes. Interactions of the wave occur with the molecules or atoms with different structure, solid particles or liquid droplets in gases. The medium may have its own emission sources; In addition, the radiation also causes some brightness of scattering medium. The radiation energy being absorbed is turned into heat, changes the thermal state of the medium and will be re-emitted.

The overall change in spectral density of the radiation flux over a spatial length dx due to the incident radiation J_i and its own intrinsic I_{is} is expressed by the

equation:

$$dJ_{\lambda} = -\beta_{\lambda} J_{\lambda} dx + \epsilon_{\lambda} I_{0\lambda s} dx. \quad (7.98)$$

where $\beta_{\lambda} = \beta_{\lambda}^A + \beta_{\lambda}^S$ is the spectral attenuation coefficient of radiation due to absorption (β_{λ}^A) and due to scattering (β_{λ}^S); ϵ_{λ} is the spectral emissivity of thermal radiation of the medium.

If its own intrinsic radiation of the medium is much less than the attenuation of the incident radiation. i.e., $\epsilon_{\lambda} I_{0\lambda s} \ll \beta_{\lambda} J_{\lambda}$, the transport equation becomes:

$$\frac{dJ_{\lambda}}{J_{\lambda}} = -\beta_{\lambda} dx$$

From this we have

$$\frac{J_{\lambda}^S}{J_{\lambda}^A} = \exp\left(-\int_0^s \beta_{\lambda} dx\right)$$

$$\frac{J_{\lambda}^A - J_{\lambda}^S}{J_{\lambda}^A} = 1 - \exp\left(-\int_0^s \beta_{\lambda} dx\right) = A_{\lambda s}$$

where $A_{\lambda s}$ signifies the absorption (and scattering) ability of the layer of thickness s for the beam of wavelength λ . The ratio generally depends on the physical properties of the medium (absorption and scattering, the concentration of the absorbing substance, wavelength, temperature, thickness, etc.).

Effect of concentration of absorbing material in the medium on the optical properties is established in the first approximation by the Bouguer-Beer law, in which the relative attenuation of the beam of rays is proportional to the volume concentration of the absorbing substance μ .

Absorption ability or absorptivity of such a medium can be determined by the formula:

$$A_{\lambda} = 1 - \exp(-\beta_{\lambda} \mu s). \quad (7.99)$$

This law holds only approximately for monochromatic radiation of low concentrations. Deviations from the law are caused by the interactions among the particles or molecules of absorbing materials. For nonmonochromatic radiation and for high concentrations of absorbing substances, the absorption coefficient depends on the concentration and length of the beam path.

The value given by

$$L_{\lambda} = \int_0^s \beta_{\lambda} dx \quad (7.100)$$

is called as the *optical thickness* of the medium. If the absorption coefficient does

$$L_{\lambda} = \beta_{\lambda} s = \frac{s}{1/\beta_{\lambda}}$$

not vary in distance, then s is the characteristic length, e.g., the layer thickness, and $1/\beta_{\lambda}$ can be regarded as the mean free path of photons. If β_{λ} is large (shorter mean-free-path), penetration depth is small, while for small β_{λ} (longer mean-free-path) the penetration depth is deep. In this way, the optical thickness is the ratio of the characteristic dimensions of the

length of the radiation penetration. When the optical thickness $L_{\lambda} \gg 1$, the medium is said optically thick (the characteristic size of the system is significantly

larger than the mean photon path length). If $L_{\lambda} \ll 1$ the medium is called

optically thin and if $L_{\lambda} \rightarrow 0$ the medium is not involved in heat exchange (transparent or diathermic medium).

Engineering calculation methods of radiative heat transfer often use the *effective thickness* of the emitting layer (l_{eff}). For a medium with a volume V and a small optical thickness ($L_{\lambda} \ll 1$)

$$l_{eff} = \frac{4V}{A}. \quad (7.101)$$

Here A is the surface area.

In many practical situations we encounter, we find Eq. (7.101) often overestimates the optical thickness of layers l . Therefore, we decided to use formula

$$l_{eff} = \frac{3.6V}{A}, \quad (7.102)$$

which reflects a real balance between the effective values l_{eff} and the equivalent thickness layer l_0 (Blokh, 1991).

Effect of optical layer thickness L on the effective thickness l is accounted for as follows:

$$l_{eff} = \frac{3.6V}{A} \frac{Le^{-L}}{L + e^{-L} + Le^{-L} - 1}. \quad (7.103)$$

For $L=0$, the effective thickness of the layer l_{eff} becomes l_0 and defined by Eq. (7.102).

7.4 Complex heat transfer

7.4.1 The complex heat transfer and basic principles of calculation

Two or more heat transfer mechanisms often act simultaneously, for example: thermal conduction and radiation (λ - r), convection and radiation (c - r), convection-conduction (c - λ), or even all three together. The usual method of complex heat transfer calculations is a summation of the heat fluxes of each heat exchange

mechanism:

$$\begin{aligned} q &= q_{\lambda} + q_c \\ q &= q_c + q_r \\ q &= q_{\lambda} + q_c + q_r \end{aligned} \quad (7.104)$$

The approach is valid only if each mechanism shown on the right-hand-side of the equation does not affect the other(s), i.e., if there is no interactions among them. This usually occurs when a magnitude of one component of the heat flux is significantly different from the other(s) (Özisik, 1973; Kokorev and Kharitonov, 1986)

There are two types of interaction effects of concern:

1. The effect of radiation in an absorbing medium appears in the similar form of the heat sources or sinks in the heat conduction or convection. This problem becomes nonlinear;
2. The interaction of radiation can change the boundary conditions.

A special case of complex heat transfer is the simultaneous transport of heat by radiation (q_r) and directional flow of electron flows direction that are emitted from a heated surface (cathode) to the other, colder (anode) surface (q_e):

$$q = q_r + q_e \quad (7.105)$$

7.4.2 Radiation heat transfer between flow of emitting gas and wall

7.4.2.1 Radiation and conduction

We now consider here a stationary system involving the absorption and conduction by the gas medium. The problem is characterized by the following parameters:

optical thickness of the medium (L , see Section 7.3.5); emissivity of the surfaces (ϵ_1 and ϵ_2); relative temperature of the cold surface to the hot surface ($\theta = T_2/T_1$); and the parameter

$$N = \frac{\lambda a}{4\sigma_0 T_1^3}$$

where λ is the thermal conductivity of the gas; a is the gas absorption coefficient; and σ_0 is Stefan-Boltzmann constant. The parameter N characterizes the interaction intensity of heat transfers by conduction and radiation: if $N \rightarrow \infty$ (T_1 at lower temperature), heat is transferred only by thermal conductivity; if $N \rightarrow 0$ (at higher temperature T_1), heat is transferred only by radiation.

Here are two extreme cases:

– Optically thin gas layer ($L \rightarrow 0$). The radiation heat is not absorbed by the gas but practically by every surface element of the medium that interacts with the radiation coming directly from the boundary surfaces. The total heat flux will be

given. with $q_r = \alpha_r (T_1 - T_2)$ and

$$q_\lambda = \alpha_\lambda (T_1 - T_2)_{\text{bv}}$$

$$q = q_r + q_\lambda = (\alpha_r + \alpha_\lambda) (T_1 - T_2), \text{ which is also written as:}$$

$$q = \epsilon_{\text{red}} \sigma_0 (T_1^4 - T_2^4) + \frac{\lambda}{\delta} (T_1 - T_2). \quad (7.106)$$

The first term on the right-hand-side of Eq. (7.106) is Eq. (7.91) with the reduced emissivity defined in Section 7.3.4.

– Optically thick gas layer ($L \rightarrow \infty$). The radiation heat is readily absorbed by the gas. Radiation properties of the surfaces affect only the layers of gas within a distance much smaller than the size of the system. In this case, the radiation heat transfer approaching the diffusion process, the analogy with the thermal conductivity of the gas can be made. The heat flux is expressed by:

$$q = \frac{4\sigma_0}{3a\lambda}(T_1^4 - T_2^4) + \frac{\lambda}{\delta}(T_1 - T_2). \quad (7.107)$$

In general, the radiation beam penetrates the surface of the medium volume and is partially absorbed. This affects the temperature distribution within the volume and thus changes the thermal conductivity under the heat transfer conditions. This is the most complicated case, and the total heat flux q cannot be obtained readily by adding q_r and q_c because of their strong interconnected behaviors.

The temperature level of the nuclear fuel depends on the thermal conductance λ/δ at a radial clearance δ between the fuel pellet and cladding as it determines the temperature drop. The value λ/δ depends on the design of fuel element (cladding diameter, gap, etc.), the properties of the cladding and fuel materials, surface conditions (roughness, coatings, presence of the oxide films), properties of the fission gas and fill-in gas, its pressure, and the metallurgical and many other processes occurring in the fuel during irradiation (Fig. 7.37).

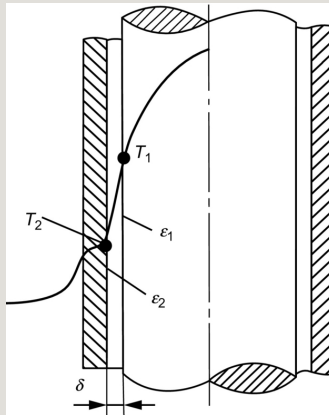


Fig. 7.37 Calculation of complex heat transfer in the gaseous fuel rod gap.

The radiation heat flux is estimated by $q_r = \alpha_r(T_1 - T_2)$, where α_r is the gap thermal conductance given by:

$$\alpha_r = \epsilon_{red} 4\sigma_0 \bar{T}^3, \quad (7.108)$$

$$\frac{\partial \epsilon_k \overline{\rho_k^k} \vec{v_k^k}}{\partial t} + \nabla \cdot \left(\epsilon_k \overline{\rho_k^k} \vec{v_k^k} \vec{v_k^k} \right) + \epsilon_k \nabla \overline{p_k^k}$$

$$= \epsilon_k \overline{\rho_k^k} \vec{g} + \nabla \cdot [\epsilon_k (\overline{T_k} + T_k^t)] + \vec{M}_{ik}$$

where

$$\overline{T} = \frac{T_1 + T_2}{2}$$

and

is the average temperature in the gap region.

For a temperature of the inner surface of cladding 350–700°C and the temperature difference in the gap 600–700°C, you may find $\alpha_r \approx 50\text{--}150 \text{ W/(m}^2 \text{ K)}$, i.e., *the heat transfer by radiation under the operating conditions is in most cases less than 10% of the total heat flux*. In evaluating the gap conductance, it is important to take into account the changes in many parameters over the nuclear reactor operation period, including the gap size, thermal conductivity of the gas in the gap, and the mass transfer of fuel due to evaporation/condensation.

7.4.2.2 Radiation and convection

Consider we have both radiation and convection in practical engineering problems. In most cases, the two heat fluxes are assumed to be independent and dealt with separately: $q = q_r + q_c$. This assumption is accurate enough if one of the two heat fluxes is significantly smaller than the other.

Sometimes there are cases where three mechanisms of heat transfer (heat conduction, convection, and radiation) are to be considered. An example is the heat transfer through an insulated circular pipe with an outer diameter of the insulation d_2 , heat transfer coefficient α_c by convection and α_r by radiation to the environment (Fig. 7.38). Temperatures on the insulation surfaces are T_{1i} and T_{2i} . The heat flow from the unit length q' (W/m) will be equal to:

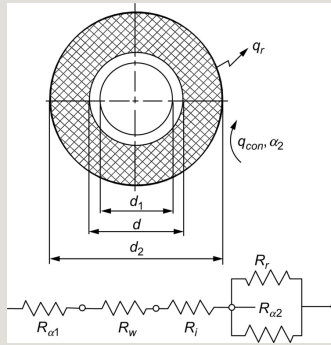


Fig. 7.38 Calculation of heat transfer from the coolant through a conduit with insulation: its equivalent electric circuit diagram.

$$q' = \frac{\pi(T_{1i} - T_{2i})}{\frac{1}{\alpha_1 d_1} + \frac{1}{2\lambda_w} \ln \frac{d}{d_1} + \frac{1}{2\lambda_i} \ln \frac{d_2}{d} + \frac{1}{\alpha d_2}} \quad (7.109)$$

Thermal resistance of the heat transfer inside the pipe is $1/(\alpha_1 d_1)$ and the thermal

$$\frac{1}{2\lambda_w} \ln(d/d_1)$$

resistance of the pipe wall can be neglected for simplicity. Thermal resistance of the heat transfer at the outer insulation surface is due to the radiation from the insulation surface and the convection:

$$\frac{1}{\alpha} = \frac{1}{\alpha_r(T_{2i})} + \frac{1}{\alpha_c}; \quad (7.110)$$

therefore, three parameters in two Eqs. (7.109), (7.110), i.e., q' the linear heat rate of the insulated pipe, α_r the radiation heat transfer coefficient with the surface insulation, and T_{2i} the surface temperature of the insulation are depending on each others. With the ambient temperature to be provided, the problem is solved by the successive approximation.

7.4.3 Contact heat transfer

7.4.3.1 Contact resistance

Nuclear fuel elements usually take the form of the fuel pellets inside the cladding, where with a gap between them the mechanical contacts are assumed. The thermal conductance of such contact is of the order of 10^3 – 10^4 W/(m² K). When the heat flux is $\sim 10^6$ W/m² and a temperature difference across the contact could be a hundred degrees or more. However, as noted in Section 7.4.2, radiation heat transfer hardly affects this temperature difference. For more information, see Holm (1967), Shvets and Dyban (1964), Shlykov (1965), Shlykov et al. (1977), and Kharitonov et al. (1973).

Thermal contact resistance plays an important role in problems of semiconductor thermoelectric generators, thermionic converter of nuclear energy into electrical energy, in devices operating in the vacuum of space. For example, see Clausing and Chao (1965) and Fried and Costello (1962).

Conventional nuclear reactor fuel materials are metal alloys, oxides, carbides, nitrides, uranium, and plutonium metals (Boeschofen, 1955; Miller, 1962; Avduevsky and Koshkin, 1992; Özisik, 1973; Popov, 1977; Spiridonov et al., 1974; Rapier et al., 1963; Waltar and Reynolds, 1981). The thermal contact resistance between the metallic cladding and the ceramic fuel (UO₂, UC, UN, etc.) is particularly a difficult issue (Miller, 1962) for the following reasons: first, the ceramic fuel does not come into close contact (i.e., plane mode) with the cladding inner surface; second, because of the ceramics' poor thermal conductivity and high hardness, the conductivity of the actual contact points may be small.

7.4.3.2 Rough surfaces

Actual contact area between two solid surfaces is essential information to evaluate contact resistance (Dyomkin, 1962; Dyl'nev, 1963; D'iachenko et al., 1963; Kaganer and Zukova, 1966; Miller, 1962; Bahrami et al., 2006). The contact resistance is a relative concept, because the actual surface roughness and waviness of the contact surfaces between solids are of a discrete nature. Some of the heat goes through the contact spots of solids and other through the gaseous gaps. Since the thermal conductivity of the contact spots is higher than that of the gaseous medium in the gap, the heat flow streamlines are highly congested toward these

local spots with the thermal contact resistance $R = \Delta T / q$, where ΔT is the temperature difference at the contact position.

For many surfaces encountered in engineering practice, a population density of the contact points, therefore, a degree of concentration of lines of the heat flow, has a definite influence on the thermal contact resistance (see Fig. 7.39A; Latyev et al., 1974).

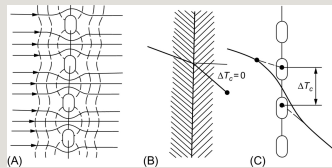


Fig. 7.39 Heat flow line (—) and isotherms (---) at the contact between two plates (A); temperature distribution in an ideal location (B); and real (C) at the contact.

Inverse of the thermal contact resistance $1/R$ is the thermal conductance ($=a$) of the contact. The total contact resistance is made up of two resistances in parallel—one of the gaseous medium in the gap (R_g) and the other of the mechanical contact spots (R_m):

$$\frac{1}{R} = \frac{1}{R_g} + \frac{1}{R_m}, \quad (7.111)$$

where R_g is determined by the gap width and conductivity λ_g of the medium filling the gap; R_m is the actual contact resistance based on the contraction of the heat flow streamlines. When the gap is $20 \mu\text{m}$ wide and filled with air,

$$R_g = \frac{\delta}{\lambda} = \frac{20 \times 10^{-6}}{3.2 \times 10^{-2}} = 6.2 \times 10^{-4} \quad (\text{m}_2 \text{ K/W}).$$

It is noted that this resistance is equivalent to the resistance of ST-3 steel plate of thickness 33 or 150 mm thick aluminum.

Eq. (7.111) is rewritten in terms of the thermal conductance (a_g and a_m) and the fraction of actual contact area S to the total surface area $\eta = S/A$:

$$\alpha = \alpha_g(1 - \eta) + \alpha_m\eta, \quad (7.112)$$

η and S depend on the characteristics of roughness and waviness of the surfaces, their mechanical properties, compression force and other parameters.

In calculations, it is usually assumed that the actual contact area S formed by a plurality of circular spots of radius a , in which the heat flow streamlines are “pulled together” (Fig. 7.39A). The corresponding additional thermal resistance associated with the curvature of the heat flow streamlines is taken into account by introducing a correction factor ψ_r .

If the mean free path of the gas molecules in the gap is commensurable with size of the gap, the gas may not be regarded as a continuous medium. Then, the discreteness of gas properties leads the temperature, instead of a linear profile, to have a distribution in the planar gap region, resulting in a temperature drop (jump) as shown in Fig. 7.39C. To characterize this distortion, we introduce a concept *length* of “a temperature jump” ($\Delta T_1 + \Delta T_2$), which is equivalent to an increase in the thickness of gas layer ($l_1 + l_2$). The length of a temperature jump would be

$l \approx \ell / \xi$, where ℓ is a mean free path length of the molecules, ξ is the accommodation coefficient (see below).

In view of the above effect, the thermal resistance at the gas gap can be written as:

$$R_g = \frac{1}{\alpha_g} = \frac{\delta_e}{\lambda} + \frac{l_1 + l_2}{\lambda} = \frac{\delta_e}{\lambda} + \frac{1}{\alpha_*}, \quad (7.113)$$

$$\alpha_* = \xi_e \frac{\gamma + 1}{\gamma - 1} \cdot \frac{p}{2} \sqrt{\frac{k}{2\pi MT}} \quad \gamma = \frac{c_p}{c_v}$$

where p is the pressure (Pa); k is Boltzmann constant ($=1.38 \times 10^{-23}$ J/K); T is the temperature (K); M is the molecular mass of the gas; ξ_e is the equivalent accommodation coefficient associated with the accommodation coefficients on the surfaces 1 and 2 by the relation $1/\xi_e = 1/\xi_1 + 1/\xi_2 - 1$.

7.4.3.3 Accommodation factor

Accommodation coefficient characterizes the energy transfer efficiency of the gas molecules to the surface and depends on the nature of the gas and the surface material. The higher the molecular weight of the gas, the higher the accommodation coefficient:

$$\xi = \frac{\mu}{2(1 + \mu)}, \quad (7.114)$$

where $\mu \equiv M_g / M_W$ is the ratio of atomic (molecular) mass of the gases and the surface material.

The amount of heat conduction through the gas layer between the fuel pellet and cladding in the nuclear fuel rods are not strongly dependent on the composition of the gas (Fenech and Rohsenow, 1963). Thickness of the gas layer, in which the temperature jump is observed at the boundary of gas and solid body, is given by

$\delta_g \approx \ell / \xi$, where ℓ is the mean free path, ξ is the accommodation coefficient, the fraction of the molecular energy that is exchanged with the wall per one collision.

Thermal conductivity at the gap, then, may be given by:

$$\alpha \sim \frac{\lambda}{\delta_g} = \frac{\lambda \xi}{l}. \quad (7.115)$$

From $\lambda \sim 1 / \sqrt{M_g}$, $\xi \sim \sqrt{M_g}$, where M_g is the atomic mass of the gas in the gap, we can see that α is weakly dependent on the type of gas. The heat transfers through the actual contact point and even due to radiation reduce the effect of this dependence. However, as the burnup increases and hence the pressure in the fuel element, this relationship given by Eq. (7.115) may be slightly modified

as indicated in the next table:

--	--

The thermal resistance R (in Eq. 7.111) decreases with increasing contact pressure of the contact surfaces. While at low contact pressures and temperatures, almost 80% of the heat is passing through a gas layer, at high temperatures and high contact pressures, more than 90% of the heat goes through the contact points.

Taking into account the factors mentioned just above, the relationship of the contact conductivity Eq. (7.112) can be written as:

$$\alpha = \frac{\lambda}{\delta_e} (1 - \eta) + \frac{1}{\pi a^2 R \psi_t \psi_k} \eta, \quad (7.116)$$

where λ is the thermal conductivity of the medium in the gap; R is the thermal resistance of an ideal contact between two infinite surfaces;

$$\delta_e = \frac{A}{\int_A \frac{dA}{\delta(A) + 2l_m}}$$

the lengths of the temperature jump;

$$\int_A \frac{dA}{\delta(A) + 2l_m} \approx (\overline{h_1} + \overline{h_2}) + 2l_m$$

; $\overline{h_1}$ and $\overline{h_2}$ are the average height of roughness; l_m —the length of temperature jump; ψ_k —correction factor taking into account tapering the roughness; a —the average radius of the contact points.

Data evaluation and modeling the equivalent gap are controversial, due to the influences of the distribution function of height and shape of roughness. The equivalent gap may be defined by profilogram surface.

The complexity of calculating the contact heat transfer with Eq. (7.116) is associated with many difficulties in determining the quantities involved among the relationship ($\delta\epsilon$, η , a , ψ_i , ψ_k).

There are two popular theories (models) for the contact resistance. One theory suggests an *elastic* deformation of roughness elements on the contact surfaces. Other is their *plastic* deformation. For further reading, see McWald and Marschall (1993), Rapier et al. (1963), Sanderson (1961), Yovanovich (1986, 1998), Yovanovich and Marotta (2003), Skipper and Wootton (1958), and Skipper (1958).

The final word, as always, experimental results play crucial roles in this area.

Part 2: Boiling Heat Transfer

In this second half of this chapter, we concentrate on boiling heat transfer phenomena first focusing on nucleate and film boiling in a nonflowing system, i.e., in a pool of a large volume, and then on convective boiling in channels, focusing on the fundamental aspects of heterogeneous nucleation and heat transfers, i.e., boiling two-phase flow heat transfer from the heated surface to fluids. It is designed again for professionals as well as for students, being aimed at helping readers to better understand the phenomena and at providing the basis on which physical modeling of the phenomena is to be made for the system safety analysis and subchannel analysis of nuclear reactors.

7.5 Boiling process and heat transfer

7.5.1 Advantages of the boiling process

Boiling is a process of evaporation of the bulk liquid. The main advantage of using a boiling process in nuclear engineering is due to a fact that quite high heat fluxes are achieved without increasing significantly the surface temperature. Mechanisms of heat removal from the heated surface is associated with conduction, liquid- and vapor/gas-phase convection, phase change of liquid into vapor with the latent heat of vaporization, and radiation. The liquid-phase motion near the surface is largely determined by the dynamics of growth of vapor bubbles. The bubble dynamics is associated with the temperature field in the region surrounding the vapor bubble; and the temperature field is a result of interaction with the bubble dynamics itself. The number of nucleation sites is determined by the conditions at the surface (surface roughness, wettability, etc.). A large number of governing parameters (geometry, properties of the liquid, vapor, surface properties, and the boundary

conditions of each phase) complicate the theoretical analysis of the boiling process. The intensity of the boiling heat transfer will be dependent on many factors difficult to control (surface roughness, the amount of dissolved gases in the liquid, wettability, etc.), which cannot be fully taken into account in theory and experiment.

There are at least three reasons for the heat transfer enhancement in the boiling. First, the strong turbulence agitation to the boundary layer at the expense of growth and separation of vapor bubbles. Second, the heat transfer by evaporation of the liquid microlayer at the bottom of the vapor bubble. Third, the transfer of the latent heat of vaporization into the growing vapor bubble. The absence of a closed mathematical description of the process of boiling heat transfer and an abundance of factors influencing the process make choices of generalized variables rather arbitrary. Correlations obtained as a result of processing and synthesis of experimental data are inevitably semiempirical, and able to describe only a certain average level of the heat transfer.

*... The fact of the successful approximation
Experimental data of some empirical formula does
not give grounds for approval of the true extent of
influences of various properties on the heat transfer
during boiling*

(Labuntsov, 1972)

7.5.2 Onset condition of boiling on a heated surface

Formation of the vapor phase in a volume of liquid is due to density fluctuations caused by the random motion of molecules.

For a spherical bubble to stay in a volume of liquid and not to collapse under the forces of surface tension, the pressure therein must be greater than the pressure of the surrounding fluid, and its size must be larger than a certain critical radius R_{cr} .

This value is calculated from the Laplace's pressure $\Delta p_1 = 2\sigma/R$, and Thomson modification, taking into account the change in the vapor pressure of the concave curved surface of radius R compared with a flat surface:

$$\Delta p_2 = \frac{2\sigma}{R} \cdot \frac{\rho_g}{\rho_f - \rho_g}$$

$\Delta p = \Delta p_1 + \Delta p_2$. A sum of pressure differences must comply with the Clausius-Clapeyron

$$\frac{\Delta p}{\Delta T} = \frac{\Delta h_{fg}}{T(v_g - v_f)}$$

equation: . Hence the critical (minimum) radius of the nucleus R_{cr} of the vapor can be obtained from:

$$R_{cr} = \frac{2\sigma T(v_g - v_f)}{\Delta h_{fg} \Delta T} \frac{\rho_f}{\rho_f - \rho_g} \quad (7.117)$$

For $\rho_g \ll \rho_f$ or $(v_f \ll v_g)$, we have

$$R_{cr} \approx \frac{2\sigma T_S}{\Delta h_{fg} \rho_f \Delta T} = \frac{2\sigma \mathcal{R} T_S^2}{\Delta h_{fg} p \Delta T}, \quad \text{with } p = \rho_f \mathcal{R} T_S, \quad \mathcal{R}: \text{ gas constant.} \quad (7.118)$$

Required wall superheating can be obtained for the formation of a vapor bubble of radius R by:

$$T_w - T_S = \Delta T \approx \frac{2\sigma T_S}{\Delta h_{fg} \rho_g R} = \frac{2\sigma \mathcal{R} T_S^2}{\Delta h_{fg} p R} \quad (7.119)$$

This equation can be used for the subcooled liquid to its saturation temperature T_S (Hahne et al., 1990).

Boiling begins on the heated surface where the surface is at an excess temperature and the liquid at saturation. The birth of a vapor bubble on a solid surface takes place at the nucleation centers where the surface energy for the vapor formation is lowest. Usually this recess is portions with weak molecular adhesion between liquid and solid. For the vapor bubble formation to occur on the surface, also a certain degree of superheating of the liquid above the saturation temperature is required. It depends on the purity of the liquid and the presence of vaporization centers, i.e., surface conditions. The centers of vaporization—cavities on the surface, are filled with gas or vapor. Under ideal conditions, superheat in the bubble of radius R is described by the classical theory:

$$\Delta T_S = T_g - T_S = \frac{\rho T_S (v_g - v_f)}{\Delta h_{fg}} \ln \left(1 + \frac{2\sigma}{pR} \right).$$

$$\frac{2\sigma}{pR} \ll 1, \quad \ln \left(1 + \frac{2\sigma}{pR} \right) \cong \frac{2\sigma}{pR}$$

Typically, for with sufficient precision. R may be regarded as the maximum radius of the cavity—the center of vaporization would be 0.2–0.4 μm . Superheating ΔT_w and the surface heat flux corresponding to the beginning boiling (q_{bbs}) in general can be calculated by the relationships:

$$\Delta T_w = T_w - T_S = \frac{\rho T_S (v_g - v_f)}{\Delta h_{fg} R e^{0.2} Pr^{0.5} (p/p_{cr})};$$

and

$$q_{bbs} = \alpha (T_w - T_S)$$

where the heat transfer coefficient α can be obtained from single-phase convective heat transfer correlations.

Size of the vapor embryos depends on the surface roughness and wettability conditions. The number and size of nucleation sites define the boiling initiation. If the nucleation sites are many and large, the boiling initiation requires small superheating. Good wettability liquid fills the surface cavity and the excess temperature rise of the surface temperature over saturation, i.e., ($T_w - T_S$) must be higher than in the case of poor wettability fluid. Good wettability fluid leads to hysteresis phenomena during boiling—a significant increase in the surface temperature before boiling and its subsequent decline from the start of boiling.

For good wettability liquids which begin to boil as the steam embryo of the critical radius:

$$R_{cr} = \left[\frac{2\sigma\lambda_f T_s (v_g - v_f)}{q\Delta h_{fg}} \right]^{0.5},$$

a recommended correlation for the amount of wall surface superheat is:

$$T_w - T_s = \frac{2\sigma T_s (v_g - v_f)}{R_m \Delta h_{fg}},$$

where R_m is the radius of the largest cavity ($R_m < R_{cr}$).

The heat flux corresponding to the beginning boiling (q_{bb}):

$$q_{bb} = \alpha \left[(T_s - T_f) + \left(\frac{2\sigma}{R_m} \right) \frac{T_s (v_g - v_f)}{\Delta h_{fg}} \right].$$

Magnitude of $2\sigma/R_m$, for example for water at 0.1 MPa ($\sigma \sim 60$ mN/m) and $R_m \approx 0.4 \mu\text{m}$, is 1.5×10^3 Pa. With good wettability of surfaces and without impurity (e.g., liquid metals, liquids with low surface tension, and the like), the high superheating is usually realized. Under these conditions, growth rate of the vapor volume is limited by (Gavrilov, 1999):

$$R = \sqrt{\frac{6Mc_f \rho_f}{k \rho_g} a \tau}, \quad (7.120)$$

where M is the molecular weight; $k = 1.38 \times 10^{-23}$ J/K is Boltzmann constant; a is the thermal diffusivity in m^2/s ; c_f is the specific heat capacity of the liquid in $\text{J}/(\text{kg K})$ and the time τ is in s. Eq. (7.120) implies that the growth rate is independent of the magnitude of superheating.

In general, the interface velocity is determined by solving Rayleigh's equation, transient energy and mass conservation equations simultaneously, considering the energy-mass balance conditions at the interface.

7.5.3 Types of boiling

Depending on the heat flux and other factors of the wall surface, vapor bubbles or a continuous layer of vapor is formed, which is accordingly called bubbly or film boiling. In the nucleate boiling, the liquid is in direct contact with the nucleation site on the surface. In the film boiling, the vapor layer separates the liquid from much of the heated wall surface. The vapor layer covering the heated wall surface transfers the heat by conduction and reduces the heat transfer rate by many times, so a transition from the nucleate boiling to the film boiling takes place at a constant heat flux and may be accompanied by a sharp increase in the surface temperature of the heating wall (heat transfer crisis or burnout, or simply “crisis”).

Various types of boiling are classified as follow:

– By the nature of the boiling—nucleate boiling and film boiling;

– The type of convection—the boiling under natural convection (in a large volume), and forced convection;

– Magnitude of the average fluid temperature (J_k^*) relative to the saturation temperature (T_s)—subcooled boiling if $\left[\frac{\rho_l \left(\frac{v_k^2}{2} \right)}{\rho_l c_p \left(\frac{v_k^2}{2} \right)} \right] \frac{\partial \theta}{\partial z} \left(\frac{v_k^2}{2} \right)$; liquid temperature close to the saturation temperature ($\rho_k \frac{v_k^2}{2} > \rho_k \frac{V_k^2}{2}$)

– On the surfaces—horizontal, vertical, inclined;

– The nature of the boiling—developed, developing, or undeveloped and unstable.

Nucleate boiling is developed for a large number of nucleation sites and undeveloped for a small number of nucleation sites. In the latter case, a large proportion of the heat is removed by the single-phase liquid flow convection. The boiling process becomes unstable, if the nucleate boiling regime is replaced by a liquid-phase random natural convection, and then back to nucleate boiling again.

7.5.4 Boling curve

Dependence of the heat flux on the temperature difference ($T_w - T_s$) is the boiling curve (Fig. 7.40), originally proposed by Nukiyama (1934). With increasing the temperature difference, the heat flux reaches a maximum and then decreases and increases again (curve ABB'C'DE). On this curve, you can highlight areas of different modes of heat transfer and the characteristic points (see Fig. 7.40).

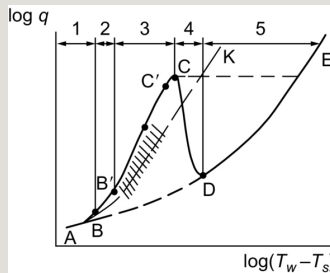


Fig. 7.40 Boiling curve for a large volume (Nukiyama curve). *Different modes of heat transfer:* 1—gravitational convection; 2—undeveloped boiling; 3—developed boiling; 4—boiling transition (from bubble to film); 5—film boiling; \\\\\\\—region stable boiling. *Typical modes:* AB—natural (free) convection; B—beginning of nucleate boiling; B'—beginning of the developed nucleate boiling; C—point of crisis; D—Leidenfrost point; C'—point of deviation from the mode of nucleation.

For the region of free convection (ABK), the heat transfer coefficient

$MH_k = - \int_C^A \rho_k (\vec{v}_k - \vec{v}_i) \cdot \vec{n}_k \cdot \frac{dCi}{\vec{n}_k \cdot \vec{n}_{kC}}$, typically with $m=1/4$ for the laminar region and $m=1/3$ for turbulent flow regime. Consequently,

$EC_{ik} = - \int_{Ci}^A \rho_k (\vec{v}_k - \vec{v}_i) \cdot \frac{\vec{v}_k^2}{2} \cdot \vec{n}_k \cdot \frac{dCi}{\vec{n}_k \cdot \vec{n}_{kC}}$. At point B, boiling begins on the surface. If the temperature of the liquid in a volume is lower than T_s , the bubbles within the liquid condense. If the fluid temperature is equal to T_s , the bubbles will rise to the liquid surface without condensing.

In region 2 (BB') with increasing heat flux or temperature difference increases the number of nucleation sites and increases the heat transfer rate, although still a considerable amount of heat removed by convection. With further increase in q or the number of nucleation sites continuously increases, an increasing portion of the heat is removed by evaporation.

In the region (B'C'), $MH_{ik} = A \Gamma_{ik} \tilde{H}_k^k$; Point C' corresponds to the deviation

from the nucleate boiling regime; and the point C is reached the maximum heat flux, called critical heat flux because further (even slight) increase in the q results in a dramatic increase in the wall surface temperature according to the line (C–E). If the surface temperature can be controlled, it will lead to an increase in vapor blanketing the surface and the heat flux decreases (CD). For the vapor flowing along the surface, it requires a significantly higher wall surface temperature (DE) to achieve the same heat flux of the nucleate boiling.

In the region of sustainable film boiling, the heat is transferred from the heated wall through the vapor by the evaporation of a thin liquid layer, steam convection, and radiation. The contribution of the radiation increases with ΔT . In the region

$$(DE) \quad EC_{ik} = \Gamma_{ik} \frac{V_i^2}{2}.$$

Influences of various factors on the boiling curve for pool boiling is illustrated qualitatively by a series of charts as illustrated in Fig. 7.41 (Chai and Shoji, 2001; Shoji, 1998; Soloviev, 1998).

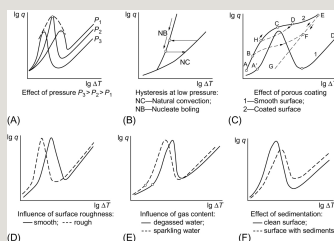


Fig. 7.41 Influence of various factors on the process of the boiling (boiling curve) in bulk fluids.

The boiling curve shifts to the right with the increase in the system pressure and the heat transfer coefficient increases with the pressure in the nucleate and film boiling regime (A). At very low pressures (R_{cr} is large), there is a delay to start boiling in the process of natural convection that requires more fluid to superheated

($T_w - T_s$). After the boiling initiation, this superheating will be reduced. With a reduction in the heat flux, a transition can occur from nucleate boiling (NB) again to the natural convection (NC)—hysteresis phenomenon (Fig. 7.41B). At sufficiently high heat flux with increasing surface superheating, a possible transition could take place from nucleate to film boiling, bypassing the transition boiling regime. On the other hand, with a decrease in the film boiling surface (or

reduction of the heat flux), the system can switch to the nucleate boiling regime, also bypassing the transitional regime—hysteresis II.

Issues related to the transition boiling regime have been studied in the last decades intensively (Gavrilov, 1999; Haddad and Cheung, 1998; Klimenko and Snytin, 1988), although a satisfactory understanding of the process has not yet been reached. Fig. 7.41C schematically shows a difference of the boiling curve on a smooth surface and a porous surface coating. On the porous surface, boiling occurs at lower heat flux density (A) than on the smooth surface (A'). If the coating has high permeability and high thermal conductivity, then the boiling curve would be ABCD. If the vapor encounters resistances in coming out of the porous structure, the process while reducing the q is on the line DH or EFG. One of the reasons for the observed hysteresis is due to a difficulty for the liquid to penetrate from the small pores into the large space. In this case, the heat transfer coefficients at EFG line is determined from thermal resistance of the porous coating δ/λ . This mode of nucleate boiling is considered to have the vapor film inside the porous layer. With low permeability porous coating, a transition to the film boiling is observed with the vapor available on the BF line at $q < q_{cr}$. The position of the curve (2) depends on the coating thickness, permeability, thermal conductivity. Data in some areas of the curve (2) for coatings can be found in industrial practices. An overview and the method of heat transfer calculation at boiling on the porous surfaces is found in Soloviev (1998).

The presence of surface roughness increases the heat transfer rate (Fig. 7.41D). The presence of gas in the liquid enhances boiling at low heat fluxes and the heat transfer during the nucleate boiling (Fig. 7.41E). Effects of deposits (e.g., corrosion products) typically come from the low thermal conductivity of the deposits, resulting in an increase ΔT and the boiling curve to shift to the right (Fig. 7.41F).

Bubbly boiling structure on a horizontal surface will change as the heat flux increases from single large steam bubbles to vapor mushroom formations (Gertner, 1965) (see Fig. 7.42).

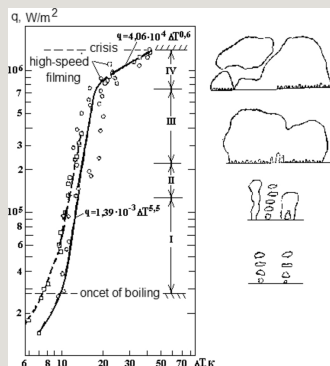


Fig. 7.42 Boiling curve and vapor bubble structure depending on heat flux: I—individual bubbles region; II—the first transition region; III—mushroom region; IV—the second transition region.

7.5.4.1 Minimum film boiling temperature

On the boiling curve illustrated in Fig. 7.43, point D, corresponding to the minimum heat flux q_{\min} and temperature T_{\min} , it is called the Leidenfrost point or minimum film boiling temperature T_{MFB} . Various names have been given to the T_{MFB} including rewetting temperature, quench temperature, Leidenfrost temperature, film boiling collapse temperature and others. Heat transfer characteristics in the vicinity of the T_{MFB} point are important in assessing the cooling process of the heated surfaces (hardening treatment by quenching) and in evaluating the ECCS for LOCA. This point separates the transition boiling and film boiling modes: in the region $T > T_{\text{MFB}}$ the liquid ceases to wet the heated surface. A conventional technique to define T_{MFB} is associated with the measurement of the lifetime (evaporation) τ of drops on the hot surface heated up to T_w . Fig. 7.44 shows a comparison of the curve $\tau = f(T_w)$ as if it were inverted boiling curve.

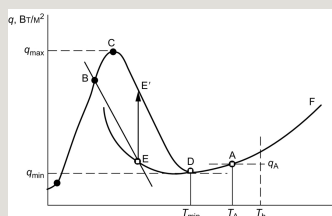


Fig. 7.43 Boiling curve: AF—film boiling; CE'—transition boiling from nucleate to film boiling; EDA—transition from film boiling; EE'—heat flux jump with

improved wetting; T_A , q_A —temperature and heat flux in the presence of liquid contact; C initiation of transition boiling.

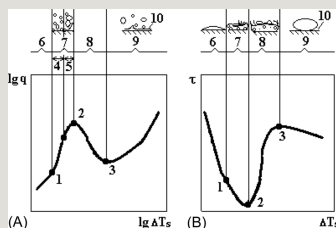


Fig. 7.44 (A) Boiling curve at saturation temperature and (B) liquid droplets evaporation time on a heated surface: 1—nucleate boiling initiation; 2—critical heat flux; 3—minimum heat flux (Leidenfrost point); 4—separated bubbles; 5—jets and steam column mode; 6—single-phase convection mode; 7—bubble-film coexisting boiling regime; 8—transition boiling regime; 9—film boiling regime; 10—vapor layer; τ —the evaporation of droplets.

It is well known that the mode of liquid contact with the heated surface is dependent not only on the temperature, but also on the liquid-wall interface conditions (surface smoothness, surface roughness, surface geometry, subcooling, surface tension, boundary conditions, etc.). It is noted that, in Fig. 7.43, the deterioration of the wettability will shift the beginning of film boiling to $T_E (<T_{\min})$ while improved wettability to $T_A (>T_{\min})$, where EDA is the transition region to the film boiling regime and the region AF is the mode of pure film boiling.

Trying to take into account the thermal properties of the heated surface and the wettability conditions of the liquid-solid system, Baumeister and Simon (1973) arrived at the following semiempirical expression:

$$q_{kz}^d = \lambda_{kz}^d \frac{\partial \tilde{T}_k^k}{\partial z}$$

where the subscript s refers to the surface material;

$\int_{A_k} \frac{\partial p}{\partial t} dA = A \frac{\partial R_k \langle p_k \rangle_k^S}{\partial z} = A \frac{\partial R_k \widehat{p}_k^k}{\partial t}$; σ is the surface tension; M_s is the atomic weight of the surface materials; λ_s is the thermal conductivity; ρ_s is the density; c_{ps} is the specific heat of the material. It is logical to assume that the influence of ΔT_{sub} (subcooling) on T_{\min} will be similar to the effect on the critical heat flux q_{cr} , i.e.,

$$\int_{A_i} \nabla \cdot \vec{T} \cdot \vec{v} dA = \frac{\partial}{\partial z} A_k \vec{v}_k \cdot \left(\vec{T}_k \cdot \vec{n}_z \right)_k^S + EF_{ik} + EP_{ik}$$
Experiments were carried out with the hot spheres (1–100 mm in diameter) that are immersed in various fluids (water, Freon, sodium, etc.) by many researchers. For water, obtained empirical relationships are summarized by the formula:

$$EF_{ik} = \tau_{ik} V_i$$

where $A=200\text{--}220^\circ\text{C}$; $B=6.3\text{--}8$. Quenching cooling mode at high ΔT_{sub} will lead to a sudden achievement of higher wettability resulting in a jump in the heat flux. It is commonly accepted that during the initial stages of the drop-surface contact, the interface temperature between the liquid and solid is dictated by the thermal properties of the liquid and solid as well as by their initial temperatures. This interface temperature T_i is given by the solution to the one-dimensional energy equation with semiinfinite body boundary conditions (Eckert and Drake, 1972):

$$EP_{ik} = EP'_{ik} - P \frac{\partial R_k}{\partial t} \cong -P \frac{\partial R_k}{\partial t}$$

The limiting temperature at which the initial contact can stay nonequilibrium or metastable, i.e., superheating of a liquid above its boiling point, between the liquid and the drop surface, is the *homogeneous nucleation temperature* T_{hn} . A detailed theory of this process was developed and reported by Skripova (1972). An empirical relationship for T_{hn} is established by Ramilison and Lienhard (1988):

$$\int_{A_i} \rho \vec{g}_z \cdot \vec{v} dA = A_k (\rho_k g_z u_{kz})_k^S = AR_k \widehat{\rho_k^k} \widehat{V_k^k} g_z$$

It is necessary to distinguish between T_{hn} ($\equiv T_{lim}$) and T_{min} ($\equiv T_{MFB}$). T_{lim} ($\equiv T_{hn}$) is determined purely by the thermodynamic conditions. T_{min} is affected by not only thermodynamic factors, but also by many other factors such as actual fluid periodical contacts with the wall, insulation of the surface, etc. Experimental data indicate that the pressure is an important parameter for thermophysical properties of the fluid, surface tension, contact angle, and surface material which can play an

important role in determining T_{\min} .

In accordance with Klimenko and Snytin (1988):

$$\int_{V_0} \nabla \cdot q \, dV = - \frac{\partial}{\partial t} A_0 \left(q_0 \cdot n_0 \right)_0 - \int_{V_0} n_0 q_0 \frac{dC}{dn_0 \cdot n_0} - \int_{V_0} n_0 \cdot q_0 \frac{dC}{n_0 \cdot n_0} \\ = - \frac{\partial A_0 q_{0n}}{\partial t} + C_0 q_{0n} + A_0 q_{0n}$$

$$C_k q_{wk} \triangleq - \int_{C_k} \frac{\vec{n}_k \cdot \vec{q}_k}{\vec{n}_k \cdot \vec{n}_{C_k}} \frac{dC}{\vec{n}_k \cdot \vec{n}_{C_k}}; A q_{ik} \triangleq - \int_{C_i} \frac{\vec{n}_k q_{ik}}{\vec{n}_{kc} \cdot \vec{n}_k} \frac{dC}{\vec{n}_{kc} \cdot \vec{n}_k}$$

where

This relationship is obtained in the range of

$$\sum_k q_{ik} + \Gamma_{ik} \widetilde{H}_k^k = 0 \\ \frac{\partial A_0 \widetilde{p}_k^k}{\partial t} \left(\widetilde{H}_k^k + \frac{V_k^{k,2}}{2} \right) + \frac{\partial A_0 R_k \widetilde{p}_k^k V_k}{\partial z} \left(\widetilde{H}_k^k + \frac{V_k^{k,2}}{2} \right) \\ - A_0 R_k \frac{\partial p}{\partial t} + \frac{\partial A_0 R_k (q_{0n} + q_{0t})}{\partial z} = + A_0 R_k \widetilde{p}_k^k V_k^k g_0 \\ + C_k q_{0n} + A_0 q_{0k} + A_0 \Gamma_{0k} \left(\widetilde{H}_k^k + \frac{V_k^{k,2}}{2} \right) + A_0 \tau_{0k} V_l + A_0 \theta_{0k} \omega_l; \quad \text{and} \\ A \frac{\partial R_{0l} \widetilde{p}_k^k V_k^k}{\partial t} + \frac{\partial A R_{0l} \widetilde{p}_k^k V_k^k}{\partial z} + A R_{0k} \frac{\partial p}{\partial z} + A l_1 \frac{\partial R_{0k}}{\partial z} \frac{\partial A}{\partial z} + A e_1 G_z - D_k \\ = A R_{0k} \widetilde{p}_k^k g_z - A \tau_{0k} - C_k \tau_{0k} + A \Gamma_{0k} V_l$$

A detailed overview of the temperature T_{\min} is available in Bernardin and Mudawar (1999), which is excerpted in Table 7.5. It shows the diversity of mechanisms related to the Leidenfrost phenomena.

Table 7.5
Possible mechanisms of the Leidenfrost phenomenon (Bernardin and Mudawar, 1999)

--

Two theories have been proposed for the analytical prediction of the minimum film boiling temperature. One theory says that the minimum temperature is a thermodynamic property of the fluid (i.e., maximum liquid temperature) and thus is primarily a function of pressure. The other theory suggests that rewetting

commences due to hydrodynamic instabilities which depend on the velocities, densities, and viscosities of both phases as well as the surface tension at the liquid-vapor interface (IAEA TECDOC, 1203, 2001).

During fast transitions, where insufficient time is available to fully develop the hydrodynamic forces, rewetting is expected to be thermodynamically controlled, while for low flows and low pressures, where sufficient time is available and the volumetric expansion of the fluid near the wall is large, rewetting is more likely to be hydrodynamically controlled. Once rewetting has occurred locally, the rewetting front can then propagate at a rate which is primarily controlled by axial conduction. These theories can be modified to include the thermal properties of the surface (IAEA TECDOC, 1203, 2001).

7.5.4.2 Leidenfrost temperature

The evaporation of superheated droplets on the surface depends on the temperature. Thus, a drop of the radius of 2 mm on the brass plate evaporates over the time:

at~100°C—35 s; at~170°C—a few seconds (the first critical temperature);

at~240°C—130 s (the second critical temperature—the temperature of the Leidenfrost);

at~500°C—60 s (spheroidal state).

In the last case, the drop is separated from the heated surface and floating on the superheated vapor layer; for estimates the following can be used:

$$g_z = -g \sin \theta$$

where T_c —thermodynamic critical temperature in K (see Table 7.6).

Table 7.6

Leidenfrost temperature T_{LFP} for saturated fluids that are in contact with the smooth clean surfaces at atmospheric

7.6 Nucleation pool boiling

7.6.1 The mechanisms of the nucleation process

Complete theory of boiling has never been established that takes into account all the factors affecting the magnitude of the heat transfer. They include primarily physical properties of the fluid, complex surface conditions (surface roughness, its size distribution, surface deposits, wettability, surface material properties, etc.). The system of differential equations and boundary conditions, describing the boiling two-phase flows, include:

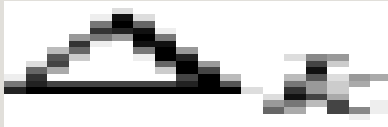
- Momentum conservation equation for the liquid and vapor phases;
- Mass continuity equation for the liquid and vapor phases;
- Energy conservation equation for the liquid and vapor phases;
- and appropriate initial and boundary conditions including those associating with the diffusion processes:
- Thermal and mechanical interactions at the phase interface;
- Continuity of the energy flow (heat flux) across the phase interfaces;

$$\Delta_k = -\rho_k g \sin \theta (X_k - X_i)$$
 where w_g is the local vapor-phase velocity on the interface is assumed to be a speed of evaporation;

- Equal temperatures at the phase interface.

Mathematical description of physical models of boiling process can only be formal because of the uncertainties of many factors involved in closure equations, the lack of accurate boundary conditions, in particular at the interfaces between vapor- and liquid-phase. Therefore, these relations serve only to establish a kind of generalized variables, which make processing of experimental data possible. A

capillary constant is often used either as a reference length



(minimum) radius of the nucleus of vapor

$$f_i = R_g \Delta_l - (1 - R_g) \Delta_v + R_g (1 - R_g) \frac{\partial(\Delta_v - \Delta_l)}{\partial \alpha} \quad (\text{Eq. 7.117})$$

(Lykov, 1954). The characteristic velocity is the speed of evaporation

$$G_z = R_g (1 - R_g) \frac{\partial(\Delta_v - \Delta_l)}{\partial z}$$

under the thermal equilibrium condition, which determines the vapor volume withdrawn from the unit interphase surface area per unit volume and per unit time (m/s).

The high heat flux density at boiling is mainly associated with the following two processes: (1) agitation of liquid steam bubbles near the surface of the heat exchange (q_{conv}); and (2) intensive evaporation of the micro liquid layer at the bottom of the vapor bubble (q_{eva}). Thus, $q = q_{conv} + q_{eva}$.

Formation of one vapor bubble of diameter d_0 , i.e., the volume

$$D_k = \int_{S_k} \vec{n}_k \cdot \vec{p}_k(x, y, z) - p_l \vec{n}_k \cdot \vec{n}_k ds$$

consumes the heat

$$\epsilon_v = 1; \epsilon_l = -1$$

. Let the number density of the existing vaporization centers per unit area be N (m⁻²), the total heat transfer area A , the separation frequency f_i , the volume of each bubble V_i , then the amount of heat removed by evaporation of the liquid will be given by:

$$q_{ev} = \sum_A^N Q f_i = \Delta h_{fg} \rho_f \sum_A^N f_i V_i = \Delta h_{fg} \rho_f N f_i \bar{V} = \Delta h_{fg} \rho_f N_g^2 f_i \bar{V}_g^2$$

As the heat flux or temperature difference (ΔT) increases, the number of

vaporization centers grows ($G_z = A^{3/2} \epsilon_k \alpha (1 - \alpha) \frac{\rho_m \partial g \cos \theta}{2 \partial z}$). The average frequency f and the detachment diameter d_0 are virtually independent of q . Therefore, the average production of vaporization centers under the developed boiling is approximately constant. In the developed boiling, the fraction of the heat

transported by the evaporation (q_{eva}/q) increases as q increases and approaches to 100%, i.e., $f_i=R_g(1-R_g)(\rho_L-\rho_V)g\cos\theta A/2$.

7.6.2 Influence of various factors on heat transfer in nucleate boiling

The effect of pressure is shown in Fig. 7.45 (Borishanskii, 1961; Borishanskii et al., 1964). With increasing pressure, the heat transfer coefficient increases, slowly

at first (up to $\Delta_k=\frac{1-\alpha_k f_i}{4}$), then (for $\rho_m=R_g\rho_V+(1-R_g)\rho_L$) the influence of pressure increases sharply.

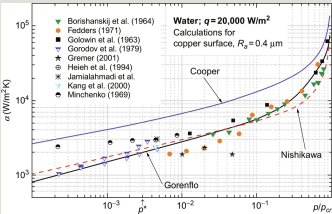


Fig. 7.45 The effect of pressure on the heat transfer coefficient of nucleate boiling (Borishanskii, 1961; Borishanskii et al., 1964): p_{cr} —critical pressure, p^* —conditionally selected pressure, $p^*=0.03p_{cr}$. Adapted from Feldmann, H., Luke, A., 2008. Nucleate boiling in water for different pressures. In: International Refrigeration and Air Conditioning Conference. Paper 982.

The reason for this pressure dependency is explained from the nature of changes in physical properties of the fluid, i.e., first of all, Δh_{fg} , σ , ρ_f , and ρ_g . Growth of the vapor bubbles at high pressure is explained by the heat transferred from liquid to the vapor bubble through the interface surface in the base layer (Labuntsov, 1960). An increase in the pressure reduces the surface tension and the heat of evaporation, facilitating nucleation and growth of the vapor bubbles, reduction in R_{cr} , and the

growing number of vaporization centers. At low pressures ($<5\times10^{-4}$, $p<0.01$ MPa), boiling initiation becomes difficult, expanding the convective heat transfer region, decreasing the bubble detachment frequency and increasing R_{cr} .

Influence of the surface roughness on the heat transfer is evaluated based on the information on active centers of vaporization (cavities), including the number density, and not only the value of the protrusions and depressions, but their size distribution and even the shape of cavities. In general, with an increase in the surface roughness for the same heat flux, we have less wall superheat, i.e., an

increase in heat transfer. However, this observation is not universal. Depending on the size and shape distributions of the cavities (caverns), the boiling curve vary. For example, Fig. 7.46B shows boiling curves for cavities of the normal distribution of sizes, of an equal size, and for a specially selected distribution of cavities in size. Thus you can control the shape of the boiling curve (i.e., the flux) with new technology of production of special surfaces with cavities and hollows (Fig. 7.46).

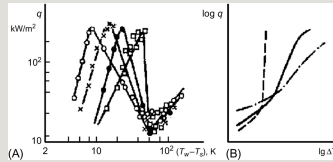


Fig. 7.46 Influence of surface roughness on the boiling curve: (A) $\square \rightarrow \bullet \rightarrow \times \rightarrow \bigcirc$ —increase roughness; (B) for the normal distribution of the cavity sizes; - - - all cavities of the same size; ---- for cavities of specially selected size distribution.

The presence of impurities in the water causes deposits on the heating surface, changing the surface roughness, which, on the one hand, leads to formation of new cavities and, consequently, to increase the heat transfer coefficient. On the other hand, the additional thermal resistance of these deposits reduces the heat transfer coefficient. In practice, however, due to the variety of operating conditions, it is difficult to estimate the thickness and thermal conductivity of the deposits. Thus, we rely on the thermal resistance of the deposits provided from industry experience.

In the context that follows, the formulas are listed which are suitable for smooth surfaces with no deposits. During boiling, the surface deposits should be considered as a sediment layer with thermal resistance. In this case,

$f_i = R_g (1 - R_g) (\rho_L - \rho_V) g \cos \theta D$, where a_p is the heat transfer coefficient that can be obtained according to the equations to be shown in the following; and R is the thermal resistance of the deposits.

Material thermal properties and thickness of the heat-transfer wall may affect effective heat transfer coefficient. The reason for this lies in the unsteady heat conduction that develops in the vicinity of the cavity center of vaporization. If the wall material has high thermal conductivity and high heat capacity c_p , it would facilitate the influx of heat of vaporization to the cavity centers and provides a high

heat transfer rate. It is noted that, when the deposits layer is thick ($\delta > 1$ mm), which is not unusual in normal industrial operations, the boiling heat transfer rate does not practically depend on the material and its conditions but is greatly influenced by the surface roughness and the presence of low conduction deposits on it. It is also noted that the heat transfer coefficient of the nucleate boiling in a large volume is essentially independent of the orientation of the heat-transfer surface, if the detachment of steam bubbles is ensured on the surface at any angles.

Modeling of boiling heat transfer of pure liquid and binary mixtures generally includes the following processes (Balakrishnan, 1998):

1. Micro-convection in the boundary layer due to an increase in bubbles at the heating surface;
2. The flow of fluid as a result of growth and detachment of the bubble, flow of the cold liquid toward the heating surface;
3. Transient heat conduction in a cooling fluid as it gets warm;
4. Vaporization of the micro layer during the bubble growth;
5. Agitation of the liquid layer due to the bubble growth, bubble detachment and the “cold” flow to the surface;
6. Turbulence generated by natural convection in the region adjacent to the center of evaporation, where there is no evaporation.

Heat transfer in the binary mixtures is usually more intense than in the pure liquids, for easier evaporation of the volatile component.

Thus, the pool boiling process in a large volume is associated with the active effects of vapor bubbles and the rate of heat transfer that can be considered as a sum of four components:

- (1) Micro-convection occurring near the surface during the growth and detachment of the vapor bubbles;
- (2) Evaporation of the liquid layer underneath the vapor bubbles, taking into account the transfer of the latent heat of vaporization to inside the vapor bubble;
- (3) Natural convection in the large volume;

(4) Thermo capillary flow (Marangoni flow).

The last component is connected to a longitudinal movement along the surface, which is caused by a temperature gradient and the surface tension at the liquid-vapor interface. It does not play a big role in the boiling at the saturation temperature, but essentially at high subcooling. In most of simple models of boiling heat transfer, the heat flux appears to be a sum of only two heat fluxes associating with the convection (q_{conv}) and evaporation (q_{eva}): $q=q_{conv}+q_{eva}$.

7.6.3 Estimate correlations

Heat transfer in the developed boiling region is calculated on the clean surface in a large volume of water by the following heat transfer coefficient:

$$h_{DE} = \frac{0.62 p^{0.16} a^{0.68}}{Pr^{0.41}} \quad (7.121)$$

where q is expressed in W/m^2 ; p in MPa; a in $W/(m^2 K)$. The range of applicability of Eq. (7.121) will be: $p=0.1-20$ MPa; $q<0.4$ MW/m^2 . The equation is applicable at temperatures from the subcooled to saturation range. Temperature difference in this case is defined as a difference between the surface temperature and the saturation temperature. Dependence of the heat transfer coefficient on the saturation temperature of water is expressed empirically by the following equation:

$$\alpha_k \triangleq \widehat{p}_k^* = \frac{(\alpha_k DE_k)^{0.5}}{\alpha_k} \quad (7.122)$$

where T_s is in K. The same applicability range for Eq. (7.121) is applied. Assuming that the same boiling heat transfer process can be determined by the flow internal mechanisms, Labuntsov (1960) proposed a correlation:

$$Nu = C Re^n Pr^{1/3}, \quad (7.123)$$

$$P_k \triangleq \frac{\hat{p}_k}{\hat{p}_k} = \frac{\langle \chi_k p_k \rangle^S}{a_k} \quad ; \quad P \triangleq a_v P_v + a_l P_l \quad \text{since}$$

$$V_k \triangleq \frac{\langle \chi_k \rho_k v_{zk} \rangle^S}{\langle \chi_k \rho_k \rangle^S} = \frac{\langle \chi_k \rho_k v_{zk} \rangle^S}{a_k \hat{\rho}_k} \quad ; \quad Pr \text{ is the Prandtl number of the liquid; and}$$

$$H_k \triangleq \frac{\hat{h}_k}{\hat{h}_k} = \frac{\langle \chi_k \rho_k h_k \rangle^S}{\langle \chi_k \rho_k \rangle^S} = \frac{\hat{\rho}_k h_k}{\hat{\rho}_k}.$$

To calculate the heat transfer during the nucleate boiling in a large volume, the following fairly simple equation could be used (Minchenko, 1960):

$$\frac{q}{A} = \frac{h_k (T_{\text{sat}} - T_{\text{wall}})}{1 + \frac{h_k (T_{\text{sat}} - T_{\text{wall}})}{q}} \quad (7.124)$$

$$P_k \triangleq \frac{\hat{p}_k}{\hat{p}_k} = \frac{\langle \chi_k p_k \rangle^S}{a_k} \quad ; \quad \text{where}$$

$$\frac{\Gamma_{ik} V_i}{\Gamma_k} \cong \frac{\Gamma_{ik} V_i}{\Gamma_k} \quad ; \quad \text{and}$$

$$\frac{\Gamma_{ik}}{\Gamma_k} \cong \frac{\Gamma_{ik}}{\Gamma_k}.$$

More widely used correlation is by Rohsenow (1952), based on the idea that the heat transfer coefficient of boiling mainly depends on the degree of turbulence in the boundary layer and the increasing uprising steam bubbles (i.e., the main

component of the heat flux is contributed by the convection). Then,

$$q = C_{sf} \tau_{wk} \quad (7.124)$$

where C_{sf} is the coefficient that depends on the thermal properties of the fluid at a temperature of saturation and surface conditions. Another form of the equation is:

$$q = C_k \tau_{wk} \quad (7.125)$$

where $\overline{C_k \tau_{wk}} \triangleq \overline{C_k} \overline{\tau_{wk}}$. For water at $T_s=100\text{--}350^\circ\text{C}$, $q=3\text{--}3200 \text{ kW/m}^2$; $n=1$; $C_{sf}=0.013\text{--}0.015$. For low pressure $C_{sf}=0.007\text{--}0.008$ as shown in Pioro (1999); for hydrocarbons, freon, C_{sf} is widely spread in $0.0014\text{--}0.0018$.

7.6.4 On the hydrodynamic theory of similarity of boiling heat transfer

Thermodynamic similarity principle provides a formula for the heat transfer coefficient of the boiling up to a constant coefficient, which is determined experimentally and is a constant for thermodynamically similar liquids. Similitude substances based on this principle were first suggested and applied to the problems of heat transfer and the crisis at boiling by Novikov (1961) and developed further by Borishanskii et al. (1964, 1973). Since the boiling heat transfer coefficient is a function of the developed heat flux and physical properties of liquid and vapor, its first approximation could be represented as a product of powers of these values:

$$h = \frac{\partial R_E}{\partial z} \quad (7.125)$$

On the saturation line any physical parameter is determined depending on the form given by:

$$\widehat{f_i} \frac{\partial \alpha_k}{\partial z} \quad (7.126)$$

Therefore, the formula (7.125) takes the form:

$$\widehat{f_i} \frac{\partial \alpha_k}{\partial z} \quad (7.127)$$

A number of experiments have shown and established that $\alpha \sim q^{2/3}$. Therefore in order for the R.H.S. of Eq. (7.127) to have the dimension of the heat transfer coefficient, $m_1 = -1/6$; $m_2 = -5/6$; $m_3 = 1/3$; $m_4 = 1/6$. Thus, the final form is:

$$\widehat{f_i} \frac{\partial \alpha_k}{\partial z} \quad (7.128)$$

The magnitude B and the function F_2 are determined from experiments. Estimates of the heat transfer coefficients for the boiling, for which there are no direct measurements, can be performed using the following equation:

$$\widehat{C_k q_{wk}} \triangleq \widehat{C_k} \widehat{q_{wk}} \quad (7.129)$$

where $\pi = p/p_{cr}$.

7.6.5 Boiling on a coated porous surface

Fig. 7.47 shows that the use of porous coating of the high permeability and high thermal conductivity layer allows significantly increasing the heat transfer coefficient of nucleate boiling and critical heat flux, where the boiling initiates on the porous surface at a lower heat flux (A) than on the smooth surface (A'). In the figure, the boiling curve 2 is for the coated surface and the line 1 for a smooth surface. The position of the curve 2 has a large uncertainty and may shift by tens and hundreds degrees (temperature) depending on the characteristics of the porous

structure. At complicated exhalation of the vapor from the capillary-porous structure, and with a decrease in the heat flux, the boiling curve can be represented by BFE (line 3). Heat transfer coefficient on the line 3 is determined by the thermal resistance of the porous coating, i.e., $\alpha \approx \lambda_s / \delta$, where λ_s is the thermal conductivity, δ is the thickness of the porous layer.

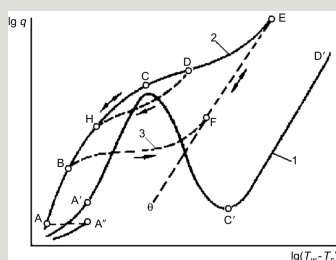


Fig. 7.47 Generalized boiling curves by Borishanskii et al. (1973): 1—to a smooth surface; 2—on the surface of a capillary-porous coating. Data from Kovalev, S.A., Solovlev, S.L., 1989. Evaporation and Condensation in Heat Pipes, Nauka, Moscow (in Russian); Kovalev, S.A., Solovlev, S.L., Ovodkov, O.A., 1985. Liquid boiling on porous surfaces. In: Proc. of School – Seminar: Heat and Mass Transfer Processes at Two-Phase Changes and at Two-Phase Flows, pp. 26–38 (in Russian); Kovalev, S.A., Solovlev, S.L., Ovodkov, O.A., 1987. Liquid Boiling on Porous Surfaces. Heat Trans. Sov. Res. 19 (1), 109–120.

The physical model of the heat transfer at boiling on the capillary-porous surface is shown in Fig. 7.48.

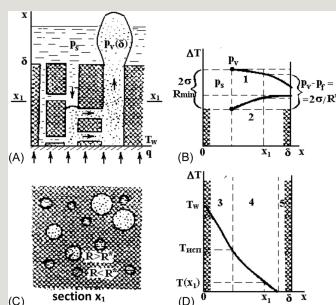


Fig. 7.48 Heat transfer model with liquid boiling on the capillary-porous surface (from Solovlev, 1998). (A) phasic motion in the porous structure; (B) pressure changes in the thickness of the porous layer $0 < x < \delta$; (C) in the horizontal section x_1 — x_1 porous structure; (D) temperature variation of the skeleton of the porous coating thickness $0 < x < \delta$. 1—vapor; 2—liquid; 3—dried layer; 4—saturation.

Modeling is based on a phasic description of the motion and heat transfer in a

porous layer. We assume a stable stationary regime of evaporation inside the capillary-porous structure, vapor and liquid flows move along separate channels, the heat is transferred by heat conduction through the skeleton of the porous coating to the liquid meniscus where the main evaporation takes place, the liquid completely wets the porous material of the coating, and the contact angle θ equals zero. Results from numerical experiments are presented by Soloviev (1998) for different characteristics of the capillary-porous structure. The capillary-porous surfaces boiling under the forced convection cooling conditions is discussed in Section 7.8.5.

7.6.6 Bulk boiling in tubes

Boiling process is often used in design of heat exchangers and steam generators in vertical or horizontal pipes. Typical examples are PWR steam generators and heat exchangers for passive heat removal systems. In many cases, the temperature

difference $\overline{C_k \tau_{wk}} \triangleq \overline{C_k} \overbrace{\tau_{wk}}$ is small and does not exceed 20–30 K.

7.6.6.1 Low pressure condition (0.1–0.3 MPa)

In this pressure range, there are two major heat exchange mechanisms: first, heat transfer increase due to the liquid-phase turbulence and vapor bubbles generation (for $q < 50 \text{ kW/m}^2$); second, heat exchange deterioration due to the formation of large vapor bubbles conglomerate covering the heated wall surface with $q > 50 \text{ kW/m}^2$.

Based on the review of publications until 1997 by Parlattan and Rohatgi (1997) for all models of vertical tube heat exchangers, simple correlations of the pool boiling heat transfer coefficients are recommended, that are easy to use in codes for nuclear system safety analysis and subchannel analysis:

$$q_{kext} \quad (7.130)$$

where q is in W/m^2 ; $\overline{C_k \tau_{wk}} \triangleq \overline{C_k} \overbrace{\tau_{wk}}$ in K. Modes of boiling, wall superheating with respect to the saturation temperature ΔT , A , and b are provided in Table 7.7.

Coefficients in Eq. (7.130)

$$\begin{aligned}
& A \frac{(\partial t_1 t_2)_1 Y_1}{\partial t} + \frac{(\partial t_1 t_2)_1 Y_1 Y_2}{\partial t} = A \alpha_1 \frac{\partial P}{\partial t} + A f_1 \left(\frac{\partial t_1}{\partial t} + g_1 \frac{\partial Y_1}{\partial t} \right) \\
& = A \alpha_1 \Omega_1 \dot{g}_1 + \frac{(\partial A R_1) (Y_1 + Y_2)}{\partial t} - A f_1 - C_1 g_1 \dot{g}_1 + A f_2 \frac{\partial P}{\partial t} + A f_2^{(2)} + A f_2 (V_1 \\
& A \frac{(\partial t_1 t_2)_1 (H_1 + \frac{Y_1^2}{2})}{\partial t} + \frac{(\partial t_1 t_2)_1 Y_2 (H_1 + \frac{Y_1^2}{2})}{\partial t} - A \alpha_1 \frac{\partial P}{\partial t} = - \frac{(\partial A \alpha_1) (\frac{\partial P}{\partial t} + g_1^2 + g_1^2)}{\partial t} \\
& + A(t_1 \Omega_1 Y_1 + C_1 g_1 \dot{g}_1 + A g_1 \dot{g}_1 + A f_2) (H_1 + \frac{Y_1^2}{2}) + A \alpha_1 Y_1 + A g_1 \dot{g}_1
\end{aligned} \tag{7.131}$$

Coefficients in Eq. (7.131)

Surface roughness is substantially more effective for vertical pipes than for horizontal pipes, although in both cases an increase in roughness causes an increase in heat transfer coefficients. Instead of Eq. (7.131), you could use less precise but simpler empirical relationship:

$$\sum_i q_i = 1; \sum_i \Gamma_{ik} = 0; \sum_i \tau_{ik} = 0; \sum_i \Gamma_i^{(W)} = 0; \sum_i |q_{ik} + \Gamma_{ik} H_i| = 0; \quad (7.132)$$

where α is in kW/m² K and q in kW/m².

7.6.6.2 High pressure region ($p > 0.3$ MPa)

Under high-pressure conditions, heat transfer coefficients are quite high (2.5×10^4 to 2.5×10^5 W/m² K). Many different authors recommended a number of formulas for a pool boiling. For instance, see IAEA TECDOC 1203 (2001). Perhaps the formula by Rassokhin (1980) is one of the most preferred, giving some leeway for calculation:

$$q_{kz} + q'_{kz} + q^{cl}_{kz} = -\lambda_k^{eff} \nabla T_k \quad (7.133)$$

$$Q_k = \rho_k(P, H_k); T_k = T_k(P, H_k); \mu_k = \mu_k(P, H_k); \lambda_k = \lambda_k(P, H_k) \quad (7.134)$$

where q is in W/m² and p in MPa.

7.6.6.3 Effect of oxide films and deposits on the outer surface of the pipe

Oxide films and deposits formed on the tube surfaces reduce the heat transfer coefficient. Determination of the composition and structure of deposits, and taking into account the impact of these factors are a complicate task. Oxide films are usually composed of hematite (Fe₂O₃) or magnetite (Fe₃O₄). The formation of oxide films on the surface of the pipe is subject to the law (Glebov et al., 1983; Man'kina, 1977):

$$\tau_{ik}, T_{kz}^d, T_{kz}^d, q_{ik}, C_k, \tau_{wk}, q_{wk}, \delta P_{ksing}, F_k^{AM}, \lambda_k^{eff} \quad (7.135)$$

where M is in g/m², T in K and τ in h. A , B , and C in Eq. (7.135) are found in Table

Table 7.9

Coefficients for Eq. (7.135)

--

_a C—0.12; Cr—1; Mo; V.

_b C—0.12; Cr—18; Ni—12; Ti.

The thermal conductivity of hematite (Fe₂O₃) and magnetite (Fe₃O₄) can be described by the following:

$$\lambda(\text{Fe}_2\text{O}_3) = 4.133 - 0.852 \times 10^{-2}T + 0.757 \times 10^{-5}T^2; \quad (7.136)$$

$$\lambda(\text{Fe}_3\text{O}_4) = 4.133 - 0.852 \times 10^{-2}T + 0.757 \times 10^{-5}T^2; \quad (7.137)$$

where λ is in W/(m K) and T in °C. Deposits usually consist of two layers: (1) firmly adjoining the surface; and (2) outer and more porous. They differ in their composition and porosity:

--

More details about the influence of deposits on heat transfer coefficient for steam generators are found in Trunov et al. (2001) for PGV-1000 of VVER.

7.7 Film pool boiling

7.7.1 Stationary film boiling

In the film boiling mode, the liquid is separated by the vapor film from the heating surface. The intensity of heat transfer is determined by convection, while at high temperature environment, by $\Delta T = T_w - T_s$ and radiation heat transfer through the vapor film. Mechanisms of vapor detachment out of the cavity on the wall surface is related to the thickness and the vapor film flow mode (laminar wave, turbulent, mixed). Therefore, the configuration and orientation of the heating surface, and the physical properties of liquid and vapor have certain importance in the gravity field. Theoretical analysis of the film boiling is simplified as compared with the analysis of nucleate boiling, because the process takes place only at the interface of the two phases and is in quite ordered a pattern. However, analysis of instability of the vapor film boundaries and the presence of irregular waves is suitable only for qualitative assessment, which is helpful in understanding the physical picture of the phenomenon, but cannot give quantitative results.

In this boiling regime, a total heat flux can be represented by a sum of convective (q_c) and radiation (radiant) (q_r) of the heat transfer: $q = q_c + q_r$. If the heat transfer coefficient refers to the temperature difference ($T_w - T_s$), then the total heat transfer coefficient of the film boiling is determined to a first approximation, by the sum of convection (a_c) and radiation (a_r) components:



$$(7.138)$$

$$A \frac{\partial \alpha_k Q_k U_k}{\partial t} + \frac{\partial A \alpha_k Q_k V_k U_k}{\partial z} = -AP \frac{\partial \alpha_k}{\partial t} - P \frac{\partial A \alpha_k V_k}{\partial z} + C_k q_{wk} + A q_{ik} + A \Gamma_{ik} H_K + A q_{kext} + D_k, \text{ W/m}^2\text{K};$$

where

$$A \frac{\partial \alpha_k Q_k}{\partial t} \left(U_k + \frac{V_k^2}{2} \right) + \frac{\partial A \alpha_k Q_k V_k}{\partial z} \left(U_k + \frac{V_k^2}{2} \right) + \frac{\partial A \alpha_k V_k P}{\partial z} = A \alpha_k Q_k g V_k + C_k q_{wk} + A q_{ik} + A \Gamma_{ik} H_K + A \tau_{wk} V_k + A q_{kext}$$

$\epsilon_w \approx 0.75$ is the surface emissivity, $T_k = T_{sat}(P)$ is the emissivity of the water surface,

The convective heat transfer coefficient a_c of the film boiling of saturated water

and other liquids is from the empirical relation by Klimenko (1984):

$$T_k < T_{\text{sat}}(P) \quad (7.139)$$

where

$$Q_k \triangleq \widehat{P}_k^k \triangleq \frac{\langle \overline{\chi_k \rho_k} \rangle^S}{\alpha_k} \quad Pr = \nu_g / a_g;$$

$$P_k \triangleq \widehat{P}_k^k \triangleq \frac{\langle \overline{\chi_k \rho_k} \rangle^S}{\alpha_k}; \quad P \triangleq \alpha_v P_v + \alpha_l P_l$$

σ , Δh_{fg} , and ρ_f are evaluated at the saturation temperature T_s , and other material properties are determined and an average temperature of vapor is given by

$$V_k \triangleq \overline{v_{zk}}^k \triangleq \frac{\langle \overline{\chi_k \rho_k v_{zk}} \rangle^S}{\langle \overline{\chi_k \rho_k} \rangle^S} = \frac{\langle \overline{\chi_k \rho_k v_{zk}} \rangle^S}{\alpha_k \widehat{\rho}_k^k} \quad C, m, n, \text{ and the form of the function } f$$

(K) in the equation are given in Table 7.10.

Table 7.10

Data necessary for Eq. (7.139)

D —the characteristic size of the flat surface (disc diameter, the width of the tape, etc.).

Eq. (7.139) gives an average value of the heat transfer coefficient across the flat wall surface. On the curved surfaces, the local values of a may differ by 20%–30%.

7.7.2 Rapid cooling of very hot bodies (hardening modes)

When a heated solid metal body is immersed into cold water, there is a series of

rapid-mode cooling called quenching that changes the characteristics of metals: hardening steels in order to acquire special steel structure, hardness, and other characteristics; production of aluminum; hardening aluminum alloys, and so on. Knowledge of these processes is necessary for the evaluation of residual stress and fatigue.

For nuclear reactor safety, investigation of similar phenomena is important for the analysis and calculation of the reactor core cooling in the event of accidents.

In metallurgical process errors with heat transfer calculations may be corrected quite easily, conducting repeated “integrated” experiments and applying appropriate corrections. However, in the nuclear power reactor it is difficult to do so or, in many cases, impossible. Therefore, the importance of the calculation of such events cannot be overestimated for the nuclear power industry. Rapid cooling of hot objects in the water involves several modes of heat transfer, which replace one another, i.e., modes of the film boiling, nucleate boiling, convection (forced and natural), and the thermal conduction. As shown in Section 7.1.4, a boiling curve has three characteristic points: (1) the minimum film boiling temperature or Leidenfrost temperature T_L (T_{MFB} or T_{LFP}); (2) the surface temperature corresponding to the critical heat flux (q_{cr}) T_c ; and (3) the onset boiling point T_b for water under normal conditions (0.1 MPa, 20°C). Consider at this point again the boiling curve (Fig. 7.49) in a large volume.

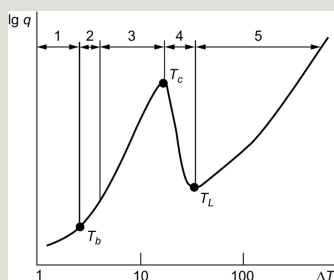


Fig. 7.49 Boiling curve in a large volume of water (0.1 MPa). Regions of various modes of heat transfer: 1—free convection; 2—undveloped boiling; 3—developed boiling; 4—transition boiling (from bubbly to film); 5—film boiling; T_b —initial boiling point; T_c —wall surface temperature corresponding to the critical heat flux q_{cr} ; T_L —Leidenfrost temperature (minimum film boiling temperature T_{MFB}).

A hot rod, submerged in cold water, will not be wetted by water due to the blanketing by the low conductivity vapor around the rod surface. Heat is

transferred to the water from the hot surface by radiation (Q_R) and vapor-phase thermal conduction (Q_i). Heat flow (Q_i) through a continuous vapor film is determined by the temperature difference ($T_w - T_f$). The contribution of radiation decreases rapidly as the

$$G \triangleq G_v + G_l$$

1. If the water is heated at the contact with the hot body to T_s ($T_f \approx 10\text{--}20^\circ\text{C}$), the vapor bubbles generated at the interface with the liquid surface quickly condense, providing a stable thin film of vapor (no bubbles!) (Fig. 7.50A).

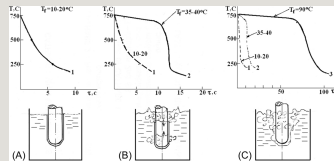


Fig. 7.50 Cooling mode of a hot rod (0.1 MPa). (A) Thin film of vapor. Quiet and rapid cooling. (B) Wetting front movement; explosive boiling. (C) Film mode with blanketing and bubbly mode. Slow cooling.

2. For water temperature at about $T_f \approx 35\text{--}40^\circ\text{C}$; at the bottom of the rod, there is the film boiling; near the liquid level, an intensive transitional or nucleate boiling, driving to the rapid formation of large quantities of steam (explosive boiling) and then a sharp cooling of the rod (Fig. 7.50B).

3. For water temperature close to T_s ($T_f \approx 80\text{--}90^\circ\text{C}$), film boiling regime is realized covered with the thick vapor film. As cooling of the rod proceeds to the transition, then the bubbly boiling regime prevails (Fig. 7.50C).

4. The transition boiling regime is realized for the surface temperatures from T_s to T_c (temperature corresponding to the critical heat flux).

5. For $T < T_c$, the bubbly mode becomes dominant with intensive heat removal, which is then replaced by the natural or forced convection mode of cooling.

Below is a calculation flow of hot body cooling immersed in water. This referenced scheme is in accordance with the modified code RELAP5/MOD2 and CFX4.4 (Yeoh and Tu, 2002) in the quasiapproximation.

The total amount of heat (Q) is assumed to consist of four components:

Q_R —heat dissipation by radiation from the body to the water;

Q_i —heat removal by conduction to the vapor;

Q_e —heat, withdrawn through liquid evaporation; and

Q_c —heat, allocated to turbulent convection.

$$H_k \triangleq \overline{H_k}^k \triangleq \frac{\langle \overline{\chi_k \rho_k h_k} \rangle^s}{\langle \overline{\chi_k \rho_k} \rangle^s} = \frac{\overline{\rho_k h_k}^k}{\overline{\rho_k}^k} \quad (7.140)$$

The individual components are calculated as follows:

1. The amount of heat transferred by radiation:

$$Q_R = \varepsilon_{1,2} \sigma_0 (T_w^4 - T_f^4) F, \quad (7.141)$$

where T_w and T_f are temperatures of the body and fluid; $\sigma_0 = 5.668 \times 10^{-8} \text{ W}/(\text{m}^2 \text{ K}^4)$; $\varepsilon_{1,2}$ is the emissivity of the surface of the body system (ε_1) and of the water (ε_2). F —body surface area (m^2).

2. The amount of heat transferred by conduction through the vapor layer to the water:

$$Q_i = \left[\frac{2}{\sqrt{\pi}} \sqrt{\lambda_f \rho_f c_{pf}} \sqrt{f} \right] (T_w - T_f) F_1, \quad (7.142)$$

where f is the frequency of the bubble formation (Kocamustafaogullari and Ishii, 1995) given by:

$$f=\frac{1.18}{d}\left[\frac{\sigma g\Delta\rho}{(\rho_f)^2}\right]^{0.25};\tag{7.143}$$

d is the detachment diameter of vapor bubble,

$$\widehat{H}_k\triangleq\frac{\langle\chi_k\rho_kv_{zk}h_k\rangle^S}{\langle\chi_k\rho_kv_{zk}\rangle^S}=\frac{\alpha_k\langle\rho_kv_{zk}h_k\rangle^S}{G_k}\tag{7.144}$$

$$b=\frac{T_S-T_e}{2\Big(1-\rho_g/\rho_f\Big)}$$

p —pressure; b is the coefficient taking into account the effect of pressure and subcooling;

$$\Phi=\left\{\begin{array}{ll} (w_e/0.61)^{0.47} & \text{for } w_e\geq 0.61\text{ m/s} \\ 1.0 & \text{for } w_e<0.61\text{ m/s} \end{array}\right.$$

Φ is the coefficient reflecting the effects of the detachment speed and diameter d ; w_e —velocity of the

$$F_1=n(\pi d^4/4)$$

water; F_1 is the fraction of the surface projected by the vapor bubbles; n —number of vapor bubbles on the unit surface:

$$X_{th}\triangleq\frac{\widehat{H}_m-h_{lsat}}{h_{vl}}\tag{7.145}$$

where

of vaporization: $\dot{Q}=\dot{G}_v\widehat{H}_m+\dot{G}_l\widehat{H}_m$;

$$A\frac{\partial\rho_m}{\partial t}+\frac{\partial AG}{\partial z}=0\tag{7.146}$$

and

$$A \frac{\partial G}{\partial t} + \frac{\partial A G^2}{\partial z} + A \frac{\partial P}{\partial z} = A \rho_m g_z - C \tau_w - \frac{A}{\delta z} \delta p_{sing}$$

3. The amount of heat used for the evaporation:

$$A \rho_m \frac{\partial H_m}{\partial t} + A G \frac{\partial \hat{H}_m}{\partial z} - A \frac{\partial P}{\partial t} = C q_w \quad (7.145)$$

4. The amount of heat being carried by turbulent flow natural convection:

$$\overline{T}_m < h_{lsat} : X_{lh} \triangleq \frac{H_l - h_{lsat}}{h_{lv}} < 0; \alpha_v = x = X = 0 \quad (7.146)$$

From experiment $T_w=f(\tau)$ —the transient surface temperature measurement enables calculation of the heat transfer coefficient $\alpha=f(\tau)$, due to

$$H_m = \hat{H}_m = H_m(\rho_m = \rho_l(P, H_l); T = T_l(P, H_l))$$

. Qualitatively, a variation of the heat transfer coefficient is shown in Fig. 7.51 (Gilles et al., 2002).

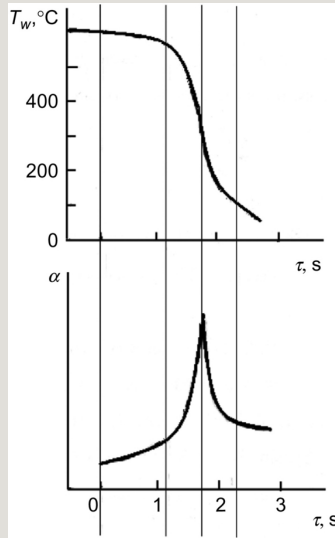


Fig. 7.51 Dependence of $T_w(\tau)$ and $\alpha(\tau)$: 1—film boiling mode; 2—bubbly mode; 3—convective cooling mode.

7.8 Convective boiling heat transfer in channels

7.8.1 Boiling modes in flow channels

Different types of flow regimes and modes of heat transfer in a vertical heated tube are shown in Figs. 7.52 and 7.53. Fig. 7.52 shows the flow conditions and heat transfer modes in a uniformly heated tube ($q=\text{const}$). The figure has been cited in many reports and books on two-phase flow and heat transfer (e.g., Wallis, 1972; Mandhane et al., 1974; Butterworth and Hewitt, 1977), which was adopted originally from Tong (1965). Fig. 7.52 is from its second edition by Tong and Tang (1997), and is self-explanatory, as it contains all the necessary information in the figure.

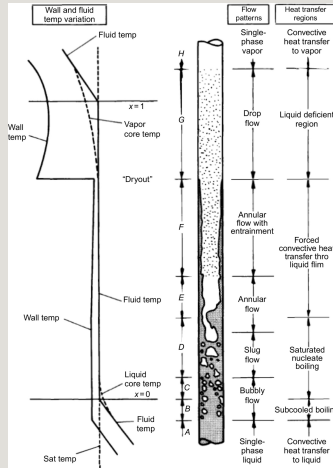


Fig. 7.52 Flow patterns and modes of heat exchange ($q=\text{const}$) (Tong and Tang, 1997). Regions of heat transfer in convective boiling in a heated channel with constant heat flux; the regions A–H are further described in Fig. 7.54. From Ahmada, M., et al., 2013. Phenomenological modeling of critical heat flux: the GRAMP code and its validation. Nucl. Eng. Des. 254, 280–290.

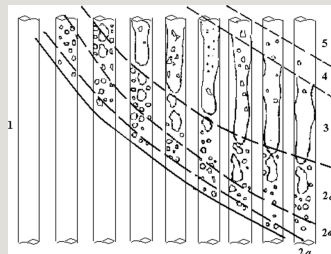


Fig. 7.53 Different flow patterns of two-phase flow in a long pipe (constant: pressure, mass flow rate, inlet enthalpy) by Hewitt and Hall Taylor (1972): 1—single-phase liquid flow; 2—bubbly, slug; 3—annular-dispersed; 4—mist; 5—single-phase vapor flow.

Fig. 7.53 shows a change in the flow patterns of two-phase flow in a long pipe with increasing heat flux from left to right, with the fluid inlet temperature and mass flow rate and the system pressure constant. In the single-phase flow region (region 1), while the liquid on the wall surface may be heated up to the saturation temperature, the wall temperature is still below the value required for vaporization in the presence of the convective heat transfer. Just downstream of the region 1, the fluid at the wall becomes superheated such that evaporation occurs in the micro

cavity centers, although the bulk flow is still subcooled, i.e., below the saturation temperature. This is an area of nucleate boiling of the subcooled liquid (2a). The difference between the saturation temperature and the mass-average temperature of

the liquid is called subcooling $\hat{H}_m > h_{f,sat}; X_m \triangleq \frac{H_v - h_{f,sat}}{h_{fg}} > 1; a_v = x = X = 1$. The upper boundary of the region 2a in Fig. 7.53 corresponds to the vapor quality $x=0$. This portion of the liquid is heated to the saturation temperature so that the average liquid-vapor flow enthalpy is equal to that of saturated liquid ($h_{f,sat}$). In the nucleate boiling of the saturated liquid region (2b) as well as in the subcooled boiling region, equilibrium steam quality (or relative enthalpy) at a distance z is determined by the heat balance

$H_m = \hat{H}_m = H_v; \rho_m = \rho_v(P, H_v); T = T_v(P, H_v)$ where $h(z)$ is the mixture enthalpy and Δh_{fg} is the latent heat. With this definition, it may have a negative or positive value.

With increasing steam quality, plug or slug flow regime prevails (region 2c). The upper boundary of this region is in transition to the dispersed-annular flow regime (region 3) where there is a change in the mechanism of heat transfer. There the process of boiling is mostly replaced by evaporation. While the boiling can be observed within a thick liquid film, the bubble generation in the thin liquid film is usually suppressed and the process of heat transfer cannot be referred to as boiling. The heat is transferred by the convection from the wall to the interface between liquid and the vapor core where evaporation takes place. The upper boundary of the region 3 in Fig. 7.53 corresponds to the complete evaporation of the liquid film and there dominates a dispersed flow mode with gradual evaporation of droplets in the superheated steam (region 4), which shifts into the single-phase vapor flow convection mode—region 5. At the location of the film dry-out, the heat transfer coefficient drops sharply where with the high heat flux the wall surface temperature may reach unacceptable values (burnout, crisis). This heat flux is called critical heat flux (q_{cr}). The line between the areas 3 and 4 corresponds to the critical heat flux associated with the dry-out of the liquid film.

When $q > q_{cr}$, the mechanism of the heat transfer varies depending on the boiling regime, i.e., either DNB, the formation of a conglomerate of bubbles of steam shielding the surface of the bulk liquid from the heated wall, or the boiling transition (BT), the liquid film dry-out. Film boiling under the forced convection mode is basically similar to that observed in the pool boiling. Heated surface is covered with a vapor film that is of low heat conduction through which the heat must be transferred.

Dependency of the two-phase forced convection heat transfer regimes on the quality (vertical axis) and heat flux (horizontal axis) is shown in Fig. 7.54 (taken from Collier and Thome, 1980).

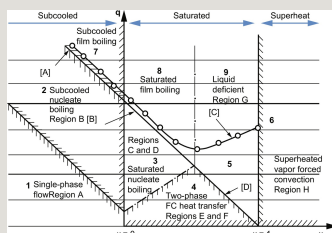


Fig. 7.54 Heat transfer regions in forced convection; Regions A—H in Fig. 7.52. 1—Single-phase fluid flow; 2—subcooled nucleate boiling ($T_i < T_s$); 3—saturated nucleate boiling $T_i = T_s$; 4—two-phase forced convection heat transfer; 5—liquid deficient region (degraded heat transfer); 6—superheated vapor forced convection; 7—subcooled film boiling ($T_i < T_s$); 8—saturated film boiling $T_i = T_s$; 9—liquid deficient and heat transfer crisis; [A]—subcooled CHF by DNB; [B]—saturated CHF by DNB ($T_i = T_s$); [C]—typical burnout locus; [D]—CHF by film dry-out.

It should be borne in mind that, in Fig. 7.54, the equilibrium quality x reflects only qualitatively the border areas. Therefore, when $x > 1$ (area 6) a thermodynamically nonequilibrium vapor flow is possible in the presence of liquid droplets. Then the boundary between the regions 9 and 6 moves to the right.

Since the void fraction (ϕ) in the flow determines the flow and heat transfer modes, it is advisable to consider the actual steam quality that takes into account the nature of the change in ϕ along the channel (for example, $q = \text{const}$), instead of the equilibrium steam quality x_e , as depicted in Fig. 7.55.

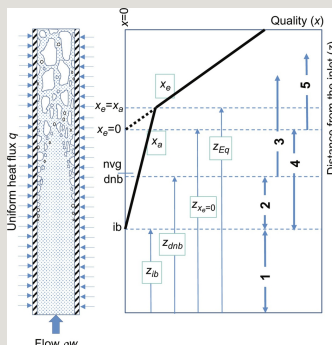


Fig. 7.55 Vapor quality, flow conditions and heat transfer. x_a —actual vapor quality; x_e —equilibrium quality; 1—single-phase flow forced convection; 2—nucleate boiling (developing); 3—developed nucleate boiling; 4—subcooled boiling; 5—saturated boiling (thermally equilibrium for $z > z_{eq}$). ib—incipient boiling initiation; nvvg—net vapor generation; dnb—developed nucleate

boiling; $1 - x = \frac{W_1}{W_g + W_1}$ —distance from the heated section inlet to the point $x_e = 0$ at which saturated nucleate boiling to begin, but the liquid is still below the saturation temperature. z_{eq} —distance to the point of $x_a = x_e$ where all the liquid is at the saturation temperature. Figure modified based on Collier, J.G., 1981. Convective Boiling and Condensation. McGraw-Hill, New York.

First, vapor bubbles appear at the location “ib.” Moving through, or migrating away from the thin boundary layer near the wall surface, the vapor bubbles condense in a bulk of highly subcooled liquid. Here, the void fraction is low, because the growth of bubble layer is limited by the high level subcooling. As a result, the subcooling decreases in the flow core and gradually attains the conditions under which the rate of vapor generation exceeds that of vapor condensation in the stream. From this point the void fraction begins to increase rapidly, which is considered the beginning of the vapor generation—nvvg (net vapor generation).

The equilibrium quality can be zero ($x_e=0$) in the nucleate boiling (beginning) region even with significantly high values of the void fraction ($\varphi \gg 0$). Thus, this mode is under thermodynamically nonequilibrium condition, i.e., where the flow contains a significant amount of vapor (by volume) in the subcooled liquid as a whole. A simple calculation assumes that the undeveloped surface boiling starts in the section in which the surface temperature is saturation temperature T_s . Then a

magnitude of the relative enthalpy $h_{lsat} < \hat{H}_m < h_{vsat}; 0 < X_m < 1; X_m = X = x = \frac{\hat{H}_m - h_{lsat}}{h_{lv}}$ (i.e., quality) can be evaluated by the convective heat transfer coefficients α_c :

– For longitudinal flow inside and outside a tube or pipe,

$$H_m = \hat{H}_m = x h_{vsat} + (1 - x) h_{lsat} \text{ since}$$

$\alpha_v = \frac{(\hat{H}_m - h_{lsat}) \rho_{lsat}}{(h_{vsat} - \hat{H}_m) \rho_{vsat} + (\hat{H}_m - h_{lsat}) \rho_{lsat}}$, where q is the heat flux, c_p is the heat capacity, α_c is calculated on the basis of the formulas for the single-phase convective heat transfer, Δh_{fg} the latent heat; and

– For transverse flow across tube bundles,

$$\rho_m = \frac{\rho_{lsat} \rho_{vsat} h_{lv}}{(h_{vsat} - \hat{H}_m) \rho_{vsat} + (\hat{H}_m - h_{lsat}) \rho_{lsat}}, \text{ where Reynolds number } (Re) \text{ is calculated from the velocity at the narrow gap; } \alpha_c \text{ is the convective}$$

heat transfer coefficient for cross-flows in the bundle.

Recently proposed method of calculating the heat transfer in the boiling channels consists of the following three modes (Kandlikar, 1990, 1991, 1998):

– Partial (or undeveloped) boiling at qualities $\overline{v}_{zk} \triangleq \frac{\chi_k \overline{v}_{zk}}{\epsilon_k}$ (region 2 in Fig. 7.55) where x_{ib} corresponds to the quality at beginning of nucleate boiling and x_{dnb} the developed nucleate boiling;

– Fully developed boiling at $j_k \triangleq \overline{\chi_k v_{zk}} = \epsilon_k \overline{v_{zk}^k}$ (region 3 in Fig. 7.55);

– Mode of a high steam quality for $j \triangleq j_v + j_l$, starting from the point of beginning net vapor generation (x_{nvg}) where

$$J_k \triangleq \langle j_k \rangle^S = \langle \epsilon_k \overline{v_{zk}^k} \rangle^S$$

Here, $J_m \triangleq J_v + J_l$; d is the pipe diameter; Re and Pr_f are for liquid-phase. Points “dnb (developed nucleate boiling)” and “nvg (net vapor generation)” are sufficiently close to each other. While these techniques are not yet widely used, the logic and additional studies may allow us to abandon the simplified representations.

7.8.2 Onset of subcooled nucleate boiling

The flow regimes and temperature change along the inner surface of a circular pipe for a uniform heat flux distribution were shown in Fig. 7.52. The mean liquid-phase temperature varies linearly along the heated length in the convective region away from the inlet according to the heat balance. Also, the wall temperature along

the inner surface of the pipe varies linearly: $v_k \triangleq \frac{J_k}{\alpha_k} = \frac{\langle \chi_k \overline{v_{zk}^k} \rangle^S}{\langle \chi_k \rangle^S}$ where α_c is the single-phase flow heat transfer coefficient. At a certain wall

superheating of $Co \triangleq \frac{\langle \epsilon_v \bar{j} \rangle^S}{\langle \epsilon_v \rangle^S \langle \bar{j} \rangle^S} = \frac{\langle \epsilon_v \bar{j} \rangle^S}{\alpha_v J}$, the water begins to boil on the surface. The subscript *ob* designates the onset of nucleate boiling. The magnitude of the wall superheating could be found by the following empirical relation in Petukhov and Shilov (1987):

$$V_{rel} \triangleq \frac{\langle \epsilon_v (\bar{v}_{zv}^v - j) \rangle^S}{\alpha_v} \quad (7.147)$$

where q is in MW/m² and p in MPa. The range of application of the formula

(7.147) is: $d=3.6-5.7$ mm; $p=0.7-17$ MPa; $J_k^* = 115-340^\circ\text{C}$; $G=11-10^4$ kg/(m² s); $q < 12$ MW/m².

In the case of flows in narrow annular channels, the onset of surface boiling occurs with the wall-superheat determined by the formula:

$$\langle j_v \rangle^S = \langle \epsilon_v j \rangle^S + \langle \epsilon_v (\bar{v}_{zv}^v - j) \rangle^S \quad (7.148)$$

Here d_e is the equivalent hydraulic diameter (mm); w_0 the flow velocity (m/s); q is the heat flux (MW/m²); p the pressure (MPa). Onset of the surface boiling is related to the flow enthalpy at onset of boiling h_{ob} , which is determined from the equation (Tarasova and Orlov, 1964):

$$V_v = CoJ + V_{gj} \quad (7.149)$$

where h is the enthalpy (kJ/kg); q the heat flux (MW/m²); d_e the equivalent hydraulic diameter of the channel (m); G is the mass flow rate (kg/m²/s). The formula is applicable to the range: $p=4.9-19.6$ MPa; $G=1300-11,000$ kg/(m² s); $q=0.43-1.3$ MW/m²; $d_e=2.9-6.3$ mm.

The enthalpy at the beginning of the surface boiling can be calculated through the vapor quality ($x_{ob} < 0$):

$$h = h_f + x_{ob} h_{fg}$$

where

$$Co = 1.74 \ln \left(\frac{1}{1 - x_{ob}} \right) + 1.74 \ln \left(\frac{1}{1 - x_{ob}} \right) + 1.74 \ln \left(\frac{1}{1 - x_{ob}} \right) + 1.74 \ln \left(\frac{1}{1 - x_{ob}} \right);$$

$$V_{gj} \neq 0, \quad V_k \triangleq \frac{\langle \chi_k \rho_k V_{zk} \rangle^S}{\langle \chi_k \rho_k \rangle^S} \cong V_k = \frac{\langle \chi_k V_{zk} \rangle^S}{\langle \chi_k \rangle^S} \quad \text{with}$$

$$H_k \triangleq \bar{h}_k \triangleq \frac{\langle \chi_k \rho_k h_k \rangle^S}{\langle \chi_k \rho_k \rangle^S} \cong \hat{h}_k = \frac{\langle \chi_k h_k \rangle^S}{\langle \chi_k \rangle^S}; \quad \text{and} \quad V_{\eta}(1 - Co a_{\eta}) = Co(1 - a_{\eta})V_l + V_{gj} \quad \text{where } p_{crit}$$

the critical pressure. In general, the subcooling at the boiling initiation can be found approximately by the equation

$$A \frac{\partial \alpha_k Q_k V_k}{\partial t} + \frac{\partial A \alpha_k Q_k V_k}{\partial z} + A \alpha_k \frac{\partial P}{\partial z} + A f_i \frac{\partial \alpha_k}{\partial z} + g_k \frac{\partial A}{\partial z} = A \alpha_k Q_k g_z - A \tau_{ik} - C_k \tau_{wk} - A \alpha_k \frac{\delta P_{ksing}}{\delta z} + A F_{ik}^{AM} + A \Gamma_{ik} V_l, \quad \text{where } \alpha_c \text{ and } \alpha_b$$

are the heat transfer coefficients in single-phase flow convection and developed boiling, respectively. In the presence of deposits on the surface having the thermal resistance R (m² K/W), the value of subcooling at the start of boiling will be equal

$$\text{to } A \frac{\partial \alpha_v Q_v V_v + \alpha_l Q_l V_l}{\partial t} + \frac{\partial A [\alpha_v Q_v V_v + \alpha_l Q_l V_l]}{\partial z} + A \frac{\partial P}{\partial z} + (g_v + g_l) \frac{\partial A}{\partial z} = A Q_m g_z - C_v \tau_{vv} - C_l \tau_{wl} - A \left(\alpha_v \delta P_{vsing} + \alpha_l \delta P_{lsing} \right) \frac{\partial A}{\partial z}.$$

7.8.3 Subcooled boiling, developing region

Heat transfer in the channels under the conditions of undeveloped subcooled boiling of water, corresponding to the region 2 in Fig. 7.55, is calculated by the formula:

$$A \left[a_l \frac{\partial \alpha_l Q_l V_l}{\partial t} + a_v \frac{\partial \alpha_v Q_v V_v}{\partial t} \right] + a_l \frac{\partial A \alpha_l Q_l V_l}{\partial z} + a_v \frac{\partial A \alpha_v Q_v V_v}{\partial z} = -A f_i \frac{\partial \alpha_l}{\partial z} - [g_v a_v - a_l g_l] \frac{\partial A}{\partial z} - A \alpha_l a_l [g_l - g_v] g_z - A [a_v - C_v a_v \tau_{vv} + C_l a_l \tau_{wl} - A a_l a_l \left(\frac{\delta P_{vsing}}{\delta z} - \delta P_{lsing} \right) + A F_{ik}^{AM} + A \Gamma_{ik} V_l]$$

where $a\omega$ is calculated by the formulae given in Section 7.6 for pool boiling in a large volume; a_c is the single-phase flow convective heat transfer coefficient.

7.8.3.1 Features of subcooled boiling at low pressures (0.1–1.0 MPa) (Wadekar, 1990)

Subcooled boiling at low pressures is characterized by large specific vapor volumes and, hence, high velocities. In this situation, the saturation temperature decreases toward the downstream region of the channel in accordance to the decrease in pressure; and in the stabilized convective heat transfer section (with $q=\text{const}$), it increases in accordance to the increase in the average bulk liquid temperature.

Fig. 7.56A shows axial temperature profile for the onset of boiling of flows with the subcooled bulk liquid. In this figure, after the surface temperature reaching the desired superheat (point A), the subcooled liquid water starts boiling and the

surface temperature decreases rapidly because of the high heat transfer coefficients. With an increase in the mass flux (Fig. 7.56B), the boiling is suppressed and the surface temperature decreases (AB). After the point B the surface temperature T_w is observed to rise (up to Point C) in accordance with increase in the bulk fluid

temperature J_k^* . This indicates that while the true vapor quality does not change, the two T_w peaks appear. Fig. 7.56C shows a wavy surface temperature profile, which should be corresponding to T_s changes along the length of the channel.

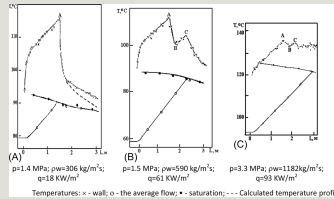


Fig. 7.56 Boiling onset with different wall temperature peaks (Wadekar, 1993). Temperatures: x—wall; o—the average flow; •—saturation; - - - calculated temperature profile.

Boiling flow heat transfer in a vertical pipe with subcooling has other features (Dougherty et al., 1990). If there is no boiling, the heat transfer coefficient α_i at the pipe inlet can be found from the correlation:

$$\frac{\partial \alpha_v}{\partial z} \cong 0; \frac{\partial V_k}{\partial z} \cong 0$$

The heat transfer coefficient for the flow of subcooled ($x=-0.3 \sim 0$) fluid is given by:

$$g_v \cong 0; \delta P_{ksing} \cong 0$$

From this it follows that when $x=0$, $\alpha=4.13\alpha_i$; at $x=-0.1$, $\alpha=1.44\alpha_i$; at $x=-0.2$, $\alpha=1.04\alpha_i$.

7.8.4 Developed boiling in channels in subcooled to saturated region

The heat transfer coefficient of the forced flow boiling is influenced mainly by two processes—convection and boiling. It is well understood that the former process can suppress the latter. There, a magnitude of the heat transfer coefficient can be similar to that of the convection heat transfer coefficient α_c at low heat flux and high velocity, and the pool boiling heat transfer coefficient α_0 at high heat flux and moderate velocity.

The method proposed by Kutateladze (1979) allows you to take into account the influences of the flow velocity and heat flux without relying on complicated criteria. First, heat transfer rates α_0 at boiling and α_c for turbulent flow convection of the liquid at T_s are compared. That is, depending on the ratio α_0/α_c the following equations are to be used:

$$A\tau_{iv} \cong -A\alpha_l\alpha_l[q_l - q_v]g_s - C_v\alpha_l\tau_{iv} + C_l\alpha_l\tau_{iv} \quad (7.150)$$

$$\tau_{iv} \cong \alpha_v\alpha_l[q_l - q_v]g \quad (7.151)$$

$$v_{iv} = C \sqrt{\frac{g \Delta \rho g}{\rho_l}} \quad (7.152)$$

Here α is the heat transfer coefficient for the considered mode, α_c is the convective heat transfer coefficient calculated according to the formulae. In Eq. (7.151), C is a function of p and, for $p < 15$ MPa, is 0.8–0.9. According to Kutateladze, Eq. (7.152) is applicable to the nucleate boiling of water at T_s and to the subcooled boiling. Eqs. (7.150)–(7.152) are applicable for $p = 2$ –20 MPa and are accurate within $\pm 35\%$. A similar approach is found in Wadekar (1990).

Instead of the formula (7.151), Yagov et al. (1998) recommended a formula that gives the best agreement with experiment for the case of boiling in a large volume of water:

$$B \sim g \Delta \rho \delta^3; D \sim C_d \rho_l \delta^2 V_{gj}^2 \quad (7.153)$$

$$V_{gj} \sim \left[\frac{g \Delta \rho \sigma}{\rho_l^2} \right]^{0.25}$$

When a two-phase mixture flows in a pipe or annular channel, heat transfer coefficients are calculated according to the formula obtained in CKTI by Borishanskii et al. (1973) and Handbook (1986):

$$V_{gj} \sim \sqrt{\frac{g \Delta \rho D}{\rho_l}} \quad (7.154)$$


where $\tau_{iv} = \alpha_v \alpha_l q_l \frac{V_{gj}^2}{C^2 \delta} = \alpha_v \alpha_l q_l (1 - Co \alpha_v)^2 \frac{(V_v - C_a V_l)^2}{C^2 \delta}$, α_c is the heat transfer coefficient of single-phase flow at the velocity w_0 in a pipe or channel; α_0 is the heat transfer

coefficient of the pool boiling; $C_a = \frac{Co(1 - \alpha_v)}{(1 - Co \alpha_v)}$ is the mixture volumetric flux where



; x is the mass quality. The range of application for water is $p=0.2-17$ MPa; $J_{cm}=1-300$ m/s; $q=0.08-6$ MW/m².

Influence of the mixture velocity becomes notable, when the following relation is

true: . In this case the heat transfer coefficient is in proportion to the mass flux to the 0.8th

power, i.e., $\alpha \sim W^{0.8}$. At lower values of this combination $A \frac{\partial X}{\partial t} + B \frac{\partial X}{\partial z} = C$ and does not depend on J_{cm} and then $Det(B - \lambda A) = 0$ (see Fig. 7.57).

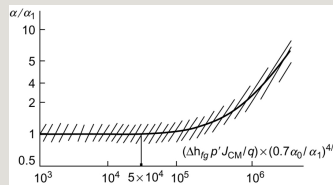


Fig. 7.57 Heat transfer in two-phase flow in channels.

It would be sufficient to use a simple formula for evaluating the boiling heat transfer of different fluids as proposed by Borishanskii et al. (1973):

$$\lambda_1 = V \quad (7.155)$$

$$\lambda_{2,3} = V \mp C_s$$

where M is molecular mass. The limit of applicability is $Y=1-20$. Accuracy will be for $F<1$, $\pm 35\%$; for $F=0$, $\pm 20\%$; at $F=40$, $\pm 5\%$.

7.8.5 Boiling on porous structures under forced convection conditions

7.8.5.1 Subcooled boiling on a capillary-porous surfaces

The concept of the process of subcooled boiling subcooled for this case is presented in Soloviev (1998).

Depending on the magnitude of the heat flux and degree of subcooling, there are three modes of heat transfer: (1) microtube mode, (2) bubble roughness mode, and (3) bubbly surface roughness mode (see Fig. 7.58). Calculation of the heat transfer coefficient for the mode 2 can be made by the method proposed by Avdeev (1982, 1985):

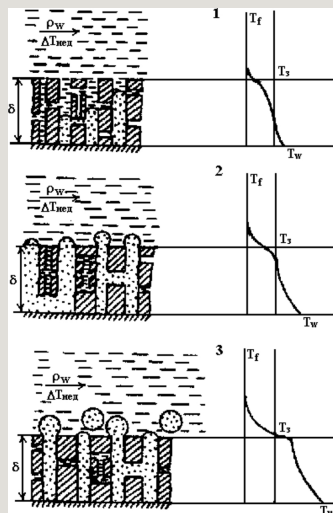


Fig. 7.58 Subcooled liquid boiling model at the capillary-porous surfaces. Mode 1—microtube mode, in which heat is transferred from the surface through pores that act as heat pipes (evaporation occurs at the base and condensation at the top); Mode 2—bubble roughness mode, in which at the outer boundary of the porous layer formed stationary steam bubbles on top of which there is a vapor condensation; Mode 3—bubbly surface roughness mode, in which at the outer boundary of the porous layer, the stationary bubbles are formed and condense on the top.

$$\lambda_1 = \frac{\lambda_s}{\varepsilon} \quad (7.156)$$

where D is the channel diameter, d is the bubble diameter, defined by the formula:

$$\lambda_1 = \frac{\lambda_s}{\varepsilon}$$

where d_s is the pore diameter; ε is the porosity; q_l and q_c are heat flux associated with evaporation and convection given by:

$$\lambda_2 = V_f$$

Heat transfer for the mode 3 can be determined by the following (Avdeev, 1982, 1985):

$$\lambda_{3,4} = W_a \mp C_a \quad (7.157)$$

where d is the detachable bubble diameter (see above).

7.8.6 Heat transfer in film boiling, and superheated vapor flow in channels

Film boiling heat transfer has been extensively investigated during the last half century. Excellent reviews are found in text books by Tong (1965), Tong and Tang (1997), Collier and Thome (1980), Delhay et al. (1981), Butterworth and Hewitt (1977), a handbook by Hetsroni (1982), and articles by Ganic and Rohsenov (1977), Mayinger and Langer (1978), Tong (1978), Sergeev (1978, 1987, 2007), Groeneveld and Snoek (1986), Groeneveld (1992), Yadigaroglu and Andreani (1989), Sakurai (1990), Andreani and Yadigaroglu (1989, 1994), and in the proceedings of the 1st International Symposium on Fundamental Aspects of Post-CHF Heat Transfer (1984). A good summary of the literature survey is given in (published in 2001 in the context of the IAEA's Coordinated Research Project on Thermohydraulic Relationships for Advanced Water Cooled Reactors (IAEA TECDOC, 1203, 2001)).

In the context that follows in this section, we discuss on a number of two-phase flow heat transfer regions depicted previously in Fig. 7.54 by region 5—liquid deficient region (degraded heat transfer), region 6—superheated vapor forced

convection, region 7—subcooled film boiling ($\lambda_{5,6} = W_s \mp C_s$), region 8—Saturated film boiling $f_i \frac{\partial \alpha_v}{\partial z}$, and region 9—liquid deficient and heat transfer crisis; in Fig. 7.53 by region 3—dispersed-annular, region 4—mist and region 5—single-phase superheated vapor; and in Fig. 7.52 by region G (liquid deficient) and region H (super heated vapor).

In boiling two-phase flows in a heated channel, a drastic deterioration of heat transfer (heat transfer crisis) may occur, which shows an increase in temperature on the heat-transfer surface, or reduction in the heat flux q . The heat transfer mode

between the onset location of the crisis and its downstream region where the flow becomes single-phase superheated vapor flow is called as film boiling. In this regime, at a constant heat flux, an increase in the surface temperatures is observed and the offset of the crisis in the region of low steam quality with increasing q (see Fig. 7.59).

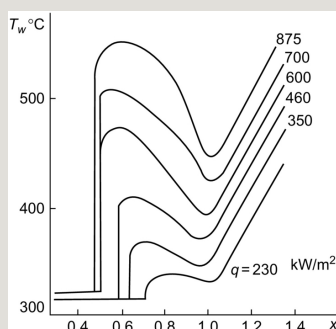


Fig. 7.59 Wall temperature dependence on the vapor quality and heat flux at $\rho_w=1400 \text{ kg/(m}^3 \text{ s)}$; $p=9.8 \text{ MPa}$.

The film boiling is characterized by an aggravated mode, temperature fluctuations due to the variable surface contact modes of liquid and vapor. This regime is implemented in the steam generator but is to be avoided in the case of nuclear fuel rod bundle cooling. Nevertheless, some experiments show that a short-term operation of fuel rods in such a regime under certain parameters is possible if the excess temperature of the fuel cladding surface and the amplitude of the oscillations do not exceed permissible limits. From this point of view, perhaps a more accurate calculation of heat transfer is necessary. The temperature jump at a crisis decreases with increasing mass flow rate and pressure, and increases with increasing heat flux. Two-phase flow structure in this region is different depending on the nature of the crisis, i.e., DNB ([A] in Fig. 7.54) or film dry-out ([D] in Fig. 7.54).

If a crisis occurs in the subcooled two-phase flow, or two-phase flow of low steam quality, i.e., due to DNB, the realized two-phase flow mode is called as “*inverted annular flow*” where the superheated vapor flow flowing along the wall separates the subcooled layer from the wall. The inverse-annular flow regime is preceded by the transition boiling section in the upstream region which is bounded by the DNB point (CHF) and the quench front or the minimum heat flux of the film boiling on the boiling curve.

As described in Section 7.5.4 on the boiling curve in the pool boiling, the location of the minimum film boiling temperature (T_{MFB}) separates the high temperature region of the inefficient film boiling or vapor cooling, from the lower-temperature region of more efficient transition boiling region. Thus it provides a limit to application of the transition boiling and film boiling correlations. T_{MFB} also represents a temperature boundary beyond which surface properties and surface conditions generally do not affect the heat transfer. Wettability or contact angle although important in nucleate and transition boiling, are not applicable in the film boiling regime, and the conduction along the surface becomes less important when nucleate and film boiling no longer occur one-by-one.

It is noted that, while the critical heat flux has been extensively studied and can be predicted fairly well by a variety of correlations, the minimum heat flux under forced convective conditions has undergone less investigation. There is no general consensus on the effect of the various system parameters on T_{MFB} under the conditions but it should be affected by flow, pressure, fluid properties, and heated surface conditions in the same way as in the pool boiling described in Section 7.5.4.

In the “*dispersed-annular flow*” regime, the crisis is usually associated with the liquid film dry-out on the heated surface. In this case, the heated wall is cooled by the vapor flow, which is superheated while flowing along the channel. In this vapor flow region, liquid droplets exist and gradually evaporate exchanging heat with the superheated vapor.

In general, the dispersed two-phase flow in this zone is in thermally nonequilibrium, and the wall surface temperature is determined by several processes: the convective heat transfer by the vapor flow, radiation, and evaporation of the droplets. The actual flow parameters depend on the evaporation of droplets and heat-transfer area in the vapor flow, whose temperature may exceed the saturation temperature. In simple calculations, thermal equilibrium between liquid and vapor phases is often assumed. There the boundary between this region and a superheated vapor flow region of the channel is considered where the equilibrium steam quality $x=1$.

Depending on the operating conditions and the channel geometry, the flowing vapor in the post-CHF zone may be superheated in the inverse-annular regime where the liquid is separated from the heated surface by the vapor film (downstream of the DNB point and the transition boiling region), or in the dispersed-annular flow regime (downstream of the film dry-out point) where the liquid droplets are distributed in the vapor core flow.

Structure of two-phase flow in the postminimum heat flux region is stable and most of the liquid phase decays into droplets toward the downstream region and the flow becomes dispersed which is a dominant flow regime in the heat transfer crisis. Higher surface temperature in this zone is due to the fact that the superheated vapor is primarily in contact with the wall.

7.8.7 Inverse-annular flow boiling and dispersed-annular flow film boiling

There are few reliable guidelines for calculation of the inverse-annular mode heat transfers. A large number of semiempirical models have been developed, most of which are very complicated. It is difficult to check many of the parameters used in these models match the final results from the individual experimental data and their validity of generalization has not been yet demonstrated. Furthermore, the experimental data do not always provide sufficient accuracy, which are adopted with the background of the models often facing a difficulty for justification.

The heat transfer in the film boiling of the subcooled liquid region is made up of three mechanisms:

- (1) convective heat transfer from the heated surface by the vapor flow convection in the vapor film along the surface;
- (2) conduction and laminar convection heat transfer from the vapor film to the vapor-liquid interface; and
- (3) thermal radiation.

The heat transfer in the dispersed-annular flow mode, which appears most often in the superheated zone of high steam quality ($x > 0.2$), generally comprises of the following components:

- (1) convective heat transfer from the wall to the bulk vapor flow;
- (2) conduction heat transfer from the wall to the liquid droplets that are in contact with the thermal boundary layer (dry contact) and that impact the wetted (or not wetted) wall;
- (3) radiation heat transfer from the wall to both bulk vapor and liquid droplets;
- (4) convective heat transfer by the bulk vapor flow to the suspended droplets in the vapor core.

A majority of the heat is transported by convection. The presence of the superheated vapor and the liquid droplets at saturation temperature T_s , results in the actual vapor flow quality x_a being lower than the equilibrium vapor quality x . Let's define a degree of thermodynamic nonequilibrium by the ratio of these two values $x_a/x=n$ (≤ 1 in the dispersed-annular regime). Then the mean temperature and enthalpy of the superheated vapor in this case is expressed by the relations:

$$\bar{T}_v = T_s + \frac{\Delta h_{fg}}{c_p} \frac{(1-n)}{n} = T_s + \frac{\Delta h_{fg}}{c_p} \cdot \frac{x-x_a}{x_a},$$

$$\bar{h}_v = h_s + \Delta h_{fg} \frac{(1-n)}{n} = h_s + \Delta h_{fg} \frac{x-x_a}{x_a}.$$

When the mass flux of the mixture is higher than $1000 \text{ kg}/(\text{m}^2 \text{ s})$, the thermodynamic nonequilibrium will be small and $n \approx 1$. The nature of the temperature distribution and the actual vapor quality in the crisis zone is shown in Fig. 7.60. The crisis zone could be defined as the region where the actual vapor quality x is higher than the critical steam quality x_{cr} at which departure from nucleate boiling (DNB) would occur. Heat transfer coefficient is usually referred to as the temperature difference ($T_w - T_s$).

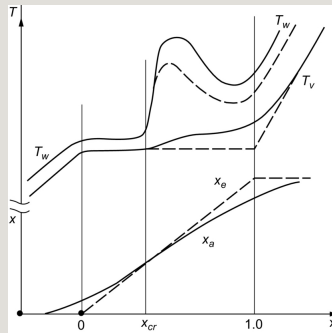


Fig. 7.60 Temperature behaviors to the vapor quality and the actual vapor quality in the crisis zone ($q=\text{const}$ and $x > x_{cr}$): — thermally nonequilibrium flow; x_a is the actual quality; - - - thermally equilibrium flow; x_e is the equilibrium quality. T_v and T_w are the vapor-phase and wall temperatures.

7.8.7.1 Heat transfer in a dispersed droplets-vapor mixture flow

When the dispersed-annular flow structure changes to the dispersed droplets-vapor

mixture flow in channels, heat transfer can be calculated by taking into account thermal nonequilibrium of the flow (Sergeev et al., 1985; Sergeev, 2002). There, the two-phase flow in the crisis region is treated by a homogeneous mixture of superheated vapor and liquid droplets. It is considered that the heat is transferred by convection from the heating surface to the vapor, and from the vapor to the droplets (droplets evaporating on the wall surface; and the radiation heat transfer is neglected). The heat transfer coefficient from the wall to the vapor and the critical steam quality (x_{cr}) are assumed to be known.

The method can be applied for flows in pipes, annular channels, and for nuclear fuel rod bundles with spacer grids with their hydraulic diameter would be 4–

$$20 \text{ mm, and } p=1.1\text{--}19.6 \text{ MPa, } \rho w = 70 - 2000 \text{ kg/(m}^2 \text{ s)}, \\ q \leq 1 \text{ MW/m}^2, T_w - T_s \leq 500^\circ\text{C and } W_\alpha = \frac{\alpha_l \rho_g^{am} V_G + \alpha_G \rho_l^{am} V_l}{\alpha_l \rho_g^{am} + \alpha_G \rho_l^{am}}.$$

The variation of actual vapor quality x_a in the *post-CHF* zone in the channel could be determined by the following differential equation:

$$C_\alpha^2 = \frac{f_l \rho_m^{am} - \alpha(1-\alpha) \rho_l^{am} \rho_g^{am} (V_G - V_l)^2}{\rho_m^{am2}} \quad (7.158)$$

where x_e is the thermodynamically equilibrium mass quality; C is an empirical constant ($C=1.5$), P_w and P_h are the wetting and heating perimeters, respectively, in m; q is the local heat flux on the j th heat transfer surface (W/m^2); ρ_w is the mass flux ($\text{kg/m}^2 \text{ s}$); parameters m and n depend on pressure:

$$m = 1.5 - 0.0001 p, \quad n = 1.5 - 0.0001 p$$

with the pressure p in bars.

For flows in pipes and rod bundles, $C=1.5$. For annular channels with one-sided heating, $C=3$. For annular channels with two-sided heating, the heat flux to the vapor at the second surface is assumed to be zero and the constant $C=3$. In the downstream of the crisis section, C is assumed to be equal 1.5 (Sergeev et al., 1985). The “actual” vapor quality distribution x_a will be obtained by integration of Eq. (7.158) for the heat-transfer crisis section, which depends on x_{cr} and

$$f_i > f_{ihyp} = \frac{\alpha(1-\alpha)\rho_g^m \rho_l^m (V_G - V_l)^2}{\rho_m^m}$$

For $n=1$ (highly superheated vapor flows, $x_a=x_e$), Eq. (7.158) has an analytical solution:

$$f_i > f_{ihyp} = \frac{\alpha(1-\alpha)\rho_g \rho_l (V_G - V_l)^2}{\rho_m} \quad (7.159)$$

$$f_i = C \alpha \rho (V_G - V_l)^2$$

where B is the constant $\tau_i = -a_i C_i \frac{\rho}{2} |V_v - V_l| (V_v - V_l)$ determined from the condition $x=x_{cr}$, and $\Phi(\xi)$ is the probability integral. Eq. (7.159) could be used for testing the numerical integration scheme of Eq. (7.158).

7.8.7.2 Procedure for calculating heat transfer in the crisis zone

– by solving the differential equation (7.158) or by the formula (7.159), the actual vapor quality x_a is obtained at a given vapor equilibrium quality x_e ;

– then with x_e and x_a , the enthalpy of superheated vapor is given by

$$q_{ik} = a_i h_{ik} (T_{sat} - T_k)$$

in a specified section of the channel;

– with the given enthalpy of superheated vapor and the saturation enthalpy from

$$a_i = \frac{6\alpha_d}{\delta_{32}}; n_d = \frac{6\alpha_d}{\pi \delta_{32}^3}$$

the steam table, n_d determines the superheated steam temperature;

– The wall temperature on the i th heat-transfer surface is calculated by:

$$\tau_{id} = -C_d (Re_d) \frac{\pi \delta_{32}^2}{4} n_d \frac{\rho_c}{2} |V_d - V_c| (V_d - V_c) \\ = -\frac{3\alpha_d}{4\delta_{32}} C_d \rho_c |V_d - V_c| (V_d - V_c)$$

, where α is the convective heat transfer coefficient to the superheated vapor; T_v is the temperature of the superheated vapor (K); T_w the wall temperature (K).

Thermal properties refer to those at the superheated vapor temperature

7.8.7.3 Annular channels

Heat transfer coefficient for annular flow channels is obtained from the following equations (Handbook PTM.24.031.05-72, 1974):

– when the inner wall of the annular channel is heated:

$$We_{crit} = \frac{\rho_c (V_d - V_c)^2 \delta_{32}}{\sigma}$$

– when the outer wall of the annular channel is heated:

$$\frac{\partial n_d}{\partial t} + \nabla \cdot n_d V_n = \Phi_n^{Nuc} + \Phi_n^{Col} + \Phi_n^{Coo} + \Phi_n^{BU}$$

– when the both inner and outer walls are heated:

For the inner wall

$$\frac{\partial u_i}{\partial t} + \nabla \cdot (u_i v_i) = \frac{2\alpha_i}{3a_i \rho_{f,i}} \left(\Gamma_d - a_{f,i} \frac{\partial p_d}{\partial t} - a_{f,i} \nabla p_d \right) + \Phi_{a_i}^{Nuc} + \Phi_{a_i}^{Col} + \Phi_{a_i}^{Coo} + \Phi_{a_i}^{BU}$$

For the outer wall



where

$$S_j(x, t) \triangleq \int_0^\infty \delta f(\delta; x, t) d\delta$$

$$\frac{\partial S_j}{\partial t} + \nabla \cdot (S_j v_j) - j D_{j-1} S_{j-1} = P_j$$

$$\phi_{a_i}^{Coz} = 12\pi \left(\frac{a_i}{d_i} \right)^2 \phi_n^{Coz}, \quad \phi_{a_i}^{BU} = 12\pi \left(\frac{a_i}{d_i} \right)^2 \phi_n^{BU}$$

$$S_j = \eta_{ij} S_i \triangleq \left(\eta_{ij} \right) S_i = \frac{a_i}{a_j} S_i = \frac{\eta_{ij}}{1}$$

$$\delta_{32} = \frac{S_3}{S_2}$$

The subscripts 1 and 2 of the thermal properties at refer to the inner and outer walls of the annular channel, respectively.

7.8.7.4 The rod bundles

Heat transfer coefficient can be represented by (Subbotin et al., 1975):

$$q_{il} = \left[n_d \pi \int_{\delta_{min}}^{\delta_{max}} \delta f(\delta) Nu(\delta) d\delta \right] \lambda_c (T_{sat} - T_c) \quad (7.160)$$

$$\Gamma_{vcl} = -\Gamma_{chl}$$

where P/D is the rod pitch to diameter ratio.

7.8.7.5 Heat transfer at the entrance region of a crisis zone

Heat transfer to the superheated vapor flow in the region from the entrance to downstream of the crisis zone, where the thermal boundary layer is formed approximately for the length of 15 hydraulic diameters, is calculated by:

$$\Gamma_{vdl} = -\Gamma_{dlv} \quad (7.161)$$

where Nu_0 is the Nusselt number for steady-state heat transfer, and Δz is the distance from the cross section of the heat-transfer crisis (Isachenko et al., 1981).

7.8.7.6 Influences of spacer elements

In this section, integration of Eq. (7.158) will be carried out with a new boundary condition given by Eq. (7.162), which takes into account an increase in the vapor quality due to an additional amount of evaporation resulting from the interactions of the flow with the spacer elements (Sergeev et al., 1990):

$$A_{\text{finel}} \frac{\partial \alpha_{\text{el}}}{\partial z} \quad (7.162)$$

where $(\Delta A/A)$ is an extent of the flow channel area blockage by the spacer, k is the multiplication factor that depends on the geometry of the spacer and its mode of settings ($0 < k < 1$). For simple spacer elements without swirl enhancing tabs, the factor k could be given by:

$$A_{\text{finel}} \frac{\partial \alpha_{\text{el}}}{\partial z}$$

If the calculated vapor quality in the spacer element section by Eq. (7.162) exceeds the value of the relative enthalpy (quality) at the same location, it is considered that

the difference $g_{\text{dl}} \frac{\partial A}{\partial z}$ is due to the evaporation of the liquid film, which is formed as a result of flow interaction with the spacer and covers the heated wall surface on the segment length:

$$A \alpha_{\text{dl}} \frac{\delta P_{\text{dlsing}}}{\delta z} \quad (7.163)$$

In this spacer region, the heat transfer is calculated using the formulas for boiling, after which the procedure described above with the solution of Eq. (7.158) is repeated, starting from the section located at a distance Δz from the spacer, where the flow is considered to be at thermally equilibrium.

The following takes into account the single-phase flow heat transfer enhancement by the spacers, suggested by Yao et al. (1982):

$$A \frac{\partial \alpha_v Q_v}{\partial t} + \frac{\partial A \alpha_v Q_v V_v}{\partial z} = A \Gamma_{vcl} + A \Gamma_{vdl} \quad (7.164)$$

where Nu_0 is Nusselt number in the absence of the spacer; Nu is Nusselt number in the presence of the spacer; z is the distance from the spacer; and d_h is the equivalent hydraulic diameter of the flow channel.

7.8.7.7 Consideration of radiation

The total heat transfer by vapor flow convection and radiation to the droplets is expressed by Sergeev et al. (1990):

$$A \frac{\partial \alpha_{cl} Q_{cl}}{\partial t} + \frac{\partial A \alpha_{cl} Q_{cl} V_{cl}}{\partial z} = A \Gamma_{clv} + A \Gamma_d - A \Gamma_e \quad (7.165)$$

where σ is Boltzmann constant, and ε the reduced emissivity of the blackbody-droplet system.

The wall temperature is obtained following the above procedure of solving Eqs. (7.158), (7.165). For the given wall temperature, reduced heat transfer coefficient is

calculated by
$$A \frac{\partial \alpha_{dl} Q_{dl}}{\partial t} + \frac{\partial A \alpha_{dl} Q_{dl} V_{dl}}{\partial z} = A \Gamma_{dlv} - A \Gamma_d + A \Gamma_e$$

The unit of various parameters used in the formulas are in the following:

A —W/(m² K); T —in °C; q —W/m²; p —MPa; h —J/kg; ρw —kg/(m² s); Δh_{fg} —J/kg; μ —N s/m²; $d_h=(d_2-d_1)$ —m; d_1, d_2 —m; λ —W/(m K); σ —N/m; ρ —kg/m³.

Range of applicability of the method is as follows:

$$\begin{aligned} n=1.1-19.6 \text{ MPa}^2; \quad T_w - T_f &\leq 500^\circ\text{C}; \quad \rho w=70-2000 \text{ kg}/(\text{m}^2 \text{ s}); \quad q \leq 1 \text{ MW}/\text{m}^2; \\ A \frac{\partial \alpha_{cl} Q_{cl}}{\partial t} + \frac{\partial A \alpha_{cl} Q_{cl} V_{cl}}{\partial z} + A \alpha_{cl} \frac{\partial T_w}{\partial z} + A \alpha_{cl} \frac{\partial T_f}{\partial z} &= A \Gamma_{clv} + A \Gamma_d - A \Gamma_e; \\ A \alpha_{cl} Q_{cl} &= A \Gamma_{clv} - A \Gamma_d + A \Gamma_e; \quad d_h=4-20 \text{ mm}. \end{aligned}$$

At lower mass flux than $1000 \text{ kg}/(\text{m}^2 \text{ s})$, the superheated vapor flow is characterized by a significant thermodynamic nonequilibrium in the presence of

liquid droplets in the vapor flow stream. In this case, the heat transfer coefficient refers to the temperature difference $(T_w - T_s)$ instead of $(T_w - T_s)$, as is commonly practiced for thermodynamic equilibrium flow. As a result, $T_w = \bar{T}_v + q/\alpha$. The superheat is calculated from a steam table, knowing \bar{h}_v :

$$\bar{h}_v = h_g + \Delta h_{fg}(x - x_a)/x_a, \quad (7.167)$$

where x is the equilibrium vapor quality; x_a —true vapor mass quality; Δh_{fg} —heat of vaporization; h_g —saturation enthalpy of vapor.

7.8.7.9 Heat transfer in the superheated zone of the helical coil pipes

The helical coil heat exchanger has a number of different features as compared with a straight tube heat exchangers. For instance, the flow in the helical coil tube shows the influence of centrifugal force and the heat transfer crisis occurs not uniformly along the perimeter of the tube. There exists a large variation of the heat transfer coefficient around the perimeter and, as a result, large temperature gradients. Nonequilibrium effects at a crisis zone are less than those of the straight tubes/pipes of identical parameters. With d the tube inner diameter and D the coil diameter, the calculation formula takes the form (in Handbook, 1983) for $d/D \geq 0.015$:

$$Nu = ad/\lambda_g = CRe_m^{0.8}Pr_w^{0.8}z \pm 25\%,$$

where $C=0.017$ for helical coil tubes; $C=0.017(1+3.18d/D)$ for pipes bent at 90 degrees:

$$z = 1 + y(1 - x)^{0.8}$$

$$y = 0.5 \left(\rho_f / \rho_g - 1 \right)$$

for $\rho_f/\rho_g < 1300$. For $d/D < 0.015$

for $\rho_f/\rho_g \leq 480$; $y=70$ for $480 < \rho_f/\rho_g$

$$Nu = 0.023 Re_w^{0.8} Pr_w^{0.8} \left[1 - 0.1 \left(\frac{\rho_f}{\rho_g} - 1 \right)^{0.4} (1-x)^{0.4} \right].$$

The formula is based on the experimental data obtained in the steam-water mixture in the range of $Re_m=5.4 \times 10^3$ to 4×10^5 ; $d/D=0.007-0.14$; $\rho_w=100-2000$ kg/(m³ s); $p=0.1-21.5$ MPa; $q=0.1-1.1$ MW/m²; $x=0-1.0$.

Another formula for calculating heat transfer is given by:

$$Nu = Nu_0 \left[1 + 0.1 \left(\frac{\rho_f}{\rho_g} - 1 \right)^{0.4} (1-x) \right] \left[x + \left(\frac{\rho_f}{\rho_g} \right) (1-x) \right]^{0.8}.$$

There Nu_0 is the Nusselt number for a single-phase flow in the coiled pipes.

7.8.7.10 Heat transfer of superheated steam

The magnitude of heat transfer rate to the superheated vapor as well as to the gases is significantly lower than that to liquids. Therefore, the temperature difference

$T_w - T_f$ becomes significant, which solicits the need to consider the heat transfer coefficients applicable to a wide spectrum of the physical properties of the flow section.

The calculation of the average heat transfer rate (for $l/d \geq 50$) in the vapor flow away from the critical region can be carried out according to the formulae, which take into account the variation of the physical properties of simplices ρ_w/ρ_f or

$$\bar{T}_v/T_w;$$

For $q \leq 0.5$ MW/m² (Eq. 7.168, Miropolskii, 1975; Eq. 7.169, Lel'chuk and Elfimov, 1968)

$$\overline{Nu} = 0.028 \overline{Re}^{0.8} \overline{Pr}^{0.4} (\rho_w/\rho_v)^{1.15}; \quad (7.168)$$

$$\overline{Nu} = 0.023 \overline{Re}^{0.8} \overline{Pr}^{0.4} (\overline{T}_v / \overline{T}_w)^{0.5} \pm 10\%, \quad (7.169)$$

where all the properties are selected on the average temperature basis of the

$$\overline{Re} = \frac{(\rho w) x d}{\mu}, \quad \overline{Pr} = \frac{\mu c_p}{\lambda}$$

superheated vapor. These equations are applicable for $\rho w = 300\text{--}1000 \text{ kg/(m}^2 \text{ s)}$; $p = 4\text{--}20 \text{ MPa}$. For $q > 0.5 \text{ MW/m}^2$, the heat transfer to the vapor is obtained based on the arithmetic mean of the results from the last two Eqs. (7.168), (7.169).

The local heat transfer coefficients for pipes can be found in Petukhov and Kurganov (1974) and Petukhov (1987):

$$\frac{Nu}{Nu_0} = \exp \left\{ -K \left[0.013 f(l/d) + 1.188 \frac{1.25 \times 10^{-4} (l/d)^{2/3}}{1 + 10^{-4} (l/d)^2} \right] \right\}, \quad (7.170)$$

Here x is the distance from the entrance of test section;

$$K = \frac{qd}{\lambda_f \overline{T} Nu_0} = \frac{T_w - \overline{T}_f}{\overline{T}_f}$$

is the coefficient characterizing the temperature variation in the flow when the heat flux is changed.

$$Nu_0 = Nu_{0e} \epsilon_1, \quad \text{where } \epsilon_1 = 1 + \frac{0.48 \left[1 + 3600 / (Re \sqrt{x/d}) \right]}{(x/d)^{0.25}} e^{-0.17 x/d}, \quad (7.171)$$

$$Nu_{\infty} = \frac{(\xi/8) Re Pr}{1 + 900/Re + 12.7 \sqrt{\xi/8} (Pr^{2/3} - 1)}; \quad \text{and} \quad (7.172)$$

$$\xi = [1.82 \ln(Re/8)]^{-2}. \quad (7.173)$$

For $Pr=0.65-1$ good results are obtained by a simple formula:

$$Nu_{\infty} = 0.0225 Re_f^{0.8} Pr_f^{0.6} \pm 2\% \quad (7.174)$$

Eq. (7.170) can be rewritten as:

$$\frac{T_w}{T_f} = 1 + K \exp \left\{ K \left[0.013 f(\nu/d) + 1.18 K \frac{1.25 \times 10^{-4} (\nu/d)^2}{1 + 10^{-4} (\nu/d)^2} \right] \right\} \quad (7.175)$$

which allows you to immediately calculate the local wall temperature for q , d , G , T_f .

Eq. (7.175) can be simplified for $x/d > 50$, in which $f(x/d) = 1$:

$$\frac{T_w}{T_f} = 1 + K \exp \{ K [0.013 + 1.4 K] \} \quad (7.176)$$

7.9 Boiling at surface deposition

7.9.1 Key processes and mechanisms

The deposits on the surfaces of the fuel elements and the steam generators are due to impurities, which enter the water mainly

- (1) with suction of cooling water in the condensers;
- (2) with compensate water to recover the losses due to leakages of water and steam and due to blowdown of the steam generator;
- (3) with impurities introduced into the water loop for adjusting changes in the water level;

(4) as the corrosion products of equipment components;

(5) in the form of fission products and particles of nuclear fuel (with infringement of hermetic fuel cladding tightness).

The deposits formed on the steam-generator tube surfaces are called scales. They differ in chemical-phase composition and structure. In the energy sector, the following types of scale (as the dominant component) are representative: (1) calcium and magnesium; (2) iron oxide; (3) iron phosphate; (4) ferromagnetic and aluminosilicate; and (5) copper.

There are two mechanisms of deposits formation on the surface during boiling: first—connected with the processes of crystallization of impurities that fall from a supersaturated solution of water; and second—sticking to the surfaces of the colloid or particulate solids (or sludge cruds). A result of the first mechanism is the formation of a dense layer of the solid phase and little porous surface. The second provides a formation of sufficiently loose sticky layer between itself and the particles surface. These particles may come off into the fluid flow and fall back again onto the surfaces, depending on the hydraulic and temperature conditions in a different part of the circuit. In nuclear power plant (NPP) systems, formation, entrainment, and migration of the particles which are sparingly soluble corrosion products, along the coolant circulation systems determine to a large extent the radiation dose distribution at the NPP (e.g., Voronov et al., 2006; British Nuclear Energy Society, 2000).

Deposits of corrosion products in nuclear power circuits are in many cases poorly soluble even in concentrated acids and alkalis. One reason for this is the deep hydration precipitation at high temperatures and pressures. Another reason is the presence in the sediments of the metal silicates. Silicic acid enters the coolant circuit from the feed water or structural materials (for steels 1H18N10 type, Si content may be up to 1%).

During the circuit loop operation, usually 20%–80% of the metal is corroded in the circulating water. The intensity of the deposits and their physico-chemical properties are dependent on the concentration of impurities (e.g., iron oxide) and dispersion spectrum of particle sizes. Most of the particles (65%–80%) have a size of 0.9–1.3 μm . The precipitation of iron oxides cannot be described simply by a single system, since there exist the processes of different nature at the same time. For example, the results of industrial research show that the formation time of iron oxides in the boiler tubes is subject to:

$$M = A \exp \left(-\frac{B}{T} \right) \tau^C, \quad (7.177)$$

where M is in g/m^2 ; T is in K; τ is in hours. The constants A , B , and C in this formula depend on the steel grade and the water pH (Table 7.12).

Table 7.12

Constants A , B , and C in Eq. (7.177)

--

In modern power plants, which are constructed with different grades of steel, strict water quality control is required. There the basic substances dissolved in water are primarily iron compounds in the form of magnetite (Fe_3O_4) and hematite (Fe_2O_3). Since the solubility of magnetite in water is higher than in vapor, the magnetite aerosol formation will be prompted out of its solution in the vapor environment. Individual particles (aerosols) of magnetite are in a shape of sphere with a diameter of $0.1\text{--}0.5\ \mu\text{m}$, which are easily stick together, forming deposits on the porous surface.

The deposits form two layers (Fig. 7.61) on the surface. The inner layer has a dense structure. It is formed by oxidation of the steel surface and its thickness varies parabolically with time. The outer, thicker layer, has a loose structure and is formed due to deposits at boiling of flowing water. Some characteristics of the layers are shown in Table 7.13.

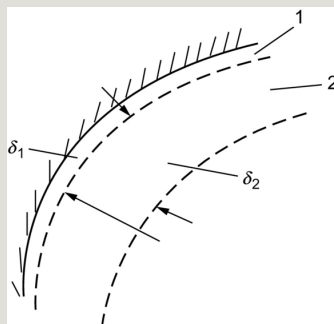


Fig. 7.61 Two layers of the deposits on the surface (internal— δ_1 and external— δ_2).

Table 7.13

Characteristics of Layers 1 and 2

--	--

Hereafter we focus on the influences of this surface deposition onto the heat transfer.

A characteristic feature of typical layer of deposited materials is the presence of large porous openings (“steam trunks” about $5\ \mu\text{m}$), the density of such holes reaches 5000 pores/ mm^2 . This structure provides a so-called “wicks boiling” (see Fig. 7.62).

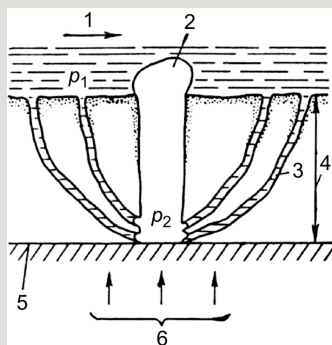


Fig. 7.62 Model Macbeth—flow circulation in the deposits with high rate of evaporation of the readily soluble compounds in vapor sediments: 1—the flow of water under pressure p_1 ; 2—exit of steam “steam trunks or steam pipe” with pressure p_2 as a result of consistent formation and the separation of the vapor bubbles; 3—capillary channels (wicks), sucking liquid to the bottom of the “steam pipe”; 4—the thickness of the sludge sediments; 5—the surface of the metal; 6—heat flux direction.

The dissolved substances in water (compounds of Cr, Ni, Mn, Zr, Cu, Al, and others) form thick solid structures which are stronger magnetite but can be peeled off from the surface at the cyclic temperature changes. The porosity of the magnetite scale is ~65%–70%, and “steam channels” occupy ~10%. When pores are filled with other compounds the process of matchlock boiling abates. It is noted that a majority of the heat transfer in this case is carried out by the thermal conduction through the layer, which causes an increase in the heated surface temperature (while maintaining the values of heat flux).

7.9.2 Composition and thermal conductivity of the sediments

The water may be present ferrous iron compound constituting FeO , compounds containing di- and trivalent iron forming Fe_3O_4 , ferric compounds, turning into Fe_2O_3 . The main parameters that determine the shape of the iron oxides are pH value of pH, temperature and redox potential of the system.

At a temperature $\leq 400^\circ\text{C}$, thermodynamically stable oxide is magnesia. Under the condition of the high oxidation potential (high oxygen concentration) and higher temperature, the stable oxides may be hematite or its hydrated forms.

Theoretical density of the magnetite Fe_3O_4 is 5180 g/cm^3 , and the density of the outer (loose) layer is $1.25\text{--}4.1 \text{ g/cm}^3$, which corresponds to the porosity of 75%–20%.

The thermal conductivity of porous sediments can be approximated by the following:

– at the location perpendicular to the direction of the heat flux

$$\frac{1}{\lambda} = \frac{1-\varphi}{\lambda_1} + \frac{\varphi}{\lambda_2}, \text{ where } \lambda_1, \lambda_2 \text{ are thermal conductivity of the sediments in the pores and } \varphi \text{ is the porosity.}$$

– at the location parallel to the direction of the heat flux (usual direction)

$$\lambda = \frac{\lambda_1 \nu [1 - \phi(1 - \nu)]}{\nu A + (1 - A)[1 - \phi(1 - \nu)][\nu + \phi(1 - \nu)]} \quad (7.178)$$

where $\nu = \lambda_1 / \lambda_2$, A is the empirical coefficient and is 0.94.

A more sophisticated method is described in Chudnovskaya et al., 1978, where the thermal conductivity of the compounds of hematite (Fe_2O_3) and magnetite (Fe_3O_4) is given by:

$$\lambda = 13.215 - 0.375 \times 10^{-1} T + 0.379 \times 10^{-4} T^2 \text{ for } \text{Fe}_2\text{O}_3 \quad (7.179)$$

$$\lambda = 4.133 - 0.852 \times 10^{-2} T + 0.757 \times 10^{-5} T^2 \text{ for } \text{Fe}_3\text{O}_4 \quad (7.180)$$

where λ in $\text{W}/(\text{m K})$, and T in $^\circ\text{C}$.

7.9.3 Effects of deposits on the flow resistance and heat transfer coefficient

The sediments on the surface of the flow circuit leads to: (1) reduction in the cross-sectional flow area of the channels, which becomes particularly noticeable for channels of a small hydraulic diameter; (2) increase in the surface roughness. Both effects are not difficult to be taken into account in the calculation of hydraulic

resistance, if the thickness of the deposits and the roughness are known although it is difficult to predict in advance such parameters due to the large number of factors that associate with them. Therefore, it is usual to rely on special experiments, empiricism, or industrial experience.

If the heat flux (q) and the heat transfer coefficient for a “clean” environment α_0 are specified, we can calculate the temperature of the outer surface of the heat-wall:

$$T_w = \bar{T}_f + q/\alpha_0,$$

where J_k^* is the average temperature of the bulk coolant.

For the surface conditions with deposits, we have similar relationship:

$T_w = \bar{T}_f + qR$, where $R = \frac{1}{K} = \frac{1}{\alpha} + \frac{\delta}{\lambda}$ is the total thermal resistance at the surface, consisting of two parts (heat transfer resistance $1/\alpha$ and thermal resistance of sediments δ/λ). There δ and λ are the thickness and thermal conductivity of scale, respectively; α is the coefficient of heat transfer from the surface of the scale to the flowing liquid.

If we keep in mind the roughness of the surface sediments and the ability to “wick boiling” layer (see above), we should assume $\alpha > \alpha_0$. Take into account $\alpha = \alpha_0$, then we obtain higher values of T_w , which can go to conservative calculations. This calculation T_w is possible, but its results should be treated with caution, i.e., it is possible to predict the value of δ on the basis of experimental data, as well as the values of λ on the basis of analysis of the composition and characteristics of the sediments. Apparently, this approach can only serve to estimates, and almost the same has to be based on an experiment or industrial experience.

7.10 Unstable boiling modes

7.10.1 Types of instabilities

1. *Unstable pool boiling* occurs in the process of surface cooling in a large volume of fluid, which may be followed by a transition from the liquid-phase convection to

the nucleate boiling regime and again to the convection. The nucleate boiling can be replaced by the film boiling and return to the nucleate boiling regime. All of these transitions at a constant heat flux lead to unstable regimes—temperature fluctuations/oscillations at the cooled surface, which adversely affect the structural integrity.

2. *Instability of boiling in a single channel* has a different (thermohydraulic or thermal fluid dynamic) nature. If boiling occurs in a separate part of the channel, its pressure drop is changed. As a result it may cause a change of flow rate. Under the certain circumstances fluctuations in flow rate and pressure can be the periodic (pulsating mode).

To avoid the unstable regimes under operation of the steam generating channel, its hydraulic characteristic should be known. The latter reflects the dependence of the total pressure drop in the channel on a flow rate (or a mass flux) at the steady-state

regime: $\Delta p = f(G) = f(\rho w)$

For stable operation of the channel, it is necessary that this characteristic was unambiguous (Fig. 7.63). The characteristics, which shows the same value of pressure drop associated with the different flow rate in a certain range of Δp , is considered as *unstable* (Habensky and Gerliga, 1994). Furthermore, it is necessary to know the enthalpy distribution along a channel length. The pulsations of the flow rate occur when the ratio $\Delta h_{ec}/\Delta h$ is below the certain value (here Δh_{ec} is the enthalpy growth within the economizer section; Δh is the total increase in enthalpy.)

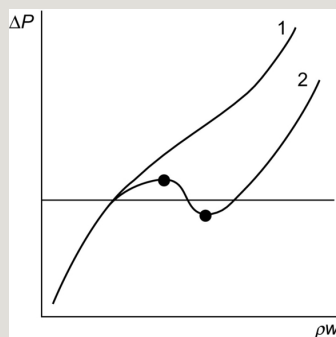


Fig. 7.63 Typical hydraulic characteristics. 1—single-valued, stable; 2—multiple-valued, unstable: •—points of extremum.

3. *Boiling instabilities in parallel channels.* In the case of flow boiling in the

separate-parallel tubes each of which has different pressure drop characteristics and is under different heating conditions. Assume these parallel flow channels are connected at an inlet plenum and at an outlet plenum, i.e., share the inlet and outlet in common. In this parallel channel system, the flow and temperature re-distributions take place showing a different enthalpy increase in different channels. It is characterized by the ratio of the enthalpy increase in i th single tube (Δh_i) to the

mean value of enthalpy for the whole tube bundle ($\Delta \bar{h}$), i.e.,

$$K_i = \Delta h_i / \Delta \bar{h}$$

and a hydraulic nonuniformity factor

$\eta_i = \zeta_i / \zeta_B$ a ratio of the hydraulic resistance (drag) coefficient of the i th

$$\zeta_i = \frac{\Delta p_i \cdot 2\rho_i}{(\rho_i w_i)^2}$$

channel to that of the whole bundle

$$\zeta_B = \frac{\Delta \bar{p} \cdot 2\bar{\rho}}{(\bar{\rho} \bar{w})^2}$$

; ρ_i is the coolant density in a tube; $\bar{\rho}$ is the mean density in the bundle. Large values of these ratios in a bundle of parallel tubes result in unstable modes.

7.10.2 Unstable pool boiling

At the low reduced pressures $p/p_{cr} < 2 \times 10^{-3}$ and the good wettability of surface cavities (centers of vapor generation) there is the significant liquid superheating as regard to the saturation temperature. At low pressures, the critical radius of the vapor nucleus reaches the high values ($R_{cr} \sim 1/\rho_g$), boiling is appeared to be complicated, and the natural convection is delayed. This phenomenon is also due to the decrease in the number of vapor generation centers (Avsentuk and Kutateladze, 1977). In some cases, a transition from the natural convection to the film boiling is possible bypassing nucleate boiling (Fig. 7.64).

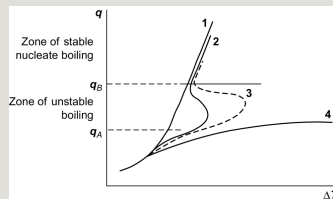


Fig. 7.64 Boiling curves at different pressures ($p_1 > p_2 > p_3$). 1—High pressures; 2, 3—low pressures; 4—transition from natural convection to the film boiling.

The S-shaped form of the boiling curve, when the q is the independent variable (for example, electric heating), determines the number of vapor generation centers per the area unit (N/A) and the surface superheating relative to the saturation temperature (ΔT), with all other factors being equal:

$$q \sim (N/A)^n (\Delta T)^m.$$

The values of (N/A) and (ΔT) are related to each other. So the increase in ($q > q_A$) also causes an increase of (N/A), which causes the ΔT decrease (curves 2, 3 in Fig. 7.64). Usually $n \sim 0.5-0.7$ and $m \sim 3$.

The mechanism of the film boiling bypassing the nucleate boiling has cavitation character—i.e., an explosive emergence of vapor bubbles is observed on the surface and the formation of a vapor film (curve 4).

7.10.3 Instability of channel boiling

In a single channel the boiling instability is primarily associated with the hydrodynamic instability, especially in circuits with natural circulation. Despite to the constant power applied to the channel, the oscillations of flow rate can be observed after onset of boiling. There are the following explanations of the reasons for this phenomenon. Let us suppose that as a result of some disturbance, the flow rate through the channel will increase slightly. This causes at all factors to be equal the decrease of vapor generation, which will reduce the value of lifting force and as well as the flow rate. However, the flow rate decrease will cause an increase in quality and lifting forces, therefore it should be resulted in further increase of flow rate. The sequence of each process will take place with some delay and causes the flow rate pulsation. If the ratio of two successive amplitudes $D=A_1/A_2 < 1$, then damping of oscillations is occurred, at $D > 1$ pulsation gain will be observed.

All these processes have to a large extent by nonlinear relationships. Since the hydraulic resistance is a nonlinear function of water and vapor velocities, and, moreover, the nonlinear function of void fraction, which, in its turn, depends on the applied power and flow rate.

The hydrodynamic characteristic of a single steam generating pipe with the certain diameter and length is described by function $\Delta p = f(\rho w)$. Here Δp is the full

hydraulic resistance of channel, which consists of two components: Δp_1 is the resistance of the economizer section; Δp_2 is the resistance of the evaporator section and $\Delta p = \Delta p_1 + \Delta p_2$.

$$\Delta p_1 = \zeta \frac{l_1 (\rho w)^2}{d \cdot 2 \rho_f}; \quad \Delta p_2 = \zeta \frac{l - l_1 (\rho w)^2}{d \cdot 2 \rho_f} \left[1 + \bar{\chi} (\rho_f / \rho_s - 1) \right] \bar{\psi}. \quad (7.181)$$

The thermal balance equation for the economizer and the evaporation sections is as follows:

$$\pi d l_1 \bar{q} = \frac{\pi d^2}{4} \rho w (h_{f, \text{sat}} - h_{in});$$

$$\pi d (l - l_1) \bar{q} = \frac{\pi d^2}{4} \rho w (h_{out} - h_{f, \text{sat}});$$

$$\begin{aligned} & \text{from where } l_1 = \frac{\Delta h \cdot d \rho w}{4 \bar{q}}, \quad \Delta h_{in} = h_{f, \text{sat}} - h_{in}, \\ & x_{out} = \frac{4 \bar{q} l}{\Delta h_{fg} d \rho w} - \frac{\Delta h_{in}}{\Delta h_{fg}}, \quad \bar{x} = \frac{x_{out}}{2}. \end{aligned}$$

After substitution of all of these relations in Eq. (7.181) by setting $\bar{\psi} = 1$ we have:

$$\Delta p = A(\rho w)^3 + B(\rho w)^2 + C(\rho w). \quad (7.182)$$

$$A = \frac{\xi \Delta h_{in}^2}{16 \Delta h_{fg} \rho_f \bar{q}} \left(\frac{\rho_f}{\rho_g} - 1 \right)$$

Here

$$B = \frac{\xi l}{2 \rho_f d} \left[1 - \frac{\Delta h_{in}^2}{\Delta h_{fg}} \left(\frac{\rho_f}{\rho_g} - 1 \right) \right];$$

$$C = \frac{\xi l^2 \bar{q}}{\rho' d^2 \Delta h_{fg}} \left(\frac{\rho_f}{\rho_g} - 1 \right)$$

In general, the solution of this equation provides one or three real root. The extremums of the curve in Fig. 7.64 are determined by differentiation of Eq. (7.182):

$$\frac{d(\Delta p)}{d(\rho w)} = 3A(\rho w)^2 + 2B(\rho w) + C = 0, \quad (7.183)$$

$$(\rho w)_{in} = \frac{-B \pm \sqrt{B^2 - 3AC}}{3A}$$

Eq. (7.183) yields . If Eq. (7.183) has no real roots, then it means that the hydrodynamic characteristic is

stable. The stability condition $B^2 - 3AC < 0$ leads us to an approximate relationship:

$$\Delta h_{in} \leq \frac{7.46 \Delta h_{fg}}{\left(\rho_f / \rho_g \right) - 1}. \quad (7.184)$$

Eq. (7.184) suggests that the region of Δh_{in} for stability increases as pressure increases, because the denominator decreases faster than the numerator. Therefore,

with decrease in pressure, a probability of unstable regimes is increasing.

7.11 Augmentation of heat transfer of surface with boiling water

7.11.1 Method of augmentation

The nuclear technology is in a constant search for new methods of heat transfer enhancement applied to the water-cooled reactors. Along with traditional methods, newly developed methods suggesting improved fluid mixing in the channel may seem yet exotic. Some of them provide possibilities in principle to increase the critical heat flux by twice or more, which will increase the specific power of the reactor, or to provide a large margin to thermal limits of the heat transfer crisis than at present, that is, to increase the reliability of the safety system installation (Perepelitsa and Sapankevich, 1976; Kalinin et al., 1986).

In general, heat transfer coefficient during the boiling is of sufficiently high value on the order of 10^4 – 10^5 W/(m² K), and there seems no sense to take care of its further increase. However, in the case of transition from nucleate boiling to film boiling mode (boiling crisis, critical heat flux—CHF) heat transfer coefficient can be reduced by one to two orders of magnitude. To prevent burnout while keeping the constant heat flux, it is necessary to apply the device and methods of heat transfer augmentation. In this regard, promising improvements may be achieved by using the means that provide the ability to increase either permissible reactor power or margins prior to the heat transfer crisis.

Classification of heat transfer enhancement methods is rather conditional. Methods vary according to the principles of physical phenomena that determine the augmentation of the process (Thome, 1990; Holpanov and Shkadov, 1990; Kaviany, 1999):

1. Provide better flow mixing by installation of special geometry devices such as twisted tube, twisted ribs on the surface of the fuel rods, fuel rod spacer grids, etc.;
2. Change surface conditions (roughness, porous coatings, and others);
3. Improve surface wettability;
4. Use additives to the water in very low concentrations (nanofluids), which do not change the properties of water, but the impact on the transport processes in the boundary layer.

7.11.2 Augmentation of heat transfer by agitation of the swirl flow

Additional two-phase flow turbulence can be generated by means of transverse or helical corrugations, ribs, inserts of various kinds of braided tapes, screws, etc. or by knurling the pipes (see Fig. 7.65; Dzubenko et al., 1988). Also see Zysin and Dorfman (1986) and Kalinin et al. (1990).

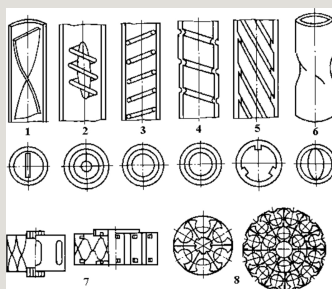


Fig. 7.65 Types of heat exchange enhancers (turbulators and swirl elements): 1—twisted ribbons; 2—swirl insert (propellers, screws); 3—helical wire; 4—corrugations (ridge) on the surface; 5—the internal edges; 6—elliptic coiled tubing; 7, 8—lattice spacer with swirlers.

In the bubbly flow regime of low qualities, such devices as baffles do not give any advantages. In the dispersed-annular flow regime, especially at high mass flux, CHF will be increased by enhancing the turbulence intensity. In case of a wrong choice of design parameter value, e.g., resulting in a narrower flow area, however, leading to an increase in velocity at the heated wall, the installation of vortex generators may reduce the critical power limit and steam quality due to the liquid film thinning effect.

In the rotating flow field by centrifugal force, the distribution of liquid droplets will be shifted toward the outer wall, which means higher concentration of the liquid-phase around it and increases the critical heat flux. It is noted that the increase in CHF depends on the fluid motion, i.e., mainly on the magnitude of the centrifugal acceleration (w^2/R), and not by subcooling. As a first approximation,

$$\alpha \sim (w^2/R)^{0.25-0.3}$$

The more intensive is the twisted flow (i.e., with the smaller pitch arrangement of the swirl element) and at the lower steam quality in the dispersed-annular flow regime, the more stable becomes the liquid film surface. The twisted flow is realized by installing the swirl elements (belt,

propeller insert, helical wire, helical ribs, twisted elliptic pipe, etc.). These elements would generate much the same twisted flow field, yielding the same order of increase in the heat transfer coefficient as a first approximation.

Heat transfer augmentation in the film flow regime in the channels has been discussed by many authors (Kalinin et al., 1990; Kamenchshikov et al., 1984; Shchukin and Halatov, 1982; Shchukin, 1980; Mitrophanova, 2002; Webb, 1993). In brief, it can be carried out in four ways: (1) agitation of wall vapor layer; (2) forced wall irrigation (water supply to the liquid film on the wall); (3) providing good wettability of the wall at high temperature differences (transition to nucleate boiling); and (4) decreasing thermal nonequilibrium stream by dispersing liquid phase.

With a help of ring orifices or knurling on the surface, the forced irrigation fluid film on the wall will be effective in reducing the flow thermal nonequilibrium. Then the heat flux from the wall is divided into two, one to the vapor-phase (q_g) and the other to the droplets depositing onto the wall (q_l):

$$q = q_g(1 - \omega) + q_l\omega = \alpha_g(T_w - T_g)(1 - \omega) + \alpha_l(T_w - T_g)\omega, \quad (7.185)$$

where ω is the proportion of the wall surface droplets irrigated; α_g and α_l are the heat transfer coefficients for the vapor-phase and the liquid droplets, and; T_g is the average temperature of the superheated vapor.

If $\alpha_l > \alpha_g$ (the heat flux), the liquid layer becomes significant that $T_w \rightarrow T_g$ and there would be the nucleate boiling but no superheating of the vapor-phase.

Heat transfer augmentation in the boiling tubes could be achieved by periodically arranged projection-type (protrusions) turbulence promoter such as carving spirals, however at a cost of increase in the flow resistance. Fig. 7.66 shows, for example, a scheme with annular projections in a tube.

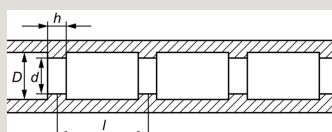


Fig. 7.66 Geometry of the tube with annular projections.

$$\alpha = F(d/D, l/D, h, \alpha_0, \alpha_1, \alpha_2), \quad (7.186)$$

where α_0 is the heat transfer coefficient at the boiling surface of a smooth pipe diameter D ; α_1 , α_2 are the heat transfer coefficients of the pure convection and the pool boiling in a large volume. α_0 can be calculated by the following equation (D.A. Labuntsova):

$$\frac{\alpha_0}{\alpha_1} = \frac{4\alpha_1 + \alpha_2}{5\alpha_1 - \alpha_2}. \quad (7.187)$$

The following equations suggested by Kalinin et al. (1990) are recommended to find α_1 and α_2 :

$$Nu_1 = 0.023 Re_f^{0.8} Pr_f^{0.4} \left(\frac{Pr_f}{Pr_w} \right)^{0.06}, \quad (7.188)$$

$$T_f = \frac{T_{in} + T_{out}}{2}$$

Here, the fluid temperature T_f is defined by

$$Nu_2 = 0.125 Re_*^{0.65} Pr^{0.33}, \quad (7.189)$$

where $Nu_2 = \alpha_2 l / \lambda$; $Re_* = ql / \Delta h_{fg} \rho_g \nu$;

$$l = c_p \rho_f \sigma T_s / \left(\Delta h_{fg} \rho_g \right)^2$$

at temperature T_s . ν , λ , c_p , and Pr are all evaluated

Eq. (7.187) is proposed when $0.5 \leq a_2/a_1 \leq 2$. If $a_2/a_1 < 0.5$ the convection heat transfer is determined by $a_0=a_1$. When $a_2/a_1 > 2$, heat transfer is determined by the boiling and $a_0=a_2$.

Shown in Fig. 7.66 are the annular projections (orifice) that increase the heat transfer coefficient by 30%–40%, while the stronger, the smaller the ratio d/D , l/D (a_2/a_1), i.e., the greater the contribution to the overall forced convection heat transfer:

$$\frac{\alpha}{\alpha_0} = 1 + 1.35 \left(1 - 0.371 \frac{l}{D} \right) \left(1 - \frac{d}{D} \right)^{0.418} \left(1 - 0.104 \frac{a_2}{a_1} \right) \quad (7.190)$$

Eq. (7.190) is valid for $(l/D)=0.25$ – 0.6 ; $(d/D)=0.88$ – 0.94 ; $a_2/a_1=0.5$ – 2.4 ; $Re=(2$ – $6) \times 10^4$; $q=(1.8$ – $8) \times 10^4$ W/m².

7.11.3 Special surface: Porous structures

With specially selected distribution of cavity sizes on the surface, you can change the boiling curve (i.e., the heat exchanges), as shown earlier. Special surface treatment technology has been developed, some forms of which are seen in Fig. 7.67. Porous coatings typically have an irregular structure and porosity.

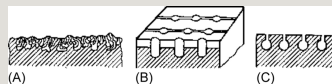


Fig. 7.67 Special (structured) heat transfer surface: (A) high flux; (B) thermoexcel; (C) Gewa.

The surface heat transfer by the boiling water is determined by interactions between the vapor flow formed by evaporation and the fluid flow that flows toward the surface. Displacement of the liquid by the vapor determines the first limiting condition—the hydrodynamic limit.

When the liquid flows toward the surface, second hydrodynamic limit occurs that is defined by the hydraulic resistance of viscous flow in a porous media structure.

Influence of coatings on the heat transfer coefficient is explained by a combination of different factors, i.e., the movements in the capillary-porous structures, increase in the number of vaporization centers, improvement in evacuation of the conglomerates of vapor through the pores of the porous layer (Thome, 1990; Soloviev, 1998). All of these effects depend on the thermophysical properties of the fluid and the surface geometry and structure of the coatings (film thickness, pore size distribution, etc.).

In general, the liquid evaporation mechanism limits the heat flux and the limitation depends on: (1) the conditions of liquid supply to the surface, (2) the removals of the vapor from the surface, and thus depends on the vapor-liquid interaction and hydraulic resistances in the case of the countercurrent flows.

When the thick porous coatings have additional hydraulic resistance to the fluid flows, the vapor-phase may reduce the possibility of heat transfer enhancement and may even lead to the opposite effect. Thin porous coatings show a possibility of enhancement by supplying liquid to the surface by capillary forces, reducing interactions between the vapor and liquid streams. The porous coating that is specially created to supply liquid arteries is even more effective. For example, specially designed porous coating of variable thickness accommodates capillary structures with the arteries, such as heat pipes, thus increasing the heat transfer rate at boiling in a large pool by three times or more as compared with a flat surface.

7.11.4 The effect of improving the wettability of the surface (superhydrophilicity)

There are proposals to use the effect of superhydrophilicity to enhance the heat exchange at boiling and condensation. Superhydrophilicity promotes the liquid spreading over the heated surface even at high temperatures. Photocatalysis is a method to decompose various organic substances by means of powerful ultraviolet (UV) irradiation. Titanium dioxide (TiO_2) is one of the substances having photocatalytic ability and unique characteristics. Another characteristics associated with titanium dioxide, published recently is superhydrophilicity. It was found that: (1) critical heat flux at the surface of the heated metal sample coated by TiO_2 is two times higher than that at the uncoated surfaces; (2) Onset temperature of wetting (Leidenfrost temperature) increases with a decrease in the contact angle.

Creation of very thin continuous stable falling films at extremely low costs has become possible, which previously could not be done with conventional surfaces. Measurement of the rate of cooling of the heated metal sample in boiling water showed that the sample coated with TiO₂ was cooled much faster than the uncoated sample, as the first film boiling regime was destroyed and followed by a transition to nucleate boiling heat transfer with a significantly higher heat transfer rate.

The influence of the wettability onto the minimum heat flux point was observed and reported by many investigators. Leidenfrost temperature increases with a decrease in contact angle and increases in sets with improved surface wettability.

7.11.4.1 The aqueous slurry: Augmentation using additives to water

Suspensions of dispersed particles of sizes 10–100 nm in water or other liquids are referred to as nanofluids. Studies of boiling water with small additions of ($\leq 0.001\%$) nanoparticles showed that the rate of heat transfer and critical heat flux (CHF) could be increased by two times. Although these experiments are not directly related to nuclear reactor applications, a possibility of this kind of heat transfer augmentation cannot be excluded (Table 7.14).

Table 7.14

Typical thermal hydraulics characteristics of PWRs and the fuel assembly

--

It is estimated that the use of this approach to the Westinghouse-type conventional fuel assembly (17×17) may allow the reactor core outlet temperature increase by 7°C (20%), and in combination with increasing mass flow by 18%, the power could be increased for~40% (1.18×1.2–1.4).

While the nanofluid technology has not been fully mastered even in the prototype installations, there are constant research and development efforts for the new methods of heat transfer augmentation to be applied to the water-cooled nuclear reactors. Along with the traditional methods including improved fluid mixing in and between subchannels, the new developed methods may seem yet exotic.

References

- Adrianov V.N. *The Fundamentals of Radiative and Complex Heat Transfer*. Moscow: Energiya; 1972 (in Russian).
- Alexeenko S.V., Nakoriakov V.E., Pokusaev B.G. *Wave Flow of Films of Liquid*. Novosibirsk: Nauka; 1992 (in Russian).
- Andreani M., Yadigaroglu G. *Dispersed flow film boiling*. Wurenlingen, Switzerland: Paul Scherrer Institut; 1989.
- Andreani M., Yadigaroglu G. Prediction methods for dispersed flow film boiling. *Int. J. Multiphase Flow*. 1994;20:1–51.
- Avdeev, A.A., 1982. Reynolds analogy in undeveloped surface boiling on porous-coated surface, *Teploenergetika* 3, 23 (in Russian)
- Avdeev A.A. Pressure drop in subcooled boiling under forced convection conditions. *Teploenergetika*. 1985;5:49 (in Russian).
- Avduevsky V.S., Koshkin V.K., eds. *Principles of Heat Transfer in Aircraft and Rocket-Space Technology*. Moscow: Mashinostroenie; 1992 (in Russian).
- Avsentuk B.P., Kutateladze S.S. Heat transfer instability on the surfaces depleted centers of vaporization. *Teplofiz. Vys. Temp*. 1977;15(1):115–120 (in Russian).
- Bahrami M., Culham J.R., Yovanovich M.M., Schneider G.E. Review of thermal joint resistances models for nonconforming rough surfaces. *Appl. Mech. Rev*. 2006;59:1–12.
- Balakrishnan A.R. *Pool boiling of saturated pure liquids and binary mixtures: effect of surface characteristics*. In: Proc. 11th IHTC Heat Transfer, vol. 1; 1998:71–87.
- Baumeister K.J., Simon F.F. Leidenfrost temperature—its

correlation for liquid metals, cryogenes, hydrocarbons and water. *ASME J. Heat Transfer*. 1973;95:166–173.

Berman B.R. *Thermal Conduction in Solids*. New York: Oxford University Press; 1976.

Berman L.D., Gordon B.G., Bogdan S.H. Experimental relationships for prediction of heat transfer at vapour condensation on the water dispersed jet. *Teploenergetika*. 1983;4:19–22 (in Russian).

Bernardin J.D., Mudawar J. The Leidenfrost point experimental study and assessment on existing models. *ASME J. Heat Transfer*. 1999;121:894–903.

Blokh A.G. *Basic Principles of Thermal Radiation Heat Transfer*. Moscow: Gosenergoizdat; 1962 (in Russian).

Blokh A.G. In: Blokh A.G., Zhuravlev Yu.A., Ryzhkov L.N., eds. *Thermal Radiation Heat Transfer Handbook*. Moscow: Ergoatomizdat; 1991 (in Russian).

Boeschofen F. *On the possibility to improve the heat transfer of uranium and aluminum surfaces in contact*. In: Proceedings of the First International Conference on the Peaceful Uses of Atomic Energy, Geneva, vol. 9; 1955:208–209.

Borishanskii B.M. The effect of pressure on heat transfer and critical loads. *Problems of Two-Phase Heat Transfer*. Moscow: GosEnergoizdat; 1961 (in Russian).

Borishanskii B.M., Kozyrev A.P., Svetlova L.S. Researches of heat transfer in nucleate boiling. *Convective Heat Transfer in Two- and Single Phase Flows*. Moscow: Energiya; 1964 p. 71 (in Russian).

Borishanskii B.M., Andrievsky A.A., Fokin B.S. The generalized dependence for calculation of heat transfer at the two-phase flow in pipes and channels. *Advances in the Researches of Two-Phase Heat Transfer and Hydraulics in Power Elements*. Leningrad: Nauka; 1973 (in Russian).

Borishansky V.M., Kutateladze S.S., Novikov I.I., Fedynsky O.S., eds. *Liquid Metal Coolants*. third ed. Moscow: Atomizdat; 1976 (in Russian).

Breber G., Palen G.W., Taborek J. Prediction of horizontal tubeside condensation of pure components using flow regime criteria. *J. Heat Transfer Trans. ASME*. 1980;102(3):471–476.

British Nuclear Energy Society. *Water Chemistry of Nuclear Reactor Systems*, No. 8. In: Proceedings of the Conference Organized by BNES, Bournemouth, UK; 2000.

Butterworth D., Hewitt G.F., eds. *Two-Phase Flow and Heat Transfer*. Oxford: Oxford Univ. Press; 1977.

Carslaw H.S., Jaeger J.C. *Conduction of Heat in Solids*. second ed. Oxford, UK: Clarendon Press; 1959.

Cess R.D. The interaction of thermal radiation with conduction and convection heat transfer. In: Irvine J.F., Hartneet J.P., eds. New York: Academic Press Inc.; 1–51. *Advances in Heat Transfer*. 1964;vol. 1.

Chai L.H., Shoji M. Boiling curves-bifurcation and catastrophe. *Int. J. Heat Mass Transfer*. 2001;44:4175–4179.

Chaikin P.M., Lubensky T.C. *Principles of Condensed Matter Physics*. Cambridge: Cambridge University Press; 1995.

Chudnovskaya I.I., Shtern Z.Yu., Zarichnyak Yu.P., Muratov B.L. *Method and results of researches of in-tube formations*. In: Proc. of the Temperature Regime and Hydraulics in Steam Generators; Leningrad: Nauka; 1978:21–32 (in Russian).

Chudnovsky A.F. *Heat and Mass Transfer in Disperse Mediums*. Moscow: GITTL; 1954 (in Russian).

Clausing A.M., Chao B.T. Thermal contact resistance in vacuum. *J. Heat Transfer Trans. ASME*. 1965;87(2):243–250.

Collier J.G., Thome J.R. *Convective Boiling and Condensation*. third ed. in 1996 Oxford: Oxford University Press; 1980.

D'iachenko P.E., Tolkacheva N.N., Andreev G.A., Karpov T.M. *The Actual Contact Area of Mating Surfaces*. Moscow: Academy of Sciences USSR; 1963 (in Russian).

Delhaye J.M., Giot M., Riethmuller M.L. *Thermohydraulics of Two-Phase Systems for Industrial Design and Nuclear Engineering*. New York: Hemisphere Publishing Co.; 1981.

Dougherty T., Fighetti C., Reddt G. *Flow boiling in vertical down flow*. In: Proc. 9th Int. Heat Transfer Conf., Jerusalem, vol. 2; 1990:9–14.

Dul'nev G.N., Novikov V.V. *Processes of Transfer in Nonuniform Mediums*. Moscow: Energoatomizdat; 1991 (in Russian).

Dul'nev G.N., Zarichniak Yu.P. *Heat Conduction of Mixture and Composite Materials*. Moscow: Energiya; 1974 (in Russian).

Dyl'nev G.N. *Heat Transfer in Radioelectronic Devices*. Moscow: Gosenergoizdat; 1963 (in Russian).

Dyomkin N.B. *The Actual Contact Area of Solid Surfaces*. Moscow: Academy of Sciences USSR; 1962 (in Russian).

Dzubenko B.V., Dreitser G.A., Ashmantas L.A. *Transient Heat Transfer in Bundles of Twisted Tubes*. Moscow: Mashinostroenie; 1988.

Eckert E.R.G., Drake R.M. *Analysis of Heat and Mass Transfer*. first ed. New York: McGraw Hill; 1972.

Fedotovskiy V.C. *Effective thermal conductivity of heterogeneous materials*. In: Proceedings of the 1st Russian National Conference on Heat Transfer, vol. 10, no. 2; Moscow: Izdatel'stvo MEI; 1994:116–120 (in Russian).

Fenech, H., Rohsenow, W.M., 1963. Thermal conductance of metallic surfaces in contact. ASME Paper 62-HT-32. See also Transactions ASME 85C, 15–24.

Florschuetz L.W., Chao B.T. On the mechanics of vapor bubble collapse. *J. Heat Transfer*. 1965;87(2):209–220.

Fried E.A., Costello F.A. Interface thermal contact resistance problem in space vehicles. *ARS J.* 1962;32(2):237–243.

Ganic E.N., Rohsenov W.M. Dispersed flow heat transfer. *Int. J. Heat Mass Transfer.* 1977;20(8):855–866.

Gavrilov P.M. Onset of boiling in highly overheated liquid. *Teplofiz. Vys. Temp.* 1999;37(4):602–605 (in Russian).

Gertner R.F. A photographic study of bubble-wise boiling in a large volume. *Teploperedacha.* 1965;87(1):20–35 (in Russian).

Gilles J., Bourouga B., Bardon J.-P. *Estimation of the part-bath heat transfer coefficient during a quenching.* In: Proc. 12th Int. Heat Transfer Conf. Grenoble, vol. 4; 2002:767–772.

Glebov V.P., Eskin V.P., Trubachev V.M., et al. *In-line Formation in Supercritical Pressure Boilers.* Moscow: Energoatomizdat; 1983 p. 240 (in Russian).

Gogonin N.I. *Velocity dependence of heat transfer at vapor condensation inside vertical tubes.* In: Proceedings of the 4th Russian National Conference on Heat Transfer, vol. 5; Moscow: Izdatel'stvo MEI; 2006:93–96 (in Russian).

Golovnyov I.F., Zamuraev V.P., Katznel'son S.S. In: Soloukhin R.I., ed. *Radiative Heat Transfer in High Temperature Gases.* Moscow: Energoatomizdat; 1984 (in Russian).

Groeneveld, D.C., 1973. Post-dry Heat Transfer at reactor Operating Conditions. AECL-4513.

Groeneveld D.C. A review of inverted annular and low quality film boiling. In: Hewitt G.F., Delhay J.M., Zuber N., eds. *Post-Dryout Heat Transfer.* Cleveland, OH, USA: CRC Press; 1992:327–366.

Groeneveld D.C., Snoek C.W. A comprehensive examination of heat transfer correlations suitable for reactor safety analysis. *Multiph. Sci. Technol.* 1986;2(1–4):181–274.

Habensky V.B., Gerliga V.A. *Flow Instability in Elements of*

Equipment. S. Petersburg, Russia: Nauka; 1994 (in Russian).

Hackford H.L. *Infrared Radiation*. New York: McGraw-Hill; 1960.

Haddad K.H., Cheung F.B. Steady-state subcooled nucleate boiling on a downward-facing hemispherical surface. *J. Heat Transfer*. 1998;120:365–370.

Hahne E., Spindler K., Shen N. *Incipience of flow boiling in subcooled well wetting fluids*. In: Proc. 9th Int. Heat Transfer Conf., Jerusalem, vol. 2; 1990:69–74.

Handbook, 1974. Methods and Correlations for Calculation of Heat Transfer and Pressure Drop in Heat Exchange Equipment of NPP. PTM 24.031.05-72 (in Russian).

Handbook, 1983. Nuclear steam generator with tubes in the form of helical coils. NPO CKTI. PTM. 1983.108.300.01-81 (in Russian)

Handbook, 1986. Heat-Exchange Equipment of NPP. Thermal and Hydraulic Calculation. NPO CKTI. PTM. 1986.108.031.05-84 (in Russian).

Harding J.H., Martin D.G., Potter P.E. *Thermophysical and Thermochemical Properties of Fast Reactor Materials* Report EUR 12402 EN, Commission of the European Communities, Nuclear Science and Technology. Brussels: ECSC-EEC-EAEC; 1989.

Hetsroni G. *Handbook of Multiphase Systems*. New York: Hemisphere; McGraw-Hill; 1982.

Hewitt G.F., Hall Taylor N.S. *Annular Two-Phase Flow*. Oxford: Pergamon Press; 1972.

Holm R. *Electric Contacts Handbook*. Berlin: Springer-Verlag; 1967.

Holpanov L.P., Shkadov V.Ya. *Hydrodynamics and Heat and Mass Transfer With the Interface*. Moscow: Nauka; 1990 (in Russian).

IAEA TECDOC 1203. *Thermohydraulic Relationships for Advanced Water Cooled Reactors*. IAEA; 2001.

Ingersoll L.R., Zobel O.J., Ingersoll A.C. *Heat Conduction with Engineering, Geological and Other Applications*. Madison: University of Wisconsin Press; 1954.

Isachenko V.I. *Heat Transfer at Condensation*. Moscow: Energiya; 1977 (in Russian).

Isachenko V.P., Osipova V.A., Sukomel A.S. *Heat Transfer*. Moscow: Energoizdat; 1981 (in Russian).

Ivanovsky M.N., Milovanov Yu.V., Subbotin V.I. About the mechanism of dropwise condensation of metal vapours. *At. Energ.* 1966;21(1):17–21 (in Russian).

Ivanovsky M.N., Sorokin V.P., Subbotin V.I. *Evaporation and Condensation of Metals*. Moscow: Atomizdat; 1976 (in Russian).

Kaganer M.G., Zukova R.I. Determination of thermal resistance in vacuum for contacts between metallic surfaces with various extent of roughness. *Inzhenerno-Fizichesky Zhurnal*. 1966;11(3):329–337 (in Russian).

Kalinin E.K., Dreitser G.A., Yarcho S.A. *Heat Transfer and Hydrodynamics in the Channels of Complex Configuration*. Moscow: Mashinostroenie; 1986 (in Russian).

Kalinin E.K., Dreitser G.A., Yarcho S.A. *Heat Transfer Intensification in the Channels*. third ed. Moscow: Mashinostroenie; 1990.

Kamenchshikov F.T., Reshetov B.A., Ryabov A.N., et al. *Mechanical Problems of Rotating Flows and Heat Transfer Intensification in Nuclear Power*. Moscow: Energoatomizdat; 1984 (in Russian).

Kandlikar S.G. A general correlation of saturation two-phase flow boiling heat transfer inside horizontal and vertical tubes. *J. Heat Transfer*. 1990;112:219–238.

Kandlikar S.G. Development of a flow boiling map for subcooled and saturated flow boiling of different fluids inside circular tubes. *J. Heat Transfer*. 1991;113:190–200.

Kandlikar S.G. Heat transfer characteristics in partial boiling, fully development boiling and significant void flow regions of subcooled flow boiling. *J. Heat Transfer*. 1998;120:395–401.

Kaviany M. *Principles of Heat Transfer in Porous Media*. second ed. New York: Springer; 1999.

Kaviany M. *Principles of Heat Transfer*. New York: John Wiley & Sons, Inc.; 2002.

Kharitonov V.V., Kokorev L.S., Del'vin N.N. About the role accommodation coefficient at contact heat transfer. *At. Energ.* 1973;35(5):360–361 (in Russian).

Kirillov P.L., ed. *Thermophysical Properties of Materials for Nuclear Engineering: A Tutorial and Collection of Data*. Vienna: IAEA; 2008.

Kirillov P.L., Bogoslovskaya G.P. *Heat and Mass Transfer in Nuclear Power Plants*. second rev. ed. Moscow: Energoatomizdat; 2000 (in Russian).

Kitzel' V.A. *Reflection of Light*. Moscow: Nauka; 1973 (in Russian).

Klimenko, V.V., 1984. Processes of two-phase heat transfer in cryogenic liquids (pool boiling, forced flow, film pool boiling) and the development of optimal methods of their calculation. Abstract of Doctor thesis, Moscow (in Russian).

Klimenko V.V., Snytin S.Yu. *Film boiling crisis on a submerged heating surface*. In: Proc. of the 1st World Conf. Exp. Heat Transfer, Fluid Mech., Thermod. Dubrovnik, September 4–9; 1988:551–563.

Klimenko A.V., Zorin V.M., eds. *Theoretical Fundamentals of Heat Engineering, Thermotechnical Experiment*. third rev. and ad. ed. Moscow: Izdatel'stvo MEI; 2001 2nd Book (in Russian).

Kocamustafaogullari G., Ishii M. Foundation of the interfacial area transport equation and its closure relations. *J. Heat Mass Transfer*. 1995;38(3):481–993.

Kokorev B.V., Farafonov V.A. *Steam Generators of Liquid Metal Cooled Nuclear Power Plants*. Moscow: Energoatomizdat; 1990 (in Russian).

Kokorev L.C., Kharitonov V.V. *Thermohydraulic Design and Optimization of Nuclear Power Plants*. Moscow: Energoatomizdat; 1986 (in Russian).

Kondrat'ev G.M. *Regular Heat Regime*. Moscow: Gostekhizdat; 1954 (in Russian).

Kudryashev, L.I., Zhemkov, L.I., 1963. Generalization of the Theory of Regular Thermal Regime for the Case of Variable Coefficients of Heat Conductivity and Specific Heat, in Collection of Scientific Papers, Heat Power Engineering (selected articles), FTD-TT-62-1200/1 + 2 + 4.

Kutateladze S.S. *Fundamentals of Heat Transfer Theory*. fifth ed. Moscow: Atomizdat; 1979 (in Russian).

Kutateladze S.S., Nakoriakov V.E. *Heat and Mass Transfer and Waves in Gas-Liquid Flows*. Novosibirsk: Nauka; 1982 (in Russian).

Kutateladze S.S., Gogonin N.I., Dorokhov A.P., Sosunov V.I. Dropwise condensation of moving vapour at the horizontal tube bundle. *Teploenergetika*. 1979;5:12–15 (in Russian).

Labuntsov D.A. Generalized dependence to at nucleate boiling heat transfer fluids. *Teploenergetika*. 1960;5:S76–S81.

Labuntsov D.A. Issues in nucleate boiling heat transfer. *Teploenergetika*. 1972;9C:C14–C19.

Labuntzov D.A. Heat transfer at dropwise condensation of pure vapours on vertical surfaces and horizontal tubes. *Teploenergetika*. 1957;7:72–80 (in Russian).

Labuntzov D.A. Heat transfer at vapour condensation on vertical surface under conditions of turbulent flow of condensate film. *Inzhenerno-Fizichesky Zhurnal*. 1960;3(8):3–8 (in Russian).

Latyev L.N., Petrov V.A., Cekhovsky V.Ya., Shestakov E.N. In: Sheindlin A.A., ed. *Radiative Properties of Solid Materials*. Moscow: Energiya; 1974 (in Russian).

Lel'chuk B.L., Elfimov G.I. Convective heat transfer in turbulent flow in tubes. *Convective Heat Transfer in Single-Phase Flow. Generalized Data to Regulatory Calculation*. Leningrad: CKTI; 1968 Issue 82, pp. 35–47 (in Russian).

Lykov A.V. *Phenomena of Transfer in Capillary-Porous Bodies*. Moscow: Gostekhizdat; 1954 (in Russian).

Lykov A.V. *The Theoretical Principles of Building Thermophysics*. Minsk: Izdatel'stvo Academy of Sciences BSSR; 1961 (in Russian).

Lykov A.V. *Theory of Heat Conduction*. Moscow: Vysshaya Shkola; 1967 (in Russian).

Lykov A.V. *Heat and Mass Transfer/Handbook*. second rev. and ad. ed. Moscow: Energiya; 1978 (in Russian).

Man'kina N.N. *Physical and Chemical Processes in the Steam-Cycle of Power Plants*. Moscow: Energiya; 1977 (in Russian).

Mandhane J.M., Gregary G.A., Aziz K. A flow pattern map for gas-liquid flow in horizontal pipes. *Int. J. Multiphase Flow*. 1974;1:537–553 (Cit. By “Two-Phase Flow and Heat Transfer”, Butterworth, D., Hewitt, G.F. (Eds.), 1977).

Mayinger F., Langer R. *PDO heat transfer*. In: Proc. 6th Int. Heat Transfer Conf., Toronto, vol. 6; 1978:181.

McWald T.H., Marschall E.A. Comparison of elastic and plastic contact models for the prediction of thermal contact conductance. *Wärme- und Stoffübertragung*. 1993;28:441–448.

Meredith R.E., Tobias C.W. Conductivity of emulsions. *J. Electrochem. Soc.* 1961;103:286–290.

Miller B.S. The features of contact heat transfer in heat-generating units of reactors. *Izvestiya Vuzov. Energetika.* 1962;24:133–139 (in Russian).

Minchenko F.P. On the issue of heat transfer in nucleate boiling. *Power Mach. Build.* 1960;6:S17–S21.

Miropol'sky Z.L. Heat transfer at condensation of high pressure vapour inside tubes. *Teploenergetika.* 1962;3:79–82 (in Russian).

Miropolskii Z.L. Heat transfer to the superheated steam with heat supply and dissipation. *Teploenergetika.* 1975;3:75–78 (in Russian).

Mitrophanova O.V. *Methods of Mathematical Modeling of Fluid Flow and Heat Transfer of Swirling Flows in the Channels With Promotions.* Diss. Doctor. Tehn. Sciences Moscow: MEPHI; 2002 (in Russian).

Moon H.C., et al. Effect of heat exchanger tube parameters on nucleate pool boiling. *J. Heat Transfer.* 1998;120(5):468–476.

Novikov I.I. Conditions for the similarity of heat transfer processes with variable fluid properties. *Problems of Two-Phase Heat Transfer.* GosEnergoizdat: Moscow; 1961 pp. S7–S14 (in Russian).

Nukiyama S. Maximum and minimum values of heat q transmitted from metal to boiling water under atmospheric pressure. *J. Soc. Mech. Eng. Jpn.* 1934;37(53–54):367–374.

Odelevsky V.I. Calculation of generalized conductivity of heterogeneous systems. *Zhurnal Tekhnicheskoy Fiziki.* 1951;21(6):667–685 (in Russian).

Özisik, 1973 Özisik M.N. *Radiative Transfer and Interactions with Conduction and Convection.* New York: John Wiley & Sons; 1973.

Parlatan Y., Rohatgi U.S. Simple model of boiling heat transfer on tubes in large pools. *J. Heat Transfer*. 1997;119:376–379.

Perepelitsa N.I., Sapankevich A.P. *Ways to Improve Parameters at Heat Transfer Crisis. Analytical Review*. Obninsk: IPPE; 1976 AR-31 (in Russian).

Petukhov B.S. *Problems of Heat Transfer*. Moscow: Nauka; 1987 pp. 68–86.

Petukhov B.S., Kurganov V.A. Analysis and generalization of experimental data on heat transfer in tubes at turbulent gas flow with variable physical properties. *Teplofiz. Vys. Temp.* 1974;12(2):304 (in Russian).

Petukhov B.S., Shilov V.K., eds. Moscow: Energoatomizdat; 383. *Handbook on Heat Exchangers*. 1987;vol. 1 (in Russian).

Pioro J.L. Experimental evaluation of constants for the Rohsenow pool boiling correlation. *Int. J. Heat Mass Transfer*. 1999;42(11):2003–2013.

Popov V.M. *Heat Transfer in a Contact Zone of Permanent Connections*. Moscow: Energiya; 1977 (in Russian).

Ramilison I.M., Lienhard J.H. Transition boiling heat transfer and the film transition regime. *ASME J. Heat Transfer*. 1988;110(3):746–752.

Rapier A.C., Jones T.M., Macintosh J.E. The Thermal conductance of uranium dioxide/stainless steel interfaces. *Int. J. Heat Mass Transfer*. 1963;6(5):397–416.

Rassokhin N.G. *Steam Generators of Nuclear Power Plants*. second ed. Moscow: Atomizdat; 1980 360 pp. (in Russian).

Rohsenow W.M. A method of correlating heat transfer data for boiling of liquids. *J. Heat Transfer*. 1952;74:969–976.

Rose J.W. On interphase matter transfer, the condensation coefficient and dropwise condensation. *Proc. R. Soc. Lond. A Math. Phys. Sci.* 1997;411(1841):305–311.

Rose J.W. Dropwise condensation theory and experiment: a review. *Proc. Inst. Mech. Eng. A: J. Power Energy*. 2002;216:115–128.

Sakurai A. *Film boiling heat transfer*. In: Proc. 9th Int. Heat Transfer Conf., Jerusalem, vol. 1; 1990:157–186.

Sanderson P.D. *Heat Transfer from uranium fuel to the Magnox Can in a gas-cooled reactor*. In: Proceedings of International Development in Heat Transfer, vol. 1; New York: ASME; 1961:53–64.

Schlünder E.U., Spalding D.B., Taborek J. *Heat Exchanger Design Handbook*. Düsseldorf: VDI-Verlag GmbH; 1983 Hemisphere Public Corp., Washington.

Schneider P.J. Conduction. In: Rohsenow W.H., Hartnett J.P., eds. *Handbook of Heat Transfer*. New York: McGraw-Hill Book Co.; 1973.

Sergeev V.V. *Post Dryout Heat Transfer in Annulus and Rod Bundles, Analytical Review, FEI OB-67*. Obninsk: Institute of Physics and Power Engineering; 1978 (in Russian).

Sergeev, V.V., 1987. Calculation of heat transfer in post dryout heat transfer in vertical cylindrical channels: Preprint IPPE-779. Obninsk: IPPE (in Russian).

Sergeev V.V. *Verification of the model of post-CHF heat transfer in dispersed flow*. In: Proc. 3rd Russian National Heat Transfer Conference, vol. 4; Moscow: MPEI Publishing House; 2002:165–168 (in Russian).

Sergeev V.V. *Transfer in Post-CHF Zone of Steam Generating Channels and Subassembly Thermohydraulics in Transient Regimes and Accidents*. (Ph.D. Thesis) Obninsk: IPPE; 2007.

Sergeev, V.V., Gal'chenko, E.F., Remizov, O.V., 1985. Engineering method of post dryout heat transfer in annular channels: Preprint IPPE-1649. Obninsk (in Russian).

Sergeev V.V., Gonin A.I., Remizov O.V. Post critical heat

transfer in the channels with spacer elements. *At. Energ.* 1990;68(6):445–447 (in Russian).

Shchukin V.K. *Heat Transfer and Hydrodynamics of Internal Flows in the Fields of Mass Forces*. second ed. Moscow: Mashinostroenie; 1980.

Shchukin V.K., Halatov A.A. *Heat Transfer, Mass Transfer and Hydrodynamics of Swirled Flows in Axisymmetrical Channels*. Moscow: Mashinostroenie; 1982 (in Russian).

Shlykov Yu.P. Prediction of contact thermal resistance of processed metallic surfaces. *Teploenergetika*. 1965;10:79–83 (in Russian).

Shlykov Yu.P., Ganin E.A., Zarevskii C.N. *Contact thermal resistance*. Energia: Moscow; 1977 (in Russian).

Shoji M. *Boiling chaos and modeling*. In: Proc. 11th Int. Heat Transfer Conf., vol. 1; 1998:3–21.

Shvets I.T., Dyban E.P. Heat transfer at contact of plain metallic surfaces. *Inzhenerno-Fizichesky Zhurnal*. 1964;7(3):3–9 (in Russian).

Siegel R., Howell J.R. *Thermal Radiation Heat Transfer*. third ed. Washington: Hemisphere Public Corp.; 1981.

Skipper R.G.S. Heat transfer within reactor fuel elements. *At. Energy Rev.* 1958;1(3):141–146.

Skipper R.G.S., Wootton K.J. *Thermal resistance between uranium and can*. In: Proceedings of the Second United Nations International Conference on the Peaceful Uses of Atomic Energy, Geneva, vol. 7; 1958:687–690.

Skipova V.P. *Metastable Liquid*. Moscow: Nauka; 1972 (in Russian).

Soloviev, S.L., 1998. Boiling and evaporation of liquid on porous surface. Diss. Doctor. tehn. Sciences. MEI, Moscow. Heat transfer in developed nucleate boiling on the capillary-porous

surfaces. In: Proc. of the Heat Transfer in Modern Technology, Institute of High Temperatures, RAS, Moscow, pp. 173–195 (in Russian).

Spalding D.B., Taborek J., eds. *Heat Exchanger Design Book*. Düsseldorf: VDI-Verlag GmbH; 1983 Washington: Hemisphere Public Corp.

Sparrow E.M., Cess R.D. *Radiative Heat Transfer*. New York: Hemisphere Public Corp.; 1978.

Spindler R. *Flow boiling*. In: Proc. 10th Int. Heat Transfer Conf., vol. 1; 1994:349–368.

Spiridonov Yu.G., Tzykanov V.A., Samsonov B.V., Fomin N.A. *Experimental Determination of UO_2 Thermal Conductivity Coefficient and of Fuel-Cladding Contact Conduction in Fuel Elements Under Reactor Irradiation/Preprint NIIR P-250*. Dimitrovgrad: NIIR; 1974 (in Russian).

Subbotin V.I., et al. *Hydrodynamics and Heat Transfer in Nuclear Power Facilities*. Moscow: Atomizdat; 1975 (in Russian).

Sukhatme S.P. *Condensation on enhanced surface horizontal tubes*. In: Proceedings of the 9th International Heat Transfer Conference, August 19–24, Jerusalem, Israel, vol. 1; 1990:305–327.

Tanasawa I. *Recent advances in condensation heat transfer*. In: Proceedings of the 10th International Heat Transfer Conference, August 14–18, Brighton, UK, vol. 1; 1994:297–312.

Tarasova N.V., Orlov V.M. *Heat transfer and hydraulic resistance in surface boiling of water in the annular channels*. In: Proc. of the Konvektivnaya Heat Transfer in Two-Phase and Single-Phase Flows; Moscow, Russia: Energy; 1964:162–186 (in Russian).

Thome J.R. *Enhanced Boiling Heat Transfer*. New York: Hemisphere; 1990.

Tong L.S. *Boiling Heat Transfer and Two-Phase Flow*. first ed. New York: John Wiley and Sons; 1965.

Todreas N.E., Kazimi M. *Nuclear Systems*. New York: Hemisphere Pub. Corp.; 2012; vols. I and II (1st time published in 1990).

Tong L.S. Heat transfer in reactor safety. *J. IHTC*. 1978;1978:285–309.

Tong L.S., Tang Y.S. *Boiling Heat transfer and Two-Phase Flow*. second ed. Cleveland, OH, USA: CRC Press; 1997.

Trunov N.B., Logvinov S.A., Dragunov Yu.G. *Hydrodynamic and Thermochemical Processes in the Steam Generators of Nuclear Power Plants With VVER*. Moscow: Energoatomizdat; 2001 (in Russian).

Voronov V.N., Larin B.M., Senina V.A. *Chemical and technological modes of NPP with VVER*. Moscow: MEI; 2006 (in Russian).

Wadekar V. *Flow boiling—a simple correlation for convective heat transfer coefficient*. In: Proc. 9th Int. Heat Transfer Conf., Jerusalem, vol. 2; 1990:87–91.

Wadekar V. *Onset of boiling in vertical up flow*. In: ASME Symp. Ser., vol. 89. Heat Transfer—Atlanta; 1993:293–299.

Wallis G.B. *One-Dimensional Two-Phase Flows*. New York: McGraw-Hill; 1972.

Waltar A.E., Reynolds A.B. *Fast Breeder Reactors*. New York: Pergamon Press; 1981.

Webb R. *Principles of Enhanced Heat Transfer*. New York: Wiley & Son; 1993.

Yadigaroglu G., Andreani M. *Two-fluid modeling of thermal-hydraulic phenomena for best-estimate LWR safety analysis*. In: Proc. NURETH-4, Karlsruhe; 1989.

Yagov V.V., Puzin V.F., Sukomel L.A. Heat transfer during developed boiling of halocarbons and high velocity of forced motion. *Teplotoenergetika*. 1998;3:11–19 (in Russian).

Yamada E., Ota H. Effective thermal conductivity of dispersed materials. *Wärme- und Stoffübertragung*. 1980;13:27–37.

Yang C., Nakayama A. A synthesis of tortuosity and dispersion in effective thermal conductivity of porous media. *Int. J. Heat Mass Transfer*. 2010;53:3222–3230.

Yao J.C., Hochreiter L.E., Leech W.J. Heat transfer augmentation in rod bundles near grid spacers. *Trans. ASME J. Heat Transfer*. 1982;104(1):76–81.

Yeoh G.H., Tu J.Y. *Improvements in reactor code RELAP5/MOD2 to predict distribution*. In: Proc. 12th Int. Heat Transfer Conf., Grenoble, vol. 4; 2002:621–626.

Yovanovich M.M. *Recent development in thermal contact, gap and joint conductance theories and experiment*. In: Proceedings of the 8th International Heat Transfer Conference, August 17–22, San Francisco, CA, USA, vol. 1; 1986:35–45.

Yovanovich M.M. Conduction and thermal contact resistances (conductances). In: Rohsenow W.M., Hartnett J.P., Cho Y., eds. *Handbook of Heat Transfer*. New York: McGraw-Hill; 1998 (Chapter 3).

Yovanovich M.M., Marotta M.E. Thermal spreading and contact resistances. In: Bejan A., Kraus D., eds. *Handbook of Heat Transfer*. New York: J. Willey & Sons; 2003 (Chapter 4).

Zhao Q., Zhang D.C., Zhu X.B., Xu D.Q., Lin Z.Q., Lin J.F. *Industrial application of dropwise condensation*. In: Proceedings of the 9th International Heat Transfer Conference, August 19–24, Jerusalem, Israel, vol. 4; 1990:391–394.

Zvetkov F.F., Grigor'ev B.A. *Heat and Mass Transfer*. second rev. and ad. ed. Moscow: Izdatel'stvo MEI; 2005 (in Russian).

Zysin L.V., Dorfman E.A. Heat transfer in the channels during the transition from convection to developed boiling. *Heat Transfer in NPP Power Equipment*. Leningrad: Nauka; 1986 pp. 143–149 (in Russian).

¹ Here we use the T_w as the temperature of the outer surface of the condensate film.

² Values characterizing the blackbody radiation will be designated by the subscript 0.

³ bb: beginning of boiling.

⁴ Former CKTI, Central Boiler and Turbine Institution in Russia (<http://english.ckti.ru/about.html>), Currently, I.I.Polzunov Scientific and Development Association on Research and Design of Power Equipment.

⁵ crud—chalk river unidentified deposit.

Pressure drops in nuclear thermal-hydraulics

Principles, experiments, and modeling

*K. Umminger**; *F. D'Auria†* · AREVA, Erlangen, Germany

† University of Pisa, Pisa, Italy

Abstract

Pressure drops in a loop are consequence of the flow (except for gravity pressure drops). The consistent combination of mass flow rate and pressure drop determines the pumping power in all systems including water cooled nuclear reactors. The complexity of the issue may be grasped considering the following items: (a) two-phase flows; (b) singularities in the flow stream or at geometric discontinuities; (c) counter-current flow (liquid and steam); (d) flow reversal; (e) flashing of subcooled fluid including the extreme conditions of typical geysering. Pressure drops in a closed loop following loss of coolant accident (e.g., pressurized water reactor conditions, mainly) determine the fluid stagnation point location which may signify zero-flow and very low heat transfer coefficient. All of this constitutes a motivation for this chapter.

Keywords

Pressure drops; Singularity pressure drop; Two-phase flow multiplier; Two-phase critical flow and pressure drops; Measurement of pressure drops; Reversible and irreversible components of local pressure drop

Nomenclature

AM accident management

ATWS anticipated transient without
scram

BD blowdown (phase of a LOCA)

BWR boiling water reactor

CCFL counter-current flow limitation

CFD computational fluid dynamics

CHF critical heat flux

CRE control rod ejection

DBA design basis accident

DC downcomer

DEGB double-ended guillotine break

ECC(S) emergency core cooling
(system)

IB-LOCA intermediate break LOCA

ITF integral test facility

LB-LOCA large break LOCA

LOCA loss of coolant accident

LOFW loss of feed water

LS loop seal

LSC loop seal clearing
(phenomenon)

NC natural circulation

NPP Nuclear Power Plant

PCT peak cladding temperature

PRZ pressurizer

PWR pressurized water reactor

RCP reactor coolant pump

RCS reactor coolant system (for
NPP)

RCL reactor coolant loop (for ITF)

RE reflood (phase of a LOCA)

RF refill (phase of a LOCA)

RIA reactivity initiated accident

RPV reactor pressure vessel

S.B. steam binding

SB-LOCA small break LOCA

SBO station blackout

SET(F) separate effect test (facility)

SG steam generator

SYS TH system thermal-hydraulics

TAF top of active fuel

TPCF two-phase critical flow

T/H or TH thermal-hydraulics

List of symbols

Most of the symbols are defined in the text or common to the scientific literature. Other symbols can be found in **Chapter 5** of the book.

Chapter foreword

Pressure drops and heat transfer are of main concern in system thermal-hydraulics. This reflects in the importance of related modeling and results of system code application to the prediction of accident scenarios in Nuclear Power Plants. Although pressure drops and heat transfer constitute key parts of the modeling for system thermal-hydraulic codes, discussed in **Chapters 5** and **9** of the book, special devoted chapters are foreseen, namely **Chapter 7** and current chapter dealing with heat transfer and pressure drop, respectively.

Pressure drop models are characterized by a long history dated since the beginning of previous century as discussed in **Chapter 2** of the book and outlined in this chapter. Furthermore, pressure drops directly affect the phenomena and the accident scenarios discussed in **Chapters 6** and **15** of the book. The discussion in this chapter shall be seen as complementary and linked to what discussed in those chapters.

Qualification is discussed in **Chapter 13** of the book and directly includes pressure drop models.

8.1 Introduction

The importance of pressure drops in nuclear reactor thermal-hydraulics (Nuclear Power Plant (NPP) design and safety aspects) constitutes the motivation for this chapter. The objective is to present the current status and the vision for the future in this area of TH science.

Apart from formulations of the laws of conservation of mass, energy, and momentum, the equations for pressure loss and heat transfer are the most important

formulations for the design of thermal-hydraulic systems.

In order to solve the basic conservation equations in thermohydraulic system codes, additional constitutive equations are required, simply because the number of unknowns is higher than the number of equations.

For NPPs, knowledge of the pressure loss in and between the individual systems and components is of decisive importance, not only in “normal” power operation, but especially for the analysis and assessment of accident situations.

In power mode the power generated in the core must be safely removed by the coolant mass flow rate. The reactor coolant pumps (RCPs) are designed so that they provide the required coolant mass flow rate in steady-state power mode. Here the pressure build-up across the pumps equals the total pressure loss across the cooling system. This means that for the design of the reactor plant, knowledge of the pressure losses across the individual components of the plant is required.

Many important phenomena expected during accident situations are highly influenced by the prevailing pressure drops, e.g.:

- break flow following loss of coolant accidents (LOCA),
- emergency core cooling (ECC) injection from passive injection systems (e.g., from accumulators),
- ECC bypass inside the reactor pressure vessel (RPV),
- loop seal clearing (LSC).

The different components of the pressure drop (static head, acceleration, friction, and local pressure loss) have a large impact on all natural circulation (NC) situations which may occur in normal operation or under accident conditions with respect to stability or even with respect to existence/establishment or stagnation/interruption of NC in the entire system or in individual components/subsystems.

The reproduction of reactor typical pressure losses is an important scaling aspect for integral test facilities. Not only the overall system pressure drop but also the adequate simulation of the pressure drops in individual components is of great importance (especially under NC conditions).

Pressure drop tests for specific components, such as spacer grid and fuel bundle are typically conducted in separate effect test facilities (SET(Fs)). So called basic

experiments are performed to systematically investigate the pressure drop as function of the geometry of the flow channel and the flow structure.

Finally the close coupling of pressure drop with heat transfer (Chapter 7) has to be mentioned.

8.2 Pressure drop components

The starting point for the pressure drops equations is the theorem of the conservation of momentum. Accordingly, the total static pressure drop, which a fluid is exposed to flowing through a flow path in steady-state conditions, is made up of the following components:

$$\Delta p = \Delta p_e + \Delta p_a + \Delta p_f + \Delta p_l \quad (8.1)$$

where Δp_e is the pressure drop due to static head—reversible component caused by different heights. Δp_a is the acceleration pressure drop—reversible (or partly reversible, or reversible in principle) component caused by change in the cross-section area or the density of the fluid. Δp_f is the friction pressure drop—irreversible component caused by shear stress on the walls. Δp_l is the local pressure drop—irreversible component caused by change in flow geometry and the flow direction.

The total pressure drop is therefore made up of the reversible components of the height (head) and (partly of) acceleration and a permanent pressure drop (referred to as pressure loss in the following), which in turn is made up of friction pressure loss and local form (shape) loss. When the fluid conditions change with time the acceleration pressure drop also includes a transient term. This term, although part of the equations at the basis of system thermal-hydraulic codes (see Chapters 5 and 11 of the book) has negligible impact upon the prediction of system performance in the majority of situations of interest.

The permanent pressure drop caused by the dissipation of kinetic or mechanical energy cannot only arise due to friction on walls and structures but also, especially in two-phase water/steam mixtures, due to irreversible momentum exchange between the phases.

Eq. (8.1) derived from the theorem of the conservation of momentum, also expresses the conservation of mechanical energy along a flow path including the reduction in energy due to dissipation.

8.3 Overview on pressure drop models and related phenomena

8.3.1 Friction pressure drop

8.3.1.1 Single-phase flow

Modeling of friction pressure drops in single-phase flows is based on empirical approach widely validated by experiments and theoretical data, see e.g., Nikuradse (1932). The irreversible pressure drop caused by sheer stress at the wall, sometimes also called distributed pressure drop, because it occurs all along the lengths of the flow channel, is determined by:

$$1 - \alpha = \frac{A_l}{A_g + A_l} \quad (8.2)$$

where f is the friction factor and D_h is the hydraulic diameter (equal to four times flow area/wetted perimeter). Pressure drops across tubes, rectangular channels, and bare rod bundles (without spacers) are typical examples for this pressure drop component.

The friction factor depends on the Reynolds number within the flow channel. Commonly used correlations some of which are discussed in the following are applicable to steady state fully developed flow.

Adiabatic single-phase flow

For fully developed laminar flow, the friction factor can be expressed as follows:

$$x = \frac{W_g}{W_g + W_l} \quad (8.3)$$

This is valid for Re numbers < 2320 .

For turbulent flow in smooth pipes a large number of friction factor correlations are available in the literature. A few commonly used are mentioned in the following:

According to Blasius (1913), the following simple formula applies in the range: $3000 < Re < 10^5$

$$1 - x = \frac{W_l}{W_g + W_l} \quad (8.4)$$

The Herman equation is appropriate for the higher range from

$$W = W_g + W_l$$

$$G = \frac{W}{A} \quad (8.5)$$

Colebrook and White (1937) (see also Colebrook, 1939) proposed an implicit equation, valid for smooth and rough pipes (considering the pipe roughness e) for the whole range of Re number above 3000:

$$D_h = 4A/p \quad (8.6)$$

The explicit equation provided by Filonenko (1948):

$$Re = \rho \times v \times D_h / \mu \quad (8.7)$$

is a good approximation of the Colebrook-White equation for smooth tubes in the range $Fr = v / \sqrt{(g \times L)}$.

Correlations for circular pipes are normally used also for the calculation of single-phase pressure drops in rectangular channels, in annuli and without existence of experimental data also in bare rod bundles applying the hydraulic diameter concept. One of the commonly used correlations for bare rod bundles is proposed by Kays (1975):

$$W_g = A_g \rho_g u_g = W \alpha \quad (8.8)$$

where K_1 is a function of pt/D (pitch to diameter) based on the work by Diessler and Taylor (1956), and f_{cir} can be calculated using correlations for circular pipes.

8.3.1.2 Two-phase flow

While the pressure drop in single-phase flow is characterized by the level of turbulence, the two-phase pressure drop is connected with the momentum exchange between the two phases and is characterized by the two-phase flow pattern. A large number of methods for the prediction of two-phase pressure drop can be found in the literature. The two-phase multiplier approach which is the basis for most of the cited methods, is the generally accepted engineering model to account for the effect of a two-phase mixture in a flow channel. The fundamental idea behind this is to calculate the pressure drop of one phase (gas or liquid) Δp_L first. To determine the two-phase pressure drop Δp_{TP} , the single-phase pressure

$$W_{TP} = W \cdot \phi = W \cdot \sqrt{1 + C}$$

drop is multiplied with a two-phase multiplier ϕ to consider the influence of the second phase. The following four basis methods to define the two-phase multiplier are commonly used:

- two methods that assume the liquid or gas phase flowing alone in the flow channel
- two methods that assume the entire mixture flowing as liquid or gas only.

Applying these basis definitions of the two-phase multipliers, the two-phase friction pressure gradients can be expressed as follows:

$$\text{Heat flux} = -K(\text{temperature gradient}) \quad (8.9)$$

The Φ_{L2} , Φ_{G2} , Φ_{LO2} , Φ_{GO2} terms constitute the two-phase pressure drop multiplier to be determined. The numerous approaches found in the literature on the calculation of two-phase pressure drop can be categorized into two general groups:

- Modifications of the single-phase friction factor based on the homogeneous model
- Empirical calculations applying the two-phase multiplier concept based on separated flow model.

In addition, there are also some direct empirical models (e.g., Lombardi and Pedrocchi, 1972). According to this approach, the two-phase pressure drop is directly determined as function of mass flux, mixture density, geometry of the flow channel, etc. without reference to a single-phase pressure drop. Furthermore flow pattern specific models have been developed to provide flow pattern specific correlations.

Finally, it has to be mentioned that modern computer codes based on two fluid models require additional correlations for the partitioning of the wall friction between the two phases (wall-to-phase for each phase) and interfacial friction models. Some of the widely used and often cited correlations are summarized in IAEA (2001), a few typical examples are outlined in the following.

Homogeneous model

Applying the homogeneous model, the two-phase flow is treated as pseudo-fluid characterized by suitable averaged properties of the liquid and gas phases. First approaches to determine the frictional pressure drops of two-phase flow were based on modifications of the friction factor for single-phase flow. For this approach, the two-phase pressure drop caused by shear stress at the wall can be expressed as:

$$q'' = -K \nabla T \quad (8.10)$$

where f_{TP} is the friction factor for two-phase flow and ρ is the density of the mixture. The friction factor is calculated applying one of the equations for single-phase flow, Eqs. (8.3)–(8.7), with the use of the mixture viscosity for the determination of the Re number. Several two-phase flow viscosity models are available; the most common ones have been introduced by:

McAdams et al. (1942):

$$q'''(r, t) - \nabla q'' = \delta / \delta t (\rho c T) \quad (8.11)$$

and Cicchitti et al. (1960):

$$q'''(r, t) - \nabla(-K \nabla(T(r, t))) = \delta / \delta t (\rho c T) \quad (8.12)$$

Additional examples for two-phase viscosity models for use in the homogeneous approach are given in IAEA (2001). Many of these models do not lead to significant different results. Homogeneous models are expected to provide good results for high mass flux flows. All homogeneous models can also be formulated in terms of two-phase friction multipliers.

Two-phase multiplier for separated flow model

The frictional pressure drop in two-phase flow is typically predicted by use of separated flow models. In the separated flow model the phases are considered to flow separately in the flow channel each with a given velocity and capturing a certain fraction of the channel cross-section area.

The study of two-phase pressure drop has been subject to numerous investigations

over the last six decades. Most of the developed methods are based on empirical calculations applying the two-phase multiplier approach. The methods by Martinelli and Nelson (1948) and Lockhart and Martinelli (1949) can be considered as origin of the two-phase friction multiplier approach. Lockhart and Martinelli (1949) defined a parameter X , known as Martinelli parameter:

$$q'''(r, z) = K_f \Sigma_f \Phi(r, z)$$

Based on the idea of Lockhart-Martinelli other researchers have then developed further correlations to account for specific geometry or flow conditions, e.g., see Fitzsimmons (1964) and Friedel (1980). The Martinelli-Lockhart-Nelson approach does not consider the interaction between the phases and does also not consider the influence of the mass flux on the two-phase multiplier.

While the correlations developed by Baroczy (1966) and Friedel (1979) consider the effect of the mass flux on the two-phase multiplier, the method introduced by Chisholm (1973), see also Chisholm (1968) and Chisholm and Sutherland (1969) accounts for the interaction between the phases.

8.3.1.3 Conclusive remarks

A not comprehensive (as already mentioned) overview of friction pressure drops has been given in this section. Additional snapshot like information which may be useful for the reader for connecting friction pressure drop with different topics in the book or in applications of nuclear thermal-hydraulics are listed in the following.

- All textbooks in nuclear thermal-hydraulics (see references in Chapters 1 and 2 of the book) provide key information about pressure drops. A pioneering, still valid and applicable document, mostly focusing upon local pressure drops, is by Idel'Chik (1960) (see also Idel'chik, 1979), and a more recent effort to summarize current technological understanding in the area of water cooled nuclear reactors has been performed within the framework of the International Atomic Energy Agency (IAEA) activities (IAEA, 2001).
- The principle approach to the calculation of friction pressure drops is based upon the definition of " τ_w " as mentioned in Chapters 5 and 11 of the book (see also

Chapter 9 of the book). The approach suffers from the difficulty in determining the derivative of fluid velocity in the direction perpendicular to the wall where the friction is acting. The difficulty occurs for Newtonian fluids and may reveal higher in the case of non-Newtonian fluids. Computational fluid dynamics (CFD) codes or approaches (see Chapter 12 of the book) did not get rid of the problem so far. The engineering approach, widely used is based upon the definition of “ f ” (friction coefficient) and the computation of hydraulic diameter and Re number (also function of the hydraulic diameter).

- The concepts equivalent diameter, and the situations “fully developed flow” and “laminar or turbulent velocity profile” in the cross sections, largely affect the computation of friction pressure drops. The related evaluations are not immune by errors and approximations (Del Frate et al., 2016) (see also the Ph.D. Thesis, Del Frate, 2016). Furthermore, the condition fully developed flow is needed to establish any meaningful/qualified correlation (e.g., for the friction coefficient); however, in no region of a water cooled reactor [either pressurized water reactor (PWR) or boiling water reactor (BWR), with the exception of the primary side of vertical parts of tubes in steam generators (SGs)] fully developed conditions occur. So errors are expected in any calculation of practical interest: this is an issue which generates the need for uncertainty quantification (Chapter 13 of the book).

- Experimental data are definitely needed to circumvent the limitations and deficiencies outlined in the previous bullet items. However experimental data are not immune of problems: measurement errors, reproducibility of test conditions, and of measured data and lack or insufficient knowledge of boundary conditions are reasons which give rise to the scatter of data; this requires an interpretation by the analysts. Powerful statistics based methods are available which do not reduce to zero the arbitrariness, e.g., when formulating a correlation (for instance, the exclusion of singular points which do not fall into a selected category may not be based upon fundamental principles of physics).

- The validity range for a correlation is at the origin of an additional problem for any empirical model based upon the analysis of experimental data. A strict interpretation of the information from a correlation would imply the use of the assigned correlation only within the ranges of parameters which are used to develop or to qualify the correlations. However, if one considers the following:

- combinations of the ranges of parameters (typically, many more than three parameters appear explicitly or implicitly, including boundary and initial condition values) used for development or available to demonstrate the qualification level of the correlation,

– expected ranges of interest in water cooled reactors, namely high pressure and large geometry,

the only applicable conclusion is that the concerned correlation is not applicable for predictions in water cooled reactor conditions. This constitutes the subject for scaling analysis and contributes to the uncertainty expected for any calculation (see Chapter 13 of the book).

8.3.2 Local pressure drop

When local obstacles, connected with flow area and/or flow direction changes occur in the flow channel, additional irreversible pressure losses, so called local or form losses, have to be considered.

Pressure drop across area changes (abrupt or continuously), bends, valves, elbows, tees, etc. are typical examples. In case of NPPs, the geometries of main interest for local pressure drop are the spacer grids, tie plates and any transition zones between individual components which are connected with change in flow area (e.g., SG U-tube inlet/exit or various bypasses in the PWR RPV) or change in flow direction [e.g., hot leg to SG inlet chamber, loop seal (LS) bends].

The local pressure drop is generally given by:

$$\Delta p / q_0''' = f(t_f, t_a) \quad (8.13)$$

where K is the local loss coefficient which is different for single-phase and two-phase flows and depending on geometrical details of the obstacle.

8.3.2.1 Area changes

Single-phase flow

One of the common flow obstacles is a sudden cross-sectional area change. Fig. 8.1 shows the flow structure for a single phase flow through a sudden expansion.

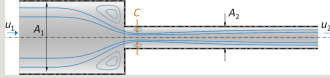


Fig. 8.1 Flow through sudden expansion.

Turbulent recirculation flow zones with mechanical energy losses are formed behind the opening of the cross-sectional area. After a transition lengths (8 to 10 times the larger tube diameter) behind the enlargement, the flow is again fully developed (VDI Heat Atlas, 2010). Based on a balance of mass, momentum, and kinetic energy and applying the Bourda-Carnot assumption, the irreversible local pressure loss can be expressed as follows:

$$q_l'' = h_s (T_{\text{wall}} - T_{\text{bulk}}) \quad (8.14)$$

and according to Eq. (8.13) the local loss coefficient is as follows:

$$Pr = \mu \times C_e / k \quad (8.15)$$

Eq. (8.15) is valid for turbulent flow. Loss coefficients for the pressure drop in laminar flow have been presented by Kays, 1950.

The flow process at a sudden contraction can be treated in a similar way with the exception that an additional effect has to be considered. Behind the point of area reduction, the flow continues to contract and forms a so called vena contracta at location C in Fig. 8.2.

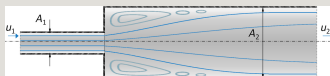


Fig. 8.2 Flow through sudden contraction.

The local pressure loss and the loss coefficient can be expressed as follows:

$$N\ddot{u} = h_s \times D_h / k \quad (8.16)$$

$$F_Q^E = \text{Engineering tolerances factor} \quad (8.17)$$

The smallest flow cross-section area A_c is not exactly known and is an empirical function of A_2/A_1 .

Two-phase flow

The “ K ” factor in two-phase flow is a function primarily of geometric characteristics of the system (this is at the origin of the definition of form loss factor for “ K ”) and of void fraction, other than fluid velocity or Re number. Related correlations have necessarily an empirical nature (see, e.g., Van Rooyen and Thome, 2013). The following should be considered before application:

- (1) range of validity, part 1: range of void fraction used in the experiment is important together with the number of boundary values used for void fraction: in other terms, extrapolation of “ K ” between two void fraction measurement is not appropriate when the distance between two points is greater than 0.05;
- (2) range of validity, part 2: the way to measure void fraction and the experimental error in the measurement should be documented;
- (3) flow reversal condition in the same geometrical configuration may give rise to a dramatically different dependence of “ K ” upon void fraction and Re than measured for direct flow;
- (4) use of the correlation shall be connected with a suitable model to predict void

fraction (i.e., consistent with the model used to generate the correlation).

8.3.2.2 Conclusive remarks

Pressure drops at geometric discontinuities either in single- or two-phase conditions are currently modeled by the application of empirically based coefficients. Assumptions are needed to determine those coefficients from experiments and, usually, no dependence is available from Reynolds number and void fractions: the impact of assumptions and of the lack of specification of dependencies upon results of prediction is unknown. This may largely contribute to the uncertainty of system thermal-hydraulics (SYS TH) code predictions, as already discussed in Chapter 1 of the book.

8.3.3 Acceleration pressure drop

The following topics are relevant for acceleration pressure drops (see also IAEA, 2001):

- Acceleration pressure drops may occur in steady-state flow conditions.
- Acceleration pressure drops are zero in case of steady flow of incompressible fluid.
- Acceleration pressure drops have theoretical formulation derived from momentum balance equation. Void fraction is the key parameter determining the related value.

8.3.4 Elevation pressure drop

Elevation pressure drops are caused in a gravity environment by different elevations of two points considered for the evaluation. In two-phase flow conditions elevation pressure drops (like acceleration pressure drops) largely depend upon void fraction: a suitable void fraction model is needed for the evaluation (e.g., qualified system thermal-hydraulic code, Chapter 11 of the book).

8.4 Relations between pressure drops, phenomena, and accident scenarios

The thermal-hydraulic phenomena (e.g., including pressure drops) in accident conditions expected in water cooled nuclear reactors are discussed in Chapter 6 of the book. Furthermore, the cross-link between phenomena, including pressure drops and accident scenarios can be found in Chapter 15 of the book. Insights

related to selected topics, noticeably the large break loss of coolant accident scenario (LB-LOCA) are discussed in this section.

8.4.1 Pressure drops in case of LB-LOCA

The distribution of Δp and flow resistances in the reactor coolant system (RCS) plays an important role in all phases of a hypothetical LB-LOCA

- Blowdown (BD),
- Refill (RF),
- Reflood (RE).

The chronology of events is described in detail in Chapter 15.

The following sections focus especially on the relation between pressure drops and the occurring flow phenomena and their impact on the heat transfer. As described in Chapter 15 the double-ended guillotine break (DEGB) in the cold leg between RCP and RPV is considered as limited or worst case with respect to peak cladding temperature (PCT) performance and is used as reference scenario for the following explanations. Most of the descriptions are referring to PWR with preferably cold leg ECC injection.

8.4.1.1 Occurrence of stagnation point during BD and RF phases

With the occurrence of the break, BD starts with pressure wave propagation/jet impingement causing load on RPV internals during the first hundred milliseconds (this will not be described in detail here). At first subcooled critical flow occurs at both ends of the break. The high mass flow rates at the break results in a sharp primary pressure decrease and saturation conditions in the hottest regions of the RCS (upper part of the core, upper plenum (UP), hot legs) are reached within the first seconds.

Due to flashing the depressurization rate is decreased; however the “saturation front” further expands and comprises the entire primary system within the next few seconds. The flow phenomena (flow direction) in the individual components are mainly influenced by the flashing processes, by the prevailing flow resistances and the critical flow via both ends of the break and to some extent by the performance of the RCP.

The loss of subcooling at the break and the reduced pressure result in a remarkable

reduction in break flow rate and therefore in a reduced depressurization rate. In any case, during the (very) first period after occurrence of the break, flow stagnation in the core region and reverse flow at the core inlet has to be expected (Fig. 8.3). The RPV or the core region provides a rather large volume at high temperature and therefore a significant source/reservoir for pronounced flashing processes.

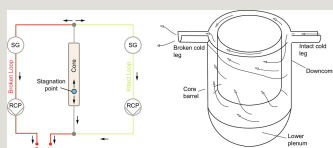


Fig. 8.3 Stagnation point in the RPV during BD and RF phases.

On the other side a simplified pressure balance analysis can demonstrate that the core is a favorite candidate for the stagnation point. Starting from the stagnation point, there are two or more (depending on the number of intact loops) flow paths to the RPV side of the break. One leads directly via the lower plenum, the downcomer (DC), and the cold leg of the broken loop to the break. In parallel, flow paths exist via the UP, the SG and RCP of the intact loops and via the DC to the break. The total break mass flow rate at the RPV side (critical flow conditions) is composed of both, the flow via the lower plenum and the flow from the cold legs of the intact loops. The flow distribution and thus the location of the stagnation point between these individual flow paths are self-regulating adjusted in such a way that the corresponding pressure drops between the stagnation point and the break location are identical. For an overall pressure balance analysis also the second main flow path via the UP, the SG and RCP of the broken loop to the pump side of the break has to be considered.

The break flow at both sides of the break is characterized by critical flow in the very first phase under subcooled and then under two-phase flow conditions. The mass flow rate via the RPV side is significantly higher compared with the pump side flow rate, as the flow resistance via the SG and especially the RCP of the broken loop is generally higher as the flow resistance via the other flow paths to the pump side of the break.

With the flow stagnation and reversal occurring within one second after the break, critical heat flux (CHF) conditions are reached in the core causing the fuel rods to experience DNB. The reduced heat transfer (film and transition boiling, see Chapter 7) leads to rise in cladding temperatures and to the occurrence of the first

PCT (blowdown PCT) even though the reactor is rapidly shutdown either by reactor trip (low pressure set point is reached) or due to core coolant voiding (decay power).

If the RCP in the intact loops continue to supply water to the RPV, a short period of positive (upward) flow at the core inlet may occur. This is going to happen when the total mass flow rate from the intact loops exceeds the break flow rate on the RPV side. The RCPs are either tripped directly with the occurrence of the break in case of LOOP or shortly afterwards on indication of certain RCP trip signals (e.g., low system pressure, low Δp over the pump). The amount of water supplied to the RPV from the intact loops depends on the T/H conditions at the RCPs and the operation/performance of the pump (timing of RCP trip, coast-down behavior, and inertia of pump masses) and also the number of intact loops (tendency for positive flow more pronounced in four-loop plants).

The positive flow into the core may improve the heat transfer in the core terminating the further cladding temperature increase and causing partial core rewet during this period (bottom up cooling around 10 s after break occurrence). With the occurrence of two-phase conditions at the RCP their effectiveness is reduced, the positive core flow is terminated, and once again flow reverses.

In the following time some additional processes, such as flashing and delivery of water from the PRZ, upper head or UP to the core may also contribute to the core cooling during the BD phase (top down cooling). At the end of BD, the RCS is completely empty with the exception of some residual water in the lower plenum of the RPV. According to the flow resistance of the individual flow paths, stagnation points are expected to occur in the region of the hot legs. From these points, steam is flowing in negative direction via the RPV to the RPV side of the break. In the intact loops steam is also flowing from these points via the SG, RCP, and the DC (positive direction) to the RPV side of the break. In the broken loop the steam directly flows from the hot leg via the broken loop to the pump side of the break. The negative steam flow through the core ends as the level in the UP reaches the upper end of the core barrel during the RF phase.

8.4.1.2 Pressure drops and RE

As described in more details in Chapter 15 of the book, the RE phase begins when the water level reaches the lower end of the core. During the RE phase the core is filled with coolant and the core cooling is reestablished (quenching) throughout the entire core region. Depending on the boundary conditions, the RE phase may last between <100 s and several minutes. There is a strong coupling between the

reflooding process and the encountering heat transfer modes and thereby with the quench front propagation and rewetting processes in the core.

During the early RE phase, coolant from the accumulators (rather high mass flow rates) enters the core initiating or intensifying the quenching process at the bottom of the core. Heat release from the hot fuel rods to the surrounding water leads to intensive steam production. The creation of steam results in an increase in pressure drop along the steam flow paths from the core to the break and an increased pressure in the core region compared to the pressure at the break or in the DC. This local pressure build-up above the water or water/steam mixture level in the core has a delaying effect on the further flooding of the core and accelerates the filling of the DC leading to a remarkable difference in water levels between the core region and the DC region. Fig. 8.4 shows corresponding results from a PKL experiment. The level in the DC is of course the driving force for the flooding process in the core. However the flooding rate and thereby the propagation of the quench front also depends on the evolution of the absolute pressures above the water levels in the core and in the DC, i.e., the pressure difference between these locations.

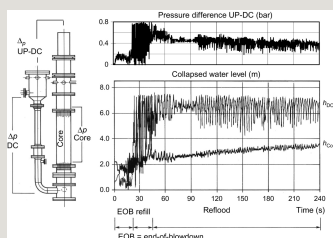


Fig. 8.4 PKL II: RPV level evolution during reflood.

The pressure in the core is on one side a function of the amount of generated steam which again depends on the decay power, the power distribution, and the quench front propagation itself and on the other side a function of the flow resistance from the core to the break location or to the condensation location in the cold legs.

The steam flowing out of the core divides in the UP in accordance with the pressure losses of the individual loops in the direction of the two ends of the break. Here, in particular, the pressure losses through the RCPs are of importance. On its way to the break location, the steam is heated up when passing the SGs that are still under hot conditions. In the broken loop it can be assumed that the steam flows

at the pump side of the break under superheated conditions into the containment. In the intact loops steam is condensed at the ECC injection points in the cold legs, depending on the amount of injected ECC, partially or completely. The thus heated emergency core cooling water flows toward the DC and from there partly toward the lower plenum and contributes to flooding the core. A partial flow also passes through the DC to the RPV side of the break and is discharged there. The pressure at the top of the DC is finally determined by the pressure loss in the primary side loops and by condensation processes in the region of the ECC injection. In addition to design-related pressure losses due to friction and form losses and local and temporal acceleration due to changes in cross-sectional areas or by evaporation and condensation processes, also certain thermal-hydraulic processes/phenomena can cause an increase in the pressure drops in the primary circuit, e.g.:

- water entrainment and steam binding (S.B.) (see Section 8.4.1.3),
- counter-current flow limitation (CCFL) phenomena (see Section 8.4.2.1),
- deposition of boron acid in the SG U-tubes (see Section 8.4.1.4),
- backward flow of ECC water via the RCP and accumulation in the LSs (see Section 8.4.1.4).

The last two mentioned phenomena are more expected in the long-term cooling phase.

Generally, pressure losses in the primary circuit have a major impact on the flooding rate and on the progression of the quench front and therefore on the PCT and the timing of the turnaround of the cladding temperatures and the complete quenching. Depending on the boundary conditions differential pressures of more than 100 mbar in configurations with cold leg breaks and cold leg injection may occur.

Fig. 8.4 shows exemplarily typical results of an experiment from the PKL II B test series with double-ended break in the cold leg and only cold-side ECC supply. The experiments of PKL II B series include, starting from a primary pressure of 40 bar, the end of BD phase, the refilling and the reflooding of the core. Shown are the measured levels in the RPV DC and in the core area and the measured differential pressure between the UP and the top of the DC. It can be seen that with the beginning of the flooding process, the levels in the DC and in the core significantly diverge. With decreasing decay power during the flooding process also the pressure difference decreases and the levels equal to itself. That is, with already

filled DC water, inventory in the core steadily increases. The flooding process itself and the potential variations/oscillations in level are subjected to a self-regulating mechanism. A rapid progress of the quench front causes intensive steam formation associated with an increase in pressure drop, and thus a slowdown of the flooding process. This in turn means a reduced steam formation, resulting in a renewed acceleration of the flooding process.

When interpreting the test results, it should be noted that the illustrated collapsed levels were directly derived from differential pressure measurements along the core or the DC neglecting other pressure loss components (friction, form losses, acceleration). It is assumed that the hydrostatic component is predominant in the measured differential pressure and the so derived collapsed levels represent the water inventory in the respective components with a good approximation. It must however be remembered in particular for the interpretation of the temporal variations that dynamic effects are included in the displayed measurement signals which partly can even lead to a phase shift between the measured differential pressures and the actual inventory fluctuations.

The course of the mixture level in the core region can be well reproduced by means of cascaded differential pressure measurements along the core (Fig. 8.5), at least by trend (at certain times). The passing of the mixture level at the respective lower pressure tapping point is indicated by a significant increase in the measured differential pressure in the respective measuring section. The progress of the quench front is determined by measuring the surface temperature detected at the fuel rod simulators (lowering the temperature to near saturation). The relation between the fictitious collapsed level (water inventory), the mixture level, and the quench front depends on the system pressure, stored energy in the rods, the decay power, and the flow pattern developing in the core above the quench front (Chapter 7).

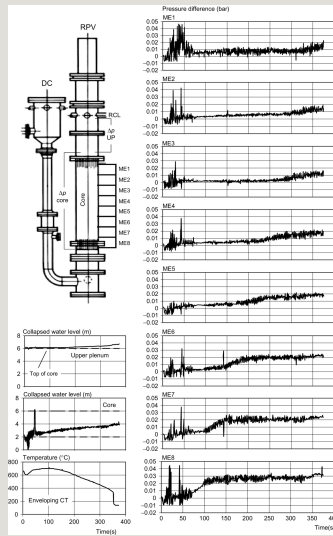


Fig. 8.5 PKL II: Δp along the core during reflood.

In conclusion, the pressure losses in the primary circuit lines have a major impact on the flooding process in the core. As part of the PKL I test series this was confirmed quantitatively by varying the flow resistance of the reactor coolant pumps (RCP simulators were used in PKL). Higher pump resistances lead to higher PCT and longer quench times. This effect is especially relevant when configurations with cold side break and cold-side ECC injection are considered. In other constellations with respect to break location and ECC injection location this influence is of lesser importance.

8.4.1.3 Steam binding

During the RE phase of LB-LOCA large vapor quantities are generated in the core when the quench front is propagating along the core. Droplets may be entrained out of the core by high steam velocities and evaporate at the hot structures in the UP, the hot legs and especially in the SG U-tubes, because the SG are normally on a higher temperature level than the primary side during this phase.

The evaporation of liquid carry over increases the pressure above the core, which again opposes the driving pressure for displacement of water from the DC to the core, reduces the core flooding rate and thus adversely effects core cooling. This effect is called “steam binding” (S.B.). While in the more common sense “S.B.” is defined as the impact of the core steam generation and water carryover on the

increase in UP pressure in general, in the literature it is mainly referring to the contribution of the pressure increase generated by the evaporation of entrained water in the SG U-tubes. In the following explanations "S.B." will be used in the latter mentioned sense. The effect of S.B. can directly be expressed by the increase in differential pressure over the loops and over the SGs, respectively.

As S.B. is directly connected with entrainment of water, the velocity of the steam and thus the system pressure is of great importance on the S.B. effect. Higher containment pressure and thus higher system pressure tends to reduce S.B. in the SG due to higher steam density. On the other side high pressure on the SG secondary side tends to increase S.B. due to the more effective evaporation process. In this connection it has to be mentioned that not only the evaporation itself leads to an increase in steam velocity and therefore to an increase in pressure drop but also the rising temperature itself (lower density, higher velocity) of the steam results in an increase in pressure drops over the SGs. The flow at the SG outlet mainly consists of superheated steam whereas the entrainment of a certain amount of water toward the SG outlet even under superheated steam conditions cannot be excluded as experiments in the FLECHT-SEASET test facility have indicated. This amount of water does not contribute to S.B. in the SGs just as well as the water deentrained on its way from the core toward the SG in the UP, the hot legs, and the SG inlet chambers.

A number of experiments in SET(Fs) (e.g., FLECHT-SEASET) and integral test facilities (e.g., BETHSY and PKL II) related to water carryover and S.B. have been performed, some of them several decades ago. SETs especially on water entrainment and deentrainment in the UP, the hot legs, and SG inlet chamber have also been performed under real plant dimensions in the UPTF facility.

Results from FLECHT-SEASET demonstrate the effect of S.B. on the pressure drop over the SG observed in a SET. Code assessment calculations against FLECHT-SEASET experiments demonstrated that the S.B. effect is over predicted.

S.B. and the impact on core cooling was also one aspect in the already cited integral experiment performed within the PKL II B program. In this test entrainment of water from the core, was only observed in the first phase of the RE phase, when high steam velocities occurred due to intense evaporation processes at the bottom of the core. In the predominant part of the RE phase almost no water entrainment (and evaporation in the SGs) took place.

The increased pressure drop in the SG is mainly due the heat up of the steam and the consequential increase in steam velocity (lower density). However the

contribution of the pressure drop over the SG to the entire pressure drop over the loop is relatively small (Fig. 8.6, top). This rather low effect of the S.B. and entrainment of water may be attributed to the relative high system or containment pressure of 4 bar postulated for the assumed scenario. An assessment of RELAP5 using this PKL experiment showed the tendency of the code to overpredict the S.B. phenomena (over prediction of pressure drop across the SG) by overpredicting the liquid entrainment from the core, finally resulting in higher core cladding temperatures in the calculation.

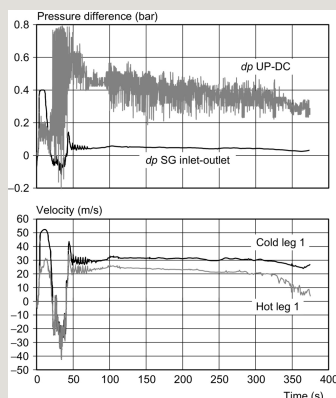


Fig. 8.6 PKL II: Δp across SG (steam binding) and loop velocities during reflow.

In general, it seems that the existing experimental database is not sufficient to completely cover the entire range of relevant parameters including all relevant phenomena associated with S.B. (water entrainment, deentrainment, heat transfer in SG U-tubes with hot walls and entrained water, possible entrainment of water into the SG outlet chamber, resulting pressure drop across the SG). Additional integral and/or SETs especially in the lower pressure range with use of adequate instrumentation are therefore desirable.

8.4.1.4 Pressure drop during long-term cooling

Continuous boiling in the RPV is expected during the long-term phase of a large cold leg break LOCA in PWR plants with sole cold leg ECC injection. In this state, the reactor core is rewetted and covered by two-phase mixture of water and steam, but due to mixing of cold ECC water with steam in the upper DC the coolant fed to the core in compensation for the evaporation is almost at saturation temperature.

The limitation of the ECC flow from the cold side via DC to the core is a consequence of the pressure balance between hot (core, UP) and cold side (break location); the hot side UP pressure acts against the flow and thereby avoids a subcooling of the core volumes. In doing so, the ECC flow theoretically only compensates for the evaporation rate in the core, regardless of the cold-side ECC flow rates as any excess ECC is lost via the break.

Thus, the boiling process in the core continues in the long term. The continuous replacement of almost boron-free steam by borated ECC water leads to a continuous increase in boron concentration in the core and the temperature-dependent limit of boron solubility in water may be reached. Locally initiated crystallization then effectuates the formation of solid boron particles which may compromise core cooling by impeding the heat transport from the rods through plate-out of boric acid at the rod cladding surfaces. An effective measure to avoid or reverse a present or developing boron enrichment process in the core is the switch-over to hot-leg ECC injection. A hot-leg ECC flow high enough may create a net flow that displaces the high boron coolant inventory from the RPV riser side via DC toward the break ("flushing" of the core).

The maximum switching time (from cold to hot leg injection) depends on the speed of the boron enrichment process and thus on the size of the mixing volume, i.e., the amount of liquid water in the RPV available for mixing with the continuously accumulating boric acid. The available mixing volume, i.e., the mixture level on the hot side again is mainly influenced by the flow resistance along the loops and its possible increase during the transient. In a cold-leg break scenario, a high flow resistance between UP (close to steam source) and cold side (break, heat sink) results in a high differential pressure between UP and break location. The hot-side swell level accounts for this pressure differential: The higher the flow resistance, the higher the pressure differential between UP and cold leg and the lower the mixture level above the lower plenum and the mixing volume available.

Of course the parameters for the UP pressure are mostly given by the PWR design concept:

- bypass flow from upper head/upper plenum to DC,
- pressure losses along the loops determined by SG U-tubing and RCPs at standstill.

In addition, certain effects possibly occurring during the transient may contribute

to the increase of the overall pressure differential between hot and cold sides. Refilling of LSs by ECC backflow via the RCPs resulting in partial or complete blockage of one or multiple cross-over legs by water or two-phase mixture increases the flow resistance (in contrast to LSC that decreases the flow resistance, see Section 8.4.2.3). S.B. (see Section 8.4.1.3) as well as plate-out of boric acid in the SG U-tubes resulting from the evaporation of coolant entrained into the U-tubes (the secondary side is at a higher temperature level) may also slowly increase the flow resistance across the SG and contribute to the overall pressure differential. In this way, high steam loads (comparably high core power in the early long-time cooling phase) in conjunction with the built-up flow resistances along the loops cause a decrease of the swell level in the core (swell level depression) and thereby a significant reduction of the mixing volumes in the RPV (Fig. 8.7).

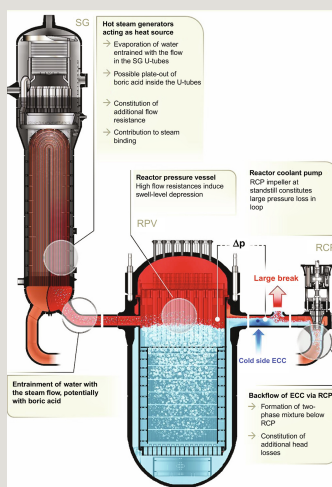


Fig. 8.7 Increase in Δp along the loops by boron deposition and LS refilling.

Systematic experimental studies on the size of the mixing volume in the RPV as function of the decay power and the flow resistance in the cross over legs (geometrically or by refilling with ECC water) were performed within previous PKL test programs. Additional concluding investigations are still ongoing. As an example, Fig. 8.8 shows schematically the impact of the refilling of one LS on the pressure difference between the UP and the upper DC and the following decrease in collapsed level in the RPV as observed in the PKL experiments.

water down flow in vertical flow sections are expected to occur in many accident sequences. CCF may also appear in inclined or even horizontal flow sections if there is a connection with inclined or vertical sections experiencing CCF. At high steam flow rates or steam velocities the water flow in the opposite direction may be impeded or even terminated/diverted in the same direction as the steam flow (cocurrent flow) due to momentum exchange between the phases. This phenomenon, called CCFL, may lead to accumulation of water, i.e., flooding or water hold-up at the CCFL location. CCFL can be considered as one of the key thermal-hydraulic phenomena in reactor safety analyses because it can prevent or at least deteriorate the backflow of water to the reactor core. The occurrence of CCFL is generally connected with an increase in pressure drop at the CCFL location. It therefore does not only lead to a displacement of water from the core to the CCFL location but it may also cause a certain suppression of the core level.

CCFL is likely to occur in complex geometries characterized by flow restrictions, bends or significant reductions of flow areas, such as upper core tie plate, hot Leg bend, inlet of SG header, or inlet of SG tubes. Additional possible CCFL positions are the RPV DC, the pressurizer (PRZ) surge line, and the ascending part of the cross over leg. Specific local modeling is necessary in system codes to obtain reliable predictions. Flooding correlations are established from experimental data and the parameters of these correlations are part of the code input deck.

Extensive experimental investigations in SET and integral test facility (ITF) have been performed during the last decades to address the CCFL issue and to provide an experimental database for the development and validation of the corresponding models. Comprehensive experiments in full scale PWR geometry on CCFL in the hot legs during reflux condenser mode in small break LOCA (SB-LOCA) conditions have been performed in UPTF. Additional investigations in UPTF addressed CCFL at the upper core tie plate and in the RPV DC during LB-LOCA. The UPTF test results and the comparison with results from smaller test facilities clearly demonstrated the dependency of CCFL occurrence on the geometrical dimensions and the importance of scaling for the investigated cases. Pronounced heterogeneous 3D flow distributions with water downflow (breakthrough) and steam upflow paths have been observed and, for example, nonuniform distribution of vertical differential pressure across the tie plate has been detected (Mayeringer et al., 1993).

CCFL in the SG U-tubes have been mainly addressed by systematic investigations in integral test facilities (e.g., LSTF, BETHSY, and PKL). As mostly PWR-prototypical SG tubing with original dimensions of the individual U-tubes is used

in the test facilities, the experimental results are largely representative of the PWR.

CCFL under reflux condenser conditions has been extensively investigated for instance in the PKL III test facility. Within parametric studies, the influences of the specific SG load (heat to be removed by the SG) and the primary pressure on the occurrence of CCFL and on the amount of water accumulated in the U-tubes due to CCFL was systematically analyzed under quasisteady state and transient conditions (secondary side cool down). As an example Fig. 8.9 shows typical results from an experiment on CCFL under reflux condenser conditions performed with a stepwise increase of the SG load from 4% to 20% of the nominal SG power at a constant primary pressure of 40 bar (realized by controlling the secondary side pressure). The measured Δp , between the in- or outlet chamber and the outlet chamber and the top of the U-tubes for three tubes with different heights as well as the measured Δp between the SG inlet and outlet chamber are shown in Fig. 8.9. In the PKL test facility 3 out of 30 U-tubes are equipped with Δp measurements on the inlet and outlet sides of each of the four SGs.

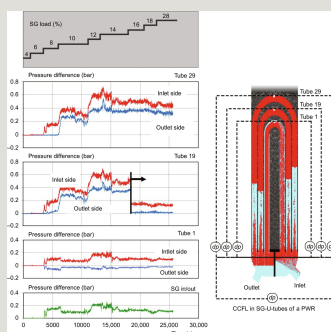


Fig. 8.9 PKL III—CCFL in SG U-tubes during reflux condenser mode of operation.

The test started in “pure” reflux condenser condition, i.e., the mixture level in the RPV was between the core exit and the lower edge of the RCL and there was no water accumulation, neither in the hot legs nor in the SG inlet chamber or in the U-tubes. Under these conditions, the measured Δp on the inlet side (CCF) and outlet side (concurrent flow) is close to zero. The onset of CCFL in the U-tubes is clearly indicated by a significant increase in Δp on the SG inlet side and by an increase in Δp between the SG inlet and outlet chamber at a SG load of 6%. It has to be mentioned that in the SG inlet chamber liquid hold-up occurred at the same power level, however shortly after the occurrence of liquid hold up in the U-tubes.

Consequently liquid hold up in the U-tubes was the result of CCFL and not simply a continuous rise of the steam/water mixture level from the inlet chamber into the U-tubes.

Fig. 8.9 also reveals a rather heterogeneous flow behavior among the individual U-tubes. While the longer tubes experience water hold up, condensate is carried over to the outlet side in the short U-tube creating a pressure drop (due to high steam/water velocities) from the top of the U-tubes to the SG outlet chamber (cocurrent water/steam flow) indicated by the negative value for the pressure difference in the outlet side of the short tube. Obviously, the steam is not condensed completely in the shorter tubes, and the remaining steam flows via the SG outlet chamber into the outlet sides of other tubes experiencing CCFL in their inlet sides. As a result, CCFL may also occur in the outlet sides of longer tubes if this steam flow rate is large enough. The entire pressure drops on the inlet side (carry-over of condensate) and the outlet side (cocurrent flow of steam and condensate) corresponds to the differences in pressure drops between the inlet and outlet side of the longer tubes which are mainly caused by the hydrostatic head of the accumulated water, whereas friction pressure drop, local pressure drop, and possible dynamic effects are also included in the measured Δp .

8.4.2.2 Pressure drop and TPCF

When a fluid passes from a high pressure region with a given thermal-hydraulic state (pressure, temperature, void) via a restriction (e.g., pipe, orifice, valve) to a lower pressure environment, the mass flow is determined by the pressure difference between the two regions as far as a certain limit for the pressure difference is not exceeded. Under these conditions a pressure reduction in the downstream region results in an increase in mass flow. However, if this pressure falls below a certain value (i.e., Δp exceeds a certain value), no further increase in mass flow takes place (Fig. 8.10).

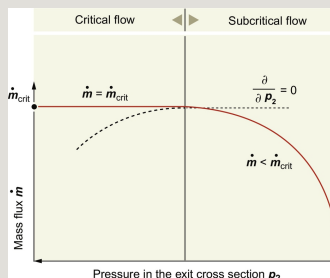


Fig. 8.10 Relation between mass flow and pressure in the exit cross section.

The resulting flow (called critical or choked flow) is then independent of the conditions in the downstream region and is for a given geometrical configuration, only a result of the conditions (e.g., pressure, temperature, void, quality, flow region) in front of the restriction. Fig. 8.11 shows schematically the pressure profile along the flow path from the inlet to the outlet of a flow duct (restriction). The pressure reduction with increasing gradient is connected to an acceleration of the two-phase mixture. The reason for critical flow is the strong expansion of the gaseous phase and can be explained on the basis of energy conservation (transposition from potential to kinetic energy). For subcritical flow the pressure in or just upstream of the exit cross section corresponds to the pressure in the downstream region p_2 . In case of critical flow a pressure jump is observed in the exit cross section. The minimum achievable pressure p_1 is called critical pressure p_c and cannot be decreased further even if the pressure p_2 is reduced.

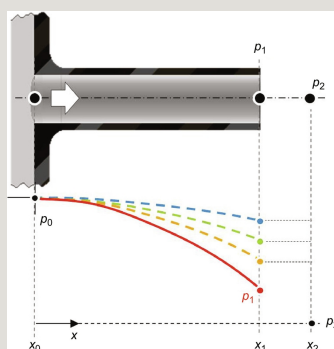


Fig. 8.11 Pressure along the flow path as function of the exit pressure.

As outlined in Chapter 6, the knowledge on the two-phase mass flow under critical flow conditions is a very important issue in reactor safety analysis concerning a broad range of accident/events and relevant for different components/structures in reactor systems, such as:

- Loss of inventory through breaks/leaks ranging from small cracks to DEGBs,
- Restrictions inside a system (e.g., surgeline or locked RCP after DEGB),
- Critical flow through valves, e.g., during

- Cycling of safety and relief valves to control primary and secondary side pressures, e.g., in SBO, LOFW, ATWS, and SB-LOCA transients.
- Depressurization of primary and/or secondary side by fully opening of corresponding valves (as AM measures).

Numerous models for critical two-phase flow have been developed for use in thermal-hydraulic system codes. The detailed description of these models which are differing among others by their complexity or by the level of assumed disequilibrium (thermal and mechanical) can be found in the open literature and is not subject to this chapter. Such critical flow models have been assessed against an extensive set of data from critical flow experiments mainly conducted in SET. A number of studies based on existing experimental results have been performed in recent years (e.g., Sokolowski and Koslowski, 2012; Bartosiewicz et al., 2011), to validate the models in the currently used codes, to investigate the range of applicability of the individual models and to identify options for further improvements in the calculation of the critical flow. It is clear that none of the existing models can cover the entire parameter range expected to occur under accident situations with respect to the geometrical configuration and with respect to the thermal-hydraulic conditions in front of the critical flow area.

A large number of SET on critical flow, the first ones already performed in the seventies of the last century, are known from the literature. The OECD/NEA has selected different experiments as reference tests for critical flow during LOCA transients (see Chapter 6 of the book). One of the most prominent test campaign often used as source of experimental data for validation of two-phase critical flow (TPCF) models was performed within an international project in the Swedish Marviken Power Station facility under almost real plant conditions (Ericson and Hall, 1978) in the years 1978–1979.

Typical results of another experimental campaign on two-phase critical BD from a pressure vessel following a pipe break, performed at the University of Pisa, are shown in Fig. 8.12. The illustrated curves represent the time trends of the pressures measured in the pressure vessel and in the exit pipe at two different positions. A method for analyzing the most important phenomena in the BD transient was applied by D'Auria and Vigni (1983) to these experimental signals to obtain values for flow rate as well as spatial and temporal trends of quality and velocity in the exit pipe.

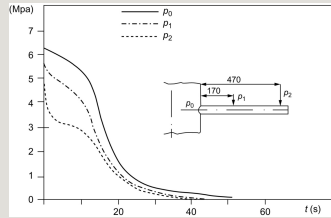


Fig. 8.12 Pressure evolution at different locations.

With the spatial profiles of the pressures (input) Fig. 8.13 shows the calculated velocity and quality profiles along the exit pipe at a certain point in time ($t=6$ s). The pressure decrease in the pipe causes, in this case, evaporation of water entering the nozzle and then a continuous increase in velocity. In the applied theoretical method, axially symmetric flow under thermodynamic and mechanic equilibrium conditions was assumed. The pressure drop due to local discontinuity and wall friction was considered by corresponding input data (pressure loss coefficient at pipe inlet, distributed friction factor between pipe wall and fluid and two-phase flow multiplier).

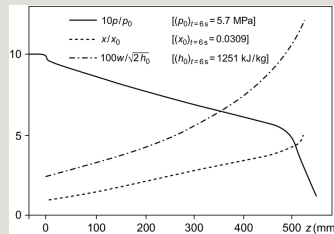


Fig. 8.13 Pressure, quality, and velocity versus distance from the nozzle inlet.

In general, most of the calculation methods for critical mass flow assume in a first approximation isentropic changes of the conditions from the inlet to the exit of the flow duct. Under these conditions (typical for ideal nozzle) the pressure drop along the flow duct only consists of acceleration effects (wall friction is neglected). Depending on the geometry and the operating conditions, the friction pressure drop may not be neglected. In constant cross section pipes with choking occurring at the pipe exit, the critical flow may be significantly influenced by the entrance losses and the wall friction in the pipes. The length of the pipe or the L/D ratio is one decisive factor to quantify the impact of friction pressure drop on the critical

flow rate.

In case of narrow wall penetrating cracks in pressurized components, the hydraulic resistance in the flow path is very important for the determination of the leakage rate. As an example, Fig. 8.14 shows the pressure distribution through a crack, calculated with a finite volume program on the basis of geometrical characteristics of the leakage path (Keim et al., 1999).

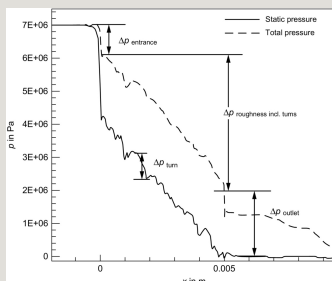


Fig. 8.14 Pressure within the crack.

The analysis of leak flow rates of through-wall cracks is also relevant in connection with the qualification of leakage detection and surveillance systems used in NPP and with respect to break preclusion concepts including leak-before-break.

8.4.2.3 The LSC

Depending on the break size and the availability of the emergency core cooling system a loss of coolant with small or intermediate break may lead to significant reduction in primary system inventory with interruption of NC and under certain boundary conditions even to core uncover and cladding temperature increase. The occurrence, extent, and termination of core uncover is closely linked with the occurrence of LSC. In contrast to LB-LOCA where the LSs are completely emptied already during the BD phase, they remain initially at least partly filled with water in SB-LOCA or intermediate break LOCA (IB-LOCA) transients.

In case of cold leg break the core level depends on the pressure drop of the steam flowing from the core to the break. As long as the LSs are filled with water the flow path via the SG and the cross over legs are blocked and the only available flow paths to the break are via the upper head—DC bypass (and via the nozzle

bypass) leading to a relative high pressure difference between the UP and the cold leg (break location).

In case of SB-LOCA a certain part of the decay power is transferred to the secondary side under so called reflux condenser conditions so that the primary pressure is mainly determined by the secondary pressure. In case of IB-LOCA the primary pressure typically drops below the secondary pressure due to the larger break size and there is no heat transfer from the primary to the secondary side for the major part of the transient. Continuous loss of inventory (assuming no or small ECC injection rates compared to the break flow rate) results in a continuous level reduction in the core.

In parallel a continuous displacement of water in the loops seals from the SG outlet side to the upward part, i.e., toward the break in the cold leg, occurs. Assuming that the pressure drop from the core outlet via the SG to the SG outlet is small, the pressure difference between both sides of the LSs and between core and DC are similar so that the level reduction on the SG side of the LS proceeds synchronously with the level in the UP/core region (manometer balance). As soon as the water level in the downward vertical part of the LS reaches the upper edge of the horizontal section, steam can flow through the corresponding loop to the break and can also push the water in the upward vertical part off the LS toward the cold leg. An additional steam flow path from the core to the break is generated in this way. This effect is called “LS clearing.”

As a consequence, the differential pressure between the UP and the DC decreases and the core and DC water levels equalize. A potentially preceding core uncover may be terminated in this way. This effect can be supported by additional displacement of water from the LSs to the DC and to the core. The described phenomena could also be observed in a PKL test simulating a SB-LOCA transient as shown in Fig. 8.15. Core uncover occurred before LSC (situation 2). Due to the relative high pressure difference between the UP and the upper DC the core level was “suppressed.” With LSC and subsequent pressure equalization between UP and DC, water from the DC and the LS was displaced into the core and the core cooling was reestablished.

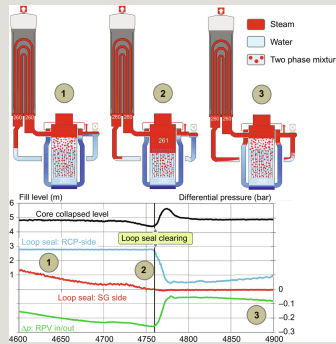
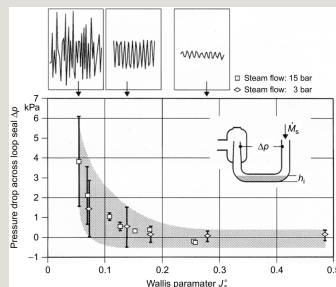


Fig. 8.15 PKL test on loop seal clearing.

Insofar LSC is an issue related to core uncover/recovery in SB- and IB-LOCA transients. The occurrence of LSC in relation to the occurrence of core uncover is mainly determined by the difference in elevation between the top of the core and the horizontal part of the LS. The timing, the dynamic of LSC as well as the number of loops involved in LSC are depending on additional parameters such as break size, and flow resistance via UP—DC bypass and by the operation of the SG secondary side (e.g., cool-down rate). LSC may also be influenced or even initiated by injection of ECC water into the cold legs causing condensation at the injection location.

In addition, SETs on LSC were performed in the 1:1 scaled UPTF in a single loop configuration in order to investigate the residual water level, the flow pattern, and the pressure drop across the LS during and after its clearance (Liebert and Emmerling, 1998). As an example, Fig. 8.16 shows the pressure drop across the LS for varying steam flow without droplet entrainment for two pressure levels. The amplitudes of differential pressure for three different steam flow rates are also illustrated.



8.4.2.4 Flow reversal in SG U-tubes

NC plays an essential role in decay heat removal for a number of operational transients and accidents in PWRs characterized by loss of forced circulation in the primary system. Loss of forced circulation occurs under loss of off-site power conditions (RCPs are no more available) or due to automatically or operator initiated shut down of the RCP, e.g., in case of LOCA. Under NC conditions decay power is transported from the core (heat source) to the SGs (heat sink) at flow rates that are significantly lower than the flow rates in normal (forced flow) operation (in the order of some percent, e.g., core flow rate in NC conditions: about 600 kg/s, for forced flow: about 20,000 kg/s).

The driving forces for NC are the temperature/density differences in the RPV between the DC and the core region and in the SGs between the inlet and the outlet side. In steady-state conditions the NC flow mass flow rates in the individual loops are adjust in a self-regulating way so that the driving forces are equalized by the irreversible pressure drops due to friction and local flow resistances. The performance of the SGs in general, and the individual U-tubes in particular, is of great importance for the overall system behavior under NC. The flow behavior of the individual U-tubes is a rather complex mechanism, mainly because of the following two aspects:

- The relatively low driving forces between the inlet and outlet plenum of the SG, typical for NC conditions.
- The existence of parallel flow channels between the inlet and outlet plenum of the SG comprising several thousands of U-tubes with different lengths.

Extensive investigations on the flow behavior in the SG performed in integral test facilities over the last decades revealed heterogeneous flow distribution among the U-tubes for many NC situations. In these tests, flow reversal was observed in some U-tubes leading to a flow from the SG outlet to the SG inlet plenum in such tubes while at the same time other U-tubes still experienced forward flow from the SG inlet to the SG outlet plenum. This heterogeneous behavior was observed under single and two-phase flow conditions and also in the transition phases from two-phase flow to reflux condensation and from reflux condenser conditions to the restart of two-phase NC. Fig. 8.17 shows a typical situation with heterogeneous flow behavior for single-phase NC. In the illustration, the short and medium tubes

represent U-tubes with forward flow and heat transfer from the primary to the secondary side mainly on the lower part of the inlet side. The long U-tube represents U-tubes with reverse flow. In such tubes the temperatures over the entire lengths correspond to the secondary side and there is almost no heat exchange between the primary and secondary sides.

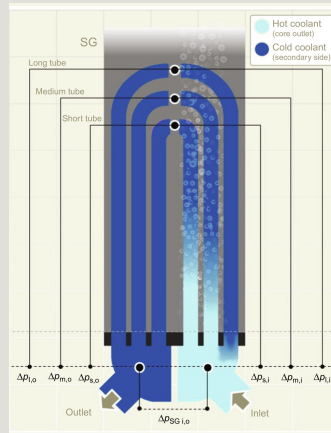


Fig. 8.17 Heterogeneous behavior in SG U-tubes (forward and reverse flow).

In the experiments the use of temperatures measured inside different U-tubes along the tubes' lengths is an appropriate method to detect the flow direction in these tubes. If a tube is subject to continuous forward flow, it displays a temperature profile that decreases from the primary side temperature at the tube inlet to the secondary temperature toward the outlet. In contrast, an equalization of the primary and secondary temperatures along the active length (no temperature profile) is an indication for flow stagnation or flow reversal.

As an example, Fig. 8.18 shows the time trends of primary side temperatures on the inlet sides of two different U-tubes of the same SG observed in a PKL experiment during a phase with steady-state single-phase NC conditions. While the evolution of the temperatures in tube 2 reflects continuous stable forward flow, the temperature drop of the primary side temperatures down to the secondary temperature is a clear indication for the interruption of forward flow in tube 1. The change in flow distribution within the SG is also reproduced by a change in differential pressure between the SG inlet and outlet plenum and a slight reduction in loop mass flow rate.

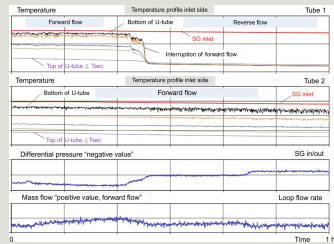


Fig. 8.18 PKL test on NC.

In NC conditions with heat transfer from the primary to the secondary side the pressure difference between the inlet and the outlet plenum is normally negative (the outlet pressure is higher than the inlet pressure). This results from the difference in gravitational heads between the down flow side (cold) and the up flow side (hot) which generally exceeds the frictional and local pressure drops along the tube at low flow rates typical for NC. At higher flow rates the frictional pressure drop exceeds the gravitational component and the resulting pressure difference over the SG reaches a positive value.

Assuming that the pressure difference between the inlet and outlet plenum is the same for all U-tubes, a negative value in NC conditions means that in tubes with no temperature profile (difference in hydrostatic head is zero) flow reversal is expected to be established in these tubes. In general, the flow behavior in the individual U-tubes is the result of the balance of the different pressure drop components including frictional, local, acceleration, and gravitational pressure drops in different U-tubes. Because of the composition of the different pressure components and the interaction between the parallel connected U-tubes the “normal” forward flow in some tubes may be disturbed, e.g., by a change in the boundary conditions. In the above mentioned PKL test, a slight change in the secondary pressure was the reason for the termination of the forward flow at least in one (of 28) U-tube.

Also mathematical models and solutions using the characteristic flow curves (differential pressure over mass flow rates) for forward and reverse flow in single U-tubes based on momentum and energy balance equations have been developed by several researchers (see also Chapter 5 and 11 of the book) with the attempt to interpret/confirm the observed heterogeneous flow behavior in the U-tubes, to demonstrate the required conditions for reverse flow and to identify the preferred U-tube positions for occurrence of reverse flow. More details on the applied

methods can be found in the corresponding literature.

It has to be mentioned that despite the possible occurrence of flow stagnation and flow reversal in some U-tubes in NC conditions, the overall net forward flow will always remain stable as long as the corresponding SG is available as heat sink. The impact on the overall heat transfer is also rather small as the loss of heat transfer in the tubes with reverse flow is compensated by the increasing heat transfer in the tubes with continuous forward flow (the SG are designed for much higher load). However, the total mass flow rate through the SG and therefore also through the core may be reduced as result of reverse flow in some U-tubes. This again leads to a higher core outlet temperature. In order to address this aspect in code calculations, the application of multitube modeling is of importance. It has to be noted that the flow behavior in the U-tubes may be even more unstable and more heterogeneous under two-phase flow conditions. Heterogeneous water/steam distribution at the tube sheet with preferred steam supply to some tubes may promote the heterogeneous flow behavior in the individual U-tubes.

8.4.2.5 Stability in boiling channels

Focus is given in this section to the qualitative role and the importance of pressure drops in the characterization of stability of fluid systems (single- and two-phase).

Currently, there are more than 80 BWR operating all over the world that provide an important contribution to the overall electricity supply from the nuclear source. The water boiled in the core produces steam that is directly used to rotate the turbine(s), thus constituting the simplest industrial system built so far that is suitable to transform fission power into electrical power. However, fundamental aspects concerned with the interaction between SYS TH and neutron kinetics obstructed or delayed (or made less effective), so far, the exploitation of this type of reactor concept. The BWR stability issue (D'Auria et al., 1997a,b) caused in the past a number of concerns and requested specific attention by technologists and researchers.

The classification of instability mechanisms provides an idea of the topic.

Different classifications can be found in the literature. These can be based upon: (a) fundamental mechanisms, (b) pattern of core oscillations, and (c) system interactions.

(a) Classification based upon thermal-hydraulic fundamental mechanisms
The static instabilities are:

- flow excursion (Ledinegg type);
- boiling crisis;
- relaxation types, including flow pattern transition, geysering, and chugging.

The dynamic instabilities are:

- density wave oscillations;
- pressure drop oscillations;
- acoustic oscillations;
- thermal oscillations.

(b) Classification based upon geometrical features of the oscillations

In this case the relationships between phases and amplitudes of the waves at different axial and azimuthal positions in the core of a reactor or of a reactor simulator are considered. Coupled neutron physics/thermal-hydraulic and pure thermal-hydraulic oscillations can be distinguished, respectively. The following classification results:

- core wide or in phase oscillations;
- regional or out-of-phase oscillations;
- single channel or local oscillations;
- punctual or not propagating oscillations (their existence can only be envisaged from the performed activity and considered documentation).

Most of the phenomena above can be explained making reference the concept of “harmonic modes” of the reactor diffusion equations.

(c) Classification based upon system design

This classification is valid primarily for coupled nuclear-thermal-hydraulic systems (BWR plants), but may occur also in pure thermal-hydraulic systems. The overall system performance and the origin of oscillations are concerned. The following classification can be introduced:

- oscillations involving core-bypass;

- oscillations involving vessel DC;
- oscillations involving the entire primary loop (also referred as loop type oscillations);
- oscillations induced by the Balance of Plant, including the control systems.

The analysis of instability phenomena may constitute a multidisciplinary subject, involving different technological areas like transient thermal-hydraulics, neutronics, fuel behavior and fuel cycle management, instrumentation, plant control and monitoring, and detailed knowledge of plant features and operating conditions.

A wide literature exists in this area, see, e.g., Ishii and Zuber (1970), Yadigaroglu and Chan (1979), D'Auria et al., 1997a,b, Vijayan (2002), and D'Auria et al. (2016). Hereafter there is no intention to duplicate the information in reports and papers devoted to the stability either in BWR and/or in boiling/condensing systems. However, it seems worth mentioning that the measurement, the modeling, and the prediction of pressure drops have a key role in this area. Sample reference data for pressure drops during stability events are given in Figs. 8.19 and 8.20: these constitute typical diagrams adopted to characterize the stability performance of a system. Change of sign or passing from positive to negative value for pressure drops (Figs. 8.19 and 8.20) implies occurrence of flow reversal. Amplitudes and frequency of pressure drop oscillation (Fig. 8.19) correspond to amplitude and frequency for mass flows.

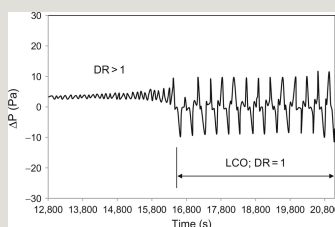


Fig. 8.19 Characterization of an instability event: pressure drop versus time (Vijayan, 2002).

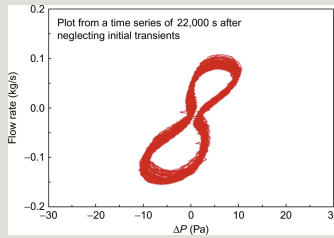


Fig. 8.20 Characterization of an instability event: pressure drop versus mass flow rate (Vijayan and Nayak, 2012).

8.5 Modeling of pressure drops and applications in TH system codes

8.5.1 SYS TH code modeling

SYS TH codes constitute the tip of the pyramid of knowledge in nuclear thermal-hydraulics as discussed in different chapters of the book. Insight into the code modeling can be found in Chapters 5, 10, and 11), including the modeling for pressure drops (i.e., the momentum equations). A few comments about modeling features are provided hereafter rather than insights into the features (noticeably including numerical aspects) of the pressure drop models.

8.5.1.1 Wall friction

Making reference to the Relap5 code, the wall friction model consists of two main parts:

- Computing the overall two-phase friction pressure drop,
- Apportioning the total wall friction into liquid and vapor components.

The wall friction model is based on a two-phase multiplier approach calculated from the HTFS-modified Baroczy correlation, which is independent of flow regime. The individual phasic wall friction components are calculated by apportioning the two-phase friction between the phases using a technique derived by Chisholm from the Lockhart-Martinelli model. The calculated phasic factors depend on flow regimes. Comments are as follows.

- Notwithstanding highly (or relatively) sophisticate mass, momentum, and energy

balance equations, i.e., the so called unequal velocities, unequal temperatures or, six partial-derivative set of equations, single-phase and two-phase pressure drops are based upon empirical correlations (basically those discussed in Section 8.3) developed during the 60s.

- The process “of apportioning” mentioned above implies that one overall data (typical the total friction pressure drop available from experiments) is split into two or more components, according to the structure of the balance equations. In the majority of the conditions of interest there is no possibility to estimate the correctness of, i.e., to validate, the apportioning process.
- Pressure drops are highly dependent upon flow regimes: flow regimes are highly dependent upon geometry and upon the condition of fully developed flow. In the case of large diameter pipes (up to around 1 m) like those constituting the hot legs and the cold legs of RCS in PWR, experiments in two-phase conditions have not been performed. Necessarily simplified flow regimes are considered in modeling which are derived from small scale experiment (scaling issue occurs as discussed in Chapter 13 of the book).

From the view point of the code user (or analyst) one may add what follows:

- *Roughness*: the related value must be supplied by the analyst and may not constitute an available data for the system to be simulated by the code; furthermore, roughness may vary during the lifetime of the system, e.g., due to corrosion, erosion oxide formation, and crud deposit.
- *Equivalent diameter*: the related value must be supplied by the user; an engineering formulation is available which is directly connected with simple geometry without possible three-dimensional effects; the value of equivalent diameter is therefore used to adapt results of code prediction, noticeably pressure drops, to measured data if available; the process is prone to some arbitrariness from the side of the code user: the fixed value for equivalent diameters also impact the calculation of heat transfer coefficient in the concerned region.

One may summarize that modeling for distributed friction pressure drops is part of the code and user effect is restricted to the (sometimes unknown) values of roughness and equivalent diameter.

8.5.1.2 Form losses

Losses due to abrupt area change are calculated using form loss models and are originated by geometric discontinuities already discussed in this chapter.

Noticeably, connection between pipes (relatively small diameter) and plena (relatively large diameters), changes of direction of flow in plena and entrance-exit of a plate (e.g., the core support plate) are characterized by form loss coefficients which constitute input for the code.

Dependency of K factor upon Re (or fluid velocity) is typically allowed in correlations to be supplied by the code user; however no dependence for K factor is envisaged in available models upon void fraction. Comments are as follows.

- The first two bullet items in the previous paragraph, i.e., current sophistication level of modeling and apportioning procedure, also apply here.
- K factor values (very) strongly depend upon details, e.g., rounded or sharp edge, which are not available in all locations of a RCS in water cooled nuclear reactors.
- At every discontinuity, whatever is its geometric complexity, different flow situations may occur, namely in two-phase conditions: cocurrent flow of steam and liquid (with steam and liquid flow configurations affected by flow pattern determined by upstream conditions), countercurrent flow of steam and liquid and flow reversal (i.e., liquid and steam flowing together in a direction opposite to the direction which characterizes the nominal operating conditions of the RCS).
- With the partial exception of core region in all water cooled reactors and the SG tube region in PWR, local pressure drops constitute the largest part of total pressure drops in RCS at any time during a transient. (*Note: partial exception in core region is introduced because of the importance of bottom, top, and spacer grids as far as the total pressure drops in the core are concerned.*)

From the view point of the code user (or analyst) one may add what follows:

- It is responsibility of code user to supply suitable data for K factors as calculation input parameters: unavailability of data (typical situation) should correspond to the execution of proper sensitivity and uncertainty analyses (this is not always possible).
- The user must consider the existence of possible large differences between direct and reverse K factors values.
- CFD codes may provide a valid support to the analysts for a systematic estimation of K factors at any geometric discontinuity (Chapter 12 of the book) although the related results are not immune by errors.

So, one may expect highly approximate calculation results: the degree of approximation changes with void fraction. Even larger impact of K factors upon calculation results may be expected if one considers the combination of fluid velocities and void fraction.

One may summarize that modeling for local pressure drops is not part of the code and user effect is decisive for attaining reasonable results from code applications.

8.5.2 Pressure drops and steady-state qualification of computational model

Establishment by code user of a correct steady-state conditions in terms of pressure (based on pressure drops) along the loop constitutes a mandatory prerequisite for the prediction of any transient scenario and of NPP performance. Acceptable errors are proposed by Bonuccelli et al. (1993). An example of current situation is discussed in the following, based upon a code application activity performed within an international framework in 2006 (Petruzzi et al., 2006).

The calculated normalized (respect to the hot leg inlet position) pressure distribution curve versus loop length related to the LOFT nuclear facility, are shown in Fig. 8.21. The activity was performed by a dozen groups of analysts using different SYS TH codes; it constitutes the second phase (of six) of the OECD/NEA/CSNI BEMUSE project, see also Glaeser et al. (2011). The following considerations apply:

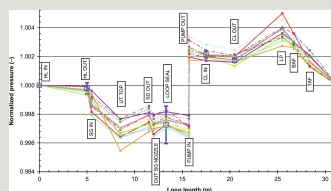


Fig. 8.21 Comparison of normalized pressure curves along the loop, BEMUSE phase II.

- Almost all calculated values are inside the uncertainty experimental bands in correspondence of the hot leg outlet position and of the LS;
- In correspondence of the cold leg inlet and outlet positions, the major part of the calculations fall outside the uncertainty bands;

- The positions characterized by a large discrepancy among the calculated results of the participants are: (a) the SG U-tubes top elevation, (b) the pump inlet and outlet, and (c) the lower plenum. No experimental value was available for those locations.

Not surprisingly large differences were observed in the comparison among various calculated data (as well as in the comparison between experimental data and code calculation) for the concerned LB-LOCA. Full documentation available by Petruzzi et al. (2006) (see also de De Crécy et al., 2008).

8.5.3 Pressure drops and pressure drop predictions/measurements during transients

In nuclear thermal-hydraulics pressure drops during a transient do not necessarily imply transient pressure drops or time-acceleration pressure drops. Namely, quasi steady conditions and related assumptions can be used to predict and to characterize pressure drops during most of the design basis accident (DBA) scenarios in NPPs as discussed in **Chapter 15** of the book. Fast changing conditions which require consideration of time acceleration pressure drop occur, for instance, in the initial tenths of seconds of LOCA, or in case of control rod ejection (CRE) event part of reactivity initiated accident (RIA).

A sample list of items connecting pressure drops and pressure drop predictions with transient conditions in NPP is provided below not in an order of importance. In this case the word transient refers to accident scenarios in water cooled nuclear reactors within the DBA category and to simulated accident scenarios in ITF.

- LS. The LS is the U-shaped part of the cold leg in PWR upstream the main coolant pumps (MCPs). The elevation of the horizontal axis of the LS is lower than the elevation of the top of active fuel (TAF) for the core. This induces the possibility of formation of a plug of liquid in the LS during accident scenarios. The plug formation constitutes a seal for the coolant flowing in the loop, hence the name LS. The depth of the LS vertical part is close to 1 m. LSC may induce level recovery in the core and in some case quenching of a previous dry-out condition. Measurement of pressure drop across the vertical part provides the information about the LS status and possible clearing occurrence.
- Bypass. Several bypass flow-paths inside the vessel of a PWR play a role primarily in case of SB-LOCA. Pressure drop measurements indicate the direction of the flow and may contribute to determine bypass flow rate.
- Flow reversal. Direct flow at any location in the primary system of either a PWR

or a BWR is connected with nominal operating conditions. However, flow reversal may occur almost anywhere in the circuit during transient conditions. The predictability of flow reversal (i.e., very important to calculate system performance in case of transients) is connected with the knowledge of related loss coefficient at abrupt discontinuities. Those coefficients may be different from “direct” coefficients at the same location and their value may reveal (much) more uncertain than the value characterizing the direct flow.

- Stability of single-phase and two-phase or boiling condensing systems. In addition to BWR stability mentioned in Section 8.4.2.5, flow oscillations, thus stability issues, are expected in one- and two-phase NC conditions in PWR (see also Chapter 15 of the book). Namely it is well established that selected groups of U-tubes in SGs may experience flow oscillations including flow reversal, thus reducing the overall transit flow area for the coolant in the core. Pressure drops are the key indicator of this phenomenon.

- Emptying and filling and DC level (SG and RPV in PWR and RPV in BWR). Change of level, namely in the PRZ of a PWR, implies changes in the dynamic response characteristics of the overall system. Empty or overfill PRZ signifies loss of control capacity for the pressure in the system. The knowledge of narrow range and wide range level in SG and in RPV of BWR allows the control of the core power. Pressure drop signal is used for detecting level.

- Advancement of quench front. Specifically in case of LOCA in either PWR or BWR, core uncover is expected which must be followed by proper recovery mainly governed by level rise in the DC of the vessel. Then quench front advancement is detectable by pressure drop measurement.

- MCPs. Values of head of MCP as well as of head during MCP rundown (coast-down) and of head in locked or free rotor conditions constitute essential parameters affecting the coolant flow in the core. Related pressure drop measurements are essential for determining the system response in case of transients.

- Sump recirculation and core pressure drops. Long-term cooling implies containment sump (PWR) or pressure suppression pool recirculation (BWR). In both cases “small” debris accumulated in the bottom of the containment may pass through filters and recirculation pumps and may produce partial core blockage. Ballooning of fuel rods may also cause partial core blockage. Cross-correlating pressure drop signals in different regions of the vessel may allow detection of core blockage. Related techniques may need to be developed.

- Measurement issue. At least three issues must be carefully addressed for a qualified transient pressure drop measurement:

- The absolute value for the range of variation expected for pressure drop measurement may be several orders of magnitude lower than the absolute pressure acting in the system at the location of pressure drop transducer terminals (i.e., the port connecting the measurement pipeline and the concerned “high” pressure system).

- The distance between the location of pressure drop transducers and the terminals (or taps) is typically of the order of several tens meters. A small (typically 5–10 mm internal diameter) measurement pipeline (hereafter called pipeline) connects the terminals with the pressure transducers. Usually bends and U-configurations cannot be avoided. Filling of the pipeline by incompressible fluid must be ensured by proper actions before the start of the transient (e.g., experiment in ITF).

- Very small leakages in the pipelines, gas liberated from liquid inside the pipelines when the absolute value of the system pressure decreases, initially undetected gas bubbles, regions of high fluid temperature in the pipe such that liquid flashing may occur when the absolute value of the system pressure decreases, may produce unqualified pressure drop signals with very few possibilities to detect the failure or to recover the right signal.

The provided overview confirms the role and stresses the importance of pressure drops in nominal and transient operation of water cooled reactors: pressure drops are not measured in all cases in NPP; however, predictive capabilities for pressure drops must be ensured in all cases and, in all cases, pressure drops are measured in ITF.

8.6 Measurement techniques

The measurement of pressure drops constitutes the focus for this chapter. Here one may state:

(a) measurable quantities exist which are derived from pressure drop type of measurement (e.g., liquid levels);

(b) quantities can be measured which are directly connected with pressure drops (e.g., fluid velocities and mass flow rates).

Techniques are considered hereafter dealing with quantities in categories (a) and (b), in addition to direct measurement of pressure drop. Furthermore, measurements in experimental loops (or test facilities) are distinguished from measurement adopted in NPP. Namely key measured quantities connected with pressure drops are:

- In test facilities: local pressure drop; collapsed level/swell level; void fraction; density; mass flow;
- In NPP systems: RPV level/loop level; Δp over MCP; mass flow.

Hereafter some comments are provided to the current state of the art in performing pressure drop measurement rather than discussing (important) details of experimental techniques including techniques for interpreting raw data from transducers. When considering the issues (or measurement drawbacks) in forthcoming sections the complexity of measurement should be considered (high temperature, high pressure, and presence in the case of NPP of radiation fields).

8.6.1 Direct measurement of pressure drops

Reference is made to direct measurements for pressure drops in ITF and in NPP. The typical configuration of interest below is constituted by two pressure taps connected by two hydraulic lines to two terminals of a pressure transducer. Pressure transmission lines have a diameter of 6–8 mm and are filled by incompressible fluid, typically liquid water. It must be ensured that liquid does not vaporize at the contact with the high temperature fluid and that (reasonably) noncondensable gases are not present to form bubbles or even are not dissolved in the fluid. Dissolved gas in the fluid (as well as steam produced at the interface between measuring liquid and hot process fluid, and gas produced during a depressurization process) may heavily affect the measured values.

8.6.1.1 Distributed (friction and acceleration)

The presence of gas or vapor in the transmission line is one reason of concern for the quality of measurement: this is also connected with the length of pressure lines (up to several tens meters) and to the many elbows and curves necessarily part of the construction of those lines. The main additional issues which may cause measurement errors for distributed friction pressure drops (acceleration pressure drops issues can be inferred as a consequence) are:

- Static pressure target. The goal of the measurement is the static pressure in the majority of cases; problems may arise because of possible influence of dynamic

pressure, e.g., caused by imperfectly aligned pressure taps.

- Elevation pressure drops. It is necessary to separate the contribution of elevation pressure drops: this is not straightforward (see also below) when two-phase flows are involved.
- Compressible fluids including two phase. It is necessary to separate the contribution of (spatial) acceleration pressure drop: this is not straightforward (see also below) when two-phase flows are involved.
- Two-phase conditions. An interpretation model is needed to estimate the average void fraction between the two taps. The model is necessarily imperfect and its quality depends upon the flow regime experienced by the process fluid.
- Long piping for transmitting pressure drop signal may generate errors in measurement in very fast transients in addition to errors possibly originated by the presence of gas or steam.

8.6.1.2 Local or at geometric discontinuities

The issues described for distributed friction pressure drops also apply to the measurement of local pressure drops at geometric discontinuities, e.g., signals used to characterize the K factors. In addition, the following issues are specific for local pressure drop measurements:

- Irreversible portion-1. Any local pressure drop implies the occurrence of a total pressure drop which is formed by a reversible and an irreversible portion. Only the irreversible portion is of technological interest and contributes to the K factor. Typically, the total pressure drop occurs immediately downstream the geometric discontinuity: the reversible portion brings to a recovery in pressure at some distance downstream. The value of the “distance downstream” causes the issue: the distance is not known and depends upon the geometric configuration and the flow conditions.
- Irreversible portion-2. The measurement of the “distance downstream” is troublesome and is possible only in selected reference situations. Hence unavoidable error must be expected from measurements.
- Special geometry. Local pressure drops also occur inside plena, e.g., lower plenum or UP in case of PWR RPV. In those situations it is impractical to install transducers along the actual flow path of the fluid. This gives origin to a hidden error when attempting to simulate fluid flow behavior in those conditions.

8.6.2 Quantities connected with pressure drops

Pressure is a scalable physical variable, which describes the force on a unit of area.

Together with the measurement of temperature, the measurement of pressure is one of the first and most used measurements in science. Pressure measurement, which is one of the so-called “conventional measurements,” continues to play a central role in the detection and recording of flow processes in thermohydraulic systems. In nuclear engineering this not only applies to detection and recording of the processes in the nuclear plants themselves but also to the test facilities used for analysis and modeling important thermohydraulic processes.

In practice the pressure at certain measuring points in the system to be investigated is forwarded to a sensor via pressure tapping points and so-called pressure sensing lines. The sensor responds to the pressure exerted on it or pressure difference with a displacement or deformation (e.g., a diaphragm). The deformation is converted via appropriate sensors (capacitive, inductive, etc.) into electrical signals proportional to the differential pressure.

Due to this measurement principal, pressure measurements generally give a pressure difference between two points or the difference in pressure between a measurement point and a reference pressure.

If the reference pressure is zero (i.e., complete vacuum) the measured value corresponds to the so-called absolute pressure, if the reference pressure equals the atmospheric pressure, the measured pressure difference corresponds to the so-called overpressure (aka positive or gauge pressure) at the measuring point concerned. However, if both measuring points are located within the system, the measurement registers the pressure difference between these two points, i.e., the pressure drop along the flow path which is mainly of interest later.

As described in Section 8.2, the total measured pressure drop is made up of several components including gravity, acceleration, and pressure losses.

$$\alpha = \frac{\Delta p_a}{\Delta p_s + \Delta p_a} \quad (8.18)$$

where Δp_s is the pressure drop due to static head. Δp_a is the acceleration pressure drop due to change in flow velocity along the flow path as a result of change in cross-sectional area or change in density. In nonsteady-state processes another term

is added to this convective acceleration, which expresses the local acceleration over time.

Under certain conditions or if certain influencing factors are ignored, the differential pressure measurement can be used not only to determine the permanent pressure loss, but other important physical variables can also be derived, such as

- Level (swell level/collapsed level)

- Mean fluid density

- Mean void fraction.

In steady-state flows of incompressible fluids in flow paths with constant cross-section, the acceleration term is omitted completely. For horizontal flows the head component of Eq. (8.18) is also omitted and the measured differential pressure in fully developed flow is the remaining pressure loss in the flow path ($\Delta p_f + \Delta p_e$).

8.6.2.1 Filling level

Using the static pressure of water columns to take differential pressure measurements of the water filling level or water reserves is a common method used both in nuclear plant and also associated testing systems. If tanks are filled with water and steam (idle system) and the two phases exist in a separated form, the differential pressure measurement is a simple and very precise method for determining the filling level; this method requires knowledge of the densities of the two phases (e.g., by means of additional absolute pressure and temperature measurements). The water filling level can be determined via the following designation.

Wherever there are high pressure levels, the static pressure of the steam can no longer be neglected and should be taken into account when determining the water filling level.

8.6.2.2 Collapsed level

It is not possible to directly determine the swell level (separation between two-phase mixes with a predominant steam proportion) by measuring the differential pressure alone; additional measuring information is required. However, conducting several differential pressure measurements in succession can pinpoint the position of the swell level to at least a segment of the corresponding differential pressure measurement. Also, if the mix level changes (increase/decrease), it is possible to at

least trace the trend of the temporal progression of the mix level. For instance, usually information can be derived from the Δp measuring signal curve about the passing of the swell level at a pressure removal point and therefore the transition to a predominant steam proportion within the associated Δp measurement (when the swell level decreases).

If a measuring range section is completely filled with a two-phase mix and if the water and steam density is known, it is possible to derive from the measured differential pressure a constant assumed mean density of the mix or the mean *void fraction*.

Strictly speaking, these considerations only apply to states or processes in which the pressure drop can be neglected due to dynamic effects (e.g., wall friction, two-phase friction).

This usually also applies to flow conditions in which a specific steam quantity flows from bottom to top through standing water in tanks or vertical pipes.

The proportion of the pressure loss (due to friction) of the measured differential pressure can be neglected, especially in small steam mass flows and higher pressure levels compared to the height (head) component. Generally, the height (head) component can be determined by also measuring the volumetric steam proportion using special two-phase measuring equipment (see below, *will be included*). The pressure loss proportion is the difference between the measured differential pressure and the height (head) component determined by measuring the steam content.

8.6.2.3 Practical applications for differential pressure measurement in NPPs

Absolute pressure and differential pressure measurements are, in combination with the temperature measurements, the main measuring methods used in nuclear plants, and are used both as operating instruments and for incident instrumentation purposes. For instance, differential pressure measurements taken via MCPs in the BWR not only supply information about the number of operational pumps, but are also used to determine the loop flow rate using the pump characteristic curve, as well as helping to protect the aggregates. During commissioning tests, pressure loss measurements via other plant parts are taken in some cases to obtain an overall picture of the total pressure loss and establish the status of individual plant components; they are also used to confirm computed values upon which the plant was designed.

8.7 Envisaged development in the area of pressure drops

The phenomena associated with the loss of pressure along with those associated to the heat exchange gave rise to major technological problems since the advent of thermal machines in the 18th century (the identification and the characterization of pressure drops and heat transfer mechanisms came much earlier during the human civilization history), as already discussed in the book, see also D'Auria (2012). Furthermore, within the areas of pressure drops and heat transfer a tight connection exists between theoretical modeling and the actual configuration of the systems.

Insights addressing the above statements can be found in this chapter and in other parts of the book. Furthermore, Reynolds, Moody, Colebrook, Darcy, Idel'chik, Martinelli, Nelson, etc. (see also **Chapter 1** of the book), are eminent scientists whose name is associated with the calculation of pressure drops.

The target for this section is to identify directions for possible improvements in the knowledge in the area of pressure drops.

Looking at the future may take benefit from the view of the past. A few sentences from the well-known, more-than 500 pages, Idel'chik Handbook (Idel'chik, 1960) are reported:

There is, almost no branch of engineering which is not somehow concerned with the necessity of moving fluids through pipes, conduits, or machinery. The degree of complexity of a hydraulic or gas-air line can be quite varied. In some cases these are largescale systems of pipes, gas mains, water conduits, steam pipes, air ducts, etc., while in other cases these are pipelines of relatively small length, but having a large number of fittings and branches, various obstructions such as throttles and adjusting devices, grids, protruding parts, etc. ... Until recently only restricted data were available on the subject, and these were scattered among various textbooks ... and in scientific papers. In many cases these data are contradictory or dated, and deal with only a limited number of local resistances. Furthermore, the coefficients of local resistances generally were given only for special geometric and physical

characteristics. In order to fill this gap, in 1954 the author published a book ... We present here in the same spirit this special handbook on the local fluid and friction resistances.

The writing of this handbook presented considerable difficulties, mainly due to the range of local resistances, their geometric boundaries, and the states of flow in them, which are much narrower than required by practice. Furthermore, much of the data obtained is insufficiently accurate and reliable; this is particularly true of the coefficients of local resistances. Therefore, it would have been better to delay the publication of this handbook until all coefficients of local resistances could have been checked and refined experimentally by some standard method, based on the contemporary level of metrology. Unfortunately, it seems unlikely that such a series of experiments would be completed in the near future.

Those words are perfectly true today, after more than half a century. Namely:

- more experiments have been done, but their number is still much less than needed with reference to the geometric and operating conditions of Water Cooled Reactors, specifically if two-phase conditions are concerned; errors, which are not always documented, are the result of experiments; measurement errors are expected to be larger in two-phase conditions;
- computational fluid-dynamic codes have been made available which, at least in single-phase conditions could be used to determine “all coefficients of local resistances,” but, errors in computed results (a bit less than $|10\%|$ of the actual value) may reveal higher than precision needs; and
- precision targets from the side of nuclear plant designers or safety analysts have not been fixed: these could be a function of Re number and void fraction and could be less than $|1\%|$ of the actual value, i.e., 10 times below established computational capabilities, and possibly much below attainable accuracy from experiments.

As defined above is the context in which an attempt is made to identify some lines of development in the evaluation of pressure losses.

8.7.1 Extension of experimental database

A nonexhaustive list of key words connected with pressure drops (PD) includes:

- Laminar or turbulent;
- Fully developed flow or nondeveloped flow;
- Transient or steady state and acceleration (in space or in time);
- Compressible or incompressible fluid;
- Single- or two-phase and (in case of two phase) two-fields or multiple fields;
- Distributed (friction) or local (i.e., at geometric discontinuity);
- Wall roughness;
- Sharp or smooth edge (in case of geometric discontinuity);
- Viscosity of fluid, Newtonian and non-Newtonian fluids;
- Velocity profile (single-phase flow) or fluid velocities and void fraction profile (two-phase flow).

The items above can be used for the design of new experiments and for planning developments in the area: (a) to identify affecting variables-parameters and related ranges; (b) to build one multidimensional table or several tables covering the identified topics and the ranges of relevant parameters. It is also clear that the characterization of items or conditions like “nondeveloped flow,” “viscosity,” “level of smoothness,” etc., may require an infinite variety of situations. In this case an attempt should be made to group the envisaged situations into a manageable number.

It is beyond the objective for the present book to pursue either the targets (a) and (b) mentioned previously. To this aim, groups of experts from nuclear regulators, designers, and scientific institutions involved with thermal-hydraulic programs should be convened. Here in the book the importance for such an activity is recognized and some guidelines are further provided in Section 8.6.2 in relation to specific topics.

8.7.2 Development in the area of two-phase flow modeling

It is clear from the picture given in the entire chapter and from the snapshot views of previous sections that two-phase flows deserves or is expected to deserve the largest attention as far as possible developments in the area of pressure drops are concerned.

Experimental and modeling researches in the 60s, even before the advent of computers, demonstrated the existence of a situation as depicted in the sketch of Fig. 8.22. Under the condition of equal mass flow rate (i.e., kg/s) the friction pressure drops for liquid get a value much lower than in the case of steam (or gas) pressure drops. The two-phase pressure drop curve is assumed to follow a trend bounded by the two curves relating to single-phase conditions. Furthermore the two-phase curve does not show up a monotonous trend and the well-known Ledinegg instability is expected.

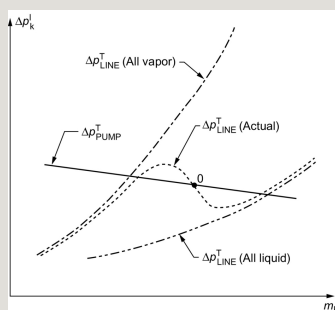


Fig. 8.22 Friction pressure drop in horizontal channel as a function of mass flow-rate for the single-phase (liquid and vapor) and two-phase conditions.

8.7.2.1 Expected-desirable developments

Significant examples of expected-desirable developments, without having the target of a systematic and comprehensive line of attack to the overall issue and assuming proper support from the execution of experiments, are:

(A) Related to distributed pressure drops. Substitution of the two-phase multiplier approach with an improved mechanistic approach where wall drag, interfacial drag, and flow regimes play the key role. Fluid velocities, void fraction, absolute pressure, and diameter-size (in addition to roughness and equivalent diameter) should be considered with suitable ranges of variations. The new approach should directly account for nondeveloped flow conditions.

(B) Related to local pressure drops. An attempt should be made first to distinguish among groups of situations: e.g., abrupt area changes in a pipe-like configuration, bends, branches, connection of pipes with reservoirs, changes in flow-path directions inside plena, component related, special situations like interface between jet pump and DC region in BWR. Then, for each group, key geometry related parameters should be identified. Then the fluid-dynamic parameters should be identified with suitable ranges of variations. Finally correlations, as far as possible of mechanistic type (i.e., considering balance equation) should be developed dealing with functional relationships between local loss coefficients and the parameters belonging to the different groups of situations.

8.7.3 Modeling improvements in TH system codes

System thermal-hydraulic codes, as discussed in Chapters 5, 9–11, 13, and 15 (balance equations, constitutive equations, special models, structure, validation, and application, respectively), constitute complex computational tools which can be imagined as repositories for the knowledge in different areas of thermal-hydraulics. This also applies in relation to the modeling of pressure drops.

The key issues related to pressure drop prediction within the validation process of SYS TH codes, i.e., comparison between measured and calculated values, appear to be:

- Lack of or insufficient information about the experimental error (e.g., experimental values are also needed to fix suitable steady-state conditions when transient calculations for closed loop are performed);
- Occurrence of nonfully developed flow conditions (within the code, these are dealt with by correlations developed or qualified for fully developed flow conditions);
- Lack or insufficient information about flow regimes or flow regimes changes;
- Need for the code user to supply information related to local pressure drop coefficients.

The first two issues apply to single- and two-phase conditions and the third issue is valid for two-phase conditions.

8.7.3.1 Envisaged developments

Traceable improvements for SYS TH codes imply resolving the listed issues even by considering the developments in the areas of experiments and two-phase flow modeling (Sections 8.6.1 and 8.6.2). Solution of the issue at the last bullet item (reduction of user effect), may bring to the need of creating a database for local pressure drop coefficients for NPP geometric conditions. In this connection, flow reversal conditions (whose consideration is essential to determine system performance in case of transients like LOCA) and component (MCPs, valves, separator dryers, accumulator lines, etc.) local pressure drops should receive proper attention.

8.7.4 Trends for CFD applications

CFD development is driven by a context much wider than nuclear thermal-hydraulics as also discussed in Chapter 12 of the book. CFD codes are widely used in various areas of nuclear thermal-hydraulics including design and safety aspects. CFD codes are also coupled with SYS TH codes and are used to support results of related calculations in selected fields. A snapshot picture connecting CFD codes and pressure drops in nuclear thermal-hydraulics can be given as follows:

(A) Validation studies (for CFD codes) focus upon three-dimensional phenomena like mixing of different fluid streams and characterization of local conditions, namely velocities densities or even void fraction when two-phase flows are involved; in a very few cases a check is made that pressure drops along the fluid paths are close enough to experimental data: in the majority of case are not even measured properly or available from experiments. Then, CFD computational tools can be found qualified in computing three-dimensional phenomena in case of some experiments without proving consistency with experimental data of pressure drops in the same experiments.

(B) CFD computational tools have the intrinsic and unique capability to predict pressure drops at geometric discontinuities: therefore it is also possible to predict the relationship between local pressure drop coefficients in various situations and Re number. As already discussed, this relationship constitutes an important input parameter for SYS TH codes.

Then, in some cases mesh convergence of CFD code results can be demonstrated as part of the adoption of best practice guidelines.

8.7.4.1 Envisaged developments

Envisaged developments for CFD codes in the area of pressure drops can be derived, as follows:

- First: precision targets which are consistent with current numerical capabilities and, possibly, with needs in nuclear thermal-hydraulics should be established, e.g., in relation to pressure drops.
- Second: capability to predict pressure drops in experiments dealing with any phenomenon, whatever one-dimensional or three-dimensional, item (A), mentioned previously, should be demonstrated. This must become a necessary part of CFD validation process.
- Third: systematic application of CFD codes to the prediction of local loss coefficients in the whole variety of situations of interest to nuclear thermal-hydraulics should be promoted. Prediction errors should be documented and, possibly, found to be lower than acceptable errors, item (B), mentioned previously. Mesh convergence tests should be documented together with guidelines for controlling or further reducing the errors.

8.8 Conclusions

The motivation for this chapter is the importance of the pressure drops in nuclear thermal-hydraulics and in reactor design and safety technology. The content of the chapter depicts the current status and the importance and the role of the prediction of pressure drops (or losses).

Furthermore,

- (a) Pressure drops are considered in all textbooks of thermal-hydraulics: selected, as far as possible, complementary information is provided in this chapter.
- (b) In the area of two-phase flow it is noted again that current modeling capabilities are based upon the two-phase multiplier approach, i.e., an averaged approach proposed and developed during the 60s, or before, in the previous century, i.e., at a time when computers did not exist and partial differential equations of two fluid models could not be handled.
- (c) Recommendation for the future and foreseen developments constitute the objective of Section 8.7 in this chapter and are not repeated here.

As a final remark, let's cite the recent paper by Yang et al. (2016), where the errors or differences between computational fluid-dynamic code predictions and experimental data relevant in nuclear technology (fuel bundle) are discussed: whatever is the CFD adopted model, errors which are inconsistent (i.e., too high,

basically larger than 10% the measured value) with the needs in nuclear thermal-hydraulics are found.

In relation to both the areas “CFD” and “two-phase system thermal-hydraulics,” the achievement of suitable or satisfactory (to the code user) predictions, e.g., in calculating mixing or transient scenarios, respectively, without the demonstration of adequate calculation of pressure drops is not acceptable.

References

- Agbodemegbe V.Y., Xu C., Akaho E.H.K., Allotey F.K.A. Correlation for cross-flow resistance coefficient using STAR-CCM+ simulation data for flow of water through rod bundle supported by spacer grid with split-type mixing vane. *Nucl. Eng. Des.* 2015;285:134–149.
- Aksan, S.N., D’Auria, F., Groeneveld, D., Kirillov, P., Saha, D., Badulescu, A., Cleveland, J. (Lead Authors), 2001. Thermohydraulic Relationships for Advanced Water Cooled Reactors. IAEA Tecdoc 1203, Vienna (A) (ISSN 1011-4289).
- Baroczy C.J. A systematic correlation for two-phase pressure drop. *Chem. Eng. Prog. Symp. Ser.* 1966;62:232–249.
- Bartosiewicz Y., Seynhaeve J.-M., Serre G. *Delayed equilibrium model and validation experiments for two-phase choked flows relevant to LOCA*. In: The 14th International Topical Meeting on Nuclear Reactor Thermalhydraulics, NURETH-14, Toronto, Ontario, Canada, September 25–30; 2011.
- Batta A., Class A.G. CFD analysis of pressure drop across grid spacers in rod bundles compared to correlations and heavy liquid metal experimental data. In: *Nucl. Eng. Des.* 2016. <http://dx.doi.org/10.1016/j.nucengdes.2016.08.040>.
- Blasius P.R.H. Das Ähnlichkeitsgesetz bei Reibungsvorgängen in Flüssigkeiten. *Mitteilungen über Forschungsarbeiten auf dem Gebiete des Ingenieurwesens.* 1913;131:1–41.
- Bonuccelli M., D’Auria F., Debrecin N., Galassi G.M. A methodology for the qualification of thermalhydraulic codes

nodalizations. In: 6th Int. Top. Meet. on Nuclear Reactor Thermalhydraulics, Grenoble (F), October 5–8; 1993.

Chisholm D. *The influence of mass velocity on friction pressure gradient during steam-water flow*. In: Proc. Thermodynamics and Fluid Mechanics Conf., vol. 182; Institute of Mechanical Engineers; 1968:336–341.

Chisholm D. Pressure gradients due to friction during the flow of evaporating two-phase mixtures in smooth tubes and channels. *Int. J. Heat Mass Transf.* 1973;16:347–358.

Chisholm D., Sutherland L.A. *Prediction of pressure gradient in systems during two-phase flow*. In: Proc. Inst. of Mechanical Engineers Symposium on Two-phase Flow Systems; Leeds, UK: Univ. of Leeds; 1969.

Cicchitti A., Lombardi C., Silvestri M., Soldaini G., Zavattarelli R. Two-phase cooling experiments: pressure drop, heat transfer and burnout experiments. *J. Energ. Nucl.* 1960;7:407–425.

Colebrook C.F. Turbulent flow in pipes, with particular reference to the transition region between the smooth and rough pipe laws. *J. Inst. Civil Eng.* 1939;11(4):133–156.

Colebrook C.F., White C.M. Experiments with fluid friction in roughened pipes. *Proc. R. Soc. Lond. Ser. A.* 1937;161(906):367–381.

D'Auria F. Perspectives in system thermal-hydraulics. *Nucl. Eng. Technol.* 2012;44(8):855–870.

D'Auria F., Vigni P. *BLOWAES: a method for evaluating blowdown two phase flowrate from pressure and thrust measurement*. In: The Second International Topical Meeting on Nuclear Reactor Thermalhydraulics, NURETH-2, Santa Barbara, January 11–14; 1983.

D'Auria F., Frogheri M., Misale M. *System codes capabilities in predicting instabilities in single phase natural circulation*. In: 4th Regional Meet. Nuclear Energy in Central Europe, Bled (SLO),

September 7–10; 1997a.

D'Auria, F., Ambrosini, W., Anegawa, T., Blomstrand, J., In De Betou, J., Langenbuch, S., Lefvert, T., Valtonen, K., 1997b. State of the Art Report on Boiling Water Reactor Stability (SOAR on BWR) (OECD-CSNI Report OECD/GD (97) 13), Paris.

D'Auria F., Lombardi-Costa A., Bousbia Salah A. *The boiling water reactor stability*. In: OECD/NEA/CSNI, THICKET Seminar, Paper 21, Budapest (Hu), June 26–July 1; 2016.

De Crécy A., Bazin P., Glaeser H., Skorek T., Joucla J., Probst P., Fujioka K., Chung B.D., Oh D.Y., Kyncl M., Pernica R., Macek J., Meca R., Macian R., D'Auria F., Petruzzi A., Batet L., Perez M., Reventos F. Uncertainty and sensitivity analysis of the LOFT L2-5 test: results of the BEMUSE programme. *Nucl. Eng. Des.* 2008;238(2008):3561–3578.

Del Frate, L., 2016. Assessment of CFD Methods for Single and Two-Phase Flows in Nuclear Reactors (Ph.D. Thesis). University of Pisa, Pisa (I).

Del Frate L., Moretti F., Galassi G., D'Auria F. Limitations in the use of hydraulic diameter. *J. Nucl. Sci. Technol.* 2016;6(1):53–62.

Diessler G., Taylor M.F. *Analysis of axial turbulent flow heat transfer through banks of rods or tube*. In: Reactor Heat Transfer Conference, TID-7529, vol. 2; 1956.

Ericson L., Hall D.G. The Marviken critical flow tests – a description and early results. In: *ENS/ANS International Topical Meeting on Nuclear, Power Reactor Safety*. Belgium: Brussels; 1978:16–19.

Filonenko G.K. *On Friction Factor for a Smooth Tube*. Russia: All Union Thermotechnical Institute (Izvestija VTI, No. 10); 1948.

Fitzsimmons D.E. *Two-Phase Pressure Drop in Piping Components*. Hanford Laboratory Rep., HW-80970; 1964.

Friedel L. *Improved friction pressure drop correlations for*

horizontal and vertical two-phase flow. In: European Two-Phase Flow Group Meeting, Ispra (I); 1979.

Friedel L. Pressure drop during gas/vapor-liquid flow in pipes. *Int. Chem. Eng.* 1980;20:352–367.

Glaeser H., D'Auria F., De Crécy A., Reventos F. *Main results of the OECD best estimate methods.* In: Uncertainty and Sensitivity Evaluation (BEMUSE) Programme, Int. Topical Meet. on Nuclear Reactor Thermal-Hydraulics (NURETH-14), Article N. 71, Toronto (Ontario, Canada), September 25–30; 2011.

IAEA, 2001. see Aksan et al. (2001).

Idel'chik I.E. *Handbook of Hydraulic Resistance – Coefficients of Local Resistance and of Friction.* Moskva-Leningrad: Gosudarstvennoe Energeticheskoe Izdatel'stvo; 1960 (Russia, Soviet Union at the time) – Translated from Russian by Israel Program for Scientific Translations, Jerusalem (Israel) 1966.

Idel'chik I.E. *Hand Book of Hydraulic Resistances.* New York, NY: Hemisphere Publishing Company; 1979.

Ikeda K. CFD application to advanced design for high efficiency spacer grid. *Nucl. Eng. Des.* 2014;279:73–82.

Ishii M., Zuber N. *Thermally induced flow instabilities in two phase mixtures.* In: 4th Int. Heat Transfer Conference, Paris (F); 1970.

Jayanti S., Reddy K.R. Effect of spacer grids on CHF in nuclear rod bundles. *Nucl. Eng. Des.* 2013;261:66–75.

Kays W.M. *Convective Heat and Mass Transfer.* New Delhi: Tata-McGraw Hill Publishing Company Ltd.; 1975.

Kays W.M. Loss coefficients for abrupt changes in flow cross section with low Reynolds number flow in single and multiple tube systems. *Trans. ASME.* 1950;72:1067–1074.

Keim E., Huber N., Kastner W. *Crack opening and leakage rates of real cracks.* In: 7th International Topical Meeting on Nuclear

Reactor Thermalhydraulics, NURETH-7, Tokyo; 1999.

Liebert J., Emmerling R. UPTF experiment – flow phenomena during full-scale loop seal clearing of a PWR. *Nucl. Eng. Des.* 1998;179:51–64.

Lockhart R.W., Martinelli R.C. Proposed correlation of data for isothermal two-phase, two-component flow in pipes. *Chem. Eng. Prog.* 1949;45:39–48.

Lombardi C., Pedrocchi E. A pressure drop correlation in two-phase flow. *J. Energ. Nucl.* 1972;19(2):91–99.

Martinelli R.C., Nelson D.B. Prediction of pressure drop during forced-circulation boiling of water. *Trans. Am. Soc. Mech. Eng.* 1948;70:695–702.

Mayinger F., Weiss P., Wolfert K. Two-phase flow phenomena in full-scale reactor geometry. *Nucl. Eng. Des.* 1993;145(1–2):47–61.

McAdams W.H., Woods W.K., Heroman Jr. R.H. Vaporization inside horizontal tubes. II. Benzene-oil mixtures. *Trans. ASME.* 1942;64:193.

Nikuradse J. Mitt. Forsch. Geb. Ing.-Wesen. *Laws of turbulent flow in smooth pipes (English translation)*. 1932;356:1.

Petruzzi, A., D'Auria, F. (Editors), De Crecy, A., Bazin, P., Borisov, S., Skorek, T., Glaeser, H., Benoit, J. P., Chojnacki, E., Fujioka, K., Inoue, S., Chung, B. D., Trosztel, I., Toth, I., Oh, D. Y., Pernica, R., Kyncl, M., Macek, J., Macian, R., Tanker, E., Soyer, A. E., Ozdere, O., Perez, M., Reventos, F., 2006. BEMUSE Programme. Phase 2 Report. Re-Analysis of the ISP-13 Exercise, Post Test Analysis of the LOFT L2-5 Experiment (OECD/CSNI Report NEA/CSNI/R(2006)2), © OECD 2006, Paris (F), pp. 1–625.

Schikorr M., Bubelis E., Mansani L., Litfin K. Proposal for pressure drop prediction for a fuel bundle with grid spacers using Rehme pressure drop correlations. *Nucl. Eng. Des.*

2010;240:1830–1842.

Sokolowski, L., Koslowski, T., 2012. Assessment of Two-Phase Critical Flow Models Performance in RELAP5 and TRACE Against Marviken Critical Flow Tests (International Agreement Report, NUREG/IA-0401).

Van Rooyen E., Thome J.R. Pressure drop data and prediction method for enhanced external boiling tube bundles with R-134a and R-236fa. *Int. J. Refrig.* 2013;36:1669–1680.

VDI Heat Atlas. *Second Edition*. Berlin Heidelberg: Springer-Verlag; 2010.

Vijayan P.K. Experimental observation on the general trends of the steady state and stability behavior of single-phase natural circulation loops. *Nucl. Eng. Des.* 2002;215:139–152.

Vijayan P.K., Nayak A.K. Introduction to instabilities in natural circulation systems. In: *Joint ICTP-IAEA Course on Natural Circulation Phenomena and Passive Safety Systems in Advanced Water Cooled Reactors*. Italy: Trieste; 2012 3-7 December 2012, paper 2349-15.

Yadigaroglu G., Chan K.C. *Analysis of flow instabilities*. In: *Proceedings of the Japan–US Seminar on Two-Phase Flow Dynamics* July 31–August 3, Kobe, Japan; 1979.

Yang L.X., Zhou M.J., Zheng Y. A comparison of the CFD simulation results in 5 x 5 sub-channel with mixing grids using different turbulence models. *Kerntechnik*. 2016;81(3):321–330.

Constitutive equations

J.J. Jeong Pusan National University, Pusan, South Korea

Abstract

The concept of constitutive equations is strictly linked with the modeling in two-phase nuclear thermal-hydraulics. This is specifically true for the commonly adopted “unequal-velocity, unequal-temperature” (UVUT) models. Constitutive equations or closure models are embedded into balance equations. Here one may distinguish within the broad category of closure equations (i.e., all the equations needed to solve the balance equations) the constitutive equations, as those equations derived from experiment. In this case constitutive equations have an empirical or a semiempirical nature. Closure equations aim at the numerical simulation of the phenomena in nuclear thermal-hydraulics. Constitutive equations are discussed in the present chapter making specific reference to models adopted in the current system thermal-hydraulic codes.

Keywords

Constitutive equations; Closure equations; Interfacial friction; Interfacial heat transfer; Flow regimes; Heat transfer regimes; Interfacial transfer terms

Chapter foreword

The concept of constitutive equations is strictly linked with the modeling in two-phase nuclear thermal-hydraulics. Balance equations derived from basic principles and discussed in Chapter 5 of the book cannot be solved without closure and/or constitutive equations. Here one may distinguish within the broad category of

closure equations (i.e., all the equations needed to solve the balance equations) the constitutive equations, as those equations derived from experiment. In this case constitutive equations have an empirical or a semiempirical nature. Constitutive equations are discussed in the present chapter, making specific reference to models adopted in the current system thermal-hydraulic codes.

The understanding of this chapter is essential for the reader in order to develop his own idea in relation to the capabilities and the limitations of the current system thermal-hydraulics codes discussed in Chapter 11. Constitutive equations and related modeling are connected with geometry of the system and are part of the scaling issue in system thermal-hydraulics (also discussed in Chapter 11).

Furthermore, constitutive equations also constitute: (a) one motivation and origin of uncertainty, discussed in Chapter 13; (b) an area needing continuous development in the future including planning of new experiments.

9.1 Introduction

There are various mathematical models that have been developed for a two-phase flow, such as homogeneous equilibrium model, drift-flux model, two-fluid model (known as the unequal-velocity unequal-temperature model or six-equation model), two-fluid three-field model (Frepoli et al., 2003), and two-fluid four-field model (Lahey and Drew, 2001). Each of these models was derived from the first principles of thermodynamics and mechanics under its own assumptions for simplification. Among these models, the one-dimensional two-fluid six-equation model has been adopted in most of the state-of-the-art system thermal-hydraulic (TH) codes, such as RELAP5/MOD3 (USNRC, 1998a,b), RELAP5-3D (Idaho National Lab., 2001, 2012a,b), TRAC-PF1 (Liles et al., 1988; Spore et al., 1993), TRACE V5 (USNRC, 2013), CATHARE 2 (Bestion, 1990), and MARS (Jeong et al., 1999).

In the two-fluid six-equation model, the mass, energy, and momentum balance equations for liquid and vapor/gas mixture phases are established separately. The six equations are represented in differential form, with time and one space dimension as independent variables, and in terms of time and volume-average dependent variables. Each phase in the two-fluid model has two interfaces, see Fig. 9.1A:

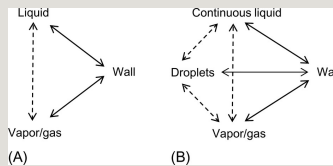


Fig. 9.1 Interfaces in (A) the two-fluid model and (B) the two-fluid three-field model.

- A variable interface between the two phases, where heat, mass, and momentum transfer occur.
- An interface with the fixed wall, where heat and momentum transfer occur.

The mathematical models used to represent the interface transfer phenomena in terms of time and volume-averaged dependent variables are called constitutive equations. The term “constitutive equations” is associated with a specific set of governing equations. For the two-fluid model, they link the six governing equations, leading to “mathematical closure” together with state equations (Meyer et al, 1967; Haar et al., 1984; Watanabe and Dooley, 1996; Harvey et al., 2000; Lemmon et al., 2010).

In this chapter, the constitutive equations of the two-fluid models, selected from RELAP5/MOD3 (hereafter, RELAP5), RELAP5-3D, TRACE V5, or CATHARE 2, are briefly presented and discussed. For the readers who want to compare with those of other system codes, including RELAP-7, WCOBRA/TRAC, TRAC-M, and ATHLET, the review papers by Roth and Aydogan (2014a,b) are recommended. They provided a systematic comparison of various system TH codes and discussed their governing equations, closure relations, numerical solutions, and code validation and limitations.

Some system TH codes, such as WCOBRA/TRAC (Thurgood and George, 1983), SPACE (Ha et al., 2011), and CATHARE 3 (Emonot et al., 2009; Bassenghi, 2013), use the two-fluid three-field model for two-phase flows, where there are three additional interfaces, as shown in Fig. 9.1B, because of the separate modeling of entrained liquid (i.e., droplets). Thus, additional constitutive equations are needed for droplet entrainment/deposition and the mass, energy, and momentum exchanges at the droplets-to-vapor interface. These are not discussed here.

9.2 Two-fluid equations and constitutive equations

The basic field equations for a one-dimensional two-fluid model consist of two phasic continuity equations, two phasic momentum equations, and two phasic energy equations. The following equations, which may differ in various system TH codes, were selected to illustrate both the basic form and constitutive terms of a two-fluid model:

- Continuity equation of k -phase

$$G \triangleq G_v + G_l \quad (9.1)$$

where $k=f$ or g (liquid or vapor phase).

- Momentum equation of k -phase

$$H_k \triangleq \overline{\overline{h_k}}^k = \frac{\langle \chi_k \rho_k h_k \rangle^S}{\langle \chi_k \rho_k \rangle^S} = \frac{\widehat{\rho_k h_k}^k}{\widehat{\rho_k}^k} \quad (9.2)$$

- Energy equation of k -phase

$$H_m \triangleq \frac{\alpha_v Q_v H_v + \alpha_l Q_l H_l}{Q_m} \quad (9.3)$$

In the right-hand side of Eqs. (9.1)–(9.3), we need to identify 14 transfer terms at least that require constitutive relations (D'Auria et al., 2012). These include:

- Wall transfers
 - Liquid-wall friction (F_{wf})
 - Gas-wall friction (F_{wg})
 - Wall-to-liquid heat transfer (Q_{wf})
 - Wall-to-gas heat transfer (Q_{wg})

- Interfacial transfers

– Interfacial mass transfer (Γ_k , vaporization or condensation; $\hat{H}_i \triangleq \frac{\langle \chi_i \rho_i v_{i,z} h_i \rangle^s}{\langle \chi_i \rho_i v_{i,z} \rangle^s} = \frac{\alpha_i \langle \rho_i v_{i,z} h_i \rangle^s}{G_i}$)

– Liquid to interface heat flux (Q_{if})

– Gas to interface heat flux (Q_{ig})

– Energy transfer to liquid due to interfacial mass transfer $\hat{H}_m \triangleq \frac{G_v \hat{H}_v + G_l \hat{H}_l}{G}$,

– Energy transfer to gas due to interfacial mass transfer $x \triangleq \frac{\alpha_v Q_v}{Q_m}$,

– Interfacial momentum transfers:

○ Interfacial friction (F_{ik}),

○ Virtual mass force ($F_{vm,k}$),

○ Differential terms of momentum equations related to pressure differences

$$X \triangleq \frac{G_v}{G}$$

between phases and interface

○ Momentum transfer to liquid due to interfacial mass transfer (ΓV_{if}),

○ Momentum transfer to gas due to interfacial mass transfer ($\Gamma_g V_{ig}$)

As can be seen in Eqs. (9.1)–(9.3), the two-fluid equations are formulated in one dimension in the direction of the flow. This means cross-section averaged flow variables are used in the governing equations. Thus the constitutive equations for the thermal-hydraulic phenomena at the wall and the two-fluid interface should be developed in terms of the cross-section averaged properties using empirical or semiempirical formulations.

All the constitutive equations in a system TH code should be developed so that they will be applicable to a wide range of flow conditions (USNRC, 1987) that

may occur during design-basis accidents of light water reactors:

- pressures from 0.1 to ~20 MPa,
- temperatures up to 1500 K,
- various flow passage geometries, including pipe, rod bundle, and annulus with equivalent diameters from 0.01 to ~1.3 m,
- subcooled liquid, two-phase mixture, and superheated vapor flows,
- various flow regimes in horizontal, vertical, and inclined ducts,
- pre-CHF and post-CHF wall heat transfer.

However, in general, most constitutive equations have been developed using experimental data from a limited range of flow conditions and parameters at reduced-scale facilities, leading to the scaling issue and uncertainties. Thus the constitutive equations are one of the key modules in a system TH code that determine overall code accuracy (Ahn et al., 2015). For example, it is known that about 50% of the uncertainties of peak cladding temperature (PCT) for a loss-of-coolant accident (LOCA) in a pressurized water reactor (PWR) come from those of interfacial and wall heat transfer models (Choi and No, 2012).

Among the 14 terms listed above, the virtual mass force (or added mass force) and differential terms of momentum equations related to the pressure differences between phases and interface are briefly discussed first.

In the CATHARE 2, TRACE, and RELAP5 codes, the virtual mass terms have been implemented as follows:

$$X_{th} = \frac{\widehat{H}_m - h_{lsat}}{h_{vl}} \quad (9.4)$$

where

$$Bo = \frac{g \Delta \rho L^2}{\sigma}$$

C_{vm} : the virtual mass which depends on the flow regime,

$$Fr = \frac{v}{\sqrt{gD}},$$

d/dt is the material derivative.

In RELAP5, the spatial derivative terms in the virtual mass force were neglected (Anderson et al., 1977; USNRC, 1998a,b). The reason for this change is that inaccuracies in approximating the spatial derivative portion of the term for the relatively coarse nodalizations used in system representations can lead to nonphysical characteristics in the numerical solution. Meanwhile, in TRACE (USNRC, 2013), the virtual mass terms have been ignored in the momentum equations because there is no evidence of significance in reactor safety problems, and they create a significant increase in the complexity of the solution procedure. They will reconsider virtual mass terms if higher order numerical methods are introduced into a future version of TRACE and a well-posed set of partial differential equations becomes important. However, for the critical flow model, the effects of virtual mass terms are considered separately. In CATHARE 2, the virtual mass term was well preserved for the well-posedness of two-fluid governing equations (Bestion, 1990, see also Chapter 5).

This difference in the three codes indicates that the virtual mass is not of primary concern from a physical point of view. The primary effects of the virtual mass are on the mixture sound speed and temporal acceleration of phasic slip. The simplified form might be adequate in the system of governing equations or it may be neglected.

Most system TH codes, such as RELAP5, TRACE, and CATHARE 2, assume the two phases have equal pressures in the mass and energy equations. This assumption is relaxed in the momentum equations in the case of horizontally stratified flow in RELAP5 and TRACE. However, CATHARE 2 always considers the effect of unequal pressures in the momentum equations by adding (or

subtracting)  into the interfacial stress terms, where

$$J_k^* = \frac{\sqrt{\rho_k} J_k}{\sqrt{g \Delta \rho D}} \quad (9.5)$$

In nonstratified flows the expression for p_i was simply chosen to provide the hyperbolicity of the system of equations. It is known that the term



has less physical significance but enhances stability in the CATHARE numerical solution method.

Then, the remaining 12 terms among the 14 listed above can be reduced to the following four groups: (i) interfacial heat and mass transfer, (ii) interfacial drag, (iii) wall heat transfer, and (iv) wall friction. The last two were already discussed in Chapters 7 and 8, respectively, in terms of physical phenomena and models. In the remainder of this chapter, they are discussed again as the constitutive equations.

Two-phase flow may exist under various flow regimes characterized by specific phase repartitions. Every flow regime has its internal structure and its transfer mechanisms. This makes it necessary to use a flow regime map (or flow pattern map) and to develop flow-regime-dependent constitutive relations for interface and wall transfers. Thus the flow regime map is discussed first in Section 9.3 followed by a discussion of the interfacial heat and mass transfer, interfacial drag, wall heat transfer, and wall friction. The effects of noncondensable gases are not included for simplicity of explanation.

9.3 Flow regime map

Extensive studies of gas-liquid two-phase flow have their origins in the petrochemical and chemical process industries. These were further investigated in the nuclear power industry for their own purposes. One of the complicated features in a two-phase flow is its liquid-gas interface structure. A particular type of geometric distribution of the liquid and gas phases in a two-phase flow is called a flow pattern or flow regime (Collier and Thome, 1994). It has an important effect on the prediction of void fraction, wall and interfacial heat transfer, interfacial drag, and pressure drop.

In most system TH codes, flow regimes are divided into pre- and post-CHF flow, depending on wall temperature. The post-CHF flow regime is used when the

temperature of a wall surface is above the minimum stable film boiling temperature and, thus, the liquid phase cannot contact the hot surface. Otherwise the pre-CHF flow regime is used.

Pre-CHF flows are typically subcategorized into vertical flows, horizontal flows, and inclined flows. Fig. 9.2 shows the schematic representation of vertical flow regimes in pipes (Collier and Thome, 1994).

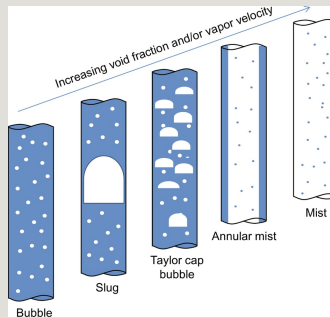


Fig. 9.2 Schematic of vertical flow regimes.

In a bubbly flow, small bubbles are dispersed as discrete bubbles in a continuous liquid phase. With increasing void fraction, the small bubbles coalesce into larger slugs, whose diameters approximately reach the pipe diameter, resulting in a slug flow. The nose of the slug bubble has a spherical cap. The length of the main gas bubble can vary considerably. The flow structure becomes unstable with increasing flow velocity. The net flow remains upward, but components of the flow travel in both directions. The instability comes from the balance of the gravity and shear forces acting in opposing directions on the thin liquid film of the Taylor bubbles. Slug bubbles are more likely in smaller pipes, while Taylor cap bubbles are more common in larger pipes. Churn flow may be formed by the breakdown of the large bubbles in slug flow.

The annular-mist regime follows with increased gas flow rate. The interfacial shear of the high-velocity gas on the liquid film dominates over gravity in the annular flow regime. When the heat transfer from the wall increases further, the liquid film disappears or dries out, finally reaching a mist flow.

Fig. 9.3 shows horizontal flow regimes. They have different characteristics due to the asymmetry of the phases resulting from the effects of gravity (Collier and

Thome, 1994). The bubble flow pattern is similar to that of vertical flow—at low liquid velocities the gas bubbles tend to travel in the upper half of the pipe, whereas at high liquid velocities the bubbles are dispersed. By increasing the vapor flow, plug flow is formed. This is similar to slug flow in a vertical pipe. The stratified or stratified wavy flow only occurs at low liquid and gas velocities, where the two phases flow separately with a relatively smooth interface. As the gas velocity is increased, the interface becomes disturbed by waves traveling in the direction of the flow. A further increase in the gas velocity causes the waves at the interface to bridge the channel and form a frothy slug that is propagated with a high velocity. A still higher gas velocity results in the formation of a gas core with a liquid film around the periphery of the pipe. This annular regime is usually accompanied by the presence of entrained droplets due to the high gas velocity.

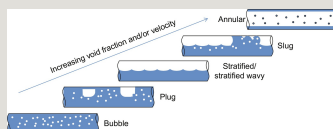


Fig. 9.3 Schematic of horizontal flow regimes.

In the post-CHF flows, the liquid phase cannot contact the hot surface. This leads to inverted flow regimes, with the gas phase in contact with the wall, as illustrated schematically in Fig. 9.4.

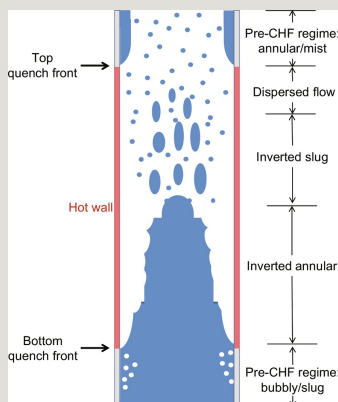


Fig. 9.4 Schematic of inverted flow regimes in post-CHF conditions (USNRC, 2013).

In inverted annular flows, there is a core of liquid in the center of the pipe surrounded by an annulus of vapor. In inverted slug flow, large slugs of liquid surrounded by vapor are present. In dispersed flows, droplets are present in a vapor flow with no liquid in contact with the wall. These flow regimes may exist in the reflood phase of an LOCA in a PWR.

The flow regime map and transition criteria have been developed to identify the flow regimes for local flow conditions. Some old flow regime maps, which are still used, are summarized in Table 9.1. The complexity and deficiencies in the understanding of various flow regimes can be seen indirectly from the various flow variables which are used for flow regime identification. This complexity results from the difficulty of observation and measurement—the flow regimes are very sensitive to flow geometry, and the transition mechanisms are not clearly known.

Table 9.1

Old flow regime maps



Traditional two-phase flow-regime criteria based on gas and liquid superficial velocities may not be suitable for the analyses of rapid transient or entrance flows by the two-fluid model. Ishii and Mishima (1984) assumed that direct geometrical parameters, such as the void fraction, were conceptually simpler, and therefore more reliable parameters could be used in flow regime criteria than the traditional parameters. They developed new flow-regime criteria for upward gas-liquid flow in vertical tubes considering the mechanisms of flow regime transitions. These became the basis for the RELAP5 and TRAC-PF1 flow regime maps.

In the remainder of this section, the vertical and horizontal flow regime maps of RELAP5 are briefly introduced first, and those of other system TH codes are also discussed. The RELAP5 flow regime maps are similar to those of the RELAP5-3D, TRACE, and SPACE codes. It is noted that, in RELAP5, the volume and junction flow regime maps are provided separately. The volume flow regime map is based on volume quantities, which is used for interfacial heat and mass transfer, wall friction, and wall heat transfer. The junction flow regime map is based on both

junction and volume quantities. It is used for the interphase drag and shear, as well as the coefficient of virtual mass. Conceptually the volume and junction flow regime maps are the same.

9.3.1 Vertical flow regime map

Fig. 9.5 shows the schematic of the RELAP5 vertical flow regime map (USNRC, 1998a). This map for both up and down flow is for volumes whose elevation angle ϕ is such that $45 < |\phi| < 90$ degrees. It is noted that, in RELAP5-3D (Idaho National Lab., 2012a), nearly the same vertical flow regime map is used for $60 \leq |\phi| < 90$ degrees and the horizontal flow regime map for $0 < |\phi| < 30$ degrees. An interpolation region between vertical and horizontal flow regimes is used for volumes whose absolute value of vertical inclination angle is between 30 and 60 degrees. Kim et al. (2007, 2010) showed that the flow regime is very sensitive to flow geometry and angle. It is clear that the approaches in the two codes may have great uncertainties.

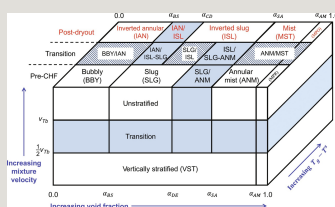


Fig. 9.5 Schematic of the RELAP5 vertical flow regime map (USNRC, 1998a).

The vertical flow regime map in Fig. 9.5 is modeled as nine regimes: four for pre-CHF heat transfer, four for post-CHF heat transfer, and one for vertical stratification. For pre-CHF heat transfer, the regimes modeled are the bubbly, slug, annular-mist, and mist-pre-CHF regimes. The mist-pre-CHF regime was added for smoothness. For post-CHF heat transfer, the bubbly, slug, and annular-mist regimes are transformed to the inverted annular, inverted slug, and mist regimes, respectively, as suggested by Ishii and Jarlais (1982). The mist-post-CHF regime was added for symmetry with the mist-pre-CHF regime.

The schematic in Fig. 9.5 is three-dimensional, to illustrate flow regime transitions as functions of void fraction (α_g), average mixture velocity (v_m), and boiling regime (pre-CHF, transition, and postdryout), where

$$Re = \frac{vD}{\nu} \tag{9.6}$$

$$We = \frac{\rho \Delta V^2 L}{\sigma} \tag{9.7}$$

When the mixture velocity is sufficiently low (~50%) in comparison with the Taylor bubble velocity (v_{Tb}), the flow is assumed to be vertically stratified. v_{Tb} is given by the correlation:



$$\tag{9.8}$$

In the pre-CHF regimes, the void fraction of bubbly-to-slug transition (α_{BS}) is given by

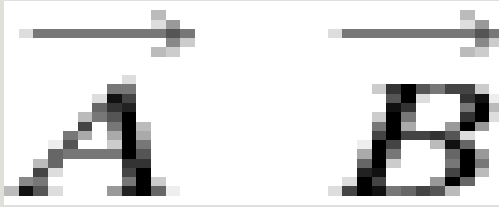


$$\tag{9.9}$$

where



$$=$$

D is the pipe diameter.

The slug-to-annular transition void fraction (α_{SA}) is given by

$$\frac{\overline{A}}{D} = \frac{\overline{B}}{D} \quad (9.10)$$

where

$$\overline{f} \triangleq \frac{1}{T} \int_T f \, dt$$

$$\tilde{f} \triangleq \overline{\rho f} / \overline{\rho}$$

The transition region between the slug flow and annular-mist flow regimes is defined by α_{DE} and α_{SA} where

$$f^k \triangleq \overline{\chi_k f_k} / \overline{\chi_k} \quad (9.11)$$

The minimum void fraction for annular-mist flow, α_{SA} , is constrained to lie between 0.5 and 0.9. For the transition between annular mist and mist pre-CHF, the value of α_{AM} is

$$\tilde{f}_k^k \triangleq \frac{\overline{\chi_k \rho_k f_k}}{\chi_k \rho_k} = \frac{\overline{e_k \rho_k f_k}}{e_k \rho_k} = \frac{\overline{\rho_k f_k}}{\rho_k} \quad (9.12)$$

If the hydrodynamic volume has heat flux from a surrounding wall to the vapor, or the reflood model is turned on for that wall, and the vapor temperature is more than 1 K superheated, then the flow regime is a post-CHF regime, in which the previous a_{BS} and a_{SA} are still effective. The transition region between inverted slug flow and inverted annular flow regimes is defined by a_{BS} and a_{CD} , where

$$\langle f \rangle^L \triangleq \frac{1}{L} \int_L f \, dl \quad (9.13)$$

9.3.2 Horizontal flow regime map

The horizontal flow regime map is for volumes whose elevation angle ϕ is such that $0 < |\phi| < 45$ degrees. This map is similar to the vertical flow regime map except that the post-CHF regimes are not included, and a horizontally stratified regime replaces the vertically stratified regime. The horizontal flow regime map therefore consists of horizontally stratified, bubbly, slug, annular-mist, and mist-pre-CHF regimes. A schematic for the horizontal flow regime map is shown in Fig. 9.6 (USNRC, 1998a). The transition criteria for the bubbly to slug and the slug to annular-mist regimes are similar to those for the vertical map.

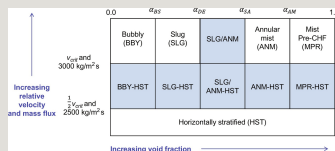


Fig. 9.6 Schematic of the RELAP5 horizontal flow regime map (USNRC, 1998a).

The bubbly-slug transition criterion is

$$\langle f \rangle^S \triangleq \frac{1}{A} \int_A f \, ds \quad (9.14)$$

The minimum void fraction for annular-mist flow, α_{SA} , is a constant

$$\langle f \rangle^V \triangleq \frac{1}{V} \int_V f \, dv \quad (9.15)$$

and the transition region between slug flow and annular-mist flow regimes is defined by α_{DE} and α_{SA} , where

$$\langle f(x, y, z, t) \rangle^{\theta} \triangleq \iiint_R g(x' - x, y' - y, z' - z, t) \cdot f(x', y', z', t) \, dx' \, dy' \, dz' \quad (9.16)$$

The annular-mist to mist-pre-CHF transition criterion is

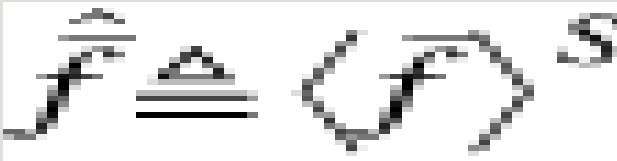
$$\widehat{f}_k^k \triangleq \frac{\overline{\chi_k \rho_k f_k}}{\chi_k \rho_k} = \frac{e_k \overline{\rho_k f_k}}{e_k \rho_k^k} = \frac{\overline{\rho_k f_k^k}}{\rho_k^k} \quad (9.17)$$

The flow is horizontally stratified if the phasic velocity difference satisfies the condition

$$\widehat{f}_k^k \triangleq \frac{\langle \chi_k f_k \rangle^S}{R_k}$$

and the mass flux satisfies the condition

$$\tilde{f}_k^k \triangleq \frac{\langle \chi_k \rho_k f_k \rangle^S}{\langle \rho_k \rangle^S}$$



where and the angle θ is defined in Fig. 9.7. If the above two conditions are not met, then the flow field undergoes a transition to the bubbly, slug, annular-mist, or mist-pre-CHF flow regime.

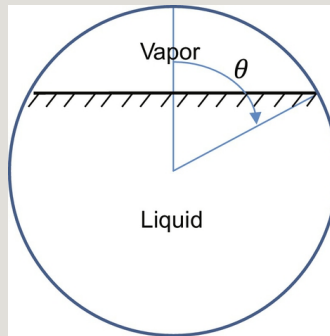


Fig. 9.7 Horizontally stratified flow.

In addition to the vertical and horizontal flow regime maps, RELAP5 provides the high mixing flow regime map, which is used in pumps, and the ECC mixer volume flow regime map.

9.3.3 CATHARE 2 and TRACE flow regime maps

In the CATHARE 2 code, only two flow regime transition criteria are explicitly written, and they are used in several closure terms (Bestion, 1990; Serre et al., 2011; Bassenghi, 2013).

The first transition is between stratified and no stratified flow, which is associated with the parameter R in Fig. 9.8. This transition depends on two criteria: the first criterion is based on the Kelvin-Helmholtz instability threshold, and the second depends on the relative effects of bubble sedimentation and of bubble turbulent mixing. The second transition is between annular and droplet flows, which is

associated with the parameter E in Fig. 9.8.

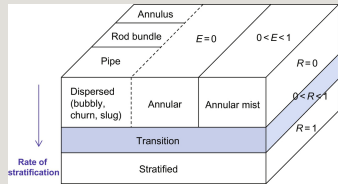


Fig. 9.8 Schematic of the CATHARE 2 pre-CHF flow regime map.

The parameters R and E are used for interpolation to establish smooth transitions of the flow regimes. The post-CHF flow regimes in CATHARE 2 are inverted annular and dispersed flow (liquid slugs and/or droplets).

The TRACE code considers three distinct classes of flow regimes (USNRC, 2013): (i) the pre-CHF flow regime consist of the bubbly/slug and the annular/mist regimes, (ii) the horizontal stratified flow regime is available for 1-D components that are either horizontal or inclined, and (iii) the post-CHF flow regime encompasses the inverted flow regimes that occur when the wall is too hot for liquid-wall contact. The TRACE pre-CHF flow regime map, which is used for interfacial heat transfer, is that of TRAC-PF1/MOD2 (Spore et al., 1993). As shown in Fig. 9.9, the flow regime is based on void fraction and mass flux, with the mass flux range limited for the Taylor cap or slug bubble flow regime. The map is similar to that of RELAP5 except that there is no vertically stratified flow regime.

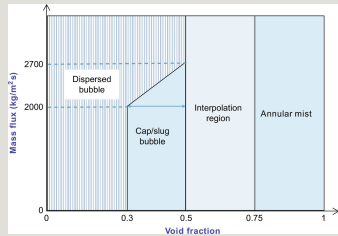


Fig. 9.9 Schematic of the TRACE pre-CHF flow regime map (USNRC, 2013).

9.3.4 Limitations of the flow regime map approach and recent

improvements

The flow regime map is very important because it determines the flow regime for a given local flow condition and, based on the flow regime, the interfacial transfer model and interfacial area per unit volume (or called interfacial area concentration, IAC) are determined.

The shortcomings caused by the traditional two-phase flow regimes and regime transition criteria were pointed out by Ishii (1975) and coworkers (Ishii and Mishima, 1980; Hibiki and Ishii, 2002; Ishii et al., 1998; Uhle et al., 1998), which can be summarized as follows:

- The flow regime transition criteria are algebraic correlations, which have been usually developed from steady-state, fully developed flows. Hence, the effects of the entrance and developing flow cannot be taken into account correctly, nor can the gradual transitions between regimes.
- The transition criteria and flow-regime-dependent IAC correlations are valid in limited parameter ranges for certain operational conditions and geometries. Most of them are obtained from simple experiments and phenomenological models. Often the scale effects of geometry and fluid properties are not correctly taken into account.
- The method based on the flow regime transition criteria is a two-step method, which requires flow configuration transition criteria and IAC correlations for each flow configuration. The compound errors from the transition criteria and IAC correlations can be very significant.

To solve such problems, the interfacial area transport equation (IATE) was introduced (Ishii, 1975; Ishii and Kojasoy, 1993; Kocamustafaogullari and Ishii, 1995). The IATE can be obtained by considering the fluid particle number density transport equation analogous to Boltzmann's transport equation (Wu et al., 1998; Morel et al., 1999). The one-group formulation was suggested first, where the dispersed bubbles are assumed to be spherical in shape (Ishii et al., 2000; Hibiki and Ishii, 2002). The one-dimensional form of the one-group IATE in a bubbly flow is given by:

$$\dot{f} = \frac{\langle \dot{V} f \rangle}{\langle V \rangle^2} \quad (9.18)$$

The four terms in the right-hand side of Eq. (9.18) indicate the rates of change of IAC due to bubble breakup, bubble coalescence, phase change, and bubble expansion, respectively.

To realistically describe the interfacial area transport in various two-phase flow regimes, the two-group transport equation was suggested (Ishii et al., 2005; Ishii and Hibiki, 2006). This is because the differences in bubble sizes or shapes cause substantial differences in their transport mechanisms and interaction phenomena. Therefore, two transport equations for two characteristic groups of bubbles were suggested: group 1 for small dispersed and distorted bubbles, and group 2 for cap/slug/churn-turbulent bubbles. The maximum bubble diameter of the group 1 bubble is given by

$$\bar{d}_{k1} \triangleq \frac{\langle \chi_k d_k \rangle^S}{\alpha_k} \quad (9.19)$$

The two-group IATEs have more complicated source and sink terms, including additional intergroup transfer terms.

In the development of the two-group IATEs, major difficulties arise from the existence of various types of bubbles and their complicated interactions (Ishii et al., 2005). Interactions between the bubbles in the same group and those between the bubbles of two different groups should be modeled, along with intergroup transfer at the group boundary, due to expansion and compression. It is also important that, in the two-group transport formulation, the particle distribution function needs to be properly averaged due to the existence of various types of bubbles in the two-group transport equation.

The source and sink terms of the interfacial area are still being developed, which are strongly dependent on flow conditions and geometries. So far, most of the experiments for interfacial area research have been performed in round tubes (Revankar and Ishii, 1992; Grossetete, 1995; Hibiki et al., 1998, 2001; Hibiki and Ishii, 2000, 2002; Fu, 2001; Ishii and Kim, 2004; Ishii et al., 2005; Yao and Morel, 2004; Smith et al., 2012a,b), a few in annuli (Hibiki et al., 2003; Jeong et al., 2008; Ozar et al., 2013a,b; Brooks et al., 2014) and rod bundles (Yang et al., 2013). Experiments on sudden area changes, elbows, bends, and large volumes are still scarce.

Considering the wide range of flow conditions that the constitutive equations of a

system TH code should cover, it is somewhat premature to use the interfacial area transport model in a system TH code because of the lack of sufficient data and validated models. Nevertheless, RETRAN-3D (CS & A, 2001) attempted to adopt the dynamic flow regime based on the IATE, which is different from Eq. (9.18) (Stuhmiller, 1986). However, there has not been sufficient validation work to recommend the model for general use. The TRACE development roadmap also includes the IATE. In CATHARE 3, the IATE is under development (Emonot et al., 2009) and to be used when the results are validated and reliable. It seems that the complete replacement of the flow regime map with IATE requires substantial work, and will take very long time.

A two-step approach for the future development of IATE is desirable. First, we need to focus on the in-depth development of the one-group IATE, which allows us a limited use for a dispersed bubbly flow but brings us enhanced accuracy. Thereafter, we may proceed with the second step, the development of two-group IATEs, including the source and sink terms, in parallel with the interfacial area transport by droplets (Thurgood and George, 1983), to cover all flow regimes. In this step, the three-field model is naturally to be used at least. Additional efforts are needed to fit the two-group IATE into the two-fluid or three-field models (Lee et al., 2013) because only one vapor velocity is defined in the two-fluid model, however, vapor velocities of two-group bubbles are needed in the two-group IATE. Sun et al. (2003) and Wang et al. (2011) have suggested some models to implement the IATE into two-fluid models. These combined efforts will be able to replace the conventional flow regime map approach with IATEs.

9.4 Interfacial heat and mass transfer

Interfacial heat and mass transfer may occur in the bulk and/or in the thermal boundary area near the wall (e.g., see Fig. 9.10). The former results from energy exchange between the two phases, determining the level of thermal nonequilibrium, while the latter is due to heat transfer at the wall. Even when the bulk liquid temperature is lower than the local saturation temperature, the liquid in the thermal boundary layer near the wall can be superheated, which may lead to subcooled boiling. The same is true for the film-wise condensation at a subcooled wall. A special model is needed for this, which will be discussed in Section 9.5. In this section, the interfacial heat and mass transfer in the bulk fluid is mainly presented. This is one of the two-phase flow phenomena that have great uncertainties because the fundamental mechanisms are not well understood yet and direct measurement is nearly impossible.

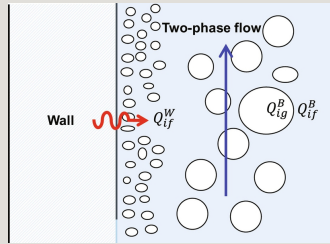


Fig. 9.10 Interface heat transfer in the bulk and near the wall for subcooled boiling (USNRC, 1998a).

In the two-fluid six-equation model in RELAP5 (USNRC, 1998a), the total volumetric vapor generation rate or interfacial mass transfer rate is given by

$$\bar{f}_k^k \triangleq \frac{\langle \chi_k \rho_k \bar{f}_k \rangle^S}{\langle \chi_k \rho_k \rangle^S} = \frac{\overline{\rho_k \bar{f}_k}^k}{\overline{\rho_k}^k} \quad (9.20)$$

where $\frac{d}{dt} \int_{V(t)} \rho \psi dV = \int_{V(t)} \rho \psi dV - \int_{A(t)} \rho \psi (\vec{v} - \vec{v}_A) \cdot \vec{n} dA - \int_{A(t)} (\rho \vec{v}) \cdot \vec{n} dA$, Γ_{ig} is the vapor generation rate in the bulk fluid, and Γ_w is the thermal boundary area near the wall. Similarly, the vapor-side interfacial heat transfer rates is given by

$$-\int_{A(t)} \rho \psi (\vec{v} - \vec{v}_A) \cdot \vec{n} dA \quad (9.21)$$

The liquid vapor-side interfacial heat transfer rate is given by



$$(9.22)$$

The bulk interface heat transfer is at the steam-liquid interface in the bulk. This represents thermal energy exchange between the fluid interface at the saturation temperature, T_s , and the bulk fluid state. For gas, the bulk interface heat transfer is

given by

$$\frac{d}{dx} \left[\lambda(T) \frac{dT}{dx} \right] = -q_v. \quad (9.23)$$

where H_{ig} is the gas interface heat transfer coefficient per unit volume and T_g is the gas temperature. For liquid, the bulk interface heat transfer is given by

$$\frac{d}{dx} \left[\lambda(T) \frac{dT}{dx} \right] = -q_l. \quad (9.24)$$

where H_{lf} is the liquid interface heat transfer coefficient per unit volume and T_f is the liquid temperature.

In general, it is assumed for simplicity that the bulk interfacial heat transfer terms and the near wall energy exchange terms each sum to zero independently. Then,

$$\frac{d}{dx} \left[\lambda(T) \frac{dT}{dx} \right] = -q_v. \quad (9.25)$$

and

$$\frac{d\Lambda}{dx} = \frac{d\Lambda}{dT} \frac{dT}{dx} = \lambda(T) \frac{dT}{dx} \quad (9.26)$$

where $\vec{f} = \vec{g}$ and \vec{q} are the vapor and liquid enthalpies associated with bulk interface mass transfer, respectively. They are defined in such a way that the interface energy jump conditions at the liquid-vapor interface are satisfied. In

particular, $\vec{F} = \vec{g}$ and \vec{q} are chosen to be h_{gs} and h_f , respectively, for the case of vaporization, and h_g and \vec{a} , respectively, for the case of condensation, where the superscript s indicates saturation. The same is true for the phasic enthalpies h_g and h_f associated with wall (thermal boundary layer) interface mass transfer.

It is also assumed that vapor appears (or, is generated) at saturation, and it follows

that $\frac{\partial \rho}{\partial t} + \nabla \cdot (\rho \vec{v}) = 0$ for boiling processes in the boundary layer near the wall (i.e., subcooled boiling). Thus, Eq. (9.26) can then be used to solve for the interface vaporization rate in the boundary layer near the walls (see Section 9.5):

$$\frac{\partial \rho \vec{v}}{\partial t} + \nabla \cdot (\rho \vec{v} \vec{v}) - \rho \vec{F} - \nabla \cdot \vec{T} = 0 \quad (9.27)$$

Similarly, since it is assumed that liquid appears at saturation, it follows that

$\frac{\partial \rho}{\partial t} + \nabla \cdot (\rho \vec{v}) = 0$ for condensation processes in the boundary layer near the wall. Eq. (9.26) can then be used to solve for the interface condensation rate in the boundary layer near the walls:

$$v^2 = \vec{v} \cdot \vec{v} \quad (9.28)$$

Using the above equations, total interfacial mass transfer rate is then represented by

$$\theta(x, \tau) = \frac{T(x, \tau) - T_s}{T_0 - T_s} = 1 - \operatorname{erf}\left(\frac{x}{2\sqrt{a\tau}}\right). \quad (9.29)$$

Eq. (9.29) shows that the interfacial mass transfer rate is directly related with the interfacial heat transfer rate.

Note that the interfacial heat transfer coefficient (IHTC) per unit volume (H_{ik}) in Eq. (9.29) is generally given by

$$\mathcal{T} \triangleq T + pI \quad (9.30)$$

where h_{ik} is the IHTC and a_i is the IAC. The former requires special models, which are empirical, semiempirical, or ad hoc. The IAC is mechanistically modeled, which depends on the flow regime. For the combined flow regimes, such as slug flow or annular-mist flow, the effects of two flow regimes are separately taken into account. For example, in the case of annular-mist flow, H_{ik} , is given by

$$q(0, \tau) = \frac{\lambda(T_0 - T_s)}{\sqrt{\pi a \tau}}. \quad (9.31)$$

where the terms in the right-hand side indicate the contributions by liquid film and droplets, respectively.

The IAC models are similar in various system TH codes. For bubbly and mist flow regimes, the model is rather clear. According to Wallis (1969) and Shapiro and Erickson (1957) the dispersed bubbles or droplets can be assumed to be spherical particles with a size distribution of the Nukiyama-Tanasawa form (USNRC, 1998a). Using the Nukiyama-Tanasawa distribution function, the IAC can be obtained as:

(9.32)

$$\frac{\partial}{\partial t} \left(\rho \left(i + \frac{\tau^2}{2} \right) \right) + \nabla \cdot \left[\rho i \left(i + \frac{\tau^2}{2} \right) \right] - \rho \left(i^2 + \frac{\tau^2}{2} \right) \nabla \cdot \left(\rho i \right) - \nabla \cdot \left(\tau \cdot i \right) + \nabla \cdot \left(\tau \cdot \frac{\tau^2}{2} \right)$$

(9.33)

where σ is the surface tension and ρ_c is the continuous-phase density. The values for We are presently taken as

(9.34)

Similarly, the IACs for other regimes can be modeled. For slug flow regime, the Taylor bubble and small bubbles are separately modeled. For annular-mist flow regime, liquid film and droplets are separately modeled, where the IAC by droplets is obtained by using Eqs. (9.32), (9.33). For inverted flow regimes, the effects of liquid core, liquid slug, and droplets are separately taken into account. Table 9.2 summarizes the IAC model in the RELAP5 code (USNRC, 1998a).

Table 9.2

The IAC model in the RELAP5 code

The IHTCs are rather complicated because of fundamental difficulties in experimental observation and modeling. In the RELAP5 code, the interfacial heat transfer is split into four cases for each flow regime based on fluid temperature: superheated liquid (SHL), subcooled liquid (SCL), superheated gas (SHG), and subcooled gas (SCG). In each regime, correlations for the four cases are provided and some of the correlations are reused.

In the bubbly flow regime, for a condition of SHL, the interfacial heat transfer is the larger of either the model for bubble growth developed by Plesset and Zwick (1954) or the model for convective heat transfer for a spherical bubble (modified by Lee and Ryley, 1968).

For the bubbly flow regime with a condition of SHG, an IHTC is assumed that is high enough that the vapor temperature will relax toward the equilibrium (saturation) condition— h_{ig} is set to 10^4 W/m² K. The same model is used for the bubbly flow regime with a condition of SCG.

Analogously, in the mist flow regime for the condition of SHG, a convective heat transfer model for a spherical droplet (Lee and Ryley, 1968) is used for the IHTC. For mist flow with SHL, it is assumed that the IHTC is high enough so that the liquid temperature will relax toward the equilibrium (saturation) condition.

In the bubbly flow regime for the SCL condition, the interfacial heat transfer is calculated by the modified Unal bubble collapse model (Unal, 1976; Riemke, 1993) and the Lahey model (Lahey, 1978).

In the slug flow regime, the interfacial heat transfers at the Taylor bubbles and the small bubbles are separately modeled. The large IHTC is used for Taylor bubbles to bring the vapor phase to saturation quickly. In the annular-mist flow regime, the interfacial heat transfers at the annular film and droplets are separately modeled. For the subcooled liquid condition, the interfacial mass transfer is calculated by the modified Brown droplet model (Brown, 1951) for the drops, and the modified Theofanous interfacial condensation model (Theofanous, 1979) for the film.

Table 9.3 summarizes the correlations for the IHTC in the RELAP5 code (USNRC, 1998a). As can be seen in Table 9.3, some of the IHTC models are on an ad hoc basis, and these need to be assessed against experimental data. Very large IHTC puts the liquid and vapor phases in thermal equilibrium. This can lead to making the system TH code numerically more stable, but with less physical results.

Table 9.3

The IHTC correlations in the RELAP5 code



The formulation of the interfacial heat transfer in the TRACE code (USNRC, 2013) is basically the same as that in RELAP5, Eqs. (9.23), (9.24). However, for the special case where the liquid is superheated with respect to saturation at the total pressure, rapid nucleation will occur at any surface, and the resulting IHTC will increase dramatically as the level of liquid superheat increases. Under these conditions, Eq. (9.24) is modified to add an additional term for flashing, which is,

$$\frac{\partial \rho v_L}{\partial t} + \frac{\partial \rho v_L v_L}{\partial x_i} + \frac{\partial p}{\partial x_j} - \rho F_j - \frac{\partial \tau_{ij}}{\partial x_i} = 0 \quad (9.35)$$

When noncondensable gases are present, several modifications are made to the IHTC models to consider the additional heat transfer resistance associated with the diffusion of the noncondensable gas.

In the TRACE code, the IHTCs (h_{ig} , h_{if} , and h_{flash}) and IAC (a_i) are dependent upon the flow regime. Each flow regime has its correlations for a_i , h_{ig} , h_{if} , and h_{flash} . Unlike the RELAP5 code that uses different IHTCs according to fluid temperature, one set of correlations is used for each flow regime and, if needed, the effect of fluid temperature is accounted. Tables 9.4 and 9.5 summarize the IAC and IHTC correlations of the TRACE code, respectively.

Table 9.4

The IAC model in the TRACE code



Table 9.5

The IHTC correlations in the TRACE code

--

9.5 Interfacial drag

The equations of motion in the two-fluid six-equations are coupled by two interfacial terms: one resulting from the interfacial drag force between the phases (F_{ik}) and the other from the momentum transfer associated with mass transfer ($V_{ik}\Gamma_{ik}$). The interfacial drag determines the slip between liquid and vapor phases, phase separation, two-phase mixture level, etc. This term is very important in a slow two-phase flow transient, such as a small-break LOCA.

The interfacial drag between the phases is generally represented as



(9.36)

where C_i is the interfacial drag coefficient. Two different models are widely used for the phasic interfacial drag computation in system TH codes: the drift-flux method and the drag coefficient method.

9.5.1 Drift-flux method

In RELAP5, TRACE, and CATHARE 2, the drift-flux approach is used in the bubbly and slug flow regimes for vertical flow. This is because lots of reliable drift-flux data are available in vertical bubbly and slug flows.

The drift-flux model specifies the distribution coefficient (C_o) and the vapor drift velocity (V_{gi}). By using appropriate assumptions, these two quantities are converted into a constitutive relation for the interfacial frictional force per unit volume (USNRC, 1998a, b, 2013). In RELAP5, the drift-flux method leads to the

following interfacial drag:

$$F_i = (-1)^k C_i |C_i V_g - C_o V_f| (C_i V_g - C_o V_f), \quad (9.37)$$

where

$$\frac{\partial \rho^2}{\partial t} + \nabla \cdot \left(\rho \vec{v} \frac{\rho^2}{2} \right) - \rho \vec{F} \cdot \vec{v} + \vec{v} \cdot \nabla p - \vec{v} \cdot \nabla T = 0 \quad (9.38)$$

$$\frac{\partial \rho u}{\partial t} + \nabla \cdot \left(\rho \vec{v} u \right) + p \nabla \cdot \vec{v} - T : \nabla \vec{v} + \nabla \cdot \vec{q} = q_{eff}$$

The drift-flux correlations (C_o and V_{gi}) from the literature based on Putney (1988a,b,c, 1989, 1991) and Chexal and Lellouche (1986) are used, which had been developed for rod bundles, small pipes ($D < 0.018$ m), intermediate pipes ($0.018 \text{ m} < D < 0.08$ m), and large pipes ($0.08 \text{ m} < D$) for a wide range of flow rates.

A similar approach is used in the TRACE code for bubbly/slug flow regime in pipes and rod bundles. Meanwhile Eq. (9.36) is used instead of Eq. (9.37) and the friction coefficient C_i is given by

$$\frac{\partial \rho h}{\partial t} + \nabla \cdot \left(\rho \vec{v} h \right) - \frac{\partial p}{\partial t} - \vec{v} \cdot \nabla p - T : \nabla \vec{v} + \nabla \cdot \vec{q} = q_{eff} \quad (9.39)$$

$$m = \mu_1^2 a / l^2$$

where μ_1 is the profile slip factor, Ps , can be considerably less than unity.

The term comes from the fact that the velocities used in the field equations in TRACE are the void-weighted area-averaged phase velocities (Brooks et al., 2012). The drift-flux parameters C_0 and V_{gj} are prepared for dispersed bubbly/slug flow and Taylor cap bubble flow in pipes (Zuber and Findlay, 1965; Wallis, 1969; Ishii, 1977; Kataoka and Ishii, 1987) and for bubbly/slug flow in rod bundles (Bestion, 1985; Salay, 2001; Coddington and Macian, 2002). It is known that the

$$\frac{1}{\theta} \frac{\partial \theta}{\partial \tau} = -m$$

Bestion model, and $C_0=1.2$, did a reasonably good job for the low-flow low-pressure conditions in rod bundles. Based on a study by Salay (2001) the Bestion model was extended to high-pressure boil-off conditions in TRACE. However, for the BWR conditions, the value of distribution parameter C_0 was set to unity, as recommended by Coddington and Macian (2002) to correct the underprediction of the void fraction.

CATHARE 2 also uses a drift-flux model to compute the interfacial drag on the bubbles in bubbly flow, where configuration-dependent parameters are additionally taken into account for the flows in rod bundles, pipes, and annuli (Bestion, 1985, 1990).

9.5.2 Drag coefficient method

The drag coefficient method, using Eq. (9.36), is used in all flow regimes except for the flow regimes that use the drift-flux method. Correlations for the drag coefficients and the IAC (see Tables 9.2 and 9.4) are needed in this method. For illustration, a description of the RELAP5 drag coefficient method follows below.

The constitutive relation for the frictional force on a body moving relative to a fluid is given by

$$\ln \theta = f(\tau) \quad (9.40)$$

where

F is the drag force,

ρ is the fluid density,

V is the velocity of body relative to the fluid,

C_D is the drag coefficient,

A is the projected area of the body.

Expressing the frictional force for a group of bodies moving relative to a fluid (e.g., bubbles moving through liquid or droplets moving through vapor) in terms of the frictional force for each body leads to the following constitutive relation for the frictional force per unit volume:

$$\vec{q} = -\lambda \nabla T \quad (9.41)$$

where

$$t_w = t_m \cos(\omega \tau)$$

ρ_c is the density of continuous phase,

S_F is the shape factor.

The additional factor of 1/4 in Eq. (9.41) comes from the conversion of the projected area of spherical particles (πr^2) into the interfacial area ($4\pi r^2$) and the shape factor is included to account for nonspherical particles. As can be seen in Eq.

(9.41), the drag is proportional to the IAC. The IAC models in Table 9.2 are used to obtain the IAC for a specific flow regime. This again shows that the flow regime map is very important for two-phase flow computations.


The drag coefficient to be used in nonvertical bubbly flow and all droplet flow situations is given by Ishii and Chawla (1979) for the viscous regime, as

$$\mathcal{T} = -\frac{2}{3}\mu \nabla \cdot \vec{v} I + \mu \left(\nabla \vec{v} + {}^t \nabla \vec{v} \right) \quad (9.42)$$

where the particle Reynolds number, Re_p , is defined as

$$\rho(p, h); T(p, h); \mu(p, h); \lambda(p, h) \quad (9.43)$$

The density, ρ_c , is given by ρ_f for bubbles and ρ_g for drops. The mixture viscosity,

ρ_m , is for the continuous phase. It is given by  for bubbles

$$\frac{\partial \rho}{\partial t} + \nabla \cdot (\rho \vec{v}) = 0$$

and $\frac{\partial \rho}{\partial t} + \nabla \cdot (\rho \vec{v}) = 0$ for mist pre-CHF, mist, and mist-post-CHF droplets. It can be seen from Eqs. (9.41), (9.43), the average bubble (or droplet) diameter is very important for determining the interfacial drag.

For nonvertical slug flow, slug flow for nonvertical geometry is modeled as a series of Taylor bubbles separated by liquid slugs containing small bubbles. The effects of Taylor bubbles and the small bubbles are separately modeled (see also Table 9.2 for the IAC). The drag coefficient for the Taylor bubbles in nonvertical slug flow is given by Ishii and Chawla (1979):

$$\frac{\partial \rho \vec{v}}{\partial t} + \nabla \cdot (\rho \vec{v} \vec{v}) + \nabla p - \rho \vec{F} - \nabla \cdot \left[-\frac{2}{3}\mu \nabla \cdot \vec{v} I + \mu \left(\nabla \vec{v} + {}^t \nabla \vec{v} \right) \right] = 0 \quad (9.44)$$

where D' is the Taylor bubble diameter and a_b is the void fraction of a single Taylor bubble in the total mixture. The drag coefficient for small bubbles in nonvertical slug flow is again given by Eq. (9.42).

Similarly, annular-mist flow is characterized by a liquid film along the wall and a vapor core containing entrained liquid droplets. The IAC model is presented in Table 9.2. The interfacial friction factor of the liquid film is described by a standard correlation in the laminar region and is based on Wallis's correlation in the turbulent region. The values of C_D are

$$\frac{\partial \rho}{\partial t} + \vec{V} \cdot \left(\rho \vec{V} \right) + \vec{V} \cdot \rho \vec{F} - \mu \left(\frac{1}{3} \vec{V} \cdot \vec{V} + \vec{V}^2 \right) = 0 \quad (9.45)$$

where

$$\frac{\partial}{\partial t} \left[\rho \left(h + \frac{V^2}{2} \right) \right] + \vec{V} \cdot \left[\rho \vec{V} \left(h + \frac{V^2}{2} \right) \right] - \rho \vec{F} \cdot \vec{V} - \vec{V} \cdot \left(T \cdot \vec{V} \right) - \vec{V} \cdot (k \nabla T) = q_{ext}$$

$$\frac{\partial \rho v_j}{\partial t} + \frac{\partial \rho v_i v_j}{\partial x_i} + \frac{\partial p}{\partial x_j} = -\rho g_j + \mu \left[\frac{\partial^2 v_j}{\partial x_i^2} + \frac{1}{3} \frac{\partial^2 v_i}{\partial x_j \partial x_i} \right]$$

is the equivalent wetted diameter.

The drag coefficient for droplets is again given by Ishii and Chawla by Eq. (9.42).

9.6 Wall heat transfer

The constitutive equations to represent wall heat transfer are of great significance in system TH codes. They link the governing equations for two-phase flow and the heat conduction equations for fuel rods, heat exchangers, and structures. The constitutive equations for radiation heat transfer are not discussed here, which becomes increasingly important in film boiling, particularly when surface temperature is greater than ~1000 K.

Wall heat transfer is dependent on the flow channel geometry, flow regime, relative wall temperature, etc., which results in very complicated logics for selecting appropriate heat transfer models. Roth and Aydogan (2014b) outlined the wall heat transfer models of various system TH codes. RELAP5-3D implements specific

models for pipes, parallel plates, rod bundles, swirl tubes, horizontal plate, and annuli. TRACE has specific correlations for four geometries: rods, plates, cylinders, and tube bundles. RELAP5-3D uses 31 heat transfer models to represent 12 heat transfer modes. On the other hand, TRACE has 20 heat transfer models for 11 heat transfer modes. CATHARE 2 takes a relatively simple approach—eight heat transfer models for six heat transfer modes, considering three geometries of rods, plates, and cylinders. Considering the complexity of the wall heat transfer models, RELAP5 was selected here to illustrate how they are implemented in a system TH code.

In RELAP5, the total wall heat flux $q_w = \frac{h_{wg}(T_w - T_{refg})}{1} + \frac{h_{wl}(T_w - T_{reff})}{1}$ is the heat flux to the vapor plus the heat flux to the liquid:

$$q_w = \frac{h_{wg}(T_w - T_{refg})}{1} + \frac{h_{wl}(T_w - T_{reff})}{1} \quad (9.46)$$

where

h_{wg} is the heat transfer coefficient to gas,

h_{wl} is the heat transfer coefficient to liquid,

T_w is the wall temperature,

T_{refg} is the gas reference temperature,

T_{reff} is the liquid reference temperature.

The reference temperatures can be the local gas or liquid temperature or the saturation temperature, depending on the heat transfer coefficient correlation being used.

The RELAP5 wall heat transfer correlations are based mainly on internal flow in pipes. Additional geometries considered are vertical parallel plates, vertical and horizontal tube bundles and horizontal flat plates. RELAP5 has a reflood heat transfer model developed by the Paul Scherrer Institute in Switzerland (Analytis, 1996). For a reflood heat structure where heat conduction to both axial and radial directions is allowed, the same wall heat transfer logic is used as for other surfaces.

A boiling curve is used in RELAP5 to select the wall heat transfer correlations when the wall surface temperature is above the saturation temperature (superheated relative to the saturation temperature based on total pressure). When a hydraulic volume is voided and the adjacent surface temperature is subcooled, steam condensation on the surface is predicted. If noncondensable gases are present, the phenomena are more complex, because while boiling is a function of the wall superheat based on the total pressure, condensation is based on the partial pressure of steam. When the wall temperature is less than the saturation temperature based on total pressure, but greater than the saturation temperature based on steam partial pressure, a convection condition exists. Fig. 9.11 illustrates these three regions.

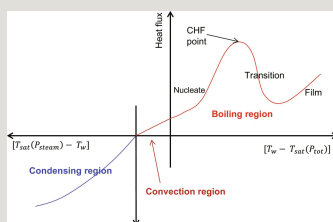


Fig. 9.11 The RELAP5 wall heat transfer curves.

9.6.1 Convection region

In the convection region, the heat transfer coefficient to liquid is the maximum among those for forced convection, laminar convection, and natural convection. The correlations are by Dittus and Boelter (1930), Kays (1955), and Churchill and Chu (1975a,b), respectively. For parallel plates the Petukhov correlation (Petukhov, 1970) is used in place of the Dittus-Boelter correlation, and the Elenbaas correlation (Incropera and DeWitt, 1990) is used instead of the Churchill-Chu correlation.

For vertical bundles, the turbulent convection coefficient is multiplied by the tube pitch-to-diameter ratio as suggested by Inayatov (1975). Horizontal bundles in RELAP5 differ from pipes in their nucleate boiling, critical heat flux, and natural convection prediction methods. Nucleate boiling predictions follow the Polley-Ralston-Grant method (Polley et al., 1981) and the prediction of critical heat flux uses the Folkin-Goldberg method (Folkin and Goldberg, 1980). Horizontal bundles use the Churchill and Chu (1975a,b) horizontal cylinder correlation.

9.6.2 Boiling region

The boiling curve uses the Chen (1966) boiling correlation up to the critical heat flux point. A table lookup method developed by Groeneveld et al. (1986) is used for the prediction of the critical heat flux. When the wall superheat exceeds the critical value, the heat flux for both the transition boiling and the film boiling regimes are calculated and the maximum value is used. This eliminates the need to predict a minimum film boiling temperature. The Chen-Sundaram-Ozkaynak correlation (Chen et al., 1977) is used for transition boiling and a modified Bromley correlation (Bromley, 1950) is used for film boiling.

The post-CHF heat transfer regimes mainly determine the PCT at the reflood phase of an LOCA in a PWR (Choi and No, 2012). They, besides droplet behaviors at that time, still have great uncertainties.

When the wall temperature exceeds that for the onset of nucleate boiling, but the bulk liquid is subcooled, subcooled nucleate boiling occurs. In this situation, the wall heat can be transferred to liquid phase only in the two-fluid formulation, but a portion of the wall heat flux is spent for vapor generation in the boundary layer near the wall. To obtain the fraction of the heat flux which causes vapor generation near a superheated wall, the Lahey method (Lahey, 1978) is used in RELAP5. The resulting vapor generation rate is given by:

$$\lambda > 0 \quad (9.47)$$

where

q'' is the total wall heat flux,

A_w is the wall surface area,

V is the cell volume,

$$\frac{\lambda_{\text{eff}}}{\lambda} = \frac{2(1-\varphi) + (\lambda_0/\lambda)(1+2\varphi)}{(2+\varphi) + (\lambda_0/\lambda)(1-\varphi)}.$$

h_{cr} is the critical enthalpy for net voids calculated using the Saha-Zuber correlation (Saha and Zuber, 1974),

$$\frac{\lambda_{\text{eff}}}{\lambda} = \frac{1}{1 - (6\varphi/\pi)^{1/3} \cdot F_i(\gamma)},$$

a pumping factor.

It was shown by Hari and Hassan (2002) that the Lahey's formulation underpredicts void fraction at low-pressure conditions. They recommended the Bowring's and Zeitoun and Shoukri's pumping factor formulations (Collier and Thome, 1994) for low-pressure conditions.

9.6.3 Condensing region

There are two methods available for calculating the condensation heat transfer coefficients for all geometries. The default method uses the maximum of Nusselt (1916) and Shah (1979). When noncondensable gases are present, the default method uses the Colburn and Hougen (1934) iteration method to solve for the interface temperature between the steam and liquid, and uses this value in the heat flux calculation. The alternate method uses Nusselt's laminar film coefficient modified for gas turbulence and noncondensable gases, using the multipliers developed by Vierow and Schrock (1992).

In the TRACE code, the total wall heat flux $\frac{d}{dt} \left(\frac{1}{T} \right) \left(\frac{1}{T} \right) \left(\frac{1}{T} \right)$ is represented by

$$\frac{\partial \rho}{\partial t} \vec{v} + \nabla \cdot (\rho \vec{v} \vec{v}) + \nabla p - \rho \vec{F} - \mu \left(\frac{1}{3} \nabla \cdot \nabla \cdot \vec{v} + \nabla^2 \vec{v} \right) = 0 \quad (9.48)$$

The second term in the right-hand side is used to represent the subcooled boiling, where the Lahey model is adopted. In Eq. (9.46), the wall heat transfer to liquid contains the subcooled boiling effect. Thus, Eqs. (9.46), (9.48) are actually the same.

For the default CHF model in TRACE, the 1995 AECL-IPPE CHF lookup table (Groeneveld et al., 1996) was selected. It is based on an extensive database of CHF values obtained in tubes with a vertical upflow of a steam-water mixture, and provides the value of the critical heat flux as a function of the local conditions.

This method was selected because of its reasonably good accuracy and wide range of applicability.

The wall heat transfer models play a crucial role in the system TH codes, requiring continuous improvement. It is well known that the model uncertainties of post-CHF heat transfer and condensation under the presence of noncondensable gases are still great, thus leading to continuous development of new models (Chatzikyriakou et al., 2010; Chikhi and Fichot, 2010; Wu et al., 2012; Huang et al., 2015). The implementation of a new model into a system TH code, however, requires very careful approach. The wall heat transfer package in a code consists of many specific models. For example, RELAP5-3D uses 31 heat transfer models. A change in one of the models, which was proved to be advanced based on the assessment against separate effect tests, may not yield expected results in a transient calculation for an integral effect test or a nuclear power plant because it may change the transient sequence, may not be used as intended, or may affect the wall heat transfer at a transition region by interpolation. Thus, a systematic assessment using integral effect tests is needed also. This causes significant delay between a new model development and its implementation in a system TH code.

9.7 Wall friction

Frictional pressure losses in a system TH code are usually divided into wall friction and form loss (or called form drag). The former models the fluid-wall shear using a friction factor approach. The latter models geometry-specific pressure losses at a sudden area change (expansion and contraction), orifice, elbow, bend, or complicated flow passage geometries, using an additive loss coefficient, of which form loss factor is usually input by the user.

Various wall friction models were introduced in Chapter 8. This chapter puts an emphasis on the method to implement the wall friction models into a system TH code. In the two-fluid formulation, the phasic pressure gradient due to wall friction can be given by

$$\frac{\partial}{\partial t} \left[\rho \left(h + \frac{v^2}{2} \right) - p \right] + \nabla \cdot \left[\rho \vec{v} \left(h + \frac{v^2}{2} \right) \right] - \rho \vec{F} \cdot \vec{v} - \nabla \cdot \left(\vec{\tau} \cdot \vec{v} \right) - \nabla \cdot \vec{q} = q_{\text{eff}} \quad (9.49)$$

and

$$\vec{\tau} = -\frac{2}{3}\mu \nabla \cdot \vec{v} \vec{I} + \mu \left(\nabla \vec{v} + {}^t \nabla \vec{v} \right); \quad (9.50)$$

where C_{wf} and C_{wg} are the wall friction coefficients for wall-liquid and wall-gas shear, respectively.

9.7.1 Single-phase flow

In the case of a single-phase flow, the wall friction coefficients of k -phase is defined by

$$\rho = \rho_k, \quad T = T_k, \quad \mu = \mu_k, \quad \lambda = \lambda_k \quad (9.51)$$

where the subscript k indicates the fluid phase (f or g) and λ_D is the friction factor. To obtain the friction factor, RELAP5 uses correlations for laminar and turbulent flows with interpolation in the transition regime. It is calculated as

$$\frac{\partial \rho Y_k}{\partial t} + \nabla \cdot (\rho Y_k \vec{v}) = \nabla \cdot (\vec{\dot{m}}_{Y_k}) + S_{Y_k} \quad (9.52)$$

where

Re is the Reynolds number,

Φ_s is a user-input shape factor for noncircular flow channels,

$\lambda_{L,2200}$ is the laminar factor at a Reynolds number of 2200,

$\lambda_{T,3000}$ is the turbulent friction factor at a Reynolds number of 3000,

ε is the surface roughness.

The turbulent friction factor is given by the Zigrang and Sylvester (1985) approximation to the Colebrook-White correlation (Colebrook, 1939). It has the advantage that it is an explicit relation for the friction factor, while the Colebrook-White correlation is a transcendental function requiring iteration for the determination of the friction factor. The friction model applies to unheated surfaces. The isothermal friction factor can be corrected for the variation of the fluid viscosity near a heated surface using the relationship used in the VIPRE code (Stewart, 1985).

In TRACE, the Churchill formula (Churchill, 1977) for the friction factor is used because it applies to all three flow regimes—laminar, transition, and turbulent:

$$\overrightarrow{\dot{m}_{Y_k}} = D_{Y_k} \nabla Y_k \tag{9.53}$$

where

$$\frac{\partial \rho Y_k}{\partial t} + \frac{\partial \rho v_j Y_k}{\partial x_j} = \frac{\partial}{\partial x_j} \left(D_{Y_k} \frac{\partial Y_k}{\partial x_j} \right) + S_{Y_k}$$

$$\sum_{k=1,n} Y_k = 1$$



Its predictions for the laminar regime are in agreement with Eq. (9.52). The predictions for transition flow are subject to some uncertainty. However, its accuracy for turbulent flow (Ebdadian and Dong, 1998) shows a maximum deviation from the Colebrook-White equation of about 3.2% for

$$Y_{k=2,n} \text{ and } \rho(p, h, Y_{k=2,n}) ; T(p, h, Y_{k=2,n}) ; \mu(p, h, Y_{k=2,n}) ; \lambda(p, h, Y_{k=2,n})$$

9.7.2 Two-phase flow

For a two-phase flow, the wall friction model based on a two-phase multiplier approach is used in RELAP5. For the normal pre-CHF flow regimes, the Lockhart-Martinelli model computes the overall friction pressure drop in terms of the liquid-alone wall friction pressure drop

$$\bar{f} = \frac{1}{T} \int_T f dt \quad (9.54)$$

or the vapor-alone wall friction pressure drop

$$f \triangleq \bar{f} + f' \quad (9.55)$$

where ϕ_f and ϕ_g are the liquid-alone and vapor-alone two-phase Darcy-Weisbach friction multipliers, respectively. The phasic wall friction pressure gradients are expressed as

$$\frac{dP}{dz} = \frac{dP}{dz} + \frac{dP}{dz} \quad (9.56)$$

for the liquid alone, and

$$\bar{f}' = 0 \quad (9.57)$$

for the vapor alone, where λ_k' indicates the liquid- and vapor-alone Darcy-Weisbach friction factors, calculated at the respective Reynolds numbers

$$\overline{cf} = c\overline{f} \text{ if } c = cte \quad (9.58)$$

and

$$\overline{\overline{f}} = \overline{f} \quad (9.59)$$

The liquid and vapor mass flow rates, respectively, are defined as

$$\overline{f\overline{g}} = \overline{f}\overline{g} \quad (9.60)$$

and

$$\frac{\partial \overline{f}}{\partial x} = \frac{\partial \overline{f}}{\partial x} \quad (9.61)$$

The two-phase multiplier ϕ_f and ϕ_g is calculated from the Heat Transfer and Fluid Flow Service (HTFS)-modified Baroczy correlation (Chaxton et al., 1972) in RELAP5. The individual phasic wall friction components are calculated by apportioning the two-phase friction between the phases using a technique derived

by Chisholm (1967) from the Lockhart and Martinelli (1949) model. The partitioning model is based on the assumption that the frictional pressure drop may be calculated using a quasisteady form of the momentum equation and the effect of individual flow regime is separately modeled. For example, in a bubbly flow at pre-CHF flow regime, the void fraction at the wall (a_{wg}) is approximated as the bulk vapor volume fraction (a_g). The wall friction coefficient for wall-gas shear (C_{wg}) is a function of a_{wg} . This indicates that the wall friction is partitioned to both liquid and vapor phases in a bubbly flow.

In TRACE, a similar approach is used for the calculation of wall friction. However, for the normal pre-CHF flow regimes (bubbly/slug and annular/mist), all of the wall drag is applied to the liquid phase alone. This is different from that in RELAP5. Thus,

$$\frac{\partial \bar{f}}{\partial t} = \frac{\partial \bar{f}}{\partial t} \quad (9.62)$$

or, in terms of the two-phase multiplier for the liquid phase considered to flow alone in the channel,

$$\rho = \rho_0 = cte \quad (9.63)$$

where the friction factor, $f_{2\phi,l}$, is calculated with

$$\rho = \rho_0 [1 - \beta(T - T_0)] \quad (9.64)$$

The wall drag coefficient is then

$$\rho = (P, T) \quad (9.65)$$

To complete the specification of the wall drag for the pre-CHF regimes, it remains

to specify the two-phase multiplier, $\frac{\partial \phi}{\partial x} + \frac{\partial \phi}{\partial y} = 0$, and the friction factor, $f_{2\phi f}$. In TRACE

code the two-phase multiplier $\frac{\partial \phi}{\partial x} + \frac{\partial \phi}{\partial y} = 0$ is a function of void fraction only, where the function depends on the flow regime. The friction factor is also dependent on the flow regime.

For two-phase flows with nucleate boiling, the pressure drop data by Ferrell and Bylund (1966) show that the two-phase multiplier when boiling is present is both significantly higher and contains a pronounced mass flux effect. Thus, an additional multiplier is devised to account for the effect.

In horizontal stratified flow, both the liquid and gas phases are in contact with the pipe wall, so the wall drag coefficient is specified for both phases. For the “inverted” post-CHF flow regimes, the wall surface temperature is beyond the minimum stable film boiling temperature, so only the gas phase is in contact with the wall. Consequently, wall-fluid shear only occurs for the gas phase and C_{wf} should be zero.

For the pre-CHF flow regimes, the two-phase frictional pressure drop models of the RELAP5 and TRACE codes are similar to each other, but the partition methods are different. In RELAP5, the wall friction is partitioned to each phase. Meanwhile, in TRACE and CATHARE 2, the wall friction is applied to the liquid phase alone for all the pre-CHF flow regimes. From a physical point of view the latter approach seems reasonable because the vapor phase does not directly touch the wall. But, this may lead to the prediction of unphysical results. For example, in the case of a steady-state bubble flow in a horizontal pipe, simple algebraic operations of the phasic momentum equations lead to the result that the vapor-phase velocity is

greater than the liquid-phase velocity if $\left[\frac{\partial}{\partial x} \left(\frac{\rho^2}{\mu} \right) \right] \left[\frac{\partial}{\partial y} \left(\frac{\rho^2}{\mu} \right) \right] \left[\frac{\partial}{\partial z} \left(\frac{\rho^2}{\mu} \right) \right] \left[\frac{\partial}{\partial t} \left(\frac{\rho^2}{\mu} \right) \right] \left[\frac{\partial}{\partial x} \left(\frac{\rho^2}{\mu} \right) \right] \left[\frac{\partial}{\partial y} \left(\frac{\rho^2}{\mu} \right) \right] \left[\frac{\partial}{\partial z} \left(\frac{\rho^2}{\mu} \right) \right] \left[\frac{\partial}{\partial t} \left(\frac{\rho^2}{\mu} \right) \right] \left[\frac{\partial}{\partial x} \left(\frac{\rho^2}{\mu} \right) \right] \left[\frac{\partial}{\partial y} \left(\frac{\rho^2}{\mu} \right) \right] \left[\frac{\partial}{\partial z} \left(\frac{\rho^2}{\mu} \right) \right] \left[\frac{\partial}{\partial t} \left(\frac{\rho^2}{\mu} \right) \right]$ (Kim et al., 2014). However, the RELAP5 approach, where C_{wg} is a nonzero coefficient, yields more reasonable results in this case. Further study is needed to improve its implementation method.

The two-phase wall friction models for bends, sudden area changes, and helically coiled tubes need further improvement (Hsu et al., 2015; Colombo et al., 2015),

requiring experimental data and correlations for an extended range of validity.

9.8 Validation of constitutive equations

The V&V process of system TH codes is discussed in detail in Chapter 13. In this section, validation of constitutive equations is briefly presented.

A system TH code usually adopts a number of mechanistic models and constitutive equations to represent various two-phase flow phenomena that may be expected to occur during design-basis accidents or anticipated transients in an light water reactor (LWR). For example, RELAP5/MOD3.3 adopts more than 200 correlations to represent two-phase flow and heat transfer processes (USNRC, 1998b). These correlations have crucial effects on the applicability and accuracy of the code and, thus, all the correlations should be validated appropriately.

As concerns the validation of the correlations, it should be noted that the calculation of any two-phase flow process usually needs several relevant correlations. For example, to predict the subcooled boiling in a vertical pipe, three correlations are involved at least: wall heat partition, interfacial drag, and interfacial heat transfer. This indicates the validation or assessment of a correlation cannot be completely separate but rather synthetic. In addition, we need to be aware that:

- (i) Each correlation was developed to represent a single phenomenon based on limited experimental data set. This leads to the *limited range* of its applicability.
- (ii) The code developers adopt one or several correlations (and combine them) to represent a phenomenon at *all possible flow conditions* that may be expected to occur during a transient. Interpolation of two or more correlations and extrapolated use of a correlation, although not desirable, might be sometimes inevitable.
- (iii) The code users use the codes for their own purposes. When they calculate a specific transient or accident, the physical phenomena of great interest may change as time goes on (i.e., as the transient advances). This means *the importance of a correlation changes according to the transient advancement*.

These features imply that constitutive equations should be validated in a synthetic approach. In this regard, the validation of constitutive equations is carried out in the framework of the code validation using separate effect tests (SETs), where key two-phase flow and heat transfer phenomena are identified first and thereafter the code (or the correlations in practice) is systematically assessed against a set of

relevant experimental data.

An internationally agreed SET validation matrix for system TH codes has been established by the OECD/NEA Committee on Safety of Nuclear Installations (OECD/NEA, 1993; Aksan, 2008). The construction of such a matrix was an attempt to collect together in a systematic way the best sets of openly available test data for code validation, assessment and improvement and also for quantitative code assessment. The experts identified 67 phenomena relevant to two-phase flow in relation to LOCAs and transients in LWRs and set up a catalog of information sheets on the experimental facilities, as a basis for the selection of the facilities and specific tests. The 67 phenomena involve 9 basic phenomena, which are evaporation due to depressurization, evaporation due to heat input, condensation due to pressurization, condensation due to heat removal, interfacial friction in vertical flow, interfacial friction in horizontal flow, wall to fluid friction, pressure drops at geometric discontinuities, and pressure wave propagation. All these are related with the constitutive equations introduced in Section 9.1–9.6. The other 58 phenomena are related with component-specific two-phase flow phenomena. Finally, they established the SET cross-reference matrix suitable for the developmental assessment of system TH codes, consisting of 2094 tests from 187 test facilities. The SET validation matrix of a recent CATHARE-2 version is known to have ~1000 tests from ~50 test facilities.

It is noted again that the validation of constitutive equations requires large amount of work and, thus, should be carried out in a systematic way.

9.9 Summary remarks

Constitutive equations suitable for the solution of an unequal-velocity, unequal-temperature (UVUT) set of balance equations and for the development of a system thermal-hydraulic are described in this chapter. Those constitutive equations are concerned with the interactions fluid-to-wall and fluid-to-gas. The fluid-to-wall related equations are also of concern in Chapters 7 and 8.

The empirical (or semiempirical) nature of the equations results from the present overview, as well as the widespread effort needed for their development in terms of time (several decades) and geographical origin of authors (from all over the world where nuclear technology is exploited).

Selected issues connected with the development and the application of constitutive equations and of interest for future investigations can be summarized as follows:

(a) The approach of two-phase multiplier for the prediction of distributed friction pressure drops in two-phase flow may benefit of deep revision where fundamental terms like τ_i and τ_w are used to build a mechanistic model with reduced (i.e., compared with current models) impact/role of empirical constants.

(b) A unified multi-D convection heat transfer surface should be constructed where, in addition to the established heat transfer regimes, phenomena or aspects (not an exhaustive list) like reflood, radiation heat transfer and transient boiling result of thermal power pulse are integrated.

(c) The development of terms including first and second (and eventually higher) order derivatives of unknowns should be promoted, eventually showing their importance (or their low impact) upon the solution the UVUT equations, including the hyperbolicity issue.

(d) An attempt should be made to connect the flow regimes to the concept of virtual mass.

(e) The pressure drop at geometric discontinuities (or abrupt area change) should also be considered part of constitutive equation packages.

(f) A special effort should be made to integrate constitutive equation modeling and water properties modeling and formulation with specific attention to the derivatives which may affect numerical solution of algebraic UVUT models: the sophistication in computing water properties should be connected with the structure and the validation of constitutive equations.

References

Ahn S.H., Aksan N., Austregesilo H., Bestion D., Chung B.D., D'Auria F., Emonot P., Gandrille J.L., Hanninen M., Horvatić I., Kim K.D., Kovtonyuk A., Petrucci A. FONESYS: the forum & network of system thermal-hydraulic codes in nuclear reactor thermal-hydraulics. *Nucl. Eng. Des.* 2015;281:103–113.

Analytis G.Th. Developmental assessment of RELAP5/MOD3.1 with separate effect and integral test experiments: model changes and options. *Nucl. Eng. Des.* 1996;163:125–148.

Aksan N. *Overview on CSNI separate effects test facility matrices for validation of best estimate thermal-hydraulic computer codes.*

In: Presented at THICKET 2008, Pisa (I)—Session III—Paper 03; 2008.

Anderson P.S., Astrup P., Eget L., Rathman O. *Numerical experience with the two-fluid model RISQUE*. In: Proceedings from Topical Meeting on Thermal Reactor Safety, Sun Valley, ID, July 31–August 4; 1977.

Baker O. Design of pipelines for the simultaneous flow of oil and gas. *Soc. Petrol. Eng.* 1953;doi:10.2118/323-G.

Bassenghi F. *Validation of the CFD Code NEPTUNE for a Full-Scale Simulator for Decay Heat Removal Systems With In-Pool Heat Exchangers*. (Ph.D. thesis) Bologna: University of Bologna; 2013.

Bestion D. *Interfacial friction determination for the 1-D six equation two-fluid model used in the CATHARE code*. In: European Two-Phase Flow Group Meeting, Marchwood, UK, 3–7 June; 1985.

Bestion D. The physical closure laws in the CATHARE code. *Nucl. Eng. Des.* 1990;124:229–245.

Bromley L.A. Heat transfer in stable film boiling. *Chem. Eng. Prog.* 1950;46:221–227.

Brooks C.S., Hibiki T., Ishii M. Interfacial drag force in one-dimensional two-fluid model. *Prog. Nucl. Energy.* 2012;61:57–68.

Brooks C.S., Ozar B., Hibiki T., Ishii M. Interfacial area transport of subcooled boiling flow in a vertical annulus. *Nucl. Eng. Des.* 2014;268:152–163.

Brown G. *Heat Transmission by Condensation of Steam on a Spray of Water Drops*. Institute of Mechanical Engineers; 1951 pp. 49–52.

Chen J.C. A correlation for boiling heat transfer to saturated fluids in convective flow. *Ind. Eng. Chem. Process Des. Dev.* 1966;5:322–327.

Chen, J.C., Sundaram, R.K., Ozkaynak, F.T., 1977. A Phenomenological Correlation for Post-CHF Heat Transfer, NUREG-0237, Washington, DC.

Chatzikyriakou D., Walker S.P., Hewitt S.P. The contribution of non-wetting droplets to direct cooling of the fuel during PWR post-LOCA reflood. *Nucl. Eng. Des.* 2010;240:3108–3114.

Chaxton, K.T., Collier, J.G., Ward, J.A., 1972. H.T.F.S. Correlation for Two-Phase Pressure Drop and Void Fraction in Tubes, AERE-R7162, UK.

Chexal, B., Lellouche, G., 1986. A Full-Range Drift-Flux Correlation for Vertical Flows (Rev. 1). EPRI NP-3989-SR, Palo Alto, CA.

Chikhi N., Fichot F. Reflooding model for quasi-intact rod configuration: quench front tracking and heat transfer closure laws. *Nucl. Eng. Des.* 2010;240:3387–3396.

Chisholm D. A theoretical basis for the Lockhart-Martinelli correlation for two-phase flow. *Int. J. Heat Mass Transf.* 1967;10:1767–1778.

Choi T.S., No H.C. An improved RELAP5/MOD3.3 reflood model considering the effect of spacer grids. *Nucl. Eng. Des.* 2012;250:613–625.

Churchill S.W., Chu H.H.S. Correlating equations for laminar and turbulent free convection from a horizontal cylinder. *Int. J. Heat Mass Transf.* 1975a;18:1049.

Churchill S.W., Chu H.H.S. Correlating equations for laminar and turbulent free convection from a vertical plate. *Int. J. Heat Mass Transf.* 1975b;18:1323–1329.

Churchill S.W. Friction factor equations spans all fluid-flow regimes. *Chem. Eng.* 1977;84:91–92.

Coddington P., Macian R. A study of the performance of void fraction correlations used in the context of drift-flux two-phase flow models. *Nucl. Eng. Des.* 2002;215:199–216.

Colebrook C.F. Turbulent flow in pipes with particular reference to the transition region between smooth and rough pipe laws. *J. Inst. Civil Eng.* 1939;11:133–156.

Colburn A.P., Hougen O.A. Design of cooler condensers for mixtures of vapors with non-condensing gases. *Ind. Eng. Chem.* 1934;26:1178–1182.

Collier J.G., Thome J.R. *Convective Boiling and Condensation*. third ed. Oxford: Clarendon Press; 1994.

Colombo M., Colombo L., Cammi A., Ricotti M.E. A scheme of correlation for frictional pressure drop in steam-water two-phase flow in helicoidal tubes. *Chem. Eng. Sci.* 2015;123:460–473.

CS & A, 2001. RETRAN-3D—A Program for Transient Thermal-Hydraulic Analysis of Complex Fluid Flow Systems, Volume 1: Theory and Numerics, Rev. 5. EPRI-NP-7500(A), Palo Alto, CA.

D'Auria F., Bestion D., Jeong J.J., Kim M. *V & V in system thermal-hydraulics*. In: ASME Verification and Validation Symposium (V & V 2012) Meeting, Las Vegas, NV, May 2–4; 2012.

Dittus F.W., Boelter L.M.K. *Heat transfer in automobile radiators of the tubular type*. Berkeley: University of California; . *Publications in Engineering*. 1930;vol. 2 pp. 443–461.

Ebadian M.A., Dong Z.F. Forced convection, internal flow in ducts. In: Rohsenow W.M., Hartnett J.P., Cho Y.I., eds. *Handbook of Heat Transfer*. third ed. New York, NY: McGraw Hill; 1998 (Chapter 5).

Emonot P., Souyri A., Gandrille J.L., Barré F. *CATHARE-3: a new system code for thermal-hydraulics in the context of the NEPTUNE project*. In: The 13th International Topical Meeting on Nuclear Reactor Thermal Hydraulics (NURETH-13), Kanazawa City, Ishikawa Prefecture, Japan, September 27–October 2; 2009.

- Fair J.R. What you need to design thermosiphon reboilers. *Pet. Ref.* 1960;39:105.
- Ferrell, J.K., Bylund, D.M., 1966. A Study of Convection Boiling Inside Channels, Final Report, Volume II. North Carolina State University, Dept. of Chemical Eng., USA.
- Folkin B.S., Goldberg Y.N. Simulation of free convection boiling crisis in vapor blanketing of a horizontal tube bundle. *Heat Transfer Sov. Res.* 1980;12(3):77–81.
- Frepoli C., Mahaffy J.H., Ohkawa K. Notes on the implementation of a fully-implicit numerical scheme for a two-phase three-field flow model. *Nucl. Eng. Des.* 2003;225:191–217.
- Fu, X., 2001. Interfacial area measurement and transport modeling in air-water two-phase flow (Ph.D. thesis). School of Nuclear Engineering, Purdue University, West Lafayette.
- Gnielinski G. New equations flow regime heat and mass transfer in turbulent pipe and channel flow. *Int. Chem. Eng.* 1976;16:359–368.
- Groeneveld D.C., Cheng S.C., Doan T. 1986 AECL-UO critical heat flux lookup table. *Heat Transfer Eng.* 1986;7(1–2):46–62.
- Groeneveld D.C., Leung L.K.H., Kirillov P.L., Bobkov V.P., Smogalev I.P., Vinogradov V.N., Huang X.C., Royer E. The 1995 look-up table for critical heat flux in tubes. *Nucl. Eng. Des.* 1996;163:1–23.
- Grossetete, C., 1995. Caractérisation expérimentale et simulations de l'évolution d'un écoulement diphasique à bulles ascendant dans une conduite verticale (Ph.D. thesis). Ecole Centrale Paris, Paris (in French).
- Ha S.J., Park C.E., Kim K.D., Ban C.H. Development of the space code for nuclear power plants. *Nucl. Eng. Technol.* 2011;43:45–62.
- Haar L., Gallagher J.S., Kell G.S. *NBS/NRC Steam Tables*:

Thermodynamic and Transport Properties and Computer Programs for Vapor and Liquid States of Water in SI Units. New York: Hemisphere; 1984.

Hari S., Hassan Y.A. Improvement of the subcooled boiling model for low-pressure conditions in thermal-hydraulics code. *Nucl. Eng. Des.* 2002;216:139–152.

Harvey, A.H., Peskin, A.P., Klein, S.A., 2000. NIST/ASME Steam Properties, Version 2.2, Users' Guide. National Institute of Standards and Technology. U.S. Department of Commerce, NIST Standard Reference Database 10, March.

Hewitt, G.F., Roberts, D.N., 1969. Studies of two-phase flow patterns by simultaneous X-ray and flash photography. AERE-M 2 1 59, HMSO, UK.

Hibiki T., Hogsett S., Ishii M. Local measurement of interfacial area interfacial velocity and liquid turbulence in two-phase flow. *Nucl. Eng. Des.* 1998;184:287–304.

Hibiki T., Ishii M. Two-group interfacial area transport equations at bubbly-to-slug flow transition. *Nucl. Eng. Des.* 2000;202:39–76.

Hibiki T., Ishii M., Xiao Z. Axial interfacial area transport of vertical bubbly flows. *Int. J. Heat Mass Transf.* 2001;44:1869–1888.

Hibiki T., Ishii M. Development of one-group interfacial area transport equation in bubbly flow systems. *Int. J. Heat Mass Transf.* 2002;45:2351–2372.

Hibiki T., Mi Y., Situ R., Ishii M. Interfacial area transport of vertical upward bubbly two-phase flow in an annulus. *Int. J. Heat Mass Transf.* 2003;46:4949–4962.

Huang J., Zhang J., Wang L. Review of vapor condensation heat and mass transfer in the presence of non-condensable gas. *Appl. Therm. Eng.* 2015;89:469–484.

Hsu L.C., Chen I.Y., Chyu C.M., Wang C.C. Two-phase pressure

drops and flow pattern observations in 90° bends subject to upward, downward and horizontal arrangements. *Exp. Thermal Fluid Sci.* 2015;68:484–492.

Idaho National Lab., 2001. RELAP5-3D Code Manual, Volume I: Code Structure, System Models and Solution Methods, INEEL-EXT-98-00834 Revision 1.3a, Idaho Falls, ID, February.

Idaho National Lab., 2012a. RELAP5-3D Code Manual, Volume I: Code Structure, System Models and Solution Methods. INEEL-EXT-98-00834, Idaho Falls, ID.

Idaho National Lab., 2012b. RELAP5-3D Code Manual, Volume IV: Models and Correlations. INEEL-EXT-98-00834, Idaho Falls, ID.

Inayatov A.Y. Correlation of data on heat transfer flow parallel to tube bundles at relative tube pitches of $1.1 < s/d < 1.6$. *Heat Transfer Sov. Res.* 1975;7(3):84–88.

Incropera F.P., DeWitt D.P. *Introduction to Heat Transfer*. New York: John Wiley & Sons; 1990 p. 501.

Ishii M. *Thermo-fluid dynamic theory of two-phase flow*. Paris: Eyrolles; 1975. *Collection de la Direction des Etudes et Recherches d'Electricite de France.*

Ishii, M., 1977. One-Dimensional Drift-Flux Model and Constitutive Equations for Relative Motion Between Phases in Various Flow Regimes. Argonne National Laboratory report ANL-77-47, USA.

Ishii M., Chawla T.C. *Local Drag Laws in Dispersed Two-Phase Flow* NUREG/CR-1230, ANL-79-105. Lemont, IL: Argonne National Laboratory; 1979.

Ishii M., Hibiki T. *Thermo-Fluid Dynamics of Two-Phase Flow*. New York, USA: Springer; 2006.

Ishii M., Jarlais G. *Inverted annular flow modeling*. In: Advanced Code Review Group Meeting, Idaho Falls, ID, July 27; 1982.

Ishii M., Kim S. Development of one-group and two-group interfacial area transport equation. *Nucl. Sci. Eng.* 2004;146:1–17.

Ishii M., Kim S., Kelly J. Development of interfacial area transport equation. *Nucl. Eng. Technol.* 2005;37:525–536.

Ishii M., Kim S., Uhle J. *Interfacial area transport: data and models*. In: Proceedings of OECD/CSNI Workshop on Advanced Thermal-hydraulics and Neutronics Codes: Current and Future Applications, Barcelona, Spain, April 10–13; 2000.

Ishii, M., Kojasoy, G., 1993. Interfacial area transport equation and preliminary considerations for closure relations, PU/NE-93-6. School of Nuclear Engineering, Purdue University, USA.

Ishii M., Mishima K. *Study of Two-Fluid Model and Interfacial Area* NUREG/CR-1873, ANL-80-111. Lemont, IL: Argonne National Laboratory; 1980.

Ishii M., Mishima K. Two-fluid model and hydrodynamic constitutive relations. *Nucl. Eng. Des.* 1984;82:107–126.

Ishii M., Wu Q., Assad A., Uhle J. *Interfacial area transport equation for two-fluid model formulation*. In: Proceedings of IMuST Meeting; 1998.

Jeong J.J., Ha K.S., Chung B.D., Lee W.J. Development of a multi-dimensional thermal-hydraulic system code, MARS 1.3.1. *Ann. Nucl. Energy.* 1999;26(18):1611–1642.

Jeong J.J., Ozar B., Dixit A., Juliá J.E., Hibiki T., Ishii M. Interfacial area transport of vertical upward air-water two-phase flow in an annulus channel. *Int. J. Heat Fluid Flow.* 2008;29:178–193.

Kataoka I., Ishii M. Drift flux model for large diameter pipe and new correlation for pool void fraction. *Int. J. Heat Mass Transf.* 1987;30:1927–1939.

Kays W.M. Numerical solution for laminar flow heat transfer in

circular tubes. *Trans. Am. Soc. Mech. Eng.* 1955;77:1265–1274.

Kim B.J., Kim J., Kim K.D. On the wall drag term in the averaged momentum equation for dispersed flows. *Nucl. Sci. Eng.* 2014;178:225–239.

Kim S., Kojasoy G., Guo T. Two-phase minor loss in horizontal bubbly flow with elbows: 45° and 90° elbows. *Nucl. Eng. Des.* 2010;240:284–289.

Kim S., Park J.H., Kojasoy G., Kelly J.M., Marshall S.O. Geometric effects of 90-degree Elbow in the development of interfacial structures in horizontal bubbly flow. *Nucl. Eng. Des.* 2007;237:2105–2113.

Kocamustafaogullari G., Ishii M. Foundation of the interfacial area transport equation and its closure relations. *Int. J. Heat Mass Transf.* 1995;38:481–493.

Kronig R., Brink J. On the theory of extraction from falling droplets. *Appl. Sci. Res.* 1950;A2:142–154.

Kuhn, S.Z., Schrock, V.E., Peterson, P.F., 1994. Final Report on U.C. Berkeley Single Tube Condensation Studies, UCB-NE-4201. U.C. Berkeley, CA.

Lahey Jr. R.T. *A mechanistic subcooled boiling model*. In: Proceedings Sixth International Heat Transfer Conference, Toronto, Canada; 293–297. 1978;1.

Lahey Jr. R.T., Drew D.A. The analysis of two-phase flow and heat transfer using a multidimensional, four field, two-fluid model. *Nucl. Eng. Des.* 2001;204:29–44.

Lee D.Y., Liu Y., Hibiki T., Ishii M., Buchanan Jr. J.R. A study of adiabatic two-phase flows using the two-group interfacial area transport equations with a modified two-fluid model. *Int. J. Multiphase Flow*. 2013;57:115–130.

Lee K., Ryley D.J. The evaporation of water droplets in superheated steam. *Trans. ASME J. Heat Transf.* 1968;90:445–456.

Lemmon E.W., Huber M.L., McLinden M.O. *NIST Standard Reference Database 23: Reference Fluid Thermodynamic and Transport Properties-REFPROP, Version 9.0*. Gaithersburg, VA: National Institute of Standards and Technology, Standard Reference Data Program; 2010.

Liles D.R., Spore J.W., Knight T.D., Nelson R.A., Cappiello M.W., Pasamehmetoglu K.O., Mahaffy J.H., Guffee L.A., Stumpf H.J., Dotson P.J. *TRAC-PF1/MOD1 Correlations and Models Technical Report NUREG/CR-5069*. Los Alamos, NM: Los Alamos National Laboratory; 1988.

Lockhart R.W., Martinelli R.C. Proposed correlation of data for isothermal two-phase, two-component flow in pipes. *Chem. Eng. Prog.* 1949;45(1):39–48.

Meyer C.A., McClintock R.G., Silvestri G.J., Spencer Jr. R.C. *ASME Steam Tables—Thermodynamic and Transport Properties of Steam*. New York: The American Society of Mechanical Engineers; 1967.

Morel C., Goreaud N., Delhay J.M. The local volumetric interfacial area transport equation: derivation and physical significance. *Int. J. Multiphase Flow.* 1999;25:1099–1128.

Nusselt W. Die Oberflächenkondensation des Wasserdampfes. *Ver. Dtsch. Ing.* 1916;60:541.

OECD/NEA, 1993. Separate Effects Test Matrix for Thermal-hydraulics Code Validation: Phenomena Characterization and Selection of Facilities and Tests. OCDE/GD(94)82, Paris.

Ozar B., Brooks C.S., Euh D.J., Hibiki T., Ishii M. Investigation of one-dimensional interfacial area transport for vertical upward air-water two-phase flow in an annular channel at elevated pressures. *Nucl. Eng. Des.* 2013a;263:362–379.

Ozar B., Brooks C.S., Hibiki T., Ishii M. Interfacial area transport of vertical upward steam-water two-phase flow in an annular channel at elevated pressures. *Int. J. Heat Mass Transf.* 2013b;57(2):504–518.

Petukhov B.S. *Heat Transfer and Friction in Turbulent Pipe Flow With Variable Physical Properties, Advances in Heat Transfer*. New York: Academic Press; 1970.503–565.

Plesset M.S., Zwick S.A. Growth of vapor bubbles in superheated liquids. *J. Appl. Phys.* 1954;25:493–500.

Polley, G.T., Ralston, T., Grant, I.D.R., 1981. Forced Crossflow Boiling in an Ideal In-line Tube Bundle, ASME 80-HT-46.

Putney, J.M., 1988a. Proposals for Improving Interphase Drag Modeling for the Bubbly and Slug Regimes in RELAP5, CERL Report RD/L/3306/R88, PWR/HTWG/P(88)622, June.

Putney, J.M., 1988b. Implementation of a New Bubbly-Slug Interphase Drag Model in RELAP5/MOD2, CERL Report RD/L/3369/R88, PWR/HTWG/P(88)597, November.

Putney, J.M., 1988c. Equations for Calculating Interfacial Drag and Shear from Void Fraction Correlations, CERL Report RD/L/3429/R88, PWR/HTWG/P(88)630, December.

Putney, J.M., 1989. Development of a New Bubbly-Slug Interfacial Friction Model for RELAP5—Final Report, National Power Report ESTD/L/0075/R89, PWR/HTWG/P(89)722, October.

Putney J.M. Development of a new bubbly-slug interfacial friction model for RELAP5. *Nucl. Eng. Des.* 1991;131:223–240.

Ranz E., Marshall W.R. Evaporation from droplets: part I and part II. *Chem. Eng. Prog.* 1952;48:141–146 173–180.

Revankar S.T., Ishii M. Local interfacial area measurement in bubbly flow. *Int. J. Heat Mass Transf.* 1992;35:913–925.

Riemke R.A. Modification to Unal's subcooled flow boiling bubble model. *Nucl. Technol.* 1993;102:416–417.

Roth G.A., Aydogan F. Theory and implementation of nuclear safety system codes. Part I: Conservation equations, flow regimes, numerics and significant assumptions. *Prog. Nucl.*

Energy. 2014a;76:160–182.

Roth G.A., Aydogan F. Theory and implementation of nuclear safety system codes. Part II: System code closure relations, validation, and limitations. *Prog. Nucl. Energy*. 2014b;76:55–72.

Ryskin G. Heat and mass transfer from a moving drop – some approximate relations for the nusselt number. *Int. Comm. Heat Mass Transfer*. 1987;14:741–749.

Saha P., Zuber N. *Point of net vapor generation and vapor void fraction in subcooled boiling*. In: Proceedings Fifth International Heat Transfer Conference, vol. 4; 1974:175–179.

Salay, M.A., 2001. Evaluation of Interfacial Drag Models for Use in TRAC-M Rod Bundle Components with Validation Against Steady-State and Transient Boil-Off Experiments (Ph.D. thesis). Univ. of Maryland, College Park, MD.

Serre G., Bestion D., Franco M., Bottin M., Marchand M. *On the stratification criterion in the CATHARE code*. In: The 14th International Topical Meeting on Nuclear Reactor Thermalhydraulics, NURETH-14, Toronto, Ontario, Canada, September 25–30; 2011.

Shah M.M. A general correlation for heat transfer during film condensation inside pipes. *Int. J. Heat Mass Transf.* 1979;22:547–556.

Shapiro A.H., Erickson A.J. On the changing size spectrum of particle clouds undergoing evaporation, combustion or acceleration. *Trans. ASME*. 1957;79:775.

Smith T.R., Schlegel J.P., Hibiki T., Ishii M. Two-phase flow structure in large diameter pipes. *Int. J. Heat Fluid Flow*. 2012a;33:156–167.

Smith T.R., Schlegel J.P., Hibiki T., Ishii M. Mechanistic modeling of inter-facial area transport in large diameter pipes. *Int. J. Multiphase Flow*. 2012b;47:1–16.

Spore J.W., Guffee L.A., Woodruff S.B., Steinke R.G. *TRAC-PF1/*

MOD2: Volume I. Theory Manual, NUREG/CR-5673.

Washington, DC: USNRC; 1993.

Stewart, C.W., 1985. VIPRE-01: A Thermal-Hydraulic Code for Reactor Cores, EPRI NP-2511-CCM, EPRI.

Stuhmiller, J.J., 1986. A Dynamic flow Regime Model of Two-Phase Flow, JAYCOR Final Report Prepared for EPRI RP888-1.

Sun X., Ishii M., Kelly J.M. Modified two-fluid model for the two-group interfacial area transport equation. *Ann. Nucl. Energy*. 2003;30:1601–1622.

Taitel Y., Bornea D., Dukler A.E. Modeling flow pattern transitions for steady upward gas-liquid flow in vertical tubes. *AIChE J.* 1980;26:345–354.

Taitel Y., Dukler A.E. A model of predicting flow regime transitions in horizontal and near horizontal gas-liquid flow. *AIChE J.* 1976;22:47–55.

Theofanous T.G. *Modeling of basic condensation processes*. In: The Water Reactor Safety Research Workshop on Condensation, Silver Springs, MD, May 24–25; 1979.

Thurgood M.J., George T.L. *COBRA/TRAC—A Thermal-Hydraulic Code for Transient Analysis of Nuclear Reactor Vessels and Primary Coolant System* NUREG/CR-3046. Washington, DC: USNRC; 1983.

Uhle J., Wu Q., Ishii M. *Dynamic flow regime modeling*. In: Proceedings of the 6th International Conference on Nuclear Engineering, Paper No. ICONE-6509, San Diego, CA, May 10–14; 1998.

Unal H.C. Maximum bubble diameter maximum bubble-growth time and bubble-growth rate during the subcooled nucleate flow boiling of water up to 17.7 MN/m². *Int. J. Heat Mass Transf.* 1976;19:643–649.

USNRC, 1987. Compendium of ECCS research for realistic LOCA analysis, NUREG-1230, Washington, DC.

USNRC, 1998a. RELAP5/MOD3 Code Manual Volume I: Code Structure, System Models, and Solution Methods, NUREG/CR-5535, Washington, DC.

USNRC, 1998b. RELAP5/MOD3 Code Manual Volume IV: Models and Correlations, NUREG/CR-5535, Washington, DC.

USNRC, 2013. TRACE V5.840 Theory Manual: Field Equations, Solution Methods, and Physical Models, Washington, DC.

Vierow K.M., Schrock V.E. *Condensation in a natural circulation loop with non-condensable gas present*. In: Japan-U.S. Seminar on Two-Phase Flow Dynamics, Berkeley, CA; 1992.

Wallis G.B. *One-Dimensional Two-Phase Flow*. New York, NY: McGraw-Hill Book Company; 1969.

Wang X., Sun X., Doup B., Zhao H. *Dynamic modeling strategy for flow regime transition in gas-liquid two-phase flows*. In: The 14th International Topical Meeting on Nuclear Reactor Thermalhydraulics, NURETH-14, Toronto, Ontario, Canada, September 25–30; 2011.

Watanabe, K., Dooley, R.B., 1996. IAPWS Release on the IAPWS Formulation 1995 for the Thermodynamic Properties of Ordinary Water Substance for General and Scientific Use, Fredericia, Denmark, September.

Wu D., Yu H., Yu J., Yu J. Reflooding characteristics investigation and predicted models improvement for the pressurized water reactor with the tight lattice core design. *Nucl. Eng. Des.* 2012;249:335–347.

Wu Q., Kim S., Ishii M., Beus S.G. One-group interfacial area transport in vertical bubbly flow. *Int. J. Heat Mass Transf.* 1998;41:1103–1112.

Yang X., Schlegel J.P., Liu Y., Paranjape S., Hibiki T., Ishii M. Experimental study of interfacial area transport in air-water two phase flow in a scaled 8×8 BWR rod bundle. *Int. J. Multiphase Flow.* 2013;50:16–32.

Yao W., Morel C. Volumetric interfacial area prediction in upward bubbly two-phase flow. *Int. J. Heat Mass Transf.* 2004;47:307–328.

Zigrang D.J., Sylvester N.D. A review of explicit friction factor equations. *Trans. ASME J. Energy Resour. Technol.* 1985;107:280–283.

Zuber N., Findlay J. Average volumetric concentration in two-phase flow systems. *Trans. ASME J. Heat Transf.* 1965;87:453–468.

Special models for nuclear thermal hydraulics

U.S. Rohatgi Brookhaven National Laboratory, Upton, NY, United States

Abstract

The balance equations supported by the closure equations may not be suitable to calculate the evolution of certain two-phase flow processes or the performance of some components, which are relevant to the accident analysis of water-cooled reactors. For this reason, special models are developed and these form a supplement to the set of balance and constitutive equations. Two main categories of special models are distinguished as phenomenon related and component related. The former category includes Two-Phase Critical Flow, Counter-Current Flow Limitation, pressure drop coefficient at geometric discontinuity, and direct contact condensation at the emergency core cooling port. The latter category includes pump, valves, steam separator, dryer, and turbine. Special models need consistency with modeling of phenomena by constitutive equations.

Keywords

Special models; Centrifugal pump; Jet pump; Steam separator; Steam dryer; Two-Phase Critical Flow (TPCF); Counter-Current Flow Limitation (CCFL); Turbine modeling; Direct contact condensation (DCC) modeling

Acronyms

BWR boiling water reactor

CCFL Counter-Current Flow
Limitation

CFD computational fluid dynamics

CSAU code scaling applicability and
uncertainty

CSNI Committee on the Safety of
Nuclear Installations

ECC emergency core cooling

ECCS emergency core cooling system

EPRI Electrical Power Research
Institute

HEM homogeneous equilibrium
model

ITF integral test facility

LBLOCA large break loss of coolant accident

LOCA loss of coolant accident

MHI Mitsubishi Heavy Industry

NEA Nuclear Energy Agency

OECD Organization for Economic Cooperation and Development

PWR pressurized water reactor

TPCF Two-Phase Critical Flow

USNRC United States Nuclear Regulatory Commission

Chapter foreword

Nuclear thermal hydraulics, as discussed in previous chapters, constitutes among the other things an ancillary discipline for nuclear reactor safety and design: whatever are the needs coming from nuclear reactor safety and design a feedback shall be expected in nuclear thermal hydraulics. In this connection, nuclear thermal hydraulics addresses the simulation of transient evolutions for two-phase mixtures: this is done through the balance equations (mass, momentum, and energy), as discussed in Chapter 5, which are supplemented by constitutive equations (see Chapter 9).

The problem arises owing to the fact that the ensemble of balance and constitutive equations do not cover all situations of interest in nuclear reactor safety and design. Therefore, “special models” are needed. Special models are distinguished into two categories dealing with:

- (a) Physical situations, which are not (or cannot be) covered by balance and constitutive equations such as Counter-Current Flow Limitation (CCFL) and Two-Phase Critical Flow (TPCF).
- (b) Performance of components or regions of the system having geometric complexity, which is not consistent with the (simple) domain of integration for the balance equations.

Therefore, special models are developed (and discussed in this chapter), which supplement balance and constitutive equations and are part of the system thermal-hydraulic code described in Chapter 11 and, in some cases, are useful for computational fluid dynamics (CFD) codes application discussed in Chapter 12.

The special models are validated as part of the system codes with procedures discussed in Chapter 13 and results of application of those models are embedded into the list of phenomena and Nuclear Power Plant (NPP) transient scenarios are discussed in Chapter 15.

10.1 Introduction

Nuclear reactors are complex systems that generate heat in the fuel. In pressurized water reactors (PWRs) the heat is convected by the coolant to steam generator where steam is produced. In boiling water reactor (BWR) the steam is produced in the core. The steam runs turbine. During abnormal situation, the reactor system

depressurizes, vapor is generated and distributes in the system, and safety injection mixes with two-phase flows. Two phase flows through various components with different configuration of the distribution of phases and interfaces.

The nuclear reactor operation and accident scenarios are simulated by thermal hydraulic codes coupled to neutronics. These codes have two-fluid one-dimensional formulation, and some have limited three-dimensional capabilities to model the vessel. However, within the reactor system, under abnormal and accident conditions, there are processes and components that cannot be modeled by these codes. These processes and components require empirical or separate analytical models. These special models have significant impact on the assessment of reactor safety systems.

Special process and component models are described in this chapter. Section 10.2 addresses process models and Section 10.3 describes special component models.

10.2 Special process models

These are the process or phenomena that are not amenable to modeling by current system formulation and require either empirical correlations or separate analytical models. In this section, some of the processes such as critical flow, Counter-Current Flow Limitation (CCFL), entrainment and de-entrainment, reflood, break flow through branch, area change losses, and grid spaces are described.

10.2.1 TPCF—Two-phase critical flow

Choked flow or critical flow conditions may occur in reactor transients either at a break or in internal flow at flow restrictions or pumps. When sonic velocities are reached at a section (often at the smallest flow cross section area) the flow becomes independent from downstream conditions. Estimation of critical flow is then of prime importance for all loss of coolant accident (LOCA) transients since the break flow rate controls the system pressure and coolant mass inventory and distribution, and consequently, the core cooling capability (see e.g., Sozzi and Sutherland, 1975).

Large classes of design basis accident scenarios involve some type of outflow from the reactor system, either through pipe break or stuck-open valves. The flow could be choked at high pressure. The choking could be subcooled choking, where flashing occurs at the break, or saturated choking, where flow at the break could be two-phase mixture or could be single-phase vapor flow choking. The computer codes for reactor simulations have generally separate correlations for subcooled

and saturated choking.

The single-phase vapor flow choking is governed by gas dynamics with choked velocity based on velocity of sound at choking plane that is either at the exit of a straight pipe or lowest area in a channel. This will not be discussed here.

$$\alpha = \frac{A_g}{A_g + A_l}$$

In the case of two-phase choking the critical flow will depend on the rate of vapor generation at choke point. The compressibility of the mixture will depend on the rate of vapor generation as fluid particles move toward the break. The rate of change of density with pressure is an inverse of sonic velocity and in case of two-phase flow, there is large change in mixture density with change in pressure, even more than in the gas phase. The sonic velocity in two-phase flow is lower than in the single-phase gas flow (Fig. 4.13 of Deych and Filipov, 1969). The measured values of the ratio of two-phase sonic velocity to vapor sonic velocity, as function of quality is shown in Fig. 10.1. There are other curves that are from different analytical models for different frequency and bubble/droplet size in this report. Similar behavior was mentioned in other studies (Kieffer, 1977). The conclusion was that the sound velocity is lower for single-component two-phase flow compared to two-component mixture and can vary with frequency.

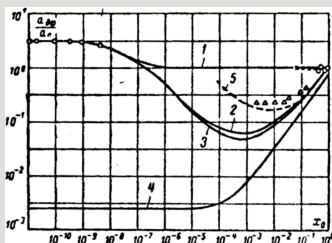


Fig. 10.1 Ratio of sound velocity in two phase to vapor sound velocity as function quality.

This vapor generation will depend on flow regime, interfacial area, interfacial momentum transfer or slip, and liquid superheat or degree of nonequilibrium. The vapor generation leads to increase in mixture velocity. It was stated by Kestin (1991) and Rohatgi and Reshotko (1975) that in case on converging-diverging nozzles the choke point could be in the diverging section contrary to single-phase flow. The vapor generation can compensate for increase in area and still accelerate the flow. However, there are no tests that measure local details of two-phase flow in critical flow tests.

The idealized situation is homogenous equilibrium model (HEM) where both phases have same velocity and same temperature. The formulation is similar to single-phase gas flow and provides the lowest sonic or choking velocity. However, this type of condition could exist in long pipe where two phases have time to get close to equilibrium conditions. HEM formulation predicts the lowest sound velocity.

$$1 - \alpha = \frac{A_l}{A_g + A_l}$$

The homogeneous thermal nonequilibrium phenomenon was addressed by two mechanistic approaches. In one case nucleation and bubble growth combination was used and in another approach critical plane pressure undershoot was estimated from experiments. The conditions at the break plane control the critical flows. It is observed that during depressurization of subcooled liquid at the break plane, there is a delay in vapor generation due to the finite rate of nucleation and bubble growth leading to fluid pressure undershooting the vapor pressure. This phenomenon was studied by Alamgir and Lienhard (1981) and Jones (1980), and expression for pressure at which vaporization will begin, as documented in TRACE, is as follows:

$$x = \frac{W_g}{W_g + W_l}$$

$$1 - x = \frac{W_l}{W_g + W_l}$$

Here subscripts *l*, *g*, *crit*, *t*, *up*, and *HEM* are liquid, vapor, critical, throat, upstream, and homogeneous equilibrium, respectively. As is seen in the expression there is an effect of rate of change of pressure of the fluid particle as it moves from upstream to the throat and of surface tension. Bernoulli equation is used to estimate flow at this pressure, which is below the saturation pressure.

There have been few studies that account for nucleation and bubble growth models to estimate vapor generation and its effect on critical flows (Rohatgi and Reshotko, 1975; Richter, 1983). While these studies provide a framework of modeling, they require a free parameter such as nucleation site density and it is not a measured quantity. It may vary by many order of magnitude values from 10^9 m^{-3} to 10^{11} m^{-3} . These analyses have used friction loss at the wall. In the case of gas flow with wall friction, the critical flow is estimated from the model and it is called Fanno equations. The reason for decrease in critical flow for gas flow is that stagnation pressure decreases and with that critical flow decreases.

There are correlations that deal with relaxation of one or other equilibrium criterion such as homogenous nonequilibrium or nonhomogenous equilibrium models. Most widely used correlations are by Moody (1966) and Henry and Fauske (1971) and HEM model is described earlier.

Moody (1965) relaxed the criterion of equal velocity but kept thermal equilibrium. His correlation is given here.

$$W = W_g + W_l$$

$$G = \frac{W}{A}$$

where H_0 is stagnation enthalpy, x is equilibrium quality, s is entropy, w and u_g are phasic velocities.

$$D_h = 4A/p$$

Fauske (1962) has suggested a slightly different slip correlation.

$$Re = \rho \times v \times D_h / \mu$$

The other widely used correlation is from Henry et al. (1970) for local conditions. They relaxed the thermal equilibrium criterion by decreasing the quality at break from equilibrium value.

$$Fr = v / \sqrt{(g \times L)}$$

where k is slip ratio. It is stated that the slip would be close to 1.0 at choke location. The critical mass flux expression was empirically obtained for low quality and valid for long pipes, and is given as

$$W_g = A_g \rho_g u_g = W \alpha$$

$$W_1 = A_1 \rho_1 u_1 = W(1 - \alpha)$$

$$\text{Heat flux} = -K(\text{temperature gradient})$$

Henry (1970) also developed correlations including pipe length. The exit quality was given as

$$q'' = -K \nabla T$$

Here x_{LT} is quality for long tube and defines as

$$q'''(r,t) - \nabla q'' = \delta / \delta t (\rho c T)$$

Henry (1970) assumed incompressible liquid and isothermal expansion of vapor phase. The critical mass flux is given as

$$q'''(r,t) - \nabla (-K \nabla (T(r,t))) = \delta / \delta t (\rho c T)$$

The decay constant B was obtained from fitting with the data and a value of 0.0523 was recommended.

There are few documents (Saha, 1978; Elias and Lellouche, 1994; Levy, 1999;

Sokolowski et al., 2012; Brittain and Karwat, 1982; Miller, 2010; OECD/NEA/CSNI, 1980) that describe various models and tests available for critical flows. Elias and Lellouche (1994) listed 66 tests with different lengths, diameters, and pressures. However, only 42 data sets were usable. The diameter of broken pipe varied from very small at 4 mm to large at 76 mm. The length varied from no pipe to 1700 mm pipe. Marviken provided a data set that was much closer to reactor system. The diameter of the pipe varied from 200 to 500 mm and length varied from 166 to 1800 mm. Elias and Lellouche's study indicated that none of the model did well with the data. The scatter plots indicated that most of the data were outside of $\pm 10\%$ of mean line.

Saha (1978) had earlier reviewed various models and concluded the following:

1. The HEM underpredicts the critical flow rates for short pipes and near liquid saturation or subcooled upstream conditions.
2. The equilibrium slip models of Fauske, Moody, and others, although successful for long tubes, underpredicted the critical flow rates for short pipes. This is particularly true if the upstream condition is subcooled or near saturation.
3. Effects of thermal nonequilibrium must be taken into account for short pipes. However, it is not clear whether the pipe length, L , or the pipe length-to-diameter ratio, L/D , or both are important in determining the effects of thermal nonequilibrium.
4. At present, there is no general model or correlation for critical flow, which is valid for a broad range of pipe lengths, pipe diameters, and upstream conditions including subcooled liquid. The more sophisticated the model used for a more precise design, the more prudent it is to consider some data benchmarking under similar conditions.

There has not been any systematic scaling study for critical flow phenomenon. The subphenomena that affect the critical mass flux have been identified but the data have not been compiled with dimensionless groups representing subcooling, flow rate, slip, wall friction, nucleation sites, geometry of break, and two-dimensional effects. Deych and Filipov (1969, Chapter 3) have provided nondimensional analyses and identified groups that control the flow conditions and critical flow. Their approach was to nondimensionalize basic two-fluid balance equations with two-phase transfer terms. They identified Strouhal (transient case), Euler, Reynolds Froude numbers, Weber, Peclet, Prandtl, Mach, and Nusselt (at interface) numbers for assessing similarity.

10.2.1.1 Models in system codes

The system codes calculate conditions at the break plane based on code models for wall and interfacial transfer terms that include wall friction. However, flow is restricted based on correlation for critical two-phase flow. These system codes include constitutive relationships based on steady-state data and flow near the choke point is rapidly changing conditions. Therefore, imposed critical flow model on break flow or possible location of choking will be sufficient.

System codes developed either 0-D or 1-D models for break flow or choked flow but in the worst conditions the accuracy of prediction cannot be better than 20% due to complex geometrical effects and to unpredictable nucleation conditions. Assessment of TRAC code with Marviken as part of code scaling applicability and uncertainty (CSAU) uncertainty estimate showed that critical flow uncertainty (or error in comparison with experimental data) was in excess of 20% (USNRC, 1989b).

These models predict area average flow rates through the break based on the conditions just upstream of the break. As these critical flow models are based on fluid properties and thermal-hydraulic conditions (pressure, temperature, void fraction), they are expected to predict break area average mass flux as independent of scale for application with same fluid. However, nonfully developed flow conditions occur upstream of the break and flow development depends, almost unavoidably, upon scale. Lack of fully developed flow will also have an impact on critical flow. In the case of power to volume scaling, the break size is scaled to volume to preserve the timescale. Ishii et al. (1998) also stated that critical velocity or mass flux is dependent on the property and thermal hydraulic conditions and the scaling should be applied to the design of the break size.

An assessment of RELAP5 and TRACE critical flow models was undertaken, e.g., by Sokolowski et al. (2012). The conclusion from this study was that code predictive accuracy was independent of the length of the pipe before the break. Another conclusion implied that same correlation worked better with one code than the other. These results indicated that the effect of length alone is not conclusive. This also means that the other two-phase flow models that estimate void vapor generation may have more important influence on the critical flow. Also the diameter effect has not been established. However, unless cross-section flow variation is significant, the diameter effect will diminish with the size of the pipe. The fact that length affects the level of thermal nonequilibrium at the break and thus affects the flow has been accepted.

10.2.2 Counter-current flow limitation (CCFL)

Counter-current flow of gas and liquid appears in many places in the reactor system, such as steam generators, core upper tie plate, hot and cold legs, and downcomer during phases of various transients (OECD/NEA/CSNI, 1993). In most cases the liquid flows down and gas flows up, and they interact at the interface. The shear at the interface that increases with gas flow rate opposes the liquid down flow. This limits the liquid down flow. CCFL is the limit of this liquid flow due to opposing gas flow. It has safety implication in getting coolant to the core and preventing heat up.

The upper plenum tie plate is a plate with holes. Similar plates exist in BWR and PWR. In both cases liquid may accumulate on the top and flow down on the top of the core. However, steam up-flow may impede or prevent this liquid down flow. The upper support plate flow is multidimensional as the steam up-flow is not uniform; the correlations are generally for average of flows over whole plate. There are data available at almost full scale from UPTF.

One of the most important phenomena for large break loss of coolant accident (LBLOCA) safety is the emergency core coolant bypass, where some of the coolant injected in the cold legs during LOCA is bypassed to broken cold leg instead of going down in the downcomer and filling the lower plenum, and flooding the core. This bypass is caused, in part, by the steam flow from the core to the broken cold leg through downcomer. This steam up-flow in the downcomer impedes and in some cases reverses the down flow of the coolant from the intact cold legs. The downcomer has counter-current flow where steam flow transfers momentum at the interface and also creates waves and entrainment at the interface. The combination of these phenomena lead to limitation of down flow of coolant for given steam up-flow, coolant subcooling, and downcomer geometry. It has also been observed that in the downcomer type geometry, the liquid coming from cold legs spreads azimuthally in the downcomer. This spreading phenomenon is much different from counter-current flow in pipes. This counter-current flow phenomenon is shown in Fig. 10.2.

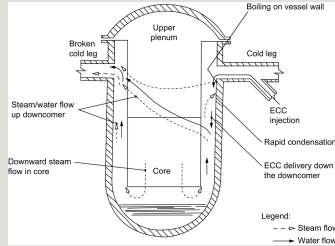


Fig. 10.2 Flow field in downcomer during refill phase.

There have been many experimental studies at different scales to address CCFL (Levy, 1999). They are in pipes and in annuli. Tests in pipes of different sizes and liquid injection methods were used to develop CCFL correlations by Wallis and Kutateladze. Wallis correlation is based on pipe diameter as length scale. Nondimensional volumetric fluxes for gas and liquid are correlated well. However, this correlation diverges from data for larger diameter pipes.

$$q'''(r, z) = K_f \Sigma_f \Phi(r, z)$$

$$q''' / q_0''' = f(t_f, t_a)$$

For pipes with diameter greater than 5 cm, the CCFL can be represented by Kutateladze correlation. It has length scale based on surface tension. Kutateladze correlation is for large pipes where waves at the interface are smaller than the pipe diameters. This is given as

$$q'' = h_s(T_{\text{wall}} - T_{\text{bulk}})$$

$$Pr = \mu \times C_e / k$$

Traditionally Wallis model is used in smaller pipe component. However recent experiences from UPTF (Wolfert, 2008; Mayinger et al., 1993) show that it can be extended to larger pipe as well, like the hot leg of PWRs.

Wallis' model predicted the reflux condensation return flow back to hot leg well in both high and low pressure range. There have been correlations similar to Wallis correlation for annular flow but were not widely used. A systematic scaling study has been done for annular geometry (Yun et al., 2004).

Different tests with annular geometry were reviewed in CSAU (Rohatgi et al., 1990) as given in Table 10.1 and Fig. 10.3. These tests were UPTF (1/1), CREARE (1/5), BCL (2/15), BCL (1/15), CREARE (1/15), and CREARE (1/30). These facilities were designed with linear scaling. A comparison of TRAC-PF1 prediction with the data (e.g., Fig. 10.4, Martinson et al., 1989, or Rohatgi et al., 1990) indicated that TRAC-PF1 overpredicted lower plenum filling rate (underpredicted emergency core cooling system (ECC) bypass) for smaller facilities. For UPTF tests, TRAC-PF1 underpredicted lower plenum filling rates.

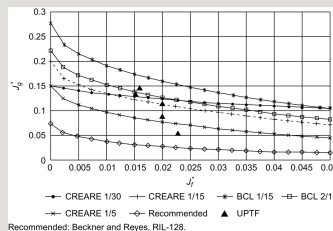


Fig. 10.3 CCFL experiments in CREARE, BCL, and UPTF (Rohatgi et al., 1990).

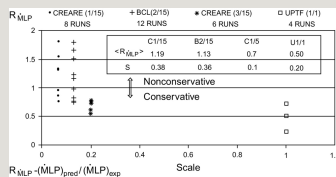


Fig. 10.4 TRAC-PF1 prediction of ECC bypass flow (Rohatgi et al., 1990).

Table 10.1

**Geometrical parameters for the CREARE, BCL and UPTF
(Rohatgi et al., 1990)**

--	--

^a Scale is the ratio of actual dimension to PWR dimension.

^b Lower plena are deeper and gaps are narrower in subscaled facilities.

Analyses of UPTF data indicated that most of the injected ECC was unaffected by steam flow as shown in Fig. 10.5. The cold water injection in the intact cold leg falls under the cold leg junction and is not impeded by steam up-flow.

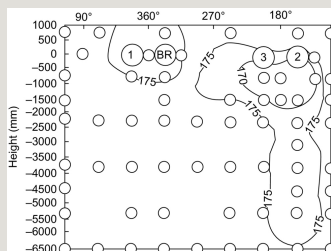


Fig. 10.5 Flow in downcomer detected in UPTF.

Yun et al. (2004) have shown that linear scaling method is not appropriate and provided a modified linear scale method. The facilities for studying CCFL

phenomena are of annular shape. The flow is multidimensional as the spread and thickness of the film are important. The annular gap has effect on flow regime expected in the downcomer; therefore the size should be such that the flow regime expected is preserved. The film thickness as it spreads under the cold leg in the downcomer is same fraction of the downcomer gap as expected in the plant. As it implies that the interfacial shear is same, the downcomer aspect ratio, that is gap and circumference ratio, should be preserved as it affects the film spreading. Yun et al. (2004) showed that data plotted in Wallis form of superficial gas velocities show that data at different sizes match.

It is recommended that UPTF or any other full-scale data can be used for code validation and for uncertainty analyses as they are available.

The pioneering investigation of this phenomenon was performed in the Semiscale facility at Idaho National Laboratory near the end of 1960s (Batt and Berta, 1978). During the simulated LOCA conditions the flashing of lower plenum liquid prevented the penetration of ECCS injected water. The coolant injected by accumulators during the blowdown period was experimentally found to be almost completely diverted toward the break, causing the bypass of the core. The resulting phenomenon was called “ECCS-core-bypass.” The ECCS core bypass is affected by many phenomena including the depressurization rate, the TPCF at the break, the pressure drops inside the vessel and the heat transfer from the reactor pressure vessel (RPV) walls. The last phenomenon is also known as the “hot wall delay.” The design of ECCS and its capability to cool the core became of concern in reference to the inability to cool the core during the LBLOCA fast depressurization observed in the experiment. Subsequent deep analyses with continuous experimental support continued until the availability of the full-scale UPTF experiments in Germany (Damerell and Simons, 1992).

10.2.3 Entrainment and de-entrainment

Nuclear reactor system has entrainment and de-entrainment phenomena taking place in different components such as core, steam generators, steam separator in BWR, and suppression pool. There are three scenarios—one in which the gas bubbles out from the interface, second, where the gas flows parallel to the interface and third, where water is separated by centrifugal forces such as in BWR separator/dryer and steam generator secondary side.

The phenomena of entrainment and de-entrainment are important as they affect the distribution of liquid in gas phase, and affect the interfacial energy, mass, and momentum transfer through the shape and size of the interface. These phenomena

occur at the interface between gas and liquid phases. The mechanism for entrainment and de-entrainment is different. The entrainment occurs due to relative velocity between gas and liquid leading to instabilities at the interface. The peaks in the waves are broken by the gas phase and results in liquid entrainment. This captured liquid may break up further until stable drop size is achieved.

There are many mechanisms of de-entrainment. In the case of horizontal flow of gas and droplet over an interface, any decrease in air velocity will decrease the shear between the gas and droplets, leading the droplets to be deposited on the interface. In the case of vertical flows, there is continuous impingement of droplets on the interface along with creation of entrainment from wavy interface. As gas slows down, the waviness will decrease, the entrainment will decrease, with a net effect of de-entrainment exceeding entrainment. In addition, if there are many steps or barriers in flow direction, the droplet will impinge and separate from the gas-droplet mixture. While gas can change direction, the droplets due to larger momentum cannot easily change the direction and impinge on the barriers. Grid spacers in the core act as a separator for droplets. These droplets impinge on solid surfaces of heated rods during accidents, providing precursor cooling prior to full-scale reflood. The phenomena of entrainment are at localized process level and generally not modeled by first principle in the system codes. Instead, the codes use correlations for net entrainment.

The system codes such as TRACE and RELAP5 have correlation for entrainment fraction, $\dot{M}_{li} = h_{li} \times D_{li} / k$, based on Ishii and Mishima correlation (Ishii and Mishima, 1989):

$$F_Q^E = \text{Engineering tolerances factor}$$

where

$$F_Q = \text{Total power peaking factor}$$

$$F_Q = F_Q^N \times F_Q^E$$

As can be seen the entrainment is based on local Weber number and Reynolds number, and depends on the diameter of the tube. The interface instabilities generally depend on the thickness of the film. Film thickness will be larger for larger diameter pipes for same void fraction and is more likely to have instability at the interface.

The other mechanism of entrainment is when gas bubbles emerge from the interface and as they leave the interface, a liquid filament is created that breaks and leads to drops. The drops have some momentum from the gas phase. However, some of the drops can fall back to the interface. A good review of this type of entrainment was provided by Bagul et al. (2013) and Ishii and Kataoka (1984). As in this situation, the liquid phase is stagnant except for activity at the interface, the entrainment ratio, $E_{fg}(h, J_g)$, is defined differently (see Fig. 10.6). It is the ratio of gas phase supplied and liquid entrained above the interface. The ratio of liquid entrainment and gas flow is shown here as function of gas space height, h . Droplets can fall back for large gas space above interface.

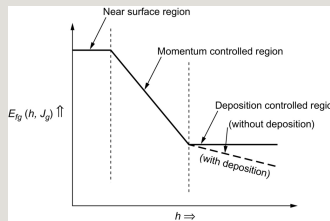


Fig. 10.6 Regions of entrainment above the separation interface. Taken from Ishii, M., Kataoka, I., 1984. Mechanistic modeling of pool entrainment phenomenon. *Int. J. Heat Mass Transf.* 27 (11), 1999–2014.

Near interface,

$$F_{\Delta H} = \Delta \text{Enthalpy}_{\text{Max}} / \Delta \text{Enthalpy}_{\text{Average}}$$

Deposition controlled region

$$F_{\Delta H_i} = \Delta \text{Enthalpy}_i / \Delta \text{Enthalpy}_{\text{Average}}$$

For intermediate region, the entrainment depends on momentum exchange and the rate is given for three different gas flow rates. For high gas flows the correlation near the interface applies.

For low flows the correlation is as follows.

$$\mathbf{P} \triangleq \widehat{\bar{\rho}} = \langle \bar{\rho} \rangle^S$$

$$\mathbf{V} \triangleq \widetilde{\bar{v}_z} = \frac{\langle \overline{\rho v_z} \rangle^S}{\langle \bar{\rho} \rangle^S} = \frac{\langle \bar{\rho} \widetilde{v_z} \rangle^S}{\langle \bar{\rho} \rangle^S}$$

For intermediate flows, a different correlation was recommended:

$$\mathbf{H} \triangleq \widehat{\bar{h}} = \frac{\langle \overline{\rho h} \rangle^S}{\langle \bar{\rho} \rangle^S} = \frac{\langle \overline{\bar{\rho} h} \rangle^S}{\langle \bar{\rho} \rangle^S}$$

$$\mathbf{Q}_k \triangleq \widehat{\bar{\rho}}_k^k = \frac{\langle \overline{\chi_k \rho_k} \rangle^S}{\alpha_k}$$

$$Q_m \triangleq \alpha_v Q_v + \alpha_l Q_l$$

Important regions of de-entrainment are steam separator and dryer in BWR and

separator in steam generator secondary side. In both cases, the vapor-liquid mixture is sent through curved channels to create centrifugal forces that separate the liquid from the steam. Most codes use empirical value of carry over and carry under fractions and from that, the amount of liquid separated from the two-phase mixture is estimated. TRACE also has a mechanistic model based on joint development undertaken by Electrical Power Research Institute (EPRI), United States Nuclear Regulatory Commission (USNRC), and General Electric. It is available in TRACE code and it consists of conservation of water mass, vapor mass, axial momentum, and angular momentum, entering and leaving the separating barrel. The model assumes a form of void distribution and vortex flow. The model does have four parameters that are determined from the tests.

The scaling issues are the effect of pipe size on entrainment in annular flow, empirical carry over, and carry under fractions for separators that are empirically obtained. For developing correlation or for model validation, full-size separate effects tests are needed.

10.2.4 Reflood

Safety of nuclear fuel in light water reactor (LWR) is ensured by keeping fuel covered with the coolant. In case of LOCAs the reactor loses inventory and may lead to degradation of cooling due to the uncovered fuel. The uncovered fuel will heat up due to decay heat. Reactors have safety injection systems such as emergency core coolant, high pressure injection, and low pressure injection to fill the vessel after the system has sufficiently depressurized to allow for such injections. Majority of the PWRs have injection in cold legs, but few designs have injection in downcomer and in hot legs. The coolant flows down in the downcomer and to lower plenum, and then to core. In the case of additional injection in the hot leg, the coolant condenses vapor in upper plenum and eventually some of this coolant flows down in the lower plenum. This hot leg injection creates an internal recirculating flow of cold coolant flowing down and two-phase mixture flowing through other part of the core (central part) and it prevents steam binding by condensing vapor in upper plenum and prevents it going to steam generator. Effects of radial power distribution and of combined coolant injection have been reported in a study from Japan (Iguchi, 1998).

These transients have generally three periods—blowdown, refill, and reflood. Blowdown period lasts about 30 s, refill period about 10 s, and reflood period lasts about 250 s. The blowdown period ends when ECC injection begins and the refill period ends when lower plenum is full. During the reflood phase the coolant starts to fill the core and quench (cool) the fuel.

The physics of quenching the core is complex. If the temperature of the clad is above the minimum stable film boiling temperature (T_{min}), the cooling will be through film boiling. However due to axial conduction and precursor cooling, the temperature of the clad can be reduced sufficiently (below T_{min}) to allow for transition and subcooled boiling. The region above subcooled boiling is still film boiling with inverted annular flow regime and dispersed droplet regime created from the breakup of the core of the inverted annular regime. The quench front or transition to subcooled boiling region moves up the core as the steam and droplet cool the core ahead of the front along with axial conduction. USNRC studies have identified the phenomena and their impact on heat transfer from the clad (Hochreiter et al., 2010; Odar, 2001).

There are two different regimes during the reflood period, based on inlet subcooling and coolant velocity, as shown in Fig. 10.7. In the case of saturated or low subcooling or low velocity core inlet flow, the vapor generation rate is high and flow regime changes from saturated boiling to dispersed boiling heat transfer. For high subcooling or higher velocity flows at the core inlet, the quenching occurs sooner and there is generally an inverse annular flow regime above the quench front. As the vapor generation increases the central liquid region breaks up, leading to dispersed film boiling regime. The droplets, in the dispersed phase, cool the vapor by evaporation and also remove clad heat if they impinge on the clad.

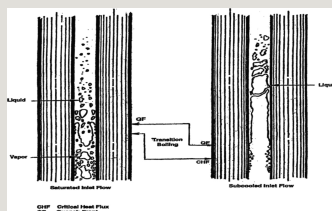


Fig. 10.7 Qualitative reflood flow regimes at different subcooling (high on the right side) and flow velocity (low on the left side).

The Hochreiter's study in support of new Rod Bundle Heat transfer Facility identified the important processes needed to be investigated in the tests for accurately modeling reflood period. It identified important processes related to local void fraction that governs interfacial heat transfer, interfacial area, fuel/clad material, transition boiling heat transfer, inlet fluid temperature and velocity, liquid entrainment, droplet size, droplet impingement heat transfer, dispersed phase heat transfer, etc. Minimum stable film boiling temperature is also important to indicate

the onset of quenching. Grid effect was not rated high but the test results showed that grid spacer improves the heat transfer due to break up of boundary layer and break up of drops.

There have been many tests to study this phenomenon. Most tests are with electrically heated fuel rod simulators without gas gap. A study (Ihle and Rust, 1987a,b) was conducted to study the effect of the gap. It concluded that fuel rod simulator without gap showed delayed quenching and higher temperatures. This is expected as the clad energy balance with gap has more resistance to heat transfer from the fuel rod leading to early quench.

The model for reflood phase in the computer codes consists of correlations for T_{min} , film boiling heat transfer, dispersed phase heat transfer, nucleate boiling, transition boiling, and conduction in the fuel rods including gap and clad. All these phenomena are based on local conditions and are not subject to any scaling issue. TRACE code has implemented Stewart and Groeneveld correlation (Stewart and Groeneveld, 1981) for T_{min} as described below. The correlation was validated with independent data. There are no terms with geometric dimensions or material properties.

$$P_k \triangleq \overline{P_k^*} \triangleq \frac{\langle X E P E \rangle^2}{\alpha_k}$$

$$P \triangleq \alpha_v P_v + \alpha_l P_l$$

The convective heat transfer in the inverted annular region is based on estimating the size of the vapor film on the wall and enhancement due to vapor-liquid interface disturbances. The correlation was further enhanced to match rod bundle data. There is also a correction for natural convection in the vapor film. It should be recognized that the film thickness determines the natural convection fluid dynamics in the vapor region, and this thickness is directly proportional to the tube hydraulic diameter.

TRACE also has a correction of 30% increase for heat transfer coefficient based on tube data for application to rod bundles. The transition from inverted annular flow

to dispersed phase is assumed to be void fraction of around 0.6. The heat transfer in dispersed phase is modeled with correlation by Forslund and Rohsenow (1968). A set of saturated and subcooled film boiling correlations were provided by Sudo (2012). The description of TRACE models (or any other system code) shows the need for well-instrumented tests with heated rod bundles.

There have been many rod bundle tests to study Reflood phenomena (Hochreiter et al., 2010). These are listed here.

- FLECHT Cosine Tests (NRC/Westinghouse)
- FLECHT Skewed Axial Power Shape Tests (NRC/Westinghouse)
- FLECHT-SEASET 21 Rod Bundle Tests (NRC/Westinghouse)
- FLECHT-SEASET 161 Unblocked Bundle Tests (NRC/Westinghouse)
- FEBA Reflood Tests (Germany)
- THTF Rod Bundle Tests (NRC/Oak Ridge National Lab)
- FRIGG Rod Loop Tests (Sweden)
- GE 9-Rod Bundle Tests (NRC/General Electric)
- NRU Rod Bundle Tests (Canada)
- ACHILLES Reflood Tests (United Kingdom)
- Lehigh 9-Rod Bundle Tests (NRC/Lehigh University)
- PERICLES Reflood Tests (France)

While these tests do simulate flow in the rod bundles, they have limitations, as pointed out by Hochreiter et al. (2010), that will make it difficult to either develop correlations or validate the models as were identified in this report and listed earlier. The tests did not measure void fractions, droplet size and velocity, and vapor temperatures. They also have different materials for clad than in the reactors. USNRC has supported a test program in Penn State University, Rod Bundle Heat transfer Test facility. This facility was designed based on the H2TS scaling approach (Zuber, 1991; Wulff, 1996). The top-down approach identified different phenomena through the transfer terms on the right side of the balance equations.

Scaling estimate identified three possible scale distortions—the presence of housing containing rod bundles that will act as an additional heat sink, electrically heated rods and gap, and finally clad material that has an effect on T_{min} .

10.2.5 Break flow in branch

There are two flow situations that differ from broken pipe flows—flow from a tank and flow through a branch. Depending on the location of break or branch, and flow regime in the main pipe, there could be either gas pull through or entrainment of the liquid. This section will address these phenomena.

One class of accidents that is simulated with system codes is small break in cold or hot legs. The break size is smaller than pipe area and could be any part of the pipe. The location of such a small break determines the loss of mass and energy from the primary system. During the transient with loss of inventory, there may be stratification of flow in the pipe with break. The flow through the break will be vapor for break at the top and with some entrainment of liquid and in case of break at the bottom, there will be liquid flow with some vapor pull through. The break in the middle will have liquid or vapor primary flow with either entrainment or gas pull through. The flow from the bottom of tank such as accumulator may have vapor pull through with vapor vortex as the level decreases. Fig. 10.8 shows various possibilities for liquid entrainments and vapor pull through.

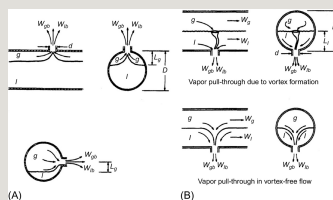


Fig. 10.8 Various possibilities for break flow from branches. (A) Illustration of liquid entrainment in break flow due to Bernoulli effect. (B) Illustrations of mechanisms for vapor pull-through a break.

It is essential that correct mass and energy discharge are calculated to characterize the fluid condition in the reactor system.

There have been studies that provided analytical models and experimental data, e.g., Zuber (1980), Reimann and Khan (1984), Schrock et al. (1986), Majumdar et al. (1999), Levy (1999), Cho and Jeun (2004), and Chung et al. (2000).

Furthermore, Zuber (1980) provided initial analyses for entrainment and vapor pull through the break. There are revised analyses with validation with data from Reimann and Khan (1984). Schrock team also conducted tests and provided revised correlation for initiation of pull through for vapor and for entrainment.

Vapor pull through and liquid entrainment require flow stratification and the presence of level for the liquid interface.

10.2.5.1 Vapor pull through

As shown earlier, there are two mechanisms of vapor pull through with vortex and without vortex. In the case of flow at the bottom of tank, there will be vapor pull through with vortex and in the case of branch in hot or cold leg, the vapor pull through will be without vortex. A study by Schrock group (Schrock et al., 1986) noted that even in the pipe flow branch, there is initially a vortex but as level decreases the vortex disappears. In some cases there is no vortex as the circulation could not be established.

The vortex free onset of vapor pull through is given by Lubin and Horwitz (1966):

$$V_k \triangleq \widetilde{\widetilde{v}}_{zk}^k \triangleq \frac{\langle \chi_k \rho_k v_{zk} \rangle^S}{\langle \chi_k \rho_k \rangle^S} = \frac{\langle \chi_k \rho_k v_{zk} \rangle^S}{\alpha_k \hat{\rho}_k^k}$$

For the case of vortex vapor pull through the correlation by Reimann and Khan (1984) is given here.

$$j_k \triangleq \overline{\chi_k v_{zk}} = \epsilon_k \bar{v}_{zk}^k$$

These correlations were compared with the data for three-flow configuration. In the case of configurations (a) and (b) there is no continuous flow such as in hot or cold legs. The pipe either has no flow or is closed on one side. The figure shows clearly the vapor pull through vortex and at lower liquid pull through without vortex. For pipe with flow higher than in the branch, there is hardly any vortex formation as shown in Fig. 10.9 for initiation of vapor pull through.

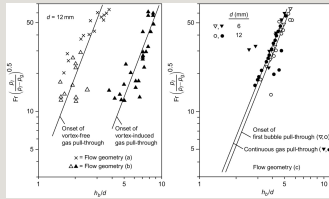


Fig. 10.9 Vapor pull through making reference to flow configurations (a), (b), and (c) in Fig. 10.7.

Reimann (Reimann and Khan, 1984) also provided a correlation for flow through the break as function of liquid level.

$$j \triangleq j_v + j_l$$

Schrock et al. (1986) developed a correlation that accounts for viscosity and surface tension in correlation for initiation of pull through as given here along with quality at the break as function of liquid level.

$$J_k \triangleq \langle j_k \rangle^S = \langle \epsilon_k \bar{v}_{zk}^k \rangle^S$$

$$J_k \triangleq J_v + J_l$$

Most of flow will be liquid but flow can be quickly choked. With information on quality a two-phase choked flow calculation can be performed.

The data from UCB, INL, and KfK are shown in Fig. 10.10.

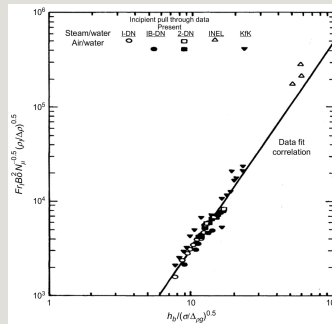


Fig. 10.10 Vapor pull through data from UCB, KfK, and INL test facilities.

10.2.5.2 Upward oriented break

In upward oriented break the vapor flow may entrain liquid through the break. As the liquid level decreases the entrainment will cease. Schrock et al. (1986) provided correlation based on their data, and data from INL and KfK (Fig. 10.10).

$$V_k \triangleq \frac{J_k}{\alpha_k} = \frac{\langle \overline{\chi_k v_{zk}} \rangle^S}{\langle \overline{\chi_k} \rangle^S}$$

$$G_k \triangleq \alpha_k Q_k V_k = \langle \overline{\chi_k \rho_k v_{zk}} \rangle^S$$

10.2.5.3 Side break

Sometimes there are breaks at the side of the pipe and the vapor pull through or liquid entrainment will depend on the relative location of the liquid level with respect to the break.

When the liquid level is above the break initiation of vapor pull through is given by following correlation that is similar to correlation for bottom break; experimental data and results from the application of the correlation are given in Fig. 10.11.

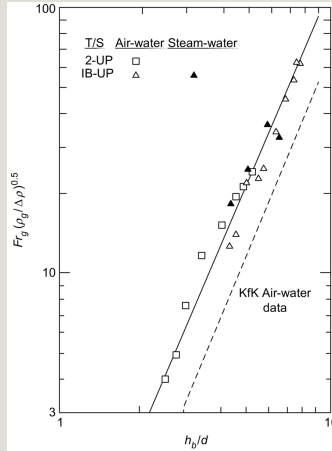


Fig. 10.11 Vapor pull through data for upward oriented break.

$$G \triangleq G_v + G_l$$

When the liquid level is below the break, the initiation of entrainment is given by the following correlation. It looks similar to the correlation for top break.

$$H_k \triangleq \overline{h_k}^k = \frac{\langle \overline{x_k \rho_k h_k} \rangle^S}{\langle \overline{x_k \rho_k} \rangle^S} = \frac{\overline{\rho_k h_k}^k}{\overline{\rho_k}^k}$$

The correlation for quality at the break was also derived from the data (Schrock et al., 1986):

$$H_m \triangleq \frac{\alpha_v Q_v H_v + \alpha_l Q_l H_l}{Q_m}$$

where $X_0=0.06$ and,

$$\overline{H}_k \triangleq \frac{\langle X_k \rho_k v_{z,k} h_k \rangle^s}{\langle X_k \rho_k v_{z,k} \rangle^s} = \frac{\alpha_k \langle \rho_k v_{z,k} h_k \rangle^s}{G_k}$$

10.2.5.4 Models in system codes

RELAP5 (USNRC, 1998) and TRACE (USNRC, 2013) codes model the branch flow or offtake, based on Smoglie's work (Smoglie, 1984). The model for liquid level with respect to branch point at the initiation of entrainment of vapor pull through is similar for all three orientations except for a constant. The expression is given here.

$$\widehat{H}_m \triangleq \frac{G_v \widehat{H}_v + G_l \widehat{H}_l}{G}$$

Here subscript k is either l for liquid or g for gas.

Furthermore,

$$\widehat{H}_k = \frac{G_k \widehat{H}_k}{G}$$

The expression for quality at the break is different for different orientation.

For top break with liquid entrainment the expression for quality is given as follows:

$$x \triangleq \frac{\alpha_v Q_v}{Q_m}$$

For bottom break with vapor pull through, the expression for quality is as follows:

$$X \triangleq \frac{G_v}{G}$$

For side break, there are two expressions depending on the location of the level with respect to the break. They are as follows:

$$X_{th} = \frac{\widehat{H}_m - h_{tsat}}{h_{vl}}$$

where,

$$\widehat{H}_m = \frac{1}{g} \left(\frac{dH}{dt} + H \frac{dG}{dt} \right)$$

10.3 Special components

Reactor system contains many components that are important for reactor performance during normal and accident conditions, such as pumps, steam separators, advance accumulator, and jet pumps. These components in the reactor system have very complicated flow and cannot be modeled by the formulations of the current system codes and require separate analyses both empirical and analytical. Some of these special components are described here.

10.3.1 Pumps

Reactor coolant pumps provide head to meet frictional losses in the loop. In addition, the torque generated also makes up for energy supplied to the coolant and any frictional losses in the pump. If there is a loss of power, the pump motor will not provide the torque and the rotating element will start to coast down depending on pump inertia and frictional losses. The pump head also decreases. In the case of reduction in pressure, the coolant may flash and a two-phase mixture flows through the pump, leading to degradation of the pump performance.

The head and torque characteristic functions have to be known in the four quadrants.

The head flow curve for the pump for single-phase flow is governed by specific speed as defined below

$$Fr = \frac{v}{\sqrt{gD}}$$

The flow direction in the pump changes from radial flow pump to axial flow pump as the specific speed increases as shown in Fig. 10.12. Here the specific speed is given in metric units.

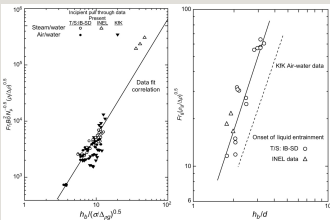


Fig. 10.12 Vapor pull through data for side oriented break.

There are many pumps in operation as shown in Table 10.2.

Table 10.2

Available data for centrifugal pumps



Pumps are generally modeled as a point (or 0-D) module. A pump is located in a node or a mesh and it adds source and/or sink terms to the momentum and energy balance equations. The model also includes angular momentum equation that predicts the rotation speed of the pump. The pump head and hydraulic torque are modeled through user-defined characteristic functions of fluid flow rate and rotational speed. The hydraulic torque is a sink term for the angular momentum equation and is multiplied by the rotation speed in a source term for the fluid energy equations. The pump head is also modeled through the user-defined characteristic functions of fluid flow rate and rotational speed. The pump head appears as a source term in the fluid momentum equations. If pump is free to rotate in reverse direction, the flow reversal can do that.

Normally, the pump performance is reported in terms of homologous curves. The parameters representing the performance are obtained from nondimensional analyses such as Buckingham π Theorem. There are five independent variables, namely pressure increase (ΔP), rotation (ω), flow rate (Q), diameter (D), and density (ρ) leading to two nondimensional groups.



$$J_k^* = \frac{\sqrt{\rho_k} J_k}{\sqrt{g \Delta \rho D}}$$

$$K_k = \frac{\sqrt{\rho_k} J_k}{(g \Delta \rho \sigma)^{1/4}}$$

We can create alternate groups that can be transformed into homologous groups by eliminating angular speed from π . In addition, the parameters can be normalized with design values so that groups remain with 1.0 and -1.0 as much as possible. The geometric parameter, D will normalize to 1.0.

$$Re = \frac{vD}{\nu}$$

We can get another set from π groups

$$We = \frac{\rho \Delta V^2 L}{\sigma}$$

This provides a general format for presenting any pump performance curves based on nondimensional analyses and normalization with design values. There are four possible flow combinations of flow and rotational speed (Choi et al., 2003).

Here, see Fig. 10.13,

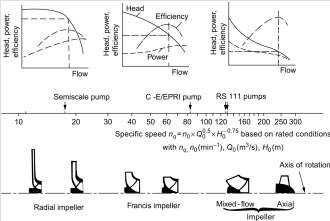


Fig. 10.13 Design characteristics for centrifugal pumps.

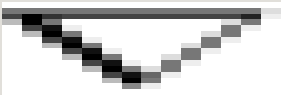


Fig. 10.14 Parameters for centrifugal pump modeling in system codes.

Single-phase pump performance is either available from manufacturer or can be obtained easily.

A study by Schneider and Winkler (1988) indicated that two-phase performance of the pumps depends on specific speed, void fraction, flow, pressure, and size. They provided some nondimensional groups to account for flow stratification, slip in phases, and flow coefficient effect on pump head degradation. An analytic study by Furuya (1985) indicated that the performance degradation occurred due to increase

in liquid velocity, slip between the phases, and void fraction change. It should be noted that this study does not include vapor compressibility, and increase in void fraction is due to relative velocity of two phases.

The pump performance degrades based on three possible phenomena in the pump channels: slip between vapor and liquid, phase separation, and vapor compressibility. The separation leads to decrease in the component of absolute velocity in the direction of rotating velocity as shown in Fig. 10.15 (Schneider and Winkler, 1988).

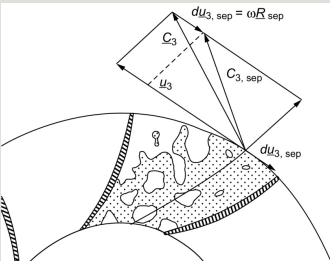


Fig. 10.15 Flow separation in blade channel.

From Euler equation for pump head.



Here u is the azimuthal velocity of impeller, c is the actual fluid velocity, and c_u is the component of fluid velocity in direction of pump speed. As seen in the figure c_u decrease due to flow separation.

Tests with full size (Chan et al., 1999) indicated that pump performance degraded rapidly around inlet void fraction of 0.35 for different inlet flows and inlet fluid temperature, as shown in Fig. 10.16.

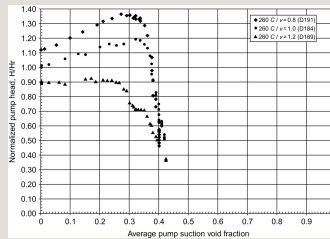


Fig. 10.16 Pump head degradation as a function of void fraction at the inlet.

The current model uses inlet void fraction-based interpolating function between single-phase and two-phase fully degraded ($\alpha > 0.9$) performance. The phase separation could also depend on the flow field upstream of the pump. The study reported in CSAU indicated that pump size, pressure, and specific speed have impact on performance degradation (Fig. 10.17).

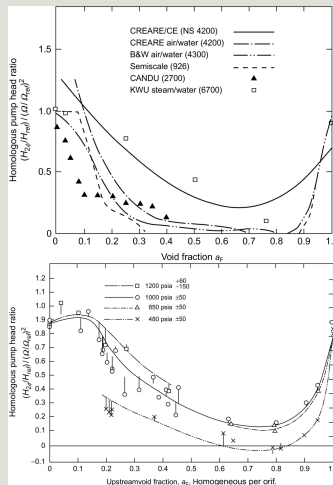


Fig. 10.17 Centrifugal pump performance, head versus entrance void relationship. Top: effect of size. Bottom: effect of pressure.

Most models only account for inlet void fraction effect on pump performance. CSAU study (USNRC, 1989a) reviewed five sets of data from small-scale pumps to 1/3 size Westinghouse pump as shown in Table 10.3. The analyses are described in Appendix I of USNRC (1989a). It was shown that pump with larger specific speed degraded less, larger pump with same specific speed degraded less, and data

at higher pressure degraded less.

Table 10.3

Degradation function for pump head based on Semiscale pump

--

The AP1000 pump is a large pump with a specific speed of 6050 in units of gpm, ft, and rpm. As shown in Table 10.2, it will have larger specific speed than any other pump. Based on CSAU analyses, it will have smaller effect of void fraction on performance. Currently, Westinghouse 1/3 scale is the largest data that is widely used. As the prototype pump (both AP1000 and regular PWR) will degrade less than Westinghouse 1/3 scale pump with same specific speed, the Westinghouse Test data may be conservative for some transients as it will lead to stagnation and flow reversal sooner during the blowdown phase of LBLOCA.

10.3.1.1 Model in system codes

The framework of pump models in TRACE and RELAP5 is based on homologous curves that are supplied through input.

Usually pump vendors give only single-phase characteristic functions in the first quadrant. It may be necessary to do experimental tests to get the pump characteristic functions in the other quadrants. Moreover, two-phase characteristic functions have also been given as user-defined functions since pump performance (head and torque) is degraded in two-phase flow conditions. Usually two-phase characteristic functions are also function of inlet void fraction. The single- and two-phase characteristics are obtained empirically along with degradation functions $M(\alpha)$ and $N(\alpha)$.

$$\frac{H}{\rho N^2 D^5} = f\left(\frac{Q}{N D^3}\right)$$



The pumps are generally modeled as a point (or 0-D) module. Turbine also adds source and/or sink terms to the momentum and energy balance equations. The sink and source terms are also modeled as user-defined functions. The degradation function is shown in Table 10.3, derived from RELAP5 []. This function can also be provided through input, see also Fig. 10.18.

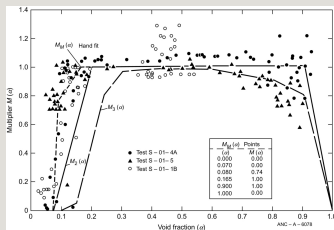


Fig. 10.18 Experimental data and modeling for the multiplier of two-phase pump performance.

The pump angular momentum balance is given as follows:

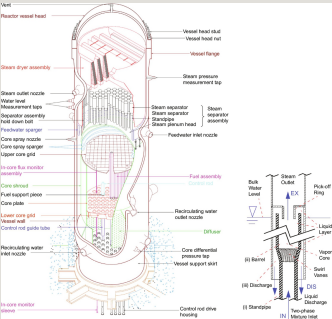
$$\vec{A} = \vec{B}$$

Here, I is the moment of inertia of moving parts; T_{hyd} and T_{frict} are hydraulic and frictional torque, respectively; and T_{fric} is the function of impeller rotational speed.

10.3.2 Separators and dryers

Separators are used to separate steam and liquid water at core exit of BWRs or at the top of PWR steam generators. These components are needed as wet steam has an adverse effect on the life of turbines. In the case of BWRs, a two-phase mixture enters the separator barrel, passing through a set of stationary swirl vanes. These vanes produce a high rotational velocity in the fluid flowing through the separator barrel. The resultant centrifugal force separates the steam-water mixture into a

water vortex on the inner wall of the separator barrel and a steam vortex in the core. The process is shown in Fig. 10.19. The separated liquid film is picked from the wall as shown in the figure. There are multiple stages of separator, each with a pick-up ring.



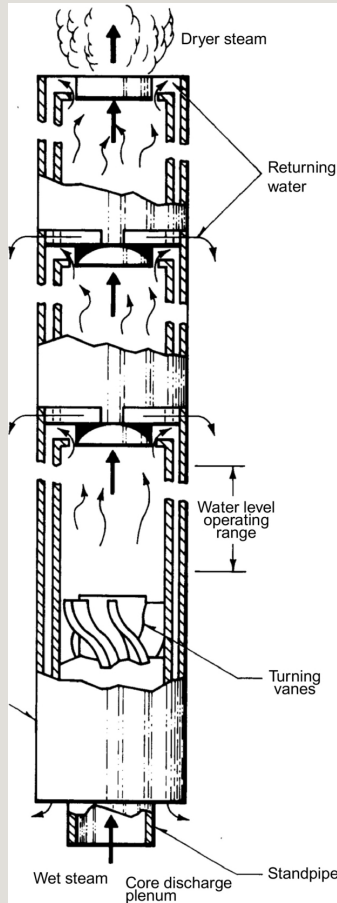


Fig. 10.19 Sketch of a BWR with detail for a single stage of steam separator.

This separation process cannot be simulated by using the 1-D two-fluid model. Special empirical models are used for the separators. The separator model determines the low void fraction mixture that goes to downcomer and high void fraction mixture going out of top outlet junction. In general, two options might be available: (i) a simple separator model in which a steam-water inflowing mixture is separated by defining the quality of the outflow streams using input specification and (ii) a mechanistic separator model, which is intended to model the centrifugal separators by solving phasic continuity equation, angular momentum equation, and axial momentum equation with some simplifying assumptions. These are discussed in next section.

A sketch of a BWR with some details of the separators can be found in Fig. 10.19.

The steam dryer uses Chevron vanes to remove the moisture, which is discharged from the steam separators. The vanes provide a curved path, which the liquid droplets must follow if they are to flow through the dryer. The liquid droplets, flowing along the curved path, hit the vanes due to their inertia and are de-entrained. The resultant liquid film flows down the vanes under the force of gravity and then back to the liquid pool surrounding the separators. The dryer efficiency depends on the steam velocity and the moisture content of the steam flow entering the dryer. Since this process cannot be simulated by using a 1-D two-fluid model, special models, which are either simple or mechanistic, are used for dryers.

10.3.2.1 Model in system codes

System codes such as RELAP5 and TRACE used supplied values for carry over quality (X_{co}) and carry under quality (X_{cu}). Carry over quality determines amount of liquid that is carried by the vapor. Carry under quality determines the amount of vapor that is carried by the discharged liquid. The purpose of this model is to predict the liquid flow rate going out with vapor and vapor going down in the downcomer.

$$\bar{f} \triangleq \frac{1}{T} \int_T f dt$$

$$\tilde{f} \triangleq \overline{\rho f} / \bar{\rho}$$

$$\vec{f}^k \triangleq \overline{\chi_k f_k} / \overline{\chi_k}$$

$$\tilde{f}_k^k \triangleq \frac{\overline{\chi_k \rho_k f_k}}{\overline{\chi_k \rho_k}} = \frac{\overline{\epsilon_k \rho_k f_k}}{\overline{\epsilon_k \rho_k}} = \frac{\overline{\rho_k f_k}}{\overline{\rho_k}}$$

This set of equation is solved for each stage of separator and will predict the mixture going into downcomer. The inlet liquid and vapor flow from the core exit are known and X_{co} and X_{cu} are specified. This is an important parameter as it will influence the core inlet subcooling and therefore, the core power.

General Electric, EPRI, and USNRC (Cheung et al., 1983) also developed a mechanistic model to predict the carry over and carry under. The model includes angular momentum conservation that leads to redistribution of liquid and vapor with liquid migrating toward the wall where it is picked up and discharged to downcomer. However some of the vapor also picked up leading to carry under. Fig. 10.19 shows the configuration of separator that is modeled. The two-phase mixture enters the separators from stand pipes. Separator has swirl vanes that create a vortex that separates the liquid toward wall and vapor in the center.

The model assumes that the axial velocity is uniform, tangential velocity is based on vortex strength, void fraction distribution is based on measurements and is related to inlet quality, X_i , pressure in gas core is uniform and in the liquid film is based on centrifugal force. The velocity and void fraction distribution are as given here.

$$\langle f \rangle^L \triangleq \frac{1}{L} \int_L f \, dl$$

where

$$\langle f \rangle^S \triangleq \frac{1}{A} \int_A f \, ds$$

$$\langle f \rangle^V \triangleq \frac{1}{V} \int_V f \, dv$$

$$\left\langle f(x,y,z,t) \right\rangle^{\hat{t}} \triangleq \frac{1}{\hat{t}} \iiint_{R^3} g(x'-x,y'-y,z'-z,t) \cdot f(x',y',z',t) dx' dy' dz'$$

AA and *BB* are based on data as given in Table 10.4.

Table 10.4

Design data for steam separator

--

In addition to this distribution, there are conservation equations for mass and momentum that can be solved for gas and liquid velocities. The carry under flow rate of liquid and gas is given as follows.

For liquid film thicker than pick-off ring and barrel wall,

$$\bar{f} \triangleq \frac{\langle \rho f \rangle^S}{\langle \rho \rangle^S}$$

$$\widehat{f}_k^{\,k} \triangleq \frac{\langle X_k f_k \rangle^S}{R_k}$$

For liquid film thinner than the pick-off ring, one gets:

$$\bar{f}_k^k \triangleq \frac{\langle \chi_k \rho_k f_k \rangle^S}{\langle \rho_k \rangle^S}$$

$$\widehat{\bar{f}} \triangleq \langle \bar{f} \rangle^S$$

From mass balance carry over can be calculated,

$$\bar{f} \triangleq \frac{\langle \rho f \rangle^S}{\langle \rho \rangle^S}$$

$$\widehat{\bar{f}}_k^k \triangleq \frac{\langle \chi_k \bar{f}_k \rangle^S}{\alpha_k}$$

Liquid and vapor mass balances are given as,

$$\bar{f}_k^k \triangleq \frac{\langle \chi_k \rho_k \bar{f}_k \rangle^S}{\langle \chi_k \rho_k \rangle^S} = \frac{\rho_k \bar{f}_k^k}{\rho_k}$$

$$\frac{d}{dt} \int_{V(t)} \rho \psi dv = \int_{V(t)} \rho \phi dv - \int_{A(t)} \rho \psi \left(\vec{v} - \vec{v}_A \right) \cdot \vec{n} da - \int_{A(t)} \left(J \cdot \vec{n} \right) da$$

Angular momentum equation provides pressure drop radial film.

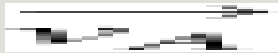
$$-\int_{A(t)} \rho \psi \left(\vec{v} - \vec{v}_A \right) \cdot \vec{n} da$$



Here v_{tw} and v_w are tangential and total velocity at the wall and r_h is hub radius.

Axial momentum balance is given as

$$\frac{d}{dx} \left[\lambda(T) \frac{dT}{dx} \right] = -q_v.$$



The details of this model are given in RELAP5 and TRACE manuals ().

10.3.3 Accumulators

Accumulators store coolant and inject when system pressure is sufficiently low to open the valve in accumulator line. Accumulators may be modeled either using standard modules (0-D, 1-D, valves, tee, walls) of the codes or by a specific accumulator model. The specific module must predict:

- Accumulator pressure as function of remaining mass and of heat released from accumulator walls (from isentropic depressurization for rapid discharge to quasi-isothermal for slow discharge).
- Flow rate delivered to the circuit as function of valve opening, accumulator pressure, primary circuit pressure, pressure losses, etc.
- Mass momentum and energy source terms in both phases in the injection mesh.
- If some specific options are actuated, the accumulator-specific module should also predict the amount of dissolved nitrogen in liquid water and the source term of nitrogen in gas mixture in the case of transport of noncondensable gas.

Recently, MHI provided model for advanced US PWR (Fig. 10.20). The advanced

accumulator has a vortex device at the bottom of the tank that replaces a valve in surge line and controls the flow rate. Similar design is used in new Korean PWR. Initially there is flow through central pipe into vortex chamber leading to radial flow in the vortex chamber exiting in surge line. After certain amount of flow has been released, there is no flow through the central pipe and only tangential flow at the bottom of the tank into the vortex chamber. This leads to vortex flow, increase in friction, and reduction in flow. MHI had a full length, half size test facility and developed a model to connect pressure difference between top of the accumulator and cold leg, liquid level for early flow and later vortex flow case. As the vortex chamber was only half size, there was some scale distortion that was estimated using computational fluid dynamics (CFD) analyses of prototype and the test facility. Scale distortion was very small. However, CFD procedure contributed additional biases.

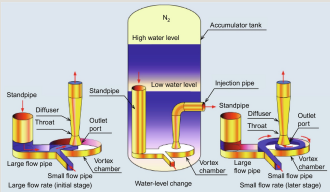
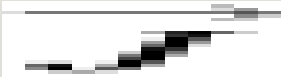


Fig. 10.20 Advanced accumulator with “vortex” device to control delivered flow rate.

The data were plotted in the form of flow coefficient and cavitation number.



$$\frac{d\Lambda}{dx} = \frac{d\Lambda}{dT} \frac{dT}{dx} = \lambda(T) \frac{dT}{dx}$$

Here, p_a , p_d , and p_{dT} are accumulator pressure, discharge pipe pressure, and total pressure in the discharge pipe, respectively.

The discharge flow rate coefficient is derived from experimental data shown in Fig. 10.21. In this case, a curve fit to the data was used in the computer codes.

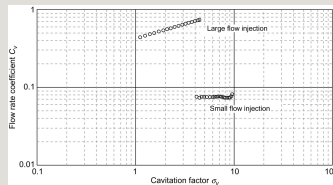


Fig. 10.21 Flow rate coefficient for the discharge from the advanced accumulator.

10.3.4 Valves, safety valves, control valves, check valves, and flow limiters

Reactor system has many valves such as safety valves, control valves, and check valves. They may be “internal” to the modeled coolant loop, or “external” when they connect the modeled coolant loop with the external space such as relief vales (e.g., containment or pressure suppression pool). These valves are either active or passive. They are characterized by the pressure loss as a function of flow rate and the flow area. In case of larger pressure difference the flow could be choked and the flow will depend on upstream conditions.

10.4 Summary remarks

Special models in nuclear thermal hydraulics, part of system codes, are discussed in this chapter, which has direct connections with Chapters 5, 9, 11, 12, and 15 as discussed in the Foreword. Physical phenomena and component-related special models are distinguished.

The motivation for special models derives from the boundaries of validity for balance and constitutive equations as well as from the use of (relatively) simple control volumes for the numerical solution. This imposes a formulation for special models directly connected with experiments. Thus, one may state that special models are empirical (or semi-empirical) by nature.

Special models are embedded into the system thermal-hydraulic codes and application of those codes to NPP transient analysis implies their use. Then, special models may be seen as modules of a feedback control system: for instance in the case of CCFL, variables calculated by the balance and constitutive equations (input to the model), like fluid velocities and void fraction, are used to determine quantities (output from the model) like the maximum liquid flow through the physical location (typically a “junction”) where the concerned special model is applied; the output from the model determines the conditions for the calculation of input variables at the new time step. Inadequate computation of the initial values of input quantities causes inadequate response of the special models, which is fed back to the overall system calculation, typically causing inadequate prediction of the system performance.

Therefore, as in many situations in nuclear thermal-hydraulics codes:

- an assigned special model may produce qualified results when embedded in one code and not when coupled to a different code,
- validation of the overall code other than validation of the individual special model is needed.

Not all special models needed for accident analysis are discussed in this chapter. This also includes special occurrences like loop seal clearing which may need detailed modeling, e.g., Tuomisto and Kajanto, (1988).

References

Alamgir M.D., Lienhard J.H. Correlation of pressure undershoot during hot water depressurization. *J. Heat Transf.* 1981;103:522–525.

Bagul R.K., Pilkhwal D.S., Vijayan P.K., Joshi J. Entrainment phenomenon in gas-liquid two-phase flow: a review. *Sadhana*. 2013;38(6):1173–1217.

Batt D.L., Berta V.T. *ECC delivery and distribution in scaled PWR experiments*. In: Consideration for the American Nuclear Society, Winter Meeting at Washington, DC, USA, 12–17 November; 1978.

Brittain, I., Karwat, H., D'Auria, F., Vigni, P., Hall, D.G.,

- Reocreux, M., 1982. Critical Flow Modelling in Nuclear Safety, NEA/OECD Report, Paris, ISBN 92-64-12366-0.
- Chan A.M.C., Kawaji M., Nakamura H., Kukita Y. Experimental study of two-phase pump performance using a full size nuclear reactor pump. *Nucl. Eng. Des.* 1999;193(1-2):159-172.
- Cheung, Y.K., Parameswaran, V., Shaug, J.C., 1983. BWR Refill-Re flood Program, Task 4.7-Model Development, TRAC-BWR Component Models, NUREG/CR-2574 (also EPRI report NP-2376, GEAP-22052, April 1983), Washington, DC.
- Cho Y.J., Jeun G.D. Modeling of liquid entrainment and vapor pull-through in header-feeder pipes of CANDU. *J. Kor. Nucl. Soc.* 2004;36:142-152.
- Choi J.S., McLaughlin D.K., Thompson D.E. Experiments on the unsteady flow field and noise generation in a centrifugal pump impeller. *J. Sound Vib.* 2003;263(3):493-514.
- Chung M.S., Chang K.S., Lee S.J. Wave propagation in two-phase flow based on a new hyperbolic two-fluid model. *J. Numer. Heat Transf. A.* 2000;38:169-191.
- Damerell, P.S., Simons, J.W., 1992. 2D/3D Program Work Summary Report, GRS-100, ISBN 3-923875-50-9, Koln.
- Deych M.Y., Filipov G.A. *The Gas Dynamics of Two Phase Media.* Fig 4-13 Moscow: Gazodinamika Dvukhfaznykh Sred; 1969.
- Elias E., Lellouche J. Two-phase critical flow. *Int. J. Multiphase Flow.* 1994;20:91-168.
- Fauske, H.K., 1962. Contribution to the Theory of Two-Phase One Component Critical Flow, Argonne National Laboratory Report, ANL-6633.
- Forslund R.P., Rohsenow M.W. Dispersed flow film boiling. *J. Heat Transf.* 1968;90:6.
- Furuya O. An analytical model for prediction of two-phase (non-condensable) flow pump performance. *ASME J. Fluids Eng.*

1985;107(1):139–147.

Henry R.E. The two-phase critical discharge of initially saturated or subcooled liquid. *Nucl. Sci. Eng.* 1970;41:336–342.

Henry R.E., Fauske H.K. The two-phase critical flow of one-component mixture in nozzles, orifices, and short tubes. *Trans. A.S.M.E. Series C, J. Heat Transfer.* 1971;93:179–187.

Henry R.E., Fauske H.K., McComas S.T. Two-phase critical flow at low qualities, part II. *Nucl. Sci. Eng.* 1970;41:92–98.

Hochreiter L., Cheung F.-B., Lin T.F., Frepoli C., Sridharan A., Todd D.R., Rosal E.R. *Rod Bundle Heat transfer Test Facility, Test Plan and Design*. NUREG/CR-6975 Washington, DC: USNRC; 2010.

Iguchi, T., 1998. Study of Thermal-Hydraulics During a PWR Reflood Phase, JAERI-Research-98-054, Tokai Mura.

Ihle P., Rust K. PWR reflood experiments using full length bundles of rods with zircaloy claddings and alumina pallets. *J. Nucl. Eng. Des.* 1987a;99:223–237.

Ihle P., Rust K. PWR reflood experiments using full length bundles of rods with zircaloy claddings and alumina pellets: Results of the SEFLEX program. *J. Nucl. Eng. Des.* 1987b;99:223–237.

Ishii M., Kataoka I. Mechanistic modeling of pool entrainment phenomenon. *Int. J. Heat Mass Transf.* 1984;27(11):1999–2014.

Ishii M., Mishima K. Droplet entrainment correlation in annular two-phase flow. *Int. J. Heat Mass Transf.* 1989;32(10):1835–1845.

Ishii M., Revankar S.T., Leonardi T., Dowlati R., Bertodano M.L., Babelli I., Wang W., Pokharna H., Ransom V.H., Viskanta R., Han J.T. The three-level scaling approach with application to the Purdue University Multi-Dimensional Integral Test Assembly (PUMA). *J. Nucl. Eng. Des.* 1998;186:177–212.

Jones Jr., O.C., 1980. Flashing Inception in Flowing Liquids, Brookhaven National Laboratory Report BNL-NUREG-51221, also NUREG/CR-1515.

Kestin J. *Spurious solutions in critical two-phase flow numerical codes*. In: International Conference on Multiphase Flow, Tsukuba, Japan, 1991; 1991.

Kieffer S.W. Sound speed in liquid-gas mixture: water-air and water-steam. *J. Geophys. Res.* 1977;82(20):2895–2904.

Levy S. *Two-Phase Flow in Complex Systems*. New York: John Wiley & Sons; 1999 (Chapter 5).

Lubin B., Horwitz M. *Vapor pull through at a tank drain with and without dielectrophoretic buffing*. In: Conference on Long Term Cryo-Propellant Storage in Space; Huntsville, AL: NASA Spatial Space Center; 1966:173.

Majumdar P., Lele H.G., Gupta S.K. *Modeling the effects of vapor pull through and entrainment in the simulation of stratified header in pressurized heavy water reactor*. In: 7th International Conference in Nuclear Engineering (ICONE-7365), Tokyo, 19–23 April; 1999.

Martinson Z.R., Gasparini M., Hobbins R.R., Petti D.A., Allison C.M., Hohorst J.K., Hagrman D.L., Vinjamuri K. *PBF Severe Fuel Damage Test 1–3 Test Results Report*. EG&G Idaho Inc. Report NUREG/CR-5354, EGG-2565 Washington, DC: USNRC; 1989.

Mayinger F., Welsa P., Wolfert K. Two-phase flow phenomena in full scale reactor geometry. *J. Nucl. Eng. Des.* 1993;145:47.

Miller J. *Fundamental of nuclear engineering-module 13*. <http://www.nrc.gov/docs/ML1214/ML12142A162.pdf>. 2010.

Moody F.J. Maximum flow rate of a single component, two-phase mixture. Trans. A.S.M.E. Series C, *J. Heat Transfer*. 1965;87:134–142.

Moody F.J. Maximum two-phase vessel blowdown from pipes. *J. Heat Transf.* 1966;87:285–295.

Odar F. *Assessment of the TRAC-M Codes Using FLECHT-SEASET Reflood and Steam Cooling Data*. NUREG-1744 Washington, DC: USNRC; 2001.

OECD/NEA/CSNI, 1980. Two Phase Critical Flow Models, CSNI Report 49, Paris.

OECD/NEA/CSNI. *A separate effects test matrix for thermal-hydraulic code validation: phenomena characterization and selection of facilities and tests*. In: OECD/GD (94) 82, Vols. I and II, Paris, France; 1993.

Reimann J., Khan M. Flow through a small break at the bottom of large pipe with stratified flow. *J. Nucl. Sci. Eng.* 1984;88:297–310.

Richter H.J. Separated two phase flow model: application to critical two phase flow. *Int. J. Multiphase Flow.* 1983;9(5):511–530.

Rohatgi U.S., Reshotko E. Non-equilibrium one-dimensional two-phase flow in variable area channels. In: Lahey R.T., Wallis G.B., eds. *Non-Equilibrium Two Phase Flow*. ASME Conference Paper; Houston, TX: ASME; 1975.

Rohatgi U.S., Neymotin B., Wulff W. *Bias in Peak Clad Temperature Predictions due to Uncertainties in Modeling of ECC Bypass and Dissolved Non-Condensable Gas Phenomena*. NUREG/CR-5354 Washington, DC: USNRC; 1990.

Saha P. *A Review of Two-Phase Steam-Water Critical Flow Models With Emphasis on Thermal Non-equilibrium*. NUREG/CR-0417 Washington, DC: USNRC; 1978.

Schneider K., Winkler F.J. Physical model for reactor coolant pumps. *J. Nucl. Eng. Des.* 1988;108:99–105.

Schrock V.E., Revankar S.T., Mannheimer R., Wang C.H. *Small Break Critical Discharge—The Role of Vapor and Liquid Entrainment in a Stratified Two-Phase Region Upstream of Break*. NUREG/CR-4761, LBL-22024 Washington, DC: Lawrence

Berkeley Laboratory, USNRC; 1986.

Smoglie, C., 1984. Two-Phase Flow Through Small Branches in a Horizontal Pipe With Stratified Flow, KFK 3861, Karlsruhe.

Sokolowski L., Kozłowski T., Calvo A. *An Assessment of Two-Phase Critical Flow Models Performance in RELAP5 and TRACE Against Marviken Critical Flow Tests*. NUREG/IA-0401 Washington, DC: USNRC; 2012.

Sozzi G.L., Sutherland W.A. *Critical flow of saturated and subcooled water at high pressure*. In: Non-Equilibrium Two Phase Flows. ASME Winter Annual Meeting, Houston, Texas, 30 Nov.–5 Dec; 1975:19–25.

Stewart J.C., Groeneveld D.C. Low quality subcooled film boiling of water at elevated pressures. *J. Nucl. Eng. Des.* 1981;67:259–272.

Sudo Y. Film boiling heat transfer during reflood phase in postulated PWR loss of coolant accident. *J. Sci. Technol.* 2012;17:516–530.

Tuomisto H., Kajanto P. Two phase Flow in full scale loops seal facility. *J. Nucl. Eng. Des.* 1988;107:295–305.

USNRC, 1989a. Regulatory Guide 1.157, Best-Estimate Calculations of Emergency Core Cooling System Performance, Washington, DC.

USNRC, 1989b. Quantifying Reactor Safety Margins, NUREG/CR-5249, Washington, DC.

USNRC, 1998. RELAP5/MOD3 Code Manual Volume IV: Models and Correlations, NUREG/CR-5535, Washington, DC.

USNRC, 2013. TRACE V5.840 Theory Manual: Field Equations, Solution Methods, and Physical Models, Washington, DC.

Wolfert K. *Scaling of thermal-hydraulic phenomena and system code assessment*. In: Seminar on the Transfer of Knowledge Gained Through CSNI Activities in the Field of Thermal-

Hydraulics, THICKET, Pisa, 5–9 May; 2008.

Wulff W. Scaling of thermohydraulic systems. *J. Nucl. Eng. Des.* 1996;163:359–395.

Yun B.J., Cho H.K., Euh D.J., Song C.-H., Park G.C. Scaling for ECC bypass phenomena during LBLOCA reflood phase. *J. Nucl. Eng. Des.* 2004;231:315–325.

Zuber N. *Problems in Modelling of Small Break LOCA*. NUREG-0724 Washington, DC: U.S. Nuclear Regulatory Commission; 1980.

Zuber N. *Appendix D: A Hierarchical, Two-Tiered Scaling Analysis, An Integrated Structure and Scaling Methodology for Severe Accident Technical Issue Resolution*. US NRC, NUREG/CR-5809 Washington, DC: USNRC; 1991.

The structure of system thermal-hydraulic (SYS-TH) code for nuclear energy applications

D. Bestion Atomic Energy Commission, Grenoble, France

Abstract

The system thermal-hydraulic (SYS-TH) codes have played and will play a major role for investigating thermalhydraulics of complex systems in various situations and particularly in safety analysis. They have integrated the available knowledge which was produced during decades from the analysis of a large number of experiments. SYS-TH codes include an interface to build a nodalization of a reactor, thermal-hydraulic balance equations, models for conduction, radiation, neutron physics, fuel thermomechanics, chemical reactions, and instrumentation and control (I&C) systems. They are used to simulate reactor thermalhydraulics in normal operation and during design basis accidents. They have proven their capability to predict with sufficient confidence many accidental transients. The main characteristics of the modeling in SYS-TH codes are presented and a state-of-the-art on the predictive capabilities identifies the main sources of uncertainty of predictions.

Keywords

System thermal-hydraulic code; Nodalization; Averaging; Modeling options; Numerical scheme; Upscaling

Nomenclature

ATWS anticipated transient without
scram

B boron

BC boundary condition

BDBA beyond design basis accident

BE best estimate

BEPU best estimate plus uncertainty

BFBT BWR full-size fine mesh
bundle test

BoP balance of plant

BWR boiling water reactor

CCFL countercurrent flow limitation

CFD computational fluid dynamics

CFL courant Friedrichs Lewy

CHF critical heat flux

CIWH condensation-induced water
hammer

CL cold leg

CPU central processing unit

DBA design basis accident

DSA deterministic safety analysis

DWO density wave oscillation

ECC emergency core cooling

ECCS emergency core cooling system

FoM figure of merit

GUI graphical user interface

HL hot leg

HX heat exchanger

I&C instrumentation and control

IBLOCAs intermediate-break loss of
coolant accidents

IC initial condition

IET integral effect test

IL intermediate leg

LBLOCAs large-break loss of coolant accidents

LOCAs loss of coolant accidents

LOFW loss of feedwater

LORHR loss of residual heat removal

LP lower plenum

LWR light water reactor

MFB minimum film boiling

NPP nuclear power plant

NVFP nonvolatile fission products

ODEs ordinary differential equations

PCT peak clad temperature

PDE partial differential equation

PSA probabilistic safety analysis

PTS pressurized thermal shock

PWR pressurized water reactor

QA quality assurance

RHR residual heat removal

SBLOCAs small-break loss of coolant accidents

SCRAM safety control rods activation mechanism

SET separate effect test

SETS stability-enhancing two-step

SG steam generator

SLB steam line break

SYS-TH system thermal hydraulics

TH thermal hydraulics (or
thermalhydraulics)

TIA transport of interfacial area

TPCF two-phase critical flow

UH upper head

UP upper plenum

UQ uncertainty quantification

Chapter foreword

The system thermal-hydraulic (SYS-TH) code (or codes) can be considered as the arrival point for research in the area, either experimental or modeling related. Thus the code (or codes) also constitutes the repository of knowledge, competence, and expertise in nuclear thermal hydraulics, as already discussed in the book.

This chapter is the pivot chapter in the book: it connects the basic information in thermal hydraulics (e.g., Chapter 3, see also Chapters 1 and 2), the modeling capabilities (e.g., Chapters 5, 7–10), the needs in nuclear technology (e.g., Chapter 4 of the book) and, noticeably, the phenomena expected in transient conditions for water-cooled reactors (e.g., Chapter 6) with the applications (see, e.g., Chapter 15), and the procedures for the application in nuclear reactor safety (see, e.g., Chapter 14). Key elements ensuring proper connection between development and application are verification, validation, and uncertainty as discussed in Chapter 13.

The SYS-TH code (or codes) have a birth time which can be localized in the early 1970s (see Chapter 2) and an expected lifetime which will cover some decades during the current century, that is, till the time when computational fluid dynamics (CFD) codes (Chapter 12) will become adequately mature and sufficiently powerful. Possibly, integration of capabilities for SYS-TH and CFD codes can be expected.

11.1 Introduction to system codes

The nuclear reactor safety technology is based on deterministic safety analysis (DSA) and probabilistic safety analysis (PSA). In order to perform DSA, fully qualified computational tools are needed. Among the computational tools, the SYS-TH codes play the major role since it is able to model the whole reactor with all interactions between circuits and between components. To some extent the SYS-TH codes are multiphysics simulation tools since they include:

- Thermal-hydraulic (or fluid) modules to model flows and heat transfers in circuits
- Conduction heat transfer in solid domain

- Fuel thermomechanics
- Neutron kinetics diffusion equations
- Pump and turbine models including simple equations for predicting rotation speed of the shaft
- Regulations, control, and protection systems including actuation of safety systems, SCRAM, opening of valves, or safety injections (SIs)
- Auxiliary circuits such as residual heat removal (RHR), volumetric and chemical control, and emergency core cooling system (ECCS) may be modeled or treated as boundary conditions (BCs)

Many types of incidents or accidents can be modeled (breaks in primary, secondary, and auxiliary circuits, station black-out, loss of RHR, loss of feedwater (LOFW), loss of heat sink, stop of pumps, inadvertent closure or opening of valves, etc.).

Point kinetics (0-D modeling) for the neutron flux in the core is usually embedded in the codes, including time constancy for the axial power profile in any region of the core. However, coupling with more detailed 3-D neutron kinetics may be available.

SYS-TH codes have the capability to cover design basis accident (DBA) and some beyond DBA (BDBA) scenario up to the condition of loss of core geometric integrity; at that point severe core damage and wide melting occur that need additional modeling capabilities usually part of severe accident codes. Coupling of system codes with severe accident codes or severe accident modules may be available. The code characteristics that are necessary and that are covered here are the following:

- Although many system codes have the capability to model light water reactor (LWR), heavy-water reactors, gas-cooled reactors, liquid metal reactors, only the steam-water flows are considered here as encountered in LWRs. However, there may be some noncondensable gases, boron, radioactive, and chemical products transported in circuits.
- Modeling capabilities are available for all water-cooled reactors, including primary circuit, secondary circuit, balance of plant (BoP), and pool in the case of research reactors.

- The physical domain of simulation of SYS-TH codes should cover the single- and two-phase flows in the pressure range from 0.001 to 22 MPa, steam and clad temperatures up to 1200°C, velocity from zero to supersonic velocities. All single- and two-phase flow regimes may be encountered, and each phase can be saturated, subcooled, or superheated. Metastable states (subcooled steam and superheated liquid) are encountered in rapid depressurization.
- All heat transfer regimes between a heating or cooling wall and a single- or two-phase flow have to be modeled, including the characteristic points of the “boiling curve,” the critical heat flux (CHF), and the minimum film boiling (MFB) temperature. Furthermore, a specific reflood model is often needed.
- Modeling of two-phase critical flow (TPCF) rate and countercurrent flow limitation (CCFL) is necessary.
- Codes should be able to cover steady states and transients. Tools are necessary to obtain a reference state of a plant or of an integral test known by a few measured data temperatures, power, pressures, and to guaranty that it is a stationary state.
- Zero-dimensional or point kinetics model should be part of the code with the capability of dealing with feedbacks, for example, void fraction, temperature, control rods, etc. The availability of coupling with a 3-D neutron kinetics model is desirable.
- Fuel modeling is available, including capabilities to calculate fuel elastic deformation and creep (ballooning) and failure, as well as the effect of ballooning upon the thermal-hydraulic performance of the concerned core region. The oxidation with hydrogen production and transport model should also be available.
- SYS-TH codes have the capability of modeling logics (so-called I&C) installed in the nuclear power plant (NPP) independently of their relevance from the safety or licensing point of view (logics are needed to calculate the “realistic” system performance).

The main known system codes for which information is available are in alphabetic order: APROS (Ylijoki et al., 2008), ATHLET (Teschendorff et al., 1996), CATHARE (Bestion, 1990a; Antoni et al., 2009), CATHENA (Luxat et al., 1996), KORSAR (Gudoshnikov and Migrov Yu, 2008), MARS (Jeong et al., 1999), RELAP5 (RELAP5/MOD3, 1995; RELAP5-3-D, 2001), SPACE (Kim et al., 2009), TRAC (Boyack, 1996), TRACE (TRACE, 2007a, b,c).

Fig. 11.1 illustrates the modeling of a three-loop pressurized water reactor (PWR) modeling of a system code by the display of code results in a plant simulator based on the CATHARE code.

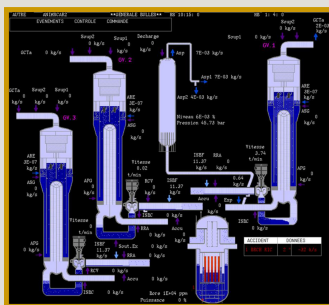


Fig. 11.1 A three-loop PWR modeled by a system code (from the plant simulator based on the CATHARE French system code). This corresponds to a situation encountered during a SBLOCA with a partial core uncover and with liquid slugs in intermediate legs.

11.2 The requirements and the domain of simulation

In order to simulate all DBAs of interest, a SYS-TH code is expected to be a multiscale, multiphysics computational tool.

Thus, the domain of simulation can be formally defined as “the set of multiphysics phenomena expected in the NPP in the case of operational and DBA conditions.”

The lists of the disciplines needed to meet the requirements are:

- Thermal hydraulics (TH) for all parts where there is fluid which may exchange mass, momentum, and energy at the boundaries. The fluid is water, steam, or steam-water mixture with possible addition of:
- Gases (i.e., N_2 , H_2 , air, and fission products), which may be transported by steam or dissolved in liquid water.
- Boron and nonvolatile fission products (B & NVFP) transport.

- Heat conduction within solid structures with exchanges with fluids.
- Neutron physics (NP).
- Chemistry, (CH) restricted to the zirconium-water reaction.
- Fuel performance (FP).
- Mechanics (ME), for example, dealing with the inertial behavior of rotors or the flapper movement in check valves.
- The I&C including the logics used to control the overall system, the subsystems, and the individual components of an NPP.

Depending on the reactor component and on the situation of interest, phenomena may be treated with more or less space resolution. Then SYS-TH codes have usually the following capabilities:

- 0-D models or lumped parameter models which may model components where velocities are low: pressurizer, upper head (UH), lower plenum (LP), upper plenum (UP), steam generator (SG) dome, inlet and outlet headers of SGs, etc.
- 1-D models for flow in components which have a privileged flow direction such as pipes, core assemblies, and annuli.
- 2-D and 3-D models for components with a 3-D velocity field as may be found in the pressure vessel (PV). An annular downcomer is usually modeled as a 2-D component and LP, core, UP, and UH are modeled as 3-D components with a relatively coarse nodalization.

Additional disciplines are involved in the DBA that are not usually treated by system codes. They are often modeled in other tools that may be coupled to SYS-TH codes:

- Mechanical loads on structures from pressure wave propagation or from pressurized thermal shock (PTS) are usually treated by other simulation tools.
- A 3-D neutron kinetics tools may substitute the “zero-dimensional” modeling capability of the system code.
- CFD codes may allow zooming in some regions of the reactor when a fine space resolution is needed for turbulent mixing (e.g., temperature mixing, boron mixing,

etc.).

- The subchannel modeling of core assemblies was traditionally treated by specific component codes although some modern system code versions have included this capability.
- Containment thermalhydraulics must also be simulated either as a simple 0-D or multi 0-D model or as a full 3-D model. The former may be treated by SYS-TH codes but the latter requires usually coupling to a specific CFD model.

SYS-TH codes are designed to be able to simulate with sufficient confidence all reactor components and all involved phenomena in the DBA domain. Identifying all dominant phenomena in each component for all reactor design and all considered DBA transients required a huge work that took decades. Such lists of phenomena and components were established for code validation matrices in OECD/NEA/CSNI documents (OECD/NEA/CSNI, 1987, 1993, 1996, 2001). A state-of-the-art report on Thermo-hydraulics of Emergency Core Cooling in Light Water Reactors was published by OECD/NEA/CSNI (1989).

11.3 Key features of system codes

SYS-TH codes considered here have three main attributes:

- SYS-TH codes are *best-estimate codes*
- SYS-TH codes are *safety codes*
- SYS-TH codes are *industrial codes*

11.3.1 Best-estimate code

A best-estimate (BE) code aims at modeling with sufficient reliability all dominant processes that take place in the domain of simulation. The modeling intends to be as close as possible to the physical reality. This is totally different from “conservative codes” which do not predict the figure of merits (FoM) but an upper bound or a lower bound of the FoM on the unfavorable side with respect to safety. For example, BE codes intend to predict the peak clad temperature (PCT) during LOCAs with the best possible accuracy when conservative codes just predict an upper limit of PCT.

The first generation of system codes was used for licensing of the first PWR and BWR (boiling water reactor) in many countries. They are being replaced by second generation BE codes for licensing.

The four first BE codes of the second generation (TRAC, RELAP5, ATHLET, and CATHARE) started to be developed in late 1970s and the 1980s and reached full maturity in the 1990s. The main objective of developing these codes was to replace evaluation models which used many conservative assumptions by the best-estimate approach for more realistic predictions of PWR or BWR accidental transients.

This constituted a very big scientific challenge since they have much higher level requirements than previous codes:

- All phenomena of all transients had to be first identified and modeled at a sufficient level of fidelity. This required a very large database and progresses in experimentation and measurement techniques were necessary.
- The selected thermal-hydraulic model had to be more sophisticated than previous models to describe the very complex physics of two-phase flows, but should remain accessible to experimental validation. A difficult compromise was made which selected the two-fluid six-equation model as the basic model for two-phase flow. This was due to the need to model both mechanical and thermal nonequilibrium with possible low mechanical coupling in stratified flow, with highly superheated steam in post-CHF conditions, with subcooled water at ECCS injection and superheated flashing water in break flow.
- 0-D and 1-D models were found able to describe most flows but a few large-scale 3-D effects were identified which required 3-D pressure vessel models and specific 2-D-3-D experimental programs.
- Closure laws for mass momentum and energy transfers at the walls and at steam-water interfaces had to be established in a huge domain of parameters, in a very large variety of complex component geometry, and for all two-phase flow regimes. This may need 150 to about 200 closure laws, which are often identified as “correlations” or “constitutive laws.” A very extensive separate effect database was necessary to develop and validate each closure law.

11.3.2 Safety code

Codes which are applied to safety demonstration for licensing must have some necessary attributes:

- The code should be developed with clearly specified quality assurance (QA) procedures
- The code must be fully documented
- The code should be verified
- The code should be validated and should prove its scalability
- The code should be complemented by uncertainty quantification (UQ) methods
- The code should have precise User Guidelines to reduce the user effect

Verification is a process for accessing the software correctness and the numerical accuracy of the solution to a given physical model defined by a set of equations. The verification is performed to demonstrate that the code numerical algorithms conform to the design requirements, that the source code conforms to programming standards and language standards, and that its logic is consistent with the design specification. This includes tracking of code errors, evaluation of numerical errors as function of node size and time step, checking of mass error and energy errors, control of code portability on different platforms and different compilers, etc.

Validation is a process for accessing the accuracy of a physical model based on comparisons between computational simulations and experimental data. The validation is performed to provide confidence in the ability of a code to predict the values of the safety parameter or parameters of interest realistically or conservatively. The validation results may be used to determine the uncertainty of some constitutive laws of the code. The validation can be conducted by the code developers and/or by the code users. The former is called developmental assessment and the latter is called independent assessment.

User Guidelines are provided to code users to give them the necessary recommendations for building an adequate nodalization and input deck, in order to perform an appropriate simulation of a thermal-hydraulic problem. User Guidelines of a system code address mainly:

- the choice of modules (0-D, 1-D, 3-D) and submodules (pumps, sources, sinks, valves, breaks, heat exchanger (HX), neutron kinetics models, etc.) to model the components of a system (test facility or reactor),
- the space resolution by giving recommendations on the mesh size for hydraulic

meshes and for heat conduction in solids,

- the time resolution by giving recommendations on the time step and time step control.

User Guidelines are necessary to eliminate or at least to reduce as far as possible the user effect. The “user effect” is what makes the difference between two sets of calculation results obtained by two code users (or two groups of code users) who use the same code to simulate the same problem (here a thermal-hydraulic system with initial and BCs), and have access to the same information for setting up the nodalization and for determining the needed input and BC values.

The *code scalability* or scale-up capability is the capacity to simulate a reactor transient with the same fidelity and accuracy as observed in SET and integral effect test (IET) simulations relative to the same situation.

UQ of a SYS-TH code is necessary when a BE code is used for safety demonstration in a BEPU methodology. The UQ methodology may use propagation of uncertainty or accuracy extrapolation methods. The propagation methods being extensively used, they require a quantification of the model uncertainties at the level of each of the closure laws.

11.3.3 Industrial code

An industrial code is a code which can be used in standardized industrial processes in a routine way. The main requirements of an industrial code are:

- The code should be highly robust and perform all simulations without code failure or with a very low rate of failures.
- The code should be developed and maintained following precise QA procedures. Successive versions should be tested and the impact of error corrections or of new capabilities should be measured and justified.
- The CPU time and response time should remain reasonable and allow many calculations with sensitivity tests to closure laws.
- When SYS-TH codes are implemented in plant simulators for operator training, real time calculations of transients which require operator actions should be obtained.

11.3.4 Some features of the first BE codes

Such system codes have a wide range of applications from research to safety and design purposes. Examples of applications are:

- Safety analysis
- Quantification of the conservative analyses margin
- Investigation of plant operating procedures and accident management
- Definition and verification of emergency operating procedures
- Investigations for new types of fuel management
- Preparation and interpretation of experimental programs
- Licensing when used together with a methodology to evaluate uncertainties of the code predictions
- Design of new reactors and systems including passive features for the third and fourth generations of NPP

System code application has been often extended to the field of severe accidents. For this purpose they are coupled with other codes, which model core degradation and fission product release.

Implementation in full scope plant simulator: simplified versions were first used to obtain real time simulations and later, thanks to the increasing computer performance, the standard versions were used.

Some features of the first second generation codes are given below.

11.3.4.1 The RELAP5 code

RELAP5 is the advanced version of the RELAP (Reactor Excursion and Leak Analysis Program) code developed at the Idaho National Engineering Laboratory. The version, RELAP5/Mod3 (see RELAP5/Mod3, 1995), includes some contributions and improvements from the member countries of the joint International Code Assessment Programme (ICAP) and its successor, the Code Application and Maintenance Programme (CAMP).

The description of the thermal hydraulics is based on a two-fluid model for two-phase flow with a flow-regime-based modeling of interfacial transport processes for mass, momentum, and energy. In the US-NRC version, only a 1-D model is

available with possible cross-flow junctions to allow some description of multi-D flows in porous bodies (core, horizontal SG, etc.). A DOE version included a 3-D pressure vessel model.

11.3.4.2 TRAC and TRACE codes

The Transient Reactor Analysis Code (TRAC), developed at the Los Alamos National Laboratory is an advanced, best-estimate computer program for the numerical simulation of postulated accident and related transient behavior in PWRs. A first preliminary version (TRAC-P1) was publicly released in 1977. Since then the code has been continuously improved (TRAC-PF1, TRAC-PF1/MOD1, and TRAC-PF1/Mod2) in order to extend the code robustness and range of applicability. A BWR version of the code was developed as a side branch at the Idaho National Engineering Laboratory following the same modeling and numerical approach as its PWR counterpart. TRACE code (TRACE, 2007a, b,c) is written in FORTRAN 90 and combines both PWR and BWR predictive capabilities. It is supposed to replace RELAP and TRAC codes for all LWRs at the US-NRC. The first validated version TRACE V5.0 (see TRACE, 2007a) was released in 2007.

The basic modeling approach for transient two-phase flow is a two-fluid model with flow regime dependent correlations for the interfacial heat, momentum, and energy transfer processes. TRAC and TRACE have a 3-D pressure vessel model.

11.3.4.3 The CATHARE code

The Code for Analysis of THERmal hydraulics during Accident of Reactor and Safety Evaluation is the French counterpart to the RELAP5 or TRAC code. The code has been developed by three partners, the French Atomic Energy Commission with the safety institute CEA & IPSN (now IRSN), the French utility EDF, and the vendor FRAMATOME (now AREVA-NP) for the BE analysis of postulated accidents in PWRs.

As in most best-estimate codes, the description of thermal nonequilibrium inhomogeneous two-phase flow is based on a two-fluid approach using mainly algebraic constitutive relations for the modeling of interfacial coupling, wall friction, and wall heat transfer processes (Bestion, 1990a). An interfacial pressure difference term has been introduced, which results in an unconditionally hyperbolic system of equations. In addition to the basic 1-D pipe component, more simplified lumped parameter models are used for tees, branches, and capacities which are needed to build complex thermal-hydraulic networks. The code is based on a two-fluid six-equation model. In the version CATHARE 2 V2.5 (Antoni et al., 2009), a

validated 3-D pressure vessel modeling is available. The code is able to model any kind of experimental facility or PWR (Western type and WWER), and is usable for other reactors (fusion reactor, RBMK reactors, BWRs, research reactors).

11.3.4.4 The ATHLET code

The thermal-hydraulic computer code ATHLET (Analysis of THERmal hydraulics of LEaks and Transients) is being developed by the Gesellschaft für Anlagen- und Reaktorsicherheit (GRS) for the safety analysis of LWRs (Teschendorff et al., 1996). The code can model the whole spectrum of design basis and BDBAs (without core degradation) like anticipated and abnormal plant transients and small to large-break loss of coolant accidents (LBLOCAs) in PWRs and BWRs. For the fluid dynamics the code user can choose between three options having different degrees of sophistication:

- The basic option is a five-equation drift flux model with separate balance equations for mass and energy and one mixture momentum equation; mechanical nonequilibrium is calculated by a full-range of drift flux correlations for horizontal and vertical flow conditions.
- A two-fluid model with separate balance equations for mass, momentum, and energy with corresponding algebraic source terms for the description of interfacial transport processes.
- A four-equation homogeneous thermal nonequilibrium model including separate mass balance equations and mixture equations for momentum and energy.

11.4 The “nodalization” concept

SYS-TH codes model the thermal-hydraulic physical system and other related coupled systems. The thermal-hydraulic system can be either the cooling circuits of a nuclear reactor, or the circuits of a test facility, to be simulated by solving systems of equations. The thermal hydraulics of the cooling circuits is generally treated by a generic method used for all components. However, some specific components having a particular geometry require some specific thermal-hydraulic models. Thermal hydraulics is also coupled to nonthermal-hydraulic systems which are also modeled in SYS-TH codes.

Since the system of interest in nuclear thermalhydraulics, that is, the reactor, is extremely complex by the geometry and by the very various physical processes, a simplified model of the reactor is established in SYS-TH codes. The fluid domain

is split into a number of meshes or “control volumes” where balance equations derived from first principles are written. This results in a discretized set of equations where physical parameters such as pressures, temperatures, and velocities are calculated in a set of nodes. Mathematically speaking, the simplification reduces the state space of the system to a finite dimension, and the partial differential equations (PDEs) of the continuous (infinite-dimensional) time and space model of the physical system into ordinary differential equations (ODEs) with a finite number of parameters. This process is often called the nodalization and includes many choices which have an important influence on the quality of predictions:

- Choice to model some component of the reactor fluid domain by either 0-D, 1-D, 2-D, or 3-D models
- Choice of the number and type of meshes (or control volumes) in each component
- Choice to model heat transfers in solid structures by either 1-D, 2-D, or 3-D models and choice of the size of meshes for heat conduction
- Choice between several options for modeling pumps, turbines, valves, safety valves, check valves, flow limiters, neutron kinetics (from point kinetics to coupling with 3-D neutron kinetics), breaks, and ECCS systems (accumulators, injection systems with pumps)
- Modeling of some systems such as separators and dryers in BWRs and in SG of PWRs
- Modeling of I&C with possible regulations
- Choice of pressure loss coefficients in all component of the circuits
- Choice to activate some CCFL option in some specific component of the circuit
- Choice of heat losses modeling
- Choice of a break flow model with possible multipliers
- Modeling of HX and choice of mesh sizes for fluid and solid walls
- Modeling of fuel either by a simple multilayer wall or by a more complex thermomechanical model which can predict fuel deformation, creeping, clad

rupture, clad oxidation, etc.

- Use of additional transport equations for noncondensable gases such as nitrogen which may be injected through accumulators, hydrogen which is produced by clad oxidation, air which may enter the system through breaks or when the system is open to containment in cold shutdown state
- Use of additional transport equations for boron concentration
- Use of additional transport equations for radioactive elements
- The coupling to containment calculation
- The coupling to possible passive systems

Such choices are necessary for building the input deck of a SYS-TH calculation. In addition to the nodalization, information is necessary to define the process to obtain an initial state—which is often a stationary and reference state—and the scenario of the transient with all necessary BCs all along the transient (break opening, automatic safety system actuations, operator actions, etc.). The time step management is also part of an input deck and it is an important choice of the user which may affect the calculation accuracy (see subsection on numerics).

The 0-D and 1-D versions of the two-fluid six-equation model are the basic models in most SYS-TH codes.

11.4.1 The 1-D modules in system codes

It is clearly the basic module of system codes since it is able to model complex two-phase flow in most components of the reactors including all pipes and also flow in core assemblies. As soon as there is a privileged direction of the flow, a 1-D model can describe the flow. There may be different closure laws depending on the duct shape. For example the CATHARE code distinguishes the pipe (used for circulation loop, surge line, SG tubes, any pipe connected to primary and secondary circuits), the annuli (for modeling annular downcomer in pressure vessel and in SGs), and the rod bundles and tube bundle (for core and riser of SGs). The 1-D system of equations is described in **Chapter 5**. This module was able to catch most phenomena of interest in many accidental transients of LWRs. However, a few limitations were encountered in low velocity situations when natural circulation effects induce 3-D velocity field with possible recirculation cells or when it is used in components which have a very complex 3-D geometry.

11.4.2 The Tee junctions

Many connections between two pipes exist in reactors and it required specific models where specific momentum balance equations have to be written. Attention was paid to phase separation phenomena when a side branch takes some fluid from a main pipe (Fig. 11.2). Due to complex pressure field and different inertia of steam and water, the quality of the side branch may be very different from the quality in the main pipe. Also in the case of stratified flow in the main pipe, the branch may be below the free surface or above and vapor pull-through below the level or water suction above the level have to be taken into account.

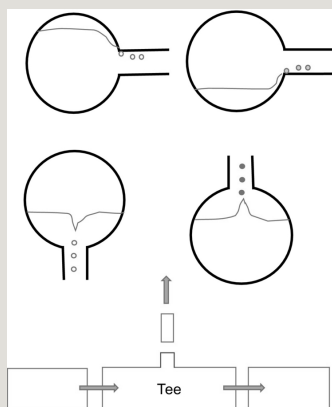


Fig. 11.2 A modeled Tee junction with illustration of the phase separation phenomena.

11.4.3 0-D modules in system codes

0-D modules exist in some system codes when some specific flow behavior cannot be treated as a current mesh or control volume of the 1-D module. For example when large capacities are connected to various pipes or ducts at various elevations and with various orientations, the CATHARE code may use a two-node volume module. It is assumed that velocities within the module are small compared to velocities at the junctions so that gravity effects play a major role in the phase repartition and the pressure field is assumed hydrostatic. The module may describe phase stratification by splitting the total volume into two subvolumes separated by a free surface, with water and bubbles below the free surface and steam with possible droplets above the free surface. This explains that scalar quantities are

calculated at two nodes. Similarly to the Tee, such module may represent phase separation phenomena at the junctions (see Fig. 11.3).

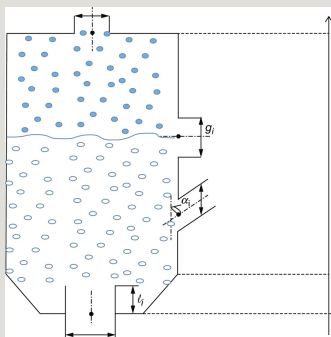


Fig. 11.3 Illustration of a 0-D two-node module for representing large capacities with phase stratification (from the CATHARE code).

Thermal hydraulics of coolant fluid in reactor circuits may be influenced by a local specific geometry, which requires some specific models. Some of them are classified as special component models or special process models. Examples of special process models are briefly described below.

11.4.4 Critical flow

Choked flow or critical flow conditions may occur in reactor transients either at a break or in internal flow at flow restrictions or pumps. When sonic velocities are reached at a section (often at the smallest flow cross-section area) the flow becomes independent from downstream conditions. Predicting critical flow is then of prime importance for all LOCA transients since the break flow rate controls the coolant mass inventory, and consequently the core cooling capability. System codes developed either 0-D or 1-D models for break flow or choked flow. They are presented in more detail in Section 11.8.1.

11.4.5 Singular pressure losses

Complex geometries, such as bends, flow limiters, valves, sudden area change, nozzles, perforated plates, spacer grids, and support plates, induce irreversible pressure losses which are called “form losses” or “singular pressure losses.” System codes do not predict these losses and the user has to enter loss coefficients in the input deck.

11.4.6 Countercurrent flow limitation

The flooding limit and the CCFL play an important role in many accident sequences since it may control the quantity of cooling water which is kept out of the core (UP, hot leg (HL), SG tubes) and which is no more available for the core cooling. The basic phenomenon is the limitation of a liquid downward flow rate by a given upward gas flow rate. The CCFL is likely to occur in complex geometry such as upper core tie plate, HL bend, inlet of SG header, inlet of SG tube, and a specific local modeling is necessary in system codes to obtain reliable predictions. Flooding correlations are established from experimental data and the parameters of these correlations are entered in the code input deck.

11.4.7 Separators

Separators are used to separate steam and liquid water at core exit of BWRs or at the top of PWR SGs. A two-phase mixture enters the separator barrel, passing through a set of stationary swirl vanes. These vanes produce a high rotational velocity component in the fluid flowing through the separator barrel. The resultant centrifugal force separates the steam-water mixture into a water vortex on the inner wall of the separator barrel and a steam vortex core. Because this process cannot be simulated by using the 1-D two-fluid model, special models are used for separators. The separator model determines the void fraction in the (bottom) liquid fall back junction and the liquid fraction in the (top) outlet junction. In general, two options might be available: (i) a simple separator model in which a steam-water inflowing mixture is separated by defining the quality of the outflow streams using empirical functions, and (ii) a mechanistic separator model, which is intended to model the centrifugal separators by solving phasic continuity equation, angular momentum equation, and axial momentum equation with some simplifying assumptions.

11.4.8 Dryers

The steam dryer uses Chevron vanes to remove the moisture which is discharged from the steam separators. The vanes provide a curved path which the liquid droplets must follow if they are to flow through the dryer. The liquid droplets, flowing along the curved path, hit the vanes due to their inertia and are deentrained. The resultant liquid film flows down the vanes under the force of gravity and then back to the liquid pool surrounding the separators. The dryer efficiency depends on the steam velocity and the moisture content of the steam flow entering the dryer. Since this process cannot be simulated by using a 1-D two-

fluid model, special models which are either simple or mechanistic are used for dryers.

11.4.9 Pumps

Pumps are generally modeled as a point (or 0-D) module. A pump is located in a node or a mesh and it adds source and/or sink terms to the momentum and energy balance equations. The angular momentum equation is added and controls the rotation speed of the pump. The hydraulic torque is generally modeled through user defined characteristic functions of fluid velocities and rotation speed. The hydraulic torque is a sink term for the angular momentum equation and is multiplied by the rotation speed in a source term for the fluid energy equations. The pump head is also modeled through user defined characteristic functions of fluid velocities and rotation speed. The pump head appears as source terms in the fluid momentum equations. The head and torque characteristic functions have to be known in the four quadrants.

Usually pump vendors give only single-phase characteristic functions in the first quadrant. It may be necessary to do experimental tests to get the pump characteristic functions in the other quadrants. Moreover two-phase characteristic functions have also to be given as user defined functions since pump performance (head and torque) are degraded in two-phase flow conditions. Usually two-phase characteristic functions are also function of inlet void fraction.

11.4.10 Turbines

Turbines, like the pumps (see above), are generally modeled as a point (or 0-D) module. Turbine also adds source and/or sink terms to the momentum and energy balance equations. The sink and source terms are also modeled as user defined functions.

11.4.11 ECC injections

ECC injection is often simply modeled as a source term (of mass, momentum, and energy) in a node or mesh. A very simple model may be used when the flow rate is a function of the pressure at injection location. The ECC injection (special) model takes care of the mixing, including interfacial transfer, between different fluids in the delivery line and in the primary system (typically).

11.4.12 Accumulators

Accumulators may be modeled either using standard modules (0-D, 1-D, valve, Tee, walls) of the codes or by a specific accumulator model. The specific module must predict:

- Accumulator pressure as function of remaining mass and of heat released from accumulator walls (from isentropic depressurization for rapid discharge to quasi-isothermal for slow discharge).
- Flow rate delivered to the circuit as function of valve opening, accumulator pressure, primary circuit pressure, pressure losses, etc.
- Mass momentum and energy source terms in both phases in the injection mesh.

If some specific options are actuated, the accumulator specific module should also predict the amount of dissolved nitrogen in liquid water and the source term of nitrogen in gas mixture in the case of transport of noncondensable gas.

11.4.13 Valves, safety valves, control valves, check valves, and flow limiters

Many valves, safety valves, control valves, and check valves exist in a reactor. They may be “internal” to the modeled circuit or “external” when they connect the modeled circuit with the external space (e.g., containment or pressure suppression pool). They are characterized by functions giving either the pressure loss as a function of flow rate and the degree of opening, or flow rate as function of upstream pressure and temperature for choked flow conditions. Most of the time, only single-phase valve characteristics are known. The valve model also must predict the behavior in abnormal two-phase conditions.

11.4.14 Breaks

The break may occur anywhere in a pressurized system and may put in communication a high pressure (typically high temperature) environment with a low pressure (typically ambient temperature and pressure) environment. Conditions for the occurrence of “critical flow” (i.e., TPCF) develop at the break. Although a number of breaks and break configurations are excluded for technological reasons (e.g., catastrophic vessel break, application of the leak before break concept in selected piping), a wide variety of break configurations may appear. This reflects in a wide variety of break shapes that cannot be controlled by thermal-hydraulic parameters and, at the same time, affects the prediction of relevant thermal-hydraulic quantities like critical flow rates. Furthermore, the capabilities to predict TPCF are not necessarily embedded into the balance

equations (with the noticeable exception of the CATHARE code, where a specific experimental database was created and used) even due to the specific ranges of validity of relevant equations: for example, friction pressure drop at very high fluid speed, or vaporization rate when steep pressure gradient occur along the flow direction and as a function of time. Owing to this, special critical flow models are needed and are provided by code developers as well as by several researchers in the open literature.

11.4.15 Spray cooling

The spray of subcooled liquid into a steam environment constitutes an efficient way to cool a space region of the NPP. Spray cooling is adopted in nominal operating conditions (e.g., cooling of the vapor region of the pressurizer in PWR in order to control the pressure) or in accident conditions (e.g., cooling of the upper core region of BWR to facilitate the liquid entering into the upper part of the core following the occurrence of accidents). Thermodynamic nonequilibrium phenomena occurring in direct contact condensation conditions are involved that are not within the domain of validity of closure equations. Furthermore, the phenomenon is controlled by aspects like the droplet size, the droplet speed distribution, and the formation of droplets clouds and the interaction of droplets with solid walls. Those aspects are not part of the balance equations; rather they are dependent upon the design and the operation of the spray nozzles. Owing to this, special models are needed and are provided by code developers.

One of the first RELAP5 nodalization schemes for LBLOCA test of LOFT facility is shown in Fig. 11.4. In the early times of system codes, the CPU cost was an issue and code users had to minimize the cost by reducing the number of control volumes. Here an SG tube was represented with only 4 upward meshes and 4 downward meshes, a HL by only 5 meshes and the core by only 13 meshes.

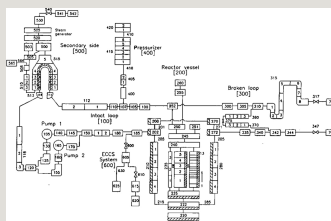


Fig. 11.4 RELAP5 nodalization scheme for large-break LOCA test at LOFT facility.

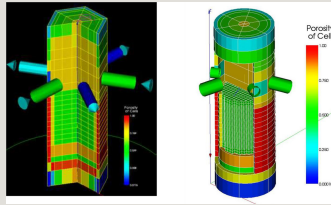


Fig. 11.6 Illustration of the nodalization of a PWR pressure vessel using a 3-D module. Left: a very coarse nodalization. Right: a finer nodalization particularly in the core.

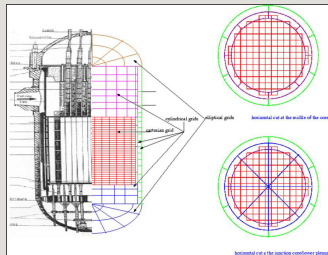


Fig. 11.7 Illustration of advanced pressure vessel modeling for system codes.

11.4.16 Importance of the nodalization

A reactor nodalization includes several thousands of figures and errors are very likely to be introduced in the input deck. Therefore, smart systems were developed in preprocessors and man-machine interface with graphical user interface (GUI), with many consistency checks to help users and to minimize the possible errors. However, the various possible choices in the nodalization process are the origin of the “user effect” which is visible in blind benchmarks, when several independent users simulate the same transient with the same code and obtain significantly different results. In order to minimize this “user effect,” more and more precise User Guidelines were established by code developers which give recommendations for many of these choices.

The process of nodalization includes a space averaging of a complex physics which affects the prediction quality in two ways:

- The space resolution is rather coarse (a few hundred to a few thousand meshes are usually modeling reactors) which gives only macroscopic information on the

physical parameters.

- The average equations are no more exact equations but are simplified equations with many closure laws which introduce many approximations and simplifications resulting in a limited accuracy of predictions.

From these two points, the former represents a limitation of the amount of information produced by the code whereas the latter is the main source of difficulties for solving reactor safety issues and represents the main source of code uncertainty.

11.5 The numerical solution methods

The successive steps to establish the model equations and to solve them are shown in Fig. 11.8. The space discretization of space and time-averaged equations for all modules (0-D, 1-D, 2-D, and 3-D) results in a set of ODEs and further time discretization leads to a set of linear algebraic equations.

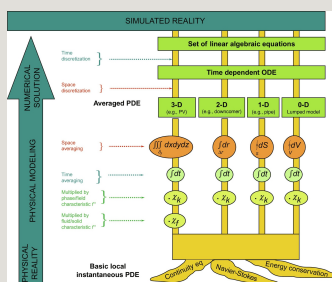


Fig. 11.8 The successive steps for establishing and solving thermal-hydraulic equations.

The numerical scheme is the set of mathematical algorithms which is used to solve the set of nonlinear PDEs. It includes the space and time discretization of equations which is used in finite-volume or finite-difference methods. Then the set of nonlinear PDEs is finally converted to a set of coupled linear equations. The converged solutions in one time step are calculated using iteration techniques in most cases.

From the physical reality to the simulated reality, both the physical modeling and the numerical scheme induce some degradation which should be kept within

acceptable and estimated limits.

The numerical method in the SYS-TH codes uses variants of finite-volume and finite-difference methods based on the ICE method of Harlow and Amsden (1968, 1971, 1975). Although all codes are rather similar in the space discretization, they differ by the time discretization which may be from semiimplicit up to fully implicit. The space discretization uses a staggered mesh and the donor cell principle in first-order scheme. Velocities are defined at vector nodes X_j and scalar quantities are defined at scalar nodes O_j (see Fig. 11.9). Mass and energy equations may be written using a conservative form and can be discretized in order to preserve a very good mass and energy conservation.

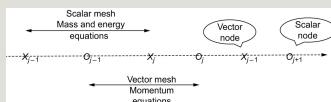


Fig. 11.9 Illustration of the space discretization for 1-D models.

These methods are known for their robustness in a wide range of two-phase flow configurations. The material Courant condition (or CFL condition) on the time step has to be respected in semiimplicit schemes to ensure the stability. On the contrary, implicit methods may use very large steps without any limitation which is very convenient for stationary initial state of a reactor, or even for very slow transients. The CATHARE code has selected this fully implicit scheme for 0-D and 1-D modules since it allows prediction of critical flow at a break with very high velocities in very small meshes required by the strong pressure gradient. This would lead to extremely small time steps with a semiimplicit scheme due to CFL limit, which prefer to model break flow by a 0-D sink modeling. In a 1-D module, the CFL limits prescribe that in a mesh with a length dX with a fluid velocity V , the time step dt should respect the condition:

$$1 - \alpha = \frac{A_l}{A_g + A_l}$$

The heat conduction in solid structures is usually implicit to avoid time step limitations. It also uses an implicit coupling to hydraulic equations.

Semiimplicit and implicit methods require an iterative solution of every time step with calculation of a Jacobian matrix. A linear system of equations is solved at each iteration. Semiimplicit methods allow the elimination of all variable increments as function of only pressure increments, which reduces the CPU time.

The semiimplicit schemes were extended to numerical schemes without CFL time step limitations: nearly implicit method in RELAP (Trapp and Riemke, 1986) and stability-enhancing two-step (SETS) method in TRAC the TRACE codes (Mahaffy, 1982).

The space and time discretization of balance equations result in a nonlinear system of equations which is often solved by a Newton-Raphson iterative method following several steps. For example, in the CATHARE code at each iteration:

- Increments of variables of heat structures and other submodules are eliminated as function of increments of fluid variables
- Increments of internal fluid variables of each element are eliminated as function of increments of junction fluid variables
- Increments of all junction variables are calculated
- All variable increments are regenerated and convergence tests are performed

The numerical scheme of a SYS-TH code should meet many requirements. Examples of common requirements are given below.

Some requirements for the numerical algorithm are mandatory such as the consistency, the convergence, and the stability.

- *Consistency*: ability of a system of discretized equations to tend toward the system of PDEs when the discretization steps tend to zero.
- *Convergence*: ability of a numerical scheme to converge to the solution when the discretization steps tend to zero.
- *Stability*: ability of a numerical scheme not to generate nonphysical instabilities.

Some other requirements are very important for system codes:

- *Robustness*: capability to converge to a solution in all physical situations of the domain of simulation without code failure. If the system code is used to design

NPPs or to assess the safety of them, this requirement is very important.

- *Mass and energy conservation*: It is not only a requirement for being accurate on mass and energy, but also to be able to predict system pressure correctly since any numerical source or sink of mass or energy will affect the pressure. The system pressure has a strong impact on reactor transient scenarios since it controls actuations of SCRAM signal, SIs, safety valve opening, accumulator discharge, and so on. Mass conservation in thermal hydraulics, and energy conservation in both thermal hydraulics and solid heat structures are then very important.

Some requirements are also important for system codes:

- Numerical efficiency criterion: The CPU time must remain compatible with the intended use of the code.

- Accuracy:

- Accuracy on mass and energy conservation is mandatory (see above).

- Accuracy of transport processes has to be sufficient with respect to some acceptance criteria, or at least requirements on space and time increments (dx and dt) may be defined to obtain a given accuracy. This may be important for transport of a temperature front (e.g., positive reactivity feedback due to flowing cold water into the reactor core by overcooling in the SG in the case of a steam line break, SLB) or for the transport of a boron concentration (e.g., positive reactivity feedback due to flowing unborated water into the reactor core in the case of SBLOCA).

- Accuracy of propagation processes has to be sufficient with respect to some acceptance criteria, or at least requirements on space and time increments (dx and dt) may be defined to obtain a given accuracy. This may be important for pressure wave propagation in water hammer situation or in condensation-induced water hammer (CIWH) where strong pressure peaks may propagate in the fluid. This may also be important for void fraction wave propagation in particular in the case of stratified flow where free surface waves may propagate either downstream or upstream depending on the conditions. In subcritical conditions, the prediction of void fraction requires the capability to predict the upstream propagation velocity correctly.

- Accuracy and numerical efficiency are tightly coupled since any numerical scheme may improve its accuracy by reducing space and time increments (dt and

dx), which also increases the resolution time.

- The numerical algorithm has to be able to deal with water level, swollen levels, and water packing. When a liquid level or swell level passes a mesh there should not be numerically induced pressure peaks that affect the transient behavior.

At last, there are several requirements related to operability (i.e., the capability to deal with different flow conditions) of the numerical algorithm to treat the physical situations of interest:

- The numerical algorithm has to be able to deal with incompressible and compressible flows with nonsimplified equations of state.
- The numerical algorithm has to be able to deal with flows with strong interfacial mass transfers (strong pressure-void fraction coupling).
- The numerical algorithm has to be able to deal with strong hydraulic-wall conduction couplings (passing DNB, rewetting).
- The numerical algorithm has to be able to deal with flows in an extended range of velocities including subsonic and supersonic velocities.
- The numerical algorithm used for thermal-hydraulic equations has to be able to deal with all the two-phase flow regimes in the whole range of void fraction and to respect some positivity constraint to keep the void fraction in the range $[0, 1]$ while preserving mass and energy conservation.
- The numerical algorithm has to be able to work in a wide range of pressures and temperatures: $0 < T_l < 350^\circ\text{C}$; $0 < T_v < 2000^\circ\text{C}$; $0.001 \text{ MPa} < P < 22 \text{ MPa}$.
- When used with additional equations for noncondensable gases, the numerical algorithm must respect some positivity constraint to keep all gas mass fractions (or molar fractions) of each component of the gas mixture (e.g., steam-air, steam-H₂, steam-N₂) in the range $[0, 1]$ while preserving mass and energy conservation.

11.5.1 State-of-the-art on numerical schemes in current system codes

The numerical schemes used in current system codes meet the mandatory requirements and differ by the robustness, accuracy, and efficiency criteria. None of them fulfill all the criteria fully satisfactorily. The schemes implemented in the current codes are robust and fairly efficient but not very accurate. The main

capabilities are the following ones:

Robustness: The schemes implemented in the current system codes solve the system of equations in a very wide range of flow configurations without code failure or with very few failures.

Accuracy: In many situations of interest, the accuracy of numerical scheme is limited by the use of nonconverged mesh size and/or time step.

Accuracy and mesh size: The advection terms being discretized at first order, this induces some numerical diffusion which is increasing with the mesh size. In particular temperature of each phase and other scalar quantities (boron concentration) are artificially diffused particularly with an implicit time discretization. In addition, most of the time, the nonspace convergence of the calculation of wall and interfacial transfer terms induce even more inaccuracy than the numerical diffusion. However, these wall and interfacial transfer terms are modeled by empirical correlations which have a rather high uncertainty. At the end, the numerical error is often acceptable since it is one order of magnitude smaller than the uncertainty due to the imperfect physical modeling.

Higher order schemes: Other more accurate schemes exist which are operational in a smaller range of flow configurations and still did not prove their robustness when the scope of application is broadened. Higher order models may be used on option in some particular cases when a temperature front or boron concentration front is transported and should not be smoothed artificially by numerical diffusion.

Accuracy and time step. It may occur that the physics of the flow creates phenomena with very small time scale. This is often due either to instabilities, to oscillations, or to pressure wave propagation. Instabilities may be generated in boiling flow such as density wave oscillation (DWO) or Ledinegg instability, or in the case of CIWH. Oscillations may be generated between loops, or gravity oscillations between the core and the downcomer. A valve opening or closure and a break opening induce pressure wave propagation with possible reflections and water hammer. Such phenomena can only be captured when a sufficiently small time step is used. It is possible that a code does not predict some of these phenomena when the time step is too large. For two-phase pressure wave propagation, the time step should be limited by the sonic velocity C_s ($dt < dx/C_s$) but time scales associated with flashing and condensation may be even smaller than this, and require even smaller time steps. Boiling instabilities at low pressure may be predicted during core reflooding when using small time step (e.g., $dt < 0.005$ s) and are not seen with a larger time step. Gravity oscillations may be artificially

damped if the time step is not small enough. This is particularly true for implicit time discretization which is dissipative.

Phase appearing and disappearing. The phase appearing and disappearing when the void fraction is close to zero or one may lead to numerical difficulties with void fractions values out of the bounds $[0, 1]$ at least during iterations. Special techniques are used in system codes to guaranty that void fractions stays within bounds without having violated mass and energy conservation. However, small time steps are often necessary to approach the bounds with sufficiently small increments. Interfacial heat and mass transfer models have to be conditioned in such a way that they cannot produce vaporization when there is no more liquid and they cannot produce condensation when there is no more steam. This looks trivial but is not so straightforward when steam is mixed with noncondensable gases.

Time step control. The time step control includes usually both a user control and a code time step management. When a physical situation requires a particular attention to small time scale processes, the user must impose a maximum time step. The numerical algorithm may not be able to obtain a convergence with this maximum time step and codes implemented procedures to decrease the time step until convergence is obtained. Then this time step may increase again if the numerics allows.

Water packing problem. Generic problem in two-phase flow modeled by the two-fluid model is the possible discontinuity of void fraction when there is a free surface level or a swell level in a vertical component or a swell level. It is found in the former case that moving the level from one mesh to the next mesh may create artificial pressure peaks, particularly when the water is subcooled and creates a countercurrent flow with steam due to condensation. This is the “water packing” problem and it is due to both an inadequate physical modeling and inadequate space discretization in such situation. Codes have developed some interface tracking methods which recognize the situation and apply modified physics and discretization. A remarkable study by Aktas (2003) provides very good behavior in TRACE.

Stability and hyperbolicity. Many instabilities exist in two-phase flow. Taylor instability and Kelvin-Helmholtz instability are very frequent and induce bubble or droplet break up, droplet entrainment from a free surface or a film surface. They govern mainly the interface structure of each flow regime and some transitions between flow regimes. Oscillations between loops, Ledinegg instabilities in parallel heated channels, DWOs may appear and have an important effect on the global behavior of a reactor transient. Kelvin-Helmholtz instability in a stratified

flow is probably the most abrupt change in the mechanical behavior. This instability is responsible for the transition from a stratified flow—which is a separate-phase flow regime with a very low coupling between phases—to a slug flow characterized by a much stronger coupling between phases. In large diameter pipes, this transition may increase the interfacial friction coefficient by several orders of magnitude in a very short time. Such instability is even more violent when associated with condensation in the case of CIWH.

A choice has to be made in SYS-TH codes to simulate or not the instabilities. The answer depends on the instability:

- Since the code intends to filter in time and space the physics, many local instabilities responsible for the flow regime transitions may be simply taken into account by using flow regime maps.
- The passage from one regime to the other may be very progressive (bubbly to slug, bubbly to churn, bubbly to stratified flow). In such case there is no difficulty to represent the smooth physical behavior.
- The onset of droplet entrainment is somewhat abrupt but induces a progressive change of phase coupling since the rate of entrainment increases also progressively.
- The transition from stratified to slug flow is more abrupt but may be smoothed in the space-time-averaged model. The objective is to be able to predict the change of flow regime without simulating the local instability with a free surface wave having a very high rate of increase up to liquid bridging.
- Large-scale instabilities which affect the system behavior should be simulated by the code. This requires that the physical processes responsible for the instability are correctly modeled. The two-fluid model has shown its capability to predict many of these instabilities (Ledinegg instability, density wave instability, coupled neutronic-thermal-hydraulic instabilities in BWR, instabilities between loops during natural circulation) provided that time step and mesh size are sufficiently small. Such large-scale instabilities do not create very steep gradients nor very sudden changes of flow parameters and do not challenge the code numerics.

Current numerical schemes can then simulate the most important instabilities and can smooth the most steep Kelvin-Helmholtz instability.

A slightly different question also associated with the stability in system codes is

the hyperbolicity of the system of equations. Since axial diffusion terms in 1-D equations are neglected, all codes use a first-order set of PDE. A necessary and sufficient condition for a first-order set of PDE function of time and space to be well posed is the hyperbolicity of the system of equations. The well posedness in the sense of Hadamard states that:

- a solution exists,
- the solution is unique,
- the solution depends continuously on initial conditions.

If a problem is ill-posed, it needs to be reformulated for numerical treatment. In order to include some smoothness in the solution. This process is known as regularization. This question is treated in Section 5.12 (Chapter 5) and the various SYS-TH codes adopted two main different approaches.

- In TRAC, RELAP5, TRACE, MARS, and SPACE codes, a very pragmatic point of view has been developed. The second-order diffusive terms that have been neglected in six-equation model are small compared to numerical diffusion and the cell size used is such that there is no need to add this second-order terms. Diffusion stabilize the high frequency void waves and many transfer terms of the equations like wall friction and interfacial friction can induce sufficient dissipation to stabilize the low frequency void waves. This point of view requires cells large enough to prevent instability through numerical diffusion. However, when decreasing the mesh size, numerical diffusion is decreased and the possible unstable nature of equation is revealed. In this approach, no convergence in cell size is possible.

- CATHARE and ATHLET use hyperbolic equations (this is demonstrated at least

$$X = \frac{W_g}{W_g + W_l}$$

for the 1-D module). Using the added mass force the $\frac{W_g}{W_g + W_l}$ term is justified by the physics of two-phase flow. The expression for f_i is clearly derived in stratified flow (Bestion and Serre, 2012) and plays an important role. It is not well known for all two-phase flow regimes and can only be approximated. A condition is added that these terms make the system hyperbolic. This method guaranties the well posedness and allows mesh convergence without creating instabilities.

This question is still a subject of controversy between two communities.

- A mathematical community does not accept the numerical regularization adopted in some codes and do not accept the physical regularization by imposing an

$$\chi = \frac{W_g}{W_g + W_l}$$

“arbitrary” condition on the term. Some of them prefer to use a two-pressure seven-equation model which is unconditionally hyperbolic.

- The engineering community accepts either the numerical or the physical regularization. The advocates of the physical regularization argue that the differential closure terms are physically based even if no universal model exists, and that it is nonsense to study the hyperbolicity of the six-equation single pressure model or the two-pressure seven-equation model without considering any of the differential closure terms.

SYS-TH code developers belong to the second community which did not observe any code failure due to predicted instabilities which could be attributed to nonhyperbolicity after having simulated a huge number of real two-phase flow situations during decades. They prefer to focus on many other real difficult problems they are obliged to face in two-phase flow modeling. Some consider discussions on hyperbolicity are like discussions on “How many angels can dance on the head of a pin?” (in France one would say “discussions on the gender of angels”).

11.6 The relation between SYS-TH code and containment

Safety analyses should prove that the containment integrity is preserved. This may be challenged by a high internal pressure, by external events, such as earthquakes, flooding, tsunamis, plane crash, and fire. In the case of severe accidents, there may be hydrogen explosion, steam explosion, and corium-concrete interaction.

As far as DBA are concerned, containment thermalhydraulics is often decoupled from reactor thermalhydraulics, at least during the short-term cooling. In all LOCAs, as long as the break flow is a choked flow, it is independent from the containment pressure. One can then simulate the reactor behavior with a system code, then simulate the containment behavior using dedicated containment codes, the break flow being a BC. Then during the long-term cooling, there may be some coupling between the reactor and the containment.

However, in a PWR LBLOCA, the pressures in primary circuit and containment are rapidly equalized and both systems are coupled. There may be a strong impact

of containment pressure on the core reflooding, the reflooding being more difficult at lower pressure. Therefore, using the single failure criterion leads to minimize the availability of containment spray system (one out of two independent trains of spray may be supposed out of service) to demonstrate that containment pressure remains below the safety limit and, on the contrary, the single failure criterion leads to maximize the availability of containment spray system, since it will induce lower pressure during the core reflooding. In PWR LBLOCAs, at the end of the refill phase, there may be some reverse gas flow from containment to primary circuit due to a strong depressurization induced by condensation on cold ECCS water from accumulators. This gas is then a mixture of air and steam and this is also a coupling between the reactor and the containment.

In any type of LOCA, the long-term cooling with possible recirculation of the water pumped from the containment, reactor, and containment are also coupled by the pressure and possible effects of sump clogging.

Some reactors, particularly generation III reactors have many systems which induce a stronger coupling between reactor and containment, such as automatic depressurization systems (ADS) which blow steam in a pool in the containment, or passive RHR systems using water pools in containment. Therefore, the coupling of system codes with containment codes became more useful and two strategies are possible:

- develop coupling between system and containment codes;
- extend system code capabilities to make them capable of simulating some containment phenomena.

The first approach is rather common and does not raise very big difficulties. The second approach is limited to the use of 0-D or a multi-0-D modeling of the containment. It is limited to the modeling of phenomena which control containment pressure and it cannot predict hydrogen explosion. It requires some specific capabilities including the following:

- Treatment of steam-air mixtures.
- Specific treatment of wall condensation in the presence of noncondensable gases.
- Models for spray cooling.
- Vaporization at a free surface in the case of a pool which may be heated by an

ADS or a HX.

11.7 The relation between SYS-TH code, component codes, and subchannel codes

System codes, component codes, and subchannel analysis codes have been developed in parallel since the 1980s in different contexts. They have different features but also overlapping domains of simulation. These legacy codes are first presented to show their characteristics and domains of simulation before drawing perspective for future of the reactor thermal-hydraulic codes.

11.7.1 System codes

The system scale is dedicated to the overall description of the circuits of the reactor for the simulation of all transients required by safety analysis. The primary and secondary circuits of a reactor are modeled by coupling 0-D, 1-D, and 3-D modules together with submodules for pumps, valves, breaks, safety systems, HX, and control systems. Pipes are treated by a 1-D model, pipe connections with Tees, large volumes with 0-D modules, and the pressure vessel may be modeled with a 3-D module using CFD for porous medium. The whole reactor is modeled using a few hundred 0-D and 1-D meshes, whereas a 3-D pressure vessel modeling currently uses about 10^3 coarse meshes. This method allows simulations of all accident scenarios, including LBLOCAs and small-break LOCAs (SBLOCAs), with a reasonable CPU time (less than 12 h of a single-processor computer).

11.7.2 Component codes

The component scale also uses CFD in porous medium. This scale is dedicated to the design, safety, and operation studies of reactor cores and tubular HX (SGs, condensers, auxiliary exchangers). Rod or tube bundles are homogenized into the control volumes using the “porosity” concept. The minimum spatial resolution is fixed by the subchannel size (of the order of 1 cm), which gives the subchannel analysis. Some component codes can either do subchannel analysis or model a core with larger radial meshes corresponding to a few rods or one assembly or several assemblies. Examples of component codes used for LWR core are COBRA-TF (Thurgood et al., 1981; Avramova, 2006, 2007), FLICA (Toumi et al., 2000), and SUBCHANFLOW (Imke et al., 2010). Example of a component code used for SG is GENEPI (Obry et al., 1990; Belliard and Grandotto, 2000). All component codes are 3-D codes in porous medium. The two-phase models in component codes may be a three-equation model with drift flux (GENEPI), a four-equation with drift flux allowing one phase being out of thermodynamic equilibrium (FLICA), a six-

equation model or even a three-field model with eight or nine equations to describe separately the liquid films and the droplets (COBRA-TF). The domain of simulation of component codes used for the core includes the following applications:

- Core instabilities in BWR with possible coupling to 3-D neutron kinetics
- Some ATWS in BWR or PWR
- SLB transients in PWR with possible coupling to 3-D neutron kinetics
- Boron dilution transients in PWR with possible coupling to 3-D neutron kinetics
- Rod ejection reactivity transient with coupling to 3-D neutron kinetics
- PWR core reflooding

The whole core is usually modeled. A usual modeling is a row of mesh for each assembly. In many applications, the component code is coupled to a system code and may also be coupled to a CFD code (SLB, boron dilution) and to a 3-D neutron kinetics. Fig. 11.10 shows a COBRA-TF core moderator density distribution in a coupled ATHLET/COBRA-TF calculation simulating the Oskarshamn-2 NPP ATWS event.

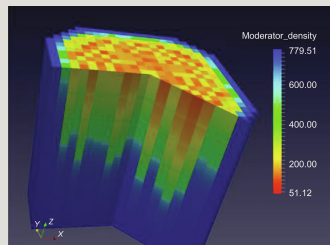


Fig. 11.10 COBRA-TF core moderator density distribution in a coupled ATHLET/COBRA-TF calculation of the Oskarshamn-2 NPP ATWS event (Jimenez and Sanchez, 2015). From Jimenez, J., Sanchez, V., 2015. Final report on BWR thermal-hydraulics at system scale and sub-channel scale. NURESAFE, D33.12.5, EC Project, Brussels, Belgium.

The domain of simulation of component codes used for the SGs and the HX includes the following applications:

- Heat transfer efficiency of the exchanger depending on the design

- Mass inventory and recirculation ratio in a SG
- Fouling in SG and in any HX
- Tube vibrations

The component codes may include some capabilities to have local mesh refinements using domain decomposition and local zoom methods (Belliard and Grandotto, 2000).

11.7.3 Subchannel analysis codes

Subchannel analysis codes model fuel assemblies with one row of meshes per subchannel. Most of the time such capabilities are included in component codes which can also use coarser meshing. Subchannel analysis is more an application of component codes rather than a type of code. The domain of application includes the following:

- Analysis of CHF tests and modeling of flows in rod bundles to predict CHF occurrence. Usually, such subchannel analysis models the various transfers between subchannels including mass transfers by crossflows, turbulent diffusion, and dispersion of mass momentum and energy. After a validation of the various radial transfers on dedicated experiments, they interpret CHF tests performed in small rod bundle tests (e.g., 5×5 bundles) and establish a correlation of CHF as function of the local average values of P , G , and X . Then they can be used to simulate a reactor core and to predict when and where CHF may occur.
- Subchannel analysis may be used in a part of a core to predict with a high resolution the highest power assembly(ies) in some transients whereas the rest of the core is simulated with a coarser meshing (e.g., one row meshes per assembly).

11.7.4 Common features and differences between codes

Component codes, subchannel codes, and 3-D modules of system codes use the porous body approach where local instantaneous equations are multiplied by a fluid characteristic function then by a phase or field characteristic function before being averaged over time and over a spatial domain. This is clearly different from CFD in open medium where equations are written only in the fluid domain possibly with a multiplication by a phase or field characteristic function before being time averaged (see Chapter 5).

Component codes, subchannel codes, and 3-D modules of system codes must

model radial transfers by diffusion, dispersion, and due to crossflows (Chandesris et al., 2013). However, since they have different applications, the role of diffusion and dispersion may be either important (in CHF investigations) or negligible compared to crossflows and to wall and interfacial heat transfers (in LOCAs).

Component codes, subchannel codes, and 3-D modules of system codes differ by the size of the meshes or control volumes. Fig. 11.11 illustrates these differences and compare also to the CFD in open medium approach.

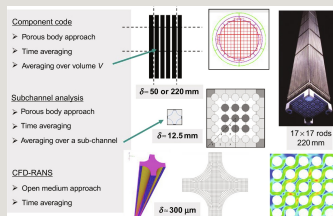


Fig. 11.11 Illustration of three modeling scales of an LWR core thermal hydraulics.

Differences may exist in the type of model and number of equations.

Differences may exist in the treatment of the momentum balance equations in the radial direction. They can be written in the same way as in the axial direction, or they may be simplified by a simple relation between pressure difference and flow rate, which is sometimes called a cross-flow junction.

Differences may exist in the numerical scheme and in the flexibility of the meshing: Cartesian grid, cylindrical grid, prismatic grid, and body fitted meshing.

11.7.5 Current trends

The CPU cost of system codes is becoming very low due to the continuous progress of computer efficiency. This allows using the 3-D modules of system codes with a finer grid. Such modules were compared to component and subchannel codes in PSBT and BFBT benchmarks (see NUPEC documents available from public literature), to predict flow in experimental tests relative to PWR and BWR rod bundles. Although this was an exercise typically devoted to component and subchannel codes, system codes have shown relatively good performance. They could be used with a meshing at the subchannel scale and one may imagine that these modules will progressively be used to replace component

codes (see Valette, 2007, 2011). This will eliminate the need of coupling between codes.

11.8 Predicting break flow and choked flow

Predicting break flow and more generally choked flow in reactor transient thermalhydraulics is of major importance in many transients. LOCAs with a break on the primary circuit lose mass and energy through the break and the severity of the transient depends a lot on the impact of the break on both the liquid mass inventory available to cool the core and on the system pressure which governs many safety automatic signals such as the SCRAM and SI signals. Choked flow with a sonic velocity is likely to occur at any break as long as there is a significant overpressure of the circuit with respect to the containment. Choked flow may occur in other components such as valves, safety valves, and flow limiters. Modeling and predicting choked flow has been a major issue for system codes. This subsection will summarize the available knowledge on choked flow understanding, modeling, and on the predictive capabilities of system codes.

11.8.1 Choked flow in single-phase gas flow

Let consider a flow through a nozzle with a convergent, a possible constant cross-section pipe, and a divergent. This represents the geometry where a choked flow may occur. If the upstream pressure P_o is constant and the downstream pressure P_d decreases, the flow rate will increase to a maximum which is reached when the sonic velocity is reached somewhere in the minimum cross-section area. A further decrease of downstream pressure does not change the flow rate and does not change any flow parameter in the zone from upstream to choked plane where the sonic velocity is reached. This single-phase situation is rather well understood and available models can predict the flow rate with a very good accuracy.

The sonic velocity is the velocity of propagation of pressure waves. In Newton-Stokes fluid, a pressure wave induces flow velocity without shear and without viscous dissipation so that a pressure wave can be predicted by Euler equation.

The case of a simple local pressure perturbation applied to a stagnant fluid may easily show that the perturbation obeys a propagation equation:

$$W = W_g + W_l$$

$$G = \frac{W}{A}$$

Using a linear analysis with a small perturbation

$$D_h = 4A / p$$

One may easily obtain the equation:

$$Re = \rho \times v \times D_h / \mu$$

which is a propagation equation at celerity c with:

$$Fr = v / \sqrt{(g \times L)}$$

Let us consider a 1-D flow in a converging diverging nozzle

$$W_g = A_g \rho_g u_g = W \alpha$$

$$W_l = A_l \rho_l u_l = W (1 - \alpha)$$

where A is the cross-section area.

Writing this system of equations in the vector form,

$$\text{Heat flux} = -K(\text{temperature gradient})$$

$$q'' = -K \nabla T$$

one may calculate the characteristic velocities of the system of equations by solving:

$$q'''(r,t) - \nabla q'' = \delta / \delta t (\rho c T)$$

which results in:

$$q'''(r,t) - \nabla \cdot (-K \nabla (T(r,t))) = \delta / \delta t (\rho c T)$$

From a point following the fluid, two waves are propagating upstream and downstream with the celerity c .

- When $V < c$, the flow is subsonic: one wave travels upstream and one wave travels downstream
- When $V > c$ the flow is supersonic and two waves are travelling downstream

A wave with period or time scale τ_w and frequency $f = 1/\tau_w$ creates local pressure variations with a wavelength $q'''(r,z) = K_f \Sigma \Phi(r,z)$.

The pressure variations induce temperature variations which induce temperature gradients and heat transfers. To determine if the pressure variations are isentropic or not one may compare the conduction time scale τ_{cond} with τ_w

$$q''' / q_0''' = f(t_f, t_a)$$

where λ is the heat conductivity (W/m/K) and C_p is the heat capacity (J/kg/K).

The heat conduction time scale τ_{cond} is usually much larger than the pressure wave time scale (except for very high frequencies) and one can consider that the pressure variations are isentropic. This is why usually one adopts the isentropic sonic velocity expression:

$$q'' = h_s (T_{wall} - T_{bulk})$$

For a perfect gas this is:

$$Pr = \mu \times C_e / k$$

Fig 11.12 illustrates the single-phase choked flow in gas with three cases depending on the value of downstream P_d :

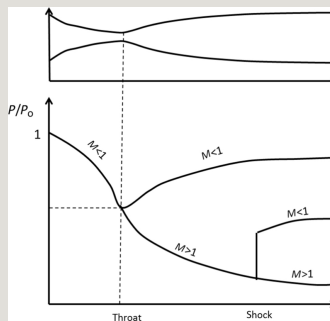


Fig. 11.12 Pressure evolution in a nozzle.

- The upper curve shows a subsonic flow in the convergent, sonic at the throat and subsonic in the divergent.
- The middle curve shows a subsonic flow in the convergent, sonic at the throat, supersonic in the divergent up to a shock where it becomes subsonic again.
- The lower curve shows a subsonic flow in the convergent, sonic at the throat and supersonic in the divergent.

Writing steady-state mass and momentum equations without wall friction and wall heat transfers (isentropic flow) and neglecting gravity effects,

$$Nu = h_s \times D_h / k$$

$$F_Q^E = \text{Engineering tolerances factor}$$

one may derive the Hugoniot equation:

$$F_Q = \text{Total power peaking factor}$$

From this equation one may easily draw the following conclusions:

- In a subsonic flow the velocity increases in a convergent and decreases in a divergent.
- In a supersonic flow the velocity decreases in a convergent and increases in a divergent.
- The sonic velocity is reached only where $dA/dz=0$ at the throat.

The total enthalpy equation is simply:

$$F_Q = F_Q^N \times F_Q^E$$

which gives for a perfect gas

$$F_{\Delta H}=\Delta \text{Enthalpy}_{\text{Max}}/\Delta \text{Enthalpy}_{\text{Average}}$$

And from this, one may obtain the flow parameters as function of upstream stagnation conditions ($V_o=0, P_o, T_o$),

$$F_{\Delta H_i}=\Delta \text{Enthalpy}_i/\Delta \text{Enthalpy}_{\text{Average}}$$

$$P\triangleq \hat{\bar{p}}=\langle \bar{\rho}\rangle^S$$

and the values at the throat T_c, p_c,ρ_c where the fluid is at sonic velocity:

$$V\triangleq \widetilde{\widetilde{v}}_t=\frac{\langle \overline{\rho v_t}\rangle^S}{\langle \bar{\rho}\rangle^S}=\frac{\langle \widetilde{\widetilde{\rho v_t}}\rangle^S}{\langle \bar{\rho}\rangle^S}$$

$$H\triangleq \widetilde{\widetilde{h}}=\frac{\langle \overline{\rho h}\rangle^S}{\langle \bar{\rho}\rangle^S}=\frac{\langle \widetilde{\widetilde{\rho h}}\rangle^S}{\langle \bar{\rho}\rangle^S}$$

$$Q_k \triangleq \widehat{\rho}_k^k = \frac{\langle \overline{\chi_k \rho_k} \rangle^S}{\alpha_k}$$

Then the mass flux and mass flow rate in choked flow conditions are given by:

$$Q_m \triangleq \alpha_v Q_v + \alpha_l Q_l$$

$$P_k \triangleq \widehat{p}_k^k \triangleq \frac{\langle \overline{\chi_k P_k} \rangle^S}{\alpha_k}$$

This is a very good model for a perfect gas in the case of a smooth and short convergent with no significant irreversible pressure losses. When singular or regular friction pressure losses are not negligible it must be corrected. Anyway one may well predict a break flow by knowing only the upstream fluid parameters P_o and T_o . In nonperfect gases, it is not valid due to variable C_p , C_v , and γ but some extrapolations of the model using an equivalent γ may give reasonable predictions.

For example, in the case of a choked flow in a reactor with pure saturated steam, which does not behave as a perfect gas, it was found that the following approximation was applicable:

$$P \triangleq \alpha_v P_v + \alpha_l P_l$$

If more accurate calculations are needed, it is still possible to solve the 1-D system of equations with mass, momentum, and energy along the nozzle.

11.8.2 Choked flow in two-phase steam water flow

A similar process exists in two-phase flow through a nozzle with a maximum flow

rate obtained when the downstream pressure is decreased beyond a limiting value. Further decrease does not change the flow rate and the flow parameters upstream of a section which is assumed to be at sonic velocity. Some experiments have observed that there is a limit where the flow rate seems to be constant but in fact it is not strictly constant but changes become very small when P_d further decreases.

Various approaches in two-phase flow tried to extend the single-phase choked flow model to two-phase models by combining three equations:

- an expression for a two-phase sonic velocity,
- a simplified momentum balance equation from upstream to choked flow section,
- a simplified energy equation from upstream to choked flow section (either isentropic evolution, or constant stagnation enthalpy or other).

Following the single-phase case, a two-phase sonic velocity expression may be obtained by deriving the mixture density with pressure under some assumption (isentropic, along saturation, etc.) or by calculating the characteristic velocities of a system of equations (also under some simplifying assumptions).

11.8.3 Sonic velocity in two-phase flow

Looking at the compressibility of a two-phase mixture, one may first consider some limiting cases.

The *homogeneous frozen model* considers a two-phase mixture with equal phase velocities and no phase change. The corresponding sonic velocity can be obtained by solving the characteristic velocities or by calculating the derivative of the mean density. One obtains:

$$V_k \triangleq \overline{v_{zk}} \triangleq \frac{\langle \overline{\chi_k \rho_k v_{zk}} \rangle^S}{\langle \overline{\chi_k \rho_k} \rangle^S} = \frac{\langle \overline{\chi_k \rho_k v_{zk}} \rangle^S}{\alpha_k \widehat{\rho_k}}$$

c_l and c_g are the sonic velocities in pure liquid and pure gas.

It has a larger compressibility than the liquid phase but also than the gas phase itself. The reason is that when pressure changes, each phase density changes but also the void fraction changes. This corresponds to a sound speed in water divided

by two as soon as there is 0.2% volume of air.

In air-water at atmospheric pressure, this expression gives a minimum sound speed of $c_{\min}=21.5$ m/s.

However, this assumes that the pressure changes are isentropic which may be far from the reality. The reason is that pressure variations induce different temperature variations in liquid and gas phases, creating heat transfers with a characteristic time scale which depends on the flow regime.

Very small bubbles or droplets of size δ may have conduction time scale τ_{cond} smaller than pressure wave time scale τ_w . Here τ_{cond} is calculated with the bubble or droplet size and no more with the wavelength:

$$\dot{j}_k \triangleq \gamma_k \overline{v_{zk}} = \epsilon_k \vec{v}_{zk}^k$$

Let us consider a wave of frequency 1 kHz, the wavelength may be of the order of 1 m when microbubbles or droplets may be of a few micrometers. As a result one may have conditions with:

$$\vec{j} \triangleq \vec{j}_v + \vec{j}_l$$

and the pressure changes are no more isentropic.

Moreover if the mixture is a fluid with its vapor, heat transfers at the interfaces will produce flashing and condensation which induce an additional compressibility since the quality changes during the pressure change.

Such heat and mass transfers can reduce even more the sonic velocity and also induce a dissipation of the wave energy. However, the homogeneous frozen model may also underestimate the sonic velocity by not considering any slip between phases.

11.8.3.1 The homogeneous equilibrium model

Another limiting case was considered where the time scales for heat transfer were assumed zero so that the thermal equilibrium is respected during pressure changes. This is the homogeneous equilibrium model (HEM). In two-phase conditions, both phases stay along the saturation curve during pressure changes. One may expect that this “homogeneous” sonic velocity will overestimate the compressibility and underestimate the sonic velocity.

This results in the following speed of sound:

$$J_k \triangleq \langle j_k \rangle^S = \langle \epsilon_k \bar{v}_{zk}^k \rangle^S$$

$$J_k \triangleq J_v + J_l$$

And the following critical mass flux:

$$v_k \triangleq \frac{J_k}{\alpha_k} = \frac{\langle \chi_k \bar{v}_{zk} \rangle^S}{\langle \chi_k \rangle^S}$$

with

$$G_k \triangleq \alpha_k Q_k V_k = \langle \chi_k \rho_k \bar{v}_{zk} \rangle^S$$

$$G\triangleq G_v+G_l$$

$$H_k\triangleq \overline{\overline{h_k}}=\frac{\overline{\langle \chi_k\rho_k h_k\rangle}^S}{\overline{\langle \chi_k\rho_k\rangle}^S}=\frac{\widehat{\overline{\rho_k h_k}}^k}{\widehat{\overline{\rho_k}}^k}$$

$$H_m\triangleq \frac{\alpha_v Q_v H_v + \alpha_l Q_l H_l}{Q_m}$$

$$\widehat{H}_k\triangleq \frac{\overline{\langle \chi_k\rho_k v_{zk} h_k\rangle}^S}{\overline{\langle \chi_k\rho_k v_{zk}\rangle}^S}=\frac{\alpha_k\overline{\langle \rho_k v_{zk} h_k\rangle}^S}{G_k}$$

$$\widehat{H}_m\triangleq \frac{G_v\widehat{H}_v+G_l\widehat{H}_l}{G}$$

$$x\triangleq \frac{\alpha_v Q_v}{Q_{FFI}}$$

$$x\triangleq \frac{G_v}{G}$$

$$x_{th} = \frac{\widehat{H}_m - h_{lsat}}{h_{vl}}$$

$$Bo = \frac{g \Delta \rho L^2}{\sigma}$$

None of these two limiting cases (frozen model and HEM) considers the slip between phases and its effect on pressure wave propagation. Let us consider a droplet in gas when a pressure wave is passing. The movement induced by the wave accelerates the gas and the liquid in different ways due to different inertia. Due to a higher density, the droplet will move with a smaller amplitude creating an additional nonequilibrium slip and additional viscous dissipation. A bubble in liquid when a pressure wave is passing will move with a larger amplitude than the liquid creating also an additional nonequilibrium slip and additional viscous dissipation. Two effects are induced:

- The response of a dispersed phase to a pressure wave propagated in a continuous phase may affect the local instantaneous slip ratio and the mixture density evolution, changing also the resulting speed of sound in the mixture.
- Due to the additional nonequilibrium slip created by a pressure wave propagation and to the related additional viscous dissipation, the waves are damped by losing mechanical energy. It is expected that the highest frequency waves are more quickly damped than low frequency waves.

The change of the sound speed by nonequilibrium slip depends on the ratio of the wave time scale τ_w and the particle interaction time τ_d in dispersed flow which is the time scale for a particle submitted to steady gravity and pressure forces to reach an equilibrium velocity difference with the continuous phase. Namely,

$$Fr = \frac{v}{\sqrt{gD}}$$

This particle interaction time is much larger for droplets than for bubbles due to density differences and it increases with the size of bubbles or droplets. Then one may expect that the impact of nonequilibrium slip on the sound speed depends on the ratio τ_d/τ_w . Combined with the fact that the impact of thermal nonequilibrium on sound speed depends on τ_{cond}/τ_w important conclusions can be drawn:

- The speed of sound in two-phase flow depends on the frequency of the wave.
- The speed of sound in two-phase flow depends on the flow regime and in particular on the size of bubbles or droplets in dispersed flow.

The speed of sound calculated from the characteristic velocities cannot take these effects into account since they do not take into account heat transfers and interfacial friction terms of the equation. Only first-order time and space derivatives are taken into account. In fact characteristic velocities correspond to the propagation velocity at the high frequency limit. High frequency waves being rapidly dissipated, choked flow may not correspond to a blockage at the characteristic velocity. Another important conclusion can be drawn:

- The speed of sound in two-phase flow which controls the choked flow can be very different from the characteristic velocity which does not take into account interfacial forces and heat and mass transfers.

The effects of the slip between phases have to be taken into account when predicting choked flow in flow regimes where the mechanical coupling between phases is relatively low:

- Bubbly flow: the coupling may be rather high due to small particle interaction time τ_d and due to the virtual mass force which tends to keep bubble acceleration close to liquid acceleration.
- Droplet flow: the coupling may be rather low due to large particle interaction time τ_d and due to the low effect of the virtual mass force when the dispersed field has a higher density than the continuous field.
- Other flows: it is still a mystery what flow regime may exist in a nozzle at high

velocity in the intermediate void fraction range. For $\alpha < 0.5$ one may expect a bubbly flow, for $\alpha > 0.9$, one may expect droplet flow with possible very thin liquid films along walls. In between no visualization could clarify what the flow regime is. One may imagine a bubbly flow changing progressively to a froth flow with liquid films between bubbles splitting progressively leaving only small droplets.

What heat transfer regime controls the flashing due to liquid-to-interface and vapor-to-interface heat transfers?

- Vapor-to-interface heat transfer plays a minor role compared to liquid-to-interface heat transfers due to lower heat capacity of vapor compared to liquid.
- Liquid-to-interface heat transfer in droplet flow may be due to heat conduction within the droplet which may have a very small time scale if the droplet is very small: a thermodynamic equilibrium may be a good approximation when τ_{cond} is much smaller than the transit time from upstream to choked flow τ_{tr} .
- Liquid-to-interface heat transfer in bubbly flow may be due to both heat conduction in the liquid surrounding the bubble and convection: time scale may be much larger than in droplet flow and nonequilibrium must be considered; according to Berne (1983), convection may be dominant at low steam quality and may be replaced progressively by conduction for higher quality.
- Liquid-to-interface heat transfer in the transition from bubbly flow to droplet flow may be progressively due to conduction since the thickness of liquid films between bubbles decreases and the conduction time scale also decreases.

11.8.3.2 Attempts to take the slip ratio into account

The slip between phases being identified as playing a role in critical flow, several attempts to take it into account were made. Based on experimental data, Fauske (1961, 1965) and Moody (1965) assume that the slip ratio at “choking” conditions is equal to:



Fauske uses $m=1/2$ and Moody uses $m=1/3$.

Over a wide range of data Fauske's empirical value shows somewhat better agreement but measurements of void (Fauske, 1961) showed that the velocity ratio may be very different from that calculated from the slip ratio correlation and no such simple slip model can fit all the data.

Trapp and Ransom (1982) calculated the characteristic velocities of a two-fluid model assuming thermodynamic equilibrium and taking into account the virtual mass force in separate gas and liquid momentum equations. This is better than the HEM model by allowing some slip between phases and better than the frozen model by considering interfacial heat and mass transfers but it overestimates these H&M transfers and cannot precisely take interfacial friction into account. Also using characteristic velocity as choked flow condition is not valid in two-phase flow.

11.8.3.3 Use of the 1-D two-fluid model

A way of taking into account all the mechanical and thermal nonequilibrium in critical flow is to use a 1-D two-fluid model in which:

- Thermal nonequilibrium is modeled through the liquid-to-interface and vapor (or gas)-to-interface heat fluxes, which control the flashing.
- Mechanical nonequilibrium is modeled through an interfacial drag force and a virtual mass force.

Such an approach does not need simplifications such as the following:

- No need to use characteristic velocities as choking criterion since one may model the convergent and divergent part of the flow and BCs may simply be the upstream flow parameters and the far downstream pressure.
- Wall friction effects are modeled and may naturally take into account geometrical effects in short or long nozzle, with a small or long L/D ratio of the minimum cross-section pipe.
- No need to use simplified momentum balance between upstream conditions and choked plane.
- No need to use simplified energy balance between upstream conditions and choked plane.

The calculation of the characteristic velocities of the CATHARE six-equation model with the virtual mass force was made using some small simplifications and gave the following speed of sound:

$$J_k^* = \frac{\sqrt{\rho_k} J_k}{\sqrt{g \Delta \rho D}}$$

with

$$K_k = \frac{\sqrt{\rho_k} J_k}{(g \Delta \rho \sigma)^{1/4}}$$

β is the virtual mass coefficient, c_l and c_g are the sonic velocities in liquid and gas.

11.8.4 Observations in two-phase choked flow experiments

Experiments reported by Henry (1968) show that there is no plane at which choking completely occurs. Apparently there is a very small increase in flow with a decrease in discharge pressure. Henry concluded by examining the details of test data closely that the downstream pressure does, in some small way, affect the flow rate and that downstream geometry does matter. Upstream geometry also clearly matters which made necessary to use the L/D as a means to predict choked flow critical pressure. For the same choke plane pressure and enthalpy, the choked flow mass velocity clearly depends on the upstream geometry. This is never true of a single-phase flow.

These departures from a true choked flow cast doubt on the idea of the “choking” condition as a real physical occurrence for two-phase flow. There are similarities between single- and two-phase cases but there are also clear differences. However, assuming choked flow with a flow rate which depends only on upstream conditions remains a very reasonable approximation in two-phase conditions.

The observations in SUPER-MOBY-DICK long nozzle tests (see Fig. 11.13) also found a similar behavior. The pressure up to a “presumed sonic section” does not seem to change for various downstream pressures and small differences in flow rate were found but within the measurement uncertainty. One can imagine a sonic

section at end of the small diameter pipe or just a little downstream followed by a supersonic flow up to a pressure recovery which is not discontinuous like in single-phase gas conditions but much more progressive.

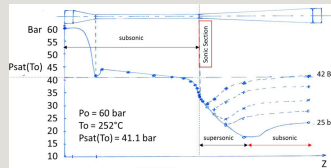


Fig. 11.13 SUPER-MOBY-DICK long nozzle tests with constant upstream conditions (subcooled water at $P_o=60$ bar, $T_o=252^\circ\text{C}$) and at various downstream pressures.

11.8.5 Choked flow prediction by system codes

System codes developed three methods for modeling break flow or choked flow:

(1) 0-D model with the use of characteristic velocity: the geometry of the flow restriction is simplified and a coarse meshing is used. A characteristic velocity is set to zero to predict the sonic velocity and simplified equations are used to predict flow evolution from upstream to the sonic section (e.g., Bernoulli equation, isentropic evolution, or constant total enthalpy). Such methods are available in TRACE (e.g., TRACE, 2007a) and RELAP5 (RELAP5, 2001) codes. There may be a set of available methods (HEM, Ransom-Trapp, Henry and Moody) depending on the upstream conditions.

(2) 1-D modeling of the flow through the nozzle: the flow from upstream to sonic section is more precisely calculated by two-fluid equations using a very fine meshing in the vicinity of the throat. This method is possible in the CATHARE code. It requires that very small meshes are used in the vicinity of the sonic section where pressure gradient is very high. Such a method is only possible with an implicit numerical scheme which allows high velocity flow in small meshes without material Courant limitation.

(3) 0-D model with empirical critical flow rate correlation: the geometry of the flow restriction is simplified and a coarse meshing is used as in Case 1. The mass flow rate is predicted using an empirical correlation as a function of upstream flow conditions. This method may be used on option in CATHARE code as a cheaper and less accurate alternative to the recommended 1-D modeling.

11.8.5.1 Using 0-D choked flow model

The use of 0-D modeling of choked flow with coarse meshing may have a good accuracy in some cases such as high quality but they have a higher uncertainty in low subcooling conditions. In semiimplicit numerical schemes such methods prevent from calculating high velocity flow in small meshes, which is CPU costly since the material Courant limit has to be satisfied. A simple discharge coefficient may be added to take geometrical effects into account. User Guidelines recommend using discharge coefficients in the domain (0.8, 1.2). The limitations are the following:

- Using characteristic velocity as speed of sound is not well based as explained above.
- 2-D or 3-D effects in abrupt area change are not modeled and can only be corrected by constant multipliers.
- In worst cases, uncertainty in predicting flow rate may be about 20%.

Whatever method is used, the prediction of break flow rate or choked flow remains a limitation for the accuracy of reactor transient simulations.

11.8.5.2 Predicting choked flow with a 1-D two-fluid modeling

When using this method with the CATHARE code to simulate critical flow experiments, it was observed:

- The choked flow condition is reached without having reached the speed of sound resulting from characteristic velocities. There might be up to a factor 2 between the velocity at the throat where the choked flow was observed and the speed of sound resulting from characteristic velocities. This confirms that the characteristic velocity of a system of equations does not account for the effects of interfacial H&M transfers and interfacial forces and cannot be used to predict choked flow conditions.
- Although the virtual mass force is affecting a lot the C_s value, it had very small effect on the predicted critical flow rate (about 1% difference between $\beta=0.5$ and $\beta=0$).
- When simulating critical flow tests with subcooled liquid upstream conditions, the liquid-to-interface heat flux, which governs the flashing, was the dominant parameter for having good predictions. If the nozzle has a pipe with a long L/D at the minimum flow area, the wall friction also influences the critical flow rate

prediction. In such conditions, one may expect to have bubbly flow with small bubbles up to choked plane and the interfacial friction was high so that the relative velocity was small.

- When the upstream subcooling was small, the predicted flow rate was also sensitive to the flashing delay model and it was not possible to reach a generally good prediction of flow rates in various geometries in such conditions.
- When simulating critical flow tests with saturated two-phase upstream conditions, the liquid-to-interface heat flux was less sensitive and the interfacial friction became progressively the dominant parameter for having good predictions when the quality increases. Moreover, in high steam quality flow where a droplet flow is expected, using a classical Weber number criterion for predicting the droplet diameter and a classical drag coefficient was sufficient to obtain good predictions of the critical flow rate.

The validation of the CATHARE code against critical flow used a set of experiments with various geometries (see Fig. 11.14) and covered all upstream conditions from subcooled liquid to high quality and pure steam flow. The prediction accuracy was better than 5% for high subcooling and high quality upstream conditions. The worse predictions were for low subcooling upstream conditions with errors up to 15%. It was also found that geometries with complex geometries (abrupt area changes, orifices, etc.) could also induce additional difficulties.

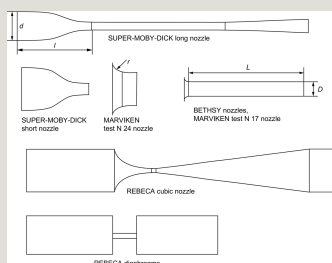


Fig. 11.14 Various critical flow experiments used for validation of the choked flow prediction by the CATHARE code.

A more in-depth analysis of the reasons of the difficulties in the predictions for low subcooling tests was conducted and the conclusions are the following:

- These most difficult conditions correspond to a void fraction range (approx. 0.5–0.9) at the choked plane where there is no information on flow regime. This does not allow a mechanistic modeling of the liquid-to-interface heat flux which is the most sensitive model controlling the quality of predictions.

- These conditions are highly sensitive to the flashing delay model. However, this delay is controlled by heterogeneous nucleation which depends on parameters which cannot be well known in all conditions such as the quality of the water, the status of the wall surface. It may also depend on the turbulence intensity which may be very small after a convergent or very high after flowing at high velocity through a small diameter pipe. Predicting the pressure fluctuations due to turbulence in such nonequilibrium turbulence is far beyond the capabilities of a 1-D six-equation two-fluid model.

- Since bubbly flow is expected in such conditions the prediction of bubble size distribution is of prime importance for a good liquid-to-interface modeling. Attempts to use a convective heat transfer and a break up criterion for defining the bubble size could not predict correctly all low subcooling tests probably because transient conduction may prevail in some conditions. However, modeling this transient conduction would require a good knowledge of the geometry of interfaces in the whole void fraction range of interest, including the void fraction range (0.5–0.9) where there is no information on the flow regime. It was also found difficult to fit a flashing model on one nozzle geometry and to predict other geometries with the same accuracy.

In summary the 1-D modeling of choked flow with the CATHARE code could provide the flow rate rather well in high subcooling and two-phase upstream conditions but encountered more difficulties with low subcooling conditions and with geometrical effects. Fig. 11.15 shows the prediction of critical mass flux in SUPER-MOBY-DICK long nozzle with a smooth convergent and with a more abrupt convergent. Calculations were performed with the standard empirical flashing model (Bestion, 1990a) and with a more mechanistic convection model. The convection model could predict better than the empirical model the smooth convergent data but has worse predictions in the abrupt convergent.

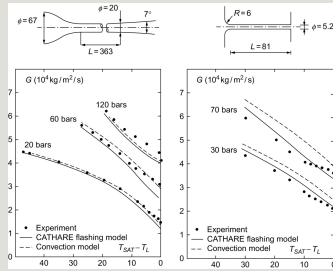


Fig. 11.15 Comparison of CATHARE code predictions with experimental data of critical mass flux G ($\text{kg}/\text{m}^2/\text{s}$) for subcooled water inlet conditions, for two nozzle geometries and with two flashing models: the CATHARE standard model and a convection model.

It was observed that the prediction of the mass flow rate is very sensitive to flashing in subcooled liquid upstream conditions and to interfacial friction in high quality flows. This 1-D method is able to capture the governing phenomena, which control the actual sonic velocity. The limitations are the following:

- Nonestablished flow conditions make more difficult the derivation of mechanistic models. The bubble size or droplet size is probably not an equilibrium size due to the very short transit time scales in comparison to coalescence and break up time scales. The slip between phases is probably not an equilibrium slip.
- Nucleation delay is difficult to model in a general way for all conditions.
- 2-D or 3-D effects (such as vena contracta) in abrupt area change are not well described in a 1-D model.
- In the worst cases the uncertainty in predicting flow rate may be about 15 %.

A state-of-the-art report on “Critical flow modelling in nuclear safety” published by OECD-NEA-CSNI (1982) recommended to develop 1-D modeling to obtain more accurate predictions than 0-D models. After the efforts spent in the 1980s, the 1-D models actually obtained some progress but not as expected.

More recently, Bartosiewicz and Seynhaeve (2014) have proposed the delayed equilibrium model (DEM) implemented in a 1-D three-field model with saturated steam, saturated liquid, and metastable liquid which performs better in low subcooling conditions than any other model. A mechanical equilibrium is assumed between the three fields and a relaxation equation controls the mass fraction of metastable liquid. The relaxation time constant was somewhat empirically

correlated. However, one may interpret the success of this model by a better capability to treat transient conduction in a model which keeps the memory of the upstream fluid temperature. This flashing model was implemented in both a 1-D model and in a 3-D CFD code (Duponcheel et al., 2015). This opens the way to a better prediction of geometrical effects.

The accurate prediction of critical flow rate at a break on a reactor circuit in a nuclear reactor may not be considered as mandatory since safety analysis of reactors should cover any kind of break sizes. However, the very limited accuracy of critical flow rate prediction by system codes may be an issue when analyzing IETs by preventing from precise validation of other code models. Moreover a precise prediction of choked flow in well-know reactor component geometry (valve, flow limiter, etc.) may be necessary for a precise analysis of some reactor transients. The continuous increase of computer power will allow in near future a 2-D or 3-D treatment of a break flow at a reasonable CPU cost which may be associated with a modern flashing modeling such as the DEM model and may predict choked flow with a significantly better accuracy than current models.

11.9 Predicting two-phase flow in horizontal pipes including stratification

11.9.1 Phenomena of interest in HL and CL of a PWR

HLs, CLs, and ILs of PWRs play an important role in accident sequences, particularly when two-phase steam water flow occurs in the loops (see Fig. 11.16). When the primary mass inventory is degraded in the case of a loss of coolant accident (LOCA) the phase coupling or decoupling controls the amount of water which is kept out of the pressure vessel and influences the occurrence of a core uncover with fuel clad temperature excursion. The formation of a liquid slug in IL after the end of natural circulation and the loop seal clearing may also induce a core uncover. Many auxiliary circuits are connected to HL and CL such as SIs, RHR circuit, and the pressurizer surge line. All these connections may also be considered as potential breaks when analyzing the safety of the reactor.

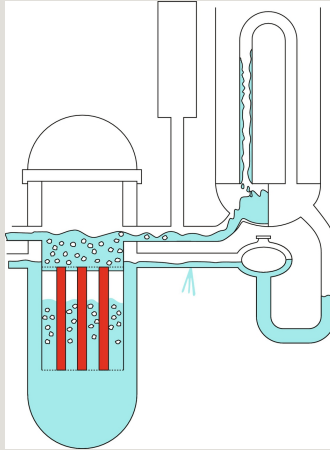


Fig. 11.16 Examples of flow situations encountered in hot legs and cold legs in accidental transients of a PWR.

The knowledge of the flow regime in horizontal pipes may play an important role in PWR accident scenarios. For example, during many LOCA transients, the flow regime in HLs or CLs influences the amount of liquid and steam lost at a break or entrained in the pressurizer surge line in the case of pressure relief valve opening. Both the primary mass inventory and the primary pressure are very sensitive to the steam quality of the break or valve flow. As an example, the quality of the flow rate at a break or steam relief valve in the pressurizer will strongly depend on the flow regime at the T junction between HL and surge line as illustrated in Fig. 11.17.

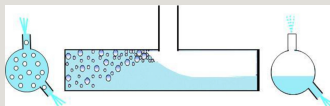


Fig. 11.17 Two different flow regimes at the pressurizer T junction or at two different break orientations.

The main phenomenon in hot and CLs is phase stratification, which dramatically decreases the mechanical coupling between phases. The interfacial friction in stratified flow is several orders of magnitude lower than in dispersed bubbly flow. Therefore, the entrainment of liquid water in the loop by steam coming from the core is minimized in stratified flow. This is a favorable feature since it keeps more

water in the core without affecting the heat release to the SGs which may continue even after the stop of two-phase natural circulation, by the reflux condensation mode. In the stratified flow regime in a horizontal pipe, there may be a nonhorizontal free surface due to interfacial friction and/or due to some interfacial waves propagating at the free surface. In many SBLOCAs there is a liquid slug formed in the IL after the end of the two-phase natural circulation. This liquid slug is then removed by the so-called loop seal clearing process and some quantity of water is kept at the bottom of the IL, which depends on the interfacial friction at the free surface and on the predicted free surface slope which determines the minimum cross-section for steam flow and then the maximum steam velocity. The slope of the free surface is the result of the interfacial friction and the slope influences the interfacial friction and the possible entrainment of water by determining the maximum steam velocity.

In the two-phase natural circulation mode, the flow at the entrance of the HL may be bubbly or stratified-bubbly—with a continuous vapor flow at the top and a bubbly flow below the free surface—when the swell level in UP decreases to the elevation of the HL. In most cases velocities are low and the flow regime changes progressively to pure stratified flow without any more bubbles.

In the case of stratified flow, waves are created at the free surface, which increase the surface roughness and the interfacial friction. Both fluvial and torrential flows may occur and a hydraulic jump may be created when there is a transition from torrential to fluvial regime.

In the case of reflux condenser mode, CCFL may occur in the HL in the zone of the bend and the SG entrance nozzle. Large amplitude waves reflecting on the bend were observed in some conditions in the MHYRESA tests (Geffraye et al., 1995). CCFL may result from liquid entrainment at the crest of large amplitude waves.

The MHYRESA hot-leg entrainment tests (Geffraye and Laroche, 1999; Ratel and Geffraye, 2000; Geffraye et al., 2000) have also shown that for a given liquid level in the UP, a hydraulic jump could be created and moved downstream when the gas flow rate is increased.

During the reflooding of a LBLOCA a mist flow enters the HL and some deposition of droplets occurs. Liquid films are created along HL walls and a continuous liquid field is collected at the bottom of the pipe. Due to the large vapor velocity, droplets may be also entrained from the crest of waves. The mist flow which enters the SG tubes is the result of this deposition and entrainment of droplets occurring first in the UP and in the HL. Prediction of the resulting droplet

flow rate entering SG tubes is of prime importance for modeling the so-called steam-binding effect (Valette et al., 2011). The vaporization of droplets in the hot SG tubes creates additional pressure losses in the loops which decreases the flooding rate in the core.

In postulated accident sequences where pumps are supposed to operate in two-phase flow conditions, the phases may be well mixed at the outlet of the pump and may tend to stratification when flowing to the pressure vessel.

Postulated small and medium size breaks in HL, IL, and CL may be oriented at the top, on the side or at the bottom of the pipe (see Fig. 11.17). The quality and mass flow rate at the break depends a lot on the position of the break and on the flow regime. In a stratified flow there may be a very large difference between a bottom break, which entrains a large flow rate but a low quality, and a top break, which entrains a high steam flow rate and a low mass flow rate. Losing a high coolant mass flow rate may induce a core uncover with fuel clad temperature excursion. Having a high steam quality at the break induces a slower loss of primary mass and decreases primary pressure (Bestion, 1989) so that actuation of SI will occur earlier. Therefore, core uncover is less likely to occur and will be shorter than in the bottom break case. This shows the importance of predicting the flow regime and more generally the vertical repartition of steam and water in horizontal pipes.

Postulated loss of RHR accidental transients at very low pressure (close to atmospheric pressure) may create high velocity steam flow in the HL. Such situations may occur during mid-loop operation with vent valves possibly open or even with an open manhole in the pressurizer or the SG header. The loss of mass inventory is controlled by water entrainment either in the pressurizer or to the SG, which depends a lot on the flow regime in the HL. Transitions from stratified to slug flow by Kelvin-Helmholtz instability or to stratified-mist flow by droplet entrainment at wave crests may occur and influence the water entrainment out of the circuit.

SI in CL, or in both CL and HL, induce direct contact condensation since subcooled water is injected into a saturated steam or steam-water mixture. Analysis of SI COSI experiments (see Janicot and Bestion, 1993) has shown that a stratified flow is created in most cases. However, the high turbulence created by SI jets induces an efficient mixing which enhances the local condensation. In the case of a very high condensation rate (when the SI flow rate is very high) in a CL there may be a condensation-induced Kelvin-Helmholtz instability with a liquid slug which may go back to the pump at high velocity. UPTF refill tests have also shown that condensation may be sensitive to the presence of small amounts of degassed

nitrogen at the accumulator injection, which limits the condensation and prevents large instabilities.

In summary the main phenomena that must be predicted with sufficient accuracy in horizontal legs are:

- Transition from bubbly to stratified flow
- Transition from stratified flow to slug flow by Kelvin-Helmholtz instability
- Transition from stratified flow to stratified-mist flow by droplet entrainment
- Transition from mist flow to stratified-mist flow by droplet deposition
- Presence of free surface waves which increase the interfacial friction
- Occurrence of fluvial and torrential flow regimes with a possible hydraulic jump
- Effects of the cross-section area changes and of orientation changes (in the bends of HL and IL) on the free surface position
- All phenomena which affect a possible free surface inclination, such as interfacial friction or wave propagation
- Remaining water mass in IL after a loop seal clearing
- Interfacial heat and mass transfers associated with DCC at SIs, which depend a lot on turbulence created by ECCS jets

Other phenomena exist in horizontal legs which are less sensitive in accidental transients. Wall friction in large diameter pipes is rather small compared to friction in other components such as the core and SGs so that they do not influence the loop flow rate a lot. Therefore, the modeling of wall friction does not require a high accuracy. In bubbly or slug flows in horizontal legs there is practically no slip between gas and liquid due to the absence of buoyancy forces, so the transition from bubbly to slug flow and the interfacial friction in these flow regimes do not require very accurate modeling.

11.9.2 Horizontal flow modeling with the two-fluid model

As already discussed in Section 5.8.3, the 1-D two-fluid one-pressure six-equation model is able to describe many important features of two-phase flow in horizontal or inclined pipes including stratification where a significant pressure difference

may exist between phases due to gravity.

The case of a stratified flow in a horizontal or inclined duct is particular since the interface has a simple shape and the pressure field in a cross-section may be reasonably approximated. The CATHARE code two-fluid six-equation model able to describe stratified flows was derived by de Crecy (1986), see also Bestion and Serre (2012) using the following assumptions:

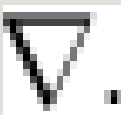
- A hydrostatic transverse pressure gradient
- Vapor and liquid densities uniform over the cross-section
- Continuity of pressure across the interface (no surface tension effect and no pressure jump induced by mass transfer)

In such conditions the derived momentum equations are:

$$Re = \frac{vD}{\nu}$$

with

$$We = \frac{\rho \Delta V^2 L}{\sigma}$$



The We term plays a very important role in stratified flow. It represents the force which tends to homogenize the free surface elevation in horizontal pipe. It controls the characteristic velocity corresponding to void fraction waves which are shallow water waves at the free surface of the stratified flow.

The “cross-momentum equation” obtained by eliminating the pressure gradient between gas momentum and liquid momentum controls the slip ratio, whereas the total mixture momentum equation (addition of the gas and liquid momentum equation) controls relations between flow rate and axial pressure gradient.

$$\overline{v}^2 = \Delta$$

In the case of horizontal steady established flow ($\overline{v}^2 = \Delta$ and zero axial gradient of velocities and void fraction) and for a constant cross-section horizontal pipe without interfacial mass transfer, one can write a simple force balance representing the equilibrium:

$$\overline{v}^2 = \Delta$$

However, this equilibrium is practically never reached in HL, IL, and CL.

In many stratified situations in HL, IL, and CL, wall friction terms are negligible but there is a level slope such that the force balance may be described by the following approximation equation:

$$\overrightarrow{A} \cdot \overrightarrow{B}$$

In the case of a stationary steep level slope such as a hydraulic jump, the inertial forces may not be negligible and the situation may be described by the following approximation equation:

$$\overline{f} \triangleq \frac{1}{T} \int_T f dt$$

11.9.3 Properties of the system of equations for stratified flow

As shown by de Crecy (1986), the characteristic equation may be written from mass and momentum equations for gas and liquid. It is here assumed that both phases are incompressible and sound speed is infinite in order to simplify the calculation of the void wave propagation velocities. It results in the following equation:

$$\widetilde{f} \triangleq \overline{\rho f} / \overline{\rho}$$

The hyperbolicity condition is:

$$\widetilde{f}^k \triangleq \overline{\chi_k f_k} / \overline{\chi_k}$$

With

$$\widetilde{f}_k^k \triangleq \frac{\overline{\chi_k \rho_k \widetilde{f}_k}}{\overline{\chi_k \rho_k}} = \frac{\overline{e_k \rho_k \widetilde{f}_k}}{\overline{e_k \rho_k^k}} = \frac{\overline{\rho_k \widetilde{f}_k^k}}{\overline{\rho_k^k}}$$

or

$$\langle f \rangle^L \triangleq \frac{1}{L} \int_L f \, dl$$

The characteristic velocities are $W+C_a$ and $W-C_a$ where:

$$\langle f \rangle^S \triangleq \frac{1}{A} \int_A f \, ds$$

$$\langle f \rangle^V \triangleq \frac{1}{V} \int_V f \, dv$$

The limit between fluvial (subcritical with respect to void waves) and torrential (supercritical with respect to void waves) occurs when $W=C_a$, or when:

$$\left(\int_{\Gamma} \left(\frac{1}{2} \rho \left(\frac{d\mathbf{u}}{dt} \right)^2 + \rho \left(\frac{d\mathbf{v}}{dt} \right)^2 \right) d\Gamma \right)^{\frac{1}{2}} = \left(\int_{\Gamma} \left(\frac{1}{2} \rho \left(\frac{d\mathbf{u}}{dt} \right)^2 + \rho \left(\frac{d\mathbf{v}}{dt} \right)^2 \right) d\Gamma \right)^{\frac{1}{2}} = \left(\int_{\Gamma} \left(\frac{1}{2} \rho \left(\frac{d\mathbf{u}}{dt} \right)^2 + \rho \left(\frac{d\mathbf{v}}{dt} \right)^2 \right) d\Gamma \right)^{\frac{1}{2}}$$

Then depending on the value of p_i , one may find nonhyperbolic flow, torrential flow, or fluvial flow as shown in Fig. 11.18.

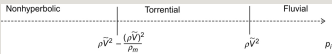


Fig. 11.18 The torrential and fluvial stratified flow regimes depending on the p_i value.

An example of two flows obtained in the MHYRESA test facility (representing a PWR HL) is shown in Fig. 11.19. The water level H increases progressively in the case of the flow rate Q4, whereas it increases suddenly with the flow rate Q6. Condition Q4 is fluvial from entrance to exit whereas condition Q6 is torrential then fluvial after a hydraulic jump.

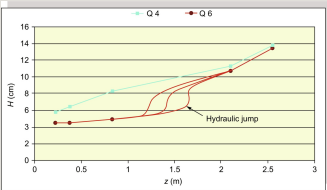


Fig. 11.19 Examples of water level evolution in the MHYRESA hot leg.

Momentum equations with the $\hat{f} \triangleq \frac{\langle \rho f \rangle^S}{\langle \rho \rangle^S}$ term presented above have the capability of the Saint-Venant equations to distinguish the two flow conditions and to predict a hydraulic jump. This is not possible when using a simple mixture momentum equation with drift flux.

11.9.4 Predicting stratification

All models for the transition from stratified flow to slug flow or intermittent flow are based on an analysis of the Kelvin-Helmholtz instability in one or two dimensions. The CATHARE model assumed that a 1-D analysis is sufficient and that the model equations contain enough information to study these instabilities.

Two kinds of linear stability analysis have been investigated (Bestion and Micaelli, 1986) a high frequency linear stability and a marginal stability analysis. They consist in determining the conditions when a void fraction wave has a positive growth rate.

High frequency analysis considers only differential terms of the equation and neglects the viscous and algebraic source terms. It corresponds to the hyperbolicity limit of the system of equations. It can be demonstrated that when the hyperbolicity is not satisfied, high frequency waves are unstable and all wave lengths are unstable. The limit overestimates the stability domain.

It corresponds to a limiting Froude number defined as:

$$\hat{f}_k^k \triangleq \frac{\langle \chi_k f_k \rangle^S}{R_k}$$

The marginal stability analysis takes into account all terms of the equation and determines the limit at which at least one wavelength becomes unstable. There is no explicit expression for this limit and it must be solved numerically.

The two limits are illustrated in the plane J_v versus J_l by adding the mechanical equilibrium equation for established flow as in Fig. 11.20. It was observed that the limit value of 0.25 for the Froude number is close to other stratification criteria

(Taitel and Dukler, 1976) and not far from the marginal stability limit.

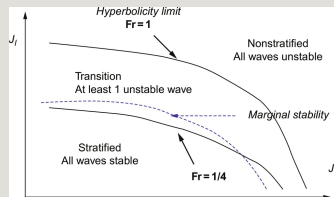


Fig. 11.20 Qualitative view of stability domains with respect to Kelvin-Helmholtz.

Therefore, it was considered that:



A rate of stratification R_1 in the range 0–1 may be defined based on the K-H instability.

However, this only considers the stability of a stratified flow; it is not sufficient to determine the flow regime. The stability of a bubbly flow regime must also be analyzed.

11.9.4.1 Stability of bubbly flow regime

A horizontal bubbly flow can remain dispersed bubbly or change to another flow regime depending on the forces acting on the bubbles in the vertical direction:

- The buoyancy force may induce bubble rising and accumulation at the upper part of the pipe, where they can coalesce. If the coalescence dominates, the bubbles will merge leading to large gas pockets that eventually lead to stratified flow, slug flow, or plug flow.
- Turbulence of the liquid tends to mix the bubbles and homogenizes the bubble concentration, preventing their accumulation at the upper part of the pipe and thus their coalescence. Bubbles are dispersed by being entrained by the liquid eddies due to the drag force and added mass force associated with the fluctuating velocity

field.

- Average drag force in the mean flow slows the movement of the bubbles whatever the direction.

Therefore, the persistence of the dispersed flow will strongly depend on the liquid turbulence intensity since it can first prevent the bubbles rising, then prevent their coalescence and it may also break the largest ones. It also depends on the bubble size: small bubbles are more likely to be entrained by eddies since the drag coefficient is higher than for large bubbles. In addition, the buoyancy force is proportional the bubble size to the cube when drag and turbulent dispersion forces are proportional to the squared bubble size.

The modeling of the transition from bubbly to stratified flow or slug flow may consist in comparing two velocity scales: V_b is the bubble rising velocity and V_t is the liquid turbulent velocity scale. One will consider that the flow will remain bubbly if the turbulent velocity is significantly larger than the rising velocity and transition to stratification may occur in the opposite situation.

For example, the bubble rise velocity was taken in CATHARE 2 as:

$$\tilde{f}_k^k \triangleq \frac{\langle \chi_k \rho_k f_k \rangle^S}{\langle \rho_k \rangle^S}$$

and the turbulent liquid velocity was taken proportional to the wall friction velocity:

$$\hat{\tilde{f}} \triangleq \langle \tilde{f} \rangle^S$$

With $\tilde{f} \triangleq \frac{\langle \rho f \rangle^S}{\langle \rho \rangle^S}$ one obtains $\hat{\tilde{f}}_k^k \triangleq \frac{\langle \chi_k \tilde{f}_k \rangle^S}{\alpha_k}$.

Experimental data sources have been used to calibrate the transition criterion. The

stratification is possible almost when $\bar{f}_k^k \triangleq \frac{\langle \chi_k \rho_k f_k \rangle^S}{\langle \chi_k \rho_k \rangle^S} = \frac{\widehat{\rho_k f_k}}{\widehat{\rho_k}}$ and impossible almost for $\frac{\widehat{\rho_k f_k}}{\widehat{\rho_k}} < \frac{\langle \chi_k \rho_k f_k \rangle^S}{\langle \chi_k \rho_k \rangle^S}$ with a transition in between. Similar criteria were adopted by other system codes.

Looking at the stability criteria for Kelvin-Helmholtz instability and for the stability of bubbly flow four cases are possible:

1. Stable stratified flow possible and stable bubbly flow impossible: in this case one can easily decide that the flow is stratified.
2. Stable stratified flow impossible and stable bubbly flow possible: in this case one can easily decide that the flow is bubbly.
3. Stable stratified flow impossible and stable bubbly flow impossible: in this case one can easily decide that the flow is intermittent (slug or plug flow).
4. Stable stratified flow possible and stable bubbly flow possible: in this case one cannot easily decide what the flow regime is.

This last case corresponds to flow conditions with rather high liquid velocity and rather low velocity difference between phases; this may occur in bubbly, slug, and stratified flows. One should know the history of the flow to determine which regime is possible and this is not possible with only the six local variables of the two-fluid model. More advanced models may provide useful additional information. If a transport equation for the interfacial area was added it could clearly allow distinguishing stratified flow from bubbly flow. A multifield model with two gas fields (continuous gas and dispersed bubbles) could also easily distinguish stratified flow from bubbly flow. In the absence of knowledge of the history, the CATHARE six-equation model preferred to select bubbly flow when both bubbly and stratified flow could be stable. This allows stratification only when stratified flow is stable and bubbly flow unstable. In PWR horizontal legs, high liquid velocities are mainly encountered when pumps are still on. Therefore, the flow at the inlet of the CL cannot be stratified due to strong perturbations in the pump. At the exit of the UP there may be either a bubbly flow or a stratified flow with bubbles below the free surface depending on the position of a possible swell level in the UP. In the latter case the CATHARE code may be partly wrong by predicting pure bubbly flow. However, this situation does not happen very often and no big discrepancy in IET prediction was observed which could be attributed to this weakness of the flow regime identification.

11.9.4.2 Interfacial friction

In horizontal bubbly flow in large diameter pipes, there is a low axial pressure gradient and consequently the mean velocity of the bubbles and of the liquid are very close. It is not difficult to predict the right slip between phases which is nearly zero. A simple extrapolation of the interfacial friction from vertical bubbly flow would be convenient. For the same reasons extrapolating the interfacial friction from vertical slug flow would be convenient in horizontal flow.

For stratified flow the interfacial friction is much lower and there can be large velocity differences between phases. The interfacial friction coefficient depends a lot on the presence of waves. The TRACE code (TRACE, 2007a) adopted only a friction coefficient for stratified smooth regime. The RELAP5 code also uses an interfacial friction coefficient for stratified flow which is similar to the wall friction (Blasius model). Several academic works may be found in the literature which correlated the interfacial friction based on experiments including wavy stratified flow. The friction coefficient depends on some gas Reynolds number or on a Froude number to take into account the roughness due to waves. However, there may be a difficulty since the roughness due to waves may depend on the axial location along the pipe since waves are created and increase progressively in amplitude as shown in Fig. 11.21.

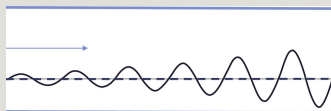


Fig. 11.21 Typical formation of a wavy stratified flow.

The average liquid level H may be constant or quasi-constant while the amplitude of waves increases. This should produce an increasing interfacial friction coefficient but there is nothing in the principal variables of the two-fluid model which can tell what the local amplitude of waves is. The time-averaged values of the void fraction and of the phase velocities are constant. Therefore, it is impossible to predict the axial increase of the interfacial friction when the wave amplitude increases. One can only adopt a homogeneous average friction coefficient which takes into account the presence of waves. However, for the same conditions, the average wave amplitude is smaller for a short pipe than for a longer pipe. It was considered that the models of the literature were not well adapted to the reactor HL, IL, and CL since they were obtained for established flow

conditions in very long pipes. Therefore, the interfacial friction coefficient of the CATHARE code was derived from experiments which represented an IL and a HL. This was supposed to be the best compromise.

One must notice that only the roughness of the waves which are not predicted by the code has to be taken into account in the averaged friction coefficient. As shown above “shallow water waves” may be predicted by the two-fluid model due to the

$\bar{f} \triangleq \frac{\langle \rho f \rangle^S}{\langle \rho \rangle^S}$ term which gives to the two-fluid equations the capabilities of the Saint-Venant equations. Such waves have a wave length longer than twice the water depth. Shorter wavelength waves may be created at the free surface of the stratified flow which cannot be predicted by the two-fluid model—they are “deep water waves”—even if the time averaging was made on a very short time interval. At least all these deep water waves should be taken into account by interfacial friction coefficients.

11.9.5 Conclusion on predictive capabilities of two-fluid model in horizontal pipes

In the classical two-fluid six-equation one-pressure model, the axial effects of gravity forces may be correctly taken into account even in the case of change of the cross-section area or of the pipe orientation (see Section 5.8.3 in Chapter 5). It can predict both fluvial and torrential flow with a possible hydraulic jump. The shallow water waves may be predicted but the presence of small wavelength “deep water waves” should be treated as a free surface roughness in the interfacial friction coefficient for a stratified flow regime.

Since phase stratification plays a dominant role, the Kelvin-Helmholtz instability and the stability of bubbly flow regime must be considered. A transition criterion based on a Kelvin-Helmholtz instability and a criterion for the transition from bubbly to stratified flow regime can be established from local flow variables. The prediction of the actual flow regime may be obtained from these two criteria except when both stratified flow and bubbly may be found stable. For this situation the two-fluid model cannot decide what the flow regime is whereas a multifield could easily determine the flow regime.

The use of a transition domain between bubbly and stratified flow or between stratified and slug flows provides a progressive change of flow regime. Then the predicted qualitative behavior is consistent with the physics but there is no quantitative control of the transition time period. Here again a multifield model could model the transition and the time period and space extension of the transition may be physically controlled. A dynamic modeling of liquid turbulence and bubble

interfacial area could be used to model precisely the time scales associated with the transition from bubbly to stratified flow. It could be more convenient to use a dynamic modeling of turbulence to better model interfacial heat transfers in all situations, particularly for direct contact condensation.

A four-field model with a continuous liquid field, a continuous gas field, a dispersed bubble field, and a dispersed droplet field, has many capabilities to improve the prediction of flow regimes, the dynamics of flow regime transitions, the mechanical behavior, and the interfacial transfers in complex situations when a phase is split into two fields. In addition it could provide a better characterization of the flow with a more precise vertical void repartition. Three-field models with two liquid fields are already being implemented in CATHARE-3 and SPACE codes. Four models already exist in the petroleum industry for liquid-gas flows in pipelines and could probably be implemented in system codes in the medium-term future.

11.10 The use of flow regime maps

Every flow regime has its internal structure and its transfer mechanisms. So it seems natural to use a flow pattern map in a code and to develop correlations for mass momentum and energy transfers which depend on the flow pattern. This is usually done via flow regime maps where specific two-phase flow patterns are identified as functions of input data such as superficial gas and liquid velocities, flow rates, or more complex dimensionless parameters. The highly empirical flow regime maps are based on a large amount of measured data for different fluids, vertical, and horizontal flow conditions and different pipe diameters. Typical examples are the flow pattern maps of **Mandhane et al. (1974)** and **Taitel and Dukler (1976)**. Nevertheless, all these flow regime maps are valid only for steady state—or quasi-steady state—and fully developed—or quasi-developed—flow conditions although rapid transient and nonestablished flows also exist in nuclear reactors under accident conditions. Having these restrictions in mind it might be justified to further simplify the flow maps as is usually done in all the codes.

As an example, the flow regime map as used in RELAP5/MOD3 for horizontal flow is shown in Fig. 11.22. Major selection parameters are void fraction α_g and total mass flux G_m .

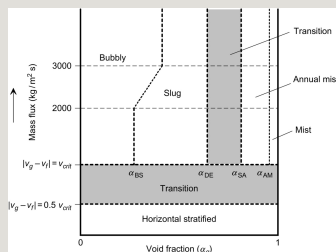


Fig. 11.22 RELAP5 flow regime map for horizontal flow.

Specifically modeled are the bubbly, slug annular-mist, mist, and stratified flow regimes. Transition criteria are also algebraic relations between flow parameters. To avoid discontinuities, some transition regions are included where all parameters are interpolated from the adjacent flow regime boundaries. This only provides artificially smooth transitions but cannot take into account the relaxation time scale associated with the flow process responsible for the transition.

11.10.1 Transition criteria

Horizontal stratified flow conditions are assumed to exist for



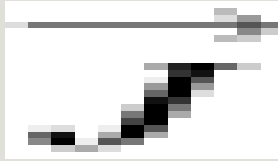
$$\text{and } \frac{d}{dx} \left[\lambda(T) \frac{dT}{dx} \right] = -q_v,$$

critical velocity according to Taitel and Dukler (1976):



where θ represents the angle between the vertical axis and the pipe axis.

The criteria for bubbly to slug, slug-to-annular mist, and annular mist to mist flow regimes are just given by limiting values of void fraction and mass flux. A classical slug-to-annular transition criterion is:



Other flow regime maps are applied for vertical flow separating pre-CHF and post-dry-out conditions. Flow regime maps provide a necessary information on interfacial structure and interfacial area based on experimental observation and with some theoretical basis and allows a mechanistic modeling of interfacial transfers.

The most important transitions correspond to interfacial area changing by several orders of magnitude, for example, at the onset of droplet entrainment or when phase stratification occurs in a bubbly flow in a horizontal pipe.

Several models are used in the various codes for the onset of droplet entrainment, for example, Steen-Wallis (Wallis, 1969) model:

$$\frac{d\Lambda}{dx} = \frac{d\Lambda}{dT} \frac{dT}{dx} = \lambda(T) \frac{dT}{dx}$$

E being the entrainment rate (droplet flow rate divided by total liquid flow rate).

The Ishii and Mishima (1984) model gives:

$$\vec{F} = \vec{g}$$

or a limiting value of the Kutateladze number:



The main reason for codes not having converged to the same correlation is probably that the validation could not clearly identify which model was the most appropriate since measurements of E is very difficult particularly in complex geometry (fuel assembly) and high pressure and temperature.

11.10.2 The limitations of flow regime maps

The main limitations of using such flow regime maps are:

- Range of validity: no observations are available in high pressure steam water flows to validate the flow maps in such reactor conditions. Also data in large diameter pipes are very limited.
- Flow geometry: very limited observation of flows in complex geometry (rod bundle) is available although geometrical effects are likely to be significant. Also effects of some singularities are not taken into account.
- Steady and established flows are necessary to establish such maps, and they are extrapolated in transient or nonestablished conditions. History effects and relaxation time constants associated with regime transitions are not taken into account.

11.11 Developing and validating closure relations

Physical models are required to close the system of equations. Closure relationships concern mass, momentum, and energy exchanges between phases and between each phase and the wall. In a first step, code developers look at the scientific literature to find such models. When they exist, they were often developed based on theoretical work and from rather academic experimental data such as air-water flow in a circular pipe with a large length to diameter ratio. They must be later confronted to more industrial flow conditions, with steam-water data in larger ducts of various shapes. Specific separate effect tests (SETs) were performed and analyzed to investigate two-phase flows in conditions more representative of the reactor transients to be simulated. Based on these data new correlations were developed when existing models were not satisfactory. The degree of empiricism depends on the understanding of the physical mechanisms

involved. In the domain where experimental and theoretical knowledge was still missing, extrapolations or interpolations were adopted by making simple assumptions.

Thermal and mechanical transfers are interconnected in steam-water two-phase flows. However, it was often assumed in a first approximation that mechanical interactions do not strongly depend on thermal exchanges. A step-by-step method was then used. Mechanical terms were first derived from experiments where thermal nonequilibrium is negligible. Interfacial heat transfer terms were then derived. Finally wall to fluid heat fluxes are correlated.

One may distinguish four different approaches used to establish the closure relations:

1. *The fully empirical approach*: representative experiments are carried out in the required range of parameters and a transfer term of the system of equations is measured together with the main variables. A correlation is then established between the transfer term and the main variables of the flow by using some fitting technique or interpolation technique. CATHARE, TRACE, and RELAP use CHF look up tables for the CHF prediction. This method may be the most accurate but it requires a lot of experimental data and it does not allow extrapolations out of the domain covered by data.

2. *Empirical approach with dimensional analysis*: correlations are here expressed with dimensionless numbers. Since many dimensionless numbers exist in two-phase flows, a preliminary analysis may allow to identifying the controlling physical processes and only the dimensionless parameters which are assumed to play a role are used in the correlation. This method was used to establish “full-range drift flux correlations” by EPRI (Chexal and Lellouche, 1986) or the Kataoka and Ishii (1987) drift flux correlation.

3. *The phenomenological or mechanistic approach*: A governing physical mechanism is assumed and an expression of the transfer term is derived theoretically. Expressions of the added mass force, or of the interfacial friction for dispersed droplet flows are examples of this method. The validity is verified a posteriori by comparison with experimental data. The quality depends on the appropriateness of the basic assumptions made on the governing processes. Very few models are of this type. The added mass force was developed from analytical calculations of a potential flow around a sphere in acceleration. The pressure difference term in stratified flow was derived from simple assumption of a transverse gravitational pressure gradient in a horizontal channel (de Crecy, 1986;

Bestion and Serre, 2012).

4. The *semiempirical approach*: Compared to the previous method, weaker assumptions are made, which allow to deriving expressions theoretically with some free parameters to tune with experimental data. The interfacial friction in bubbly-slug and churn flow regimes in pipes and rod bundle developed for the CATHARE code (Bestion, 1990a,b) are of this type. Interfacial heat transfer expressions for direct contact condensation at ECCS are also of this type (Janicot and Bestion, 1993).

First versions of the system codes used mainly the mechanistic approach but, after an extensive validation, the degree of empiricism of closure relations was progressively increased reflecting the lack of knowledge and the complexity and diversity of the physical mechanisms involved in such a large variety of two-phase flows. Therefore, the quality and reliability of the closure laws are mainly the result of an extensive validation database in the most representative experiments. Extrapolation beyond the validated domain remains somewhat hazardous.

Looking at closure laws in current system codes, one can observe the following:

- Codes rarely selected the same correlation for the same transfer. First versions of the codes used many academic mechanistic models which were often modified through empirical corrections after comparison with experimental data of the validation.
- Even when the various codes do not use the same basic correlation, they often converged to the same degree of empiricism in the selected final correlation. The level of empiricism just reflects the degree of understanding of basic processes or the lack of knowledge.
- A high accuracy is not required for all models and more attention was paid to the most sensitive models in accidental transients and an effort was made to improve them using corrections based on experimental validation. The sensitivity of transient scenarios of interest being not equal for all the models, it results that the accuracy and reliability of the models is not equal for all the models. As a consequence, when a new situation is investigated with different sensitivities, it is often necessary to pay more attention to some closure laws which are found not accurate enough.

11.12 Predicting CCFL

The two-fluid model either with a drift flux model or with two-momentum equations is able to predict the CCFL and a flooding limit. It results from the force balance with dominant effects of gravity, acceleration, and interfacial friction forces. However, this does not guaranty that the CCFL will be predicted correctly in a reactor transient since it is likely to occur in complex geometries within the reactor circuits where standard interfacial friction laws are no more valid due to local geometrical effects. For example in a PWR, CCFL is likely to occur at the following locations (see Fig. 11.23):

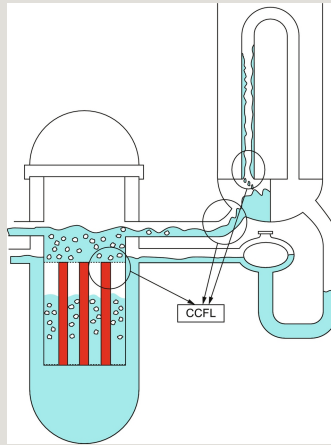


Fig. 11.23 Example of locations where CCFL may occur in accidental transients of a PWR.

- Upper tie plate in a PWR core
- SG tube inlet in a PWR
- HL bend of a PWR

All system codes developed local treatment to obtain a predetermined flooding curve (Wallis type or Kutateladze type). Such flooding correlation can be put on a general form:

$$\frac{d}{dt} \int_{V(t)} f dv = \int_{V(t)} \frac{\partial f}{\partial t} dv + \int_{A(t)} f \vec{v}_A \cdot \vec{n} da$$

When the exponent of the Bond is zero, it is a Wallis type correlation and when it is 1 it is a Kutateladze type correlation.

A drift flux model was made consistent with a flooding correlation in the ATHLET code (Sonnenburg, 1989)

$$\int_{A(t)} \vec{v}_A \cdot \vec{n} \, d\alpha = \frac{dV(t)}{dt}$$

An interfacial friction model was made consistent with a flooding correlation in the CATHARE code (Freitas and Bestion, 1993)



The coarse nodalization and the use of 1-D models makes it impossible for system codes to predict CCFL and flooding limits which depend on small-scale 3-D geometrical effects. CCFL is for interfacial friction what form losses are for wall friction. System codes are not predictive for form losses and for CCFL since the user must know the solution which depends on the actual geometry and representative experiments are necessary to establish the adequate flooding correlations. Data are plotted as in Fig. 11.24 to determine the values of C and M and the flooding correlation is determined. Then it is translated into a drift flux model or an interfacial friction correlation. Using such drift flux or interfacial friction correlations in system codes make them capable to predict the correct flooding limit. Many experimental programs were devoted to the determination of the flooding limits in various reactor components to determine the flooding correlation as illustrated in Fig. 11.24.

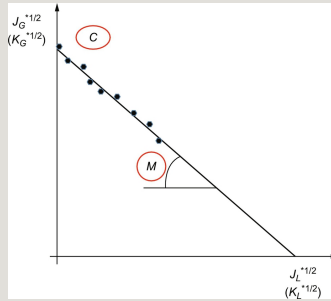


Fig. 11.24 Determination of CCFL and flooding curve from experimental data.

11.13 Upscaling capabilities of system codes

The reactor safety demonstration requires the analysis of complex problems related to accident scenarios. Experiments cannot reproduce at a reasonable cost the physical situation without any simplification or distortion and the numerical tools cannot simulate the problem by solving the exact equations. Only reduced scale experiments are feasible to investigate the phenomena and only approximate system of equations may be solved to predict time and/or space averaged parameters with errors due to imperfections of the closure laws and to numerical errors. Therefore, complex methodologies are necessary to solve a problem including a PIRT analysis, a scaling analysis, the selection of scaled IETs or combined effect tests (CET) and SETs, the selection of a numerical simulation tool, the verification and validation of the tool, the code application to the safety issue of interest, and the use of an uncertainty method to determine the uncertainty of code prediction. This global approach is illustrated in Fig. 11.25.

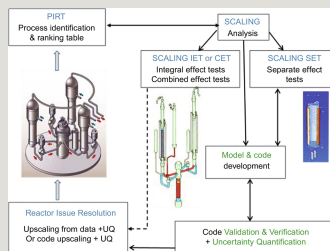


Fig. 11.25 General methodology for solving a complex reactor thermal-hydraulic issue using experiments, codes, and UQ methods.

11.13.1 PIRT

Phenomena identification is the process of analyzing and subdividing a complex SYS-TH scenario into several dominant processes or phenomena. Usually, there is a parameter of interest in the thermal-hydraulic scenario which may be a safety criterion (e.g., a PCT, a reactivity insertion, a thermal or mechanical load, etc.). Ranking means here the process of establishing a hierarchy between identified processes with regards to its influence on the parameter of interest. PIRT is a formal method described by Wilson and Boyack (1998). When PIRT-identified dominant processes of a reactor transient, the code should take care to model these processes with sufficient fidelity.

11.13.2 Scaling

When dominant phenomena are identified and ranked, experiments are designed to simulate at reduced scale and power the reactor transient in IET facilities and in SET facilities. Scaling of an experiment is the process of selecting the nondimensional numbers to be respected for having a good similarity with the reactor behavior at least for the dominant processes. For application in nuclear reactor safety, a first comprehensive scaling methodology named H2TS (“Hierarchical Two-Tiered Scaling”) was developed by a Technical Program Group of the USNRC under the chairman Zuber (1991).

Simulation tools are most often used to extrapolate from experiments to reactor situation—this is the upscaling process—and the degree of confidence on this extrapolation is part of the scaling issue. When dominant phenomena are affecting the whole behavior of the system, a system code is necessary. This is the case of many transients like LOCAs, SLB, LOFW, loss of electrical power, loss of residual heat removal (LORHR), etc. When local complex 3-D phenomena are playing a dominant role, CFD codes may be required or even a coupling of system and CFD codes.

11.13.3 Distortion in IET

Although IETs are designed to represent correctly dominant phenomena, distortions exist of phenomena which may play a nonnegligible role in the transient of interest. Let us consider an example. A classical scaling of IET used the K_V -scaling or power-to-volume scaling where the same reduction factor λ is applied to power, volume, and flow rate. If vertical scale is preserved, channels are thin and tall. This is not a problem in core and SGs since one may just reduce the number of

rods (resp. tubes) and respect the hydraulic diameter, this preserves all nondimensional numbers that are important for friction losses, heat transfers, flow regime, and interfacial transfers. Namely,

$$\int_{V(t)} \nabla \cdot \vec{a} \, dv = \int_{A(t)} \vec{a} \cdot \vec{n} \, da$$

Horizontal legs of a PWR should respect a Froude similarity in order to respect the stratification criterion. This induces some distortions of Reynolds and Kutateladze numbers:

$$\int_{V(t)} \nabla \cdot \vec{B} \, dv = \int_{A(t)} \vec{B} \cdot \vec{n} \, da$$

One may expect that droplet entrainment occurrence will not be respected which plays a significant role in a LBLOCA reflooding. Also the aspect ratio or shape of the bend and inlet header of SG is not respected and one may expect distortions in the CCFL in such components and this may induce a wrong liquid mass repartition in some small-break or intermediate-break LOCAs.

This CCFL distortion problem can be solved by using system codes provided that they are able to predict with the same reliability the CCFL in reactor geometry and in IET geometry. Fig. 11.26 shows a set of experiments which were used for CATHARE code validation. It includes CCFL tests in the same geometry as the BETHSY IET but also reduced scale and scale 1 data in reactor geometry. This is a typical case where the system code can solve the distortion in an IET by validation on SETs.

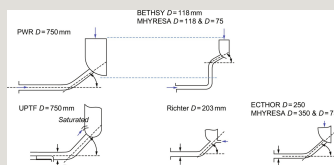


Fig. 11.26 SETs used in the CATHARE code validation to solve the BETHSY

11.13.4 Code upscaling capability

Distortion may be encountered in thermal-hydraulic codes due to some simplifying assumptions which are not satisfied in all conditions of interest. The two-fluid model is used in most system codes and it has extended capabilities to model correctly. However, some situations have countercurrent of droplets and liquid films which may not be predicted with only one liquid velocity. Many other limitations of the current models were mentioned here above and they may induce various small distortions to a simulated transient. In reactor safety analysis, these distortions should be taken into account at least in the UQ. Measuring the accuracy of code predictions in many SETs is a good way of identifying the impact of all these small distortions.

Codes which are validated on some scaled SETs and IETs may have the capability to predict the phenomena of interest at reactor scale provided that some conditions are satisfied. This is called the upscaling or scaling-up capabilities. Among the main conditions to satisfy one may find:

- The code has modeled the dominant phenomena of a transients of interest.
- The model has been validated on scaled IETs which represent the dominant phenomena, and the code predicts well qualitatively and quantitatively the main phenomena.
- In the favorable case where several scaled IETs at different scales have simulated the transients of interest, the code must predicts the scale effect or the absence of scale effect.
- The code has proved that closure laws have a good upscaling capability by validation of all important phenomena at local or component scale against several SETs at different scales.
- The code closure laws validation domain covers the entire prototypical thermal hydraulic range of interest. This includes the pressure and temperature domain, the flow quality, and the flow geometry. When the reactor domain is not fully covered, physical arguments should be given to justify that the code extrapolation to reactor domain of parameters is reliable. For example, when scale 1 data are not available,

validation should at least cover several scales.

- Since scaled IETs have necessarily some scale distortions, the code should be able to predict correctly the distorted and nondistorted phenomena. This may require a validation of the distorted (in IETs) phenomena in nondistorted SETs.
- The uncertainty of code prediction should take into account the uncertainty due to IC and BC, material properties, physical models, numerical errors, and should also estimate the uncertainty due to nonmodeled phenomena or code distortions due to limitations of the physical model.

11.14 Predictive capabilities of SYS-TH codes

11.14.1 Status of current system codes

The current generation of best-estimate system codes fully met the difficult challenge of replacing the previous conservative evaluation models to provide more accurate and reliable safety analyses of most accidental transients of interest for LWRs.

A huge effort was spent to provide sufficient experimental data to develop and validate the 150-to-200 closure laws of the system of equations. This experimental program considerably improved the knowledge of the two-phase flow phenomenology at system, component and local levels. The SETs covered all local and component physical situations. The various IET facilities were necessary to validate the global consistency of the models and to identify remaining weaknesses. For example, phenomena such as phase separation in separating Tee junction, or geometry-dependent CCFL required additional SET investigations to better simulate IET tests.

Today the industrial versions of first system codes which have been developed since the late 1970s such as RELAP5, CATHARE, TRAC then TRACE, ATHLET and a few other more recent codes are fully mature and are able to predict qualitatively and quantitatively well all dominant processes of all accidental transients of interest. Best-estimate plus uncertainty methodologies can be used for licensing provided that the code version is qualified, fully verified, and validated and that uncertainty evaluation method is applied.

Uncertainties methods demonstrated also a good maturity in the BEMUSE international benchmark (De Crécy et al., 2007). Fig. 11.27 shows the PCT in the LOFT L2.5 LBLOCA test. Data are compared to CATHARE prediction with the base case calculation, an upper bound and a lower bound calculation. This was obtained with an uncertainty propagation method using 100 calculations with all input uncertain parameters (IC, BC, material properties, and closure laws) being randomly sampled. The Wilks theorem was used to determine the 95th percentile PCT with 95% level confidence. Today CPU time is no more an issue for system codes and 1000 calculations were performed of the first peak giving the pdf of the PCT shown in Fig. 11.28.

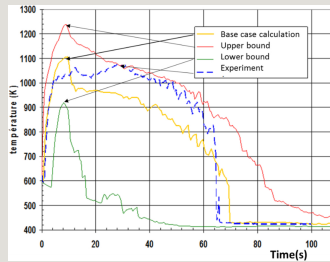


Fig. 11.27 Peak clad temperature in the LOFT L2.5 LBLOCA test. Data are compared to CATHARE prediction with the base case calculation, an upper bound and a lower bound calculation obtained by uncertainty propagation (BEMUSE exercise).

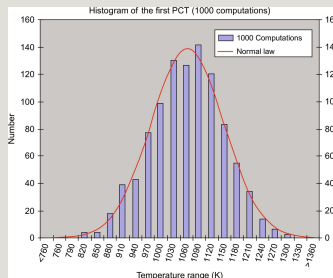


Fig. 11.28 Probability density function of the peak clad temperature in the LOFT L2.5 LBLOCA test obtained by 1000 uncertainty propagation CATHARE calculations (BEMUSE exercise).

This example is characteristic of the common uncertainty band of system codes for the PCT in LOCAs which is often of the order of ± 150 or even ± 200 K. This limited accuracy is due to significant uncertainty of boundary and initial conditions and of material properties (such as UO_2 conductivity) and also for an important part to the limitations of the physical modeling.

The main sources of the physical modeling uncertainty are due to four main reasons:

1. The extreme complexity of two-phase flow with so many flow regimes and heat transfer regimes, with a very large diversity of interface geometry, with many possible bifurcations (CHF, quenching, flow regime transitions, etc.). In regard to this measurement techniques are limited to characterize all these processes and

experimental uncertainty may be rather large.

2. The extreme complexity and diversity of flow geometries in the various components of LWRs. The physics being highly nonlinear, small geometrical details may have a very significant effect on macroscopic processes (CHF dependent on spacer grid design details, CCFL dependent on small-scale details of the geometry).

3. The two-fluid six-equation model used in 0-D, 1-D, and 3-D modules has inherent limitations. Some phenomena cannot be described (effects of flow nonestablishment, history effects on the flow regime, countercurrent flow of liquid films and droplets, combined effects of coalescence break up nucleation, and collapse on interfacial area) which are partly responsible for the final uncertainty of the physical model. Further progress would require additional equations, such as a multifield modeling and transport equations for interfacial area or for turbulent scales.

4. The macroscopic description of flows in system codes may not describe all small-scale geometrical effects in a general way with a high accuracy.

Other limitations are listed below.

- The accuracy of the various models is not uniform since more attention was paid to the most sensitive models in accidental transients. Looking at heat transfers from fuel rods to the fluid in a core, some heat transfer regimes such as liquid forced convection or nucleate boiling have good heat transfer coefficients and can easily remove and transfer the rod power. Then no specific effort to accurately model these transfers with all possible effects were made.
- A rather high degree of empiricism was necessary for some models reflecting a lack of understanding of all governing physical processes.

These two reasons make system code application to new transient situations or new geometry somewhat hazardous. New experimental programs with industrial configuration are still required for any new reactor design.

11.14.2 Capabilities of system codes seen from the validation

An optimistic view of the code capabilities results from the assessment calculations including both SETs and IETs. SETs have well-specified BCs and many measured flow parameters provided enough data for a good validation of closure laws. Then, IETs are necessary to check the general consistency of all

models, to verify that all important phenomena are modeled, to validate the nodalization in conditions close to reactor application.

SETs are generally well calculated since they were extensively used for the development or the improvement of the closure relations. SET with well-specified BCs are the only way to determine the validity and accuracy of each closure relation.

Many IETs are also well calculated. One can consider three main cases:

- All the important phenomena are well predicted with a good timing and a good accuracy.
- The most important phenomena are predicted. The timing and the accuracy are not perfect but it does not prevent from clear conclusions on safety issues.
- Some important phenomena are not predicted or are predicted with a very bad accuracy.

The first type of calculation is still exceptional but the second type became more and more frequent and the third type was progressively eliminated.

Calculations of many integral tests with system codes allowed to point out and to solve some problems:

- Problems in modeling a component: Problem may come from an inadequate choice of module to model a component. All codes have several types of modules with specific capabilities. The user must select a module depending on the transient to calculate. For example, a common modeling of a pressurizer with the CATHARE code uses a simple two-node volume module which is sufficient for all LOCA transients where the pressurizer is rapidly empty. For transients such as a LOFW with PORV opening or a multiple SGTR with pressurizer regulations, a more sophisticated modeling is available and must be selected. Such errors were minimized after having developed precise User Guidelines.
- Physical process not predicted by the code: physical mechanisms can be encountered which cannot be quantitatively predicted by system codes. For example, when CCFL occurs in a zone with a complex geometry the corresponding flooding correlation must be established first from experimental tests having the exact geometry before it is implemented in the code. A specific CCFL model is implemented in system codes where the equations are forced to

find a prescribed flooding limit correlation given by the user on option for a particular node. This requires that the possible occurrence of CCFL was suspected in a particular region of a circuit and that representative experiments were performed to measure the flooding curve. When CCFL is not suspected or when no data exist, prediction errors are possible. Experimental data now exist for most important reactor components where CCFL is expected to occur and User Guidelines may recommend adequate flooding correlations.

- Transients highly sensitive to a certain physical process: The loop seal clearing in some PWR CL small-break transients is an example of possibly sensitive process. The formation of a liquid slug in the IL of a PWR is a common feature of many SBLOCA transients. This occurs in particular after the rupture of the natural circulation when the reflux condenser mode starts. The primary circuit steam is divided into two parts separated by two liquid slugs in loop seals and in the vessel bottom. These two subsystems are practically uncoupled from the energetic point of view. They follow a thermal equilibrium defined by a saturation temperature resulting from local energy exchanges. In the hot subsystem—core, HLs, SG tubes—the temperature level is generally stabilized just above the secondary pressure. In the cold subsystem the energy balance generally depends on the presence of a CL break and of SIs, both of them giving a trend to a temperature and pressure decrease. Such a depression of the cold part moves water from core to downcomer and induces a core uncover with a clad temperature excursion. This dangerous situation stops when the liquid level in the descending part of the IL reaches the horizontal part. The loop seal clearing occurs either simultaneously or at different times in the different loops. After loop seal clearing the pressure in hot and CLs are nearly equal again. When the process is slow it is very sensitive to small asymmetries between the loops. Once it happens in one loop a stable state may be reached preventing from its occurrence in the other loops. Codes have many difficulties to predict these nonsymmetrical behavior correctly. It is a typical problem of predictability with small causes having big effects. Such situations were identified by the extensive application of system codes to integral tests. It should be accounted for in an UQ methodology.

11.14.3 Was the two-fluid model the right choice?

The present generation of system codes is based on the two-fluid model. This choice was made after having identified unacceptable drawbacks of previous models. In the domain of simulation of system codes for reactor accidental transients, all kinds of thermal and mechanical nonequilibrium may exist.

Subcooled liquid with direct contact condensation after ECCS injection have to be

modeled. Superheated vapor has to be modeled mainly when post-CHF heat transfer occurs in the core. Meta-stable superheated liquid and subcooled vapor exist in flashing flows with a small relaxation time constant (of the order of 10^{-3} s). Only models with two mass balance equations plus two energy balance equations can model all these situations.

Mechanical nonequilibrium is also encountered in most situations with possible weak coupling between phases. Using only one momentum equation with a drift flux models is sufficient for many situations, particularly when the coupling between phases is rather strong. Two-momentum equations are necessary in other cases particularly when inertial forces play a role in the slip ratio. Droplets created in a core during a reflooding are entrained by steam but do not reach the equilibrium slip velocity before leaving the core due to high inertia. Better capabilities—than with the drift flux model—are also found for stratified flows by writing two-momentum equations, which allow to represent wave propagation phenomena, fluvial and torrential regimes and.

The choice of the two-fluid model promoted a very extensive experimental program required for validating all closure relations. Due to this effort, the choice of the two-fluid model was a success.

Multifield models are expected to have better capabilities for annular-dispersed flows or stratified-dispersed flow. The main reason of not having chosen a three-field model in the 1970s and 1980s was probably the high CPU cost at that time. Today a three-field model does not penalize the CPU time too much so that most recent system codes such as SPACE developed by KAERI in Korea (No et al., 2013) or COSINE developed by SNPSDC in China (Liu et al., 2013) are based on three-field models.

11.14.4 The evolution of 3-D modeling in system codes

System codes like RELAP and ATHLET codes first developed “cross-flow junctions” between 1-D modules to represent some multidimensional flow features. 1-D equations are written in the main direction of the flow and simplified momentum equations are used in the transverse direction to allow mass exchanges between several parallel channels. This simplified approach of 3-D flows may be sufficient in some cases particularly for porous body like a reactor core when only small crossflows exist due to high resistance to transverse velocity.

Explicit 3-D modules exist as an option in the codes TRACE, RELAP5, CATHARE, and SPACE for the reactor pressure vessel. They represent a

straightforward extension of the 1-D modules for cylindrical or Cartesian coordinates. The main objective of such 3-D modules is the modeling of large-scale 3-D effects in a pressure vessel during LBLOCA such as downcomer penetration of ECCS water and reflooding of the core with transverse power profile effects.

Due to the heavy computational effort needed, the 3-D modules are being used mainly for fast (short) transients like LBLOCA but with the increasing computer power CATHARE 3-D Module is now also used for SBLOCA and many other transients. In most applications, rather coarse nodalization schemes (about 1000 nodes for a CATHARE Pressure Vessel 3-D nodalization) are applied and consequently the advantage of a 3-D modeling of the flow processes might be offset to a certain extent. However, large-scale 3-D effects can be better modeled than with 1-D models.

Using such coarse nodalization is far from being converged in space. Then these 3-D modules must validate together the physical model, the numerical scheme, and the reference vessel nodalization using scale 1 experiments such as UPTF tests. This does not prevent from compensating errors but such 3-D modules are a progress compared to parallel channel representation with cross-junction connections.

The computer power continuous increase now allows much finer nodalizations with a core nodalization which may be one mesh/assembly and 40 axial meshes, that is, 6000–10,000 meshes for the core. Forty axial meshes were found to provide a reasonably good convergence of PCT (a few degrees) during LOCA simulations whereas ten axial meshes could result in numerical errors of about 30 K. One considers that the industrial use of a system code allows transient simulations within hours (say <12 h) of common engineer computers so that many sensitivity tests can be performed or uncertainty propagation using a Monte-Carlo type method (a 100 runs are usually performed) can be performed.

Previous validation was limited to some UPTF tests for LBLOCA refill and PERICLES, SCTF, or CCTF tests for reflooding. They provided sufficient validation for LBLOCA. If the use of 3-D modeling is extended in such a way to cover many transients a better modeling and a SET validation is required (Bestion, 2014). The wall friction and interfacial friction terms have to be modeled in a core with a more general formulation of friction tensors taking into account the nonisotropy of the geometry. Radial transfers (Chandesris et al., 2013) in a quasi-vertical flow have to be better modeled and validated. Radial transfers of phase momentum may be due to:

- Transport by mean transverse velocity when there are crossflows
- Radial diffusion (molecular+turbulent) of momentum
- Radial dispersion of momentum by subscale transverse velocity
- Interfacial transfers between phases due to radial void dispersion force

The radial transfers of phase enthalpy may be due to:

- Transport terms by mean transverse velocity if there are crossflows
- Radial diffusion (molecular+turbulent) of energy
- Radial dispersion of energy by subscale transverse velocity

11.15 Drift flux, two-fluid, and TIA in system codes

11.15.1 The point of view of time scale analysis

The time scale analysis of physical processes is a useful tool to justify or not some simplifying assumptions made in the modeling of the complex two-phase flow phenomena.

When several processes are coupled in a sequential way, the processes with the largest time scales play the major role and require a good modeling, whereas the processes with the smallest time scales may be simplified. Let us take an example.

The slip between phases in bubbly-slug-churn flows depends first on the bubble size which is controlled by coalescence, break up nucleation, collapse. A relaxation

time scale $\frac{\partial \rho}{\partial t} + \nabla \cdot (\rho \vec{v}) = 0$ to reach an equilibrium bubble size (or bubble size distribution) or more generally an equilibrium interfacial area density exists which is not necessarily well known.

For a given bubble size, an equilibrium slip is obtained with a relaxation time scale

$\frac{\partial \vec{v}}{\partial t} + \vec{v} \cdot \nabla \vec{v} = 0$. This is the same as the particle interaction time τ_i in dispersed flow which is the time scale for a particle submitted to steady gravity and pressure forces to reach an equilibrium velocity difference with the continuous phase

$$Fr = \frac{v}{\sqrt{gD}}$$

These two time scales may be compared to a transit time scale in a reactor component of length L . Comparing these time scales one may identify various situations:

$$v^2 = \vec{v} \cdot \vec{v}$$

• If $\theta(x, \tau) = \frac{T(x, \tau) - T_s}{T_0 - T_s} = 1 - \operatorname{erf}\left(\frac{x}{2\sqrt{a\tau}}\right)$, or if $\mathcal{T} \triangleq T + pI$ it may be better to write a transport of interfacial area (TIA) equation to model the relaxation process which controls the evolution of the size distribution.

• If $q(0, \tau) = \frac{\lambda(T_0 - T_s)}{\sqrt{\pi a \tau}}$, and $q(x, \tau) = \frac{2\lambda(T_0 - T_s)}{\sqrt{\pi}} \exp\left(-\frac{x^2}{4a\tau}\right)$, one may use an equilibrium algebraic expression of the interfacial area A_i . This approximation is used in current two-fluid models either with two-momentum equations or with a drift flux

where it is assumed that $\frac{\partial p}{\partial t} + \nabla \cdot (\rho \vec{v}) = 0$ is zero.

• If $\frac{\partial}{\partial t} \left[\left(\frac{\rho^2}{2} \right) + \rho \nabla \cdot \left(\frac{\rho^2}{2} \right) \right] - \rho \vec{v} \cdot \nabla \cdot \left(\frac{\rho^2}{2} \right) + \rho \vec{v} \cdot \nabla \cdot \left(\frac{\rho^2}{2} \right) = 0$ the use of two separate momentum equations is better than the drift flux algebraic relation to model this relaxation process which controls the slip between phases.

• If $h = u + \frac{p}{\rho}$ then one may use an equilibrium algebraic expression of the slip between phases such as the drift flux model. $\frac{\partial p}{\partial t} + \nabla \cdot (\rho \vec{v}) - \rho \vec{v} \cdot \nabla \cdot \vec{v} = 0$ is assumed equal to zero.

The experience gathered so far allows a picture of those time scales depending on the flow regime:



Only the bubbly-slug-churn flows could be well modeled by the drift flux approach.

Droplet flows (such as in a reflooding process) and separate-phase flow (annular and stratified flows) have a rather long time scale $\frac{\partial \bar{\rho}}{\partial t} + \nabla \cdot (\bar{\rho} \bar{\mathbf{v}}) = 0$ before reaching an equilibrium slip and the use of two-momentum equations in the six-equation models provided a clear added value compared to previous drift flux models.

The relaxation time scale $\frac{\partial \bar{\rho}}{\partial t} + \nabla \cdot (\bar{\rho} \bar{\mathbf{v}}) = 0$ to reach an equilibrium interfacial area density may be rather long in dispersed flow such bubble-slug-churn and droplet flows. In such cases, the use of TIA may bring an added value. However, this would require an extensive experimental program to measure $\frac{\partial \bar{\rho}}{\partial t} + \nabla \cdot (\bar{\rho} \bar{\mathbf{v}}) = 0$ in all the geometries and all the flow regime of interest, which is not yet available.

11.15.2 Comparing drift flux with two-momentum equations

The prediction of interfacial transfers of mass, momentum, and heat depends a lot on our capacity to predict the nature of interfaces—which depend on the flow regime—and of the velocity difference between phases. The dispersed flows, bubbly flow or droplet flows, may have various bubble and drop sizes and predicting the slip between phases and thermal nonequilibrium depends a lot on the capacity to predict these sizes.

A drag force on a single bubble may be easily modeled if we know the size δ of the bubble through correlations of this type:



where D is the drag force, Re_b is the bubble Reynolds number, C_d is the drag coefficient, ρ_l is the liquid density, v_b is the bubble velocity, and v_l is the liquid velocity. Similar drag force models are available for droplets.

If there is two-phase flow with a population of n bubbles per unit volume having the same size—called a monodispersed flow—one may easily express the resulting interfacial friction per unit volume τ in 1-D two-fluid set of equations:

$$\frac{\lambda_{eff}}{\lambda} = \frac{2(1 - \varphi) + (\lambda_0/\lambda)(1 + 2\varphi)}{(2 + \varphi) + (\lambda_0/\lambda)(1 - \varphi)}.$$

One can obtain a “cross-momentum equation” by eliminating the pressure gradient term between the two-phase momentum equations:

$$\frac{\lambda_{\text{eff}}}{\lambda} = \frac{1}{1 - (6\varphi/\pi)^{1/3} \cdot F_i(\gamma)},$$

$$\frac{\partial \rho}{\partial t} + \nabla \cdot (\rho \vec{v}) = 0$$

Let us consider a quasi-steady flow and quasi-established flow

$$\frac{\partial \rho \vec{v}}{\partial t} + \nabla \cdot (\rho \vec{v} \vec{v}) + \nabla p - \rho \vec{F} - \mu \left(\frac{1}{3} \nabla \nabla \cdot \vec{v} + \nabla^2 \vec{v} \right) = 0$$

without strong geometrical complexity

$$\frac{\partial}{\partial t} \left[\rho \left(h + \frac{v^2}{2} \right) - p \right] + \nabla \cdot \left[\rho \vec{v} \left(h + \frac{v^2}{2} \right) \right] - \rho \vec{F} \cdot \vec{v} - \nabla \cdot (T \cdot \vec{v}) - \nabla \cdot \lambda \nabla T = q_{\text{ext}}$$

and without big interfacial mass transfer ($\Gamma_{iv} V_i$ term is negligible) this cross-momentum equation is simplified:

$$\mathcal{T} = -\frac{2}{3} \mu \nabla \cdot \nabla T + \mu (\nabla^2 \vec{v} + \nabla \nabla \cdot \vec{v})$$

In such conditions, the force balance between phases is reduced to an equilibrium between drag force, the buoyancy (gravity force-Archimedes force), and wall friction forces. Considering a dispersed gas phase and a continuous liquid as encountered in bubbly, slug and churn flow, in a vertical channel at moderate velocity, wall friction terms may be significantly smaller than interfacial friction due to a much higher interfacial area than wall friction area. Then a rough approximation in vertical upward oriented flow leads to:

$$\rho = \rho(p, h); T = T(p, h); \mu = \mu(p, h); \lambda = \lambda(p, h)$$

This simple balance between buoyancy and drag forces has a clear similarity with the drift flux models where the drift velocity models are of the following form:

$$\frac{\partial \rho Y_k}{\partial t} + \nabla \cdot \left(\rho Y_k \vec{v} \right) = \nabla \cdot \left(\vec{m}_{Y_k} \right) + S_{Y_k}$$

where δ is a length scale characteristic of the bubble size. This expression can be obtained from a balance between buoyancy B and drag force D applied to a bubble of size:

$$\vec{m}_{Y_k} = D_{Y_k} \nabla Y_k$$

If the drag coefficient is assumed constant and if δ is proportional to the Laplace scale, one obtains the form of Zuber and Findlay (1965) model for churn-turbulent bubbly flow:

$$\frac{\partial \rho Y_k}{\partial t} + \frac{\partial \rho v_j Y_k}{\partial x_j} = \frac{\partial}{\partial x_j} \left(D_{Y_k} \frac{\partial Y_k}{\partial x_j} \right) + S_{Y_k}$$

If the drag coefficient is assumed constant and if δ is bounded by the duct diameter, one obtains the form of Zuber and Findlay model for slug flow:

$$\sum_{k=1,n} Y_k = 1$$

From the drift flux equation, V_{gj} general expression and simplified cross-momentum equation, one can obtain an expression of the interfacial friction which

is consistent with a drift flux model:

$$Y_{k=2,n}$$

$$Y_{k=2,n}$$

This simply shows that a drift flux approach can be equivalent to a full two-fluid six-equation model when the approximations made in the simplified cross-momentum equation are valid. When some simplifications are not justified a full two-fluid six-equation model may have better capabilities.

In situations where inertial forces are not negligible compared to buoyancy, drag, and friction forces, the drift flux may be significantly worse than the full six-equation model. For example:

- Droplet flow: a water droplet created at a quench front during a core reflooding process is entrained by steam but it does not reach an equilibrium slip within the core (see Fig. 11.29).

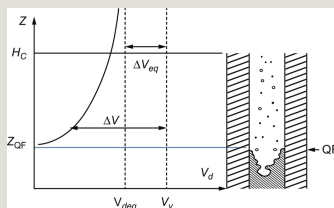


Fig. 11.29 Qualitative and simplified droplet velocity evolution within a core during a reflooding process. At quench front (QF), the initial drop velocity may be close to zero. Then V_d increases as droplet is entrained by vapor at

$$\alpha = \frac{A_g}{A_g + A_l}$$

velocity V_v . The equilibrium velocity difference ΔV_{eq} is not reached at the elevation H_c at top of the core.

- Stratified flow: in a stratified flow, due to a weak coupling between phases, many situations cannot be predicted precisely by an algebraic slip since the



term is not negligible and also some acceleration terms may play a significant role in the phase slip.

$$\bar{f} = \frac{1}{T} \int_T f dt$$

- Transient flow: when is no more valid in cross-momentum equation, the algebraic slip relation is not valid.

$$f \triangleq \bar{f} + f'$$

- Nonestablished flow: when is no more valid in cross-momentum equation, the algebraic slip relation is not valid.
- High condensation and flashing flows: such flows are usually accelerating flows and the term $\Gamma_{iv} V_i$ is no more negligible.

11.15.3 Polydispersion effects

Dispersed flows, bubbly flow or droplet flows, usually have a population of bubbles or droplets covering a rather large range of sizes. There may be a maximum size beyond which an instability will break the bubble or droplet. Below the maximum size, the size distribution may depend on many processes including nucleation, vaporization, condensation, coalescence, entrainment from films or droplet creation by film sputtering in a reflooding process and deposition.

A size repartition may be defined by a probability density function $f(\delta)$ such that:



When $f(\delta)$ is known one can express the liquid-to-interface heat transfers as:

$$\overline{f'} = 0$$

which is expected to be more precise than the monodispersed expression calculated for a Sauter mean diameter d_{32} :

$$\overline{cf} = c\overline{f} \text{ if } c = cte$$

Similarly

$$\overline{f} = \overline{f}$$

is expected to be more precise than the monodispersed expression:

$$\overline{f\overline{g}} = \overline{f} \overline{g}$$

However, taking the polydispersion into account induces a huge modeling effort and many experimental data which are not available. A monodispersion approximation able to predict an average or an equivalent bubble size or droplet size may be a more reasonable compromise. One may notice that the equivalent size for heat transfers may be different from the equivalent size for interfacial friction. The prediction of a slip between phase depends mainly on the larger drops or bubbles while the total interfacial heat and mass transfers are dominated by the smallest drops or bubbles.

11.15.4 Perspective for using TIA in future system codes

A dynamic modeling of interfacial area (IA) in system codes may be a way to go beyond limitations of current codes by taking into account time scales associated with coalescence, break up phenomena, and flow regime transitions. The

experience gained in developing a dynamic modeling of IA was summarized by Bestion and Serre (2013):

- The analysis of some flow regimes with new measurement giving access to IA and bubble size distribution has confirmed that almost all flows have nonestablished bubble size repartition. In such condition an algebraic IA modeling has limitations, a TIA equation may bring some added value, and a polydispersion modeling would be necessary to get a very significant progress.
- The IA data and TIA models available cannot yet improve system codes since the validation covers only a very small fraction of the flow situations of interest.
- A mechanistic modeling of polydispersion still requires a very long effort and requires that many new data are produced. This may be envisaged only in a long-term perspective.
- The modeling of some important flow regime transitions such as onset of droplet entrainment or bubbly-to-stratified flow would require first a multifield modeling to separate the dispersed field (bubbles or drops) from continuous liquid or gas before benefiting from the use of TIA for the dispersed field.

However, in a medium term perspective TIA may be used in a more heuristic way to improve system code predictions provided that:

- The modeling is simplified to use also SET data without IA measurement. This does not allow complex modeling with many additional transport equations and many closure laws.
- One must accept some empiricism in TIA equation closure laws.
- A step-by-step strategy may be used for TIA implementation in system codes where TIA may be used in one component whereas algebraic IA models are still used in other components.
- Investigations are focused on some important flow conditions such as core flow.

The void fraction range $[0; 0.8]$ in core rod bundle geometry (probably in some kind of bubbly-slug-churn flow) might benefit from TIA by taking into account the effect of boiling on the bubble size distribution. It is observed that the slip ratio is smaller when there is depressurization than at constant pressure due to many small bubbles being created by flashing. Such effect cannot be modeled with algebraic IA and could be modeled by a simple TIA equation. In this case, the unknown would

be empirically fitted on rod bundle data with various heat fluxes and with both constant pressure and during slow blowdown.

In order to support this modeling effort, new experiments in core geometry would be necessary starting with a characterization of a flow regime map for rod bundle. Very few data were reported and only in adiabatic low pressure low temperature air-water conditions. All effects of pressure, temperature, and boiling or flashing must be investigated before having reliable information in reactor conditions.

Multifield models have to be developed in parallel to be able to improve modeling of annular-mist flow, stratified-mist flow, bubbly-to-stratified flow regime transition, and stratified to stratified-mist flow transition. In all these flow conditions, one phase is split into a continuous field and a dispersed field and TIA could be used for the dispersed field provided that both fields are treated separately.

11.16 Three-field models in system codes

11.16.1 The situations of interest for three-field models

The annular-mist flow is clearly better described by a three-field model with separate balance equations for droplets and continuous liquid. This approach has been developed for a long time in the context of dry-out investigations for BWRs. The COBRA-TF (Thurgood et al., 1981; Glück, 2008a, 2008b) component code has been developed with a three-field model for a long time. The NASCA component code (Ninokata et al., 2000) also uses a three-field model. COBRA-TF was used in combination with system codes in COBRA-TRAC or in the MARS system code (Jeong et al., 1999). Fig. 11.30 shows a typical evolution of flow regimes in a boiling channel. The domain of annular-mist flow is characterized by the splitting of the liquid phase into two separate fields:

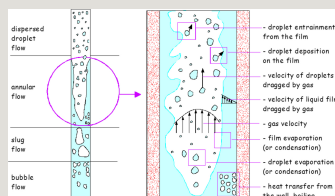


Fig. 11.30 Flow regime evolution in boiling channel with a zoom on the phenomena in the annular-mist flow.

- the films along the walls with low velocities due to friction along walls;
- the droplets in the steam core with much higher velocities.

Characteristic transit times of the two liquid fields may be different by one or two orders of magnitude. A countercurrent flow of films and droplets may also happen in some transient cases. Droplets are entrained from the crest of waves at the surface of liquid films. Droplets are then entrained in the steam flow, and may be radially dispersed by steam turbulent eddies. Some droplets may later be deposited on films by turbulent eddies. The rate of entrainment E (ratio of droplet mass flow rate to total liquid mass flow rate) is the result of the combined effects of deposition and entrainment. In boiling flow, the dry-out occurs when the deposition does not compensate the film vaporization and droplet entrainment. In two-fluid models with a single-liquid field models are necessary for predicting:

- The rate of entrainment E : E models need to assume some kind of equilibrium between entrainment and deposition to be able to express E as a function of only local values of V_v , V_l , and a although almost all situations of interest in boiling flow are nonequilibrium situations with a region where entrainment is larger than deposition followed by a region with more deposition than entrainment when the film thickness decreases. This is the main drawback of the one-liquid field modeling of annular-mist flows. Also countercurrent flow of films and droplets is not predicted by existing correlations.
- Interfacial friction: models must be able to predict an average liquid velocity of film and droplets and a total liquid fraction for film and droplets. Although good mechanistic models exist for drag force applied to droplets and for interfacial friction on film interface, it is very difficult to find the right combination of both models to express the interfacial friction since the velocity of each liquid field is not known.

The three-field model has much better capabilities in such annular-mist flow provided that good entrainment and deposition models are available. Dry-out investigation benefited a lot from such three-field models (see Frepoli et al., 2003; Jayanti and Valette, 2005).

In CATHARE-3, a three-field model has been developed in order to improve the simulation of the reflooding phase of an LB LOCA (see Fig. 11.31) at different locations such as the core, the vessel UP, and the HLs. This requires additional experimental data for validation with information on droplet entrainment and deposition in such components. The interest for PWR was shown when revisiting

LBLOCA with a three-field model (Valette et al., 2011). Oscillatory reflooding is observed at the beginning of the process of a gravity driven reflooding. When water from the accumulators first enters the core, a large quantity of vapor is generated due to the heat transfer from the hot rod cladding. This initiates flow oscillations between the downcomer and the core. At each oscillation, some water may be lost at the break on one side and some water is entrained out of the core to the UP on the other side. The amount of coolant lost at the break depends on the oscillation amplitude and affects the core reflooding efficiency, by reducing the water head in the downcomer. On the other hand, droplets entrained out of the core are vaporized when meeting hot walls in the UP, in HLs or in the SG tubes. This is unfavorable for the reflooding because this liquid cools UP or SG instead of the core on one hand and it increases steam binding on the other hand. The BETHSY 6.7C test belongs to the standard list of assessment tests for CATHARE-2. The use of CATHARE-3 aims to improve the simulation of at least the following points. At the top of the core, during reflooding, liquid drops are carried up by the vapor while a liquid film may flow down along rods, contributing to the top-down quenching of the upper part of the core. The use of only one velocity for the droplets and the film does not allow an accurate simulation of this process.

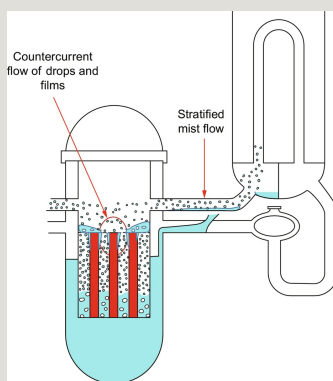


Fig. 11.31 Sketch of a reflooding phase of a PWR LBLOCA. Separate drops and continuous liquid field coexist at top of the core, in upper plenum in hot legs and in SG headers.

Furthermore, separate calculation of droplets and continuous liquid enables to improve the simulation of deentrainment and reentrainment of droplets through the UP, the HLs and the SGs, which contribute to the steam binding. When these droplets vaporize out of the core they increase the steam flow rate and the associated pressure loss by acceleration and friction mainly in SG tubes and in the

main coolant pumps, reducing the velocity of the reflooding process. The transit time for droplets from the top of the core to the SG tubes where they vaporize may also have an effect on the damping or excitation of oscillations during reflooding. If this vaporization occurs during flow reversal in the core it may amplify the oscillation, and if it is out of phase it may damp the oscillation. It is clear that a simple two-fluid model cannot predict correctly this transit time since the only liquid velocity is an average between the very small continuous liquid velocity and the rather high droplet velocity. This may be a reason of the rather poor prediction of oscillations in gravity reflooding tests.

Better predictions are also expected by using three-field models instead of two-fluid models in other transients with droplets such as low pressure transient such a LORHR.

Although three-field models are available in CATHARE-3 and SPACE system codes, it is too early to draw conclusions on the benefit compared to two-fluid model since there is a limited experience gathered so far and additional validation on HLs is still required.

However, it is expected that three-field models will become soon a new standard for system codes. Since it modifies only a small part of the flow regime map, it requires a moderate additional modeling validation effort.

References

Aktas, B., 2003. Level tracking in thermal-hydraulic simulations of nuclear reactors. Ph.D. Thesis, The Pennsylvania State University, State College, PA, USA.

Antoni O., Farvacque M., Geffraye G., Kadri D., Lavalie G., Ramon B. *CATHARE 2 V2.5.2: a single version for various applications*. In: NURETH 13, Kanazawa, Japan; 2009.

Avramova M. *CTF Input Manual*. State College, PA, USA: The Pennsylvania State University; 2006.

Avramova M. *CTF Theory Manual*. State College, PA, USA: The Pennsylvania State University; 2007.

Bartosiewicz Y., Seynhaeve J.M. *Delayed equilibrium model (DEM) of flashing choked flows relevant to LOCA and*

implementation in system codes. In: Conference ICONE 22 Praha, Czech Republic, Paper 30957; 2014.

Belliard M., Grandotto M. *Computation of two-phase flow in steam generator using domain decomposition and local zoom methods*. In: ICONE 8, Baltimore, MD, USA; 2000.

Berne, P., 1983. Contribution à la modélisation du taux de production de vapeur par auto-vaporisation dans les écoulements diphasiques en conduites. Thèse de Doctorat, Ecole des Arts et Manufactures, Paris, France.

Bestion D. Fluid dynamic effects in the fuel element top nozzle area and two-phase flow in piping junctions. In: Krishner W., ed. *Proceedings of the Seminar on the Commission Contribution to Reactor Safety Research, 20–24 November*. Varese, Italy: Elsevier Applied Science; 1989.

Bestion D. The physical closure laws in the Cathare code. *Nucl. Eng. Des.* 1990a;124:229–245.

Bestion D. *Recent developments on interfacial friction models*. In: European Two-Phase Flow Group Meeting, Varese, Italy, 21–24 May; 1990b:229–245.

Bestion D. *Validation data needs for CFD simulation of two-phase flow in a LWR core*. In: CFD4NRS-5, Zurich, Switzerland, September; 2014.

Bestion D., Micaelli J.C. *A two-fluid stratified model suitable for pressurized water reactor safety code*. In: 4th Miami International Symposium on Multiphase Transport and Particulate Phenomena, Miami, FL, USA, 15–17 December; 1986.

Bestion D., Serre G. On the modelling of two-phase flow in horizontal legs of a PWR. *Nucl. Eng. Technol.* 2012;44(8):871–888.

Bestion D., Serre G. *Transport of interfacial area in system codes: status and perspectives*. In: 15th International Topical Meeting on Nuclear Reactor Thermalhydraulics, NURETH-15, Pisa, Italy,

May 12–15; 2013.

Boyack B. *Methodology, status and plans for development and assessment of TUF and TRAC code*. In: USNRC and OECD/CSNI Workshop on Transient Thermal-Hydraulic and Neutronic Codes Requirements, Annapolis, MD, USA, 5–8 November; 1996.

Chandesris M., Mazoyer M., Serre G., Valette M. *Rod bundle thermalhydraulics mixing phenomena: 3-D analysis with CATHARE 3 of various experiments*. In: 15th International Topical Meeting on Nuclear Reactor Thermalhydraulics, NURETH-15, Pisa, Italy, May 12–15; 2013.

Chexal, B., Lellouche, G., 1986. A full range drift-flux correlation for vertical flows (revision 1). EPRI Report NP-3989-SR, Palo Alto, CA, USA.

De Crecy F. Modeling of stratified two-phase flow in pipes, pumps and other devices. *Int. J. Multiphase Flow*. 1986;12:307–323.

De Crécy, A., Bazin, P. (Eds.), Glaeser, H., Skorek, T., Joucla, J., Probst, P., Chung, B., Oh, D.-Y., Kynck, M., Pernica, R., Macek, J., Meca, R., Macian, R., D'Auria, F., Petruzzi, A., Perez, M., Reventos, F., Fujioka, K., 2007. Bemuse phase III report, uncertainty and sensitivity analysis of the LOFT L2-5 test. OECD/CSNI Report NEA/CSNI/R(2007)4, Paris, France, October.

Duponcheel M., Seynhaeve J.M., Bartosiewicz Y. *Implementation and assessment of the delayed equilibrium model for computing flashing choked flows in a multifield CFD code*. In: NURETH-16, 16th International Topical Meeting on Nuclear Reactor Thermal Hydraulics, Chicago, IL, USA, August 30–September 4; 2015.

Fauske, H.K., 1961. Contribution to the theory of two-phase one-component critical flow. ANL-6633, Argonne Nat. Lab., Chicago, IL, USA.

Fauske H.K. The discharge of saturated water through tubes.

Chem. Eng. Progr. Symp. Ser. 1965;61:210.

Freitas R., Bestion D. *On the prediction of the flooding phenomenon with the Cathare code*. In: 6th Int. Topical Meeting on Nuclear Reactor Thermal Hydraulics, NURETH 6, Grenoble, France, October 5–8; 1993.

Frepoli C., Mahaffy J.H., Hochreiter L.E. Calculation of dry out and post-dry out heat transfer in rod bundles using a three field model. *Nucl. Eng. Des.* 2003;224:131–148.

Geffraye G., Laroche S. *Analysis of the MHYRESA hot-leg entrainment tests*. In: Ninth International Topical Meeting on Nuclear Reactor Thermal Hydraulics (NURETH-9), San Francisco, CA, USA, October 3–8; 1999.

Geffraye G., Bazin P., Pichon P., Bengaouer A. *CCFL in hot legs and steam generators and its prediction with the CATHARE code*. In: Proceedings of the 7th International Topical Meeting on Nuclear Reactor Thermal Hydraulics (NURETH-7), Salt Lake City, Utah, USA, September 10–15; 1995.

Geffraye G., Faydide B., Laroche S., Ratel G. *Analysis of the MHYRESA hot-leg entrainment tests*. In: 8th International Conference on Nuclear Engineering (ICONE-8), Baltimore, MD, USA, April 2–6; 2000.

Glück M. Validation of the sub-channel code F-COBRA-TF part I: recalculation of single-phase and two-phase pressure loss measurements. *Nucl. Eng. Des.* 2008a;238:2308–2316.

Glück M. Validation of the sub-channel code F-COBRA-TF part II: recalculation of void measurements. *Nucl. Eng. Des.* 2008b;238:2317–2327.

Gudoshnikov A.N., Migrov Yu A. Verification of the computer code KORSAR taking into account the effect of non-condensable on thermal-hydraulic processes. *Therm. Eng.* 2008;55(11):971–977.

Harlow F.H., Amsden A.A. Numerical calculation of almost

incompressible flow. *J. Comput. Phys.* 1968;3:80.

Harlow F.H., Amsden A.A. *Fluid Dynamics*. In: second ed. Los Alamos, NM, USA: Los Alamos Scientific Laboratory; 1971 Los Alamos Scientific Laboratory Monograph, LA-4700.

Harlow F.H., Amsden A.A. Flow of interpenetrating material phases. *J. Comput. Phys.* 1975;18:440.

Henry, R.E., 1968. A study of one and two-component two-phase critical flows at low qualities. ANL 7430, Chicago, IL, USA, March.

Imke U., Sanchez V., Gomez R. *Subchanflow: a new empirical knowledge based sub channel code*. In: Annual Meeting on Nuclear Technology, Berlin, Germany; 2010.

Ishii M., Mishima K. Two fluid model and hydrodynamic constitutive relations. *Nucl. Eng. Design*. 1984;82:107–126.

Janicot A., Bestion D. Condensation modelling for ECC injection. *Nucl. Eng. Des.* 1993;145:37–45.

Jayanti S., Valette M. Calculation of dry out and post-dry out heat transfer in rod bundles using a three field model. *Int. J. Heat Mass Transf.* 2005;48:1825–1839.

Jeong J.J., Ha K.S., Chung B.D., Lee W.J. Development of a multi-dimensional thermal-hydraulic system code, MARS 1.3.1. *Ann. Nucl. Energy*. 1999;26(18):1611–1642.

Jimenez, J., Sanchez, V., 2015. Final report on BWR thermal-hydraulics at system scale and sub-channel scale. NURESAFE, D33.12.5, EC Project, Brussels, Belgium.

Kataoka I., Ishii M. Drift flux model for large diameter pipes and new correlation for pool void fraction. *Int. J. Heat Mass Transf.* 1987;30(9):1927–1939.

Kim K.D., Lee S.W., Bae S.W., Moon S.K., Kim S.H. *Development of physical models and correlation packages for the SPACE code*. In: The 13th International Topical Meeting on Nuclear Reactor

Thermal Hydraulics (NURETH-13), Kanazawa City, Ishikawa Prefecture, Japan, September 27–October 2009; 2009.

Liu L., Fu X., Du Z., Yu N., Yang Y. In: COSINE Validation Experiment Plan: 1st Phase, 21st International Conference on Nuclear Engineering, Vol. 4: Thermal Hydraulics, Chengdu, China, July 29–August 2; 2013.

Luxat J.C., Richards D.J., Liu W.S., Hanna B., Leung R.K., Krishnam V.S. *Methodology, status and plans for development and assessment of TUF and CATHENA codes*. In: USNRC and OECD/NEA/CSNI Workshop on Transient Thermal-Hydraulic and Neutronic Codes Requirements, Annapolis, MD, USA, 5–8 November; 1996.

Mahaffy J.H. A stability enhancing two-step method for fluid flow calculations. *J. Comput. Phys.* 1982;46:329–341.

Mandhane J.M., Gregory G.A., Aziz K. A flow pattern map for gas-liquid flow in horizontal pipes. *Int. J. Multiphase Flow.* 1974;1:537–553.

Moody F.J. Maximum flow rate of a single component two-phase mixture. *Int. Heat Transf., Trans. ASME Ser. C.* 1965;87(1):134.

Ninokata H., Mishima K., Sadatomi M., So A., Yamamoto Y., Nishida K., Yabushita Y., Hara T., Kusuno S. Development and improvement of transient subchannel analysis code NASCA. Developmental status. 655–656. *Nihon Kikai Gakkai Nenji Taikai Koen Ronbunshu.* 2000;1.

No H.C., Ha S.J., Kim K.D., Lim H.S., Lee E.H., Jin H.G. Korean development of advanced thermal-hydraulic codes for water reactors and HTGRs. *Nucl. Technol.* 2013;181(1):24–43.

Obry P., Cheissoux J.L., Grandotto M., Gaillard J.P., De Langre E., Bernard M. *An advanced steam generator design 3-D code*. In: Thermal Hydraulics of Advanced Heat Exchangers, 1990 ASME Winter Annual Meeting, Dallas, TX, USA, 25–30 November; 1990.

OECD/NEA/CSNI. Critical flow critical flow modelling in nuclear safety. In: *A State of the Art Report by a Group of Experts of the NEA Committee on the Safety of Nuclear Installations*. Paris, France: Nuclear Energy Agency; 1982.

OECD/NEA/CSNI, 1987. CSNI code validation matrix of thermo-hydraulic codes for LWR LOCA and transients. CSNI Report No. 132, Paris, France.

OECD/NEA/CSNI, 1989. Thermo-hydraulics of emergency core cooling in light water reactors – a state-of-the-art report. CSNI Report No. 161, Paris, France.

OECD/NEA/CSNI, 1993. Separate Effects test matrix for thermal-hydraulic code validation: phenomena characterization and selection of facilities and tests, I. OCDE/GD(94)82, Paris, France.

OECD/NEA/CSNI, 1996. CSNI code validation matrix of thermo-hydraulic codes for LWR LOCA and transients. CSNI Report No. 132-Rev.1, Paris, France.

OECD/NEA/CSNI, 2001. Validation matrix for the assessment of thermal-hydraulic codes for VVER LOCA and transient. NEA/CSNI/R(2001)4, JT00108841, Paris, France.

Ratel G., Geffraye G. *Analysis with CATHARE code of stratified flow regime in the MHYRESA hot leg entrainment test*. In: 38th European Two-Phase Flow Group Meeting, Karlsruhe, Germany, May 29-31; 2000.

RELAP5/MOD3. In: Washington, DC, USA: USNRC; . *Code Manual, Models and Correlations*, NUREG/CR-5535. 1995;Vol. 4.

RELAP5-3-D. *Code Development Team, RELAP5-3-D Code Manual Volume I: Code Structure, System Models and Solution Methods*. Idaho Falls, ID, USA: Idaho National Engineering and Environmental Laboratory; 2001.

Sonnenburg H.G. *Full-range drift flux model based on drift-flux theory with envelope theory*. In: Fourth International Topical

Meeting on Nuclear Reactor Thermal Hydraulics, NURETH-4, Karlsruhe, Germany, October 10–13; 1989.

Taitel Y., Dukler A.E. A model for predicting flow regime transitions in horizontal and near-horizontal gas-liquid flow. *AIChE J.* 1976;22(1):47–66.

Teschendorff V., Austregesilo H., Lerchl G. *Methodology, status and plans for development and assessment of ATHLET code*. In: USNRC and OECD/NEA/CSNI Workshop on Transient Thermal-Hydraulic and Neutronic Codes Requirements, Annapolis, MD, USA, 5–8 November; 1996.

Thurgood, M., Crowell, K., Kelly, J., 1981. COBRA-TF equations and constitutive models. FATE-81-106, Pacific Northwest Laboratory, USA.

Toumi I., Bergeron A., Gallo D., Royer E., Caruge D. FLICA-4: a 3-D two-phase flow computer code with advanced numerical methods for nuclear applications. *Nucl. Eng. Des.* 2000;200:139.

TRACE. V5.0, *Theory Manual*. Washington, DC: USNRC; 2007a.

TRACE. V5.0 *User Manual*. Washington, DC, USA: USNRC; 2007b.

TRACE. V5.0 *Assessment Manual*. Washington, USA: USNRC; 2007c.

Trapp J.A., Ransom V.H. A choked-flow calculation criterion for nonhomogeneous, nonequilibrium two-phase flows. *Int. J. Multiphase Flow*. 1982;8(6):669–681.

Trapp J.A., Riemke R.A. A nearly-implicit hydrodynamics numerical scheme for two-phase flow. *J. Comput. Phys.* 1986;66:66–82.

Valette M. *Analysis of boiling two phase flow in rod bundle for NUPEC BFBT benchmark with 3-fields NEPTUNE system code*. In: Proceedings of the 12th International Topical Meeting on Nuclear Reactor Thermal Hydraulics (NURETH-12) Pittsburgh, PA, USA, September 30–October 4; 2007.

Valette M. *PSBT simulations with Cathare 3*. In: 14th International Topical Meeting on Nuclear Reactor Thermal Hydraulics, NURETH-14, Toronto, Ontario, Canada, September 25–30; 2011.

Valette M., Pouvreau J., Bestion D., Emonot P. Revisiting large break LOCA with the CATHARE 3 three field model. *Nucl. Eng. Des.* 2011;241(11):4487–4496.

Wallis G.B. *One-Dimensional Two Phase Flow*. New York, NY, USA: McGraw Hill; 1969.

Wilson G.E., Boyack B.E. The role of the PIRT process in experiments, code development and code applications associated with reactor safety analysis. *Nucl. Eng. Des.* 1998;186:23–37.

Ylijoki, J., Normann, S., Silde, A., 2008. Validation of APROS version 5.08. Research Report, VTT-R-03692-08, Espoo, Finland.

Zuber, N., 1991. Appendix D: a hierarchical, two-tiered scaling analysis, an integrated structure and scaling methodology for severe accident technical issue resolution. NUREG/CR-5809, November, US Nuclear Regulatory Commission, Washington, DC.

Zuber N., Findlay J.A. Average volumetric concentration in two-phase systems. *J. Heat Transf.* 1965;87(4):453–468.

An overview of computational fluid dynamics and nuclear applications

Y. Hassan *Texas A&M University, College Station, TX, United States*

Abstract

Numerical equation solvers have been developed rather than complex codes in the area of computational fluid dynamics (CFD). As a further difference related to system thermal hydraulics, turbulence can be modeled directly (only its effects are computed by system thermal-hydraulic codes) by empirically supported models and convergence of results can be in principle demonstrated when mesh size is reduced down to a fixed value. So-called spatial resolution in phenomena modeling can be ensured. Grid generation methods are adopted instead of code-user-nodalizations in system thermal hydraulics. The CFD user has access to suitable numerical ports for enhancing modeling capabilities. Best practice guidelines (BPG) do exist to orient the applications. These partly substitute the validation in the area of system thermal hydraulics. Coupling between system thermal hydraulics and CFD codes constitutes a common practice to simulate complex systems and to achieve the needed spatial resolution in selected regions of nuclear power plants.

Keywords

Computational fluid dynamics (CFD); Spatial resolutions; Best practice guidelines (BPG); Turbulence modeling; Mesh generator; Numerical solver algorithm

Nomenclature

ABWR advanced BWR

AIAA The American Institute of
Aeronautics and Astronautics

ALE Arbitrary Eulerian-Lagrangian

ANS American Nuclear Society

ANSYS see CFX

AMD computer identification

AP600 advanced PWR (600 MWe)

ASCLIM Consortium in EU dealing
with CFD

ASME American Society of

Mechanical Engineering

ASTAR Consortium in EU dealing
with CFD

ATI axial turbulence intensity

BDBA beyond design basis accident

BEPU best estimate plus uncertainty

BIC boundary and initial conditions

BPG best practice guidelines

BSL baseline (also Standard “Menter
baseline two-equation model,”
Menter (1994))

BWR boiling water reactor

CASL Research Project financed by

DOE in the US

CD-adapco see STAR-CCM +

CFD computational fluid dynamics

CFDS see FLOW 3D

CFD4NRS Working Group for CFD
(and set of activities) at OECD/NEA/
CSNI

CFX CFD code

CHF critical heat flux

CHT conjugate heat transfer

CILC crud-induced localized
corrosion

CIPS crud-induced power shift

CPU central process unit

CSNI Committee on the Safety of
Nuclear Installations

DBA design basis accident

DDES delayed DES

DES detached eddy simulation

DNB Departure from Nucleate
Boiling

DNS direct numerical simulation

DOE Department of Energy

EARSM explicit algebraic RSM

EASM explicit algebraic stress model

EB elliptic blending (related to RSM)

ECC emergency core cooling

ECCI ECC injection

ECORA consortium in EU dealing
with CFD FLOWMIX-R

EDF Electricité de France

ELES embedded LES

EOHL end of heated length

EPRI electrical power research
institute

ERCOFTAC Network of CFD
specialists (see corresponding
website)

ESP electric submersible pump

EUBORA consortium in EU dealing with CFD

EVM eddy viscosity model

FAD fuel assembly distortion

FLOWMIX-R consortium in EU dealing with CFD

FLOWNET network of CFD specialists (see corresponding website)

FLOW 3D CFD code

FLUENT CFD code

FSI fluid structure interaction

FSM flow simulation methodology

GFR gas fast reactor

GIS grid-induced separation

GGDH general gradient diffusion
hypothesis

GTRF grid to rod fretting

H hydrogen

HPC high performance computing

IBM immersed boundary method

ICM interfacial capturing method (or
model)

IDDES improved DDES

ISP International Standard Problem

ITM interfacial tracking model (or method)

KAERI Korean Atomic Energy Research Institute

k-kL two-equations RANS model (L is the integral scale length of turbulence), Rotta (1972)

LANL Los Alamos National Lab

LBM lattice Boltzmann method

LDV laser doppler velocimetry

LES large eddy simulation

LEVM linear eddy viscosity model

LHGR linear heat generation rate

LHS latin hypercube sampling

LIME lightweight integrating
multiphysics environment

LLM logarithmic law mismatch

LMFBR liquid metal fast breeder
reactor

LOCA loss of coolant accident

LRR Launder-Reece-Rodi (related to
RSM)

LvK von-Karman length scale

MANIVEL test facility used for CFD
benchmark

MARNET network of CFD specialists
(see corresponding website)

MCPR minimum critical power ratio

MILES monotone integrated LES

MMS method of manufactured
solution

MSD modeled stress depletion

MVG mixing vane grid

NEA Nuclear Energy Agency

NLEVM nonlinear eddy viscosity
model

NPARC network of CFD specialists
(see corresponding website)

NRC Nuclear Regulatory
Commission

NRS nuclear reactor safety

NS Navier-Stokes

NTF nuclear thermal fluid

ODE ordinary differential equations

OECD Organization for Economic
Cooperation and Development

OMEGA test facility used for CFD
benchmark

ORNL Oak Ridge National Lab

PAHR post accident heat removal

PCI pellet clad interaction

PCMI pellet clad mechanical interaction

PIRT phenomena identification and ranking table

PIV particle image velocimetry

PTS pressurized thermal shock

PTV particle tracking velocimetry

PWR pressurized water reactor

QNET-CFD network of CFD specialists (see corresponding website)

RANS Reynolds average Navier-Stokes

RCS reactor coolant system

REV representative elementary
volume

RIA reactivity initiated accident

RMS root mean square

RNG renormalization group (method
to renormalize the NS equations)

RPV reactor pressure vessel

RSICC Radiation Safety Information
Computational Center

RSM Reynolds stress model

SA Spalart-Allmaras (model)

SAS scale-adaptive simulation

SG steam generator

SGDH simple gradient diffusion hypothesis

SGS subgrid scale

SMC second moment closure

SP standard problem (CFD exercise)

SRS scale resolving simulation

SSG simple support grids or
Speziale-Sarkar-Gatski (related to
RSM)

SST shear stress transport

STAR-CCM + CFD code

SYS TH system thermal-hydraulics
(codes)

UQ uncertainty quantification

TAMU Texas A&M University

TBL turbulent boundary layer

THERFAT consortium in EU dealing
with CFD

TNT Kok's $k-\omega$ model for turbulent/
nonturbulent interfaces (Hellsten,
2004)

TPCF two-phase critical flow

T/C thermocouple

URANS unsteady RANS

(U)RANS see URANS

VOF volume of fluid

VLES very large eddy simulation

VR virtual reactor (e.g., by CASL)

V & V verification and validation

WALE wall adapting local eddy

WG working group

WGAMA working group of OECD/
NEA/CSNI

WMLES wall-modeled LES

ZDES zonal DES

Chapter foreword

Computational fluid dynamics (CFD) constitutes a self-standing complex technology; see also the discussion in **Chapters 1 and 2**. CFD-related technology is a cross-cutting subject for researches, development, and application in areas like chemistry, aeronautics, aerospace, military, mechanics (noticeably, car industry), naval, meteorologies including climate and ocean. As such, a huge number of roadmaps for development can be identified since the time when computer power became suitable for performing CFD calculation, i.e., around the 1970s of past century. Furthermore, dozens of textbooks and thousands of CFD-related papers can be found in the literature.

Thus, a comprehensive state of the art, e.g., documenting CFD model capabilities and perspectives is a prohibitive task, well beyond the scope for this chapter.

The nuclear thermal hydraulics was not the origin or the main motivation for CFD. However, CFD may be seen as the major area where researches and investments are ongoing in nuclear thermal hydraulics. Namely, making reference to two-phase flows, the CFD research resembles a building site with work in progress: a number of targets have been achieved and, at the same time, new directions are identified for development.

In addition, one may note that:

- Fundamental or balance equations for CFD, typically identified as Navier-Stokes equations, derive from principle of thermodynamics and mechanics in the same way as in the case of system codes (see e.g., **Chapters 5 and 11**);
- CFD analyses provide support for, or receive support from, system thermal hydraulics code calculations for suitable application of the best estimate plus uncertainty (BEPU) approach as discussed in **Chapter 14**.
- CFD analyses are relevant for sectors in nuclear technology other than thermal hydraulics.

Within the area of nuclear thermal hydraulics, large efforts have been made by OECD/NEA/CSNI, as testified by the CFD4NRS series of Workshops:

(1) CFD Codes for Application to Nuclear Reactor Safety (CFD4NRS), Garching, Sept. 2006, NEA/CSNI/R(2007)3 to be found in NEA website.

(2) Experiments and CFD Code Application to Nuclear Reactor Safety (XC4NRS), Grenoble, Sept. 2008, NEA/CSNI/R(2009)12, to be found in NEA website.

(3) CFD for Nuclear Reactor Safety Applications (CFD4NRS-3), Bethesda, Sept. 2010, NEA/CSNI/R(2011)14 to be found in NEA website.

(4) CFD for Nuclear Reactor Safety Applications (CFD4NRS-4), Daejeon, Sept. 2012, NEA/CSNI/R(2014)4, to be found in NEA website.

(5) CFD for Nuclear Reactor Safety Applications (CFD4NRS-5), Zürich, Sept. 2014, NEA/CSNI/R(2016)1, to be found in NEA website.

(6) CFD for Nuclear Reactor Safety Applications (CFD4NRS-6), Cambridge, MA (hosted by MIT), Sept. 2016, to be found in NEA website.

Additional OECD/NEA/CSNI key documents dealing with CFD are considered in the text (e.g., Mahaffy et al., 2007a,b; OECD/NEA/CSNI/R(2014)3, 2014; Smith et al., 2015; Bestion et al., 2016).

Then a CFD chapter in a modern nuclear thermal hydraulics book is essential; other motivations for this chapter can be found in **Chapter 1**. However, this chapter shall be seen as the work-in-progress building site (see the introductory statements in **Section 12.6** for more detail): topics and question marks are listed with an attempt to provide an evaluation in some cases, rather than picturing a reality which risks to become obsolete in a few years; this includes mentioning sectors in nuclear technology, which have a connection with thermal hydraulics (e.g., fretting corrosion). Furthermore, in a work-in-progress building site, the same component can be found in different locations; similarly, in this chapter repetitions are not excluded even though an attempt is made to look at the same topic from different viewpoints. Definitely, a work-in-progress chapter seems to reflect the CFD technology status better than a synthesis of (nonexisting) consolidated achievements.

A hint for the reader: a look to the list of acronyms gives an idea of the multitarget

nature and complexity of CFD area.

Part 1. Computational fluid dynamics for nuclear thermal hydraulics: The current overview

12.1 Introduction

In the nuclear field, views on the CFD are poles apart. Some think that the CFD is promising and can play a key role in nuclear thermal fluid problems now and in the near future, while others think that the CFD is not reliable compared to the experiment and it will take a very long time until it plays a key role in this field. Anyway, it is true that in recent years numerous applications of CFD have been actively performed in the nuclear field. In this chapter, leaning to the first view, we address what we have to keep in mind for the CFD to be a promising tool and to play an important role in the nuclear thermal hydraulics.

There are numerous issues and questions relating to the use of CFD in the nuclear thermal hydraulics. These can be categorized into application-related and validation-related ones, each of which can be classified into CFD and physics viewpoints. In addition, the stance, i.e., CFD users, experimentalists, system code users, vendors, utilities, regulators, etc., changes the emphasis on the questions/issues.

Traditionally, system codes (SYS TH codes, see e.g., **Chapter 11**) and subchannel analysis codes have been successful to a degree for the nuclear safety analysis. However, because their main role is to combine numerous empirical correlations based on very simple governing equations to evaluate the synthetic effect, the expected level of accuracy was relatively low. The validation is performed against global variables (pressure, temperature, void fraction, liquid level, and so on; see **Chapter 13**) in a relatively large control volume (components, subchannels, and so on). On the other hand, in recent years, as the computing power increases, the CFD code has become a viable tool to predict the more detailed thermal fluids behavior in the nuclear system with a higher accuracy than system and subchannel codes.

However, because the nuclear system, in general, involves very complex phenomena characterized as high turbulence and/or multiphase not only during transient events and accidents but also in normal operating conditions, the models used in the CFD code for the nuclear system problems still involve empirical

closure models, such as RANS equations with turbulence closure models for turbulence calculations and two-fluid model equations with closure models for two-phase calculations, rather than less-empirical models, such as wall-resolved LES/DNS turbulence models and interfacial tracking models (ITMs), respectively, because of practical feasibility. Once some assumptions and related modeling are involved in the CFD code, we need to understand more about the phenomenon of our interest because the assumptions and modeling have to have the capability of reflecting key phenomenon.

In this chapter, we provide a critical (as far as possible) overview for the CFD applications in the nuclear thermal-hydraulic fields and some recommendations for better use.

12.2 CFD analysis procedure

Now, we address a CFD analysis procedure, which can be generally applied to validation and application (prediction). This is important to CFD analysts. Selected steps are (Faragher, 2004):

- Understand the problem and set the simulation strategy;
- Generate the geometry and the mesh;
- Set the boundary and the initial conditions;
- Run the CFD solver;
- Postprocess and interpret the results;
- Refine the mesh;
- Perform the sensitivity studies;
- Document the analysis.

12.2.1 Understand the problem (phenomena) and set the simulation strategy

When applying the CFD to nuclear thermal-hydraulic problems, it is important to understand the characteristics of the phenomenon. These may include physical conditions, turbulence, flow separation, swirling, secondary flows, multiphase flows, etc. Based on these, we set the simulation strategy by considering objectives

of the analysis, required level of accuracy (qualitative information/incremental quantities/absolute quantities), geometry (simplification and/or omission) flow domain and boundary conditions, turbulence models (steady/unsteady, RANS/hybrid RANS-LES, LES, closure models), solvers, heat transfer, heat conduction (conjugate heat transfer/heat flux), memory and CPU resources, etc.

12.2.2 Generate the geometry and the mesh

In many nuclear thermal-hydraulic problems, we need to consider the geometrical simplification. Unlike the system code where geometry-related information must be supplied by code user in an averaged manner (see e.g., the local pressure drop coefficient at any geometric discontinuity), the geometry is very important because it plays a role in boundary condition in the CFD calculation.

The mesh is a key factor affecting the accuracy of the calculation results. However, it has infinite degrees of freedom, thus representing quantitatively the geometry and hard to directly compare with other mesh configurations.

12.2.3 Set the boundary and the initial conditions

Flow and thermal variables (and turbulent variables) should be specified on the boundaries of the flow domain. Material properties should be specified for all solids and fluids in the simulation.

If the CFD-level boundary and initial conditions are not given in validation problem or if we have to impose the boundary and initial conditions in application problems, it should be reasonable and its sensitivity should be examined afterward.

12.2.4 Postprocess and interpret the results

Because CFD has all the information in the computational domain, it is difficult to determine what results should be extracted and visualized. If the calculation purpose is validation, i.e., comparison with measured data, it may be clear. Otherwise, we need to consider various ways to get more insights.

12.2.5 Refine the mesh (rerun) and perform a sensitivity analysis (rerun)

Refining mesh is usually prior to other sensitivity study. Depending on the mesh type, this process may be easy or impossible. However, demonstrating the convergence of results when mesh size is decreased must be considered an implicit requirement for CFD code application in nuclear thermal hydraulics (e.g., something that cannot be achieved by SYS TH codes). An important thing is what

variable in what region needs to be used to evaluate the mesh sensitivity.

The sensitivity of the computed results may be examined with respect to variables such as flow conditions, initial and boundary conditions, mesh type, configuration and density, turbulence models, and computer system. Practically, all of these cannot be performed. The round robin benchmark exercise can support some of these; however, it cannot cover this individual sensitivity studies.

12.2.6 Document the analysis

Documentation is very important because it is a tool to communicate with others. The document should include not only the findings from the analysis but also each process in detail so that other analysts can repeat it. To go further toward the problem-specific best practice, this individual document is very important. Qualified analyses should include results of sensitivity studies, possible demonstration of convergence of results (when the mesh size is decreased), and quantification of expected uncertainty (UQ).

12.3 Methodological aspects—Physical models

In this section, we briefly explain CFD methodologies that can be used or considered in the nuclear field. In fact, it is impossible to describe all aspects of CFD in this chapter because there are numerous CFD methodologies depending on problems that we want to deal with.

12.3.1 Single-phase modeling

In most problems in nuclear field flows are turbulent. To accurately simulate the turbulent flows, the broad range of time and space scales should be suitably captured or modeled. Considering the geometrical complexity (broad range of scales) and high Re in typical nuclear thermal fluid problems, it is a key to adopt methodology with efficiency (even practicality or possibility) as well as accuracy. The basic starting point is steady RANS modeling, which solves the time-averaged Navier-Stokes equations and the closure models for the turbulence stress resulting from the averaging procedure. Numerous studies on the turbulence closure models have been performed in various industrial problems for the last fifty years. What we need to have in mind when applying the steady RANS turbulence models are:

- (i) no unique turbulence closure model to be appropriate for different problems;

(ii) the steady RANS turbulence model is a steady model; thus, when large unsteady effect is involved as a key phenomenon in a given problem, it is not expected to be successful to this problem.

Once the problem involves locally, in critical regions, or globally unstable unsteady turbulent phenomena, we need to consider unsteady turbulence models. However, it is sometimes challenging to characterize any unsteady phenomenon. There are numerous unsteady turbulence models, which can, however, be classified into unsteady RANS, hybrid RANS-LES, LES, and DNS. These should be selected carefully considering the main physics and efficiency.

Another important factor in the CFD turbulence simulation is near-wall treatment. The wall function method is typically used because of its efficiency and reasonable accuracy. Since each solver has slightly different enhanced near-wall treatment method, users need to understand how it works before using it. In the near-wall treatment, it is important to generate the near-wall mesh, so that the assumptions (basic requirements) of the near-wall treatment adopted are satisfied, and then to evaluate whether the assumptions are applicable to this problem.

12.3.2 Two-phase modeling

Once multiphase phenomena are involved in the problem of our interest, change of governing equations may be needed. Depending on how to deal with interface, there are various methodological changes. In multiphase modeling, there are large differences depending on whether the interface is treated statistically or deterministically. The statistical approach requires numerous modeling, while the deterministic approach requires enormous CPU resources. We do not get into the details of respective methods within the multiphase CFD in this chapter. Please refer to Chapters 5, 9, and 11 for further details.

12.4 Characteristics of the CFD analysis

To successfully apply the CFD to nuclear thermal-hydraulic problems, we need to understand the characteristics of the CFD analysis different from other numerical and experimental analyses and then use the advantages fully.

12.4.1 Applications

The validated CFD-based numerical experiment can give us various insights because we can use all variables over the entire region, which is different from the physical experiments. Thus, we may need to spend more time on the development of how to use the numerical experimental results fully using the benefit of the

numerical experiment.

An ideal image of the CFD use may be that like a system code, the CFD simulates flow and heat transfer phenomena (covering all transient and accident scenarios) in the entire reactor coolant system of the reactor. However, this may not be attainable at least within a few decades (50 years is a guess). In this sense, the CFD may not play a key role in the applied nuclear thermal hydraulics field. However, CFD can do what lumped codes cannot do and can do more specifically and efficiently what experiments can do. In fact, various different aspects of CFD use in this field have been considered.

First, we can directly use the CFD-calculated data for the target analysis, for example, production of the thermal-hydraulic data (pressure, temperature fluctuations) for the structural analysis, production of rod surface temperature (heat transfer coefficient) for the crud analysis tool. Next, we can use the data to determine the input parameters for lumped volume codes (subchannel and system codes). For example, we can use the CFD-calculated pressure drop data for the new design of the mixing vane grids to impose the resistance coefficient in the subchannel or system codes. For another example, we can adjust the loss coefficient based on the CFD-calculated three-dimensional flow distribution. Also, we can use the CFD calculation results to develop physical models needed in lumped volume codes. Some (CFD) research groups started development or application of ITM to produce the correlations needed in the lumped volume code. Also, CFD can provide insight for the new design of components or new experimental designs. So, it can help people reduce the trial and error in making the experimental apparatus. In addition, CFD can increase the physical understandings of or help identify complex phenomena that cannot be imagined by people's insight. Also, CFD can be used to check the system code results especially for the 3D flow distributions. For example, NRC adopted CFD to check the flow distribution obtained by system codes for refueling storage tank problem (Boyd, 2016). Depending on the purpose, the level of accuracy can change.

12.4.2 Validations

The capabilities and the advantages of CFD over SYS TH codes addressed in the previous section are only valid when the CFD method is validated for the test appropriately mimicking a given problem. The validation process for the CFD is basically similar to that of the system code (see e.g., Chapter 13); however, there are many more difficulties in CFD validation (Smith et al., 2015). In the CFD-level

benchmark experiment, problem specification needs to be much more elaborate than the system code. Initial and boundary conditions and geometrical information should be accurately provided. For the data measurement, the data should cover not only target regions and target variables but also supplementary variables and regions. However, in the previous experience, it is not easy to identify the target regions and the target variables. Also, physically important phenomena for nuclear thermal hydraulics are not necessarily part of the capabilities of the CFD codes and methods. Thus, benchmark experiments, which are supposed to address physically important phenomena and the CFD calculations, should give rise to a feedback process, not to a serial process. If any experiment is for the CFD benchmark the CFD needs to be involved in its design process. Furthermore, phenomena identification and ranking table (PIRT, e.g., see Chapter 13) for the system code is not suitable for the CFD code in most cases. Although numerous experiments have been performed for the validation of the system code (models), most of them are not suitable for the CFD validation. Thus, in many cases, new experiment should be performed. CFD validation experiments and other experiments (developing physical models, for the study of physical phenomena, for the validation of system codes) are needed.

The CFD validation is not just comparing the CFD-calculated results with the measured data for a given problem. For successful CFD validation, we need to consider several things from experimental point of view, CFD point of view, and both points of view. Here, we address some (selected) important things for each point of view. From the experimental point of view, a general requirement for data accuracy (with errors) should be satisfied. Beyond this, the specific problem-related issues should be reflected well. Among these, at first, the benchmark experiment should be representative of the prototype. This becomes problematic when the main discrepancies between the CFD calculations and the experiment are due to the difference between the experimental and the prototypic conditions (geometry and thermal fluid conditions). Next, the measured variables in the experiment should reflect key phenomenon and target variables at target range.

From the CFD calculation point of view, it is very important to follow the general CFD best practice guidelines (BPG)—for mesh sensitivity, mesh quality, turbulence models and near-wall treatment, numerical schemes, and so on—to reduce the user errors and evaluate the selected CFD methods in a right way. Beyond this, we need to use an advantage of the CFD—availability of all variables in the computational domain—to understand the overall phenomenon made in the selected CFD world. This will help both experimental design and interpretation of discrepancies between the CFD results and measured data.

From both points of view, it should be stressed that the reliable and effective CFD validation needs closer collaboration between experimentalists and CFD analysts. Both ways from experiment to CFD and from CFD to experiment can greatly reduce time and cost at the end. Each party needs to be willing to provide not only results (data) but also the limitations (errors and uncertainty) and phenomenological insights to another and try to understand the other party to achieve a common goal effectively.

On the other hand, several round robin benchmark exercises have been performed, as discussed in Part 2 of this chapter. The round robin exercise has a great advantage because various numerical methods (especially, various turbulence models, codes, and mesh configurations) can be considered and compared for the same problem. In fact, through the previous round robin benchmark exercise, some meaningful conclusions could be derived (see Part 2 of this chapter). In several benchmark applications where different CFD codes or procedures are involved, the ranking method was adopted to evaluate and compare the results. It seems very objective; however, it also has limitations. We need to consider qualitative analysis along with such quantitative measures.

Some findings relevant to the application of CFD methods, models, and codes, which are discussed in Part 2 of this chapter, are summarized below.

12.4.2.1 Capabilities of steady RANS

The main insight from Phase 2 of EPRI round robin benchmark (EPRI, 2014, 2015) was that appropriate steady RANS approaches with wall function could reasonably predict two key variables in the PWR fuel rod bundle with split-type mixing vane grids: the grid span pressure loss and rod surface temperature distributions. Here, the appropriate steady RANS approach indicates that:

(i) fluid and solid region meshes are suitable for the complex geometry of the grid and wall-function requirement;

(ii) conjugate heat transfer is considered;

(iii) the “reasonable” prediction specifically means that:

○ the pressure loss errors for SSG and MVG spans are within about 5% and about 10%, respectively;

○ the circumferentially averaged rod inner-surface temperature errors with elevation for different rods are within -2 to 3 K and the RMS errors around the

circumference (with elevation for different rods) are within the range 2–4 K.

Overall, the CFD calculations under the trim mesh with extrusion layers consistently showed good result. In addition, the effect of turbulence-anisotropy was relatively reduced in the MVG wake region.

12.4.2.2 Limitations of steady RANS

On the other hand, the steady RANS approaches showed limitations:

(i) they could not capture well central rod circumferential temperature distribution patterns in the far wake probably because of the cross-flow reorientation (and dumping) due to the interaction between asymmetric, cross-flows with test section wall;

(ii) they showed quite large local maximum rod inner-surface temperature error (ranging 4–9 K with elevation, see Section 12.8.1 in the Part 2 of this chapter), probably because of unsteady, large-scale cross-flow fluctuation effect. In addition, it should be pointed out again that in the actual applications to PWR fuel rod bundles where the test section wall is not present except near the core barrel, the unsteady, large-scale cross-flow fluctuation effect on the circumferential temperature variation magnitude may be of greater importance than the test section wall effect on the flow pattern changes.

12.4.2.3 Final remarks from EPRI round robin

The steady RANS approaches showed reasonable capabilities in predicting the circumferentially averaged rod surface temperature and the grid span pressure loss. However, if the purpose of the simulation is to predict the local surface temperature distribution in the far downstream (e.g., crud-induced localized corrosion), we may need to adopt higher level unsteady turbulence models. Concurrently, we may need to perform experiments with a larger lateral domain to see the test section wall effect and with a longer axial domain (comparable to typical PWR span) to see decaying patterns of the rod temperature distribution in the real target region.

12.5 Summary remarks

The CFD cannot play a system code-like role in the nuclear thermal-hydraulic analysis in the near future. However, the CFD can contribute to the nuclear thermal-hydraulic analysis in different ways from other numerical and experimental analyses. In this context, the nuclear CFD analysts have tried to find

the problems (physics) that CFD models can simulate and have applied those models to various problems in various aspects (e.g., Smith et al., 2015). In some problems, they successfully used and have established some level of best practices.

Finally, to increase the contribution of the CFD to the nuclear thermal hydraulics field, we need to keep in mind the following points:

- We need to set timely goals—near-term, mid-term, and long-term goals. Depending on the time-based goals, we can have totally different strategies.
- We do not need to confine ourselves to accustomed methodologies just because new methodologies need new strict validations.
- We need more specific application examples and need to develop problem-specific BPG as many as possible. As the number of BPG increases, the applications will accelerate.
- We need to construct open systems where the communications, accumulations, and collaborations can be actively performed. Their best form (web-based or hypertext) and contents should be identified.
- The CFD analyst need to fully understand the problem (physics), physical models, as well as the numerical factors.
- We need to develop efficient CFD assessment methods.

These cannot be done by one person or one group. Collaborations between CFD analysts, with experimentalists, with system or subchannel code analysts are essential.

Part 2. Insights into computational fluid dynamics for nuclear power plant applications

12.6 CFD-related elements and definitions

This section aims at substantiating the statement in the Sword to Chapter 12 describing the CFD technology as a building site with work in progress. Namely,

the pieces, or the equivalent of bricks, compounds, components, and subcomponents of different nature (electrical, chemical, metal, and plastic industrial products in the building site) for the CFD technology are defined or just mentioned below; this includes acronyms which are considered in other parts of the chapter and are defined at the end of the chapter. The current technological status is that various pieces are not integrated at the time of writing of the book. In the subsequent sections (i.e., starting from Section 12.7) snapshot type of details and insights are given.

The list of CFD topics (including open issues and question marks) to be considered for a comprehensive presentation of its role in nuclear thermal hydraulics is as follows:

○ “CFD.” Definition: Collection of solvers of physical models in a user interface. Physical models. Governing equations: Porous medium & Open medium. Averaging: volume-averaging, time-averaging, filtered Navier-Stokes equations. Interface models. Statistical model (two-fluid model) and ITM (VOF, level set). Multicomponent models. Lagrangian-Eulerian method.

○ “Application-1.” (i) Contents—(i-1) local, detailed results: providing data for other analyses (e.g., thermal fatigue, vibration, CILC analysis); (i-2) 3D phenomena, e.g., asymmetric distribution of flows in the reactor pressure vessel; improvement of 1D-based model (in system code); (ii) Format/method: coupling with system code.

○ “Application-2.” (i) A part of multiphysics and multiscale analysis, i.e., needing coupling with separate analyses and codes in different areas or related calculation results; (ii) As a fully integrated and self-standing multiphysics and multiscale analysis.

○ “Application-3.” What system codes (and experiments) cannot do (well).

○ “Nuclear Thermal Fluids Problems.” Design evaluation and optimization; experimental design evaluation; safety and performance analyses; methodology evaluation in regulatory process (e.g., Boyd, 2016).

• Introduction to CFD discussion – Background. Many uses of CFD computational tools are possible. A broad spectrum of applications can be derived from the analysis of the literature. Various aspects having different origin and implication are relevant: some of these are discussed in Foreword, Abstract, and in the Introduction to Part 1 of this chapter.

- **CFD code.** A code can be seen as the collection of multiple numerical solvers for fluid dynamics, heat transfer, and the interface in the case of two-phase flows. Coupling among different solvers may be needed, as well as coupling between CFD codes and codes in other areas, like structural analysis, chemical reaction, and radiation heat transfer (see **Section 12.10**, below).

- **Solver:** A solver is a generic term indicating a piece of mathematical software, possibly in the form of a stand-alone computer program or as a software library that “solves” a mathematical problem. A solver takes problem descriptions in some sort of generic form and calculates their solution. In a solver, the emphasis is on creating a program or library that can easily be applied to other problems of similar type (e.g., see also Wikipedia-related definitions).

- **Assessment of “CFD code.”** Assessment is used here as synonymous of the second “V” in the acronym V&V (i.e., validation). Open question is: Is assessment right? Namely, assessment of “System code” makes sense (**Chapter 13**), but assessment of “CFD code” is very ambiguous because in many cases we use partial CFD codes, e.g., because the word CFD is sometimes associated with codes like GOTHIC, GASFLOW, and COBRA, e.g., see **Westinghouse (2014)**, **Thurgood et al. (1983)**, and **Xiao et al. (2016)**, respectively.

- **Introduction – Motivation.** Open question is: Is the right image of CFD available to decision makers and end users? Streamlines for addressing the questions are:

- Possibly, more focus is provided on multiphysics than on CFD itself;

- The image of CFD is biased by the idea of system codes;

- There is the misunderstanding that the products are dependent on purpose;

- The application targets may reveal either too ambitious or too loose;

- There can be overconfidence in the results or the temptation to neglect the related implications;

- A broad spectrum of CFD codes and methods is available for application and the selection of the best code or the best method may reveal difficulty;

- In all cases difficulties may arise in demonstrating the validation of the process of code application or the quality level of results.

- **Differences of CFD codes from system (SYS TH) codes.** The following

differences are emphasized

(1) Governing equations are very important in CFD code applications, while the governing equations are fixed in SYS TH codes and modeling effects connected with constitutive equations (see Chapter 9) are dominant;

(2) Meshing has infinite degree of freedom and a key factor affecting the results in CFD codes;

(3) Typically, solutions of balance equations in SYS TH codes are obtained in control volumes bounded by solid walls; this is not the case for CFD codes;

(4) Averaging is needed in control volumes in the case of SYS TH codes;

(5) Limitation of CPU resources is an important factor for the selection of methods in the case of CFD code; the same limitation may not apply in the case of modern SYS TH codes;

(6) Application range should be selected carefully in the case of CFD codes; application ranges for SYS TH codes may be broader and properly fixed by the validation process;

(7) The spectrum of application models in CFD codes may reveal wider (i.e., encompassing the boundary of interest for nuclear thermal hydraulics);

(8) The validation process for CFD codes may reveal more complex than for SYS TH codes

(9) the computational domain and boundary condition effects are critical to accuracy in both CFD and SYS TH codes; however the criticalities and the impact upon accuracy of results may be different;

(10) CFD codes are in principle able to provide new phenomenological results; this capability is not expected from the application of SYS TH codes.

- What system (SYS TH) codes cannot do:

- full prediction of three-dimensional phenomena;

- prediction of local (transient) phenomena;

- detailed consideration (modeling) of geometrical effects.

- The Ideal and the real in CFD NTF.

- The ideal: we assume that the results are accurate and reliable; we trust in three-dimensional and local calculated data; we assume that all information in the computational domain are available to the (CFD) analysts; we accept all transient data, i.e., whatever characteristics of fluctuation intensity and frequency values; we obtain positive results from sensitivity study performed by adopting the method that showed good agreement with benchmark data;

- The real: We need to calibrate models to match the results of experiments if available (e.g., for the validation process); we note that even calibration cannot produce good results in most cases; we realize that broad methodology comparisons (e.g., through round robin benchmark) are needed but are not available; we realize that higher level calculations (HPC, High Performance Computing) are required and not available: namely, HPC results are needed for the systematic calibration for the lower level calculations;

- What CFD codes can do. In general, CFD can do what system code and/or experiments cannot do (3D effect, local phenomenon) or cannot do well, i.e., in a satisfactory way. Specific additional examples are given below.

- Finding new problems/issues: this includes phenomena-finding like fluid velocity reversal in rod bundle with split-type mixing vane grids;

- Reducing conservatism: specifically in relation to local phenomena like occurrence of CHF or DNB conditions and formation of crud layer over fuel pins (so-called CILC occurrence);

- Developing/Improving models: examples are constituted by “weak” models used by SYS TH codes like those used for two-phase critical flow (TPCF) (e.g., Guyot et al., 2016) or for heat transfer in highly time-dependent transient conditions (RIA) (see e.g., Baudin et al., 2016).

- Explaining the reason/causes: one example is to analyze and measure the void fraction at the inlet of an electric submersible pump (ESP) and the effect of the gas in the head delivered by the first stage of this pump (Pineda et al., 2016).

- Providing data that would be used in other analyses: examples are the coupling with other codes (Section 12.10 below), like thermal fatigue, formation of crud. In this connection a right balance should be achieved between detail level requested and level of detail (complexity, cost, and qualification) available from CFD

analysis.

○ Evaluating CFD: this means to evaluate other CFD results with higher level turbulence simulations, e.g., achieved by HPC or by the application of LES level turbulence models; within the same framework, for a specific problem this implies evaluating the results from lower level turbulence models (such as steady RANS) or enabling the improvement of them by a priori and a posteriori tests.

• Variety of problems: The variety of problems which can be addressed by CFD analysis includes the following (only representative examples are given) analyses of:

○ Single-phase/multiphase;

○ Chemical reaction;

○ Conditions ranging from supersonic flow with shock waves to low-Froude-number buoyant jets or mixed convection are possible

○ Natural convection;

○ Fluid-structure interaction (FSI);

○ Steam generator tube vibration;

○ Fuel rod wear due to grid-to-rod fretting (GTRF).

• List of NRS single-phase problems. A list of nuclear reactor safety issues of interest for CFD applications is derived by a recent document published by OECD/NEA/CSNI (OECD/NEA/CSNI/R(2014)3, 2014). The list includes:

○ Boron dilution (DBA conditions);

○ Mixing: stratification/hot-leg heterogeneities (NPP normal operation conditions), also multiphase conditions;

○ Heterogeneous flow distribution (e.g., NPP normal operation conditions in SG inlet plenum causing vibrations, the analysis of HDR experimental data, etc.);

○ BWR/ABWR low plenum flow (NPP normal operation conditions), also multiphase conditions;

- Pressurized thermal shock, PTS, (DBA), also multiphase conditions;
 - Induced break, e.g., by pipe whip or missile generated by the break of components like main coolant pump (DBA);
 - Thermal fatigue, e.g., caused at any T-junction (NPP normal operation conditions);
 - Hydrogen distribution (BDBA), also multiphase conditions;
 - Chemical reactions/combustion/detonation (BDBA), also multiphase conditions;
 - Special considerations for advanced (including gas-cooled) reactors (DBA/BDBA), also multiphase conditions.
- Difficulties in nuclear thermal fluid problems. When we apply the CFD methods to nuclear thermal fluids problems, we encounter several difficulties, as discussed by Boyd (2016):
- Complex geometry: This makes it difficult to generate computational grids and cause the computational load. In general, the geometry is simplified; however, to ensure the reliability of the simplified geometry results, additional efforts are required.
 - Uncertain and complex flow behaviors.
 - Uncertain boundary and initial conditions.
 - Lack of benchmark data (CFD grade, full-scale data).
 - Lack of similar research and references.
- Reactor core performance-related challenging problems. A nonexhaustive list includes pellet-clad interaction (PCI), grid-to-rod fretting, crud formation (CILC), cladding integrity in case of reactivity insertion accident (RIA), cladding integrity in case of loss of coolant accident (LOCA), namely when challenged by the occurrence of ballooning, occurrence of departure from nucleate boiling, (DNB) phenomenon. Reference literature related to listed topics is given by, see e.g., Kothe et al. (2010), Kothe (2011), and Kothe (2015).
- Various aspects—Safety, Operation, Design. Detailed information can be found

in the CASL (the Consortium for Advanced Simulation of Light Water Reactors) website, see e.g., Kothe et al. (2010), Kothe (2011), and Kothe (2015). A summary list of safety aspects in nuclear thermal hydraulics, part of CASL, is given in Fig. 12.1.

Various Standpoints. Stakeholders in the area of CFD can be listed as follows: CFD User Community (Utility Owner-Operators, Reactor Vendors, Fuel suppliers, Engineering providers, and National Laboratories), Regulatory Authority, Universities and Research Laboratories, and Public.

Safety	Operating	Design
<ul style="list-style-type: none">• DNB safety limit• Reactivity coefficients• Shutdown margin• Enrichment• Internal gas pressure• PCMI• RIA fragmentation• Non-LOCA runaway oxidation• LOCA: PCT, oxidation, H release, long-term cooling• Seismic loads• Holddown force• Criticality	<ul style="list-style-type: none">• DNB operating limit• LHGR limit• PCI• Coolant activity• Gap activity• Scurie term• Control rod drop time• RIA fuel failure limit	<ul style="list-style-type: none">• Crud deposition• Stress/strain/fatigue• Oxidation• Hydride concentration• Transport loads• Fretting wear• Clad diameter increase• Cladding elongation• Radial peaking factor• 3D peaking factor• Cladding stability

Fig. 12.1 CASL: list of safety, design, and operational aspects in nuclear technology relevant to CFD (Kothe, 2015). Courtesy of Oak Ridge National Laboratory, U.S. Dept. of Energy.

• Operational and Safety Issues limiting reactor performance. Recent orientations for NRS applications can be found in the CASL DOE project in United States, as given in Fig. 12.2, Kothe et al. (2010), Kothe (2011), and Kothe (2015). Phenomena expected within the DBA in water-cooled reactor are proposed by OECD/NEA/CSNI and listed in Table 12.1, see Aksan et al., 1993; the same phenomena are updated and discussed in detail in Chapter 6. Making reference to Table 12.1, phenomena in row 10 are of special interest for CFD applications.

	Power uprate	High burnup	Life extension
Operational			
CRUD-induced power shift (CPS)	X	X	
CRUD-induced localized corrosion (SILC)	X	X	
Grid-to-rod fretting failure (GTRF)		X	
Pellet-clad interaction (PCI)	X	X	
Fuel assembly distortion (FAD)	X	X	
Safety			
Departure from nucleate boiling (DNB)	X		
Cladding integrity during loss of coolant accidents (LOCA)	X	X	
Cladding integrity during reactivity insertion accidents (RIA)	X	X	
Reactor vessel integrity	X		X
Reactor internals integrity	X		X

Fig. 12.2 CASL: list of key phenomena challenging CFD applications in nuclear technology (Kothe, 2015). Courtesy of Oak Ridge National Laboratory, U.S. Dept. of Energy.

Table 12.1

List of phenomena for separate-effect tests derived from accident analysis of water-cooled reactors (Aksan et al., 1993)

- Deficiencies that CFD code validation for NRS applications frequently encounters.

Deficiencies in CFD code validation have been the target of recent activities performed within the CSNI-WGAMA framework, see e.g., OECD/NEA/CSNI/R(2014)3, (2014), Smith et al. (2015), and Bestion et al. (2016). A summary list of deficiencies is summarized as follows in those reports (not an exhaustive list and including some modifications introduced by the present author):

- PIRT for the intended application is not available in a systematic way.
- Quantified estimates of experimental (measurement error) and numerical uncertainties (approximations introduced by numerical methods) are not provided.
- Validation metrics, figures of merit, or target values for the error for the intended application are not defined.
- Experiments, selected for validation at some of the tiers, do not meet all intended requirements one would like to have on validation experiments. Since validation experiments are very expensive, experiments intended for other purpose (e.g., for the study of physical phenomena or for the development of physical models), or very old experiments performed in (today) dismantled facilities are sometimes used. The last deficiency also prevents feedback between CFD simulations and experiments.
- For some physical phenomena identified in the PIRT (when this is available) the experiments at the basis of the PIRT evaluation are not identified: in those cases, new experiments must be proposed.
- Validation simulations cannot provide information on boundaries of regions of acceptability of the conceptual model from regions where the model cannot be applied or where its application is questionable. In other terms boundary of validity for the applicability of the codes is not available.

- Main questions and issues.

Selected key questions and (unresolved) issues that should be considered by the CFD community of code and model developers as well as by users and (possibly) by end users are summarized in the following:

○ Main Question 1: From where do we start (e.g., for developing a new CFD model)? What we (e.g., CFD code-user or model developer) can do and what do we need (goal-directed activity to be performed)? Triggering statements and recommendations to address the questions in nuclear thermal hydraulics are as follows: There is no single starting point, and a wide basis of competences, information, and data is needed to start. Concerned knowledge elements must be connected among each other and should constitute a system at the end. The assimilation of information available from recognized technical literature is essential. For instance, system code-based V&V, UQ, and general CFD methodologies discussed in international agreed CSNI reports (Mahaffy et al., 2007a,b; OECD/NEA/CSNI/R(2014)3, 2014; Smith et al., 2015; Bestion et al., 2016) must be considered. Proper importance must be given to review the activity by senior experts and taking into account previous research and data. In some cases the target of activities should be limited by the statement “change unknown knowns into known unknowns.”

○ Main question 2: What are the differences in methodological approaches between CFD and other areas? E.g., CFD model development vs. experiments design, planning, and execution; CFD vs. SYS TH codes; CFD code “A” vs. CFD code “B.” A hint for addressing this question may be taken from considering the topics listed below:

(1) CFD-level experiments must be defined and planned. Experiments used to develop and to validate SYS TH codes must be considered. Phenomena (relevant to nuclear thermal hydraulics) should be targeted, possibly defining a series of intermediate targets.

(2) Specific set of experiments must be planned for CFD code validation: those experiments must be independent from experiments used or considered to develop the CFD models.

(3) System codes V&V and UQ must be considered.

(4) An attempt should be made to define the meaning of CFD scaling. Possibly, the scaling activities performed in relation to SYS TH codes (see e.g., ongoing efforts by CSNI and ASME) should be considered.

(5) etc.

○ Main Question 3: What do we need to do in the future? Some recommended directions are listed below:

(1) Right goal setting: this includes distinguishing short-term and long-term targets; different (simultaneous) directions for research could reveal necessary.

(2) Goal set 1: qualitative and quantitative targets should be distinguished; this includes different acceptance methods and thresholds for results.

(3) Accumulation of experience in the application of specific methodologies, like BPG: Develop problem-specific BPG as many as possible and consider knowledge management techniques.

(4) Collaboration (understanding) is needed among experts of different physics: neutronics, fuel performance analysis, reactor kinetics, chemistry, system code, structural mechanics, etc.

(5) Collaboration is needed among CFD users and analysts: the round robin benchmark exercise is recommended.

(6) Goal set 2: Active (CFD main solver) and passive applications (CFD parts) are concerned: for instance, without considering 3D effect and local effects, the results can never be accurate.

(7) An “open system” should be designed and constructed where the accumulation of experiences, the collaboration among CFD players, and the accessibility of data are possible. This should imply not only the form (e.g., web-based, hypertext) but also the contents (e.g., provide a common methodology and share results of interest). Furthermore, it may be impossible to explain all the reasons of respective selections, but selected experiments should be shared as well as experienced in considering those experiments within the model development and validation processes. The assumptions at the basis of the methodologies should be made known. The reasons for good results with main factors to produce them should be explained. The question “Bad results, why?” should be asked frequently; what was not considered should be revealed. Great courage is required to do these!

(8) Implicit knowledge should be changed into explicit one.

(9) The importance of experts should be increased as well as their impact upon the conduct of activities: suggestions by senior experts may save years of failing

attempts to get solutions for given problems.

(10) More understanding in physics is definitely needed (e.g., turbulence dissipation, pressure drops at geometric discontinuities).

(11) More understanding of CFD methods including numerical solution methods and the interaction between those methods and the computer features is needed.

12.7 CFD methods

12.7.1 CFD procedure

A typical procedure for performing CFD analysis is given in Fig. 12.3.

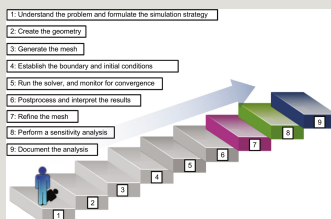


Fig. 12.3 Typical CFD analysis procedure, Faragher, 2004.

- Procedure of CFD NTF applications (NRS issues). The topics for performing CFD applications indicated in Fig. 12.3 are further discussed in this paragraph. When a problem (rather, an issue) for CFD application is assigned, related phenomena identification (PIRT) should be performed. The problem definition requires the identification of the CFD role. Then CFD methodologies (physical models) should be selected and related assessment should be planned: this may require the availability of CFD-grade benchmark experiments and suitable/applicable V&V and UQ procedures. Review of results should be planned. Implications of results should be considered. Problem-specific BPG should be used and experience from their application should be documented. However, V&V and UQ procedures are not so simple: phenomena are mixed and occur simultaneously in the reality; some phenomena may simply be unknown, especially for emerging issues or new applications; CFD needs, e.g., boundary and initial condition values may not be consistent with available information; few CFD-grade experiments are available; no efficient CFD-level V&V and UQ procedures exist, so far; BPG application is resource and time consuming, i.e., beyond what is available; scaling

issues should be identified and addressed. In addition, according to Boyd (2016), a general procedure for the CFD applications to the nuclear thermal fluids problems can be summarized as follows: First, the key phenomena should be clarified because this step critically affects the selection of the CFD models. Especially for an emerging issue, this step is very important. Next, the selected CFD methods or models become a CFD methodology for the problem. A thorough assessment for the selected CFD methodologies should be performed. The verification and validation and uncertainty quantification are key parts in the assessment step. Feedback by trial and error and the multitude of V&V can establish best practice guideline specific for the problem.

12.7.2 Problem definition and identification of CFD role

The following additional items should be considered when a coupled CFD/SYS TH code application is planned (Bestion, 2012).

- Identification of important flow process. The following steps are undertaken when a coupled CFD/SYS TH code application is performed: (1) Identification of the target basic process of interest in the reactor system, (e.g.,) fluid temperature field in a component, clad temperature, local heat transfer, mechanical load on some structure, velocity field in a component, system peak pressure, etc.; (2) Identification of the other basic processes expected in the process of interest; (3) Identification of the main nondimensional numbers, which characterize the important flow process; (4) Identification of space and time domain of interest for the concerned; (5) Identification of two-phase flow characteristics and kind of two-phase flow regime likely to occur in the domain of interest; this should also include the number and the kind of expected separate fields; (6) Identification of the fluid motion nature, i.e., steady or transient; in case of transient, the minimum timescale of interest should be identified; (7) Fixing the minimum space scale of interest in the process.
- Isolation of CFD issues. First, the CFD computational domain and the boundary conditions (also initial conditions) are defined: examples of computational domain in RCS: RPV lower plenum, RPV downcomer, cold leg (e.g., to solve PTS problems), and SG tube. Second, the issue of Boundary and Initial Condition (BIC) needs to be addressed: this may be a complex step and different solutions are possible, e.g., one-way/two-ways coupling. Third, the sources of uncertainty should be identified. Any of the steps above may have large effect on the CFD results.
- Features of Nuclear Thermal Fluids (NTF) problems: All problems in nuclear

field involve fluid and/or heat transfer. Therefore the following issues should be addressed:

- Geometry: this is typically “large,” “complex,” and “multiscale” (i.e., with phenomena expected in the range from mm to m).
- Flows: complex three-dimensional flows are expected. The flow nature can be steady (time independent) and/or unsteady (time dependent). Multiple flow physics are concerned: in relation to heat transfer, natural, mixed and forced convection; in relation to flow motion, laminar, turbulent, and transition flows; in relation to the number of phases, single-phase and multiphase (having a variety of flow regimes); in relation to the number of components, single and multicomponent flows (e.g., various gases moving in the same space region); in relation to fluid properties, incompressible and compressible flows. One difficulty comes from observing that all the listed conditions may occur simultaneously for the simulation of a unique phenomenon.
- Multiple physics: the following areas are involved: chemistry (corrosion), neutron physics, and structural mechanics (e.g., fluid-structure interaction, fatigue).
- CFD Boundary/Interface conditions. Related to CFD analysis within a coupled CFD/SYS TH computational framework, the following problems occur: (1) lack of data: more details are needed for a 2D analysis than for a 1D; (2) 2D and 3D situations imply more difficulties in gathering experimental data suitable for validation than in the case of 1D; (3) sensitivity analysis and uncertainty evaluation techniques and approaches; (4) when the governing equations change (case of CFD analyses), problems at the interface can occur: e.g., in open and porous medium approach, the interface between REV-averaged equation and RANS equation may reveal inconsistent; in Zonal Hybrid RANS-LES models problems are expected at the interface between RANS and LES regions.
- Multiphase interface. In multiphase modeling, large difference in results may occur, depending on whether the interface is treated statistically or deterministically: the statistical approach requires a large modeling effort; the deterministic approach typically requires enormous CPU resources.
- Simplification. The simpler is the model and the approach, the easier is the validation process. However, basic assumptions (simplifications) need justification, e.g., that the simplification would not affect the main physics. Then we have to know what the key phenomena are and what mechanism is important a priori (i.e., before performing the analysis). Furthermore, the effect of simplification should be

traceable during the entire code application.

12.7.3 Selection of physical models

- Selecting basic model options for two-phase flow CFD application. In the case of two-phase flow application, Bestion (2012) proposes the following steps: specify (1) the time and space resolution of the simulation; (2) the choice of a number of fields; (3) the list of wall transfers (mass, momentum, and energy), which may play a significant role in the whole process; (4) the list of interfacial and interfield transfers (mass, momentum, and energy) which may play a significant role in the whole process; and (5) the list of turbulent transfers (mass, momentum, and energy) which may play a significant role in the whole process;

- Selection of physical models in CFD NTF applications. The following items should be considered:

- Understanding of physical phenomena involved and understanding of CFD models and capabilities: the phenomena should be consistent with the capabilities of the models.

- Physical models that are expected (i.e., known) to capture the main physical phenomena must be available.

- Single-Phase CFD: The most important methodological factors in the single-phase CFD are turbulence model and computational grid. We may consider the following unavoidable steps or options in relation to turbulence modeling.

If we start from Navier-Stokes equations we have (standard symbols are used, see also Chapter 5):

$$\alpha = \frac{A_g}{A_g + A_l} \quad (12.1)$$

Filtered or time-averaged Navier-Stokes equation:

$$1 - \alpha = \frac{A_l}{A_g + A_l} \quad (12.2)$$

Putting $x = \frac{W_g}{W_g + W_l}$ and rewriting:

$$1 - x = \frac{W_l}{W_g + W_l} \quad (12.3a)$$

$$W = W_g + W_l \quad (12.3b)$$

or

$$G = \frac{W}{A} \quad (12.3c)$$

where

$$D_h = 4A/p$$

Note:

Reynolds decomposition (for time-averaging only) gives:

$$Re = \rho \times v \times D_h / \mu \quad (12.4)$$

Decomposition of variables:

$$Fr = v / \sqrt{(g \times L)}$$

If we start from momentum equation:

$$W_g = A_g \rho_g u_g = W \alpha \quad (12.5)$$

Filtered or time-averaged Navier-Stokes equation:

$$W_1 = A_1 \rho_1 u_1 = W (1 - \alpha) \quad (12.6)$$

Rewriting, we get:

$$\text{Heat flux} = -K(\text{temperature gradient}) \quad (12.7)$$

For RANS, overbar means time averaging. Introducing the Reynolds

decomposition:
$$q'' = -K \nabla T$$

$$q'''(r,t) - \nabla q'' = \delta / \delta t (\rho c T) \quad (12.8)$$

RANS equation:

$$q'''(r,t) - \nabla (-K \nabla (T(r,t))) = \delta / \delta t (\rho c T) \quad (12.9)$$

For LES, overbar means filtered integration.

Filtered equation:

$$\overline{q'''}(r, z) = K_f \Sigma_f \Phi(r, z) \quad (12.10)$$

Some of the possible (multiple and theoretically based) directions for CFD solutions-calculations-applications can be understood by comparing Eqs. (12.3c), (12.6), (12.9), and (12.10).

12.7.4 Turbulence models

The following statements provide a picture in relation to turbulence models, e.g., see mainly Smith et al. (2015), then, Rotta (1972), and Roelofs et al. (2013).

- CFD simulations of NRS problems almost always involve turbulent flow conditions. However, laminar situations may occur (even for short time) during the simulation of a “turbulent scenario” (e.g., flow reversal conditions in RCS).

- The turbulence community has assembled and classified a large selection of generic flow situations (jets, plumes, flow through tee junctions, swirling flow, etc.), and made recommendations of which turbulence models are most appropriate. Care is needed to ensure that in NRS applications the turbulence model has been chosen appropriately.

- CFD is not capable, for the time being, of modeling entire reactor systems, which means that sections of the system must be isolated for CFD treatment. The range of scales can be large (e.g., in containments), and/or the flow phenomena rather special (e.g., ECC injection). It is necessary to extend the database of recognized flow configurations to include those particular conditions and build a suitable validation database.

- In most industrial applications of CFD, RANS models are employed. However, due to the averaging procedure, information is lost, which has to be fed back into the equations via an appropriate turbulence model. The lowest level of turbulence models offering sufficient generality and flexibility are two-equation models. They are based on the description of the dominant length and timescale by two

independent variables. More complex models have been developed, and offer more general platforms for the inclusion of physical effects. The most complex are second moment closure (SMC) models. Here, instead of two equations for the two main turbulent scales, the solution of seven transport equations for the independent Reynolds stresses and one length (or related) scale is required.

○ The challenge for the user of a CFD method is to select the optimal model for the application at hand from the models available in the CFD method. It is not trivial to provide general rules and recommendations for the selection and use of turbulence models for complex applications. Two equation models offer a good compromise between complexity, accuracy, and robustness. The most popular models are the standard k - ϵ model and different versions of the k - ω model. However, the latter shows a severe free-stream dependency, and is therefore not recommended for general flow simulations, as the results are strongly dependent on the user input.

○ An important weakness of standard two-equation models is that they are insensitive to streamline curvature and system rotation. Particularly for swirling flows, this can lead to an overprediction of turbulent mixing and to a strong decay of the core vortex. There are curvature correction models available, but they have not been generally validated for complex flows. On the other hand, SMC models are much less robust; they are often recommended to perform a first simulation based on the k - ϵ model and use this as a starting point for the SMC approach. However, such an approach is hardly feasible for transient simulations, which are usually required for NRS applications.

○ The first alternative to RANS is URANS (Unsteady RANS) or VLES (very large eddy simulation). The former is more descriptive of the actual technique of application: i.e., to carry out an unsteady RANS analysis, even if the boundary conditions are steady. Thus, if steady-state RANS calculation does not converge, it may be that some unsteady behavior is present in the flow, such as periodic behavior, plume or jet meandering, and vortex shedding. A URANS calculation can often identify the unsteady component, but it has to be remembered that averaging over all turbulence scales remains implicit in the method, and may not be appropriate to reliably capture the nonsteady phenomena.

○ The amount of information to be provided by the turbulence model can be reduced if the large time and length scales of the turbulent motion are resolved explicitly. In LES, the equations are filtered over the grid size of the computational cells. All scales smaller than that provided by the resolution of the mesh are modeled using a suitable subgrid scale (SGS) model, and all scales larger than the

cells are computed explicitly. Away from boundaries, LES appears trustworthy, even with very simplistic SGS models, such as Smagorinsky. In the wall regions, pure LES becomes very inefficient due to the need to scale the lateral dimensions in the same way as in the normal direction to capture the smaller scale eddies. This is not necessary in RANS because the mean flow parallel to the wall changes much less abruptly than in the normal direction. Also, lack of sophistication of the SGS models may be tolerated in the bulk flow, but near walls the SGS stresses become much more important, and need to be accounted for accurately.

○ An alternative to a full LES application is to entrust the entire boundary layer treatment to a RANS model for the “attached” eddies and only use LES away from the walls where the eddies are “detached.” This approach has become known as detached eddy simulation (DES) and leads to considerable savings in CPU time. The case for continued use of LES in near-wall regions, probably in combination with a more complex SGS model, has to be judged in terms of possible information lost using DES versus the extra computational effort. This remains an active research area, particularly in the aerospace industry.

○ The scale-adaptive simulation (SAS) model is a hybrid approach similar to DES, but operates without an explicit grid dependency. The controlling parameter is the ratio of the turbulent length scale L , for example, derived from the two-equation k - ϵ RANS model of Rotta (Rotta, 1972) and the von-Karman length scale L_vK , which is determined in the usual way from the first and second velocity gradients. In regions where the flow tends to be unstable, L_vK is reduced, increasing the length scale ratio, L/L_vK . This leads to a reduction in the eddy viscosity. The flow will become more unstable, and hence transient in these regions, with vortices down to the scale of the local grid size being resolved, resulting in a LES-like behavior. In stable flow regions, L_vK remains large, which leads to high values for the eddy viscosity. In these areas, the model acts like a RANS model. Due to the model's ability to resolve the turbulent spectrum, it is termed a “scale-adaptive simulation” model. It has similarities to the DES model, but has the advantage that it is not based on the local grid size and therefore avoids grid sensitivity problems.

○ As way of illustration, the picture in Fig. 12.4 shows how each approach to turbulence modeling is expected to capture an instantaneous velocity signal, produced experimentally or using direct numerical simulation (DNS).

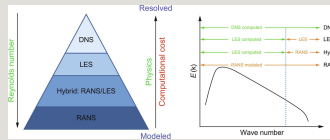


Fig. 12.4 CFD modeling approaches (Roelofs et al., 2013).

○ As a general observation, LES simulations do not easily lend themselves to the application of grid refinement studies, for either the time or space domains. The main reason is that the turbulence model adjusts itself to the resolution of the grid. Two simulations on different grids may not be compared by asymptotic expansion, as they are based on different levels of the eddy viscosity and therefore on a different resolution of the turbulent scales. From a theoretical standpoint, the problem can be avoided if the LES model is not based on the grid spacing but on a prespecified filter width. This would allow grid-independent LES solutions to be obtained. However, LES remains a very expensive approach to turbulence modeling, and systematic grid and time step studies too prohibitive, even for a prespecified filter. It is one of the disturbing facts that LES does not lend itself naturally to the application of BPGs.

○ Note: when the laminar and turbulence transitions exist, large-scale unsteady flow conditions occur (e.g., flows in a tight rod bundle), causing specific problems in modeling.

12.7.5 Characterization of turbulent situations

Various turbulent situations may occur. An attempt is made below to characterize some situations.

- Turbulent flow types/classifications (1): Depending on turbulent flow types, suitable turbulence models are different. The model may depend on whether the flow is stable or unstable and whether the unstable flow is local or global (see e.g., Menter, 1992; Menter, 1994; Menter and Esch, 2001; Menter et al., 2003a; Menter et al., 2003b; and Menter and Egorov, 2005). However, it is not easy to categorize turbulent flows in many NTF problems; coexistence of several types of turbulence situations affecting one another may occur. Steady RANS can be used to scale or to resolve different turbulent situations.

○ Example: difficulties in classifying the turbulent flow type in NTF problems, the T-junction mixing problem.

The flow condition in the case of T-Junction is not easily categorized into one of

the three recognized groups: stable, globally unstable, and locally stable. In principle, it can be computed with SAS and DDES models in SRS mode. This means that the instability in the interaction zone between the two streams is sufficiently strong to generate unsteady resolved turbulence. However, it was also observed that these simulations are extremely sensitive to the details of the numerical method employed or the shielding function used. The SAS model provided “proper” solutions only when a pure Central Difference scheme was selected, but went into URANS mode in the case of the Bounded Central Difference scheme. The DDES model provided correct solutions when a nonconservative shielding function is used but produces only weak unsteadiness in the case of a conservative shielding function. It is therefore recommended to apply the ELES model, where modeled turbulence is converted into synthetic resolved turbulence in both pipes upstream of the interaction zone at predefined RANS-LES interfaces. In addition, the turbulence model is switched from SST to WMLES at these interfaces. This then avoids the need for the flow instability of the interacting streams to generate resolved scales (Menter, 1994).

- Turbulent flow types/classifications (2): One choice may be to consider the issue both for single and global effects. Indeed, the rather complex configurations arising in industrial situations have led people to consider canonical situations that may be identified in industrial flows.

(1) The first level of complexity consists of flows dominated by a single and identified phenomenon and a single and identified regime for a given identified geometry. Usual isolated effects lead to the consideration of: simple shear flows (attached shear flows (boundary layer, wall jet); free shear flows (mixing layers; wake; plume, plane or round jets); impinging flows. The related regimes may be stably (unstably) stratified flows, flows dominated by buoyancy leading to mixed or natural convection, or forced convection. Geometries are rather simple ones and may refer to canonical configurations including plane wall; round tube; plane or round jets; the related flows are driven by a nearly two-dimensional strain.

(2) The second level of complexity includes configurations with secondary flows, and configurations with a strong coupling between turbulence and another key physical phenomenon such as rotation or chemical processes (e.g., combustion). This also includes flows with strong turbulence state variation (transition between laminar and turbulence state or occurrence of unsteadiness that cannot be considered as fully developed turbulence).

(3) Strong Unsteady Flows: The two previous items mainly refer to steady flows. More complex flows involve strongly unsteady flows for which the timescale of

variations is of the order of turbulence time. Unsteadiness may originate from unsteady boundary conditions; from flow separations, from coupling between turbulence, and from other phenomenon (e.g., acoustics or material vibrations). These circumstances are seldom compatible with the hypotheses of turbulence modeling and the predictive capacity of this latter will be very difficult to access, see e.g., Mahaffy et al. (2007a,b) and OECD/NEA/CSNI/R(2014)3 (2014).

- Coexistence of turbulent and laminar flows and turbulence-laminar transitions. T-junction mixing problems with low ratio of branch to main pipe flow rate may occur when branch flow is due to the leak from the valve. In these conditions the flow in branch pipe is laminar and the main pipe flow is turbulent. Laminar to turbulent transition occurs around the mixing zone. For modeling purposes, turbulence model should cover laminar, turbulent, and transition regions. In such situation: (a) if one applies the Smagorinsky SGS model, even if the flow is laminar, the second invariant of the strain rate tensor is large near the wall and the eddy viscosity exists; (b) in WALE model, in pure pipe shear flows, the eddy viscosity vanishes (this situation is ensured only in the simple pipe-like flows: for laminar flows with complex 3D velocity gradient this is not ensured; in this case, dynamic turbulence model should be considered).

- Wall function. Wall function is based on the streamwise flows in attached boundary layer parallel to the channel wall; thus, when flow separation or impinging occurs we cannot ensure the accuracy of the results. For these cases, strict evaluation should be performed. Note that it does not necessarily mean that the wall function does not work for these cases (e.g., for the rod bundle problem the pressure loss across the grid can be predicted accurately using the wall function). Definitely, the important point when we evaluate the wall function is to use right condition for the first y^+ .

- Statistically steady (stable) vs. unsteady (unstable): Although turbulent flow is unsteady, steady RANS model can be successfully applied to problems with statistically steady turbulent flows (or stable flows). However, there is a region where large-scale unsteady flow is dominant and is related to target region and variables. In these cases, we should consider unsteady turbulence models. For globally unstable flows, even unsteady RANS can capture the physics, but shows large errors. For locally unstable flows RANS cannot capture the unstable flows, thus requiring the use of scale-resolving simulation models (SAS, Hybrid RANS-LES, LES);

- 3D CFD models (Bestion, 2008):

The question marks arising for identifying and classifying CFD models can be

derived from Fig. 12.5.

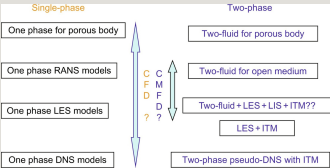


Fig. 12.5 Classification of 3D CFD models (Bestion, 2008).

• Two-phase CFD. According to Bestion (2012), two-phase CFD is a promising way for extending the simulation capabilities for many nuclear reactor thermal-hydraulic issues. However, this is a rather new technology and a long effort is still required before reaching a good maturity and reliability of the tools and application methods. Various methods exist and many modeling options are offered to users but only some combinations of options constitute physically consistent approaches, see e.g., Fig. 12.6. Scientists who wish to develop new applications of two-phase CFD and analysts who must evaluate these applications should consider the classification of various modeling approaches. Clear identification of the simplifying assumptions and range of applicability of each approach and consistency checks are needed. Specific checklists for applications of two-phase CFD to nuclear reactor thermal-hydraulic issues are needed (e.g., considering Fig. 12.6).

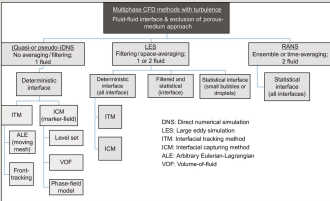


Fig. 12.6 A view of multiphase CFD methods (Bestion, 2012).

12.7.6 Coupling

In many nuclear thermal hydraulics application the CFD codes and models are applied (and are applicable only) in combination with other numerical tools

including primarily SYS TH codes. This originates the issue of “coupling” discussed below. Multiphysics and/or multiscale coupling can be considered.

○ Multiphysics coupling. Examples are (i) neutron physics and CFD in core analysis; (ii) crud deposition and growth: CFD, chemistry, and (possibly) neutron physics are needed; (iii) T-junction mixing: CFD and structural analyses should be connected. What is needed in those situations is a clear understanding of the CFD roles (as already mentioned in the text above).

○ Multiscale coupling. CFD codes' capabilities in predicting mesoscale phenomena may be linked to SYS TH codes capabilities in predicting macroscale phenomena. As already discussed above in this chapter, this needs: (i) identification of space region in RCS or RPV for CFD application; (ii) identification of CFD computational domain and/or CFD isolation; (iii) identification and characterization of BIC. The characterization of BIC may reveal a problem because information needed for CFD running is not available for the space outside the CFD computational domain (BIC affects noticeably the CFD results into the CFD domain).

○ Multiscale and multiphysics coupling. This is the combination of the above two.

- Example-1, notes in multiphysics coupling – CFD application range. In crud modeling problem, CFD plays a role in providing rod surface temperature. The typical assumptions used are that flow is single-phase and the geometry change due to crud deposit growth is negligible. However, the surface roughness and the equivalent diameter of the region may change with the presence of crud. This may affect flow pattern, pressure drops, and local heat transfer coefficient, and thus local temperature field. All of this may also generate secondary flows (the circumferential gradient of axial velocity generates the secondary flows) which may not be considered by the application.

- Example-2, nuclear reactor core behavior. The following areas are concerned: neutron physics, thermal fluids (CFD part), fuel performance, chemistry, crud formation and induced Corrosion, CILC, structural mechanics, materials, and reactor physics (including core control). A synthetic outline of the concerned topics can be derived from Figs. 12.7 and 12.8 (Kothe et al., 2010; Kothe, 2011; Kothe, 2015).

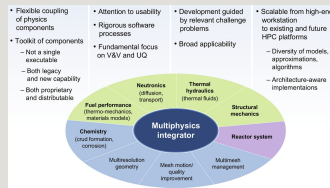


Fig. 12.7 The CASL virtual reactor: a code system for scalable simulation of nuclear reactor core behavior (e.g., Kothe, 2015).

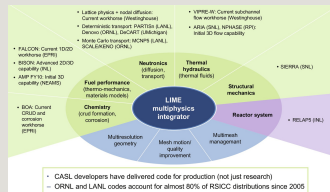


Fig. 12.8 The CASL virtual reactor (VR) builds on a foundation of mature validated and widely used software (e.g., Kothe, 2015).

12.7.7 CFD assessment: V&V and UQ

• V&V

International or National institutions (in the latter case, looking at an international consensus) deal with V&V and UQ, see e.g., the three elements diagram in Fig. 12.9 (AIAA, 1998).

Performance-based V&V capability. It is infeasible to apply system code level V&V strategies to CFD. New methodologies are required. When planning a “new” V&V methodology, for any code prediction, the first question one might ask is whether or not we can trust the prediction for the intended purpose. The issues outlined above provide some of the areas where legitimate questions regarding the validity of the solution must be explored. When dealing with problem-specific models with a history of benchmarking and analysis, other concerns can be outlined. If compromises or simplifications are needed for a practical solution and assumptions are made to fill gaps in one's knowledge about boundary conditions or modeling approaches, what is the impact on the final results? All of these concerns, as well as concerns related to verification, such as ASME standard V&V 20 (ASME, 2009) provide methods for estimating uncertainties but are very expensive to follow for large and complex scenarios. In some cases, the test data sufficient for the task of validation are not available and it is common for compromises to be

made in the area of verification and validation. Estimates of uncertainty are commonly limited in scope and based on only a subset of potential uncertainties. It can be difficult to determine whether or not the predictions are adequate if the uncertainty is not quantified. Methods to determine whether or not a code is adequate for a given analysis and the methods for determining the uncertainty are common considerations for nuclear safety analysts (e.g., see Theofanous et al. (1984), Nourbakhsh and Banerjee (2013), and Banerjee (2013)). When discussing these methods for CFD applications, additional practical concerns come into play. Many analyses are completed using large computer systems and significant amounts of CPU time. Methods to propagate uncertainties with systematic approaches such as Monte Carlo methods or even the more efficient Latin Hypercube sampling approaches can become impractical for many CFD models due to the large computational requirements. Efficient techniques to estimate uncertainty for nuclear safety CFD analyses need to be demonstrated (Boyd, 2016).

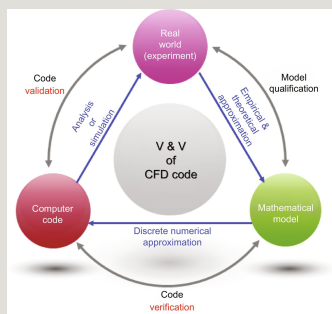


Fig. 12.9 Verification and validation (V&V) in CFD (AIAA, 1998).

• UQ

Discussion about UQ for CFD calculation started more recently within the international community. Elements and descriptions of activities in progress can be derived from Bestion et al. (2016).

12.7.8 CFD experiments

- Overview of experimental data for validation. The following checklist applies (Bestion, 2012).

- (1) Check whether available experimental data cover all basic flow processes

identified in phenomena-identification process. If required, plan and design new experiments to cover all processes.

(2) For two-phase flows, check that the available experimental data cover all important wall transfers, interfacial transfers, and turbulent transfers identified in phenomena-identification process. Check that they can be used to validate all important transfer models in a separate effect way. If required, plan and design new experimental programs in order to be more exhaustive.

(3) Check that the instrumentation and the experimental tests provide enough information to get initial conditions and boundary conditions for the simulation.

(4) Check that the instrumentation and the experimental test provide sufficient local information on flow parameters of interest to validate closure laws for wall, interfacial, and turbulent transfers identified in the phenomena-identification process.

- Identification/definition of CFD-grade experiments. CFD grade experiments are performed having in mind the CFD validation. Those experiments should be discriminated from other purpose experiments like those aiming at physics developing correlations and system code validation (1D model). CFD-grade experiments must use nonintrusive techniques: LDV, PIV, and PTV techniques and instruments are assumed to be available.

- Geometry is a key issue. Specific issues are: (1) test section size; (2) boundary condition measurements (e.g., 2D field data, mean and turbulence information needed); (3) measuring regions and variables (target region and variables; figure of merits); (4) field data may be needed; (5) test conditions (real vs. measurable).

- Note-1: Simplification in designing experiments may not be simple: oversimplification can sometimes make problem more challenging to the CFD method (see the discussion below in relation to EPRI-NESTOR benchmark. Wall effect may become important in a reduced size test section, e.g., wall effect in a rod bundle with mixing vane grids. (3) A stepwise approach (bottom to top) for design of experiments is desirable, but sometimes top-to-bottom approach can be efficient. Scaling issue must be addressed in both cases.

- Note-2: Different from system code scaling, local phenomenon is at the center of the attention of CFD experiments.

12.7.9 Best practice guidelines (CFD application)

The use of approved/endorsed BPG is essential in NRS applications of CFD. Additional notes are reported below.

- Problem-specific BPG (Boyd, 2016). Many problems (e.g., multiphase PTS problems) have multiple layers of interacting two-phase phenomena as well as single-phase phenomena, each with their own unique best-practice modeling approach. These types of complexities complicate the selection of models and solvers and ultimately lead analysts to pursue compromised approaches. Problem-specific best-practice guidelines can take years to develop and require updates as new methods and models are developed and tested. It is common for compensating errors to mask underlying problems in the model and these issues can cause problems when models are scaled from test facilities to full-scale conditions. These types of complexities make it difficult for a reviewer to answer the question of whether or not a CFD prediction can be trusted for the intended application.

- Acceptability of CFD prediction. NRS application of CFD to individual NPP unit (e.g., licensing process) implies the use of validated/approved methodology. In this case the well-known scaling problem comes into play and scaling capabilities shall be demonstrated for the methodology (of CFD application) other than for the results of the CFD application.

- Extrapolation/extrapolability of the CFD methodology: This is topic of current interest to the scientific community. No conclusive/meaningful statement can be provided (i.e., in addition to the qualitative identification of the issue).

- Extrapolation/extrapolability of CFD results: This is topic of current interest to the scientific community. No conclusive/meaningful statement can be provided (i.e., in addition to the qualitative identification of the issue).

12.8 Applications of CFD—Examples

12.8.1 PWR rod bundle problem—EPRI CFD round robin benchmark exercise

We consider below an example of the CFD application. This is related to flow and heat transfer in a PWR rod bundle with mixing vane grids; crud-related and DNB-related issues are concerned. Local information (hot spot) is available from experiments that only CFD can produce. Bullet items in the following summarize key aspects of the EPRI CFD round robin. The complete report can be found in EPRI (2014) and EPRI (2015).

• EPRI-led CFD round robin benchmark exercise. The EPRI-led CFD round robin benchmark exercise against the NESTOR experiment for a PWR rod bundle has been recently completed (the steps of the activity can be derived from Fig. 12.10). This project has great advantages in that (i) the round robin type validation enables us to test and compare various CFD methodological factors and thus to obtain overall insights into CFD capabilities and limitations; and (ii) the NESTOR experiment has broad-range, accurate measurements of rod inner-surface temperatures as well as flow field under the thermal-hydraulic conditions comparable to typical PWR ones. In this section, we summarize the capabilities and limitations of CFD methods (steady RANS approaches) especially for split-type mixing vane grids, based on the submitted CFD results along with NESTOR data (EPRI, 2014, 2015).

	PHASE 1	PHASE 2
	SSG bundle configuration	MVG bundle configuration
Isothermal (NESTOR-MANIVEL experiment)	Exercise 1	Exercise 1
Thermal (NESTOR-OMEGA experiment)	Exercise 2-1	Exercise 2-1
	Exercise 2-2	Exercise 2-2
	Exercise 2-3	Exercise 2-3

Fig. 12.10 Structure of EPRI-led CFD round robin benchmark.

(1) Structure of the exercise. The benchmark exercise consists of two phases depending on the rod bundle types as shown in Fig. 12.10: Phase 1 is for the SSG rod bundle with only simple support grids (SSG) and Phase 2 is for the MVG rod bundle with SSGs and alternating split-type mixing vane grids (MVGs) (Fig. 12.11). For each phase, we considered four problems—one problem for the isothermal case (MANIVEL) and three problems with different thermal-hydraulic boundary conditions (OMEGA) for the thermal case to check the consistencies of the CFD results. In this discussion we focus only on Phase 2, i.e., the MVG bundle with split-type mixing vanes.

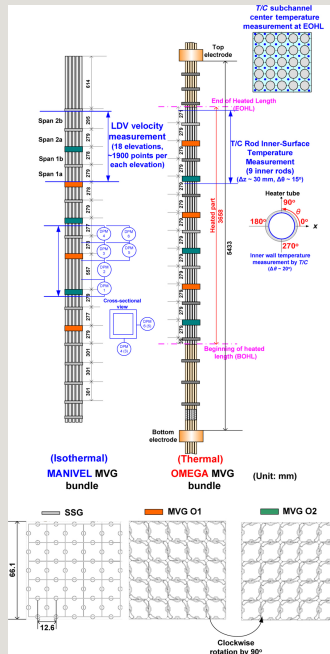


Fig. 12.11 Test section and measurement information of the MVG bundle (Phase 2) in NESTOR experiment.

(2) NESTOR experiment. In the NESTOR-MANIVEL experiment, the grid span pressure drop and the mean and RMS axial velocities were measured (see Fig. 12.11, left) and in the NESTOR-OMEGA experiment rod inner-surface temperature and fluid temperature at subchannel centers at the end of heated length were measured (see Fig. 12.11, right).

(3) Test conditions. For an isothermal problem, Reynolds numbers based on the regular subchannel hydraulic diameter (Re_{sc}) is 101,000. For thermal problems in Phase 2, Reynolds numbers based on the regular subchannel hydraulic diameter and average temperature (Re_{sc}) are in the range 450,000–580,000. Detailed thermal-hydraulic conditions are provided in the EPRI Phase 2 report (EPRI, 2015).

(4) Participants. In Phase 2, seven organizations (ANSYS, AREVA, CD-adapco, EDF, Penn State University, Texas A&M University, and Westinghouse) participated. Two commercial CFD codes (ANSYS Fluent and STAR-CCM+) and one open-source CFD code (Code_Saturne) were used as CFD solvers by the participants. They considered only steady RANS approach due to large-scale

problems in this benchmark. The Phase 2 analysis report (EPRI, 2015) provides the detailed information about CFD methods adopted.

- **Capabilities of steady RANS.** The main insight from Phase 2 round robin benchmark was that appropriate steady RANS approaches with wall function could reasonably predict two key variables in the PWR fuel rod bundle with split-type mixing vane grids—the grid span pressure loss and rod surface temperature distributions. Here, the appropriate steady RANS approach indicates that (i) fluid and solid region meshes are suitable for the complex geometry of the grid and wall-function requirement and (ii) conjugate heat transfer is considered. Also, the “reasonable” prediction specifically means that (i) the pressure loss errors for SSG and MVG spans are within about 5% and about 10%, respectively; and that (ii) the circumferentially averaged rod inner-surface temperature errors at different elevations for different rods are within $[-2$ to 3 K], Fig. 12.12B, and the RMS errors around the circumference (at different elevations for different rods) are within 2–4 K. Overall, the CFD calculations under the trim mesh with extrusion layers consistently showed good results. In addition, the effect of turbulence anisotropy was relatively reduced in the MVG wake region.

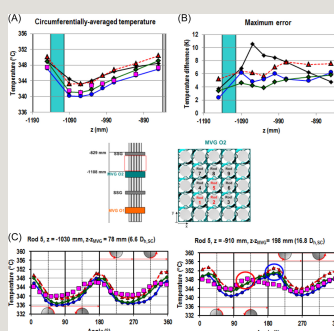


Fig. 12.12 Inner-surface temperatures around the central rod (Rod 5) in the MVG O₂ wake: (A) comparison of circumferentially averaged temperature; (B) the maximum errors of the circumferential distributions of the inner-surface temperature distribution, and (C) comparison of circumferential distributions of the inner-surface temperature at intermediate (*left*) and far wake (*right*) regions: pink symbols indicate measured data, and lines with symbols indicate CFD calculation results.

- **Limitations of steady RANS.** On the other hand, the steady RANS approaches showed limitations: (i) they could not capture well central rod circumferential temperature distribution patterns in the far wake (see Fig. 12.12 right) probably

because of the cross-flow reorientation (and dumping) due to the interaction between asymmetric, cross-flows with test section wall, and (ii) they showed quite large local maximum rod inner-surface temperature error (ranging 4–9 K with elevation), Fig. 12.12B probably because of unsteady, large-scale cross-flow fluctuation effect. In addition, it should be pointed out again that in the actual applications to PWR fuel rod bundles where the test section wall is not present except near the core barrel, the unsteady, large-scale cross-flow fluctuation effect on the circumferential temperature variation magnitude may be of greater importance than the test section wall effect on the flow pattern changes.

12.8.1.1 Experimental data

It was found that NESTOR experiment had several advantages over other experiments. The representative ones were as follows:

- It was in full-length axial domain (with fully heated length for thermal cases) comparable to the actual PWR rod bundle that CFD calculations could be directly assessed by comparing the results with data measured at upper spans (target region). As a result, it was found that steady RANS approach could provide a reasonable accuracy in this general application.
- A direct comparison of target variable, i.e., rod (inner-) surface temperature, was possible, thus providing important findings that could not or hardly be obtained by the comparison of the flow field only. They were mismatch of the patterns and overprediction of the magnitude in the circumferential temperature distribution as well as importance of conjugate heat transfer.
- Data measured over several spans enabled us to check the representativeness (consistency) of the results and phenomena.
- A typical split-type MVG (used before in industry) was adopted in the experiment; thus, the effects due to atypical geometries were reduced. For example, rod-contact structures with a cylindrical button shape in the OECD-KAERI CFD benchmark (Smith et al., 2013) induced stronger unsteady effect (vortex shedding) than that expected in typical spring and dimple structures. In fact, the Axial Turbulence Intensity (ATI) in the OECD-KAERI CFD benchmark (ATI about 0.22 at $z\text{-}z_{\text{MVG}}=1 D_h$ and about 0.14 at $z\text{-}z_{\text{MVG}}=4 D_h$) was much higher than that of NESTOR (ATI about 0.12 at $z\text{-}z_{\text{MVG}}=2.4 D_h$ and 0.09 at $z\text{-}z_{\text{MVG}}=4.9 D_h$) and Yang and Chung (1998) (ATI in the range 0.12–0.14 at $z\text{-}z_{\text{MVG}}$ about $2 D_h$ and ATI in the range 0.09–0.1 at $z\text{-}z_{\text{MVG}}$ about $4 D_h$) experiments with typical springs and dimples. Here, D_h is a test section hydraulic diameter, not an inner-subchannel

hydraulic diameter ($D_{h,SC}$).

However, the NESTOR experiment also showed several limitations for the CFD validation. The related important ones and associated recommendations are as follows:

- The asymmetrical effect due to the test section wall, which also holds for the previous, typical split-type MVG rod bundle test with a small-size (4×4, 5×5, or 6×6) array, exists. The resulting qualitative cross-flow pattern change and complex far-wake flow patterns in the experiment may not be representative of typical physics in the actual PWR rod bundle and turned out to be challenging to CFD calculations. Thus, we may need to increase our understanding of the involved physics by improved experiments as well as advanced CFD methods.

- The simple support grid (SSG) installed between MVGs for the structural integrity prevented us from seeing the phenomenon at farther wake region ($D_{h,SC} > 25$) of great interest in the real applications, such as prediction of CHF and crud deposition. However, previous experimental investigations (Yang and Chung, 1998) and CFD studies (Blowe et al., 2015; Bieder et al., 2014) showed that the vane-driven cross-flow effects reach the next grid even for a long MVG span without the SSG in the middle. The far-wake physics in the longer MVG span without the SSG should be measured and compared with CFD calculations in the future.

- Since the lateral flow field was not measured, important phenomena like swirl decay and cross-flow pattern change along the rod bundle could not be directly evaluated. The lateral velocities (covering both the gap and near-rod regions) need to be measured.

- In addition, the full-length axial domain, although it was an advantage of this experiment in that we could do the comprehensive and practical CFD assessment, prevented us from clarifying the source of discrepancies between the measurement and the CFD calculations. Especially, the spatial aperiodicity probably due to the different MVG inlet velocities made it difficult to identify whether a certain discrepancy was in common or what factors caused discrepancies. Thus, upstream (MVG inlet) flow condition-controlled experiments may be more desirable to identify and understand the related problems. For example, we can basically consider a fully developed MVG inlet condition from very long bare rod section; furthermore, we can put a long (without SSG in the middle) MVG span with 90°-rotated MVG as in a typical PWR and without MVG rotation for the reference at the upstream of the target MVG span.

Among these limitations, the first item, i.e., the wall effect in the 5×5 array test, needs to be discussed in more detail for the more realistic CFD assessment and more improved experimental design for the split-type MVG rod bundle problem in the future.

The most critical wall effect may be due to the cross-flows from inward peripheral vanes at edge- and corner-subchannels near the wall. The cross-flows generated in these regions are quite different from those in inner subchannels in that (i) they have less axial flows upstream of the vane (because they are near the wall) and thus less cross-flows and (ii) they do not have the same swirl structures as those of other inner subchannels because they only have one vane not a pair. Thus, as the distance from the MVG increases, each inner subchannel becomes affected by the wall cross-flows (different from the inner subchannel cross-flows in magnitude and pattern) depending on the vane direction and relative distance to the wall. Consequently, each subchannel has asymmetrical lateral flow patterns (swirl patterns), and the overall cross-flow pattern could change qualitatively and globally in 5×5 array test. On the other hand, considering geometrical configuration in the actual PWR rods, except rods near the barrel, rods are very far from the wall. Thus, this phenomenon may not be a representative one in the actual PWR rod bundle.

To remove or minimize the wall cross-flow effect, we can simply consider much larger lateral domain experiment; however, this seems practically undesirable. Instead, we may be able to find a way under the existing 5×5 test facility. For example, we can remove the inward peripheral vanes near the wall of 5×5 test section under the hypothesis that it is more desirable to remove the wall cross-flows than to involve wrong (in pattern and magnitude) wall cross-flows so that the lateral flow patterns in central subchannels in 5×5 test represent that at a typical subchannel in the actual PWR rod bundle. In fact, Navarro and Santos (2009) compared lateral velocity vector fields between models with and without peripheral vanes obtained from their CFD calculations. They showed that without peripheral vanes the swirl pattern in inner subchannels was maintained at the far wake (of $18D_{h,SC}$), while with peripheral vanes the lateral flow patterns were irregular at the same axial location. From this result, they argued that the case without peripheral vanes is more representative of typical inner subchannel flow behavior in the actual PWR rod bundle.

12.8.1.2 Adopted CFD methods

Now, we address lessons and recommendations about respective CFD methodological factors for typical split-type MVG rod bundle problems.

Mesh

The round robin benchmark enabled us to see the characteristics and effects of various types and configurations of mesh, which was a key advantage of this approach (Kang and Hassan, 2016). However, direct comparisons of mesh between different types and between different configurations even for the same mesh type were impossible in most cases, and the mesh sensitivity results for each submitted mesh were not reported. Furthermore, compared to the trim mesh type, limited numbers of other types of mesh were considered. Thus, it is difficult to derive detailed conclusions about the mesh.

Nonetheless, a qualitative finding was clearly observed that the calculation results strongly depended on the mesh types (rather than turbulence closure models). For hexahedral mesh considered, the pressure loss across the grid and turbulent fluctuations was largely underpredicted for both SSG and MVG spans. On the other hand, trim mesh calculations showed much more improved results of these variables. Especially RMS axial velocity fluctuations just downstream of the MVG (at $z\text{-}z_{\text{MVG}}=25\text{ mm}$) were comparable to the measured ones (see Smith et al., 2013). The dependence on the mesh type observed in this benchmark was also observed in the OECD-KAERI CFD benchmark (e.g., by Lee et al., 2014) although the vane-upstream grid structures used in OECD-KAERI benchmark were different.¹

However, this does not necessarily mean that a certain type of mesh is superior to other types of mesh. For split-type MVG problems that are characterized as (i) the high complexity in the grid region, (ii) axially large difference in the geometry complexity, (iii) vane-driven high velocity gradient in the near wake, and (iv) critical effect of in and near-grid region flows on the downstream flows, efficiently generating consistent, high-quality mesh is important. From this point of view, trim mesh (with extrusion layer) that seems able to provide consistent (less dependent on the participants) and good quality and that is less time-consuming to generate may be a good choice. On the other hand, the large discrepancies of the hexahedral mesh calculations are likely due to the strong nonorthogonality of mesh in- and near-grid regions (EPRI, 2015; Benhamadouche, 2015). The structured hexahedral mesh seems difficult to keep uniform quality for geometry with large difference of complexity in streamwise direction and at near-wall (of grid structures and vanes as well as rod) and high velocity-gradient regions.

Also, a detailed mesh sensitivity study is strongly recommended to get more detailed conclusions about mesh. For example, although the flow field results were quite similar among different participants under trim mesh, the pressure loss across the MVG ranged from -3% to 11% . Thus, we need to investigate what factors in

mesh configuration are important to improve the pressure loss results: for example, effect of the local mesh refinement in the region where the higher velocity gradient is expected and the effect of y_+ in the mesh adjacent to the grid structure (under the wall function assumption) using/adjusting the extrusion (prism) layer(s) shape and size.

Turbulence closure models

It could be inferred from the comparative results in this benchmark that the use of anisotropic model was essential in the SSG wake where the cross-flow effect was small or negligible, while it was not critical to the MVG wake where cross-flows are still effective. However, this conclusion may need to be reconsidered because of the following reasons:

- In the hexahedral mesh, the flows (both mean and RMS velocities) in- and near-grid regions were not captured well. The mean axial velocity variations at $z_{\text{MVG}}=25$ mm showed smaller than the measured ones (Smith et al., 2013; Lee et al., 2014), which may indicate that predicted cross-flows and swirls were weaker probably because of the low quality of the mesh at in- and near-grid regions. Thus, the comparison among different turbulent closure models (SSG-RSM and $k-\epsilon$ model with linear production) of the flow evolution downstream (swirl decay and cross-flow interactions) from wrong upstream flows may not be so meaningful. For a meaningful comparison between turbulence closure models, the starting point of the swirls and cross-flows should have better quality results, for example, by adopting the better quality of mesh.
- In the trim mesh, which showed better quality results than hexahedral mesh at the near wake, only linear and quadratic $k-\epsilon$ models were considered. Since quadratic nonlinear eddy viscosity models (NLEVMs) reflect only the normal Reynolds stress anisotropy effect, other Reynolds stress anisotropy effects related to the streamline curvature and swirls, which can be included by cubic terms, were not considered. Thus, the similar results between linear and quadratic $k-\epsilon$ models may only indicate that in the MVG wake, the effect of the normal Reynolds stress anisotropy is not critical.

Thus, the following recommendations can be made relating to turbulence closure models in the future research. Here, the premises of these recommendations are that mesh quality is good enough to capture the main flow physics in- and near-grid regions, and that unsteady effect is negligible.

- For nonlinear eddy viscosity models (NLEVMs), which are computationally

efficient (only marginal increase in computational time from the base two-equation closure models) and robust, we can consider the following:

○ Cubic models can be considered for more general turbulence anisotropy related to swirls and cross-flow interactions with curved wall and each other. Here, it is worth noting that we may need a recalibration process of the existing cubic models for this specific problem. Recall that that modified quadratic k - ϵ model (Baglietto et al., 2006) that showed good results for bare rod bundle problems was obtained by calibrating some coefficients in the existing SZL quadratic k - ϵ model (Shen et al., 1991) for the rod bundle geometry.

○ Different scale-determining equations (with calibrations) can be considered. Only k - ϵ model was considered in this benchmark. Use of other scale-determining equations, such as those in BSL k - ω model, may have a significant influence on the downstream flow evolution because key physics may be dictated by factors other than anisotropy of the turbulence (Gatski and Jongen, 2000).

○ Alternatively, explicit algebraic Reynolds stress models (EARSMs) (e.g., BSL EARSMS) can be considered. This is because compared to NLEVMs, which can be considered as nonlinear extensions of the ordinary LEVMs, and coefficients are determined by experimental and/or higher level turbulence model results, EARSMS, which can be considered as a truncation of RSMs, can easily combine more physics, such as nonlinear pressure-strain rate correlation models and anisotropic dissipation rate models, existing in original RSMs (Gatski and Jongen, 2000; Hellsten and Wallin, 2009). In fact, BSL EARSMS was highly ranked at near-flow field prediction in OECD-KAERI benchmark under unsteady RANS frame (Lee et al., 2014).

- Use of RSMs may be a more desirable option because their (theoretically) higher degree of universality may be more suitable for split-type MVG rod bundle problem that involves various (and even unidentified) complex phenomena although they require more computing resources than two equation-based models and are not computationally robust.

○ SSG-RSM (Speziale et al., 1991) may be more preferable than LRR-RSM (Launder et al., 1975) because the SSG-RSM is more accurate than the LRR-RSM for most flows including swirl flows (Speziale et al., 1991; Lu and Semião, 2003). Furthermore, use of an elliptic blending RSM (EB-RSM) can be considered for a better prediction of the inhomogeneous near-solid fluid behaviors (Benhamadouche et al., 2015).

○ In addition, ω -based RSM (e.g., BSL RSM) can be considered because ω -based model sometimes showed better results than ϵ -based RSM for flow separation (ANSYS, 2010).

○ It should also be noted that although RSMs (especially, SSG-RSM) were more successful than EVMs for confined swirl flows in pipe, e.g., Mimouni et al. (2008), it does not necessarily guarantee their success in typical split-type MVG rod bundle problems. This is because the former problem (Mimouni et al., 2008) is swirl decay in confined circular pipe wall and the swirl is generated by swirl-type vanes without asymmetrical upstream structures, while the latter is unconfined swirl decay within partially concave wall with neighboring cross-flows and with asymmetric structures just upstream of the vane, where other physics may be dominant.

Unsteady turbulence models

Transferring from steady RANS models to higher level unsteady turbulence models leads to an enormous increase in computational resources. Applying directly the unsteady turbulence models to actual full-scale problems seems practically infeasible. Note that most of the previous problems used in the validation of higher level turbulence models had one-order lower Reynolds number than typical PWR one. Therefore, we need enough considerations about steady RANS turbulence models before transferring to higher level turbulence models. On the other hand, in parallel with a deeper study on the steady RANS closure models, considering higher level unsteady turbulence models seems still necessary. This is because (i) they can provide better understanding of the complex rod bundle flow physics that may include strong unsteady effects that cannot be captured by steady RANS approach; and (ii) once higher-level turbulence models, such as LES, turned out to be accurate, it may be possible to calculate turbulence budget to calibrate the RANS closure models for this specific problem.

Relating to this benchmarking study, consideration of unsteady turbulence models seems necessary for some unresolved issues in a 5×5 MVG rod bundle with a typical split-type vane pair arrangement. Specifically, we need to focus on the followings when using unsteady turbulence models:

- Whether they can increase the turbulence fluctuations, especially at the intermediate and far wake regions of the split-type MVG;
- Whether they can capture the qualitative cross-flow pattern change (or circumferential distribution pattern of the rod inner surface temperature) around

the central rod;

- Whether they can reduce the amplitude of the circumferential rod inner-surface temperature distribution possibly by capturing the large-scale, unsteady cross-flow effect;
- Whether they can improve the prediction of the second peaks along the dimple line at the near wake.

However, from the previous studies (e.g., OECD-KAERI CFD benchmark), not all unsteady turbulence models showed good accuracy. Most unsteady RANS turbulence models were not so successful. Even LES showed large differences between calculations, and some LES results were worse than those from URANS or hybrid RANS-LES methods. It should be, however, pointed out that the OECD-KAERI benchmark (Smith et al., 2013) adopted different geometries from this benchmark. Especially different upstream structures (cylindrical button shape) are expected to generate the large-scale vortex shedding just upstream of the vane; thus, just downstream of the vane, low-level turbulence models, i.e., steady RANS models that could not capture such vortex shedding at all and some unsteady models that could not capture it in a right way showed larger variations than the measured mean axial velocity profile. On the other hand, the MVG with conventional spring and dimples, like MVG adopted in this benchmark, may not have such a large-scale unsteady flow structures just upstream of vane. Actually, $z_{\text{MVG}}=25 \text{ mm}$ ($2.1D_{h,SC}$), steady RANS results showed quite similar level of variations with the measured mean axial velocity profile although some peaks were missed. Thus, in this benchmark exercise, we may obtain an unsteady trend different from the OECD-KAERI CFD benchmark.

Conjugate heat transfer

It was evident that conjugate heat transfer (CHT) calculation produced more physical outer-surface heat flux in the benchmark. However, direct quantitative comparison with CHT and without CHT (i.e., with uniform outer-surface heat flux) with other conditions the same was not performed in the benchmark, which may be needed in the future work.

Near-wall treatment

Assessment of the near-wall treatment was limited in this benchmark. It was only found that wall function approach could be a reasonable option. However, the wall function approach may not be suitable for the strong flow separation and impingement of cross-flow prediction; thus, the possibility of the enhancement by

use of the low Reynolds number model can be considered.

Others

The effects of temperature-related factors, such as effects of a turbulent Prandtl number, gradient methods, like simple gradient diffusion hypothesis, SGDH, and general gradient diffusion hypothesis, GGDH, for RSMs, buoyancy, and thermal properties, may lead to slight quantitative difference, which was included in Phase 1 (EPRI, 2014) and Phase 2 (EPRI, 2015) reports under the hexahedral mesh, but not with other types of mesh. Thus, we need detailed sensitivity studies for these factors under mesh with a better quality in the future.

12.8.1.3 Concluding remarks

Several advantages of the NESTOR experiment and the round robin benchmark enabled us to find the capabilities of the steady RANS approach for full axial, 5×5 rod bundle with typical split-type MVGs by comparing several isothermal and thermal variables. An important insight about capabilities of the steady RANS approach was that appropriate steady RANS calculations with wall function could reasonably predict two key variables in the PWR fuel rod bundle with split-type mixing vane grids—the grid span pressure loss and rod (inner-)surface temperature distributions. Here, the appropriate steady RANS approach means that (i) fluid and solid region meshes are appropriate (i.e., the mesh is fully resolved and suitable for the near-wall treatment, and the mesh type is appropriate for the complex geometry of the grid), (ii) conjugate heat transfer is considered. Also, the “reasonable” prediction specifically means that (i) the pressure loss errors for SSG and MVG spans are within about 5% and about 10%, respectively; and that (ii) the circumferentially averaged rod inner-surface temperature discrepancies with elevation for different rods are within [−2 K, 3 K], and the RMS errors around the circumference (with elevation for different rods) are within the range 2–4 K.

However, the steady RANS approach could not capture well the corner subchannel center fluid temperatures at the end of heated length and central rod circumferential temperature distribution patterns in the far wake probably because of not capturing the qualitative cross-flow pattern change due to the laterally confined test section, and showed quite large local maximum rod inner-surface temperature errors (ranging 4–9 K with elevation) probably because of unsteady, large-scale cross-flow fluctuation effect.

Thus, if the purpose of simulation is to obtain the global (axial and radial) distributions of the rod surface temperature in the core, appropriate steady RANS calculations can achieve the purpose quite satisfactorily. However, if the purpose

of simulation is to obtain the accurate circumferential and axial distributions of the surface temperatures for each rod, as required in the level IV in-core crud risk assessment (EPRI, 2014), the limitations mentioned above need to be resolved.

Furthermore, we discussed the limitations of the current experiment methods as well as the CFD methods and provided the recommendations for the future research of typical split-type MVG rod bundle. Especially, for the experiment to reflect right physics and to achieve right CFD validation the effect of test section sidewall (and related inward-peripheral vanes) should be considered more carefully; and a longer MVG span without SSG needs to be considered. For CFD methods, in parallel with higher-level unsteady turbulence models (e.g., hybrid RANS-LES and LES) relating to vane-upstream structure effects, large-scale unsteady fluctuations of the cross-flow across the rod bundle, and possibly qualitative cross-flow change, more systematic RANS turbulence models (e.g., cubic NLEVMs, EARSMs, and RSMs) relating to the generated swirl decay and cross-flow interaction, were recommended.

Finally, it is worth noting that the round robin benchmark was suitable for identifying the overall characteristics and effects of CFD methodological factors, but not for accurate individual effect; thus, the detailed sensitivity study should be performed.

12.8.2 Example of nontraditional approach: LBM and IBM applications

Immersed boundary methods (IBM) and lattice Boltzmann methods (LBM) may be seen as nontraditional approaches in CFD applications (although the tradition of CFD application is not “so long”).

In particular, in recent years, the lattice Boltzmann method has been widely applied to numerous fluid dynamics and heat transfer problems as an alternative to conventional CFD methods based on the Navier-Stokes equation. This is because the LBM has advantages over the conventional methods, such as simplicity in implementation due to its simple algorithm and effective parallelization (with the domain decomposition) due to its locality. Following this trend, the LBM has started to be applied to various nuclear thermal hydraulics problems. In their work, see e.g., Fig. 12.13, Li et al. (2016), present some basic LBM applications to nuclear-related problems and provide some insights and notes.

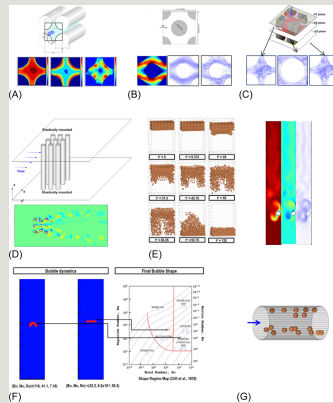


Fig. 12.13 Applications of lattice Boltzmann method: (A) flow in a rod bundle (with LES), (B) flow across a tube bundle (with LES), (C) flow in a pebble bed (with LES), (D) flow-induced vibration (with IBM), (E) particle sedimentation (with IBM), (F) bubble rising (with phase-field model), and (G) particulated flows (with IBM) (Li et al., 2016).

Key items for LBM (and IBM) applications can be summarized as follows:

- Complex geometry problems. Turbulent flows in nuclear reactor geometries can be considered for LBM (and IBM) application as an alternative or a support to Large Eddy simulation (LES).
- Moving boundary problems. Fluid-structure interaction problems and particle-fluid interaction problems are within the principle capabilities of Immersed Boundary Method (IBM). The same can be repeated for two-phase flow with phase-field flow regimes.
- Future. Various potential applications of the Lattice Boltzmann Method to nuclear thermal fluids problems can be envisaged.

12.8.3 Overall data evaluation

An overall view of experiments and CFD applications to experiments brings the following synthesis.

- Synergy of efforts. The progress in the development and the capabilities of CFD methods can be largely enhanced if an “open system” is adopted: this implies cooperation among developers of CFD methods and models as well as cooperation between experimentalists, developers, and analysts (i.e., those who apply the code), as well as experts in NRS and licensing of NPP. The cooperation should be

solid, i.e., not only in format but also in content. Namely accessibility to valued codes, models, and data should be guaranteed to the overall community of experts and an alive system should be created and operated.

- Trade-offs in CFD NTF applications. The following aspects are relevant in CFD applications to experiments: (1) Accuracy vs. Efficiency: acceptable calculation accuracy and efficiency (i.e., computational resources) are needed; this implies the definition of target accuracy; (2) Experiment vs. Numerical analysis: qualified CFD tools may substitute experiments in some cases; however, experiments are indispensable for progressing the knowledge; (3) CFD code vs. System code: synergic use of CFD and SYS TH codes appears the best choice consistent with the current state of the art; (4) Partial application vs. Entire application: this is related to CFD simulation of NPP; present CFD capabilities do not allow an “Entire” application; (5) Using results vs. Using methods: using results without knowing the method should be discouraged; method capabilities and limitations must be associated with the use of result; (6) Breadth vs. Depth: depth of analysis should be preferred to wide range investigations namely in the domain of NRS; (7) Individual vs. Collective: collective efforts are needed for a qualified application of CFD; (8) Means vs. Ends: means models and grids and related hypotheses are more important than results; results in relation to which qualification cannot be demonstrated are useless; (9) Quantity vs. Quality: quality is more important than quantity, see also item (6) above; (10) Short-term vs. Long-term: long-term effort and dedication to the effort (of producing qualified results) are more important than any short-term achievement; (11) Specific vs General: specific and general topics may have the same importance for the development of CFD technology; (10) Tradition vs. Change: the best estimate approach requires the application of the best estimate techniques; therefore change shall be preferred to tradition always, however, maintaining suitable qualification level; (11) Single-phase vs Two-phase: single-phase qualification should come first; both single- and two-phase applications are of interest in nuclear thermal hydraulics; (12) Steady (stable) vs. Unsteady (unstable) turbulence models: both steady and unsteady turbulence models are needed; however qualification of steady models should come first; (13) New design evaluation vs. Old design evaluation: quality and control of results comes (only or primarily) for old design evaluations; so applicability of CFD codes and methods should be demonstrated for old design; (14) Understanding physics vs. Safety analysis: understanding physics and understanding safety analysis constitute independent matters; both of them are essential for a suitable CFD application; (15) NTF problems vs. General CFD problems: inspiration to solve NTF problems should come from a profound knowledge of general CFD problems.

- High-Performance Computing (HPC) and new experiments. Whatever discussed above may become reality only if a suitable computational power is available as well as powerful numerical techniques fully integrated with the computer hardware characteristics. So, (i) higher numerical accuracy constitutes a moving target, (ii) numerical experiments are welcome and need to be continuously updated, (iii) reference data for lower level models are welcome even though the level should increase, (iv) new finding in physics should be expected and new basic experiments must be designed and performed (also in view of the availability of more powerful measurement techniques), (v) Improving lower level turbulence closure models by a priori and a posteriori tests is recommended.

12.9 CFD applications to nuclear thermal fluids problems

12.9.1 Introductory remarks

The status in the application of CFD methods and models to NPP technology including NRS can be derived from the series of workshop named CFD4NRS listed in the Foreword to this chapter. Key statements are reported below.

- CFD is to an increasing extent being adopted in nuclear reactor safety analyses as a tool that enables specific safety-relevant phenomena occurring in the reactor coolant system to be better described (Hassan and Smith, 2008).

- The use of computational methods for performing safety analyses of reactor systems has been established for nearly 40 years. Very reliable codes have been developed for analyzing the primary system in particular, and results from these analyses are often used in the safety assessment of nuclear power systems undertaken by the regulatory authorities. Similarly, but to a lesser extent, programs have also been written for containment and severe accident analyses. Such codes are based on networks of 1D or even 0D cells. However, the flow in many reactor primary components is essentially 3D in nature, as is natural circulation, mixing, and stratification in containments. CFD has the potential to treat flows of this type, and to handle geometries of almost arbitrary complexity. Already, CFD has been successfully applied to such flows, and to a limited extent has made up for a lack of applicable test data in better quantifying safety margins. Consequently, CFD is expected to feature more prominently in reactor safety analyses in the future.

- Computational methods have been used in the safety analysis of reactor systems for nearly 40 years. During this time, very reliable numerical programs have been developed for analyzing the primary system, and similar programs have also been

written for modeling containments and severe accident scenarios. Such codes model the reactor components as networks of 1D or even 0D cells. It is evident, however, that the flows in many reactor primary components are essentially 3D in character, as is natural circulation, mixing, and stratification in containments. CFD has the potential to numerically simulate flows of this type and to handle geometries of almost arbitrary complexity. Consequently, CFD is expected to feature more prominently in reactor thermal-hydraulics analyses in the future (OECD/NEA/CSNI/R(2014)3, 2014).

- Traditional approaches to NRS analysis, using system codes for example, have been successful because of the very large database of mass, momentum, and energy exchange correlations that have been built into them. The correlations have been formulated from essentially 1D special-effects tests, and their specific ranges of validity have been very well scrutinized. Analogous data relating to 3D flow situations are very sparse by comparison. Consequently, the issue of the validity range of CFD codes for 3D NRS applications is first to be addressed before the use of CFD may be considered as routine and trustworthy, as it is, for example, in the turbo-machinery, automobile, and aerospace industries. Assessment of the reliability of CFD methodology in NRS applications represented the primary focus of the WG2 group (OECD/NEA/CSNI/R(2014)3, 2014).

- The application of CFD to nuclear thermal fluids problems is a broad topic that is hard to deal with in a chapter. There are numerous CFD-related problems (OECD/NEA/CSNI/R(2014)3, 2014) that involve a broad spectrum of the CFD method. Hence, only addressing basic concepts of respective CFD methods can make a series of books.

- What we expect from the CFD analysis is to approach more realistic phenomena. In some cases, it is expected that more detailed 3D phenomena obtained from CFD analysis can improve previous 1D models. The CFD plays a certain role like an experiment in the 1D model development. If the CFD is more time and cost-effective for a certain phenomenon or problem than experiment, it has a clear advantage over experiment in that it can provide all detailed information within the computational domain. Another prerequisite for this application is the accuracy and reliability of the CFD methods and results. In other cases where it is almost impossible to include 3D effect in 1D frame, CFD can be a part or even a main tool in the entire analysis process for a given problem. The former case is needed when only using CFD in the entire analysis process is neither time nor cost-effective.

12.9.2 Applications of CFD

12.9.2.1 Usage of CFD: OECD/NEA/CSNI report

Selected nuclear reactor safety issues supposed to be addressed by CFD codes with or without the coupling with system thermal-hydraulics (SYS TH) codes are listed in Table 12.2 (OECD/NEA/CSNI/R(2014)3, 2014).

Table 12.2

NRS problems requiring CFD w/without coupling to SYS TH codes

--

DBA, design basis accident; *BDBA*, beyond design basis (or severe) accident;
M CPR, critical power ratio.

12.9.2.2 CFD application procedures for nuclear thermal fluids problems

A general procedure for the CFD applications to the nuclear thermal fluids problems can be summarized as follows: First, the key phenomena should be clarified because this step critically affects the selection of the CFD models. Especially for an emerging issue, this step is very important. Second, the selected CFD methods or models become a CFD methodology for the problem. Third, a thorough assessment effort for the selected CFD methodologies should be performed. The verification and validation (V&V) and uncertainty quantification are key parts in the assessment step. Feedback by trial and error and the multitude of V&V can establish best practice guideline specific for the problem.

12.9.2.3 Issues and notes

Selected issues and notes (or topics) are reported below which have already been implicit or explicit part of discussion in other parts of the chapter. The issues and notes are:

- Boundary and initial conditions are also important.

- The simpler method requires more thought and multiple assessment procedures because more empirical models are involved.
- Application scope should be clear.

Examples of CFD application scopes

- Understanding of 3D phenomena (Qualitative) evaluation of lower level code models
 - In-vessel mixing phenomenon: help identify the mixing laws used in the actual schemes (systems codes, coupled system, 3D core thermal-hydraulic and neutronics codes) in use
- For the part that needs 3D information
 - In-vessel mixing phenomenon: one could imagine integration of a CFD code into the coupled chain: i.e., system, CFD, core 3D thermal-hydraulic and neutronics codes operating together
- Main:
 - In-vessel mixing phenomenon: if the capability of CFD codes is assessed for core thermal-hydraulic simulation, one could imagine the use of CFD for lower plenum and the core, coupled to 3D neutronics codes.

Variety of problems

- Single-phase/multiphase
- Chemical reaction
- Conditions ranging from supersonic flow with shock waves to low-Froude-number buoyant jets or mixed convection are possible
- Natural convection
- Fluid-structure interaction (FSI)—Steam generator tube vibration; fuel rod wear due to grid-to-rod fretting (GTRF).

Necessity of geometry simplification

Induced break (This scenario is of direct safety relevance because it involves the potential for a steam generator tube rupture during a severe accident scenario,

which could lead to the release of fission products bypassing the containment): The complexity and expanse of the geometry to be modeled: at least one hot leg with the pressurizer surge line, the primary side of the steam generator, including both plena (inlet and outlet), the SG tubes, and possibly the vessel upper plenum.

Difficulties in nuclear thermal fluid problems (Boyd, 2016)

When we apply the CFD methods to nuclear thermal fluids problems, we encounter several difficulties:

- (1) Complex geometry: This makes it difficult to generate computational grids and cause the computational load. In general, the geometry is simplified; however, to ensure the reliability of the simplified geometry results, additional efforts are required.
- (2) Uncertain and complex flow behaviors
- (3) Uncertain boundary and initial conditions
- (4) Lack of benchmark data (CFD grade, Full-scale data)
- (5) Lack of similar research and references

12.9.3 CFD models

12.9.3.1 Single-phase model (OECD/NEA/CSNI/R(2014)3, 2014)

Applications of CFD to single-phase thermal fluids problems

The most important methodological factors in the single-phase CFD are constituted by the turbulence models and the computational grids, as already discussed in Section 12.6; see also Table 12.2. The list of NRS single-phase problems is as follows:

- Boron dilution (DBA)
- Mixing: stratification/hot-leg heterogeneities (operational) (also multiphase)
- Heterogeneous flow distribution (e.g., in SG inlet plenum causing vibrations, HDR experiments, etc.) (operational)
- BWR/ABWR low plenum flow (operational) (also multiphase)

- PTS (Pressurized thermal shock) (DBA) (also multiphase)
- Induced break (DBA)
- Thermal fatigue (e.g., T-junction) (operational)
- Hydrogen distribution (BDBA) (also multiphase)
- Chemical reactions/combustion/detonation (BDBA) (also multiphase)
- Special considerations for advanced (including gas-cooled) reactors (DBA/BDBA) (also multiphase)

12.9.3.2 Two-phase model

CFD can be applied to multiphase thermal fluids problems. The classification of Eulerian fluid dynamic simulation approaches for two-phase flows can be found in Table 12.3. The following list is based on OECD/NEA report (OECD/NEA/CSNI/R(2014)3, 2014).

Table 12.3

Classification of Eulerian fluid dynamic simulation approaches for two-phase flow (Bestion, 2012)

O, open medium approach; *P*, porous medium approach; *1*, one fluid; *2*, two fluid; *n*, multifield; *F*, filtered interface; *D*, deterministic interface; *DNS*, direct numerical simulation; *S*, Statistical interface; *R*, Reynolds averaged, *V*, volume averaged or integrated.

- DNB, Dry-out, and CHF (M)
- Subcooled boiling (M)
- Two-phase pressurized thermal shock (M)
- Direct contact condensation: steam discharge in a pool (M)

- Pool heat exchangers: thermal stratification and mixing problems (H)
- Containment thermal hydraulics (H)
- Two-phase flow features in BWR cores (M)
- Atmospheric transport of aerosols outside containment (M)
- DBA reflooding (M)
- Pipe flow with cavitation (M)
- External reactor pressure vessel cooling (M)
- Behavior of gas-liquid interfaces (M)
- Pipe break-in vessel mechanical load (M)
- Specific features in passive reactors (M)

For each NRS problem, we need to check what is the issue, what is the benefit from the use of multiphase CFD, and how mature the current CFD level is.

There are numerous approaches in multiphase CFD. To select and apply them in a right way, we need to understand the details of each method: advantages/disadvantages, differences from other methods, etc.

For multiphase flows, we need to select and determine not only the governing equations (e.g., time-averaged, spatial averaged NS) but also the interface treatments (e.g., deterministic, statistical, or filtered). Here, we need to know compatibility between the combinations selected, e.g., in relation to:

- Interfacial transfer (mass, momentum, energy);
- Turbulence transfer (based on the selected models);
- Wall transfer (momentum and energy transfer by wall function)
- RANS turbulence model is not compatible with deterministic interface capturing method because the motion and change in the interface are determined by eddies, which cannot be captured by RANS turbulence models.
- In principle, the RANS turbulence models can be compatible with all flow

regimes if the multiphase flow is statistically steady or quasisteady; however, in practice, the level of information loss (inaccuracy) can vary with flow structures (Bestion, 2012): good accuracy for dispersed bubbly flow or dispersed droplet flow; bad accuracy for separated-phase flows such as stratified flow and annular flow; Furthermore, for flow regimes with large bubbles (slug and churn flow) regime,

- RANS turbulence models with statistical approach are very empirical, thus requiring much more complex assessment process.
- RANS cannot simulate strong unsteady flows. LES and quasi-DNS are required.

Turbulence modeling in two-phase conditions seems to be presently limited to extrapolations of the single phase k -epsilon models by adding interfacial production terms. The limits of such approaches have already been reached, and multiscale approaches are necessary to take account of the different nature of the turbulence produced in wall shear layers, and the turbulence produced in bubble wakes. Certainly, more research effort is required in this area; see also Fig. 12.5 and related discussion above.

In the area of two phase, the closure laws in 3D, sometime three-fluid, to include a dispersed phase, are needed and are currently being adopted. These equations require closure laws representing the exchange of mass, momentum, and energy between the phases. Namely, except for rather particular flow regimes (separated phases, dispersed second phase), general purpose expressions for such closure laws require extensive further development.

12.9.4 Phenomenological issues

12.9.4.1 Stratification and buoyancy effects

Buoyancy forces develop in the case of heterogeneous density distributions in the flow. Most of the events concern thermally stratified flows, which result from differential heating (e.g., in heat exchangers), or from incomplete mixing of flows of different temperatures (e.g., thermal stratification). Other contributions to this report have underlined the possible occurrence of stratification and buoyancy forces. For single-phase flows, one can recall stratified flow developing in the case of pressurized thermal shock, hot leg heterogeneities, thermal shock, induced break, and for natural convection in many relevant safety situations for GFR and

LMFBRs and within the context of the design of PAHR (post accident heat removal). For two-phase flow problems, the reader may also refer to **Mahaffy et al. (2007a,b)**.

Stratification may be one of the significant phenomena in the case of thermal shock, under some small break LOCA conditions (e.g., performance of AP-600) and for water-hammer condensation. Stratification and buoyancy effects may lead to thermal fatigue, to modification of condensation rates, and to difficulties in predicting the associated mixing processes.

12.9.5 Turbulence

12.9.5.1 Steady RANS turbulence modeling

From the very early days of industrial CFD practice to the present time, the treatment of turbulence has been based on statistical closure models of the Reynolds-averaged Navier-Stokes (RANS) equations. The limitations of computing power available have rendered this the only feasible option, although the complexity and sophistication of the closure models employed have increased in line with advancing power. Although a large amount of research capability has been invested in steady RANS models over the past few decades, to date, no practicable model has emerged that is competent across a broad range of flows featuring diverse states of strain. Over one hundred RANS models or model variants have now been published. Many of these variants have been devised to fix a problem in a preceding model, but few are widely successful beyond that class of flows against which they are calibrated.

Here, we consider RANS turbulence closure models under the three categories:

- Linear eddy viscosity models (LEVIM)
- Nonlinear eddy viscosity models (NLEVIM)
- Reynolds stress models (RSM)

Linear eddy viscosity models (LEVIM)

Among the various RANS turbulence models, the k - ϵ is currently the most popular together with its variants (e.g., realizable, RNG) and similar linear approaches such as the k - ω and shear stress transport (SST) models. However, it is well known that the usual formulations of these models assume isotropic eddy diffusivity in modeling the Reynolds stress tensor, and therefore anisotropic effects are not accounted for. A consistent overview of selected Turbulence model is provided below:



Comments on LEVM

Adopting an isotropic eddy diffusivity in modeling the Reynolds stress tensor means that since the viscosity is a scalar, each component of the stress affects its strain to the same extent. For this reason, flows, where turbulent intensity gradients and hence the augmentation effects of secondary strain rates are important, cannot be accurately predicted. The most evident example is the secondary flow that originates in noncircular ducts due to the gradients of turbulent shear stresses (Baglietto and Ninokata, 2004).

An important weakness of the standard two-equation models is that they are insensitive to streamline curvature and system rotation. Particularly, for swirling flows, this can lead to an overprediction of turbulence mixing, i.e., overly dissipative, and to a strong decay of the core vortex. There are curvature correction models available, but they have not been generally validated for complex flows (ANSYS, 2010).

Nonlinear eddy viscosity models (NLEVM)

It is well known that a significant development in the turbulence modeling theory since the 1990s is the nonlinear eddy viscosity turbulence model (NLEVM), which is essentially equivalent to the explicit algebraic stress model (EASM).

Theoretical background

The NLEVM describes the Reynolds stresses explicitly in an algebraic expression in terms of the mean strain and rotation (spin) tensors as:

$$q''' / q_0''' = f(t_f, t_a) \quad (12.11)$$

Many EARSMS and NLEVMs are used in combination with different k - ε models, but several authors have also proposed combinations with k - ω models and other types of two-equation models. Specifically, in Eq. (12.11), nonlinear terms consist of second-order (quadratic) terms and third-order (cubic) terms, which reflect the normal stress anisotropy of the turbulence structure and the effect of the streamline curvature and the rotation, respectively (Xu and Ma, 2009). Several NLEVMs have been developed according to flow characteristics by selecting appropriate nonlinear

terms.

Advantages

The advantage of NLEVM lies in that, with a well-developed robust CFD code for the conventional two-equation turbulence models, it can be readily implemented to simulate complex turbulent flows by merely adding the nonlinear terms into the expression for the Reynolds stress (In et al., 2003) without significantly consuming the CPU (about 10% increase) and losing the computational robustness (Xu and Ma, 2009). Thus, for the problem of flow in a rod bundle with mixing vanes, it needs to be validated.

Notes

However, it should be emphasized that a careful calibration is needed for the scale-determining part of the model when it is coupled with a nonlinear stress-strain relationship, either NLEVM or EARSMS (Hellsten and Wallin, 2009).

EARSMS or NLEVMs that are simply combined with an existing two-equation model developed originally in the context of linear eddy-viscosity modeling may show unexpected problems if insufficient attention is paid to the recalibration of the scale-determining model. Both EARSMS and NLEVMs need the turbulent kinetic energy k and timescale ($\tau=k/\epsilon$), which must be obtained from a scale-determining model. As an example, strongly unphysical velocity profiles were obtained around outer edges of turbulent layers using the Wallin and Johansson EARSMS (Wallin, 2000; Wallin and Johansson, 2000), the Wallin model in combination with the $k-\omega$ TNT model (Kok, 2000), or the $k-\omega$ BSL model (Menter, 1994), without any recalibration (Hellsten and Bezaud, 2005; Hellsten, 2005).

Reynolds stress models

Overview

The Reynolds stress model (RSM) is the most elaborate turbulence model in (U)RANS turbulence models. Abandoning the isotropic eddy-viscosity hypothesis, the RSM closes the Reynolds-averaged Navier-Stokes equations by solving transport equations for the Reynolds stresses, together with an equation for the dissipation rate. This means that five additional transport equations are required in 2D flows and seven additional transport equations must be solved in 3D.

Advantages

Specifically, RSM can show better performance involving the following types of flows:

- Free shear flows with strong anisotropy, like a strong swirl component, including flows in rotating fluids,
- Flows with sudden changes in the mean strain rate,
- Flows where the strain fields are complex and reproduce the anisotropic nature of turbulence itself,
- Flows with strong streamline curvature, secondary flows, and
- Buoyancy flows.

All of these are based on a higher degree of universality by considering each Reynolds stress tensor.

Disadvantages

However, the penalty for this flexibility is a high degree of complexity in the resulting mathematical system, thus leading to *reduced numerical robustness*, requires increased computational resources. Thus, people typically start with a more stable turbulence closure model, such as k - ϵ model, and then run the RSM. The RSM may require more iterations to converge than the k - ϵ and the k - ω models due to the strong coupling between the Reynolds stresses and the mean flow.

Notes

The fidelity of RSM predictions is still limited by the closure assumptions employed to model various terms in the exact transport equations for the Reynolds stresses. The modeling of the pressure-strain and dissipation-rate terms is particularly challenging and often considered to be responsible for compromising the accuracy of RSM predictions.

In addition, the RSM might not always yield results that are clearly superior to the simpler models in all classes of flows to warrant the additional computational expense.

Variants of RSM

Some variants exist in RSM. These vary depending on modeling of the pressure-strain term. Examples are provided in the following:

- The LRR RSM (Launder, Reece, Rodi) (Launder et al., 1975), with a linear pressure-strain term, and SSG RSM (Speziale, Sarkar, Gatski), (Speziale et al., 1991), with a quadratic pressure-strain term, are used well.
- The SSG RSM has been demonstrated to give superior performance in a range of basic shear flows, including plane strain, rotating plane shear, and axisymmetric expansion/contraction. This improved accuracy should be beneficial for a wider class of complex engineering flows, particularly those with streamline curvature.
- The quadratic pressure-strain model, i.e., the SSG RSM, does not require a correction to account for the wall-reflection effect in order to obtain a satisfactory solution in the logarithmic region of a turbulent boundary layer.
- However, the SSG RSM can be only used with wall-modeled near-wall treatment, while the linear pressure-strain model can be used with wall-resolved treatment or a two-layer model. Thus, if it is important to resolve the viscous sublayer, only the linear pressure-strain model (LRR RSM) can be chosen.
- The CFX code also provides ω -based RSMs, such as the SMC- ω (underlying the Wilcox k - ω model, Wilcox, 1998) and the baseline RSM (BSL RSM, underlying the BSL k - ω model) because the ω -equation allows a more accurate near-wall treatment.

12.9.5.2 Unsteady RANS (URANS) turbulence modeling

When the flow is not statistically stationary, Reynolds averaging is not same as time-averaging and thus, the simulation must be time-dependent (Ramesh et al., 2006) (see also Diwan et al., 2006). In fact, it has become common to call RANS modeling URANS whenever the computed solution is time dependent. The approach then is to apply an existing RANS model and to aim at resolving some of the unsteady features of the flow without recalibration of model coefficients (Fröhlich and von Terzi, 2008). Although the URANS is still theoretically disputable, it has been proven to be successful in numerous real applications.

Theoretical background

The URANS is based on the following triple decomposition:

$$q'' = h_s (T_{\text{wall}} - T_{\text{bulk}}) \quad (12.12)$$

where $\bar{u}_i(x_i)$ is the mean value defined as

$$Pr = \mu \times C_e / k$$

, $\hat{u}_i(x_i, t)$ is deterministic or coherent contribution, and $u_i(x_i, t)$ is random, turbulent fluctuation. In the actual calculation, the mean and the coherent component in Eq. (12.12) are lumped together and thus,

$$N\ddot{u} = h_s \times D_h / k \quad (12.13)$$

Using the above decomposition, the URANS equations can be derived as (Johnson, 2008) (see also Labois and Lakehal, 2011):

$$F_Q^E = \text{Engineering tolerances factor} \quad (12.14)$$

It should be noted that

$$F_Q = \text{Total power peaking factor} \quad (12.15)$$

$$F_Q = F_Q^N \times F_Q^E$$

where F_Q^N is Reynolds stress.

Since it is practically impossible to attain ensemble average in an experiment, we cannot directly compare $\tau_{ijURANS}(x_i, t)$ results, i.e.:

$$F_{\Delta H} = \Delta \text{Enthalpy}_{\text{Max}} / \Delta \text{Enthalpy}_{\text{Average}} \quad (12.16)$$

Turbulent kinetic energy is also evaluated as:

$$F_{\Delta H_i} = \Delta \text{Enthalpy}_i / \Delta \text{Enthalpy}_{\text{Average}} \quad (12.17)$$

where

$$\mathbf{P} \triangleq \widehat{\widehat{\mathbf{P}}} = \langle \bar{\mathbf{P}} \rangle^S \quad (12.18)$$

Since the URANS model in usual CFD code typically calculates $\langle u_i \rangle$ and τ_{ij}^{URANS} and their average and RMS values, to compare Reynolds stress τ_{ij}^{TRANS} or turbulent kinetic energy with experimental ones, additional calculations need to be performed using Eqs. (12.16)–(12.18). For example, the coherent part of kinetic energy is obtained by time averaging the sum of the squares of the resolved velocity component fluctuations and the noncoherent part of kinetic energy is obtained by time-averaging the URANS computed instantaneous turbulent kinetic energy.

Theoretical issues

One theoretical issue is that the triple decomposition (Eq. 12.12) is valid under the assumption that there is a clear spectral gap between deterministic (coherent) and turbulent fluctuation. In other words, the deterministic component should have larger timescale than the maximum timescale of turbulent fluctuation.

$$\mathbf{V} \triangleq \widetilde{\widetilde{\mathbf{v}_z}} = \frac{\langle \bar{\rho} \mathbf{v}_z \rangle^S}{\langle \bar{\rho} \rangle^S} = \frac{\langle \bar{\rho} \tilde{\mathbf{v}}_z \rangle^S}{\langle \bar{\rho} \rangle^S}$$

Modeling of $\widetilde{\widetilde{\mathbf{v}_z}}$, i.e., in terms of steady RANS turbulence closure models without modification, may cause another problem. This is because coefficients in steady RANS turbulent transport equations were determined by statistically stationary experiments or DNS results. In general, most previous RANS turbulence models are basically adjusted to reproduce the spreading rate of mixing layers in steady RANS simulations, i.e., the

Reynolds stress predicted by the models implicitly contains contributions not only from the turbulent or random motions but also from the coherent motions of the flow (Spalart, 2000), and thus the models are, in general, overly dissipative (Menter et al., 2003a,b) when used in URANS simulations.

Especially, using an isotropic linear eddy viscosity model makes the overly dissipative characteristics more clear. This is because the Boussinesq approximation adopted in linear eddy viscosity model assumes that anisotropy and strain are aligned. The production term in the transport equation of kinetic energy continuously changes with the maximum and the minimum when anisotropy and strain are aligned and perpendicular, respectively. However, unsteady flow with large-scale fluctuations strain is generally not aligned with the anisotropy tensor. Thus, the linear eddy viscosity model always has the maximum production term, thereby showing overly dissipative characteristics in unsteady flows.

Also, URANS can often capture the instability, but the difference from DES or LES is that grid refinement does not extend the energy cascade. The solution converges to the smooth solution of the modeled equations, instead of generating smaller and smaller eddies. Typically, both the three-dimensionality and the shedding modulations are suppressed by the smoothing effect of the RANS model (Travin et al., 1999).

12.9.5.3 Near-wall treatment of (U)RANS

Wall-modeled (U)RANS (wall function methods)

In this treatment, standard wall function is based on the assumption that the first grid point of the wall is located in the universal law of the wall or logarithmic layer. The wall function eliminates the need to resolve the very thin viscous sublayer, thus leading to reduction in the number of cells and to a more moderate (and desirable) aspect ratio of the cells (ratio of the longest to the smallest side in a structured grid).

On the other hand, standard wall function formulations are difficult to handle because it should be ensured that the computational grid resolution near the wall satisfies the wall function requirements. If the grid becomes too coarse the resolution of the boundary layer is no longer ensured. If the resolution becomes too fine, the first grid spacing can be too small to bridge the viscous sublayer. In this case, the logarithmic assumptions are no longer satisfied. The user should ensure that both limits are not overstepped in the grid generation step. Also, high aspect ratios can result in numerical problems due to round-off errors.

The lower limit on the grid resolution for standard wall functions is a severe detriment to a systemic grid refinement process, as required by the best practice approach. In other words, instead of an improved accuracy of the solution with grid refinement, the solution will deteriorate from a certain level on, leading eventually to a singularity of the numerical method. Standard wall functions are therefore not recommended for systematic grid refinement studies. Recently, alternative formulations like scalable wall functions (Menter and Esch, 2001) have become available, which allow for systematic grid refinement when using wall functions (ANSYS, 2010).

The wall function approach for the near-wall region is simple but becomes less reliable when the flow conditions depart too much from the ideal conditions underlying the wall functions. Examples are as follows (FLUENT, 2006):

- Pervasive low-Re number or near-wall effects (e.g., flow through a small gap or highly viscous, low-velocity fluid flow);
- Massive transpiration through the wall (blowing/suction);
- Severe pressure gradients leading to boundary layer separations;
- Strong body forces (e.g., flow near rotating disks, buoyancy-driven flows);
- High three-dimensionality in the near-wall region (e.g., Ekman spiral flow (Ekman, 1905) strongly skewed 3D boundary layers).

Wall-resolved (U)RANS

The use of low-Reynolds number formulations of turbulence models for the integration of the equations through the viscous sublayer is generally more accurate because no additional assumptions are required regarding the variation of the variables near the wall. On the other hand, most low-Reynolds number turbulent models are quite complex and can reduce the numerical performance or even destabilize the numerical method. In addition, classical low-Re models require a very fine near-wall resolution of y^+ around 1 at all wall nodes. This is quite difficult to ensure for all walls of a complex industrial application. In the case that significantly coarser grids are used, the wall shear stress and the wall heat transfer could be reduced significantly below their correct values (ANSYS, 2010).

Low Reynolds number model

The low-Reynolds number approach employs a turbulence model that is valid

throughout the boundary layer including the viscous sublayer. Turbulence models need to be modified to resolve the viscous layer by using a damping function.

The mesh must be sufficiently fine to resolve the viscous sublayer, and there is little or no need for modeling to obtain the wall boundary conditions. The computational expense associated with this approach can be significant, particularly for large Reynolds numbers (FLUENT, 2006).

Two-layer model (for ε -based RANS models)

The two-layer model is an alternative to the low-Reynolds number model, allowing the k - ε model to be applied in the viscous sublayer.

In this model, the computation is divided into two layers. In the layer adjacent to the wall, the turbulent dissipation rate (ε) and the eddy viscosity are specified as functions of wall distance. The values of ε specified in the near-wall layer are blended smoothly with the values computed from solving the transport equation far from the wall. In contrast, the k -equation is solved in the entire flow region.

This explicit specification of ε and eddy viscosity is arguably no less empirical than the damping function approach in low Reynolds number models and the results are often as good or better (CD-adapco, 2006).

Enhanced near-wall treatment

Most commercial codes have the enhanced near-wall treatment method so that low Re number (mainly ω -based models but also ε -based models in STAR-CCM+) or two-layer models (ε -based models) may not be deteriorated by coarse mesh.

12.9.5.4 Large eddy simulations

Large eddy simulation (LES) was pioneered in the 1960s and much progress has been achieved over the last few decades. Although important subgrid scale models were already developed in the 1990s, the main applications of such models are mainly confined to building-block flows. Actual applications to engineering problems have not been performed prevalently. This is mainly because LES simulations still require enormous amount of computational cost for engineering application.

This fact can also be confirmed by viewing the LES models in commercial CFD codes. Most CFD codes only contain very simple SGS models, Smagorinsky

model, or WALE model (although the FLUENT code contains a dynamic Smagorinsky model and a dynamic kinetic energy equation model).

However, since the LES still requires a large computational cost compared to (U)RANS simulations, its applications have been mainly simple flows rather than complex engineering flows. Furthermore, in wall-bounded flows, demanded grid resolution near the wall become enormous, comparable to DNS.

Thus, for practical applications, one can employ several wall models, such as the wall stress model similar to wall function methods as in RANS model, zonal models, or hybrid methods, where the near-wall region is solved by a (U)RANS equation and far from the wall LES is performed.

Wall-modeled LES

Large eddy simulations (LES) of wall-bounded flows become prohibitively expensive at high Reynolds numbers if one attempts to resolve the small but dynamically important vertical structures in the near-wall region. The Reynolds number scaling of the required number of grid point is nearly the same as for DNS.

An attractive alternative to compute high-Reynolds number flows is using wall-layer models (wall-modeled LES), in which only the outer layer is resolved, while the near-wall region is modeled.

Three broad classes of approaches are presently used (Piomelli, 2008): (1) bypassing this region altogether using wall function (equilibrium stress model), (2) solving a separate set of equations in the near-wall region, weakly coupled to the outer flow (zonal approaches), and (3) simulating the near-wall region in a global, Reynolds-averaged, sense (hybrid RANS-LES method).

Zonal methods can also be included in hybrid methods (layering RANS-LES method) (Fröhlich and von Terzi, 2008).

Wall stress model

To circumvent the severe near-wall resolution requirement, LES can be combined with a wall (-layer) model. In this approach, LES is conducted on a relatively coarse grid designed to resolve the desired outer flow scales. The dynamic effects of the energy-containing eddies in the wall layer (viscous and buffer regions) are determined from a wall model calculation, which provides to the outer flow LES a set of approximate boundary conditions, often in the form of wall shear stresses. Wall models, which supply wall stresses to the LES, are called wall stress models

(Wang and Moin, 2002) or equilibrium stress models (Piomelli, 2008).

The simplest wall stress models are analogous to the wall functions commonly used in RANS approaches except that they are applied in the instantaneous sense in unsteady calculations. The wall function provides an algebraic relationship between the local wall stresses and tangential velocities at the first off-wall velocity nodes.

This approach was first employed in a channel flow simulation by Schumann (1975) who assumed that streamwise and spanwise velocity fluctuations are in phase with the respective surface shear stress components.

A number of modifications to Schumann's model have been made by, for example, Groetzbach (1987) and Werner and Wengle (1991) (whose power law model was adopted in commercial CFD code like STAR-CCM+) to eliminate the need for a priori prescription of the mean wall shear stress and to simplify computations, and by Piomelli et al. (1989) to empirically account for the phase shift between the wall stress and near-wall tangential velocity due to the tilting of near-wall eddies.

Comments and recommendations

The wall stress approach can give reasonably accurate results in attached flows, with mild pressure gradient and curvature (Piomelli, 2008). However, since the assumption underlying the approximate boundary condition (i.e., turbulence is in equilibrium) is quite strong, it may fail catastrophically in the following flows:

- Rotating flows where turbulence is damped on one side and amplified on the other.
- Flow with shallow separation, e.g., flow over a contoured ramp.
- Flow with strong pressure gradient.
- In attached flows, even in the presence of fluid-dynamical nonequilibrium, the logarithmic law approximate boundary condition can give more accurate results.
- Oscillating freestream (where fluid is dynamically nonequilibrium, but the boundary layer is still attached)

Zonal model

The “algebraic” wall stress models mentioned above all imply the logarithmic law or law of the wall for the mean velocity, which is not valid in many complex flows.

To incorporate more physics into the model, wall stress models based on boundary-layer approximations have been proposed, e.g., Cabot and Moin (2000), Balaras et al. (1996), Cabot (1996), Wang and Moin (2002), and Gungor and Menon (1996).

In this method, turbulent boundary-layer (TBL) equations are solved numerically on an embedded near-wall mesh to compute the wall stress. These equations are forced at the outer boundary by the instantaneous tangential velocities from LES, while no-slip conditions are applied at the wall. The turbulent viscosity is modeled by a RANS type model, such as the mixing length model with wall damping.

Comments and recommendations

Zonal models have had success in flow in which the outer layer drives the inner layer. However, they have been less successful when the perturbation is propagated from the wall outward.

Hybrid RANS-LES models (as wall models)

In hybrid RANS-LES methods, the RANS equations are solved in the inner layer, while the filtered LES equations are solved away from the wall. The main issue is the disparity of scales between the LES and RANS regions.

In the wall stress and zonal models, the outer layer imposes its scales on the inner one, which therefore contains eddies as small as the filter size.

In hybrid methods, on the other hand, the inner layer has its own time scale and length scale (determined by the URANS equations applied there), which are generally much larger than those of the outer-layer eddies.

The lack of resolved eddies in the interface region results in the logarithmic law mismatch (LLM). Since the total stress is determined by the global momentum balance, the decrease in the eddy viscosity that occurs beyond the RANS/LES nominal interface, if not accompanied by a corresponding increase of the resolved Reynolds stress, must result in an increase in the mean velocity gradient.

To reduce or remove the LLM, various methods have been developed, e.g.:

- Introducing artificial fluctuation (e.g., stochastic forcing) at the interface (Piomelli et al., 2003; Keating and Piomelli, 2006).
- Introducing additional filtering at the interface (Hamba, 2003, 2006).

Comments and recommendations

Hybrid RANS-LES methods seem to be the most effective in flow conditions that facilitate the rapid amplification of any instability, whether due to numerical or natural causes, such as separation, concave curvature, and adverse pressure gradients. In such cases, the eddy generation at the interface is greatly increased, and accurate results can be obtained.

Hybrid RANS-LES methods are the least accurate in attached, thin shear layers, where the instability mechanisms are comparatively weak (due to logarithmic law mismatch).

Summary of wall-modeled LES

It is unreasonable to expect that wall-modeled LES, which bypasses the inner layer, could ever be as accurate as wall-resolved LES because even in equilibrium flows, the inner layer is the region where most of the production occurs and the eddies are created that grow and advect into the outer layer, affecting the momentum transfer too.

Despite this intrinsic shortcoming, wall-modeled LES is able to predict with reasonable accuracy a wide variety of flows.

In many cases, the physics of the outer layer is reproduced well, despite the fact that the inner layer is bypassed, as long as the grid is fine enough to resolve the outer-flow integral scale.

Unless the integral scale in the outer layer is resolved well, $\Delta > \delta/15$, uniformly accurate results cannot be obtained.

12.9.5.5 Very large eddy simulation

Overview

Based on the initial successes of LES in predicting prototypical flows, attempts have been made to apply traditional LES to complex flows of industrial relevance. However, due to computational affordability, the resulting computational grids necessarily had to be coarse, too coarse to resolve the desired amount (about 80%) of kinetic energy (Fröhlich and von Terzi, 2008). This was called very large eddy simulation (VLES) by some researchers (e.g., Ferziger, 1996). Within the framework of this chapter, we restrict the VLES to its original intent, i.e., LES

with traditional SGS models on coarse grids.

Notes

The VLES has two fundamental problems. First, the LES cutoff is now located within or even below the wavenumber range of the most energetic modes. Modeling the interaction between resolved motion and unresolved motion is very delicate in this case, and there is little hope for success. Second, the numerical discretization scheme, mostly disregarded in the classical (explicit) LES model development, impacts the scales near the grid scale, which are the physically relevant ones with VLES (Fröhlich and von Terzi, 2008).

Comments and recommendations

Despite the failure of the naive approach, the idea to predict the large-scale unsteadiness of the flow at minimum cost (e.g., Smagorinsky, 1963) remains attractive and such coherent structure capturing, as it was called by Ferziger (1996), is the aim of many hybrid LES/RANS methods. This, however, requires a substantially more sophisticated modeling approach. In the literature, the acronym VLES has occasionally been used synonymously for a wide range of methods (e.g., Drikakis, 2002) such that this term is no longer descriptive.

However, the VLES can be used to generate inflow conditions for LES, e.g., Meri et al., 1999; Meri and Wengle (2002), and Howard and Pourquie (2002).

12.9.5.6 Hybrid RANS-LES method

URANS turbulence models are overly dissipative, thus rendering only a single mode of unsteady structures. Also, VLES turbulence models do not resolve turbulence production fully, whereas dissipation is largely overpredicted. Despite the failure of such approaches, the idea of predicting the large-scale unsteadiness of the flow at minimum cost remains attractive and such coherent structure capturing is the main motivation of many hybrid RANS-LES methods. This however requires a substantially more sophisticated modeling approach than URANS or VLES.

Numerous hybrid methods have been developed. These are

- based on (U)RANS closure models, by adding the characteristics of resolved turbulence scales mainly related to grid size, which is a main property of LES SGS model, or

- based on LES SGS models, by adding the characteristics of broad turbulence scales coverage, which is a main property of a (U)RANS closure model.

These approaches are possible because the governing equations (momentum and energy equations) have the same form, except that Reynolds averaging and filtering operations were applied in URANS and LES, respectively. Although Reynolds averaging and filtering has quite different physical meaning, the difference is not revealed explicitly in the actual calculation process except in the turbulence stress term.

Classifications

In the hybrid RANS-LES method, the calculation for a node can be performed (i) by selecting (switching) either RANS turbulence models or LES SGS models, or (ii) by blending two model effects (in turbulence stresses or some physical values). This kind of hybrid method is often called a global or unified approach.

On the other hand, one can simulate pure LES calculations in one domain region and pure RANS calculations in the remaining parts of the domain and then match values in the interfaces. This kind of hybrid method is called a zonal (or segregated) approach.

It should be noted that in global (or unified) models without using blending concepts, usually RANS and LES regions separately exist as in zonal model. However, they are different from zonal models in the following ways.

- Interfaces in global (or unified) models are determined by wall distance and grid size or additionally in a solution-dependent manner for each time calculation, not by predetermined separate domains as in zonal methods.
- Communication at interfaces in global (or unified) models is achieved in a turbulence stress level (i.e., unresolved turbulence values), such as turbulence kinetic energy and turbulence dissipation, in contrast to a governing equation level (i.e., resolved scales) in zonal (or segregated) models.

Also, it should be pointed out that: (i) if the interface is determined only by wall distance and grid size, it will not change (hard interface) over time, once grid is generated, whereas, (ii) if it is determined by solution-dependent values in addition, it may change with time (soft interface) (Fröhlich and von Terzi, 2008).

On the other hand, zonal approaches in the wall-modeled LES can be regarded as a global (or unified) hybrid RANS-LES method with hard interface because they

solve the near-wall flow region using RANS and the flow region from the outer layer using LES, and they communicate unresolved turbulence scales with each other. Thus, the zonal approach can be called layering RANS-LES models (Fröhlich and von Terzi, 2008). It also needs to be mentioned that layering RANS-LES models can have soft interface by specifying the wall distance in a solution-dependent coordinate system (e.g., Breuer et al., 2008a; Breuer et al., 2008b) or by using the ratio of kinetic energy to total turbulent kinetic energy (Kniesner et al., 2007).

12.9.5.7 Detached eddy simulation

Although most hybrid methods were developed for general purposes, some hybrid models can be used as wall layer models for LES simulation. Among them, detached eddy simulation (DES) has been the most widely used in CFD society and also included in many commercial CFD codes, such as CFX, FLUENT, and STAR-CCM+ because of its simplicity to implement in previous RANS turbulence models through simple modification.

Original SA-DES can be classified into a global (or unified) hybrid RANS-LES method with hard interface because the interface is determined by wall distance and grid size.

One advantage of DES is that it uses the same transport equation for RANS and LES turbulence stress and instead chooses the length scale in the dissipation term of the equation from either wall distance (originally for RANS turbulence closure models) or grid size-related length scale.

Use of DES

The DES was originally developed for massively separated flows in the aerodynamic field to apply RANS calculations in an attached boundary layer region and LES calculations in separated flows. This use of DES can be called *Natural DES*. DES can also be used as a wall layer model for LES. Hereafter, this use of DES will be called *wall-modeled DES*. The difference between the natural and wall-modeled DES is that in wall-modeled DES applied to wall-attached flows, the RANS region is usually limited to a region in the outer layer as in wall-modeled LES, while in natural DES mainly applied to massively separated flows, such as airfoil, the RANS region is desired to cover all boundary layers, which is because intermediately resolved wall grids may cause the early transition to LES, thus inducing the early separation (which is called grid-induced separation (GIS) due to modeled stress depletion (MSD) (Spalart, 2009).

Variants of DES

Subsequent enhancements, such as delayed (SA-) DES (DDES), zonal (SA-) DES (ZDES), and shielding SST-DES, were mainly for the prevention of the GIS in terms of natural DES. In contrast, improved DDES (IDDES) was developed to relieve the LLM by changing the length scale.

Comments and recommendations

If a hybrid RANS-LES method like DES is used as a wall-layer model, grids in the LES region should be finely resolved enough to satisfy the LES SGS model conditions.

If one wants to use entirely coarse grids (finer than URANS but coarser than LES), one should not use DES methods because the DES becomes VLES outside the boundary layer region. Alternatively, one can use blending hybrid RANS-LES methods like flow simulation methodology (FSM), e.g., Zhang et al. (2000), Fasel et al. (2002), and Hussaini et al. (2006), or hybrid methods using weighted sum (Xiao et al., 2004), see also Fu et al. (2010) and Xiao et al. (2003) because these methods consider a RANS correction of LES in coarser regions.

12.9.5.8 Scale-adaptive simulation

The scale-adaptive simulation (SAS) is regarded as an improved URANS. The improved URANS aimed at resolving a substantial part of the turbulent fluctuations but do not contain an explicit dependency on the computational grid like LES. RANS models involve only physical length scales, while LES models contain explicitly or implicitly a length scale related to the numerical grid, which determines the size of resolved fluctuations.

The SAS modeling is based on the use of a second mechanical scale in the source/sink terms of the underlying turbulence model. In addition to the standard input from the momentum equations in the form of first velocity gradient (such as strain rate tensor and vorticity tensor), SAS models rely on a second scale, in the form of higher velocity derivatives (second derivatives).

SAS models satisfy the following requirements (Menter and Egorov, 2005):

- (a) Provide proper RANS performance in stable flow regions.
- (b) Allow the breakup of large unsteady structures into a turbulent spectrum.

(c) Provide proper damping of resolved turbulence at the high wave number end of the spectrum (resolution limit of the grid).

Functions (a) and (b) are achieved without explicit grid or time step dependency in the model. Naturally, function (c) must be based on information on the grid spacing, other information concerning the resolution limit (dynamic LES model, etc.), or numerical method (MILES) damping.

Characteristics

Flows or flow conditions where SAS mode is active are:

- Flows where steady-state solution cannot be obtained;
- Flows where the use of smaller time steps results in unsteady solutions.

One could argue that the occurrence of unsteady regions in URANS simulation is the result of a nonlocal interaction which cannot be covered by the single-point RANS closure. Flows where SAS mode is not active, i.e., they return to URANS mode, are

- Attached or mildly separated boundary layers, and
- Undisturbed channel/pipe flows.

This behavior of SAS is ideal for many technical applications, as flows for which the model produces steady solutions are typically those where a well-calibrated RANS model can produce accurate results.

Contrary to DES, SAS cannot be forced to go unsteady by grid refinement.

SAS has the advantage of being relatively “safe” as it has a RANS fall-back position in case of overly coarse grids/time steps or insufficient flow instability.

This is not the case with the DES model, which introduces a grid dependency into the RANS portion of the model to ensure an LES mode under certain conditions.

On the other hand, DES models can more easily be forced into unsteady mode which can be of significant advantage for otherwise stable flows.

Note

However, it has been shown in many simulations, such as the backstep simulation,

that enforcing unsteadiness by grid refinement requires an in-depth understanding of the flow, the turbulence model, and its interaction with the grid in order to produce reliable results. Nevertheless, there will be cases where the grid sensitivity of DES will be advantageous, as it allows unsteady simulations where SAS might produce a steady-state flow field.

Variants of SAS

Several SAS models were developed:

- Original SAS model.
- SST-SAS model.
- k -epsilon SAS model.

12.9.6 Efficiency of turbulence modeling

Computational power has dramatically increased over the last few decades. A consequence of this is the rapid increase in the size of subsequent datasets, with *unsteady 50–100 million point grid* simulations now being conducted with increasing regularity (Sagaut and Deck, 2009).

General estimation of the computational cost of each turbulence model for a given Reynolds number is impossible because it depends on the problem (especially geometry). However, approximate estimation may be possible. Regarding computational efficiency, the following issues are evident:

- High-level turbulence models are more expensive than low-level ones because they contain more equations to be solved and more parameters to be evaluated. In other words, computational cost increases with RANS, Hybrid RANS-LES, and LES in that order.
- In the same context, unsteady turbulence simulation is more expensive than steady turbulence simulation. This is only valid for RANS-related turbulence models.
- Wall-resolved near-wall treatments are more expensive than wall-modeled ones.

In addition to turbulence models, the following also affect computational cost:

- Thermal simulation is more expensive than isothermal simulation because additional energy equations need to be included.

- Simulations with lower order schemes are faster than those with higher order schemes.
- Calculations in structured mesh are faster than those in unstructured mesh.

Table 12.4 shows a comparison of computational cost of turbulence modeling strategies for flows over an airliner or a car (Spalart, 2000).

Table 12.4

Comparison of turbulence modeling strategies for flows over an airliner or car (Spalart, 2000)

--

12.9.6.1 (U)RANS turbulence modeling

Linear eddy viscosity models (LEVM)

In RANS turbulence closure models, the number of transport equations is a dominant factor affecting computational cost for the same near-wall treatment. The standard $k-\epsilon$ model clearly requires more computational effort than the Spalart-Allmaras model since an additional transport equation is solved. The realizable $k-\epsilon$ model requires only slightly more computational effort than does the standard $k-\epsilon$ model. However, due to the extra terms and functions in the governing equations and a greater degree of nonlinearity, computations with the RNG $k-\epsilon$ model tend to take 10%–15% more CPU time than with the standard $k-\epsilon$ model. Like the $k-\epsilon$ models, the $k-\omega$ models are also two-equation models, thus requiring about the same computational effort as $k-\epsilon$ models.

LEVM versus NLEVM

The advantage of nonlinear eddy-viscosity model (NLEVM) lies in that, with a well-developed robust CFD code for the conventional two-equation turbulence models, it can be readily implemented to simulate complex turbulent flows by merely adding the nonlinear terms into the expression for the Reynolds stress, without significantly consuming the CPU (about 10% increase) and losing the

computational robustness (Xu and Ma, 2009).

LEVM versus RSM

Compared to k - ϵ and RNG k - ϵ models, the Reynolds stress model (RSM) requires additional memory and CPU time due to an increased number of transport equations. On average, a calculation using the RSM requires 50%–60% CPU time and 15%–20% per iteration more than that using the k - ϵ model (FLUENT, 2006).

Near-wall treatment (wall-modeled) versus wall-resolved RANS

Wall-resolved RANS requires much more stringent grid resolution especially for the wall-normal direction. The viscosity-affected sublayer is a region where effective transport properties change at a rate typically two or more orders of magnitude faster than elsewhere in the flow. So, if one adopts the same numerical strategy, a much finer mesh is required. Consequently, while the viscous-affected sublayer typically occupies only around 1% of the flow, resolving that region can require between 3 and 300 times as much computational time (depending on the flow problem, the mathematical model of turbulence, and the type of CFD solver adopted) as would be required if the mesh density could be kept comparable with that in the fully turbulent part of the flow (Craft et al., 2006).

RANS versus URANS

For the same grids, i.e., the same wall treatment, URANS needs slightly more computational time because of time advancement, but it is not so critical. For example, in computational cost estimations for flows over an airliner or car (e.g., see Spalart, 2000), 3D URANS requires more computational steps by $10^{0.5}$ for the same grids.

LES and hybrid RANS-LES

Cost estimates for LES can be found in various references available from the literature, e.g., Chapman (1979), Reynolds (1990), Spalart (2000), Piomelli and Balaras (2002), and Piomelli (2008).

Core flow region in LES

The cost estimate is based on the consideration that in LES the *integral scales of motion must be accurately resolved*. The classical picture of turbulence starts from a sequence of bifurcations in a laminar flow, each of which renders more eddies of smaller and smaller scales. The kinetic energy is found to be of the form

$$H \triangleq \tilde{h} = \frac{\langle \rho h \rangle^S}{\langle \bar{\rho} \rangle^S} = \frac{\langle \bar{\rho} h \rangle^S}{\langle \bar{\rho} \rangle^S}$$
 , where length scale $1/k$ corresponds to the wave number k , f is a damping function (for high k), and l_k is the Kolmogorov length scale, at which the smallest turbulent eddies dissipate into heat. Most of the kinetic energy is contained within the (large) integral scales, l_i , from which energy is transported by the cascade process down to the Kolmogorov scales. In most flows, the large-scale flow forms coherent structures, containing most of the energy, typically spanning a range of scales from l_i to l_r where l_r is the (intermediate) Taylor scale. These coherent structures consist of relatively closely bounded vortex filaments that move collectively in the flow, being responsible for most of the large-scale mixing and dynamics. Dimensional analysis suggests that

$$Q_k \triangleq \widehat{\bar{\rho}}_k^k = \frac{\langle \overline{\chi_k \rho_k} \rangle^S}{\alpha_k}$$
 and
$$Q_m \triangleq \alpha_v Q_v + \alpha_l Q_l$$
 where ε is the dissipation; by assuming equilibrium between production,

$$P_k \triangleq \widehat{\bar{\rho}}_k^k \triangleq \frac{\langle \overline{\chi_k \rho_k} \rangle^S}{\alpha_k}$$
 and

dissipation, it follows that
$$P \triangleq \alpha_v P_v + \alpha_l P_l$$
 These relations suggest that

$$V_k \triangleq \overline{\bar{v}}_{zk}^k \triangleq \frac{\langle \overline{\chi_k \rho_k v_{zk}} \rangle^S}{\langle \overline{\chi_k \rho_k} \rangle^S} = \frac{\langle \overline{\chi_k \rho_k v_{zk}} \rangle^S}{\alpha_k \widehat{\bar{\rho}}_k^k}$$
 a DNS will require whereas an LES would only require

$$j_k \triangleq \overline{\chi_k v_{zk}} = \varepsilon_k \bar{v}_{zk}^k$$
 cells. Hence, LES is cheaper than DNS, although still expensive compared to RANS (Fureby et al., 2008; Fureby, 2009).

Region far away from wall in wall-bounded flows

In wall-bounded flows, the integral scale, away from the walls, is proportional to the boundary layer thickness, δ ; a reasonable estimate of the grid spacing in each

direction is then
$$j \triangleq j_v + j_l$$
 For boundary layer flows, the boundary layer thickness is represented by
$$J_k \triangleq \langle j_k \rangle^S = \langle \varepsilon_k \bar{v}_{zk}^k \rangle^S$$
 Thus, the number of grid points required to resolve the outer layer is proportional to $Re_{0.4}$ (Piomelli, 2008).

Computational cost of outer and inner layers in LES

The cost estimate in LES is shown in Fig. 12.14, in which the CPU time required to compute a turbulent boundary layer is estimated for three different codes: (1) a Cartesian code with a staggered, second-order discretization; (2) a colocated finite-

volume code suited for body-fitted grids, also second order in space and time; and (3) an unstructured, second-order accurate, finite-volume code. The cost per time step and grid point was measured on an AMD Opteron processor for calculation at a given Re , and the scaling laws derived above were used to extend the cost estimate to higher Re . From this figure, one can observe that even at moderate Reynolds numbers (Re about 10^4), over 50% of the resources are used to resolve only 10% of the flow. For $Re > 5 \times 10^4$ a vanishing fraction of the grid points is used in the outer layer.

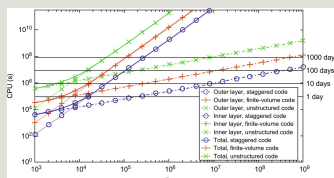


Fig. 12.14 Cost, in CPU seconds, of the LES of flat-plate boundary layer flow. Calculations were performed on an AMD Opteron, using two in-house codes and an open source unstructured one. Actual mileage may vary (Piomelli, 2008).

As a consequence of this unfavorable scaling, wall-resolved LES are limited to very moderate Reynolds numbers. Only if massive computational resources (clusters with thousands of processors) are available, calculations at Reynolds numbers of marginal engineering interest (Re around 10^5) are possible. Resolved LES is clearly not suitable for designs in which substantially more rapid computation is required, or to evaluate and compare possible designs within strict time limits, or to study aerodynamic or geophysical flows at $Re = 10^6 - 10^9$ (Piomelli, 2008).

Wall-resolved LES

Assuming that a nested grid system is used, with mesh spacing that increases in all directions as one moves away from the wall, Chapman (1979) estimates that the number of points required to resolve the inner layer is proportional to $Re^{1.8}$ (Piomelli, 2008).

Wall-modeled LES

Wall stress models are the least expensive models, in terms of computational

requirements. The cost of this kind scales like the cost of the outer layer, $Re^{0.6}$. Zonal models require between 10% and 20% more CPU time for the solution of the boundary-layer equations, and significantly more memory. The cost of hybrid RANS/LES methods is higher, since the wall-normal direction must be well resolved (the SA model, for instance, requires that the first point be at $y_+ \sim 1$), so that the number of grid points in the wall-normal direction is proportional to $\log(Re)$, resulting in a cost that scales approximately like $Re^{0.6} \log(Re)$ (Piomelli, 2008).

In WMLES, the resolution of the outer layer is, in fact, an often overlooked issue. Bypassing the wall layer is sometimes viewed as justification to use excessively coarse grids everywhere; however, many of the simulations demonstrate that *unless the integral scale in the outer layer is resolved well*, uniformly accurate results cannot be obtained. Several calculations (see e.g., Keating and Piomelli, 2006; Radhakrishnan et al., 2006, 2008; Radhakrishnan and Piomelli, 2008) show how grid sizes greater than $\delta/15$ do not result in grid-dependent results, and often give incorrect predictions of the Reynolds stresses (Piomelli, 2008).

DES

Hutton (2009), after consultation with colleagues who are experienced practitioners of DES, estimates that a hybrid solution to a problem is of the order of 10^3 – 10^4 times more expensive than a steady RANS solution. It is difficult to be more precise because the computational effort depends strongly upon the complexity of the problem, the quality of the solution sought, and indeed the expertise of the person running the solution.

Subgrid-scale (SGS) models

There are many kinds of subgrid-scale models in explicit LES. According to SGS models selected, computation cost varies. Table 12.5 shows the CPU time used by various models in a pseudo-spectral channel code, compared to that required by the Smagorinsky model and by a simulation with no model. The calculation of the SGS model, for the dynamic eddy viscosity model, requires a small amount of total CPU time, only 7% more than the Smagorinsky model. As more complex models are used, however, the calculation of the SGS stresses may require a substantial amount of CPU time. Two-coefficient models require over 30% of the CPU time only for the model evaluation. It is not clear whether the benefits gained by such models outweigh their additional cost.

Table 12.5

CPU time required by various SGS models

The CPU time is normalized by that of an LES that used the Smagorinsky model (Piomelli, 1999).

12.10 CFD coupling

The following CFD couplings are considered below:

- Coupling of CFD code with neutron physics codes
- Coupling of CFD code with structural mechanics codes
- Coupling CFD with System (SYS TH) codes: porous medium approach

Validation of CFD-type computer codes on separate-effect experiments is discussed thoroughly in Mahaffy et al. (2007a,b) as already mentioned. The processes of validation in the context of nuclear reactor simulations are, in majority of cases, beyond the possibilities of present hardware capabilities if a CFD code is used alone. Use of a less detailed, less demanding system analysis code to produce initial and boundary conditions for the CFD code is a practical alternative. Such multiscale coupling is indispensable in the case of demonstration simulations and, of course, application of a CFD code to real industrial problems. Moreover, in such problems it is very frequently necessary to simulate not only thermal hydraulics, but also phenomena belonging to different fields of physics or even to chemistry. Furthermore, in this type of multiphysics coupling, problems with different spatial and temporal scales appear.

General methods of coupling are treated in several books and papers, e.g., Zienkiewicz (1984), Hackbush and Wittum (1995), Cadinu et al. (2007), and Ibrahimbegovic and Markovic (2003). Most generally, couplings are distinguished between those taking place on the same domain, by changing the differential equations describing the corresponding physical phenomena (this approach is frequently realized by means of a single computer code), or coupling on adjacent

domains by matching boundary conditions at their interfaces. In this case, either the models are combined to produce a comprehensive model for the coupled problem (joint, or *simultaneous solution strategy*), or there are modules solving the individual problems, and coupling is effected via an outer iteration (changing of parameters, boundary conditions, or geometries after each step or selected steps of the outer iteration—*partitioned solution strategy*). Whenever an outer iteration is used, the problem of the optimum level of explicitness of the coupling has to be faced, especially when two-way coupling is required. Generally, explicit coupling is easy to program compared with implicit coupling, but is more prone to numerical instabilities.

Independently of the details of the particular coupling strategy, validation and assessment of the coupled code are required. The individual codes usually solve problems with different spatial and timescales and, particularly if two-way coupling is required, it is not enough to validate or assess the codes individually. Design of corresponding experiments must take into account different requirements concerning density of instrumentation (when multiscale coupling of codes is tested) or requirements of different type of instrumentation (in the case of multiphysics coupling).

There are several examples of coupled CFD or CFD-type codes with system codes, as can be seen in the Table 12.6, reproduced from Cadinu et al. (2007).

Table 12.6

Examples of CFD coupled codes (Cadinu et al., 2007)

--

12.11 CFD validation

An assessment matrix for a given application should comprise three groups of items (OECD/NEA/CSNI/R(2014)3, 2014) (Section 6):

- Verification problems with “highly accurate” CFD solutions;

- Validation experiments and their CFD simulations;
- Demonstration simulations, possibly with some suitable supporting experiments.

Assessment can be performed as (Fig. 12.15):

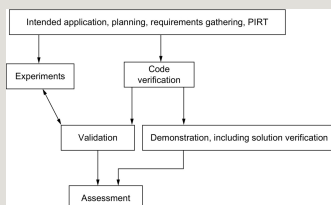


Fig. 12.15 Applicability demonstration for CFD codes (OECD/NEA/CSNI/R(2014)3, 2014).

- Verification or solving the equation correctly;
- Validation or solving the correct equations;
- Demonstration of the capability to solve a given class of problems.

12.11.1 Assessment matrix

The assessment matrix can consist of (OECD/NEA/CSNI/R(2014)3, 2014):

- “Exact” solutions and corresponding CFD calculations;
- Validation experiments and corresponding CFD calculations;
- Demonstration CFD simulations, and possibly prototype experiments;

Any assessment matrix should be strictly problem dependent: that is, any particular matrix must contain at least part of a computational path (numerical algorithm and/or physical model) considered for the intended application of the code.

As a consequence, a separate assessment matrix should be prepared for every selected nuclear safety issue where CFD simulation can be beneficial. This is a very demanding task. Fortunately though, many items (particular matrices) will be the same in the majority of such groups of matrices associated with different applications, since the same numerical algorithm and physical models will often be

used.

Whereas verification should be performed mainly by code developers, validation and demonstration are strictly application dependent and must therefore be performed, or at least overseen, by users. Validation and demonstration are the principal themes of this document. A review of several available general-purpose databases comprising experimental data is presented below under appropriate subheadings.

Then, specific application areas, namely boron dilution, pressurized thermal shocks, thermal fatigue, and aerosol transport in containments, are dealt with in more detail. Some corresponding experiments are presented, together with available calculations. On the basis of analysis of experimental data and results of CFD simulations, a statement on the appropriateness of a given CFD code to the intended class of problems can be stated. This step completes the description of the existing assessment bases.

Examples of established assessment bases for NRS applications

A list of experiments already adopted (i.e., boron dilution, PTS and core) or envisaged areas needing experiments to demonstrate the applicability and the qualification of CFD codes to NRS problems is given below (OECD/NEA/CSNI/R(2014)3, 2014) (Section 5):

- Boron dilution: University of Maryland experiments and corresponding simulations (ISP-43); ROCOM experiments (FLOMIX-R); Gidropress Facility (FLOMIX-R); Vattenfall Experiments (FLOMIX-R);
- Pressurized Thermal Shock (PTS):
 - Creare 1:5 (Tests 100, 101, 103, 104, 106) and 1:2 (tests May 105, May 106), USA;
 - IVO (FORTUM) 2:5 (Tests T9, T10, T12, T16, T44, T45, T47, T51, T106, T111 to T116), Finland;
 - Purdue 1:2 (Runs 0-1C, 0-1C-R, 0IV, 0-2C, 0-2C-R, 0-2 V, CE-1C, W-1C, B&W-1C, CE-2C, W-1C-90, CE-1C-PS, CE-3C-0), USA;
 - HDR 1:1 (Tests T32.11 to T32.15, T32.18 to T32.22, T32.31 to T32.34, T32.36,

T32.41, T32.51, T32.52, T32.57, T32.58, T32.61), Germany

○ UPTF 1:1 (Runs 020, 021, 023, 025, 026), Germany

- Core benchmark: MATIS-H facility and KAERI facility.
- Thermal fatigue: T-junctions in *Liquid-Metal Reactors and Light Water Reactors*; Parallel jets,
- Aerosol transport in containments;
- Sump clogging;

12.11.2 Deficiencies in assessment

Validation of CFD codes for NRS application frequently encounters deficiencies, which includes, but is not restricted to (OECD/NEA/CSNI/R(2014)3, 2014):

- PIRT for the intended application is not prepared.
- Quantified estimates of experimental and numerical uncertainties are not provided.
- Validation metrics, figures of merit, or target values for the intended application are not clearly defined.
- Experiments, selected for validation at some of the tiers, do not meet requirements put on validation experiments. Since validation experiments are very expensive, experiments intended for other purpose (e.g., for study of physical phenomena or for development of physical models), or very old experiments performed on already nonexistent facilities (which excludes feedback between CFD simulations and experiments), are sometimes used.
- For some physical phenomena identified in the PIRT, suitable experiments are missing so that new experiments must be proposed.
- Validation simulations cannot provide information on boundaries of regions of acceptability of the conceptual model from regions where the model cannot be applied, or where its application is questionable.

Identification of gaps in technology and assessment bases

An assessment matrix for a given application should comprise three groups of items (OECD/NEA/CSNI/R(2014)3, 2014) (Section 6):

- Verification problems with “highly accurate” CFD solutions;
- Validation experiments and their CFD simulations;
- Demonstration simulations, possibly with some suitable supporting experiments.

12.11.2.1 Additional notes: Validation in computational simulation of nuclear system thermal fluids behavior

The notes below are intended to provide an overview of efforts of and some insights into the numerical validation (focusing on the CFD method) relating to the nuclear system thermal fluids behavior. In addition to general CFD validation requirements, we stress out the importance of considering the physics in specific problems for the validation procedure. We provide specific examples to support the respective main points addressed using the previous CFD validation experiences from our groups and other groups.

For the last few decades, the broad applications of the computational simulation to predict nuclear system thermal fluids behaviors have been performed. Traditionally, system codes and subchannel analysis codes have been successful to a degree for the nuclear safety analysis. However, because their main role is to combine numerous empirical correlations based on very simple governing equations to evaluate the synthetic effect, the expected level of accuracy was relatively low. The validation is performed against global variables (pressure, temperature, void fraction, liquid level, and so on) in a relatively large control volume (components, subchannels, and so on). On the other hand, in recent years, as the computing power increases, the CFD code has become a viable tool to predict the more detailed thermal fluids behavior in the nuclear system with a higher accuracy than system and subchannel codes.

However, because the nuclear system, in general, involves very complex phenomena characterized as high turbulence and/or multiphase during not only transient events and accidents but also normal operating conditions, the models used in the CFD code for the nuclear system problems still involve empirical closure models, such as RANS equations with turbulence closure models for turbulence calculations and two-fluid model equations with closure models for two-phase calculations, rather than less-empirical models, such as wall-resolved LES/DNS turbulence models and ITMs, respectively, because of practical feasibility. Once some assumptions and related modeling are involved in the CFD

code, we need to understand more about the phenomenon of our interest because the assumptions and modeling have to have capability of reflecting key phenomenon.

The CFD validation is not just comparing the CFD-calculated results with the measured data for a given problem. For successful CFD validation, we need to consider several things from experimental point of view, CFD point of view, and both points of view. Here, we address some (selected) important things for each point of view. From the experimental point of view, a general requirement for data accuracy (with errors) should be satisfied. Beyond this, the specific problem-related issues should be reflected well. Among these, at first, the benchmark experiment should be representative of the prototype. This becomes problematic when the main discrepancies between the CFD calculations and the experiment are due to the difference between the experimental and the prototypic conditions (geometry and thermal fluid conditions). Next, the measured variables in the experiment should reflect key phenomenon and target variables at target range.

From the CFD calculation point of view, it is very important to follow the general CFD BPG—for mesh sensitivity, mesh quality, turbulence models and near-wall treatment, numerical schemes, and so on—to reduce the user errors and evaluate the selected CFD methods in a right way. Beyond this, we need to use an advantage of the CFD—availability of all variables in the computational domain—to understand the overall phenomenon made in the selected CFD world. This will help both experimental design and interpretation of discrepancies between the CFD results and measured data.

From both points of view, it should be stressed that the reliable and effective CFD validation needs closer collaboration between experimentalists and CFD analysts. Both ways from experiment to CFD and from CFD to experiment can greatly reduce time and cost at the end. Each party needs to be willing to provide not only results (data) but also the limitations (errors and uncertainty) and phenomenological insights to another and try to understand the other party to achieve a common goal effectively.

12.11.3 Verification matrix

Code verification activities can be subdivided into Numerical Algorithm Verification and Software Quality Assurance Practices. Here, only the Numerical Algorithm Verification will be discussed in which CFD solutions are compared with “correct answers,” which are highly accurate solutions for a set of well-chosen test problems.

Designing and performing the Numerical Algorithm for verification imposes the need for highly accurate solutions. Then, there is a hierarchy of confidence in these “highly accurate solutions,” ranging from high confidence of exact analytical solutions and/or application of the Method of Manufactured Solutions (MMS), through semianalytic benchmark solutions (reduction to numerical integration of ODEs) to highly accurate benchmark numerical solutions to PDEs.

12.11.4 Requirements for assessment

12.11.4.1 Validation and demonstration matrices

According to the tiered approach to validation of conceptual models, four progressively simpler levels of validation experiments can be distinguished:

- complete system,
- subsystem cases,
- benchmark cases,
- unit problems.

Related experiments should be selected or proposed for each intended application of the CFD code, with at least one suitable experiment (or a set of experiments in the case of unit problems and benchmark cases) at each level.

12.11.4.2 Requirements for validation of experimental data

According to the ECORA BPG, experimental data for validation of a CFD code should be complete (geometry, boundary and initial conditions, well analyzed as to the physical phenomena involved), high quality (accurate within given error bounds, repeatable, consistent), and publicly available.

12.11.4.3 Demonstration simulations

Demonstration simulations are frequently similar to subsystem or complete system cases when there is no or very limited experimental support. Only very approximate conclusions on applicability of the conceptual model can therefore be formulated. Nevertheless, demonstration simulations are very important from the viewpoint of application, since such simulations can support decisions on funding of verification and validation activities, or even of purchase of a CFD code. Especially at the complete system levels, multiscale and multiphysics coupling is frequently required, and balance of resource constraints, including time, level of

effort, available expertise and desired fidelity is very important. In many cases, a demonstration simulation is the first step in application of a CFD code to an NRS issue; such simulation can provide an insight into problems very probably encountered in future, more serious, application of the code. These problems can then be taken into account during planning of the code validation activity.

When demonstration simulations of the same problem are performed with two or more CFD codes, some idea on effectiveness of algorithms can be deduced. Since requirements put on the demonstration simulations are very relaxed in comparison with the validation simulations, it is not in fact possible to speak about “deficiencies,” with the exception of formulation of the initial and boundary conditions (which are either deduced from system code calculations or defined as “the most unfavorable” from the point of view of the intended application), fineness of the computational grid, selection of time steps, and selection of physical models. An important role in the evaluation of demonstration simulations is played by expert judgment, which should take into account all the mentioned deficiencies.

12.11.5 Insights into the assessment process

The overall procedures of CFD analysis for the simulation of heat transfer and fluid flows in a rod bundle with mixing vane grids is considered in this section.

Overall steps of CFD methodology development and validation for the rod bundle problem are presented in Fig. 12.16. First, we have to clearly set objectives of CFD analysis and then set a validation strategy, i.e., choose benchmark problems for the validation of CFD methods. For each benchmark problem, we must clearly describe the problem and then set the CFD solution strategy, which includes choice of CFD methods of turbulence models, computational domain, boundary conditions, numerical schemes, grid types, and resolution. This choice is initially based on previous CFD exercises on this and similar problems and general CFD guidelines. Then, we implement the CFD calculations based on the CFD methods selected and analyze the results by comparing them with experimental results. Changing a specific choice in CFD methods, we iterate the application and analysis until we find the *optimized CFD methods in terms of accuracy and efficiency*.

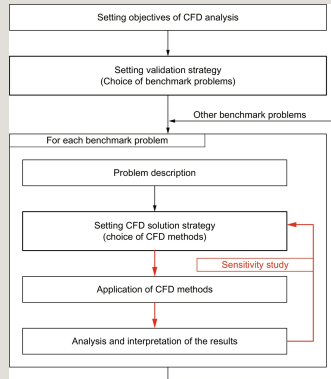


Fig. 12.16 Overall steps of CFD methodology development and validation.

12.11.5.1 Setting objectives of CFD analysis (Step 1)

First, we *set objectives of CFD analysis* clearly, e.g., design of a component, safety analysis, interpretation of experimental data, validation of numerical grid structure, validation of a model, demonstration of CFD code-user quality, user training (many calculation analyses actually fall in this category), finalizing the development of a CFD model, development of BPG or demonstration of quality for BPG, etc.

12.11.5.2 Setting validation strategy (Step 2)

The next step is to *set validation strategy*. Here, one needs to thoroughly review previous experiments and CFD analyses relating to the topic to efficiently and specifically set the strategy. Collecting available experimental tests and identifying unresolved CFD issues, one must select and organize experiments as benchmark problems. During the choice process, several problems, not a single problem, are often considered. This is because one problem cannot be complete in terms of data coverage and quality and because data provided sometimes need to be cross-checked through other tests at similar conditions. In addition, attacking one complex problem often does not clearly reveal the source of discrepancy, if one exists, because the problem may involve several complex interactions. In this case, we can take the stepwise approach from simple to complex problems.

12.11.5.3 Problem description (Step 3)

Once experimental tests to be benchmarked are determined, for each problem CFD methods are applied and validated. Before applying CFD methods, *each*

benchmark problem should be clearly defined. The following information should be described in detail:

- Purposes of the experiment,
- Geometry, and
- Boundary conditions

In addition, any uncertainties (incompleteness) relating to the above information must be clearly stated. This can play an important role in the result analysis procedure.

12.11.5.4 Setting CFD solution strategy (Step 4)

Then, we need to *set CFD solution strategy* for a given problem, which includes many choice procedures, such as choice of computational domain, choice of boundary conditions, choice of turbulence models including near-wall treatment, choice of numerical schemes, choice of geometrical representation, and choice of computational grids. It should be pointed out that the choice of any CFD method does not necessarily coincide with the actual implementation. In other words, in the implementation of CFD methods, geometry and computational domain are first generated and the grid is, then, created mainly by using preprocessing tools. Then, the choices of other CFD methods may follow.

In this step, *knowledge about CFD methods previously used for this or similar problems and general guidelines* is very important because it provides for an effective initial choice of CFD methods, which can reduce uncertainties and thus the number of methods requiring sensitivity study. Thus, we identify main CFD methodological issues, which can preliminary affect the results, especially target variables in the region of interest.

12.11.5.5 Application of CFD methods (Step 5)

In the process of *application of CFD methods selected*, i.e., implementing the CFD solution strategy with a particular code, *user errors should be minimized* and *appropriate convergence criteria* must be selected. These issues are not specific to rod bundle problems, but are general to all CFD simulations.

Minimizing user errors

Before running the code, a potential source of user errors should be checked. Such errors may be minimized by using a formal check list or by letting another CFD

analyst check through the code input data.

For example, the following types of questions can be considered (Gallagher and Woodburn, 2003):

- Have boundary conditions not only been properly defined, but also properly applied?
- Has the appropriate system of units been used?
- Is the geometry correct?
- Are the correct physical properties specified?
- Have the intended physical and mathematical models, such as gravity force, rotation, and user-defined functions, been used?
- Have default parameters been changed which may affect the solution?
- Has the appropriate convergence criterion been defined?

Choice of convergence criteria

The choice of convergence criteria also needs to be considered in the application of a CFD method, i.e., running the CFD code, because most computer programs use iterative methods to solve the algebraic system of equation (e.g., the equation for the pressure). Here, convergence indicates the criterion adopted to terminate an iterative process, not the convergence of discretized equation to differential equation.

The following convergence criteria are typically used (COST, 2007):

- (Scaled) residuals;
- Target variables;
- Integral balance of mass, momentum, and energy.

The termination criterion is usually based on the residuals of the corresponding equations. These residuals should tend toward zero. Scaling of the residuals is usually done with the residuals after the first iteration. The scaled residual then shows how much the initial error has dropped. In industrial applications, typically a termination criterion of 0.001 is used, which, in general, is too high to have a

converged solution. A reduction of the residuals of *at least four orders of magnitude* is recommended. For validation purposes of turbulence or other physical models much lower threshold criteria should be used.

General guidelines for convergence control are as follows (Gallagher and Woodburn, 2003):

- Be aware that different codes have different definitions of residuals.
- Always check the convergence on global balances (conservation of mass, momentum, and turbulent kinetic energy) where possible, such as the mass flow balance at inlet and outlet and at intermediate planes within the flow domain.
- Check not only the residual itself but also the rate of change of the residual with an increasing iteration count.
- Convergence of a simulation should not be assessed purely in terms of the achievement of a particular level of residual error. Carefully define solution-sensitive target quantities for the integrated global parameters of interest and select an acceptable level of convergence based on the rate of change of these (such as mass flow, lift, drag and moment forces on a body).
- For each problem class, test the effect of converging to different levels of residual on the integrated parameter of interest (this may be a single calculation that is stopped and restarted at different residual levels). This test demonstrates at what level of residual the parameter of interest can be considered to have converged and identifies the level of residual that should be aimed at in similar simulations of this problem class.
- Monitor the solution in at least one point of a sensitive area to see if the region has reached convergence.

For calculations that are proving difficult to converge, the following advices may be helpful (Gallagher and Woodburn, 2003):

- Use more robust numerical schemes during the first (transient) period of convergence and switch to more accurate numerical schemes as the convergence improves.
- When using RSM, start with a stable turbulence model like the k - ϵ model.
- Reduce parameters controlling convergence, for instance, under-relaxation

parameters or the CFL number.

- If the solution is heavily under-relaxed, increase relaxation factors at the end to see if the solution holds.
- Check whether switching from a steady to a transient calculation has any effect.
- Consider using a different initial condition for the calculation.
- Check the numerical and physical suitability of boundary conditions.
- Check whether the grid quality in areas with large residual has any effect on the convergence rate.
- Look at the residual distribution and associated flow field for possible hints, e.g., regions with large residuals or unrealistic velocity levels.

12.11.5.6 Analysis and interpretation of the results (Step 6)

Most commercial CFD codes have useful postprocessing tools, which allow various flow and heat transfer phenomena to be visualized or plotted in graphical form. The step of results analysis covers:

- Checking credibility of results,
- Checking needs of sensitivity studies, and
- Using various variables which help understand the phenomena.

Checking the credibility of the results in the validation process can be directly implemented because the main target variables are usually given in the experiment. However, if the objective of the simulation is to provide detailed data in a new spacer grid design, checking credibility may involve several steps, such as checks on conserved variables, visual confirmation that velocities and pressure are smoothly distributed, and comparison with other similar problem results (Gallagher and Woodburn, 2003).

As discussed in the step of setting the CFD solution strategy, a *sensitivity study* is not confined to only computational grid resolution, but is also applied to all computational methods selected in the CFD solution strategy step, such as turbulence modeling, near-wall treatment, numerical schemes, grid types, boundary conditions, and geometrical representation. In practicality, performing a

sensitivity study about all procedures is impossible, since an interpretation of the results must focus on finding the CFD method most regarded as affecting the target variables.

Analysis using multiple variables helps understand the phenomena more clearly.

12.12 CFD scaling

12.12.1 The scaling issue

The word scaling can be used in a number of contexts: two of these are reported here.

(1) Scaling of an experiment is the process of demonstrating how and to what extent the simulation of a physical process (e.g., a reactor transient) by an experiment at a reduced scale (or at different values of some flow parameters, such as pressure and fluid properties) can be sufficiently a representative of the real process in the reactor.

(2) Scaling applied to a numerical simulation tool is the process of demonstrating how and to what extent the numerical simulation tool validated on one or several reduced scale experiments (or at different values of some flow parameters, such as pressure and fluid properties) can be applied with sufficient confidence to the real process.

One should emphasize that scaling is meant here in terms of the prediction of a result for the reactor from a scaled experiment, as defined by Oberkampf and Roy in their book on V&V (Oberkampf and Roy, 2010).

When solving a reactor thermal-hydraulic problem, the answer to the scaling issue may be:

1. Purely experimental: the experiments can tell what would occur in the reactor with sufficient accuracy and reliability;
2. Purely numerical: only numerical simulations are used to solve the problem (usually this is not acceptable);
3. Both experiments and simulation tools are used to solve the issue (this is the best practice).

The first case is not common and is not considered here since CFD simulation tools

are not involved. The second case is also not common, due to the limited reliability and accuracy of thermal-hydraulic simulation tools. So we will focus here on the third case, in which both experiments and simulation tools are used to try to resolve the issue. This means that the simulation tool is used to extrapolate from experiments to the reactor situation, and that the degree of confidence in this extrapolation is itself part of the scaling issue.

The extrapolation to a reactor situation made by a single-phase CFD tool introduces several new aspects and raises several questions:

- How to guarantee that a CFD code can extrapolate from a reduced-scale validation experiment to the full-scale application?
- How to extrapolate nodalization from a reduced-scale validation experiment to the full-scale application?
- How to extrapolate:
 - from one fluid to another?
 - to a different value of the Re number and/or to a different value of any other nondimensional number important in the physical processes taking place?
- In any case, numerical simulation of scaled experiments has a given accuracy defined by the error on some target parameters, and one should determine how the code error changes when extrapolating to the reactor situation.

Therefore, scaling associated with a CFD application is part of the CFD code uncertainty evaluation, and is a necessary preliminary step in this uncertainty evaluation. Both scaling and uncertainty are closely related to the process of Validation and Verification. The definition of a metric for the validation is also part of the issue.

12.13 Conclusions and recommendations

12.13.1 Conclusions of OECD/NEA/CSNI report (OECD/NEA/CSNI/R(2014)3, 2014)

Hereafter conclusions are reported that have been agreed within a wide scientific community (OECD/NEA/CSNI) in relation to the CFD technology. The reported conclusions are (obviously) consistent with the text of the chapter. Minor editorial changes are introduced, namely to adapt the original text to the content of this

chapter.

The use of computational methods for performing safety analyses of reactor systems has been established for nearly 40 years. Reliable codes have been developed for analyzing the primary system in particular, and results from these analyses are often used to support the safety assessment of nuclear power systems undertaken by the regulatory authorities. Similarly, but to a lesser extent, programs have also been written for containment and severe accident analyses. Such codes are based on networks of 1D or even 0D cells. However, the flow in many reactor primary components is essentially 3D in nature, as is natural circulation, mixing, and stratification in containments. CFD has the potential to treat flows of this type and to handle geometries of almost arbitrary complexity. Already, CFD has been successfully applied to such flows, and to a limited extent has made up for a lack of applicable test data in better quantifying safety margins. Consequently, CFD is expected to feature more prominently in reactor safety analyses in the future.

The traditional approaches to nuclear reactor safety analysis, using system codes for example, take advantage of the very large database of mass, momentum, and energy exchange correlations that have been built into them. The correlations have been formulated from essentially 1D special-effects experiments, and their range of validity is well known, and (as far as possible) controlled internally within the numerical algorithms. Herein lays the trustworthiness of the numerical predictions of such codes. Analogous databases for 3D flows are very sparse by comparison, and the issue of the trust and reliability of CFD codes for use in NRS applications has therefore to be addressed before the use of CFD can be considered as trustworthy.

A list of NRS problems for which it is considered CFD analysis is required or its application is expected to result in positive benefits in terms of better understanding and improved safety margins is provided in OECD/NEA/CSNI (2014) and also discussed in this chapter. The list contains safety issues of relevance to fluid flows in the core, primary circuit and containment, both under normal and off-normal operating conditions including accident sequences. The list contains both single-phase and two-phase safety items, though in the latter case reference is made to the document dealing with the Extension of CFD Codes to Two-Phase Flow Nuclear Reactor Safety Problems, Mahaffy et al. (2007a,b) and OECD/NEA/CSNI (2014) (see also Bestion et al., 2016).

Recognizing that CFD is already an established technology outside of the nuclear community, a list of the existing assessment bases from other application areas has also been included in OECD/NEA/CSNI (2014) and their relevance to NRS issues

discussed in the same report. It is shown that these databases are principally of two types: those concerned with aspects of trustworthiness of CFD code predictions in general industrial applications (ERCOFTAC, QNET-CFD, FLOWNET), and those focused on specialized topics (MARNET, NPARC, AIAA). The usefulness and relevance of these databases to NRS have been assessed. In addition, most CFD codes currently being used for NRS analysis have their own, custom-built assessment bases, the data being provided from both within and external to the nuclear community. Application of CFD to NRS problems can benefit indirectly from these databases. The continuing efforts to extend them can lead to a well-maintained NRS-specific database, a valuable addition.

Descriptions of the existing CFD assessment bases have been established specifically within the nuclear domain and their usefulness discussed. Typical examples are experiments devoted to the boron dilution and in-vessel mixing issues (ISP-43, ROCOM, Vattenfall 1/5th Scale Benchmark, UPTF TRAM C3), pressurized thermal shock (UPTF TRAM C2), and thermal fatigue in pipes (THERFAT, Forsmarks), all of which have already been the subject of benchmarking activities. The EU Framework Programs, such as ASTAR, ECORA, EUBORA, FLOWMIX-R and ASCHLIM, have also provided direct NRS-specific data and/or have each focused on relevant aspects of the CFD modeling.

The technology gaps which need to be closed to make CFD a more trustworthy analytical tool have also been identified in OECD/NEA/CSNI (2014). These include, for example, lack of a proper uncertainty methodology; limitations in the range of application of turbulence models, for example in stratified and buoyant flows; coupling of CFD with neutronics and system codes, needed to keep simulations to a manageable size; and generally computer power limitations in simulating long transients. Particular application areas for which CFD simulations need to be improved are in stratified flows, containment modeling, aerosol transport and deposition, and liquid-metal heat transfer. In other areas, such as in-vessel mixing, the models may be adequate but grid resolution is inadequate due to the current lack of machine power, a situation that will certainly improve with time.

The computational overhead of performing CFD simulations in comparison with system code transient computations may still be regarded as a definite limitation of the potential for directly using CFD in licensing procedures, even for single-phase applications for which the underlying models are well established. The uncertainty quantification methodology for system codes generally requires 50–100 computations to be carried out, and the statistical method of Latin Hypercube

Sampling (LHS) is becoming widespread in order to optimize the efficiency of the random parameter sampling. This cannot, at the present time, be mirrored with CFD, and until it can, a different methodology needs to be established. However, in the spirit of BPGs, at least mesh independency must be demonstrated, and some limited study of sensitivity to input parameters should be attempted. The issue of access to the source code of CFD software, particularly in regard to the commercial codes, will also have to be addressed before CFD is accepted as an analysis tool by the regulatory bodies.

There is a distinct lack of quality validation data for aerosol transport, even though the phenomenon was identified as a key process in containment modeling, and one that can only be treated mechanistically by the use of CFD. The experiments carried out at the PHEBUS facility as part of the EU 5th Framework Programme PHEBEN produced only data of an integral nature, and as such very limited in regard to validating CFD models. Comprehensive, local aerosol deposition data appear only to be available for pipes (straight and elbowed), and for some nonnuclear applications, such as atmospheric pollution. This is one key area where future CFD assessment needs to be focused.

Important new information has been provided by the material presented at the CFD4NRS series of Workshops (here listed in the Foreword), in which numerical simulations with a strong emphasis on validation were particularly encouraged, and the reporting of experiments which provided high-quality data suitable for CFD validation. Participation in the workshops has enabled a list of existing databases to be assembled of possible candidates for future benchmarking activities for:

- (1) primary circuits,
- (2) core-flow regions,
- (3) containments,

in relation to which data of the type needed for CFD benchmarking already exists or are likely to be available in the near future.

This updated document represents a continuing process in establishing an assessment database for the application of CFD to NRS problems, but in many places reflects the time and manpower restriction for issuing the concerned OECD/NEA/CSNI report (this also applies to this chapter), and considerable further work still needs to be done in terms of both presentation and technical content. Sections

of the OECD/NEA/CSNI report, as well as of this chapter, remain unbalanced in terms of detail, reflecting not only the subjective inputs of the authors but also whether the safety issue being addressed is of a country-specific nature or of more common concern. Part of the recommended obligation to regularly update the provided information shall include an attempt to equilibrate the information level. In addition, similar information appears in different sections of the report and of the chapter. This was done to avoid excessive page turning or scrolling, but gives the OECD/NEA/CSNI document (and this chapter) an appearance of disjointedness if read in a continuous manner.

CFD remains a very dynamic technology, and with its increasing use within the nuclear domain there will be ever greater demands to document current capabilities and prove their trustworthiness by means of validation exercises. It is therefore expected that any existing list of specific assessment databases will soon require further updating. In order to prevent the important information assembled in the OECD/NEA/CSNI document and in this chapter from becoming obsolete, the following recommendations are made:

- Extend the process of consolidating the information contained here through continuous updating. This process is necessary to ensure that the NRS assessment database is readily accessible to all, and as dynamic and mobile as the CFD technology itself.
- Set up a forum for numerical analysts and experimentalists to exchange information in the field of NRS-related activities relevant to CFD validation, e.g., like the one provided by the series of CFD4NRS workshops (see e.g., Foreword to this chapter).
- New blind CFD benchmarking exercises should be defined, both to encourage the release of previously restricted CFD-grade data from experiments, to test the skills of the CFD practitioners, and perhaps persuade the software developers to improve their models, where these have proved lacking. To this end, it is encouraging to note that representatives of the large commercial software houses actively participate in the benchmarks.

Finally, it seems worthwhile to extend the alarm given in the following statement of OECD/NEA/CSNI (2014) report to this chapter. The Special CFD Group, which was first set up in 2007 and initially comprised of the chairmen of the original three Writing Groups (WG) together with the NEA secretariat, can continue to act as the central organizing bodies for the above activities provided new members are appointed to replace the “old guard.” The timescale for this process is (i) *overdue*

for the WG1 chairman (J. H. Mahaffy reached pensionable age in 2009); (ii) *imminent* for the WG2 chairman (B. L. Smith reached pensionable age in 2012); and *within sight* for the WG3 chairman (D. Bestion will reach pensionable age in 2017). It is important to ensure a smooth transition to a new group membership before the existing expertise is lost.

12.13.2 Final-summary remarks

The complex CFD subject is discussed in this, work-in-progress type (see the Chapter foreword), chapter: question marks and identification of critical issues are part of the text; however, an attempt is made to clarify some important topics in relation to nuclear thermal hydraulics. Any reader who has completed the reading of the chapter should not believe he has acquired the understanding of the CFD subject: he must integrate his learning with information from literature (e.g., including listed references) and by direct application of CFD methods. The chapter shows the multiple directions of the R & D research in the concerned area.

The CFD technology and the related development are tightly connected with the computer power and with the related characteristics. Thus a fast CFD development can be noted in the last few decades and in the recent years. This makes difficult to fix the current status: it is just like trying to make a meaningful picture of a fast moving object.

Furthermore, CFD has the origin, the scientific background, and the application areas much wider than nuclear thermal hydraulics.

A single summary sentence to outline the current status in CFD technology in relation to nuclear thermal hydraulics is the following: The computational power of CFD codes is enormous, even beyond the actual needs in NPP technology, and so are the perspectives for further development; however, V & V of tools and methods is insufficient and there is a lack of uncertainty quantification and, whenever applicable, of scaling capability demonstration (in the last two area efforts are ongoing by the international community, e.g., Bestion et al., 2016).

In the area of nuclear thermal hydraulics, keywords are: CFD; Spatial resolutions; BPG (BPG); Turbulence Modeling; Mesh generator; Numerical solver algorithm.

For the future: It seems useless to recommend efforts in one direction or in another, e.g., preferring one model or one approach to others: too many players are involved and the (science and technology) market, including the fashion topics, will fix the development. However, restricted to nuclear thermal hydraulics, it

seems that a tight cooperation among physical model developers, experts in numerics and in computer-related aspects, code users, designers, and reactor safety experts has the potential to dramatically reduce the time needed for the achievement of a mature computational technique.

References

AIAA. *Guide for the Verification and Validation of Computational Fluid Dynamics Simulations (G-077-1998e)*. AIAA Standards; 1998.978-1-56347-354-8.

Aksan, S.N., D'Auria, F., Glaeser H., Pochard, R., Richards, C., Sjoberg, A., 1993. Separate effects test matrix for thermal-hydraulic code validation: facility and experiment characteristics, Vol II. OECD/NEA/CSNI Report OCDE/GD(94)83, Paris, France, September.

ANSYS. *ANSYS CFX-Solver Theory Guide – Release 13.0*. Canonsburg: ANSYS Inc; 2010.

ASME. *Standard for Verification and Validation in Computational Fluid Dynamics and Heat Transfer, V V 20–2009 (reaffirmed 2016)*. ASME; 2009.9780791832097.

Aumiller D.L., Tomlinson E.T., Bauer R.C. Coupled RELAP5-3D/CFD methodology with a proof-of-principle calculation. *J. Nucl. Eng. Des.* 2001;205(1–2):83–90.

Baglietto E., Ninokata H. *CFD modelling of secondary flows in fuel rod bundles*. In: Conf. NUTHOS-6, AESJ, Nihon Genshiryoku Gakkai, Japan; 2004.

Baglietto E., Ninokata H., Misawa T. CFD and DNS methodologies development for fuel bundle simulations. *Nucl. Eng. Des.* 2006;236:1503–1510.

Balaras E., Benocci C., Piomelli U. Two layer approximate boundary condition for large eddy simulation. *J. AIAA*. 1996;34:1111–1119.

Banerjee S. *What can we expect from DNS and LES?* In: Invited at

NURETH-15 Conf., Pisa, Italy; 2013.

Baudin N., Colin C., Ruyer P., Sebillieu J. Turbulent flow and transient convection in a semi-annular duct. *Int. J. Thermal Sci.* 2016;108:40–51.

Benhamadouche S. *On the use of (U)RANS and LES approaches for turbulent incompressible single phase flows in nuclear engineering applications*. In: The 16th International Topical Meeting on Nuclear Reactor Thermal Hydraulics (NURETH-16), Chicago, IL, USA; 2015.

Benhamadouche S., Malouf W.J., Arenas M. *Effects of spatial discretisation and RANS turbulence modelling on the numerical simulation of a flow through a square-edged orifice in a round pipe*. In: E-proceedings of the 36th IAHR World Congress, The Hague, NL; 2015.

Bestion D. *Extension of CFD codes to two-phase flow safety problems*. In: Workshop CFD4NRS-4 Grenoble, France, Sept. 10–12; 2008.

Bestion D. Applicability of two-phase CFD to nuclear reactor thermal hydraulics and elaboration of Best Practice Guidelines. *J. Nucl. Eng. Des.* 2012;253:311–321.

Bestion D., de Crecy A., Camy R., Barth A., Bellet S., Badillo A., Niceno B., Hedberg P., Muñoz Cobo J.L., Moretti F., Scheuerer M., Nickolaeva A. *Review of uncertainty methods for computational fluid dynamics application to nuclear reactor thermal hydraulics*. In: NEA/CSNI/R(2016)4, Paris, France; 2016.

Bieder U., Falk F., Fauchet G. LES analysis of the flow in a simplified PWR assembly with mixing grid. *J. Prog. Nucl. Ener.* 2014;75:15–24.

Blowe T.N., Kang S.K., Hassan Y.A. *CFD methodologies for a PWR fuel rod assembly*. In: 16th International Topical Meeting on Nuclear Reactor Thermal Hydraulics (NURETH-16), Chicago, IL, USA; 2015.

Boyd C. Perspectives on CFD analysis in nuclear reactor regulation. *J. Nucl. Eng. Des.* 2016;299:12–17.

Breuer M., Jaffrézic B., Arora K. Hybrid LES–RANS technique based on a one-equation near-wall model. *J. Theor. Comput. Fluid Dyn.* 2008a;22(3–4):157–187.

Breuer M., Peller N., Rapp Ch., Manhart M. Flow over periodic hills—numerical and experimental study in a wide range of Reynolds numbers. *Int. J. Computers Fluids.* 2008b;38:433–457.

Cabot W. *Near wall model in large eddy simulation of flow behind a backward facing step.* In: Annual Research Briefs, Center for Turbulence Research, NASA, Stanford University, CA, USA; 1996.

Cabot W., Moin P. Approximate wall boundary conditions in the large-eddy simulation of high reynolds number flow. *J. Flow. Turb. Comb.* 2000;63(1):269–291.

Cadinu F., Kozłowski T., Nam Dinh T. *Relating system-to-CFD coupled code analyses to theoretical framework of a multiscale method.* In: Proceedings of ICAPP 2007, Nice, France, May 13–18, Paper 7539; 2007.

CD-adapco, 2006. STAR-CCM+ provider: STAR-CAT5 at COE; also CD-adapco - the leading provider of CAD-embedded and advanced multidisciplinary turbomachinery simulations exhibit at the annual ASME Turbo Expo in Barcelona.

Chapman D.R. Computational aerodynamics development and outlook. *AIAA J.* 1979;17(12):1293–1313.

Christensen H. MS, Royal Technical University of Denmark (1954). In: *Doctoral Dissertation.* Massachusetts Institute of Technology; 1961.

COST. Best practice guideline for the CFD simulation of flows in the urban environment. In: Franke J., Hellsten A., Schlünzen H., Carissimo B., eds. *COST Action 732: Quality Assurance and Improvement of Microscale Meteorological Models.* European

Cooperation in Science and Technology; 2007:16–18.

Craft T.J., Gerasimo A.V., Launder B.E., Robinson C.M.E. A computational study of the near-field generation and decay of wingtip vortices. *Int. J. Heat Fluid Flow*. 2006;27:684–695.

Diwan S.S., Chetan S.J., Ramesh O.N. *On the bursting criterion for laminar separation bubbles, Laminar-Turbulent Transition*. In: Proceedings of the IUTAM Symposium; Springer; 2006:401–407.

Drikakis D. Embedded turbulence model in numerical methods for hyperbolic conservation laws. *Int. J. Numer. Methods Fluids*. 2002;39(9):763–781.

Ekman V.W. On the influence of the Earth's rotation on ocean currents. *Arch. Math. Astron. Phys*. 1905;2:1–52.

EPRI. *Computational Fluid Dynamics Benchmark of High Fidelity Rod Bundle Experiments: Industry Round Robin Phase 1 – Rod Bundle With Simple Support Grids*. CA, USA: Palo Alto; 2014 2014.3002000504.

EPRI. *Computational Fluid Dynamics Benchmark of High Fidelity Rod Bundle Experiments: Industry Round Robin Phase 2 – Rod Bundle with Mixing Vane Grids*. CA, USA: Palo Alto; 2015 2015.3002005401.

Faragher J. *Probabilistic methods for the quantification of uncertainty and error in computational fluid dynamics simulations*. In: DSTO-TR-1633, Sydney, Australia; 2004. <http://dspace.dsto.defence.gov.au/dspace/handle/1947/4214>.

Fasel H.F., Seidel J., Wernz S. A methodology for simulations of complex turbulent flows. *J. Fluids Eng*. 2002;124(4):933–942.

Ferziger J.H. Large Eddy Simulation, Simulation and Modeling of Turbulent Flow. In: Gatski T.B., Hussaini M.Y., eds. NY, USA: Oxford Univ. Press; 1996. *ICASE/LArc Series in Comp. Science and Eng.*.

FLUENT. *Fluent 6.3 User Guide*. Lebanon, NH USA: Fluent Inc.,

Centerra Resource Park; 2006.

Fröhlich J., von Terzi V. Hybrid LES/RANS methods for the simulation of turbulent flows. *Prog. Aerosp. Sci.* 2008;44:349–377.

Fu S., Xiao Z.X., Huang J.B., Zhang Y.F. Investigation of practical flow control methodologies with RANS/LES hybrid methods, chapter. 41–58. *Progress in Hybrid RANS-LES Modelling, Volume 111 of the series Notes on Numerical Fluid Mechanics and Multidisciplinary Design.* 2010;vol. 111.

Fureby C. Large eddy simulation modelling of combustion for propulsion applications. *Philos. Trans. R. Soc. A Math. Phys. Eng. Sci.* 2009;367:2957–2969. doi:10.1098/rsta.2008.0271.

Fureby C., Henriksson M., Parmhed O., Sjökvist L., Tegnér J. *CFD predictions of jet engine exhaust plumes.* In: AIAA 2008-2345; 2008.

Gallagher P., Woodburn P. *An overview of European research in CFD-based fluid loading and fluid structure interaction.* In: MARNET-CFD Offshore Technology Conference; 2003.

Gatski T.B., Jongen T. Nonlinear eddy viscosity and algebraic stress models for solving complex turbulent flows. *Prog. Aerosp. Sci.* 2000;36:655–682.

Gibeling H., Mahaffy J. *Benchmarking simulations with CFD to 1-D coupling.* In: Joint IAEA/OECD Technical Meeting on Use of CFD Codes for Safety Analysis of Reactor Systems, Including Containment, Pisa, Italy; 2002.

Graf U. Implicit coupling of fluid-dynamic systems: Application to multidimensional countercurrent two-phase flow of water and steam. *Nucl. Sci. Eng.* 1998;129(3):305–310.

Grgic D., Bajcs T., Oriani L., Conway L.E. *Coupled RELAP5/GOTHIC model for accident analysis of the IRIS reactor.* In: IAEA Technical Meeting on Use of Computation Fluid Dynamics (CFD) Codes for Safety Analysis of Reactor Systems, Pisa, Italy,

Nov. 11–15; 2003.

Groetzbach G. Direct numerical and large eddy simulation of turbulent channel flows. In: Cheremisinoff N.P., ed. Houston, TX: Gulf Publishing; 1337–1391. *Encyclopedia of Fluid Mechanics*. 1987;vol. 6.

Gungor A., Menon S. *Direct Simulation of subgrid turbulence in high-re, wall-bounded flows*. In: 36th AIAA Fluid Dynamics Conference and Exhibit, Fluid Dynamics and Co-located Conferences, San Francisco, CA, USA; 1996.

Guyot M.K., Ormiston S.J., Soliman H.M. Numerical analysis of two-phase flow from a stratified region through a small circular side branch. *Int. J. Multiphase Flow*. 2016;87:175–183.

Hackbush W., Wittum G. *Numerical treatment of coupled systems*. In: Eleventh-GAMMA Seminar Kiel (G), vol 51, Jan. 20–22; 1995.

Hamba F. A hybrid RANS/LES simulation of turbulent channel flow. *Theor. Comput. Fluid Dyn*. 2003;16:387–403.

Hamba F. A hybrid RANS/LES simulation of high-Reynolds-number channel flow using additional filtering at the interface. *Theor. Comput. Fluid Dyn*. 2006;20(2):89–101.

Hassan Y.A., Smith B.L., eds. Topical issue on CFD4NRS. *Nucl. Eng. Des*. 2008;238:771–785.

Hellsten, A., 2004. New Two Equation Turbulence Model for Aerodynamics Application. Dissertation for the degree of Doctor of Science in Technology, Helsinki University of Technology, Espoo, Finland.

Hellsten A. New advanced k-omega turbulence model for high-lift aerodynamics. *AIAA J*. 2005;43(9):1857–1869.

Hellsten A., Beazard H. Behaviour of nonlinear two-equation turbulence models at the free-stream edges of turbulent flows. In: Rodi W., Mulas M., eds. *Engineering Turbulence Modelling and Experiments*. Amsterdam: Elsevier; 2005.

Hellsten A., Wallin S. Explicit algebraic Reynolds stress and non-linear eddy viscosity models. *Int. J. Comput. Fluid Dyn.* 2009;23:349–361.

Howard R.J.A., Pourquie M. Large eddy simulation of an Ahmed reference model. *J. Turbul.* 2002;3:N12.
doi:10.1088/1468-5248/3/1/012.

Hussaini M.Y., Thangam S., Woodruff S.L., Zhou Y. Development of a continuous model for simulation of turbulent flows. *J. Appl. Mech.* 2006;73(3):doi:10.1115/1.2173006.

Hutton A.G. The merging role of large eddy simulation in industrial practice: challenges and opportunities. *Philos. Trans. R. Soc., A.* 2009;367:2819–2826.

Ibrahimbegovic A., Markovic D. Strong coupling methods in multi-phase and multi-scale modeling of inelastic behavior of heterogeneous structures. *Comput. Methods Appl. Mech. Eng.* 2003;192:3089–3107.

In W.K., Oh D.S., Chun T.H. *Simulation of turbulent flow in rod bundles using eddy viscosity models and the reynolds stress model.* In: Proc. 10th Int. Topical Meeting on Nuclear Reactor Thermal Hydraulics (NURETH-10), Seoul, South Korea, Oct. 5–9; 2003.

Jeong J.J., Sim S.K., Ban C.H., Park C.E. Assessment of the COBRA/RELAP5 code using the LOFT L2-3 large-break loss-of-coolant experiment. *Ann. Nucl. Energy.* 1997;24(14):1171–1182.

Johnson R.W. Modeling strategies for unsteady turbulent flows in the lower plenum of the VHTR. *Nucl. Eng. Des.* 2008;238:482–491.

Kang S.K., Hassan Y.A. Computational fluid dynamics (CFD) round robin benchmark for a pressurized water reactor (PWR) rod bundle. *Nucl. Eng. Des.* 2016;301:204–231.

Keating A., Piomelli U. A dynamic stochastic forcing method as a wall-layer model for large-eddy simulation. *J. Turbul.*

2006;7:12.

Kliem S., Höhne T., Rohde U., Weiss F.-P. *Main steam line break analysis of a VVER-440 reactor using the coupled thermohydraulics system/3D-neutron kinetics code DYN3D/ATHLET in combination with the CFD code CFX-4*. In: Proc. 9th Int. Topl. Mtg. Nuclear Reactor Thermal Hydraulics (NURETH-9), San Francisco, CA, USA, October 3–8; 1999.

Kniesner B., Jester-Zürker R., Jakirlić S., Hanjalić K. *RANS–SMC and hybrid LES/RANS modelling of a backward-facing step flow subjected to increasingly enhanced wall heating*. In: Fifth Int. Symp. on Turbulence and Shear Flow Phenomena, Garching, Germany, 27–29 August; 2007.

Kok J.C. Resolving the dependence on freestream values of the k - ω turbulence model. *AIAA J.* 2000;38:1292–1295.

Kothe D.B. *CASL: the consortium for advanced simulation of light water reactors*. In: 2nd DOE/NRC/NEI Workshop on U.S. Nuclear Power Plant Life Extension R & D, Washington, DC, USA, Feb. 22–24; 2011.

Kothe D.B. *CASL, CASL: The Consortium for Advanced Simulation of Light Water Reactors Various Presentations*. Oak Ridge, TN, USA: ORNL; 2015.

Kothe D.B., Szilard R., Turinsky P. *CASL: The Consortium for Advanced Simulation of Light Water Reactors*. Oak Ridge, TN, USA: US Department of Energy; 2010.

Labois M., Lakehal D. Very-large eddy simulation (V-LES) of the flow across a tube bundle. *Nucl. Eng. Des.* 2011;241:2075–2085.

Laufer J. Structure of fully developed turbulent pipe flow. *NASA Tech. Note.* 1953;2954.

Launder B.E., Reece G.J., Rodi W. Progress in the development of a Reynolds stress turbulence model. *J. Fluid Mech.* 1975;68:537–566.

Lee J.R., Kim J., Song C.-H. Synthesis of the turbulent mixing in a rod bundle with vaned spacer grids based on the OECD-KAERI CFD benchmark exercise. *Nucl. Eng. Des.* 2014;279:3–18.

Li Q., Luo K.H., Kang Q.J., He Y.L., Chen Q., Liu Q. Lattice Boltzmann methods for multiphase flow and phase-change heat transfer. *Prog. Energy Combust. Sci.* 2016;52:62–105.

Lu P., Semião V. A new second-moment closure approach for turbulent swirling confined flows. *Int. J. Numer. Methods Fluids.* 2003;41:133–150.

Mahaffy, J. H., Chung, B., Dubois, F., Ducros, F., Graffard, E., Heitsch, M., Henriksson, M., Komen, E., Moretti, F., Morii, T., Mühlbauer, P., Rohde, U., Scheuerer, M., Smith, B.L., Song, C.-H., Watanabe, T., Zigh, G., 2007a. Best practice guidelines for the use of CFD in nuclear reactor safety applications. OECD Report, NEA/CSNI/R(2007)5, Paris, France.

Mahaffy, J.H., Chung, B., Dubois, F., Ducros, F., Graffard, E., Heitsch, M., Henriksson, M., Komen, E., Moretti, F., Morii, T., Mühlbauer, P., Rohde, U., Scheuerer, M., Smith, B.L., Song, C.-H., Watanabe, T., Zigh, G., 2007b. Best practice guidelines for the use of CFD in nuclear reactor safety applications. OECD Report, NEA/CSNI/R(2014)11, Paris, France.

Menter F.R. *Improved two equation k - ω turbulence model for aerodynamics flows*, NASA Technical memorandum 103975, Houston (Tx, US). 1992.

Menter F.R. Two-equation eddy-viscosity turbulence models for engineering applications. *AIAA J.* 1994;32:8.

Menter F.R., Egorov Y. *A scale-adaptive simulation model using two-equation models*. In: AIAA Paper 2005-1095, Reno, NV, USA; 2005.

Menter F.R., Esch T. Advanced turbulence modeling in CFX. *CFX Update*. 2001;20:4–5.

Menter F.R., Kuntz M., Langtry R. *Ten years of industrial*

experience with the SST turbulence model. In: 4th International Symposium on Turbulence, Heat and Mass Transfer, ICHMT 4, Antalya, Turkey; 2003a.

Menter F.R., Kuntz M., Bender R. *A scale-adaptive simulation model for turbulent flow prediction*. In: AIAA Paper 2003-0767, Reno, NV, USA; 2003b.

Meri A., Wengle H. DNS and LES of turbulent backward-facing step flow using 2ND- and 4TH-order discretization. In: *Advances in LES of Complex Flows*. Netherlands: Springer; 2002:99–114.

Meri A., Wengle H., Raddaoui M., Chauve M.-P., Schiestel R. Large-eddy simulation of non-equilibrium inflow conditions and of the spatial development of confined plane jet with co-flowing streams. In: Rodi W., Laurence D., eds. *Engineering Turbulence Modelling and Experiments*. Proceedings of the 4th International Symposium on Engineering Turbulence Modelling and Measurements, Porticcio-Ajaccio, Corse, France, 24–26 May, pp. 197; Amsterdam, NL: Elsevier; 1999.

Mimouni S., Archambeau F., Boucker M., Laviéville J., Morel C. A second-order turbulence model based on a Reynolds stress approach for two-phase flow—part I: adiabatic cases. *Sci. Technol. Nucl. Install.* 2009. 2008;1–14.

Navarro M.A., Santos A.A.C. *Numerical evaluation of flow through a 5×5 PWR rod bundle: effect of the vane arrangement in a spacer grid*. In: International Nuclear Atlantic Conference, INAC, Rio de Janeiro (Brazil); 2009.

Nourbakhsh H., Banerjee S. *Assessing the adequacy of thermal–hydraulic analyses for safety decisions*. In: NURETH-15 Conf., Pisa, Italy, May; 2013.

Oberkamp W.L., Roy C.J. *Verification and Validation in Scientific Computing*. USA: Cambridge University Press; 2010.

OECD/NEA/CSNI/R(2014)3, 2014. Containment Code Validation Matrix. Report NEA/CNSI/R(2014)3, pp. 86–202.

Pineda H., Biazussi J., López F., Oliveira B., Carvalho R.D.M., Bannwart A.C., Ratkovich N. Phase distribution analysis in an Electrical Submersible Pump (ESP) inlet handling water–air two-phase flow using Computational Fluid Dynamics (CFD). *J. Pet. Sci. Eng.* 2016;139:49–61.

Piomelli U. Large-eddy simulation, achievements and challenges. *Prog. Aerosp. Sci.* 1999;35:335.

Piomelli U. Wall-layer models for large-eddy simulations. *Prog. Aerosp. Sci.* 2008;44:437–446.

Piomelli U., Balaras E. Wall-layer models for large-eddy simulations. *Annu. Rev. Fluid Mech.* 2002;34:349–374.

Piomelli U., Ferziger J., Moin P., Kim J. New approximate boundary conditions for large eddy simulations of wall-bounded flows. *Phys. Fluids A.* 1989;1:1061.

Piomelli U., Balaras E., Pasinato H., Squires K.D., Spalart P.R. The inner-outer layer interface in large-eddy simulations with wall-layer models. *Int. J. Heat Fluid Flow.* 2003;24:538–550.

Radhakrishnan S., Piomelli U. Large eddy simulation of oscillating boundary layers: model comparison and validation. *J. Geophys. Res.* 2008;113:C02022doi:10.1029/2007JC004518.

Radhakrishnan S., Piomelli U., Keating A., Silva Lopes A. Reynolds-averaged and large-eddy simulations of turbulent non-equilibrium flows. *J. Turbul.* 2006;7(63):1–30.

Radhakrishnan S., Piomelli U., Keating A. Wall-modeled large-eddy simulations of flows with curvature and mild separation. *ASME J. Fluids Eng.* 2008;130:101203.

Ramesh O. N., Manisekaran S., Shivsai Ajit, Dixit S., 2006, The structure of the sink flow turbulent boundary layer, American Physical Society, 59th Annual Meeting of the APS Division of Fluid Dynamics, November 19-21, 2006APS.DFD.KL008R

Reynolds W.C., 1990, Whither Turbulence? Turbulence at the Crossroads, Lumley J.L. (Editor) Springer-Verlag, Heidelberg, p.

Roelofs F., Gopala V.R., Jayaraju S., Shams A., Komen E.
Review of fuel assembly and pool thermal hydraulics for fast
reactors. *Nucl. Eng. Des.* 2013;265:1205–1222.

Rotta J.C. *Turbulente Strömungen*. Stuttgart, Germany: BG
Teubner; 1972.

Sagaut P., Deck S. Large eddy simulation for aerodynamics:
status and perspectives. *Phil. Trans. R. Soc. A.* 2009;367:2849–
2860.

Schultz R., Weaver W.L. *Using the RELAP5-3D advanced systems
code with commercial and advanced CFD software*. In: Proc. 11th
Int. Conf. on Nuclear Engineering, Tokyo, Japan, April 20–23;
2003.

Schumann U. Subgrid scale model for finite difference
simulations of turbulent flows in plane channels and annuli. *J.
Comput. Phys.* 1975;18:376–404.

Shen Y.F., Cao Z.D., Ganglu Q. An investigation of crossflow
mixing effect caused by grid spacer with mixing blades in a rod
bundle. *Nucl. Eng. Des.* 1991;125:111–119.

Smagorinsky J. General circulation experiments with the
primitive equations. *Mon. Weather Rev.* 1963;91:99–110.

Smith, B.L., Song, C.-H., Chang, S.-K., Lee, J.R., Kim, J.W.,
2013. Report of the OECD/NEA KAERI rod bundle CFD
benchmark exercise. NEA/CSNI R(2013)5, Paris, France.

Smith B.L., Andreani M., Bieder U., Ducros F., Graffard E.,
Heitsch M., Henriksson M., Höhne T., Houkema M., Komen E.,
Mahaffy J.H., Menter F., Moretti F., Morii T., Mühlbauer P.,
Rohde U., Scheuerer M., Song C.-H., Watanabe T., Zigh G.
*Assessment of CFD Codes for Nuclear Reactor Safety Problems –
Revision 2*. NEA/CSNI/R(2014)12 Paris, France: Nuclear Energy
Agency; 2015.

Spalart P.R. Strategies for turbulence modelling and

simulations. *Int. J. Heat Fluid Flow*. 2000;21:252–263.

Spalart P.R. Detached eddy simulation. *Annu. Rev. Fluid Mech.* 2009;41:181–202.

Spalart P.R., Allmaras S.R. In: A one-equation turbulence model for aerodynamic flows. 30th Aerospace Sciences Meeting and Exhibit, 439 pp; 1992.

Speziale C.G., Sarkar S., Gatski T.B. Modelling the pressure-strain correlation of turbulence: an invariant dynamical systems approach. *J. Fluid Mech.* 1991;277:245–272.

Theofanous T.G., Nourbakhsh H.P., Gherson P., Iyer K. *Decay of Buoyancy-Driven Stratified Layers With Applications to Pressurized Thermal Shock*. NUREG/CR-3700 Washington, DC, USA: USNRC; 1984.

Thurgood M.J., Kelly J.M., Guidotti T.E., Kohrt R.J., Crowell K.R. *COBRA/TRAC- A Thermal-Hydraulics Code for Transient Analysis of Nuclear Reactor Vessels and Primary Coolant Systems Equations and Constitutive Models*, Pacific Northwest Laboratory. Pacific Northwest Laboratory, NUREG/CR-3046, PNL-4385 Washington, DC, USA: USNRC; 1983.

Travin A., Shur M., Strelets M., Spalart P. Detached-eddy simulations past a circular cylinder. *Flow Turbul. Combust.* 1999;63:293–313 Kluwer Academic Publishers, The Netherlands.

Wallin, S., 2000. Engineering turbulence modelling for CFD with a focus on explicit algebraic Reynolds stress models. Technical Reports from Royal Institute of Technology, Department of Mechanics, Stockholm, Sweden.

Wallin S., Johansson A.V. An explicit algebraic Reynolds stress model for incompressible and compressible turbulent flows. *J. Fluid Mech.* 2000;403:89–132.

Wang M., Moin P. Dynamic wall modeling for LES of complex turbulent flows. *Phys. Fluids*. 2002;14:2043–2051.

Weiss P., Sawitzki M., Winkler F. UPTF, a full-scale PWR loss-of-coolant accident experiment program. *Atomkernenergie Kerntechnik*. 1986;49(1/2):61–67.

Werner H., Wengle H. *Large eddy simulation of turbulent flow over and round a tube in a plate channel*. In: 8th Symp. Of Turbulent Shear Flow, Munich, Germany; 1991.

Westinghouse, 2014. GOTHIC code, NS-ES-0002, ©2014 Westinghouse Electric Company LLC.

Wilcox D.C. *Turbulence Modeling for CFD*. La Canada, CA, USA: DCW Industries; 1998.

Wilcox D.C. *Basic Fluid Mechanics*. San Diego, CA, USA: DCW Industries; 2007.

Xiao X., Edwards J.R., Hassan H.A. *Inflow boundary conditions for LES/RANS simulations with applications to shock wave boundary layer interactions*. In: AIAA paper 2003–0079, Reno, NV, USA; 2003.

Xiao X., Edwards J.R., Hassan H.A. Blending functions in hybrid large-eddy/Reynolds-averaged Navier-stokes simulations. *AIAA J.* 2004;42(12):2508–2515.

Xiao, J., Travis, J., Royl, P., Necker, G., Svishchev, A., Jordan, T., 2016. GASFLOW-MPI: a scalable computational fluid dynamics code for gases, aerosols and combustion volume 2: users' manual (revision 1.0). KIT Scientific Report 7711, Karlsruhe, Germany.

Xu J., Ma H. Applications of URANS on predicting unsteady turbulent separated flows. *Acta Mech. Sinica*. 2009;25(3):319–324.

Yang S.K., Chung M.K. Turbulent flow through spacer grids in rod bundles. *J. Fluids Eng.* 1998;120:786–791.

Zhang H.L., Bachmann C.R., Fasel H.F. *Application of a new methodology for simulations of complex turbulent flows*. In: Fluids Conference and Exhibit, Fluid Dynamics and Co-located

Conferences, Denver, CO, USA; 2000.

Zienkiewicz O. *Methode der Finiten Elemente*. Leipzig: Carl Hanser Verlag; 1984.

¹ In the OECD-KAERI CFD benchmark (Smith et al., 2013; see also Lee et al., 2014), the under-prediction of the RMS velocity fluctuation was attributed to the limitation of steady RANS turbulence models where RMS values can be obtained only from the modeled term of the turbulent kinetic energy. However, in OECD-KAERI benchmark, SP09 (steady RANS $k-\varepsilon$ model with hexahedral mesh that seemed similar to that used in this benchmark) showed such large under-prediction at the near-wake ($z_{ZMVG} = 1$ and $4D_h$), while SP18 (steady RANS $k-\varepsilon$ model with trim mesh with extrusion layer) showed comparable results (scores) to other unsteady RANS calculation results of SP17 (unsteady RANS SST $k-\omega$ with polyhedral mesh) and SP19 (unsteady RANS BSL EARSM with hybrid mesh).

Part Four

Applications of thermal-hydraulics in nuclear technology

Verification and validation of system thermal-hydraulic computer codes, scaling and uncertainty evaluation of calculated code results

H. Glaeser GRS, Garching, Germany

Abstract

The approximations of system thermal-hydraulic (SYS TH) codes necessitate proper verification and validation (V&V) processes. Validation by predictions of complex phenomena can only be performed after the availability of relevant experimental data. Since many experiments used to validate a code are in small scale compared with a nuclear reactor, the scaling effects have to be considered. Therefore, scaling effects or addressing the scaling issues must be part of the validation activity. Deviations between calculation results and experimental data are observed. Consequently, various sources of uncertainty are identified and uncertainty methods for their quantification have been developed. International programs highlighted the validation, scaling and qualification of uncertainty methods. The chapter discusses V&V, scaling and the evaluation of uncertainty including the effects of the code users.

Keywords

Verification and validation (V&V); Scaling and addressing the scaling issues; Uncertainty and uncertainty methods; Code-user effect; Code-user qualification and training; Separate effect test facilities (SETF); Integral effect test facilities; International Standard Problems

Nomenclature

AEA/AEAT Atomic Energy Agency/
Technology (UK)

AEKI Atomic Energy Agency
(Hungary)

ANS American Nuclear Society

BEMUSE Best Estimate Methods—
Uncertainty and Sensitivity
Evaluation

BWR boiling water reactor

CCFL counter-current flow limitation

CEA Commissariat a L'Energie
Atomique (France)

CFD computational fluid dynamics

CFR Code of Federal Regulation

CIAU code with the capability of
internal assessment of uncertainty

CSAU code scaling, applicability,
and uncertainty

CSNI Committee on the Safety of
Nuclear Installations

DVI direct vessel injection (line)

DSA deterministic safety analysis

ECC emergency core cooling

ECCS emergency core cooling systems

EMDAP evaluation model development and assessment process

ENUSA Empresa Nacional del Uranio, SA (Spain)

FCM fractional change metric

FFTBM fast Fourier transform-based method

FRC fractional rate of change

FSA fractional scaling analysis

GRS Gesellschaft für Anlagen- und Reaktorsicherheit (Germany)

H2TS hierarchical two-tiered scaling

IAEA International Atomic Energy Agency

IPSN Institut de Protection et de
Sûreté Nucléaire (France)

IRSN Institut de Radioprotection et
Sûreté Nucléaire (France)

IRWST in-containment refuelling
water storage tank

ISP International Standard Problem

IT integral test

ITF integral test facility

I/O input/output

JNES Japan Nuclear Energy Safety
Organization

KAERI Korean Atomic Energy
Research Institute

KINS Korean Institute for Nuclear
Safety

LB large break

LOCA loss of coolant accident

LWR light water reactor

NPP nuclear power plant

NRC Nuclear Regulatory
Commission (USA)

NRI Nuclear Research Institute
(Czech Republic)

OECD Organization for Economic
Cooperation and Development

PDF probability density function

PIRT phenomena identification and ranking table

PREMIUM Post-BEMUSE Reflood Model Input Uncertainty Methods

PSI Paul Scherrer Institute
(Switzerland)

PWR pressurized water reactor

QAM quantity accuracy matrix

SB small break

SET separate effects test

SYS System

TH Thermal-Hydraulics

UMAE uncertainty method based on accuracy extrapolation

UMS uncertainty method study

UNIPi University of Pisa (Italy)

UPC University of Barcelona (Spain)

USNRC United States Nuclear
Regulatory Commission (see also
NRC, USA)

V&V verification and validation

WWER water-cooled and water-
moderated energy reactor

Symbols

$$\alpha = \frac{A_g}{A_g + A_l} \text{ Wallis}$$

number = dimensionless superficial
velocity based on downcomer
annulus circumference

$$1 - \alpha = \frac{A_l}{A_g + A_l} \text{ Kutateladze}$$

number = dimensionless superficial
velocity based on surface tension

A_{DC} flow cross section of downcomer

Bo Bond number

d_{av} downcomer average diameter

d_{outer} downcomer outer diameter

Fr Froude number

g gravity

L characteristic geometrical length

M mass flow rate

W average downcomer annulus
circumference

$\theta_{\text{ECC-BCL}}$ angle between ECC injection
leg and broken loop

ν kinematic viscosity

ρ density

σ surface tension

Subscripts

g vapor

l liquid

s steam

w water

x either steam or water

Chapter foreword

Validation (and verification, i.e., what is included in the acronym V&V), scaling, and uncertainty constitute crosscutting issues from development to application in system thermal-hydraulics (SYS THs). The unavoidable approximations introduced at the development level of any code model, including the lack of direct consideration of turbulence, the averaging, and the application of theorems from mechanics of continuum to the noncontinuum two-phase flows impose a validation process. The difficulty to perform experiments (even to be used for validation) at the same conditions (size, geometry, pressure, and power) of the prototype nuclear power plants (NPPs) needs to deal with the scaling issue. Differences between measured and calculated values of transient variables and consequently expected deviations in predicting accident scenarios in NPPs are a reason to deal with uncertainty.

Thus, this chapter is connected with Chapters 5, 9, and 10 of the book where modeling features are discussed in addition to Chapters 7 and 8. The chapter is also connected with Chapter 11 where system code validation, scaling, and uncertainty analysis is already mentioned. The validation procedures described in this chapter are based on phenomena described in Chapter 6 of the book.

Finally, validation, scaling, and uncertainty constitute very basic and important elements for the best estimate plus uncertainty (BEPU) approach described in

Chapter 14 and should be considered when interpreting results of calculations presented in Chapter 15 of the book.

The reader may recognize that validation, scaling, and uncertainty are linked among each other and needs suitable understanding prior to the application of thermal-hydraulic models and code to the evaluation of safety of nuclear installations.

13.1 Introduction

This chapter deals with important steps before performing safety analyses using thermal-hydraulic computer codes calculating the physical behavior of a steam-supply system of a NPP. Verification and validation are means to prove the quality of a computer code. Since many experiments, which are used to validate a code, are in small scale compared with a nuclear reactor, the scaling effects have to be considered. Since initial and boundary conditions, geometry, reactor plant operating parameters, fuel parameters, and scale effects may not be exactly known, and the SYS TH computer codes approximate the physical behavior, the code predictions are not exact but uncertain. Agreement of calculated results with experimental data is often obtained by choosing specific code input options or changing parameter values in the model equations. These selected parameter values usually have to be changed again for different experiments in the same facility or a similar experiment in a different facility in order to obtain agreement with data. To make calculation results useful, for example to be compared with limits of acceptance, the uncertainty in the predictions has to be calculated separately. Therefore, uncertainty analysis methods were developed to estimate safety margins if best estimate codes are used to justify reactor operation. These uncertainty analyses are used more and more instead of the former conservative analysis methods using conservative computer models and/or conservative initial and boundary conditions with the intention to cover all existing uncertainties.

This chapter describes the verification, validation, scaling, and uncertainty evaluation to perform safety analyses because of their strong interrelation.

13.2 Verification and validation of thermal-hydraulic system computer codes

Evaluation of nuclear reactor safety is based on deterministic safety analysis (DSA) and probabilistic safety analysis (PSA). In order to perform DSA, properly qualified computational tools are needed. Verification deals with the question “are the correct equations implemented and solved correctly?” while validation deals

with the question “are the calculated results in agreement with experimental results?” Among the computational tools, the current emphasis is on the SYS TH codes. These codes consist of three major modules: the input/output (I/O) module, the governing equation solver, and closure models. The governing equation solver consists of the following three key modules:

- Thermal-hydraulics (or fluid) balance equations solved in the fluid domains
- Fourier equations for conduction of heat transfer in solid material
- Neutron diffusion equations

Parts of the system code are the “special models” which supplement the capabilities of the various sets of equations. Deviations in the prediction of the same scenario by the same code used by different users may come from different options and selections of input parameters by these users.

This book focuses on water-cooled nuclear reactors, including research reactors, heavy water-cooled/moderated reactors, and graphite-moderated boiling reactors designed and operated in Russia. Any calculation method or tool, including computer codes, applied within the nuclear reactor safety issue shall undergo proper verification and validation (V&V).

The quality of a calculation depends upon: (a) the quality of the code, (b) the quality of the nodalization, (c) the adequacy of the adopted computer-compiler installation, (d) the quality of the input data, and (e) the qualification level of the code-user. Furthermore, any calculation by a best estimate SYS TH code should be supported by uncertainty evaluation, specifically when results are relevant to safety or licensing.

Attention should also be exercised that scaling-related qualification is performed to be part of the validation. Qualitative and quantitative accuracy evaluation, including identification and ranking of thermal-hydraulic phenomena, is also considered for performing verification and validation.

13.2.1 Verification of computer codes

Verification of computer codes is performed within a code development process to show that the code behaves as intended, i.e.,

- that it is a proper mathematical representation of the conceptual model or the design

- that the equations are correctly encoded and solved
- corresponds to the description in the documentation

The verification is performed to demonstrate that the design of the code numerical algorithms conforms to the design requirements, that its logic is consistent with the design specification, and that the source code conforms to programming standards and language standards. Physical phenomena and processes to be simulated are represented by a set of equations and closure relations.

Verification of computer codes consists of:

- (1) the verification of the code design or concept and
- (2) the verification of the source code (ANS, 1987; IAEA, 2009, 2015).

In general, the verification of the code design is performed to ensure that the numerical methods, the transformation of the numerical equations into a numerical scheme to provide solutions, and user options and their restrictions are appropriately implemented in accordance with the design requirements. The verification of the code design includes a review of the design concept, basic logic, flow diagrams, numerical methods, algorithms, and computational environment. If the code is run on a hardware or software platform other than that on which the verification process was carried out, the continued validity of the code verification should be assessed (portability). When the code design contains the integration or coupling of codes, then the verification of the code design should ensure that the links and/or interfaces between the codes are correctly designed and implemented to meet the design requirements.

Verification of the source code is performed to demonstrate that it conforms to programming standards and language standards, and that its logic is consistent with the design specification. The comparison with measured values is not part of the verification; such a process is included in the validation process.

Practical instruments to verify the source code are review, inspection, and audit. Checklists may be provided for review and inspection. Examples for checklists for reviews and inspections of verification of the code design as well as the source code are given in ANS (1987) and IAEA (2015).

Comparisons with independent calculations are carried out where practicable to verify that the mathematical operations are performed correctly. Audits will be

performed on selected items to ensure quality. A review and inspection of the entire code may not be practicable for verification purposes due to its large size. In such cases, verification of individual modules or parts of the code can be conducted, and this should include a careful inspection of all interfaces between the modules.

Any noncompliance of the code or its documentation with the design requirements should be reported to and should be corrected by the code developer. The impact of such noncompliances on results of analyses that have been completed before the correction and used as part of the safety assessment for a plant should be assessed.

13.2.2 Validation of computer codes

Validation is the process carried out by comparing code calculation results with experimental measurements or measurements in a reactor plant if available. A code or code model is considered validated when sufficient testing has been performed to ensure an acceptable level of predictive accuracy over the range of conditions over which the code may be applied. Accuracy is a measure of the difference between measured and calculated quantities taking into account uncertainties and biases in both. Bias is a measure, usually expressed statistically, of the systematic difference between a true mean value and a predicted or measured mean. Uncertainty is a measure of the scatter in experimental or predicted data. The acceptable level of accuracy is judgmental and will vary depending on the specific problem or question to be addressed by the code. The procedure for specifying, qualitatively or quantitatively, the accuracy of code predictions is also called code qualification or code assessment.

13.2.2.1 Validation process

Validation is mandatory to be performed on all computer codes that are used for the DSA of NPPs. The purpose of validation is to provide confidence in the ability of a code to predict, realistically or conservatively, the values of the safety parameter or parameters of interest. Analysis methods that are used for safety demonstration of the fulfillment of the regulatory acceptance criteria must be validated for their respective scope of application. If calculation methods are used for analyzing the effectiveness of preventive or mitigative accident management measures, these shall also be validated for their respective scope of application.

The major sources of information that should be used to assess the quality of computer code predictions are analytical solutions, experimental data, NPP transients, and benchmark calculations, i.e., code-to-code comparisons. Those

code-to-code comparisons can be used for validation purposes provided that, at least, one of the codes has been validated.

It is recommended for complex analysis, to perform the validation process in two steps: the development phase, in which the assessment is performed by the code developer, and the independent validation phase, in which the validation is done by someone who is independent of the developer of the code. Both phases are necessary for an adequate validation procedure. If possible, it is recommended that the data used for the independent validation of the code and the data that are used for the validation by the code developers should be selected from different experiments. Where possible, users should do validation exercises without having any prior knowledge of the experimental results to preclude any deliberate tuning of code calculations to yield better agreement with experimental results. Validation exercises are a very good means for users of a code to get experience in applying the code.

The validation process should ideally include four different types of test calculation:

(1) Basic tests. Basic tests are simple test cases that may not be directly related to a NPP. These tests may have analytical solutions or may use correlations or data derived from experiments.

(2) Separate effects tests (SET). Separate effects tests address specific phenomena that may occur at a NPP but do not address other phenomena that may occur at the same time. SETs should ideally be performed at full scale. In the absence of analytical solutions or experimental data, other codes that are known to model accurately the limited physics represented in the test case may be used to determine the accurate solution.

(3) Integral tests (ITs). Integral tests are test cases that are directly related to the behavior of the system of a NPP. All or most of the relevant physical processes as well as their interactions are represented. However, these tests are usually carried out at a reduced scale, the tests may use substitute materials or may be performed at low pressure.

(4) NPP level tests and operational transients. Nuclear power plant level tests are performed on an actual NPP. Validation through operational transients together with NPP tests are important means of quantifying the plant model.

The validation tests should ideally cover the entire range of values of parameters,

conditions, and physical phenomena that the code is intended to cover. The scope of the independent validation exercise performed by the code user should be consistent with the intended purpose of the code and the range of experimental data available. The scope of validation should also be in accordance with the complexity of the code and the complexity of the physical processes that it represents. The code user should also evaluate qualitatively or quantitatively the accuracy of the results of the calculations. For complex applications, a validation matrix should be available for code validation because a code may predict one set of test data with a high degree of accuracy but may be extremely inaccurate for other data sets. The validation matrix should include test data from different experimental facilities at different scale and different sets of conditions in the same facility. It should ideally include basic tests, SETs, ITs, and NPP level tests. If sufficient data from full-scale experiments are not available, data from reduced scale experiments will be used, with appropriate consideration of scaling (see Section 13.3).

Internationally agreed integral test facility (ITF) matrices for validation of realistic thermal hydraulic system computer codes were established in the OECD/NEA/CSNI validation matrix (CSNI, 1996) containing a total number of 177 PWR and BWR specific ITs selected as potential source for thermal hydraulic code validation. ITF development is mainly for pressurized water reactors (PWRs) and boiling water reactors (BWRs). A separate activity was for Russian pressurized water-cooled and water-moderated energy reactors (WWER) (CSNI, 2001). First, the main physical phenomena that occur during considered accidents are identified, test types are specified, and test facilities suitable for reproducing these aspects are selected. Second, a list of selected experiments carried out in these facilities has been set down. The criteria to achieve the objectives are outlined.

The SET are designed to validate specific phenomena of the whole physical model independently from the others. SETs may address:

- A specific basic flow process (flashing, critical flow, direct contact condensation, counter-current flow limitation (CCFL), lower plenum voiding, etc.)
- A specific closure term for a given flow or for a given range of flow parameters
- The specific behavior of a specific reactor component (separator, break, valve, loop seal, etc.). This is called a component test
- A specific flow process occurring in a specific reactor component during a selected time span of an accidental transient identified as a phenomenological

phase

Due to the variety of models, the variety of flow regimes and the variety of geometrical configurations, a SET validation matrix has a large number of tests. The OECD/NEA/CSNI SET matrix (CSNI, 1994) contains 67 thermal-hydraulic phenomena and 1094 tests from 185 test facilities as potential source for thermal hydraulic code validation. Subsequent experiments have been performed in the meantime to investigate different reactor designs.

The number and the selection of tests in the test matrix used for validating specific computer codes do not need to use all these experiments contained in the international validation matrices. The number of tests used should be justified as being sufficient for the intended application of the code. The range of validity and the limitations of a computer code, which are established as a result of validation, should be documented in a validation report which should be referenced in licensing documentation. However, code users may perform additional validation to demonstrate that the code satisfies the objectives for their specific application. This, however, necessitates the availability of experimental data as well as experimental documentation or the results of NPP data, like start-up tests.

When experiments are used for validation of the computer codes, care should be exercised when planning an experiment to ensure that the measured data are as suitable as possible for the purpose of code validation. The safety parameters that will be calculated using the code should be considered when the experiment and its instrumentation are planned. To ensure that the code is validated for conditions that are as close as possible to those in a NPP, it should be ensured that the boundary conditions and initial conditions of the test are appropriate. Consideration should be given to scaling laws. A scaled experimental facility cannot be used to represent all the phenomena that are relevant for a full size facility (see Section 13.3). Thus, for each scaled facility that is used in the assessment process, the phenomena that are correctly represented and those that are not correctly represented should be identified. The effects of phenomena that are not correctly represented should be addressed in other ways. The uncertainty in the experimental data should be reported in the documentation of the experiment. When performing a validation against experimental data, allowance for errors in the measurements should be included in the determination of the uncertainty of the computer code.

13.2.2.2 Qualification of input data

The input data for a computer code include a representation of all or parts of the

NPP. There is usually a degree of flexibility in how the plant is modeled or nodalized. The intention is to be flexible in calculating different reactor types and different scenarios. The input data that are used to perform safety assessment calculations should conform to the best practice guidelines for using the computer code as described in the user manual and should be independently checked. The input data should be a compilation of actual information found in as-built and valid technical drawings, operating manuals, procedures, set point lists, pump performance charts, process diagrams and instrumentation diagrams, control diagrams, etc. Users who prepare input data to model validation tests should be suitably qualified and should make use of all available guides. These include the specific code user guide, generic best practice guides for the type of code, and guidance from experienced users. The validation process itself often enables the determination of best practices. This may include nodalization schemes, model options, solution methods, and mesh size. Those who generate input data sets for safety analysis calculations should use the best practice guidelines established during the validation process.

13.2.2.3 Qualitative and quantitative assessment of validation calculations

A realistic or “best estimate” computer code or analysis method may be deemed validated if the applicability and sufficient accuracy of the code applied has been demonstrated for the respective application within the framework of the validation scope performed and documented.

Qualitative judgment of agreement between the code calculation and the data is generally divided into four categories:

Excellent agreement: The calculation lies within or near the data uncertainty band at all times during the phase of interest.

Reasonable agreement: The calculation sometimes lies within the data uncertainty band and shows the same trends as the data. Code deficiencies are minor.

Minimal agreement: Significant code deficiencies exist. Some major trends and phenomena are not predicted. Incorrect conclusions may be drawn based on the calculation when data are not available.

Unacceptable agreement: A comparison is unacceptable when a significant difference between calculation and the data is present, and the difference is not

understood. Such a difference could follow from errors in either the calculation or the presentation of the data, or an inadequate code model of the phenomenon.

A code is considered to be of adequate applicability when it shows either excellent or reasonable agreement with the highly ranked phenomena, sometimes identified as the dominant phenomena, for a transient of interest. If the code gives minimal or unacceptable agreement, additional work must be performed, ranging from additional code development to additional analysis to understand the phenomena.

Quantitative judgment of agreement between code results and data can be performed in different ways. The Japan Atomic Energy Research Institute comparing the submissions of International Standard Problem No. 26 (ISP-26), calculating an experiment on the LSTF facility, a 5% cold leg break experiment LSTF-SB-CL-18, performed one accuracy quantification study. Seventeen time-averaged deviations between selected, calculated, and measured results were performed for the different participants:

$$x = \frac{W_s}{W_s + W_l}$$

The limit chosen for ISP-26 (LSTF-SB-CL-18) was, for example:

good agreement: limit=0.1

acceptable agreement: limit=0.2

poor agreement: limit>0.2

Such an accuracy quantification method has not generally been used because of the dependence of results on the number and type of included variables, the dependence on the chosen time span, error compensation may not be detected, erroneous initial and boundary conditions may not be taken into account, and a lack of information about qualitatively correct trends in the calculation.

University Pisa, using the fast Fourier transform-based method (FFTBM) with imposed acceptability limits (Ambrosini et al., 1990) has proposed another accuracy quantification method. The FFTBM has been developed to perform quantitative accuracy evaluation of the results of SYS TH codes. The idea is to perform the comparison between the measured and the calculated results from the

time domain toward the frequency domain in order to get a figure of merit independent of the time duration of the scenario. The main FFTBM output is the average accuracy related to an individual or the total accuracy related to a set of variables. Kunz et al. (2002) discuss the comparison of the FFTBM with other methods suitable for quantifying accuracy, and Prosek et al. (2005) present application results.

For conservative safety analysis methods used in licensing applications of NPPs, experimental results should be bounded in the direction of regulatory acceptance criteria, like the peak cladding temperature (PCT) of 1200°C for loss of coolant accidents (LOCAs). Conservative is understood here in the unfavorable direction to acceptance criteria of safety parameters. That means the result of a conservative code should always be closer to the acceptance criterion than the realistic value.

13.2.2.4 International Standard Problems

A special and challenging case of validation activities is occurring during an International Standard Problem (ISP), where comparison exercises are performed between different participants. Two kinds of comparison exercises can be organized between participants for code calculations, following the definition made generally in the CSNI, benchmarks, and ISPs. The benchmark exercise corresponds to calculations of a physical case defined theoretically for which no experimental reference exists. The comparisons are performed between each participant calculations, but there is no way to decide which one is really the best. In an ISP the calculations are centered on experimental results. Comparisons between each participant are still part of the exercise, but the final quality of the predictions is judged on the basis of the experimental results themselves which play consequently a key role. As a consequence, the specifications relative to the experimental results should follow detailed requirements in the ISP process. The mode for distribution of experimental data becomes also very important. A specific CSNI Report 17 (CSNI, 2004) discusses all these points and provides recommendations on each of them. 26 out of the 52 ISPs performed within the CSNI between the years 1973 and 2012 were from primary and secondary SYS THs and six from containment thermal-hydraulics. The others were from fuel behavior during LOCA (2) and severe accidents (19); 1 proposal was cancelled. Brief descriptions of all CSNI Standard Problems up to ISP 43 can be found in report CSNI (2000); further reports about CSNI Standard Problems are available on the CSNI web site www.oecd-nea.org/nsd/docs.

The recommendations on the ISP specifications emphasized particular important features. Here are some of them:

- The experimental facility description provided to the ISP participants should be sufficiently detailed including layout, drawings, component characteristics that are necessary. Before proposing an ISP one must be sure that no proprietary interdiction is on the required data.

- The instrumentation should be detailed. Location, type, accuracy, data acquisition system, sampling, response time should be supplied to the participants.

- The test conditions should be well known; initial and boundary conditions should be provided with sufficient detail for running the prediction calculations in a meaningful way.

One can observe that those recommendations are still topical and that partial nonobservance is, even now, sometimes the source of shortcomings in the results. The governing idea has been to put the ISP participant in the same situation as when the user of a code is proceeding to a plant calculation for solving a safety issue. Therefore, in the last ISPs, results like those from characterization tests giving, for example, pressure drops, pump characteristics, heat losses and their distributions, etc., have been added in the specifications to the test conditions. Furthermore, for ISPs in relation to actual plant transients, additional specifications were supplied such as the timing and degree of interventions from operators as well as plant auxiliary system conditions with their uncertainty bands.

The distribution of test results is also a key point in the ISP performance. Different options have been used which change the nature and the outcome of the ISP. Depending of those options, ISPs are classified in open, blind, semiblind, or double-blind ISPs. These categories are explained in more details:

- *Open ISP*: This is an ISP where the participant gets all the experimental data from the very beginning. All information is open. The calculations are performed, while the experimental results are known.

- *Blind ISP*: on the contrary to open ISP, the participants in the blind ISP have no access to the test results except the test boundary and initial conditions in the general meaning discussed above. Actual test results remain locked until the calculations are finished and sent to the ISP organizer. The participants are doing their calculation in a blind situation in the same way they are doing the calculations of plant accidents where no experimental data is available. Blind ISPs are consequently recommended because they reflect better the real conditions in which an analyst will find himself for plant analysis. Furthermore, this is reinforced by the very frequent observation that calculations are generally better when

experimental results are available at the time of the calculation. This is due to adjusting of the computer model and/or of the input data to account for the specific test results. Calculations in blind situation may avoid most of this kind of “tuning effect.”

In reality, even in blind situations, some tuning of the code may be obtained by using tests which have been already performed on the same experimental facility and which may be more or less similar to the one proposed for the ISP. For this reason, distinction was made in ISPs between real blind participants and participants who in fact had opportunities to perform extensive analysis of other tests and who could therefore not be considered as completely blind. This is also why the concept of double-blind ISP was created.

– A *double-blind ISP* is an ISP for which the participant has not access to the results of the ISP test or to the results of any other tests performed on the experimental facility (except the characterization tests considered as normal additions to tests conditions). This situation represents in fact the exact real situation of the analyst performing plant calculations. Consequently, double-blind ISPs are especially challenging to both the codes and the code users, and correspondingly more valuable in assessing code performance. However, such ISP can only be performed in the very rare situations where no test results have been already published, i.e., when starting a new facility. In this situation, meeting the high quality of standard requested for ISP is considerably difficult for the organization running the facility as it requires a perfect control of the experimental procedure, which is in fact in contradiction with the learning phase generally experienced on a brand new experiment. Consequently, very few double-blind ISPs have been practically organized.

From the preceding discussion, it appears clearly that the “more” blind an ISP is, the more significant the conclusions may be. However, there are cases where the generalization of this statement is in fact an oversimplification.

– A *semi blind ISP* concept has been introduced, for example, when the prediction of the tests involves two types of interacting phenomena and when the uncertainties on one of these phenomena will preclude the conclusions, which can be drawn on the other one. In these specific cases, it has often been decided, for preserving the ISP efficiency that the results concerning the first phenomena will be opened, and the results of the second will be blind. This *semibind* procedure has been for instance used for fuel behavior ISPs where thermal-hydraulic conditions were often open and fuel results were blind so that uncertainties on thermal-hydraulics will not prevent to draw conclusions on fuel.

As another example where blind ISPs are not providing necessarily the most significant conclusions, we can mention ISPs dealing with physical areas where the knowledge is at an early stage or dealing with areas where phenomena are particularly complex. In such cases, blind calculations would give unusable results and valuable ISPs could only be open ones. In those specific areas, even if the ISPs results look encouraging, it should be kept in mind that for such ISP, an open exercise has been chosen because of the difficulties expected in blind calculations and that consequently, one could also expect similar difficulties in similar plant calculations, which will be performed by the analysts in a necessarily blind-like situation.

The comparisons between the calculations and the experiment and between the calculations themselves are the constitutive part of the ISPs. It provides the basis for drawing conclusions on the capabilities and the deficiencies of existing calculation tools in an international framework. It is also during the analysis that the most detailed discussions can take place between experts.

13.2.2.5 User effects

The user of state-of-the-art SYS TH computer codes must make many choices in setting up an input deck and running a calculation. Such a flexibility is by purpose to be able to apply such a code for different events and purposes. One experience from International Standard Problems is, however, that large differences of code results from different code users applying the same code version and the same specifications (e.g., initial and boundary conditions, geometry) have been observed. These differences are considered as code user effects (CSNI, 1995). In other arenas, e.g., plant calculations, some of these elements may better be classified as code, scale, plant state, etc., uncertainties. Uncertainty analyses are supposed to quantify some of these user effects. The focus is here on quantifying user effects of experienced code users and qualified input decks but not exactly known values for several input parameters. Mistakes in the input deck and code deficiencies in calculating important phenomena should not be included in these uncertainty quantifications. The main source of quantifying code model uncertainties is therefore the experience of experts during the validation process.

The development of thermal-hydraulic advanced codes was expected to decrease this effect of code users, but the last thermal-hydraulic ISPs have shown that there was still a significant “user effect” in applying these advanced codes. Detailed studies of this effect have been made on different ISPs. In addition to the identification of the user effect, ISPs have contributed largely to its understanding. ISPs are really providing data that are absolutely unique on this crucial subject. In

recent comparisons of international applications of uncertainty evaluations, we have seen significant user effects, too.

Ways to reduce user effects have been proposed within the CSNI working groups (CSNI, 1995, 1998; Shotkin, 1997; D'Auria, 1998). User training by performing validation, mentoring, and instruction are the most effective and easiest ways to improve the quality of code predictions. Users need a good knowledge of the physical modeling and limitations of the codes, the facility to be described, and an understanding of major phenomena expected to occur during the transient. User Guidelines that are based on the results of a systematic code validation program are also a way to reduce the user effect. They prevent an inadequate use of a code and avoid mistakes. However, these guidelines cannot give detailed recipes for all existing conditions. They cannot substitute for a trained and experienced code user.

Another way to reduce code user effects is quality assurance. Preparation and testing of an input deck requires at least 6 months for an experienced code user. Clear quality assurance strategy is necessary. Often, incomplete or error-ridden input decks are used. It is common practice to use existing input decks. However, a warning should be issued to share existing decks between different users to save time who then introduce only minor modifications without complete checking of the major part and without understanding for what purpose the available input decks have been developed.

Even though some suggested ways to reduce the user effect have been proposed, it remains that we are quite far from controlling it completely. The user effect has also appeared as a generic question and not only in the thermal-hydraulics area where it has been discovered. In particular, the several ISPs that have been recently performed in the severe accident area have shown the same importance for this effect.

13.2.2.6 Counterpart and similar tests

The development and the assessment of system codes used in the safety analysis of water-cooled reactors have to rely mainly on experimental data from scaled, separate effects, or integral system test facilities. Data from full size plants are not usually available for code validation except for mild operational transients. The typicality of the experimental data acquired in scaled test facilities is however often questioned due to inherent scaling distortions stemming from design and simulation constraints. In order to assure the adequacy of system codes in predicting a realistic system response, the code assessment process is thus diversified over a wide range of test data from test facilities having different

scaling ratios and/or design concepts.

In addition, it is considered beneficial to verify the code scalability aspects against a set of data from tests performed in different facilities but under “similar” initial and boundary conditions. This would partially separate the code assessment process from physical assumptions emphasizing instead the influence of configurational and geometric scaling aspects.

The word “similar” has been however the subject of many discussions in the past, and some authors tried to indicate which of the minimum set of initial and boundary conditions have to be preserved between the various test facilities in order to classify that series of tests as “Counterpart Tests.” Counterpart tests are tests specified from the beginning as counterpart tests to be performed in different test facilities with scaled initial and boundary conditions. It should be noted then that some tests are more suitable than others to be the subject of a counterpart test: in particular tests where the influence of facility distortions (e.g., heat losses) are less important.

The difficulty in the specification of a counterpart test connected with generally strict and fixed test programs makes it difficult to have a large number of these test series. Nevertheless, looking at the integral facilities test programs it is possible to identify some tests which although they do not meet exactly the conditions for a counterpart test do maintain a great similarity in the initial and boundary conditions. These tests here referred to as “Similar Tests” can reveal important scaling influences that would otherwise been lost.

The most relevant counterpart test activity was performed during a time frame of about 20 years. Selecting small break (SB) counterpart tests, for example, five IT facilities and seven experiments, are involved. The ITFs are

- LOBI (simulator of a German four loops PWR by two unequal loops)
- SPES (simulator of a US three loops PWR by three equal loops)
- BETHSY (simulator of a French three loops PWR by three equal loops)
- LSTF (simulator of a US four loops PWR by two equal loops)
- PSB (simulator of Russian four loops VVER-1000 by four equal loops)

Four of the involved ITF are equipped with vertical U-tubes steam generators, and the fifth one, PSB, is equipped with horizontal tube steam generators. The

concerned experiment is a SB-LOCA simulating a break in one cold leg, without activation of the high-pressure injection system.

A few remarkable results taken from the SB-LOCA counterpart test database (e.g., see D'Auria et al., 1994; Blinkov et al., 2005; D'Auria and Galassi, 2010) are reported in Figs. 13.1–13.3 for the system pressure, water mass inventory, and rod surface temperature. These figures were produced by University of Pisa. The objective is to give an impression of the counterpart test database. Each of the three diagrams shows the comparison between seven experiments out of five test facilities and seven calculated trends. This gives an impression of the capabilities of computational tools to calculate phenomena at different scale with a comparable level of accuracy.

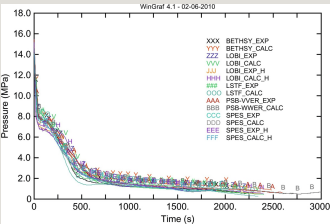


Fig. 13.1 Upper plenum pressure of SB-LOCA counterpart test database and calculations. Courtesy of D'Auria, F., Galassi, G.M., 2010. Scaling in nuclear reactor system thermal-hydraulics. Nucl. Eng. Des. 240, 3267–3293.

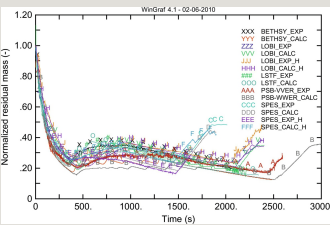


Fig. 13.2 Normalized residual water mass of SB-LOCA counterpart test database and calculations. Courtesy of D'Auria, F., Galassi, G.M., 2010. Scaling in nuclear reactor system thermal-hydraulics. Nucl. Eng. Des. 240, 3267–3293.

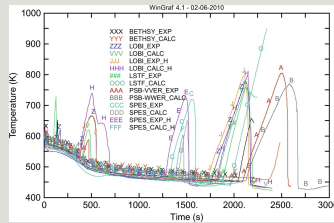


Fig. 13.3 Heater rod surface temperature of SB-LOCA counterpart test database and calculations. Courtesy of D'Auria, F., Galassi, G.M., 2010. Scaling in nuclear reactor system thermal-hydraulics. Nucl. Eng. Des. 240, 3267–3293.

Some selected interesting aspects of these counterpart tests are:

- Occurrence of three dry-out conditions due to:

(a) pump seal blockage, consequential drop of water level in the core region, and clearance of the pump seal and consequently recovery of water level in the core region

(b) water inventory loss via the SB and water inventory recovery by accumulator injection

(c) water inventory recovery by Low Pressure Injection System (LPIS)

- For all these ITF experiments, the scaled initial power condition was considered in the design. However, only LOBI and SPES were able to simulate scaled full initial power, the others had reduced scaled initial power (10%–14%). Seven experiments in five ITF are part of the SB counterpart test program.

- Measured data from the seven experiments fulfilled the objectives of the tests, are consistent, and discrepancies among the corresponding time trends could be explained. However, in principle, all thermal-hydraulic phenomena are scale dependent with regard to geometry. For instance, two-phase pressure drop depends on diameter because flow regimes depend on diameter. Then, a number of phenomena depending on volume to surface ratio are scale dependent. Noticeable examples are found for liquid penetration (i.e., downflow) in the downcomer, or across the upper core plate in the case of hot leg injection. It strongly depends upon the geometric dimensions of the components for counter-current flow, see also Sections 13.3.2 and 13.3.3 of this chapter as well as Glaeser and Karwat (1993). In case of small-scale experiments, liquid penetration is interfered by more intense steam-water interaction compared with large scale where more separate steam-

water flow passages are possible. Consequently, higher ECC water penetration to the core region is possible for cooling the core.

- Accuracy in the predictions by using more than one code was independent upon scaling using an appropriate ratio of experimental and calculated value Y_{exp}/Y_{calc} . “Y” is a generic parameter value representing a thermal-hydraulic phenomenon under investigation (D'Auria et al., 1988).

Analyses of counterpart tests in PWR for scenarios different from SB-LOCA and performed in ITF, scaled according to time-preserving laws, can also be found in the literature (e.g., Bazin et al., 1992) dealing with natural circulation.

13.2.3 Conclusions

Verification and validation of a computer code are important activities to assure its quality. On the other hand, performing validation calculations is a very good exercise for the users of a code to improve the understanding and handling of the code to set-up the input data.

The results of a systematic code validation are an important basis to determine the uncertainty of the results obtained by a code calculation. In assessing the uncertainty of a code, user effects should be minimized. Different methods are appropriate for assessing the uncertainty of the results from the validation by comparing calculation results with experimental data. Dependent on the methods used for evaluating the uncertainty, differences between calculation and experimental results are used directly, or uncertainty ranges and distributions of relevant model parameters are derived (see Section 13.4).

13.3 Scaling of thermal-hydraulic phenomena and relation to system code validation

In the last five decades, large efforts have been undertaken to provide reliable thermal-hydraulic system codes for the analyses of transients and accidents in NPPs. Many SETs and integral system tests were carried out to establish a database for code development and code validation. In this context, the question has to be answered, to what extent the results of downscaled test facilities represent the thermal-hydraulic behavior expected in a full-scale nuclear reactor under accident conditions. Scaling principles, developed by many scientists and engineers, present a scientific-technical basis and give a valuable orientation for

the design of test facilities. However, it is impossible for a downscaled facility to reproduce all physical phenomena in the correct temporal sequence and the kind and strength of their occurrence. The designer needs to optimize a downscaled facility for the processes of primary interest. This leads compulsorily to scaling distortions of other processes with less importance. Due to distortions, phenomena may dominate small-scale facility behavior, but these may be less important for large-scale tests. For example, due to different surface to volume ratio the heat losses and wall effects are higher in small-scale facilities. Therefore, the computer code to be applied for safety analyses is the necessary and important tool to scale physical phenomena. Consequently, a goal-oriented code validation strategy is required, based on the analyses of SETs and integral system tests as well as transients occurred in full-scale nuclear reactors. The CSNI validation matrices and international experimental programs are an excellent basis for fulfilling this task. SETs in full scale, like on the upper plenum test facility (UPTF) test facility, have here an important role.

Because a full-scale IT including physical interactions over the whole coolant system of a NPP is usually impossible, the scaling of the test facilities becomes a fundamental issue. The question of scaling has to be considered not only in the design of the test facilities; it has also to be taken into account in the code development process.

The codes must describe the results from SETs and integral system tests of different scale (for example, volume scaling of integral system tests range from 1:48 to 1:2070). When a code model describing, for example, the counter-current flow in the downcomer of a PWR, was developed mainly on the basis of results of the 1:1 scaled UPTF separate effects experiments must also describe this phenomenon in down-scaled integral system tests (scale-down capability). For the full range of transients and accidents, the interactions of the code models can be checked only on the results of down-scaled integral system test facilities. On the other hand, code models developed mainly based on the results of down-scaled experiments, must describe the thermal-hydraulic processes expected in the full-scale reactor plant (scale-up capability).

13.3.1 Scaling concepts

The transfer of experimental results—obtained in a scaled-down test facility—to reality in a large-scale industrial plant is a common challenge of engineering. A sufficient similarity of parameters is needed controlling the processes in the test rig and the real plant. This similarity can be geometric, mechanic, thermal-hydraulic, static, or dynamic.

Several methods have been proposed to develop scaling laws. One of the most known methods is based on the nondimensional form of the governing differential equations describing the thermal-hydraulic processes. In this method the differential equations are made nondimensional by choosing proper reference values for various physical quantities in the equations. From these equations nondimensional numbers, respectively, similarity groups can be obtained. For example, the derivation of the nondimensional Reynolds and Grashof numbers is the simplest case, namely for the steady-state single-phase flow (Glaeser and Wolfert, 2012).

Compared with this simple example for a single-phase flow the development of scaling laws for two-phase processes is much more complicated. Not only the number of differential equations but also the high number of constitutive equations describing the interfacial interactions and the interactions of the two phases with the channel wall hamper enormously the derivation of scaling laws. Some examples of scaling laws used for the design of integral system tests facilities and SETs facilities can be found in Glaeser and Wolfert (2012).

To obtain information about the overall system behavior and about the interaction of the different system components of a nuclear steam-supply system, integral system tests have been performed for more than four decades. However, because a full-scale ITF is usually not feasible, the facility scaling becomes a fundamental issue.

The Nahavandi scaling principle is most popular for LOCA test facilities (Nahavandi et al., 1979, see Table 13.1). Ishii and Kataoka (1983) have presented similarity groups for two-phase flow, which can be obtained from the set of balance equations directly or the perturbation analyses. Similarity between test facility and prototype is assumed if these dimensionless numbers are identical for facility and prototype. Two typical similarity groups are shown below for illustration, where g is gravitational acceleration, H is enthalpy, ρ is density, u is flow velocity, and l is characteristic length.

Table 13.1

Scaling ratios proposed by Nahavandi et al. (1979)

--

S, area-model/area-prototype.

Subcooling number (subcooling/latent heat)

$$1 - x = \frac{W_l}{W_g + W_l}$$

Froude number (inertia/gravity force)

$$W = W_g + W_l$$

Similarity criteria, such as given above, cannot be fulfilled in total. Nevertheless, they present a scientific-technical basis and give a valuable orientation for the design of test facilities. Ishii and Kataoka (1983) presented scaling criteria specifically for the coolant loops of PWRs under single- and two-phase natural circulation conditions. Ishii et al. (1998) presented the Ishii scaling for the test facility PUMA, simulating the simplified BWR by introducing scaling of geometric length.

The hierarchical two-tiered scaling (H2TS) (Zuber, 1991) creates a hierarchy among scaling factors and scaling design. The “first tier” or top-down scaling analysis examines synergistic effects on the system by interactions between the constituents. A phenomena identification and ranking table (PIRT) process is applied, involving expert judgment. The “second tier,” or bottom-up scaling analysis, provides similarity criteria for specific processes, such as flow pattern transitions and flow-dependent heat transfer. The focus is on developing similarity criteria to scale individual processes of importance to system behavior as identified in the first tier. Closure equations addressing local phenomena are considered to obtain similarity criteria.

The fractional scaling analysis (FSA) proposed by Zuber et al. (2007) considers

fractional rate of change (FRC) and fractional change metric (FCM). The first quantifies the intensity of each transfer process (agent of change), which changes a state variable by a fraction of its total change during a selected transient, and allows the ranking of the agents of change. The second is representative for scaling the fractional change of a state variable. The FCM is used for scaling the fractional change of a system state variable, like pressure. These scaled state variable trajectories representative for different transients show similarities that do not show up when the same variables are represented versus time. FRC and FCM are similar to the “specific frequency” and “time ratio” in the H2TS, respectively.

It is claimed that FSA can replace complex computer codes and to establish a different framework for the analysis of complex scenarios. However, that obviously overburdens this method. FSA is a scaling analysis, not a prediction tool (Wulff et al., 2005). As stated in Wulff et al. (2005), FSA provides the quantitative hierarchy that may supersede the widely used, but subjectively generated PIRT. FSA can be used to compare computer code simulations by an independent analytical infrastructure (D'Auria and Galassi, 2010).

Reyes (2015) and Reyes et al. (2015) to address the time dependency of scaling distortion, propose a dynamical system scaling (DSS). The strategy is to convert the transport equations to a process space through a coordinate transform and exploit the principle of covariance to derive similarity relationships between the prototype and model. After the transformation, the target process can be expressed in the process-time space as a three-dimensional phase curve called geodesics. If a similarity is established between model and prototype, these two-phase curves will overlap at any moment of the transient. Any deviation of the process curves represents the deviation of the scaling as a function of time. By specifying the ratios of the conserved quantity and the process (called 2-parameter transform), the generalized framework can be converted to a specific scaling method such as the power-to-volume scaling. But this generalized approach provides the benefit of identifying the distortion objectively and quantitatively at any moment of the transient.

DSS computes scaling distortion as a function of dimensionless process time via the (flat-space) geodesic separation between the prototype and test facility geodesic process curves. The same normalizing factor, the process action, is applied to all quantities when computing dimensionless process time. This allows comparing the prototype and test facility process curve trajectories throughout the entire transient which reveals that distortion is a dynamic quantity. It may increase and/or decrease as the responses evolve. The geodesic separation can then be integrated to yield a

single measure which accounts for all distortion present between the two facilities or between a code calculation and experimental results. DSS can make use of a simplified transient analysis model for optimization of an experiment over the entire duration of a transient process (Yurko et al., 2015).

An overview about different scaling approaches for the design of thermal-hydraulic integral test facilities (ITFs) is given in a published article of D'Auria and Galassi (2010). The importance of system computer codes for the scaling issue is emphasized there, too. A state-of-the art report on scaling collected extensive information on the topic (CSNI, 2016b).

It is impossible for a down-scaled facility to reproduce all the physical phenomena during a transient process in a real scale plant. The designer needs to optimize a down-scaled facility for the processes of greatest interest. However, this leads compulsorily to distortions of other processes with less importance.

The H2TS, FSA, and DSS aim to the design of an experimental facility. A different objective is the scaling application of SYS TH computer codes to the process of determining the safety of NPPs.

13.3.2 Integral system tests

The LOBI Programme (Riebold et al., 1984) has demonstrated the impact of test facility scaling very impressively. The LOBI facility was volume scaled 1:712. The tests were performed with two different gap widths of the annular-shaped downcomer. In the first test series, a downcomer gap width of 50 mm was used what resulted in 6.3 times too large downcomer volume and therefore in a strong distortion of the mass distribution in the scaled system. The intention was to preserve as far as possible counter-current flow as well as hot wall-related phenomena during the refill period. In the second test series, a downcomer of 12 mm gap width was installed. The 12 mm was chosen as a compromise between the volume-scaled downcomer (7 mm gap width) and a downcomer which would yield the same pressure drop due to wall friction as in the reference reactor (25 mm gap width for the scaled facility). The influence of downcomer gap width and downcomer volume was shown by comparing the results. Both tests simulated a double-ended cold leg break with cold leg accumulator injection. Overall initial and boundary conditions were generally equal or directly comparable for the two tests.

No significant influence of downcomer gap width on the SYS TH behavior occurred during the very first blowdown period when subcooled fluid conditions

persisted in the downcomer region. However, the course of the transient was strongly affected during the subsequent saturated blowdown and refill periods. Water evaporation had also started in the cold regions of the system due to the depressurization rate. The relatively higher-density fluid persisting near the core entrance and the reestablishment of positive mass flow through the core were much more pronounced in the case of the large downcomer where the initial liquid inventory in the downcomer is about 3.6 times larger than in the case of the small downcomer. This in turn ensured enhanced cooling of the heater rod bundle during the late blowdown. Therefore, completely different conditions existed in the primary system at the time when ECC injection from the accumulator started. Conversely, a smaller downcomer width tended to inhibit ECC water penetration and lower plenum refill, which led to nearly stagnation conditions in the core and relatively poor core cooling.

Extremely poor core cooling was observed in the smaller 1:1600 scale SEMISCALE facility. In contrast to the results of the UPTF test facility with a geometrical scaling of 1:1, the SEMISCALE test results have shown that penetration of ECC water into the downcomer during cold leg ECC injection was completely prevented by CCFL. The multidimensional flow in the annulus downcomer of a large PWR could not be reproduced by the small tubular downcomer of the SEMISCALE facility. No effect of cold leg ECC injection on core cooling has been observed, what was misleading with respect to large-scale behavior.

These examples show very clearly that the thermal-hydraulic behavior of a down-scaled ITF cannot be extrapolated directly to obtain nuclear plant behavior. Although the facilities have been designed in different volume scaling, ranging from 1:2070 to 1:48 (Table 13.2), the experimental results of these facilities are not solving the scaling problem. A combination of integral system tests with SETs in full reactor scale is indispensable. The computer codes shall be validated to calculate integral and separate effects experiments over the whole available scaling range in good agreement with the data. Therefore, the SYS TH computer code is an important scaling tool to perform safety analysis for power reactors.

Table 13.2

PWR integral system test facilities and main characteristics

--

^a Full power scaling not possible.

Another effect of scaling of geodetic height of a test facility for passive emergency core cooling systems (ECCS) relying on gravity was observed from the APEX test facility. The design of the AP1000 reactor uses gravity-driven passive safety systems to provide emergency core cooling (ECC) and containment cooling in case of an accident for an extended period of time. The APEX test facility at Oregon State University in USA simulates accident behavior of an AP1000 reactor plant. Height scaling of APEX is 1:4 (see Table 13.2). That is the reason for a drawback. The incontainment refuelling water storage tank (IRWST) injection to the AP1000 reactor coolant system starts when the pressure in the primary system is lower than the pressure in the IRWST due to its water head. The scaling of APEX delays the IRWST injection start. NUREG-1826 report “APEX-AP1000 Confirmatory Testing To Support AP1000 Design Certification” (nonproprietary) (NRC, 2005a) states that the IRWST injection start occurs for:

- AP1000 at reactor pressure 0.198 MPa (28.7 psia)=10.0 m height of liquid level in the IRWST
- APEX at reactor pressure 0.125 MPa (18.2 psia)=2.5 m (=1/4) height of liquid level in the IRWST

Such a delayed IRWST injection may have a negative effect on core cooling on the APEX tests. Core-uncovery was observed in tests investigating failure of two ADS4 valves to open on the nonpressurizer side (beyond design basis accident in the United States) in combination with either a double-ended direct vessel injection (DVI) break or a 2 in. break at the bottom of a cold leg, for example. The explanation for the behavior on the APEX test facility is the height scaling of the test facility: APEX has a reduced IRWST head due to 1/4-scaled height. Timing of IRWST injection would be earlier with 1:1 height scaling.

13.3.3 Separate effects tests

In addition to the integral system tests, SETs are being performed for investigating particular phenomena. There are several reasons for the importance and high value of this test type.

First, it has been recognized that the development of individual code models often requires some iteration, and that a model, despite well-conceived, may need

refinement as the range of applications is widened. To establish a firm need for the modification or further development of a model it is usually necessary to compare predictions with SETs data rather than to rely on inferences from IT comparisons.

Second, a key issue concerning the application of best estimate codes to LOCA and transient calculations is the quantification of the uncertainties in predicting safety-relevant parameters. Most methods for determining these uncertainties rely on assigning uncertainties to the modeling of individual phenomena. This concept has placed a new emphasis on SETs above that originally envisaged for model development.

The advantages of SETs are:

- Clear boundary conditions
- Measurement instrumentation can be focused on a particular phenomenon
- Reduced possibility of compensating modeling errors during validation
- More systematic evaluation of the accuracy of a code model across a wide range of conditions up to full reactor plant scale
- Steady state and transient observations possible

A further incentive to conduct SETs in addition to experiments carried out on integral system test facilities is the difficulty encountered in the upscaling of predictions of phenomena from down-scaled ITs to real plant applications. Where a phenomenon is known to be highly scale dependent and difficult to model mechanistically, there is a strong need for conducting SETs at full scale.

Only a few selected results from experiments on the 1:1 scaled UPTF can be presented here in the following sections to show some scaling effects and differences to observations from small-scale experiments.

13.3.3.1 UPTF tests

UPTF (Weiss et al., 1986, 1990; GRS, 1992, 1993) in Germany was a full-scale (1:1) representation of the primary system of a 1300 MWe PWR with four-loop system. It was a fluid-dynamic facility especially designed for studying multidimensional two-phase flow effects in components of large volume like downcomer, upper plenum, entrance region of the steam generator, and main coolant pipes. The steam generation in the core and the entrained water flow during

emergency cooling were simulated by feeding steam and water via nozzles in the so-called core simulator. The behavior of the steam generators was simulated by a controlled removal or feed of steam and water from or to the steam generator simulator from outside. The required steam was provided by a fossil fired power station.

13.3.3.2 Vertical heterogeneous counter-current steam-water flow in the downcomer

In order to illustrate the scaling dependence of thermal-hydraulic phenomena in the downcomer for heterogeneous vertical steam-water counter-current flow, some results are presented. That phenomenon is considered to be important for efficient core cooling by the ECC systems during a LOCA when a break of a pipe of the main coolant system occurs. The previous insight of downcomer phenomena during cold leg ECC injection had been developed particularly based on the USNRC ECC Bypass Programme. It contained steam-water tests which were performed at 1/30, 1/15, 2/15, and 1/5 length scale at the Battelle Columbus Laboratories and CREARE. Steady-state CCFL tests with steam upflow and ECC water downflow as well as transient tests involving lower plenum flashing and two-phase upflow were carried out.

Empirical flooding correlations based on experimental data of these down-scaled test facilities have been developed, using two dimensionless phase velocities: a modified Wallis parameter

$$G = \frac{W}{A}$$

containing W as average downcomer annulus circumference and the Kutateladze number

$$D_h = 4A/p$$

In spite of the variation of scale of the test facilities between 1/30 and 1/5, the

extrapolation to full-scale downcomer geometry was still not clear.

To provide CCFL and ECC bypass data for full reactor geometry, tests on UPTF were carried out. The result of a UPTF experiment, simulating the downcomer behavior during the end-of-blowdown and the refill phases for a large cold leg break, is shown in Fig. 13.4.

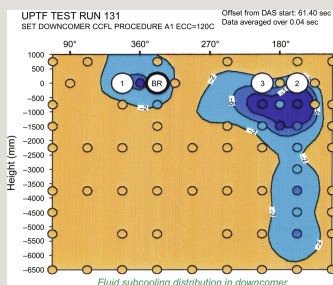


Fig. 13.4 Counter-current flow conditions in full-scale downcomer for strongly subcooled ECC water, distribution of subcooled temperatures.

The test was carried out at a reactor typical steam upflow of 320 kg/s and ECC water injection (subcooling 115 K) into the three intact loops. The contour plot shows isotherms of fluid temperatures (subcooling) in the downcomer projected in a plane. The two-dimensional presentation shows strongly heterogeneous steam-water flow conditions which were not observed in small-scale experiments. The ECC water delivered from the cold legs 2 and 3, which are located opposite the broken loop connection, penetrates the downcomer without being strongly affected by the upflowing steam. Most of the ECC water delivered from cold leg 1, which is located close to the broken loop, however, flows directly to the break bypassing the core.

To demonstrate the effect of the facility scaling on downcomer CCFL, the data obtained from UPTF and CREARE with 1/5 scaling are compared in reference (GRS, 1992; Glaeser and Wolfert, 2012). Slightly subcooled ECC water was used in this UPTF test and saturated ECC water on CREARE. Due to the strongly heterogeneous flow conditions in the full-scale downcomer of UPTF the water delivery curve of UPTF is significantly higher than for CREARE.

The main findings with respect to downcomer behavior during the end-of-blowdown and refill phases of a large cold leg break with cold leg or downcomer

ECC injection can be summarized as follows:

- A significant scale effect on downcomer behavior can be observed
- Steam-water flow conditions in the downcomer are highly heterogeneous at full scale
- Heterogeneous or multidimensional behavior increases water delivery rates at full-scale relative to previous tests on down-scaled facilities
- CCFL correlations developed from the down-scaled tests are not applicable to full-scale downcomers
- Downcomer CCFL correlations for cold leg ECC injection based on down-scaled test results underpredict the water penetration to the lower plenum at full scale
- Due to strong heterogeneous flows in a real downcomer, a CCFL correlation has to account for the location of the ECC injection relative to the broken cold leg

In order to describe the *vertical asymmetric heterogeneous gas/liquid counter-current flow* in the full-scale downcomer, the Kutateladze-type flooding equation was extended by Glaeser (1992) correlating the local steam velocities of the multidimensional flow field with the superficial steam velocity. A *geometrical lateral distance between the legs with ECC injection and the broken loop is introduced in the gas upflow momentum term*. This term relates the local upward gas velocity at the water downflow locations to the superficial gas velocities. The superficial gas velocity can be calculated from the steam mass flow rate.

$$Re = \rho \times v \times D_h / \mu$$

$$Fr = v / \sqrt{(g \times L)}$$

If there is more than one ECC injection location, the arithmetic mean value of all distances L between the ECC injection legs and the broken leg has to be used in the

correlation. However, only those injection locations can be considered where water can flow downward. This means that the modified dimensionless gas velocity obtained by using the value of L for the individual injection location has to be below the onset of penetration point. Otherwise, the respective ECC injection leg cannot be included in the arithmetic mean value L . More details of the derivation and application of the Glaeser-correlation can be found in Glaeser (1992) and Glaeser and Karwat (1993).

The resulting lowest gas velocity for zero water penetration (onset of penetration) is shown in Fig. 13.5 (legend provided in Table 13.3) compared with the downcomer circumference scale. Water downflow is impossible for gas velocities above the curve. Three different flooding correlations are applicable for three different scaling regions. These are the classical Wallis- and Kutateladze-type as well as the Glaeser-correlation. The range of applicability is dependent on the dimensionless annulus circumference, which governs the different flooding correlations. It can be seen that it is impossible to extrapolate counter-current flow correlations from small-scale data below one-ninth downcomer circumference scale (equivalent to 1/81 flow cross-section scale) to reactor scale. The full-scale UPTF data were needed to clarify the influence of scaling on the ECC flooding phenomenon.

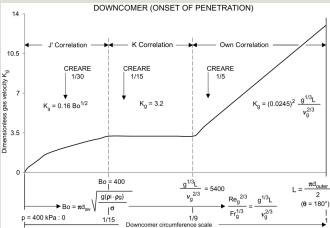


Fig. 13.5 Downcomer flooding correlation for zero penetration of liquid (total bypass).

Table 13.3

Legend for Fig. 13.5

13.3.3.3 Calculated results for importance of downcomer counter-current flow on maximum cladding temperature and quench time

The downflow of ECC water injected into the cold legs or at the top of the downcomer counter-current to steam flowing upward was considered as highly important in the PIRTs, especially for a large break (LB) in one cold leg scenario. As described before, that phenomenon had a significant effect on the cooling of the heater rod bundles representing the core of a reactor in small-scale experimental facilities, like SEMISCALE and LOBL.

A statistical uncertainty and sensitivity analysis for a 2%×100% cold leg break on the Zion NPP was performed using the ATHLET computer code (Glaeser et al., 2008). Of interest here was to get information on the importance of counter-current flow in the downcomer on the maximum cladding temperature. Such information can be obtained from the statistical GRS-uncertainty and sensitivity method, see Section 13.4. Validation of differently scaled experiments up to 1:1 UPTF separate counter-current flow experiments in the downcomer was performed. The interfacial shear multiplier was adjusted to calculate the counter-current flow in good agreement. Interfacial shear had to be reduced significantly for UPTF experiments during nondispersed flow in the downcomer and the core compared with small-scale experiments in order to calculate the downflow water mass flow in agreement with the data. The interfacial shear in the upper plenum and core region was adjusted in order to calculate water flow coming locally via the hot legs from the steam generators and the pressurizer. These extended ranges for interfacial shear were used for the Zion calculations. The upper bound of the uncertainty ranges from small-scale experiments remained. The multipliers for the downcomer derived from 1:1 scale UPTF calculations are in the range of 0.05–3.0 for the reactor instead of 0.33–3.0 used for the 1:50 scale LOFT experiments. The ranges for the core, tie plate, and upper plenum are 0.01–2.5 instead of 0.2–2.5 for LOFT.

Different to earlier PIRTs, it turned out, that no significant effect of downcomer counter-current flow on the cladding temperature is to be seen in the reactor calculation.

Fig. 13.6 shows the uncertainty band (tolerance interval) of calculated maximum cladding temperature versus time and the time span of accumulator injection.

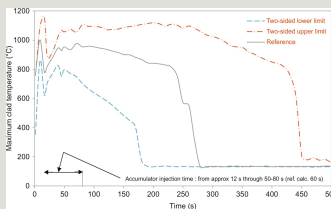


Fig. 13.6 Calculated uncertainty band of maximum cladding temperature of Zion reactor, 2%×100% cold leg break.

The importance measures are shown in Fig. 13.7 during the blowdown phase and Fig. 13.8 during the reflood phase. The length of the bars indicate the importance, positive sign tends to increase cladding temperature with increasing input parameter values, and vice versa. More effect on the cladding temperature comes from the core and tie plate counter-current flow, even more on the quench time (Fig. 13.9). A reason may be that the time of limitation of water downflow through the downcomer counter-current to significant steam upflow is relatively short during such a LB transient in reactor scale.

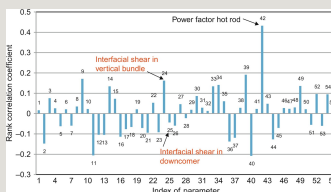


Fig. 13.7 Importance measures of 55 uncertain input parameters for maximum cladding temperature during blowdown phase.

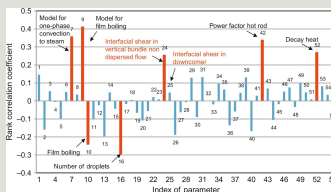


Fig. 13.8 Importance measures of 55 uncertain input parameters for maximum cladding temperature during reflood phase.

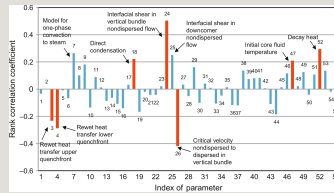


Fig. 13.9 Importance measures of 55 uncertain input parameters for quench time.

13.3.3.4 Vertical counter-current flow of saturated steam and water for homogeneous flow conditions at the upper core tie plate and in the upper plenum

To study the counter-current flow at the upper core tie plate and the liquid hold up above the tie plate in case of saturated steam/water upflow a series of UPTF tests were carried out. The core simulator with controlled injection of steam and water adjusted reactor typical steam/water upflow. Steam and entrained water upflow is of higher relevance for counter-current flow in the reactor than steam upflow only. This effect has not been investigated in vertical counter-current SETs prior to UPTF.

The test results indicate that:

- Steam/water upflow, two-phase pool above the tie plate, and water fall back through the tie plate is uniform across the core area
- Flooding curves for both full-scale and subscale test facilities are similar
- Water downflow to each fuel assembly is scale-invariant
- For homogeneous flow conditions at the tie plate the flooding curve can be defined by applying the Kutateladze number as scaling parameter

Consequently, the effects of scaling on vertical counter-current steam-water flow is dependent on the two-phase flow distribution, either heterogeneous or homogeneous. Heterogeneous flows are highly scaling dependent but homogeneous flows not.

13.3.3.5 Flow conditions in the hot leg during reflux condenser mode

Heat is transferred from the core to the secondary side of the steam generators by evaporation of water in the core and subsequent condensation of the steam in the U-tubes of the steam generators in the reflux condenser mode. A portion of the condensate flows back from the steam generator to the upper plenum counter-currently to the steam through the hot leg. That condensate serves cooling the core. Due to momentum exchange between the steam-flow and the water-flow in the hot legs flooding may occur, which could prevent or at least deteriorate the water flow back to the core.

The Kutateladze-type equation considering instabilities of the gas-liquid interface in horizontal counter-current flow conditions can be transferred into the Wallis-type equation (Glaeser, 1992). This is possible for horizontal or inclined flow since the gravity force of unstable waves and droplets act perpendicular to the main flow directions of steam and water and counter the pressure difference between the bottom of such a wave and the crest due to different steam velocities at the wave crest and bottom (Glaeser and Karwat, 1993). Hence, *the Wallis correlation is applicable to horizontal counter-current flow over the whole scaling region what is different to vertical heterogeneous counter-current flow.*

The UPTF test has demonstrated that a substantial margin exists between the flooding limit and the typical conditions expected in a PWR during reflux condenser mode of a SB-LOCA. This is the case in a full-reactor scale hot leg (Glaeser and Karwat, 1993; see Fig. 13.10). This steam mass flow results from a 2% core decay power scaled from 8 to 0.3 MPa pressure of UPTF.

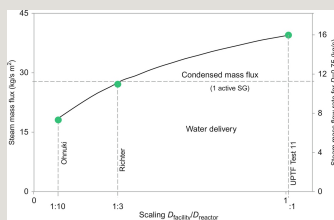


Fig. 13.10 Counter-current flow limitation compared with reactor steam mass flow in the hot leg.

GRS used these full-scale UPTF test series data of counter-current flow in the hot leg for the code development and validation of their ATHLET computer code when they became available in the year 1984. Prior to that, the code was developed and validated using small-scale LOBI and LOFT experiments. A new correlation

for the geometry of the horizontal tube including the inclined tube section at the steam generator inlet was developed and validated against a variety of UPTF experiments. For example, saturated water was supplied from the steam-generator side and, simultaneously, saturated steam from the vessel side, i.e., from the upper plenum was supplied in UPTF Test 11. The steam mass flow rate was increased gradually until occurrence of the CCFL. Good correspondence for a horizontal tube with original diameter demonstrated that the velocities of the two phases including the CCFL are determined realistically by the new correlation.

With the new correlation, further experiments were analyzed successfully, e.g., the depletion of the steam generator U-pipes during a small-break experiment in the LOBI test facility. After completion of the model validation calculations, the new correlation was included in the ATHLET code. Based on the same findings the vendor made similar improvements in his version of SRELAP5. Some licensing calculations were repeated in order to find out the effect of the changed correlation in ATHLET. A medium break size of 160 cm² (3.6%) in the cold leg of the KONVOI plants was selected for demonstration. It turned out that no heat-up was calculated compared with the old model due to improved back-flow of condensate from the steam generator toward the upper plenum to fill the core region and serve better cooling of the core (see Fig. 13.11).

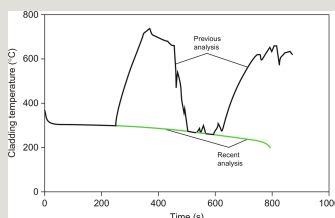


Fig. 13.11 Application of counter-current flow results of UPTF on ATHLET calculations for small break LOCA (160 cm² break in cold leg of PWR 1300 MW electric) with respect to maximum cladding temperature in the core.

13.3.4 Conclusions and future trends

Some information about scaling in nuclear reactor SYS THs is presented. Some phenomena strongly depend on geometrical scale, like heterogeneous vertical steam-water CCFL. The SYS TH computer code is an important scaling tool to perform safety analysis for power reactors. Strong connections are therefore

between scaling, code validation, setting up the nodalization and uncertainty evaluation, as well as code user qualification and expertise.

Power and volume scaling is the dominant approach. The concept of scaling hierarchy by Zuber may be applied. Full height is often used for test facilities. The alternative Ishii scaling allows to reduce the cost of an experimental facility, and to reduce the influence of heat release from structures or the distortion due to different surface to volume ratio on the course of a transient. However, the Ishii scaling may need confirmation by a scaling preserving the time in order to provide confidence in the simulation of important phenomena and the timing of sequences of an accident scenario.

The examples presented show very clearly that the thermal-hydraulic behavior of a down-scaled ITF cannot be extrapolated directly to obtain nuclear plant behavior. Although the ITFs have been designed in different volume scaling, ranging from 1:2070 to 1:48, the experimental results of these facilities are not solving the scaling problem. A combination of integral system tests with separate effect tests in full reactor scale is indispensable. The computer codes shall be validated to calculate integral and separate effects experiments over the whole available scaling range in good agreement with the data. Therefore, the SYS TH computer code is an important scaling tool to perform safety analysis for power reactors.

The refinement of the thermal-hydraulic system codes, the completion of the validation and the quantification of the uncertainties in the simulation of full size plant accidents are tasks for the next years.

Another important effort in the analytical work will be focused on the development of two-phase flow computational fluid dynamics (CFD) codes. Due to the high resolution in space and the possibility for three-dimensional description of the single- and two-phase flow phenomena the scaling issue will become less important. Parallel to the progress in the development of the computer hardware with regard to reducing calculation time the application area of these codes will be extended.

The development of the two-phase flow CFD codes is a great challenge for the analytical teams in the next decades and may contribute to the motivation of young scientists working in the field of nuclear technology.

13.4 Current uncertainty methods

13.4.1 Introduction

The safety analysis used to justify the design and construction of water-cooled NPPs demonstrates that the plants are designed to respond safely to various postulated accidents in a deterministic thermal-hydraulic safety evaluation. These postulated accidents include LOCAs in which the pressure boundary containing the water, which takes heat away from the reactor core, is breaking and a range of other transients in which conditions deviate from those in normal operation.

The equations of state and heat transfer properties of water including relevant two-phase phenomena vary very substantially over the conditions that will occur in such accidents. These events can therefore only be simulated by computer codes.

Initial and boundary conditions, geometry, reactor plant operating parameters, fuel parameters, and scale effects may not be exactly known. The models of the thermal-hydraulic computer codes approximate the physical behavior, and the solution methods in the codes are approximate. Therefore, the code predictions are not exact but uncertain. Agreement of calculated results with experimental data is often obtained by choosing specific code input options or changing parameter values in the model equations. These selected parameter values usually have to be changed again for different experiments in the same facility or a similar experiment in a different facility in order to obtain agreement with data. A single “best estimate” calculation with an advanced realistic code would give results of one code run of unknown accuracy. To make such results useful, for example, if they are to be compared with limits of acceptance, the uncertainty in the predictions then has to be calculated separately. Uncertainty analysis methods therefore were developed to estimate safety margins if best estimate codes are used to justify reactor operation. A particular stimulus was the USNRC's revision of its regulations in 1989 to permit the use of realistic models with quantification of uncertainty in licensing submissions for ECCS (CFR, 1989).

In addition, uncertainty analysis can be used to assist research prioritization. It can help to identify models that need improvement and areas where more data would be needed. It can make code development and validation more cost-effective.

The alternative is to use conservative computer codes and/or conservative initial and boundary conditions to introduce unquantified conservatisms to bound uncertainties. This may lead to unrealistic results. A list of ECCS evaluation models is provided in Appendix C of CFR (1989) to follow the conservative approach in the United States. That approach is not part of this section dealing with uncertainty evaluation rather than trying to bound computational results of safety

parameters conservatively toward the direction of regulatory acceptance criteria (CFR, 1989). An uncertainty analysis quantifies the uncertainty of a result of a safety parameter, and the range toward the acceptance criterion determines the margin. Such a procedure is not nonconservative. It is quantifying the conservatism of a calculation result.

13.4.2 Common methods

Within the uncertainty methods considered, uncertainties are evaluated using either

(1) Propagation of input uncertainties: code scaling, applicability, and uncertainty (CSAU) method and GRS (Gesellschaft für Anlagen- und Reaktorsicherheit) method or

(2) Extrapolation of output uncertainties: uncertainty methodology based on accuracy extrapolation and code with the capability of internal assessment of uncertainty (UMAE/CIAU).

For the “propagation of input uncertainties,” uncertainty is obtained following the identification of uncertain input parameters with specified ranges and/or probability distributions of these parameters, and performing calculations varying these parameters. The propagation of input uncertainties can be performed by either deterministic or statistical methods. For the “extrapolation of output uncertainty” approach, uncertainty is obtained from the output uncertainty based on comparison between calculation results and relevant experimental data.

A short description of these methods is provided in the following sections. These methods have been described in several publications. Detailed comprised information on the different methods and their applications can be obtained from the IAEA Safety Series No. 52 (IAEA, 2008).

13.4.2.1 CSAU method

The CSAU methodology was proposed to investigate the uncertainty of safety-related output parameters. It supplies a complete framework to go through the whole process of an uncertainty analysis. The output parameters in the demonstration cases of this method were only single-valued parameters, such as PCT or minimum water inventory, no time dependent values were provided. Prior to this, a procedure is used to evaluate the code applicability to a selected plant scenario. Experts identify all the relevant phenomena. Following this step, the most important phenomena are identified and are listed, based on an examination of experimental data and code predictions of the scenario under investigation, ranking

them as highly important. In the resulting PIRT, ranking is accomplished by expert judgment. The PIRT and code documentation are evaluated, and it is decided whether the code is applicable to the plant scenario. The CSAU methodology is described in detail by Boyack et al. (1990). Demonstration applications have been performed for a LB-LOCA and a SB-LOCA for a PWR (Boyack et al., 1990; Ortiz and Ghan, 1992).

An optimized nodalization to capture the important physical phenomena should be used for all calculations. This nodalization represents a compromise between accuracy and cost, based on experience obtained by analyzing SETs and integral experiments. No particular method or criteria are prescribed for this task.

Only parameters important for the highly ranked phenomena are selected for consideration as uncertain input parameters. The selection is based on a judgment of their influence on the output parameters. Additional output biases are introduced to consider the uncertainty of other parameters not included in the variation calculations.

Information from the vendor of NPP components as well as from experiments and previous calculations was used to define the mean value and probability distribution or standard deviation of uncertain input parameters, for both the LB- and the SB-LOCA analyses. Additional biases can be introduced in the output uncertainties.

Distributions values of uncertain input parameters are uniform and normal which were used in the two applications performed for demonstration. Output uncertainty is the result of the propagation of input uncertainties through a number of code calculations.

A statistical method for uncertainty evaluation has not been proposed in the CSAU but has been widely used in the past. A response surface approach was used in the demonstration applications. The response surface fits the code predictions obtained for selected parameters and is further used instead of the original computer code for performing the variation calculations. Such an approach then entails the use of a limited number of uncertain parameters in order to reduce the number of code runs and the cost of analysis but was limited to results of point values, like PCT in the demonstrations. However, within the CSAU framework the response surface approach is not prescribed and other methods can be applied.

Scaling is considered by the CSAU, identifying several issues based on test facilities and code assessment. The effect of scale distortions on main processes,

the applicability of the existing database to the given NPP, the scale-up capability of closure relationships, and their applicability to the NPP range is evaluated at a qualitative level. Biases are introduced if the scaling capability is not provided.

13.4.2.2 Statistical (GRS) method

The statistical method again propagates potential uncertain input parameters to uncertain output parameters by code calculations. The main advantage to use these tools is that the number of calculations is independent of the number of uncertain parameters to be investigated. The number of calculations depends only on the chosen tolerance limits or intervals of the uncertainty statements of the results. Not using these statistical tools necessitates a drastic increase of code calculations with the number of uncertain parameters when uncertain values of the selected input parameters have to be combined.

Choosing combinations of parameter values at will by the expert and performing the respective code runs does not allow to make quantitative tolerance/confidence statements about the combined influence of the identified uncertainties. Such statements could not be made without the tools from statistics, not even after a very large number of code runs. It simply is a matter of efficiency to exploit what is known from statistics in order to reach the target uncertainty coverage and confidence at minimum cost or to extract the most of information from the expended number of runs. The features of the statistical method are:

(1) The uncertainty space of input parameters like computer code models, initial and boundary conditions, geometry, reactor plant operating parameters, fuel parameters, scale effects, and solution algorithms are defined by their uncertainty ranges and probability distributions. These are sampled at random according to the probability distributions of the uncertain parameters. Code calculations are performed by sampled sets of parameters.

(2) The number of code calculations is determined by the requirement to estimate a tolerance and confidence interval for the quantity of interest, such as PCT or cladding temperature versus time. Following a proposal by GRS, Wilks' formula (Wilks, 1941, 1942) is used to determine the number of calculations to obtain the uncertainty bands.

(3) Statistical evaluations are performed to determine the sensitivities or importance of input parameter uncertainties on the uncertainties of key results, i.e., parameter importance analysis.

The smallest number n of code runs to be performed is according to Wilks' formula (Wilks, 1941, 1942):

$$W_g = A_g \rho_g u_g = W \alpha$$

which is the size of a random sample (number of calculations) such that the maximum calculated value in the sample is an upper statistical tolerance limit. The required number n of code runs for the a =upper 95% fractile is 59 at the b =95% confidence level.

For two-sided statistical tolerance intervals (investigating the output parameter distribution within an interval) the formula is:

$$W_l = A_l \rho_l u_l = W (1 - \alpha)$$

The minimum number for a 95%/95% two-sided tolerance interval is 93. The minimum number of calculations can be found in Table 13.4.

Table 13.4

Minimum number of calculations n for one- and two-sided statistical tolerance limits

--

Upper statistical tolerance limits are the upper b confidence for the chosen a fractile. The fractile indicates the probability content of the probability distributions of the code results (e.g., a 95% means that PCT is below the tolerance

limit with at least $a=95\%$ probability). One can be $b\%$ confident that at least $a\%$ of the combined influence of all the characterized uncertainties is below the tolerance limit. The confidence level is specified because the probability is not analytically determined. It accounts for the possible influence of the sampling error due to the fact that the statements are obtained from a random sample of limited size. The 95% probability for the uncertainty evaluation comes from US NRC Regulatory Guide 1.157 “Best Estimate Calculations of Emergency Core Cooling System Performance” that an acceptance criterion has not to be exceeded with a probability of 95% or more. The same value is stated in the IAEA Specific Safety Guide No. SSG-2 “Deterministic Safety Analysis for Nuclear Power Plants” (IAEA, 2009). In addition it says: “Techniques may be applied that use additional confidence levels, for example, 95% confidence levels.”

For regulatory purposes, where the margin to licensing criteria is of primary interest, the one-sided tolerance limit may be applied, that is, for a 95th/95th percentile, a minimum of 59 calculations should be performed.

As a consequence, the number n of code runs is independent of the number of selected input uncertain parameters, only depending on the percentage of the fractile and the desired confidence level percentage. The number of code runs for obtaining sensitivity measures is also independent of the number of uncertain input parameters. As an example, 100 runs were carried out in the analysis of a reference reactor, using 50 parameters. More description can be found in references of Hofer (1993) and Glaeser (2008).

The total number of (n) code runs is performed varying simultaneously the values of all uncertain input parameters, according to their distribution. For each instant of time the n values of the considered output parameters are ordered from the lowest to the highest values:

$$\text{Heat flux} = -K(\text{temperature gradient})$$

That “order statistics” is used when Wilks' formula is applied. On the basis of ordering of the output values, the tolerance limits are obtained at a confidence level of 95% by selecting the output values in Table 13.5.

Table 13.5

**Selection of tolerance limits at the 95% confidence level
depending on number of code runs performed**



For the selected plant transient, the method can be applied to an integral effects test simulating the same scenario prior to the plant analysis. If experimental data are not bounded, the set of uncertain input parameters has to be modified or ranges and distributions changed.

Experts identify significant uncertainties to be considered in the analysis, including the modeling uncertainties and the related parameters, and identify and quantify dependencies between uncertain parameters if present. Probability density functions (PDFs) are used to quantify the state of knowledge of uncertain parameters for the specific scenario. Uncertainties of code model parameters are derived based on validation experience. Therefore, experts performing the validation should determine the probability distributions of model uncertainties.

The scaling effect is quantified as a model uncertainty. Additional uncertain model parameters can be included or PDFs can be modified, accounting for results from differently scaled SET analysis.

Input parameter values are simultaneously varied by random sampling according to the PDFs and according to dependencies between them, if dependencies are relevant. A set of parameters is provided to perform the required number n of code runs. For example, the 95% fractile and 95% confidence limit of the resulting distribution of the selected output quantities are directly obtained from the n code results, without assuming any specific distribution. No response surface is used.

Statistical uncertainty and sensitivity analysis provides statements on:

- Uncertainty range of code results that enables to determine the margin between the bound of uncertainty range closest to an acceptance criterion and the acceptance criterion. The 95% fractile, 95% confidence limit for output parameters versus time are provided.

- Sensitivity measures about the influence of input parameters on calculation results, i.e., a ranking of importance versus time is provided which
- allows a ranking of input parameters on output uncertainty as result of the analysis instead of setting up a prior PIRT
- guides further code development
- prioritizes experimental investigations to obtain more detailed information

The sensitivity or importance measures give useful information about those input parameters influencing the uncertainty of computer code results most. That information can be used to find out which ranges and distributions of input uncertainties should potentially be determined more accurately. These sensitivity measures, using regression or correlation techniques from the sets of input parameters and the corresponding output values, allow ranking of the uncertain input parameters in relation to their contribution to output uncertainty. The ranking of parameters is therefore a result of the analysis, not of prior expert judgment, like a PIRT. Nevertheless, a PIRT may be performed to define uncertainty ranges and distributions for a limited number of input parameters, which are considered to be important or to identify important code models to be validated.

The same ordered statistical method using Wilks' formula for setting up the number of code calculations followed later the AREVA Method (Martin and Dunn, 2004), ASTRUM (Automatic Statistical TReatment of Uncertainty)—Method of Westinghouse (Muftuoglu et al., 2004), KREM in Korea, ESM-3D in France and several more. The AREVA method has been licensed by USNRC in the year 2003 and the ASTRUM Method in 2004.

Number of calculations for statistical methods to meet more than one regulatory acceptance limit

A controversial international discussion took place about the number of calculations to be performed using ordered statistical methods during the years 2003–2005. That issue was mainly brought up when more than one regulatory acceptance criterion or limit has to be met, like PCT, local oxidation of fuel rods, and core average zirconium-water reaction for LOCAs. Wald (1943) extended Wilks' formula for multidimensional joint/simultaneous tolerance limits or intervals. However, it seems that a direct and satisfactory extension of the concept of tolerance limits for safety-relevant applications in nuclear safety is not necessary. A slightly modified concept has therefore been proposed by Krzykacz-Hausmann from GRS, introducing a lower confidence limit (Glaeser et al., 2008).

The lower confidence limit according to Clopper-Pearson (Brown et al., 2001) for the binomial parameter is now the unknown probability that a result is lower than a regulatory acceptance limit. Instead of direct joint tolerance limits for the outputs of interest, one considers the lower confidence limit for the probability of “complying with the safety limits for all outputs,” i.e., “meeting the regulatory acceptance criteria.” Basis is that both of the following statements are equivalent:

1. The Wilks' (probability $a=95\%$ and confidence $b=95\%$) limit for the results is below the regulatory acceptance limit
2. The lower $b=95\%$ confidence limit for the probability that the value of the result stays below the regulatory acceptance limit is greater or equal $a=95\%$

The regulatory acceptance limits are incorporated into the probabilistic statements. It turns out that

(1) in the one-dimensional case, i.e., for a single output parameter, this concept is equivalent to the one-sided upper tolerance limit concept.

(2) the necessary number of model runs is also the same in the general case, i.e., independent of the number of outputs or criteria involved and of the type of interrelationships between these outputs or criteria. Therefore, the number of necessary model runs is the same as in the one-dimensional tolerance limit case, even if several output parameters are involved. In the one-dimensional case the lower 95%-confidence interval for the probability of “complying with the regulatory limit” corresponds to the two step procedure: (1) compute the tolerance limit as usual and (2) compare this tolerance limit with the given regulatory limit. In other words: The statement “there is a 95% confidence that the probability of complying with the regulatory limit x_{reg} exceeds 95%” is equivalent to the statement “the computed 95%/95% tolerance limit x_{TL} lies below the regulatory limit x_{reg} .” In the multidimensional case there is no such direct correspondence or equivalence.

The principal advantage of the confidence interval or limit (or “sign-test”) approach seems to be that it can directly be used in the multidimensional case, i.e., multiple output or several output variables, too. The multidimensional extensions of the tolerance limit approach suffer from

(1) not being unique because the runs with the highest value for checking the first limit has to be eliminated for comparison with the next limit, and so on

(2) require substantially increased calculation runs and

(3) are in most cases not necessary since functions of several variables can be reduced to the one-dimensional case

Much more influence on the uncertainty range of computational results has the specified input uncertainty ranges. Less important is the distribution of these input uncertainties. Therefore, high requirements are on the specification and the justification for these ranges. Investigations are underway to transform data measured in experiments and posttest calculations into thermal-hydraulic model parameters with uncertainties. Care must be taken to select suitable experimental and analytical information to specify uncertainty distributions. The selection of suitable experiments is important for the UMAE/CIAU method as well.

13.4.2.3 UMAE/CIAU method

The CIAU method is based on the principle that it is reasonable to extrapolate code output deviations of relevant experimental tests to real plants, as discussed by D'Auria et al. (1995) and D'Auria and Giannotti (2000). The development of the method implies the availability of qualified experimental data. A first step is to check the quality of code results with respect to experimental data by using a procedure based on fast Fourier transform method. Then a method (UMAE) is applied to determine both quantity accuracy matrix (QAM) and time accuracy matrix (TAM).

Considering ITFs of a reference light water reactor (LWR) and qualified computer codes based on advanced models, the method relies on code capability qualified by application to facilities of increasing scale. Direct data extrapolation from small-scale experiments to the reactor scale is difficult due to the imperfect scaling criteria adopted in the design of each scaled-down facility. Only the accuracy (i.e., the difference between measured and calculated quantities) is therefore extrapolated. Experimental and calculated data in differently scaled facilities are used to demonstrate that physical phenomena and code predictive capabilities of important phenomena do not change when increasing the dimensions of the facilities. However, available IT facility scales are far from reactor scale.

One basic assumption is that phenomena and transient scenarios in larger-scale facilities are close enough to plant conditions. The influence of the user and the nodalization upon the output uncertainty is minimized in the methodology. However, user and nodalization inadequacies affect the comparison between measured and calculated trends; that deviation is considered in the extrapolation

process and contributes to the overall uncertainty.

Calculations of both ITs and plant transients are used to obtain uncertainty from accuracy. Nodalizations are set-up and qualified against experimental data by an iterative procedure, requiring that a reasonable level of accuracy be satisfied. Similar criteria are adopted in developing plant nodalization and performing plant transient calculations. The demonstration of the similarity of the phenomena exhibited in test facilities and plant calculations, taking scaling laws into consideration, leads to a qualified nodalization of the plant.

It is not possible to establish a correspondence between each input and each output parameter without performing additional specific calculations. That is, however, beyond the scope of the UMAE. The process starts with the experimental and calculated database. Following the identification (e.g., from the CSNI validation matrix) of the physical phenomena involved in the selected transient scenario, relevant thermal-hydraulic aspects are used to evaluate the acceptability of code calculations, the similarity among experimental data, and the similarity between plant calculation results and available data. Statistical treatment is pursued in order to process accuracy values calculated for the various test facilities and to obtain uncertainty ranges with a 95% probability level. These are superimposed as uncertainty bands bracketing the qualified base calculation using the above mentioned qualified nodalization.

The scaling of both experimental and calculated data is claimed to be explicitly assessed within the framework of the analysis. In fact, the demonstration of phenomena scalability is necessary for the application of the method and the evaluation of the uncertainty associated with the prediction of the NPP scenario.

Comparison of thermal-hydraulic data from experimental facilities of a different scale constitutes the basis of the UMAE checking whether the nodalization and code calculation results are acceptable. An adequate experimental database including the same phenomena as in the selected test scenario of the NPP is needed for the application of this method. For a successful application it is necessary that the accuracy of the calculations does not dramatically decrease with increasing scale of the experimental facilities. The demonstration that accuracy improves when the dimensions of the facility in question are increases would need a sufficiently large database which is not fully available now.

The extension of the method to internal assessment of uncertainty CIAU can be summarized in two parts (D'Auria and Giannotti, 2000):

(1) Consideration of plant state: Each state is characterized by the value of six relevant quantities (i.e., a hypercube) and the value of the time since the transient start

(2) Association of an uncertainty to each plant state

In the case of a PWR the six quantities are: (a) upper plenum pressure; (b) primary loop mass inventory (including the pressurizer); (c) steam generator secondary side pressure; (d) cladding surface temperature at 2/3 of core active height (measured from the bottom of the active fuel), where the maximum cladding temperature in one horizontal core cross section is expected; (e) core power; and (f) steam generator downcomer collapsed liquid level. If levels are different in the various steam generators, the largest value is considered.

A hypercube and a time interval characterize a unique plant state for the purpose of uncertainty evaluation. All plant states are characterized by a matrix of hypercubes and a vector of time intervals. Y defines as a generic thermal-hydraulic code output plotted versus time. Each point of the curve is affected by a quantity uncertainty and a time uncertainty. Owing to the uncertainty, each point may take any value within the rectangle identified by the quantity and time uncertainties. The value of uncertainty—corresponding to each edge of the rectangle—can be defined in probabilistic terms. This shall satisfy the requirement of a 95% probability level acceptable to NRC staff for comparing best estimate predictions of postulated transients with the licensing limits in 10 CFR 50.

The basic assumption of the CIAU is that the uncertainty in code prediction is the same for each plant state. A quantity uncertainty matrix (QUM) and a time uncertainty vector (TUV) can be set-up by means of an uncertainty methodology, like UMAE.

Possible compensating errors of the used computer code are not taken into account by UMAE and CIAU, and error propagation from input uncertainties through output uncertainties is not performed and is not the purpose of that method. A high effort is needed to provide the database for deviations between experiment and calculation results in CIAU. That time and resource consuming process has been performed only by University of Pisa for the codes CATHARE and RELAP5 up to now. The database is available only there. That is the reason why this method is only used by University of Pisa up to now.

13.4.3 International validation of uncertainty methods

Several international programs have been performed within OECD/CSNI in order to apply uncertainty methods, to compare their applications by different participants and derive conclusions and recommendations.

13.4.3.1 Uncertainty method study

International validation and comparison exercises in applying uncertainty methods have been performed. The first was the uncertainty method study (UMS) with the objectives:

- 1. To gain insights into differences between features of the methods by:
 - comparing the different methods, step by step, when applied to the same problem
 - comparing the uncertainties predicted for specified output quantities of interest
 - comparing the uncertainties predicted with measured values
 - allowing conclusions to be drawn about the suitability of methods
- 2. To inform those who will take decisions on conducting uncertainty analyses, for example, in the light of licensing requirements.

The United Kingdom was given the task of leading the study. The study was performed from May 1995 to June 1997.

Methods compared

The methods compared in the UMS are summarized in Table 13.6. The methods may be divided into three groups according to their basic principles (Wickett et al., 1998):

Table 13.6
Summary of methods compared in the UMS study

- The University of Pisa method, the uncertainty method based on accuracy

extrapolation (UMAE), extrapolates the accuracy of predictions from a set of integral experiments to the reactor case or experiment being assessed, see previous Section 13.4.2.

The other methods rely on identifying uncertain models and data and quantifying and combining the uncertainties in them. They fall into two kinds:

- The AEA Technology method that characterizes the uncertainties by “reasonable uncertainty ranges” and attempts to combine these ranges with a bounding analysis.
- Methods which assign probability distributions to uncertainty ranges for uncertain input parameters and sample the resulting probability density at random in the space defined by the uncertainty ranges (see Section 13.4.2.2). In the UMS, the GRS, IPSN, and ENUSA methods are of this kind. The probability used here is due to imprecise knowledge and is not probability due to stochastic or random variability.

Chosen experiment

The International Standard Problem (ISP) 26 experiment, LSTF-SB-CL-18, was used. LSTF-SB-CL-18 is a 5% cold leg SB-LOCA experiment conducted in the ROSA-IV Large-Scale Test Facility (LSTF). The LSTF is located at the Tokai Research Establishment of JAERI and is a 1/48 volumetrically scaled, full height, full pressure simulator of a Westinghouse type 3423 MWth PWR. The experiment simulates a loss of off-site power, no high-pressure injection (HPIS), the accumulator system initiates coolant injection into the cold legs at a pressure of 4.51 MPa, the low pressure injection system initiates at 1.29 MPa. Thus, the experiment considers a beyond design basis accident. Because of the ISP the experiment was already well documented.

Although ISP 26 was an open ISP participants in the UMS have not used experimental measurements from the test, for example, the break flow or the secondary pressure. In the same way other experiments performed in the LSTF were not used. This means not allowing the related measurements to influence the choice of input uncertainty ranges and probability distributions of the input uncertainties. Submissions included a written statement of the justification used for input uncertainty ranges and distributions used and were reviewed at workshops. All other assumptions made were listed and reviewed.

Comparison of calculated uncertainty ranges

The participants were asked to make uncertainty statements, based on their calculation results, for:

(1) Functions of time

- Pressurizer pressure
- Primary circuit mass inventory
- Rod surface temperature for B18 rod (4, 4) position 8 (TW359 TWE-B18448)

(2) Point quantities

- First peak clad temperature
- Second peak clad temperature
- Time of overall peak clad temperature (the higher of the two)
- Minimum core pressure difference at DP 50 DPE300-PV

As a result of the short time scale of UMS and limited funding some of the uncertainty ranges derived from experimental data for the calculations have been less well refined and, as a consequence, wider than would have been the case, for example, if the calculations were for a plant safety analysis. This affected the AEAT and ENUSA CCFL ranges, for example.

Functions of time

The uncertainty ranges calculated for pressurizer pressure, primary inventory, and hot rod surface temperature for LSTF B18 rod (4, 4) at position 8 are shown in Figs. 13.12–13.14.

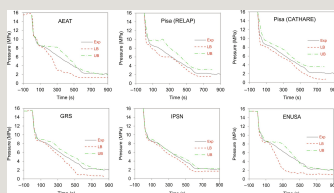


Fig. 13.12 Uncertainty ranges and data for pressurizer pressure. From Wickett, T., Sweet, D., Neill, A., D'Auria, F., Galassi, G., Belsito, S., Ingegneri, M., Gatta, P., Glaeser, H., Skorek, T., Hofer, E.,

Kloos, M., Chojnacki, E., Ounsy, M., Lage Perez, C., Sánchez Sanchis, J.I., 1998. Report of the uncertainty methods study for advanced best estimate thermal hydraulic code applications, Volume 1 (Comparison) and Volume 2 (Report by the participating institutions). NEA/CSNI/R(97)35, Paris, France.

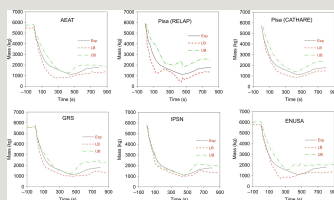


Fig. 13.13 Uncertainty ranges and data for primary mass. From Wickett, T., Sweet, D., Neill, A., D'Auria, F., Galassi, G., Belsito, S., Ingegneri, M., Gatta, P., Glaeser, H., Skorek, T., Hofer, E., Kloos, M., Chojnacki, E., Ounsy, M., Lage Perez, C., Sánchez Sanchis, J.I., 1998. Report of the uncertainty methods study for advanced best estimate thermal hydraulic code applications, Volume 1 (Comparison) and Volume 2 (Report by the participating institutions). NEA/CSNI/R(97)35, Paris, France.

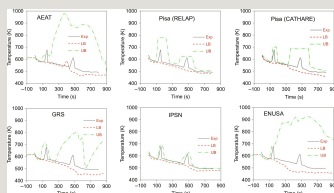


Fig. 13.14 Uncertainty ranges and data for hot rod temperature. From Wickett, T., Sweet, D., Neill, A., D'Auria, F., Galassi, G., Belsito, S., Ingegneri, M., Gatta, P., Glaeser, H., Skorek, T., Hofer, E., Kloos, M., Chojnacki, E., Ounsy, M., Lage Perez, C., Sánchez Sanchis, J.I., 1998. Report of the uncertainty methods study for advanced best estimate thermal hydraulic code applications, Volume 1 (Comparison) and Volume 2 (Report by the participating institutions). NEA/CSNI/R(97)35, Paris, France.

Clad temperature ranges

The AEAT and ENUSA predictions are remarkably similar. The same code (RELAP5), the same base input deck, and mostly the same input uncertainties were used. However, they applied different methods, i.e., bounding (AEAT) versus statistical treatment (ENUSA) of the uncertainties, and the numbers of the input uncertainties are different (7 by AEAT and 25 by ENUSA).

The two applications of the Pisa (UMAE) method using different computer codes (RELAP and CATHARE) are broadly similar. The clad temperature ranges for the second dry-out are similar. Those ranges for the first dry-out calculated by CATHARE gave a narrower range because the base case calculation did not predict the dry-out. However, the UMAE still generated a successful uncertainty range for this quantity because of the first dry-out measured on those experiments

considered for accuracy extrapolation to the LSTF experiment.

Of the probabilistic methods, IPSN gave the narrowest ranges. This is attributed to the choice of parameters made and the parameter ranges used. An actuation of the CCFL option in the CATHARE code (at the upper core plate and the inlet plena of the steam generators) was needed to predict the first dry-out.

The large uncertainty ranges for clad temperature calculated by AEAT, ENUSA, and GRS prompted discussion among the participants about the reasons for them.

In the case of AEAT and ENUSA this may be in part due to unrealistically large uncertainty ranges for CCFL parameters, agreed upon in order to complete the study on time. When AEAT discounted CCFL uncertainty completely the calculated uncertainty range for peak clad temperature changed from 584-1142 K to 584-967 K. Another contribution may come from the used RELAP5 version MOD 3.2, calculating higher peak clad temperatures than MOD 2 and MOD 3.2.2, see under “follow-on activity.”

The measured maximum clad temperature during the second heat-up is well below that of the first. In the GRS calculations, many of the 99 calculated time histories exhibit the contrary, namely a maximum during the second heat-up. The uncertainty of the maximum temperature during the second heat-up is about double of that during the first. In some code runs a partial dry-out occurs due to fluid stagnation in the rod bundle which causes an earlier second heat-up, and as a consequence, a larger increase of the clad temperature.

The large uncertainty is striking, and the sensitivity measures indicate which of the uncertainties are predominantly important. These sensitivities are presented in Volume 2 of reference Wickett et al. (1998). Main contributions to uncertainty come from the critical discharge model and the drift in the heater rod bundle. Other contributions that are worth mentioning come from the bypass cross section upper downcomer-upper plenum. As a consequence, improved state of knowledge about the respective parameters would reduce the striking uncertainty of the computed rod surface temperature in the range of the second core heat-up most effectively.

UMS follow-on activity

After the closure of the UMS and after the report by Wickett et al. (1998) was issued University of Pisa performed comparison calculations of experiment LSTF-SB-CL-18 using different versions of the RELAP 5 code, i.e., MOD 2, MOD 3.2, and MOD 3.2.2. Mod2 was used by the University of Pisa, and MOD 3.2 by AEA Technology as well as ENUSA in this study. It turned out that MOD 3.2 calculated

a 170 K higher peak clad temperature compared with MOD 2 and MOD 3.2.2 using the same input deck. This may contribute to the relative high upper limit of the uncertainty ranges calculated by AEAT and ENUSA. That explanation is also in agreement with the AEAT peak clad temperature of 787 K at 300 s for their reference calculation using nominal values for the input parameters, without calculating the first heat-up. The measured second peak is 610 K at 500 s.

A new application was performed by GRS using revised probability distributions for the most important uncertain parameters, which were identified by importance measures in the UMS analysis, contraction coefficient of critical discharge flow and drift in the heater rod bundle. A newer ATHLET version Mod 1.2, cycle A was used instead of Mod 1.1, Cycle A. The result was a shorter duration of the second heat-up and lower peak clad temperatures during the second heat-up (Fig. 13.15).

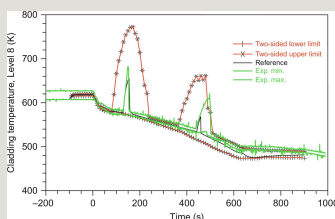


Fig. 13.15 Revised calculated uncertainty range compared with measured minimum and maximum values of rod clad temperature by GRS.

Due to these findings lower differences of uncertainty ranges by different participants are expected.

Conclusions and recommendations of UMS Study

Five uncertainty methods for advanced best estimate thermal hydraulic codes have been compared. Most of the methods identify and combine input uncertainties. Three of these, the GRS, IPSN, and ENUSA methods, use probability distributions, and one, the AEAT method, performs a bounding analysis. One of the methods, the University of Pisa method, is based on accuracy extrapolation from integral experiments. To use this method, stringent criteria on the code and experimental database must be met.

Where the predictions of the methods differ, the differences have been accounted for in terms of the assumptions of the methods and the input data used. The calculated ranges bound the experimental results with some exceptions. The possible causes of these discrepancies have been identified.

Comparison between the calculations

The differences between the predictions from the methods will come from a combination of:

- the method used
- the underlying accuracy of the reference calculation and the modeling used
- the completeness of the identification and selection of uncertainties
- the conservatism of the input (e.g., uncertainty ranges, probability distributions) used
- in the Pisa method optimization of the nodalization and possibly from the different number of experiments investigated (5 experiments with CATHARE, 10 experiments with RELAP)

Of these, differing degrees of conservatism of the input, particularly where data are sparse, probably account for the major differences between the specified uncertainty ranges. For example, critical two-phase flow data from LSTF were not used, and data for the geometry of the LSTF orifice were not available.

The ideal is for a specified uncertainty range that fully reflects the accuracy of the underlying modeling. The input uncertainties mainly responsible for the differences are probably those identified as important by the sensitivity studies of the methods. These are: choked flow and CCFL (AEAT and ENUSA) and choked flow and drift in the heater rod bundle (GRS). Further work to refine input uncertainty ranges for these will affect the calculated uncertainty ranges. An example performed by GRS is presented here. It follows that it is very important how the methods are applied. Due to these findings lower differences of uncertainty ranges by different participants are expected in the future. In all cases appropriate knowledge, skill, experience, and quality standards must be applied.

Other Conclusions of UMS

For some of the methods described here the present study was the first full

application. For all of them it constituted a pilot study that allowed a better understanding of the basic assumptions of the method.

The information gained in the UMS about the methods described and how they can be applied can be used to inform decisions on the conduct of uncertainty analyses, for example, in the light of licensing requirements.

13.4.3.2 Best estimate methods—uncertainty and sensitivity evaluation (BEMUSE) programme

Objectives of BEMUSE

The high level objectives of the work are:

- To evaluate the practicability, quality, and reliability of best-estimate (BE) methods including uncertainty and sensitivity evaluation in applications relevant to nuclear reactor safety
- To develop common understanding from the use of those methods
- To promote and facilitate their use by the regulatory bodies and the industry

Operational objectives include an assessment of the applicability of best estimate and uncertainty and sensitivity methods to ITs and their use in reactor applications. The justification for such an activity is that some uncertainty methods applied to BE codes exist and are used in research organizations, by vendors, technical safety organizations, and regulatory authorities. Over the last years, the increased use of BE codes and uncertainty and sensitivity evaluation for design basis accident (DBA), by itself, shows the safety significance of the proposed activity. Uncertainty methods are used worldwide in licensing of LOCAs for power uprates of existing plants, new reactors, and new reactor developments. End users for the results are expected to be industry, safety authorities, and technical safety organizations.

Main steps of BEMUSE

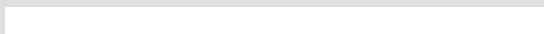
The programme was divided into two main steps, each one consisting of three phases. The first step is to perform an uncertainty and sensitivity analysis related to the LOFT L2-5 test, and the second step is to perform the same analysis for a NPP LB-LOCA. The program started in January 2004 and was finished in September 2010.

- Phase 1: Presentation “a priori” of the uncertainty evaluation methodology to be used by the participants; lead organization: IRSN, France
- Phase 2: Reanalysis of the International Standard Problem ISP-13 exercise, posttest analysis of the LOFT L2-5 large cold leg break test calculation; lead organization: University of Pisa, Italy (CSNI, 2006)
- Phase 3: Uncertainty evaluation of the L2-5 test calculations, first conclusions on the methods and suggestions for improvement; lead organization: CEA, France (CSNI, 2007)
- Phase 4: Best-estimate analysis of a NPP-LBLOCA; lead organization: UPC Barcelona, Spain (CSNI, 2008)
- Phase 5: Sensitivity analysis and uncertainty evaluation for the NPP LB-LOCA, with or without methodology improvements resulting from phase 3; lead organization: UPC Barcelona, Spain (CSNI, 2009)
- Phase 6: Status report on the area, classification of the methods, conclusions and recommendations; lead organization: GRS, Germany (CSNI, 2011)

The participants of the different phases of the programme and the used computer codes are given in Table 13.7.

Table 13.7

BEMUSE participants and used codes



From CSNI, 2011. BEMUSE phase VI report, status report on the area, classification of the methods, conclusions and recommendations. NEA/CSNI/R(2011)4, Paris, France.

Used methods

Two classes of uncertainty methods were applied. One propagates “input uncertainties,” and the other one extrapolates “output uncertainties.”

The main characteristics of the statistical methods based upon the propagation of input uncertainties is to assign probability distributions for these input uncertainties, and sample out of these distributions values for each code calculation to be performed. The number of code calculations is independent of the number of input uncertainties but is only dependent on the defined probability content (percentile) and confidence level. The number of calculations is given by Wilks' formula (see Section 13.4.2.2). By performing code calculations using variations of the values of the uncertain input parameters, and consequently calculating results dependent on these variations, the uncertainties are propagated in the calculations up to the results. Uncertainties are due to imprecise knowledge and the approximations of the computer codes simulating thermal-hydraulic physical behavior.

The methods based upon extrapolation of output uncertainties need available relevant experimental data and extrapolate the differences between code calculations and experimental data at different reactor scales (see Section 13.4.2.3). The main difference of this method compared with statistical methods is that there is no need to select a reasonable number of uncertain input parameters and provide uncertainty ranges (or distribution functions) for each of these variables. The determination of uncertainty is only on the level of calculation results due to the extrapolation of deviations between measured data and calculation results.

The two principles have advantages and drawbacks. The first method propagating input uncertainties is associated with order statistics. The method needs to select a reasonable number of variables and associated range of variations and possibly distribution functions for each one. Selection of parameters and their distribution must be justified. Uncertainty propagation occurs through calculations of the code under investigation. The “extrapolation on the outputs” method needs to have “relevant experimental data” available to derive uncertainties. The sources of deviation between calculation and data cannot be derived by this method. The method seeks to avoid engineering judgment as much as possible.

In BEMUSE, the majority of participants used the statistical approach, associated with Wilks' formula. Only University of Pisa used its method extrapolating output uncertainties. This method is called the CIAU method, Code with (the capability of) Internal Assessment of Uncertainty. The reason why other participants do not use this method is the high effort needed to get the database for deviations between experiment and calculation results in CIAU. That time and resource consuming process has been performed only by University Pisa for the codes CATHARE and RELAP5 for the time being. The database is available only there.

Selected results

Application to LOFT L2-5 experiment

Based on procedures developed at University of Pisa, a systematic qualitative and quantitative accuracy evaluation of the code results have been applied to the calculations performed by the participants for LOFT test L2-5 in BEMUSE phase 2. The test simulated a 2%×100% cold leg break. LOFT was an experimental facility with nuclear core. A FFTBM was performed to quantify the deviations between code predictions and measured experimental data (CSNI, 2006). Participants carefully pursued the proposed criteria for qualitative and quantitative evaluation at different steps in the process of code assessment during the development of the nodalization, the evaluation of the steady-state results, and the measured and calculated time trends. All participants fulfilled the criteria with regard to agreement of geometry data and calculated steady-state values.

The results of uncertainty bands for the four single-valued output parameters first PCT, second PCT, time of accumulator injection, and time of complete quenching for the calculations of the LOFT L2-5 test are presented in Fig. 13.16 (CSNI, 2007). It was agreed to submit the 5/95 and 95/95 estimations of the one-sided tolerance limits, that is, to determine both tolerance limits with a 95% confidence level each. They are ranked by increasing band width. It was up to the participants to select their uncertain input parameters.

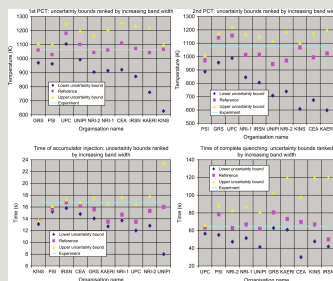


Fig. 13.16 Uncertainty analysis results of LOFT L2-5 test calculations for four single-valued output parameters, first PCT, second PCT, time of accumulator injection and time of complete quenching compared with experimental data. From CSNI, 2007. BEMUSE phase III report, uncertainty and sensitivity analysis of the LOFT L2-5 test. NEA/CSNI/R(2007)4, Paris, France; CSNI, 2011. BEMUSE phase VI report, status report on the area, classification of the methods, conclusions and recommendations. NEA/CSNI/R(2011)4, Paris, France.

The following observations can be made:

- First PCT: The spread of the uncertainty bands is within 138-471 K. The difference among the upper 95%/95% uncertainty bounds, which is important to compare with the regulatory acceptance criterion, is up to 150 K and all but one participant cover the experimental value. One participant (UPC) does not envelop the experimental PCT due to a too high lower bound. Two reasons can explain this result: Among all the participants, on the one hand, UPC has the highest reference value; on the other hand, its band width is among the narrowest ones. KINS attribute their low lower uncertainty bound to a too high value of maximum gap conductance of the fuel rod.

- Second PCT: In this case, one participant (PSI) does not envelop the experimental PCT, due to a too low upper bound. The reasons are roughly similar to those given for the first PCT: PSI, as several participants, calculates a too low reference value but has also the specificity to consider an extremely narrow upper uncertainty band. The spread of the uncertainty bands is within 127–599 K. The difference among the upper 95%/95% uncertainty bounds, which is important to compare with the regulatory acceptance criterion, is up to 200 K.

- Time of accumulator injection: Four participants among 10 calculate too low upper bounds (KINS, PSI, KAERI, and UPC), whereas CEA finds an upper bound just equal to the experimental value. These results are in relationship with the prediction of the cold leg pressure reaching the accumulator pressure 4.29 MPa. The band widths vary within the range 0.7–5.1 s for all the participants except for UNIFI which finds a much larger band, equal to 15.5 s. This is mainly due to the consideration of time error for the pressure transient calculated by UNIFI.

- Time of complete quenching: All the uncertainty bands envelop the experimental value, even if the upper bound is close to the experimental value for one participant. The width of the uncertainty range varies from 10 s to more than 78 s. If the core is not yet quenched at the end of the calculation as it is the case for two participants (KAERI, KINS), or if there are several code failures before the complete quenching (IRSN), the upper bound is plotted at 120 s in Fig. 13.16.

First suggestions for improvement of the methods have not been proposed as result of the exercise; however, recommendations for proper application of the statistical method were given, see under “Conclusions and recommendations of BEMUSE programme.”

Application to Zion NPP

The scope of phase 4 was the simulation of a LB-LOCA in a NPP using experience

gained in phase 2. Reference calculation results were the basis for uncertainty evaluation, to be performed in the next phase. The objectives of the activity are (1) to simulate a LB-LOCA reproducing the phenomena associated to the scenario and (2) to have a common, well-known basis for the future comparison of uncertainty evaluation results among different methodologies and codes (CSNI, 2008).

The activity for the Zion NPP was similar to the previous phase 2 for the LOFT experiment. The UPC team together with UNIPI provided the database for the plant, including RELAP5 and TRACE input decks. Geometrical data, material properties, pump information, steady-state values, initial and boundary conditions, as well as sequence of events were provided. The nodalization comprised generally more hydraulic nodes and axial nodes in the core compared with the LOFT applications.

Results of reference calculations

The base case or reference calculations are the basis for the uncertainty evaluation. The calculated maximum cladding temperatures versus time shows Fig. 13.17. The highest difference in calculated maximum PCTs between the participants is 167 K (EDO “Gidropress”: 1326 K, KAERI: 1159 K), what is lower than the difference of BEMUSE phase 2 calculations of the LOFT test.

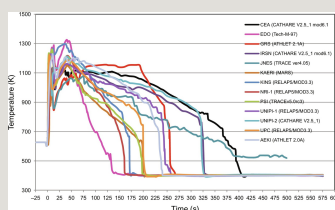


Fig. 13.17 Calculated maximum cladding temperature versus time for the Zion NPP. From CSNI, 2008. BEMUSE phase IV report, simulation of a LB-LOCA in Zion nuclear power plant. NEA/CSNI/R(2008)6, Paris, France; CSNI, 2011. BEMUSE phase VI report, status report on the area, classification of the methods, conclusions and recommendations. NEA/CSNI/R(2011)4, Paris, France.

Single parameter sensitivity

A list of sensitivity calculations was proposed by UPC and performed by the participants to study the influence of different parameters, such as material properties, initial and boundary conditions upon the influence of relevant output

parameters in the scenario under investigation, i.e., a LB-LOCA of a cold leg (CSNI, 2008).

Fig. 13.18 contains values for difference in PCT as well as calculated difference in reflood time $\Delta t_{\text{Reflood}}$, what is meant as difference in total quench time, for the minimum and maximum values of the input parameter range. This shows the highest difference in calculated cladding temperature using the same variation in maximum linear power of $\pm 7.6\%$ of the nominal value. The differences are up to 100 K, mainly between different codes with the exception of UPC using RELAP5 mod 3.3.

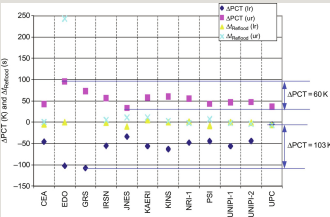


Fig. 13.18 Largest effect of same variation of maximum linear power by $\pm 7.6\%$ on differences of participant's calculated PCT and $\Delta t_{\text{Reflood}}$ for NPP Zion. From CSNI, 2011. BEMUSE phase VI report, status report on the area, classification of the methods, conclusions and recommendations. NEA/CSNI/R(2011)4, Paris, France.

Results of uncertainty analysis

Phase 5 dealt with a power plant (CSNI, 2009) like phase 4. There was no available documentation concerning the uncertainties of the state of the plant, initial and boundary conditions, fuel properties, etc. To solve this situation, it was agreed to provide common information about geometry, core power distribution, and modeling. In addition, a list of common input parameters with its uncertainty was prepared. This was done due to the results of phase 3, calculating the LOFT experiment, showing quite a significant dispersion of the uncertainty ranges by the different participants. The CEA, GRS, and UPC teams prepared this list of common uncertain input parameters with their distribution type and range for the NPP. These parameters were strongly recommended to be used in the uncertainty analysis when a statistical approach was followed. Not all participants used all proposed parameters. On the other hand, some considered only these given parameters without any model uncertainty. The list is shown in Table 13.8.

Table 13.8

Common input parameters associated with a specific uncertainty, range of variation, and type of probability density function

--

From CSNI, 2009. BEMUSE phase V report, uncertainty and sensitivity analysis of a LB-LOCA in Zion nuclear power plant. NEA/CSNI/R(2009)13, Paris, France; CSNI, 2011. BEMUSE phase VI report, status report on the area, classification of the methods, conclusions and recommendations. NEA/CSNI/R(2011)4, Paris, France.

The main results of the calculated uncertainty bands can be seen for the single-valued code results maximum PCT in Fig. 13.19. This temperature is defined as the maximum fuel cladding temperature value, independently of the axial or radial location in the active core during the whole transient. It is the main parameter to be compared with its regulatory acceptance limit in LOCA licensing analyses. For comparison purposes it was agreed to submit the 5%/95% and 95%/95% estimations of the one-sided tolerance limits, that is, to determine both tolerance limits with a 95% confidence level each.

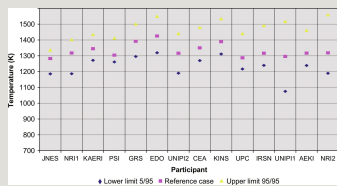


Fig. 13.19 Calculated uncertainty bands of the maximum PCT of Zion NPP LB-LOCA. From CSNI, 2009. BEMUSE phase V report, uncertainty and sensitivity analysis of a LB-LOCA in Zion nuclear power plant. NEA/CSNI/R(2009)13, Paris, France; CSNI, 2011. BEMUSE phase VI report, status report on the area, classification of the methods, conclusions and recommendations. NEA/CSNI/R(2011)4, Paris, France.

Comparing results for the maximum PCT, there is an overlap region of 17 K (i.e., between 1221 and 1238 K). This region is very small. EDO, JNES, and PSI considered only the proposed common input parameters from Table 13.8 without model uncertainties.

Results of sensitivity analysis

Sensitivity analysis is here a statistical procedure to determine the influence of uncertain input parameters on the uncertainty of the output parameter (result of code calculations). Each participant using the statistical approach provided a table of the most relevant parameters for four single-valued output parameters and two time trends (maximum cladding temperature and upper-plenum pressure), based on their influence measures. To synthesize and compare the results of these influences, they are grouped in two main “macro” responses. The macro response for core cladding temperature comprise first, second, and maximum PCT, maximum cladding temperature as function of time before quenching and time of complete core quenching. The summary of the total ranking by participants is shown in Fig. 13.20. Such information is useful for further uncertainty analysis of a LB-LOCA. High ranked parameters are fuel pellet heat conductivity, containment pressure, power after scram, critical heat flux, and film boiling heat transfer.

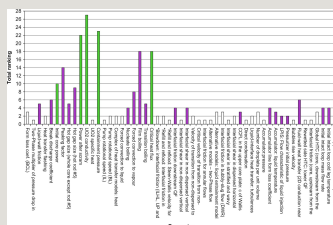


Fig. 13.20 Total ranking of the influence of input uncertainties on cladding temperature per uncertain input parameter for Zion NPP LB-LOCA. From CSNI, 2009. BEMUSE phase V report, uncertainty and sensitivity analysis of a LB-LOCA in Zion nuclear power plant. NEA/CSNI/R(2009)13, Paris, France; CSNI, 2011. BEMUSE phase VI report, status report on the area, classification of the methods, conclusions and recommendations. NEA/CSNI/R(2011)4, Paris, France.

Conclusions and recommendations of BEMUSE programme

The methods used in this activity are considered to be mature for application, including licensing processes. Differences are observed in the application of the methods, consequently results of uncertainty analysis of the same task lead to different results. These differences raise concerns about the validity of the results obtained when applying uncertainty methods to system analysis codes. The differences may stem from the application of different codes and uncertainty methods. In addition, differences between applications of statistical methods may

mainly be due to different input uncertainties, their ranges, and distributions. Differences between CIAU applications may stem from different data bases used for the analysis. However, as it was shown by all BEMUSE phases from 2 to 5, significant differences were observed between the base or reference calculation results. Furthermore, differences were seen in the results using the same values of single input parameter variations (e.g., in BEMUSE phase 4, see Fig. 13.18).

When a conservative safety analysis method is used, it is claimed that all uncertainties are bounded by conservative assumptions. Differences in calculation results of conservative codes would also be seen, due to the user effect, such as different nodalization and code options, like for best estimate codes used in the BEMUSE programme. Difference of code calculation results have been observed for a long time and have been experienced in all International Standard Problems where different participants calculated the same experiment or a reactor event. The main reason is that the user of a computer code has a big influence on how a code is used. The objective of an uncertainty analysis is to quantify the uncertainties of a code result. An uncertainty analysis may not compensate for code deficiencies. Necessary precondition is that the code is suitable to calculate the scenario under investigation.

Consequently, before performing uncertainty analysis, one should concentrate first of all on the reference calculation. Its quality is decisive for the quality of the uncertainty analysis. More lessons were learnt from the BEMUSE results. These are:

- The number of code runs, which may be increased to 150–200 instead of the 59 code runs needed when using Wilks' formula at the first order for the estimation of a one-sided 95%/95% limit tolerance. More precise results are obtained, what is especially advisable if the upper tolerance limit approaches regulatory acceptance criteria (e.g., 1200°C PCT).
- For a proper use of Wilks' formula, the sampling of the input parameters should be of type simple random sampling (SRS). Other types of parameter selection procedures like “Latin-Hypercube-Sampling” or “Importance-Sampling” may therefore not be appropriate for tolerance limits.
- Another important point is that all the code runs should be successful. At a pinch, if a number of code runs fail, the number of code runs should be increased so that applying Wilks' formula is still possible. That is the case supposing that the failed code runs correspond to the highest values of the output (e.g., PCT).

In addition to the above recommendations, the most outstanding outcome of the BEMUSE programme is that a user effect can also be seen in applications of uncertainty methods, like in the application of computer codes. In uncertainty analysis, the emphasis is on the quantification of a lack of precise knowledge by defining appropriate uncertainty ranges of input parameters, which could not be achieved in all cases in BEMUSE. For example, some participants specified too narrow uncertainty ranges for important input uncertainties based on expert judgment, and not on sufficient code validation experience. Therefore, skill, experience, and knowledge of the users about the applied suitable computer code as well as the used uncertainty method are important for the quality of the results.

Using a statistical method, it is very important to include influential parameters and provide distributions of uncertain input parameters, mainly their ranges. These assumptions must be well justified. This has been the experience from the UMS Study already. An important basis to determine code model uncertainties is the experience from code validation. This is mainly provided by experts performing the validation. Appropriate experimental data are needed. More effort, specific procedures, and judgment should be focused on the determination of input uncertainties.

This last point has been an issue of recommendation for further work. Especially, the method used to select and quantify computer code model uncertainties and compare their effects on the uncertainty of the results are studied in a common international investigation using different computer codes, the CSNI Post-BEMUSE Reflood Model Input Uncertainty Methods (PREMIUM) programme (CSNI, 2016a).

13.4.3.3 Post-BEMUSE Reflood Model Input Uncertainty Methods Programme

The objective of the PREMIUM exercise was to find a better means than coarse expert judgment in order to quantify the uncertainty ranges and distributions of relevant model input parameters. The PREMIUM benchmark application was focused on determination of uncertainties of the physical models involved in the prediction of the core reflood, which is an important phase during a loss of coolant-accident (LOCA) scenario (CSNI, 2016a). PREMIUM generally addresses the solution of inverse problems in modeling and simulation, where model input parameters are estimated including their uncertainty from values of model output magnitudes. The solution of the inverse problem includes the processes of model calibration (adapting a model by a correction) and model uncertainty quantification. PREMIUM is focused on the last topic. PREMIUM has been

organized in five consecutive phases.

In Phase I (coordinated by UPC and CSN, Spain), the participants presented and described their methods of model uncertainty quantification. Two methods were offered to the participants (including assistance for their application): CIRCÉ, developed by CEA, France and FFTBM, developed by University of Pisa, Italy. Several participants used these methods, and others used their own quantification methods, like iteration of several input model parameters to bound relevant experimental parameters. The features of the two series of reflood experiments FEBA and PERICLES were also described in this phase.

In Phase II (coordinated by University of Pisa, Italy) participants identified influential code input parameters, from the point of view of reflood, and made a preliminary quantification of their variation range. Phase II coordinators proposed a methodology for the identification of influential parameters, based on a set of quantitative criteria, and presented a preliminary list of possibly influential parameters on reflood. Some participants modified the proposed criteria or established their own criteria.

Each participant obtained a list of influential model parameters to be quantified, assigning ranges of variation to the parameters, based on sensitivity calculations of test 216 of FEBA, and using as responses cladding temperatures and quench front propagation. The influential model parameters obtained by the participants were typically wall and interfacial heat transfer coefficients, interfacial friction coefficient, heat transfer enhancement at the quench front, and droplet diameter.

In Phase III (coordinated by GRS, Germany), the uncertainty of influential input parameters (identified in Phase II) was quantified. Participants obtained uncertainties in the form of ranges or probability distributions. The uncertainties obtained depend strongly on the quantification method. Additionally, they depend on:

- The responses used for quantification of input uncertainties
- The set of input parameters being quantified
- The TH code and the specific model being used

The dependency on the quantification method was stronger than on the used TH code. The results exhibited a significant user effect and a large variability and discrepancy among participants. In some cases, extremely small uncertainty ranges

were found for model parameters, which are physically nonrealistic. They were obtained by participants who performed a calibration of the code models, additionally to the uncertainty quantification, i.e., by a majority of users of the CIRCÉ method.

In Phase IV (coordinated by CEA and IRSN, France), uncertainties calculated for model parameters in Phase III were propagated through the code simulation for the selected tests of FEBA and PERICLES experiments and compared to the experimental results. The objective was to confirm (using FEBA) and validate (using PERICLES) the model uncertainties.

For FEBA tests, most of participants obtained by propagation, uncertainty bands enveloping the experimental values. The width of the bands varied significantly among the participants. The uncertainty bands were highly influenced by the responses used in the quantification and the selected input parameters.

For PERICLES tests, the results were less satisfactory. Considering all the contributions, the fraction of experimental values, which were enveloped by uncertainty bands, was clearly lower than for FEBA, and far from the expected value. Therefore, the direct extrapolation of the model uncertainties calculated for FEBA to PERICLES gave poor results. This result can be explained in terms of significant differences between the two facilities and the analyzed tests.

The quality of the nominal calculation was found important in the final results of the propagation calculations. A good nominal calculation facilitated enveloping the experimental data by the calculated uncertainty bands. Reasons for deviations between nominal calculation and experimental value should be clarified.

The results were highly dependent on the parameter uncertainties derived in Phase III, and therefore were strongly related to the quantification method, rather than to the TH code.

Quantification methods may have the option of performing calibration, as well as quantification, of the models. Applying such option means a calibration of the code models. Some participants in Phase IV compared results with and without the calibration option for the FEBA application, concluding that results improve for PERICLES when there is no calibration. This outcome is completely in line with the validation strategy of “best estimate” TH codes to include several experiments of one test facility, and of differently scaled test facilities.

As in Phase III, a user effect was observed in Phase IV results. Participants using

the same method and the same version of the same system code obtained uncertainty bands, which were significantly different. Differences in the input deck, influential on the nominal calculations, and in the choice of input parameters and responses, could account for the discrepancies.

In Phase V (coordinated by CSN and UPC, Spain), the main conclusions, lessons learned, and recommendations have been collected, and the final report of PREMIUM has been produced (CSNI, 2016a).

A majority of CIRCÉ users obtained envelop calculations, which were globally satisfactory for FEBA results, but not for PERICLES results. For the nominal calculation, most participants predict a too rapid quench front progression for FEBA. However, a majority of participants predict a too slow quench front progression for PERICLES.

CIRCÉ users estimate median values for their input parameters, different from the nominal values. The median values produce what is called a “calibrated calculation.” This corresponds to a “calibration” of models of the system code. Theoretically, this action corrects systematic deviations of the nominal calculation with respect to the experiment used for the quantification. This effect can be especially observed for the prediction of the quench front progression.

The calibrated value of the input parameters found for FEBA is applied to PERICLES. But the prediction of the quench front progression is often different for FEBA and PERICLES. Therefore, the calibrated calculation leads to a deviation to the measured quench front on PERICLES. In addition, the intention of CIRCÉ is to derive narrow uncertainty bands. In order to get more representative ranges and distributions, more suitable experiments should be included for deriving the input uncertainties.

The intention of PREMIUM was to use one or a series of six experiments of the same test facility (FEBA) to derive model input uncertainties and use these for the uncertainty evaluation of another experiment (PERICLES). Using only one experimental facility is not recommended for a validation strategy and to derive input model uncertainties based on the experience from that validation. In the case of PREMIUM, an application of methods to derive input uncertainties inversely from output magnitudes was the objective, and it was considered that it can be extrapolated to a similar experiment, PERICLES. That assumption failed obviously because of differences of the two experimental facilities.

In order to get more representative ranges and distributions of model input

parameters, more suitable experiments should be considered for deriving the input uncertainties. Very well known BEPU framework like the CSAU (Boyack et al., 1990) or the evaluation model development and assessment process (EMDAP) (NRC, 2005b) should be taken into account in the task, see also Section 13.4.2.1 of this chapter. Two issues are important here:

- A strategy to collect experimental databases for TH code model input uncertainty evaluation
- Combine results of input uncertainty quantification from several experiments

13.4.4 Applications in licensing

Best estimate computer codes plus uncertainty evaluation is more and more used in licensing of NPPs. Mostly the ordered statistical method has been used. Applications of uncertainty analyses in licensing cases have been performed up to now in the following countries: Argentina (CIAU), Belgium (ordered statistics), Brazil (output uncertainties and statistical method as well as CIAU), China, France (ordered statistics), Great Britain (ordered statistics), Korea (ordered statistics), Lithuania (ordered statistics), Netherlands (statistical method), Spain (ordered statistics), Taiwan (ordered statistics), and the United States (ordered statistics).

Significant activities for use in licensing are performed in these countries: Canada, Czech Republic, Germany, Hungary, Japan, Russia, Slovak Republic, and Ukraine.

The change from the conservative analysis to the BEPU evaluation according to the change of 10 CFR §50.46 “Acceptance criteria for emergency core cooling systems for light water nuclear power reactors” in the United States had a big economic effect. The demonstration of the CSAU for a large cold leg break resulted in much lower PCTs than the conservative calculation applying Appendix K for the ECC evaluation models. The total 95% probability PCT of the CSAU demonstration in the year 1988 was 856°C (second peak was the highest). Uncertainties were determined for the single values blowdown peak, first reflood peak and second reflood PCTs. The calculation shows a large margin to the acceptance criterion 1200°C. Consequently, the utilities applied for power uprates. Increasing the maximum linear heat generation rates from 299 W/cm to 495 W/cm resulted in a total 95% probability PCT of 1081°C, still below the acceptance criterion. Power uprates were applied and approved for a significant number of plants which made it unnecessary to build new plants in the United States. The CSAU demonstration was performed for a generic Westinghouse four-loop plant which generates 3411 MW normal full thermal power.

13.4.5 Conclusions of uncertainty methods

The safety demonstration method “uncertainty analysis” is becoming common practice worldwide, mainly based on ordered statistics. Basis for applications of statistical uncertainty evaluation methods is the development of the GRS method.

Several activities are carried out on an international world-wide level, like in OECD and IAEA. Comparison of applications of existing uncertainty methods have been performed in the frame of OECD/CSNI Programmes. Differences were observed in the results of uncertainty analysis to the same task. These differences are sometimes reason for arguing about the suitability of the applied methods. Differences of results may come from different methods. When statistical methods are used, differences may be due to different input uncertainties, their ranges, and distributions. However, differences are already seen in the basic or reference calculations.

When a conservative method is used, it is claimed that all uncertainties, which are considered by an uncertainty analysis, are bounded by conservative assumptions. That may only be right when conservative code models or conservative input parameters for relevant code models are used in addition to conservative initial and boundary conditions. In many countries, however, a best estimate code plus conservative initial and boundary conditions are accepted for conservative analysis in licensing. Differences in calculation results of best estimate and even conservative codes would also be seen, comparing results of different users of the same computer code due to different nodalizations and code options the user is selecting. That was observed in all International Standard Problems where code users calculated the same experiment or a reactor event. The main reason is that the user of a computer code has a big influence in applying a code. A user effect can also be seen in applications of uncertainty methods.

Another international discussion took place about the number of calculations to be performed using ordered statistics methods. That issue was mainly brought up when more than one acceptance criterion has to be met. However, much more influence on the results is by the specification of uncertainty ranges of these input parameters. Therefore, high requirements are on their specification and the justification for these ranges. The international OECD/NEA/CSNI PREMIUM (Post-BEMUSE REflood Models Input Uncertainty Methods) Project deals with this issue.

13.5 Summary remarks

The verification and validation of an analysis method, here a computer code, is necessary before applied for safety analyses. The SYS TH computer code is an important scaling tool to perform safety analysis for power reactors. The question has to be answered, to what extent the results of down-scaled test facilities represent the thermal-hydraulic behavior expected in a full-scale nuclear reactor under accident conditions. It was shown very clearly that the thermal-hydraulic behavior of a down-scaled ITF cannot be extrapolated directly to obtain nuclear plant behavior. Although the ITFs have been designed in different volume scaling, ranging from 1:2070 to 1:48, the experimental results of these facilities are not solving the scaling problem. A combination of integral system tests with SETs in full reactor scale is indispensable. The computer codes shall be validated to calculate integral and separate effects experiments over the whole available scaling range in good agreement with the data. Therefore, the SYS TH computer code is an important scaling tool to perform safety analysis for power reactors. Strong connections are therefore between scaling, code validation, setting up the nodalization and uncertainty evaluation, as well as code user qualification and expertise.

A future important effort in the analytical work will be focused on the development of two-phase flow CFD codes. Due to the high resolution in space and the possibility for three-dimensional description of the single- and two-phase flow phenomena the scaling issue may become less important. Parallel to the progress in the development of the computer hardware with regard to reducing calculation time the application area of these codes will be extended. The development of the two-phase flow CFD codes is a great challenge for the analytical teams in the next decades and may contribute to the motivation of young scientists working in the field of nuclear technology.

Because of the long calculation time of CFD codes, uncertainty analysis using statistical methods will be very time consuming. Other methods may be necessary or response surface methods may be used for uncertainty analysis of CFD codes.

When no BEPU evaluation is performed, a conservative safety analysis approach anticipates that all unquantified uncertainties are bounded by conservative assumptions. An uncertainty analysis quantifies the uncertainty of a result of an assigned safety parameter and the bound toward the acceptance criterion determines the margin. Such a procedure cannot be considered as nonconservative. Rather, it is quantifying the conservatism of a calculation result. Uncertainty analysis will be more used in licensing applications beyond the early application to LB scenarios in the future. That is promoted by the USNRC, for example. Other

institutions prefer to continue to follow the conservative approach with settled conservative assumptions and fewer calculations to be performed. However, power uprates and optimized fuel strategies may need to apply more the BEPU approach for safety analysis.

Wide range cooperative international activities have been performed connected with V&V, scaling, and uncertainty. Selected international activities and programs received proper emphasis in the chapter. The following additional specific topics, objective of international activities, are linked with V&V, scaling, and uncertainty:

- User effects: user effects are expected in the applications of codes and in performing uncertainty analysis. The skills of users of a code or an uncertainty method determines to a great deal the quality of the results. Aksan et al. (1993) identify user effects and qualification and Ashley et al., CSNI (1998) and D'Auria (1998) discuss training in order to reduce the user effect.
- International Standard Problems have been performed within the time frame from 1973 to 2015 and about 32 “problems” (each one constituting an international project) deal with thermal-hydraulics directly related to the issues of validation and scaling. Useful references are by Reocreux (2012) and by Choi et al., CSNI (2012) the last one dealing with the documentation of the latest ISP in the area of SYS THs.
- Experimental programs involving ITF and SET have been performed addressing scaling which are necessary for code validation and the assessment of uncertainty methods, as discussed in this chapter. Mull et al. (2007) provide one example of final report of an international activity. Counterpart tests are also carried out within the framework of international cooperation, based on experiments in ITF (e.g., Belsito et al., 1994).

References

Aksan S.N., D'Auria F., Staedtke H. User effects on the thermal-hydraulic transient system codes calculations. *Nucl. Eng. Des.* 1993;145(1–2) Also OECD ‘Status’ Report NEA/CSNI R(94)35, Paris, France, January 1995.

Ambrosini W., Bovalini R., D'Auria F. Evaluation of accuracy of thermal-hydraulics codes calculations. *Energia Nucl.* 1990;7:2.

ANS, 1987. American National Standard Guidelines for the

verification and validation of scientific and engineering computer programs for the nuclear industry. ANSI/ANS-10.4-1987.

Bazin P., Deruaz R., Yonomoto T., Kukita Y. *BETHSY-LSTF counterpart test on natural circulation in a pressurized water reactor*. In: ANS National Heat Transfer Conference, San Diego, USA; 1992.

Belsito S., D'Auria F., Galassi G.M. Application of a Statistical model to the evaluation of Counterpart Test data base. *Kernteknik*. 1994;59(3).

Blinkov V.N., Melikhov O.I., Kapustin A.V., Lipatov I.A., Dremine G.I., Nikonov S.M., Rovnov A.A., Elkin I.V. *PSB-VVER counterpart experiment simulating a small cold leg break LOCA*. In: Proceedings of the International Topical Meeting on Nuclear Reactor Thermal Hydraulics (NURETH-11), Avignon, France; 2005.

Boyack B.E., Catton I., Duffey R.B., Griffith P., Katsma K.R., Lellouche G.S., Levy S., May R., Rohatgi U.S., Shaw R.A., Wilson G.E., Wulff W., Zuber N. Quantifying reactor safety margins. *Nucl. Eng. Des.* 1990;119:1–117.

Brown L.D., Cai T.T., Gupta A. Interval estimation for a binomial proportion. *Stat. Sci.* 2001;16(2):101–133.

CFR, 1989. 10 CFR 50.46, Acceptance criteria for emergency core cooling systems for light water nuclear power reactors, to 10 CFR Part 50, Code of Federal Regulations, US Office of the Federal Register.

CSNI, 1994. Aksan, N., D'Auria, F., Glaeser, H., Pochard, R., Richards, C., Sjöberg, A. Separate effects test matrix for thermal-hydraulic code validation, (a) Volume I: phenomena characterization and selection of facilities and tests, (b) Volume II: facility and experiment characteristics. NEA/CSNI/R(93)14/Part 1 and Part 2, Paris, France.

CSNI, 1995. Aksan, S.N., D'Auria, F., Städtke, H. User effects on

the transient system code calculations. NEA/CSNI/R(94)35, Paris.

CSNI, 1996. Annunziato, A., Glaeser, H., Lillington, J., Marsili, P., Renault, C., Sjöberg, A. CSNI integral test facility validation matrix for the assessment of thermal-hydraulic codes for LWR LOCA and Transients. NEA/CSNI/R(96)17, Paris, France.

CSNI, 1998. Ashley, R., El-Shanawany, M., Eltawila, F., D'Auria, F. Good practices for user effect reduction. NEA/CSNI/R(98)22, Paris.

CSNI, 2000. CSNI International Standard Problems (ISP), brief descriptions (1975–1999). NEA/CSNI/R(2000)5.

CSNI, 2001. Validation matrix for the assessment of thermal-hydraulic codes for VVER LOCA and transients. NEA/CSNI/R(2001)4, Paris, France.

CSNI, 2004. International standard problem procedure. CSNI Report 17 Revision 4, NEA/CNI/R(2004)8, Paris.

CSNI, 2006. BEMUSE phase II report, re-analysis of the ISP-13 exercise, post-test analysis of the LOFT L2-5 test calculation. NEA/CSNI/R (2006)2, Paris, France.

CSNI, 2007. BEMUSE phase III report, uncertainty and sensitivity analysis of the LOFT L2-5 test. NEA/CSNI/R(2007)4, Paris, France.

CSNI, 2008. BEMUSE phase IV report, simulation of a LB-LOCA in Zion nuclear power plant. NEA/CSNI/R(2008)6, Paris, France.

CSNI, 2009. BEMUSE phase V report, uncertainty and sensitivity analysis of a LB-LOCA in Zion nuclear power plant. NEA/CSNI/R(2009)13, Paris, France.

CSNI, 2011. BEMUSE phase VI report, status report on the area, classification of the methods, conclusions and recommendations. NEA/CSNI/R(2011)4, Paris, France.

CSNI, 2012. Choi, K.Y., Baek, W.P., Cho, S., Park, H.S., Kang, K.H., Kim, Y.S., Kim, H.T. International Standard Problem No. 50, Volume 1, Analysis of blind/open, calculations. NEA/CSNI/R(2012)6, Paris, France.

CSNI, 2016a. OECD/NEA Post-BEMUSE reflood model input uncertainty methods (PREMIUM) Benchmark. Final Report, NEA/CSNI/R(2016)18, Paris, France.

CSNI, 2016b. Scaling in system thermal-hydraulics applications to nuclear reactor safety and design: a state-of-the-art report. NEA/CSNI/R(2016)14, Paris, France.

D'Auria F., Galassi G.M. Scaling in nuclear reactor system thermal-hydraulics. *Nucl. Eng. Des.* 2010;240:3267–3293.

D'Auria F., Giannotti W. Development of code with capability of internal assessment of uncertainty. *Nucl. Technol.* 2000;131(1):159–196.

D'Auria F., Karwat H., Mazzini M. *Planning of counterpart tests in LWR experimental simulators*. In: Proceedings of the ANS National Heat Transfer Conference, Houston, USA; 1988.

D'Auria, F., Galassi, G.M., Ingegneri, M., 1994. Evaluation of the data base from high power and low power small break LOCA counterpart tests performed in LOBI, SPES, BETHSY and LSTF facilities. University of Pisa Report, DCMN NT 237(94), Pisa, Italy.

D'Auria F. *Proposal for training of thermal-hydraulic system codes users*. In: IAEA Specifications Meeting on User Qualification and User Effects on Accident Analysis for Nuclear Power Plants—Vienna (A), 31 August–4 September; 1998.

D'Auria F., Leonardi M., Glaeser H., Pochard R. *Current status of methodologies evaluating the Uncertainties in the prediction of thermal-hydraulic phenomena in nuclear reactors*. In: International Symposium on Two Phase Flow Modelling and Experimentation, Rome, Italy, October 9–11; Pisa: Edizioni ETS; 1995:501–509.

Glaeser H. Downcomer and tie plate countercurrent flow in the Upper Plenum Test Facility (UPTF). *Nucl. Eng. Des.* 1992;113:259–283.

Glaeser H. GRS method for uncertainty and sensitivity evaluation of code results and applications. *Sci. Technol. Nucl. Install.* (Q1):2008;1–7 Article ID 798901.

Glaeser H., Karwat H. The contribution of UPTF experiments to resolve some scale-up uncertainties in countercurrent two phase flow. *Nucl. Eng. Des.* 1993;145:63–84.

Glaeser H., Wolfert K., 2012, Scaling of thermal-hydraulic phenomena and system code assessment, seminar on the transfer of competence, knowledge and experience gained through CSNI activities in the field of thermal-hydraulics. OECD/NEA Head-quarters, Issy-les-Moulineaux, France, 25–29 June.

Glaeser, H., Krzykacz-Hausmann, B., Luther, W., Schwarz, S., Skorek, T., 2008. Methodenentwicklung und exemplarische Anwendungen zur Bestimmung der Aussagesicherheit von Rechenprogrammergebnissen. GRS-A-3443, Garching, Germany.

GRS, 1992. 2D/3D program work summary report. Gesellschaft für Anlagen- und Reaktorsicherheit (GRS) mbH, GRS-100, Garching, Germany.

GRS, 1993. Reactor safety issues resolved by the 2D/3D Program. Gesellschaft für Anlagen- und Reaktorsicherheit (GRS) mbH GRS-101, Garching, Germany.

Hofer, E., 1993. Probabilistische Unsicherheitsanalyse von Ergebnissen umfangreicher Rechenmodelle. GRS-A-2002, Garching, Germany.

IAEA, 2008. Best Estimate safety analysis for nuclear power plants: uncertainty evaluation, safety report series 52. International Atomic Energy Agency, Vienna, Austria.

IAEA, 2009. IAEA safety standards series: deterministic safety analysis for nuclear power plants, Specific Safety Guide No. SSG-2. International Atomic Energy Agency, Vienna, Austria.

IAEA, 2015. Verification and validation of thermal-hydraulic system codes for nuclear safety analyses. IAEA Consultancy, unpublished report, Vienna, Austria, 2015.

Ishii, M., Kataoka, I., 1983. Scaling criteria for LWR's under single-phase and two-phase natural circulation. ANL-83-32, NUREG/CR-3267, Argonne National Laboratory, Chicago, IL, USA.

Ishii M., Revankar S.T., Leonardi T., Dowlati A., Bertodano M.L., Babelli I., Wang W., Pokharna H., Ransom V.H., Viskanta R., Han J.T. The three-level scaling approach with application to the Purdue University Multi-Dimensional Integral Test Assembly (PUMA). *Nucl. Eng. Des.* 1998;186:177–211.

Kunz R.F., Kasmala G.F., Mahaffy J.H., Murray C.J. On the automated assessment of nuclear reactor systems code accuracy. *Nucl. Eng. Des.* 2002;211(2–3):245–272.

Martin R.P., Dunn B.M. *Application and licensing requirements of the Framatome ANP RLBLOCA methodology*. In: International Meeting on Updates in Best Estimate Methods in Nuclear Installation Safety Analysis (BE-2004), Washington, DC, USA; 2004.

Muftuoglu K., Ohkawa K., Frepoli C., Nissley M. *Comparison of realistic large break LOCA analyses of a 3-Loop Westinghouse plant using response surface and statistical sampling techniques*. In: Proceedings of ICONE12, 25–29 April, Arlington, VA, USA; 2004.

Mull, T., Umminger, K., Bucalossi, A., D'Auria, F., Monnier, P., Toth, I., Schwarz, W., 2007. Final Report of the OECD-PKL Project, AREVA NP GmbH, NTCTP-G/2007/en/0009, Erlangen, Germany, November.

Nahavandi A.N., Castellana F.S., Moradkhanian E.N. Scaling

laws for modeling nuclear reactors systems. *Nucl. Sci. Eng.* 1979;72:75.

NRC, 2005a. APEX—AP1000 confirmatory testing to support AP1000 design certification (non-proprietary). Office of Nuclear Regulatory Research, U.S. Nuclear Regulatory Commission, Washington, DC.

NRC, 2005b. USNRC regulatory guide 1.203, transient and accident analysis methods. U.S. Nuclear Regulatory Commission, Office of Nuclear Regulatory Research, Washington, DC, USA.

Ortiz, M.G., Ghan, L.S., 1992. Uncertainty analysis of minimum vessel liquid inventory during a small break LOCA in a Babcock and Wilcox plant: an application of the CSAU methodology using the RELAP5/MOD3 computer code. Rep. NUREG/CR-5818, EGG-2665, Idaho Natl Engineering Lab., Idaho Falls, ID, USA.

Prosek A., D'Auria F., Richards D.J., Mavko B. Quantitative assessment of thermal-hydraulics codes used for heavy water reactor calculations. *Nucl. Eng. Des.* 2005;236:295–308.

Reocreux M. *Historical perspective on the role and the achievements of CSNI in the field of thermal-hydraulics*. In: THICKET-3: seminar on the transfer of competence, knowledge and experience gained through CSNI in the field of thermal-hydraulics, OECD/NEA Headquarters, Issy-les-Moulineaux, France, 25–29 June; 2012.

Reyes J.N. *The dynamical system scaling methodology*. In: International Topical Meeting on Nuclear Reactor Thermal Hydraulics (NURETH-16), Chicago, IL, USA; 2015.

Reyes J.N., Frepoli C., Yurko J. *The dynamical system scaling methodology: comparing dimensionless governing equations with the H2TS and FSA methodologies*. In: International Topical Meeting on Nuclear Reactor Thermal Hydraulics (NURETH-16), Chicago, IL, USA; 2015.

Riebold W.L., Addabbo C., Piplies L., Staedtke H. *LOBI Project: Influence of Primary Loops on Blowdown, Part 1*. Ispra, Italy: EU Joint Research Centre; 1984.

Shotkin L.M. How the code analyst can influence the calculation and use good practices to minimize pitfalls. *Nucl. Technol.* 1997;117:40–48.

Wald A. An extension of Wilk's method for setting tolerance limits. *Ann. Math. Statist.* 1943;14:45–55.

Weiss P., Sawitzki M., Winkler F. UPTF, a full-scale PWR loss-of-coolant accident experiment program. *Atomkernenerg. Kerntech.* 1986;49.

Weiss P., Watzinger H., Hertlein R. UPTF experiment: a synopsis of full-scale test results. *Nucl. Eng. Des.* 1990;121:219–234.

Wickett, T., Sweet, D., Neill, A., D'Auria, F., Galassi, G., Belsito, S., Ingegneri, M., Gatta, P., Glaeser, H., Skorek, T., Hofer, E., Kloos, M., Chojnacki, E., Ounsy, M., Lage Perez, C., Sánchez Sanchis, J.I., 1998. Report of the uncertainty methods study for advanced best estimate thermal hydraulic code applications, Volume 1 (Comparison) and Volume 2 (Report by the participating institutions). NEA/CSNI/R(97)35, Paris, France.

Wilks S.S. Determination of sample sizes for setting tolerance limits. *Ann. Math. Stat.* 1941;12:91–96.

Wilks S.S. Statistical prediction with special reference to the problem of tolerance limits. *Ann. Math. Stat.* 1942;13:400–409.

Wulff W., Zuber N., Rohatgi U.S., Catton I. *Application of fractional scaling analysis (FSA) to loss of coolant accidents (LOCA)—Part 2: system level scaling for system depressurization*. In: International Topical Meeting on Nuclear Reactor Thermal Hydraulics (NURETH-11), Avignon, France; 2005.

Yurko J., Frepoli C., Reyes J.N. *Demonstration of test facility design optimization with the dynamical system scaling methodology*.

In: International Topical Meeting on Nuclear Reactor Thermal Hydraulics (NURETH-16), Chicago, IL, USA; 2015.

Zuber N., 1991. A hierarchical, two-tiered scaling analysis. US NRC, NUREG/CR-5809, Washington, DC, USA.

Zuber N., Rohatgi U.S., Wulff W., Catton I. Application of fractional scaling analysis (FSA) to loss of coolant accidents (LOCA) methodology development. *Nucl. Eng. Des.* 2007;237:1593–1607.

Best-Estimate Plus Uncertainty (BEPU) approach for accident analysis

F. D'Auria University of Pisa, Pisa, Italy

Abstract

The Best Estimate Plus Uncertainty (BEPU) constitutes an approach or a procedure aimed at making feasible the application of nuclear thermal hydraulics to the licensing and the safety evaluation processes of Nuclear Power Plants (NPPs). The features of BEPU are such to make attractive the application to address any design and operational issue in NPP technology. The triggering idea for BEPU came from the adoption of Best Estimate system thermal hydraulics codes for accident analysis in NPP technology. Key features of BEPU can be summarized as: procedures for nodalization development, code and nodalization validation, addressing the scaling issue, evaluation of uncertainty, demonstrating the analyst qualification, integrating the needs from licensing, coupling of codes from different disciplines and validation of the related software, considering the latest established findings from R & D.

Keywords

Best Estimate Plus Uncertainty (BEPU); Validation of procedures; Acceptance criteria; Qualification of analysts; Needs from licensing; Quantification of safety and design margins; Optimization of emergency operating procedures; Optimization of accident management procedures

Acronyms

ALARA As Low as Reasonably Achievable

ANL Argonne National Laboratory

ANS American Nuclear Society

AOO anticipated operational occurrence

ARN Autoridad Regulatoria Nuclear

ASME American Society of Mechanical Engineering

ATWS anticipated transient without scram

BEMUSE Best Estimate Methods Uncertainty and Sensitivity

Evaluation

BEPU Best Estimate Plus Uncertainty

BIC boundary and initial conditions

BOP Balance of Plant

BOT Break Opening Time

CBA (only used in Fig. 14.3) PIE
used for structure mechanics
assessment

CD core damage

CDF core damage frequency

CFD Computational Fluid Dynamics

CO containment

CSA (only used in Fig. 14.3) PIE
used for thermal hydraulics safety
assessment

CSNI Committee on the Safety of
Nuclear Installations

DBA Design Basis Accident

DDET Deterministic Dynamic Event
Tree

DiD defense in depth

DM design margins

DSA Deterministic Safety Analysis
(or Assessment)

EC European Commission

ECCS emergency core cooling

systems

EM evaluation model

ENS European Nuclear Society

ENV environment

ESF engineered safety features

ET event tree

EU European Union

EUR European Utilities
Requirements

FP fission product

FSAR Final Safety Analysis Report

FT fault tree

GRNSPG Nuclear Research Group in
San Piero a Grado (of University of
Pisa)

HRA human reliability analysis

IAEA International Atomic Energy
Agency

IDPSA Integrated Deterministic and
Probabilistic Safety Assessment

IEEE Institute of Electrical and
Electronics Engineers

IRIDM Integrated Risk Informed
Decision Making

I & C Instrumentation and Control
(system and components)

JSME Japan Association of
Mechanical Engineering

KNS Korean Nuclear Society

KWU KraftWerk Union (NPP
designer Company)

LBLOCA large break loss of coolant
accident

LOCA loss of coolant accident

MCP Main Coolant Pump

MIT Massachusetts Institute of
Technology

NEA Nuclear Energy Agency (part of
OECD)

NPP Nuclear Power Plant

NPSH Net Positive Suction Head

OECD Organization for Economic
Cooperation and Development

Ph.W Phenomenological Windows

PIE postulated initiating event

PREMIUM Post BEMUSE reflood
models input uncertainty methods

PS primary system

PSA Probabilistic Safety Analysis (or
Assessment)

PTS pressurized thermal shock

PWR pressurized water reactor

QA quality assurance or qualitative evaluation (*only related to discussion about Fig. 14.3*)

Q-SM quantity for (characterizing) safety margins

RCA (only used in Fig. 14.3) PIE used for assessment of radiological releases

RCS reactor coolant system

RPV reactor pressure vessel

RTA relevant thermal hydraulic aspects

SBO Station Black-Out

SM safety margins

SMAP OECD/NEA/CSNI Safety
Margin Project

SM2A SMAP follow-up project

SRS Safety Report Series

SYS TH system thermal hydraulic
(code)

TM technical meeting or workshop

UMS Uncertainty Method Study

UNIPi University of Pisa (Italy)

US United States

USNRC United States Nuclear
Regulatory Commission

V & V verification and validation

WENRA Western Association of Nuclear Regulatory Authorities

Acknowledgments

This chapter took inspiration from the BEPU application to produce the BEPU-based Chapter 15 of FSAR of Atucha-2 NPP in Argentina. The activity was performed during a time period larger than 3 years and involved more than 50 scientists, including recognized international experts, working at NA-SA (the Company owner of the Atucha-II NPP) and at University of Pisa (UNIFI), GRNSPG (Nuclear Research Group in San Piero a Grado). The current author coordinated the group and acknowledges the contribution of any individual who participated in the development, application, and revision of the BEPU. Special thanks are due to O. Mazzantini who managed the activity from the side of NA-SA and provided an invaluable technical and scientific support. Thanks are also due to M. Dusic for his endless effort in supporting the development of BEPU techniques.

Chapter foreword

The Best Estimate Plus Uncertainty (BEPU), procedure or approach, shall be seen as the final outcome of research and development in nuclear system thermal hydraulics (SYS TH); this is also the tip of the iceberg of competence in nuclear thermal hydraulics or a crossway into the thermal hydraulics universe defined in the Introduction (Chapter 1) of the book. All chapters of the book can be used to support BEPU features and, in different terms, constitute virtual parts of this chapter. In addition, each chapter of the book can be used as a triggering chapter for the BEPU presentation.

Although an attempt is made in this chapter to avoid “copy & paste” of descriptions taken from other chapters of the book, the need and the wish to produce a self-standing chapter made unavoidable some repetitions: this is specifically true in the case of the list of references.

An opening idea of complexity of BEPU already emerges from the above statements. The difficulty to define what BEPU is can also be connected with its multitopic origin. Therefore emphasis is given in the chapter to the description of concepts which may help in providing a suitable vision for BEPU.

BEPU shall also be seen as an industrial product ready for applications in nuclear technology. Then, an archival BEPU document implies: (a) demonstration of a common understanding among involved technologists; (b) achieving a suitable (e.g., enough detailed) developmental and application framework; (c) availability of experts qualified for the exploitation in Nuclear Power Plant (NPP) applications. At the present time whatever part of items (a) and (c) is missing or incomplete, and a narrow BEPU developmental framework, item (b), has been constituted. Therefore, this chapter shall not have the ambition to develop an applicable BEPU framework. Rather the objective should be to provide the basis for developing such framework.

BEPU shall be seen as part of the overall Nuclear Reactor Safety context, namely for each analytical part. BEPU involves or is applicable for Deterministic Safety Assessment (DSA) and Probabilistic Safety Assessment (PSA): DSA concepts are part of other chapters of the book; so some fundamental PSA concepts are discussed in this chapter.

14.1 Introduction

The words Best Estimate Plus Uncertainty, i.e., BEPU, since their origin, constituted the attribute of a calculation performed by a SYS TH code. Three items provide a pedagogic definition of BEPU:

(a) *Best Estimate (BE) versus Conservative*: The word Conservative has been always used in engineering calculations to mask a lack of knowledge, or, in some cases to achieve resistance capabilities and strengths of a system higher than what is strictly needed by the design. The words “Best Estimate” do not imply the removal of the conservatism; rather they impose the minimum conservatism consistent with the actual technological knowledge.

(b) *Limitations of system codes*: Thermal-hydraulic system codes constitute the reference computational tools for the application of BEPU. The features and the capabilities of those codes are such to envisage an unavoidable error in any prediction. This is specifically true for the application of codes to the transient analysis of accidents in NPPs.

(c) *Uncertainty*: The unavoidable errors expected from the application of computational tools in thermal hydraulics (also referred above) need to be quantified to determine their acceptability. Then, the word “uncertainty” appears: uncertainty is the prediction of the error expected in NPP calculation results. Specific methods, or procedures or methodologies, are needed and have been developed and qualified to determine the uncertainty; acceptability or the error (i.e., of the uncertainty) is directly or indirectly linked with uncertainty evaluation.

Historical appearance of the acronym BEPU occurred toward the end of 1990s; at that time both the SYS TH codes and the uncertainty methods were thought mature enough to allow practical applications. Unfortunately, the presumed achievement of maturity for codes and uncertainty methods was not a common understanding at the time and is still debated today within the scientific and the technological community engaged in the nuclear reactor safety area.

Progresses in proving the capabilities of the codes continued during the current millennium as well as in further demonstrating the qualification level of uncertainty methods. In the same period institutions in the area of nuclear reactor safety issued documents, i.e., IAEA (2002), IAEA (2010a), and USNRC (2005), opening or promoting the application of BEPU, as further discussed in Section 14.2.1 and in Chapters 2 and 13, see also D'Auria et al. (2006). Practical applications of BEPU for the new NPPs, even due to the very small number of new units entered in operation in the period 2000–15, are restricted to two pioneering efforts:

- Final Safety Analysis Report (FSAR), Chapter 15—Accident Analysis—large break loss of coolant accident (LBLOCA), in Angra-2 NPP in Brazil (KWU-Siemens, 1997).
- FSAR, Chapter 15—Accident Analysis—all transients where analytical support is needed, in Atucha-2 NPP in Argentina, UNIPU-GRNSPG (2008), e.g., UNIPU-GRNSPG (2008).

BEPU also constituted the topic of international conferences like ANS (2000) and ANS (2004), and of literature papers, e.g., Martin and Nutt (2011), D'Auria et al. (2012a), and D'Auria et al. (2012b).

Notwithstanding the promising situation depicted in the previous statements, BEPU never became a spread technology or an internationally recognized technology at all, so far. This is the framework within which this chapter is prepared. For the benefit of the reader, this statement must be supplemented by the

consideration that almost any topic discussed in the book is functional or essential for the implementation of BEPU.

Therefore driving motivations, constraints, and objectives (see also below) for this chapter are to collect important elements of BEPU and to avoid restating what already presented in different chapters of the book.

Thus, BEPU constitutes the natural evolution of the initially adopted conservative approach and one potentially productive star system part of the nuclear thermal-hydraulics universe (see Chapter 1). Namely, BEPU is suitable to impact nuclear reactor safety and to contribute to establish the safety and the acceptability of NPP (D'Auria, 2012; see also Menzel et al., 2015 and Menzel et al., 2016). The BEPU is also the only possible framework where the knowledge gained in the development and the validation of SYS TH codes as well as in setting up and qualifying uncertainty methods is exploited.

14.1.1 The licensing framework

Licensing (of nuclear plants) establishes the legal aspects of (nuclear) reactor safety. Requirements including acceptance criteria and assumptions to perform analyses are part of the licensing process. The licensing environment (ENV) is responsibility of regulatory authorities in individual countries: it does not contain explicit or implicit obstacles to the adoption of BEPU, e.g., see USNRC (2013) (continuously updated NUREG-0800 document, or Standard Review Plan, or suggestions to the staff of regulators to perform the review of accident analysis) for details.

While the originating words BE and uncertainty have a traceable/evident physical and technological meaning, the acronym BEPU implies or fits with a licensing ENV better than its originating words. This is because of the natural mission of the BEPU approach to establish actual safety margins (SM) from NPP assessment activity, i.e., considering the errors and the approximations in current understanding, and in accordance with requirements. “Independence-of-the-analysis,” or independence between licensors and licensees in relation to the evaluation of NPP safety, constitutes by itself a safety requirement and an intrinsic feature for BEPU analysis. Thus, in the common understanding:



The favorable picture for BEPU is again not consistent with the lack of, or the inadequate, exploitation of BEPU strengths within the licensing ENV at the time when this book is published.

14.1.2 Objective and structure

The objective of this chapter is to collect relevant elements and attributes of BEPU avoiding emphasis in the description of those concepts which are part of other chapters of the book. So, description of individual pieces of a puzzle is concerned rather than attempting an organized array of the puzzle and providing an overall vision, not justifiable by current progress and by the interest from nuclear technology stakeholders (list of “nuclear technology stakeholder” is provided in the Chapter 2 making reference to nuclear thermal hydraulics).

An outline of the connection between other chapters of the book and BEPU, or what is discussed in relation to BEPU in this chapter, is given below:

- **Chapter 1** presents the universe of nuclear thermal hydraulics, which is the framework where BEPU has been developed.
- **Chapter 2** deals with the history in nuclear thermal hydraulics. The appearance of the BEPU acronym is identified together with the expected timeframe for its applications.
- The definitions in **Chapter 3** are consistent with the definitions needed for introducing the BEPU concepts.
- The nuclear technology needs, **Chapter 4**, including design and safety, shall be used to justify the development and the application of the BEPU approach.
- **Chapters 5, 7, 8, 9, and 10** deal with selected models and selected equations, which are part of a BE SYS TH code. The concerned codes, adopted for accident analysis, play a pivot role in the application of a BEPU approach.
- **Chapter 6**, dealing with expected phenomena within the Design Basis Accident (DBA) envelope, is embedded into the series of **Chapters 5–10**: phenomena constitute an input for the development of the SYS TH code. At the same time, identification and characterization of phenomena are directly relevant to uncertainty evaluation and to the application of BEPU approach.

- The structure of SYS TH codes and of Computational Fluid Dynamics (CFD) codes, Chapters 11 and 12, respectively, discuss computational tools needed for the BEPU approach.
- Verification and validation (V & V), scaling, and uncertainty methods are key elements for the application of a BE SYS TH code within the BEPU approach and are discussed in Chapter 13.
- Chapter 15 deals with the description of accident scenarios. The related analyses are not necessarily performed by pursuing a BEPU approach; however, the discussed ones are results expected from the application of a BEPU process. Uncertainty evaluation is not (necessarily) part of the analyses.
- BE analyses are used to support the description of occurred accidents in NPP, Chapter 16. Typically, no uncertainty evaluation is performed for those accidents and concerned situations are beyond DBA types. Therefore little or no interest from the side of the BEPU approach results from this chapter, unless some contribution for the validation of the SYS TH codes.

The structure of this chapter is based upon the objective stated above and upon the content of other chapters. Therefore,

- “Bases and Background,” *Chapter 2 in the following*, aims at providing a picture of issues from nuclear technology which may originate BEPU. Noticeably, various possible definitions for BEPU are given in Section 14.2.3.
- Features of BEPU are outlined in *Chapter 3 in the following*. Key terms needed for the characterization of BEPU are given in Section 14.3.1 and are distinguished from relevant topics which need a solution, discussed in Section 14.3.5. An already adopted BEPU roadmap is discussed in Section 14.3.4.
- Envisaged perspectives for expanding BEPU from the current accident analysis to any analysis needs in licensing are discussed in *Chapter 4 in the following*. Emphasis is deserved in this chapter to the extension of BEPU to any analytical part needs in licensing, noticeably Section 14.4.2.

14.2 Bases and background

Bases and background for BEPU are either the bases and the background for nuclear thermal hydraulics as already presented in the Chapter 1, or the key topics of nuclear thermal hydraulics itself as discussed in the Chapter 1 above (i.e., in this

chapter). Nevertheless, a BEPU-focused vision for bases and background is provided hereafter.

14.2.1 The historical perspective

Chapter 2 deals with a history perspective which includes BEPU appearance and key related milestones. Hereafter, the BEPU history is summarized by three tiers of documents.

(I) *BEPU application status*—three historical cornerstone periods distinguished:

(I-a) *Around the year 2000*: pioneering BEPU LBLOCA application for Angra-2 new NPP in Brazil, e.g., KWU Siemens (1997); see also Galetti and D'Auria (2000), Galetti and D'Auria (2004), and Galetti and D'Auria (2005).

(I-b) *Period 2000–15* (current time): various LBLOCA applications for license renewal of existing NPP, see e.g., Glaeser (2010).

(I-c) *Around the year 2010*: pioneering BEPU application for “all” transients in FSAR for Atucha-2 new NPP in Argentina, e.g., UNIPI-GRNSPG (2008); see also D'Auria et al. (2012a) and Petruzzi et al. (2016).

(II) *Institutional documents*—three groups distinguished to be considered as keysamples:

(II-a) *USNRC documents*: These noticeably include Regulatory Guides (RG) and NUREG, having different worth and applicability contexts, i.e., RG 1.203 and 1.206 identified in references by USNRC (2005) and USNRC (2007), and Standard Review Plan or NUREG-0800 identified as USNRC (2013).

(II-b) *IAEA documents*: Hierarchy classified documents are issued by IAEA. So, having in mind that applicability and licensing worth are different, BEPU-relevant documents are SRS 23, SRS 52, and SSG-2, identified by references, IAEA (2002), IAEA (2008), and IAEA (2010a). Furthermore, a variety of technical projects and workshops dealing with BEPU are continuously conducted or held and imply the production of papers and reports by individual authors.

(II-c) *OECD/NEA/CSNI documents*: Noticeably, UMS, BEMUSE and more recently, PREMIUM projects have been completed within the framework of CSNI activities connected with BEPU, as documented in references OECD/NEA/CSNI (1998), OECD/NEA/CSNI (2011), and OECD/NEA/CSNI (2016), respectively. As in the case of IAEA workshops, various seminar and conferences have been held

by OECD/NEA in the area as testified by the production of papers and reports by individual authors.

(III) *Scientific and technological literature*: A variety of papers and web-reachable documents can be found in relation to BEPU from all over the world, from all countries where nuclear technology is exploited for electricity production (China, EU, India, Korea, Japan, Russia, South America, and United States). Hereafter an indicative variety of documents is listed following the increasing order for the date of publication; proposals for BEPU application to research reactor safety assessment and PHD theses are also part of the picture: D'Auria et al. (2003, 2010, 2012b), Prošek and Mavko (2003), Bousbia Salah et al. (2004), Muftuoglu et al. (2004), Bucalossi (2008), Camargo et al. (2008), Yamaguchi et al. (2009), Ponomarenko et al. (2009), Bucalossi and Petruzzi (2010), Bucalossi et al. (2010), Mendizabal and Pelayo (2010), Pradhan and Bang (2011), D'Auria and Mazzantini (2011), Unal et al. (2011), Rao et al. (2012), Han et al. (2012), Hwang et al. (2012), Guyer (2013), Nainer et al. (2013), OECD/NEA/CSNI (2013), Cacuci and Arslan (2014), Adu et al. (2015), Martorell et al. (2015), Menzel et al. (2015), Shih et al. (2015), and Menzel et al. (2016).

The listed documents and papers, as already stated, provide a view for the BEPU (current year 2016) state of the art.

14.2.2 The nuclear reactor safety requirements

Chapter 4 deals with reactors' safety needs connected with the area of nuclear thermal hydraulics: this is suitable to establish a correspondence between knowledge available and knowledge needed for technological advancements in the areas of nuclear reactor design and safety. BEPU applicability is foreseen in both areas of design and safety. Hereafter the attention is focused toward fundamental requirements in the area of nuclear reactor safety.

The safety demonstration nuclear reactor is attained by safety analysis and assessment. Safety analysis and assessment (distinction between analysis and assessment discussed in Section 14.2.3) largely rely on conservatism. Conservatism in input data does not imply conservatism in output data or results of analysis/assessment used for safety demonstration. The amount of possible conservatism in output data shall be seen as a question mark (and BEPU must be used to quantify the possible amount of conservatism). Issues connected with the use of conservative methods are:

(a) *Conservatism and ignorance*: Conservatism is generally synonymous with

ignorance or lack of knowledge: otherwise, knowledge should be continuously adapted to the advancements of scientific community.

(b) *Conservatism and calculated value of safety parameters*: Conservatism introduced in any set of variables at the input level within any calculation process does not result inevitably in conservatism in the output variables which are concerned in safety assessment. Within a complex system analysis framework the following possibilities can be considered when a single (transient scenario) calculation is concerned: (i) one or more conservative values for input parameters are necessary and are introduced in assessment; (ii) the same conservative input parameter may generate a conservative result for one output quantity and a nonconservative result for a different output quantity; (iii) two assigned conservative input parameters may have an impact of different sign upon the value of an assigned output quantity; (iv) the same input conservative value may generate a conservative value for an assigned output quantity during an assigned time span and a nonconservative value for a different time span.

(c) *Quantification of conservatism*: It is desirable to quantify the conservatism in the evaluation of SM. Here the paradox is that a BEPU calculation is needed (i.e., a calculation performed with a method which is alternative to the conservative method) to estimate the “amount of conservatism.” It seems necessary to add here that currently the demonstration of the amount of conservatism is not needed in a licensing analysis: the conservatism in the output of a conservative calculation is an expert-based belief.

(d) *Misleading conservatism*: Misleading conservatism may appear when concerned conservative assumptions cannot occur at the same time. An example is maximum boron concentration in the coolant and maximum burn-up of fuel. Those two situations cannot occur at the same time and may produce an overconservative (misleading) result.

(e) *Usefulness of a conservative calculation*: Noticeably, the result of a conservative calculation does not depict and does not aim at depicting the expected NPP scenario following an assigned postulated initiating event (PIE). Rather a conservative calculation aims at calculating SM and may not be used, e.g., by operators, to understand the NPP expected performance.

One additional established requirement in nuclear safety assessment is the “independence” of the assessment, i.e., independence between the analysis performed by the owner/vendor/designer of the NPP and the analysis performed by, or on the behalf of, the regulator. Conservative analysis from owner/vendor/

designer is eventually justified by the experience gained in long-lasting time for design development. The information from design, construction, and operation expertise is typically not available for independent assessor: in this case, independent values for conservatism not derived by designer expertise cannot be easily introduced.

In relation to both the considered requirement, BEPU analysis/assessment is needed to justify conservatism and to comply with the request for “independence.”

14.2.3 Envisions for BEPU

On the one side, it is straightforward to discuss the outcomes of a BEPU calculation; on the other side it is difficult to explain what BEPU is. Hereafter some generic BEPU-definition statements are given, followed by a series of paragraphs independent (or nearly independent) among each other, dealing with the discussion of various BEPU-related peculiarities.

BEPU definition statements are:

- The BEPU is a logical process or an approach which connects the understanding in nuclear reactor safety (see also licensing below) with nuclear thermal hydraulics.
- The starting point for BEPU is the understanding of the phenomena. Thus, BEPU implies the identification of the accident scenarios, which are part of the “design basis envelope.”
- BEPU implies the existence of qualified computational tools including numerical codes dealing with different disciplines, input decks, or nodalizations and a method to evaluate the uncertainty. The words “different disciplines” imply the coupling among codes and the ability to qualify the resulting coupled codes.
- BEPU needs the existence of qualified procedures for the application of the computational tools.
- BEPU needs the existence of qualified code users and of maven (the equivalent of citizens for the small town) capable of evaluating the results and of establishing whether additional analyses are needed.
- BEPU needs the existence of “legal” acceptance criteria (e.g., suitable licensing framework).

- The application of BEPU implies the deep knowledge of the licensing process in the country where the NPP is installed and in the country where the same plant has been designed. Furthermore, advancements in licensing process by different international institutions shall be continuously considered.
- The structure of the Final Safety Analysis Report must be adapted to BEPU and connections shall be identified among different chapters: this is specifically true in relation to the design of the core, the experimental data drawn during the commissioning period of the plant, and the design of operational and emergency procedures.
- Due to the above, any BEPU report as well as any BEPU finding should be a living document or periodically updated.

14.2.3.1 The objective of BEPU

Let us distinguish first the words “assessment” and “analysis.” Both analysis and assessment in nuclear thermal hydraulics and reactor safety and design applications imply calculations performed by suited software (also referred above as computational tools). However, analyses are typically performed by NPP owner/designer/vendor and assessment is performed by regulators (or organizations supporting the regulators) to confirm the results of analyses as defined above. Then, the words “safety assessment” rather than “safety analysis” are more suitable for the BEPU approach.

The objective of BEPU is to remove conservatism when performing assessment calculations. The conservatism is replaced by uncertainty evaluation. Quality and qualification are key words for calculation and uncertainty evaluation. Ultimate objective of BEPU in nuclear reactor safety is to calculate SM according to the latest BE methods properly qualified. Ultimate objective for BEPU in nuclear reactor design is to optimize the plant construction and operational parameters, considering the best available analytical techniques and the errors associated with their use.

14.2.3.2 BEPU as the attribute of a calculation

Considering the origin of the acronym, as already stated in Chapter 1 of the book, BEPU is the attribute of a calculation. In this connection BEPU is also known as the “option 3” of the IAEA SSG-2 (IAEA, 2010a), see Table 14.1. A safety or design-related calculation can be performed according to the following possibilities:

Table 14.1

Possibilities to perform a safety analysis or a safety assessment calculation (IAEA, 2010a)

^a Realistic input data are used only if the uncertainties or their probabilistic distributions are known. For those parameters whose uncertainties are not quantifiable with a high level of confidence, conservative values should be used.

- (1) Adopting a conservative code, conservative boundary and initial conditions (BIC) values, and conservative consideration for engineered safety features (ESF) including emergency core cooling systems (ECCS).
- (2) Adopting a BE code, conservative BIC values, and conservative consideration for ESF including ECCS.
- (3) Adopting a BE code, realistic BIC values, and conservative consideration for ESF including ECCS. In this case, an uncertainty method is needed. This is the BEPU or “the option 3” calculation.
- (4) All as above at “option 3,” plus removing the conservative consideration for ESF including ECCS. In this case devoted PSA analyses bring to a “risk-informed” calculation.

14.2.3.3 A quality assurance (QA) framework

The BEPU approach can be compared with a QA framework. The following characteristics are applicable to QA and to BEPU:

- (1) existence of technological tools to be inserted into a framework;
- (2) key role of qualification;
- (3) existence of a regulatory ENV;

(4) expected relevance, including financial value, for the outcome of the technological processes associated with its use (noticeably NPP design and safety evaluations).

14.2.3.4 BEPU elements and features: the simplified list

A condensed set of elements which provide a simplified vision for BEPU can be found in Fig. 14.1. Namely, the cross correlation among SYS TH code, nodalization, V & V process, scaling, uncertainty, and analysts (or code users) can be derived, all aimed at achieving a licensing target. Furthermore, “rules” are needed within a multiphysics and multiscale ENV where nuclear SYS TH plays a pivot role. A more comprehensive list of BEPU elements is provided in Section 14.3.2.

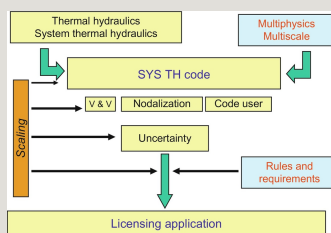


Fig. 14.1 Selected key elements for the BEPU approach and interrelations.

14.2.3.5 Accident analysis and licensing connection

Accident analysis and, according to proposed nomenclature, assessment of accident analysis are part of the current licensing process. Conservative accident analysis or assessment implies a (in certain sense) weak connection with the overall licensing framework because the safety is controlled by the amount and by the proper use of conservatism and not by the process; the BEPU accident analysis or assessment implies a strong connection. Two examples are considered:

(I) A conservative accident analysis (Chapter 15 of FSAR) may not help to fix the technical specifications (so-called tech spec values) for ESF (e.g., Chapter 16 of FSAR) because a conservative calculation does not predict the actual-expected plant performance; rather conservative calculations ensure, or better aim at demonstrating that under certain (conservative) assumptions, selected safety thresholds are not overpassed. On the contrary, a BEPU analysis where Instrumentation and Control (I & C) is properly simulated can be used to fix “tech

spec” values: this can be done for instance to fix tolerable excursion of pressurizer level during nominal NPP operation.

(II) A conservative accident analysis documented in (Chapter 15 of FSAR) may not have any relation with the conservative analysis, supported by ruled conservatism, performed to estimate the pressurized thermal shock (PTS) in reactor pressure vessel (RPV) walls and documented in (Chapter 6 of FSAR). On the contrary, an integrated BEPU analysis, avoiding conservatism in (Chapters 6 and 15 of FSAR), may show the existence of wide margins for PTS which do not pose PTS risks, e.g., impacting directly the planning of the NPP surveillance.

14.2.3.6 DSA & PSA connection within BEPU and severe accident role

The roles of Deterministic Safety Analysis (DSA) and of Probabilistic Safety Analysis (PSA) (in both cases, the word Analysis shall be used interchangeably with the word Assessment) within the nuclear reactor safety framework, are outlined in Chapter 2. Furthermore, the information from Table 14.1 does not allow any distinction between the roles of PSA when “option 2” (application of conservatism) or “option 3” (BEPU application) is pursued.

Within the entire book, DSA is concerned. Therefore, a few notes related to PSA are introduced below.

Probabilistic Safety Analysis (PSA) has typically not been included in the FSAR for NPPs built till the 1970s. However, many plant-specific PSA applications have been completed for those plants. For some of reactors constructed since 1980, PSA analyses are documented together with an evaluation of severe accidents. The principal objectives of these analyses are to demonstrate that the design poses an acceptably low risk of core damage (CD) accidents and to identify opportunities for improvements during the design phase.

Typically, a PSA analysis addresses CD, containment (CO) failure, and offsite consequences, corresponding to Level 1, Level 2, and Level 3 PSA, respectively. This is done at nominal full-power operation for both internal and external events. In addition, PSA analysis addresses other modes of operation (low-power, shutdown, and other than full-power and shutdown modes of operation).

In the case of Level 1 PSA, the thermal-hydraulic and other supporting engineering evaluations are performed to determine the accident progression parameters (e.g., timing, temperature, pressure). These analyses determine the requirements for mitigating the accident and improving the design and operation of systems and

components. The same analyses can also be used to determine timings and the requirement for operator actions.

Within the Level 2 PSA, the probability, the composition, the magnitude, and the timing of fission product (FP) releases from the plant, should an accident occur, are calculated. Level 2 PSA implies a combination of deterministic and probabilistic analyses. Severe accident progression analysis (i.e., the description of the physical, mechanical, and chemical processes that may occur in primary system (PS) during the progression of a core melt event including the identification and the characterization of phenomena and of the relationship between those phenomena and the phenomena, which affect the CO response) is performed mainly in order to support development of the CO event trees (ETs) including the determination of branch probabilities and, as end result, determining the so-called (FP) source term for each individual accident sequence. Severe accident progressions can be subdivided into in-vessel and ex-vessel phases or time periods.

In Level 3 PSA offsite consequences are calculated in relation to FP release categories, basically considering the source term identified in Level 2. Release categories are distinguished based on the radiological and chemical characteristics of radioactive products. For each release category, the timing, the energy, the isotopic content, and the magnitude of release could be established based on plant-specific, thermal-hydraulic calculations using severe accident codes. The expected end result in this case is to establish the impact of an accident upon population and ENV.

Typically, detailed acceptance criteria for results of PSA are not set by regulators. Rather, targets are given for core damage frequency (CDF) and large release frequency.

The severe accident evaluation section of FSAR (Chapter 19) describes the NPP features adopted to prevent and to mitigate a severe accident, the performance of the CO as a FP barrier during a severe accident, and the accident management scenarios including the evaluation of severe accident mitigation measures. The present generation of nuclear reactors (i.e., those reactors designed after the year 2000) includes specific design featured to prevent at least some severe accidents (e.g., anticipated transient without scram (ATWS), mid-loop operation, Station Black-Out (SBO), and fire events). In relation to severe accident mitigation design features and related issues of analysis exist in order to address a variety of severe accident challenges. These include hydrogen control, core debris coolability, high-pressure melt ejection, fuel-coolant interaction, CO bypass, CO performance, dedicated CO vent penetration, and equipment survivability. As support to severe

accident management (SAM) programs deterministic severe accident analyses are needed for both preventive and mitigative SAM measures and SAM guidance. DSA are needed also as support to PSA Level 2, source term assessment, and equipment qualification programs: BEPU analyses may reveal unavoidable for design and optimization purposes (and in some cases are conducted with partial consideration of all BEPU tools and procedures, see also BEPU elements in Section 14.3.2).

A probability-based accident classification is envisaged and discussed in IAEA (2002) (SRS 23); different classes of accidents characterized by different probabilities can also be found in the US regulation, e.g., USNRC (2007) and USNRC (2013). Namely, different classes of probability are connected with different classes of severity and/or accident consequences, e.g., Anticipated operational occurrences (AOOs) and DBA, which also imply different acceptance criteria.

Now the following question applies:



Let us first clarify that BEPU can be used and has been used to demonstrate the amount of conservatism within a DSA framework, e.g., Stanev and D'Auria (2001) and D'Auria et al. (2001). Then, an attempt is made to answer the question (at least partially) considering each of the three levels of PSA.

No internationally agreed or comprehensive and technologically acceptable answer to the question can be reported. Insights can be found in the paper by Dusic et al. (2014): this addresses the “option 4” in Table 14.1; the related framework, i.e., the integration between DSA and PSA, is discussed in Section 14.4.1.

The following statements may help in deriving an answer to the question:

- Conservative DSA types of analysis imply rigid calculation frameworks which may not require as input those parameters which are important for probabilistic analysis.
- The amount of conservatism (within a conservative analysis framework) can be assumed so “high” to overshadow the impact of probability upon the results of the

(conservative) analysis: for instance if one assumes a one minute delay in the actuation of one diesel generator driving ECCS pump(s) and the actuation is successful for the concerned safety parameter, the actuation of the second diesel generator (with any associate probability) is not influent upon the safety evaluation.

- BEPU (so far) is a DSA-only framework, with meaning to be derived from this chapter: this brings an additional difficulty in addressing the question.

- A BEPU calculation appears not justified in relation to an event which has low (or no) probability of occurrence. For instance a BEPU calculation for loss of coolant accident (LOCA) in PWR assuming maximum fuel burn-up and void coefficient associated with Beginning-Of-Cycle conditions is not justified.

- The capabilities of computational tools in both DSA and PSA areas and the technological infrastructure needed for a valuable BEPU calculation, including the needed validation efforts, suggest a mutual role for PSA and BEPU analyses.

Therefore, a formal and history of technology-based answer to the question is as follows:

$$r = \frac{W_2}{W_2 + W_1}$$

One consequence one may draw is that current PSA Level 2 results, generally based on conservative DSA type of analysis, do not account for real or expected NPP system performance.

Then a perspective answer to the question may be worthwhile. To this aim the sketch in Fig. 14.2 can be considered: for BEPU application the current barrier existing between DSA and PSA is expected to be broken and interactions among corresponding elements shall be created.

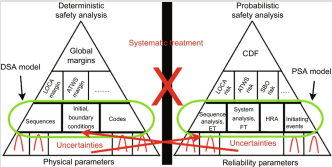


Fig. 14.2 Barrier (to be broken) between DSA and PSA and key potential connections (IAEA, 2015a).

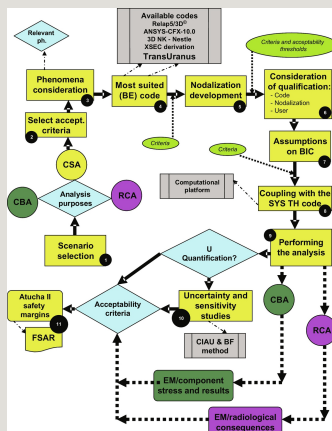


Fig. 14.3 Flow diagram for the BEPU approach pursued for the safety assessment of the Atucha-2 NPP.

The characterizations of the role of PSA into a BEPU (DSA) analysis and of the potential role of BEPU analysis for PSA constitute potential elements for the current state of art in the technology. However, no additional details are provided in this chapter with the noticeable exception of Section 14.4.1 addressing possible extensions of the BEPU framework.

14.2.3.7 BEPU as exploitation of database

The development and the application of BEPU depend upon the availability of suitable database in the concerned technological area, i.e., nuclear thermal hydraulics at present time, e.g., see Pla et al. (2016). Fig. 2.11 in Chapter 2 is considered here.

Specific databases are needed and can be classified according to their use: verification, validation, scaling analysis, uncertainty analysis, and code user qualification, e.g., Petruzzi and D'Auria (2014) and Petruzzi and D'Auria (2016). The following are examples of databases to be gathered and considered for a suitable BEPU application, see also Chapter 13:

- (a) *Basic experiments*, for code development and independent V & V activity.
- (b) *Separate effect experiments*, for code development and independent V & V activity including nodalization qualification.
- (c) *Integral experiments*, mostly for independent V & V activity and nodalization qualification.
- (d) *NPP transient measurement data*, mostly for confirming code and nodalization validation, typically in a narrow range of variation for key parameters and addressing the scaling issue.

Definitely, a large variety and a huge mass of data have been gathered in nuclear thermal hydraulics as also resulting from **Chapters 1 and 2**: BEPU can be seen as a means for the systematic exploitation of the various sets of data.

14.2.3.8 The BEPU as the civilization

The complexity of BEPU and of explaining the BEPU framework is considered by D'Auria (2013): a parallel is created having, on the one side, the BEPU technology and the thermal hydraulics/nuclear reactor safety, and, on the other side, the human civilization and a hypothetical town.

Bricks, compounds of bricks, buildings, and infrastructures including transport lines and standing vehicles, constitute the ghost (empty, or free from humans) city or the hypothetical town. This resembles the existing/established knowledge which has been acquired so far in nuclear thermal hydraulics.

A wild traveler, i.e., the researcher in nuclear thermal hydraulics in the near future when the expertise used to establish the current knowledge may have been lost, enters the (marvelous) empty town. He will find empty shops, dormitories, offices, gas stations, and even bus and metro lines without passengers. Presumably the wild traveler does not know what to do and has no ideas about how to operate the perfect components he can see. The wild traveler may feel frustrated. He has no access to laws, manuals, and rules (or whatever is part of the knowledge of the retired experts which has not been transferred to the follow-up generation), e.g., when moving across the desert roads prior to his arrival into the ghost city. Also, he might not expect anybody controlling his actions and eventually no fine for the possible “imperfect-precision” of his actions.

Then he will expect problems in implementing the possible task of making alive the ghost town, and/or he will need long time (compared with his working life) to

perform the task. In order to realistically accomplish the task, a group of “coordinated individuals” is needed (i.e., not a group of wild travelers): they should have in mind the principles of civilization including reasons for staying together and, possibly, a strategy for the sustainability. Once “coordinated individuals” enter the ghost city rules are created and established. The effort by the “coordinated individuals” may have a success and the empty town becomes a living town. Under those circumstances, the wild traveler may become a citizen.

The word civilization may be used to gather all the actions and activities which transform the ghost city into a living town. In a similar way the BEPU approach includes all the steps needed for the application of nuclear thermal hydraulics within nuclear reactor safety. The wild traveler or the thermal hydraulics expert becomes a citizen or a nuclear reactor safety analyst when he is capable to apply BEPU.

Now, what is BEPU? The BEPU definitely allows a nuclear thermal-hydraulic specialist to become a maven. A comprehensive explanation of BEPU is equivalent to the explanation of the process bringing the empty town to become alive and populated by citizens (not wild travelers). Finally, one may state:

$$1 - x = \frac{w_1}{w_{sc} + w_1}$$

Therefore, even the bases for BEPU may require a deep description, i.e., inconsistent with the framework and the size of the present document.

14.3 Elements and structure of BEPU for the accident analysis

In this section the BEPU concept is restricted to the accident analysis part of safety evaluation for individual NPP and to the current status in its application in technology. The main objective of the chapter, like the previous one, is to contribute or provide information suitable for characterizing BEPU avoiding as far as possible duplication of information from other chapters.

14.3.1 Selected key terms

A wide variety of terms, noticeably involving acronyms, which are related to the definition of BEPU, have already been used in previous sections of this chapter and

in other chapters, namely Chapter 3. Hereafter, a series of terms which are essential for understanding BEPU are listed together. Added descriptions for each term are provided to focus on the connection with BEPU.

14.3.1.1 DBA & BDBA

The DBA framework fixes the boundary for specific (restrictive) nuclear safety requirements, thus reflecting on SYS TH code development, related V & V including scaling, uncertainty evaluation, and application procedures. One key BEPU basis is constituted by the V & V requirements.

14.3.1.2 Deterministic & probabilistic accident analysis

Definitely BEPU approach and related procedures are originated within the Deterministic Safety Assessment (DSA) technology. The need and the importance to connect PSA and DSA within BEPU are discussed in different parts of this document (e.g., see Section 14.3.2).

14.3.1.3 Risk informed regulation

The words “risk informed” (regulation) were introduced in the 1990s and reflected in a key document issued by IAEA, e.g., IAEA (2011). Adopting some oversimplification one may state that (full) integration of DSA and PSA also includes the consideration of risk-informed regulation.

14.3.1.4 Safety margins

The evaluation of safety margins (SM) is the key goal for safety analyses including NPP licensing process. The evaluation of SM implies the calculation of related quantities or Q-SM. A number of additional variables are needed to be computed in order to calculate the Q-SM. BEPU aims at achieving qualified calculations of SM. BEPU types of analysis shall be considered also for NPP design and operation, as already discussed in this document. Then one may state that BEPU is expected to provide a framework where the calculation of all physically relevant quantities is required and proper qualification is pursued: i.e., Q-SM values shall have qualification and qualification is expected for non Q-SM values. Additional discussion can be found in Section 14.4.3 of this document, see also D'Auria et al. (2015).

14.3.1.5 Sensitivity & uncertainty

Sensitivity and uncertainty are key activities to estimate the error expected or characterizing SYS TH code calculation results. The difference between sensitivity and uncertainty is shortly outlined hereafter, having in mind the uncertainty methods based on the propagation of input errors as discussed in Chapter 13 (see also Adu et al., 2015).

Sensitivity analyses may be worthwhile when carried out in relation to *any* input parameter within *any* range of variation; uncertainty analysis shall be carried out in relation to those input parameters which are at the origin of the uncertainty in code calculations and related ranges of variations shall be properly defined to account for the approximations unavoidable in the overall (calculation) process.

Both sensitivity and uncertainty are of interest within a BEPU approach.

14.3.1.6 Accuracy & uncertainty

Accuracy is the known error which characterizes the comparison between measured and calculated values, e.g., Ambrosini et al. (1987) and Kalli et al. (1995); uncertainty is the unknown error which characterizes the calculation (or prediction) of NPP transient performance, e.g., IAEA (2008).

Gathering of accuracy database is necessary to show the qualification of a BEPU process, and uncertainty is part of the BEPU acronym.

14.3.1.7 Reliability & uncertainty

Reliability and reliability analyses constitute key concepts or even established technologies inside the PSA framework and are not considered. Here the word reliability is restricted to passive thermal-hydraulic systems and to physical phenomena expected during their operation.

In this situation, e.g., passive systems and phenomena, reliability can be calculated with methods similar to those adopted for uncertainty analysis, see e.g., D'Auria and Galassi (2000), Jafari et al. (2003), and Marques et al. (2005). The comment here is that reliability analysis related to the design of a system and uncertainty analysis related to the error of a calculation.

Reliability analysis is important within a BEPU approach where passive systems are considered.

14.3.1.8 Bounding approach

Bounding approach are not frequently used terms to signify one analysis where

minimum conservatism is adopted, see e.g., Zhang et al. (2011). In an oversimplified way one may state that bounding approach is an intermediate step between conservative and best-estimate approach. The bounding approach is not expected to have a role within a BEPU process.

14.3.1.9 BE & conservative code

The meaning of BE and conservative code is discussed in other parts of the book, e.g., Chapters 1, 2, and 13, see also Table 14.1 in this chapter, where “option 1” and “option 2” deal with conservative analyses. BEPU can be (and must be) used to quantify the amount of conservatism as already stated (Stanev and D'Auria, 2001; D'Auria et al., 2001). Only BE codes are of interest within the BEPU framework.

14.3.1.10 Conservative & realistic input data

Conservative and realistic input data can be used for BE codes as foreseen by the “option 2” and the “option 3” in Table 14.1 in this chapter. Only realistic input data, properly characterized by errors, i.e., input uncertain parameter ranges, are of interest within the BEPU framework.

14.3.1.11 Conservative & realistic assumptions

Realistic assumptions are considered at any step of the application of a BEPU process. However, conservative assumptions are part of BEPU approaches when related to the intervention of ECCS, according to the “option 3” in Table 14.1 in this chapter.

14.3.2 The elements

Let us define a BEPU element as follows: any software, procedure, or a dataset which is needed to perform a BEPU application in the area of NPP accident analysis. The key elements for BEPU shall be derived from the envision provided in Section 14.2.3 and from selected key terms in Section 14.3.1.

A not exhaustive (minimum) list of BEPU elements is provided hereafter: the nuclear thermal-hydraulics framework should be considered as element “zero” of BEPU and is not part of the list; furthermore, items are given not necessarily in the logical order of application or in any order of importance.

- Computational tools/SYS TH codes—design and development

- Computational tools/SYS TH codes—V & V procedures
- Computational tools/SYS TH codes—procedures for application
- Computational tools/nodalizations (or input decks)—development
- Computational tools/nodalizations—V & V procedures
- Computational tools/code-coupling software—design and development
- Uncertainty methods/design and development
- Uncertainty methods/qualification procedures
- NPP parameters database
- PIE
- Phenomena/physical aspects which characterize PIE
- Databases for code and nodalization qualification
- Scaling demonstration/procedures and database
- Users of computational tools/qualification
- DSA—PSA integration
- I & C modeling
- Documentation requirements for each elements
- Licensing framework—acceptance criteria, SM, procedures, etc.

Additional notes are provided hereafter for some of the elements (e.g., those not considered in other chapters or in Sections 14.2 and 14.3).

Procedures for SYS TH V & V: In addition to the information in Chapter 13, the recently completed activity within the framework of IAEA shall be considered in relation to V & V procedures for SYS TH codes involved within the application of a BEPU approach, e.g., IAEA (2016).

Procedures for SYS TH code application: The application of SYS TH code to the

BEPU accident analysis is not straightforward: the availability of a code, eventually of a specific NPP input deck (or nodalization) and of analysts capable of running the code, does not guarantee the achievement of valid or acceptable results. A variety of checks are needed (see also below). When an NPP nodalization is available to perform accident analysis, i.e., ready for the final stage of the code application process, the Kv-scaled procedures already introduced to support the application of an uncertainty method are recommended or necessary (D'Auria et al., 1995). The procedure implies the comparison between calculated NPP transient performance and experimental data gathered from a suitable Integral Test Facility (ITF) where a scaled-down experiment has been performed simulating the concerned NPP transient. Examples of Kv-scaled applications, including substeps and conditions for the analysis, can be found in the papers by Martinez-Quiroga and Reventos (2014) and Martinez-Quiroga et al. (2014).

Nodalizations development and qualification: The nodalization or input deck is tightly connected with the SYS TH code when accident analysis is performed. Importance for nodalization qualification and related requirements can be found in the paper by Bonuccelli et al. (1993): criteria are proposed for the acceptance of nodalization development, for the achievement of steady state and for demonstrating acceptability of transient results (“on-transient qualification”).

Code coupling software design and development: Coupling among codes derived for various technologies is essential for performing BEPU analyses; see also Fig. 2.8 in Chapter 2 and related discussion. Creating the interface between different software aiming at calculating time transients implies new software and related qualification, e.g., see D'Auria et al. (2004) and D'Auria et al. (2010), both related to coupling in the areas of thermal hydraulics and neutron physics.

NPP parameters databases: BEPU databases must be created and managed. A wide variety of databases are needed as discussed by D'Auria (2001), Petruzzi et al. (2012), Kovtonyuk et al. (2013), Petruzzi and D'Auria (2014), and D'Auria (2015); see also “BEPU as the exploitation of database” in Section 14.2.3.

PIE: Internal and external PIE need to be properly considered aiming at NPP safety evaluation. Within the thermal-hydraulics area internal PIE are of interest. These are discussed in Section 14.3.3, e.g., see IAEA (2002). The BEPU framework and procedures have the capability to make “robust” and consistent the consideration of external PIE.

Phenomena and physical aspects: Thermal-hydraulic phenomena expected to be relevant within the DBA envelope are discussed in Chapter 6 (OECD/NEA/CSNI,

1993, 1996) (see also references listed in Chapter 1). Phenomena and physical aspects constitute the link between BEPU and the experimental reality.

SYS TH code user training and qualification: The availability of a qualified code and of a qualified nodalization, as well as of qualified uncertainty procedure, does not guarantee a qualified BEPU calculation in nuclear thermal hydraulics (NPP accident analysis). A qualified group of code users and analysts is needed as discussed by Aksan et al. (1993), D'Auria (1998), Ashley et al. (1998), and Petruzzi et al. (2011), and in the IAEA (2016), technical guidance document.

I & C modeling: The full modeling of the I & C of the concerned NPP constitutes an essential requirement for the application of a BEPU approach as discussed by D'Auria et al. (2012b). Following any PIE, I & C of existing NPP has the task and the capability to bring the current operating status far from the original one which characterizes the PIE under concern. This causes a variety of consequences in the analysis of accidents, as also discussed in IAEA (2015b) (a synthesis of concerned items is provided below):

- The effectiveness and efficiency of regulatory design reviews are decreased owing to the extreme difficulty that vendors have in producing a fully standardized and documented design.
- Uncertainties intervene in the licensing processes and analyses which currently discourage the adoption (and the consideration) of new systems and technology to analyze I & C.
- Difficulties emerge with the reuse of previously licensed technical solutions for a large spectrum of applications and hence affect the validity of actual safety evaluations.
- Limitations exist in the development of competency on a global basis (i.e., it is difficult to create an expertise “parallel” to the expertise of the licensee), thus making the resolution of complex licensing issues more difficult.

Procedures within licensing framework: Procedures shall be derived from the licensing framework. However specific procedures need to be introduced consistently with the licensing framework. A sample, and not exhaustive list of procedures, basically providing an idea of the types of procedures, includes:

- Harmonizing the regulations in the country where the NPP is built and the country where the same NPP is designed or where licensing experience exists.

- Establishing a direct connection between technical specifications for the operation of components (typically Chapter 16 of FSAR) and the results of safety analysis (i.e., Chapter 15 of FSAR).
- Establishing the duration of transient calculations, consistently with the need to demonstrate the licensing requirements.
- Application of uncertainty methods including cases where wide SM are predicted by BE calculation.
- Establishing the list of PIE, based on available or specific PSA (see discussion in Section 14.3.3).

14.3.3 The concerned events

An idea of the PIE can be derived from IAEA (2002); see also USNRC (2005):

Grouping by principal effect leading to potential degradation of fundamental safety functions leads to the following event categories considered typically in the reactor design:

- Increase in heat removal by the secondary side,
- Decrease in heat removal by the secondary side,
- Decrease in flow rate in the reactor coolant system (RCS),
- Increase in flow rate in the RCS,
- Anomalies in distributions of reactivity and power,
- Increase in reactor coolant inventory,
- Decrease in reactor coolant inventory,
- Radioactive release from a subsystem or component.

Each category of events is typically subdivided into several more specific events. Events which are expected to occur during the plant lifetime are called AOOs (anticipated transients). Some of those events are also analyzed under the assumption of a complete failure of the fast reactor shutdown system and are called ATWS. Additional variations for each individual event are obtained by considering various plant operational states (e.g., burn-up or boron concentration when the PIE

occurs) at the time of the accident. “Radioactive releases” include events which do not represent the consequences of another event given above; i.e., the release is a direct result of the failure of the component which contains radioactive material.

Grouping by principal cause of the initiating events considered in the reactor design leads to the following categories:

- Reactivity anomalies due to control rod malfunctions,
- Reactivity anomalies due to boron dilution or cold water injection,
- Coast down of the main circulation pumps,
- Loss of PS integrity (LOCA),
- Interfacing systems LOCA,
- Loss of integrity of secondary system,
- Loss of power supply,
- Malfunctions in the PSs,
- Malfunctions in the secondary systems,
- ATWS,
- Accidents in fuel handling,
- Accidents in auxiliary systems,
- Accidents due to external events.

14.3.4 The needed resources

The following resources typologies are needed to perform a BEPU application

- Computational tools: codes in various areas, see e.g., Fig. 2.8 in Chapter 2;
- Computational tools: nodalizations (or input decks) to run the codes;
- Computational tools: software for coupling the codes;
- Uncertainty Method;

- Computers;
- Group of Analysts and Experts;
- Databases to demonstrate qualification and applicability of computational tools as well as to apply uncertainty method.

In order to provide an idea for the amount of resources needed for BEPU application, the following can be considered, in each case distinguishing between *minimum number of analysts-experts* ① (not necessarily working full time all together), *rough man-years effort* ② (equivalent effort including availability of computational tools and management effort), and *minimum time needed* to complete the activity in years ③:



Experience related to activities at items (A) and (B) is available, e.g., Galetti and D'Auria (2005), and UNIPI-GRNSPG (2008); the framework related to item (C) can be found in the paper by D'Auria et al. (2015), see also Section 14.4.2.

14.3.5 The roadmap

The BEPU roadmap can be considered as the end result of the BEPU planning, the origin of the BEPU application, and the consistent assembly of BEPU features. Thus, a variety of roadmaps can be envisaged. In the case considered below, the BEPU approach was pursued having access to the original designer delivered information, but independently from designer.

A sketch of the BEPU roadmap at the basis of the application for Chapter 15 of the FSAR of the Atucha-2 NPP can be found in Fig. 14.3.

Atucha-2 info: *KWU-Siemens-AREVA German design, about 800 MWe, vessel type, natural uranium, heavy water coolant and moderator, 2 loops with SG for power production and 4 loops for moderator cooling, full power operation attained in 2015, final license for operation attained in 2016.*

Three parallel paths are possible for each PIE (see Fig. 14.3):

- CSA (yellow color): Scenarios which are used for assessing the design and demonstrating the acceptability of ECCS, safeguards, or countermeasures, i.e., evaluation of systems performance associated with the integrity limits for the safety barriers against radioactive releases.
- RCA (pink color): Scenarios which are used as bounding (of other scenarios) for estimating the radiological impacts and demonstrating compliance with regulatory limits set at the territorial boundaries of the NPP unit.
- CBA (green color): Scenarios which are used for assessing the structural design of components or structures for demonstrating stability or integrity, i.e., implying the calculation of mechanical design loads and stresses.

The diagram shall be entered at item 1 in Fig. 14.3 for a logical interpretation. A preventive safety study is performed including probabilistic analysis where the boundary conditions of “enveloping transients” for safety analysis are identified. The “purposes for the analysis” of those transients shall be introduced according to the safety needs. Three areas are concerned, corresponding to CSA, RCA, and CBA, respectively:

(a) “Typical” ECCS design confirmation analysis (CSA in the diagram), e.g., aiming at demonstrating compliance with criteria in 10 CFR 50.46, USNRC (and German) requirements. In this case well-established acceptance criteria (e.g., PCT<2200°F) are used and standard BEPU SYSTEM analyses (e.g., see Chapter 15) are performed.

(b) Radiological protection analysis aiming at evaluating the radiological impact of any transient (RCA in the diagram), ARN (Argentinean Regulatory Body) requirements. In this case, among others, the maximum dose expected at the assigned territorial boundaries of the NPP had to be determined. This implies the solution of issues per, each PIE, like (b1) number of failed fuel rods; (b2) amount of radioactivity in the primary loop; (b3) amount of radioactivity in the CO; (b4) amount of radioactivity in the reactor building following assigned CO leakages; (b5) consideration of leakages from reactor building; (b6) use of meteorological categories including history of measurement on the site; (b7) passing from radioactivity to doses assuming persons standing at the site boundary; (b8) consideration of worst impact on the surrounding population also to exclude the need for evacuation (case of DBA).

(c) Structural mechanical analysis aiming at evaluating the stress and strain status of safety-relevant components and structures (CBA in the diagram), American Society of Mechanical Engineering (ASME) requirements. This implied among the other things calculation of the pressure wave from the break and consequent loads on internals and calculation of PTS based on realistic accident evolutions.

In relation to each of the above areas acceptance criteria must be identified (item 2 in the diagram). These are derived from legal requirements in the country (Argentina in this case).

The selection of computational tools, item 3 in the diagram, is based upon the phenomena which need to be analyzed. This constitutes a key item for the entire process: complexity of identified phenomena requires suitable level of sophistication which could not be handled via conservative-simplified codes or approaches. Furthermore, the need for a variety of computational tools emerged at this level of the process. Actually, addressing the item 3 brought to the need for a BEPU study: the physical complexity of the transient following the selected PIE could not be calculated by conservative methods without having access to the expertise of the original designers of the NPP. Applications of BE codes and of the latest available technological knowledge were the only possible alternative to perform assessment independent upon the original NPP designer.

Items 4, 5, 6, 7, and 8 are the direct consequences of the application of a set of computational tools. Namely,

- Selection of the most suited numerical codes was necessary (item 4).
- Input decks or nodalizations were developed in relation to each code, as needed (item 5).
- The issues of demonstrating the qualification for the codes, the nodalizations and (not least) the users or analysts were considered (item 6).
- Assumptions and acceptability criteria related to the quality and the level of detail for the values of relevant BIC had to be formulated (item 7). Examples are: (a) the burn-up level of each fuel assembly; (b) the dimensions of the RPV following thermal dilatation caused by nominal power operation.

The use of different codes implies the need of coupling (e.g., neutron cross section generation and three-dimensional neutron kinetics, three-dimensional neutron kinetics and thermal hydraulics, structural mechanics and thermal-hydraulics,

etc.), item 8.

Specific software and related qualification demonstration are needed. Rules are needed to perform the analyses once computational tools, i.e., codes and nodalizations including coupling-software, and suitable users are available or ready, item 9. Those rules refer to unavoidable consideration of conservatism although a BE process is pursued, including topics like single failure and “worst” failure. Results are expected in relation to the three areas (a), (b), and (c) defined under item 1.

Uncertainty analysis is performed, item 10, and is part of the results. Compliance with acceptance criteria shall be demonstrated.

Pursuing the BEPU approach implied a specific consideration of the modalities to write Chapter 15 of the FSAR (e.g., amount of information provided in each section, cross-connection among topics, etc.), item 11.

Additional synthesis information related to the diagram in Fig. 14.3 is provided below. In the first step, as a function of the selected scenario and of the purpose of the analysis, the complexity of the evaluation model (EM) may range from a simplified qualitative evaluation (EM/QA) to a complete combination of the three possible modules (EM/CSA+EM/RCA+EM/CBA). In order to evaluate the plant safety performance, acceptance criteria are properly selected according to established international practice.

The two main aspects, which have been considered for developing the EM with the ability of adequately predict plant response to PIEs, are intrinsic plant features and event-related phenomena characteristics. “Sets of requirements” connected with the two aspects are discussed below. The first set of requirements for the EM is imposed by the design characteristics of the NPP, its systems, and components. Requirements on the capability of simulating automatic systems are of particular importance for AOOs, in which control and limitation systems play a key role on the dynamic response of the plant. It shall be noted that the concerned modeling features are consistent with the requirements which impose the design of the limitation system according to the same standard as the reactor protection system. However, this rule does not apply to control systems. Nevertheless, the best response of the plant cannot be calculated without the detailed modeling of the control system. This has been considered in the present framework. The second set of requirements is derived from the expected evolution of the main plant process variables and the associated physical phenomena. For the proposed approach, this is performed through the process of identifying the Phenomenological Windows

(Ph.W) and the relevant thermal-hydraulic aspects (RTA). The relevant timeframe for the event is divided into well-defined intervals, i.e., the Ph.W, where the behavior of relevant safety parameters, i.e., the RTA, is representative of the physical phenomena. For the adequate simulation of the identified phenomena, computational tools were selected from those which have previous qualification using an appropriate experimental data base. Satisfactory qualification targets provide basis for acceptability of the postulated application.

14.3.6 Selected relevant topics

Different issues, or questionmarks, or “BEPU topics to be addressed” occur when pursuing the BEPU roadmap (Section 14.3.5). Those are in addition to the terms and the elements considered in Sections 14.3.1 and 14.3.2, including PIE (discussed in Section 14.3.3). Again a not exhaustive list of BEPU topics is provided below.

- (1) Initial power.
- (2) Decay power.
- (3) Maximum Linear Heat Generation Rate.
- (4) Gap model.
- (5) Hydrogen production and clad embrittlement.
- (6) Clad burst and FP release, transport and deposition.
- (7) Ballooning including coolability after ballooning.
- (8) Radiation heat transfer.
- (9) Nuclear fuel modeling (pellet crack) including High Burn-up and plutonium-uranium mixed oxides fuel.
- (10) Assumptions on NPP conditions (e.g., single failure).
- (11) Mechanical loads.
- (12) Long-term cooling including the debris effect.

Some insights into some of the BEPU topics are given with the aim to characterize the topic rather than providing a suitable answer for applications.

The core power, item (1), is indirectly measured in any NPP and the measurement is affected by errors. The amount of approximation (or error) can be $\pm 2\%$ or, agreed everywhere, $< 6\%$. Then possible values to be considered for initial power are 100%, 102%, and so on up to 106%. A technological procedure is needed within the BEPU approach to fix a suitable value.

It is difficult to avoid some conservatism in the case of decay power, item (2): all (regulatory-body) recognized decay-power curves imply some level of conservatism. Actual conservatism need to be quantified and eventually eliminated.

Maximum linear heat generation rate, item (3), in the hot bundle and/or in the hot rod is typically calculated based on regulatory-body suggested procedures and controlled, as far as possible, by core instrumentation. In a BEPU approach the maximum reasonable local power can be calculated by coupled three-dimensional thermal hydraulics and neutron physics models, thus avoiding the conservatism embedded within the possible regulatory body-suggested procedure. The approval of the new procedure by regulators may be the key issue in this connection.

Ballooning, item (7), is an expected phenomenon, e.g., following LBLOCA-DBA, for nuclear fuel. This constitutes the most expected mechanism causing release of radioactive products into the PS in DBA conditions. Then, proper models are needed within a BEPU calculation framework and properly accounting for actual fuel properties, e.g., determined by burn-up and thermal-hydraulic parameters.

Mechanical loads and possible presence of debris in the CO, items (11) and (12), respectively, need proper modeling within a BEPU approach. Namely mechanical loads in case of LBLOCA can be generated by the propagation into the vessel of the depressurization wave from the break (see also discussion in Section 14.3.5): mechanical loads cause stresses acting on the internal components and upon the vessel supports. Consideration of debris is needed to demonstrate the long-term cooling capabilities of ECCS and must be considered together with sump fluid temperature effects. This imposes the calculation of the level in the CO sump and the evaluation of consistency between the ECCS pump Net Positive Suction Head (NPSH) and the NPSH available from the system (i.e., generated by the level into the CO sump).

14.4 BEPU perspectives in safety-licensing demonstration

An idea of current BEPU framework can be derived from this chapter, including

related background information and selected elements, terms, and topics (namely Chapters 2 and 3). The present one shall be considered a “perspective” section of this chapter where bases for possible BEPU developments are discussed.

Two converging directions for BEPU development are considered: the former, Section 14.4.1, can be defined as a PSA-platform-based where DSA analytical features of current BEPU are exploited; the latter, Sections 14.4.2 and 14.4.3, consists in the proposal of extending the BEPU concept to the whole safety analysis needed for individual NPP. The BEPU visions considered below are still preliminary, or not ready for applications, and need endorsement by the technological community.

14.4.1 Integration of DSA and PSA

Current status of integration between DSA and PSA has been discussed in Section 14.2.3. Related trends primarily originated from the PSA area of expertise can be found in documents IAEA (2010b), EC-EURATOM (2013), and Zimmermann (2011), in the last case summarizing an OECD/NEA/CSNI activity.

Since 2005, the IAEA and the OECD/NEA have organized ten meetings, to develop the understanding of BEPU and the integration of DSA and PSA, e.g., IAEA-TM (2005), IAEA-TM (2006), IAEA-TM (2007), IAEA-TM (2008), IAEA-TM (2009), IAEA-TM (2010), IAEA-TM (2012), IAEA-TM (2013), OECD/NEA/CSNI-TM (2005), and OECD/NEA/CSNI-TM (2011). Participants at the 2012 meeting (IAEA-TM, 2012) provided conclusive remarks summarized in the following paragraphs.

The first attempts to bridge the gap between DSA and PSA were the Deterministic Dynamic Event Tree (DDET) (Amendola and Reina, 1984) and the Cell to Cell Mapping Technique (Aldemir, 1991). However, these techniques either required very large computer facilities or could not be applied to the complexity of a NPP.

14.4.1.1 DSA-PSA integration—IAEA and OECD/CSNI technical meetings

Integrating PSA and DSA was a major factor in the OECD/NEA/CSNI Safety Margin Project, SMAP, and in its subsequent study SM2A, e.g., see Zimmermann (2011). The motivation for this study was the observation that plant modifications, such as a plant upgrade, erode SM but the extent of the erosion remains unquantified if only licensing-conservative analyses are performed. SMAP proposed a framework for the evaluation of generalized SM that relies on a combination of PSA and DSA. In this approach, fault sequences and parameters

are not enveloped (bounded). Rather, the transients are analyzed using a BEPU approach and discarding of events in the ET is avoided as far as practicable. It allows for using “option 4,” already introduced in Table 14.1, integrating PSA and DSA in a consistent manner involving the application of DDET.

Both PSA and DSA have matured with time and constitute “state-of-the-art” frameworks for developing the designs and demonstrating the safety of NPPs, but there is only limited experience of applying combined approaches. Preserving the mature techniques and combining them is the objective of Integrated Deterministic and Probabilistic Safety Assessment (IDPSA), see also IAEA (2011), dealing with Integrated Risk Informed Decision Making (IRIDM).

Application of DSA in PSA

As already discussed in this chapter, the recognized key objective of a PSA level 1 and level 2 is the calculation (or the confirmation) of the probability and of the consequences of any PIE. In the case of PSA level 3 the radiological consequences are of interest. When the calculation of consequences is concerned, DSA tools and methods are needed. So PSA analysis cannot be performed without DSA type of knowledge and expertise. This is illustrated by more specific situations in Table 14.2 (*the statement by G.T. Klope from ANL, Chicago area, US, 2013, is relevant: “If this sounds like the PSA has become a deterministic analysis, so be it. Level 2 PSA work is a 50-50 mix if not a 65-35 mix of deterministic-probabilistic analyses.”*).

Table 14.2

Examples of challenging DSA aspects as far as the PSA application is concerned

--

Table 14.2 shows that techniques developed within DSA are relevant to PSA applications. For instance:

- Codes used for calculating the CD time or the CD consequences in PSA applications should either be the same as used for DSA or should be developed

based on the same technological background (e.g., qualification, application of the best knowledge in numerics, etc.).

- The calculation of time of intervention of a system (related setpoints are part of the technical specification for the NPP operation) is affected by an error to be quantified by DSA uncertainty methods. This is also true for the time required for operator action: if an operator action is calculated at 35' after the PIE start, i.e., after the 30' grace period for operator intervention, the error in estimating the 35' is needed. This might bring the request for operator action within the 30' grace-period (i.e., within the no operator action boundary).

Application of PSA in DSA

DSA applications aim at characterizing the NPP scenarios following a PIE. The probability of PIE should be known apriori to make meaningful the DSA application (e.g., the maximum ground acceleration for the earthquake consistent with the NPP site). The importance of PSA application in this connection is underlined by the fact that the PIE probability is associated with acceptance criteria.

In addition to this, a list of situations within the DSA framework, which would benefit from PSA applications, is provided below:

- (1) Probability of Single Failure: a very low probability Single Failure may reveal less probable than two or more high probability failures.
- (2) When searching for the worst position for break (e.g., LBLOCA, SBLOCA, and SGTR) no use is made of probability consideration which might exclude some (several) break locations.
- (3) The Break Opening Time (BOT) in case of LOCA may affect the load on pressure vessel internals: it is important to calculate the probability distribution for BOT and perform consequently the DSA calculation (current practice is to assume “unrealistic” very low value for BOT and to not calculate load on internals).
- (4) When performing DSA for LBLOCA the consequential events like SBO or the failures of components like Main Coolant Pump (MCP) or vessel internals should be calculated with PSA techniques like the fault tree (FT) and proper probability should be considered when creating the input of the DSA calculation.
- (5) Following any PIE the control systems can bring the NPP scenario far from the initial state. This implies the need to calculate the probability of the NPP status at

any time after the PIE (thus, the need to model the control system in both DSA and PSA studies).

(6) Events which are part of the accident analysis by DSA shall be classified with their own probability (i.e., not only category-of-event probability): ideally, a suitable DBA envelope should be created in the “Farmer” variables space (probability vs consequences) (Farmer, 1967).

Furthermore,

- It is well established that a large variety (maybe all) of DSA code input parameters has a statistical nature. This shall be recognized also in relation to output quantities;
- When performing conservative calculation the probability associated with the conservative value should be calculated (to avoid overconservatism or even lack of conservatism).

Thus PSA techniques are well needed within the DSA processes.

14.4.1.2 The proposal for “option 4” (in Table 14.1) by Dusic et al. (2014)

The “option 4” presented in Table 14.1 is not developed further, e.g., in the current version of IAEA SSG-2 (IAEA, 2010a). The SSG-2 only indicates that “option 4” is an attempt to combine insights from probabilistic safety analyses with a deterministic approach, which results in a risk-informed safety analysis: in the “options 1–3,” the availability of safety systems is based on conservative assumptions whereas, in “option 4,” the availability of safety systems is derived by probabilistic means.

“Option 4” integrates the system availability, and the single failure criterion in particular, into a risk informed safety analysis. The main differences between the applications of “option 4” and “option 3” are envisaged to be as follows (i.e., making reference to “option 4”):

1. The availabilities of safety systems are determined using probabilistic arguments.
2. All sequences in the ETs associated with the PIE are systematically evaluated and not only those which incorporate a single failure.

3. If all the sequences meet the acceptance criterion with the standard tolerance level (typically 95/95), it follows that the acceptance criterion for the PIE is met. If there are sequences which do not meet it, it is necessary to determine whether or not the acceptance criterion for the PIE, i.e., for all the sequences together, is still met.

4. Even if all sequences meet the acceptance criterion with the standard tolerance level, the fulfillment of the acceptance criteria for the next class with an increased tolerance level (e.g., 99/95) needs to be checked. This helps in ensuring that there are no cliff-edge effects.

5. Those sequences which failed the acceptance criterion at the standard tolerance level and have low enough frequencies can be reclassified into the next higher class. There, they are compared to the acceptance criterion of that class with the increased tolerance level.

6. If a sequence is reclassified to a beyond design basis plant condition, it does not need to be analyzed. If it is a single failure sequence, this is equivalent to not requiring the single failure criterion under well-specified conditions.

As an extension of “option 3” the proposed “option 4” would tighten the requirements for those sequences that do fulfill the acceptance criteria of its class with the standard “option 3” tolerance level. In doing that, “option 4” addresses possible cliff-edge effects. On the other hand, it would allow certain sequences having a low enough probability of occurrence to be reclassified into the next higher class, where they would be compared with the acceptance criteria of that class (or some more stringent ones if appropriate) with an increased tolerance level.

Definitely, “option 4” provides a systematic methodology to identify design deficiencies of various types and to find possible ways to solve them, including the possibility of design extensions. Completeness and consistency of the plant design are therefore better addressed with “option 4” than with former methodologies. This option is still a research option and will remain so for some time.

14.4.2 From ALARA to BEPU

ALARA is an acronym for As Low As Reasonably Achievable. This is a radiation safety principle for minimizing radiation doses and releases of radioactive materials by employing all reasonable methods, components, and procedures.

ALARA is not only a sound safety principle, but is also a regulatory requirement for all radiation safety programs.

The ALARA principle has already been introduced as a cross-connecting path or a condition to pass from principles to applications and design in Nuclear Reactor Safety Technology, e.g., Fig. 2.1 in Chapter 2. The same principle shall be taken at the origin of BEPU (D'Auria et al. 2015): the ALARA shall be translated for the analytical-calculation domain into the words As Accurate As Reasonably Achievable. The BEPU framework presented in Chapters 2 and 3 is consistent with this definition, i.e., a boundary-moving frontier in the application of computational methods into the licensing process.

14.4.3 BEPU for the entire FSAR

An idea has been launched, e.g., D'Auria and Debrecin (2014), D'Auria et al. (2015), Menzel et al. (2015), and Menzel et al. (2016), for a systematic application of BEPU to each area of FSAR where an analytical-computational activity is required.

The first step for the implementation of the idea, making reference to an individual NPP, is the identification and the characterization of FSAR parts where numerical analyses are needed, e.g., USNRC (2007) and USNRC (2013) (the last document continuously updated). Further steps include: list of key technological areas, status of computational activities in each technological area (thus identifying computational areas), transfer of BEPU concepts into each computational area, gathering expertise and database for each area, planning BEPU licensing-consistent calculations, performing calculations, and documenting results proving NPP safety compliance.

In order to provide an idea of the complexity of the process, a rough list of key technological areas in licensing is given below in alphabetical order.

- Chemistry (of nuclear fluids)
- Civil Engineering
- Climatology (including siting needs)
- Control Rod mechanisms
- Corrosion

- Component (nuclear) qualification and degradation of capacities (turbine, condenser, MCP, Reactor Pressure Vessel, Valves, Alternator, etc.)
- Computational tools, i.e., corresponding to fundamental expertise in related disciplines:
 - Atmospheric diffusion
 - CFD
- CO
- Cross-Section Derivation
- Fuel (nuclear) performance
- Monte Carlo type of codes
- Probability and Reliability
- Severe Accident
- Structural Mechanics (including PTS)
- System Thermal hydraulics
- Three-dimensional neutron physics, namely three-dimensional
- DSA (licensing aspects, e.g., SM, acceptance criteria)
- Earthquake and Tsunami
- Electric Engineering (including machinery)
- Emergency Preparedness
- Emergency Operating Procedures (design, implementation, and operator training)
- Fire protection
- FSAR writing and assessment (report format and structure)
- Fuel (nuclear)

- Fuel movement including loading and unloading machines, spent fuel cask, etc.
- Fuel Cycle (out-of and in-reactor fuel performance)
- Geology including stability of slopes
- Hazards, industrial and natural (including site vicinity and aircraft)
- Human Factors
- Man-Machine interface
- Hydrology and Floods
- In-service Inspection
- I & C, including electronic engineering
- Knowledge of EUR, IAEA, WENRA, US NRC, ASME, ANS, IEEE, CSNI frameworks of requirements (the acronyms relate to selected established international or national institutions which are in charge of issuing rules and procedures for demonstrating the safety of NPP)
- Licensing (legal-binding bases and procedures, defense in depth (DiD) application)
- Materials (other than nuclear fuel)
- Meteorology
- Mining (licensing of)
- Neutron Physics including cross section derivation
- Nuclear Instrumentation (core)
- Plant procedures (for normal operation) including plan for training of personnel
- PSA (licensing aspects) and Risk Analysis
- Quality Assurance
- Radioprotection (including Doses and impact of Doses)

- Robotics (Accessibility to remote Radioactive Zones)
- Security
- Seismology
- Severe Accident (including SAM Guidelines and NPP design against Severe Accident)
- Catastrophic (including natural and man-originated) events
- Shielding (from radiations)
- Simulator (for NPP)
- Siting
- Structural mechanics (Creep, Aging, etc.)
- Thermal hydraulics (Bases, Experiments & Numerics)
- Thermodynamic Machinery (Turbine, Pump, Condenser, etc.)
- Transportation of nuclear fuel and high radioactivity waste
- Uncertainty Analysis
- Waste Management (Nuclear Materials)

Assembling the top-level competence in relation to each of the listed technological areas constitutes an obligation to demonstrate the safety of any nuclear installation. On the other hand the difficulty to achieve related targets by established NPP design/owner/vendor companies is recognized.

Innovation introduced by BEPU proposal for the entire FSAR

The first key innovation is that safety analysis shall be carried out by expert technologists independent of the owner, vendor, or the designer for the concerned NPP.

The second key innovation is that the latest analysis techniques shall be adopted as

well as the latest findings from researches (consistently with the here presented BEPU approach).

The third key innovation is the objective of homogeneity in the nuclear reactor safety technology matters: analyses including calculation processes shall not be limited to the accident analysis, but encompass whatever topic connected with the design, the construction, and the operation of the NPP.

The fourth key innovation, discussed with some details in the following sections, consists in creating a technological connection (system or control) between BEPU safety analysis and the hardware of the NPP.

The first innovation is challenged by the (almost) insurmountable issue of the proprietary data and information: NPP Designer and Owners do not share data even though Regulatory Authorities impose mandatory requirements for the availability of data. Owing to the reasons directly connected (but not only) with intellectual properties, analytical capabilities and market competition, NPP sensible data remain not available to the screening of experts independent from the NPP designer or owner, e.g., see D'Auria and Debrechin (2014).

The second innovation is connected with the unavoidable situation that very few Regulatory Authorities exist in the world which have the capability to invest in research and may follow the myriad developments in each of the listed technological areas. On the other hand the industry may have same limitation and no interest in proposing innovation first-of-a-glance. Unavoidably a lag of 10–30 years establishes between applicable (qualified) research findings and application. This is frustrating for the specialists in the various sectors and undue for the safety: this situation can be observed for any of the three major nuclear tragedies, see Chapter 16.

Third innovation: owing to historical reasons, accident analysis received suitable attention by nuclear reactor safety technology actors. However, accidents, i.e., not only the three major tragedies, happened either in peripheral areas or following precursory events which brought the NPP in conditions outside those considered for accident analysis. Therefore homogenization of safety areas is needed: this implies the systematic identification of topics and their consideration for analysis.

So far the strategic objective of safety analysis is to demonstrate the acceptability of the NPP against assigned criteria. Here, fourth innovation: it is proposed that “each” outcome of safety analysis becomes a target for physical measurement of the NPP status (see following paragraphs).

14.4.3.1 The extended definition and the application of safety margin concepts

The safety margin for nuclear reactors is defined as the difference or the ratio in physical units between the limiting value of an assigned parameter (typically, the threshold value for the connected acceptance criterion) the surpassing of which leads to the failure of a system or component, and the actual value of that parameter during the life of the plant.

The existence of suitable margins ensures that NPPs operate safely in all modes of operation and at all times during their life. The most important SM relate to physical barriers designed to protect against the release of radioactive material, such as fuel matrix and fuel cladding (typical limiting values are associated with Departure from Nucleate Boiling Ratio (DNBR), fuel temperature, fuel enthalpy, clad temperature, clad strain, clad oxidation), RCS boundary (pressure, stress, material condition), CO (pressure, temperature), and surrounding public dose.

Nowadays, a safety analysis is in most cases performed using both the deterministic and the probabilistic approach. The deterministic approach typically considers a reduced number of limiting transients for which conservative rules for system availability and parameter values are often applied. The accident phenomenology and the related timing are estimated as complete as necessary. In turn, the probabilistic approach emphasizes the completeness of the set of different scenarios and BE methods. The approaches have been developed rather independently from each other. This then poses the problem of integrating the two approaches consistently into a single comprehensive methodology necessary to explore SM in a general sense. Hence, a generalization of the concept of safety margin is needed in order to make this concept operable in both the probabilistic and the deterministic fields of application while maintaining the traditional meaning to the maximum extent possible. Furthermore, the concepts of SM and quantifying changes in SM appear as key components of the discussions for modifications in plant design parameters and operational conditions. This includes, for example, power uprates, life extensions, use of mixed oxide fuels, different cladding materials, design and operation of passive systems, and changes to technical specifications. Some of these modifications impact SM in deterministic analyses, while others impact the reliability of systems and components, and yet others impact SM and reliability simultaneously.

The concept of “Safety Margin” is embedded into the picture of nuclear reactor

safety technology framework, as depicted in Fig. 2.1 of Chapter 2. The concepts “Safety Limits” and “Licensing Margins” are also connected with the definition of SM.

The connections between BEPU and the extended SM definition

As a difference from conservative analysis, the BEPU analysis allows the calculation of the expected NPP transient performance. This applies for the adoption of BEPU to all parts of safety analysis (FSAR) where a computational activity is needed (as discussed in this section).

Thus a wide variety of “actual” SM values are the outcome of BEPU analysis and constitute the first connection between BEPU (for the entire FSAR) and the extended SM definition.

The second connection derives from the complexity and the resources needed for BEPU analyses. The BEPU complexity and resources justify an impact on the NPP hardware which: (a) has negligible cost compared with the overall BEPU cost; (b) creates an additional barrier against the release of the FPs and is expected to cause a substantial reduction in CDF.

The multidimensional space to evaluate SM (i.e., the “extended” SM definition)

In the following, the words SM have the broader meaning coming from the “extension” of the concept and are used in combination with the words design margin (DM). The concepts of SM (and DM) are expected to be introduced in relation to the following aspects (minimum list, to be taken as example and excluding security-related issues):

- the control of the “nuclear chain reaction”;
- the amount of “radioactive source”;
- the “likelihood of an accident”;
- the prevention of (each among several) “failures” of systems and components;
- the prevention of (each among several) “possibility of escalation” of any off-normal condition of operation;
- defending (each among several) the Barriers and the Safety Features (see below) introduced “to prevent loss of radioactivity.”

It becomes clear that the definition of SM and DM shall be given within a multidimensional space. The multidimensional space implies a multiphase concept, because of the many design-safety-licensing involved aspects, and a multifield concept, because of the many involved technological fields covering nuclear reactor safety and design.

The multidimensional space can be defined for SM, noting that risk space shall be taken as synonymous of safety space. The key dimensions for the space embracing the definition of SM can be defined as:

- (A) The key elements characterizing the nuclear reactor safety technology.
- (B) The technological sectors or the key scientific disciplines at the basis of nuclear reactor safety and NPP design and operation.
- (C) The systems, the subsystems, and the components which constitute the NPP.
- (D) The time spans which form the life of the NPP.

The technological areas for BEPU analyses (see above) are expected to be covered; furthermore, human factors shall be considered as part of any of the “dimensions” above. Key elements (A1)–(A6), (B1)–(B5), (C1)–(C19), and (D1)–(D7) are defined hereafter:

- (A1) Safety Principles, i.e., SP-1 to SP-10, i.e., according to established documents (e.g., IAEA framework).
- (A2) DiD Levels, i.e., DL-1 to DL-5, i.e., according to established documents (e.g., IAEA framework).
- (A3) Safety Barriers, i.e., SB-1 to SB-6, i.e., according to established documents (e.g., IAEA framework).
- (A4) Safety Functions, i.e., SF-1 to SF-19, i.e., according to established documents (e.g., IAEA framework).
- (A5) PSA Elements, i.e., PE-1 to PE-n, i.e., according to results of safety analysis.
- (A6) DSA Elements, i.e., DE-1 to DE-m, i.e., according to results of safety analysis.

The values “m” and “n” shall be associated with the results and the procedures of

the applicable DSA and PSA.

(B1) Radioprotection;

(B2) Thermal Hydraulics;

(B3) Structural Mechanics;

(B4) Neutron Physics;

(B5) Civil and Electrical Engineering.

An attempt is made to minimize the number of disciplines. Several SM and DM are expected in relation to each discipline.

(C1) RPV;

(C2) RCS piping;

(C3) Balance of Plant (BOP) piping;

(C4) Core;

(C5) Core components;

(C6) RPV components except core;

(C7) RCS components;

(C8) BOP components;

(C9) CO;

(C10) CO components;

(C11) Core components;

(C12) Reactor building;

(C13) Auxiliary buildings;

(C14) Reactor building and auxiliary building components;

(C15) Site (parameters);

(C16) Site structures and components;

(C17) Off-site (NPP-related relevant parameters);

(C18) Off-site structures and components (NPP related);

(C19) I & C.

The value “19” associated to the identification of systems and subsystems, and component of the NPP is somewhat arbitrary. Modification in this number will not affect the procedure. Furthermore, each of the listed items should be intended as Ci-j where “i” ranges between 1 and 19 (present proposal) and “j” can assume any value connected with the level of detail of the (BEPU) analyses.

(D1) Site selection;

(D2) NPP design;

(D3) NPP construction;

(D4) NPP licensing;

(D5) NPP operation;

(D6) NPP maintenance;

(D7) NPP decommissioning.

The items from (D1) to (D7) should be considered as an outcome of the established knowledge within nuclear reactor safety and design technologies.

The expected total number of “new” SM and corresponding NPP hardware devoted instruments is in the range of a couple ten thousands.

14.5 Conclusions

The description of BEPU in nuclear thermal hydraulics involves a wide variety of concepts. At the present time, when only pioneering applications of BEPU have been completed, the reader may consider this document (i.e., this chapter) as an attempt to introduce a definition of the BEPU process or approach. Because of the

complexity associated with BEPU this chapter may resemble an unfinished mosaic of terms, elements, topics, and technological areas: a much larger effort is needed to provide a suitable shape for the mosaic.

BEPU is needed to assess the conservatism in the design and operation of NPP. Possibly, suitable conservatism can only be introduced by NPP designers or owners based on expertise which comprises operation of similar plants, proprietary BE analyses, and measured data. In other terms, designers/owners of NPP are expected to own best-estimate information and to sell (or make available, e.g., to regulator) “suitable” conservative information, which covers the best available data and prevents the disclosure of proprietary information. It is clear that a licensor (or any institution supporting the licensor) may not have the expertise of the designer/vendor and may not fix suitable conservative values for parameters which are input to the analyses for safety demonstration. Thus, BEPU may reveal as the only logical approach for the licensor for an independent assessment of the licensee submission: the uncertainty in input parameters is derived “independently” and substitutes, and eventually is consistent with, the conservatism of the licensee based on proprietary BE information.

The BEPU process or approach takes origin from the area of SYS TH.

The first key conclusion is that BEPU implies the best, i.e., the deepest possible, exploitation of analytical-numerical techniques consistently with the needs in NPP design and safety. Licensing constitutes an essential component for BEPU also owing to the established set of rules and acceptance criteria which contribute to ensure quality in the BEPU applications.

Two main achievements from the document associated with the first conclusion can be mentioned:

(I) The identification and characterization of BEPU aspects: this is done primarily in Section 14.2.3, the envisions for BEPU, in Sections 14.3.1 and 14.3.2, where selected key terms and elements are described, and in Section 14.3.5 where a BEPU roadmap already used for industrial application is discussed. This includes the motivation for BEPU and provides an idea of the computational effort necessary for the application.

(II) The expected future development for BEPU: on the one hand there is the full integration between Deterministic Safety Assessment (i.e., the technology area where the origins of BEPU can be located) and Probabilistic Safety Assessment including the Risk Informed “branch”; on the other hand a more ambitious vision

includes the connection of BEPU with all areas of nuclear reactor safety and licensing where an analytical support is needed. In this last case an extended definition of the Safety Margin concepts is expected to link with the outcomes of results of BEPU analyses. Noticeably, the extended definition of SM implies modifications of the hardware as a consequence of the BEPU analyses. This brings a strong motivation for BEPU application; although concerned NPP modification shall have a negligible impact on the construction and operation cost of a single power unit, huge and traceable impacts upon the safety are expected.

The second key conclusion is devoted to the complexity of the approach. The design and the application of a BEPU approach imply a complexity which is consistent with the complexity of the objective system, i.e., the NPP. The complexity is connected with computational tools, the database, the regulation, and the expertise which are needed for the application.

The third conclusion deals with finalized BEPU applications within the NPP accident analysis frameworks: the completed LBLOCA applications, e.g., the licensing of Angra-2 NPP in Brazil, and the recent application for all the DBA transients in Chapter 15 of the FSAR for the Atucha-2 NPP in Argentina demonstrate the feasibility of the approach and prove its industrial worth and interest.

The fourth conclusion summarizes key findings from the chapter or key identification concepts for BEPU: BEPU \Leftrightarrow ALARA, BEPU \Leftrightarrow CIVILIZATION, BEPU \Leftrightarrow V & V, Scaling and Licensing rules.

The last conclusion deals with the apparent obstacle in the spread of BEPU, e.g., for all new (NPP) built-designed, somewhat in contradiction with the previous conclusion: the needed “deep expertise,” “numbers of wide databases,” “sophistication of computational tools,” and the lack of “fixed boundaries for V & V,” and of “certainty for the requested resources,” have so far prevented the exploitation of the approach. Otherwise, the old-fashioned conservatism in the computational analyses and the conservative approaches has been kept alive. All of this does not match the parallel between the ALARA principle and the BEPU techniques which is discussed above.

References

Adu S., Horvatovic I., Darko E.O., Emi-Reynolds G., D'Auria F.
Application of best estimate plus uncertainty in review of

research reactor safety analysis. *Nucl. Tech. Radiat. Protect.* 2015;30(1):75–82.

Aksan S.N., D'Auria F., Staedtke H. User effects on the thermal-hydraulic transient system codes calculations. *Nucl. Eng. Des.* 1993;145: 1&2.

Aldemir T. In: Apostolakis G., ed. *Utilization of the cell-to-cell mapping technique to construct Markov failure models for process control systems*. New York: Elsevier; 1991:1431–1436.

Ambrosini W., Bovalini R., D'Auria F., Petrini P. *Advancements in evaluating accuracy of thermal-hydraulic codes calculations*. In: 9th Meeting of CSNI Task Group on the Status and Assessment of Codes for Transients and ECCS, Paris, 1–3 June; 1987.

Amendola A., Reina G. *DYLAM-1, A Software Package for Event Sequence and Consequence Spectrum Methodology*. Ispra: EUR-924, CEC-JRC; 1984.

ANS. In: International Meeting on Best-Estimate Methods in Nuclear Installation Safety Analysis (BE-2000), Washington, DC, 10–13 November; 2000.

ANS. In: International Meeting on Best-Estimate Methods in Nuclear Installation Safety Analysis (BE-2004), Washington, DC, 14–18 November; 2004.

Ashley, R., El-Shanawany, M., Eltawila, F., D'Auria, F., 1998. Good Practices for User Effect Reduction, OECD/CSNI Report NEA/CSNI/R(98)22, Paris.

Bonuccelli M., D'Auria F., Debrecin N., Galassi G.M. *A methodology for the qualification of thermal-hydraulic codes nodalizations*. In: International Topical Meeting on Nuclear Reactor Thermal Hydraulics (NURETH-6), Grenoble; 1993.

Bousbia Salah A., Vedovi J., D'Auria F., Ivanov K., Galassi G.M. Analysis of the Peach Bottom Turbine Trip 2 experiment by coupled Relap5-Parcs three dimensional codes. *Nucl. Sci. Eng.* 2004;148:337–353.

Bucalossi A. *Current use of Best Estimate Plus Uncertainty Methods on Operational Procedures Addressing Normal and Emergency Conditions*. Brussels: European Commission, JRC EUR 23717 EN; 2008.

Bucalossi A., Petruzzi A. Role of best estimate plus uncertainty methods in major nuclear power plant modifications. *J. Nucl. Sci. Technol.* 2010;47:8.

Bucalossi A., Petruzzi A., Kristof M., D'Auria F. Comparison between best-estimate-plus-uncertainty methods and conservative tools for nuclear power plant licensing. *Nucl. Technol.* 2010;172:29–47.

Cacuci D., Arslan E. Reducing uncertainties via predictive modeling: FLICA4 calibration using BFBT benchmarks. *Nucl. Sci. Eng.* 2014;176(3):339–349.

Camargo C., Galetti M.R., D'Auria F., Mazzantini O. *Exploitation of BEPU approach for licensing purposes, ENS-TOPSAFE*. In: International Topical Meeting on Safety of Nuclear Installations, Dubrovnik, 30 September–3 October; 2008.

D'Auria F. *The role of the experimental database in the validation of thermal-hydraulic system codes*. In: Invited at FLUIDOS 2001 – VII Int. Sem. on Recent Advances in Fluid Mechanics, Physics of Fluid and Associated Complex Systems, Buenos Aires, 17–19 October; 2001.

D'Auria F. Perspectives in system thermal-hydraulics. *Nucl. Eng. Technol.* 2012;44:855–870.

D'Auria F. *Nuclear thermal-hydraulics: from fundamentals to applications*. In: Conferencia pronunciada por el Dr. F. D'Auria el 18 de marzo (2013) en la Academia Nacional de Ciencias de Buenos Aires - Anticipo de Anales de la Academia Nacional de Ciencias de Buenos Aires, Buenos Aires; 2013.

D'Auria F. *Presentation at panel 'Data, Data Science and Data-Driven Thermal-Hydraulics'*. In: NURETH-16 Conf., Chicago, IL, 30 August–4 September; 2015.

D'Auria F., Debrecin N. *Perspectives in licensing and nuclear reactor safety technology*. In: Third International Scientific and Technical Conference "Innovative Designs and Technologies of Nuclear Power" (ISTC NIKIET-2014), Moscow, 7–10 October; 2014.

D'Auria F., Mazzantini O. The best estimate plus uncertainty challenge in the current licensing process of present reactors. *Sci. Technol. Nucl. Ins.* 2011;ID 958218.

D'Auria F., Debrecin N., Galassi G.M. Outline of the uncertainty methodology based on accuracy extrapolation (UMAE). *Nucl. Technol.* 1995;109(1):21–38.

D'Auria, F. (Project Coordinator), Bousbia Salah, A., Galassi, G.M., Vedovi, J., Reventos, F., Cuadra, A., Gago, J.L., Sjoberg, A., Yitbarek, M., Sandervag, O., Garis, N., Anher, C., Aragones, J.M., Verdù, G., Mirò, R., Hadek, J., Macek, J., Ivanov, K., Uddin, R., Sartori, E., Rindelhardt, U., Rohde, U., Frid, V., Panayotov, D., 2004. Neutronics/Thermal-Hydraulics Coupling in LWR Technology – CRISSUE-S: (Vol 1- Data Requirements and Databases Needed for Transient Simulations and Qualification), OECD/NEA Report No 4452, three volumes, Paris.

D'Auria F., Bousbia Salah A., Petrucci A., Del Nevo A. State of the art in using Best Estimate calculation tools in Nuclear Technology. *Nucl. Eng. Technol.* 2006;38:11–32.

D'Auria F., Muellner N., Parisi C., Petrucci A. BEPU approach in licensing framework, including 3D NK applications. In: Er M.J., ed. *New Trends in Technologies: Devices, Computer, Communication, and Industrial Systems*. 2010:197–216 © 2010, ISBN 978-953-307-212-8 (Chapter 11).

D'Auria F., Camargo C., Mazzantini O. The best estimate plus uncertainty (BEPU) approach in licensing of current nuclear reactors. *Nucl. Eng. Des.* 2012a;248:317–328.

D'Auria F., Camargo C., Muellner N., Lanfredini M., Mazzantini O. The simulation of I & C in accident analyses of nuclear

power plants. *Nucl. Eng. Des.* 2012b;250:656–663.

D'Auria F., Glaeser H., Kim M. *A vision for nuclear reactor safety*. In: 46th Jahrestagung Kerntechnik Annual Meeting on Nuclear Technology, Berlin, 5–9 May; 2015.

D'Auria F. *Proposal for training of thermal-hydraulic system codes users*. In: IAEA Spec. Meet. on User Qualification and User Effects on Accident Analysis for Nuclear Power Plants, Vienna; 1998.

D'Auria, F., Galassi, G.M., 2000. Methodology for the evaluation of the reliability of passive systems. University of Pisa Report, DIMNP - NT 420(00)-rev. 1, Pisa, October.

D'Auria, F., Galassi, G.M., Giannotti, W., 2001. Confirmatory safety analyses carried out by Relap5 and Cathare codes related to the Kozloduy VVER 440/230 unit no. 3, University of Pisa Report, DIMNP - NT 440(01)-rev.1, Pisa, November.

D'Auria F., Galassi G.M., Giannotti W., Petrucci A., Moussavian K., Pierro F., Lo Nigro A., Muellner N. *Qualification and application of coupled reactor cooling systems and containment nodalizations*. In: IAEA TM Progress in Development and Use of Coupled Codes for Accident Analysis, Vienna, 26–28 November; 2003.

Dusic M., Dutton M., Glaeser H., Herb J., Hortal J., Mendizábal R., Pelayo F. Combining insights from probabilistic and deterministic safety analyses in option 4 from the IAEA Specific Safety Guide SSG-2. *Nucl. Technol.* 2014;188:63–77.

EC-EURATOM, 2013. ASAMPSA2 Best Practices Guidelines for L2 PSA Development and Application, Volume 2 - Best Practices for the Gen II PWR, Gen II BWR. Extension to Gen III Reactors. Technical Report ASAMPSA2/WP2-3/D3.3/2013-35, Brussels.

Farmer F.R. Siting criteria – a new approach. *Atom.* 1967;128:152–170.

Galetti M.R., D'Auria F. *Licensing experience with BE in Brazil: regulatory audit analysis*. In: IAEA TM Use of a Best-Estimate Approach in Licensing With Evaluations of Uncertainties, Pisa, 12–16 September; 2005.

Galetti M.R., D'Auria F. *Questions arising from the application of best-estimate methods to the Angra-2 NPP licensing process in Brasil*. In: International Meeting on Best-Estimate Methods in Nuclear Installation Safety Analysis (BE-2000) IX, Washington, DC, 10-13 November; 2000.

Galetti M.R., D'Auria F. *Technical and regulatory concerns in the use of best estimate methodologies in LBLOCA analysis licensing process*. In: International Meeting on Best-Estimate Methods in Nuclear Installation Safety Analysis (BE-2004) IX, Washington, DC, 14–18 November.; 2004.

Glaeser H. *Evaluation of licensing margins of reactors using best estimate methods including uncertainty analysis*. In: IAEA Regional Workshop on Application of Deterministic Best Estimate (BE) Safety Analysis for Advanced NPP, AERB, Mumbai, 13–17 December; 2010.

Glaeser, H., 2011. BEMUSE Phase 6 Report – Status Report on the Area, Classification of the Methods, Conclusions and Recommendations, NEA/CSNI (2011)4, Paris.

Guyer, B.L., 2013. Nuclear Power Plant Performance Assessment Pertaining to Plant Aging in France and the United States, PhD Thesis at MIT, Boston, MA.

Han B.S., Bang Y.S., Kim K., Seul K.W., Woo S.W. *Prediction of number of breached rods following a LBLOCA of CANDU plants using a BEPU approach*. In: Int. Conf. ICAPP, Chicago, IL; 2012.

Hwang M., Bae S.W., Chung B.D. *APR1400 LBLOCA uncertainty quantification using Monte Carlo method and comparison with Wilks' formula*. In: Int. Conf. ICAPP, Chicago, IL; 2012.

IAEA, 2002. Accident Analysis for Nuclear Power Plants, IAEA Safety Reports Series, SRS No 23, Vienna.

IAEA, 2008. Best Estimate Safety Analysis for Nuclear Power Plants: Uncertainty Evaluation, IAEA Safety Report Series, SRS No 52, Vienna.

IAEA. *Deterministic Safety Analysis for Nuclear Power Plants*. Vienna: SSG-2; 2010a.

IAEA. *Development and Application of Level 2 Probabilistic Safety Assessment for Nuclear Power Plants*. Vienna: SSG-4; 2010b.

IAEA. *A Framework for an Integrated Risk Informed Decision Making Process*. Vienna: INSAG-25; 2011.

IAEA, 2015a. Consultancy Activity for Connecting DSA and PSA (un-published material), Vienna.

IAEA, 2015b. Technical Challenges in the Application and Licensing of Digital Instrumentation and Control Systems in Nuclear Power Plants, Nuclear Energy Series, NP-T-1.13, Vienna.

IAEA, 2016. Verification and Validation of System Codes for Nuclear Safety Analyses, draft to be issued, Vienna.

IAEA TM, 2013. TM on Best Estimate Plus Uncertainty (BEPU) Methods in Safety Analyses, Pisa, 10–14 June.

IAEA-TM, 2005. TM on Use of a Best Estimate Approach in Licensing with Evaluation of Uncertainties, Pisa, 12–16 September.

IAEA-TM, 2006. TM on Effective Integration of Deterministic and Probabilistic Safety Analysis in Plant Safety Management, Barcelona, 4–8 September.

IAEA-TM. *TM on Advanced Safety Assessment Methods for Nuclear Reactors*. Daejeon: KAERI; 2007 30 October–2 November.

IAEA-TM. *TM on the Use of Safety Margins and Advanced Safety Assessment Methods in Plant Modifications*. Budapest: HAEA; 2008 15–19 September.

IAEA-TM, 2009. TM on Application of Deterministic Best Estimate Safety Analysis, Pisa (I), 21–25 September.

IAEA-TM. *TM (in cooperation with OECD/NEA/CSNI) on Application of Advanced Safety Assessment Methods*. Bled: SNSA; 2010 7–11 June.

IAEA-TM, 2012. TM (in cooperation with OECD/NEA/CSNI) on Combining Insights From Deterministic and Probabilistic Safety Analyses, Pisa, 11–15 June.

Jafari J., D'Auria F., Kazeminejad H., Davilu H. Reliability evaluation of a natural circulation system. *Nucl. Eng. Des.* 2003;224:79–104.

Kalli H., Miettinen A., Purhonen H., D'Auria F., Frogheri M., Leonardi M. *Quantitative code accuracy evaluation of ISP 33*. In: 7th International Topical Meeting on Nuclear Reactor Thermal Hydraulics (NURETH-7), Saratoga Springs, NY, 10–15 September; 1995.

Kovtonyuk A., Fiori F., Petruzzi A., Kovtonyuk M., D'Auria F. *Use of qualified experimental database for a system code assessment*. In: International Topical Meeting on Nuclear Reactor Thermal-Hydraulics (NURETH-13), Pisa, 13–17 May; 2013.

KWU-Siemens, 1997. FSAR: Final Safety Analysis Report Central Nuclear Almirante Álvaro Alberto, Unit 2 - Rev. 0, Erlangen, September.

Marques M., Pignatelli J.F., Saignes P., D'Auria F., Burgazzi L., Muller C., Bolado-Lavin L., Kirchsteiger C., La Lumia V., Ivanov I. Methodology for the reliability evaluation of a passive system and its integration into a probabilistic safety assessment. *Nucl. Eng. Des.* 2005;235:2612–2632.

Martin R.P., Nutt W.T. Perspectives on the application of order-statistics in best-estimate plus uncertainty nuclear safety analysis. *Nucl. Eng. Des.* 2011;241:274–284.

Martinez-Quiroga V., Reventos F. The Use of System Codes in Scaling Studies: Relevant Techniques for Qualifying NPP Nodalizations for Particular Scenarios. *Sci. Technol. Nucl. Ins.* 2014 ID 138745.

Martinez-Quiroga V., Reventos F., Freixa J. Applying UPC scaling-up methodology to the LSTF-PKL counterpart test. *Sci. Technol. Nucl. Ins.* 2014 ID 292916.

Martorell S., Lazaro A., Marton I., Sanchez F., Villanueva J.F., Carlos S. A procedure to develop EBEPU methodology merging PSA based assumptions and BEPU methods. In: *Safety and Reliability of Complex Engineered Systems*. London: Taylor & Francis; 2015.

Mendizabal R., Pelayo F. *BEPU methodologies and plant technical specifications*. In: ASME 2010 3rd Joint US-European Fluids Engineering Summer Meeting, Montreal, Québec, Canada, 1-5 August; 2010.

Menzel F., Sabundjan G., D'Auria F., Madeira A. *Using of BEPU methodology in a final safety analysis report*. In: Int. Conf. INAC-ENFIR, Sao Paulo, 5–9 October; 2015.

Menzel F., Sabundjan G., D'Auria F., Madeira A. *Application of best estimate plus uncertainty (BEPU) methodology in a final safety analysis report (FSAR) of a generic plant*. In: 11th International Conference of the Croatian Nuclear Society, Zadar, 5–8 June; 2016.

Muftuoglu K., Ohkawa K., Frepoli C., Nissley M. *Comparison of realistic large break LOCA analyses of a 3-loop Westinghouse plant using response surface and statistical sampling techniques*. In: ICONE12, Arlington, VA, 25–29 April; 2004.

Nainer O., Pun-Quach D., Sermer P., Phan B., Hoppe F.M. A BEPU analysis separating epistemic and aleatory errors to compute accurate dry-out power uncertainties. *Nucl. Technol.* 2013;170–183.

OECD/NEA/CSNI. *A Separate Effects Test Matrix for Thermal-*

Hydraulic Code Validation: Phenomena Characterization and Selection of Facilities and Tests. Paris: OECD/GD (94) 82; . 1993; Vols. I and II.

OECD/NEA/CSNI, 1996. Code Validation Matrix of Thermo-Hydraulic Codes for LWR LOCA and Transients, CSNI Report 132-rev. 1, originally published in 1987, Paris.

OECD/NEA/CSNI, 1998. [Authors: Wickett, T. (Ed.), D'Auria, F., Glaeser, H., Chojnacki, E., Lage, C. (Lead Authors), Sweet, D., Neil, A., Galassi, G.M., Belsito, S., Ingegneri, M., Gatta, P., Skorek, T., Hofer, E., Kloos, M., Ounsy, M., Sanchez, J.I]. Report of the Uncertainty Methods Study for Advanced Best Estimate Thermal-Hydraulic Code Applications, Vols. I & II OECD/CSNI Report NEA/CSNI/R(97)35, Paris.

OECD/NEA/CSNI. *BEMUSE Phase 6 Report – Status Report on the area, Classification of the Methods, Conclusions and Recommendations*. Paris: NEA/CSNI (2011)4; 2011 see also Glaeser, 2011.

OECD/NEA/CSNI. *Workshop on best estimate methods and uncertainty evaluations*. In: Proceedings [Workshop held in Barcelona, Spain, 16–18 November 2011], NEA/CSNI (2013)8, Paris; 2013.

OECD/NEA/CSNI. *PREMIUM Benchmark Report*. to be issued Paris: NEA/CSNI; 2016.

OECD/NEA/CSNI-TM. In: Workshop on Evaluation of Uncertainties in Relation to Severe Accidents and Level 2 PSA, Aix-en-Provence, 7–9 November; 2005.

OECD/NEA/CSNI-TM. In: Workshop on Best Estimate Methods and Uncertainty Evaluations, UPC and CSN, Barcelona, 16–18 November; 2011.

Petruzzi A., D'Auria F. *Supporting qualified database for V&V and uncertainty evaluation of best-estimate system codes*. In: ASME-JSME Int. Conf. on Nuclear Engineering (ICONE-22), Prague, 7–11 July; 2014.

Petruzzi A., D'Auria F. Standardized consolidated calculated and reference experimental database (SCCRED): a supporting tool for V&V and uncertainty evaluation of best-estimate system codes for licensing applications. *Nucl. Sci. Eng.* 2016;182(1):13–53.

Petruzzi A., D'Auria F., Bajs T., Reventos F. *International training program in support of safety analysis: 3C S.UN.COP - Scaling, uncertainty and 3D thermal-hydraulics/neutron-kinetics coupled codes seminars*. In: International Congress on Advances in Nuclear Power Plants (ICAPP 2011), Nice, 2–6 May; 2011 Paper 11451.

Petruzzi A., Fiori F., Kovtonyuk A., D'Auria F. *Supporting qualified database for uncertainty evaluation*. In: International Congress on Advances in Nuclear Power Plants (ICAPP 2012), Chicago, IL, 24–28 June; 2012 Paper 12085.

Petruzzi A., Cherubini M., Lanfredini M., D'Auria F., Mazzantini O. The BEPU evaluation model with RELAP5-3D for the licensing of the Atucha-II NPP. *Nucl. Technol.* 2016;193:113–160.

Pla P., Tanarro J., Ammirabile L., Strucic M., Wastin F. *Long term preservation of knowledge in the area of nuclear thermal-hydraulics – The new STRESA database*. In: 11th Int. Conf. of Croatian Nuclear Society, Zadar, 5–8 June; 2016.

Ponomarenko G.L., Ryzhov S.B., Bykov M.A., Moskalev A.M. *Use of BEPU technique for analyses of BDBAs with cooling in WWER-1000*. In: Int. Conf. ICONE-17, Brussels; 2009.

Pradhan S.K., Bang Y.S. *Best estimate prediction of NFR with uncertainty following a LBLOCA of CANDU plants*. In: KNS Spring Meeting, Taebaek, 26–27 May; 2011.

Prošek A., Mavko B. *Review of best estimate plus uncertainty methods of thermal-hydraulic safety analysis*. In: Int. Conf. Nuclear Energy for New Europe, Portoroz; 2003.

Rao R.S., Kumar A., Gupta S.K., Lele H.G. Uncertainty and

sensitivity analysis of TMI-2 accident scenario using simulation based techniques. *Nucl. Eng. Technol.* 2012;44(7):807–816.

Shih C., Yang J.H., Wang J.R., Lin H.T., Chiang S.C., Liu C.C., Tien K. *BEPU Analysis and Benchmark With IIST 2% SBLOCA Experiment Using TRACE/DAKOTA*. Washington, DC: USNRC NUREG/IA 0456; 2015.

Stanev I., D'Auria F. *Analysis of LOCA D=200 mm for Kozloduy – Units 3&4 with Relap5/mod3.2 and Cathare Codes. Evaluation of the Results Uncertainty*. In: IAEA TCM on Safety Margins of Operating Reactors and Implications for Decisions Makers Including Consideration of Uncertainties of Analysis, Vienna, 15–19 October; 2001 (also IAEA TECDOC No 1332, Jan 2003 – ISBN 92-0-118102-7).

Unal C., Williams B., Hemez F., Atamturktur S.H., McClure P. Improved best estimate plus uncertainty methodology, including advanced validation concepts, to license evolving nuclear reactors. *Nucl. Eng. Des.* 2011;241(5):1813–1833.

UNIPI-GRNSPG, 2008. A Proposal for Performing the Atucha II Accident Analyses for Licensing Purposes – The BEPU Report – Rev. 3, Pisa [endorsed 2010 by Regulatory Authority in Argentina].

USNRC. *Transient and Accident Analysis Methods*. RG 1.203 Washington, DC: USNRC; 2005.

USNRC. *Combined License Application for Nuclear Power Plants (LWR Edition)*. RG 1.206 Washington, DC: USNRC; 2007.

USNRC. *Standard Review Plan for the Review of Safety Analysis Reports for Nuclear Power Plants*. Washington, DC: NUREG 0800; 2013.

Yamaguchi A., Mizokami S., Kudo Y., Hotta A. *Uncertainty and conservatism in safety evaluations based on a BEPU approach*. In: NURETH-13 Conf., Kanazawa; 2009.

Zhang J., Schneidesch C., Segurado J. *Towards an industrial*

application of statistical uncertainty analysis methods to multi-physical modelling and safety analyses. In: Proc. OECD/CSNI Workshop on Best Estimate Methods and Uncertainty Evaluations, Barcelona, Spain, NEA/CSNI/R(2013)8/Part2, Paris; 2011.

Zimmermann M.A. *Safety margin assessment (SM2A): stimulation for further development of BEPU approaches.* In: OECD/NEA/CSNI Workshop on Best Estimate Methods and Uncertainty Evaluations, Barcelona, November; 2011.

Applications of SYS TH codes to nuclear reactor design and accident analysis

F. D'Auria; G.M. Galassi University of Pisa, Pisa, Italy

Abstract

Envisaged Nuclear Power Plant transient performances are translated via experiments and expert judgement into lists of accidents. Accident scenarios are at the origin of phenomena. Phenomena are characterized by parameters or variables. The parameter values can be translated into requirements for predictive capabilities in thermal-hydraulics. The safety acceptance criteria consist of threshold parameter values. These are established by logical processes typically independent upon thermal-hydraulics knowledge. A global vision of nuclear reactor thermal-hydraulics is provided in the chapter from the side of phenomena and accident scenarios: 12 reactor types are considered for the characterization of 47 accident scenarios cross-linked with 113 phenomena and 15 sets of “homogeneous” variable time trends.

Keywords

Design Basis Accident (DBA); Reactor thermal-hydraulic performance; Accident scenarios; Phenomena in thermal-hydraulics; Accident analysis; Parameters representing phenomena; List of accidents; Acceptance criteria; Safety margins

Acronyms

ABWR advanced boiling water reactor

AC alternate current

ACC accumulator

ADS automatic depressurization system

AFW auxiliary feedwater

AM accident management

AMP accident management procedure

ANSI American National Standards Institute

AOO anticipated operational occurrence

AP1000 advanced pressurized water reactor (Westinghouse design)

APR1400 advanced pressurized water reactor (KEPCO design)

ATLAS integral simulator for PWR in Korea

ATWS anticipated transient without scram

BAF bottom of active fuel

BC bubble condenser (containment type) facility in Russia

BD blowdown

BD-SAT saturated blowdown

BD-SBC subcooled blowdown

BIC boundary and initial conditions

BL broken loop

BOC beginning of cycle and bottom of core (elevation of FA hydraulic entrance)

BOL beginning of life

BOP balance of plant

BWR boiling water reactor

CANDU Canadian Deuterium Uranium Reactor designed in Canada

CCF counter current flow

CCFL counter current flow limitation

CCVM CSNI code validation matrix

CET core exit thermocouples

CHF critical heat flux

CL cold leg

CLL collapsed liquid level

CMT core make-up tank(s)

CONT containment

CRE control rod ejection

CRGT control rod guide tube

CSNI Committee on the Safety of Nuclear Installations

CVCS Chemical and Volume Control System

DBA design basis accident

DC downcomer

DCC direct contact condensation

DEGB double-ended guillotine break

DEHL double-ended hot leg (break)

DG diesel generator

DiD defense in depth

DNB departure from nucleate boiling

DWI density wave instability

ECCI emergency core cooling
injection

ECCS emergency core cooling system

EOC end of cycle

EOP emergency operating
procedures

EPR European Pressurized Water
Reactor (AREVA design)

ERVCS External Reactor Vessel
Cooling System

ESF engineered safety features

FA fuel assembly

FC fuel channel

FCB fuel channel blockage

FCO forced convection

FP fission products or fission power

FWLB feed water line break

GF gravity feed

HEBR header break

HFP hot full power

HL hot leg

HOSG horizontal steam generator

HPCS high-pressure core spray

HT heat transfer

HTC heat transfer coefficient

HZP hot zero power

I imposed (related to TSE)

I & C instrumentation and control

IAC interim acceptance criteria

IAFB inverted annular film boiling

IBLOCA intermediate break LOCA,
see also MBLOCA

IC isolation condenser

IHE intermediate heat exchanger

ILOCA interfacing LOCA

IRWST in containment reactor water storage tank

ISP international standard problem

ITF integral test facility

JP jet pump

KWU KraftWerk Union (NPP designer)

LBLOCA large break LOCA

LCC/SW loss of component cooling service water

LOBI integral facility for PWR in Italy

LOCA loss of coolant accident

LOFA loss of flow accident (also
MCP-trip)

LOFW loss of feedwater

LOOSP loss of on- and off-site power

LP lower plenum

LPCI low-pressure coolant injection

LPCS low-pressure core spray

LPIS low-pressure injection system

LS loop seal

LSTF integral facility for PWR in
Japan

LWR light water reactor

MBLOCA medium break LOCA, see also IBLOCA

MCP main coolant pump

MI mass inventory

MOC middle of cycle

MOX Mixed Uranium Plutonium nuclear fuel

MPTR multiple pressure tube rupture

MSIV main steam isolation valve

MSLB main steam line break

MSSV main steam safety valves

nc noncondensable

NC natural circulation

NCO natural convection

NEA Nuclear Energy Agency

NPP Nuclear Power Plant

NPSH Net Positive Suction Head

OECD Organization for Economic
Cooperation and Development

ONB onset of nucleate boiling

OTSG once through steam generator

PCCS passive containment cooling system

PCEI parallel channel effects and instabilities

PCT peak cladding temperature

PD pressure drop

PDGD pressure drop at geometric discontinuity

PH phenomenon

PHW phenomenological window

PHWR pressurized heavy water reactor designed by KWU (G)

PIE postulated initiating event

PIUS process intrinsic ultimate safety (reactor design concept)

PKL integral facility for PWR in Germany

PORV pilot operated relief valve

PRHR passive residual heat removal

PRISE primary to secondary leakage (in VVER)

PRZ pressurizer

PS primary side (of RCS) or primary system

PSA Probabilistic Safety Assessment

PSB integral facility for VVER in Russia

PSD power spectral density

PSP pressure suppression pool

PT pressure tube

PTS pressurized thermal shock

PWR pressurized water reactor
(equipped with UTSG)

PWR-O PWR equipped with OTSG

PWR-V PWR equipped with HOSG
(VVER type)

QF quench front

R resulting (related to TSE)

RBMK boiling water cooled and

graphite moderated reactor designed
in Russia

RC reactor cavity

RCS reactor coolant system (includes
PS and SS in PWR)

RE reflood

RF refill

RHR residual heat removal

RIA reactivity initiated accident

RL recirculation loop

RPV reactor pressure vessel

RST rod surface temperature

RTA relevant thermal-hydraulic aspect

SAMP severe accident management procedure

SANB saturated nucleate boiling

SBLOCA small break LOCA

SBO station blackout (or loss of on-site power)

SETF separate effect test facility

SG steam generator

SGTR steam generator tube rupture

SH-D shutdown (accident conditions)

SIS safety injection system

SIT safety injection tank (see also accumulator)

SMR small modular reactor

SNB subcooled nucleate boiling

SRV steam relief valves

SS secondary side (or secondary system)

SSC structures, systems, and components

SYS TH system thermal-hydraulics

TAF top of active fuel

TMI-2 Three Mile Island (unit 2)

TOC top of core (top of core upper plate, above TAF)

TPCF two-phase critical flow

TSE time sequence of events

TT turbine trip

UCSP upper core support plate (see also UTP)

UH upper head

UP upper plenum

USAEC United States Atomic Energy Commission

USNRC United States Nuclear
Regulatory Commission

UTP upper tie plate (see also UCSP)

UTSG U-tubes steam generator

VVER water-cooled water-
moderated energy reactors designed
in Russia

WDVB wetwell-to-drywell vacuum
breakers

WWER see VVER

Acknowledgments

The authors wish to acknowledge the invaluable effort made by A. Capperi from University of Pisa for having drafted most of the figures in the text. He had to become aware of the connection between accident scenarios and phenomena.

Chapter foreword

The connection between thermal-hydraulics and accident analysis constitutes the framework for this chapter. In order to connect the fundamental thermal-hydraulic

concepts, noticeably the models and the equations, with the transient performance of Nuclear Power Plants (NPP), a virtual top-down or bottom-up approach can be pursued.

Within the former approach envisaged NPP, accident performances, hereafter referred as accident scenarios, are translated via experiments and expert judgment into lists of accidents, then into phenomena applicable to each accident, then into parameters or variables characterizing physical quantities, and finally into requirements for predictive capabilities in thermal-hydraulics. The safety acceptance criteria, established by logical processes independent upon thermal-hydraulics knowledge, constitute a necessary element to achieve the goals of the approach.

Within the latter approach competences developed in thermal-hydraulics, also derived from NPP design and safety technology, are applied to estimate the transient performances of reactors. In this case the knowledge of fundamental physics triggers the process for characterizing the thermal-hydraulic evolutions of two-phase fluids during accidents. The safety acceptance criteria need proper consideration in this approach, too.

The first approach provides the roadmap for this chapter. However, an interaction with the second approach cannot be avoided.

The process of connecting calculated variables and phenomena could be done using a couple of accident scenarios (i.e., not 47 scenarios as used in the text) with full calculation details. This does not include the description of scenarios and does not give an idea of the interest toward accident scenarios by the scientific community.

Very many acronyms are used throughout the text (see also Section 15.5.1). In a number of cases, the acronym is not identified the first time it is used (this is mostly the case of tables and figures). Although an attempt is made to use acronyms recognized in the literature, the reader is recommended to become familiar with the acronyms listed at the end of the chapter.

The present chapter constitutes the tip of the virtual pyramid of knowledge developed in nuclear thermal-hydraulics. Therefore all chapters of the book have some connection with the present one. This is specifically true for **Chapter 6** where phenomena are characterized and for **Chapter 11** where the features of system codes (i.e., needed to predict accident scenarios) are discussed. The bases for code application, noticeably V&V, scaling, and uncertainty discussed in **Chapter 13** are

also important here. However, uncertainty of predictions for the transient scenarios presented in this chapter is not under consideration.

15.1 Introduction

The key motivation for nuclear thermal-hydraulics is the design of nuclear reactors and the safety demonstration. Water cooled reactors are of concern in the book.

Thermal-hydraulic design of nuclear reactors implies, or has implied, for thermal-hydraulics support (to other disciplines) in

- (a) selecting the components, e.g., core, pumps, steam generators, turbine, condenser, needed to transform the fission power into electrical power;
 - (b) fixing the layout of the whole system, e.g., mutual position between core (heat source) and steam generator (heat sink), pressurizer location also to allow for spray line, pump location to maximize the Net Positive Suction Head (NPSH) from the loop, condenser location to optimize the thermal efficiency;
 - (c) searching for the optimum configuration of individual components, e.g., the core constituted by thin fuel pins, the helicoidally shaped steam separators to facilitate steam liquid separation by inertia forces;
 - (d) fixing the normal operational parameters, like working pressure, maximum and average linear heat flux for the fuel pins in the core, pressure drops, level in the pressurizer, in the down-comer of BWR and of steam generators in PWR;
 - (e) designing each component, e.g., the fuel pin, the number of tubes in steam generators, the size of hot and cold legs, the flow paths inside the pressure vessels, as well as the size and the number of headers (in pressure tubes reactor types like CANDU and RBMK); and
 - (f) determining expected loads, e.g., pressure and pressure drops including pressure wave propagation originated by opening/closure of valves, thermal stresses originated by cooling/heating rates and thermal fatigue.
- Safety demonstration of nuclear reactors implies, among the other things:
- (g) the calculation of the transient performance of reactors;
 - (h) namely, the proof of suitable design/construction for emergency core cooling systems (ECCS), e.g., the volume and the number of accumulators, and, more in

general of engineered safety features (ESF), e.g., the pressure set point for the operation of steam relief valves (SRV), the closure time for main steam isolation valves (MSIV);

(i) the design of emergency operating procedure (EOP) and the accident management procedure (AMP);

(j) an interaction with safety and licensing processes to fix requirements and procedures for the related analyses, e.g., list of design basis accidents (DBA), acceptable probability for failures and demonstration that consequences of failure are within the acceptability domain.

The above list of thermal-hydraulic applications, incomplete and/or not comprehensive, may be taken as another demonstration, or even one origin, for the universe in nuclear thermal-hydraulics introduced in the Chapter 1. The impossibility to describe all applications of nuclear thermal-hydraulics in one chapter (even though in one book) is also a consequence from the list.

The complexity of some topics, namely those which require the analysis of accident performances of nuclear reactors, imposed the development of system thermal-hydraulic (SYS TH) codes as outlined, for instance, in Chapters 2 and 10.

The scope for the present chapter is restricted to the transient analyses in Light Water Reactors (LWR), i.e., BWR and PWR including evolutionary and similar design like EPR, AP1000, ABWR, AP1400, and VVER, partly accomplishing the content of item (g), as listed previously; in a few cases transient analyses of CANDU, RBMK, and PHWR (Pressurized Heavy Water Reactor equipped with vertical channels core and pressure vessel) are presented. The scope can be further specified as “addressing the capabilities of the SYS TH codes (discussed in Chapter 11), constituting a cross-connection among accident scenarios (DBA area), and results of those codes and phenomena (discussed in Chapter 6, see also Section 15.1.1).” The consideration of Beyond DBA (BDBA) conditions is within the scope for the chapter till the situation where irreversible degradation of core or the loss of geometric integrity occurs. Therefore, proofs of qualification of the discussed SYS TH code calculated results and the evaluation of uncertainty of calculations are outside the scope for the present chapter.

15.1.1 The connection with phenomena

Thermal-hydraulic phenomena expected to occur in LWR (and VVER) in DBA conditions have been classified in the documents OECD/NEA/CSNI (1993) and

OECD/NEA/CSNI (1996a), respectively, related to separate effect test facilities (SETF) and integral test facilities (ITF), see also OECD/NEA/CSNI (2001), related to VVER (as also discussed Chapter 2). Containment-related phenomena can be found in the report OECD/NEA/CSNI (1999). So-called computer code validation matrices (CCVM) have been created based on the correspondence between phenomena and experiments. Therefore, the concerned phenomena have been the object of experimental investigations and are considered in various reports, papers, or textbooks, see for instance, the report (USNRC, 1988), the CSNI documents dealing with International Standard Problems (ISP) (e.g., OECD/NEA/CSNI-ISP, 2000, and more recently OECD/NEA/CSNI-ISP-50, 2012), the textbook (Levy, 1999), and the papers (like D'Auria and Galassi, 1990a; D'Auria and Ingegneri, 1997; Del Nevo et al., 2012a,b; Mascari et al., 2012; Reventos et al., 2012).

The idea here is to create a correspondence between thermal-hydraulic phenomena, variables to characterize the phenomena, and results of code calculations related to accident analyses.

15.1.2 Objective and structure

The objective for this chapter is to close a logical circle, the starting point of the circle being the definitions and the fundamental concepts given in Chapter 3. These are followed by needs in nuclear reactor design and safety (Chapter 4), expected phenomena for DBA in LWR and advanced water cooled designs (Chapter 6), equations and models (Chapters 5, 7–10), and by computational tools which make use of the equations and models (e.g., Chapters 11 and 12 where applicable). In this connection Chapters 1 and 2 provide a general framework suitable for the understanding of the nuclear thermal-hydraulics discipline; the remaining two chapters discuss the conditions for the applicability of those codes to the accident analysis, noticeably, the needs for qualification and the need to supplement the calculation results by uncertainty (Chapter 13), and the connection with the licensing process (Chapter 14).

Additional objective is to provide essential information to the reader in relation to the links among phenomena, the predicted accident evolutions in nuclear reactors and the variables, or time trends or parameters, which are the direct outcomes of SYS TH code calculations and are suitable for the characterization of phenomena.

Although a complex process is pursued to establish those links, it seems worthwhile to emphasize that only a narrow sector of system thermal-hydraulics is

involved in this chapter. This is the item (g) from the list above (i.e., safety analysis), supplemented by one noticeable example from the item (d) (i.e., design analysis) (e.g., see Section 15.4.12.1).

Four main tables (plus one) have been created as bases for the document:

- **Table 15.1** deals with a minimum-reasonable list of accidents or transient scenarios resulting from NPP calculations performed by system thermal-hydraulic codes.

Table 15.1

List of NPP accident scenarios calculated by system thermal-hydraulics codes

--

- **Table 15.2** deals with the full list of transient thermal-hydraulic phenomena derived from existing OECD/NEA/CSNI and IAEA documents.

Table 15.2

List of phenomena

--

- **Tables 15.3 and 15.4** (the last one supported by **Table 15.5**) deal with the links *phenomena to accident scenarios* and *phenomena to parameters*.

Table 15.3

Cross-link between phenomena and accident scenarios

--

Table 15.4

Phenomena and variables calculated in accident scenarios

--

Table 15.5

**List of “equivalent ADDED accident SCENARIOS” for
phenomena characterization**

--

*, Thermal-hydraulic details of CRGT; **, fundamental blowdown; +, various phenomena analyzed; ++, design principles of OTSG.

Tables 15.1 and 15.2 are embedded into Section 15.2 which also constitutes the link with Chapter 6 and with the licensing/safety processes for NPP (partly discussed in Chapter 14).

Tables 15.3–15.5 constitute the key content of Section 15.3: variables (or time trends) are used to characterize transient scenarios (e.g., listed in Table 15.1) and phenomena (e.g., listed in Table 15.2).

The information gathered in Tables 15.1–15.5 is used in Section 15.4 of the present chapter for characterizing the accident scenarios and for connecting those accident

scenarios with phenomena and parameters.

15.2 Accident scenarios and phenomena

Events, or accidents, or transients, or, better, postulated initiating events (PIE) are mandatory elements to address the safety requirements for NPP issued by Regulatory Authorities. The acceptance criteria for the design of the ECCS (see e.g., USAEC, 1971, already discussed in **Chapter 2**) constitute a suitable example: the fulfillment of those criteria must be based upon expected transients for the concerned NPP unit. Thus, PIE are introduced.

At their origin PIE have a weak link or no link at all with thermal-hydraulics. However, it comes out that PIE unavoidably cause single- or two-phase coolant evolutions, which determine the NPP performance and allow the definition of safety margins. Then, PIE are characterized by phenomena: this establishes the tight link between safety requirements, PIE, and nuclear thermal-hydraulics.

Insights into the concept of PIE and the origins of PIE are discussed in **Sections 15.2.1–15.2.5**, primarily derived from IAEA (2002a, 2003). Furthermore a list of events suitable for the purpose of the present chapter (i.e., showing the link between PIE and nuclear thermal-hydraulics) is provided in **Table 15.1**, **Section 15.2.3**. The list of phenomena and the connection between each phenomenon and at least one NPP type can be derived from **Table 15.2** in **Section 15.2.5**.

15.2.1 Establishing PIE

The basic objective for nuclear safety, as already discussed in **Chapter 2**, is the protection of individuals, the society, and the environment from radiations. In order to achieve the objective, the following fundamental safety functions have to be performed (not an exhaustive list):

- (a) control of reactivity;
- (b) removal of residual heat from the fuel; and
- (c) confinement of radioactive materials.

Control of reactivity generally means all the measures taken to avoid inadvertent nuclear criticality, loss of reactivity control, inadvertent power excursions, or reduction in shutdown margin. Removal of heat from the nuclear fuel necessitates

that adequate cooling of the fuel be ensured. Confinement of the radioactive materials implies the introduction of suitable barriers and the demonstration that those barriers remain effective under selected circumstances, including the consequences of PIE.

The knowledge and the understanding of the framework for the defense in depth (DiD) (e.g., IAEA, 1996, 2005a) including the concepts of prevention and mitigation are essential for a robust and consistent description of the current status of nuclear safety and for industrial applications. This is well beyond the purpose for this section; rather snap-shot information is provided hereafter in relation to the process to establish PIE (interested reader may refer to the listed references).

According to INSAG-10 (IAEA, 1996), DiD consists of a hierarchical deployment of different levels of equipment and procedures in order to maintain the effectiveness of physical barriers placed between radioactive material and workers, the public, or the environment, during normal and off-normal operation. To this aim several successive physical barriers (generally, five levels are recognized) for the confinement of radioactive material are in place in any NPP: should one level fail, the subsequent level comes into play.

Therefore one may state, IAEA, 2002a: “Once a release of radioactive material is foreseen, either as a routine part of normal operation or as the consequence of an accident sequence, this release will be controlled for the normal operation case and limited or delayed, as much as possible, for the accident condition case.”

The need to prove the safety of NPP in conditions different from the nominal operation of the system, open the way to the definition of PIE. The consideration of the levels of DiD implies the derivation and the fulfillment of the concepts of prevention and mitigation and, among the other things, impose the way for the design and the optimization of ESF and ECCS.

PIEs, either incidents or accidents, may therefore be initiated whenever a failure, malfunction or faulty operation of a system or component creates harm or endangers one or more of the established safety functions. Thus, the term PIE refers to an unintended event, including operating errors or equipment failures, which, directly or indirectly, endanger fundamental safety functions. Such an event necessitates protective actions (automatic, manual, on-site, and/or off-site) to prevent or to mitigate the undesired consequences to plant equipment, plant personnel, the public, and the environment.

For the purposes of accident analysis, it is reasonable to group all initiating events

into categories. There are different sets of criteria for grouping, thus leading to different event lists. The grouping of transients aims at constituting consistent sets of events which form the DBA envelope. Grouping possibilities (IAEA, 2002a) include

- (a) principal effect on potential degradation of fundamental safety functions;
- (b) principal cause of the initiating event;
- (c) frequency and potential consequences of the event; and
- (d) relation of the event to the original NPP design (for existing plants).

Each category of events is typically subdivided into several more specific events. In some cases a deeper event subdivision is adopted: events which are expected to occur during the plant lifetime are called anticipated operational occurrences (AOO) or anticipated transients. AOO which are associated with the failure of the scram system are called anticipated transients without scram (ATWS).

Grouping based on the degradation of safety functions implies listing of safety functions and the search for mechanisms which harm or damage the integrity of the functions.

Grouping by principal cause of the initiating events considered in the reactor design brings, for instance, to the categories exemplified in Table 15.1.

Grouping by frequency and potential consequences implies a preliminary PSA study, where probability of the event and consequences are estimated. A relationship between probability, consequence, and acceptance criteria is established for each event: the combination of high probability and high consequence for an assigned event is not allowed. Design modifications are needed should such a situation occur.

Grouping in relation to the original plant design reveals necessary in order to upgrade the safety of an existing NPP according to new regulations, new computational methods, or needs for design modernization (e.g., power uprating, replacing of key components, etc.).

The achievement of a meaningful list of PIE implies the consideration of different (all) grouping possibilities, including the last one when applicable. A large number of individual accident scenarios may result such that a detailed computational analysis may not reveal practicable. Limiting scenarios bounding and enveloping

phenomena and ranges of variations of parameters which characterize those phenomena are typically preselected before full application of calculation procedures (e.g., BEPU, see Chapter 14). In the process of identifying limiting scenarios, the following substeps are recommended (IAEA, 2002a):

- accident analyses done for similar designs;
- engineering judgment and expert reviews;
- “bottom-up” methods in reliability analysis such as failure modes and effects analyses;
- real operating experience to determine the reliability of equipment;
- “near misses” or precursor events; and
- actual events occurred in NPP similar to the concerned one.

15.2.2 Acceptance criteria

Acceptance criteria at the same time constitute the motivation for the analysis of PIE and drive the analysis by imposing precision targets and in some cases methods for the analysis. Acceptance criteria are full responsibility of Regulatory Authority and not the subject for the present book (or chapter). However, because of their importance, a few notes derived from IAEA (2002a) are reported as follows.

Acceptance criteria set: (a) the numerical limits on the values of predicted parameters, (b) the conditions for plant states during and after an accident, (c) the performance requirements on systems, and (d) the requirements on the need for, and the ability to credit, actions by the operator.

Acceptance criteria, as already discussed, are applied to licensing calculations whatever its type (i.e., conservative and best estimate). In the case of BEPU approach (Chapter 14), specific additional criteria may be needed, e.g., criteria for accepting the validation of a computational tool and of the analysts, criteria for deciding the applicability of uncertainty method when wide safety margins are predicted from the “nominal” BE calculation. These criteria may be developed by the analysts on the behalf of the designer or owner for the NPP and approved by the regulatory body.

The analyst may set analysis targets to limit economic loss from AOO. An

example would be the prevention of fuel dry-out for a loss of flow.

As a key feature, more stringent criteria apply for events with a higher probability of occurrence: for instance if DBA and AOO are distinguished based on their frequency, a “no consequential containment damage” criterion is appropriate for DBA, whereas a “no cladding damage” criterion would be appropriate for AOO; similarly, a “no boiling crisis” criterion is appropriate for AOO whereas “cladding temperature less than 1204°C” criterion (in addition to others) is used for LOCA DBA.

In relation to basic acceptance criteria fixed by analysts (on the behalf of vendor/designer/owner), which are more restrictive than the legal acceptance criteria fixed by Regulatory Authorities, the following can be mentioned:

(a) The dose to individuals and the public, different for AOO and DBA. These may be given together with the specifications for the duration of the calculated exposure and for the atmospheric conditions to be assumed.

(b) An event must not generate a more serious plant condition without an additional independent failure (having low or acceptable probability). Thus an AOO must not evolve into a DBA and a DBA must not evolve into a BDBA or a severe accident.

(c) Systems necessary to mitigate the consequences of an accident must not be made ineffective because of conditions caused by the accident, e.g.:

(c1) The containment must not be damaged in an LOCA to the extent that it cannot perform its function because of

- the dynamic effects of whipping of primary coolant pipes;
- jet forces from the break;
- pressure generated internally by the break or by combustion of hydrogen;
- pressure within internal compartments; and
- high temperatures due to the break or due to combustion of hydrogen.

(c2) ECCS pipes must not be damaged by the dynamic forces in an LOCA to the extent that the system becomes ineffective.

(c3) If the functioning of any shutdown (non-ECC) system is necessary in an LOCA, it must not be damaged by the dynamic effects of the pipe break.

(d) Systems designed for accident mitigation must not be the origin for the plant components to loads or conditions that would exceed the design or failure limits for the accident condition, e.g., thermal and mechanical loads, water hammer, and pressure wave induced loads upon RPV internals.

(e) The pressure in the coolant systems must not cause a pressure boundary failure in addition to the accident (e.g., stuck open SRV).

(f) In the case of AOO the probability of failure of the fuel cladding resulting from a heat transfer crisis must be insignificant.

(g) For DBA the fuel damage must be limited in order to ensure coolable core geometry; dispersal of fuel and fission products must be prevented in case of reactivity initiated accidents (RIA).

(h) If operator intervention is necessary in an event, it must be demonstrated that the operator has sufficient time, adequate EOP and corresponding training, and reliable information available to initiate and complete the intended action.

(i) Sufficient time and adequate means must be available to implement AMP in BDBA conditions, i.e., attempting to prevent the loss of geometric integrity for the core (similar conditions apply for the management of severe accident, not considered here).

(j) Accident analysis needs to be continued to the point in time that the plant can be shown to have reached a safe and stable shutdown state, so that:

- the core remains subcritical;
- the core remains in a coolable geometry and there is no further fuel failure (i.e., in the long term, before possible fuel removal from the RPV);
- thermal power is being removed by the appropriate heat removal systems till possible fuel removal from the RPV; and
- releases of fission products from the containment have ceased, or an upper bound of further releases can be estimated.

Furthermore, proper attention shall be given to ECCS acceptance criteria other

than related to PCT. This may require additional specifications (i.e., acceptance criteria not necessarily part of regulatory documents), like, in case of LOCA:

- keeping structural integrity of fuel following unavoidable ballooning of clad and coolable geometry for fuel channels;
- keeping structural integrity for the RPV internals (e.g., tolerable stresses in case of pressure wave propagation from the break, as already mentioned);
- assuming loss of shutdown capability by control rods, thus ensuring suitable boron concentration for the long term;
- in relation to tolerable thickness for crud and oxide; and
- in relation to maximum burn-up and percentage of mixed uranium-plutonium (MOX) fuel.

The role of nuclear thermal-hydraulics is evident to show fulfillment of the listed acceptance criteria. Some of those criteria are assessed in safety analysis; others may be the subject of specific design calculations.

Examples of criteria (e.g., 64 generalized design criteria) can be found in USNRC (1995). Four categories of events together with selected acceptance criteria are defined on the basis of event frequency and potential radiological consequences (ANSI, 1995). Acceptance criteria applicable for WWER reactors are summarized for two categories of event (IAEA, 1997): AOO and “postulated occurrences.”

15.2.3 The accident scenarios: AOO and DBA

A set of PIE representative for the envelope of AOO and DBA in NPP is considered in this section. As already mentioned:

- the idea is to close a virtual circle including accident scenarios, phenomena, and thermal-hydraulic variables;
- LWR transients (i.e., primarily PWR and BWR) with a few examples of other reactor types which adopt water as coolant (i.e., CANDU, VVER, RBMK, and PHWR) are selected.

Table 15.1 (5 columns and 45 rows) has been created with the objective to gather a

comprehensive set of accident scenarios (i.e., according to IAEA, 2002a), which is suitable for characterizing phenomena (i.e., based on the list derived in Chapter 6, see also below). Namely, the column 1 of the table identifies the sections of the present chapter which include the categories of accident scenarios; in columns 2 and 5 individual NPP accident scenarios are reported resulting from calculations described in the literature; columns 3 and 4 deal with elements to characterize the selected individual NPP accident scenarios.

An attempt has been made, in the selection of documents/references associated with accident scenarios (column 5 of the table), to encompass the widest possible range of variation for the nature of the document and for the target of the NPP calculation. Therefore, documents have been selected in the last column ranging from journal papers, to internationally agreed reports (e.g., IAEA and OECD), to industry analysis reports, to technology/research project reports, to reports supporting regulations, without distinguishing between simplified and sophisticated approaches. Furthermore no emphasis is given to the quality of calculations; otherwise recent documents are preferred to “old” documents, but examples of old documents are included. The common contents for all documents are constituted by the availability of time trends of variables used to characterize accident scenarios: those variables are adopted here to fix the link between accident scenarios and phenomena.

Table 15.1 also provides an idea of the variety of situations where nuclear thermal-hydraulics is applied to the accident analysis including approaches for the application.

15.2.4 Other events: external, “low power,” not core related

The current section is introduced having in mind the target to characterize the boundaries (i.e., the narrow field) for the performed activity within the sector of nuclear reactor safety.

Events important for the evaluation of the overall risk of an individual NPP include the following:

- Originated by natural causes “external” to the NPP like earthquake and flooding, or impact of a meteorite also hitting the surroundings of the NPP.
- Originated by industrial activities “external” to the NPP like accidental explosion of a truck and arrival of dangerous gas cloud (explosive or poisoned), or impact of an aircraft and including erroneous management of military weaponry.

- Originated by “internal” accidental events like fire of a diesel generator gasoline tank or missiles generated by the failure of rotating machinery.
- Not originated at full power: A shutdown transient is actually part of Table 15.1 (i.e., row 43); however, a systematic evaluation of possible events and characterization of phenomena in not full power conditions was not performed.
- Originated by human sabotage. A large variety of situations may be invented by the human mind to create an accident in NPP, ranging from using chemical explosive, to the injection of de-borated water into the RCS, to coercing the actions of operators.

Furthermore, “Radioactive releases” include events which do not represent the consequences of another event given above; i.e., the release is a direct result of the failure of the component which contains radioactive material. This is the case of the fall of an irradiated fuel assembly during its moving inside or outside the containment, as well as any cooling failure occurring into the spent fuel pool.

In all those cases nuclear thermal-hydraulics may support the needed analysis for NPP safety demonstration; however, related accident scenarios and phenomena are not considered within the present framework (i.e., not part of Table 15.1).

Noticeably and out of the present framework, the Fukushima Daiichi accident (some details given in Chapter 16) is originated by an external PIE (see e.g., D'Auria et al., 2012). However, thermal-hydraulic phenomena took place: those phenomena occurred in the condition before “loss of geometric integrity for the core” are discussed in Chapter 16.

15.2.5 The transient thermal-hydraulics phenomena

Phenomena have been established within the framework of activities performed within international institutions, see also below. Phenomena of interest for the present chapter deal with the condition DBA, before the occurrence of the loss of geometric integrity for the core. The DBA concept has already been discussed in the book: namely, the diagram in Fig. 2.9 of Chapter 2 may be of help. The concerned condition covers some BDBA situations, e.g., in terms of probability of occurrence of a selected PIE, and in cases outside the DBA boundary, when AMPs are utilized to prevent core degradation (e.g., fast depressurization of secondary side of SG).

The nuclear thermal-hydraulic phenomena are collected and characterized in Chapter 6. The list of phenomena considered hereafter is similar but does not

necessarily coincide with the list in Chapter 6.

Four categories of phenomena are distinguished in Table 15.2: basic (B), separate effect (S), integral effect (I), and addressing the design of “new reactors” (A). Both Reactor Coolant System (RCS) and containment phenomena are considered within the four categories.

Originating documents for deriving Table 15.2 are:

- the CSNI SETF CCVM (OECD/NEA/CSNI, 1993);
- the CSNI ITF CCVM (OECD/NEA/CSNI, 1987, 1996a); consideration is also given to OECD/NEA/CSNI (1989b);
- the CSNI VVER CCVM (OECD/NEA/CSNI, 2001);
- various CSNI reports for containment (OECD/NEA/CSNI, 1986, 1989a, 1999, 2014); phenomena from those reports are considered also combining as far as possible with phenomena from other listed sources;
- the OECD advanced reactor phenomena classification (OECD/NEA/CSNI, 1996b);
- the IAEA list of phenomena for advanced reactors (IAEA, 2009a); consideration is also given to IAEA (2001) (Tecdod 1203), IAEA (2002b) (Tecdod 1281), IAEA (2005b) (Tecdod 1474), and IAEA (2012) (Tecdod, 1677).

The phenomena are listed in alphabetic order in Table 15.2. In order to keep compact the same table a higher use is made of acronyms than in the original documents.

Three phenomena have been added, which are not explicitly reported in the list of originating documents: these are reported into clear green rows in Table 15.2.

In some cases the distinction between ITF and SETF phenomena is only formal (i.e., there should be no consequences in the application of the related information).

Table 15.2 includes 113 “independent-phenomena” (i.e., labeled rows in the first column of the table):

- 9 basic phenomena [B-1 to B-9] originated from the OECD SETF CCVM;

- 61 SETF phenomena [S-1 to S-61]: 58 among those are originated from the OECD SETF CCVM plus 3 ones added [S-25, S-30, and S-42, clear green rows in Table 15.2] within the present context and dealing with horizontal heated channels, internal pumps, and convection flows inside containment, respectively;
- 30 ITF phenomena [I-1 to I-31] originated from the OECD ITF CCVM; and
- 13 “advanced reactor” phenomena [A-1 to A-13] derived from above-cited OECD and IAEA documents.

The considered phenomena, namely the “advanced reactor” phenomena, plus the S-42 phenomenon (already mentioned) are assumed to characterize the reactor containment scenarios, too; these include full pressure and pressure suppression containment and the bubble condenser adopted in some NPP equipped with VVER-440; however, no phenomenon is related to the ice-containments, which are excluded from the present framework.

Making reference to basic phenomena, the possible steam generation at abrupt discontinuities (i.e., caused by the reversible part of the total pressure drop) is included in the phenomenon B-3-EV1. Downstream a geometric discontinuity (e.g., in the presence of a sharp edge possibly combined with high Re flow), the local pressure may fall below the saturation pressure corresponding to the fluid temperature; vaporization may occur and void may appear which become subcooled void because of the sudden pressure recovery. Subcooled voids may affect the total pressure drop and, if present, the TPCF in the downstream pipe (D’Auria et al., 2003b).

15.3 The cross-link between accident scenarios and phenomena

Within the top-down approach in nuclear system thermal-hydraulics, four hierarchical levels are considered in relation to the topic Accident Analysis: [Level 1] accident scenarios; [Level 2] phenomenological windows; [Level 3] phenomena, and [Level 4] time trends of variables or parameters. It is sometimes useful to introduce the fifth topic, called Relevant Thermal-hydraulic Aspect (RTA) (see Billa et al., 1991). The RTA topic shall appear between the phenomena and the time trends as outlined as follows.

- *Accident scenarios* are (those) listed in Table 15.1.
- *Phenomenological windows* are introduced, as an example whenever appropriate,

in order to characterize time spans inside accident scenarios.

- *Phenomena* are introduced in **Chapter 6** and are listed in **Table 15.2**: phenomena are originated from internationally agreed and recognized definitions; otherwise RTA is introduced between phenomena and time trends: for instance, the phenomenon I-19-PRZ (Pressurizer thermal-hydraulics) can be characterized by the RTA “PRZ emptying” and “PRZ filling.” RTA is not used in the present chapter.

- *Variables, or time trends (of variables), or parameters* are introduced in order to characterize accident scenarios and phenomena (with the help of phenomenological windows) and are discussed later.


The targets here are to outline the thermal-hydraulics features of accident scenarios in water cooled nuclear reactors and to complement the description of phenomena provided in **Chapter 6**. As already mentioned, the list of phenomena is derived from internationally established documents and the overall number (113) should be considered the minimum number of phenomena expected within the DBA envelope making reference to the concerned list of water cooled reactors.

15.3.1 The procedure

The cross-connection between phenomena and accident scenarios is defined in **Table 15.3**. One-hundred-thirteen (113) phenomena are listed in the first column of **Table 15.3** and forty-five (45) accidents scenarios are given in the top row of the table. Namely, two accident scenarios from **Table 15.1** are reported in each cell of the top row in the following way: accident scenarios 1 (bottom) and 2 (top) are reported in the first cell; accident scenarios 3 (bottom) and 4 (top) are reported in the second cell, and so on up to the 23rd cell which contains only the scenario number 45 from **Table 15.1**. Furthermore, making reference to the first column, each phenomenon has two rows, A and B, to connect with the bottom and the top scenario (listed in the first row of **Table 15.3**), respectively.


Then, **Table 15.3** includes the following symbols:

- “•” means “phenomenon part of the concerned accident scenario and characterized by at least one figure from corresponding calculation results part of the paper(s) referenced in **Table 15.1** and discussed in the section of the present chapter also reported in **Table 15.1**.”



- “” means “phenomenon part of the concerned accident scenario and

characterized to some extent by corresponding calculation results part of the paper(s) referenced in Table 15.1 and discussed in the section of the present chapter also reported in Table 15.1.”



- “” means “phenomenon part of the concerned accident scenario and corresponding calculation results (i.e., typically not considered in available time trends of paper(s) referenced in Table 15.1).”



- “” (red star) and “” (clear blue star) mean “phenomenon associated with accident scenario in Table 15.4, third and fourth step for building Table 15.4, respectively; no star implies entering into the fifth step for building Table 15.4.”

The role of Table 15.3 within the present context is to establish one-by-one mutual correspondence between phenomena and accident scenarios and to provide a visual mapping of the correspondence.

The target for Table 15.4 is to characterize the phenomena listed in Table 15.2 and the accident scenarios listed in Table 15.1, throughout the use of parameters. The activity shall consider the cross-link between phenomena and accident scenarios established in Table 15.3.

In general terms one may state that:


- Accident scenarios in NPP can be characterized in terms of:
 - nuclear reactor design and boundary and initial conditions;
 - adopted computational tools, including SYS TH code, nodalization, use options, target of the analysis;
 - imposed and resulting time sequence of events;
 - phenomenological windows and phenomena; and
 - time trends of variables or parameters.
- Phenomena expected in case of accidents in NPP can be characterized in terms of:
 - Phenomena expected in case of accidents in NPP can be characterized in terms of;


- physical models and equations;
- ranges of variations of influential parameters; and
- time trends of variables or parameters.

Time trends of variables (or parameters) appear in both lists. So, the idea for Table 15.4 is to consider the comprehensive list of phenomena in Table 15.2 and the minimum reasonable number of transient scenarios listed in Table 15.1, in addition to the information from Table 15.3 as already mentioned.

In order to achieve the target, phenomena are listed first; then each accident scenario is associated with one or more phenomena. Furthermore, in Table 15.4:

- Time trends of variables (or parameters) representative of accident scenarios are reported in the 15 columns on the right side.
- “A” in the variables column/cell indicates that the variable is selected to represent the accident scenario in the figures part of Sections 15.4.2–15.4.12.
- “P” in the variables column/cell indicates that the variable is selected to represent the phenomenon in the figures part of Sections 15.4.2–15.4.12.
- Cells in clear yellow associate the accident scenario and the section where the accident scenario is outlined (consistently with Table 15.1).

The first step for building-up Table 15.4 consists in associating each accident scenarios listed in Table 15.1 with one phenomenon (i.e., creating the clear yellow cells: so, 45 clear-yellow-cells sets are part of Table 15.4; the related phenomenon and accident scenario are characterized by the “” in Table 15.3).

The second step [for building-up Table 15.4] consists in associating the remaining 68 phenomena (i.e., 113–45), with one of the sections describing accident scenarios in Table 15.1 (i.e., filling the fourth column starting from left). Then, one of the accident scenarios described in the section (i.e., from Table 15.1) is associated with the phenomenon (“” in Table 15.3).

The third step [for building up Table 15.4] consists in characterizing the clear yellow-labeled phenomena. In this step the cross-link is established between those phenomena (i.e., 45 phenomena, second column from left) and the parameters calculated from accident scenarios (last 15 columns).

The fourth step [for building up Table 15.4] consists in ensuring that each phenomenon (i.e., 113 phenomena listed in the second column) has at least one characterizing “P.” In the case of clear yellow-marked phenomena, the step implies checking that at least one “P” appears in the last 15 columns: if this condition is not true an accident scenario, selected among those listed in Table 15.1, is added in the third column and a corresponding “P” is placed in 1 (or more) of the 15 columns. In the case of nonmarked phenomena one scenario is selected for the third column and the corresponding “P” is added in 1 (or more) of the last 15 columns. In both cases use is made of the information in Table 15.3.

The fifth eventual step [for building up Table 15.4] is needed when no parameter is found (or reported) from the database of accident scenarios (i.e., references cited in Table 15.1). In this case a list of “equivalent ADDED accident SCENARIOS” shall be created.

The first and second steps have been carried out considering “key” expected phenomena part of the accident scenario: this is the reverse procedure compared with what done to derive the phenomena list at the basis of the cited originating documents.

The third and fourth steps imply the prior identification of parameters (variable time trends), which are “suitable” to characterize each phenomenon. This is done in Sections 15.4.2–15.4.12 where each phenomenon is listed and suitable parameters are listed in square brackets.

The role of Table 15.4 (and of the supporting Table 15.5) is to establish the bases for the description of accident scenarios considering phenomena and available parameters in Sections 15.4.2–15.4.12.

The overall process streamlined by Tables 15.1–15.5, may appear intricate and arbitrary. This is also connected with the existence of multiple solutions occurring when piecing together phenomena and accident scenarios; for instance as a limit case, the basic phenomenon B-7 (Pressure drop at geometric discontinuities including containment) can be associated with every scenario. The process is controlled by the variables available from the calculations documented in the selected references (last column of Tables 15.1 and 15.5). However, as a result (i.e., the expected outcome from the process), an overall picture of transient thermal-hydraulics applied to nuclear reactor safety is derived. Furthermore, the reader may identify the section where any phenomenon is visualized with the help of variables characterizing the accident scenarios; the reader may also recognize the complexity of nuclear system thermal-hydraulics.

In the present process for building Table 15.4, the fifth step has been necessary.

Thirteen (13) phenomena (i.e., taken from Table 15.2) needed an “equivalent ADDED accident SCENARIO.” These are given in Table 15.5 together with the related (new) reference documents. The listed phenomena, with two noticeable exceptions, are actually part of the modeling resources adopted to calculate the accident scenarios in Table 15.1: i.e., proper parameters needed to depict those phenomena (i.e., A-4-DL and I-14-NC5 in Table 15.5) are not part of reference documents provided in Table 15.1. Furthermore, the “equivalent ADDED accident SCENARIOS” (column 5 in Table 15.5) is not necessarily an NPP calculation. Rather, the related support references include parameter trends suitable for the characterization of phenomena. In Table 15.1, reference documents (last column) deal with calculation of accident scenarios in nuclear reactors; otherwise in Table 15.5 reference documents (last column deal with characterization of concerned phenomenon).

The bold characters accident scenarios listed in the fourth and the fifth column of Table 15.5 are added in Table 15.4; “P” is added in Table 15.4, where appropriate, considering the availability of parameters from documents in the last column of Table 15.5.

The tight connection among phenomena, accident scenarios, and time trends of variables (or parameters) is the first (obvious) result from the process documented in Table 15.4 (supported by added information in Table 15.5).

15.4 The characterization of phenomena and accident scenarios

15.4.1 Background

The results from the cross-link procedure for relevant phenomena and accident scenarios in nuclear thermal-hydraulics are outlined in this chapter. Two sub-steps are distinguished for describing the outcomes of the activity:

(A) The accident scenarios identified by the sections of the chapters in the first column of Table 15.1 are outlined by the use of time trends (typically consisting of the variables indicated in columns 15 to 1 going from right to left in Table 15.4).

(B) The phenomena associated with each section (fourth column of Table 15.4 starting from left) are directly connected with variables describing the accident scenarios.

The activity at the step (A) does not substitute the thermal-hydraulic analysis needed to check the consistency of any set of calculation results and shall not be considered neither an exhaustive description nor an acceptable description of the concerned accident scenario.

The activity at the step (B) is based upon variables available from the (arbitrarily selected) references listed in Tables 15.1 and 15.5.

Each of Sections 15.4.2–15.4.12.12, except Sections 15.4.12.1–15.4.12.4, 15.4.12.8, and 15.4.12.12 (dealing with single aspects of accident scenarios), is divided into three parts, the first two parts accomplishing the step (A), the third one accomplishing the step (B):

- (Part 1) Qualitative accident scenario
- (Part 2) Quantitative accident scenario: variable trends and TSE
- (Part 3) Phenomena connection with accident scenario

In part 1, thermal-hydraulic characteristics of the accident scenario are listed, having in mind the various classes of water cooled reactors. In a few cases, references in addition to those reported in Tables 15.1 and 15.5 are cited.

In part 2, a reasonable minimum number of diagrams, typically less than three, and a table with the sequence of imposed and resulting events are used to depict the accident scenario, where “imposed (I)=part of boundary conditions” and “resulting (R)=obtained from thermal-hydraulic calculation.” The calculated variable trends are derived from references in Tables 15.1 and 15.5. The reported time for events is valid for a single accident scenario and is expected to be representative for the category of accidents considered in the section (i.e., typically the result of a BE calculation where uncertainty is *not* evaluated).

Related to part 3, it shall be recalled that phenomena may be associated with different accident scenarios with the exception of some of the integral phenomena (“I”-labeled in Table 15.2), which are specific for selected accident scenarios: each phenomenon can occur or can be relevant in one or more (or all) accident scenarios and in one or more reactor types, as well. So, phenomena are preferably connected to the accident scenario, which is the topic of the section. Insights into phenomena based on information in addition to what available from references cited in Tables 15.1 and 15.5 are provided in some cases and properly referenced. Finally, not all relevant phenomena, which are expected in the concerned scenario, are necessarily

part of the section where the scenario is described. Summing up and related to figures in part 3 of each section:

- Black characters are used for phenomena listed in the section (i.e., each of the 113 phenomena in Table 15.2 is considered one time in the figures).
- In some cases (e.g., Section 15.4.5) clear green characters are used for identifying phenomena already described in different sections (i.e., which are black in other sections).
- White characters into clear blue boxes are used for phenomena, which are not part of the section and are part of sections where those phenomena could not be visualized (see e.g., Fig. 15.13).
- Red characters are used for information other than phenomena (e.g., PHW).

The structure of Sections 15.4.12.1–15.4.12.4, 15.4.12.8, and 15.4.12.12, related to single aspects or single components of accident scenarios, includes

- (a) topics and facts for the concerned aspect and
- (b) phenomena connection with accident scenario (same as in other sections).

15.4.2 The LBLOCA and the IBLOCA

The LBLOCA in PWR with UTSG is discussed first. The IBLOCA (or MBLOCA) and the scenarios in other reactor types are discussed in the second part of the section.

15.4.2.1 Qualitative accident scenario: LBLOCA

The key features of an LBLOCA and key connected facts, CL break in PWR UTSG between MCP and RPV, are:

- Occurrence of a large break having area till the guillotine break (or “2×100% A”) of the largest pipe in the system, i.e., either the pipe connected with the RPV or the header if the RPV is not part of the system: the break is typically located in the most challenging position as far as core integrity is concerned. TPCF is a key phenomenon (e.g., Réocreux, 1974; D'Auria and Vigni, 1980; Bartosiewicz et al., 2010).
- Mechanical loads of RPV internal components and external supports and structures caused by pressure wave propagation and jet impingement in the initial

tenths of seconds after the break, and strongly affected by the break opening time (e.g., Vigni and D'Auria, 1979).

- Void generation (also) in the core region caused by the arrival of the depressurization wave which cause lack of moderation and “decay-power” production with the noticeable exception of those RCS where a typically slight positive void reactivity coefficient causes a power peak (PWR with high-boron concentration in the core at BOL or BOC conditions).
- Fast depressurization of RCS, the magnitude is in the order of MPa/s, occurs in the early period, a few seconds, after the break occurrence.
- Accident subdivided into three PHW, or phases, called Blowdown, Refill, and Reflood (BD, RF, and RE, respectively, within the present context; these other than PHW also constitute thermal-hydraulic phenomena).
- Flashing and somewhat homogeneous conditions occur in the RCS for a couple dozen seconds since the transient starts.
- Excursion occurs in the value of fuel pin surface temperature (RST). This cannot be avoided and must be controlled to prevent the irrecoverable loss of core integrity (i.e., brittle rupture of clad and release of volatile and nonvolatile fission products into the coolant). Otherwise, clad ballooning and rupture with release of part of volatile fission products cannot be avoided in existing reactors.
- Stagnation point occurs. The concept of stagnation point is simple: in a closed pressurized loop, the occurrence of a “full size double-ended break” in one point causes two flow streams directed toward the two ends; a region creates unavoidably where the two streams take origin. This is the stagnation region or the stagnation point. Flow velocities are close to zero in the stagnation point and HTC is very low. Furthermore, simple pressure balance analysis shows that favorite region for stagnation point is the loop region with the highest value for pressure drops. Hence the core region in a PWR constitutes a candidate region for the location of the stagnation point. Finally, in a complex loop subject to two-phase flow conditions stagnation point may continuously shift during the transient (i.e., a moving stagnation point condition occurs). This is due to changes during the transient in the repartitions of pressure drops along the paths of the two streams (each path going from the stagnation point to the break), which are different.
- Additional key LBLOCA characterizing phenomena or events are early core rewet, ECC bypass, steam binding, and occurrences of BD PCT and RE PCT.

- Role of selected SSC is that PRZ depressurizes later than RPV and piping owing to TPCF occurrence in surgeline; PRZ stored water may contribute to core cooling in the early period of the accident, i.e., by contributing to the early core rewet in the upper region of core; SG behaves as a heat source early during the transient and till full recovery and have a minor role till the end of reflood because of steam present in the PS part of SG tubes and consequent (very) low HTC (i.e., typically less than $100 \text{ W/m}^2 \text{ K}$); MCP work in flow reversal mode (namely in BL) and two-phase conditions soon after the break and have a role in determining the location of the stagnation point; containment pressurizes and liquid level forms in the sump, needed for long-term cooling.

- Design of selected ESF (including ECCS) and actuation modalities are largely based upon the concerned accident scenario (i.e., noticeably the accumulators). ACC and LPIS are key ECCS to protect the RCS keeping the concerned accident parameter values within DBA conditions.

Classifications of LOCA imply approximations and any parameter selected for the classification may reveal questionable. Hereafter, the following rough “blow-down” (or depressurization)-based classification is proposed making reference to the dimensional parameter A_R/V (where A_R is the break area [m^2] and V the volume of the PS excluding the PRZ [m^3]) evaluated in m^{-1} :



The origin of the LOCA issue is the high pressure of RCS needed to ensure a suitable thermal efficiency for the electricity production by fission. The geometric configuration of nuclear reactor systems, the nominal-operational value of the pressure, and the linear power of fuel rods play the key role for the evolution of the transient.

The LOCA classification of existing commercial reactors based upon geometric configuration brings to the following classes:

(A) RPV equipped nuclear systems to be distinguished in:

- A1: without SG, or the BWR class; further subdivision can be:
 - A1-1 with external pumps;

- A1-2 with external pumps and jet pumps; and
- A1-3 with internal pumps (ABWR).
- A2: with SG, or the PWR class; further subdivision can be:
 - A2-1 equipped with UTSG;
 - A2-2 equipped with OTSG;
 - A2-3 equipped with HOSG (or VVER); and
 - A2-4 PHWR with moderator cooling loop.

(B) Pressurized channel-type nuclear systems to be distinguished in:

- B1: RBMK type, solid graphite moderated and
- B2: CANDU type, (low pressure) heavy water moderated.

For almost all categories, the size and the nominal power of the RCS may bring further differences in relation to: the numbers of loops, of MCP and of pressure channels, and the SG size.

The nominal operational value of pressure brings to two LOCA-classes of reactors characterized by initial pressure values around 7 and 15 MPa, respectively. A1 and B1 reactors from the previous classification (geometric configuration based) belong to the former class and remaining ones belong to the latter class.

All concerned reactor cores are equipped with fuel rods. The maximum value for design linear power, also controlled by LOCA evolutions, is around 45 kW/m and equal in all classes.

Nine main classes of water cooled nuclear reactors are distinguished from the previously mentioned process, as far as expected LOCA scenarios are concerned. The design of ESF and related EOP, including passive systems, introduces further differences inside each class. Then, one may expect that a few dozen transient scenarios (i.e., two to four in each class to demonstrate the worst one) need to be analyzed to cover the LBLOCA performance for all existing NPP.

A similar classification procedure can be repeated (this is *not* done hereafter) in relation to each of the selected accident scenarios (Sections 15.4.3–15.4.12.12)

causing an overall number of transient scenarios needed to characterize all existing water cooled reactors in the order of 1000.

15.4.2.2 Quantitative accident scenario: variable trends and TSE - LBLOCA

The LBLOCA scenario for a PWR equipped with UTSG can be derived from Table 15.6 and Figs. 15.1–15.3, taken from AP1000 calculation (Queral et al., 2015), row 14 in Table 15.1. Differences between a standard PWR and AP1000 are emphasized in the TSE Table 15.6 and in the discussion later. The following can be stressed:

Table 15.6

LBLOCA in PWR with UTSG: (selected) imposed and calculated time sequence of events

- The three PHW (Fig. 15.1), BD, RF, and RE, are typical of LBLOCA in any PWR.

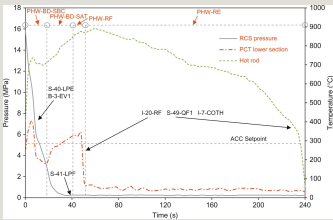


Fig. 15.1 LBLOCA in PWR (AP1000) and phenomena characterization: RCS pressure and RST (two positions).

- Containment pressurization is not part of the documented calculation results.
- The emptying of the PRZ, depending upon the location of the stagnation point,

may contribute to the early cooling of the core; the same applies to LP and UH flashing.

- The loads upon RPV internals and containment structures must be calculated to ensure core integrity after the initial phases of the transient.
- HPIS in standard PWR and PRHR in AP1000 have a modest impact upon the early phases of the LBLOCA (i.e., up to 300 s). The same is true for ESF in the SS of SG (e.g., AFW).
- A correspondence can be identified between ACC in standard PWR and in AP1000. In this connection, CMT draining and, later-on, IRWST draining may be seen as corresponding to LPIS actuation (tank feeding) and LPIS sump recirculation.
- The sump recirculation must be demonstrated taking into account of challenges to the pump (LPIS and/or RHR) cavitation put by liquid temperature in the sump and by debris eventually passing the filters installed at the pump suction location.
- The opening of vent valves in PWR equipped with OTSG mitigates the effect of steam binding (see also Fig. 15.5).

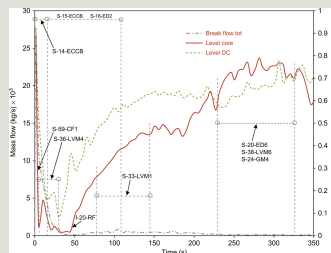


Fig. 15.2 LBLOCA in PWR (AP1000) and phenomena characterization: break flowrate and DC/core level.

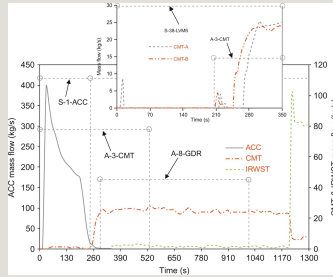


Fig. 15.3 LBLOCA in PWR (AP1000) and phenomena characterization: ACC, CMT, and IRWST flowrate.

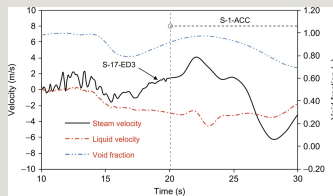


Fig. 15.4 LBLOCA in PWR and phenomena characterization: fluid velocities and void fraction in HL.

- The opening of ADS in AP1000 also mitigates the effects of steam binding.
- In the case of AP1000, pressure oscillations (e.g., caused by condensation) may occur in the circulation between CMT and RPV and following interactions between RCS and containment.

The quantitative description of the transient scenario is made with reference to a DEGB LBLOCA in CL for a 1000 MWe typical PWR equipped with UTSG, considering six (groups of) quantities.

(I) RPV and PRZ pressure. Five periods can be distinguished in the RPV pressure:

(I-a) Pressure wave propagation lasting around 1 s after the start of break opening. This depends upon the concerned location, i.e., close to the break or far away. Pressure undershoots and recovery due to flashing-boiling may occur.

(I-b) Subcooled blowdown. The period having duration of a few seconds ends when the local pressure achieves, one after the other, the saturation pressure corresponding to HL and CL (or UP and LP) coolant temperature at nominal

conditions. Depressurization rate is of the order of MPa/s.

(I-c) Saturated blowdown, with void fraction close to zero at the break. Coolant boiling hitches the pressure decrease in the RPV and depressurization rate is much slower than in the previous period (i.e., in the order of $(1/10)$ MPa/s). Time duration of the period is in the order of 10 s.

(I-d) Saturated blowdown, with void fraction close to unity at the break. Steam flow at the break accelerates again the depressurization rate up to values close to 1 MPa/s. However, the decrease of the absolute pressure in the RPV and the arrival at the break of the liquid injected by ECCS slow down the depressurization rate to values of $(1/10)$ MPa/s.

(I-e) Pressure equalization in RPV and containment. The conditions for TPCF occurring in previous periods disappear (roughly when RPV pressure achieves a value twice the value in the containment and “Bernoulli-flow” establishes at the break). The transition TPCF \rightarrow “Bernoulli-flow” may occur during a time period of a few seconds. The “Bernoulli-flow” condition at the break remains valid for the entire reactor recovery period (several dozen minutes or even hours), with RPV pressure typically above containment pressure due to continuous energy production in the core. Local condensation phenomena and pressure oscillations in the containment may change this situation during short-time periods.

ACC and LPIS actuations typically occur during the period (I-d).

The PRZ pressure remains above the RPV pressure since the beginning of the transient and till the emptying of the PRZ. The occurrence of TPCF conditions in the surgeline (surgeline diameter in the range $1/5$ to $1/10$ of CL diameter) is at the origin of the difference between RPV and PRZ pressure. Pressure equalization in RPV and PRZ typically occurs during the period (I-d).

The SG pressure remains close to nominal-initial conditions till the start of the period (I-e).

(II) RST in hot rod at PCT location. The RST time performance may be (very) different in different regions of the core. Different time performances also occur in the same rod at different elevations. Other than the geometrical coordinates in the core, RST is affected by burn-up (and, in some situations by the amount of boron in the core, i.e., when large amounts may cause reactivity excursions following coolant flashing in the core in the early period of the transient). The local linear power (i.e., q' in the units of kW/m) largely affects RST. The following time periods can be distinguished in the RST time trend.

(II-a) Possible initial fall starting from the initial value: This can occur owing to time changes in the two quantities which control the RST (i.e., fission power and coolant HTC). The decrease in fission power may be faster than the decrease in HTC.

(II-b) CHF occurrence and start of RST excursion till possible BD PCT. CHF cannot be avoided during LBLOCA. Film boiling conditions establish causing RST increase till a possible turnaround point, BD PCT, determined by RCS intrinsic cooling. Overall time duration for the first two periods is less than 10 s and the BD PCT is in the order of 900°C. Occurrence of stagnation point in the RCS largely affects RST value during periods (II-a) and (II-b). Clad ballooning with consequent ductile break may occur in this period as well as in the forthcoming periods.

(II-c) Possible (partial or complete) early core rewet. RST decrease after BD PCT may be caused by LP flashing and/or coolant flow entering the core from PRZ and UH. This phenomenon is (again) largely affected by the location of the stagnation point. So, the number of loops and the mutual position of the loop with break and the loop with PRZ affect the phenomenon. The phenomenon is more pronounced in the case of short core (e.g., like in the nuclear reactor LOFT utilized for LBLOCA experiments in the 1970s and 1980s; Reeder, 1978). The duration of the early core rewet phenomenon is in the order of 10 s and causes lowering of RST for a few tens kelvin till the full quench (i.e., RST back at values close to coolant saturation temperature).

(II-d) RST increase till RE PCT. Following the occurrence at (II-b) (i.e., with or without the occurrence of early rewet), RST increases till the main turnaround point called RE PCT or simply PCT. The slope of the RST versus time curve remains positive in this period and decreases close to the occurrence of the PCT. Various phenomena (see also below) contribute to the RST value. A key role is taken by the ACC actuation. The period is controlled by the refill conditions and duration at the core PCT location can be of the order of dozen seconds. It must be demonstrated that PCT value remains below 2200°F and other criteria for ECCS design are fulfilled (namely for H₂ production which implies a time duration for film boiling conditions).

(II-e) “Precursory cooling” till conditions for rewet. Following (RE) PCT occurrence, the effect of ECCS injection causes improved cooling conditions for the clad still not sufficient for the recovery (rewet). This is called precursory cooling and involves droplet transport into the core. QF is progressing typically in a bottom-up direction. CCFL may occur at the UTP (or UCSP) of the core. The

precursory cooling period duration is affected by several parameters including location of the observed clad region and distances from QF and spacer grids. Typical values are in the range from a few seconds to a few minutes with RST decreases in the range from a few tens kelvin to a few hundred kelvin. Steam binding and level in UP are expected in this period.

(II-f) Rewet and Return to Nucleate Boiling. Once the local conditions for rewet are locally established, the QF may cross the observed position and RST suddenly drops to values close to the saturation temperature at the RCS (and containment) pressure. The process occurs in a few seconds and RST changes can be up to a few hundred kelvin.

(II-g) Long-term cooling. After the occurrence of the rewet, satisfactory cooling conditions are expected to establish in the core and the RST remains connected with coolant temperature. All of this occurs during the so-called long-term cooling period.

(III) Coolant flow at core inlet and outlet. Core flow is essential for removing power during nominal operation. MCP provides the power to establish the pressure distribution in the RCS and design flow-rate across the core. Following LBLOCA occurrence, the pressure distribution in RCS depends upon the critical pressure (and the fluid velocities) at the break location (i.e., TPCF conditions). The MCP in the broken loop and in the intact loops typically starts their coast-down due to (presumable) loss of electrical power at within tenths of seconds after the break occurrence. They have some role in establishing the location of the stagnation point in the primary loop. However, cavitation starts almost immediately after the break occurrence and even MCP in the intact loops have little role in determining core flow: the effect of MCP inertia typically expires within 10 s. Three main periods can be distinguished for core inlet flowrate:

(III-a) Decay from nominal value and occurrence of flow reversal. In a few seconds (limit has been set to 10 s), flow rate reverses its direction at core inlet and becomes fully driven by break pressure. This condition ends when RF starts. Vaporization including flashing in LP may cause positive peaks during this period.

(III-b) RF and RE till equalization of pressure between RCS and containment. Positive value for core flow-rate occurs, needed for the advancement of the QF, which is driven by the ECCS injection flows.

(III-c) NC occurrence between core and DC. The DC level is established by the intervention of ECCS (it does not overpass the location of the CL pipe in the

broken loop, because of the large break). This determines the NC conditions sufficient for the end of RE and for removing core decay power in the long term.

Core outlet flowrate, owing to the possible occurrence of the stagnation point in the core, is disconnected from core inlet flow-rate till the end of the period (III-b). During the period (III-a) core outlet flow may remain positive (i.e., same direction as during nominal conditions) also following vaporization of (part of) core coolant inventory. During the period (III-b) and part of the period (III-c), the net core flow at top of the core may be close to zero. However, upward steam flow and downward liquid flow may occur. The steam flow may cause CCFL at the UTP leading to the formation of liquid level in the UP. During the period (III-c) a stable steam, or two-phase mixture flow, may establish and the core outlet flow is again connected with the core inlet flow.

(IV) Mass inventory in PS and SS. The discussion mentioned previously allows a simple description of the time trend of mass inventory in the RCS PS. Mass inventory decreases following the break occurrence till a value in the range 10%–30% of the initial value. Its increases start with the RF period at the moment when break flow becomes lower than ECCS injected flow. At the end of the RE period the RPV and some regions of the loop (e.g., the loop seal) are full of liquid. The performance of mass inventory in RCS PS is reflected by the core and/or the RPV downcomer level.

Mass inventory of SG SS remains nearly constant during the LOCA event (i.e., till the end of the period (II-f)). Later on the mass inventory in the SG is controlled by proper EOP aimed at the recovery and long-term cooling of the RCS.

(V) Containment pressure. The pressure in full pressure containment system increases soon after the break occurrence due to the energy flow from the RCS. It attains a peak value in the range 0.4–0.6 MPa at the time 10–30 s into the transient. Then it starts to decrease, owing to the following reasons:

- increase in the power removal by condensation on the walls and structures;
- heat and mass losses to the environment;
- actuation of specific ESF in the containment (noticeably, spray systems); and
- actuation of ECC in RCS which also results in subcooled (related to the containment pressure) liquid to the break suitable for condensing steam in the containment.

During the early containment pressure decrease period (i.e., at a time 1–2 min since the break occurrence), containment and RCS pressures equalize as discussed in item (I-e).

(VI) Sump containment level. A devoted “sump compartment” is designed and constructed in the containment to collect the liquid coolant in the containment including the condensate. At the bottom of the sump there is the suction of LPIS (or RHR) pumps for the ensuring the core long-term cooling. Condensate level starts to form immediately after the break and a level of a couple of meter (or more) is expected to exist when RHR or LPIS pumps start suctioning liquid from the sump at a time which is 15'–30' since the break occurrence (see also Table 15.6, row 22). A nearly stable level in the sump is expected to remain for several hours since the event occurrence allowing core cooling and the full recovery of the NPP.

As already mentioned thermal-hydraulic challenges associated with the liquid suction from the sump by LPIS or RHR pumps are the presence of debris and the temperature of the liquid which may cause cavitation.

The depicted scenario for RPV pressure and RST, variables (I) and (II), is consistent with the curves in Fig. 15.1. Namely, RST at two locations in the core are reported.

The core inlet flow, variable (III), is not given in the considered curves below. However, an idea of core outlet flow can be drawn from Fig. 15.4 where fluid velocities in one HL are reported.

The trend of mass inventory in RCS PS, variable (IV), can be derived from the level curves given in Fig. 15.2.

Consistent LBLOCA time trends for pressure and level in containment, variables (V) and (VI), can be found in Section 15.4.12.2.

In addition typical time trends for liquid delivery by ECCS can be found in Fig. 15.3. Flowrate and modality of actuation of ACC are qualitatively similar in standard PWR and in AP1000. CMT flow during the draining period and IRWST flow in AP1000 replace (roughly) LPIS flow in short- and long-term cooling mode.

15.4.2.3 Phenomena connection with accident scenario: LBLOCA

The phenomena listed in the second and the third columns of Table 15.7 are

connected with LBLOCA from the cross-link process in Tables 15.3–15.5. Those phenomena are associated with variables in the fourth column of the table.

Table 15.7

Phenomena visualized by variables representative of the accident scenario LBLOCA

^a Characterized by accident scenarios other than the LBLOCA in PWR.

Phenomena are associated with the time trends of the PWR LBLOCA, namely AP1000 calculation, e.g., Figs. 15.1–15.3, except those at rows, 8, 13, 14, 20, and 24 in Table 15.7. Namely, additional diagrams, Figs. 15.4 and 15.5, have been introduced (i.e., based on the cross-link in Tables 15.3 and 15.4 and the reference documents in Tables 15.1 and 15.5):

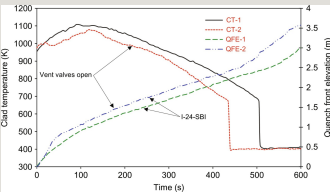


Fig. 15.5 REFLOOD-APR1400 and phenomena characterization: quench front and RST.

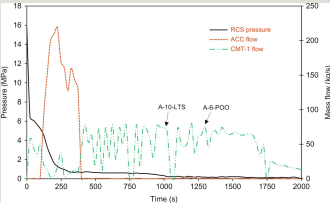


Fig. 15.6 SBLOCA in PWR (AP1000) and phenomena characterization: RCS

pressure and flows from ACC and CMT.

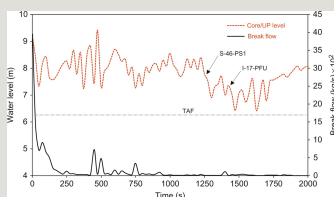


Fig. 15.7 SBLOCA in PWR (AP1000) and phenomena characterization: break flow and RPV level (core side).

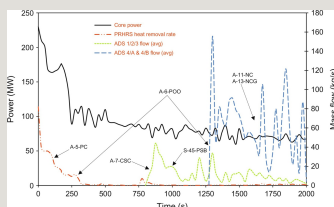


Fig. 15.8 SBLOCA in PWR (AP1000) and phenomena characterization: core and PRHR power and ADS flows.

- “Entrainment/De-entrainment—Hot Leg with ECCT” is characterized through the LBLOCA in PWR calculation at row 18 in Table 15.1, D'Auria and Galassi (2001), Fig. 15.4.
- “Horizontal heated channel HT” is characterized through the LOOSP in CANDU calculation at row 22 in Table 15.1, Tong et al. (2014), Fig. 15.22.
- “Jet pump behavior” and “QF propagation/rewet—channel walls, water rods” are characterized through the SBLOCA in BWR calculation at row 38 in Table 15.1, Analytis and Coddington (2002), Fig. 15.13.
- “Steam binding” is characterized through the added scenario REFLOOD-APR1400 data at row J in Table 15.5, Damerell and Simons (1993a), Fig. 15.5.

All the phenomena in Table 15.7 are visually characterized based on NPP calculations (Table 15.1) or specific data (typically SETF data in Table 15.5) related to water cooled reactors. The following additional notes apply.

(1) Accumulator behavior (visualized, Fig. 15.3). The ACC initial (design) pressure is determined considering the ECC bypass phenomenon. A too high initial pressure causes more coolant to the break. A too low initial pressure causes unacceptable RST excursion. Compromise is needed. The ACC liquid and gas volume must be consistent with the RCS PS volume and with the core power.

(2) Behavior of Core Make-up Tanks (visualized, Fig. 15.3). CMT are part of the passive systems of AP1000. The combination ACC, CMT, ADS, PRHR, and IRWST in AP1000 (roughly) substitutes ACC, LPIS, and HPIS in standard PWR. Recirculation phase of CMT is an NC phenomenon (gravity-driven) initiated by different liquid density in suction and delivery lines. The CMT draining is also gravity driven and is made stable by the formation of a thin (thickness of the order of mm) saturated liquid layer which prevents a direct contact (thus avoiding DCC) between steam coming from the core and liquid in the CMT. The break of the layer is expected to cause oscillations which may challenge the cooling process of the core.

(3) Blowdown (visualized, Fig. 15.1). This constitutes a PHW and a phenomenon at the same time and is described by pressure trend in the present section.

(4) Core thermal-hydraulics (partially visualized, Fig. 15.1 and BWR related). This is described by PWR RST trend in the present section. The three-dimensional core TH performance (i.e., void, temperature, fluid velocities, and—burn-up affected—local linear power) must be noted. In relation to time trends no differences occur between BWR and PWR cores.

(5) ECC bypass/Downcomer penetration (indirectly visualized, Fig. 15.2). Large values of break flowrate (and fluid velocities) coupled with DC emptying caused by (fast) depressurization are at the origin of the phenomenon in the early period of the LBLOCA scenario. This shall be associated with CCFL in DC (phenomenon S-4-CCF2, row C in Table 15.5).

(6) Entrainment/De-entrainment—Core (indirectly visualized, Fig. 15.2). The transport of liquid droplets by steam and two-phase mixture (e.g., entrainment) occurs in the core at high steam velocities. De-entrainment in the core consists in the deposition of liquid on the solid surfaces. Spacer grids have an influence upon both entrainment and de-entrainment. The phenomenon is more pronounced during the RF PHW, which corresponds to the (indirect) characterization in Fig. 15.2.

(7) Entrainment/De-entrainment—Downcomer (indirectly visualized, Fig. 15.2). What reported for core at the item mentioned earlier is applicable for downcomer.

(8) Entrainment/De-entrainment—Hot leg with ECCI (visualized, Fig. 15.4). The occurrence of this phenomenon is expected in PWR with HL injection. The calculation of different countercurrent velocities in HL for liquid and steam implies the availability of a model for entrainment/De-entrainment.

(9) Entrainment/De-entrainment—UP (indirectly visualized, Fig. 15.2). What reported for core at the item (6) is applicable for UP. In this case, UTP plays a role for entrainment and de-entrainment and CRGT play a role primarily for de-entrainment.

(10) Evaporation due to depressurization (visualized, Fig. 15.1). The RCS pressure during BD is the result of various phenomena. The evaporation due to depressurization provides a key contribution to the instantaneous pressure value. The evaporation at geometric discontinuities (part of the present phenomenon) is further discussed in Section 15.4.4.

(11) Global multi-D fluid temperature, void, and flow distribution—UP (indirectly visualized, Fig. 15.2). Any TH quantity calculated in the core at any time during the transient (noticeably during the calculation period considered in the reported figures) is the results of multi-D fluid temperature, void, and flow distribution. Core level in Fig. 15.2 for the short period identified in the figure satisfies this condition. What is written in relation to phenomenon (4) above also applies here.

(12) Gravity-driven reflood (visualized, in Fig. 15.3, considering the connection with the time trends given in Fig. 15.1). Reflood caused by the CMT injection is “gravity driven.” RST time trends constitute a direct indication for this phenomenon.

(13) Horizontal heated channel HT (visualized, Fig. 15.22). A CANDU reactor calculation is at the origin of Fig. 15.22; LOOSP (not LBLOCA) constitutes the target for the calculation. The relationship between void fraction and RST provides an indication of HT in a horizontal channel. Flow stratification puts a challenge for the modeling of the phenomenon: in the same channel cross-section, fuel rods in nucleate boiling and in film boiling, e.g., with RST differing for hundreds kelvin, coexist.

(14) Jet pump behavior (indirectly visualized, Fig. 15.13). An SBLOCA BWR calculation is at the origin of Fig. 15.13. The JP position relative to core in the RPV, thus the geometric design of the JP, is established based on TH analyses, namely LOCA (this is *not* evident from Fig. 15.11, where DC level and not level inside JP are reported). The upper elevation of the JP is sufficiently close to TAF

(TOC reported in the figure): the head generated by the subcooled fluid inside JP during LBLOCA compensates the saturated mixture level on the core side and keeps “covered” the core. The JP bottom elevation is fixed in order to allow radially uniform fluid velocity in the BOC region during nominal operation.

(15) Liquid-Vapor mixing with condensation—Core (indirectly visualized, Fig. 15.2). Direct contact condensation conditions occur during the RF PHW in LP, core region, and UP. The time trend of core (and DC) level provides an indication of the time when the process occurs.

(16) Liquid-Vapor mixing with condensation—Lower Plenum (indirectly visualized, Fig. 15.2). What reported for core at the item listed earlier is applicable for LP.

(17) Liquid-Vapor mixing with condensation—UP (indirectly visualized, Fig. 15.2). What reported for core (item 15) is applicable for UP.

(18) Lower Plenum entrainment (indirectly visualized, Fig. 15.1). The transport of liquid droplets by steam and two-phase mixture (e.g., entrainment) occurs in the LP at high steam velocities. High steam velocities occur during the flashing. Entrainment into the core region is beneficial for core cooling during BD.

(19) Lower Plenum flashing (indirectly visualized, Fig. 15.1). The flashing process is a consequence of the fast depressurization.

(20) QF propagation/rewet—fuel rods (visualized, Fig. 15.1). RST time trends provide a direct visualization of the reflood process, including the advancement of the QF. Additional information in Fig. 15.5 and in the description of RST trend in this section.

(21) QF propagation/rewet—Channel walls, Water rods (indirectly visualized, Fig. 15.13). The phenomenon refers to the different quench time for fuel rods, fuel channel box (or pressure tube), and water rods (dummy tubes inside FA in BWR, also used for the insertion of cluster control rods in PWR). Channel walls are considered in the calculation which originates Fig. 15.13 (details of the different behavior of the channel wall, or the pressure tube wall, and the fuel clad during the heat-up process in the core can be observed in Fig. 15.22 related to CANDU).

(22) Refill including loop refill in PWR-O (visualized, Fig. 15.2). The level in the core region characterizes the RF phenomenon.

(23) Reflood (visualized, Fig. 15.1). RE is the phenomenon and the PHW which shall be related to the overall system performance during LOCA. Otherwise, QF propagation and rewet relate to the core and the local clad TH conditions. However, RE phenomenon is visualized by RST time trends and what reported at item (20) applies.

(24) Steam binding (visualized, Fig. 15.5). Steam binding in the late period of reflood is originated by liquid vaporized from the contact with superheated structures like the RPV internals and the SG tubes. The vaporization causes pressure increase and liquid-level depression in the core, this delaying the QF advancement. The QF time trend provides a direct visualization for the phenomenon. Data derived from the 2D/3D experimental program are shown in Fig. 15.5: the actuation of vent valves between core and DC mitigates the steam binding consequences, all other conditions being the same for the two reflood experiments. The differences between the corresponding curves provide a quantitative evaluation of the phenomenon.

(25) TPCF—Breaks (visualized in Fig. 15.2). The performance of TPCF at the break can be derived from the description of the pressure trend in the present section.

15.4.2.4 LBLOCA in reactors other than PWR with UTSG

LBLOCA in reactors other than PWR equipped with UTSG, here including the standard PWR and the AP1000, may evolve in different ways from a quantitative view-point (i.e., compared with what described earlier). However, key phenomena qualitatively evolve according to the provided discussion.

Notes related to LBLOCA in those reactors in addition to, or as a replacement for what stated earlier, are:

- PWR with OTSG: Steam binding is avoided or controlled by the opening of vent valves between core and downcomer inside RPV.
- PHWR, CANDU, and RBMK (in the last two cases following break of header upstream the core): The occurrence of fission power peak within a few seconds after the break is expected with a magnitude controlled by the break opening time. In the case of PHWR, the delayed flashing of initially subcooled moderator is at the origin of the fission power excursion.
- CANDU and RBMK: The occurrence of TPCF in channel feeders (case of break of header in the channel inlet region) is expected.

- BWR and ABWR: The pressurization is limited inside containments by steam condensation in the PSP (wet-well region).
- VVER-440 (part of the PWR-V category in Table 15.2): Some of the reactors are equipped with bubble condenser containment type (in one NPP ice condensers are installed) to cope with LBLOCA.
- VVER-440: A venting-to-the-atmosphere system is installed in the containment to prevent pressure rise above around 0.25 MPa.

15.4.2.5 IBLOCA or MBLOCA in PWR

IBLOCA (also called MBLOCA) are typically originated by break areas smaller than “1×100 A” (according to the classification at beginning of the section) (e.g., see OECD/NEA/CSNI, 2011). Key aspects during the transient are qualitatively similar to LBLOCA and include the following: (a) transient subdivision into three PHW; (b) occurrence of PCT; (c) need for ACC to cool the core; and (d) negligible role for SG.

The IBLOCA analysis is needed for the safety evaluation of reactors to find the worst accident scenario, e.g., to find the highest PCT as a function of the break area.

When the break area becomes smaller than a certain value (see also earlier), the SG role becomes important in keeping cooled the core and SBLOCA phenomenology takes place as discussed in Section 15.4.3.

15.4.3 The SBLOCA class

The SBLOCA scenario in PWR with UTSG is discussed first. Differences in the scenarios in other reactor types are outlined in the second part of the section.

15.4.3.1 Qualitative accident scenario: SBLOCA

Let us start the SBLOCA scenario description by emphasizing one difference related to LBLOCA. One may approximately state that the duration of a typical LBLOCA (till the RCS and containment pressure equalization, or till the full quench of the core) is in the order of 100 s; then, the duration of an SBLOCA (till the RCS and containment pressure equalization) is in the order of 1000 s. However, SBLOCA characterized by several thousand second duration, are part of the DBA envelope and are analyzed (see e.g., Congiu et al., 1996; D'Auria et al.,

1996b).

SBLOCA scenarios depend upon (a) break area; (b) break location; and (c) ESF actuations as fixed by EOP and operator actions. This causes a large variety of potential scenarios resulting in different safety margins and safety implications. Issues like pressurized thermal shock (PTS) occurrence, recriticality or boron dilution occurrence, MCP operation modality, occurrence of PORV or SRV stuck open and partial availability of AFW, or their combination determine the evolution of an SBLOCA.

The first outcome is that the attempt to define a “typical” SBLOCA may reveal meaningless and even misleading. Nevertheless, a typical SBLOCA needs to be identified having in mind the purposes of the present document (i.e., to characterize the scenario and to connect with phenomena).

An SBLOCA originated by an around 3% break in CL is considered for the qualitative characterization of the scenario. Key features for the scenario can be listed as follows:

- MCP is assumed to stop early into the transient. The stop may be caused by the scram occurrence, which may cause a perturbation to the electrical grid. Alternatively, MCP may be stopped following EOP. MCP in operation bring to (a) wider safety margin to the occurrence of DNB in the core; (b) a tight thermal coupling between PS and SS; and (c) higher mass loss at the break. The key drawback for the MCP-on (other than the difficulty to ensure a sufficient reliability for the electrical grid) shall be associated with the time when the stop occurs (either due to cavitation or following a nonthermal-hydraulic event): the stop may cause void collapse and DNB in the core with SG conditions not necessarily suitable for establishing NC.
- NC establishes between core and SG when MCP coast-down is nearly completed. Flow regimes in RCS during NC are discussed in Section 15.4.12.4.
- Three subsequent RPV level (core side) depressions are envisaged and constitute three potential DNB local occurrences in the core (i.e., not necessarily wide spread in the core):

- Loop Seal (LS) controlled: This occurs when RCS pressure is around the saturation value corresponding to the fluid temperature in CL at nominal conditions. The origin of this is the mutual position between the LS bottom and the TAF: LS bottom is around 1.5 m below the BAF owing to construction constraints

for the mechanical design of the loops including the MCP geometrical configuration. Conditions may establish in the RCS where LS is full of liquid and two-phase mixture or steam are present in other parts of the loop. The liquid in the loop seal creates a plug which puts an obstacle to NC causing a depression in the core level. The situation may stay for a few dozen seconds causing an RST excursion typically less than 200 K. Further level depression in the core causes pressure rise in the HL region which “clears” the LS (LS clearing occurrence) restoring NC.

- ACC controlled: This occurs primarily when HPIS is not available (this may signify a BDBA condition) or not sufficient to compensate the mass loss from the break. The RCS pressure is close to the ACC actuation pressure. As already mentioned, the ACC design pressure is determined primarily based on LBLOCA conditions. However, mass depletion in PS may occur during SBLOCA such that ACC intervention is needed to prevent RST excursion. A proper design of ACC pressure avoids or limits the RST excursion.

- LPIS controlled: Once ACC are empty and mass loss continues at the break, a new core-level depression event is expected when RCS pressure achieves the LPIS actuation value. In this case the eventual RST excursion rate is higher than in the previous cases, mostly because of the low-pressure condition. Again, a proper design for LPIS intervention conditions (primarily head for the LPIS pumps) avoids or limits the RST excursions (see e.g., Belsito and D'Auria, 1997).

- SG has the key role for keeping cooled the core. SG SS constitutes the heat sink for the NC loop, where core constitutes the heat source. SG level and pressure are typically controlled (feed and bleed) to attain a depressurization corresponding to around 50 K/h. PS pressure is connected with SG pressure.

- Core bypass affects SBLOCA scenarios (see e.g., D'Auria and Galassi, 1990a). In the RPV, bypass flow-paths which connected the following regions can be identified (where the direction is identified in nominal operating conditions; this direction may change when MCP stop):

- LP to UP, e.g., water rods guiding the cluster control rods.

- DC to UP, caused by unsealed connection of HL nozzles and barrel.

- DC and UH and UH to UP (including via CRGT) or UP to UH. This is needed to create a circulation in the UH region and affects the initial coolant temperature inside UH.

- PRZ behavior has a role primarily in case of SBLOCA originated by a break in the PRZ (e.g., PORV stuck open, see **Chapter 16** and the description of the Three Mile Island event).

- Break flow may be controlled by stratified conditions upstream the break. Thus the mutual position of the possible break nozzle and the CL axis largely affect the break flow during the transient. Phenomena like vapor pull through and liquid carry-over may occur with break nozzle located at the bottom or at the top of the CL.

- Mixing at ECC ports. Under the conditions of low flows, mixing between cold liquid injected by ECC and the coolant at the location of the ECC port into the RCS have a role in the motion of the mixed fluid and may affect the global system performance, e.g., by controlling NC flow across the core or the homogeneity of core cooling.

- Nitrogen and boron effects. N_2 may enter the RCS following ACC liquid delivery. N_2 may concentrate in the U-tubes of SG decreasing the HT capabilities and affecting NC flow. Changes in boron concentration may occur, namely boron dilution as discussed in **Section 15.4.12.8**.

A variety of TH topics, PHW or phenomena (not necessarily part of the list in **Table 15.2**), are associated with SBLOCA. An attempt is made to summarize a following comprehensive list of those topics, including a short outline or reference to more detailed discussions:

- MCP-on or MCP-off: The preferred industry solution nowadays appears the condition MCP-off following the recognition of an SBLOCA by I & C and/or by operators.

- MCP-restart: Some EOP or AMP includes the possibility of MCP restart to improve the instantaneous conditions of core cooling.

- NC and related phases: Discussed in **Section 15.4.12.4**.

- NC in the presence of many parallel and interacting loops in AP1000. The following NC loops may simultaneously establish in case of AP1000: core-SG, core-CMT, and core-PRHR and in late phase of the transient core-IRWST. Interactions among the loops may generate inducing complex phenomena difficult to analyze.

- PTS occurrence: Discussed in Section 15.4.12.3.
- Boron dilution occurrence: Discussed in Section 15.4.12.8.
- RPV bypass flow-paths: As a difference from LBLOCA bypass flow paths inside the RPV may largely affect the SBLOCA scenario, see the qualitative description earlier.
- Specific AM strategies and AMP are related to SBLOCA: Discussed in Section 15.4.11.
- PRZ filling and simultaneous core uncover: Phenomenon S-7-CCF5 in Table 15.2 (or row 17 in Table 15.4), discussed in this section, see also the TMI-2 scenario in Chapter 16.
- Stratification in two-phase—horizontal pipes: Mentioned in the present section and in Section 15.4.12.4.
- Stratification in single-phase, including co-current and counter-current flows and formation of saturated layer at the possible interface with steam: Phenomenon S-35-LVM3 in Table 15.2 (or row 60 in Table 15.4), discussed in Section 15.4.12.3 and mentioned in Section 15.4.2 in relation to CMT draining.
- Vapor pull through and liquid carryover at break: Outlined in this section and part of phenomenon S-45-PSB in Table 15.2 (or row 78 in Table 15.4), discussed in this section.
- Heat losses, structural heat release (see also I-26-SHH in Table 15.2), flashing of dead ends connected with the RCS and (small) leakages through imperfectly closed valves. These shall be carefully accounted for in calculating SBLOCA scenarios and introduce distortions in the experimental simulation by ITF (see e.g., D'Auria et al., 1985).

15.4.3.2 Quantitative accident scenario: Variable trends and TSE - SBLOCA

As a difference from the DEGB LBLOCA a spectrum of break sizes characterizes the SBLOCA. This reflects in a variety of NPP analyses and in a larger number of typical scenarios. So, a few SBLOCA scenarios are considered for the quantitative analysis below. In all cases the ratio A_R/V is within the boundaries for SBLOCA

classification proposed in Section 15.4.2.

Five main phenomenological windows may be distinguished in typical SBLOCA in standard UTSG equipped PWR (not reported in the following figures because of specific features of the concerned NPP calculations). As a further difference with LBLOCA, PHW in SBLOCA shall not be considered sequential and time intersections may occur.

(I) Subcooled BD: from transient start till emptying of PRZ.

(II) NC: from MCP stop till reactor recovery (end of transient). NC is characterized by different “modes” including one-phase, two-phase, two-phase with siphon condensation and Reflux-Condenser.

(III) RCS PS boil-off: from the end of subcooled BD (or from the end of ACC injection) till the time when LPIS flow becomes larger than break flow (loop refill occurs).

(IV) SG control: starting from the time when SG pressure and level are controlled by EOP (or operators) and till reactor recovery (end of transient).

(V) Coupling PS and SS: when PS pressure is driven by SG pressure (NC allows full transfer of core power to SG heat sink).

The SBLOCA scenario for a PWR equipped with UTSG can be derived from Table 15.8 (related to an SBLOCA having approximately 3% break area in standard PWR, including notes related to AP1000), Figs. 15.6–15.8 taken from AP1000 calculation (Yang et al., 2012a) (row 35 in Table 15.1, 10" break or, approximately, 6% break), Figs. 15.9 and 15.10 taken from APR1400 calculation (Kim and Choi, 2014) (row 36 of Table 15.1, 6" break, or approximately, 3% break), Fig. 15.11 taken from Three Mile Island Unit 2 accident calculation (Bandini and De Rosa, 2014) (row 37 in Table 15.1, PORV stuck open), Fig. 15.12, related to LSTF experiments (Nakamura et al., 2009) (rows F and I in Table 15.5), and Figs. 15.13 and 15.14 taken from BWR calculation (Analytis and Coddington, 2002) (at row 38 in Table 15.1).

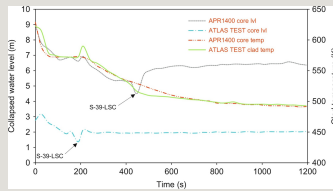


Fig. 15.9 SBLOCA in PWR (APR1400) and phenomena characterization: RST and RPV level (core side) in reduced height facility experiment (ATLAS) and in reactor.

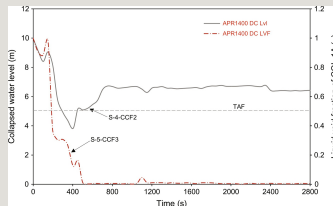


Fig. 15.10 SBLOCA in PWR (APR1400) and phenomena characterization: RPV level (DC side) and liquid fraction in CL.

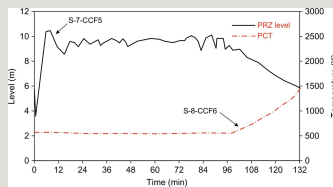


Fig. 15.11 SBLOCA in PWR-O (TMI-2) and phenomena characterization: PRZ level and RST.

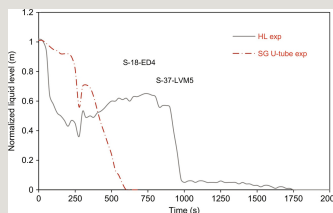


Fig. 15.12 SBLOCA in LSTF (ITF) and phenomena characterization: level in SG mixing chamber and U-tubes.

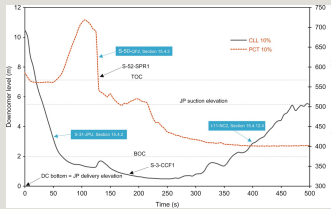


Fig. 15.13 SBLOCA in BWR and phenomena characterization: downcomer level and RST.

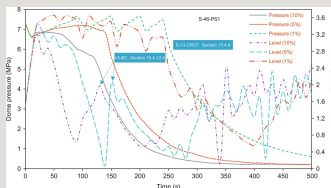


Fig. 15.14 SBLOCA in BWR, 1%, 5%, and 10%, and phenomena characterization: RPV pressure and collapsed level in the high-power channel.

Table 15.8

SBLOCA in PWR equipped with UTSG: (selected) imposed and calculated time sequence of main events

--

Making reference to the reported time trends and in addition to what stated for the qualitative analysis of the SBLOCA, the following can be added:

- ACC flowrate partially (only) compensates break flow.
- PRHR removes (in AP1000) a low part of the core power. So SG cooling remains important in AP1000.

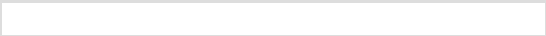
- RPV level (core side) is not expected to fall below TAF in the considered AP1000 scenario.
- LS clearing is calculated at a time in the prototype (APR1400) different from time measured in the test facility.
- LS filling is at the origin of the level depression which cause the occurrence of the first CHF condition in the ATLAS experiment.
- ADS actuation (in AP1000), ADS 1–3 and later on ADS 4, is needed for the IRWST draining and the long-term cooling.

15.4.3.3 Phenomena connection with accident scenario: SBLOCA

The phenomena listed in the second and the third columns of Table 15.9 are connected with SBLOCA from the cross-link process in Tables 15.3–15.5. Those phenomena are associated with variables given in Figs. 15.6–15.12 in the fourth column of the table.

Table 15.9

Phenomena visualized by variables representative of the accident scenario SBLOCA



^a Characterized by accident scenarios other than the SBLOCA in standard PWR.

The following phenomena are outlined in this section or (visually) described through the use of calculated accident scenarios and related time trends (whenever possible):

- (1) Behavior of emergency heat exchangers including PRHR and IC (visualized, Fig. 15.8). PRHR removes a part of core power.
- (2) Behavior of large pools of liquid (indirectly visualized, Fig. 15.8). PRHR is immersed in a pool. Natural convection flows inside the pool, liquid temperature

stratification, and boil-off in the pool (late stage of an accident) are part of the calculation.

(3) CCF/CCFL—Channel inlet orifice (indirectly visualized, Fig. 15.13). This is related to a BWR and is expected in the SBLOCA4 scenario (row 38 in Table 15.1), during the DC liquid-level depression period.

(4) CCF/CCFL—Downcomer (indirectly visualized, Fig. 15.10). Level depression in DC during depressurization is typically associated with boiling: The upward steam flow causes the conditions for CCF occurrence.

(5) CCF/CCFL—HL and CL (visualized, Fig. 15.10, for CL). Low liquid fraction (or high void fraction) causes the conditions for CCF occurrence.

(6) CCF/CCFL—SG tubes (visualized in Section 15.4.12.4, related to NC). NC constitutes a key phenomenon and a PHW during SBLOCA. CCFL-induced filling and draining of U-tubes is part of siphon condensation process described in Section 15.4.12.4, see also phenomenon (11) later.

(7) CCF/CCFL—Surgeline (visualized, Fig. 15.11). PRZ filling and RCS mass inventory decrease including core-level depression constitute typical conditions which establish when PORV cycles or remains stuck open (SBLOCA in PRZ in the last case). This is the well-known event occurring in the TMI-2, as also discussed in Chapter 16.

(8) CCF/CCFL—UTP (associated with S-38-LVM6, visualized in Section 15.4.4, see also Fig. 15.11 related to TMI-2). CCF and CCFL at UTP typically induce liquid-level formation in UP and consequent liquid-vapor mixing with condensation (this phenomenon is called S-38-LVM6 in Table 15.2 and visualized in Fig. 15.2). The phenomenon S-8-CCF6 has been associated with a loss of feedwater (LOFW) scenario where/when MI depletion occurs in PS (i.e., an RCS configuration characteristic for SBLOCA).

(9) Critical and supercritical flow in discharge pipes (indirectly visualized, Fig. 15.8). The phenomenon occurs in a typically 10-m long pipe downstream a relief valve. Such a pipe is installed downstream the ADS-1 to 3 valves in AP1000 RCS in order to allow steam condensation in the IRWST (a similar pipe is *not* present in ADS-4 in order to minimize pressure differences between PS and containment to allow IRWST discharge). A critical section established at the valve location and supercritical steam flow, $Mach > 1$, is expected in the downstream pipeline, together with formation of pressure shock fronts.

(10) Entrainment/De-entrainment—SG Mixing Chamber (indirectly visualized, Fig. 15.12). Experiments devoted to the study of the performance of the SG mixing chamber (or inlet and outlet plenum) have been performed in experimental facilities including LSTF as reported in row F of Table 15.5, see also following phenomenon (13).

(11) Entrainment/De-entrainment—SG Tubes (visualized in Section 15.4.12.4, related to NC). NC constitutes a key phase and a PHW during SBLOCA. Entrainment and de-entrainment inside U-tubes are part of siphon condensation process described in Section 15.4.12.4, see also earlier phenomenon (6).

(12) Liquid temperature stratification (indirectly visualized in Fig. 15.6). The CMT recirculation and draining occurrences imply the calculation and the occurrence of liquid stratification inside the tank.

(13) Liquid-Vapor mixing with condensation—SG Mixing Chamber (indirectly visualized, Fig. 15.12). Experiments devoted to the study of the performance of the SG mixing chamber (or inlet and outlet plenum) have been performed in experimental facilities including LSTF as reported in row I of Table 15.5, see also earlier phenomenon (10).

(14) Loop seal filling and clearance (visualized, Fig. 15.9). The role of LS can be found in qualitative and quantitative descriptions of SBLOCA above. The core-level depression associated with LS formation causes a dry-out occurrence (namely in the upper region of the core, also shown in the figure), which is quenched by the LS clearing.

(15) NC RPV and containment systems and various system configurations (visualized, Fig. 15.8). The IRWST draining is part of a global NC condition, which establishes between core and containment system of AP1000.

(16) Phase separation at branches, including effect on TPCF (visualized, Fig. 15.8). Phase separation at branches is expected in different location during SBLOCA in PWR, e.g., at PRZ surgeline connection with HL. The TPCF in ADS-1 to 3 is affected by phase separation at the branch between suction pipeline (upstream the discharge valve) and the RCS, or the HL pipe.

(17) Phase separation/vertical flow with and without mixture level—Core (indirectly visualized, Fig. 15.7). Boiling in the core, including subcooled boiling, is expected following the SBLOCA induced depressurization even in situations where the RPV level in the core region remains above TAF.

(18) Pool formation in UP (visualized, Fig. 15.7). The “UP pool formation” phenomenon may be originated by CCFL at UTP and implies nonuniformity in the distribution of void fraction along the RPV axis. A deep nonuniformity in the void fraction does not appear from the diagram in Fig. 15.7. However, the formation of a time-varying level in UP constitutes the result of the calculation.

(19) Spray effects—Core including cooling and distribution (visualized, Fig. 15.13). This is related to a BWR and is expected in the SBLOCA4 scenario (row 38 in Table 15.1), following the actuation of HPCS and, later on, of LPCS.

(20) Stratification of boron (visualized, Fig. 15.60). Boron mixing and transport including stratification in vertical components (like DC, liquid pools, etc.) constitute expected SBLOCA phenomena. Boron-related phenomena are described in Section 15.4.12.8.

(21) Tracking of noncondensable gases (indirectly visualized, Fig. 15.8). The establishment of global NC conditions, which establishes between core and containment system of AP1000, implies the effect of noncondensable gases.

15.4.3.4 SBLOCA in reactors other than PWR with UTSG

SBLOCA in reactors other than PWR equipped with UTSG, here including the standard PWR and the AP1000, may evolve in different ways from a quantitative view-point (i.e., compared with what described earlier). However, key phenomena qualitatively evolve according to the provided discussion (D’Auria et al., 1996a).

Notes related to SBLOCA in those reactors in addition to, or as a replacement for what stated earlier, are:

- The NC in reactors like BWR, PWR-O, PWR-V (VVER), CANDU, PHWR, and RBMK shows different characteristics from PWR-UTSG. This is discussed in Section 15.4.12.2.
- Single-phase or two-phase stratification in two-phase horizontal pipes, in the presence of nuclear fuel, is typical of CANDU reactors, see also discussion in Section 15.4.2.
- The presence of fuel boxes in BWR, PHWR, and VVER-440 affects the SBLOCA scenario also by causing a specific NC flow path, i.e., between core active region and bypass region.
- Cooling of the core by moderator during SBLOCA occurs in CANDU and

PHWR.

- The actuation of ADS is foreseen during BWR SBLOCA. The ADS actuation causes the SBLOCA to evolve into an IBLOCA with break in the steam region. The ADS actuation is needed to allow the intervention of the low-pressure ECCS and the system recovery.

15.4.4 The LOFW

The LOFW scenario in PWR with UTSG is discussed considering the three parts proposed in Section 15.4.1. The following preliminary notes apply:

- The LOFW accident scenario is EOP and operator action dependent, like all or most of long-lasting accidents (e.g., time duration >about 30'). So, different LOFW evolutions shall be expected in individual NPP units.
- No loss of integrity for RCS occurs.
- Low (or no) role for the containment because of item listed earlier.
- Part of group of four scenarios where similarities in system performance are expected (at least in relation to some periods and some phenomena), e.g., LOFA (or MCP-trip), LOFW, SBO, and LOOSP (respectively, Sections 15.4.12.9, present section, 15.4.5, and 15.4.6).

Differences in the scenarios in other reactor types are outlined in the second part of the section.

15.4.4.1 Qualitative accident scenario: LOFW

Feedwater allows power removal from SG SS during the nominal operation. The loss of FW is immediately detectable because of the decrease in the level in the affected SG. In a few seconds scram and isolation of the turbine occur. Then, the recovery procedures for the system are actuated. Key features for the scenario can be listed as follows:

- Core cooling by natural circulation, assuming MCP-trip occurs early into the transient.
- During the initial dozen seconds PS pressure may increase till the opening of the PORV and SS pressure increase may also cause opening of SRV.
- MI decrease in PS may occur due PORV opening. Typically this does not cause

DNB situations in the core. MI recovery may occur due to the HPIS intervention.

- RCS recovery is based upon feed and bleed of SG.

15.4.4.2 Quantitative accident scenario: variable trends and TSE - LOFW

Four main phenomenological windows may be distinguished during typical LOFW in standard UTSG equipped PWR:

(I) Loss of heat sink and PS pressurization lasting a few dozen seconds.

(II) Affected SG boil-off, till AFW restoration: this may take a few minutes.

(III) SG feed and bleed and PS recovery till the actuation of RHR (PS pressure around 2 MPa): this may take a couple hours.

(IV) Long-term cooling: from the previous event till the time when stable cooling conditions are reached at nearly atmospheric pressure: this may take a few hours.

The LOFW scenario in case of unavailability of AFW for a PWR equipped with UTSG can be derived from the TSE in Table 15.10 and Figs. 15.15 and to 15.16 taken from OECD/NEA/CSNI (2011) (row 21 in Table 15.1). The recovery of RCS is achieved by feed and bleeds in PS; namely, combined operations of HPIS and PRZ discharge valves allow the recovery.

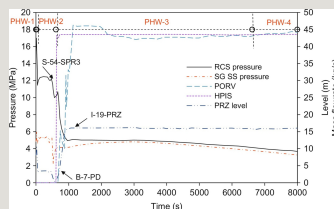


Fig. 15.15 LOFW in PWR and phenomena characterization: PS and SS pressure, PRZ level, and HPIS and PORV flowrates.

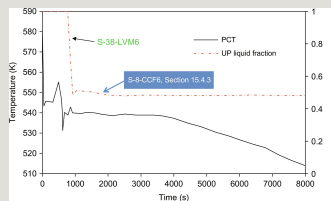


Fig. 15.16 LOFW in PWR and phenomena characterization: liquid fraction in UP and RST.

Table 15.10

LOFW in PWR equipped with UTSG: (selected) imposed and calculated events

--

Making reference to the reported time trends and in addition to what stated for the qualitative analysis of the LOFW, the following can be added:

- Following an initial peak during PHW-1, PS pressure stabilizes at a value close to saturation temperature in UP during the PHW-2.
- The operator control of the PORV (at around 670 s into the transient as from Table 15.10) causes the PS pressure to fall at the SS pressure.
- The situation of pressure equalization is achieved without causing core uncover (Fig. 15.16).
- Following the pressure equalization, the RCS configuration can be synthesized as follows (Figs. 15.15 and 15.16):
 - PORV bleed flow balanced by HPIS feed flow;
 - liquid level at top of PRZ (consistently with the condition PORV open);
 - UP level formation and core level below TAF (row 11 in Table 15.10); and

- RST not experiencing dry-out (however, margin to DNB not known).
- Further lowering of the RCS pressure causes ACC intervention during PHW-4 and, later on, the RHR-LPIS actuation and the recovery of the unit.

15.4.4.3 Phenomena connection with accident scenario: LOFW

The phenomena listed in the second and the third columns of Table 15.11 are connected with LOFW from the cross-link process in Tables 15.3 and 15.4. Those phenomena are associated with variables in Figs. 15.15 and 15.16, as reported in the fourth column of the table.

Table 15.11			
Phenomena visualized by variables representative of the accident scenario LOFW			

^a The use of Fig. 15.16 is finalized to the visualization of the phenomenon S-8-CCF6 from Table 15.9.

The following phenomena are outlined in this section or (visually) described through the use of calculated accident scenarios and related time trends (whenever possible):

(1) Pressure drops at geometric discontinuities including containment (visualized, Fig. 15.15). The transient evaluation of PDGD is needed to calculate fluid velocity in any location of a thermal-hydraulic system (e.g., RCS and containment) and occurs in any accident scenario. As already mentioned, the phenomenon has been (arbitrarily) assigned to LOFW and is visualized through the HPIS flowrate. Furthermore, two parts for the total pressure drop at any geometric discontinuity shall be distinguished known as reversible and irreversible contribution. Only the latter term contributes to PDGD and is considered in calculations by SYS TH codes through the “K-loss” coefficient. The reversible part may be at the origin of local evaporation if the saturation pressure associated with upward liquid

temperature is higher than the pressure low-value which establishes within a short distance (typically mm) at the discontinuity. In the case of the inlet of a cylindrical nozzle/pipe where TPCF occurs at the outlet, vapor generated in at the entrance may largely affect TPCF. This local phenomenon is called cavitation at sharp edge (D'Auria et al., 2003a). Thus, the evaporation occurrence at geometric discontinuity is also relevant to phenomenon B-3-EV1 in Section 15.4.2.

(2) PRZ thermal-hydraulics (visualized, Fig. 15.15). PRZ performance is relevant during all scenarios in PWR. The situation of PRZ full and PS emptying depicted in Figs. 15.15 and 15.16 is possible in the case of PORV continuous operation and occurrence of CCFL at the surpline connection with HL.

(3) Spray effects—PRZ (indirectly visualized, Fig. 15.15). During LOFW with MCP in operation, the PRZ pressure can be controlled by spray line to prevent the PORV opening or to mitigate the mass loss from the PORV.

Furthermore, phenomenon S-8-CCF6 from Table 15.9 is visualized in Fig. 15.16.

15.4.5 The SBO

The SBO accident scenario is part of group of four scenarios where similarities in system performance are expected (at least in relation to some periods and some phenomena), e.g., LOFA (or MCP-trip), LOFW, SBO, and LOOSP (respectively, Sections 15.4.12.9, 15.4.4, present section, and 15.4.6).

SBO evolves into LOOSP when the on-site electrical power generation (i.e., from Diesel Generators) is lost. However, the distinction in terms between SBO and LOOSP is not always recognized within the international community.

15.4.5.1 Qualitative accident scenario: SBO

Qualitative accident scenario for SBO reflects the scenario described for LOFW. Furthermore, following scram (i.e., assuming the availability of the scram function):

Basically, in case of SBO:

- LOFW and MCP-trip occur.
- PRZ PORV actuation and SRV actuation in SG are not avoidable.
- Diesel Generators (DG) enter in operation at the earliest time, typically a few

seconds after the event.

- AFW is the key system to recover the plant.
- NC is the only mechanism to remove decay power from the core.
- PHW is basically those identified in case of LOFW (Section 15.4.4).

15.4.5.2 Quantitative accident scenario: variable trends and TSE - SBO

PHW in case of SBO is similar to those identified in the case of LOFW (as already mentioned) and is indicated in Figs. 15.17 and 15.18.

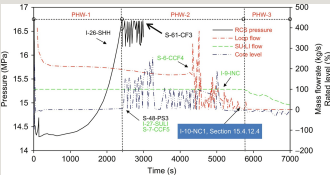


Fig. 15.17 SBO in PWR with UTSG and phenomena characterization: RCS-PS pressure, flowrate in one loop, and across PRZ Surgeline and core level.

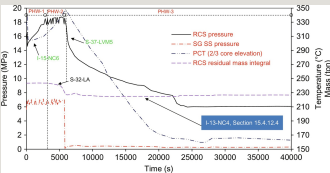


Fig. 15.18 SBO in PWR with HOSG and phenomena characterization: RCS-PS and SS pressure, RST, and RCS-PS MI.

Typical SBO scenarios for a PWR equipped with UTSG can be derived from the TSE in Table 15.12 and Figs. 15.17 and 15.18 taken from Bittan (2015) and D'Auria et al. (2006), rows, 33 and 34 in Table 15.1, respectively.

Table 15.12

SBO in PWR equipped with UTSG: (selected) imposed and calculated events



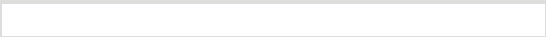
Following SBO occurrence scram occurs (almost instantaneously). Loss of flow in PS occurs together with partial loss of the heat sink (no FW available). This causes a boil-off condition in both PS and SS. Openings and cycling of PORV and SRV in PRZ and SG are expected. Specific EOP can be designed to mitigate the consequences and to recover the RCS.

15.4.5.3 Phenomena connection with accident scenario: SBO

The phenomena listed in the second and the third columns of Table 15.13 are connected with SBO from the cross-link process in Tables 15.3–15.5. Those phenomena are associated with variables in Figs. 15.17 and 15.18, as reported in the fourth column of the table.

Table 15.13

Phenomena visualized by variables representative of the accident scenario SBO



The following phenomena are outlined in this section or (visually) described through the use of calculated accident scenarios and related time trends (whenever possible):

(1) Liquid accumulation in horizontal SG tubes (indirectly visualized, Fig. 15.18). Horizontal tubes in VVER-440 and VVER-1000 are connected with inlet and outlet headers at different elevations. Condensation is at the origin of liquid formation in the horizontal tubes and may affect NC. Additional information, not in the form of time histories, can be derived from fundamental research

documented in the papers at row H of Table 15.5, Hyvarinen (1996), and Schaffrath et al. (2001).

(2) Phase separation/vertical flow with and without mixture level—Pipes and Plena (visualized, Fig. 15.17). The mixture core level allows the (direct) visualization for the phenomenon. Phase separation without mixture level shall be taken as a synonymous of Collapsed Liquid Level (CLL). CLL established in a saturated liquid occurs in the absence (or low) of thermal power exchange and depressurization rate. Otherwise mixture level establishes which is effective for ensuring nucleate boiling conditions. Mixture level formation in the secondary side of HOSG by Melikhov et al. (2011).

(3) Structural heat and heat losses (indirectly visualized, Fig. 15.17). The release of structural heat and the value of heat losses constitute a challenge in the experimental simulation of RCS. In scaled ITF, the values of thermal power from passive structures and heat losses to environment per unit core power are (much) greater than in the NPP. Furthermore, the values of both quantities can be affected by errors. Rather than a phenomenon, structural heat and heat losses shall be seen as a boundary condition affecting various phenomena and creating distortions in the simulation of accident scenarios in NPP by ITF. Structural heat and heat losses may play a relevant role in all transients.

(4) TPCF—Valves (indirectly visualized, Fig. 15.17). Opening of PORV and SRV of SG causes TPCF. The geometric complexity of flow paths in valves, including the possible occurrence of multiple critical sections and/or changes in critical section location during a transient, makes necessary the experimental evaluation of TPCF in valves. The TPCF during PORV cycling causes the pressure fluctuations shown in Fig. 15.17.

In Figs. 15.17 and 15.18, phenomena which are not part of Table 15.13 are indicated in clear green (see also discussion in Section 15.4.1).

Furthermore, phenomena I-10-NC1 and I-13-NC4 from Section 15.4.12.4, Table 15.27 are visualized in Figs. 15.17 and 15.18 (white characters in light blue label), respectively.

15.4.6 The LOOSP

The LOOSP accident scenario is part of group of four scenarios where similarities in system performance are expected (at least in relation to some periods and some phenomena), e.g., LOFA (or MCP-trip), LOFW, SBO, and LOOSP (respectively,

Sections 15.4.12.9, 15.4.4, 15.4.5, and present section).

LOOSP is the follow-up of SBO when the on-site electrical power generation (i.e., from Diesel Generators) is lost. However, the distinction in terms between SBO and LOOSP is not always recognized within the international community.

Reactor protection system is designed to avoid the occurrence of LOOSP (i.e., stopping the accident severity to the level of SBO). Therefore LOOSP is a BDBA. The interest for the accident scenario in the present chapter is till the time when core damage occurs.

15.4.6.1 Qualitative accident scenario: LOOSP

The qualitative accident scenario in the case of LOOSP is the same as SBO roughly for about 1 h after the event occurrence:

- Decay power produced by core is removed by NC to the SG.
- PRZ pressure stabilizes close to the opening/closure pressure of PORV: this causes coolant MI loss.
- SG pressure stabilizes close to the opening/closure pressure of SRV: SG emptying occurs in a time between 0.5 and 1 h.
- PORV cycling causes the well-known condition of PRZ full of coolant and core-level depressed: CCFL at surgeline connection with HL in combination with depressurization at PRZ top caused by valve opening are at the origin of the phenomenon. It may be noted here that the presence of a large volume PRZ in the RCS is not beneficial for core cooling during the LOOSP scenario.

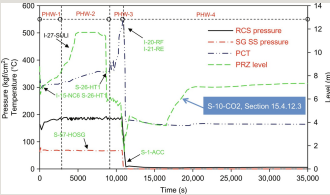
In the absence of the actuation of any AM procedure (e.g., timely PS and/or SS depressurization) MI lost causes dry-out in core region and severe core damage at time which is around 2 h after the occurrence of the event. The actuation of AMP (see later, also discussed in Section 15.4.11) may largely shift the time of core damage.

15.4.6.2 Quantitative accident scenario: variable trends and TSE - LOOSP

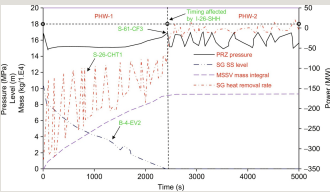
PHW in case of LOOSP is similar to those identified in the case of LOFW (as already mentioned) and is indicated in Figs. 15.19–15.22.

Typical LOOSP scenarios can be derived from the TSE in Table 15.14, PWR with

in Table 15.1).



and SS pressure, RST (PCT elevation), and PRZ level.



lost from MSSV.

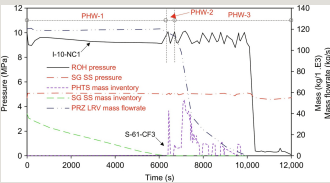


Fig. 15.21 LOOSP in CANDU and phenomena characterization: PS and SS pressure and MI and flowrate across the PRZ relief valve.

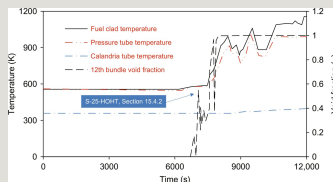


Fig. 15.22 LOOSP in CANDU and phenomena characterization: core void fraction and RST.

Table 15.14

LOOSP in PWR with UTSG: (selected) imposed and calculated events

--

Possible objectives for (quantitative) LOOSP analyses are:

- A. to estimate times of first PORV and SRV opening, loss of SG heat sink, stop of NC, core uncover, core temperature above (licensing) acceptable value, and core loss of geometric integrity;
- B. CET values and timing for possible start of AMP; and
- C. to estimate the applicability and validity of AMP.

The estimation of validity of SAMP for mitigation of severe accident consequences may constitute an objective for application of severe accident computational tools.

The calculation in Fig. 15.19 shows the effectiveness of selected AMP to keep the core coolable for more than 10 h.

The calculations in Figs. 15.20–15.22 show timing (predicted or foreseeable) for core damage in the range between 2 and 4 h applicable for current PWR and CANDU, in the last case considering the intrinsic availability of the heat sink constituted by the moderator.

15.4.6.3 Phenomena connection with accident scenario: LOOSP

The phenomena listed in the second and the third columns of Table 15.15 are connected with LOOSP from the cross-link process in Tables 15.3 and 15.4. Those phenomena are associated with variables in Figs. 15.19 and 15.21, as reported in the fourth column of Table 15.15. In Fig. 15.19 one phenomenon from Section 15.4.12.3 is also visualized (clear blue label). Figs. 15.19–15.21 include identification of phenomena visualized in different accident scenarios (clear green) and Fig. 15.22 allows visualization of a phenomenon in Section 15.4.2 (clear blue label).

Table 15.15

Phenomena visualized by variables representative of the accident scenario LOOSP



The following phenomena are outlined in this section or (visually) described through the use of calculated accident scenarios and related time trends (whenever possible):

- (1) Surgeline hydraulics (indirectly visualized, Fig. 15.19). Emptying and filling of PRZ, as well as mass and energy exchange between PRZ and HL are affected by surgeline hydraulics. This phenomenon also determines the conditions for CCFL (in the surgeline) and the consequent filling of PRZ (see also Doi et al., 2012).
- (2) Wall to fluid friction (indirectly visualized, Fig. 15.19). The transient evaluation of wall to fluid friction is needed to calculate fluid velocities at any location of a thermal-hydraulic system (e.g., RCS and containment) in single- and two-phase conditions. The phenomenon occurs in any accident scenario. It has been (arbitrarily) assigned to LOOSP and is visualized through the core

15.4.7 The SGTR

The SGTR is originated by the leakage from one or more tubes or the (guillotine) rupture of those tubes in SG. In the case of VVER, the acronym PRISE includes leakages and ruptures (“Primary to Secondary”), which can also occur through the headers which support the tubes in HOSG.

A Steam Generator Tube Rupture (SGTR) in a Pressurized Water Reactor (PWR) as well as a PRISE in VVER can lead to radioactivity release to the environment bypassing the containment. The radioactivity may be transported via the secondary system, exiting through the SRV of the affected Steam Generator. That is the main reason why SGTR historically have been treated in a special way within Deterministic Safety Analysis (DSA), focusing on the radioactive release more than in the possible core damage, as it is done in the other LOCA. This also constitutes the motivation for the present section.

Section 15.4.12.5 in this chapter deals with correlations between MSLB and SGTR and includes mentioning of the multiple SG tube rupture. Therefore focus for the present section is the single-tube rupture.

15.4.7.1 Qualitative accident scenario: SGTR

In a single-tube SGTR event, the pressurizer pressure and level start to decrease simultaneously with the decrease of the Main Feedwater flow of the faulted SG to compensate the extra mass flow from the ruptured tube. In this phase, the operator can guess which SG is the faulted one with the help of radiation monitors in the steam lines.

The operators can start to manage the transient before the scram decreasing the turbine load and therefore the reactor power. They can also increase the charge flow and stop the letdown trying to compensate the break flow of the ruptured tube. Once the reactor is shutdown (manually or automatically), the operators have to identify (or confirm the identification) the faulted SG and isolate it stopping the AFW and closing the Main Steam Isolation Valve and the turbo-driven pump steam feed.

Once the faulted SG is isolated, the main goal is to stop the faulted tube leak via primary and secondary pressure equalization. Therefore, in a first step, the PS is cooled down via SS depressurization through intact SG SRV or steam dump to the condenser. Then the PS is depressurized to the faulted SG pressure via PRZ spray or PORV.

The following topics are relevant for the SGTR, accident scenario:

A. Radioactivity release. The radioactivity release to the environment with containment bypass is of main concern for the accident scenario as already mentioned.

B. Accident parameters. Boundary conditions for the accident like elevation the rupture and time of detection of the event may affect the overall scenario and the radioactivity release. The elevation of the break affects the release of radioactive materials into the liquid or steam phase of the SG SS. In the former case lower release to the environment and delay in detection of the accident may be expected. Moreover, the level in the affected SG SS should be kept above the elevation of the break, although identification of break elevation is typically not possible. The time of detection of the event depends upon settings of operation set-points for system or parameters like PRZ and SG level and CVCS, also affected by unavoidable leakages between PS and SS during nominal operation. SGTR detection time including time needed to identify the faulted SG may range between a few minutes and a couple of dozen minutes.

C. Boron. Flow reversal at the rupture (i.e., from SS to PS) may cause on the one hand stop of radioactivity release into the SG and on the other hand inlet of deborated liquid into the primary coolant. So the EOP design aim at keeping close the PS and SG pressure with suitable margin to avoid inlet of SS water into the PS. It may be noted that “boron risk” for core integrity depends upon the time into the fuel cycle period: higher at BOC and lower at EOC (consequences of boron dilution also discussed in Section 15.4.12.8).

D. Pressurized Thermal Shock. Fast PS depressurization and overfeed by HPIS (highly borated water) may cause an overall decrease of PS to SS mass transfer and radioactivity lost from PS, but create the potential for PTS. EOP design take into account of such risk (PTS discussed in Section 15.4.12.3).

E. Integrity of SS challenged. Overfeeding of SG SS, i.e., the broken SG because of the break flow and because of the need to minimize radioactivity release to environment (as discussed in item B.) and the intact SG in order to ensure (or to make easier) the control of PS pressure, may be part of the EOP design (see also “quantitative” description of the accident scenario later). This causes the condition of “solid” SS with risk for water hammer and/or condensation induced water hammer (IAEA, 2009b).

15.4.7.2 Quantitative accident scenario: variable trends and TSE—

SGTR

The TSE table related to the Doel-2 SGTR accident is reported in Table 15.16 as summarized by Reocreux (2008).

Table 15.16

SGTR in PWR equipped with UTSG: events from Doel-2 accident (1979)

Typical SGTR scenarios can be derived from Table 15.16 and Figs. 15.23 and 15.24, Doel-2, PWR with UTSG taken from OECD/NEA/CSNI (1988) (row 41 in Table 15.1) and Fig. 15.25, VVER-440, taken from IAEA (2009b) (row 31 in Table 15.1).

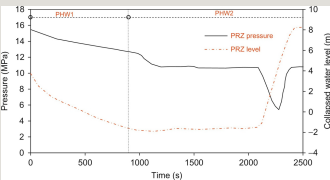


Fig. 15.23 SGTR in PWR with UTSG and phenomena characterization: PRZ pressure and level.

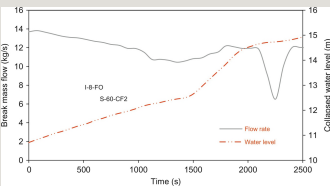


Fig. 15.24 SGTR in PWR with UTSG and phenomena characterization: break flow and affected SG level.

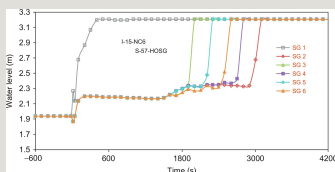


Fig. 15.25 PRISE in VVER-440 (PWR with HOSG) and phenomena characterization: level in SG SS.

The time histories in Figs. 15.23 and 15.24, either calculation results or data measures during the Doel-2 event, give an idea of the management of the event. Three PHW are distinguished identified in Table 15.16 as diagnosis phase, mitigation phase part 1 (getting the control of the RCS) and mitigation phase part 2 (toward the RCS recovery).

The PRISE in VVER-440, Fig. 15.25, has been calculated under the condition of isolation for the feedwater flow to the affected SG, and of trip of the main coolant pump associated with the defective SG. In addition, cooldown through BRU-K (condenser dump valve) on intact loops, primary system depressurization, and termination of the HPSI system intervention were imposed. The time histories in Fig. 15.25 show (a) the asymmetric SG performance and (b) the occurrence of the over-feed condition for all SG.

15.4.7.3 Phenomena connection with accident scenario: SGTR

The phenomena listed in the second and the third columns of Table 15.17 are connected with SGTR from the cross-link process in Tables 15.3 and 15.4. Those phenomena are associated with variables in Figs. 15.24 and 15.25, as reported in the fourth column of Table 15.17.

Table 15.17

Phenomena visualized by variables representative of the accident scenario SGTR

The following phenomena are outlined in this section or (visually) described through the use of calculated accident scenarios and related time trends (whenever possible):

(1) Flow through openings (visualized, Fig. 15.24). The phenomenon deals with RCS shutdown conditions when the PS is open to the containment (Section 15.4.12.11). Modeling features needed to predict shutdown conditions flow at openings may be the same (or similar) needed to predict flows at SGTR break when TPCF conditions are not established and flow reversal (i.e., from SS to PS) occurs.

(2) NC with horizontal SG (visualized, Fig. 15.25). Natural circulation during SGTR is expected in the loop with the affected SG. In intact loops the MCP may be in operation to allow RCS pressure control by spray in PRZ.

(3) Thermal-hydraulics of horizontal SG, PS, and SS (visualized, Fig. 15.25). Heat transfer across SG is essential to recover RCS following SGTR. One may also state that SGTR is a special SBLOCA, and SBLOCA is characterized by the importance in the role of SG. Asymmetric SG performance is expected during SGTR and can be noted from Fig. 15.25.

(4) TPCF—Pipes (visualized, Fig. 15.24). TPCF at the rupture location occurs during the “undetected period” (i.e., nominal RCS conditions with anomalies in PRZ and SG levels) and, once the SGTR scenario occurrence is recognized, in the period when SS pressure remains below the critical pressure that establishes at the rupture location. The geometric shape of the rupture may have a role in TPCF values (see Féburie et al., 1993).

15.4.8 The MSLB and the FWLB

In spite of specific control program, two guillotine pipe breaks of feed water system piping have occurred in 1990 and 1993 at Unit 1 and Unit 2 of Loviisa NPP in Finland. These two pipe breaks and inspections performed have revealed that wall thinning can be very local in nature, and wall thinning of similar components in parallel lines can be completely different (Korhonen and Hietanen, 1994). After the first guillotine pipe break, the extent of control program was increased to comprise about 600 items to be inspected in each unit every year. This did not avoid the second guillotine break in 1993.

An MSLB constituted the topic of the first benchmark organized by OECD/NEA/NSC to demonstrate the capabilities of coupled three-dimensional neutron kinetics thermal-hydraulics codes. The MSLB was assumed in the Three Mile Island unit 1 and implied the calculation of recriticality or return-to-power (e.g., D'Auria et al., 2003a).

The earlier two statements give an idea of the importance of the MSLB issue in PWR. In the case of BWR, (a) the MSLB may cause the largest (pressure and temperature) loads for containment, (b) the opening of ADS, e.g., following an SBLOCA is equivalent to an MSLB. Furthermore, qualitative aspects may not be distinguishable between MSLB and FWLB. Namely, full pipe cross-section MSLB creates a faster depressurization transient than a full pipe cross-section FWLB.

MSLB complementary topics also relevant in other accident scenarios are discussed in this section:

(a) Transient three-dimensional neutron flux calculated for nonhomogeneous core conditions during MSLB is visualized.

(b) Snap-shot information about thermal-hydraulics of the OTSG is given, connected with the OECD/NEA/NSC TMI-1 benchmark and with the phenomena listed in Table 15.2 (also part of Table 15.19).

15.4.8.1 Qualitative accident scenario: MSLB and FWLB

Depressurization of the SG SS constitutes the first effect of MSLB (and FWLB): from the blowdown analysis view point the SS of SG has similar features as the RPV of a BWR (e.g., including initial pressure and average void fraction in the

system). Specific topics of interest for MSLB (and/or FWLB) are:

A. MSLB and RIA. Fast depressurization implies fast temperature decrease in SS. This causes a step coolant temperature decrease in PS, which propagates into the reactor core inducing a positive reactivity perturbation (further discussed in this section).

B. MSLB and SGTR. Pressure wave propagation from the break location and fluid-dynamic loads associated with high fluid velocity may challenge the integrity of SG tubes, i.e., creating the conditions for SGTR discussed in Section 15.4.12.5.

C. MSLB and PTS. Continuous operation of MCP after the event in combination with possible actuation of HPIS may create the condition for large fluid temperature decreases and negative temperature gradients inside DC of RPV, i.e., the potential for PTS, discussed in Section 15.4.12.3.

D. In some NPP all steam lines and all FW lines cross the containment in the same zone: isolation valves are installed in each line. The break of one pipe in that region may affect the integrity of other pipes: a hypothetical situation of multiple SL and FW line break is created, which may also challenge the maximum pressure allowable for the containment.

E. The MSLB originated by a break downstream the location of isolation valve constitutes the reference design accident for the turbine building. Pressurization of the building is terminated by closure of MSIV: design of accident detection system and of called ESF shall be consistent with the maximum allowable pressure in the building.

15.4.8.2 Quantitative accident scenario: variable trends and TSE—MSLB and FWLB

Typical MSLB and FWLB scenarios can be derived from Table 15.18 (MSLB in PWR), and Fig. 15.26, MSLB in PWR with UTSG, taken from Jeong et al. (2006) (row 26 in Table 15.1), Fig. 15.27, FWLB in APR1400 experimental simulator, taken from Bae et al. (2014) (row 10 in Table 15.1), Fig. 15.28, MSLB in PWR with UTSG and OTSG, taken from Jeong et al. (2006) and D'Auria et al. (2003a) (rows 26 and 27 in Table 15.1, respectively), and Fig. 15.29 taken from Sankovich and McDonald (1971) and Guimaraes (1992) (rows L and M in Table 15.5, respectively).

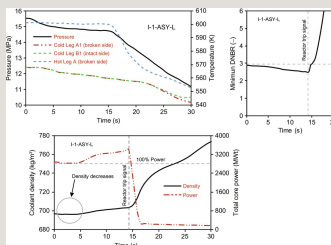


Fig. 15.26 MSLB in PWR with UTSG and phenomena characterization. Top left: PRZ pressure, coolant temperature in HL and CL. Bottom: power and average coolant density in the core. Top right: DNBR.

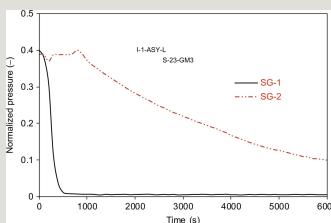


Fig. 15.27 MSLB in PWR with UTSG (simulation of ITF experiment) and phenomena characterization: asymmetry in SG pressure and long-term system performance.

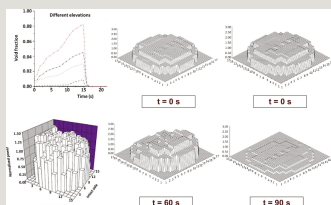


Fig. 15.28 MSLB in PWR with UTSG (left) and OTSG (right) and phenomena characterization: three-dimensional performance of neutron flux and (detail in top left) local void production in the hot FA.

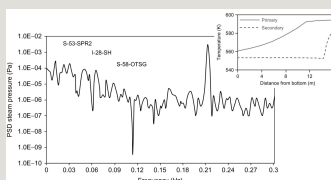


Fig. 15.29 Thermal-hydraulics of OTSG (associated, in the present document to MSLB accident scenario): PSD of the OTSG outlet pressure and (detail) temperature profile along the axis for PS and SS fluid.

Table 15.18

MSLB in PWR with UTSG: (selected) imposed and calculated events

--

Table 15.19

Phenomena visualized by variables representative of the accident scenario MSLB (and FWLB)

--

Typical RCS performance during MSLB can be derived from Fig. 15.26. The break occurrence causes a cold water plug arriving into the core in a few seconds, which causes a smooth fission power excursion and scram. Fluid temperature in HL is affected about 10 s after the event. DNBR achieves a minimum just before scram, that is, owing to the slight power increase.

The expected asymmetric performance of SG following FWLB is depicted in Fig. 15.27 (related to the ATLAS facility simulating APR1400). The same diagram gives an idea of the time needed for the recovery of the RCS.

The three-dimensional core power (or thermal neutron flux, or fission power) at different times during the transient can be seen from the sketches in Fig. 15.28 (left related to UTSG PWR, same calculation at the origin of Fig. 15.26; right related to OTSG PWR where a stuck withdrawn CR is assumed in the same region of the

core where [cold] flow the broken SG is coming). Occurrence of subcooled voids in the hot FA of the core can also be seen in Fig. 15.28, left.

A simplified overview of the OTSG thermal-hydraulic performance, which is relevant to any transient scenario and to phenomena listed in Table 15.2 can be derived from Fig. 15.29. On the basis of a suitable thermal-hydraulic model, the study of the pressure spectrum derived from NPP data (this shows a maximum at the frequency of 0.21 Hz) brought to the proposal of design modification for minimizing the oscillations. The oscillations were originated by density wave propagating through the boiling length.

15.4.8.3 Phenomena connection with accident scenario: MSLB and FWLB

The phenomena listed in the second and the third columns of Table 15.19 are connected with MSLB and FWLB from the cross-link process in Tables 15.3–15.5. Those phenomena are associated with variables in Figs. 15.26–15.29 and with Figs. 15.68 and 15.14 taken from other sections of this chapter, as reported in the fourth column of Table 15.19.

The following phenomena are outlined in this section or (visually) described through the use of calculated accident scenarios and related time trends (whenever possible):

(1) Asymmetric loop behavior (visualized, Figs. 15.26 and 15.27). The basic nature of MSLB and FWLB accident scenarios induces asymmetric loop (RCS) behavior. This also reflects in radial and azimuthal nonuniformities in thermal-hydraulics and neutron flux in the core (Fig. 15.28).

(2) Asymmetry due to the presence of a dam (indirectly visualized, Fig. 15.68). Dams are located in primary loop to keep a certain collapsed liquid level during RCS maintenance and refueling. Dams may introduce asymmetries in the loop performance and constitute part of the modeling for reactor shutdown analyses (Section 15.4.12.11).

(3) CRGT flashing (indirectly visualized, Fig. 15.14). Flashing of CRGT located in the lower plenum of BWR is delayed related to flashing of surrounding liquid in the LP. The reason for this is the higher subcooling inside CRGT (i.e., related to LP fluid) caused by high-pressure liquid continuous injected by an RPV external source for ensuring the high-pressure sealing and to prevent leakages of RPV fluid. Flashing is expected during depressurization caused by ADS opening in Fig. 15.14 (i.e., an MSLB type of situation). Geometric details about CRGT can be found in

the paper by Sehgal and Bechta (2016); blowdown studies dealing with the influence of subcooling can be found in the fundamental studies by Aumiller et al. (2000), Kolev (2006), and Ylonen (2008) (cited at row E in Table 15.5).

(4) Global multi-D fluid temperature, void, and flow distribution—SG SS (indirectly visualized, Fig. 15.27). An FWLB transient causes multi-D transient inside the SG. The modeling of the phenomenon affects the calculation of pressure shown in Fig. 15.27. Primary system parameters (Figs. 15.26 and 15.28) are also affected by multi-D modeling of SG SS through the HT across tubes.

(5) Spray effects—OTSG-SS (indirectly visualized, Figs. 15.28 and 15.29). The thermal-hydraulics of OTSG includes spray effects (in SG vertical tubes) and superheating for steam at the outlet of SG. Namely, feedwater in the OTSG is introduced through 32 spray nozzles connected to 14-inch semicircular headers (Sankovich and McDonald, 1971). Spray effect is part of the modeling capabilities to calculate OTSG performance at nominal conditions and during any accident scenario. The same considerations apply to the OTSG phenomena S-53-SPR2, I-28-SH, and S-58-OTSG in Table 15.19.

(6) Superheating in OTSG SS (visualized, Fig. 15.28). See discussion at item (5).

(7) Thermal-hydraulics of OTSG, PS and SS (visualized, Figs. 15.28 and 15.29). See discussion at item (5).

15.4.9 The RIA—reactivity excursion class of accident scenarios

A variety of RIA may occur in each NPP and are of interest to nuclear thermal-hydraulics. A comprehensive listing of RIA situations considered for each NPP as well as related accident scenarios is well beyond the purpose of the section. Chernobyl event discussed in Chapter 16 constitutes an RIA case. RIA and related scenarios are also part of safety demonstration for NPP. This constitutes the motivation for the section.

15.4.9.1 Qualitative accident scenario: RIA-CRE

Selected accident scenarios associated with RIA and relevant issues and topics (not an exhaustive list, including repetitions from other sections) are (see also D'Auria et al., 2004):

A. Background issue 1: RIA analysis (as a difference from majority of accidents) needs the consideration of instantaneous core status. Conditions like HZP, HFP

must be distinguished. For instance in LOCA analysis starting from HFP causes a challenge upon ESF more severe than starting from HZP. This is not necessarily true in the case of RIA where a number of initial core status need proper consideration (e.g., including cold zero power and intermediate status with the presence of neutron sources triggering the fission reaction).

B. Background issue 2: Beginning of Cycle (BOC), End of Cycle (EOC) conditions, as well as intermediate conditions (MOC) and BOL, need proper consideration in RIA analyses (see also the earlier item).

C. Background issue 3: Material composition of nuclear fuel including presence of plutonium (MOX fuel) is important for RIA analyses. Namely, transient production of poison materials like xenon and samarium needs proper consideration.

D. Background issue 4: RIA analysis needs three-dimensional transient modeling including suitable thermal-hydraulics (proper consideration of the phenomenon “Global multi-D fluid temperature, void, and flow distribution—Core”) and neutron physics models considering local material properties, noticeably nuclear cross-sections. The same analytical capabilities are needed for ATWS analyses discussed in Section 15.4.10 (rows 1–3 in Table 15.1).

E. Background issue 5: RIA analyses are needed for a number of component designs. For instance, (i) to confirm the acceptability of the design (worth) of a single CR, (ii) to confirm the design of a group of CR which move together; and (iii) to fix the maximum tolerable boron concentration at BOC.

F. Background issue 6: During an RIA transient nuclear fuel structure and geometric configuration may change (e.g., fuel fragmentation, ballooning, etc.). This requires specific consideration.

G. Example 1 for accident scenario, instability in BWR: oscillations in neutron flux coupled with oscillations in thermal-hydraulic parameters like local velocity, pressure, temperature, and void fraction may occur (and did occur in NPP) in BWR core (D'Auria et al., 1997b, see also Chapter 16 and the discussion about LaSalle-2 and Oskarshamn-2 events).

H. Example 2 for accident scenario, MSIV closure in BWR. Void collapses in the core happen following pressure wave generated at the closing of the valves. The accident scenario is qualitatively similar to the turbine trip event (discussed in Section 15.4.12.10, see also row 44 in Table 15.1), this one mitigated by the quick

opening of the condenser dump valves.

I. Example 3 for accident scenario, boron dilution in PWR. A boron diluted plug may form in certain SBLOCA transients, namely during the NC mode called reflux condenser (Section 15.4.12.4). Reactivity excursion may occur when the boron diluted liquid is transported into the core although mixing with borated fluid in the RPV may occur, as discussed in Section 15.4.12.8 (row 4 in Table 15.1).

J. Example 4 for accident scenario, MSLB in PWR. Cold liquid plug may be generated following the fast depressurization of one SG, inducing positive reactivity excursion in the core region, as discussed in Section 15.4.8 (rows 10, 26, and 27 in Table 15.1).

K. Example 5 for accident scenario, FP excursion following LOCA in PHWR, CANDU, and RBMK. Following an LOCA, an FP excursion may take place when (slight) positive void reactivity is tolerated in the core design. This is discussed in relation to CANDU by Rouben (1997) (row 11 in Table 15.1), in relation to PHWR by D'Auria et al. (2008a) (row 17 in Table 15.1), for details see Pecchia et al. (2011), and in relation to RBMK, by D'Auria et al. (2005) (row 13 in Table 15.1), see also D'Auria et al. (2008d).

L. Example 6 for accident scenario, CRE in any reactor design. Control Rod Ejection is a key event to demonstrate the safety of NPP and is discussed later.

Pioneering research to set-up the bases for transient three-dimensional coupled thermal-hydraulic and neutron kinetics calculations has been carried out at Pennsylvania State University (e.g., Ivanov and Baratta, 1999). An idea of the performed activity can be derived from Fig. 15.30, including the following diagrams: (a) power differences calculated in each FA by two methods; (b) axial power distribution at HZP; and (c) axial power distribution for the same core at HFP. The availability of qualified distributions for concerned quantities is a prerequisite to perform transient RIA analyses.

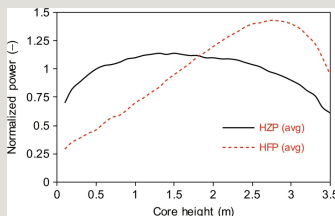


Fig. 15.30 RIA background analysis for a core of a PWR. Left: differences in radial/azimuthal core power calculated by two methods. Right: axial peaking factors at HZP and HFP.

15.4.9.2 Quantitative accident scenario: variable trends – CRE

CRE scenario is triggered by a failure in control rod drive mechanisms or in connected hardware. The ejection of one rod occurs in time period less than 1 s and the event is terminated by scram a few seconds after the triggering (TSE table not reported).

Typical CRE scenario can be derived from Figs. 15.30 and 15.31, CRE in PWR with UTSG (HZP and HFP conditions), taken from Todorova and Ivanov (2003) (row 8 in Table 15.1). Issues to be addressed from the (quantitative) analysis of the CRE are:

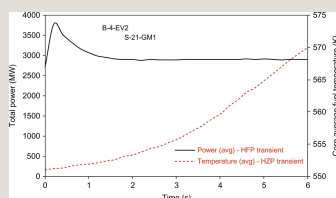


Fig. 15.31 CRE in PWR with UTSG and phenomena characterization: core power and fuel average temperature.

- Generation of local voids in transient subcooled boiling HT mode (e.g., D'Auria et al., 2004). Example of subcooled void fraction time history can be found in Fig. 15.28.
- Generation of pressure pulse in the RPV. This can be “absorbed” in PRZ, provided a suitable flow area is available in the surgeline (D'Auria and Galassi, 2004).
- Simultaneous (or delayed) occurrence of CRE and SBLOCA with break located in the upper head of the RPV, consequence of rod ejection. Break opening makes milder the pressure pulse in RPV.
- Possible occurrence of transient CHF and consequent RST excursion and possible change in fuel thermal properties (also mentioned in “background issue

6,” earlier) (D'Auria et al., 2004).

- Local feedback (around the ejected CR) of transient values for coolant temperature, density, and void and nuclear fuel parameter values like average temperature also affected by gap and pellet conductance and by possible changes in geometric configuration.

15.4.9.3 Phenomena connection with accident scenario: CRE

The phenomena listed in the second and the third columns of Table 15.20 are connected with MSLB and FWLB from the cross-link process in Tables 15.3 and 15.4. Those phenomena are associated with variables in Figs. 15.26–15.29 and with Figs. 15.68 and 15.14 taken from other sections of this chapter, as reported in the fourth column of Table 15.19.

Table 15.20

Phenomena visualized by variables representative of the accident scenario CRE



The following phenomena are outlined in this section or (visually) described through the use of calculated accident scenarios and related time trends (whenever possible):

- (1) Evaporation due to heat input (indirectly visualized, Fig. 15.31; visualized, Fig. 15.28). The basic phenomenon occurs in all scenarios where void is produced in the core region. Subcooled voids are generated following CRE and constitute an example for connecting accident scenario and phenomenon.
- (2) Global multi-D fluid, temperature, void, and flow distribution—Core (indirectly visualized, Fig. 15.31). The consideration of three-dimensional core performance is essential in the case of CRE, as discussed earlier. The time histories shown in Fig. 15.31 constitute the result of a calculation where global multi-D fluid, temperature, void, and flow distribution are taken into account.

(3) Parallel channel effects and instabilities PCEI (visualized, Fig. 16.3A and B in Section 16.4.3 of Chapter 16). The instability in BWR is an important topic in nuclear thermal-hydraulics (i.e., deserving a specific section like Boron, PTS, etc.). This is discussed in Chapter 16, including NPP data and proper literature references.

15.4.10 The ATWS

ATWS is an NPP system condition following an assigned PIE where scram is not fully actuated following the occurrence of related signals, that is, failure of scram on demand (a more comprehensive definition of ATWS can be found elsewhere). ATWS may be considered as an attribute of selected accident scenarios. For instance, the following transients can be defined: MCP-trip/ATWS, CRE/ATWS, SGTR/ATWS, MSLB/ATWS, and SBLOCA/ATWS. The common practice in NRS is to associate (relatively) “high” probability transient scenarios with the ATWS condition. Therefore, one should not find realistic analyses for LBLOCA/ATWS or LOOSP/ATWS.

The key feature of any ATWS is the interaction between thermal-hydraulics and neutron physics parameters: coupled three-dimensional modeling and calculations are needed.

15.4.10.1 Qualitative accident scenario: ATWS

Basic ATWS topics are:

A. Core operation in nominal conditions is typically associated with the best configuration for total reactivity (here intended as the capacity which ensures the highest thermal neutron flux). This is true when the same fluid has both the functions of coolant and moderator; i.e., the statement does not apply in the case of CANDU, PHWR, and RBMK. The same statement applies only partially to BWR and may not apply even in PWR when the boron concentration is very high. The connection between initial statement and ATWS is as follows: the ATWS implies a starting PIE, thus the perturbed system may not be in the best configuration; consequently, core power decrease following ATWS is expected. Unluckily, other system parameters may also not have their most effective value as far as core power removal function is concerned (e.g., low coolant flow following MCP-trip or low heat sink capability following LOFW). Thus ATWS puts a challenge to the integrity of the system.

B. The overall capability of relief valves in PS and SS (including in the latter case the condenser dump) is designed to remove maximum thermal power produced in

the core. Therefore, the opening of relief valves ensures protection for the structural integrity of the RCS

C. A specific issue associated with ATWS in the case of BWR consists in the overheating of the PSP water. Following an assigned PIE and the ATWS condition, MSIV closure occurs and SRV operate within design conditions: the issue arises because SRV discharge the two-phase fluid into the pool and the same pool is used as suction from ECCS pumps. Average heating of the pool above a given threshold (typically 80°C) induces problems for the availability of pumps. Then (only) a few dozen seconds are allowed for the operation of SRV with core at nearly nominal power.

D. Doppler effect or total power reactivity coefficients constitute intrinsic design features mitigating ATWS scenario.

E. Additional (independent) scram including devoted high-pressure boron tank constitute typical ESF to protect or to mitigate the risk associated with ATWS.

Notwithstanding the availability of ATWS-specific ESF, ATWS analyses are performed and may be requested within the licensing framework.

15.4.10.2 Quantitative accident scenario: variable trends and TSE —ATWS

An overview of typical ATWS scenarios can be derived from the TSE in Table 15.21, and Fig. 15.32, ABWR, taken from Ferng et al. (2010) (row 1 in Table 15.1) and Fig. 15.33, ABWR, taken from Huang et al. (2007) (row G in Table 15.5).

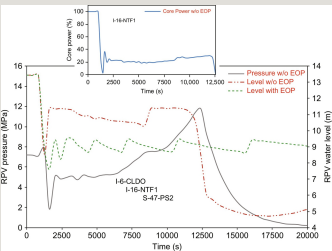


Fig. 15.32 ATWS in ABWR and phenomena characterization: RPV pressure and level. Detail core power.

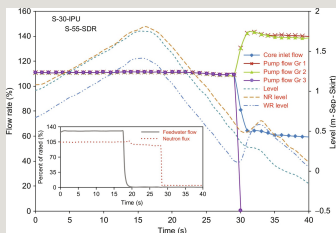


Fig. 15.33 ATWS type of condition in ABWR and phenomena characterization: RPV levels and flow from different groups of internal pumps. Detail: core power and FW flow.

Table 15.21

Typical ATWS in water cooled nuclear reactor: (selected) imposed and calculated events

--

Table 15.21 does not refer to any specific ATWS. Rather it provides an idea for timings expected for ATWS scenarios.

The data in Fig. 15.32 (not resulting from a three-dimensional coupled neutron physics thermal-hydraulic analysis) show ATWS duration of the order of 3 h, although core power is lower than the nominal value. One purpose for the concerned calculation is to determine the time available to operator to delay the boron injection.

The data in Fig. 15.33 are related to what has been called an ATWS-similar accident scenario. The reason is that scram occurs about 10 s after the stop in FW flow (detail in Fig. 15.33). The motivation for Fig. 15.33 is the availability of curves showing different performances for RPV internal pumps.

15.4.10.3 Phenomena connection with accident scenario: ATWS

The phenomena listed in the second and the third columns of Table 15.22 are connected with LOOSP from the cross-link process in Tables 15.3–15.5. Those phenomena are associated with variables in Figs. 15.32 and 15.33, as reported in

the fourth column of Table 15.22.

Table 15.22

Phenomena visualized by variables representative of the accident scenario ATWS



The following phenomena are outlined in this section or (visually) described through the use of calculated accident scenarios and related time trends (whenever possible):

- (1) Collapsed-level behavior in downcomer (visualized, Fig. 15.32). Collapsed liquid level typically occurs in conditions where pressure is increasing. The prediction of the level is important because connected with actuation of various NPP signals
- (2) Internal pump behavior (visualized Fig. 15.33). Different internal pumps may rotate at different speeds inducing further three-dimensional phenomena inside RPV.
- (3) Nuclear thermal-hydraulics feedback and spatial effect (visualized, Fig. 15.32). Nuclear thermal-hydraulic feedback can be observed from any ATWS calculation-based analysis. Spatial effects visualization need a three-dimensional calculation (e.g., by Kliem et al., 2009, at row 3 in Table 15.1).
- (4) Phase separation/vertical flow with and without mixture level—Downcomer (visualized Fig. 15.32). Phase separation is connected with (mixture and collapsed) level formation and entrainment-de-entrainment processes. Mixture-level formation is properly visualized from results of LOCA analyses (e.g., Fig. 15.13).
- (5) Steam dryer behavior (indirectly visualized, Fig. 15.33). Steam dryer performance is affected by level formation, specifically when vaporization processes occur owing to depressurization. Steam dryer (and separator) behavior affects the formation of level in downcomer due to pressure drops occurring inside.

Steam dryer integrity is challenged during accidents like MSLB, as discussed by Yan and Bolger (2009).

15.4.11 The AM procedures and selected related accident scenarios

Accident management and AMPs constitute important fields for the application of nuclear thermal-hydraulics. This shall be seen as the key motivation for the present section.

Basically, AM and AMP can be characterized by the following two statements: (a) they come into play during an accident in NPP following unexpected events or failures of systems and components including multiple failures of ESF; (b) they aim at ending further progression of any accident condition throughout prevention and mitigation actions, by adopting any resource available at NPP (including human resources), minimizing at the design-level (case of AMP) modifications needed to the hardware of existing NPP.

Historically:

- AM studies started after the TMI-2 event in 1979 (e.g., Petrangeli et al., 1993; D'Auria et al., 1997a).
- AMP have been interpreted as time follow-up of EOP, although AMP and EOP constitute integrated set of actions.
- Within the context at the item above, AMP are associated withbdba and EOP with DBA in licensing nuclear safety technology.
- Two areas have been distinguished for AM and AMP: out of DBA envelope but before core degradation and after core degradation. In the latter case the term SAMP is introduced.

In the present section only AM and AMP dealing with the “before-core-degradation” conditions are considered.

15.4.11.1 Qualitative accident scenarios: needing AM or following AM actions

The actuation of AMP is part of accident scenarios discussed in other sections of this document (see, e.g., LOOSP, Fig. 15.19 and SGTR with consequential MSLB, Fig. 15.53). Namely, the reference databases for AM in Table 15.1 include rows 12, 31, 34, and 40: related sections (other than the present one) deal with AM

information.

An idea of AM actions and issues having connection with nuclear thermal-hydraulics can be drawn from the following statements:

A. PS depressurization (e.g., Petrangeli et al., 1993). This is common practice in BWR and part of design-related EOP: e.g., any SBLOCA scenario may end-up with opening of ADS valves allowing the intervention of LPCI and LPCS and the recovery of the system. The same action may reveal troublesome in PWR because PS depressurization through RPV is not feasible and depressurization through PRZ causes the coolant accumulation in the PRZ owing to the CCFL occurrence in the surgeline.

B. SS depressurization (e.g., Madeira et al., 2003). This is an effective AM for PWR provided it is performed under proper RCS conditions: (i) depressurization of a steam filled SG may not bring-down the PS pressure owing to ineffective heat transfer across U-tubes and it is only effective if subsequent SG flooding is possible; (ii) depressurization of a liquid full SG in case PS is empty is also not effective owing to ineffective heat transfer across U-tubes and, in addition, may take long time not consistent with needs from core cooling (i.e., to prevent or to mitigate RST excursions).

C. Combination of PS and SS depressurizations (can be called consequential RCS depressurization) (e.g., Muellner et al., 2007). This may reveal the best action to prevent accident progression and to avoid core damage. The use of consequential depressurization stages combined with passive cooling of RCS is at the basis of the safety technology for the AP1000 reactor.

D. Coolant delivery from FW tank (e.g., Madeira et al., 2003). In all NPP as part of BOP, an FW tank, also called degasser-condenser, is installed downstream the main condenser and upstream the main feedwater pumps. The tank (or the group of tanks) has a volume of the order of 1000 m³ (in a 1000 MWe unit). The pressure is kept, during NPP operation at nominal power, at around 0.5 MPa and slightly subcooled liquid is present. Feeding the FW tank into a depressurized RCS (either PS or SS) reveals effective in removing decay power for a few hour without the need of external power.

E. Core Exit Thermocouples (CET). CET signal may be necessary to trigger the actuation of AMP (Toth et al., 2010): 400–600°C is the typical range of CET signals for entering thebdba virtual region and start of the AM devoted systems. The (thermal-hydraulics) issue is that superheated steam temperature at core outlet

is not easily or timely detectable owing to the influence of thermal inertia of solids present in the UP (e.g., the CRGT) and of phenomena like de-entrainment and deposition of droplets which may overshadow the fluid temperature at the location of the thermocouple. Refinement of measurement techniques is in progress allowing a straightforward connection between RST at PCT location and CET signals.

Complex AMP involving action with large asymmetries among performances or conditions of loops (PS and SS) have recently been the topic of experimental programs (see e.g., Mull et al., 2007).

15.4.11.2 Quantitative accident scenarios: needing AM or following AM actions

No typical TSE can be defined for an AMP or for an accident scenario where AM occurs. However, AM and AMP imply importance for the human (operator) actions; therefore time duration for accident scenarios involving AM are expected in the range of several minutes or hours rather than seconds.

Typical results from thermal-hydraulics analyses of transient with AMP can be derived from Fig. 15.34 dealing with CANDU, taken from Mehedinteanu (2009) (row 12 in Table 15.1), and Fig. 15.35 dealing with VVER-1000 taken from D'Auria et al. (2006) (e.g., row 40 in Table 15.1).

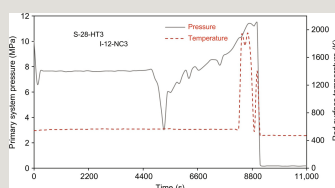


Fig. 15.34 Accident scenario with AM action in CANDU: PS pressure and RST.

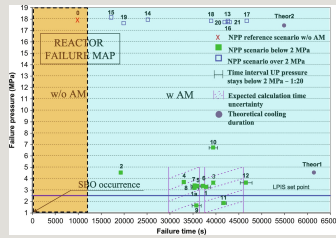


Fig. 15.35 Accident scenario with AM action in VVER-1000: reactor failure map following different AM actions.

In the case of CANDU, Fig. 15.34, the AM based upon an innovative system allows the prevention of core damage following scenarios which in the absence of such a system evolve into severe accidents. The concerned procedure involves: (a) the PS depressurization through the pressurizer with the two-phase mixture discharge into the degasser-condenser; (b) the subsequent “re-pumping” of the water into the RCS by the pressure difference intrinsically created.

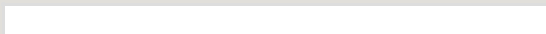
A study was performed to confirm the applicability of AMP developed for PWR with UTSG to the VVER-1000 (Fig. 15.35). Among various findings, it was demonstrated that core integrity (so-called grace-period) in case of LOOSP may be shifted for the Balakovo-3 Unit from less than 3 h (and possible RPV failure at high pressure) to more than 12 h (and possible RPV failure at low pressure) (see also Cherubini et al., 2008b). No major modification for the NPP is needed: the combination of PS and SS depressurizations allows the FW tank liquid to enter the SG keeping cooled the core. The execution of the VVER-1000 AM) study also involved an experimental program (Bucalossi et al., 2012) and contributed to the creation of a database for code validation and uncertainty in system thermal-hydraulics (Petruzzi and D'Auria, 2016).

15.4.11.3 Phenomena connection with accident scenarios: needing AM or following AM actions

The phenomena listed in the second and the third columns of Table 15.23 are connected with LOOSP from the cross-link process in Tables 15.3 and 15.4. Those phenomena are associated with variables in Fig. 15.34 as reported in the fourth column of Table 15.23.

Table 15.23

Phenomena visualized by variables representative of accident scenario involving actuation of AMP



The following phenomena are outlined in this section or (visually) described through the use of calculated accident scenarios and related time trends (whenever possible):

(1) HT [condensation]—SG structures (indirectly visualized, Fig. 15.34). The HT with condensation in SG occurs during various accident scenarios. In case of the concerned AM-related scenarios, the PS depressurization causes temperature decrease in PS which brings steam condensation in the SS.

(2) NC core bypass, hot and cold bundles (indirectly visualized Fig. 15.34). Different channels in the core need to be modeled in a variety of accident scenarios for reactors like BWR, CANDU, and RBMK. In the case of long-lasting accident scenarios relevant to AM, different flow conditions occur in various channels typically driven by NC.

15.4.12 Additional accident scenarios and related topics

Accident scenarios in addition to those considered in Sections 15.4.2–15.4.11 are analyzed here together with related topics, with the objective to complete the characterization of phenomena listed in Table 15.2. The words “related topics” include subjects of special interest to thermal-hydraulics which constitute phenomena, phenomenological windows or system, and components, part of accident scenarios. Six topics are considered:

(a) Critical Heat Flux (CHF) in Section 15.4.12.1. CHF is also part of phenomenon S-26-HT1 in Table 15.2 and is discussed with suitable detail in Chapter 7.

(b) Containment performance in Section 15.4.12.2. Containment is a key safety feature for NPP. The system performance is at the basis of phenomena I-18-PRB and S-42-NCOC in Table 15.2.

(c) PTS in Section 15.4.12.3. PTS involves the integrity of the RPV (in water

cooled reactor equipped with RPV) and implies an integrated analysis by thermal-hydraulics, structural mechanics and material damage by neutron fluence. Only thermal-hydraulics aspects are considered here. PTS-related phenomena are S-22-GM2, S-34-LVM2, and S-35-LVM3 (in the last case in relation to CL) in Table 15.2.

(d) Natural Circulation (NC) in Section 15.4.12.4. NC constitutes a PHW part of different accident scenarios where pump trip occurs. It is discussed by phenomena I-10-NC1 to I-15-NC6 and A-11-NC in Table 15.2.

(e) Boron dilution in Section 15.4.12.8. Boron mixing, transport, and stratification are considered by phenomena S-2-BO and A-12-BO in Table 15.2. In Section 15.4.12.8, attention is given to the boron dilution event, part of the boron transport. Consequences of boron dilution upon the fission power are mitigated by boron mixing.

(f) Nuclear fuel in Section 15.4.12.12. Nuclear fuel constitutes the motivation for safety analyses. The words “nuclear fuel” include the fuel rods, the Fuel Assemblies (FA), and the overall core. Thermal- or thermodynamics-related properties, like conductivity and heat capacity, gap conductance, quantities connected with reactor physics like enrichment, composition (e.g., MOX), and neutron cross-sections, material properties and related interactions like density and radiation-induced swelling, structural mechanics effects like ballooning, and system effects like burn-up, crud and oxide formation are of interest and have a connection with thermal-hydraulics.

The description of accident scenarios and related topics is provided according to the structure proposed in Section 15.4.1. Furthermore, AM could also have been part of this list. However, overall accident scenarios are involved. Thus AM is discussed in Section 15.4.11.

15.4.12.1 Calculation of CHF aimed at core design optimization

CHF is at the center of the attention in Chapter 7 and in several accident scenarios, see also the report (IAEA, 2001). Moreover, heat transfer and CHF are visualized in a number of diagrams in this chapter (e.g., Figs. 15.1, 15.9, 15.13, and 15.22). The purpose here is not to duplicate any discussion, rather, to confirm the relevance of the CHF phenomenon in nuclear thermal-hydraulics.

CHF topics and facts

Selected key topics associated with CHF phenomenon and CHF evaluation are:

- CHF value is one key parameter at the basis of the design, that is, the diameter and the length, of fuel rods part of the core of water cooled reactors.
- Maximum linear power (q'_{\max}), then attainable core power, and margin to dry-out are affected by CHF. Gathering scale-one experimental data for fuel assembly constitute the best practice to determine q'_{\max} and margin to dry-out. Therefore any nuclear fuel vendor/designer has access to an SETF to optimize parameters like number and configuration of spacer grids (specific CHF grids may be added to increase CHF at nominal operating conditions, as well as CHF expected following a transient), rod-to-rod distance and fluid velocities.
- CHF occurrence affects PCT value and related time following LBLOCA. In this connection, transient CHF value may differ from CHF determined under steady-state conditions.
- Complex phenomena and occurrences, not necessarily part of thermal-hydraulics, affect the CHF values like burn-up and associated swelling for the nuclear fuel pellets with changes in fuel rod gap size, ballooning, crud deposit, oxidation, etc.
- It is difficult to ensure the prediction of CHF value with an error less than 10% (or, any CHF prediction is affected by an error of 10% or greater).

Phenomena connection with accident scenario: CHF

CHF phenomenon-related information can be derived from Fig. 15.36 taken from PWR-core basic experiment (Visentini et al., 2014) (row 5 in Table 15.1), including the transient CHF formula (right side of the diagram) proposed by Sakurai et al. (1990).

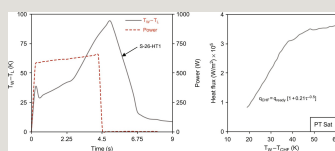


Fig. 15.36 CHF in basic test facility: transient conditions. Left: wall temperature and imposed power. Right: heat flux and wall temperature in nucleate boiling and film boiling (the legend "PT Sat" implies data in saturation conditions).

The phenomenon identified in the second and the third columns of Table 15.24 is connected with CHF from the cross-link process in Tables 15.3 and 15.4. The

phenomenon is associated with variables in Fig. 15.36.

Table 15.24

Visualization of CHF phenomenon



Only one phenomenon is outlined in this section and visually described through the use of experimental data (time trends) in basic facilities:

(1) HT [NCO, FCO, SNB, SANB, CHF/DNB, post-CHF]—Core, SG, structures (partly visualized, Fig. 15.36). The phenomenon deals with convection heat transfer and, namely, with boiling heat transfer. The phenomenon constitutes the subject for Chapter 7 and is visualized by a number of time trends related to accident scenarios, as already mentioned. In the paper by Visentini et al. (2014), several heat transfer regimes are considered, too. Noticeably, in the case of post-CHF (or film boiling conditions), radiation hat transfer may play an important role.

15.4.12.2 Containment performance

As in the case of CHF, containment is at the center of the attention in nuclear reactor safety (although no specific chapter of the book is devoted to containment), and in several accident scenarios, see also the reports (OECD/NEA/CSNI, 1989a, 1999, 2014; IAEA, 2009a). Moreover, containment-related phenomena are visualized in a number of diagrams in this chapter (e.g., Figs. 15.3 and 15.8). The purpose here is not to duplicate any discussion, rather, to confirm the relevance of the containment phenomena in nuclear thermal-hydraulics.

Containment topics and facts

Selected key topics associated with containment performance and containment phenomena are:

- Containment is at the same time a dynamic system, a safety component, and a

barrier to protect the environment and to mitigate the consequences of accidents. Containment can also be defined a passive system.

- Classification of containment systems is beyond the purpose for the present document. However, one may briefly recall the existence of full pressure and PSP or BC type containments (see e.g., Blinkov et al., 2012), of vented containments also called confinements, namely in the case of VVER-440 and RBMK NPP.
- Containment systems equipped with PSP and BC are used in BWR and VVER-440, respectively. In both cases, the objective is to reduce the maximum pressure which builds-up in the containment following an LOCA with an assigned (containment) building volume. Otherwise, the presence of BC and PSP is at the origin of possible oscillations and consequent loads upon structures caused by steam condensation processes.
- The importance of containment venting (venting is available in VVER-440 and RBMK NPP) resulted from the Fukushima event, see also Chapter 16.
- Containment systems are expected to withstand mechanical loads originated by pipe-whip, jet thrust, jet impingement, H₂ burning and deflagration, other than by pressurization, temperature gradients in the structures and by steam condensation into liquid pools. In all cases thermal-hydraulic analyses are necessary.
- A variety of thermal-hydraulic phenomena are expected to occur in containment systems during accidents in water cooled nuclear reactors. Examples of key phenomena are, in addition to steam condensation in PSP and BC subsystems, film-wise and drop-wise condensation in structures, natural convection in wide spaces, temperature stratification in pools and in steam-gas spaces, H₂ transport, and formation of liquid pools (e.g., in the sump). Furthermore the natural convection motions are also governed by pressure drops at geometric discontinuities having different three-dimensional shapes.

Phenomena connection with accident scenario: Containment

The containment-related phenomena for water cooled nuclear reactors considered in the present section can be derived from Fig. 15.37 taken from ABWR calculation (Chen and Yuann, 2015) (row 7 in Table 15.1) with the addition of the upper detail dealing with the check valve performance, taken from Hammersley et al. (2000) (row A in Table 15.5), Fig. 15.38, dealing with density lock performance, taken from Tasaka et al. (1992) (row B in Table 15.5), and Fig. 15.39, taken from AP1000 calculation (Hung et al., 2015) (row 6 in Table 15.1).

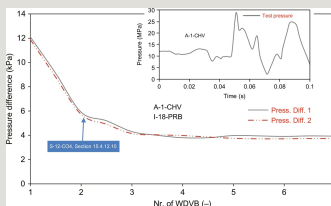


Fig. 15.37 ABWR containment performance following FWLB: dry-well/wet-well pressure difference with various operable WDVb. The upper detail shows the pressure differential across a check valve during an SETF experiment.

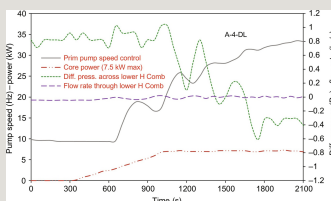


Fig. 15.38 Experimental simulation of PIUS-related density lock behavior: various system parameters during a start-up transient.

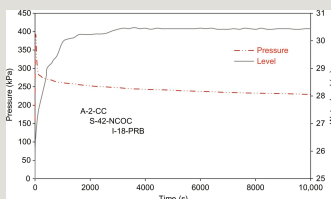


Fig. 15.39 DEHL break in AP1000: containment pressure and sump level.

Related to the ABWR calculation in Fig. 15.37, the WDVb leakage is modeled by a flow path connecting the lower dry-well and the wet-well airspace. There are eight WDVb installed in the containment. The key result is that three WDVb are enough to provide sufficient venting area to mitigate the negative pressure difference (allowed design threshold is 13.7 kPa); otherwise, if only one WDVb is operable, the peak value in the case of steam line accident (not shown in the figure) is expected to be greater than the design value.

The performance of an individual check valve in case of a separate effect

experiment can be deduced from the upper detail. A 2" check valve having 40 ms closing time is installed downstream a pressure vessel (initial pressure set at 12 MPa). The measured pressure response at a position downstream the valve is given in the figure. The peak observed pressure following check valve closure is seen to be 29 MPa.

In the case of PIUS (Fig. 15.38), the primary loop is connected to a neutron poison pool (borated water) through a lower and a upper vertical section, termed density lock, in which stable density stratification is established during power operation. The penetration of the poison water into the primary loop is prevented by keeping a balance between the pool static head and the loop differential pressure between the two density locks. Any perturbation in the primary loop causes inlet of borated liquid. The feasibility design of the system implies the demonstration of start-up process without inlet of borated water into the loop. The feasibility of the density lock-based system is confirmed from experimental data (e.g., time trends reproduced in Fig. 15.38).

Typical time trends for pressure and liquid level for containment during a DEHL break in AP1000 are reported in Fig. 15.39. The formation of liquid pool in the sump allows long-term core cooling for any PWR.

The phenomena listed in the second and the third columns of Table 15.25 are connected with containment performance from the cross-link process in Tables 15.3–15.5. Those phenomena are associated with variables given in Figs. 15.49–15.51 in the fourth column of the table.

Table 15.25			
Phenomena visualized by variables representative of the containment performance			

The following phenomena are outlined in this section or (visually) described through the use of calculated accident scenarios and related time trends (whenever possible):

(1) Behavior of check valves (visualized, Fig. 15.37). Check valves can be associated with different systems in an NPP. The association of check valves and BWR containment derives from the available paper (i.e., row 6 in Table 15.1). It is shown that check valves (smooth) operation controls the differential pressure loading upon internal structures. In addition (detail in the figure) large pressure waves can be expected from the dynamic operation (e.g., fast closure) of check valves.

(2) Behavior of containment emergency systems, PCCS (indirectly visualized, Fig. 15.39). PCCS affects the containment pressure in AP1000.

(3) Behavior of density locks (visualized, Fig. 15.38). Density locks shall be considered as a historic device (giving origin to the phenomenon in concerned documents). Density locks were proposed for the PIUS reactor concept after the Chernobyl accident, and experiments were performed in Japan. Density locks may ensure what was called “intrinsic” safety: any operation of the primary system outside the pressure range imposed by the height of the honeycomb (i.e., the physical component/structure which forms the density lock) causes highly borated liquid inlet into the core region and stop of the fission reaction. The PIUS concept was abandoned before the end of the past century, and density lock thermal-hydraulic performance is documented in the cited reference.

(4) Natural convection and H₂ distribution (indirectly visualized, Fig. 15.39). NCO and H₂ distribution contribute to the containment pressure. Direct visualization would imply the availability of local values of fluid velocities or concentration.

(5) Pressure-temperature increase and boiling due to energy and mass input (visualized, Fig. 15.37). Containment pressure and pressure differentials between compartments are affected by energy and mass exchanges. The concerned time trends deal with differential pressure build-up originated by steam flows and condensation in the PSP of an ABWR.

15.4.12.3 Pressurized thermal shock (PTS)

PTS topics and facts

An idea of thermal-hydraulic aspects which characterize Pressurized Thermal Shock can be derived from Fig. 15.40 (bases for the work by Araneo et al., 2011), Fig. 15.41 (Araneo et al., 2011; Kinoshita et al., 2012), and Fig. 15.42 (Araneo et al., 2011).

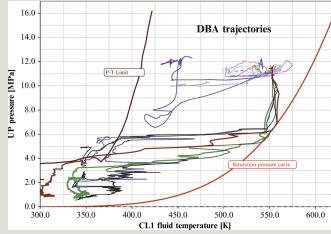


Fig. 15.40 PTS thermal-hydraulic aspects: identification of the worst transient based on trajectories in the phase space and limit thresholds at system level.

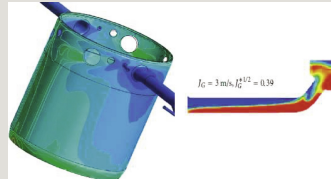


Fig. 15.41 PTS thermal-hydraulic aspects which need CFD. Left: results from liquid mixing for the estimation of PTS; Right: liquid (red) and air (blue) interacting in the HL (CCFL numerical simulation).

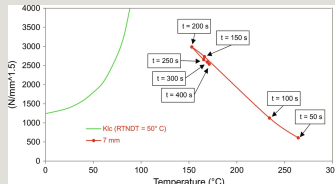


Fig. 15.42 PTS thermal-hydraulic aspects: calculation of safety margin for RPV considering limit thresholds at local level.

Selected relevant PTS topics are outlined hereafter:

A. PTS constitutes a possible mechanism which causes the loss of integrity of RPV. As already stated the combination of pressure, temperature, and neutron fluence loads may trigger the propagation of a microfracture inside the RPV leading to its rupture in a brittle mode. Zones of the RPV close to the irradiation region (the core), affected by flaws (sometimes, unknown, or undetected) greater than a critical value are prone to PTS. Welding regions with impurities at an elevation close to TAF possible origin of PTS concern.

B. PTS may occur in the presence of single-phase, noticeably MSLB, and two-phase conditions, noticeably SBLOCA or LBLOCA. In the case of PTS occurring during LBLOCA pressure may have a small role and key triggering parameters for stresses the temperature gradient into the walls of the RPV.

C. PTS is of low interest in the case of BWR because of the large downcomer and the low fluence expected for the vessel.

D. The capability to calculate locally liquid-liquid mixing (e.g., liquid streams having different temperatures and velocities) and liquid-gas interactions (e.g., including mixing and phase changes in liquid and gas streams flowing cocurrently and counter-currently) is needed for a realistic estimation of the PTS loads (see the color pictures in Fig. 15.41).

E. Various procedures are available from the literature to evaluate the PTS loads and the risk. Those procedures typically include several steps (e.g., Araneo et al., 2011; see also the paper at row 28 in Table 15.1; Jang, 2007). Three of steps directly connected with thermal-hydraulics are outlined with the support of Figs. 15.40–15.42:

- Search for the worst DBA transient (Fig. 15.40).
- Evaluation of local fluid temperature (Fig. 15.41). This needs the application of CFD codes (discussed in Chapter 12).
- Evaluation of the safety margins quantified by the minimum distance between the trajectory corresponding to the worst accident scenarios and a limit curve derived from material and stress status of the vessel (Fig. 15.42).

Phenomena connection with accident scenario: PTS

The PTS scenario for a PWR equipped with UTSG can be derived from Figs. 15.43 and 15.44 taken from SGTR, MSLB, and SBLOCA calculations (Jang, 2007; rows 28, 39, and 42 in Table 15.1).

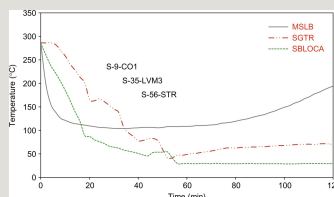


Fig. 15.43 PTS in PWR: average fluid temperature in RPV downcomer following MSLB, SGTR, and SBLOCA.

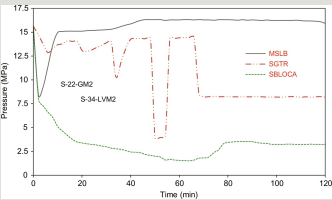


Fig. 15.44 PTS in PWR: pressure in RPV following MSLB, SGTR, and SBLOCA.

The three typical transients, possibly at the origin of PTS, are considered in a PWR with UTSG. The accident scenarios are the MSLB, the SGTR, and the SBLOCA. Reference, plausible average temperature, and pressure time trends are reported.

The MSLB and the SGTR scenarios are characterized by repressurization during the transient with moderate final coolant temperature. The SBLOCA-type transient results in the lowest final coolant temperature but the relatively low pressure. From temperature and pressure variations shown in the figures, it is presumed that the pressure effect is dominant in the MSLB-type transient and the temperature effect is dominant in the SBLOCA-type transient.

The phenomena listed in the second and the third columns of Table 15.26 are connected with PTS from the cross-link process in Tables 15.3 and 15.4. Those phenomena are associated with variables given in Figs. 15.42 and 15.43 in the fourth column of the table.

Table 15.26

Phenomena visualized by variables representative of the phenomenon PTS

Table 15.27

Phenomena visualized by variables representative of the phenomenon, or PHW, NC



The calculation of average temperatures and pressures (Figs. 15.43 and 15.44) focusing on PTS evaluation, implies the calculation of local phenomena as discussed at item D. earlier (Fig. 15.41). Therefore, phenomena associated with PTS in Table 15.26 (phenomena at rows 1, 3, 4, 5, 6, and 7) are assumed to be indirectly visualized in Figs. 15.43 and 15.44.

The following phenomena are outlined in this section or (visually) described through the use of calculated accident scenarios and related time trends (whenever possible):

- (1) Condensation in stratified conditions—Horizontal Pipes (indirectly visualized, Fig. 15.43). This phenomenon can be combined with phenomena (6) and (7) in the present list. Injection from ECCS is at the origin of the phenomenon and incomplete mixing and condensation create more severe conditions for PTS. In the HL the phenomenon may occur because of simultaneous presence of steam flowing from core to SG and condensed liquid flowing counter-currently from SG to core (i.e., not necessarily connected with ECCS injection), as from the sketch on the right side of Fig. 15.41.
- (2) Condensation in stratified conditions—PRZ (indirectly visualized, Fig. 15.19). PRZ level rise in the condition of constant pressure or increasing pressure implies condensation at the liquid-steam interface.
- (3) Condensation in stratified conditions—SG-PS (indirectly visualized, Fig. 15.51). The phenomenon is expected with liquid-level formation inside U-tubes. The siphon-condensation mode of NC is controlled by this phenomenon.
- (4) Global multi-D fluid temperature, void, and flow distribution—Downcomer (indirectly visualized, Fig. 15.44). Namely the global multi-D fluid temperature

distribution can be “directly” observed in the supporting diagram of Fig. 15.41. This phenomenon can be combined with the phenomenon (5) in the present list, with main reference to the global multi-D void distribution.

(5) Liquid-Vapor mixing with condensation—Downcomer (indirectly visualized, Fig. 15.44). See also phenomenon (4) in the present list. This phenomenon deals with two-phase conditions in the downcomer (e.g., expected in the case of SBLOCA rather than MSLB or SGTR).

(6) Liquid-Vapor mixing with condensation—ECCI in HL and CL (indirectly visualized, Fig. 15.43). See also phenomenon (1) in the present list.

(7) Stratification in horizontal flow—Pipes (indirectly visualized, Fig. 15.43). See also phenomenon (1) in the present list.

15.4.12.4 Natural Circulation

Natural circulation is a phenomenon or a phenomenological window part of accident scenarios and it is not an accident scenario. It is inserted into the list of Sections 15.4.2–15.4.12.12, which deal with accident scenarios owing to the following reasons:

(a) NC is at the basis of the thermal-hydraulic design and the safety demonstration of water cooled reactors; NC is important for the thermal-hydraulics discipline, too.

(b) NC focused studies, including experiments, have been performed in order to identify and characterize various phenomena which otherwise are expected to occur in different accident scenarios (primarily SBLOCA, but NC conditions are expected during each accident scenario where MCP is stopped).

Furthermore, NC constitutes the key topic of documents and reports already considered for deriving the list of phenomena in Table 15.2 (i.e., OECD/NEA/CSNI, 1996b; IAEA, 2001, 2002b, 2005b, 2009a, 2012). It is not the objective here to duplicate the content of those reports.

The structure of the following discussion is according to Section 15.4.1 and specific for Sections 15.4.12.1–15.4.12.4, 15.4.12.8, and 15.4.12.12.

NC topics and facts

Reference is made hereafter to the documents at row 30 in Table 15.1, namely, IAEA (2005b). Three elements characterize the NC:

(I) the presence of gravity;

(II) the presence of a heat sink and a heat source; and

(III) the geometrical configuration of the concerned NC system.

This is shown in Fig. 15.45 where (to the aim of NC analysis in nuclear systems):

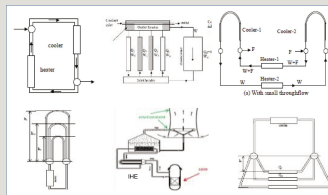


Fig. 15.45 Loop configurations of nuclear systems for NC.

- the top-left sketch is basically applicable to PWR, PWR-O, PWR-V, PHWR and to passive systems like IC and PRHR;

- the top-middle sketch is basically applicable to BWR, RBMK and to the SS of UTSG; and

- the top-right sketch is basically applicable to CANDU.

Furthermore, sketches characterizing possible multiple NC flow paths are also given in Fig. 15.45.

- The bottom-left sketch is related to all reactors with UTSG (namely PWR, PHWR, and CANDU) and to PWR-V: multiple NC flow paths are possible between the heat source (core) and the heat sink (SG). This also includes flow reversal or NC stop in groups U-tubes and of horizontal tubes (experimentally observed in the case of UTSG).

- The bottom-right sketch is related to core NC in case of CANDU: NC is possible with moderator tank constituting the heat sink. In this case unstable NC paths may establish in a channel-to-channel mode, where the loop is closed by the header and the heat sink is constituted by the moderator.

- The top-central sketch shows multiple NC paths possible in BWR: one of the

central channels in the sketch may be interpreted as the core bypass region or the space between fuel boxes where liquid moderator flows upward in nominal operating conditions. NC may establish between core assemblies and bypass (with downward liquid flow). Unstable NC may also establish between high-power assemblies and low-power assemblies.

- The bottom-central sketch shows a series of NC loops. Namely power produced in the core can be removed to the environment by three NC loops (present case). This has also been called dual NC system; specific models have been developed (e.g., D'Auria et al., 1998). Among the other things, (a) the optimum position for the Intermediate Heat Exchanger (IHE) can be determined: a high elevation for the IHE improves NC in the loop with core and degrades the NC in the downstream loop, so optimization is needed; (b) the stability performance of the overall system, tightly coupled loops must be determined; furthermore, a perturbation (instability occurrence, see later) in the last loop may reflect on the first one.

The complexity of the NC phenomenon already derives from the geometry outline. Additional NC topics considered in IAEA (2005b) are:

A. The NC flow regimes expected for PWR UTSG at various PS coolant mass inventories (Fig. 15.46). The following flow regimes are characterized and can be considered phenomenological windows in case of SBLOCA scenario with continuous coolant mass decrease in PS:

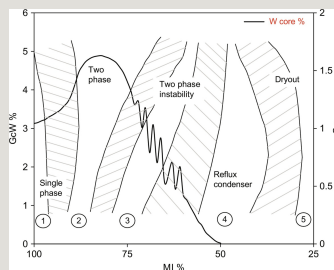


Fig. 15.46 NC flow regimes in PWR with UTSG at decay power.

- One-phase NC: The entire PS is in single phase and PRZ is losing mass to compensate the break flow. The heat sink of SG is available. Flow reversal in U-tubes may occur (De Santi et al., 1986), causing an increase of pressure drops (because of reduced cross flow area) for the overall system under natural

circulation. The phase ends when PS achieves the saturation pressure corresponding to the HL fluid temperature in nominal conditions.

- Two-phase NC: This includes the rising part of the curve, the region of the maximum value, and the first part of the descending region in Fig. 15.46. The phase starts with void formation due to simultaneous boil-off in the core and break induced depressurization. The rising part is due to a positive balance between driving head (i.e., the difference in average density of the coolant in the hold-ascending and the cold-descending loop regions) and pressure drops when MI decreases; then, a zero balance results in the peak region; further mass reduction causes a negative balance between driving head and pressure drops. Flow reversal in U-tubes may occur (see e.g., D'Auria, 2012) with same consequences (pressure drop increase in the overall loop) outlined for one-phase NC.

- Siphon condensation: CCFL at U-tube entrance, liquid formation inside the U-tubes due to condensation (or heat removal from SS), liquid level rise till the top in the concerned U-tubes, sudden liquid draining caused by the “siphon-effect,” are at the origin of siphon-condensation oscillations in RCS of PWR (D'Auria and Galassi, 1990b). Phase shift may occur among different groups of U-tubes. Oscillations are reflected all along the loop and are associated with the presence of the U-tube. Thus, siphon condensation oscillations are expected in PWR equipped with UTSG.

- Reflux condensation: When MI is further reduced a new stable NC regime establishes, called reflux condensation or reflux condensing mode. In this situation flowrate at core inlet is almost zero. At core outlet, upward two-phase mixture and downward liquid flow occur simultaneously: two-phase mixture produced in the core from liquid vaporization flows to the SG; condensate flows back to the core. The mechanism is consistent with flooding curve and CCFL at UTP, at the UP-HL connection, at the HL bend, and at U-tubes connection with SG inlet chamber. The mechanism allows core power removal at MI values as low as 40% the nominal value.

B. The NC flow map derived from collecting experimental data from several PWR-ITF experiments (Fig. 15.47; Cherubini et al., 2008a; proposed by D'Auria et al., 1994). Basically, upper and lower boundaries have been found for NC flowrate (i.e., the ratio G/P [NC flowrate at core inlet over core power] vs. MI/V [mass inventory in PS over coolant mass volume]) in PWR considering several experimental conditions, including scaling for ITF design. The flow map allows the evaluation of the NC performance of different nuclear systems by comparing with the spectrum of experimental data valid for PWR UTSG. The following key

remarks apply (i.e., making reference to the NC core flow as a function of PS MI with core power at decay values around 3% of the nominal value):

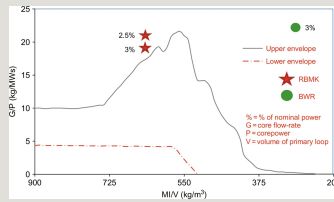


Fig. 15.47 NC flow map in PWR with UTSG at decay power with consideration of BWR and RBMK.

- NC calculated flowrate for any PWR UTSG is bounded by the upper and lower curves with values (as expected) around the mean region of the map.
- PWR with OTSG (here called PWR-O) are characterized by low NC performance in two-phase region because of the presence of the so-called candy-cane in HL: this causes degradation of NC flow (compared with U-Tube PWR) when MI is below 90% the nominal value.
- PWR with HOSG (VVER, here called PWR-V) are characterized by suitable NC performance, i.e., there is no important difference related to PWR with UTSG; in the case of VVER-440 additional complexity arises in the curve because of the presence of loop seal in the HL (in addition to loops seal in CL).
- CANDU reactors are characterized, as expected, by low NC performance compared with PWR equipped with UTSG. The reason is the presence of long pipes upstream and downstream each horizontal channel which causes large increase in friction pressure drops. This is true notwithstanding higher (potential) driving head owing to the relative elevation between the core and the UTSG (compared with PWR). The low NC performance in the case of CANDU is derived from considering “only” the flow between core and SG: the NC induced by channel to channel flow (bottom-right sketch in Fig. 15.45, where the moderator tank constitutes the heat sink) is not accounted in this evaluation.
- BWR and RBMK loop configurations are different from PWR. Furthermore, (a) NC is part of the BWR normal operation conditions; (b) NC occurs between core and bypass and between core and DC; (c) only two-phase conditions in the core with RCS pressure and DC (or steam drum in the case of RBMK) level close to

nominal can be compared with data in Fig. 15.47. This signifies one point in the map for each of BWR and RBMK (D'Auria and Galassi, 2014). The points show high values for NC flows in both cases.

C. The stability of NC flows (Fig. 15.48; Vijayan, 2014). NC flows in industrial systems including NPP are characterized by low driving forces, i.e., compared with systems where pumps are installed. This makes the NC systems “prone to instability” namely when boiling and condensation processes occur. Type-I and Type-II instabilities are distinguished in Fig. 15.48, left diagram as originally proposed by Fukuda and Kobori (1979), for DWI-related oscillations; low-flow and low-power characterize Type-I while (relative) high-power and high-flow characterize Type-II. A typical stability map is shown in the right side of Fig. 15.48. The effects of various system and BIC-related parameters are studied and affect the stability (or the instability) region. Examples are the length of cooler and heater, the L/D of piping, the orientation (related to the gravity force) of cooler and heater, the inlet (stabilizing if increased) and the outlet (destabilizing if increased) local pressure drop for the heat source, the time constants for conduction heat transfer (namely for heaters).

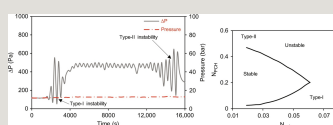


Fig. 15.48 NC flows: the stability issue. Left: characterization of “type-I” and “type-II” instability. Right: typical stability map for DWI.

D. The reliability evaluation for passive systems and the NC phenomenon (no supporting figure) (D'Auria et al., 2014). In Chapter 1, the subject of reliability of passive system has been excluded from the scope of the book. Nevertheless, a few notes are provided hereafter. The design of passive systems including IC and PRHR is based upon the NC phenomenon. The NC (as already stated) depends upon the existence of a heat source and a heat sink at different elevations in a gravity environment. The reliability of the TH phenomenon appears equal to one. This is *not* the case, specifically when boiling and condensation phenomena are involved in an NC system. Furthermore, a passive system suitable for applications in nuclear reactor safety may never operate at steady-state conditions: either the core power (decay heat) or the fluid temperatures or the levels in pool, where a heat exchanger of a passive system is immersed, change with time. This is in addition to possible changes in pressure or in other operating conditions (position

of the stem of a valve) associated with a specific accident scenario. Thus, an infinite number of combinations (time functions) occur to generate the driving force in an NC system. One may expect a zero driving force occurring in some cases which leads to stop in NC flow. This subject has been extensively studied (references can be found in Chapter 1) and reliability values less than unity have been found for NC systems.

NC stop constitutes one example of situations challenging the reliability of the phenomenon. When boron dilution is involved, NC restart (after the stop) may put at risk the core integrity (further discussed in Section 15.4.12.8).

Phenomena connection with accident scenario: NC

The NC scenario for a PWR equipped with UTSG can be derived from Fig. 15.49 taken from PWR calculation (IAEA, 2005b) (row 30 in Table 15.1, data elaboration by D'Auria and Galassi), Fig. 15.50 (Cho et al., 2009) (row J in Table 15.5, ATLAS experimental data), and Fig. 15.51 (Takeda et al., 2013) (row K in Table 15.5, LSTF experimental data).

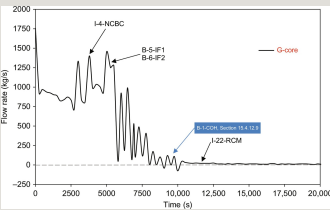


Fig. 15.49 NC in PWR: core flowrate.

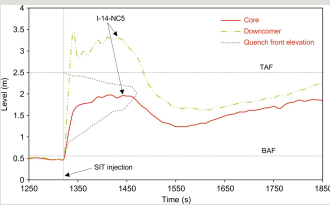


Fig. 15.50 NC in ATLAS test facility: core and DC levels and quench front.

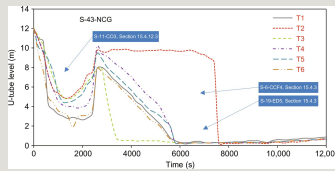


Fig. 15.51 NC in LSTF test facility: levels in SG tubes (loop B).

The NC scenario calculated for a PWR with UTSG can be derived from the core flowrate shown in Fig. 15.49. Starting from a situation PS full of coolant in liquid phase (one-phase NC) at time zero, PS MI inventory is decreased from 100% till about 40% at 20,000 s. The resulting NPP scenario is consistent with the description of NC flow regimes related to Fig. 15.46 (one-phase, two-phase, siphon condensation oscillations, and reflux condenser modes can be observed).

The scenario of NC between core and DC can be derived from Fig. 15.50 and includes the QF progression during reflood. Data measured in the ATLAS facility related to LBLOCA simulation in APR1400 are reported in the figure. Reflood is caused by the injection of accumulators (here called SIT). Vent valves between core and downcomer are open at about 600 s into the transient. During the early phase of reflood the bottom-up QF progression is delayed related to the liquid-level rise in the core (IAFB condition typical of high reflood rates). Top-down QF progression can also be observed from the figure.

The performance of SG tubes during NC in the presence of noncondensable gases can be derived from Fig. 15.51. Data measured in different SG tubes are shown. The concerned transient is an SBLOCA with AM. The NC mass flow rate temporarily decreased following ACC flow increase due to SG depressurization. The gas entered the primary system at the end of liquid delivery from ACC at about 2500 s. The consequence of gas entrance was a decrease in heat transfer between PS and SS (the PS depressurization rate decreased when gas entered the system). The noncondensable gases accumulated differently in the two loops of the facility. This contributed to the creation of a nonuniform performance of U-tubes which occurred (in the case of loop B, shown in the figure) till about 7500 s into the transient.

The phenomena listed in the second and the third columns of Table 15.27 are connected with NC from the cross-link process in Tables 15.3–15.5. Those phenomena are associated with variables given in Figs. 15.49–15.51 in the fourth column of the table.

The following phenomena are outlined in this section or (visually) described through the use of calculated accident scenarios and related time trends (whenever possible):

- (1) Boiler condenser mode of NC (visualized, Fig. 15.49). This is basically equivalent to two-phase NC discussed under item A. earlier; see also Fig. 15.46.
- (2) Channel and bypass axial flow and void distribution (indirectly visualized, Fig. 15.13). This is related to the BWR core during SBLOCA. Additional information, not in the form of time histories, can be derived from fundamental research documented in the papers at row D of Table 15.5, Kok et al. (1997), and Yang et al. (2012b).
- (3) Interfacial friction in horizontal flow (indirectly visualized, Fig. 15.49). The transient evaluation of interfacial friction in horizontal flow is needed to calculate fluid velocities at any location of a thermal-hydraulic system (e.g., RCS and containment) in two-phase conditions. The phenomenon occurs in any accident scenario. It has been (arbitrarily) assigned to NC and is visualized through the core inlet flowrate (i.e., also the HL flowrate where horizontal flow is encountered).
- (4) Interfacial friction in vertical flow (indirectly visualized, Fig. 15.49). The transient evaluation of interfacial friction in vertical flow is needed to calculate fluid velocities at any location of a thermal-hydraulic system (e.g., RCS and containment) in two-phase conditions. The phenomenon occurs in any accident scenario. It has been (arbitrarily) assigned to NC and is visualized through the core flow-rate (see also Melikhov et al., 2011) for interfacial friction effect in HOSG SS.
- (5) Intermittent two-phase NC (visualized, Fig. 15.49). This is basically equivalent to the siphon condensation NC flow regime discussed under item A. earlier; see also Fig. 15.46.
- (6) NC, one-phase, and two-phase—PS and SS (NC PS visualized, Fig. 15.49; NC SS indirectly visualized, Fig. 15.17). The phenomenon includes NC occurring in PS and SS of PWR. The PS NC is described under item A., earlier. The SS NC is at the basis of SG performance in nominal operating conditions and in case of any accident scenario.
- (7) NC core and downcomer (indirectly visualized, Fig. 15.13). This is related to the BWR RPV during various accident scenarios (e.g., SBLOCA).

(8) NC core gap, downcomer, and dummy elements (indirectly visualized, Fig. 15.18). This is related to the VVER RPV and core during various accident scenarios (e.g., SBO).

(9) NC core, vent valves, downcomer (visualized, Fig. 15.50). The NC inside RPV equipped with vent valves constitutes the focus for this phenomenon. This is of interest for reflood PHW following LBLOCA and also considered in Section 15.4.2 (see Fig. 15.5 and related discussion).

(10) Noncondensable gas effect including effect on condensation HT in RCS (visualized, Fig. 15.51). The injection of noncondensable gas in PS (e.g., coming from ACC) enhances the disuniformity in the performance of SG tubes.

(11) Reflux condenser mode and CCFL (visualized in Fig. 15.49). This is a stable NC flow regime discussed under item A. earlier; see also Fig. 15.46.

Furthermore, phenomena S-6-CCF4 and S-19-ED5, discussed in Section 15.4.3, related to SBLOCA are visualized in Fig. 15.51.

15.4.12.5 MSLB combined with SGTR

Two key motivations for this section shall be mentioned:

- After any assigned accident scenario is triggered, the probability of another (independent) accident to occur may remain the same (or increase, see next item) as in nominal operating conditions: in other words, following any event a new DBA framework could be considered.
- In some cases an accident can be the consequence of a previous event. Examples of consequential accidents are:
 - SBO following LOCA owing to weakness of the electrical net;
 - SBLOCA (e.g., due to PORV stuck open) following LOFW or SBO;
 - LCC/SW following SBO also inducing SBLOCA due to break in MCP seal circuit;
 - LOCA following earthquake (in this case the trigger is an external event);
 - ATWS following some AOO (only because scram is requested);
 - SBLOCA following CRE which causes an opening in the RPV;

- MSLB induced by a TT in PWR which causes SRV stuck open in SG; and
- SGTR (or PRISE) following MSLB because of induced fluid-dynamics loads including pressure wave loads.

A systematic listing of consequential accidents is well beyond the framework for the current document. The characterization of phenomena in consequential accidents can be based upon the cross-link in Table 15.3 (i.e., “summing” phenomena expected from two accident scenarios). However, additional specific studies may be needed for characterizing phenomena during combined accident scenarios

In the present section the attention is focused upon SGTR induced by MSLB in PWR.

Qualitative accident scenario: SGTR with consequential MSLB

Qualitative accident scenarios for SGTR and MSLB are discussed in Sections 15.4.7 and 15.4.8 and not repeated hereafter. Combination of the two scenarios, actually SGTR can be a consequence of MSLB (SGTR at the origin of MSLB is also possible in case of stuck open SRV in the affected SG), does not bring to phenomena not identified in Table 15.3, specifically when a single tube is concerned. However, the recovery of the NPP shall be different in MSLB and in MSLB with consequential SGTR.

Furthermore, MSLB combined with SGTR and multiple SGTR accident scenarios have similar features from a thermal-hydraulics view point: namely, multiple SGTR causes the opening of SRV, which (for short time) is equivalent to a rupture of the steam line.

Quantitative accident scenario: variable trends—SGTR with consequential MSLB

SGTR with consequential MSLB is discussed in the following. No TSE is provided because it is largely affected by peculiarities of individual NPP and by calculation assumptions for the event including the number of broken tubes.

The SGTR with consequential MSLB for a three-loop PWR equipped with UTSG can be derived from Figs. 15.52 and 15.53, taken from Jimenez et al. (2013) (row 29 in Table 15.1).

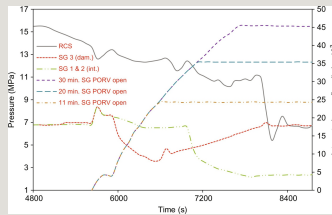


Fig. 15.52 SGTR with temporarily stuck open SRV in the affected SG in PWR with UTSG: PS and SS (damaged and intact) pressure and mass lost from affected SRV (three sensitivity cases).

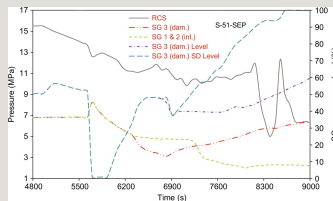


Fig. 15.53 SGTR with stuck open SRV in the affected SG in PWR with UTSG: PS and SS (damaged and intact SG) pressure and mass lost from affected SRV (three sensitivity cases).

Temporarily stuck open SRV in the affected SG is considered in the former figure, which includes two additional sensitivity calculations (only in the right diagram of the figure) dealing with the time-period of SRV stuck open. Failed stuck open SRV in the affected SG is considered in the latter figure, which includes one additional sensitivity calculation (only in the right diagram of the figure) where no cooldown of intact SG is actuated (black line).

Making reference to Fig. 15.53, it shall be noted that whatever is condition for cooldown of intact SG, the release of radioactive fluid to the environment cannot be stopped without direct depressurization of PS via the PRZ PORV. However, the situation without cooldown results in a lower narrow level in the affected SG, thus lower mass release from the stuck open SRV.

Calculated scenarios in both figures show the importance of a timely actuation of PS depressurization for minimizing the release of radioactivity to the environment (this is evaluated in the various sensitivity calculations in the paper by Jimenez et al., 2013).

The complexity of the scenario also results from the reported variables as well as

the importance of predicting correctly the phenomenon “separator behavior.”

Phenomena connection with accident scenario: SGTR with consequential MSLB

The phenomenon identified in the second and the third columns of Table 15.28 is connected with SGTR with consequential MSLB from the cross-link process in Tables 15.3 and 15.4. This phenomenon is associated with variables in Fig. 15.52, as reported in the fourth column of the table.

Table 15.28

Phenomenon visualized by variables representative of the accident scenarios during SGTR induced by MSLB



The following phenomenon is outlined in this section and visually described through the use of calculated accident scenarios and related time trends:

(1) Separator behavior and flooding, steam penetration, liquid carry-over (visualized Fig. 15.53). The separator and the steam-liquid separation process are directly connected with the (narrow) level formation at the top of the downcomer in the secondary side of SG. The subset of phenomena flooding, steam penetration, and liquid carry-over reported for S-51-SEP of importance for BWR is also important in the current scenario.

15.4.12.6 Fuel channel blockage

The blockage of a fuel channel (e.g., caused by deposition and chemical attack or by pieces of solid material present in the coolant) may occur at the inlet of any fuel assembly. Closure or flow obstruction of a valve eventually installed upstream or downstream a power generation channel may also generate an FCB event. The issue may become of safety concern in the case of channel-type reactors (discussed hereafter) and research reactors (Adorni et al., 2005; Adu et al., 2015).

Qualitative accident scenario: FCB

Selected topics for FCB transients of interest to thermal-hydraulics are:

A. The blockage may be partial or total. In case of partial blockage, the target of analysis may be the characterization of the “amount of blockage,” which causes ONB (case of research reactors), or CHF or damage to the fuel.

B. In case of total blockage (or blockage section higher than a threshold value), the damage of the fuel cannot be avoided.

C. The item above occurs because early detection is difficult or impractical (possible detection is discussed by D'Auria et al., 2008c, in relation to RBMK, see also Section 15.4.12.7).

D. Coolant (fast) vaporization in the affected channel and radiation heat transfer toward the channel walls are important phenomena.

E. Propagation of the damage to neighboring channels is a safety concern. The FCB accident constitutes one plausible precursor event for the MPTR discussed in Section 15.4.12.7.

Quantitative accident scenario: variable trends and TSE – FCB

The FCB scenario for an RBMK from Table 15.30 (in Section 15.4.12.7 related to MPTR originated by FCB, not repeated here) and Figs. 15.54 and 15.55, taken from D'Auria et al. (2005) (row 9 in Table 15.1).

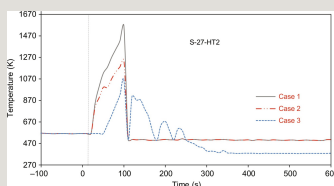


Fig. 15.54 FCB in RBMK and phenomena characterization: RST at different axial elevations.

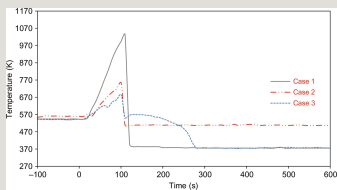


Fig. 15.55 FCB in RBMK and phenomena characterization: PT wall temperatures at different axial elevations.

Typical timing for the event can be seen in Figs. 15.54 and 15.55 and in Table 15.30. Other than radiation heat transfer phenomenon, nuclear fuel material performance (including possible ballooning and H₂ production) and mechanical resistance of PT at high temperature (creep phenomenon) are of interest during the transient. Fuel and PT failures shall be determined based on variable time histories reported in the previous diagrams. Moreover, during the event a local (channel related) neutron flux perturbation is expected due to coolant vaporization (coolant is not moderator in the RBMK) and to increase in fuel temperature.

Phenomena connection with accident scenario: FCB

The phenomenon identified in the second and the third columns of Table 15.29 is connected with FCB from the cross-link process in Tables 15.3 and 15.4. This phenomenon is associated with variables in Fig. 15.54, as reported in the fourth column of the table.

Table 15.29
Phenomenon visualized by variables representative of the accident scenarios during FCB

--

Table 15.30
FC blockage event in RBMK at the potential origin of MPTR:

^a Or quantity as defined in the second column.

The following phenomenon is outlined in this section and visually described through the use of calculated accident scenarios and related time trends:

(1) HT [radiation]-core (visualized, Fig. 15.54). Fuel rod surface temperatures above about 600°C (or 900 K) imply radiation heat transfer. Absorbing media are the coolant (steam and droplets) and mainly the PT walls which is heated up by radiation (Fig. 15.55). Practical problems associated with the characterization of the radiation HT phenomenon are the complexity of the geometry involved, the status of irradiating and absorbing surfaces, and the difficulty in distinguishing between radiation and film boiling contributions to HT.

15.4.12.7 MPTR

Multiple pressure tube rupture is a potential catastrophic accident in pressure tube reactors: the rupture of one pressure tube (possible) propagates to neighboring tubes destroying the entire core. MPTR may be triggered by loss of integrity of the wall caused by pressure load (e.g., propagation of a defect in the material), by combined temperature and pressure load (e.g., overheating of one fuel assembly due to channel blockage), and by temperature only (e.g., pressure may be low and fuel melt may occur). MPTR must be avoided at the design stage level of the reactors. Making reference to the pressure tube water cooled reactor: (a) MPTR is excluded in PHWR, e.g., Atucha type reactor mostly because pressure difference across one single tube is “low” (i.e., less than 0.1 MPa); (b) MPTR is possible in CANDU; however, the presence of water in-between the pressure tubes makes realistic (although with negligible probability), the event only in case of fuel melt in one channels with propagation of the rupture only in the gravity force direction; (c) MPTR may occur in RBMK following the rupture of one pressure tube because the surrounding graphite blocks may not absorb the pressure and the displacement loads and may transmit those loads neighboring tubes. Attention is focused hereafter to RBMK.

Qualitative accident scenario: MPTR

The sketch in Fig. 15.56, taken from D'Auria et al. (2005), see also D'Auria et al. (2008b), gives an idea of the MPTR. Geometric details and operating conditions for RBMK core can be found in the cited references.

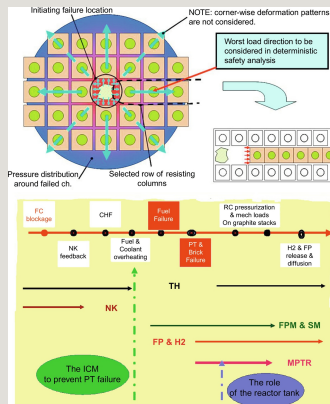


Fig. 15.56 Sketch for modeling MPTR in the core of an RBMK. *CFD*, computational fluid dynamics; *CHF*, critical heat flux; *FC*, fuel channel; *FP*, fission products; *FPM*, fuel pin mechanics; *ICM*, individual channel monitoring; *MPTR*, multiple pressure tube rupture; *NK*, neutron kinetics; *PT*, pressure tube; *RC*, reactor cavity; *SM*, structural mechanics; *TH*, thermal-hydraulics.

Selected topics for MPTR transients of interest to thermal-hydraulics are:

- A. “Hot” and “cold” graphite stacks surrounding pressure tubes are part of the core. Namely, coolant in the channels where CR is located is kept below the boiling point by suitable circulation flow. Temperature of graphite is a function of the radial and axial coordinates.
- B. The thickness of the gap between adjacent graphite blocks and upon neutron fluence.
- C. The gas, helium or nitrogen or a mixture helium-nitrogen, circulates inside the gaps among graphite stacks.
- D. Mechanical, thermal, and neutron-related properties of materials constituting the core are largely a function of core life.
- E. The deformation characteristic of the fuel channels and associated graphite stack depend upon the type of load (uniform, punctual, etc.) and upon the location of the

triggering rupture. Furthermore, other than the pressure tube that constitutes the most resistant part of the ensemble, the graphite blocks, the fuel bundles, and the central bar inside each fuel assembly contribute to the overall stiffness.

F. The detection of the event is not immediate and so the occurrence of scram.

The outline at the earlier listed items and Fig. 15.56 shows that MPTR is a multidisciplinary scenario where thermal-hydraulics, neutron physics, materials, and structure mechanics play a role.

Quantitative accident scenario: variable trends and TSE—MPTR

MPTR is typically triggered by the rupture of one tube. This may be originated by FCB discussed in Section 15.4.12.6. The single-tube rupture may evolve into an MPTR. Bases for MPTR analyses in RBMK can be derived from the TSE in Table 15.30, and Figs. 15.57 and 15.58 taken from D'Auria et al. (2005) (row 25 in Table 15.1).

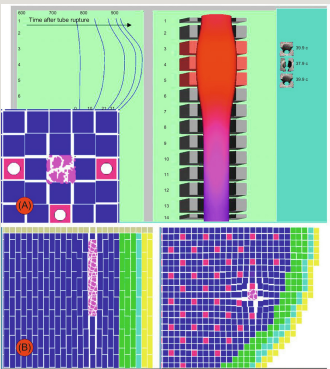


Fig. 15.57 MPTR accident scenario in RBMK: (A) tube deformation process after the blockage event; (B) “stabilized” situation at the end of the analysis.

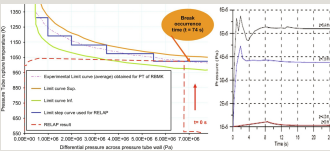


Fig. 15.58 MPTR accident scenario in RBMK. Left: trajectory in the temperature-DP space to determine rupture time. Right: pressure in the gap along the axis of the affected channel.

The FCB accident scenario, plausible trigger for MPTR, is not easily detectable. Detection may occur after the rupture of the pressure tube: early detection is discussed by D'Auria et al. (2008c). Then, MPTR, if not prevented at a design level evolves in a few seconds.

Pressurization of the interassembly region after the pressure tube rupture (conditions for rupture calculated in Fig. 15.58, left) occurs with a large-axial gradient as indicated in Fig. 15.58, right. Thereafter, the possible MPTR occurrence becomes a matter of interest for structural mechanics: strain and stressed in graphite stacks and in intact pressure tubes are involved (sketch in Fig. 15.57).

Coupled three-dimensional thermal-hydraulic, neutron physics, and structural mechanical calculation allowed the conclusion that design features of RBMK core are such to prevent the MPTR (D'Auria et al., 2005). The steel cylinder surrounding the graphite core stacks constitutes the ultimate resistant element effective in avoiding the propagation of the rupture.

This conclusion may not apply in the case of some elements located in the periphery of the core. In this situation MPTR occurrence depends upon a specific direction for the pressure tube rupture axis. Therefore, the probability of MPTR is calculated to be negligible.

Phenomena connection with accident scenario: MPTR

The phenomenon identified in the second and the third columns of Table 15.31 is connected with MPTR from the cross-link process in Tables 15.3 and 15.4. This phenomenon is associated with variables in Fig. 15.58, as reported in the fourth column of the table.

Table 15.31

Phenomenon visualized by variables representative of the accident scenarios during MPTR

--

The following phenomenon is outlined in this section and (visually) described through the use of calculated accident scenario and related time trends:

(1) Pressure wave propagation (visualized, Fig. 15.58). The pressure tube rupture causes a pressure wave propagating from the PS at high pressure into the reactor tank of the RBMK core passing through the region which separates the graphite stacks. The region has a small thickness which causes the axial pressure gradient that can be observed in Fig. 15.58. Moreover the pressure wave: (a) can be visualized for tenths of a second and (b) is at the origin of loads on graphite stacks around the broken pressure tube as illustrated in Figs. 15.56 and 15.57.

15.4.12.8 Boron Dilution

The motivations for a specific boron section have been given under item (e) in Section 15.4.12. Wide literature exists in relation to the use of boron in nuclear technology and in reactor safety (e.g., Ebert, 1995; Pla et al., 2010). Selected topics and connection with thermal-hydraulics are discussed hereafter.

Boron topics and facts

Boron connected topics/facts, which have a relation with thermal-hydraulics, are:

A. Dilution: Boron dilution is associated with the boiling and condensation processes. The steam is free of boron (distillation type of process) and the condensation of steam produces a boron diluted liquid. The boron diluted liquid may accumulate in loop seals in a time period when NC is close to zero and pushed toward the core when NC restarts (further discussion below in this section).

B. Transport: Boron transport occurs at global level in the core. Any motion of borated fluid mass into the PS shall be called boron transport.

C. Mixing: Boron mixing occurs locally in the primary system, noticeably in CL, DC, and LP when masses of fluid having different boron concentration enter in contact.

D. Deposition: Boron deposition occurs in boiling regions (i.e., subcooled boiling length in PWR core). Boron deposition causes crud formation and may affect the local fission power production.

E. Stratification: Boron stratification may be induced by liquid temperature stratification (different liquid density and temperature cause differences in boron concentration) or, in the long term (weeks or months), by gravity effect in a

stagnant tank at constant temperature. However, following Graffard and Goux (2006) and Nourbakhsh and Cheng (1995), the boron stratification is the phenomenon occurring in DC. This should be intended as a special situation of boron mixing (item C.).

F. Crystallization: High boron concentration flowing across geometric discontinuities may cause deposit and obstructions of the flow section.

G. Neutron reactivity excursion: Neutron flux excursion induced by boron may occur when a liquid diluted boron plug arrives in the core or when boron crud detaches from fuel rods.

H. System quantities associated with boron can be emphasized as follows for a large UTSG PWR unit:

- Boron concentration at BOL/BOC conditions: up to ≈ 2000 ppm.
- Volume occupied by coolant/moderator in the core: ≈ 20 m³.
- Reactivity worth associated with boron in the core at BOC/BOL: up to $\approx \$40$. This is the reactivity that could be inserted in the case all borated liquid is substituted by unborated liquid.
- Reactivity associated with all control rods: $< \$20$.
- Mass of liquid (potentially unborated) in each loop seal: ≈ 10 m³.

In Section 15.4.12.4, the possibility of NC stop is mentioned. During the NC stop (typically short, i.e., a few dozen seconds) boron diluted plugs of liquid may form in the loops seals. Once NC restarts (e.g., due to positive imbalance between ECCS and break flowrates) the diluted boron plug may be transported toward the core. The NC stop and restart is illustrated in Fig. 15.59 and the consequences of boron diluted plug motion are discussed hereafter.

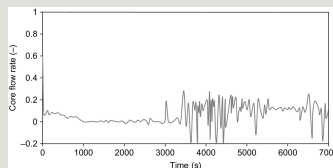


Fig. 15.59 NC stop and restart calculated for a PWR with UTSG: the NC restart may cause the motion of boron diluted plug toward the RPV.

Phenomena connection with accident scenario: Boron

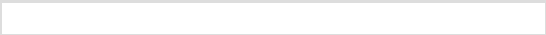
Boron phenomenon-related information can be derived from Fig. 15.60, left, taken from PWR-core basic calculation by Jimenez et al. (2015) (row 4 in Table 15.1). The boron mixing and stratification in downcomer can be (color plot) observed at a representative time snap-shot in the right side of the figure, taken from PWR calculation by Graffard and Goux (2006) (row 4 in Table 15.1).

It shall be noted that the right picture and the left time trend (actually obtained from different and not connected PWR calculations) in Fig. 15.60 can be considered as results of consequential analyses, started with the movement of the possible unborated boron plug transported toward RPV by NC restart in Fig. 15.59.

The phenomenon identified in the second and the third columns of Table 15.32 is the outcome of the cross-link process in Tables 15.3 and 15.4. The phenomenon is associated with variables in Fig. 15.60.

Table 15.32

Visualization of boron-related phenomenon



The following phenomenon is outlined in this section and (visually) described through the use of calculated accident scenarios and related time trends:

(1) Boron mixing and transport (indirectly visualized, Fig. 15.60). Three-dimensional analyses are needed for a comprehensive evaluation of boron-related phenomena. Namely transport of boron and formation of diluted boron plugs can be calculated by one-dimensional model. However, three-dimensional analyses are needed for mixing and stratification (or mixing in vertical components) (i.e., at the basis of results shown on the right-hand side of Fig. 15.60). The calculation of the effect of boron upon fission power also needs coupled three-dimensional thermal-hydraulics and neutron-physics calculation (i.e., at the basis of results shown on the left-hand side of Fig. 15.60).

The statements at items C. and E. also apply to the phenomenon A-12-BO of Table 15.9. This is directly visualized in the right sketch of Fig. 15.60.

15.4.12.9 LOFA and MCP-trip and LCC/SW

The MCP-trip accident scenario is part of group of four scenarios where similarities in system performance are expected (at least in relation to some periods and some phenomena), e.g., LOFA (or MCP-trip), LOFW, SBO, and LOOSP (respectively, present section, Sections 15.4.4–15.4.6). One may state that MCP-trip is related to the stop of one MCP and LOFA relates to the stop of all MCP. However, in the general cases the terms MCP-trip and LOFA are used interchangeably.

The interest toward the Loss of Component Cooling Service Water (LCC/SW) derives from considering that the scenarios involve actions and events occurring at very uncertain times (OECD/NEA/CSNI, 2011). In this way a connection can be delineated in the present section between thermal-hydraulics and PSA.

EOP are designed to account for MCP-trip or LOFA and LCC/SW.

Qualitative accident scenario: LOFA/MCP-trip and LCC/SW

MCP-trip

A partial LOFA is an AOO that may be caused by a mechanical or electrical failure in a pump motor, a fault in the power supply to the pump motor, or a pump motor trip caused by anomalies such as overcurrent or phase imbalance. The resulting decrease in reactor coolant flow, which occurs while the plant is at power, degrades the core heat transfer, and reduces the DNB margin. The following cases may occur:

- Partial loss of forced reactor coolant flow.
- Complete loss of forced reactor coolant flow.
- MCP rotor seizure.
- MCP shaft break.

RCS pressure increases and is limited by PRZ spray (actuation possible in case of availability of at least one MCP or of external pump). The margin to DNB is challenged.

LCC/SW and PSA connection

The loss of CCW and/or SW impacts the plant operation due to the loss of cooling of essential equipment, most notably, MCP and ECCS. When SW is lost, one of the consequences is the loss of CCW, although there are also some additional effects. Most notably, SW provides cooling water to DG, which become unavailable in loss of SW scenarios but not in loss of CCW due to other causes. Also, some containment systems like fan coolers can be affected by loss of SW but not by loss of CCW. The loss of SW has a frequency given by $1.88\text{E-}03 \text{ y}^{-1}$ (Zion NPP, OECD/NEA/CSNI, 2011).

Upon the loss of CCW/SW, the MCP is first affected. Even if the reactor coolant pumps are stopped, lack of water injection to the seals combined with loss of cooling water to the pump thermal barrier may lead to seal damage resulting in a seal LOCA (a particular case of small LOCA, conditioned by the loss of equipment). In the case that a seal LOCA occurs as a consequence of the loss of CCW, safety injection systems (SIS) are needed to compensate the loss of inventory. However, both HPIS and LPIS are unavailable while CCW is not recovered and ACC are the only available injection systems.

Sequences without seal LOCA were not significant contributors to core damage since the intervention of the AFW system (failure probability $3.4\text{E-}05$) was considered enough to prevent the exceedance of the cladding temperature limit, even without CCW recovery. The global frequency of sequences without seal LOCA and with AFW failure is about $5.05\text{E-}8$ which is below the cut-off level. The analysis then focused on seal LOCA sequences.

Following the seal LOCA event (originated by LCC/SW) a set of events or occurrences like manual scram, cooling of SG via SRV and CCW recovery, are considered together with assumptions like

- If the MCP is not stopped before high-temperature fluid reaches the seal package, all the seals are assumed damaged and reactor coolant is lost at the maximum rate.
- The failure of a sealing stage does not condition the failure of other stages.
- The failure of a sealing stage is assumed to occur simultaneously in all the four pumps.

Quantitative accident scenario: variable trends and TSE—LOFA/MCP-trip and LCC/SW

MCP-trip

Typical LOFA scenario can be derived from the TSE in Table 15.33, PWR with UTSG, and Fig. 15.61, EPR, taken from AREVA (2014) (row 20 in Table 15.1) and Fig. 15.62, VVER-440, taken from Groudev and Stefanova (2006) (row 24 in Table 15.1).

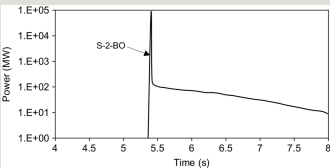


Fig. 15.60 Effect of transport of boron diluted plug into the RPV of a PWR with UTSG. Left: core power. Right: snapshot imagine for boron concentration in DC.

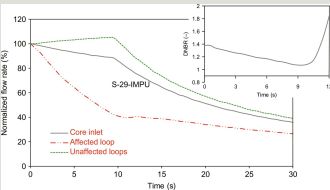


Fig. 15.61 Partial LOFA in EPR: flowrates in the primary loop and detail of DNBR time trend.

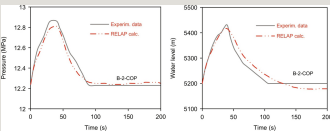


Fig. 15.62 Partial LOFA (trip of one MCP) in VVER-440. Left: PS pressure. Right: PRZ level.

Table 15.33

MCP-trip in PWR with UTSG: (selected) imposed and calculated

It may be noted that the EPR information derives from an available licensing analysis (Fig. 15.61), and the VVER-440 time trends in Fig. 15.62 include comparison with measured data in the Kozloduy NPP unit 4.

LCC/SW and PSA connection

Typical LCC/SW scenarios, PSA relevant, can be derived from Fig. 15.63, PWR with UTSG, taken from OECD/NEA/CSNI (2011) (row 19 in Table 15.1).

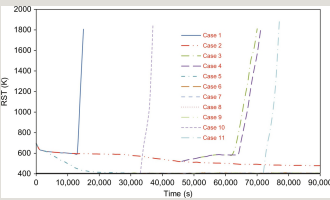


Fig. 15.63 LCC/SW sequences in PWR with UTSG: RST at PCT location from 11 PSA-related calculations.

It was assumed that CCW system recovery occurs at the time of the seal LOCA, so that safety injection systems are available, if they do not fail for reasons different from LCC/SW. The depressurization of the SG SS, if not failed, is assumed to occur 600 s after the LOCA.

Rather than providing a comprehensive documentation of the results (this can be found in the cited document), the main objective for Fig. 15.63 is to show the link between PSA and thermal-hydraulics.

Phenomena connection with accident scenario LOFA/MCP-trip and LCC/SW

The phenomena listed in the second and the third columns of Table 15.34 are

connected with LOFA/MCP-trip from the cross-link process in Tables 15.3 and 15.4. Those phenomena are associated with variables in Figs. 15.61 and 15.62, as reported in the fourth column of Table 15.34.

Table 15.34

Phenomena visualized by variables representative of the accident scenarios LOFA/MCP-trip and LCC/SW



The following phenomena are outlined in this section or (visually) described through the use of calculated accident scenarios and related time trends (whenever possible):

(1) Condensation due to heat removal (visualized, Fig. 15.49). The basic phenomenon occurs (at least) in all scenarios where SG SS removes thermal power from a PS where voids are present. All two-phase NC regimes satisfy this condition. Reflux condensing mode of NC and related flows in HL of UTSG PWR constitute an example of the effect of condensation.

(2) Condensation due to pressurization (indirectly visualized, Fig. 15.62). The basic phenomenon occurs each time there is a pressure increase. Pressure increase is connected with PRZ level increase, typically in MCP-trip, LOFW, SBO, and LOOSP.

(3) Impeller pump behavior (visualized, Fig. 15.61). Centrifugal pump performance constitutes a phenomenon occurring in all transients in all reactors (an exception could be an SMR without MCP). So-called homologous curves for centrifugal pumps, derived from experiments in one- and two-phase conditions, determine the predicted behavior of impeller pump.

15.4.12.10 Turbine trip

Turbine trip (TT) constitutes an expected (almost yearly) event during the life of

NPP. It is not usually characterized with the word “accident.” Rather, the term AOO is adopted or even operational transient.

The turbine is the key component of the BOP in an NPP. In this case “key” means the most expensive. Thermal efficiency of the plant is also affected by the turbine design. Materials of the wings and related stresses in nominal operation are the best available from current technology and the highest achievable, respectively. The turbine is installed on the same rotating axis as the alternator (i.e., an electromechanical component). Losing the load is a typical instantaneous process of electrical nets, where instantaneous means 10^{-3} s or less. In this situation, turbine over-speed may occur with mechanical damage. In order to protect the turbine a fast closing valve must be installed in the steam line upstream the machine. The fast closing of this valve is one main origin for thermal-hydraulics issues associated with turbine trip.

Qualitative accident scenario: Turbine trip

Selected topics for turbine trip transients of interest in thermal-hydraulics are:

A. Closing of turbine inlet valve after the “electric” event must be associated with fast opening of condenser dump valve.

B. The opening of the condenser dump valve causes high-pressure (then, superheated) steam entering the condenser. Although condenser may have a capacity to remove thermal power higher than needed in nominal operating conditions, the entrance of superheated steam may locally decrease the condensation HTC. The associated thermal-hydraulic issue is addressed within the framework of the component design.

C. The fast closing of the turbine inlet valve causes a positive pressure, wave which propagates upstream in the steam line. This causes condensation in the SG SS in a PWR and in the RPV of a BWR. Condensation in the SG causes a negative temperature perturbation for the PS coolant in a PWR, somewhat mitigated by the thermal inertia of the SG tubes and weakened by mixing before reaching the core. Otherwise condensation in the RPV of a BWR causes void collapse and has a direct impact on fission power which may exhibit an excursion after turbine trip.

D. In the case of BWR, turbine trip is also associated with PSP temperature increase, because in the attempt to avoid a large decrease in thermal power production (to minimize xenon effects), SRV valves are open and deliver steam to the PSP. Liquid temperature in the PSP cannot increase above a certain threshold (typically below 80°C) to avoid endangering the function of ECC pumps in case

these are called in operation. Thus, turbine can be kept in standby with core nearly at full power for a short-time period.

E. Turbine axis mechanical inertia can be considered for a few seconds for keeping the electrical power supply to crucial RCS components like MCP. Noticeably, the Chernobyl event (Chapter 16) was originated by the planning of a test to confirm availability of electrical power supply after TT.

Quantitative accident scenario: variable trends and TSE—Turbine trip

Typical turbine trip accident scenario can be derived from the TSE in Table 15.35, including PWR with UTSG and BWR and Fig. 15.64, SMR, taken from Haratyk and Gourmel (2015) (row 44 in Table 15.1) and Figs. 15.65 and 15.66, BWR, taken from Bousbia-Salah and D'Auria (2002) (row 45 in Table 15.1).

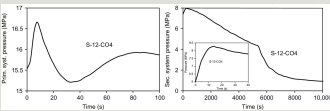


Fig. 15.64 Turbine trip accident scenario in SMR. Left: PS pressure short term. Right: SS pressure, long term with focus on initial 40 s.

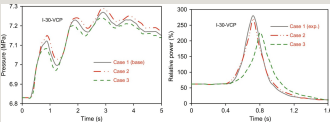


Fig. 15.65 Turbine trip accident scenario in BWR including measured NPP data. Left: RPV pressure with different assumptions about condenser dump valve history. Right: core power considering different condensation models.

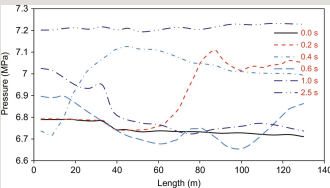


Fig. 15.66 Turbine trip accident scenario in BWR. Pressure profile in Steam Line at time 0 (before the event) and times 0.2, 0.4, 0.6, 1.0, and 2.5 s after the event.

Table 15.35

Turbine trip in PWR with UTSG and BWR: (selected) imposed and calculated events

--

The turbine trip transient evolves in a few seconds, as from Table 15.35. Later on, specific EOP or operator actions affect the transient evolution (e.g., Fig. 15.64).

In the case of BWR the positive pressure wave entering the RPV from the steam line propagates toward the core following two paths: (a) crossing steam dryers, then separator region, then upper plenum and entering the core from the top; and (b) entering DC downward separators, then lower plenum and entering the core from the bottom. The first path is shorter but wave propagation velocity is faster in the second path where liquid is present till core inlet. Both the two pressure waves contribute to the void collapse in the core and to the pressure rise. A three-dimensional RPV model is needed for predictions.

Phenomena connection with accident scenario: Turbine trip

The phenomena listed in the second and the third columns of Table 15.36 are connected with Turbine Trip from the cross-link process in Tables 15.3 and 15.4. Those phenomena are associated with variables in Figs. 15.64–15.66, as reported in the fourth column of the table.

Table 15.36

Phenomena visualized by variables representative of the accident scenarios during turbine trip

--

The following phenomena are outlined in this section or (visually) described through the use of calculated accident scenarios and related time trends (whenever possible):

(1) Condensation in stratified conditions—SG SS and BWR PSP (indirectly visualized, Fig. 15.64). Condensation in stratified conditions in SG SS and in PSP may occur in several scenarios, noticeably when pressure is increasing (SG SS) and SRV are discharging steam into the pool. Visualization in Fig. 15.64 is connected with the concerned phenomenon in SG SS. The PSP-related phenomenon is indirectly visualized in Fig. 15.37 and discussed with more detail by Wulff et al. (1992) (see also Chapter 16).

(2) Steam line dynamics (visualized, Fig. 15.66). Steam line has a length of about 100 and a number of bends. Venturi nozzles and valves are installed in the line making complex the dynamics of the propagation of pressure wave. Reflection of pressure waves (geometric discontinuities and walls) is not within the capabilities of existing system thermal-hydraulic codes.

(3) Void collapse and temperature distribution during pressurization (indirectly visualized, Fig. 15.66). The pressure and power pulse in the RPV are direct consequence or at the origin of void collapse.

15.4.12.11 Accidents during shutdown conditions

NPP operate or are designed to operate the largest part of their life at full power conditions. However, nominal conditions include all needed status like start-up and shutdown. In those situations either decay power is produced or fission core power is varied to achieve decay power (shutdown period) or the full power (start-up procedure). Let us call all NPP nominal operational conditions not at full power as shutdown conditions.

Then, shutdown conditions may arise at any pressure in the range from ambient pressure to full-nominal pressure and RCS may be tight (i.e., under pressure) or open to the containment with a variety of openings (i.e., RPV open for refueling).

Owing to a number of reasons, not last the attention given to full power conditions, it has been clear since the 1990s that shutdown conditions may largely contribute to the overall risk of NPP or even may produce a contribution to risk higher than the full power operation. This started technological research in all areas including thermal-hydraulics.

Before showing parameter time histories related to shutdown, let us note the following:

- A key target (not the only one) for accident scenario calculations starting from full power is the demonstration of suitable design for ESF. For instance, in the case of LBLOCA, the analysis must demonstrate that the pressure of ACC and the volume of injected liquid are suitable to keep the RST below the licensing limit. This implied and implies the evaluation of phenomena like TPCF, CCFL in downcomer, and reflood, including NC during reflood and QF progression. A positive outcome of the thermal-hydraulic analysis is constituted by the demonstration that phenomena are understood, calculation is qualified and performance of the ESF is according to the design.
- In the case of shutdown conditions, the key target for the analysis of accident scenario is to evaluate what happens if one or more ESF fail. For instance, a typical target of calculation in the case of RPV open is to find the time when the core uncovers following a full stop of cooling water. The calculation does not need sophisticated computational tools and complex phenomena are not expected.

In the former case, thermal-hydraulic competences are needed to confirm the suitability of the concerned ESF or to improve its design. In the latter case, the only action possible is to improve the reliability of the concerned ESF (i.e., an action that has little or no connection with thermal-hydraulics).

Furthermore, in some cases, accidents during shutdown periods are classified according to scenarios: noticeably, the event in Doel-2 (OECD/NEA/CSNI, 1988) is classified as SGTR, although it happened during a shutdown period.

Nevertheless, shutdown conditions constitute a “fashion-interest” for thermal-hydraulics.

Qualitative accident scenario: SHUTDOWN

Any PIE and associated evolution like LBLOCA, SBLOCA, SGTR, MSLB, etc., may happen during shutdown. Phenomena expected during an assigned event starting at full power shall also be expected for the same event occurring during shutdown. For instance, the distinction between an SBLOCA occurring at full power and an SBLOCA occurring during shutdown is possible, but outside the context for the present chapter.

Selected topics for shutdown transients of interest in thermal-hydraulics are:

A. In some shutdown situations the barrier constituted by the RCS is not available and one may also imagine situations when both the RCS and the containment barrier are not available (to allow refueling, maintenance, etc.). This justifies the importance of shutdown transients for NPP risk studies.

B. The evolution of some shutdown transients is expected at atmospheric pressure: this may put a challenge to some existing models.

C. A shutdown transient may occur when more than one opening exists between RCS and containment. This implies a coupled containment-RCS calculation considering the possibility that natural circulation or natural convection motion established between the two openings.

D. In case of stop in the operation of a service pump when the RPV is open, selected questions of interest to thermal-hydraulics are:

- When flow is lost at core entrance?
- When subcooling is lost at core outlet?
- When core wide void appear?
- When core uncover occurs?
- When RST reaches unacceptable and unrecoverable value after core uncover?

Quantitative accident scenario: Variable trends—SHUTDOWN

Typical SHUTDOWN scenarios can be derived from Fig. 15.67, PWR with UTSG, taken from Haste et al. (2010) and Fig. 15.68, APR1400, taken from Son and Shin (2007) (row 43 in Table 15.1 for both documents).

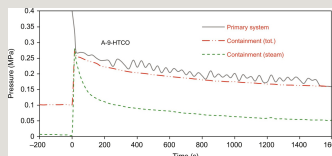


Fig. 15.67 Shutdown accident scenario, LOCA in UTSG PWR: PS and containment pressures.

Very different timings of events can be seen for the two considered transients: less than 1/2 h in Fig. 15.68 and more than 20 h in Fig. 15.68.

In the former calculation, i.e., an LOCA during shutdown, the coupling between RCS and containment is evident. In the latter case the PSA-oriented calculation should be noted: the target is the evaluation of different actions (e.g., no actions, HPIS and Gravity Feed, GF, actuation) following a loss of flow. In the reported calculation two SG are unavailable, PZR head vent, reactor head vent, PRZ manway, and SG inlet manways are open.

RCS pressure increase when HPIS is adopted is due to pump head. However, HPIS tank is exhausted at a time well before emptying of the same tank by gravity. GF is better in a case where many openings are present. In different RCS configuration different use of available (water) resources are preferable.

One expected problem occurring when recovery is attempted by gravity feed liquid is reported (by Son and Shin, 2007), when the number or the size of the RCS openings is not enough: even though the GF supplies RCS cooling water continuously, the amount of cooling water from the IRWST to the cold leg in each loop is not sufficient enough to prevent core damage because the pressurizer manway is not large enough to make large pressure difference to induce sufficient amount of cooling water from IRWST to the CL.

Phenomena connection with accident scenario: SHUTDOWN

The phenomena listed in the second and the third columns of Table 15.37 are connected with SHUTDOWN from the cross-link process in Tables 15.3 and 15.4. Those phenomena are associated with variables in Figs. 15.67 and 15.68, as reported in the fourth column of the table.

Table 15.37

Phenomena visualized by variables representative of the accident scenarios during SHUTDOWN

--

The following phenomena are outlined in this section or (visually) described through the use of calculated accident scenarios and related time trends (whenever possible):

(1) HT condensation in containment structures, with or without noncondensable (indirectly visualized, Fig. 15.67). Pressure in containment in long-lasting transients is affected by heat transfer by condensation in the structures including the presence of noncondensable gases.

(2) SG siphon draining (indirectly visualized, Fig. 15.68). Various openings in the PS cause a variety of emptying modes.

15.4.12.12 The nuclear fuel behavior

The motivations for a specific “nuclear fuel” section have been given under item (f) in Section 15.4.12. One may state that nuclear fuel and nuclear fuel performance constitute established technologies. Even a summary outline of those technologies (selected aspects are listed under item (f) in Section 15.4.12) is well beyond the purposes here. Wide literature exists: fundamental materials-related issues can be found in OECD/NEA/NSC (2015), and analyses involving transient nuclear fuel behavior are discussed by Adorni et al. (2011), Rozzia et al. (2011), and Lisovsky et al. (2015).

Nuclear fuel topics and facts

Selected nuclear fuel topics/facts which have a relation with thermal-hydraulics are:

A. The geometrical configuration of nuclear fuel rod, namely diameter and height (including the distance TAF to BAF) is strictly associated with linear power production (q' , kW/m), other than thermal neutrons motion and mean-free path inside the pellet. Related to (current) optimized pin design, an increase in diameter causes a decrease in the volumetric power density of the core, and a decrease in diameter creates a challenge for the structural integrity.

B. Linear power production (q') controls the maximum fuel temperature in nominal operating conditions, then the energy stored in the fuel. Therefore, PCT in case of LBLOCA and namely what is called blowdown-PCT is directly affected by q' .

C. Burn-up has a complex influence upon material, mechanical, thermal, and reactor physics properties of fuel pins. Burn-up increase above certain limits undermines the fuel capability to remain intact following events like CRE or

LOCA.

D. Formation of oxide and crud on the rod external surface increases RST in normal operation. The increase in LOCA PCT associated with oxide and crud can be of the order of 200 K.

E. Ballooning is the main expected mechanism for clad rupture in case of LBLOCA. Other than release of (primarily) gaseous FP into the coolant, ballooning causes obstruction in the flow inside an FA. Obstruction may be at the origin of inadequate cooling for neighboring pins (see e.g., Ammirabile and Walker, 2014).

F. Brittle rupture of fuel clad must be avoided and H₂ produced by the chemical reaction between clad material and water must be controlled during any DBA accident. PCT and time of quench directly affect brittle fracture and H₂ production.

G. Spacer grid design and number have large influence in the interaction between coolant and fuel in nominal operating conditions and during accidents.

Nuclear fuel is part of any NPP calculation.

Phenomena connection with accident scenario: Nuclear fuel

Specific nuclear fuel information can be derived from Fig. 15.69, taken from CANDU fuel-related experiments (Horhoianu et al., 1998) (row 11 in Table 15.1).

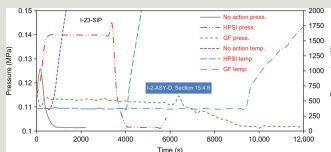


Fig. 15.68 Shutdown accident scenarios, loss of cooling with recovery actions in APR1400. Left axis: PS pressure. Right axis: RST.

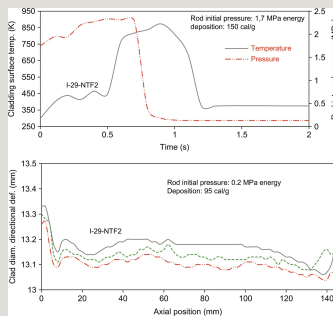


Fig. 15.69 Nuclear fuel behavior. Top: clad internal pressure and RST. Bottom: clad diametric deformation along three axial directions

Results from irradiation tests (energy deposition up to 265 cal/g) in research reactor performed in stagnant water at room temperature are shown in Fig. 15.69. Tests included the effects of initial element internal pressure and a range of energy deposition on the fuel element behavior.

Cladding failure mechanism and the failure threshold have been established: the fuel failure mechanism is a burst type and is very similar to LOCA failure mechanism.

The phenomenon identified in the second and the third columns of Table 15.38 is the outcome of the cross-link process in Tables 15.3 and 15.4. The phenomenon is associated with variables in Fig. 15.69.

Table 15.38

Visualization of nuclear fuel behavior



The following phenomenon is outlined in this section and (visually) described through the use of calculated accident scenarios and related time trends:

(1) Thermal-hydraulics—Nuclear fuel feedback (visualized, Fig. 15.69, top).

Feedback between coolant/moderator thermal-hydraulic parameters and nuclear fuel occurs in any NPP transient. The snapshot outline at items A. to G. gives an idea of the interactions.

15.5 Outcomes from the performed process

15.5.1 Resources for the cross-link between phenomena, accident scenarios, and time histories

Accident scenarios in NPP are understood and described by the use of parameter (or variable or quantity) time trends (or time histories), which are typically calculated by system thermal-hydraulics codes (discussed in Chapter 10). Phenomena have been derived to prove the qualification level of those computer codes.

A process has been completed in this document aiming at connecting accident scenarios, phenomena, and parameters resulting from NPP calculations.

Items which are part of the present chapter of the book can be summarized as follows:

- 12 water cooled reactor designs: PWR-UTSG, PWR-OTSG, PWR-HOSG (VVER-440 and VVER-1000), BWR, CANDU, PHWR, RBMK, plus AP1000, APR1400, EPR, SMR, and ABWR.
- 23 main accident scenarios (from Table 15.1) and connected sections in Chapter 4.
- 7 accident scenarios-related topics (e.g., NC, CHF, Boron, PTS, Fuel, AM, Containment).
- 45+2 accident scenarios [rows] and 47+21 leading reference documents in Tables 15.1 and 15.5 (“+” related to Table 15.5), to connect reactor designs and accident scenarios.
- 113 phenomena in Table 15.2.
- 5085 (=45×113) boxes in Table 15.3 cross-connecting accident scenarios and reactor designs with phenomena.

- 15 sets of “homogeneous” variable time trends, resulting in about 30 individual time trends distinguished in the top row of Table 15.4.
- 1695 (=15×113) boxes in Table 15.4 cross-connecting accident scenarios and phenomena with parameters.
- 158 documents part of the list of references, including 68 “process leading” documents cited in Tables 15.1 and 15.5.

One might also note the uncomfortable (for the reader) list of acronyms, including about 180 items, which was used to describe the process.

The process starts with the development of Tables 15.1 and 15.2, respectively, from:

- (a) considering reactor designs and DBA analysis results: namely, Table 15.1 includes a list of accident scenarios supported by referenced NPP calculations; and
- (b) the list of phenomena already part of Chapter 6 and available from OECD/NEA/CSNI and IAEA devoted reports.

Table 15.3 is developed by cross-connecting the accident scenarios, part of Table 15.1, and the phenomena, part of Table 15.2. The “filling of Table 15.3” provides a demonstration that all phenomena are part of at least one accident scenario. Moreover looking at Table 15.3 one may note that LBLOCA and SBLOCA are the accident scenarios where the largest number of phenomena is expected to occur.

The parameters used to characterize the accident scenarios are connected with phenomena in Table 15.4. Following the process of “filling of Table 15.4,” some phenomena (i.e., those listed in Table 15.5) could not be characterized by suitable parameters derived from NPP calculations. Thus Table 15.5 was developed including time histories referring to accident scenarios but not part of NPP calculations: available experimental and design analysis data were considered.

The data in Tables 15.1–15.5 are at the origin of Chapter 4: the sections connected with accident scenarios in Table 15.1 are considered.

As already mentioned in the Foreword, the process of connecting calculated variables and phenomena could be done using a couple of accident scenarios instead of 47 scenarios, having access to full calculation details (e.g., in-house calculation). Such a simplified process does not include the description of scenarios covering the DBA envelope and does not give an idea of the interest

toward accident scenarios by the scientific community.

15.5.2 Key achievements

The main outcome from the performed activity is a vision for the nuclear thermal-hydraulics universe mentioned in **Chapter 1**. This is based on phenomena, reactor design features, and results from the calculations by system thermal-hydraulics codes: connection with the licensing and the PSA processes comes from the nature of considered NPP calculations (i.e., the DBA envelope). A confirmation of the complexity of nuclear thermal-hydraulics shall be associated with the main outcome.

What else can be derived from the performed study?

Phenomena (i.e., expected in case of accidents in water cooled nuclear reactors) have been identified and characterized, also as a result of **Chapter 6**. They are derived from experiments and expertise which are continuously updated. Variables, results of computer code application to NPP analyses, have been associated with phenomena: whether the phenomena are properly modeled to produce a calculated accident scenario constitutes a question mark not addressed by the study. Then the achievements are:

- (1) Each qualified calculation should imply the demonstration that the concerned phenomena are properly modeled: i.e., a parameter time histories can be calculated not necessarily based upon phenomena part of the used models.
- (2) Ranking of phenomena as proposed in some approaches to accident analysis is not an outcome from the study: rather, all identified phenomena must be modeled according to their best knowledge.

One may also state that the phenomena-scenarios cross-link process is one part of activity needed to ensure the qualification of a calculation.

15.5.2.1 Application of system thermal-hydraulics codes

A few notes are given below in relation to the application of system thermal-hydraulic codes to the accident analysis of NPP considering the content of other chapters of the book.

First, the connection between modeling and phenomena in system thermal-hydraulics is not part of the present chapter: this is discussed in **Chapters 5–10**.

Second, the systematic relationship between phenomena (identified in Chapter 6 and partly characterized in the present chapter) and model features constitutes the topic of code manuals which also include the demonstration of code predictive capabilities.

Third, the listed phenomena constitute the basis for code validation, as discussed in Chapter 13.

Fourth, the study summarized in this chapter allows the confirmation that system thermal-hydraulics codes constitute the repository for the expertise associated with considered phenomena and the best (unique) tool to calculate accident scenarios.

Finally, the list of technology significant achievements from the application of system thermal-hydraulics codes to the accident analysis in water cooled reactor (not given here) might complement the present chapter as well as Chapters 11 and 13. This may also constitute a suitable prerequisite for the BEPU framework discussed in Chapter 14.

15.6 Conclusions

Two main objectives have been pursued in this chapter: (a) the description of accident scenarios; and (b) the association of thermal-hydraulics phenomena to accident scenario. Reference NPP units at the basis of the analyses documented in this chapter are PWR-UTSG, PWR-OTSG, PWR-HOSG (VVER-440 and VVER-1000), BWR, CANDU, PHWR, RBMK, AP1000, APR1400, EPR, SMR, and ABWR.

The accident scenarios are part of the nuclear reactor safety technology restricted, within the present framework, to the DBA or to the situation “before loss of core integrity.”

The thermal-hydraulics phenomena derive from OECD/NEA/CSNI and IAEA documents: the phenomena already described in Chapter 6 have been considered. In some cases more than one phenomenon deals with similar transient evolutions of two-phase flows, or in different terms, duplication in the definition of a few phenomena may have occurred. This might be connected with modeling features needed for establishing predictive capabilities and/or different validation framework. Notes are added to point out similarities, rather than reducing the number of phenomena.

The accident scenarios are depicted based on results of system thermal-hydraulics

code calculations: related time histories are associated with phenomena. No emphasis is given in the process to the quality of the calculations as well as to the needed evaluation of uncertainty. However, due importance is given to experimental programs: among the others, data or information from BC, PKL, LSTF, ATLAS, PSB, and LOBI experiments, in addition to data measured in NPP (e.g., Doel-2 SGTR) have been considered.

The main outcomes can be summarized as follows:

- A global vision of nuclear reactor thermal-hydraulics is provided from the side of phenomena and accident scenarios: 12 reactor types are considered for the characterization of 47 accident scenarios cross-linked with 113 phenomena: the phenomena are largely affected by geometry and boundary conditions and need suitable modeling capabilities (not discussed in the present chapter).
- The knowledge and the understanding of phenomena is a prerequisite for performing meaningful accident analysis. However, the process of associating time histories and phenomena does not include the demonstration that the phenomenon is part of the modeling or, in case it is part of the modeling, no quality proof is ensured.

The expected impact of the document is a contribution to the knowledge and the knowledge management in nuclear system thermal-hydraulics: the complexity of the cross-link process may give an idea of the complexity of subject (i.e., highly system geometry and boundary conditions dependent). However, the gathered information can be used as a part of the qualification process for system code calculations. All of this may constitute a guidance to formulate and to address the following issues or questions in relation to each NPP accident scenario calculation:

- a. What are phenomena expected to be relevant in the scenario? (The list in Table 15.2 to be considered: in general terms all phenomena should be considered.)
- b. Are any of the phenomena expected to be relevant in the scenario part of the adopted calculation model? For instance, in case of SBLOCA with two-phase conditions occurring in the hot leg of a PWR, importance should be given to the phenomenon “liquid and vapor mixing with condensation in SG mixing chamber.” Namely what equations (or equation parameters) are developed to account for those phenomena?
- c. What are the qualification bases for the phenomena expected to be relevant? Namely, what experiments may be used to demonstrate a suitable knowledge for

the phenomenon including addressing the scaling issue?

The distinction between a code calculation and a qualified code calculation should involve the answer (or the capability to answer) the questions/issues a. to c.

References

Adorni M., Bousbia-Salah A., Hamidouche T., Pierro F., Di Maro B., D'Auria F. Analysis of partial and total flow blockage of a single fuel assembly of an MTR research reactor core. *Ann. Nucl. Energy*. 2005;32.

Adorni M., Del Nevo A., D'Auria F., Mazzantini O. A procedure to address the fuel rod failures during LB-LOCA transient in Atucha-2 NPP. *Sci. Technol. Nucl. Ins.* 2011;2011.

Adu S., Horvatovic I., D'Auria F., Nyarko B.B.J.B., Geoffrey E.-R., Emmanuel O.D. *Analysis of channel blockage of MNSR reactor using the system thermal-hydraulic code RELAP5/MOD3.3*. In: 24th Int. Conf. Nuclear Energy for New Europe, Portoroz, 14-17 September; 2015.

Ammirabile L., Walker S.P. Dynamic ballooning analysis of a generic PWR fuel assembly using the multi-rod coupled MATARE code. *Nucl. Eng. Des.* 2014;268.

Analytis G.Th., Coddington P. Analysis and sensitivity studies of postulated SBLOCA in the Mühleberg (KKM) BWR/4 by Trac-BF1. *Ann. Nucl. Energy*. 2002;29.

ANSI. *Revision and Addendum to Nuclear Safety Criteria for the Design of Stationary Pressurized Water Reactor Plants*. ANSI-N18.2A-1995 New York: ANSI; 1995.

Araneo D., Ferrara P., Moretti F., Rossi A., Latini A., D'Auria F., Mazzantini O. Integrated software environment for pressurized thermal shock analysis. *Sci. Technol. Nucl. Ins.* 2011.

AREVA, 2014 (date of downloading), US EPR Final Safety Analysis Report, section 15-3-1, Partial loss of forced reactor coolant flow, AREVA ©.

Arkoma A., Hänninen M., Rantamäki K., Kurki J., Hämäläinen A. Statistical analysis of fuel failures in large break loss-of-coolant accident (LBLOCA) in EPR type nuclear power plant. *Nucl. Eng. Des.* 2015;285.

Aumiller D.L., Tomlinson E.T., Clarke W.G. *A new assessment of RELAP5-3D using a General Electric level swell problem.* In: RELAP5 Users Seminar, Jackson Hole, W, 12–14 September; 2000.

Bae B.-U., Kim S., Park Y.-S., Kang K.H. Integral effect test and code analysis on the cooling performance of the PAFS (passive auxiliary feed-water system) during an FLB (feed-water line break) accident. *Nucl. Eng. Des.* 2014;275.

Bandini G., De Rosa F. ASTEC validation on TMI-2 and LOFT LP-FP-2. *Nucl. Eng. Des.* 2014;272.

Bartosiewicz Y., Giot M., Seynhaeve J.M. *Revisiting modeling techniques and validation experiments for two-phase choked flows relevant to LOCA.* In: International Topical Meeting on Nuclear Thermal-Hydraulics, Operation and Safety (NUTHOS-8) N8P0317, Shanghai, 10–14 October; 2010.

Beckmeyer R.R., Gregory M.V., Buckner M.R. *Complete BWR-EM LOCA analysis using the WRAP-EM system.* In: ANS Meeting, Atlanta, GA; 1979.

Belsito S., D'Auria F. *Comparison of advanced computer codes in the simulation of CHF occurrence in PMK facility.* In: 4th World Conf. Experimental Heat Transfer, Fluid Mechanics and Thermodynamics - Brussels (B), 2–6 June; 1997.

Billa C., D'Auria F., Debrecin N., Galassi G.M. *Application of Relap5/mod2 to PWR international standard problems.* In: ANS Winter Meeting, San Francisco, CA, 10–15 November; 1991.

Bittan J. *Simulation of thermal-hydraulics accidental transients: evaluation of MAAP5.02 versus CATHAREv2.5.* In: 7th European Review Meeting on Severe Accident Research (ERMSAR-2015), Marseilles, 24–26 March; 2015.

Blinkov V.N., Melikhov O.I., Melikhov V.I., Davydov M.V., Wolff H., Arndt S. Experimental studies for the VVER-440/213 bubble condenser system for kola NPP at the integral test facility BC V-213. *Sci. Technol. Nucl. Ins.* 2012.

Borisov E., Grigorov D., Mancheva K. Study of long-term loss of all AC power supply sources for VVER-1000/V320 in connection with application of new engineering safety features for SAMG. *Ann. Nucl. Energy.* 2013;59.

Bousbia-Salah A., D'Auria F. Analysis of the Peach Bottom 2 BWR Turbine trip experiment by Relap5/3.2 code. *Nucl. Technol. Radiat. Prot.* 2002;17:1–2.

Bucalossi A., Del Nevo A., Moretti F., D'Auria F., Elkin I.V., Melikhov O.I. Investigation of accident management procedures related to loss of feed-water and station blackout in PSB-VVER integral test facility. *Nucl. Eng. Des.* 2012;250.

Chen Y.-S., Yuann Y.-R. Negative pressure difference evaluation of Lungmen ABWR containment by using Gothic. *Ann. Nucl. Energy.* 2015;75.

Chen C.-H., Wang J.-R., Lin H.-T., Shih C. ATWS analysis for Maanshan PWR using TRACE/SNAP code. *Ann. Nucl. Energy.* 2014;72.

Cherubini M., Giannotti W., Araneo D., D'Auria F. Use of the natural circulation flow map for natural circulation systems evaluation. *Sci. Technol. Nucl. Ins.* 2008a.

Cherubini M., Muellner M., D'Auria F., Petrangeli G. Application of an optimized AM procedure following a SBO in a VVER-1000. *Nucl. Eng. Des.* 2008b;238.

Cho S., Park H.-S., Choi K.-Y., Kang K.-H., Baek W.-P., Kim Y.-S. Core thermal-hydraulic behavior during the reflood phase of cold leg LBLOCA experiments using the ATLAS test facility. *Nucl. Eng. Technol.* 2009;41:10.

Congiu C., D'Auria F., Frogheri M., Galassi G.M., Madeira A.,

Zhao H. Relevant thermal-hydraulic aspects in four 1% Small break LOCA experiments in LOBI facility. *Kerntechnik*. 1996;61:4.

D'Auria F. *Natural circulation situations relevant to NPP*. In: Joint ICTP-IAEA Course on Natural Circulation Phenomena and Passive Safety Systems in Advanced Water Cooled Reactors, Trieste, December; 2012.

D'Auria, F., Galassi, G.M., 2004. Best-Estimate Analysis of the Angra-2 ATWS Event Category, University of Pisa Report, DIMNP—NT 526(04)-rev.4, Pisa.

D'Auria F., Galassi G.M. *Natural circulation situations relevant to Nuclear Power Plants*. In: IAEA Training Course on Natural Circulation Phenomena and Passive Safety Systems in Advanced Water Cooled Reactors SANESS-GCNEP, Mumbai, India, 29 September–3 October, Paper ID L19; 2014.

D'Auria F., Gago J.L., Galassi G.M., Grgic D., Spadoni A. Three Mile Island Unit 1 Main Steam Line Break three dimensional neutronics/thermalhydraulics Analysis: application of different coupled codes. *Nucl. Technol.* 2003a;142:1.

D'Auria, F., Galassi, G.M., Giannotti, W., 2003b. Transient Analyses of the BETHSY 4.2b Test Carried Out by the Code Cathare 2, University of Pisa, DIMNP NT 516(03), Pisa.

D'Auria, F. (Project Coordinator), Bousbia-Salah, A., Galassi, G.M., Vedovi, J., Reventos, F., Cuadra, A., Gago, J.L., Sjoberg, A., Yitbarek, M., Sandervag, O., Garis, N., Anhert, C., Aragones, J.M., Verdù, G., Mirò, R., Hadek, J., Macek, J., Ivanov, K., Uddin, R., Sartori, E., Rindelhardt, U., Rohde, U., Frid, V., Panayotov, D., 2004. Neutronics/Thermal-hydraulics Coupling in LWR Technology – CRISSUE-S, Vol II: State-of-the-Art Report (see also Volumes I and III), OECD/NEA Report No 5436, Paris.

D'Auria, F. (Editor), Soloviev, S., Novoselsky, O., Moskalev, A., Radkevitch, V., Malofeev, V., Parisi, C., Cherubini, M., Pierro, F., Moretti, F. (Lead Authors), 2005. Deterministic Safety Technology in RBMK – EC TACIS Project R2.03/97 < Software

Development for Accident Analysis of VVER and RBMK Reactors in Russia > Final Technical Report, Part B, University of Pisa – DIMNP NT 580 (05), Pisa, ISBN 88-902189-0-8.

D'Auria, F. (Editor), Melikhov, O., Suslov, A., Bykov, M., Elkin, I., Araneo, D., Cherubini, M., Del Nevo, A., Giannotti, W., Muellner, N. (Lead Authors), 2006. Accident Management Technology in VVER-1000, University of Pisa – DIMNP NT 581 (06), Pisa, ISBN 88-902189-0-9, pp. 1–1250.

D'Auria F., Gabaraev B., Novoselsky O., Radkevich V., Filinov N., Mazzini D., Moretti F., Pierro F., Vigni A., Parafilo L., Kryuchkov D. The Multiple Pressure Tube Rupture (MPTR) issue in RBMK safety technology. *Nucl. Eng. Des.* 2008a;238.

D'Auria F., Cherubini M., Pierro F., Giannotti W. The Individual Channel Monitoring (ICM) proposal to improve the safety performance of RBMK. *Nucl. Eng. Des.* 2008b;238.

D'Auria F., Gabaraev B., Radkevitch V., Moskalev A., Uspuras E., Kaliatka A., Parisi C., Cherubini M., Pierro F. Thermal-hydraulic performance of primary system of RBMK in case of accidents. *Nucl. Eng. Des.* 2008c;238.

D'Auria, F., Mazzantini, O., Cherubini, M., Giannotti, W., Parisi, C., Moretti, F., Melideo, D., Del Nevo, A., Galassi, G.M., Araneo, D., Terzuoli, F., Adorni, M., Muellner, N., Petruzzi, A., Lazzarini, D., Santoro, R., Bousbia-Salah, A., 2008d. DEGB LBLOCA (2 X 100% Break in CL) in Atucha-2 NPP, University of Pisa Report, DIMNP NT 628(08)-rev. 1, Pisa.

D'Auria F., Galassi G., Pla P., Adorni M. The Fukushima Event: the outline and the technological background. *Sci. Technol. Nucl. Ins.* 2012;507921.

D'Auria F., Pirro F., Araneo D., Galassi G.M. *Reliability of TH passive safety systems*. In: IAEA Training Course on Natural Circulation Phenomena and Passive Safety Systems in Advanced Water Cooled Reactors SANESS-GCNEP, Mumbai, India, 29 September–3 October, Paper ID L20; 2014.

Damerell, P.S., Simons, J.W., 1993a. 2D/3D Program Work Summary Report, GRS Report No. 100, NUREG/IA 0126, Washington, DC.

Damerell, P.S., Simons, J.W., 1993b. Reactor Safety Issues by the 2D/3D Program, GRS Report No 101, NUREG/IA 0127, Washington, DC.

D'Auria F., Galassi G.M. Assessment of RELAP5/MOD2 code on the basis of experiments performed in LOBI facility. *Nucl. Technol.* 1990a;90(3).

D'Auria F., Galassi G.M. Flowrate and density oscillations during two-phase natural circulation in PWR typical conditions. *Nucl. Eng. Des.* 1990b;122.

D'Auria, F., Galassi, G.M., 2001. Best Estimate Analysis and Uncertainty Evaluation of the Angra-2 LBLOCA DBA, University of Pisa Report, DIMNP - NT 433(01), Pisa (I)-rev.1, July, Submitted to CNEN, Rio de Janeiro.

D'Auria F., Ingegneri M. *Qualitative and quantitative analysis of Cathare-2 code results of counterpart test calculations in LOBI, SPES, BETHSY and LSTF facilities.* In: 8th Int. Top. Meet. on Nuclear Reactor Thermalhydraulics (NURETH-8), Kyoto, 30 September–4 October; 1997.

D'Auria, F., Vigni, P., 1980. Two-Phase Critical Flow Models, CSNI Report No. 49, Paris.

D'Auria F., Galassi G.M., Oriolo F., Vigni P. *Assessment of scaling principles for the simulation of small break LOCA experiments in PWRs.* In: Spec. Meet. on Small Break LOCA Analyses in LWR, Pisa, 23–27 June; 1985 (also Nuclear Engineering and Design, Vol 102, 1987).

D'Auria F., Frogheri M., Leonardi M. *Natural circulation performance in western type and eastern type PWR.* In: XI Annual Simulator Conference, San Diego, CA, 10–14 April; 1994.

D'Auria F., Galassi G.M., Gatta P., Mastrantonio L., Marsili P.

Comparison between small LOCA scenarios in Eastern and Western type PWRs. In: ASME-JSME Int. Conf. on Nuclear Engineering (ICONE-4), New Orleans, LO, 10–14 March; 1996a.

D'Auria, F., Clement, P., Faluomi, V., Staedtke, H., Vanhoenacker, L., 1996b. Lesson learned from OECD/CSNI ISP on Small Break LOCA, OECD-CSNI Report OECD/GD (97) 10, Paris.

D'Auria F., Galassi G.M., Mastrantonio L. *Accident management studies in the WWER-1000 plant.* In: ASME-JSME Int. Conf. on Nuclear Engineering (ICONE-5, 2458), Nice, 26–30 May; 1997a.

D'Auria, F. (Editor), Ambrosini, W., Anegawa, T., Blomstrand, J., In De Betou, J., Langenbuch, S., Lefvert, T., Valtonen, K., 1997b. State of the Art Report on Boiling Water Reactor Stability (SOAR ON BWRs), OECD-CSNI Report OECD/GD (97) 13, Paris.

D'Auria, F., Galassi, G.M., Spadoni, A., 1998. Optimisation of the Elevation of a Heat Exchanger in Dual Natural Circulation (in Italian), University of Pisa Report, DCMN - NT 363(98), Pisa.

De Santi G., Piplies L., Sanders J. *Mass flow instabilities in LOBI steam generators U-tubes under natural circulation conditions.* In: 2nd Int. Meet on NPP Thermal-Hydraulics and Operation, Tokyo; 1986.

Del Nevo A., Rozzia D., Moretti F., D'Auria F. OECD/NRC PSBT benchmark: investigating the CATHARE2 capability to predict void fraction in PWR fuel bundle. *Sci. Technol. Nucl. Ins.* 2012a.

Del Nevo A., Adorni M., D'Auria F., Melikhov O.I., Elkin I.V., Schekoldin V.I., Zakutaev M.O., Zaitsev S.I., Benčík M. Validation of advanced computer codes for VVER technology: LB-LOCA transient in PSB-VVER facility. *Sci. Technol. Nucl. Ins.* 2012b.

Doi T., Futatsugi T., Murase M., Hayashi K., Hosokawa S.,

Tomiyama A. Countercurrent flow limitation at the junction between the Surge Line and the pressurizer of a PWR. *Sci. Technol. Nucl. Ins.* 2012.

Ebert, D. (Ed.), 1995. Proceedings of the OECD/CSNI Specialists Meeting on Boron Dilution Reactivity Transients Held in State College, Pennsylvania, PA, 18–20 October, NUREG/CP-0158, Washington, DC.

Féburie V., Giot M., Granger S., Seynhaeve J.M. A model for choked flow through cracks with inlet subcooling. *Int. J. Multiphase Flow.* 1993;19.

Ferng Y.-M., Liu Y.-T., Shih C. Investigating the execution of EOPs in LOTDFP + ATWS + LOCA scenarios for an ABWR using MAAP code. *Nucl. Eng. Des.* 2010;240.

Freixa J., Manera A. Verification of a TRACE EPRTM model on the basis of a scaling calculation of an SBLOCA ROSA test. *Nucl. Eng. Des.* 2011;241.

Fukuda K., Kobori T. Classification of two-phase flow stability by density-wave oscillation model. *Nucl. Sci. Technol.* 1979;16.

Graffard, E., Goux, F., 2006. CFX code application to the French reactor for inherent boron dilution safety issue, CFD4NRS, Garching, 5–7 September.

Groudev P., Stefanova A. Validation of Relap5/Mod3.2 model on trip of one main coolant pump for VVER 440/V320. *Nucl. Eng. Des.* 2006;236.

Guimaraes L.N.F. *Non-Linear Dynamics of a Once-Through Steam Generator*. (PhD Dissertation) Knoxville, TN: University of Tennessee; 1992.

Hammersley R.J., Elicson G.T., Henry R.E. *Two phase flow and water hammer transient assessment with the TREMOLO computer code*. In: Conf. Best-Estimate Methods in Nuclear Installation Safety Analysis (BE-2000), Washington, DC, November; 2000.

Haratyk G., Gourmel V. Preliminary accident analysis of

Flexblue® underwater reactor. *Nucl. Sci. Technol.* 2015;1:6.

Haste T.J., Birchley J., Richner M. Accident management following loss of coolant accident during cooldown in a Westinghouse two-loop PWR. *Nucl. Eng. Des.* 2010;240.

Horhoianu G., Ionescu D.V., Sefan I., Olteanu G. CANDU type fuel behavior during rapid overpower transients. *Nucl. Eng. Des.* 1998;179.

Huang H.-W., Shih C., Yih S., Chen M.-H., Lin J.-M. Model extension and improvement for simulator-based software safety analysis. *Nucl. Eng. Des.* 2007;237.

Hung Z.-Y., Ferng Y.-M., Hsu W.-S., Pei B.-S., Chen Y.-S. Analysis of AP1000 containment passive cooling system during a loss-of-coolant accident. *Ann. Nucl. Energy.* 2015;85.

Hyvarinen J. Heat transfer characteristics of horizontal steam generators under natural circulation conditions. *Nucl. Eng. Des.* 1996;66.

IAEA, 1996. Defense in Depth in Nuclear Safety, INSAG-10, Vienna

IAEA, 1997. Guidelines on the Pressurized Thermal Shock Analysis for WWER Nuclear Power Plants, EBP-WWER-08, Vienna.

IAEA, 2001. Thermohydraulic Relationships for Advanced Water Cooled Reactors, TECDOC 1203, Vienna.

IAEA, 2002a. Accident Analysis for Nuclear Power Plants, IAEA Safety Reports Series No 23, Vienna.

IAEA, 2002b. Natural Circulation Data and Methods for Advanced Water Cooled Nuclear Power Plants Designs, TECDOC 1281, Vienna.

IAEA, 2003. Accident Analysis for Nuclear Power Plants with Pressurized Heavy Water Reactors, IAEA Safety Reports Series No 29, Vienna.

IAEA, 2005a. Assessment of Defense in Depth for Nuclear Power Plants, IAEA Safety Reports Series No 46, Vienna.

IAEA, 2005b. Natural Circulation in Water Cooled Nuclear Power Plants, TECDOC 1474, Vienna.

IAEA, 2009a. Passive Safety Systems and Natural Circulation in Water Cooled Nuclear Power Plants, TECDOC 1624, Vienna.

IAEA [Authors: Bukin, N., D'Auria, F., Elter, J., Gudoshnikov, A., Kantee, H., Kostka, P., Kristof, M., Kvidza, B., Macek, J., Makihara, Y., Matejovic, P., Misak, J., Sartmadjiev, A., Spalj, S.], 2009b. Safety Analysis of WWER-440 Nuclear Power Plants: Potential Consequences of a Large Primary to Secondary System Leakage Accident, IAEA Tecdoc 1610, Vienna, February.

IAEA, 2012. Natural Circulation Phenomena and Modeling for Advanced Water Cooled Reactors, TECDOC 1677, Vienna.

Ivanov K., Baratta A. *Coupling methodologies for best estimate safety analysis*. In: Int. Conf. on Mathematics, Computation, Reactor Physics and Environmental Analysis (M & C), Madrid; 1999.

Ivanov, K.N., Beam, T.M., Baratta, A.J., Irani, A., Trikouros, N., 1999. Pressurized Water Reactor Main Steam Line Break (MSLB) Benchmark - Final Specifications, NEA/NSC/DOC(99)8, Paris.

Jang C. Treatment of the thermal-hydraulic uncertainties in the pressurized thermal shock analysis. *Nucl. Eng. Des.* 2007;237.

Jeong J.J., Lee W.J., Chung B.D. Simulation of a main steam line break accident using a coupled system thermal-hydraulics three dimensional reactor kinetics and hot channel analysis code. *Ann. Nucl. Energy*. 2006;33.

Jimenez G., Queral C., Rebollo-Mena M.J., Martínez-Murillo J.C., Lopez-Alonso E. Analysis of the operator action and the single failure criteria in a SGTR sequence using best estimate

assumptions with TRACE 5.0. *Ann. Nucl. Energy*. 2013;58.

Jimenez G., Herrero J.J., Gommlich A., Kliem S., Cuervo D., Jimenez J. Boron dilution transient simulation analyses in a PWR with neutronics/ thermal-hydraulics coupled codes in the NURISP project. *Ann. Nucl. Energy*. 2015;84.

Khadamakar H.P., Patwardhan A.W., Padmakumar G., Vaidyanathan G. Flow distribution in the inlet plenum of steam generator. *Nucl. Eng. Des.* 2011;241.

Kim Y.-S., Choi K.-Y. An analytical investigation of loop seal clearings for the SBLOCA tests. *Ann. Nucl. Energy*. 2014;68.

Kinoshita I., Murase M., Tomiyama A. Numerical simulation of size effects on countercurrent flow limitation in PWR hot leg models. *Sci. Technol. Nucl. Ins.* 2012.

Kliem S., Mittag S., Rohde U., Weiß F.-P. ATWS analysis for PWR using the coupled code system DYN3D/ATHLET. *Ann. Nucl. Energy*. 2009;36.

Kok H.V., Van der Hagen T.H.J.J., Mudde R.F. Measurements of the void-fraction distribution in a simulated fuel assembly and the role of the void-fraction on the dynamics of a natural circulation loop. *Ann. Nucl. Energy*. 1997;24:16.

Kolev N.I. Uniqueness of the elementary physics driving heterogeneous nucleate boiling and flashing. *Nucl. Eng. Technol.* 2006;38:2.

Korhonen R., Hietanen O. *Erosion corrosion on the parallel feed water discharge lines at the Loviisa VVER 440*. In: Specialists Meeting on Erosion and Corrosion of NPP Materials, Kiev; 1994.

Levy S. *Two-Phase Flow in Complex Systems*. New York: John Wiley & Sons Inc.; 1999.

Lisovsky O., Cherubini M., Lazzerini D., D'Auria F. Base irradiation simulation and its effect on fuel behavior prediction by TRANSURANUS code: application to reactivity initiated

accident condition. *Nucl. Eng. Des.* 2015;283.

Madeira A., D'Auria F., Alvim A.C.M. A PWR recovery option for a total loss of feed-water beyond design basis scenario. In: 10th Int. Top. Meet. on Nuclear Reactor Thermalhydraulics (NURETH-10), Seoul, 5–9 October; 2003.

Mascari F., Vella G., Woods B.G., D'Auria F. Analyses of the OSU-MASLWR experimental test facility. *Sci. Technol. Nucl. Ins.* 2012.

Mehedinteanu S. The evaluation of RCS depressurization to prevent core melting in pressure tube reactors (CANDU-type). *Ann. Nucl. Energy.* 2009;36(4):537–545.

Melikhov V.I., Melikhov O.I., Parfenov Y., Nerovnov A. Simulation of the thermal hydraulic processes in the horizontal steam generator with the use of the different interfacial friction correlations. *Sci. Technol. Nucl. Ins.* 2011.

Muellner N., Cherubini M., Kromp W., D'Auria F., Petrangeli G. A procedure to optimize the timing of operator actions of accident management procedures. *Nucl. Eng. Des.* 2007;237.

Mull, T., Umminger, K., Bucalossi, A., D'Auria, F., Monnier, P., Toth, I., Schwarz, W., 2007. Final Report of the OECD-PKL Project, AREVA NP GmbH, NTCTP-G/2007/en/0009, Erlangen.

Munoz-Cobo J.L., Escrivá A., Mendizabal R., Pelayo F., Melara J. CSAU methodology and results for an ATWS event in a BWR using information theory methods. *Nucl. Eng. Des.* 2014;278.

Nakamura H., Watanabe T., Takeda T., Maruyama Y., Suzuki M. Overview of recent efforts through ROSA/LSTF experiments. *Nucl. Eng. Technol.* 2009;41:6.

Nourbakhsh H.P., Cheng Z. *Mixing phenomena of interest to boron dilution during small break LOCAs in PWRs.* In: Int. Conf. NURETH-7, Saratoga Springs, NY; 1995.

OECD/NEA/CSNI, 1986. Pressure Suppression System Containments, a State of Art Report, CSNI Report 126, Paris.

OECD/NEA/CSNI, 1987. CSNI Code Validation Matrix of Thermo-Hydraulic Codes for LWR LOCA and Transients, CSNI, 132, Paris.

OECD/NEA/CSNI, 1988. ISP-20 - Steam Generator Tube Rupture Behavior, Nuclear Power Plant Doel 2, Belgium, CSNI report No. 154, Paris.

OECD/NEA/CSNI, 1989a. Containments for Pressurized Water Reactors: A State-of-the-Art-Report (SOAR), CSNI Report 166, Paris.

OECD/NEA/CSNI, 1989b. Thermo-hydraulics of Emergency Core Cooling in Light Water Reactors-A State of the Art Report, OECD/CSNI 161, Paris, October.

OECD/NEA/CSNI, 1993. A Separate Effects Test Matrix for Thermal-Hydraulic Code Validation: Phenomena Characterization and Selection of Facilities and Tests, OECD/GD (94) 82, Vols. I and II, Paris.

OECD/NEA/CSNI, 1996a. Code Validation Matrix of Thermo-Hydraulic Codes for LWR LOCA and Transients, CSNI Report 132-rev. 1, originally published in 1987, Paris.

OECD/NEA/CSNI, 1996b. Relevant Thermal-Hydraulic Aspects of Advanced Reactor Design – Status Report, OECD/GD(97)8, Paris.

OECD/NEA/CSNI, 1999. State-of-the-Art Report (SOAR) on Containment Thermalhydraulics and Hydrogen Distribution, CSNI/R(1999)16, Paris.

OECD/NEA/CSNI, 2001. Validation Matrix for the Assessment of Thermal-Hydraulic Codes for VVER LOCA and Transients, NEA/CSNI/R(2001)4, Paris.

OECD/NEA/CSNI, 2009. BEMUSE Programme, Phase V report, Uncertainty and Sensitivity Analysis of a LBLOCA in Zion Nuclear Power Plant, NEA/CSNI/R(2009)13, Paris.

OECD/NEA/CSNI, 2011. Safety Margins Evaluation, SMAP

Framework Assessment and Application, NEA/CSNI/R82011)3, Paris.

OECD/NEA/CSNI, 2014. Containment Code Validation Matrix, CSNI/R(2014)3, Paris.

OECD/NEA/CSNI-ISP, 2000. CSNI International Standard Problems (ISP) Brief Descriptions (1975-1999), CSNI/R(2000)5, Paris.

OECD/NEA/CSNI-ISP-50, 2012. International Standard Problem No. 50, ATLAS Test, SB-DVI-09: 50% (6-inch) break of DVI line of the APR-1400 final integration report, Volume I, analysis of blind/open calculations, CSNI/R(2012)6, Paris.

OECD/NEA/NSC, 2015. State-of-the-Art Report on Multi-scale Modelling of Nuclear Fuels NSC/R/(2015)5, Paris, October.

Park H.S., No H.C., Bang Y.S. Analysis of experiments for in-tube steam condensation in the presence of non-condensable gases at a low pressure using the RELAP5/MOD3.2 code modified with a non-iterative condensation model. *Nucl. Eng. Des.* 2003;225.

Pecchia M., Parisi C., D'Auria F., Mazzantini O. Development and application of MCNP5 and KENO-VI Monte Carlo models for the Atucha-2 PHWR analysis. *Sci. Technol. Nucl. Ins.* 2011.

Petrangeli G., Tononi R., D'Auria F., Mazzini M. The SSN: an emergency system based on intentional depressurization for PWRs. *Nucl. Eng. Des.* 1993;143: (also, CSNI Spec. Meet. on Intentional Coolant System Depressurization, Garching (G), 12–14 June 1989).

Petruzzi A., D'Auria F. Standardized consolidated calculated and reference experimental database (SCCRED): a supporting tool for V&V and uncertainty evaluation of best-estimate system codes for licensing applications. *Nucl. Sci. Eng.* 2016;182:1–2.

Pla P., Parisi C., D'Auria F. Boron dilution and boron transport

after SBLOCA in PWR and VVER-1000 nuclear reactors. In: *Boron Dilution in Pressurized Water Reactors*. Saarbrücken, Germany: Lambert Academic Publishing, LAP GmbH & Co.; 2010:978-3-8383-8373-6.

Queral C., Montero-Mayorga J., Gonzales-Cadelo J., Jimenez G. AP1000 large break LOCA BEPU analysis with Trace code. *Ann. Nucl. Energy*. 2015;85.

Reeder D.L. *LOFT System and Test Description (5.5 Foot Nuclear Core 1 Loss-of-Coolant Experiments)*. TREE-NUREG- 1208 Idaho Falls, ID: EG&G Idaho; 1978.

Réocreux M. *Contribution à l'étude des debits critiques en écoulement diphasique eau-vapeur*. (PhD thesis) Grenoble: Université Scientifique et Médicale de Grenoble; 1974.

Reocreux M. *A few examples of ISPs addressing reactor specific problems*. In: OECD/NEA/CSNI, THICKET Seminar, Pisa, 5–9 May; 2008.

Reventos F., Pla P., Matteoli C., Nacci G., Cherubini M., Del Nevo A., D'Auria F. Consistent posttest calculations for LOCA scenarios in LOBI integral facility. *Sci. Technol. Nucl. Ins.* 2012.

Rouben B. *Coupled neutronics-thermal-hydraulics LOCA analysis*. In: Seminar at Chulalongkorn University, Bangkok; 1997.

Rozzia D., Adorni M., Del Nevo A., D'Auria F. Capabilities of TRANSURANUS code in simulating power ramp tests from the IFPE database. *Nucl. Eng. Des.* 2011;241.

Sakurai A., Shiotsu M., Hata K. A general correlation for pool film boiling heat transfer from a horizontal cylinder to sub-cooled liquid: Part 1 – A theoretical pool film boiling heat transfer model including radiation contributions and its analytical solution. *J. Heat Transf.* 1990;112.

Sankovich M.F., McDonald B.N. *Once through steam generation*. In: XVI Nuclear Congress, Rome, 25–26 March; 1971.

Schaffrath A., Krussenberg A.-K., Fjodorow A., Gocht U.,

Lischke W. Modeling of condensation in horizontal tubes. *Nucl. Eng. Des.* 2001;204.

Sehgal B.R., Bechta S. Severe accident progression in the BWR lower plenum and the modes of vessel failure. *Ann. Nucl. Energy.* 2016;93:28–34.

Seul K.W., Bang Y.S., Kim I.G., Yonomoto T., Anoda Y. Simulation of multiple steam Generator Tube Rupture (SGTR) event scenario. *Kor. Nucl. Soc.* 2003;35:3.

Son Y.-S., Shin J.-Y. Thermal-hydraulic analysis on the effect of operator action in the loss of shutdown cooling system accident in a PWR. *Nucl. Eng. Des.* 2007;237.

Takeda T., Ohwada A., Nakamura H. Measurement of non-condensable gas in a PWR small-break LOCA simulation test with LSTF for OECD/NEA ROSA Project and RELAP5 post-test analysis. *Exp. Thermal Fluid Sci.* 2013;51.

Tasaka K., Tamaki M., Imai S., Kohketsu H., Anoda Y., Murata H., Kukita Y. Atmospheric-pressure small-scale thermal-hydraulic experiment of a PIUS-Type reactor. *Nucl. Sci. Technol.* 1992;29:12.

Todorova N.K., Ivanov K.N. Investigation of spatial coupling aspects for coupled code application in PWR safety analysis. *Ann. Nucl. Energy.* 2003;30.

Tong L.L., Chen J.B., Cao X.W., Deng J. Thermal-hydraulic behavior under Station Blackout for CANDU-6. *Prog. Nucl. Energy.* 2014;74.

Toth I., Prior R., Sandervag O., Umminger K., Nakamura H., Muellner N., Cherubini M., Del Nevo A., D'Auria F., Dreier J., Alonso J.R., Amri A. *Core Exit Temperature Effectiveness in Accident Management of Nuclear Power Reactor*. Paris: OECD/NEA NEA/CSNI/R(2010)9; 2010 November.

USAEC. *Interim Acceptance Criteria (IAC) for ECCS*. Washington, DC: USAEC; 1971.

USNRC, 1988. Compendium of ECCS Research for Realistic LOCA Analysis, NUREG-1230, Washington, DC.

USNRC. *Domestic Licensing of Production and Utilization Facilities, Code of Federal Regulations 10, Part 50*. Washington, DC: US Government Printing Office; 1995.

USNRC, 1998. Risk Assessment of Severe Accident-Induced Steam Generator Tube Rupture, NUREG-1570, Washington, DC.

Vigni P., D'Auria F. Unsteady two-phase jet forces (in Italian). *Ingegneria Nucleare*. 1979;10.

Vijayan P.K. *Local phenomena associated with natural circulation*. In: IAEA Training Course on Natural Circulation Phenomena and Passive Safety Systems in Advanced Water Cooled Reactors SANESS-GCNEP, Mumbai, India, 29 September–3 October, Paper ID L04/05; 2014.

Visentini R., Colin C., Ruyer P. Experimental investigation of heat transfer in transient boiling. *Exp. Thermal Fluid Sci*. 2014;55.

Wulff, W., Cheng, H.S., Mallen, A.N., Rohatgi, U.S., 1992. BWR Stability Analysis with the BNL Engineering Plant Analyzer, USNRC NUREG/CR-5816 (also BNL-NUREG-52312), Washington, DC.

Yan J., Bolger F. Acoustic impact on steam dryer induced by main steam line break in boiling water reactor. *Nucl. Eng. Des*. 2009;239.

Yang J., Wang W.W., Qiu S.Z., Tian W.X., Su G.H., Wu Y.W. Simulation and analysis on 10-in. cold leg small break LOCA for AP1000. *Ann. Nucl. Energy*. 2012a;46.

Yang X., Schlegel J.P., Liu Y., Paranjape S., Hibiki T., Ishii M. Measurement and modeling of two-phase flow parameters in scaled 8 x 8 BWR rod bundle. *Int. J. Heat Fluid Flow*. 2012b;34.

Ylonen A. *Large Break Blowdown Test Facility Study*. Lappeenranta: Lappeenranta University of Technology; 2008.

Yu X.-G., Park H.S., Kim Y.S., Kang K.H., Cho S., Choi K.-Y.
Systematic analysis of a station blackout scenario for APR1400
with test facility ATLAS and MARS code from scaling
viewpoint. *Nucl. Eng. Des.* 2013;259.

Yun B.J., Cho H.K., Euh D.J., Song C.-H., Park G.C. Scaling for
the ECC bypass phenomena during the LBLOCA reflood phase.
Nucl. Eng. Des. 2004;231.

Thermal-hydraulics aspects of key nuclear accidents

G.M. Galassi; F. D'Auria *University of Pisa, Pisa, Italy*

Abstract

Accidents in Nuclear Power Plants have the potential for tremendous impact on the population and the environment. This has been specifically true for those events which evolved into severe accidents, noticeably Three Mile Island, Chernobyl, and Fukushima, i.e., the key topic for the present chapter. These accidents deserved and received deep attention from the scientific and technological community: in each case thousands of documents have been published. Nuclear thermal-hydraulics has been used for understanding the accident progressions and, specifically in the case of Three Mile Island, attained indications for new research activities and developments. Owing to this motivation the “stability” events occurred in La Salle and Oskarshamn are also part of this chapter; however, stability events have little or no safety implications and no radiological consequences.

Keywords

Three Mile Island accident; Chernobyl accident; Fukushima-Daiichi accident; La Salle stability event; Oskarshamn stability event; Accidents in nuclear technology; Accident in Nuclear Power Plants

Acronyms

ABB Asea Brown Boveri

ADS Automatic Depressurization
System

AESJ Atomic Energy Society of
Japan

AIRS Advanced Incident-Reporting
System

APRM Average Power Range
Monitor

BAF bottom of the active fuel

BOC beginning of cycle

BoP balance of plant

BWR boiling water reactor

B & W Babcock and Wilcox

CANDU Canadian deuterium
uranium reactor

CCFL counter-current flow limitation

CD core damage

CERTA consolidation of integral
system test experimental databases
for reactor thermal-hydraulic safety
analysis

CHF critical heat flux

CL cold leg

CNRA Committee on Nuclear
Regulatory Activities

CR control rod

CSNI Committee on the Safety of Nuclear Installations

CST condensate storage tank

DC direct current

DEGB double-ended guillotine break

DG diesel generator

DWOs density wave oscillations

EC European Commission

ECCS emergency core cooling systems

EFW emergency feed-water

EOP emergency operating

procedures

EPRI Electrical Power Research
Institute

ERV electromagnetic relief valve

ESF engineered safety features

FINAS Fuel Incident Notification and
Analysis System

FW feed-water

GE general electric

HL hot leg

HPCI high-pressure coolant injection

HPI high-pressure injection

HTGR high-temperature gas reactor

IAC Interim Acceptance Criteria

IC isolation condenser

INES International Nuclear and
Radiological Event Scale

IRS International Reporting System
for Operating Experience

IRSRR Incident-Reporting System
for Research Reactors

ITDB Incident and Trafficking
Database

ITF integral test facility

I & C instrumentation and control

LBLOCA large break loss of coolant accident

LOCA loss of coolant accident

LOFW loss of feed-water

LOOSP loss of on-site and off-site power

LPCS low-pressure core spray

LPI low-pressure injection

LPRM local power range monitor

LWR light water reactor

MCP main coolant pump

MCR main control room

MOX mixed oxide (uranium and plutonium) nuclear fuel

MPTR multiple pressure tube rupture

MSIV main steam isolation valves

NC natural circulation

NEA Nuclear Energy Agency

NEWS Nuclear Events Web-based Systems

NISA Nuclear and Industrial Safety Agency

NIKIET NPP Design Institution in Russia

NK neutron kinetics

NMED Nuclear Material Events
Database

NPP Nuclear Power Plant

OECD Organization for Economic
Cooperation and Development

OTSG once through steam generator

PCIS primary containment isolation
system

PHW Phenomenological Window

PORV pilot-operated relief valve

PRZ pressurizer

PS primary side

PSP pressure suppression pool

PWR Pressurized Water Reactor

RB reactor building

RBMK Graphite-moderated, Boiling
Water-Cooled, Channel-Type Reactor

RCIC Reactor Core Isolation Cooling

RCS reactor coolant system

RHR Residual Heat Removal

RPV Reactor Pressure Vessel

RR research reactors

SBLOCA Small Break Loss of Coolant
Accident

SBO station blackout

SBWR Simplified Boiling Water
Reactor

SC suppression chamber or PSP

SD steam drum

SETF separate effect test facility

SG Steam Generator

SGTS Standby Gas Treatment System

SRV steam relief valve

SS secondary side

SSI soil structure interaction

STRESA Storage of Thermal REactor
Safety Analysis Data

SYS TH system thermal-hydraulics

TAF top of active fuel

TEC Toledo Edison Corporation

TEPCO Tokyo Electrical Power
Company

TG turbo-generator

TH thermal-hydraulics

TMI-2 Three Mile Island Unit 2

TPCF two phase critical flow

UK United Kingdom

USSR Union of Socialist Soviet
Republics

USA United States of America

USAEC United States Atomic Energy
Commission

USNRC United States Nuclear
Regulatory Commission

UTSG U-tubes steam generator

VV vent valves

WB IRS Web-Based Incident-
Reporting System

WWER Water-Cooled Water-
Moderated Energy Reactors

Acknowledgments

A summary work from huge database information, like the present one, cannot be performed without the contribution of several experts. So thanks are due to all authors of references. Special thanks are due to N. Garis (from SKi in Sweden) and to P. Lien (from NRC in the US) for their prompt and effective replies to the request from authors in relation to the events of Oskarshamn and La Salle, respectively.

Chapter foreword

Accidents in Nuclear Power Plants (NPPs) have the potential for tremendous impact on the population and the environment. This has been specifically true for those events which evolved into severe accidents, noticeably Three Mile Island, Chernobyl, and Fukushima, i.e., the key topic for this chapter. These accidents deserved and received deep attention from the scientific and technological community: in each case thousands of documents have been published and can be found in the web.

So, it is not the purpose for this chapter to duplicate any of those documents, nor the reader may expect any investigation bringing new light to the established knowledge of the concerned NPP transient performances.

Nevertheless, nuclear thermal-hydraulics has been employed for understanding the accident progressions and, specifically in one case, attained indications for new research activities and developments. Owing to these motivations, key NPP accidents, including the three technology disasters already listed and the “stability” events occurred in La Salle and Oskarshamn, constitute part of this chapter of the Book. Namely stability events have little or no safety implications and no radiological consequences.

The chapter can be seen as a collection of thermal-hydraulic aspects relevant to the design of the involved NPP, the operating conditions and the time evolutions during the accidents. The reader shall be warned that only (or mostly) the thermal-hydraulic aspects in the design of the concerned systems or before the occurrence of severe core degradation are considered; little or no effort has been completed to establish the relative importance or contributions of those aspects for the occurrence or during the events.

16.1 Introduction

The exploitation of nuclear technology for electricity production, regrettably, is linked with the occurrence of unplanned (not necessarily unexpected) events which caused the irreversible damage of the plant and, at least in two cases, unjustifiable radiological impact on the environment. Those events are called severe accidents and are worldwide-known (nuclear) technology catastrophes:

- Three Mile Island Unit 2, Mar. 1979
- Chernobyl Unit 4, Apr. 1986
- Fukushima Daiichi Units 1–4, Mar. 2011

Two additional events, which did not cause core damage neither radiological releases, are relevant for nuclear thermal-hydraulics and are considered in this chapter:

- La Salle Unit 2, Mar. 1988
- Oskarshamn Unit 2, Feb. 1999

The five listed events have been deeply investigated with comprehensive reports issued and available to the scientific community. It is not the purpose here to duplicate those reports not even to give a systematic view of the involved Nuclear Power Plants and transient scenarios.

Nuclear thermal-hydraulics as discussed in **Chapter 1** of the Book constitutes a pillar discipline for nuclear reactor safety. Therefore, it seems worthwhile to discuss the mutual impact between those accidents and nuclear thermal-hydraulics. Namely, thermal-hydraulics competences helped the understanding of the events; on the other hand the same events imposed the reconsideration of the capabilities of thermal-hydraulics.

Noticeably, following Three Mile Island accident a strong impulse was generated to investigate loss of coolant accident (LOCA) scenarios originated by the opening of small ruptures in the primary coolant system, i.e., compared with the size of recirculation lines including hot and cold legs. In those conditions, as a difference with respect to transient scenarios established after large breaks, gravity forces become more important and accident times may largely expand allowing or making unavoidable the intervention of operators. This may trigger the occurrence of phenomena which have minor relevance or no relevance at all in the case of the so-called Large Break LOCA, large break loss of coolant accident (LBLOCA).

The objectives for this chapter of the book are:

(a) to clarify the role of thermal-hydraulics as far as the occurrence and the progression of those accidents are concerned, i.e., insignificant, possibly with one exception

(b) to create a link between phenomena detected during the course of the events and those which are part of the established accident analysis, i.e., discussed in Chapters 6 and 15 of the book

Before addressing the stated objectives, snapshot (i.e., necessarily incomplete) and a-posteriori (i.e., years or decades after the events) visions are provided of the technology, industrial, or political conditions at the respective dates of the events. The given pictures may not have a direct relevance to thermal-hydraulics, however may help in the understanding of those events.

16.1.1 Three Mile Island (1979), TMI-2, e.g., see Henry (2011)

The US Nuclear Regulatory Commission (USNRC) had issued Interim Acceptance Criteria (IAC, actually USAEC issued those criteria) in 1971 as discussed in Chapter 2 of the Book. The criteria are applicable for the design of emergency core cooling systems (ECCS), irrespective of the accident type. Lately in 1974, within a study supported by USNRC, Rasmussen demonstrated the importance of non-LBLOCA transients in the overall risk for the operation of NPP (more details and references are also provided in Chapter 2 of the book).

Precursor situations and events to the TMI-2 accident are systematically described, e.g., by Rogovin and Frampton (1980). Two of those precursors are recalled here: (a) A director of one NPP Owner Company in Belgium wrote to the USAEC Chair (Dopchie, 1971) asking “whether the USAEC has ever investigated the consequences of a rupture or valve opening or failure to close affecting the vapor space of a Westinghouse pressurizer”, even specifying that “...the difficulty occurs because the pressurizer water level would rise due to boiling in the core.”; (b) An incident occurred at the Davis Besse Nuclear Power Station on Sep. 24, 1977, see, e.g., TEC (1977) and Tambling and Harpster (1977). The accident involved, as in TMI-2, the loss of feed-water (LOFW) condition, the operator undetected stuck open pilot-operated relief valve (PORV), and the operator stop of main coolant pump (MCP).

The TMI-2 accident has been the subject of a wide variety of international publications including textbooks, i.e., Osif et al. (2004), in addition to Henry

(2011), already mentioned.

16.1.2 Chernobyl (1986), e.g., see Imanaka (Ed.) (2002)

The understanding of the complex and isolated Chernobyl event may start from the consideration of two facts or realities. The former is the dual mission of the RBMK reactor. NPP equipped with RBMK reactors could be used for electricity production and plutonium generation: military and civil purposes are part of the deployment of nuclear technology (see also Chapter 2). The latter is the occurrence of the event at a time when the more than 40-year cold war confronting the USA and USSR was in place in a country, the Ukraine, which was strategic in that context.

Safety features of the NPP which are relevant to the event have been reviewed by D'Auria (Ed.) et al. (2005). Nevertheless the event was driven by a sequence of human decisions in such a way to resemble the crash of an airplane voluntarily caused by the pilot.

Potential precursors for the event are proposed, e.g., by Potter (1990): among the precursors, the complete loss of electrical power at the Kursk RBMK Nuclear Power Plant is cited; flow of cooling water dropped to about 20% of normal, but little damage reported; this event might have prompted the ill-fated experiment that triggered the Chernobyl accident. Technological details of the accident can be found by Adamov et al. (1988) and Martinez Val et al. (1990), as also cited by Malko (2002).

16.1.3 La Salle (1988), see, e.g., Wulff et al. (1992), Oskarshamn (1999), see Thulin (2000)

“Although events related to unstable behavior occurred every now and then, stability was not a major issue for many years,” as pointed out by D'Auria et al. (2009). Furthermore, “stability problems may only arise during start-up or during transients which significantly shift the operating instructions for boiling water reactor (BWR). The same instructions contain rules on how to avoid operating points (regions) that may produce power-void oscillations.” The knowledge at the basis of the above statements was established since the beginning of 1960s when NPP equipped with BWRs entered in commercial operation.

So, why La Salle and Oskarshamn events? The answer for both events is: core power uprating and modifications of fuel assemblies introduced by vendors different from the original designer and/or increase in burn-up, enlarged the region where instability may occur: a simplified analysis (D'Auria et al., 1987), showed

that a single unstable channel inserted in a whatever large core may challenge the stability of the overall system. The additional answer for Oskarshamn is that recommendations issued as a consequence of the La Salle event were not implemented (e.g., see Blomstrand et al., 1990; OECD/NEA/CSNI, 1990; D'Auria (Ed.) et al., 1997).

La Salle event precursors and followers are discussed by D'Auria (Ed.) et al. (1997). Namely, followers can be explained by the previous statement: “more” uprating and burn-up and use of MOX fuel triggered new events. Details about La Salle are also discussed during an international Workshop convened after the event (OECD/NEA/CSNI, 1990) having the main objective to fix countermeasures to the occurrence of stability and, eventually, to mitigate the consequences.

16.1.4 Fukushima Daiichi (2011), see, e.g., IAEA (2014)

The Fukushima event provoked a lethal knockout for nuclear technology in many Countries, i.e., the impact upon the public and the decision makers was (much) greater than from any other previous accident. Reasons for this were the amount of radioactivity release, the cost for the recovery, the on-live video recording and broadcasting of the reactor building explosions, and, not last, the location of the accident in a country considered leader and master in managing the nuclear technology. Furthermore, consequences of the disaster could have been (much) heavier and out of control in case of winds blowing in the direction of highly populated areas.

However, the following facts appear relevant to characterize the framework for the accident:

- The economic growth of Japan took an evident boost from the exploitation of nuclear technology for electricity production during at least five decades before the accident.
- Established (internationally agreed and accepted) value for probability of core melt was estimated to be around 10^{-4} /reactor-year, see, e.g., USNRC (1990); therefore, there should be no wonder that a core melt occurs 25 years after the previous core melt (i.e., following the Chernobyl event) with about 400 reactors in operation all over the world.
- On the one side, earthquakes have been classified having a magnitude higher than the design value for the Fukushima reactors, see, e.g., Wikipedia (2015) (and related references); on the other side Fukushima is located close to one of the most

dangerous and active geological faults on the earth. Again, there should be no wonder for the occurrence of the deadly earthquake and associated tsunami in 2011.

The tsunami caused the worsening of the event from station blackout (SBO) to loss of on-site and off-site power (LOOSP). However the SBO duration for the Fukushima Daiichi NPP, in the absence of any effective rescue action, was a few tens of hours, see, e.g., D'Auria et al. (2012a), and the comprehensive document by IAEA (2014). This might have not prevented the core meltdown occurrence even without the tsunami caused damage of the on-site emergency power generation capability.

Precursors for the Fukushima event are systematically discussed in OECD/NEA/CNRA (2014), with proper focus upon SBO events, i.e., occurred in NPP units of Vandellós, Blayais, Forsmark-1, and Brunsbüttel. However, a broad series of precursor events is constituted by the earthquakes hitting Japanese NPP, i.e., Kashiwazaki-Kariwa as discussed by Nishikawa et al. (2014).

Sequence of events in the involved Fukushima Daiichi units have been clarified at the time of the present writing with a few noticeable exception, e.g., related to the origin of the explosion in the unit-4: the reader may find the established knowledge in IAEA (2014), and an initial guess related to the accident evolutions can be found in D'Auria et al. (2012a). A textbook dealing with Fukushima Daiichi nuclear accident is available, too (AESJ, 2015) at the time of the present writing.

16.1.5 Structure and content

The structure and the content of this chapter of the book are derived from the previous introductory remarks:

- **Section 16.2** aims at streamlining the narrow industrial sector for the concerned NPP accidents; in the same chapter the databases dealing with details of the accidents are cited, i.e., in addition to the provided (necessarily limited) list of references.
- **Section 16.3** includes two parts: the former deals with the description of selected thermal-hydraulic features part of the design of the plants which have some role in the accidents; the latter deals with established descriptions of time sequences for the accidents.
- **Section 16.4** aims at creating the link between the four accidents and the nuclear thermal-hydraulics.

In all cases an attempt is made, with the exception of the second part of Section 16.3, to avoid replicating information which can be found in the scientific literature. Finally, some conclusions are proposed in Section 16.5.

16.2 An overview of nuclear accidents

Accidents, or incidents, or events, or transients have occurred and occur within the framework of each industrial sector created by the human civilization, noticeably in the transport sector, as well as in the space (e.g., meteorites), the atmospheric (e.g., tornados, flooding), and the ground or the ocean (e.g., earthquake) environments where we live. In a variety of situations energy and momentum exchanges occur involving single- and multiphase fluids where the knowledge and the expertise in thermal-hydraulics can be exploited to enlighten the events or to take mitigation measures.

The first step in this chapter is to move down from industry or nature-related accidents into nuclear technology accidents. Before entering nuclear technology one may note, for instance, that the French Government database for accident called ARIA (i.e., see ARIA, 2016) includes more than 40,000 (forty thousands) industrial accidents and has links with a dozen additional databases. Furthermore, the International Disaster Database EM-DAT (i.e., see EM-DAT, 2016) considers natural and industrial disasters, and natural hazards are classified in the US National Geophysical Data Center (i.e., see NGDC, 2016).

Then, the objective for this section is to provide boundaries for the description of the selected nuclear technology accidents, at the same time giving ideas about, (a) how broad can be the field of investigation of accidents in nuclear technology and (b) how narrow is the sector for those accidents.

When considering nuclear accidents it seems worthwhile to distinguish among the following (more than 10) categories:

- Military, explosive weapon
- Military, radiation
- Military, power reactor, e.g., submarine, or air carrier reactor (peace or war mission)
- Military, industrial installations/activities necessary for or supporting any of the above, e.g., mining, enrichment, transportation

- Civil, research reactors, RR
- Civil, NPP (operation)
- Civil, nuclear fuel fabrication
- Civil, nuclear fuel reprocessing
- Civil, nuclear fuel waste
- Civil, industrial installations and activities (including researches) necessary for or supporting any of the above, e.g., mining, enrichment, transportation (including illicit trafficking), construction, or dismantling stages for NPP
- Civil, medical applications

Related to military applications, the deliberate explosion of a nuclear weapon (first category) shall not be confused with an accident in the transport of a nuclear weapon (fourth category) or with the deliberate use of radioactive materials during a conflict (e.g., bullets, second category). Nuclear submarine accidents of Russian fleet constitute the topic of “Bellona report 2.96,” by Nilsen et al. (1997).

In the case of civil applications, a higher number of RR has been built than NPP; RR may receive less attention from Regulatory Authority and from industry in relation to safety than NPP because of the lower industrial worth and the lower overall amount of stored radioactive material. Therefore, a larger number of events involving RR shall be expected than involving NPP.

Thermal-hydraulics and nuclear system thermal-hydraulics may play a role for each of the listed categories of events. However the discussion in this chapter of the Book is restricted to the sixth category in the provided list, i.e., accidents in civil NPP: namely databases for civil nuclear technology accidents are cited in the next section and (only) five major events are considered in Sections 16.3–16.5.

16.2.1 The data base of events

Examples of databases for accidents connected with civil nuclear industry include (not a comprehensive list, not reported below with any order of priority):

- The IAEA Incident and Trafficking Database (ITDB, 2016) established in 1995
- The IAEA Nuclear Events Web-based Systems (NEWS, 2016); this provides

information on all significant events in NPP, RR, nuclear fuel cycle facilities, and occurrences involving radiation sources or the transport of radioactive material. NEWS makes available event descriptions, ratings according to with the International Nuclear and Radiological Event Scale (INES)

- The USNRC Nuclear Material Events Database (NMED, 2011) covering the period 1990–2011; this contains records from all the US noncommercial power reactor incidents and events, including medical events, involving the use of radioactive byproduct material; nine categories of events are distinguished (not given here)
- The joint IAEA and OECD/NEA International Reporting System for Operating Experience (IRS), e.g., IAEA (2016a): 31 participating countries exchange experience to improve the safety of Nuclear Power Plants by submitting event reports on unusual events considered important for safety; in 2006 the Web-Based Incident-Reporting System (WB IRS) replaced the former Advanced Incident-Reporting System (AIRS)
- The joint IAEA and OECD/NEA Fuel Incident Notification and Analysis System (FINAS), e.g., IAEA (2016b), related to safety relevant events in dual cycle facilities
- The IAEA Incident-Reporting System for Research Reactors (IRSRR), e.g., IAEA (2016c), collecting safety-related information on unusual events occurred in RR
- The EC regional network to enhance nuclear safety through improvement of the use of lessons learned from Operating Experience from NPP operation. The database-network is called European Clearinghouse on Operating Experience Feedback for Nuclear Power Plants (EC, 2016a)

In addition to databases related to nuclear reactor accidents or radiological relevant events, “thermal-hydraulics-accident” databases exist which are derived from experiments performed in integral test facilities (ITFs) and Separate Effects Test Facilities (SETF). Namely one may consider OECD/NEA (2016), in relation to the database available from NEA and (EC, 2016b; Addabbo et al., 2002) in relation to the CERTA project and the database available from EC. Both ITF and SETF (see also Chapter 6 of the book) at the origin of the data concerned by the mentioned projects are scaled models for NPP: related experiments are expected to reproduce transient scenarios in prototype nuclear reactor systems.

16.3 The NPP systems and the nuclear events

Starting from this point in the chapter only four events are considered which constitute a narrow

The chapter is subdivided into two main parts, as already stated. Thermal-hydraulics is the key word in the following although, as already stated, its role may not be essential for explaining the triggering or the consequences of those events.

- The first part (Section 16.3.1) deals with an outline of the nuclear systems (NPP) where the accidents took place. The configuration of those systems as well as the design features and the operating conditions are established and known from the scientific literature: there is no motivation here to duplicate related information. Rather, thermal-hydraulic aspects parts of the design (including the design of operating conditions) are compared with similar systems to create the basis for a deep understanding of the thermal-hydraulics role during the events.
- The second part (Section 16.3.2) deals with a description of the events. Here, taking information from the relevant literature could not be avoided, for the sake of the consistency and comprehensiveness of the present chapter. Nonetheless the attention is focused on the time periods of the accidents before the occurrence of loss of core integrity (with the exception of the La Salle event where this event did not occur) and incomplete information is given in relation to the periods after that occurrence.

The information from both Sections 16.3.1 and 16.3.2 shall be intended as preparatory for the thermal-hydraulic analysis at the basis of the discussion in Section 16.4. Furthermore, information related to the concerned systems and the events can be found in the already cited references which are not necessarily recalled hereafter.

16.3.1 Selected peculiarities in the design of the involved systems

16.3.1.1 The PWR of TMI-2

It is well known that the PWR concept was exploited first for application in submarines, see the nontechnical book titled “Rickover, Father of the Nuclear Navy,” i.e., Allen and Polmar (2007). The system configuration suitable for US Navy revealed of strategic and commercial interest for civil applications:

- slightly enriched uranium in the oxide material is used as fuel: slender Zircaloy

pins contain the fuel

- pressurized water is used as coolant and moderator
- the coolant circulating in the core transfers thermal power to heat exchanger(s) where steam is produced on the secondary side, i.e., the U-tubes shaped steam generators (SG) and runs the turbine(s)

The TMI-2 NPP is equipped with a Babcock and Wilcox (B & W) reactor. The key thermal-hydraulic design features which differentiate the B & W reactor from the Westinghouse reactor, widely spread solution in the world (i.e., adopted by other vendors) for the production of electricity, hereafter called standard PWR, are the following:

- (1) Two once through steam generators (OTSG) for a standard 1000 MWe NPP unit are adopted instead of three or four U-tubes shaped SG (UTSG)
- (2) Two cold legs (CLs) per SG are installed instead of one
- (3) Vent valves (VV) are installed in the barrel inside the Reactor Pressure Vessel (RPV)
- (4) The ECCS includes high-pressure injection (HPI), Accumulators and low-pressure injection (LPI); the ECCS design characteristics, as well as the related emergency operating procedures (EOP), are different between a B & W and a standard PWR; however, both of ECCS design characteristics and EOP are within the spectrum for standard PWR.

The design solutions at items (2) and (3) have some impact upon the LBLOCA. The presence of two cold legs per each OTSG (compared with the solution of three UTSG for the same size NPP unit) implies smaller flow area per unit power in case of double-ended guillotine break (DEGB) in CL. The VV allow the mitigation of the steam-binding phenomenon during the reflood phase. Both solutions had negligible or no impact upon the evolution of the TMI-2 event. The design solution at item (4) did not impact the TMI-2 event.

The design solution at item (1) has an impact upon the evolution of the TMI-2 event. The following motivations or effects are associated with the presence of OTSG (details about the operation features of OTSG can be found in Section 15.4.8 of Chapter 15 of the Book and additional information under the key word “OTSG” in the same chapter):

- about 30 K superheated steam is produced by the secondary side, while saturated steam is produced in a standard PWR
- it is possible to control the power at the turbine in a range wider than in a standard PWR with shorter time constant
- contrary to the natural circulation working condition typical for the UTSG, a pump-driven flow is established in the secondary side of the OTSG
- smaller fluid mass inventory per unit power is stored in the secondary side: this reflects in differences in the transient performance, namely following a LOFW occurrence
- a reverse U-shaped hot leg pipe, also called candy-cane constitutes a peculiarity for the B & W primary loop configuration
- the presence of the candy-cane, and in general the overall layout of primary loop, causes some detriment in the natural circulation between core and SG when mass inventory of the Reactor Coolant System (RCS) is decreased compared with a standard PWR, as discussed by D'Auria et al. (1994) and D'Auria and Frogheri (2002)

16.3.1.2 The RBMK of Chernobyl-4

The boiling light water-cooled, graphite-moderated channel type, large electrical power production (up to 1500 MWe) RBMK reactor is designed by NPP Design Institution in Russia (NIKIET). One may state that the RBMK reactor is the evolution of the world first NPP built in Obninsk (5 MWe power produced from a water-cooled graphite-moderated reactor), as discussed by Rachkov et al. (2014), see also Schmid (2015).

The RBMK configuration was of little concern for (former) Western specialists in nuclear technology before the Chernobyl event although related books had been published, e.g., Margoulova (1969) and Dollezhal and Emeljanov (1980).

The design features of RBMK are still recognized as a key motivation for the Chernobyl-4 event notwithstanding a number of technical papers assessing and confirming the safety of RBMK, e.g., Adamov et al. (1995, 1996a), Almenas et al. (1998), Uspuras and Kaliatka (2006), and D'Auria et al. (2008a).

Hereafter, four key issues, relevant to thermal-hydraulics which have been connected to the Chernobyl-4 event, are outlined.

- No or inadequate containment

Issue: the containment of RBMK is nonexistent, or it has not the same features of full pressure containment in light water reactor (LWR) built in (former) Western Countries.

Discussion:

(a) RBMK NPP units are equipped with a pressure-resistant building or reactor cavity building which envelopes the core and not the overall RCS pressure boundary: this should not be interpreted as a severe limitation. In the case of LWR, namely PWR, the core and the rest of the RCS are coupled by a few large diameter (typically 1 m) pipes, HL and CL, while in RBMK thousands of small diameter pipes (typically 0.1 m) connect the region where radioactive products are present, the core, with large pressure components like headers and drums. The headers and drums are outside the pressure cavity, while SG and pressurizer (PRZ) are inside the containment: radioactivity transport from core to those large components in case of failure of nuclear fuel is more difficult in the former case than in the latter case. In any case, whatever can be interpreted the difference between the reactor cavity in RBMK and the containment in LWR, this difference had no role during the Chernobyl-4 event, see item (c) below.

(b) RBMK reactor cavity building is not full pressure (i.e., is not tight) and has connecting valves with the environment: the use of containment venting systems allowing controlled radioactivity releases to the environment proved to be important after Fukushima event and is under consideration for future NPP. The venting to the environment had no role during the Chernobyl-4 event, see item (c) below.

(c) There is no proof that any LWR containment would have resisted to the energy impulse produced during the Chernobyl-4 event.

Conclusion: the possible inadequacies of the containment had no role during the Chernobyl-4 event.

- Positive void coefficient

Issue: RBMK have positive void coefficient in the core, and this makes the core vulnerable to reactivity excursions.

Discussion:

(a) The maximum value of void coefficient is equivalent to five times the prompt criticality, e.g., Malko (2002), which means a system disruptive value if instantaneously occurring. In the reality, the maximum void coefficient value must

be associated with the complete emptying of thousand (pressure) channels each having an equivalent diameter of about 0.01 m and a length of about 8 m.

(b) Positive values for void coefficient are achieved in PWR, beginning of cycle (BOC) condition, due to large amount of boron.

(c) Positive values for void coefficient are tolerated during the entire life of Canadian deuterium uranium reactor (CANDU) reactors which has some neutron physics features (namely, moderator physically separated from coolant) qualitatively close to those of the RBMK core.

(d) A full three-dimensional coupled “thermal-hydraulics neutron physics” analysis (Parisi, 2008) related to the Smolensk-3 NPP unit which included some safety upgrading compared with the Chernobyl-4 unit, has shown that the void coefficient alone cannot justify an energy release consistent with the Chernobyl-4 event.

Conclusion: void coefficient had a role during the Chernobyl-4 event. However, a decisive impact upon the triggering of the explosion does not result from analyses performed so far.

- Inadequate control rod (CR) design

Various types of CR are part of the large RBMK core (about 14 m diameter and 8 m height) and have different functions. CR can be inserted into nonpressurized devoted channels part of the graphite-bounded array of holes which constitute the core of RBMK. In principle the gravity fall of CR is possible with RBMK cores.

Issue: the bottom part of CR which is inserted from the top into the core is made of nonabsorbent material for neutrons. This may cause positive reactivity occurrence and start of the insertion because water, a neutron absorber in RBMK core, is removed when CR are inserted and replaced by nonabsorbent material.

Discussion: some boundary parts of CR are made of nonabsorbent material for neutrons, and this constitutes a flaw in the design.

Conclusion: CR design is established as one origin of the Chernobyl-4 reactivity excursion. However, as in the case of void coefficient a clear cause-effect relationship between CR insertion and the actual explosion does not result from detailed analyses performed so far

- Use of graphite as moderator

Issue: graphite is prone to fires and is abandoned as safety acceptable material for the core of nuclear reactors.

Discussion:

(a) The above statement/issue is valid for water-cooled reactors and does not apply to gas reactors which are still in operation. The new design high-temperature gas reactor (HTGR) still includes graphite as moderator.

(b) The presence of graphite implies the need to estimate and control the radiation exposure damage during the nominal operation of the reactor, see, e.g., IAEA (2000), and to evaluate the mechanical resistance in case of multiple pressure tube rupture (MPTR), e.g., D'Auria et al. (2008b).

Conclusion: graphite had no role in the triggering of the Chernobyl-4 event. However the days-long graphite fire caused by air inlet into the damaged core caused the worldwide diffusion of radioactivity products. Without graphite burning, the radiological consequences of the Chernobyl-4 event could have been locally heavier but not crossing the geographical boundaries of the (former) Soviet Union.

16.3.1.3 The BWR of La Salle-2 and Oskarshamn-2

The La Salle-2 NPP unit is a standard general electric (GE) BWR-5 equipped with vessel internal jet pump for enhancing core circulation and a Mark-II type of containment system. Thermal-hydraulics features are described by Lahey and Moody (1993).

The Oskarshamn-2 NPP unit is an Asea Brown Boveri (ABB) BWR with external circulation pumps. The thermal power is 1800 MW which corresponds to an electrical power of about 630 MW.

A stability event can be triggered by any system or component of the NPP including those systems and components part of the balance of plant (BoP). Any minor (whatever small, time-dependent) perturbation in the circulating fluid shall be considered as possible origin of a stability event. The reactor core where one- to two-phase change occurs and where the feedback between circulating flow and neutron flux oscillations is possible, constitutes the instability vulnerable region: e.g., oscillations in thermal neutron flux or fission power and coolant-moderator density may grow, as a function of time, in amplitude and may challenge the structural integrity of the fuel.

One may note that stability occurrences are not connected (as well understood) with the type of recirculation system (jet-pumps or external recirculation).

16.3.1.4 The BWR of Fukushima-1 to -4

Noticeably, the nuclear event which occurred in the Fukushima Daiichi NPP hit four units. The Unit 4 was in refueling stage at the time of the event, and all fuel assemblies part of the core were located in the spent fuel pool. Nevertheless, an explosion occurred in the Unit 4 which destroyed the reactor building: the origin is presumably explosive gas coming from (underground) paths connecting with the neighbor units. Hereafter the events occurred in Units 1–3 are considered further.

The Fukushima Daiichi Units 1–3 are GE BWR-3, GE BWR-4, and (GE)-Toshiba BWR-4, respectively. All units are equipped with a Mark-I (toroidal) type of containment system. Thermal-hydraulics features are described by Lahey and Moody (1993).

Related to the set of engineered safety features (ESF) and ECCS which had some role during the events, all the units are equipped with high-pressure coolant injection (HPCI), low-pressure core spray (LPCS), boron injection, Automatic Depressurization System (ADS), and Residual Heat Removal (RHR) systems. Furthermore, Unit 1 is equipped with isolation condenser (IC), namely two IC trains, i.e., a passive system without moving parts, and Units 2 and 3 are equipped with turbine driven, i.e., a passive system with moving parts, Reactor Core Isolation Cooling (RCIC) systems. Design pressure for containment is 4.35 MPa for Unit 1 and 3.92 MPa for Units 2 and 3.

16.3.2 The outline of the events

Details about the events can be found in a wide variety of documents including those already cited, see also the textbook Sehgal (Ed.) (2012), for the technological descriptions of severe accidents in TMI-2, Chernobyl-4, and Fukushima-1–4 reactors. The sections below are not intended to replace any of the established (or official) reconstruction of the events and are introduced with the motivation of comprehensiveness and consistency of the present book. Boundaries for the discussion (partly already mentioned) are:

- information is extracted from selected references
- emphasis is given to events which are relevant to the thermal-hydraulics analysis in Section 16.4
- the time period before core degradation is concerned, and no discussion is provided in relation to the (safety relevant) release and transport of radioactive products and to the doses to the exposed workers, the population, and the environment.

Thus, an effort is made to keep all details of the sequence of the events: in each case the origin of the information is cited.

16.3.2.1 1979 TMI-2 event

The source of information for the TMI-2 event is EPRI (1980). The chronology of the event is reported in Table 16.1: a few details considered irrelevant for the present context are omitted compared with what available from the original source of information. The introduced nomenclature is assumed to be self-explanatory, e.g., in the first row of Table 16.1 “condensate pumps.”

Table 16.1

TMI-2 chronology of main events (till core melt occurrence)

--

Unrecoverable core condition—core melt (not understood at the time).

The TMI-2 event started with the unit at nominal (or nearly nominal) power.

The description of the event continues with suitable level of detail (EPRI, 1980) till 16:29:23, i.e., till 08:00:00 pm of Mar. 28, 1979. At that time a forced recirculation had been reestablished using MCP 1A. RCS pressure was in the range 1000–1100 psig. Thermal power was removed by SG-A at SG-B remained isolated. Noticeably at time 02:22:00 the PORV was closed, thus terminating the SBLOCA condition: the core lost its integrity about 30 min earlier.

The TMI-2 event was a LOFW which evolved into an undetected SBLOCA. The primary mass loss was associated to the stuck open PORV and the unbalance between letdown and make-up flows into the RCS. Stop of the MCP was the decisive action to achieve the unrecoverable core condition in a RCS already in degraded conditions. The misinterpretation of the occurrences by the operator crew created a synergy between the complexity of the scenario and the severity of the consequences.

Italic characters in Table 16.1 are used to emphasize “a-posteriori” the relevant actions or occurrences. These can be summarized as follows:

- LOFW occurrence, time 0
- (Undetected) SBLOCA occurrence, time 10 s
- Stopping by operator of make-up flow to the RCS, including HPIS, starting from time 3 min and in various subsequent actions
- Insufficient SG SS cooling due to system malfunctions (e.g., maintenance errors as discovered lately) and nonoptimized operator interventions
- Stop of MCP, starting at time 1 h 13 min and continuing till 1 h 40 min: in this period the unrecoverable core condition occurred

16.3.2.2 1986 Chernobyl-4 event

The source of information for the Chernobyl-4 event is Adamov et al. (1996b); the reports by Malko (2002) and Gorbachev (2002) were also consulted. The chronology of the event is given in Table 16.2: a few details considered irrelevant for the present context are omitted compared with what available from the original source of information. The introduced nomenclature is assumed to be self-explanatory.

Table 16.2

Chernobyl-4 chronology of main events starting from the reactor at nominal power (till core explosion)

--

Two explosions occurred and the core was destroyed.

^a In the accident reconstruction by Gorbachev (2002), it is reported that AZ-5 (manual scram) button was pressed a first time between 24:23:20 and 24:23:30 following hearing of the first explosion by operators. The second push of the button was at 24:23:41 and coincided with the second more intensive explosion. Therefore, according to Gorbachev (2002), the accident reconstruction in the table is inadequate after 24:23:39.

The Chernobyl-4 event started with the unit experiencing a complex transient condition. Therefore, the reported chronology starts from time “0” when the unit

was at nominal power.

The following information related to loop configuration and planned coast-down experiment is essential to follow the chronology in the table:

- The core consists of two halves: each one half is cooled by a cooling loop.
- One cooling loop includes two steam drums and four MCP (three of these used for normal operation).
- Nominal flow for each of the six (simultaneously in operation) MCP is 7000 t/h.
- The coast-down test (to demonstrate suitable MCP delivery flow during coast-down) had to be carried out in a power range of 700–1000 MWth.

Various authors, e.g., Pakhomov et al. (1991), Arpott and Green (1992), and Kiselev and Checherov (2001), as cited by Malko (2002), estimated the energy of the largest power burst from the Chernobyl explosion to be 1.0 TJ, equivalent to the energy of explosion of approximately 200 tons of the trinitrotoluene.

As a conclusion and following Adamov et al. (1996a), “the accident was caused by the coincidence of the following main factors: the positive reactivity effect and the deficiencies in the CR system design that resulted in positive reactivity introduction under the conditions, in which the reactor had been put before the accident.” in 2002, Gorbachev (2002) reports that “it is necessary to start the official reconsideration of the accident chronology, taking into account the new circumstances opened during the last years.”

16.3.2.3 1988 La Salle-2 and 1999 Oskarshamn-2 events

The description of La Salle-2 and Oskarshamn-2 events is given below with a lower level of detail than the other events. Although each plant component may have a role for triggering and sustaining the instability occurrences, emphasis is given hereafter to the performance of the core region.

La Salle 2

On Mar. 9, 1988, LaSalle Unit 2 underwent a dual recirculation pump trip event, as taken from USNRC (1988b). Before the event, the Unit 2 reactor was operating at steady-state conditions at approximately 84% power, with 76% rated core flow using both recirculation pumps, and with the CRs withdrawn to the 99%.

The initiating transient was caused by an instrument maintenance technician who

was performing a surveillance test. The technician opened a wrong valve. This produced a high “indicated” level signal to the feed-water control system and the response led to a trip of both recirculation pumps. The CRs remained in the 99% position.

As a result of the rapid power decrease, the feed-water heater level control system was unable to control the level in the feed-water heaters and began isolating extraction steam from the heaters. This resulted in a positive reactivity addition which, in turn, caused an increase in power, further reducing the margin to stability. Oscillations occurred as detected by the Average Power Range Monitor (APRM) signal [oscillating between 25% and 50% power (25% peak-to-peak) every two to three seconds]. The operators attempted to restart a recirculation pump in order to increase core flow and prevent instability, but this action was unsuccessful. Approximately 7 min after the recirculation pump trip the reactor automatically scrammed on APRM high power (118% trip). The sequence of events, thanks to P. Lien (Lien, 2016), has been taken from USNRC (1988a) and is given in Table 16.3.

Table 16.3

La Salle-2 chronology of main events (till scram occurrence)

--

Oskarshamn-2

On Feb. 25, 1999, the reactor operated at full power (1800 MWth) with a recirculation flow of 5493 kg/s. Fuel assemblies in the core were SVEA-64, ATRIUM-9, and ATRIUM-10B.

Maintenance work was under way with the batteries in the switchyard. During this maneuver the voltage was shortly interrupted. In Oskarshamn 2 unit two indicators were affected: one was the indicator “station not connected to the grid,” and the other was “station disconnected from the grid.” The general situation occurred that the external grid was lost, two of five feed-water preheaters were bypassed and preparation for supplying “in-house electricity consumption only” was initiated by

controlling of the turbine valves and the dump valves.

Bypass of the FW preheaters caused the FW temperature to decrease. The automatic level control maintained a high FW flow. The reactor responded to the decreasing FW temperature by increasing the reactor power. The reactor reached the E25 limitation at 108% power a few times. Each time the recirculation flow was reduced and the E25 signal reset.

About 2 min after the beginning of the event, manual partial scram and forced reduction in coolant flow was initiated. Core instability started with growing amplitude during about 20 s. Automatic scram was initiated at APRM=132% and Coolant flow=50%. The instability continued during 18 s.

The sequence of events, thanks to N. Garis (Garis, 2016), has been taken from Thulin (2000), and given in Table 16.4.

Table 16.4

Oskarshamn-2 chronology of main events (till scram occurrence)

--

16.3.2.4 2011 Fukushima Daiichi-1 to -4 events

The source of information for the Fukushima Daiichi Units 1–3 are TEPCO (2012), IAEA (2014), and AESJ (2015). The chronology of the event is reported in Tables 16.5–16.7 for the three units, respectively: details considered irrelevant for the present context are omitted compared with what available from the original source of information. The introduced nomenclature is assumed to be self-explanatory.

The earthquake occurred at 14:46 of Mar. 11, 2011; however, the time of scram signal due to earthquake was recorded for all three units at 14:47. Important issues like evacuation decision, entering radiations affected areas, injection of seawater into RPV, and containment venting are not given (due) priority attention in the

following. A few relevant chronology events after the loss of core geometric integrity are shown in brown color.

Fukushima Unit 1 event

The Fukushima-1 event started with the unit at nominal operating power, as given in Table 16.5. IC was not damaged by the earthquake.

Table 16.5

Fukushima-1 (Daiichi NPP) chronology of main events (till core loss of geometric integrity)

--

The unit was lost owing to core melt.

Fukushima Unit 2 event

The Fukushima-2 event started with the unit at nominal operating power, Table 16.6. RCIC was not damaged by earthquake.

Table 16.6

Fukushima-2 (Daiichi NPP) chronology of main events (till core loss of geometric integrity)

--

The unit was lost due to core melt and containment damage.

Fukushima Unit 3 event

The Fukushima-3 event started with the unit at nominal operating power, Table 16.7. RCIC was not damaged by earthquake.

Table 16.7

Fukushima-3 (Daiichi NPP) chronology of main events (till core loss of geometric integrity)

--

The unit was lost owing to core melt.

Summing up

In relation to start of core melt and “externally recorded” explosions and including Fukushima Unit 4, the following synthesis picture is derived:

--

- ^a Since time 00:00:00.
- ^b Date.
- ^c Flammable gas (primarily H2).
- ^d High-pressure failure.

It would be difficult for any NPP unit in the world to ensure core integrity when a longer than 10 days loss of off-site power occurs. On the other hand, the multiple Fukushima events impacted the whole world industry and technology as well as the energy policies in individual Countries owing (not least) to financial implications associated with the accident consequences, e.g., D'Auria et al. (2015).

16.4 The thermal-hydraulics aspects of the nuclear events

The idea is to connect the time evolutions of NPP accident scenarios with the thermal-hydraulics phenomena discussed in the book (e.g., Chapter 6).

Two main goals can be associated with this chapter:

- (1) To confirm that information derived from NPP events is valuable for the assessment of numerical computational tools including nodalizations and codes, as suggested by IAEA (2016d), see also D'Auria et al. (2012b);
- (2) To confirm that NPP data do not contradict the findings from scaling studies, see, e.g., D'Auria and Galassi (2010), Mascari et al. (2015), and D'Auria et al. (2016).

In relation to the first goal the following shall be observed: (a) the creation of a database for validation implies collecting design data (e.g., RCS geometry, operating conditions values, and material data), boundary conditions data (e.g., pump operation information), and recorded instrument data; (b) there is no attempt (here) to create a database, rather to confirm that a suitable database can be gathered; (c) the level of information detail to be expected from NPP data is not comparable with what achieved from scaled-down test facilities; nevertheless NPP data are of high value for code validation.

Furthermore, thermal-hydraulics (support) analysis can be essential for the understanding of accident scenarios at any time during the events. So the question arises “why we stop the thermal-hydraulics accident analysis at the conditions before core melt?” The answer is based upon there consequential statements:

- Thermal-hydraulics is a complex subject characterized by incomplete fundamental knowledge (turbulence, bubble movements, two-phase flow regimes).
- Experiments-based qualification is essential to prove the validity of any application.
- A step change in qualification occurs between the situations “before core loss of geometric integrity” and “after core loss of geometric integrity.”

In order to link phenomena and NPP scenarios, phenomenological windows (PHW) are introduced, i.e., time spans during the accidents where one or a few key phenomena occur. Arbitrariness in the selection of time duration for PHW is

unavoidable.

In each section below at least one publication is cited dealing with the thermal-hydraulics of the concerned event.

In all cases below “time 0” is 0.0 s and corresponds to time 00:00:00 in Tables 16.1–16.7. An attempt is made to use the same wording as in Chapter 6 of the book: in order to provide specific details different words are used in some cases. Acronyms adopted in the list below and not yet used in this chapter are counter-current flow limitation (CCFL), core damage (CD), critical heat flux (CHF), instrumentation and control (I & C), natural circulation (NC), neutron kinetics (NK), primary side (PS), thermal-hydraulics (TH), two phase critical flow (TPCF) and can be found in the list of acronyms. The star indicates that the concerned phenomenon also occurs during other listed PHW during the same event.

16.4.1 TMI-2 LOFW-SBLOCA

The thermal-hydraulics of the TMI-2 accident has been widely studied by the scientific community as already mentioned, for instance, see Broughton et al. (1989), and more recently Bandini and De Rosa (2014). The TMI-2 phenomenological windows are identified (time duration) and characterized (key phenomenon or phenomena) as follows:

TM-PHW-1 : 0.0–60.0 s
(1 ') «» RCS pressure rise

Other key phenomena:

- Heat transfer across OTSG in nominal operation (e.g., including steam superheating in SS)
- Critical flow through valves (TPCF through PORV)*
- Heat transfer across SG with SS loosing mass inventory

TM-PHW-2 : 1 ' – 6 ' «» RCS
pressure decrease/PRZ level rise

Other key phenomena:

- Condensation due to HPIS actuation
- Degradation of SG heat transfer due to SG SS dry
- CCFL at surge-line connection with HL*
- Condensation in PORV drain tank
- Pressurization of PORV drain tank

TM-PHW-3	6' -	
85'		«» PRZ
full/CCFL in surge-line		

Other key phenomena:

- Mixture level formation in the core
- Centrifugal pump behavior in single and two-phase conditions*

TM-PHW-4 85' -
110'
of SG heat sink

«» Restoration

Other key phenomena:

- Stop of circulation in loop B
- SG-B depressurization (due to steam condensation and reduced heat transfer from PS)
- SG-A heat transfer with increasing PS void fraction

[illegible]

Other key phenomena:

- MCP performance during coast-down
- NC performance in RCS
- Core level and dry-out occurrence
- Core film boiling
- H2 production
- H2 distribution in RCS

PHW 1–5 during the TMI-2 accident can be found in Fig. 16.1A–D (Fig. 16.1A: RPV, SG-A, and SG-B pressure & PRZ level, 0 to CD with identification of all PHW; Fig. 16.1B: RPV pressure during PHW-1; Fig 16.1C: RPV pressure and PRZ level during PHW-2; Fig. 16.1D: RPV, SG-A, and SG-B pressure & PRZ level, during PHW-3, PHW-4, and PHW-5).

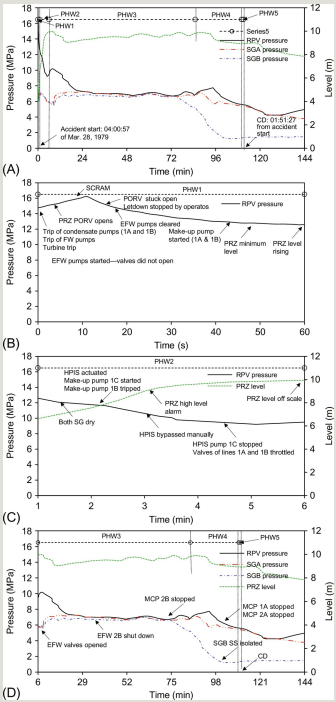


Fig. 16.1 (A) TMI-2 accident, pressure in RPV, SG-A, and SG-B and level in PRZ. Identification of PHW. (B) TMI-2 accident, pressure in RPV, PHW1. (C) TMI-2 accident, pressure in RPV and level in PRZ, PHW-2. (D) TMI-2

accident, pressure in RPV, SG-A, and SG-B and level in PRZ, PHW3, PHW4, and PHW5.

16.4.2 Chernobyl-4 reactivity excursion

A thermal-hydraulic analysis of the Chernobyl RBMK reactor prior the accident has been performed by Mokizuki (2007). The Chernobyl-4 phenomenological windows are identified (time duration) and characterized (key phenomenon or phenomena) as follows:

CH-PHW-1: 0.0-23:28
(h) «» Controlled power
reduction

Other key phenomena:

- Three-dimensional core performance (TH & NK)
- CR performance*
- System I & C

CH-PHW-2: 23:28-
24:03 «» Uncontrolled
power reduction & power rise

Other key phenomena:

- Neutron poisons (Xenon) concentration growth

CH-PHW-3: 24:03-
24:23:48 «» Establishing
system TH conditions

Other key phenomena:

- Core heat transfer in high-flow low-power conditions

CH-PHW-4: 24:23:48—

CD «» Fission power excursion

Other key phenomena:

- Subcooled nucleate boiling transient heat transfer in core

PHW 1–4 during the Chernobyl-4 accident can be found in Fig. 16.2A and B (Fig. 16.2A: core power, core inlet flowrate, 0 to CD with identification of all PHW; Fig. 16.2B: core power, core inlet flowrate, and core inlet subcooling during PHW-3 and PHW-4).

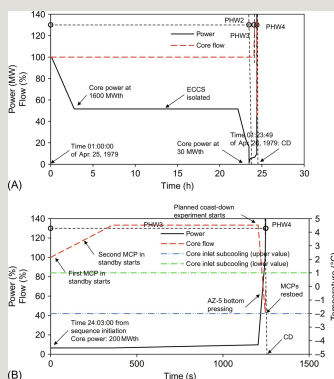


Fig. 16.2 (A) Chernobyl-4 accident, core power and core inlet flowrate. Identification of PHW. (B) Chernobyl-4 accident, core power, core inlet flowrate, and (reasonable) boundaries for core inlet subcooling, PHW3 and PHW4.

16.4.3 La Salle-2 and Oskarshamn-2 boiling stability

From a thermal-hydraulics viewpoint a similar event occurred in La Salle-2 and Oskarshamn-2 reactors as it results from Table 16.8. Thermal-hydraulic analyses for both event have been published in the literature, e.g., Wulff et al. (1990) and Kozlowski et al. (2014), respectively, related to La Salle and Oskarshamn.

Table 16.8

Summary of core performance in the case of La Salle-2 and Oskarshamn-2 events

16.4.3.1 La Salle-2

The review performed after the event revealed APRM peak-to-peak oscillations ranging from 20% to about 75% power during the event. The oscillation amplitude was at least 100% peak-to-peak when the scram occurred. The peaking factor for axial power distribution in the core increased from 2.11 before the event to 2.65 at the time of the local power range monitor (LPRM) alarm. The phenomenological windows are identified (time duration) and characterized (key phenomenon or phenomena) as follows:

LS-PHW-1:0.0-4'«» Controlled power reduction

Other key phenomena:

- Three-dimensional core performance (TH & NK)*
- Reduction of core inlet flow and subcooling
- MCP coast-down

LS-PHW-2:4'-Scram event«» Stability

Other key phenomena:

- Natural circulation in the RPV
- Margin to CHF
- Core power oscillation characteristics (frequency and amplitude)

16.4.3.2 Oskarshamn-2

The Oskarshamn-2 phenomenological windows are identified (time duration) and characterized (key phenomenon or phenomena) as follows:

OS-PHW-1: 0.0–118 s
 «» Step-changes in core power

Other key phenomena:

- Three-dimensional core performance (TH & NK)*
- Positive drift in core power
- Reduction of core inlet flow and subcooling
- MCP coast-down
- Reduction in FW flow and temperature
- Controlled power reduction

OS-PHW-2: 118 s–
 Scram «» Stability event

Other key phenomena:

- Natural circulation in the RPV
- Margin to CHF
- Core power oscillation characteristics (frequency and amplitude)

PHW 1 and 2 during the La Salle-2 and the Oskarshamn-2 events can be found in

- Natural circulation through IC
- RPV pressure drop caused by IC cooling

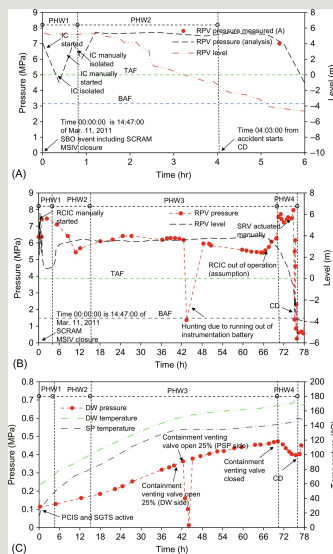
F1-PHW-2: 48'—

CD «» LOOSP evolution

Key phenomena:

- RPV pressure increase following IC isolation & SRV operation
- RPV level decrease (due to coolant loss through SRV)
- Core dry-out

PHW 1 and 2 during the Fukushima Unit 1 event can be found in Fig. 16.4A (Fig. 16.4A: RPV pressure and level).



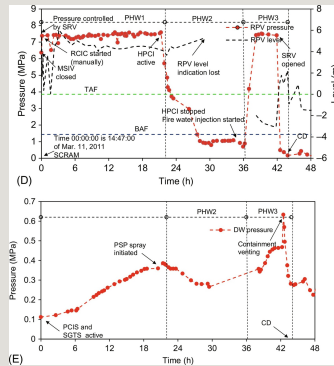


Fig. 16.4 (A) Fukushima-1, RPV pressure and level (core side), identification of PHW. (B) Fukushima-2, RPV pressure and level (core side), identification of PHW. (C) Fukushima-2, pressure and temperature in the containment. (D) Fukushima-3, RPV pressure and level (core side), identification of PHW. (E) Fukushima-3, RPV pressure in the containment.

F2-PHW-1: 0.0–4 h «» SBO/
 LOOSP evolutions (SRV cycling
 controlled)

Key phenomenon:

- Core cooling ensured by RCIC and SRV operation

F2-PHW-2: 4–
 15 h «» LOOSP-RCIC
 overcooling

Key phenomena:

- RPV pressure undershoot and recovery
- Containment (PSP) temperature rise (caused by RCIC turbine discharge)

F2-PHW-3: 15–
 70 h «» LOOSP-RCIC “stable”
 cooling

Key phenomena:

- RPV pressure (below SRV set-point)
- Core cooling ensured (level above TAF)
- Containment pressure and temperature rise*

F2-PHW-4 : 70–

CD «» LOOSP-RCIC out of operation

Key phenomena:

- RPV pressure rise
- SRV manual actuation and RPV pressure fall
- RPV level fall
- Core dry-out

PHW 1–4 during the Fukushima Unit 2 event can be found in Fig. 16.4B and C (Fig. 16.4B: RPV pressure and level all PHW; Fig. 16.4C: containment pressure and temperatures all PHW). An explanation of the negative peak at about 42 h is provided in Table 16.6.

F3-PHW-1 : 0.0–

22 h «» SBO/LOOSP evolutions (SRV cycling controlled)

Key phenomenon:

- Core cooling ensured by RCIC and SRV operation
- Containment pressure and temperature rise*

F3-PHW-2 : 22–

36 h «» LOOSP evolution–

HPCI actuated

Key phenomena:

- RPV pressure decrease
- Core cooling ensured by HPCI

F3-PHW-3: 36–

CD «» LOOSP evolutions
–Lack of core cooling

Key phenomena:

- RPV pressure increase
- Core dry-out

PHW 1–3 during the Fukushima Unit 3 event can be found in Fig. 16.4D and E (Fig. 16.4D: RPV pressure and level all PHW; Fig. 16.4E: containment pressure and temperatures all PHW).

16.4.5 Final remarks

The exploitation of the listed phenomena and of concerned database needs a follow-up analysis (see also the “caution statement” in the Foreword) including the steps below:

(1) Identification of physical quantities which characterize the phenomena: i.e., typically, the unknowns of balance equations discussed in Chapter 5 of the Book, but also connected quantities, like pressure, void fraction, level in various components of RCS, mass inventory, rod surface temperature, heat flux, mass flow, superficial velocities.

(2) Identification of ranges of variations for those quantities in the concerned PHW, e.g., pressure change between 15.0 and 8.0 MPa.

(3) Combining the ranges of variations of selected key quantities, e.g., related to PHW-xx and PHW-yy (two examples given), respectively,

- Ranges in core region: pressure 6.0–8.0 MPa, void fraction 0–0.4, liquid velocity

5.0–6.0 m/s, linear heat flux 2.0–3.0 kW/m

- Ranges in HL-PRZ connection: HL diameter 0.8 m, surge-line diameter and mutual position related to HL 0.2 m and vertical angle, pressure 10.0–9.0 MPa, liquid velocity in HL 1.0–2.0 m/s, void fraction in HL 0.7–0.8.

(4) Confirm scaling: demonstrate that experimental database gathered in ITF or SETF having, as far as possible, the same ranges of variations of parameters in NPP exist & demonstrate “no-contradiction” between data relationships from scaled experiments and NPP.

(5) Confirm code capabilities: demonstrate that code calculations performed without adjusting input parameters (but considering related uncertainties or errors) produce results which are in qualitative and quantitative agreement with NPP data according to established procedures and acceptability thresholds as discussed in Chapters 6, 13, and 14 of the book and according, e.g., to Petruzzi et al. (2006).

The following summary notes are derived from the thermal-hydraulic investigation of the concerned NPP events.

16.4.5.1 TMI-2

All phenomena occur quicker in TMI-2 related to UTSG equipped NPP. In this case “quicker” means whatever is expected in a UTSG PWR in a time scale of the order of ten seconds occurs in TMI-2 (OTSG PWR) in a time scale of the order of one second. Definitely the quick progression of the accident (e.g., PORV opening and “undetected” stuck open condition occurring in a few seconds since the start of the transient) might have contributed to mislead the operators.

The understanding of CCFL, namely, CCFL at the connection between HL and PRZ surge-line, was clear to the scientific community at the time of the accident. Nevertheless the knowledge was not of “textbook” type: i.e., this was not spread necessarily to the industry and countermeasures were not necessarily planned in the emergency procedures.

The natural circulation performance of OTSG equipped PWR is definitely not the same as UTSG equipped PWR, i.e., in terms of NC mass flux in the core at an assigned decay power value and with a decreasing mass inventory in PS. This is a conceivable motivation for keeping the MCP in operation during the TMI-2 event. This is true although advantages and disadvantages of the conditions MCP-on and MCP-off were not well established at the time of the transient as well as the connected EOP. In the case of TMI-2 one may conclude that MCP in operation

delayed the occurrence of core failure related to the condition of MCP stopped. In the case of UTSG PWR undergoing the same TMI-2 LOFW+undetected SBLOCA event, the condition MCP stopped appears more reasonable to prevent or to delay an irreversible core cooling degradation.

16.4.5.2 Chernobyl-4

As well clear the Chernobyl event was a normal operation situation (i.e., not even an “event”) till the time when the fission power fell to “zero” owing to an operator error, e.g., about 1 h before the uncontrolled reactivity excursion (see Table 16.2). At this moment the reactor was pushed toward a beyond design condition with core keeping its geometric integrity till the explosion. Such a time period (i.e., “about 1 h”) is of interest for the notes below.

The thermal-hydraulic situation of the RCS (including core and piping till the steam drums) can be depicted by the following statements applicable to the whole period:

- (a) Core power was much lower than nominal full power value.
- (b) Pressure was at (or close to) the nominal full power value.
- (c) Core flow was varied by operators and lower or equal to nominal value (i.e., corresponding to full power).
- (d) The ratio [core flow]/[core power] was for all time higher or much higher than the value corresponding to nominal or full power condition.
- (e) The core inlet subcooling was apparently lower than the value corresponding to nominal full power.
- (f) The FW flow was higher than the value corresponding to the actual core power.
- (g) The level in the steam drums was lower (on average in the period) than the value corresponding to nominal full power condition.

The thermal-hydraulic situation can be depicted as “coolant forced circulation through the core,” i.e., low-temperature difference between core inlet and outlet and, therefore, low subcooling at core inlet. Under these circumstances key questions for thermal-hydraulics are, i.e., related to the time a few seconds before the explosion:

- What was the quality at core outlet?
- What was the margin to DNB in the core?

The answer to both questions is not straightforward because of the possibility that the MCP (or some of those) were in a cavitation conditions. Furthermore, a comprehensive answer requires further investigations which are beyond the purpose for the present effort. So, rather than answering the questions a few thermal-hydraulics related statements addressing the questions are provided below (i.e., making reference to a few seconds before the explosion):

(1) In case there was no pump cavitation and all MCP were pumping the (slight) subcooled liquid into the core according to the best information gathered so far (see, e.g., Table 16.2), the sudden boiling of the coolant, i.e., a phenomenon taken to explain the positive reactivity insertion at the origin of the explosion, cannot be justified.

(2) The margin to DNB (again in case of no steam at core entrance) considering the items (a), (c), and (d) was well above a reasonable value acceptable for safety.

(3) The RBMK core is very large, i.e., 14 m diameter and about 8 m distance between bottom of the active fuel (BAF) and TAF (and includes more than 1500 pressure channels): thermal-hydraulics conditions, i.e., coolant and fuel temperatures, are necessarily different from bottom to top and from center to periphery: so, the assumption of uniform-simultaneous vaporization of the entire coolant mass in the core is not easily defensible and application of three-dimensional thermal-hydraulics is needed, see, e.g., Parisi (2008).

(4) Time constants for the evolution of thermal-hydraulic phenomena, including flashing or fast-sudden vaporization, are much longer (i.e., order of magnitude of seconds) than time constants associated with neutron flux changes if a prompt-critical situation is created (i.e., order of magnitude of milliseconds or less): the assumption of a (relatively slow, possible) reactivity insertion due to thermal-hydraulic phenomena only, like flashing, appears inconsistent with a reactivity impulse (or, better, a fast reactivity increase) lasting fractions of 1 s needed to justify the neutron flux power peak.

(5) The formation of local super-critical regions involving parts of the core is possible, e.g., according to Malko (2002). The propagation of local disturbance in neutron flux to the entire core is expected to be much faster than the evolution of any phenomenon connected with thermal-hydraulics, e.g., including the

depressurization caused by the eventual rupture of one or a few pressure channels. This makes difficult the explanation of a spatial nonsymmetric neutron flux spike as the origin of a nonsymmetric explosion.

16.4.5.3 La Salle-2 and Oskarshamn-2

Data after scram (time of accident end for the concerned cases), or RCS recovery by suited EOP, can also be of interest for the purposes of the present chapter although these are not considered.

Stability constitutes a complex issue in nuclear thermal-hydraulics (as already mentioned) and full predictive capabilities (e.g., by SYS TH codes) are not available. However capabilities to analytically reproduce detected events do exist (Bousbia Salah et al., 2010) (see also Chapters 1, 2, and 10 of the book). Four main origins for the complexity can be distinguished:

- the large number of different physical mechanisms which may trigger the instability occurrence (D'Auria et al., 2014)
- the possible interaction among various physical mechanisms during a stability event
- the influence upon instability of parameters known with some approximation (or affected by errors) like the local material properties of nuclear fuel (e.g., gap conductance) also affected by burn-up, see also Lombardi-Costa et al. (2008)
- the influence of a variety of systems, the so-called BoP, e.g., located several hundred meters away from the core (upon the instability scenario in the core)

It seems worth noting at this point, not necessarily connected with the events in La Salle and Oskarshamn: (a) the distinction between static and dynamic instabilities, as well as between “Type I” and “Type II” instabilities (Van der Hagen et al., 2000); (b) the relevance of the density wave oscillation (DWO, dynamic) stability mechanism (Lahey and Moody, 1993); (c) the detection of local instability in a prototype full height simulator of BWR which are static at the center of the core and may not detectable at the core boundaries (D'Auria and Pellicoro, 1996; see also D'Auria (Ed.) et al., 1997).

16.4.5.4 Fukushima-1 to -3 events

The evolution of the SBO and, later on of the LOOSP transients in Fukushima Daiichi Units 1–3 is fully consistent with the thermal-hydraulics knowledge at the

time of the events. Definitely no flaw in the thermal-hydraulics knowledge can be connected with the Fukushima scenarios or, in other words, no better destiny for the Units 1–3 cores could be expected under the assigned events and circumstances. This statement is substantiated by the issues below.

- **IC in Fukushima-1.** The IC is a passive system without moving parts during its design operation. IC was adopted in early BWR and reconsidered for future NPP including Simplified BWR, SBWR. The IC correctly entered into operation in the Fukushima-1 NPP following the SBO occurrence. After the LOOSP event and some nonoptimized operator actions the IC went out of operation. The IC heat sink in Fukushima-1 NPP could have been sufficient for about 10 h, i.e., a time period less than the actual duration of the LOOSP condition. Furthermore, the SBWR IC has been the target system for a reliability study (D'Auria and Galassi, 2000) where it was found that was the reliability of the thermal-hydraulic performance (i.e., independent of the actuation of any mechanical system) is below unity, see also Jafari et al. (2003). This implies that the integrity of the Fukushima-1 core was not ensured even in the case of an IC fully operative.

- **RCIC in Fukushima-2 and -3.** The RCIC is a passive system with moving parts (i.e., the turbine) during its design operation. Turbine-driven RCIC is adopted in most of the existing BWR. The RCIC correctly entered into operation in the Fukushima-2 and -3 NPP following the SBO occurrence. One may state that the LOOSP condition was not decisive in damaging the operability of the system in both units. Rather a combination of causes brought to the condition RCIC out-of-operation (i.e., not failed) in each of units -2 and -3:

- In the Fukushima-2 unit, RCIC apparently failed after nearly three full-days operation, in any case after (much) longer time than any conceivable design target.

- In the Fukushima-3 unit, the operators substituted RCIC with (still turbine driven) HPCI. Then, being afraid of a failure of the HPCI, they attempted to set-up conditions (low pressure) for the use of fire water for core cooling. Irreversible core damage occurred when this operation was in progress.

- **PSP performance.** Dry-well and wet-well constitute the BWR containment and PSP is part of the wet-well (torus, or Mark I, type in the case of the three concerned Fukushima units). Whatever was measured in the containment of any of the here units, namely in relation to the PSP, till the time of core damage is discussed within the internationally recognized reports OECD/NEA/CSNI (1986) and OECD/NEA/CSNI (1999) available well before the Fukushima event.

- **Containment venting.** Containment venting is a desirable feature for containments, contrary to the tight (full pressure resistant) concept which characterizes the containment design for most of the existing NPP. This is well established by early Soviet Union NPP, e.g., IAEA (1999). Equipped with low-pressure vented containments (confinement is the word sometimes used). Drawback of controlled containment venting is the radioactivity releases of gaseous fission products including noble gases. Advantage of containment venting is to lower the containment pressure making more easily achievable the target of containment integrity. The proper design of venting system may largely enhance the advantage and reduce the drawback.

16.5 Conclusions

Industrial accidents occur within the framework of any activity connected with human civilization. Natural disasters add-up to those accidents and in some cases interactions (i.e., between human caused and natural disasters) occur, Fukushima being one example. Huge databases of accidents exist. The five NPP events selected for consideration in the present document although important for nuclear technology form a (very) narrow area in the overall spectrum of industrial accidents. Furthermore, in two over five considered cases, Chernobyl and Fukushima, large radiological impact upon the environment was the consequence, in one case, Three Mile Island, a (very) moderate consequential radiological impact happened, and in two cases, La Salle and Oskarshamn, no impact at all occurred.

The thermal-hydraulics investigation limited to the time period of the event where the core remained intact, where applicable, constitutes the only clue among the five events in the present chapter.

The documented study did not lead to innovation in the area of accident analysis or to the identification of limitations or deficiencies in the thermal-hydraulics knowledge. Rather, the study can be used to demonstrate the importance of: (a) thermal-hydraulics in the understanding of accident evolutions: this is needed to plan preventive and mitigative countermeasures; (b) accident database to prove the validation and the scaling capabilities of thermal-hydraulic computational tools: steps needed in this direction, in addition to the present activity, have been outlined.

Insights into each accident are possible from a thermal-hydraulic analysis, and (summary) final remarks are considered in the previous section: in no case, misuse of thermal-hydraulics or lack or insufficient knowledge was among the main root

causes for the event. A further synthesis is provided hereafter, distinguishing each event:

- TMI-2, 1979: this constituted a historical cornerstone for the development of the current thermal-hydraulics; the deficiencies in spreading of thermal-hydraulics knowledge rather than deficiencies in the knowledge itself are among the causes for the accident. This is applicable, e.g., considering the lack (at the time) of suitable emergency procedure in the situation when the pressurizer is full of liquid and the core is voided.

- Chernobyl-4, 1986: thermal-hydraulics phenomena, i.e., sudden voiding of the core to generate positive reactivity and liquid flashing to generate the disruptive pressure wave, have been called to explain the explosion. However, coupled three-dimensional neutron-physics and thermal-hydraulic analysis considering the large core dimensions could not support, so far, a full explanation of the detected event features (noticeably the event-generated energy within a fraction of a second).

- La Salle-2, 1988: boiling channel and/or boiling system instability constituted a well-known phenomenon at the time of the event. A large number of parameters affect the stability performance and, in some cases, (very) small changes in the value of those parameters bring any system to cross the stability boundary. Because of this, full predictive capability of core unstable performance did not exist at the time of the accident and does not exist about 30 years later, notwithstanding enormous progresses made as far as computational tool capabilities are concerned. Thermal-hydraulics analyses allowed the identification of the most dangerous regions of the core power-to-flow map and the characterization of countermeasures to suppress the oscillations. Thermal-hydraulics studies also contributed to demonstrate that stability shall not be considered a key safety issue in the operation of BWR.

- Oskarshamn-2, 1999: what written for La Salle-2 can be repeated. In addition, countermeasures proposed as a follow-up of La Salle event were not fully considered in the operation of Oskarshamn.

- Fukushima-1 to -3, 2011: a long-lasting event originated by loss of on-site and off-site electricity occurred. The words “long lasting” signify beyond any expectation or (very) far from design conditions. Whatever happened during the event in the three units of Fukushima Daiichi, at least till the moment of core degradation, was consistent with the established knowledge in thermal-hydraulics. Establishing suitable containment venting, as well as additional safety barriers needs support from thermal-hydraulics studies.

References

- Adamov E.O., Vasilevskji V.P., Ionov A.I., et al. Analysis of the accident development first stage at the fourth unit of the Chernobyl Nuclear Power Plant. *At. Energ.* 1988;64(1):24–28 (in Russian).
- Adamov E.O., Cherkashov Yu.M., Mironov Y.V., Nikitin Y.M., Bourlakov E.V., Kukharkin N.E. *RBMK reactors during severe accidents and related assessment techniques*. In: ICHMT Seminars, Thermal Science Online, Issue 1; 1995 ISSN 961-91393-0-5.
- Adamov E.O., Cherkashov Yu.M., Ponomarev-Stepnoy N.N., Bourlakov E.V. *Upgrading of RBMK reactors: safety enhancement measures*. In: IAEA International Conference, One Decade After Chernobyl: Nuclear Safety Aspects, Vienna, April 1–3; 1996a.
- Adamov E.O., Cherkashov Yu M., Podlazov L.N., Nikitin Yu M., Stenbok I.A., Novoselsky O.Yu., Ionov A.I., Ponomarev-Stepnoy N.N., Bouriakov E.V., Malkin S.D., Krayushkin A.V., Babaitsev M.N., Checherov K.P., Abagyan A.A., Vasekin V.N., Kisil'I M. *Chernobyl Accident Causes, overview of studies over the decade*. In: IAEA International Conference, One Decade After Chernobyl: Nuclear Safety Aspects, Vienna, April 1–3; 1996b.
- Addabbo C., Annunziato A., Aksan N., D'Auria F., Galassi G.M., Dumont D., Gaul H.P., Umminger K., Nilsson L., Hofmann D., Riikonen V., Rigamonti M., Steinhoff F., Guba A., Toth I. *Development and Establishment of the CERTA Network Database* European Commission Report, CERTA/SC/D8 EUR 20421 EN, Brussels, September. 2002.
- AESJ. *The Fukushima-Daiichi Nuclear Accident Final Report of AESJ Investigation Committee*. Tokyo: Springer; 2015.978-4-431-55160-7.
- Allen T.B., Polmar N. *Rickover Father of the Nuclear Navy*. Washington, DC: Potomac Books Inc.; 2007.

Almenas K., Kaliatka A., Uspuras E. *Ignalina RBMK-1500. A Source Book, Extended and Updated Version*. Kaunas: Lithuanian Energy Institute; 1998.9986-492-35-1 pp. 1–198.

ARIA. <http://www.aria.developpement-durable.gouv.fr>. 2016.

Arpott D.G., Green C.D. *Chernobyl unique safety valve for a reactor clear explosion*. In: Proceedings of the British National Conference on The Legacy of Nuclear-Lessons for the UK held at the Council House, Bristol, UK, March 11; 1992.

Bandini G., De Rosa F. ASTEC validation on TMI-2 and LOFT LP-FP-2. *Nucl. Eng. Des.* 2014;272:163–172.

Blomstrand J., Eklund R., Nylund O. *Flow stability investigation of SVEA BWR fuel Workshop on Boiling Water Reactor Stability, Brookhaven, NY*. 1990 (see also OECD/NEA/CSNI, 1990).

Bousbia Salah A., D'Auria F., Hamidouche T. Natural circulation cooling and safety features in engineering and industrial applications. *Insights into Natural Circulation, Phenomena, Models and Issues*. Saarbrücken, Germany: LAP Lambert Academic Publishing; 2010.

Broughton J.M., Kuan P., Petti D.A., Tolman E.L. A scenario of the Three Mile Island unit 2 accident. *Nucl. Technol.* 1989;87:34–53.

D'Auria F., Galassi G.M. Scaling in nuclear reactor system thermal-hydraulics. *Nucl. Eng. Des.* 2010;240(10):3267–3293.

D'Auria, F. (Ed.), Soloviev, S., Novoselsky, O., Moskalev, A., Radkevitch, V., Malofeev, V., Parisi, C., Cherubini, M., Pierro, F., Moretti, F. (Lead Authors), 2005. Deterministic Safety Technology in RBMK—EC TACIS Project R2.03/97 (Software Development for Accident Analysis of VVER and RBMK Reactors in Russia). Final Technical Report—Part B. University of Pisa, Pisa, ISBN 88-902189-0-8, pp. 1–838.

D'Auria F., Gabaraev B., Soloviev S., Novoselsky O., Moskalev A., Uspuras E., Galassi G.M., Parisi C., Petrov A., Radkevich V.,

Parafilo L., Kryuchkov D. Deterministic accident analysis for RBMK. *Nucl. Eng. Des.* 2008a;238:975–1001.

D'Auria F., Gabaraev B., Novoselsky O., Radkevich V., Filinov N., Mazzini D., Moretti F., Pierro F., Vigni A., Parafilo L., Kryuchkov D. The multiple pressure tube rupture (MPTR) issue in RBMK safety technology. *Nucl. Eng. Des.* 2008b;238:1026–1061.

D'Auria F., Lombardi-Costa A., Bousbia Salah A. *The Boiling Water Reactor Stability—updated*. In: IAEA/ICTP Course on Natural Circulation in Water-cooled Nuclear Power Plants, International Center for Theoretical Physics (ICTP)—Lecture ID T12 & T13, Trieste, June 22–26; 2009.

D'Auria F., Galassi G., Pla P., Adorni M. The Fukushima event: the outline and the technological background. *Sci. Technol. Nucl. Install.* 2012a;507921.

D'Auria F., Bestion D., Jeong J.J., Kim M. *V & V in system thermal-hydraulics*. In: ASME Verification and Validation Symposium (V & V 2012), Las Vegas, NV, May 2–4; 2012b.

D'Auria F., Del Nevo A., Muellner N. *Insights into natural circulation stability*. In: IAEA Training Course on Natural Circulation Phenomena and Passive Safety Systems in Advanced Water Cooled Reactors, SANESS-GCNEP, Mumbai, September 29–October 4, Paper ID L08; 2014.

D'Auria F., Glaeser H., Kim M. *A vision for nuclear reactor safety*. In: 46th Jahrestagung Kerntechnik Annual Meeting on Nuclear Technology, Berlin, May 5–9; 2015.

D'Auria, F. (Ed.), Bestion, D., Lien, P., Nakamura, H. (Lead Authors), 2016. Scaling State of Art Report in Nuclear Thermal-hydraulics. OECD/NEA/CSNI Report to be Issued, Paris.

D'Auria F., Frogheri M. Use of natural circulation map for assessing PWR performance. *Nucl. Eng. Des.* 2002;215(1–2):111–126.

D'Auria F., Galassi G.M. *Methodology for the evaluation of the reliability of passive systems* University of Pisa Report, DIMNP-NT 420(00)-rev. 1, Pisa, October. 2000.

D'Auria F., Pellicoro V. *Local instability in BWR reactor simulator*. In: Int. Conf. on Nuclear Engineering (ICONE-4), New Orleans, LA, vol. 3; 1996.

D'Auria F., De Sanctis N., Di Marco P., Lahey Jr. R.T., Podowski M.Z. A linear model to study fluid dynamic instabilities in boiling channels due to density oscillations. *Heat Technol.* 1987;5(3-4):55-72.

D'Auria F., Frogheri M., Leonardi M. *Natural circulation performance in western type and eastern type PWR*. In: XI Annual Simulator Conference, San Diego, CA, April 10-14; 1994.

D'Auria, F. (Ed.), Ambrosini, W., Anegawa, T., Blomstrand, J., In De Betou, J., Langenbuch, S., Lefvert, T., Valtonen, K., 1997. State of the Art Report on Boiling Water Reactor Stability (SOAR ON BWRS). OECD-CSNI Report OECD/GD(97)13, Paris.

Dollezhal N.A., Emeljanov I.Ya. *The Channel Nuclear Power Reactor*. Moscow: Atomizdat; 1980 (in Russian).

Dopchie, H., 1971. Letter from Association Vincotte, to C. K. Beck, AEC, Subject: Possible Inadequacy of ECCS Protection Against Break of Vapor Line on Pressurizer, Belgium, April 27.

EC. <https://clearinghouse-oef.jrc.ec.europa.eu/>. 2016a.

EC. <http://stresa.jrc.ec.europa.eu/>. 2016b.

EM-DAT. <http://www.emdat.be>. 2016.

EPRI. *Analysis of Three Mile Island Unit 2 Accident*. Palo Alto, CA: NSAC-80-1 (NSAC-1 Revised); 1980.

Fernandez-Moguel L., Birchley J. Analysis of the accident in the Fukushima Daiichi nuclear power station Unit 3 with MELCOR-2.1. *Ann. Nucl. Energy*. 2015;83:193-215.

Garis N., 2016. Personal communication to F. D'Auria in relation to Oskarshamn-2 event, Stockholm.

Gorbachev, B.I., 2002. The causes and the scenario of the Chernobyl Accident and radionuclide release on the CHNPP Unit 4 site. Article in the Edited Report by Imanaka T. (Ed.).

Henry R.E. *TMI-2: An Event in Accident Management for Light-Water-Moderated Reactors*. LaGrange Park, IL: ANS; 2011.

IAEA. *Final Report of the Programme on the Safety of WWER and RBMK Nuclear Power Plants*. Vienna: IAEA-EBP-WWER-15; 1999.

IAEA. *Irradiation Damage in Graphite Due to Fast Neutrons in Fission and Fusion Systems*. Vienna: TECDOC-1154; 2000 pp. 1–176.

IAEA. *The Fukushima Daiichi Accident Report by the Director General, GC(59)14*, Vienna. 2014.

IAEA. <http://www-ns.iaea.org/home/ni/databases.asp#irs>. 2016a.

IAEA. <http://www-ns.iaea.org/home/ni/databases.asp#finas>. 2016b.

IAEA. <http://www-ns.iaea.org/home/ni/databases.asp#irsrr>. 2016c.

IAEA. *The V & V for System Thermal-Hydraulics Codes SRS Report to be Issued*, Vienna. 2016d.

Imanaka T., ed. *Recent Research Activities About the Chernobyl NPP Accident in Belarus, Ukraine and Russia*. Kyoto: Research Reactor Institute, Kyoto University; 2002.

ITDB. <http://www-ns.iaea.org/security/itdb.asp>. 2016.

Jafari J., D'Auria F., Kazeminejad H., Davilu H. Reliability evaluation of a natural circulation system. *Nucl. Eng. Des.* 2003;224:79–104.

Kim S.I., Park J.H., Ha K.S., Cho S.-W., Song J.H. Analysis of Fukushima unit 2 accident considering the operating conditions of RCIC system. *Nucl. Eng. Des.* 2016;298:183–191.

Kiselev A.N., Checherov K.P. The model of destruction process of the unit 4 the chernobyl power plant. *At. Energ.* 2001;91(6):425–434 (in Russian).

Kozlowski T., Wysocki A., Gajev I., Xu Y., Downar T., Ivanov K., Magedanz J., Hardgrove M., March-Leuba J., Hudson N., Ma W. Analysis of the OECD/NRC Oskarshamn-2 BWR stability benchmark. *Ann. Nucl. Energy.* 2014;67:4–12.

Lahey Jr. R.T., Moody F.J. *The Thermal-hydraulics of a Boiling Water Reactor*. Hinsdale, IL: ANS Monograph; 1993.

Lien, P., 2016. Personal communication to F. D'Auria in relation to La Salle-2 event, Washington, DC.

Lombardi-Costa A., Pereira C., Ambrosini W., D'Auria F. Simulation of a hypothetical out-of-phase instability case in boiling water reactor by Relap5/Parcs coupled codes. *Ann. Nucl. Energy.* 2008;35:947–957.

Malko, M.V., 2002. The Chernobyl Reactor: Design Features and Reasons for Accident. Article in the Edited Report by Imanaka, T. (Ed.).

Margoulova Th. *Le Centrales Nucléaires (translated in French in 1977)*. Moscow: Editions MIR; 1969.

Martinez Val J.M., Aragones J.M., Mingues E., Perlado J.M., Velarade G. An analysis of the physical causes of the chernobyl accident. *Nucl. Technol.* 1990;90:371–388.

Mascari F., Nakamura H., Umminger K., De Rosa F., D'Auria F. *Scaling issues for the experimental characterization of Reactor Coolant System in Integral Test Facilities and role of system codes as extrapolation tool*. In: Int. Conf. NURETH-16, Chicago, IL, August 30–September 4; 2015.

Mokizuki H. Analysis of the Chernobyl accident from 1:19:00 to

the first power excursion. *Nucl. Eng. Des.* 2007;237:300–307.

NEWS. <http://www-ns.iaea.org/tech-areas/emergency/news.asp>. 2016.

NGDC. <http://www.ngdc.noaa.gov/hazard/hazards.shtml>. 2016.

Nilsen, T., Kudrik, I., Nikitin, A., 1997. Bellona Report 2.96. The Russian Northern Fleet Nuclear Submarine Accidents. © Bellona. <http://spb.org.ru/bellona/ehome/russia/nfl/nfl8.htm>.

Nishikawa T., Inoue H., Motohashi S., Ebisawa K. Lessons Learned from Kashiwazaki-Kariwa NPP after Niigataken Chuetsu-Oki Earthquake (2007) in view of SSI effect. In: Hsu T.T.C., Wu C.-L., Li J.-L., eds. *Infrastructure Systems for Nuclear Energy*. Chichester: John Wiley & Sons, Ltd; 2014.

NMED. <https://ire.org/nicar/database-library/databases/nuclear-material-events-database-nmed/>. 2011.

OECD/NEA, 2016. <https://www.oecd-neo.org/dbprog/ccvm/indexset.html>, SETF data; and <https://www.oecd-neo.org/dbprog/ccvm/>, ITF data.

OECD/NEA/CNRA. *Report on Fukushima Daiichi NPP Precursor Events*. Paris: NEA/CNRA(2014)1; 2014.

OECD/NEA/CSNI. *Pressure Suppression System Containments, a State of Art Report* CSNI Report 126, Paris. 1986.

OECD/NEA/CSNI. In: Proceedings of Int. Workshop on Boiling Water Reactor Stability, Held in Brookhaven, New York; 1990 CSNI Report 178, Paris.

OECD/NEA/CSNI. *State-of-the-Art Report (SOAR) on Containment Thermalhydraulics and Hydrogen Distribution*. Paris: CSNI/R(1999)16; 1999.

Osif B.A., Baratta A.J., Conkling T.W. *TMI 25 Years Later: The Three Mile Island Nuclear Power Plant Accident and Its Impact*. University Park, PA: The Pennsylvania State University; 2004.

Ozdemir O.E., George T.L., Marshall M.D. Fukushima Daiichi Unit 1 power plant containment analysis using Gothic. *Ann. Nucl. Energy*. 2015;85:621–632.

Pakhomov S.A., Krivokhvatsty K.S., Sokolov I.A. Assessment of the prompt energy release by the accident at the reactor of the Chernobyl NPP based on estimation of the ratio of activities of Xenon-133 and Xenon-133m in the air. *Radiokhimiya*. 1991;33(6):125–132 (in Russian).

Parisi C. *PhD Thesis in Nuclear Engineering*. Pisa: University of Pisa; 2008.

Petruzzi, A., D'Auria, F. (Eds.), De Crecy, A., Bazin, P., Borisov, S., Skorek, T., Glaeser, H., Benoit, J.P., Chojnacki, E., Fujioka, K., Inoue, S., Chung, B.D., Trosztel, I., Toth, I., Oh, D.Y., Pernica, R., Kyncl, M., Macek, J., Macian, R., Tanker, E., Soyer, A.E., Ozdere, O., Perez, M., Reventos, F., 2006. BEMUSE Programme—Phase 2 Report. Re-analysis of the ISP-13 Exercise, Post-Test Analysis of the LOFT L2-5 Experiment. OECD/CSNI Report NEA/CSNI/R(2006)2, June 19, Paris, pp. 1–625.

Potter, W.C. (Principal Investigator), 1990. Soviet Decision Making for Chernobyl: An Analysis of System Performance and Policy Change, Contract No. 802-12. University of California, Los Angeles, CA.

Rachkov V.I., Kalyakin S.G., Kukharchuk O.F., Orlov Yu I., Sorokin A.P. From the first nuclear power plant to fourth-generation nuclear power installations [on the 60th anniversary of the World's First nuclear power plant]. *Therm. Eng.* 2014;61(5):327–336.

Rogovin M., Frampton Jr. G.T. Washington, DC: USNRC GPO Sales Program; . *Three Mile Island: A Report to the Commissioners and to the Public*. 1980;vol. II, part I.

Schmid S.D. *Producing Power—The Pre-Chernobyl History of Soviet Nuclear Industry*. Cambridge, MA: MIT Press; 2015.

Sehgal B.R., ed. *Nuclear Safety in Light Water Reactors—Severe Accident Phenomenology*. Amsterdam: Elsevier Inc.; 2012.

Sevón T. A Melcor model of Fukushima Daiichi Unit 1 accident. *Ann. Nucl. Energy*. 2015;85:1–11.

Tambling T.N., Harpster T.L. *Inspection Report No. 50-346/77-32: Davis-Besse Nuclear Power Station, Unit 1, Docket 50-346, November*. 1977.

TEC, 1977. Toledo Edison Corporation—Licensee Event Report, NP-32-77-16, Docket 50-346, October.

TEPCO. *Fukushima Nuclear Accident Analysis Report, Tokyo, June 20*. 2012.

Thulin, E., 2000. Report from the Oskarshamn-2 stability event of 99-02-25. ABB Atom AB, SPD-99-237-rev.0., Vasteras (in Swedish).

USNRC. *Inspection on March 16 Through 24, 1988, to La Salle County Station at La Salle Site Marseilles, IL* Augmented Inspection Team Report No 50-373/880008; 50-374/880008. 1988a.

USNRC. *Information Notice No. 88-39: LaSalle Unit 2 Loss of Recirculation Pumps With Power Oscillation Event, Washington, DC, June 15*. 1988b.

USNRC. *Severe Accident Risk: An Assessment for Five US Nuclear Power Plants* NUREG-1150, Washington, DC. 1990.

Uspuras E., Kaliatka A. *Accident and Transient Processes at NPPs With Channel Type Reactors, Monograph*. Kaunas: Lithuanian Energy Institute; 2006. 9986-492-87-4 pp. 1–299.

Van der Hagen T.H.J.J., Stekelenburg A.J.C., Van Bragt D.D.B. Reactor experiments on type-I and type-II BWR stability. *Nucl. Eng. Des.* 2000;200:177–185.

Wikipedia, 2015. List of 20th-Century Earthquakes & List of 21st-Century Earthquakes.

Wulff W., Cheng H.S., Mallen A.N. *Causes of Instability at La Salle and Consequences Form Postulated Scram Failure*BNL-NUREG 45273, Brookhaven, NY. 1990.

Wulff W., Cheng H.S., Mallen A.N., Rohatgi U.S. *BWR Stability Analysis With the BNL Engineering Plant Analyzer*USNRC NUREG/CR-5816 (also BNL-NUREG-52312), Washington, DC. 1992.



Subject Index

Note: Page numbers followed by *f* indicate figures, *t* indicate tables, *b* indicate boxes, and *np* indicate footnotes.

A

Acceleration pressure drop 503–504

Acceptance criteria 961, 970–972

Accident analysis, BEPU 921

- elements and structure for 921, 924–926, 931–932

 - concerned events 926–927

 - resources typologies 927

 - roadmap 928–931

 - selected terms 921–923

- in FSAR 908

- licensing connection 915–916

- probability-based classification 918

- in SAM 917–918

- in SYS-TH code 924–925

Accident management (AM)

- cross reference matrix 320–321*t*

- safety concepts 123–124

- SAMG 123–124

Accident management procedure (AMP) 13–14, 1037–1041, 1039–1040*f*, 1040*t*

Accident scenarios 955, 958–961*t*

- accident management with 1037–1041, 1039–1040*f*, 1040*t*

ATWS 1033

- in ABWR 1035–1036*f*

- phenomena connection with 1035–1037, 1035–1036*f*, 1036*t*

- in PWR with UTSG 1007–1008, 1009*t*, 1010*f*

- qualitative characterization 1033–1034

- quantitative characterization 1034–1035

- in water cooled nuclear reactor 1034*t*

boron dilution 1070–1072, 1071–1072*f*, 1072*t*

CHF 1041–1042, 1043*t*, 1043*f*

containment performance 1041, 1043–1047, 1045–1046*f*, 1047*t*

CRE

- phenomena connection 1032–1033, 1032*f*, 1033*t*

- in PWR with UTSG 1032*f*

- qualitative characterization 1030–1031

- quantitative characterization 1031–1032

fuel channel blockage 1063

- phenomena connection 1064–1065, 1064–1065*f*, 1065*t*

- qualitative characterization 1063–1064

- quantitative characterization 1064

- in RBMK 1064–1065*f*, 1068*t*

LBLOCA

- phenomena connection with accident scenario 984*f*, 989*f*, 990–994, 990–991*t*

- in PWR with UTSG 983*t*, 984*f*, 989*f*

- qualitative characterization 980–982

- quantitative characterization 982–989

- in reactors other than PWR with UTSG 994

LOFA/MCP-trip 1072–1073

- phenomena connection with 1075–1076, 1075–1076*f*, 1076*t*

- in PWR with UTSG 1074*t*

- qualitative characterization 1073–1074

- quantitative characterization 1074

LOFW

- phenomena connection with 1010–1011, 1010*f*, 1011*t*

- in PWR with UTSG 1007–1008, 1009*t*, 1010*f*
- qualitative characterization 1008
- quantitative characterization 1008–1009

LOOSP 1015

- in CANDU 1017–1018*f*
- phenomena connection with 1016–1018*f*, 1018–1019
- in PWR with UTSG 1016–1017*f*, 1018*t*
- qualitative characterization 1015–1016
- quantitative characterization 1016–1017

MPTR 1065–1066

- phenomena connection 1068–1070, 1070*t*
- qualitative characterization 1066
- quantitative characterization 1066–1068
- in RBMK 1067*f*, 1069*f*

MSLB and FWLB 1024

- phenomena connection with 1026–1027*f*, 1028–1029, 1028*t*
- in PWR with UTSG 1025*t*, 1026–1027*f*
- qualitative characterization 1024–1025
- quantitative characterization 1025–1028

MSLB combined with SGTR 1060–1063, 1062*f*, 1063*t*

natural circulation 1041, 1052–1060, 1053–1058*f*, 1059*t*

- in ATLAS test facility 1058*f*
- characterization 1052–1053
- complexity of 1053–1057
- loop configurations of nuclear systems 1053*f*
- in LSTF test facility 1058*f*
- phenomena connection with accident scenario 1057–1060, 1057*f*, 1059*t*
- in PWR with UTSG 1054*f*, 1057*f*
- stability issue 1056*f*
- stop and restart calculated for PWR with UTSG 1071*f*

nuclear fuel behavior 1083–1084

- phenomena connection with 1084–1085, 1085*f*, 1085*t*
- topics and facts 1084

and phenomena *See* (Phenomena in thermal-hydraulics)

pressurized thermal shock 1041, 1047–1052, 1048–1050*f*, 1051*t*

phenomena connection with accident scenario 1049–1052, 1050*f*, 1051*t*

in PWR 1050*f*

thermal-hydraulic aspects 1047–1049, 1048–1049*f*

RIA scenarios

PWR 1031*f*

quantitative characterization 1031–1032

reactivity excursion class of 1029–1033

SBLOCA

phenomena connection with 1000–1004*f*, 1002–1007, 1004–1005*t*

in PWR with UTSG 998–999*t*, 1000–1002*f*

qualitative characterization 995–997

quantitative characterization 998–1002

in reactors other than PWR with UTSG 1007

SBO 1011–1012

phenomena connection with 1012–1013*f*, 1014–1015, 1014*t*

in PWR with UTSG 1012–1013*f*, 1013*t*

qualitative characterization 1012

quantitative characterization 1012–1014

SGTR 1019

phenomena connection with 1022–1024, 1022*f*, 1023*t*

in PWR with UTSG 1021*t*, 1022*f*

qualitative characterization 1020

quantitative characterization 1021

shutdown 1080–1083, 1082*f*, 1083*t*

during shutdown conditions 1080–1083, 1082*f*, 1083*t*

time histories 1086–1087

turbine trip 1077

in BWR 1079*f*

phenomena connection 1079–1080, 1080*t*

in PWR 1078*t*

qualitative characterization 1077

quantitative characterization 1077–1078

in SMR 1078*f*

Accumulators 632–633

advanced US PWR 633, 633*f*

in CFD 633

flow rate coefficient 634, 634*f*

Accuracy 24–25, 65, 68*f*, 71, 115, 117–118, 123, 131, 147–148, 151*f*, 159–160, 163*np*, 208, 249, 346, 458, 462, 467, 540, 552, 564, 581, 583, 586, 601–602, 645–647, 650, 659, 662–664, 671–672, 682–684, 686, 689–690, 702, 707, 709–711, 734–739, 743, 755, 758, 768, 773, 775, 777–778, 784, 790, 793, 797, 810–813, 817–818, 835–836, 838, 840–842, 845, 847, 854, 865–866, 871–874, 875*t*, 876, 881, 884, 922–923

Accuracy extrapolation 56, 131, 647, 865, 874, 875*t*, 876, 881

Advanced boiling water reactor (ABWR), ATWS scenario in 1035–1036*f*

Advanced light water reactor (ALWR)

check valves 341

CMT behavior 343

containment emergency systems 337–338

containment structures, condensation 337

critical and supercritical flow 341

CRP objectives 333–334

density locks 341

emergency heat exchangers and ICs 341–342

gravity-driven cooling and accumulator behavior 340

IAEA 332

identification and characterization 334, 335–336*t*

large pools 334–336

liquid temperature stratification 341

NC 339

noncondensable gases, condensation HT 336–337

OECD/NEA framework 333–334

passive safety system

classification 332

definition 332

use of 332–333

steam-liquid interactions 339–340

stratification and mixing of boron 342–343

thermo-fluid dynamics and PDs 338

ALARA *See* As Low As Reasonably Achievable (ALARA)

AMP *See* Accident management procedure (AMP)

Analysis of THERmal hydraulics of LEaks and Transients (ATHLET)
code 649, 666, 703, 713

Analytical thermal hydraulics

abrupt area change model 112

CCFL 111–112

choked flow model 111

closure laws/constitutive equations 111

components 112

engineering factors 110

heat transfer correlations/look-up tables 111

ISPs 113

main code 111

nodalization/nodalization diagram 113

nuclear factors 109

system codes 110–111

user effect/good practices 113

user-specified coefficients 111–112

Anticipated operational occurrence (AOO) 970–973

Anticipated transient without scram (ATWS) scenarios 970, 1033

in ABWR 1035–1036^f

phenomena connection with 1035–1037, 1035–1036^f, 1036^t

in PWR with UTSG 1007–1008, 1009^t, 1010^f

qualitative characterization 1033–1034

quantitative characterization 1034–1035

in water cooled nuclear reactor 1034^t

AOO *See* Anticipated operational occurrence (AOO)

As low as reasonably achievable (ALARA) concept 69, 937, 944

ATHLET code *See* Analysis of THERmal hydraulics of LEaks and
Transients (ATHLET) code

Augmentation, HT

agitation of the swirl flow

annular projections 480–481, 481^f

film flow regime 480

- heat exchange enhancers 479, 480*f*
- heat transfer coefficient 479
- porous structures 482, 482*f*
- principles 479
- superhydrophilicity
 - aqueous slurry 483, 484*t*
 - characteristics 483
 - photocatalysis 483
- Automatic depressurization system (ADS) 667

B

- Balance equations
 - CFD approach 174
 - characteristic velocities and hyperbolicity
 - CATHARE 1-D 6-equation model 233
 - Hadamard's classification 231
 - PDE 231
 - cross-momentum equation 229
 - drift flux model 227–229
 - 1-D two-fluid equations 222–223
 - 6-equation model 230–231
 - 3-field models, system codes
 - 1-D 3-field equations 239
 - gas-continuous liquid-droplets 239–240*b*
 - LBLOCA simulation 238–239
- HEM
 - 1-D 226–227*b*
 - predictive capabilities 227
 - single-phase liquid to single-phase steam 226–227
- local instantaneous equations
 - Leibniz rule and Gauss theorem 176
 - mass momentum and total energy 175, 175*t*
 - multicomponent fluid flow 179
 - 1-component 1-phase flow equations 179*b*
 - properties of 180
 - single-phase single-component fluid 178

- $V(t)$ limited by a surface $A(t)$ 175, 175f
- one-to two-fluid models 223–225, 225t
- single-phase modeling
 - characteristics and modeling needs 181, 182t
 - DNS 183
 - locality and universality 183
 - RANS-type models 181
 - scale/eddy-resolving-type models 181–183
- space averaged 1-D equations
 - definition 209–211, 209–210f
 - energy balance, phase k 215–218
 - interface pressure 214, 214f
 - mass balance, phase k 211
 - momentum balance, phase k 211–215
 - stratified flow 218–220, 218f, 220f
- space-time-averaged 1-D equations
 - control volumes 188
 - energy equation 191–192
 - mass balance equation 190
 - momentum equation 192–195
 - 1-component 1-phase flow 195b
 - portion of a duct 189, 190f
 - predictive capabilities 195–196
- TIA
 - flow regime transitions 234–235
 - interfacial transfers 235
 - monodispersed approximation 235–236
 - nonestablished flows 234
 - polydispersed dynamic modeling 237–238
 - predictive capabilities 238
 - turbulent scales 234
- time-averaged single-phase equations
 - closure of 187–188
 - incompressible flow 186–187
 - 1-component 1-phase flow equations 188b

- Reynolds averaging-time averaging 184–185
- time-averaged two-fluid equations
 - bubble/drop, dispersed phase 206–207
 - momentum and total energy 205, 205_t
 - predictive capabilities 208
 - RANS two-fluid equations 207–208_b
- time-space averaged 1-D equations 221–222
- two-phase flow developments 96–97
- two-phase flow modeling
 - applicability and degree of maturity 203, 204_t
 - deterministic interface 200
 - Eulerian fluid dynamic simulation approaches 196–198, 197_t
 - factors influencing 199–200
 - filtered interface 200
 - hybrid LES method 202
 - LES with deterministic interface 201
 - LES with statistical interfaces 202
 - locality and universality 203
 - pseudo-DNS method 200–201
 - RANS method (U-RANS) 201
 - statistical interface 200, 200_f
 - time space and phase averaging 198–199, 198_f
- Ballooning 534, 642, 745, 931–932, 972, 981, 983_t, 987, 1030, 1041–1042, 1064, 1084
- Basic phenomena 254, 255–257_t, 258–265, 349–351, 586–587, 747–748_t, 975
- BDBA *See* Beyond design basis accident (BDBA)
- BE code *See* Best estimate (BE) code
- BEPU *See* Best estimate plus uncertainty (BEPU)
- Bernoulli (or Bernouilli) flow or equation 65, 599, 614_f, 682, 986
- Best estimate (BE) code 645
 - computer codes 840, 865
 - in NPPs 897
 - vs. conservative code 908, 923
 - features of first 647–649

realistic input data 923

Best estimate methods-uncertainty and sensitivity evaluation
(BEMUSE) programme

in CIAU 884

high level objectives 882

LOFT L2-5 experiment 884–886, 885*f*

parameter sensitivity 887, 888*f*, 889–890*t*

participants and used codes 883*t*

reference calculations 887

steps 882, 883*t*

used methods 882–884

Wilks' formula 884

Zion NPP 886, 887*f*

Best estimate plus uncertainty (BEPU) 834, 971

application status 911

attribute of calculation 914–915

Atucha-2 NPP 929*f*

bases and background 911

envisions for 913–921

historical perspective 911–912

nuclear reactor safety requirements 912–913

bounding approach 923

as civilization 920–921

definition 908, 913–914

DSA 131

elements and structure, for accident analysis 921, 924–926,
931–932

concerned events 926–927

resources typologies 927

roadmap 928–931

selected terms 921–923

emergency operating procedures 938

as exploitation of database 920

features and elements 915, 916*f*

institutional documents 911

in LBLOCA 932

- licensing framework 909
- in NPP 907
- nuclear thermal-hydraulics 30–31
- objectives 910–911
- realistic assumptions 923
- reliability analysis 923
- safety assessment calculation 915t
- safety-licensing demonstration 932
 - ALARA principle 937
 - DSA and PSA integration 933–936
 - FSAR 937–943
- scientific and technological literature 912
- structure 910–911
- SYS-TH code 78–79, 79f, 907–908
- Beyond design basis accident (BDBA) 122, 642, 921, 957
- Blind ISP 842–843
- Blowdown rewet *See* Early rewet
- Boiling heat transfer
 - advantage 420
 - boling curve
 - factors influencing 425, 425f
 - Leidenfrost temperature 430–431t, 432
 - minimum film boiling temperature 426–432, 427–428f
 - NC hysteresis phenomenon 425–426, 425f
 - Nukiyama curve 424, 424f
 - vapor bubble structure and 426, 427f
 - convective
 - film boiling, and superheated vapor flow 459–462, 460f
 - inverse-annular flow boiling and dispersed-annular flow
 - film boiling 462–470, 463f, 468t
 - modes, flow channels 448–454, 450–453f
 - porous structures under forced convection conditions 458–459, 459f
 - subcooled boiling, developing region 455–456, 456f
 - subcooled nucleate boiling, onset of 454–455
 - subcooled to saturated region 456–458, 458f

enhancement in 420–421

film pool

rapid cooling, hot bodies 444–448, 446*f*, 449*f*

stationary 443–444, 445*t*

good wettability liquids 422–423

nucleation pool

bulk boiling 440–443, 441*t*, 443*t*

coated porous surface 439–440, 439–440*f*

estimate correlations 437–438

factors influencing 434–436, 434–435*f*

hydrodynamic theory of similarity 438–439

mechanism 433–434

surface deposition

composition and thermal conductivity 473–474

low resistance and heat transfer coefficient 474–475

processes and mechanisms 470–473, 472*t*, 472–473*f*

types of 423–424

unstable modes

instability, channel boiling 477–478

types of 475–476, 475*f*

unstable pool boiling 476–477, 476*f*

vapor bubble formation 421–422

Boiling water reactor (BWR) 596, 850, 1104

cross reference matrix

LOCA 322–323*t*

transients 324–325*t*

entrainment and de-entrainment 607, 610

Fukushima-Daiichi accident 1112–1113

ITF 838

La Salle and Oskarshamn events 1112

SBLOCA in 1003–1004*f*

separators and dryers 628, 628–629*f*

TT accident scenario 1079*f*

Boron

phenomenon-related information 1071–1072, 1071–1072*f*,
1072*t*

risk 1020

topics and facts 1070–1071

transport 1070

Break flow models

in branch 613, 614*f*

side break 617–618, 617*f*

in system codes 618–619

upward oriented break 616, 616*f*

vapor pull through 614–616, 615–616*f*

Break opening time (BOT) 76, 934, 980, 983*t*, 994, 998–999*t*

Bubbly flow regime, stability of 694–696

Buckingham theorem 116–117, 620–622

Buoyancy forces 785

Burnout 108, 295, 423, 449–451, 452*f*, 479 *See also* Critical heat flux (CHF)

Burnup (or burn-up) -effects- 15–16, 53–54, 76, 106, 124, 308, 419, 746*f*, 913, 918, 926–927, 930–932, 972, 986, 992, 1041–1042, 1084, 1104–1105, 1144

BWR *See* Boiling water reactor (BWR)

C

Calandria tube 1018*f*

Canadian deuterium uranium (CANDU) reactors

AM action in 1039, 1039*f*

calculation 993

LBLOCA 994

LOOSP accident scenario in 1017–1018*f*

NC performance 1053, 1055

Carry over (for liquid) 509, 518, 610, 630, 632, 962–963*t*, 997, 1063, 1063*t* *See also* Entrainment/de-entrainment

Carry under (for steam) 610, 630–631, 962–963*t*

CASL virtual reactor 761*f*

CATHARE code *See* Code for Analysis of THERmal hydraulics during Accident of Reactor and Safety Evaluation (CATHARE) code

Cavitation 15–16, 65, 303, 633–634, 634*f*, 784, 985, 987–988, 995, 1011, 1114–1116*t*, 1143

Cavitation at sharp edge 1011

CCFL *See* Counter-current flow limitation (CCFL)

CCVM *See* Computer code validation matrices (CCVM)

Cell to cell mapping technique 933

Centrifugal pumps

- available data for 621*t*
- design characteristics 622*f*
- modeling in system codes 623*f*
- performance head vs. entrance void relationship 626*f*

CET *See* Core exit thermocouples (CET)

CFD *See* Computational fluid dynamics (CFD)

CFD scaling 749, 817–818

Check valves 634

Chernobyl accident 1104, 1142–1143

- chronology of events 1117–1120, 1118–1119*t*
- RBMK of 1110–1112
- reactivity excursion 1133, 1134*f*

CHF *See* Critical heat flux (CHF)

Choked flow

- with 1-D two-fluid modeling 683–686
- experiment, two-phase 681–682
- prediction by system codes 682–686
- in single-phase gas flow 671–676
- in two-phase steam water flow 676

CHT *See* Conjugate heat transfer (CHT)

CIAU *See* Code with Internal Assessment of Uncertainty (CIAU)

COBRA-TF 720–721

- core moderator density distribution 669*f*

Code for Analysis of THERmal hydraulics during Accident of Reactor and Safety Evaluation (CATHARE) code 648–652, 657*f*, 660–661, 666, 683, 684*f*, 685, 690, 695–696, 698, 703–704, 707*f*

- CATHARE 2 code, flow regime map 561, 562*f*

Code scaling applicability and uncertainty (CSAU) 601–602, 865–867

- geometrical parameters 605*t*
- in NPPs 867

Code-user qualification 835

Code with Internal Assessment of Uncertainty (CIAU) 871–872, 884

Cold legs (CLs) 686–689

Collapsed liquid level (CLL) 1014

Complex heat transfer

- accommodation factor 418–420

- contact resistance 416

- principles of calculation 412–413

- radiation and

 - conduction 413–415, 414*f*

 - convection 415–416, 415*f*

- rough surfaces 416–418, 417*f*

Computational fluid dynamics (CFD) 596, 732–735, 864 *See also*

Computational multifluid dynamics (CMFD)

- accumulators 633

- analysis procedure 735, 750–751, 751*f*

- applications 738, 764–780

 - data evaluation 775–777

 - nontraditional approach 775

 - in nuclear technology 746*f*

 - to nuclear thermal fluids problems 777–805

 - to single-phase thermal fluids problems 780–782

- assessment 761–763

- balance equations 174

- best practice guidelines (BPG) 763–764

- boundary and initial conditions 736

- capabilities of steady RANS 740

- code 742–743

 - to NRS problems 809

 - vs. SYS-TH code 743

- coupling 759–760, 806–807, 807*t*

 - assessment matrix 808–810

 - deficiencies in assessment 809–811

 - insights into the assessment process 812–817

 - verification matrix 811

- definition 742

- demonstration simulations 812

EPRI round robin 741
experiments 763
geometrical simplification 735
limitations of steady RANS 740–741
methodology development and validation 813–817, 813*f*
modeling scales 91
multiphase CFD method 760*f*
NTF 744
 applications 775
nuclear thermal-hydraulics 29
OECD/NEA/CSNI report 818–821
phenomenological issues 785
physical models selection 752–755
problem definition and identification of CFD role 751–752
PWR rod bundle problem 764–775, 767*f*
refining mesh 736
role in nuclear thermal hydraulics 742–750
safety, design, and operational aspects in nuclear
technology 746*f*
scaling issue 817–818
sensitivity analysis 736
simulation strategy 735
single-phase model 737, 780–782
steady RANS turbulence modeling 785–790
stratification and buoyancy effects 785
synergy of efforts 775
SYS-TH 65–66
3D model classification 745, 759*f*
trade-offs in 775
turbulence 785–801
turbulence model *See* (Turbulence model)
turbulent situation characterization 757–759
two-phase model 737–738, 759, 782–784
uncertainty analysis 899
UQ for CFD calculation 763
validation 739–741, 807–817

- in computational simulation 810–811
 - and demonstration matrices 811–812
 - of experimental data 812
- verification and validation in 761, 762*f*
- Computational multifluid dynamics (CMFD)
 - deterministic interface 200
 - Eulerian fluid dynamic simulation approaches 196, 197*t*
 - factors influencing 199–200
 - filtered interface 200
 - LES with
 - applicability and degree of maturity 203, 204*t*
 - deterministic interface 201
 - hybrid 202
 - locality and universality 203
 - statistical interfaces 202
 - pseudo-DNS method 200–201
 - RANS method (U-RANS) 201
 - statistical interface 200, 200*f*
- Computer codes 848
 - reactor simulations 597
 - thermal-hydraulic 834
 - validation 836–847
 - counterpart and similar tests 844–847
 - input data 839
 - ISP 841–843
 - process 837–839
 - qualitative and quantitative assessment 840–841
 - user effects 843–844
 - verification 835–836
- Computer code validation matrices (CCVM) 957, 975
- Condensation curve 382–383, 383*f*
- Condensation heat transfer
 - coefficient of condensation
 - dependency of 380–381, 382*f*
 - drop-wise condensation 382, 383*f*

- temperature distribution 380–381, 381*f*

- condensation curve 382–383, 383*f*

- direct contact of phases

- dispersed liquid spray jet 397

- liquid subcooled jet 396–397

- nuclear reactor safety analysis 396

- subcooled liquid 396

- droplet-wise condensation 383–385, 384*f*

- enhancement of

- horizontal tubes 398, 398*f*

- ribbed and corrugated pipes 397–398, 398*f*

- film-wise condensation

- film flow regimes 385–386, 386*f*

- horizontal tubes and rod bundles 389–390, 390*f*, 392

- inside tube 392–393, 392–393*f*

- laminar flow 386–387

- laminar-wavy flow 387–388, 389*f*

- metal vapor 391

- superheated and wet vapor 390

- turbulent-wave flow 388–389

- vertical surface 391, 391*f*

- pure steam 379–380, 380*f*

- vapor-gas mixture 393–395, 394–395*f*

Condensation induced water hammer (CIWH) 15–16, 341, 662–665, 1020

Conduction heat transfer

- composite and dispersed media

- bi-component regular structure system 378, 378*f*

- quasihomogeneous dispersion medium 377

- transverse and longitudinal arrangement 377–378, 377*f*

- conditions of uniqueness 366

- differential equation 365–366

- heat exchange and 363–365, 364*f*

- mechanisms 362–363, 363–364*f*

- steady-state process

- critical diameter, thermal isolation 369–370, 369*f*

- cylindrical wall 367–368
- plane wall 367
- simple form in one-dimension 366
- spherical geometry 368–369
- temperature dependence, thermal conductivity 370–371, 370–371*f*, 371*t*
- temperature field and heat flux 361–362, 361*f*, 362*t*
- transient
 - heating/cooling 372–373, 372*f*, 374*t*
 - periodic changes, temperature 375–376
 - regular thermal regime 375, 376*f*
 - surface temperature 374–375
- Conjugate heat transfer (CHT) 773
- Conservative accident analysis 912–913, 915–916
- Constitutive equations
 - CATHARE 2 553
 - continuity equations 551
 - definition 550
 - energy equation of k-phase 551
 - flow regime map
 - annular-mist regime 555
 - bubbly flow 554–555
 - CATHARE 2 code 561, 562*f*
 - definition 554
 - horizontal flow 555, 555*f*, 559–561, 560*f*
 - IATE 563–564
 - inverted flow regimes 555, 556*f*
 - limitations 563
 - old flow regime maps 555–556, 557*t*
 - post-CHF flow 554
 - pre-CHF flow 554
 - RELAP5 556–557
 - TRACE code 561–562, 562*f*
 - vertical flow 554, 554*f*, 557–559
 - interfaces, two-fluid model 550, 550*f*
 - interfacial drag

- drag coefficient method 574–575
- drift-flux method 574–575
- interfacial heat and mass transfer
 - bubbly flow regime 569
 - in bulk/thermal boundary 564–565, 565*f*
 - IAC 567, 568–569*t*, 570, 573*t*
 - IHTC 567–568, 570, 571–572*t*, 574*t*
 - Nukiyama-Tanasawa distribution function 567
 - RELAP5 code 565, 567–568, 568–569*t*
 - slug flow regime 569–570
 - TRACE code 570, 573–574*t*

momentum equation 551

RELAP5 553

TRACE 553

two-fluid six-equation model 549–550

unequal-velocity, unequal temperature 587

validation of

- correlations 586

- limitation 586

- SET validation matrix 586–587

wall friction

- friction factor approach 581

- single-phase flow 582–583

- two-phase flow 583–585

wall heat transfer

- boiling region 579–580

- condensing region 580–581

- convection region 578–579

- RELAP5 578, 579*f*

Containment performance, accident scenarios 1041, 1043–1047, 1045–1046*f*, 1047*t*

Control rod ejection (CRE)

- phenomena connection 1032–1033, 1032*f*, 1033*t*

- in PWR with UTSG 1032*f*

- qualitative characterization 1030–1031

- quantitative characterization 1031–1032

Control valves 634

Convective boiling heat transfer

capillary-porous surfaces 458–459, 459*f*

critical heat flux 449–451

film boiling and superheated vapor flow

dispersed-annular flow 461

dispersed two-phase flow 461

inverted annular flow 461

minimum film boiling temperature 461

wall temperature dependence 460, 460*f*

in forced convection 451, 452*f*

inverse-annular flow boiling and dispersed-annular flow film boiling

annular channels 465

components 462

in crisis zone 464–465

dispersed droplets-vapor mixture flow 463–464

entrance region, crisis zone 465–466

radiation 467

rod bundles 465

simplified calculation method 467–468, 468*t*

spacer elements 466

superheated steam 469–470

superheated zone, helical coil pipes 468–469

temperature distribution 463, 463*f*

single-phase flow 448–449

subcooled nucleate boiling

at low pressures 455–456, 456*f*

onset of 454–455

subcooled to saturated region 456–458, 458*f*

two-phase flow 448–449, 451*f*

vapor quality 451–452, 453*f*

Core exit thermocouples (CET) 1038

Core Make-up Tanks (CMTs) 992

Counter-current flow limitation (CCFL) 596, 653, 838

analytical thermal hydraulics 111–112

- BCL and UPTF 604, 605*t*, 606*f*
- CCF 515–516
- CREARE 604, 605*t*, 606*f*
 - definition 515–516
 - determination 704, 704*f*
 - distortion problem 707
 - flow field in 602–603, 603*f*
 - Kutateladze correlation 604
 - LBLOCA 602–603
 - occurrence 515–516
 - PKL III test 516–518, 517*f*
 - prediction 702–704, 703*f*
 - PWRs 604
 - vs. reactor steam mass flow 863*f*
 - SG U-tubes 516
 - steady-state tests 855
 - UPTF test 516
 - validation process 838
 - Wallis correlation 603–604
- Counterpart (CP) tests 117, 845–847
 - in PWR 847
 - SB-LOCA database 846*f*
- CRE *See* Control rod ejection (CRE)
- Critical flow
 - definition 346–347
 - LOCA 347
- Critical flow models
 - Fanno equations 599
 - RELAP5 and TRACE models 602
 - two-phase flow in 598
- Critical heat flux (CHF) 1041
 - convective boiling heat transfer 449–451
 - evaluation 1042
 - LB-LOCA 506
 - phenomenon-related information 1042, 1043*t*

- post flow 554, 559
- pre flow 554, 558–559
- spacer grids and 513–515
- in test facility 1043f

Crud (and oxide) 53–54, 145, 471, 471*np*, 531, 738, 744–745, 759–760, 768, 972, 1041–1042, 1070–1071, 1084

CSAU *See* Code scaling applicability and uncertainty (CSAU)

D

DBA *See* Design basis accident (DBA)

DDES model 757

Decay heat 66, 90, 106, 124, 263, 278–279, 286, 298–299, 336, 341–343, 350, 610, 1056

Deep water waves 697

Defense in depth (DiD) 966, 968

- ITF 69

- safety concepts 126

- SYS-TH 49

Delayed equilibrium model (DEM) 686

Departure from nucleate boiling (DNB) 55, 60*t*, 91, 108, 255–257*t*, 295, 310*t*, 322–323*t*, 327*t*, 451, 452*f*, 460–463, 506, 662, 744–745, 746*f*, 747–748*t*, 764–768, 783, 940, 962–963*t*, 995–996, 1008–1009, 1042, 1043*t*, 1073, 1143

Deposit(s) 239, 242, 426, 433, 435–436, 442–443, 454–455, 470–472, 471*np*, 472–473*f*, 474–475, 531, 760, 1042, 1070

DES *See* Detached eddy simulation (DES)

Design basis accident (DBA) 642, 644, 666–667, 921, 968–970, 972–973

- classification 120

- licensing basis 119

- phenomenology

- HPIS 120–121

- LBLOCA 120

- LOOP scenario 121

- loss of FW 121

- MSLB accident 122

- SBLOCA 120–121

- SBO scenario 121–122

- SGTR 122
- TPCF 597
- uncertainty and sensitivity evaluation 882
- Design basis (DB) and licensing basis
 - acceptance criteria/design criteria 118
- BDBAs 122
- DBA
 - classification 120
 - high pressure injection system 120–121
 - LBLOCA 120
 - loss of FW 121
 - loss of offsite power scenario 121
 - main steam line break accident 122
 - SBLOCA 120–121
 - SGTR 122
 - station blackout scenario 121–122
- definition 119
- quality attributes/availability/reliability 119–120
- structures, systems and components (SSCs) 118
- verification and validation 123
- Detached eddy simulation (DES) 756, 805
 - use of 799
 - variants of 799
- Deterministic Dynamic Event Tree (DDET) 933
- Deterministic & probabilistic accident analysis 922
- Deterministic safety analysis (DSA) 641, 907–908, 919, 922, 1019
 - BE codes 130
- BEPU
 - and accident role 916–919
 - methodology 131
- codes and methodologies 130
- conservative methodology 130
- deterministic safety analysis 129
- FSAR 132
- IAEA 933–936

- integration of 933–936
- inverse methods 131
- NPPs 837
- OECD/NEA/CSNI 933–936
- PSA applications 934–936
- risk-informed regulation 922, 936
- safety analyses 129
- safety margin/safety limit 130
- SYS-TH 834–835
- DiD *See* Defense in depth (DiD)
- Direct numerical simulation (DNS) 756
- Direct numerical solution (DNS)
 - pseudo method 200–201
 - single-phase modeling 183
- Dispersed-annular flow film boiling
 - annular channels 465
 - components 462
 - in crisis zone 464–465
 - dispersed droplets-vapor mixture flow 463–464
 - entrance region, crisis zone 465–466
 - radiation 467
 - rod bundles 465
 - simplified calculation method 467–468, 468t
 - spacer elements 466
 - superheated steam 469–470
 - superheated zone, helical coil pipes 468–469
 - temperature distribution 463, 463f
- Double-blind ISP 842–843
- Drag coefficient method 574–575
- Drift-flux model 703
 - balance equations 227–229
 - interfacial drag 574–575
 - two-phase flow developments 103
- Droplet-wise condensation 383–385, 384f
- Dry-out 95, 100, 106, 108, 120–121, 124, 260, 449–451, 452f, 460–462, 534, 720–722, 783, 845, 876, 971, 1006, 1009, 1016, 1042,

1068t, 1114–1116t, 1133, 1138, 1140–1141 *See also* Critical heat flux (CHF)

DSA *See* Deterministic safety analysis (DSA)

Dynamical system scaling (DSS) 851

E

Early core rewet *See* Early rewet

Early rewet 987

ECCS *See* Emergency core cooling system (ECCS)

Element 1 152

Element 2

- bottom-up scaling approach 155

- CFD software 155

- importance 153

- plant operating envelope 152, 153f

- power-to-volume scaling 154

- scaled experimental and prototype envelopes 157–158, 157f

- top-down scaling approach 155

- validation data 153–154, 154f

- validation matrix approach 156, 156f

- validation pyramid 156–157, 157f

Element 3 158

Element 4

- bottom-up code adequacy 161–163

- code and calculation documentation 159

- code verification 159

- reduction of numerical error 160–161

- top-down code adequacy 163–164, 164t

Elevation pressure drop 504

Embedded LES (ELES) model 757

Emergency core coolant (ECC) injection model 654

Emergency core cooling system (ECCS) 604, 853–854, 914, 961, 972, 989

- BEPU process 923

- design/construction for 956

- downcomer counter-current to steam flowing 858–859

- ECCS-core-bypass 606–607
- injection flow 987–988
- NPSH 932
- TRAC-PF1 prediction 606*f*
- Emergency operating procedures (EOP) 123–124
- Empirical approach, with dimensional analysis 701
- Engineered safety features (ESF) 914
- Enhanced HT *See* Augmentation, HT
- Entrainment/de-entrainment
 - BWR 607, 610
 - nuclear reactor system 607–610, 609*f*
 - thermal-hydraulic phenomena
 - core 272
 - downcomer 273–274
 - hot leg with ECC injection 274–275
 - parameters 271
 - SG mixing chambers 274
 - SG tubes 274
 - source of 271
 - upper plenum 272–273
- EPRI CFD round robin 741, 764–775
- Equal velocities equal temperatures (EVET) *See* Homogeneous equilibrium model (HEM)
- Eulerian fluid dynamic simulation approach 782–783*t*
- Evaluation model (EM) 151
- Evaluation Model Development and Application Process (EMDAP) 150–151, 151*f*
- Experimental data base (EDB) 69
- Experimental thermal hydraulics
 - analytical support 114
 - CP tests 117
 - databases 114
 - FSA 116
 - H2TS 116
 - IET/ITF 114
 - Ishii three-level scaling approach 116

- Kv-scaled calculation 117–118
- power-to-volume scaling 115
- scaling 115
- scaling distortion 116–117
- SET 113–114
- system codes 117
- Explicit algebraic Reynolds stress models (EARSMS) 772, 788–789
- Explicit algebraic stress model (EASM) 788

F

- Feedwater line break (FWLB) accident scenario 1024
 - phenomena connection with 1026–1027*f*, 1028–1029, 1028*t*
 - in PWR with UTSG 1025*t*, 1026–1027*f*
 - qualitative characterization 1024–1025
 - quantitative characterization 1025–1028
- 3-Field models, system codes
 - gas-continuous liquid-droplets 239–240*b*
 - LBLOCA simulation 238–239
 - 1-D 3-field equations 239
- Film boiling and superheated vapor flow
 - dispersed-annular flow 461
 - dispersed two-phase flow 461
 - inverted annular flow 461
 - minimum film boiling temperature 461
 - wall temperature dependence 460, 460*f*
- Film pool boiling
 - rapid cooling, hot bodies
 - boiling curve 444–446, 446*f*
 - components 447
 - cooling mode 446–447, 446*f*
 - heat transfer coefficient 448, 449*f*
 - stationary 443–444, 445*t*
- Film-wise condensation
 - film flow regimes 385–386, 386*f*
 - horizontal tubes and rod bundles 389–390, 390*f*, 392
 - inside tube 392–393, 392–393*f*

- laminar flow 386–387
- laminar-wavy flow 387–388, 389*f*
- metal vapor 391
- superheated and wet vapor 390
- turbulent-wave flow 388–389
- vertical surface 391, 391*f*
- Final safety analysis report (FSAR) 132, 908
 - BEPU for 937–943
 - plant-specific PSA applications 917
- Flow limiters 634
- Flow regime map 698–700
 - annular-mist regime 555
 - bubbly flow 554–555
 - CATHARE 2 code 561, 562*f*
 - definition 554
 - for horizontal flow 698, 699*f*
 - annular-mist to mist-pre-CHF transition 560
 - bubbly-slug transition 560
 - RELAP5 559–560, 560*f*
 - schematic representation 555, 555*f*
 - stratified flow 560–561, 561*f*
- IATE 563–564
- inverted flow regimes 555, 556*f*
- limitations of 563, 700
- old flow regime maps 555–556, 557*t*
- post-CHF flow 554
- pre-CHF flow 554
- RELAP5 556–557
- TRACE code 561–562, 562*f*
- transition criteria 699–700
- vertical flow
 - post-CHF 559
 - pre-CHF 558–559
 - RELAP5 554*f*, 557
 - schematic representation 554, 554*f*

- Flow reversal, SG U-tubes
 - characteristic flow curves 527
 - heterogeneous behavior 525, 526f
 - NC 524–525
 - PKL test 525, 527f
- Fluid density 175, 263, 538, 576
- Fluid properties 268, 346, 388, 461, 563, 602, 752, 817
- Fluid viscosity 263, 582
- Fouling *See* Deposit(s)
- Fourier (law) 22–23, 105, 178, 183, 361–362
- Fourier transform-based method (FTBM) 841, 884
- Fractional change metrics (FCM) 850–851
- Fractional rate of change (FRC) 850–851
- Fractional scaling analysis (FSA) 116, 850–851
- Friction pressure drop
 - applications of 500–501
 - single-phase flow
 - adiabatic 497–498
 - distributed 496–497
 - two-phase flow
 - homogeneous model 499
 - pressure gradients 498
 - separated flow model 499–500
- FSAR *See* Final Safety Analysis Report (FSAR)
- Fuel channel blockage (FCB), accident scenario 1063
 - phenomena connection 1064–1065, 1064–1065f, 1065t
 - qualitative characterization 1063–1064
 - quantitative characterization 1064
 - in RBMK 1064–1065f, 1068t
- Fukushima-Daiichi accident 1105–1106, 1144–1145
 - BWR of 1112–1113
 - chronology of events 1123–1130, 1124–1129t
 - PHW 1139–1140f
 - SBO and LOOSP 1138–1141, 1139–1140f
- Fully empirical approach, closure relation 701

G

- Geometric discontinuity, pressure drops at *See* Local pressure drop
- Glaeser-correlation 857
- Grid-induced separation (GIS) 799
- GRS-uncertainty method 60*t*, 80–81*t*, 859, 867–871, 875*t*, 897

H

Heat transfer (HT)

augmentation

- agitation of the swirl flow 479–482, 480–481*f*
- method of 478–479
- porous structures 482, 482*f*
- superhydrophilicity 483, 484*t*

boiling

- advantages of 420–421
- boiling curve 424–432, 424*f*, 427*f*, 430–432*t*
- heated surface, onset condition 421–423
- types of 423–424

complex

- accommodation factor 418–420
- contact resistance 416
- principles of calculation 412–413
- rough surfaces 416–418, 417*f*

condensation

- coefficient of condensation 380–382, 381–383*f*
- condensation curve 382–383, 383*f*
- direct contact of phases 395–397
- droplet-wise condensation 383–385, 384*f*
- enhancement of 397–399, 398*f*
- film-wise condensation 385–393, 386*f*, 389*f*
- pure steam 379–380, 380*f*
- vapor-gas mixture 393–395, 394–395*f*

conduction

- composite and dispersed media 376–379, 377–378*f*
- conditions of uniqueness 366

- differential equation 365–366
- heat exchange and 363–365, 364*f*
- mechanisms 362–363, 363–364*f*
- steady-state process 366–371
- temperature field and heat flux 361–362, 361*f*, 362*t*
- transient 372–376, 372*f*, 374*t*, 376*f*
- convective boiling
 - film boiling, and superheated vapor flow 459–462, 460*f*
 - inverse-annular flow boiling and dispersed-annular flow
 - film boiling 462–470, 463*f*, 468*t*
 - modes in flow channels 448–454, 450–453*f*
 - porous structures under forced convection conditions 458–459, 459*f*
 - subcooled boiling, developing region 455–456, 456*f*
 - subcooled nucleate boiling, onset of 454–455
 - subcooled to saturated region 456–458, 458*f*
- definition 363, 364*f*
- enhancement 348
- film pool boiling
 - rapid cooling, hot bodies 444–448, 446*f*, 449*f*
 - stationary 443–444, 445*t*
- nucleation pool boiling
 - bulk boiling 440–443, 441*t*, 443*t*
 - coated porous surface 439–440, 439–440*f*
 - estimate correlations 437–438
 - factors influencing 434–436, 434–435*f*
 - hydrodynamic theory of similarity 438–439
 - mechanism 433–434
- radiation
 - in absorbing and emitting environments 411–412
 - arbitrary arrangement 409–410
 - body and shell 410
 - characteristics 407–409, 408*f*
 - conduction and 413–415, 414*f*
 - convection and 415–416, 415*f*
 - Planck's law 402–406, 403*f*, 403*t*, 406*f*

- principles 399–402, 400–401*f*
- surface deposition boiling
 - composition and thermal conductivity 473–474
 - low resistance and heat transfer coefficient 474–475
 - processes and mechanisms 470–473, 472*t*, 472–473*f*
- unstable boiling modes
 - instability of channel boiling 477–478
 - types of 475–476, 475*f*
 - unstable pool boiling 476–477, 476*f*
- Heat transfer coefficient (HTC)
 - multi-D heat transfer coefficient surface 63–64
 - nuclear thermal-hydraulics 22
- Heat transfer deterioration (HTD) 348
- Heat transfer developments
 - heat conduction 105–106
 - heat convection
 - CHF/boiling crisis/post-CHF convection modes 108
 - definition 106
 - heat transfer coefficient 106
 - pre-CHF convection modes 107, 107–108*f*
 - heat radiation 109
 - importance of 104
 - 1D/3D option 105
 - power generation 105
 - Prandtl and Nusselt numbers 108–109
 - scope of 104
- Heavy water 8, 34*ge*, 332, 344–345, 642, 835, 928, 957, 982
- HEM *See* Homogeneous equilibrium model (HEM)
- Hierarchical two-tiered scaling (H2TS) 613, 850, 852
 - experimental thermal hydraulics 116
- High-performance computing (HPC) experiment 777
- High performance light water reactor (HPLWR)
 - vs.* LWR 344
 - plant characteristics 344
 - safety analysis study 344

- Homogeneous equilibrium model (HEM) 598, 601, 677–680
 - 1-D 226–227*b*
 - predictive capabilities 227
 - single-phase liquid to single-phase steam 226–227
 - two-phase flow developments 102–103
- Homogeneous frozen model 676
- Homologous curves (for pump performance) 112, 620–622, 625, 1076
- Horizontal flow modeling, with two-fluid model 690–691
- Horizontal flow regime map
 - annular-mist to mist-pre-CHF transition 560
 - bubbly-slug transition 560
 - RELAP5 559–560, 560*f*
 - schematic representation 555, 555*f*
 - stratified flow 560–561, 561*f*
- Hot legs (HLs) 686–687, 689
- H2TS *See* Hierarchical two-tiered scaling (H2TS)
- Hutze (better, hütze) nozzle 274, 284
- Hybrid RANS-LES 805
 - and LES 803
 - method 798–799
 - model 796

I

- IBLOCA *See* Intermediate break LOCA (IBLOCA)
- Immersed boundary method (IBM) 775
- Industrial code, SYS-TH code 647
- Inertia (of liquid droplets) 15–16, 24, 70*f*, 95, 98, 169, 206–207, 223–224, 231, 268–273, 299, 303–304, 365, 385–386, 388, 389*f*, 396, 506, 619, 627, 630, 644, 651, 654, 678–679, 691, 712, 850, 956, 987, 1077
- Input uncertainties 882–883, 892*f*
- Instability of channel boiling 476*f*, 477–478
- Integral effects test (IET) 114, 707–708, 711
 - distortion in 706–707
- Integral phenomena 980
- Integral system tests

- APEX test facility 853–854
- ECCS 853–854
- LOBI programme 852
- PWR and characteristics 853t
- thermal-hydraulic ITF 852–853
- UPTF test facility 852
- Integral test facility (ITF) 114, 838, 1108
 - BWRs 838
 - light water reactor 872
 - PWRs 838
 - SYS-TH code application 924–925
 - thermal-hydraulic 851
- Integral tests (ITs) 837
 - uncertainty and sensitivity methods 882
- Interfacial area concentration (IAC)
 - IHTC 567
 - Nukiyama-Tanasawa form 567
 - RELAP5 code 567, 568–569t
 - TRACE code 570, 573t
- Interfacial area transport equation (IATE) 563–564
- Interfacial drag
 - drag coefficient method 574–575
 - drift-flux method 574–575
- Interfacial friction 577, 586–587, 696–697
- Interfacial heat transfer coefficient (IHTC)
 - bubbly flow regime 569
 - complications 568
 - IAC 567
 - RELAP5 code, correlations 570, 571–572t
 - slug flow regime 569–570
 - TRACE code, correlations 570, 574t
- Interim Acceptance Criteria for ECCS 54
- Intermediate break LOCA (IBLOCA) 995
- Intermediate Heat Exchanger (IHE) 1053
- Intermediate legs (ILs) 686–688

Internal pump 962–963*t*, 969*t*, 975, 982, 1035, 1036*t*, 1036*f*, 1037

International Atomic Energy Agency (IAEA) 6, 16, 25, 46, 57, 60–61, 60*t*, 69, 71, 75*f*, 76, 123, 126–129, 132, 246–247, 249–250, 332–334, 344–345, 500, 866, 868, 897, 911, 914–915, 922, 924, 933–936, 938, 974–975, 1086, 1088, 1107–1108

International standard problem (ISP) 113

blind ISP 842

double-blind ISP 842–843

open ISP 842

semi blind ISP 843

specifications 841–842

thermal-hydraulic 844

UMS 874–875

validation activities 841

International validation, uncertainty methods 873–896

BEMUSE programme 882–894

PREMIUM programme 894–896

UMS 874–881

Interphase thermal resistance 384–385, 384*f*

Inverse-annular flow film boiling

annular channels 465

components 462

in crisis zone 464–465

dispersed droplets-vapor mixture flow 463–464

entrance region, crisis zone 465–466

radiation 467

rod bundles 465

simplified calculation method 467–468, 468*t*

spacer elements 466

superheated steam 469–470

superheated zone, helical coil pipes 468–469

temperature distribution 463, 463*f*

Ishii three-level scaling approach 116

Isolation Condenser (IC) 335–336*t*, 336, 341–342, 708, 962–963*t*, 1003, 1004–1005*t*, 1052, 1056, 1113, 1123, 1124–1125*t*, 1138, 1139–1140*f*, 1144

ISP *See* International standard problem (ISP)

ITF *See* Integral test facility (ITF)

J

Jet impingement 15–16, 144, 494, 980, 1044

Jet pumps 619

Jet thrust 15–16, 1044

K

Kelvin-Helmholtz instability 664–665, 689, 693, 694*f*, 697

K-factor 62–63

Kolmogorov (dissipative) scale 181–183, 187, 201, 803

Kursk RBMK Nuclear Power Plant 1104

Kutateladze correlation 604

Kutateladze-type flooding equation 857, 862

Kv-scaled 68*f*, 117–118, 924–925

L

Large-break LOCA (LBLOCA) scenario 602–603, 649, 689, 713, 722–723, 908, 1103

in BEPU 932

blowdown (BD) and refill (RF) phases

CHF 506

reactor coolant pump 506

reactor pressure vessel 506

stagnation point 504–506

in CCFL 602–603

Element 1 152

long-term cooling

boron deposition and LS refilling 513, 514*f*

boron enrichment process 513

emergency core cooling injection 511–513

phenomena connection with accident scenario 984*f*, 989*f*, 990–994, 990–991*t*

PWR 667

in PWR with UTSG 983*t*, 984*f*, 989*f*

qualitative characterization 980–982

quantitative characterization 982–989

- in reactors other than PWR with UTSG 994
- reflood (RE) and
 - early phase 507
 - emergency core cooling injection 507–508
 - PKL II 507, 507*f*, 509, 510*f*
- spacer grids and CHF 513–515
- steam binding
 - definition 509
 - FLECHT-SEASET experiments 511
 - PKL II 511, 512*f*
- test of LOFT facility 656, 656*f*, 709*f*
- Large eddy simulation (LES) 775, 776*f*, 794–797, 804*f*
 - applicability and degree of maturity 203, 204*t*
 - core flow region in 803
 - cost of outer and inner layers in 804
 - deterministic interface 201
 - hybrid 202
 - and hybrid RANS-LES 803
 - locality and universality 203
 - model 756, 757*f*
 - statistical interfaces 202
 - wall-modeled 794–795, 797, 805
 - wall-resolved 805
- Large-scale test facility (LSTF), SBLOCA in 1002, 1003*f*
- La Salle events 1104–1105, 1143–1144
 - BWR of 1112, 1137*f*
 - chronology of events 1120, 1121*t*
 - thermal-hydraulics analyses 1135*t*, 1136, 1137*f*
- Lattice Boltzmann method (LBM) 775, 776*f*
- LBLOCA scenario *See* Large-break LOCA (LBLOCA) scenario
- LBM *See* Lattice Boltzmann method (LBM)
- LES *See* Large eddy simulation (LES)
- LEVM *See* Linear eddy viscosity models (LEVM)
- Licensing framework, BEPU
 - acceptance criteria 909

- conservative accident analysis 915–916
- procedures 926
- Licensing needs 75–76, 75*f*
- Light water reactor (LWR) 872
 - nuclear fuel 610
- Linear eddy viscosity models (LEVM) 785–788, 802
 - vs. RSM 802
- Linear stability analysis 693
- Licensing requirements 17, 21, 45, 147, 266, 874, 881, 926
- LLM *See* Logarithmic law mismatch (LLM)
- LOCA *See* Loss of coolant accident (LOCA)
- Local form loss coefficients 62–63
- Local pressure drop
 - area changes
 - single-phase flow 502–503, c502*f*
 - two-phase flow 503
 - Reynolds number and void fractions 503
- Locked rotor (resistance) 623
- LOFT L2-5 test 882, 884–886
 - uncertainty analysis results 885*f*
- LOFW accident scenario *See* Loss of feed water (LOFW) accident scenario
- Logarithmic law mismatch (LLM) 796
- Long-term cooling 987–988, 1008
- Look-up table for CHF 63, 108, 111, 124, 701
- Loop seal clearing (LSC)
 - definition 522–523
 - IB-LOCA 521–522
 - PKL test 523, 523*f*
 - SB-LOCA 521–522
 - two-phase flow developments 101
 - UPTF test 524, 524*f*
- LOOSP *See* Loss of on-site and off-site power (LOOSP)
- Loss of component cooling service water (LCC/SW) 1073–1074, 1076*t*
- Loss of coolant accident (LOCA) 597, 602–603, 671, 686–687, 841,

1103

- blowdown 100
- classification 981–982
- IB-LOCA 521–522
- Nahavandi scaling principle 849–850
- PREMIUM 894
- reflood 100
- rewet 100
- SB-LOCA 521–522
- uncertainty methods 882
- uncovered fuel 610

Loss of feed water (LOFW) accident scenario

- LOFW-SBLOCA, Three Mile Island accident 1131–1133, 1132*f*
- phenomena connection with 1010–1011, 1010*f*, 1011*t*
- in PWR with UTSG 1007–1008, 1009*t*, 1010*f*
- qualitative characterization 1008
- quantitative characterization 1008–1009

Loss of flow accident (LOFA) scenario 1072–1073

- phenomena connection with 1075–1076, 1075–1076*f*, 1076*t*
- in PWR with UTSG 1074*t*
- qualitative characterization 1073–1074
- quantitative characterization 1074

Loss of on-site and off-site power (LOOSP) accident scenario 1015

- in CANDU 1017–1018*f*
- Fukushima-Daiichi accident 1138–1141, 1139–1140*f*
- phenomena connection with 1016–1018*f*, 1018–1019
- in PWR with UTSG 1016–1017*f*, 1018*t*
- qualitative characterization 1015–1016
- quantitative characterization 1016–1017

Low pressure injection system (LPIS) 996

Low Reynolds number model 793

LSTF *See* Large-scale test facility (LSTF)

Lumped parameter models 103

M

Main steam line break (MSLB) accident scenario 1024

- phenomena connection with 1026–1027f, 1028–1029, 1028t
- in PWR with UTSG 1025t, 1026–1027f
- qualitative characterization 1024–1025
- quantitative characterization 1025–1028
- with SGTR 1060–1063, 1062f, 1063t
- MCP-trip accident scenario 1072–1073
 - phenomena connection with 1075–1076, 1075–1076f, 1076t
 - in PWR with UTSG 1074t
 - qualitative characterization 1073–1074
 - quantitative characterization 1074
- Measurement error or Experimental error 9, 27, 501, 503, 536, 540, 542, 746
- Mechanistic approach, closure relation 701
- Mechanistic separator model 628–629
- Medium-break LOCA (MBLOCA) *See* Intermediate break LOCA (IBLOCA)
- Mesh generator 770–771
- Method of Manufactured Solution (for Verification) 159, 811
- MHYRESA test 692, 693f
 - hot-leg entrainment test 688
- Mixing vane grids (MVGs)
 - bundle in NESTOR experiment 766f
 - problems characterization 770
- Moderator tank 74f, 1053, 1056
- Modern accident analysis
 - accident, definition 132
 - Chernobyl accident 133
 - classification and treatment 132–133
 - Fukushima accident 133
 - TMI-2 accident 133
- Monodispersed approximation, TIA
 - algebraic interfacial area 236
 - dispersed phase fraction 235
 - dynamic interfacial area modeling 236
 - predictive capabilities 238
- Multi-D heat transfer coefficient surface 63–64

Multiple pressure tube rupture (MPTR), accident scenario 1065–1066, 1112

phenomena connection 1068–1070, 1070*t*

qualitative characterization 1066

quantitative characterization 1066–1068

in RBMK 1067*f*, 1069*f*

Multiplier (two-phase flow) 22–23, 26, 59, 60*t*, 103, 498–500, 520–521, 530–531, 542, 544, 580, 583–585, 627*f*, 650, 683, 859, 889–890*t*

N

Nahavandi scaling principle 849–850

Natural circulation (NC)

ALWR 339

flow reversal 524–525

instability and

Ledinegg excursive instability mechanism 349–351

pseudoboiling PH 351

single-phase flow 349–351

at subcritical pressures 350–351

two-phase flow 349–351

target phenomena 247

two-phase flow developments 99

Natural circulation (NC), accident scenario 1041, 1052

in ATLAS test facility 1058*f*

characterization 1052–1053

complexity of 1053–1057

dual system 1053

loop configurations of nuclear systems 1053*f*

in LSTF test facility 1058*f*

performance in CANDU 1053, 1055

phenomena connection with accident scenario 1057–1060, 1057*f*, 1059*t*

in PWR with UTSG 1054*f*, 1057*f*

during SGTR 1023

stability issue 1056, 1056*f*

stop and restart calculated for PWR with UTSG 1071*f*

Natural DES 799

Navier-Stokes equation 737, 753, 775

NC *See* Natural circulation (NC)

Near-wall treatment, CFD 773

enhanced 794

of (U)RANS 792–794

vs. wall-resolved RANS 803

NESTOR experiment 764–765

advantages 768, 774

experimental data 768–769

limitations for the CFD validation 768–769

MVG bundle in 766*f*

Net Positive Suction Head (NPSH) 932, 956

Neutron flux, point kinetics 641

NLEVMs *See* Nonlinear eddy viscosity models (NLEVMs)

Nodalization concept, SYS-TH codes model 649–659

Nonlinear eddy viscosity models (NLEVMs) 771, 788–789

NPSH *See* Net Positive Suction Head (NPSH)

Nuclear accidents

databases 1107–1108

overview 1106–1108

Nuclear events

NPP systems and 1108–1130

thermal-hydraulics aspects of 1130–1145

Nuclear fuel behavior 1041, 1083–1084

phenomena connection with 1084–1085, 1085*f*, 1085*t*

topics and facts 1084

Nuclear power plants (NPPs) 596, 833, 955, 1108–1109

accident performances *See* (Accident scenarios)

accuracy & uncertainty 922–923

BE, computer codes 897

BEPu, for FSAR 907, 939

Chernobyl-4 events 1110–1112, 1117–1120, 1118–1119*t*

in CSAU 867

in DSA 837

- Fukushima-1 to-4 events 1112–1113, 1123–1130, 1124–1125*t*
- I&C modeling 925–926
- independence-of-the-analysis 909
- La Salle-2 and Oskarshamn-2 events 1112, 1120–1122, 1121–1123*t*
- LB-LOCA 886
- licensing applications 841, 897
- licensing framework 909
- NPP LB-LOCA 882
 - input uncertainties 892*f*
- parameters databases 925
- PIE 925
- radioactive releases 973–974, 1019
- risk evaluation 973
- SM 909
- special process models 635
- steam-supply system 834
- thermal-hydraulic system codes 848
- TMI-2 events 1109–1110, 1113–1117, 1114–1116*t*
- uncertainty analysis 887–888
- validation process 837–839

Nuclear power plants (NPPs) and thermal-hydraulics

- accident prevention and accident mitigation requirements 148
- calculational envelope 148, 149*f*
- design 145
- Element 1 152
- Element 2
 - bottom-up scaling approach 155
 - CFD software 155
 - importance 153
 - plant operating envelope 152, 153*f*
 - power-to-volume scaling 154
 - scaled experimental and prototype envelopes 157–158, 157*f*
 - top-down scaling approach 155
 - validation data 153–154, 154*f*

- validation matrix approach 156, 156*f*

- validation pyramid 156–157, 157*f*

- Element 3 158

- Element 4

- bottom-up code adequacy 161–163

- code and calculation documentation 159

- code verification 159

- reduction of numerical error 160–161

- top-down code adequacy 163–164, 164*t*

- EM 151

- EMDAP 150–151, 151*f*

- figures-of-merit 144–145, 150

- PIRT informed R&D process 148–150, 149*f*

- primary safety requirements 147

- requirement's 48–49, 146–147

- role of 146–147

- safety 145–148

- software tool selection and software development 164, 165*f*

- stages of 148–150, 149*f*

- Nuclear reactor

- core behavior 761*f*

- entrainment and de-entrainment 607–610, 609*f*

- thermal-hydraulic design of 956

- Nuclear reactor safety (NRS)

- demonstration of 956–957

- requirements

- BEPU applicability 912, 914

- licensing framework 909

- SM concept 940

- single-phase problem 745, 780–781*t*

- technology 641

- Nuclear system thermal fluids behavior, computational simulation of 810–811

- Nuclear technology 1102

- CFD applications in 746*f*

- CFD safety, design, and operational aspects in 746*f*

Nuclear thermal fluids (NTF)

CFD 744

problems 752

CFD applications to 777–805

difficulties in 745, 780

Nuclear thermal hydraulics 596

accident management and AMP 13–14

accident phenomenology 12–13

analytical thermal hydraulics

abrupt area change model 112

CCFL 111–112

choked flow model 111

closure laws/constitutive equations 111

components 112

engineering factors 110

heat transfer correlations/look-up tables 111

ISPs 113

main code 111

nodalization/nodalization diagram 113

nuclear factors 109

system codes 110–111

user effect/good practices 113

user-specified coefficients 111–112

balance equations 24–25

BEPU approach 30–31

CFD codes 29

CFD role in 742–750

challenges 32

chemistry 15

components

accumulators 632–634, 633–634^f

coolant pumps 619–627, 621^t, 622–623^f

separators and dryers 628–632, 628–629^f, 631^t

valves 634

constitutive equations 27–28

- containment and RCS 11–12
- DBA envelope 31
- design basis and licensing basis
 - acceptance criteria/design criteria 118
 - BDBAs 122
 - DBAs 120–122
 - definition 119
 - quality attributes/availability/reliability 119–120
 - SSCs 118
 - verification and validation 123
- DSA
 - BE codes 130
 - BEPU methodology 131
 - codes and methodologies 130
 - conservative methodology 130
 - deterministic safety analysis 129
 - FSAR 132
 - inverse methods 131
 - safety analyses 129
 - safety margin/safety limit 130
- education and training 8
- electronics including instrumentation and control (I&C) 16
- experimental thermal hydraulics
 - analytical support 114
 - CP tests 117
 - databases 114
 - FSA 116
 - H2TS 116
 - IET/ITF 114
 - Ishii three-level scaling approach 116
 - Kv-scaled calculation 117–118
 - power-to-volume scaling 115
 - scaling 115
 - scaling distortion 116–117
 - SET 113–114

- system codes 117
- experiments and instrumentation 9
- features for 3
- framework 924
- HTC 22
- HT developments
 - heat conduction 105–106
 - heat convection 106–108, 107–108f
 - heat radiation 109
 - importance of 104
 - 1D/3D option 105
 - power generation 105
 - Prandtl and Nusselt numbers 108–109
 - scope of 104
- journals, conferences, and the web 7–8
- key actors and stakeholders 46–47
- mechanics 15–16
- modern accident analysis
 - accident, definition 132
 - Chernobyl accident 133
 - classification and treatment 132–133
 - Fukushima accident 133
 - TMI-2 accident 133
- need for 23–24
- neutron physics 14
- nuclear fuel 16
- nuclear safety, licensing process, and DBA (moving)
boundaries 10–11
- numerical methods and computer science 10
- objective 47
- origin of 4–5
- passive systems, reliability, and stability issues 12
- pressure drops 26–27
- PSA 14, 134
- radioprotection 14–15
- reference books 6–7

- rudimentary thermal-hydraulics 6
- safety concepts
 - AM 123–124
 - damage 125
 - defense in depth 126
 - energy sources 124–125
 - EOP 123–124
 - heat extraction safety relevance 124
 - inherent safety/passive safety/active safety 127–128
 - International institutions 128–129
 - safety barriers 126
 - safety functions 125
 - safety objectives/safety culture 123
 - safety systems/safety-related systems 126–127
- SAMGs 123–124, 134
- scientist contribution 6
- severe accidents 11
- single-and two-phase flows 5
- special process models
 - break flow, in branch 613–619
 - CCFL 602–607
 - entrainment and de-entrainment 607–610
 - reflood 610–613
 - TPCF 597–602
- start-up and shutdown phenomena 13
- supporting plant operation 134–135
- SYS-TH 4, 28–29, 45
- target NPP and the RR types 8–9
- terminology 3
- thermal-hydraulic phenomena 25
- two-phase flow developments
 - balance equations 96–97
 - blowdown/reflood/rewet 100
 - boron dilution accidents 101–102
 - boron dilution/deboration 102

- critical flow and choked flow 100
- drift-flux model 103
- empirical database and instrumentation 92
- equilibrium/subcooling/super-heating 94
- extensive properties 93
- flow-regime definition 97–99, 98–99*f*
- homogeneous model 102–103
- hydraulic diameter/Reynolds and Froude numbers 95
- importance of 90
- intensive properties 93
- interfacial area/interfacial area concentration 94
- loop seal clearing 101
- lumped parameter models 103
- mass velocity 94
- multiscale and multiphysics 91
- NC 99
- pressure drop 95
- reflux condenser mode 101
- separated flow model 103
- steam binding 101
- turbulence and 91–92
- two-fluid model 103–104
- void fraction/quality 93–94
- water properties 92–93
- V&V, scaling, and uncertainty 30
- Nuclear thermal-hydraulics 1103
- Nucleation pool boiling
 - bulk boiling
 - high pressure region 442
 - low pressure condition 441–442, 441*t*
 - oxide films and deposits, effect of 442–443, 443*t*
 - coated porous surface 439–440, 439–440*f*
 - components 436
 - effect of
 - material thermal properties and thickness 436

- pressure 434, 434*f*
- surface roughness 435, 435*f*
- estimate correlations 437–438
- hydrodynamic theory of similarity 438–439
- mechanism 433–434
- Numerical solver algorithm 742
- NURETH (series of conferences in thermal-hydraulics) 46–47, 58, 60*t*

O

- OECD-KAERI CFD benchmark 770, 770*np*, 773
- OECD/NEA/CSNI 4, 6, 16, 25, 51, 55–56, 69–70, 77, 90, 92, 102, 113–115, 117, 128, 131, 133, 332, 532–533, 602, 644, 730, 733, 745–746, 749, 758, 778, 780–784, 807–810, 808*f*, 818–821, 838, 861, 865, 867, 874, 898, 957, 958–961*t*, 961, 974, 995, 1008, 1021, 1043, 1052, 1073–1074, 1081, 1086, 1088, 1105, 1145
- Once-through steam generators (OTSGs)
 - MSLB in PWR with 1027*f*
 - thermal-hydraulics of 1027*f*, 1028–1029
- 1-D models
 - space discretization for 660*f*
 - in SYS-TH code 650–651
- 1-D two-fluid model 628–630, 680–681
 - choked flow with 683–686
- 1-D two-fluid equations 222–223
- Open ISP 842
- Ordinary differential equations (ODEs) 649–650
- Oskarshamn events 1104–1105, 1143–1144
 - BWR of 1112, 1137*f*
 - chronology of events 1121–1122, 1122–1123*t*
 - thermal-hydraulics analyses 1135*t*, 1136–1138, 1137*f*
- OTSGs *See* Once-through steam generators (OTSGs)
- Output uncertainties 882–884
- Oxidation 125, 297–299, 471–473, 642, 650, 746*f*, 870–871, 940, 1042

P

- Parameter sensitivity calculations 887

PCT 888*f*

sensitivity analysis 891

uncertainty analysis 887–890, 889–890*t*

Partial differential equations (PDEs) 649–650, 659

Passive Residual Heat Removal (PRHR) 67, 962–963*t*, 985, 992, 997, 998–999*t*, 1001, 1001*f*, 1003, 1004–1005*t*, 1005, 1052, 1056

Passive safety system

ALWR

classification 332

definition 332

use of 332–333

thermal-hydraulics 66–67

Peak cladding temperature (PCT) 645, 841, 887

uncertainty bands 891*f*

Zion NPP LB-LOCA 891*f*

Phenomena identification and ranking table (PIRT) 705, 850, 858–859

applicability, Element 4 163

CSAU method 866

Element 1 152

informed R&D process 148–150, 149*f*

Phenomena in thermal-hydraulics 975

accident scenarios and 961–975, 964–966*t*

acceptance criteria 970–972

AOO and DBA 972–973

background 979–980

CHF 1042, 1043*f*, 1043*t*

containment performance 1044–1047, 1045–1046*f*, 1047*t*

LBLOCA 990–994, 990–991*t*, 991*f*

natural circulation 1057–1060, 1057*f*, 1059*t*

nuclear fuel behavior 1084–1085, 1085*f*, 1085*t*

PIE establishment 963–970

pressurized thermal shock 1049–1052, 1050*f*, 1051*t*

procedure 976–979

risk evaluation 973

time histories 1086–1087

variables calculation 967–968*t*

equivalent ADDED accident SCENARIOS 969*t*, 978

list of 962–963*t*

transient 974–975

Phenomenological approach, closure relation 701

Phenomenological windows (PHW) 975–977, 998, 1008, 1041,
1052–1053, 1130

Chernobyl-4 1133

Fukushima Units 1–3 1138

La Salle-2 1136

Oskarshamn-2 1136

TMI-2 1131

PIE *See* Postulated initiating event (PIE)

Pipe-whip 15–16, 745, 1044

PIRT *See* Phenomena identification and ranking table (PIRT)

Polydispersed dynamic modeling

 multifield approach 238

 predictive capabilities 238

 statistical moments 237

Polydispersion effects 718–719

Porous body 180, 184, 196, 670, 671*f*, 713, 759*f*

Post-BEMUSE REFlood Model Input Uncertainty Methods
(PREMIUM) programme

 LOCA 894

 phases of 894–896

Postulated initiating event (PIE) 913, 925, 961

 establishments 963–970

Power-to-volume scaling 115

Precursory cooling 987

Pressure drop

 acceleration 503–504

 accident situations 495

 CCFL

 CCF 515–516

 definition 515–516

 occurrence 515–516

 PKL III test 516–518, 517*f*

 SG U-tubes 516

 UPTF test 516

 CFD applications 543–544

components of 495–496

direct measurement

distributed (friction and acceleration) 536

local/geometric discontinuities 536–537

elevation 504

experimental database 540–541

flow reversal, SG U-tubes

characteristic flow curves 527

heterogeneous behavior 525, 526*f*

NC 524–525

PKL test 525, 527*f*

friction

applications of 500–501

single-phase flow 496–498

two-phase flow 498–500

LB-LOCA

long-term cooling 511–513, 514–515*f*

RE and 506–509, 507*f*, 510*f*

spacer grids and CHF 513–515

stagnation point, BD and RF phases 504–506, 505*f*

steam binding 509–511, 512*f*

local

area changes 502–503, 502*f*

Reynolds number and void fractions 503

LSC

definition 522–523

IB-LOCA 521–522

PKL test 523, 523*f*

SB-LOCA 521–522

UPTF test 524, 524*f*

modeling improvements, TH system codes 542–543

pressure drop predictions/measurements and 533–535

quantities connected with

collapsed level 538–539

conventional measurements 537

- filling level 538
- physical variables 538
- practical applications 539
- reactor coolant pumps 495
- separate effect test facilities 495
- stability, boiling channels
 - classification 528–529
 - vs. mass flow rate 529, 530*f*
 - vs. time 529, 529*f*
- steady-state qualification and 532–533, 533*f*
- SYS-TH code modeling
 - form losses 531–532
 - wall friction 530–531
- TPCF and
 - within crack 521, 522*f*
 - critical/choked flow 518–519
 - mass flux 518, 518*f*
 - pressure evolution 520, 520*f*
 - pressure profile 518–519, 519*f*
 - SET 519–520
 - velocity and quality profiles 520–521, 521*f*
- two-phase flow developments 95
- two-phase flow modeling
 - expected-desirable developments 542
 - friction 541–542, 541*f*
- Pressure vessel modeling, for SYS-TH code 658*f*
- Pressurized thermal shock (PTS) 1020, 1041
 - computational fluid dynamics 1048*f*
 - phenomena connection with accident scenario 1049–1052, 1050*f*, 1051*t*
 - in PWR 1050*f*
 - thermal-hydraulic aspects 1047–1049, 1048–1049*f*
- Pressurized water reactor (PWR) 596, 604, 643*f*, 656, 686–687, 687*f*
 - accidental transients of 703*f*
 - cross reference matrix

- accident management, nondegraded core 320–321*t*
- large breaks 310*t*
- with OTSG 314–316*t*
- small and intermediate breaks 312–313*t*
- transients 317–318*t*
- IBLOCA/MBLOCA in 995
- ITF 838
- LBLOCA 667, 722*f*
- nodalization 657–659, 658*f*
 - for SBLOCA simulation 657*f*
- pressurized thermal shock in 1050*f*
- reflood 610
- RIA scenarios 1031*f*
- separators and dryers 628
- Three Mile Island accident 1109–1110
- with UTSG
 - ATWS scenario in 1007–1008, 1009*t*, 1010*f*
 - CRE in 1032*f*
 - LBLOCA scenario in 983*t*, 984*f*, 989*f*
 - LOFW scenario in 1007–1008, 1009*t*, 1010*f*
 - LOOSP accident scenario in 1016–1017*f*, 1018*t*
 - MSLB and FWLB accident scenario in 1025*t*, 1026–1027*f*
 - NC accident scenario in 1054*f*, 1057*f*
 - SBLOCA scenario in 998–999*t*, 1000–1002*f*
 - SBO accident scenario in 1012–1013*f*, 1013*t*
 - SGTR accident scenario 1021*t*, 1022*f*
 - TT accident scenario 1078*t*
- Pressurized water reactor (PWR) rod bundle problem 764–775, 767*f*
 - adopted CFD methods 769
 - conjugate heat transfer 773
 - mesh 770–771
 - near-wall treatment 773
 - turbulence closure models 771–772
 - unsteady turbulence models 772–773
 - experimental data 768–769

Principle of thermodynamics, mechanics 24, 174, 179

Probabilistic safety analysis (PSA) 641, 907–908, 919

- BEPU approach 916–919, 929*f*
- DSA applications 933–934
- IAEA 933–936
- integration of 933–936
- OECD/NEA/CSNI 933–936
- reliability & uncertainty 923
- risk-informed regulation 922, 936
- SYS-TH 834–835

Probabilistic safety assessment (PSA)

- nuclear thermal-hydraulic 14, 134
- SYS-TH code 77

PSA *See* Probabilistic safety analysis (PSA) *See also* Probabilistic safety assessment (PSA)

Pseudocritical line (PCL) 345–346, 345*f*

Pseudo-DNS method 200–201

PTS *See* Pressurized thermal shock (PTS)

Pump *See* Reactor coolant pumps

PWR *See* Pressurized water reactor (PWR)

Q

Quality assurance (QA) framework 915

Quantity uncertainty matrix (QUM) 873

Quench front (propagation) 26, 100, 231, 242, 255–257*t*, 273, 310*t*, 322–323*t*, 327*t*, 461, 506–509, 534, 555–556, 611, 717–718, 747–748*t*, 894–896, 991*f*, 1058*f*

R

Radiative heat transfer

- in absorbing and emitting environments 411–412
- arbitrary arrangement 409–410
- body and shell 410
- characteristics
 - brightness coefficient 408, 408*f*
 - emissivity 407
 - reflective surfaces 407, 408*f*

- reflectivity 408
- transparency (transmissivity) 409
- conduction 413–415, 414*f*
- convection 415–416, 415*f*
- Planck's law
 - diffuse emitter 406
 - fundamental constants 402, 403*t*
 - graphical representation 403*f*
 - Kirchhoff's law 405
 - Lambert's cosine law 405
 - radiation characteristics 406
 - relative emittance 405, 406*f*
 - Stefan-Boltzmann law 404
- principles
 - absorption of 401, 401*f*
 - electromagnetic spectrum 399, 400*f*
 - integral radiation 400
 - radiation types 401, 401*f*
 - thermal radiation flux 402
- RANS *See* Reynolds-averaged Navier-Stokes (RANS)
- RBMK
 - FCB accident scenario in 1064–1065*f*, 1068*t*
 - MPTR accident scenario in 1067*f*, 1069*f*
 - reactor, Chernobyl accident 1110–1112
- RCS *See* Reactor coolant system (RCS)
- Reactivity Initiated Accident (RIA) scenarios
 - PWR 1031*f*
 - quantitative characterization 1031–1032
 - reactivity excursion class of 1029–1033
- Reactor coolant pumps
 - available data for 620, 621*t*
 - centrifugal pump head 620, 625*f*
 - vs. entrance void relationship 626*f*
 - degradation function 627*t*
 - design characteristics 622*f*

experimental data and modeling 627*f*

flow separation 624*f*

frictional losses 619

hydraulic torque 620

modeling in system codes 623*f*

two-phase pump performance 627*f*

vapor pull through data 619, 620*f*

Reactor coolant system (RCS)

configuration 1009

consequential depressurization 1038

fast depressurization of 981

intrinsic cooling 987

pressure and RST 984*f*

recovery 1008

Reactor Excursion and Leak Analysis Program (RELAP) code 648

RELAP5 models

branch flow 618

critical flow 602

pump models 625

Reactor Excursion and Leak Analysis Program (RELAP) code,
RELAP5 648, 656, 656*f*, 696, 699*f*, 713

correlations

IAC 567, 568–569*t*

IHTC 570, 571–572*t*

horizontal flow regime map 559–560, 560*f*

interfacial heat and mass transfer 565, 567–568, 568–569*t*

vertical flow regime map 554*f*, 557

wall friction 585

wall heat transfer 578, 579*f*

Reactor pressure vessel (RPV) 986, 996

bypass flow-paths 996–997

depressions

ACC control 996

loop seal control 996

LPIS control 996

PWR with UTSG 1072*f*

Reactor system *See* Nuclear reactor

Recriticality 308, 780–781*t*, 995, 1024

Reflood, nuclear fuel

- flow velocity 611*f*

- qualitative flow 611*f*

- rod bundle tests 612–613

- TRACE code 612

- transients periods 610

- uncovered fuel 610

Reflux condensing mode 998, 1030, 1054, 1076

Relevant thermal-hydraulic aspect (RTA) 975–976

Reliability of passive systems 12, 67, 247, 250, 333, 1056

Return to Power 122, 1024, 1025*t*

Rewet 22–23, 100, 255–257*t*, 298–301, 324–325*t*, 349, 426–428, 432, 506–507, 511–512, 662, 747–748*t*, 962–963*t*, 981, 987, 990–991*t*, 992–994

Reynolds-averaged Navier-Stokes (RANS) method 755

- approach 741

- equation 785

- model 756, 758, 772–773

- single-phase modeling 181

- steady 774

 - capabilities of 740, 765

 - limitations of 740–741, 765

- time-averaged two-fluid equations 207–208*b*

- turbulence model 737, 770*np*, 785–790

- two-layer model 794

- two-phase flow modeling 201

- vs.* URANS 803

Reynolds stress model (RSM) 772, 789

- advantages 789

- disadvantages 789

- fidelity of 790

- vs.* LEVM 802

- variants of 790

RPV *See* Reactor pressure vessel (RPV)

RSM *See* Reynolds stress model (RSM)

S

Safety acceptance criteria 955

Safety analysis method 893, 912–913

Safety analysis report (SAR) 147–148

Safety code, SYS-TH code 646–647

Safety-licensing demonstration, BEPU 932

- ALARA principle 937

- DSA and PSA integration 933–936

- FSAR 937–943

Safety Margin Project (SMAP) 933

Safety margins (SM) 922

- applications 940–943

- definition 940–943

- design margin 941

- extended SM 940–941

- multidimensional space 941–943

- NPP assessment activity 909

Safety valves 634

Saint-Venant equation 697

SAM *See* Severe accident management (SAM)

SAS model *See* Scale-adaptive simulation (SAS) model

SBLOCA *See* Small-break LOCA (SBLOCA)

Scale-adaptive simulation (SAS) model 756, 800

- characteristics 800–801

- requirements 800

- variants of 801

Scaling distortion

- dynamical system scaling 851

- experimental thermal hydraulics 116–117

Scaling evaluation, SYS-TH codes 848–849, 863–864

- H2TS 850

- integral system tests 852–854

- scaling concepts 849–852, 850t

- SETs 854–862

- Scaling State of Art Report (S-SOAR) 69
- Second moment closure (SMC) models 755
- Semi blind ISP 843
- Semiempirical approach, closure relation 702
- Separated flow model
 - nuclear thermal hydraulics 103
 - two-phase multiplier 499–500
- Separate effect phenomena 25
- Separate effects test (SET) 701, 707–708, 711, 837, 863–864
 - advantages 854
 - blowdown phase 860–861, 860f
 - code models 854
 - downcomer counter-current flow and quench time 858–861, 858f
 - experimental thermal hydraulics 113–114
 - flow conditions in hot leg during reflux condenser mode 862
 - homogeneous flow conditions at upper core tie plat 861
 - quench time 860–861, 861f
 - reflood phase 860–861, 860f
 - target phenomena 253
 - TPCF and 519–520
 - UPTF tests 855
 - validation matrix 586–587
 - vertical counter-current flow of saturated steam 861
 - vertical heterogeneous counter-current steam-water flow 855–857, 856f
 - water-cooled reactors 747–748t
 - Zion reactor 859f
- Separate effect test facility (SETF) 69, 495, 1108
- SET *See* Separate effects test (SET)
- SETF *See* Separate effect test facility (SETF)
- Severe accident management (SAM) 917–918, 938
- Severe accident management guidelines (SAMG)
 - safety concepts 123–124, 134
- SGS model *See* Suitable subgrid scale (SGS) model
- Shear stress transport (SST) model 785–788

- Shutdown accident scenarios 1080–1083, 1082*f*, 1083*t*
- Single-phase gas flow, choked flow in 671–676
- Single-phase model
 - CFD 737, 780–782
 - characteristics and modeling needs 181, 182*t*
 - direct numerical solution 183
 - locality and universality 183
 - RANS-type models 181
 - scale/eddy-resolving-type models 181–183
- Single-phase thermal fluids problem, applications to CFD 780–782
- Single-phase vapor flow choking 597
- Slip ratio 266–267, 600, 678, 680, 712, 720
- Small-break LOCA (SBLOCA) 688
 - counterpart test database 845
 - heater rod surface temperature 847*f*
 - normalized residual water mass 846*f*
 - upper plenum pressure 846*f*
 - phenomena connection with 1000–1004*f*, 1002–1007, 1004–1005*t*
 - in PWR with UTSG 998–999*t*, 1000–1002*f*
 - qualitative characterization 995–997
 - quantitative characterization 998–1002
 - in reactors other than PWR with UTSG 1007
- Small modular reactors (SMRs), TT accident scenario 1078*f*
- Sonic velocity, in two-phase flow 676–681
- Space averaged 1-D equations
 - definition 209–211, 209–210*f*
 - energy balance, phase *k* 215–218
 - interface pressure 214, 214*f*
 - mass balance, phase *k* 211
 - momentum balance, phase *k* 211–215
 - stratified flow 218–220, 218*f*, 220*f*
- SPACE code 698
- Space discretization, for 1-D models 660*f*
- ‘Spacer grids’ and ‘Grids,’ 26, 61, 63, 463, 479, 495, 501, 513–515, 532, 653, 709, 816–817, 987, 992, 1042, 1084

Space-time-averaged 1-D equations

- control volumes 188
- energy equation 191–192
- mass balance equation 190
- momentum equation 192–195
- 1-component 1-phase flow 195*b*
- portion of a duct 189, 190*f*
- predictive capabilities 195–196

Spalart-Allmaras (SA) model 785–788, 802

Special process models

- break flow, in branch 613–619
- CCFL 602–607
- entrainment and de-entrainment 607–610
- reflood 610–613
- TPCF 597–602

Stagnation point concept 981

Stationary film boiling 443–444, 445*t*

Station blackout (SBO) accident scenario 1011–1012

- Fukushima-Daiichi accident 1138–1141, 1139–1140*f*
- phenomena connection with 1012–1013*f*, 1014–1015, 1014*t*
- in PWR with UTSG 1012–1013*f*, 1013*t*
- qualitative characterization 1012
- quantitative characterization 1012–1014

Statistical (GRS) method

- features 867
- minimum number of calculations 868, 868*t*, 870–871
- order statistics 869, 869*t*
- uncertain input parameters 893–894

Steady-state CCFL tests 855

Steam generator tube rupture (SGTR) accident scenario 1019

- MSLB with 1060–1063, 1062*f*, 1063*t*
- phenomena connection with 1022–1024, 1022*f*, 1023*t*
- in PWR with UTSG 1021*t*, 1022*f*
- qualitative characterization 1020
- quantitative characterization 1021

- Steam separator and dryer model 628–632, 628–629*f*
 - in BWR 607, 610, 628–629*f*
 - design data 631*t*
 - system codes 630–632
- Steen-Wallis model 700
- Stratification prediction 693–697
- Stratified flow
 - interfacial friction 696
 - properties of the system of equations for 691–693
- Stress tensor 175–176, 181, 182*t*, 185, 192, 194, 205, 207, 212, 217, 785–789
- Subcooled nucleate boiling
 - at low pressures 455–456, 456*f*
 - onset of 454–455
- Suitable subgrid scale (SGS) model 756, 805, 806*t*
- Sump compartment 988
- Supercritical pressure 344–345, 349–351
- Super critical water cooled reactors (SCWRs)
 - critical flow
 - definition 346–347
 - LOCA 347
- HPLWR
 - vs. LWR 344
 - plant characteristics 344
 - safety analysis study 344
- HT characteristics 348
- instability and NC
 - Ledinegg excursive instability mechanism 349–351
 - pseudoboiling PH 351
 - single-phase flow 349–351
 - at subcritical pressures 350–351
 - two-phase flow 349–351
- pressure loss characteristics 348
- thermal-physical properties
 - IAPWS-97 and IAPWS-95 346
 - PCL 345–346, 345*f*

- pressure and temperature, function 345, 345*f*
- tight lattice geometry
 - boil-off 349
 - reflooding 349
- Superhydrophilicity
 - aqueous slurry 483, 484*t*
 - characteristics 483
 - photocatalysis 483
- SUPER-MOBY-DICK long nozzle test 682*f*
- Surface deposition and boiling
 - characteristics, layers 471–472, 472*t*
 - circuit loop operation 471
 - composition and thermal conductivity 473–474
 - impurities entry 470
 - layers of 471–472, 472*f*
 - low resistance and heat transfer coefficient 474–475
 - mechanisms of 471
 - modern power plants 471
 - scales 470
 - wicks boiling 472, 473*f*
- Surface tension 385–386, 398, 421, 423, 428–429, 432, 434–436, 567, 599, 604, 615–616, 690, 858*t*
- System thermal-hydraulic (SYS-TH) code 641–642, 743, 833, 957
 - accident analysis, BEPU 907–908, 924–925
 - accident scenarios and phenomena *See* (Accident scenarios)
 - accumulators 655
 - application of 1087–1088
 - BEPU approach 78–79, 79*f*
 - best-estimate code 645
 - breaks 655–656
 - capabilities 644
 - vs. CFD code 743
 - CFD-like approaches 65–66
 - characteristics 642
 - closure laws in 702
 - closure relations

- approaches 701–702
- development and validation 701–702
- code modeling
 - form losses 531–532
 - wall friction 530–531
- and component codes 668–669
- connection with phenomena 957
- and containment 666–667
- countercurrent flow limitation 653
- coupling with 72–73, 74*f*
- critical flow conditions 652–653
- DBA domain 644
- drift flux with two-momentum equations 715–718
- dryers 654
- ECC injection 654
- elements for reflection 82
- energy and entropy balance 64–65
- features and differences between codes 670
- history for
 - 1960–70 54
 - 1970–80 54–55
 - 1980–90 55–56
 - 1990–2000 56–57
 - 2000–10 57–58
 - 2010–20 58
 - before 1960 54
 - 2013 and 2015 58–59
 - current trends 61
 - definitions 50–51
 - DiD framework 49
 - DSA 49–50
 - key elements 59, 59*f*
 - key words 59–60, 60*t*
 - NPP design 49
 - NRS technology 48–49, 48*f*

- nuclear thermal-hydraulics, role of 50
- PSA 49–50
 - regulator history, United States 52–54, 52^f
 - safety objective 48–49
- industrial code 647
- licensing needs 75–76, 75^f
- local form loss coefficients/K-factor 62–63
- modeling and structure 73–74
- multi-D heat transfer coefficient surface 63–64
- nodalization
 - concept 649–659
 - importance 659
- nodalization qualification 925
- NPP accident scenarios 958–961^t
- NRS problems requiring CFD with/without coupling to 780–781^t
- numerical solution methods 659–666
 - stability and hyperbolicity 664–665
 - state-of-the-art 663–666
- objective and structure 958–961
- 1-D modules in 650–651
- passive systems 66–67
- physical modeling uncertainty 709–710
- point of view of time scale analysis 714–715
- polydispersion effects 718–719
- precision targets 65
- predictive capabilities of
 - capabilities of system codes 711–712
 - evolution of 3-D modeling 713–714
 - status of current system codes 708–711
 - two-fluid model 712–713
- pressure vessel modeling for 658^f
- PSA and 77
- pumps 654
- PWR model 643^f
- requirements and domain of simulation 643–644

- safety code 646–647
- scaling and system code validation 848–849, 863–864
 - integral system tests 852–854
 - scaling concepts 849–852
 - SETs 854–862
- scaling issue and experiments 67–69, 67–68*f*
- sensitivity and uncertainty 922
- separators 653
- severe accident and 77–78
- singular pressure loss 653
- spray cooling 656–659
- subchannel analysis codes 669–670
- synthesis of 80, 80–81*t*
 - and system codes 668
- tee junctions 651, 651*f*
- three-field models in 720–723
- TIA in future system codes 719–720
- turbines 654
- uncertainty analysis 71–72, 71*f*
- uncertainty methods 864–873, 897–898
 - CSAU method 866–867
 - international validation 873–896
 - licensing, applications in 897
 - statistical (GRS) method 867–871
 - UMAE/CIAU method 871–873
- upscaling capabilities of 704–708
 - code upscaling capability 707–708
 - distortion in IET 706–707
 - PIRT 705
 - scaling 706
- user effect and training 78
- V&V process 69–71, 70*f*, 834–848, 924
- 0-D modules in 652, 652*f*

SYS-TH code *See* System thermal-hydraulic (SYS-TH) code

Target phenomena, nuclear thermal-hydraulics

accumulator behavior 304–305

ALWR

check valves 341

CMT behavior 343

containment emergency systems 337–338

containment structures, condensation on 337

critical and supercritical flow 341

CRP objectives 333–334

density locks 341

emergency heat exchangers and ICs 341–342

gravity-driven cooling and accumulator behavior 340

IAEA 332

identification and characterization 334, 335–336

large pools 334–336

liquid temperature stratification 341

NC 339

noncondensable gases, condensation HT 336–337

OECD/NEA framework 333–334

passive safety system 332

steam-liquid interactions 339–340

stratification and mixing of boron 342–343

thermo-fluid dynamics and PDs 338

boron mixing and transport 307–308

CCF/CCFL

channel inlet orifices 285

downcomer 286–287

flooding 283–284

flow behavior 284

hot and cold legs 285–286

occurrence 258

PRZ surge line 287

SG tubes 286

UTP 284–285

classification of

- CCFL 254
- constitutive equations 252–253
- integral tests 253
- LOCA phenomena 254
- SETs 253
- two-phase flow model 252
- condensation
 - heat removal 261–262
 - horizontal pipe 281
 - pressurization 261
 - PRZ 280
 - SG primary side 280
 - SG secondary side 280
- critical flow
 - in breaks 265–266
 - definition 265
 - in pipe 266–267
 - in valves 266
- ECC bypass/downcomer penetration 305–306
- entrainment/de-entrainment
 - core 272
 - downcomer 273–274
 - hot leg with ECC injection 274–275
 - parameters 271
 - SG mixing chambers 274
 - SG tubes 274
 - source of 271
 - upper plenum 272–273
- evaporation
 - depressurization 259
 - heat input 259–261
- global multidimensional fluid temperature, void, and flow distribution
 - core 290–291
 - downcomer 291
 - SG secondary side 291–292

- upper plenum 289–290
- guide tube flashing 302
- HPLWR
 - vs. LWR 344
 - plant characteristics 344
 - safety analysis study 344
- HT
 - forced convection 293–294
 - natural convection 293–294
 - nucleate boiling/dryout, departure 295
 - post-CHF 295–297
 - radiation 297–298
 - SG tubes and on structures 298
 - subcooled and nucleate boiling 294
- IAEA 247
- integral facilities
 - BWR 322–325*t*
 - PWR 310*t*, 312–317*t*, 320–321*t*
 - VVER 327–331*t*
- interfacial friction in
 - horizontal flow 263
 - vertical flow 262–263
- liquid-vapor mixing with condensation
 - computer code models 276
 - core 276
 - downcomer 276–277
 - ECC injection 279
 - lower plenum 277–278
 - reactor safety 275
 - SG mixing chambers 278–279
 - upper plenum 277
- loop seal filling and clearance 305
- LP entrainment 309
- LP flashing 301–302
- NC 247

- noncondensable gas effect 308
- one-and two-phase impeller-pump behavior 302–303
- one-and two-phase jet-pump behavior 303
- parallel channel instabilities 306–307
- PDs, geometric discontinuities 263–264
- phase separation at branches 270–271
- phase separation/vertical flow with and without mixture level
 - core 268–269
 - downcomer 269
 - pipes and plena 268
- pressure wave propagation 264–265
- QF propagation/rewet
 - channel walls and water rods 301
 - fuel rods 300–301
 - reflooding 299
- SCWRs
 - boil-off, tight lattice geometry 349
 - critical flow 346–347
 - HT characteristics 348
 - instability and NC 349–351
 - pressure loss characteristics 348
 - reflooding, tight lattice geometry 349
 - thermal-physical properties 345–346, 345f
- separator behavior 303–304
- spray effects
 - core 281–282
 - OTSG secondary sides 283
 - PRZ 282–283
 - subitems 281
- steam dryer behavior 304
- stratified flow, horizontal pipes 270
- wall-to-fluid friction 263
- Thermal conduction *See* Conduction heat transfer
- Thermal hydraulics (TH) 643
 - computer codes 834

- limitations 908
- design, nuclear reactors 956
- 3-D models, modules 24–25, 180, 184, 196, 242, 644, 650, 657–659, 658*f*, 668, 670–671, 710, 713–714
- Three Mile Island accident 1103–1104, 1142
 - chronology of events 1113–1117, 1114–1116*t*
 - LOFW-SBLOCA 1131–1133, 1132*f*
 - PWR of 1109–1110
- Time-averaged single-phase equations
 - closure of 187–188
 - incompressible flow 186–187
 - 1-component 1-phase flow equations 188*b*
 - Reynolds averaging-time averaging 184–185
- Time-averaged two-fluid equations
 - bubble/drop, dispersed phase 206–207
 - momentum and total energy 205, 205*t*
 - predictive capabilities 208
 - RANS two-fluid equations 207–208*b*
- Time-space averaged 1-D equations 221–222
- Time uncertainty vector (TUV) 873
- TPCF *See* Two-phase critical flow (TPCF)
- TRAC *See* Transient reactor analysis code (TRAC)
- TRACE code 648, 696
 - correlations
 - IAC 570, 573*t*
 - IHTC 570, 574*t*
 - flow regime map 561–562, 562*f*
 - interfacial heat and mass transfer 570, 573–574*t*
 - wall friction 584–585
- TRACE models
 - branch flow 618
 - critical flow 602
 - pump models 625
 - reflood 612
- Transient heat conduction
 - heating/cooling

- Bi«1 373
- Bi»1 373, 374^t
- body, arbitrary shape 372, 372^f
- finite body 373–374
- semiinfinite body 372, 372^f
- periodic changes, temperature 375–376
- regular thermal regime 375, 376^f
- surface temperature 374–375
- Transient reactor analysis code (TRAC) 648
- Transport of interfacial area (TIA)
 - flow regime transitions 234–235
 - interfacial transfers 235
 - monodispersed approximation
 - algebraic interfacial area 236
 - dispersed phase fraction 235
 - dynamic interfacial area modeling 236
 - predictive capabilities 238
 - nonestablished flows 234
 - polydispersed dynamic modeling
 - multifield approach 238
 - predictive capabilities 238
 - statistical moments 237
 - turbulent scales 234
- Turbine modeling 625–627
- Turbine trip (TT), accident scenario 1077
 - in BWR 1079^f
 - phenomena connection 1079–1080, 1080^t
 - in PWR with UTSG/BWR 1078^t
 - qualitative characterization 1077
 - quantitative characterization 1077–1078
 - in SMR 1078^f
- Turbulence model 755–757
 - closure 771–772, 785
 - efficiency of 801–805
 - κ - ω model 785–788

realizable κ - ε model 785–788

RNG κ - ε model 785–788

SA model 785–788, 802

SST κ - ω model 785–788

standard κ - ε model 785–788

strategy 802*t*

unsteady 772–773

URANS 790–792, 802–805

Turbulent boundary-layer (TBL) equation 796

Two-fluid model, horizontal flow modeling with 690–691

Two-layer model, RANS 794

Two-phase choking 597–598, 598*f*

flow experiment 681–682

Two-phase critical flow (TPCF) 596, 1015, 1024

choked flow *See* (Critical flow models)

within crack 521, 522*f*

critical/choked flow 518–519

DBA 597

energy and entropy balance 65

HEM 598

LOCA 597

mass flux 518, 518*f*

nucleation and bubble growth models 598–599

pressure evolution 520, 520*f*

pressure profile 518–519, 519*f*

SET 519–520

single-phase vapor flow choking 597

in system codes 601–602

two-phase choking 597–598, 598*f*

velocity and quality profiles 520–521, 521*f*

Two-phase flow modeling

applicability and degree of maturity 203, 204*t*

balance equations 96–97

blowdown/reflood/rewet 100

boron dilution accidents 101–102

- boron dilution/deboration 102
- critical flow and choked flow 100
- deterministic interface 200
- development in
 - expected-desirable developments 542
 - friction 541–542, 541*f*
- drift-flux model 103
- empirical database and instrumentation 92
- equilibrium/subcooling/super-heating 94
- Eulerian fluid dynamic simulation approaches 196–198, 197*t*
- extensive properties 93
- factors influencing 199–200
- filtered interface 200
- flow-regime
 - definition 97
 - horizontal channels 97–98, 98*f*
 - vertical channels 97–98, 99*f*
- homogeneous model 102–103
- hydraulic diameter/Reynolds and Froude numbers 95
- importance of 90
- intensive properties 93
- interfacial area/interfacial area concentration 94
- LES with
 - deterministic interface 201
 - hybrid 202
 - statistical interfaces 202
- locality and universality 203
- loop seal clearing 101
- lumped parameter models 103
- mass velocity 94
- multiscale and multiphysics 91
- NC 99
- pressure drop 95
- pseudo-DNS method 200–201
- RANS method (U-RANS) 201

- reflux condenser mode 101
- separated flow model 103
- statistical interface 200, 200*f*
- steam binding 101
- time space and phase averaging 198–199, 198*f*
- turbulence and 91–92
- two-fluid model 103–104
- void fraction/quality 93–94
- water properties 92–93
- Two-phase model, CFD 737–738, 782–784
- Two-phase steam water flow, choked flow in 676

U

- UMAE/CIAU method 871–873
- UMS *See* Uncertainty method study (UMS)
- Uncertainty analysis
 - reliability analysis 923
 - SYS-TH 71–72, 71*f*
- Uncertainty method
 - BEPU process 908
 - accuracy and 922–923
 - reliability and 923
 - sensitivity and 922
 - SYS-TH codes 864–873, 897–898
 - CSAU method 866–867
 - international validation 873–896
 - licensing, applications in 897
 - reference calculations 887, 893
 - statistical (GRS) method 867–871
 - UMAE/CIAU method 871–873
- Uncertainty method study (UMS) 881
 - calculated uncertainty ranges 875
 - clad temperature ranges 876–880, 877–879*f*
 - functions of time 876
 - chosen experiment 874–875
 - code validation 893–894

- comparison between calculations 881
- follow-on activity 880, 880f
- methods compared 874–875, 875t
- objectives 874

Unstable boiling modes

- hydraulic characteristics 475, 475f
- instability of boiling
 - parallel channels 476
 - single channel 475, 477–478
- unstable pool boiling 475–477, 476f

Unstable pool boiling 475–477, 476f

Unsteady RANS (URANS) 755, 757

- near-wall treatment of 792–794
- vs. RANS 803
- turbulence modeling 790–792, 802–805
- wall-modeled 792–793
- wall-resolved 793

Unsteady turbulence models 772–773

Upper plenum test facility (UPTF) 604, 605t, 606f, 848, 855

- counter-current flow 863f
- flow in 607f
- full-reactor scale hot leg 862

URANS *See* Unsteady RANS (URANS)

User effect/validation 843–844

US NRC 648, 868, 938

UVUT 23, 32, 103–104, 241, 587

V

Validation pyramid 156–157, 157f

Valves *see specific types of valves*

Verification and validation (V&V) processes 833

- computer codes 835–836
 - counterpart and tests 844–847
- input data 839
- ISP 841–843
- process 837–839

- qualitative and quantitative assessment 840–841
 - user effects 843–844
- definition 834
- DSA and PSA 834–835
- qualitative and quantitative accuracy evaluation 835
- Vertical asymmetric heterogeneous gas/liquid counter-current flow 857
- Vertical flow regime map
 - post-CHF 559
 - pre-CHF 558–559
 - RELAP5 554*f*, 557
 - schematic representation 554, 554*f*
- Very large eddy simulation (VLES) 755, 797
- Virtual reactor (VR), CASL 761*f*
- VLES *See* Very large eddy simulation (VLES)
- Void (fraction)-quality relationship 93–94
- Vortex in accumulators 632–634
- VVER-440 994
- VVER-1000, AM action in 1039, 1040*f*
- V&V processes *See* Verification and validation (V&V) processes

W

- Wall-bounded flows, wall in 804
- Wall friction
 - factor approach 581
 - single-phase flow 582–583
 - two-phase flow
 - Darcy-Weisbach friction factors 583–584
 - HTFS-modified Baroczy correlation 584
 - RELAP5 585
 - TRACE 584–585
- Wall function method 792–793
- Wallis correlation 603–604, 862
- Wall-modeled DES 799
- Wall-modeled LES (WMLES) 794–795, 797, 805
- Wall-modeled (U)RANS 792–793

Wall-resolved LES 805
Wall-resolved (U)RANS 793
Wall-resolved RANS vs. near-wall treatment 803
Wall stress approach 795–796
Wall stress model 795
Water-cooled and water-moderated energy reactors (WWER) 838
 large breaks 327*t*
 small and intermediate leaks 328–330*t*
 transients 331*t*
Water Cooled Nuclear Reactors 4–5, 144, 241, 483, 500, 504, 531, 533–535, 835, 976, 982, 1034*t*, 1044, 1087
Water-cooled reactor, separate-effect test 747–748*t*
Water hammer 15–16, 147, 264, 279, 341, 662–663, 780–781*t*, 785, 969*t*, 971, 1020
Water packing 73, 276, 662, 664
Wave 15–16, 255–257*t*, 258, 264–265, 335–336*t*, 504–505, 586–587, 644, 662–663, 672–673, 677–679, 747–748*t*, 928, 956, 962–963*t*, 971–972, 980, 983*t*, 986, 1025, 1030, 1046, 1061, 1070, 1070*t*, 1077–1078, 1080, 1146
Wilks (formula) 56, 861, 867–871, 883–884, 893
WMLES *See* Wall-modeled LES (WMLES)

Z

0-D choked flow model 682–683
0-D modules in SYS-TH code 652, 652*f*
Zion NPP
 application to 886
 maximum cladding temperature vs. time 887*f*
 uncertainty bands 891*f*
Zonal model 796



Author Index

Note: Page numbers followed by *f* indicate figures, *t* indicate tables, and *np* indicate footnotes.

A

- Abagyan, A.A. 1117
Abdul-Razzak, A. 57
Abu-Zeid, M.A. 15–16
Adamov, E.O. 1104, 1110, 1117, 1120
Addabbo, C. 852, 1108
Adorni, M. 957, 974, 1063, 1083–1084, 1105–1106
Adrianov, V.N. 402
Adu, S. 912, 922, 1063
Agbodemegbe, V.Y. 515
Ahn, S.H. 73, 552
Akaho, E.H.K. 515
Aksan, S.N. 55, 73, 78, 113, 344–345, 499–500, 503–504, 552, 586–587, 899, 925, 1108
Aktas, B. 664
Alamgir, M.D. 598–599
Aldemir, T. 933
Alexeenko, S.V. 385
Allen, E.J. 266–267
Allen, T.B. 1109
Allison, C. 131
Allison, C.M. 91, 113, 134–135, 604

Allmaras, S.R. 786–788*t*
Allotey, F.K.A. 515
Almenas, K. 1110
Alonso, J.R. 1038
Alvim, A.C.M. 1038
Ambrosini, W. 10, 259, 344–345, 841, 922, 1144
Amendola, A. 933
Ammirabile, L. 92, 344–345, 920, 1084
Amri, A. 1038
Amsden, A.A. 659–660
Analytis, G.Th. 578, 958–961*t*, 992, 998–1000
Anderson, M. 344–345
Anderson, P.S. 553
Andreani, M. 57, 459–460, 733, 739, 741, 746, 749, 755–757
Andreev, G.A. 416–417
Andrievsky, A.A. 438, 439*f*, 457–458
Andrs, D. 7
Anegawa, T. 66, 528–529, 1030
Anhert, C. 14, 65, 73, 91, 925, 1030–1032
Annaratone, D. 7
Annunziato, A. 92, 114, 1108
Anoda, Y. 15–16, 958–961*t*, 969*t*, 1044
Antoni, O. 642, 648–649
Apostolakis, G. 14, 134, 145–146, 933
Aragones, J.M. 133, 1104
Araneo, D. 15–16, 102, 958–961*t*, 1047, 1049, 1055–1056
Archambeau, F. 772
Ardron, K.H. 347
Arenas, M. 772
Arias, F.J. 108
Aritomi, M. 7
Arkadov, G. 14
Arkoma, A. 958–961*t*
Arndt, S. 1043
Aronson, A. 15

Arora, K. 799
Arpott, D.G. 1120
Arslan, E. 912
Ashley, R. 55, 78, 113, 899, 925
Ashmantas, L.A. 479
Assad, A. 563
Astrup, P. 553
Atamturktur, S.H. 912
Aumiller, D.L. 807*t*, 969*t*, 1029
Austregesilo, H. 73, 552, 642, 649
Avdeev, A.A. 458–459
Avduevsky, V.S. 416
Avramova, M. 668–669
Avsentuk, B.P. 476
Avvakumov, A. 14
Aydogan, F. 550, 577–578
Aziz, K. 341, 448, 698

B

Babaitsev, M.N. 1117
Babelli, I. 850
Bachmann, C.R. 800
Badillo, A. 733, 746, 749, 763, 819, 822
Badulescu, A. 499–500, 503–504
Bae, B.-U. 958–961*t*, 1025
Bae, S.W. 642, 912
Bae, Y.Y. 344–345, 958–961*t*, 1025
Baek, J.-S. 15
Baek, W.-P. 969*t*, 1057
Baglietto, E. 771, 788
Bagul, R.K. 608
Bahrami, M. 416–417
Bajorek, S.M. 52–53
Bajs, T. 8, 57–58, 78, 113, 807*t*, 925
Baker, L. Jr. 15
Baker, O. 557*t*

Balabanov, E. 6
Balakrishnan, A.R. 436
Balaras, E. 796, 803
Ban, C.H. 550–551, 807*t*
Bandini, G. 958–961*t*, 998–1000, 1131
Banerjee, S. 7, 201, 761
Bang, Y.S. 912, 958–961*t*, 969*t*
Bankoff, S.G. 283
Bannwart, A.C. 744
Baranyai, G. 15–16
Baratta, A.J. 14, 91, 1031, 1104
Bardon, J.-P. 448
Barna, I.F. 15–16
Baroczy, C.J. 500
Barré, F. 550–551, 564
Barth, A. 733, 746, 749, 763, 819, 822
Bartosiewicz, Y. 180, 196, 208, 519–520, 686, 980
Bassenghi, F. 550–551, 561, 562*f*
Batet, L. 17–18, 91, 101–102, 123, 131, 134–135, 533
Batt, D.L. 606–607
Batta, A. 515
Baudin, N. 744
Bauer, R.C. 807*t*
Baumeister, K.J. 428–429
Bazin, P. 131, 533, 688, 847
Beam, T.M. 1025*t*
Bechta, S. 969*t*, 1029
Beckmeyer, R.R. 958–961*t*
Bejan, A. 419–420
Bellet, S. 733, 746, 749, 763, 819, 822
Belliard, M. 668–669
Belov, A. 15–16
Belsito, S. 899, 996
Benčík, M. 957
Bender, R. 757, 792

Benedict, M. 15
Bengaouer, A. 688
Benhamadouche, S. 63, 770, 772
Benocci, C. 796
Benoit, J.P. 532–533, 1141
Bergeron, A. 668–669
Berman, B.R. 360
Berman, L.D. 397
Bernard, M. 668–669
Bernardin, J.D. 429, 430–431*t*
Berne, P. 680
Berry, R.A. 7
Berta, V.T. 606–607
Bertodano, M.L. 850
Bessette, D. 6, 92
Bestion, D. 7, 17–18, 65, 73, 94, 111, 123, 180, 196–198, 208, 220, 222, 238–239, 549–553, 561, 575, 642, 648–649, 666, 685, 689–690, 693, 701–704, 713–714, 719–720, 722–723, 733, 746, 749, 751–752, 759, 759–760*f*, 763, 782–783*t*, 784, 819, 822, 1130
Beus, S.G. 563
Bezard, H. 789
Biazussi, J. 744
Bieder, U. 733, 739, 741, 746, 749, 755–757, 768
Billa, C. 975–976
Birchley, J. 958–961*t*, 1082, 1138
Bird, R.B. 6
Bittan, J. 958–961*t*, 1012
Bittermann, D. 344
Blasius, H. 497
Blinkov, V.N. 845, 1043
Bloch, H.P. 7
Blokh, A.G. 402, 412
Blomstrand, J. 1104–1105
Blowe, T.N. 768
Bobkov, V.P. 6, 111, 581
Boelter, L.M.K. 111, 571–572*t*, 578–579

Boeschofen, F. 416
Bogdan, S.H. 397
Bogoslovskaya, G.P. 370
Bois, G. 201
Bolado-Lavin, L. 12, 923
Bolger, F. 1037
Bonuccelli, M. 55, 123, 532, 925
Borishanskii, B.M. 434, 434*f*, 438, 439*f*, 457–458
Borishansky, V.M. 385, 388–389
Borisov, E. 958–961*t*
Borisov, S. 131
Bornea, D. 557*t*
Bottin, M. 561
Boucker, M. 202, 772
Boure, J.A. 174
Bourlakov, E.V. 1110, 1117, 1120
Bourouga, B. 448
Bousbia Salah, A. 529, 908–909, 912, 958–961*t*, 1063, 1077–1078, 1104, 1144
Bovalini, R. 841, 922
Boyack, B. 642
Boyack, B.E. 152, 154–155, 705, 866, 896–897
Boyd, C. 738, 742, 745, 750, 761, 764, 780
Breber, G. 392, 392*f*
Breitung, W. 15
Breuer, M. 799
Brittain, I. 265, 601
Bromley, L.A. 111, 579
Brooks, C.S. 564, 575
Broughton, J.M. 1131
Brown, G. 569–570, 571–572*t*
Brown, L.D. 870–871
Brücher, W. 14–15
Bubelis, E. 515
Bucalossi, A. 912, 1039
Buchanan, J.R. 564

Buchlin, J.M. 7
Buckner, M.R. 958–961*t*
Bukin, N. 1020–1021
Bungartz, H.-J. 15–16
Burgazzi, L. 12, 923
Burtseva, T. 53–54
Butterworth, D. 448
Bykov, M.A. 912

C

Cabot, W. 796
Cacuci, D. 912
Cacuci, D.G. 7
Cadinu, F. 806–807, 807*t*
Cai, T.T. 870–871
Calastri, A. 56, 66, 99
Calvo, A. 601–602
Camargo, C. 16, 58, 73, 74*f*, 76, 78–79, 131, 909, 911–912, 925–926
Cammi, A. 585
Camp, A.L. 15
Camy, R. 733, 746, 749, 763, 819, 822
Cao, X.W. 958–961*t*, 992, 1016
Cao, Z.D. 771
Caplan, J.S. 15
Cappiello, M.W. 549–550
Carissimo, B. 815
Carlos, S. 912
Carlsrlow, H.S. 360
Caruge, D. 668–669
Carvalho, R.D.M. 744
Castellana, F.S. 849–850, 850*t*
Catton, I. 154–155, 850–851, 866, 896–897
Cekhovsky, V.Ya. 417
Celik, I. 160
Cess, R.D. 6, 402

Chai, L.H. 425
Chaikin, P.M. 261, 360
Chan, K.C. 529
Chandesris, M. 201, 670, 713–714
Chang, H. 61
Chang, K.S. 613
Chao, B.T. 396, 416
Chapman, D.R. 803, 805
Chatzikyriakou, D. 581
Chauve, M.-P. 797
Chawla, T.C. 576–577
Checherov, K.P. 1117, 1120
Cheissoux, J.L. 668–669
Chen, C.-H. 958–961t
Chen, I.Y. 585
Chen, J.B. 958–961t, 992, 1016
Chen, J.C. 111, 579
Chen, M.-H. 969t, 1034
Chen, Q. 775, 776f
Chen, Y. 344–345, 347
Chen, Y.-S. 958–961t, 1044
Cheng, H.S. 1104, 1134
Cheng, L.-Y. 15
Cheng, S.C. 111, 579
Cheng, X. 344
Cheng, Z. 1070
Cheremisnoff, N.P. 795
Cherkashov, Yu.M. 1110, 1117, 1120
Cherubini, M. 16, 102, 911, 957, 958–961t, 1038–1039, 1055, 1064, 1066, 1083–1084
Chetan, S.J. 790
Cheung, F.B. 426, 611–613
Cheung, Y.K. 630
Chexal, B. 574–575
Chiang, S.C. 912
Chikhi, N. 581

Chisholm, D. 500, 584
Cho, H.K. 17–18, 604, 969*t*
Cho, S. 958–961*t*, 969*t*, 1016, 1057
Cho, S.-W. 1138
Cho, Y. 419–420
Cho, Y.I. 583
Cho, Y.J. 613
Choi, J.S. 622
Choi, K.-Y. 958–961*t*, 969*t*, 998–1000, 1016, 1057
Choi, T.S. 552, 579
Chojnacki, E. 73
Chu, H.H.S. 578–579
Chudnovskaya, I.I. 474
Chudnovsky, A.F. 376–377
Chun, T.H. 788–789
Chung, B.D. 57, 575, 958–961*t*, 992, 998–1000
Chung, M.K. 768
Chung, M.S. 613
Churchill, S.W. 578–579, 582–583
Churkin, A. 344–345
Chyu, C.M. 585
Cicchitti, A. 499
Clarke, W.G. 969*t*, 1029
Class, A.G. 515
Clausing, A.M. 416
Clement, P. 995
Coddington, P. 57, 575, 958–961*t*, 992, 998–1000
Colburn, A.P. 580
Colebrook, C.F. 497, 582
Colin, C. 744, 958–961*t*, 1042
Collier, J.G. 6, 90, 451, 459–460, 554–555, 580
Colombo, L. 585
Colombo, M. 585
Comolet, R. 302
Congiu, C. 995

Conkling, T.W. 1104
Coste, P. 180, 196, 208
Costello, F.A. 416
Courtin, S. 15–16
Craft, T.J. 803
Crowell, K.R. 743
Cuadra, A. 15
Cuervo, D. 958–961*t*, 1071
Culham, J.R. 416–417
Cummings, J.C. 15
Cumó, M. 6–7, 9

D

Dai, Q. 61
Darko, E.O. 912, 922
D'Auria, F. 6, 8, 12, 14–18, 45, 48, 51, 55–58, 66–69, 67*f*, 72–73, 74*f*, 76, 78–79, 79*f*, 99, 102, 113, 117–118, 123, 131, 259, 265, 291–292, 499–500, 503–504, 520, 528–529, 532–533, 539, 551–552, 841, 844–845, 847, 851, 871–873, 899, 908–909, 911–912, 918, 920, 922–927, 937, 939, 957, 958–961*t*, 974–976, 980, 995–997, 1011, 1020–1021, 1024–1025, 1030, 1037–1039, 1047, 1049, 1054–1056, 1063–1064, 1066, 1070, 1077–1078, 1083–1084, 1104–1106, 1108, 1110, 1112, 1130, 1144
D'iachenko, P.E. 416–417
Damerell, P.S. 55–56, 606–607, 969*t*, 992
Daum, R. 53–54
Davilu, H. 12, 67, 923, 1144
Davydov, M.V. 1043
de Alfonso, E. 131
de Crecy, A. 131, 532–533, 733, 746, 749, 763, 819, 822
de Crecy, F. 218–220, 690–691, 701
de Langre, E. 7, 15–16, 668–669
De Rosa, F. 958–961*t*, 998–1000, 1130–1131
De Sanctis, N. 1104–1105
De Santi, G. 1053
DeWitt, D.P. 6, 578–579
Debrecin, N. 55–56, 117–118, 123, 131, 291–292, 532, 924–925, 937, 939, 975–976

Deck, S. 801
Deen, N.G. 202
Del Frate, L. 500
Del Nevo, A. 9, 91, 102, 131, 908–909, 957, 1038–1039, 1083–1084, 1144
Delhaye, J.M. 6, 174, 176, 189, 208–209, 459–460, 563
Del'vin, N.N. 416
Deng, J. 958–961t, 992, 1016
Dennhardt, L. 102
Deruaz, R. 847
Dewitt, D.P. 6, 578–579
Deych, M.Y. 597–598, 601
Dhotre, M.T. 202
Di Marco, P. 1104–1105
Di Maro, B. 1063
D'iachenko, P.E. 416–417
Diamond, D. 15
Diessler, G. 497–498
Dittus, F.W. 111, 571–572t, 578–579
Divo, E. 64
Diwan, S.S. 790
Dix, G.E. 290
Dixit, A. 564
Dixit, S. 790
Doan, T. 111, 579
Doi, T. 1019
Dollezhal, N.A. 1110
Dong, Z.F. 583
Dooley, R.B. 550
Dopchie, H. 1103–1104
Dorfman, E.A. 479
Dorokhov, A.P. 379
Dotson, P.J. 549–550
Dougherty, T. 455–456
Doup, B. 564
Dowlati, A. 850

Downar, T. 1134
Dragunov, Yu.G. 443
Drake, R.M. 428–429
Dreier, J. 57, 1038
Dreitser, G.A. 478–481
Dremin, G.I. 845
Drew, D.A. 549–550
Drikakis, D. 797
Du, K. 347
Du, Z. 712–713
Ducros, F. 733, 739, 741, 746, 749, 755–757
Duffey, R.B. 154–155, 866, 896–897
Dukler, A.E. 557t, 694, 698–699
Dulikravich, G.S. 64
Dul'nev, G.N. 377–378
Dumaz, P. 344
Dumont, D. 1108
Dunn, B.M. 870
Duponcheel, M. 686
Dusic, M. 918, 936
Dutton, M. 918, 936
Dyban, E.P. 416
Dyl'nev, G.N. 416–417
Dyomkin, N.B. 416–417
Dzubenko, B.V. 479

E

Ebadian, M.A. 583
Ebert, D. 1070
Ebisawa, K. 1105–1106
Eckert, E.R.G. 428–429
Edlund, M.C. 6
Edwards, J.R. 800
Eget, L. 553
Egorov, Y. 757, 800
Eklund, R. 1104–1105

Ekman, V.W. 793
Elfimov, G.I. 469
Elias, E. 601
Elicson, G.T. 969*t*, 1044
Elkin, I.V. 845, 957, 1039
El-Shanawany, M. 55, 78, 113, 925
Eltawila, F. 55, 78, 113, 925
Elter, J. 1020–1021
El-Wakil, M.M. 6, 92–93
Emeljanov, I.Ya. 1110
Emi-Reynolds, G. 912, 922
Emmanuel, O.D. 1063
Emmerling, R. 524, 524*f*
Emonot, P. 73, 238–239, 550–552, 564, 689, 722–723
Erickson, A.J. 567
Erk, S. 6
Esch, T. 757, 793
Escrivá, A. 958–961*t*
Eskin, V.P. 442
Espinosa-Paredes, G. 91
Etherington, H. 6
Euh, D.J. 564, 604, 969*t*
Ézsöl, G. 15–16

F

Fabic, S. 154
Fair, J.R. 557*t*
Falk, F. 768
Faluomi, V. 995
Farafonov, V.A. 363
Faragher, J. 735, 751*f*
Farvacque, M. 642, 648–649
Fasel, H.F. 800
Fauchet, G. 768
Fauske, H.K. 347, 600, 680
Faydide, B. 688

Féburie, V. 1024
Fedotovskiy, V.C. 377–378
Fedynsky, O.S. 385, 388–389
Fenech, H. 6, 92–93
Fernandez-Moguel, L. 1138
Feng, Y.-M. 958–961*t*, 1034, 1044
Ferrara, P. 1047, 1049
Ferrell, J.K. 585
Ferreri, J.C. 10
Ferziger, E.H. 10
Ferziger, J.H. 795, 797
Fichot, F. 581
Fighetti, C. 455–456
Filinov, N. 958–961*t*, 1030, 1112
Filipov, G.A. 597–598, 601
Filonenko, G.K. 497
Findlay, J.A. 54, 575, 717
Findlay, J.L. 230
Fiori, F. 69, 925
Fischer, K. 276
Fjodorow, A. 969*t*, 1014
Fletcher, C.D. 276
Florschuetz, L.W. 396
Fokin, B.S. 438, 439*f*, 457–458
Folkin, B.S. 579
Fomin, N.A. 416
Forge, A. 17–18
Forslund, R.P. 54, 612
Frampton, G.T. 1103–1104
Franco, M. 561
Franke, J. 815
Freitas, C.J. 160
Freitas, R. 703–704
Freixa, J. 91, 101–102, 113, 117–118, 131, 134–135, 924–925, 958–961*t*
Frepoli, C. 549–550, 611–613, 722, 851, 870, 912

Frid, V. 14, 65, 73, 91, 911, 925, 1030–1032
Fried, E.A. 416
Friedel, L. 500
Frogheri, M. 66, 528–529, 922, 995, 1055, 1110
Fröhlich, J. 790, 795, 797–799
Fu, S. 800
Fu, X. 712–713
Fujioka, K. 131, 533
Fukuda, K. 1056
Fulgosi, M. 201
Fulwood, R.R. 14
Fureby, C. 803
Furness, R.H. 347
Furuya, O. 623
Futatsugi, T. 1019

G

Gabaraev, B. 958–961t, 1030, 1064, 1066, 1110, 1112
Gago, J.L. 958–961t, 1011, 1024–1025
Gaillard, J.P. 668–669
Gajev, I. 1134
Gal'chenko, E.F. 464
Galassi, G.M. 17–18, 51, 55–56, 66–68, 67–68f, 99, 102, 117–118, 123, 131, 500, 532, 845, 851, 899, 912, 924–925, 957, 958–961t, 974–976, 995–997, 1011, 1024–1025, 1037, 1054, 1056, 1105–1106, 1108, 1110, 1130, 1144
Galassi, M.C. 207–208
Galeazzi, S. 291–292
Galetti, M.R. 911–912, 927
Gallagher, J.S. 550
Gallaway, T. 159–160
Gallo, D. 668–669
Gandrille, J.L. 73, 550–552, 564
Ganglu, Q. 771
Ganic, E.N. 459–460
Ganin, E.A. 416
Garis, N. 1122

Gasparini, M. 604
Gatski, T.B. 771–772, 790, 797
Gatta, P. 877–879*f*
Gaul, H.P. 1108
Gavrilov, P.M. 423, 426
Geffraye, G. 642, 648–649, 688
Geoffrey, E.-R. 1063
George, T.L. 550–551, 564, 1138
Gerasimo, A.V. 803
Gerliga, V.A. 475
Germain, P. 131
Gertner, R.F. 426
Getman, A. 14
Ghan, L.S. 866
Gherson, P. 761
Ghia, U. 160
Giannotti, W. 56–57, 72, 102, 131, 871–873, 912, 958–961*t*, 1055, 1066
Gibeling, H. 807*t*
Gilles, J. 448
Giot, M. 6, 174, 176, 189, 208–209, 459–460, 980, 1024
Glaeser, H. 17–18, 48, 56, 58, 73, 79, 112, 131, 532–533, 847, 857, 862, 868–869, 871–872, 911, 918, 922, 927, 936–937, 1130
Glasstone, S. 6
Glebov, V.P. 442
Glück, M. 720–721
Gnielinski, G. 574*t*
Gocht, U. 969*t*, 1014
Gogonin, N.I. 379, 391, 393
Goldberg, Y.N. 579
Golovnyov, I.F. 408
Gomez, R. 668–669
Gommlich, A. 958–961*t*, 1071
Gonin, A.I. 463, 466–467
Gonzales-Cadelo, J. 958–961*t*, 982–986
Gopala, V.R. 755–757, 757*f*

Gorbachev, B.I. 1117, 1119^{np}, 1120
Gordon, B.G. 397
Goreaud, N. 563
Gourmel, V. 958–961^t, 1077–1078
Goux, F. 958–961^t, 1070–1071
Govier, G.W. 341
Graf, U. 807^t
Graffard, E. 733, 739, 741, 746, 749, 755–757
Graham, R.W. 6
Grandotto, M. 668–669
Granger, S. 1024
Grant, I.D.R. 579
Grassi, W. 259
Green, C.D. 1120
Gregary, G.A. 448
Gregory, G.A. 698
Gregory, M.V. 958–961^t
Grgic, D. 807^t, 958–961^t, 1011, 1024–1025
Griffith, P. 154–155, 866, 896–897
Grigor'ev, B.A. 370, 375
Grigorov, D. 958–961^t
Gröber, H. 6
Groeneveld, D.C. 7, 111, 459–460, 499–500, 503–504, 579, 581, 612
Groetzbach, G. 795
Groudev, P. 958–961^t, 1074
Gruber, P. 6, 92
Guba, A. 131, 1108
Gudoshnikov, A.N. 642, 1020–1021
Guffee, L.A. 549–550, 561–562
Guidotti, T.E. 743
Guillen, D.P. 7, 159–160
Guimaraes, L.N.F. 969^t, 1025
Gulich, J.F. 7
Gungor, A. 796
Guo, T. 557

Gupta, A. 870–871
Gupta, S.K. 613, 912
Guyer, B.L. 912
Guyot, M.K. 744

H

Ha, K.S. 549–550, 642, 720–721, 1138
Ha, S.J. 550–551, 712–713
Haar, L. 550
Habensky, V.B. 475
Hackbush, W. 806–807
Hackford, H.L. 399
Haddad, K.H. 426
Hadek, J. 14, 65, 73, 91, 925, 1030–1032
Hafner, W. 276
Hagrman, D.L. 604
Hahne, E. 421
Halatov, A.A. 480
Hall, D.G. 265
Hall Taylor, N.S. 451^f
Hämäläinen, A. 958–961^t
Hamba, F. 796
Hamidouche, T. 1063, 1144
Hammersley, R.J. 969^t, 1044
Han, B.S. 912
Han, J.T. 850
Hanjalić, K. 799
Hanna, B. 642
Hanninen, M. 73, 344–345, 552, 958–961^t
Hara, T. 720–721
Haratyk, G. 958–961^t, 1077–1078
Hardgrove, M. 1134
Harding, J.H. 405
Hari, S. 580
Harlow, F.H. 659–660
Harpster, T.L. 1103–1104

Hartneet, J.P. 402
Hartnett, J.P. 419–420, 583
Harvey, H.A. 550
Hassan, H.A. 800
Hassan, Y. 7–8, 113, 580, 768, 770, 777
Haste, T.J. 958–961*t*, 1082
Hata, K. 1042
Hayashi, K. 1019
He, Y.L. 775, 776*f*
Healy, R.J. 15
Hedberg, P. 733, 746, 749, 763, 819, 822
Heitsch, M. 733, 739, 741, 746, 749, 755–757
Hellsten, A. 772, 789, 815
Hemez, F. 912
Henriksson, M. 733, 739, 741, 746, 749, 755–757, 803
Henry, R.E. 55, 347, 600, 969*t*, 1044, 1103–1104
Herb, J. 918, 936
Heroman, R.H. 499
Herrero, J.J. 958–961*t*, 1071
Hertlein, R. 855
Herviou, K. 14–15
Hetsroni, G. 459–460
Hewitt, G.F. 6, 448, 451*f*, 459–460
Hewitt, S.P. 581
Hibiki, T. 6, 174, 203–205, 208–209, 236, 563–564, 575, 958–961*t*, 969*t*, 998–1000, 1060
Hietanen, O. 1024
Hobbins, R.R. 604
Hochreiter, L. 53, 466, 611–613, 722
Hofer, E. 56
Hofmann, D. 1108
Hofmeister, J. 349
Hogsett, S. 564
Höhne, T. 208, 733, 739, 741, 746, 749, 755–757, 807*t*
Hohorst, J.K. 91, 113, 134–135, 604
Holbert, K.E. 7

Holm, R. 416
Holmes, B.J. 266–267
Holmstrom, H.L.O. 6, 249–251, 254, 333
Holpanov, L.P. 479
Hoppe, F.M. 912
Horhoianu, G. 958–961*t*, 1084
Hortal, J. 918, 936
Horvatic, I. 73, 552, 912, 922, 1063
Horwitz, M. 614
Hosokawa, S. 1019
Hotta, A. 912
Hougen, O.A. 580
Houkema, M. 733, 739, 741, 746, 749, 755–757
Howard, R.J.A. 797
Howell, J.R. 410
Hsu, L.C. 585
Hsu, T.T.C. 1105–1106
Hsu, W.-S. 958–961*t*, 1044
Hsu, Y.Y. 6
Hu, T. 61
Huang, H.-W. 969*t*, 1034
Huang, J. 581
Huang, J.B. 800
Huang, X.C. 111, 581
Huber, M.L. 550
Huber, N. 521
Hudson, N. 1134
Hung, Z.-Y. 958–961*t*, 1044
Hussaini, M.Y. 797, 800
Hutton, A.G. 805
Hwang, M. 912
Hyvarinen, J. 969*t*, 1014

I

Ibrahimbegovic, A. 806–807
Idel'chik, I.E. 500, 539–540

Iguchi, T. 610
Ihle, P. 612
Ikeda, K. 515
Imai, S. 969t, 1044
Imanaka, T. 1104
Imke, U. 668–669
Imre, A.R. 15–16
In De Betou, J. 528–529, 1030
In, W.K. 788–789
Inayatov, A.Y. 579
Incropera, F.P. 6, 578–579
Ingegneri, M. 957
Ingersoll, A.C. 370, 372, 376–377
Ingersoll, L.R. 370, 372, 376–377
Inoue, H. 1105–1106
Inoue, S. 532–533, 1141
Ionescu, D.V. 958–961t, 1084
Ionov, A.I. 1104, 1117
Irani, A. 1025t
Irvine, J.F. 402
Isachenko, V.I. 382f, 388–389, 393–394, 397
Isachenko, V.P. 465–466
Ishii, M. 5–6, 174, 203–205, 208–209, 236, 447, 529, 556–557, 563–564, 575–577, 608, 700–701, 850, 958–961t, 969t, 998–1000, 1060
Ivanov, I. 12, 923
Ivanov, K. 14, 91, 912, 958–961t, 1031–1032, 1134
Ivanovsky, M.N. 385
Iyer, K. 761

J

Jackson, J.D. 344–345
Jacobson, S. 308
Jaeager, J.C. 360
Jafari, J. 12, 67, 923, 1144
Jaffrézic, B. 799

Jakirlić, S. 799
Jakob, M. 6
Jamet, D. 201
Jang, C. 958–961t, 1049
Janicot, A. 689, 702
Jankowski, M. 6
Jarlais, G. 557
Jayanti, S. 515, 722
Jayaraju, S. 755–757, 757f
Jeong, J.J. 17–18, 123, 549–552, 564, 642, 720–721, 807t, 958–961t, 1025, 1130
Jester-Zürker, R. 799
Jeun, G.D. 613
Jimenez, G. 958–961t, 982–986, 1061, 1063, 1071
Jimenez, J. 958–961t, 1071
Jin, H.G. 712–713
Jo, J. 305–306
Johansson, A.V. 789
Johnson, R.W. 159–160, 791
Jones, T.M. 416, 419–420
Jongen, T. 771–772
Jordan, T. 743
Joo Er, M. 912
Joshi, J. 608
Joucla, J. 131, 533
Juliá, J.E. 564
Just, L.C. 15

K

Kadri, D. 642, 648–649
Kaganer, M.G. 416–417
Kajanto, P. 635
Kaliatka, A. 1064, 1066, 1110
Kalinin, E.K. 478–481
Kalli, H. 922
Kalyakin, S.G. 1110

Kamenchshikov, F.T. 480
Kandlikar, S.G. 453–454
Kang, K.H. 958–961^t, 969^t, 1016, 1025, 1057
Kang, Q.J. 775, 776^f
Kang, S.K. 768, 770
Kantee, H. 1020–1021
Kapat, J.S. 64
Kapustin, A.V. 845
Karpov, T.M. 416–417
Karwat, H. 17–18, 265, 847, 857, 862
Kasahara, F. 102, 134–135
Kasmala, G.F. 841
Kassab, A.J. 64
Kastner, W. 521
Kataoka, I. 575, 608, 701
Katsma, K.R. 154–155, 866, 896–897
Katznel'son, S.S. 408
Kaviany, M. 376–379, 479
Kays, W.M. 497–498, 578–579
Kazeminejad, H. 12, 67, 923, 1144
Kazimi, M. 6, 92–93
Keating, A. 796, 805
Keim, E. 521
Kell, G.S. 550
Kelly, J. 557, 563–564, 743
Kestin, J. 598
Khadamakar, H.P. 969^t
Khan, M. 613–615
Khan, S.A. 56, 133
Kharitonov, V.V. 413, 416
Kieffer, S.W. 597–598
Kim, B.J. 585
Kim, I.G. 958–961^t
Kim, J. 15, 585, 770–772, 795
Kim, J.W. 768, 770–771, 770^{np}, 773

Kim, K. 912
Kim, K.D. 73, 550–552, 585, 642, 712–713
Kim, M. 17–18, 48, 79, 123, 551–552, 922, 927, 937, 1130
Kim, S. 557, 563–564, 958–961*t*, 1025
Kim, S.B. 15
Kim, S.H. 642
Kim, S.I. 1138
Kim, Y.S. 958–961*t*, 969*t*, 998–1000, 1016, 1057
Kimber, G. 113
Kinoshita, I. 1047
Kirchsteiger, C. 12, 923
Kirillov, P.L. 6, 111, 344–345, 370, 499–500, 503–504, 581
Kiselev, A.N. 1120
Kisil'I, M. 1117
Kitzel', V.A. 408
Klein, S.A. 550
Kliem, S. 807*t*, 958–961*t*, 1037, 1071
Klimenko, A.V. 402
Klimenko, V.V. 426, 429
Kloos, M. 877–879*f*
Knief, R.A. 7
Kniesner, B. 799
Knight, T.D. 549–550
Knoll, G.F. 14–15
Kobori, T. 1056
Kocamustafaogullari, G. 447, 563
Kohketsu, H. 969*t*, 1044
Kohrt, R.J. 743
Kojasoy, G. 557
Kok, H.V. 969*t*, 1060
Kok, J.C. 789
Kokorev, B.V. 363
Kokorev, L.C. 413
Kokorev, L.S. 416
Kolev, N. 7, 969*t*, 1029

Komen, E. 733, 739, 741, 746, 749, 755–757, 757*f*
Koncar, B. 207–208
Kondo, M. 15–16
Kondrat'ev, G.M. 375
Korhonen, R. 1024
Koshizuka, S. 344
Koshkin, V.K. 416
Kostka, P. 1020–1021
Koszela, Z. 15–16
Kothe, D.B. 745, 746*f*, 760, 761*f*
Kovtonyuk, A. 69, 72–73, 552, 925
Kovtonyuk, M. 925
Kozłowski, T. 519–520, 601–602, 806–807, 807*t*, 1134
Kozyrev, A.P. 434, 434*f*, 438
Kraus, D. 419–420
Krayushkin, A.V. 1117
Krepper, E. 207–208, 238
Kress, T.S. 145–146
Krishnam, V.S. 642
Krishner, W. 689
Kristof, M. 912, 1020–1021
Krivokhvatsty, K.S. 1120
Kromp, W. 1038
Kruse, A. 345*f*, 346
Krussenberg, A.-K. 969*t*, 1014
Kryuchkov, D. 958–961*t*, 1030, 1110, 1112
Krzykacz-Hausmann, B. 870–871
Kuan, P. 1131
Kudo, Y. 912
Kudrik, I. 1107
Kudryashev, L.I. 375
Kuhn, S.Z. 574*t*
Kukharchuk, O.F. 1110
Kukharkin, N.E. 1110
Kukita, Y. 847, 969*t*, 1044

Kumar, A. 912
Kuntz, M. 757, 792
Kunz, R.F. 841
Kupiec, C.F. 15
Kurganov, V.A. 469
Kurki, J. 958–961t
Kusuno, S. 720–721
Kutateladze, S.S. 6, 104, 385, 388–389, 456–457, 476
Kvidza, B. 1020–1021
Kyncl, M. 131, 533
Kyrki-Rajamäki, R. 344

L

La Lumia, V. 12, 923
Labois, M. 201, 791
Labuntsov, D.A. 420–421, 434–435, 437
Labuntzov, D.A. 388–389, 391–392
Lage, C. 73
Lahey, R.T. 5–6, 97, 174, 549–550, 569, 571–572t, 579–580, 599, 1104–1105, 1112–1113, 1144
Lakehal, D. 58, 180, 196, 201–202, 208, 791
Lamarsh, J.R. 6, 14
Landau, L. 6
Landry, R. 6, 92
Lanfredini, M. 16, 58, 76, 78–79, 909, 911–912, 925–926
Langenbuch, S. 528–529, 1030
Langer, R. 459–460
Langtry, R. 757, 792
Larin, B.M. 471
Laroche, S. 688
Latini, A. 1047, 1049
Latyev, L.N. 417
Launder, B.E. 772, 790, 803
Laurence, D. 797
Lavialle, G. 642, 648–649
Lavieville, J. 772

Lazaro, A. 912
Lazzerini, D. 16, 1083–1084
Lebaigue, O. 201
Lee, D.Y. 564
Lee, E.H. 712–713
Lee, H.-D. 17–18
Lee, J.R. 770–772
Lee, K. 569, 571–572*t*
Lee, S. 17–18
Lee, S.C. 283
Lee, S.J. 613
Lee, S.W. 642
Lee, W.J. 549–550, 642, 720–721, 958–961*t*, 1025
Leech, W.J. 466
Lel'chuk, B.L. 469
Lele, H.G. 613, 912
Lellouche, G.S. 154–155, 866, 896–897
Lellouche, J. 601
Lemmon, E.W. 550
Leonardi, M. 871–872, 922, 1055, 1110
Leonardi, T. 850
Lerchl, G. 234, 642, 649
Leung, L.K.H. 111, 344–345, 581
Leung, R.K. 642
Leveque, C. 113
Levy, H.W. 15
Levy, S. 6, 154–155, 601, 603–604, 613, 866, 896–897, 957
Lewis, E.E. 10
Lewis, M.J. 249–251, 254, 333
Lhuillier, D. 237
Li, J.-L. 1105–1106
Li, Q. 775, 776*f*
Li, Y. 61
Liebert, J. 524, 524*f*
Lien, P. 1120

Lienhard, J.H. 429, 598–599
Lifchitz, E. 6
Lightfoot, E.N. 6
Liles, D.R. 549–550
Lillington, J. 250–251, 332–333
Lilly, D.K. 202
Lim, H.S. 712–713
Lin, H.T. 912
Lin, H.-T. 958–961*t*
Lin, J.F. 385, 398–399
Lin, J.-M. 969*t*, 1034
Lin, T.F. 611–613
Lin, Z.Q. 385, 398–399
Lipatov, I.A. 845
Lischke, W. 969*t*, 1014
Lisovsky, O. 16, 1083–1084
Litfin, K. 515
Liu, C.C. 912
Liu, L. 712–713
Liu, Q. 775, 776*f*
Liu, W.S. 642
Liu, Y. 564, 958–961*t*, 969*t*, 998–1000, 1060
Liu, Y.-T. 958–961*t*, 1034
Llopis, C. 17–18, 102, 123, 134–135
Lo Nigro, A. 912
Lockhart, R.W. 95, 499–500, 584
Loginov, N.I. 6
Logvinov, S.A. 443
Lombardi, C. 498–499
Lombardi-Costa, A. 529, 1104, 1144
López, F. 744
Lopez-Alonso, E. 958–961*t*, 1061, 1063
Lubbesmeyer, D. 251–253
Lubensky, T.C. 360, 379
Lu, P. 772

Lubin, B. 614
Lucas, D. 208
Luo, K.H. 775, 776*f*
Luther, W. 859, 870–871
Luxat, J.C. 642
Lykov, A.V. 6, 372, 376–377

M

Ma, H. 788–789, 802
Ma, W. 1134
Macek, J. 131, 533, 1020–1021
Macian, R. 131, 533, 575
Macintosh, J.E. 416, 419–420
Macken, N.A. 285–286
Madeira, A. 909, 912, 937, 995, 1038
Magdeleine, S. 201
Magedanz, J. 1134
Mahaffy, J. 181, 549–550, 661, 722, 733, 739, 741, 746, 749, 755–757, 807*t*, 841
Majumdar, P. 613
Makhin, V.M. 6
Makihara, Y. 1020–1021
Malkin, S.D. 1117
Malko, M.V. 1104, 1111, 1117, 1120, 1143
Mallen, A.N. 1104, 1134
Malofeev, V. 14
Malouf, W.J. 772
Mancheva, K. 958–961*t*
Mandhane, J.M. 448, 698
Manera, A. 102, 131, 958–961*t*
Manhart, M. 799
Manisekaran, S. 790
Man'kina, N.N. 442
Mannheiner, R. 613–616, 618
Mansani, L. 515
Maraczy, C. 344

Marchand, M. 561
March-Leuba, J. 1134
Margoulova, Th. 6, 1110
Markovic, D. 806–807
Marotta, M.E. 419–420
Marques, M. 12, 923
Marschall, E.A. 419–420
Marshall, M.D. 1138
Marshall, S.O. 557
Marshall, W.R. 574t
Marsili, P. 250–251, 332–333, 352
Martens, R. 14–15
Martin, D.G. 405
Martin, R.M. 114, 134–135
Martin, R.P. 53, 131, 870, 909
Martineau, R.C. 7
Martinelli, R.C. 95, 499–500, 584
Martinez Val, J.M. 133, 1104
Martínez-Murillo, J.C. 958–961t, 1061, 1063
Martinez-Quiroga, V. 117–118, 924–925
Martinson, Z.R. 604
Marton, I. 912
Martorell, S. 912
Maruyama, Y. 969t, 998–1000
Mascari, F. 957, 1130
Mastrantonio, L. 1037
Matejovic, P. 1020–1021
Mathieu, B. 201
Matteoli, C. 957
Mavko, B. 841, 912
May, R. 866, 896–897
Mayinger, F. 7, 459–460, 516, 604
Mazoyer, M. 670, 713–714
Mazzantini, O. 16, 58, 73, 74f, 76, 78–79, 131, 909, 911–912, 925–926, 1030, 1047, 1049, 1083–1084
Mazzini, D. 958–961t, 1030, 1112

Mazzini, M. 847, 1037–1038
McAdams, W.H. 499
McClintock, R.G. 550
McClure, P. 912
McComas, S.T. 600
McDonald, B.N. 969_t, 1025, 1029
McLaughlin, D.K. 622
McLinden, M.O. 550
McPherson, G.D. 154
McWald, T.H. 419–420
Meca, R. 131, 533
Mehedinteanu, S. 958–961_t, 1039
Melara, J. 958–961_t
Melideo, D. 1030
Melikhov, O.I. 845, 957, 1014_t, 1039, 1043, 1060
Melikhov, V.I. 1014_t, 1043, 1060
Mendizabal, R. 912, 918, 936, 958–961_t
Menon, S. 796
Menter, F.R. 729, 733, 739, 741, 746, 749, 755–757, 786–788_t,
789, 792–793, 800
Menzel, F. 909, 912, 937
Meredith, R.E. 378
Meri, A. 797
Meyer, C.A. 550
Mi, Y. 564
Micaelli, J.C. 693
Michal, R. 5
Miettinen, A. 922
Mieusset, T. 131
Migrov Yu, A. 6, 642
Mikhailov, Yu.A. 6
Miller, B.S. 416–417
Miller, J. 601
Milovanov, Yu.V. 385
Mimouni, S. 180, 196, 207–208, 772
Minchenko, F.P. 437

Mingues, E. 133, 1104
Miro, J. 17–18
Mirò, R. 14, 65, 73, 91, 925, 1031–1032
Mironov, Y.V. 1110
Miropol'sky, Z.L. 392, 467, 469
Mišák, J. 6, 75f, 1020–1021
Misale, M. 528–529
Misawa, T. 771
Mishima, K. 556, 563, 608, 700, 720–721
Mitrophanova, O.V. 480
Mittag, S. 958–961t, 1037
Mizokami, S. 912
Modro, M. 17–18
Moieni, P. 14, 134
Moin, P. 795–796
Mokizuki, H. 1133
Monasterolo, U. 66
Monnier, P. 102, 899, 1038
Montero-Mayorga, J. 958–961t, 982–986
Moody, F.J. 6, 97, 174, 347, 599, 680, 1112–1113, 1144
Moon, H.C. 441
Moon, S.K. 642
Moore, K.V. 7, 54
Moradkhanian, E.N. 849–850, 850t
Morel, C. 174, 201, 203, 207–209, 236–238, 563–564, 772
Moretti, F. 500, 733, 739, 741, 746, 749, 755–757, 763, 819, 822, 957, 958–961t, 1030, 1039, 1047, 1049, 1112
Morii, T. 733, 739, 741, 746, 749, 755–757
Moskalev, A. 1064, 1066, 1110
Moskalev, A.M. 912
Motohashi, S. 1105–1106
Moussavian, K. 912
Mudawar, J. 429, 430–431t
Mudde, R.F. 969t, 1060
Muellner, M. 1039
Muellner, N. 16, 58, 76, 78–79, 909, 912, 925–926, 1038, 1144

Muftuoglu, K. 870, 912
Mühlbauer, P. 733, 739, 741, 746, 749, 755–757
Mühlbauer, T. 91
Mulas, M. 789
Mull, T. 102, 899, 1038
Mullen, E. 287
Muller, C. 12, 923
Muñoz Cobo, J.L. 733, 746, 749, 763, 819, 822, 958–961*t*
Murase, M. 1019, 1047
Murata, H. 969*t*, 1044
Muratov, B.L. 474
Murray, C.J. 841
Murray, R. 7

N

Nacci, G. 957
Naff, S. 6, 92
Nahavandi, A.N. 849–850, 850*t*
Nainer, O. 912
Nakamura, H. 969*t*, 998–1000, 1038, 1057, 1130
Nakayama, A. 377
Nakoriakov, V.E. 385
Nam Dinh, T. 806–807, 807*t*
Navarro, M.A. 769
Naviglio, A. 7
Necker, G. 743
Neil, A. 131, 874, 876–880, 877–879*f*
Nelson, D.B. 95, 499–500
Nelson, R.A. 549–550
Nerovnov, A. 1014*t*, 1060
Neymotin, B. 604, 605*t*, 606*f*
Neymotin, I. 305–306, 604, 605*t*, 606*f*
Niceno, B. 180, 196, 202, 207–208, 238, 733, 746, 749, 763, 819, 822
Nickolaeva, A. 733, 746, 749, 763, 819, 822
Nikitin, A. 1107

Nikitin, Y.M. 1110, 1117
Nikonov, S.M. 845
Nilsen, T. 1107
Nilsson, L. 1108
Ninokata, H. 7, 720–721, 771, 788
Nishida, K. 720–721
Nishikawa, T. 1105–1106
Nissley, M.E. 53, 870, 912
No, H.C. 552, 579, 712–713, 969t
Normann, S. 642
Nourbakhsh, H.P. 761, 1070
Novikov, I.I. 385, 388–389, 438
Novikov, V.V. 377
Novog, D. 344–345
Novoselsky, O.Yu. 958–961t, 1030, 1110, 1112, 1117
Nukiyama, S. 6, 424
Nuñez-Carrera, A. 91
Nusselt, W. 6, 580
Nutt, W.T. 909
Nyarko, B.B.J.B. 1063
Nylund, O. 1104–1105

O

O'Dell, L.D. 53, 131
Oberkampf, W.L. 817
Obry, P. 668–669
Odar, F. 611
Odelevsky, V.I. 376–377
O'Dell, L.D. 53, 131
Oh, D.S. 788–789
Oh, D.Y. 131, 533
Ohkawa, K. 549–550, 870, 912
Ohwada, A. 969t, 1057
Oka, Y. 7, 344
Okrent, D. 10
Olek, S. 251–253

Oliveira, B. 744
Olteanu, G. 958–961*t*, 1084
Oriani, L. 807*t*
Oriolo, F. 997
Orlov Yu, I. 1110
Orlov, V.M. 454
Ormiston, S.J. 744
Ortiz, M.G. 866
Osif, B.A. 1104
Osipova, V.A. 465–466
Ota, H. 378
Ounsy, M. 131, 874, 876–880, 877–879*f*
Ozar, B. 564
Ozdemir, O.E. 1138
Ozdere, O 532–533, 1141
Özisik, M.N. 413, 416
Ozkaynak, F.T. 111, 579

P

Padmakumar, G. 969*t*
Païdoussis, M.P. 7, 15–16
Pakhomov, S.A. 1120
Palen, G.W. 392, 392*f*
Panayotov, D. 14, 65, 73, 91, 925, 1030–1031
Parafilo, L. 958–961*t*, 1030, 1110, 1112
Parameswaran, V. 630
Paranjape, S. 564, 958–961*t*, 969*t*, 998–1000, 1060
Parfenov, Y. 1014*t*, 1060
Parisi, C. 14, 912, 925, 1030, 1064, 1066, 1070, 1110–1111, 1143
Park, C.E. 550–551, 807*t*
Park, G.C. 604, 969*t*
Park, H.S. 958–961*t*, 969*t*, 1016, 1057
Park, I.-K. 17–18
Park, J.H. 557, 1138
Park, Y.-S. 958–961*t*, 1025
Parlatan, Y. 441

Parmhed, O. 803
Pasamehmetoglu, K.O. 549–550
Pascal, G. 92, 114
Pasinato, H. 796
Patankar, S.V. 6, 10
Patwardhan, A.W. 969^t
Pecchia, M. 1030
Pedrocchi, E. 498–499
Pei, B.-S. 958–961^t, 1044
Pelayo, F. 912, 918, 936, 958–961^t
Peller, N. 799
Pellicoro, V. 1144
Pereira, C. 1144
Perepelitsa, N.I. 478
Perez, M. 131, 533
Perez-Ferragut, M. 91, 113, 134–135
Perić, M. 10
Pericas, R. 91, 131
Perlado, J.M. 133, 1104
Pernica, R. 131, 533
Peskin, A.P. 550
Peterson, J.W. 7
Peterson, P.F. 574^t
Petrangeli, G. 1037–1039
Petrini, P. 922
Petrov, A. 1110
Petrov, V.A. 417
Petruzzi, A. 8, 57–58, 69, 72–73, 78, 113, 131, 533, 552, 908–909, 911–912, 920, 925, 1039
Petti, D.A. 604, 1131
Petukhov, B.S. 454, 469, 578–579
Phan, B. 912
Piagentini, A. 72
Pichon, P. 688
Pierro, F. 912, 958–961^t, 1030, 1063–1064, 1066, 1112
Pigford, T.H. 15

Pignatelli, J.F. 12, 923
Pilkhal, D.S. 608
Pineda, H. 744
Piomelli, U. 795–796, 803–805, 804*f*, 806*t*
Pioro, I.L. 6, 344–345
Pioro, J.L. 437–438
Piplies, L. 852, 1053
Pirro, F. 1056
Pla, P. 14, 92, 108, 114, 134–135, 920, 957, 974, 1070, 1105–1106
Planck, M. 6
Plesset, M.S. 569, 571–572*t*
Pochard, R. 17–18, 871–872
Podlázov, L.N. 1117
Podowski, M.Z. 1104–1105
Pokharna, H. 850
Pokusaev, B.G. 385
Polley, G.T. 579
Polmar, N. 1109
Ponomarenko, G.L. 912
Ponomarev-Stepnoy, N.N. 1110, 1117, 1120
Popov, V.M. 416
Porraccia, A. 17–18
Potter, P.E. 405
Potter, W.C. 1104
Pourquie, M. 797
Pouvreau, J. 238–239, 689, 722–723
Powers, D.A. 145–146
Pradhan, S.K. 912
Prandtl, L. 6
Pretel, C. 17–18, 101–102, 123, 134–135
Preusche, G. 6, 92
Price, S.J. 7, 15–16
Prior, R. 1038
Probst, P. 131, 533
Prosek, A. 841, 912

Pun-Quach, D. 912
Purhonen, H. 922
Putney, J.M. 574–575
Puzin, V.F. 457

Q

Qiu, S.Z. 65, 958–961*t*, 969*t*, 998–1000, 1060
Queral, C. 958–961*t*, 982–986, 1061, 1063

R

Raad, P. 160
Rachkov, V.I. 1110
Raddaoui, M. 797
Radhakrishnan, S. 805
Radkevich, V. 958–961*t*, 1030, 1064, 1066, 1110, 1112
Ralston, T. 579
Ramesh, O.N. 790
Ramilison, I.M. 429
Ramon, B. 642, 648–649
Ransom, V.H. 680, 850
Rantamäki, K. 958–961*t*
Ranz, E. 574*t*
Rao, R.S. 912
Rapier, A.C. 416, 419–420
Rapp, Ch. 799
Rassokhin, N.G. 442
Ratel, G. 688
Rathman, O. 553
Ratkovich, N. 744
Razumovskiy, V. 344–345
Rebollo-Mena, M.J. 958–961*t*, 1061, 1063
Reddt, G. 455–456
Reddy, K.R. 515
Reece, G.J. 772, 790
Reeder, D.L. 987
Reichardt, H. 6

Reimann, J. 613–615
Reina, G. 933
Remizov, O.V. 463, 466–467
Renault, C. 250–251, 332–333
Reocreux, M. 11, 899, 980, 1021
Reshetov, B.A. 480
Reshotko, E. 599
Rettig, W.H. 7, 54
Revankar, S.T. 564, 613–616, 618, 850
Reventos, F. 8, 17–18, 57–58, 78, 91, 101–102, 108, 113–114, 117–118, 123, 131, 134–135, 532–533, 924–925, 957
Reyes, J.N. 851
Reynolds, A.B. 416
Reynolds, O. 6
Reynolds, W.C. 803
Richards, C. 250–251, 332–334, 745, 747–748^t, 838
Richards, D.J. 642, 841
Richner, M. 958–961^t, 1082
Richter, H.J. 599
Ricotti, M.E. 585
Riebold, W.L. 852
Riegel, B. 275
Riemke, R.A. 569, 661
Riethmuller, M.L. 174, 176, 189, 208–209, 459–460
Rigamonti, M. 1108
Riikonen, V. 1108
Rindelhardt, U. 14, 65, 73, 91, 925, 1030–1032
Ríos, M. 134–135
Rithmuller, M.L. 6
Rizwan-Uddin 14, 65, 73, 91
Roache, P.J. 159–160
Roberts, D.N. 557^t
Robinson, C.M.E. 803
Rodi, W. 772, 789–790, 797
Rodionov, A. 14
Roelofs, F. 755–757, 757^f

Rogovin, M. 1103–1104
Rohatgi, U.S. 17–18, 154–155, 305–306, 441, 599, 604, 605*t*, 606*f*,
850–851, 866, 896–897, 1104
Rohde, U. 733, 739, 741, 746, 749, 755–757, 807*t*, 958–961*t*, 1037
Rohsenow, W.M. 54, 419–420, 437–438, 459–460, 583, 612
Rosal, E.R. 611–613
Rose, J.W. 385
Rossi, A. 1047, 1049
Roth, G.A. 550, 577–578
Rotta, J.C. 731, 755–757
Rouben, B. 958–961*t*, 1030
Rovnov, A.A. 845
Roy, C.J. 817
Royer, E. 111, 581, 668–669
Royle, P. 15
Rozzia, D. 957, 1083–1084
Rust, K. 612
Ruyer, P. 207–208, 238, 744, 958–961*t*, 1042
Ryabov, A.N. 480
Ryley, D.J. 569, 571–572*t*
Ryzhkov, L.N. 412
Ryzhov, S.B. 912

S

Sabundjan, G. 909, 912, 937
Sadatomi, M. 720–721
Sagaut, P. 801
Saha, D. 499–500, 503–504
Saha, P. 580, 601
Saignes, P. 12, 923
Sakurai, A. 459–460, 1042
Salay, M.A. 575
Salvat, M. 123
Salvatores, S. 6
Samsonov, B.V. 416
Sanchez, F. 344, 912

Sanchez, V. 344, 668–669
Sanders, J. 1053
Sanderson, P.D. 419–420
Sandervag, O. 1038
Sankovich, M.F. 969t, 1025, 1029
Santoro, R. 1030
Santos, A.A.C. 769
Sapankevich, A.P. 478
Sarkar, S. 772, 790
Sartmadjiev, A. 1020–1021
Sartori, E. 14, 65, 73, 91, 925, 1030–1032
Saunders, J. H. 15
Sawitzki, M. 855
Schäfer, M. 15–16
Schaffrath, A. 969t, 1014
Schekoldin, V.I. 957
Scheuerer, M. 208, 733, 739, 741, 746, 749, 755–757, 763, 819, 822
Schiestel, R. 797
Schikorr, M. 515
Schlegel, J.P. 564, 958–961t, 969t, 998–1000, 1060
Schlunder, E.U. 359
Schlünzen, H. 815
Schmid, S.D. 1110
Schneider, G.E. 416–417
Schneider, K. 623–624
Schneider, P.J. 360
Schneidesch, C. 923
Schoen, B. 102
Schollenberger, S. 102
Schrock, V.E. 580, 613–616, 618
Schulenberg, T. 344, 349
Schultz, M.A. 6
Schultz, R.R. 15–16, 163, 276, 807t
Schumann, U. 795
Schwarz, S. 859, 870–871

Schwarz, W. 102, 138, 1038
Scott, H.H. 14
Sebilleau, J. 744
Sefan, I. 958–961*t*, 1084
Segurado, J. 923
Sehgal, B.R. 11, 969*t*, 1029, 1113
Seidel, J. 800
Semião, V. 772
Senina, V.A. 471
Sergeev, V.V. 459–460, 463, 466–467
Sermer, P. 912
Serre, G. 94, 220, 238, 519–520, 561, 666, 670, 690, 701, 713–714, 719–720
Sesonske, A. 6
Seul, K.W. 912, 958–961*t*
Sevón, T. 1138
Seynhaeve, J.M. 519–520, 686, 980, 1024
Shabana, E.A. 15
Shah, M.M. 580
Shams, A. 755–757, 757*f*
Shapiro, A.H. 567
Shaug, J.C. 630
Shaw, R.A. 866, 896–897
Shchukin, V.K. 480
Sheindlin, A.A. 417
Shen, N. 421
Shen, Y.F. 771
Sherman, M.P. 15
Shestakov, E.N. 417
Shih, C. 912, 958–961*t*, 969*t*, 1034
Shilov, V.K. 454
Shin, J.-Y. 958–961*t*, 1082–1083
Shiotsu, M. 1042
Shivsai Ajit 790
Shkadov, V.Ya. 479
Shlykov, Yu.P. 416

Shoji, M. 425
Shotkin, L.M. 844
Shtern, Z.Yu. 474
Shur, M. 792
Shvetz, I.T. 416
Sidorov, V. 14
Siebe, D.A. 287
Siegel, R. 410
Silde, A. 642
Silva, Lopes, A. 805
Silvestri, G.J. 550
Silvestri, M. 499
Sim, S.K. 807t
Simon, F.F. 428–429
Simons, J.W. 55–56, 606–607, 969t, 992
Singh, M.P. 7
Situ, R. 564
Sjoberg, A. 14, 65, 73, 91, 925, 1030–1032
Sjoden, G.E. 7
Sjökqvist, L. 803
Skipper, R.G.S. 419–420
Skorek, T. 131, 533
Skripova, V.P. 429
Smagorinsky, J. 797
Smith, B.L. 202, 733, 739, 741, 746, 749, 755–757, 777
Smith, T.R. 564
Smogalev, I.P. 111, 581
Smoglie, C. 618
Snell, V. 6
Snoek, C.W. 459–460
Snytin, S.Yu. 426, 429
So, A. 720–721
Sogalla, M. 14–15
Sokolov, I.A. 1120
Sokolowski, L. 15–16, 601–602

Sol, I. 17–18, 101–102, 114, 123, 134–135
Soldaini, G. 499
Soliman, H.M. 744
Soloukhin, R.I. 408
Soloviev, S.L. 6, 425–426, 432*t*, 440, 440*f*, 458, 482, 1110
Son, Y.-S. 958–961*t*, 1082–1083
Song, C.-H. 61, 604, 733, 739, 741, 746, 749, 755–757, 770–772, 969*t*
Song, J.H. 1138
Sonnenburg, H.G. 17–18, 703
Sorensen, J.N. 145–146
Sorokin, A.P. 1110
Sorokin, V.P. 385
Sosunov, V.I. 379
Souyri, A. 344, 550–551, 564
Soyer, A.E. 532–533, 1141
Sozzi, G.L. 597
Spadoni, A. 958–961*t*, 1011, 1024–1025
Spalart, P.R. 786–788*t*, 792, 796, 799, 802–803, 802*t*
Spalding, D.B. 6, 359, 385, 392, 402
Spalj, S. 1020–1021
Sparrow, E.M. 6, 402
Spaziani, D. 102, 134–135
Specreijse, S.P. 789
Spencer, R.C. 550
Speziale, C.G. 772, 790
Spindler, K. 421
Spindler, R. 453*f*
Spiridonov, Yu.G. 416
Spore, J.W. 549–550, 561–562
Squarer, D. 344
Squires, K.D. 796
Sridharan, A. 611–613
Staedtke, H. 55, 78, 113, 852, 899, 925, 995
Stanev, I. 918, 923
Starflinger, J. 349

Stefanova, A. 958–961*t*, 1074
Steinhoff, F. 17–18, 1108
Steinke, R.G. 549–550, 561–562
Stekelenburg, A.J.C. 1144
Stenbok, I.A. 1117
Stephenson, R. 6
Stewart, C.W. 582
Stewart, J.C. 612
Stewart, W.E. 6
Strelets, M. 792
Strucic, M. 92, 114, 134–135, 920
Struwe, D. 344
Stuhmiller, J.H. 214, 234
Stuhmiller, J.J. 564
Stumpf, H.J. 287, 549–550
Su, G.H. 65, 958–961*t*, 969*t*, 998–1000, 1060
Subbotin, V.I. 385, 465
Sudo, Y. 612
Sugimoto, J. 91
Sukhatme, S.P. 389, 392, 397–398
Sukomel, A.S. 465–466
Sukomel, L.A. 457
Sun, D.C. 65
Sun, H. 285
Sun, X. 564
Sundaram, R.K. 111, 579
Suslov, A. 958–961*t*, 1012, 1016
Sutherland W.A. 597
Suzuki, M. 969*t*, 998–1000
Svetlova, L.S. 434, 434*f*, 438
Svishchev, A. 743
Sweet, D. 131, 874, 876–880, 877–879*f*
Sylvester, N.D. 582
Szilard, R. 745, 760

T

Taborek, J. 359, 385, 392, 392*f*, 402
Taitel, Y. 557*t*, 694, 698–699
Takeda, T. 969*t*, 998–1000, 1057
Tamaki, M. 969*t*, 1044
Tambling, T.N. 1103–1104
Tanaka, M. 64
Tanarro, J. 92, 114, 920
Tanasawa, I. 389
Tang, Y.S. 448, 450*f*
Tanker, E. 532, 1141
Tapley, J. 64
Tarasova, N.V. 454
Tasaka, K. 969*t*, 1044
Taylor, M.F. 497–498
Tegnér, J. 803
Terzuoli, F. 1030
Teschendorff, V. 17–18, 642, 649
Thangam, S. 800
Theofanous, T.G. 15, 569–570, 571–572*t*, 761
Thielen, H. 14–15
Thome, J.R. 451, 459–460, 479, 482, 503, 554–555, 580
Thompson, D.E. 622
Thulin, E. 1104–1105, 1122
Thurgood, M.J. 550–551, 564, 743
Tian, W.X. 65, 958–961*t*, 969*t*, 998–1000, 1060
Tien, K. 912
Tobias, C.W. 378
Todd, D.R. 611–613
Todorova, N.K. 958–961*t*, 1031–1032
Todreas, N.E. 6, 92–93
Tolkacheva, N.N. 416–417
Tolman, E.L. 1131
Tomiya, A. 1019, 1047
Tomlinson, E.T. 807*t*, 969*t*, 1029
Tong, L.L. 958–961*t*, 992, 1016

Tong, L.S. 6, 90, 92–93, 448, 450f, 459–460
Tononi, R. 1037–1038
Toth, I. 131, 1038, 1108
Toumi, I. 668–669
Toutant, A. 201
Trapp, J.A. 661, 680
Travin, A. 792
Travis, J.R. 15
Trikouros, N. 1025t
Trosztel, I. 532–533, 1141
Trubachev, V.M. 442
Trunov, N.B. 443
Tu, J.Y. 447
Tuomisto, H. 635
Turinsky, P. 745, 760
Tuzson, J. 15–16
Tzykanov, V.A. 416

U

Uhle, J. 563
Ui, A. 131
Umminger, K. 9, 91, 102, 1038, 1108, 1130
Unal, C. 912
Unal, H.C. 569, 571–572t
Uspuras, E. 1064, 1066, 1110

V

Vaidyanathan, G. 969t
Valette, M. 238–239, 670–671, 689, 713–714, 722–723
Valtonen, K. 1030
Van Bragt, D.D.B. 1144
Van der Hagen, T.H.J.J. 969t, 1060, 1144
Van Rooyen, E. 503
Vanhoenacker, L. 995
Vasekin, V.N. 1117
Vasilevskji, V.P. 1104

Vedovi, J. 912
Velarade, G. 133, 1104
Vella, G. 957
Venn, J. 149*f*
Verdù, G. 14, 65, 73, 91, 925, 1030–1032
Vierow, K.M. 580
Vigni, A. 958–961*t*, 1030, 1112
Vigni, P. 15–16, 56, 66, 99, 259, 265, 520, 980, 997
Vijayan, P.K. 344–345, 529, 529–530*f*, 608, 1056
Villanueva, J.F. 912
Vinjamuri, K. 604
Vinogradov, V.N. 111, 581
Visentini, R. 958–961*t*, 1042
Viskanta, R. 850
von Terzi, V. 790, 795, 797–799
Voronov, V.N. 471
Vyskocil, L. 207–208

W

Wadekar, V. 455, 456*f*, 457
Wagner, R. 131
Wagner, W. 345*f*, 346
Wald, A. 870–871
Walker, S.P. 581, 1084
Wallin, S. 772, 789
Wallis, G.B. 6, 54, 90, 174, 448, 567, 575, 599, 700
Waltar, A.E. 416
Wang, C.C. 585
Wang, C.H. 613–616, 618
Wang, H. 61
Wang, J.-R. 912, 958–961*t*
Wang, L. 581
Wang, M. 795–796
Wang, W. 850
Wang, W.W. 958–961*t*, 969*t*, 998–1000, 1060
Wang, X. 564

Wastin, F. 92, 920
Watanabe, K. 550
Watanabe, T. 733, 739, 741, 746, 749, 755–757, 969*t*, 998–1000
Watzinger, H. 855
Weaver, W.L. 807*t*
Webb, R. 480
Weisman, J. 6, 92–93
Weiss, F.P. 516, 807*t*, 855, 958–961*t*, 1037
Welsa, P. 604
Wengle, H. 795, 797
Werner, H. 795
Wernz, S. 800
White, C.M. 497
Wickett, T. 73
Wilcox, D.C. 786–788*t*, 790
Wilks, S.S. 131, 867–868
Williams, B. 912
Wilson, G.E. 152, 154–155, 705, 866, 896–897
Winkler, F. 855
Winkler, F.J. 623–624
Wittum, G. 806–807
Wolfert, K. 516, 604
Wolff, H. 1043
Woo, S.W. 912
Woodruff, S.B. 549–550, 561–562
Woodruff, S.L. 800
Woods, B.G. 957
Woods, W.K. 499
Wootton, K.J. 419–420
Wu, C.-L. 1105–1106
Wu, D. 581
Wu, Q. 563
Wu, Y.W. 958–961*t*, 969*t*, 998–1000, 1060
Wulff, W. 154–155, 305–306, 604, 605*t*, 606*f*, 613, 850–851, 866, 896–897, 1104, 1134
Wysocki, A. 1134

X

Xiang, Y. 65
Xiao, J.T. 15
Xiao, X. 800
Xiao, Z. 564
Xiao, Z.X. 800
Xiaojing, L. 344–345
Xu, C. 515
Xu, D.Q. 385, 398–399
Xu, J. 788–789, 802
Xu, Y. 1134

Y

Yabushita, Y. 720–721
Yadigaroglu, G. 5, 7, 57–58, 201, 459–460, 529
Yagov, V.V. 457
Yamada, E. 378
Yamada, K. 344–345
Yamaguchi, A. 912
Yamamoto, Y. 720–721
Yamanouchi, A. 7
Yan, J. 1037
Yan, Y. 53–54
Yang, C. 347, 377
Yang, J. 958–961*t*, 969*t*, 998–1000, 1060
Yang, J.H. 912
Yang, L.X. 544
Yang, S.K. 768
Yang, X. 564, 958–961*t*, 969*t*, 998–1000, 1060
Yang, Y. 712–713
Yao, J.C. 466
Yao, W. 564
Yarcho, S.A. 478–481
Ybarrondo, L.J. 154
Yeoh, G.H. 447

Yih, S. 969*t*, 1034
Yitbarek, M. 14, 65, 73, 91, 925, 1030–1032
Ylijoki, J. 642
Ylonen, A. 969*t*, 1029
Yonomoto, T. 847, 958–961*t*
Yoon, H.-Y. 17–18
Young, M.Y. 53
Yovanovich, M.M. 416–417, 419–420
Yu, H. 581
Yu, J. 581
Yu, N. 712–713
Yu, X.-G. 958–961*t*, 1016
Yuann, Y.-R. 958–961*t*, 1044
Yun, B.J. 604, 969*t*
Yur'ev, Yu.S. 6
Yurko, J. 851

Z

Zaepffel, D. 237
Zaitsev, S.I. 957
Zakutaev, M.O. 957
Zamuraev, V.P. 408
Zarevskii, C.N. 416
Zarichniak, Yu.P. 377–378
Zarichnyak, Yu.P. 474
Zavattarelli, R. 499
Zerkak, O. 91
Zhang, C. 347
Zhang, D.C. 385, 398–399
Zhang, H.L. 800
Zhang, J. 581, 923
Zhang, P. 65
Zhang, Y.F. 800
Zhao, H. 564, 995
Zhao, M. 347
Zhao, Q. 385, 398–399

Zhao, R. 61
Zhemkov, L.I. 375
Zheng, Y. 544
Zhou, M.J. 544
Zhou, Y. 800
Zhu, X.B. 385, 398–399
Zhukov, A.V. 6
Zhuravlev, Yu.A. 412
Zienkiewicz, O. 806–807
Zigh, G. 733, 739, 741, 746, 749, 755–757
Zigrang, D.J. 582
Zimmermann, M.A. 933
Zobel, O.J. 370, 372, 376–377
Zorin, V.M. 402
Zou, L. 7
Zuber, N. 6–7, 18, 54, 62, 154–155, 230, 459–460, 529, 575, 580, 613, 717, 850–851, 866, 896–897
Zukova, R.I. 416–417
Zvetkov, F.F. 370, 375
Zwick, S.A. 569, 571–572t
Zysin, L.V. 479